Neutron Thermalization and Reactor Spectra

Vol. I

Proceedings of a Symposium, Ann Arbor, 17–21 July 1967

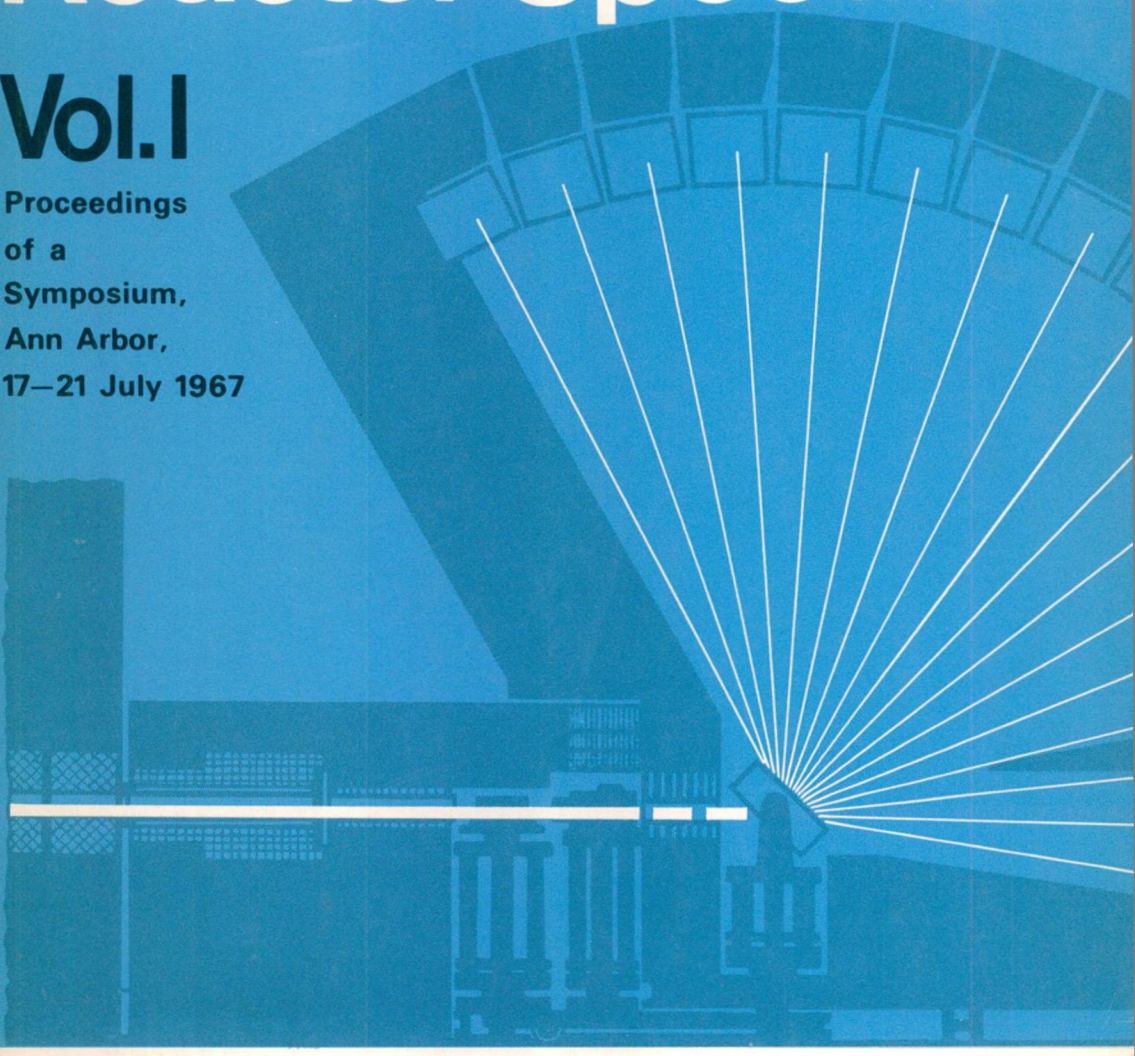

INTERNATIONAL ATOMIC ENERGY AGENCY, VIENNA, 1968

NEUTRON THERMALIZATION AND REACTOR SPECTRA

VOL. I

The following States are Members of the International Atomic Energy Agency:

AFGHANISTAN
ALBANIA
ALGERIA
ARGENTINA
AUSTRALIA
AUSTRIA
BELGIUM
BOLIVIA
BRAZIL
BULGARIA
BURMA
BYELORUSSIAN SOVIET SOCIALIST REPUBLIC
CAMBODIA
CAMEROON
CANADA
CEYLON
CHILE
CHINA
COLOMBIA
CONGO, DEMOCRATIC REPUBLIC OF
COSTA RICA
CUBA
CYPRUS
CZECHOSLOVAK SOCIALIST REPUBLIC
DENMARK
DOMINICAN REPUBLIC
ECUADOR
EL SALVADOR
ETHIOPIA
FINLAND
FRANCE
GABON
GERMANY, FEDERAL REPUBLIC OF
GHANA
GREECE
GUATEMALA
HAITI
HOLY SEE
HUNGARY
ICELAND
INDIA
INDONESIA
IRAN
IRAQ
ISRAEL
ITALY
IVORY COAST
JAMAICA
JAPAN
JORDAN
KENYA
KOREA, REPUBLIC OF
KUWAIT
LEBANON
LIBERIA
LIBYA
LUXEMBOURG
MADAGASCAR
MALI
MEXICO
MONACO
MOROCCO
NETHERLANDS
NEW ZEALAND
NICARAGUA
NIGERIA
NORWAY
PAKISTAN
PANAMA
PARAGUAY
PERU
PHILIPPINES
POLAND
PORTUGAL
ROMANIA
SAUDI ARABIA
SENEGAL
SIERRA LEONE
SINGAPORE
SOUTH AFRICA
SPAIN
SUDAN
SWEDEN
SWITZERLAND
SYRIAN ARAB REPUBLIC
THAILAND
TUNISIA
TURKEY
UGANDA
UKRAINIAN SOVIET SOCIALIST REPUBLIC
UNION OF SOVIET SOCIALIST REPUBLICS
UNITED ARAB REPUBLIC
UNITED KINGDOM OF GREAT BRITAIN AND NORTHERN IRELAND
UNITED STATES OF AMERICA
URUGUAY
VENEZUELA
VIET-NAM
YUGOSLAVIA

The Agency's Statute was approved on 23 October 1956 by the Conference on the Statute of the IAEA held at United Nations Headquarters, New York; it entered into force on 29 July 1957. The Headquarters of the Agency are situated in Vienna. Its principal objective is "to accelerate and enlarge the contribution of atomic energy to peace, health and prosperity throughout the world".

Printed by the IAEA in Austria
January 1968

PROCEEDINGS SERIES

NEUTRON THERMALIZATION AND REACTOR SPECTRA

PROCEEDINGS OF THE SYMPOSIUM ON
NEUTRON THERMALIZATION AND REACTOR SPECTRA
HELD BY THE
INTERNATIONAL ATOMIC ENERGY AGENCY
AT ANN ARBOR, MICHIGAN, 17-21 JULY 1967

VOL. I

In two volumes

INTERNATIONAL ATOMIC ENERGY AGENCY
VIENNA, 1968

NEUTRON THERMALIZATION AND REACTOR SPECTRA
(Proceedings Series)

ABSTRACT. Proceedings of a Symposium organized by the IAEA and held at Ann Arbor, Michigan, USA, 17 - 21 July 1967. The meeting was attended by 143 participants from 24 Member States and one international organization.

Contents: (Vol.I) Theory of neutron thermalization (15 papers); Scattering law (20 papers); Angular, space, temperature and time dependence of neutron spectra (9 papers). (Vol.II) Measurement of thermal neutron spectra and spectral indices, and comparison with theory (17 papers); Time-dependent problems in neutron thermalization (12 papers).

Each paper is in its original language (61 English, 1 French and 11 Russian) and is preceded by an abstract in English with one in the original language if this is not English. Discussions are in English.

(Vol. I: 656 pp., Vol. II: 530 pp., 16 × 24 cm, paper-bound, 473 figures)
(1968)

Price: Vol.I: US $13.50; £4.15.4
Vol.II: US $11.00; £3.17.8

NEUTRON THERMALIZATION AND REACTOR SPECTRA,
IAEA, VIENNA, 1968
STI/PUB/160

FOREWORD

Neutron thermalization, which concerns the approach to thermal equilibrium and the equilibrium distribution of neutrons in matter, is being studied in many research centres. Better understanding of this subject, together with a thorough knowledge of reactor spectra, promotes improved reactor calculations and technology.

For many years the International Atomic Energy Agency has encouraged and taken part in the exchange of information on these topics. Several symposia of the Agency have included them, for example the Symposium on Inelastic Scattering of Neutrons (Bombay, December 1964) and that on Pulsed Neutron Research (Karlsruhe, May 1965).

The Symposium on Neutron Thermalization and Reactor Spectra was held by the Agency on 17 - 21 July 1967, at Ann Arbor, Michigan, USA. Such a symposium was timely, for research has now reached a remarkable stage of maturity, where advanced experimental methods and mathematical techniques, giving very precise measurements, can provide a deep insight into the process of neutron thermalization. This is evident in the papers.

One hundred and forty-three theoreticians and experimentalists from 24 countries and one international organization participated, and 66 contributed and five review papers were presented. The present proceedings contain these papers and the record of the discussions. Each of the five sessions began with a review paper prepared independently of the contributed papers; the review paper gives a useful analysis of the present state of knowledge in the topic dealt with in the session.

In the first session, on "Theory of Neutron Thermalization", some refined approaches to the explanation of thermalization phenomena were presented. The inclusion of elastic scattering, fission and slowing-down kernels in transport and Boltzmann equations bridges the gap between theory and practical problems of interest to reactor physicists and designers. Challenging problems exist in the theoretical explanation of pulsed and neutron wave propagation experiments, and some interesting solutions were put forward. Since a thorough knowledge of the scattering law for solid and liquid moderators is the basis for reactor calculations, a session was devoted to new results in theoretical and experimental research on this topic. Two sessions were entitled "Angular, Space, Temperature and Time Dependence of Neutron Spectra" and "Measurements of Thermal Neutron Spectra and Spectral Indices, and Comparison with Theory". They dealt with current problems close to reactor technology and with mathematical tools for investigating processes in thermalizing media. In the session on "Time-dependent Problems in Neutron Thermalization", the results of recent research using pulsed and neutron wave techniques showed that these methods are becoming increasingly important in the investigation of neutron thermalization.

The Symposium was held at the kind invitation of the United States Government. Gratitude is also expressed to the authors of the papers, the chairmen of the sessions, and the discussion participants. The Secretariat of the Symposium is particularly thankful to the staff of Michigan University and to Professor P. Zweifel, whose help was invaluable in the preparation of the Symposium.

EDITORIAL NOTE

The papers and discussions incorporated in the proceedings published by the International Atomic Energy Agency are edited by the Agency's editorial staff to the extent considered necessary for the reader's assistance. The views expressed and the general style adopted remain, however, the responsibility of the named authors or participants.

For the sake of speed of publication the present Proceedings have been printed by composition typing and photo-offset lithography. Within the limitations imposed by this method, every effort has been made to maintain a high editorial standard; in particular, the units and symbols employed are to the fullest practicable extent those standardized or recommended by the competent international scientific bodies.

The affiliations of authors are those given at the time of nomination.

The use in these Proceedings of particular designations of countries or territories does not imply any judgement by the Agency as to the legal status of such countries or territories, of their authorities and institutions or of the delimitation of their boundaries.

The mention of specific companies or of their products or brand-names does not imply any endorsement or recommendation on the part of the International Atomic Energy Agency.

CONTENTS

THEORY OF NEUTRON THERMALIZATION (Session A)

Advances in neutron thermalization theory: A review (SM-96/103) 3
I. Kuščer
Discussion 26
Existence of a diffusion length in a finite prism of pure moderator (SM-96/3) 27
M.M.R. Williams
Discussion 42
Time-dependent thermalization with elastic scattering (SM-96/41) ... 45
M. Borysiewicz and J. Mika
Discussion 52
Использование системы полиномов Лагерра и присоединенных к ним функций для решения некоторых термализационных задач (SM-96/83) 53
Н.И. Лалетин, И.Г. Пасынков
Discussion 61
Energy-dependent Boltzmann equation with fission and slowing-down kernels (SM-96/63) 63
B. Nicolaenko and P.F. Zweifel
Discussion 79
Asymptotic behaviour of neutron transport processes (SM-96/6) 81
J.H. Hejtmanek
Discussion 93
Neutron wave propagation with a one-term degenerate thermalization kernel (SM-96/60) 95
H.G. Kaper, J.H. Ferziger and S.K. Loyalka
Discussion 110
Invariant embedding and propagation of neutron waves in a semi-infinite medium (SM-96/67) 113
A. Mockel
Relationship between pulsed, poisoning and wave experiments (SM-96/49) 125
P. Michael and M.N. Moore
Discussion 143
Некоторые методы решения задач теории термализации нейтронов (SM-96/38) 145
Л.В. Майоров, Г.Я. Труханов
Discussion 158
О нахождении решений некоторых задач переноса (SM-96/84) 159
В.И. Лебедев

Decay of a thermal neutron pulse in a finite coherent moderator (SM-96/39) 169
V. Ardente and G. Rossi
Discussion 181
Model for thermalization (SM-96/58) 183
P.B. Daitch and J.D. Jenkins
Discussion 191
Средняя плотность нейтронов в неоднородных средах (SM-96/35) 193
А.В. Степанов
Slowing-down and heating-up of neutrons in beryllium (SM-96/77) 223
A.K. Ghatak, I.C. Goyal, P.S. Grover and L.S. Kothari
Discussion 232

SCATTERING LAW (Session B)

Scattering law studies for moderators: A review (SM-96/104) 235
W. Gläser
Discussion 259
Calculations of the thermal scattering law for solids and liquids (SM-96/23) 261
R.G. Jarvis
Discussion 269
Analytical evaluation of the large time contribution to neutron scattering cross-sections (SM-96/51) 271
A.G. Gibbs and C.W. Lindenmeier
Discussion 282
Quasi-classical approximation for scattering from molecules (SM-96/65) 283
G.C. Summerfield and P.F. Zweifel
Amplitude of the two-quantum term in the scattering law for molecular gases (SM-96/68) 293
J.M. Carpenter and R.A. Schaefer
Neutron scattering from molecular nitrogen (SM-96/96) 303
J.A. Young
Multiple scattering in neutron double-differential cross-section measurements (SM-96/53) 311
E.L. Slaggie
Discussion 321
Temperature effect on neutron scattering kernels (SM-96/8) 323
L. Finkelstein
Neutron scattering in beryllium (SM-96/54) 333
J.U. Koppel and J.A. Young
Discussion 340
Изучение неупругого рассеяния нейтронов в графите при различных температурах (SM-96/80) 343
И.П. Еремеев, В.И. Мостовой, И.П. Садиков, М.Н. Северов, А.А. Чернышов
Discussion 359

Scattering laws for heavy water at 540°K and light water at 550°K (SM-96/19) 361
B. C. Haywood and D. I. Page
Discussion 372
Experimental scattering law for various reactor materials (SM-96/21) 373
I. M. Thorson
Discussion 388
Epithermal neutron inelastic scattering and scattering law for H_2O (SM-96/64) 389
G. J. Kirouac, W. E. Moore, L. J. Esch, K. W. Seemann and M. L. Yeater
Discussion 406
Inelastic neutron scattering in metal hydrides, UC and UO_2, and applications of the scattering law (SM-96/46) 407
S. N. Purohit, S. S. Pan, F. Bischoff, W. A. Bryant, C. Lajeunesse, M. L. Yeater, W. E. Moore, G. J. Kirouac, L. J. Esch and N. C. Francis
Discussion 434
Slow neutron scattering and thermalization by benzene (SM-96/76) ... 437
D. Sprevak, J. U. Koppel and J. A. Young
Calculated scattering law and thermal neutron spectrum for benzene (SM-96/71) 457
R. S. Marsden and H. L. McMurry
Molecular model for polyphenyls and its use in calculating reactor parameters (SM-96/40) 467
V. Ardente, R. Cuniberti, A. Kind and G. Rossi
Inelastic scattering of neutrons from benzene and water (SM-96/1) 477
D. K. Ross, F. P. Szabo and Y. Sanalan
Angular scattering by CH_2, $ZrH_{1.85}$ and C_6H_6 (SM-96/75) 493
J. R. Beyster, G. M. Borgonovi and G. W. Carriveau
Discussion 507
Neutron thermalization in diphenyl (SM-96/55) 509
J. M. Neill, H. Antunez and D. Sprevak
Discussion 517

ANGULAR, SPACE, TEMPERATURE AND TIME DEPENDENCE OF NEUTRON SPECTRA (Session C)

Methods currently used to compute spatially dependent thermal neutron spectra; A review (SM-96/101) 521
H. C. Honeck
Discussion 534
Importance of upscattering in the calculation of neutron spectra (SM-96/74) 537
D. Bollacasa and D. T. Goldman
Discussion 552

Integral and angular characteristics of thermal and neutron leakage spectra (SM-96/69) 555
J. M. Kallfelz and R. Kladnik
Discussion 568
Effect of scattering anisotropy on the calculation of pulsed-neutron decay constants (SM-96/50) 571
J. Dorning
Discussion 589
Effet de la non-uniformité du flux en ralentissement sur l'intégrale de résonance (SM-96/33) 591
P. Benoist, A. Kavenoky et M. Livolant
Thermalization calculations in a cylindrical shell (SM-96/90) 603
S. A. Kushneriuk, C. S. Kalman and A. M. Malecki
Discussion 616
Monte Carlo analyses of time-dependent neutron thermalization in organic moderator (SM-96/29) 617
E. Cupini and V. G. Molinari
Discussion 627
Neutron rethermalization studies in H_2O and ZrH_n (SM-96/12) 629
J. Saastamoinen
Calculations on the fundamental time-decay constant of water and polyethylene (SM-96/72) 643
G. W. Griffing
Discussion 652

Chairmen of sessions and secretariat of the Symposium 655

THEORY OF NEUTRON THERMALIZATION

(Session A)

ADVANCES IN NEUTRON THERMALIZATION THEORY
A review

I. KUŠČER
INSTITUTE OF PHYSICS,
UNIVERSITY OF LJUBLJANA,
LJUBLJANA, YUGOSLAVIA

Abstract

ADVANCES IN NEUTRON THERMALIZATION THEORY: A REVIEW. Parallel with further development of pulsed-neutron experiments and related techniques, thermalization theory has devoted much attention to eigenvalue problems of the transport equation, to problems of relaxation times and relaxation lengths, and to the related problem of neutron waves.

The pictures of eigenvalue spectra are now reasonably clear, although not always rigorously established. In each of the three quoted cases part of the spectrum covers a continuum corresponding to singular eigenfunctions. Outside the continuum there may be a finite or sometimes infinite set of discrete eigenvalues, associated with regular eigenfunctions. These eigenvalues disappear one by one by reaching the edge of the continuum if a characteristic parameter of the system is varied in a certain sense. Thus all the space-eigenvalues disappear if too much absorber is added to the medium. Discrete time-eigenvalues cease to exist if the size of the system is made sufficiently small. And no regular neutron waves (associated with discrete wavelengths and attenuation lengths) are possible beyond a critical frequency.

The puzzling phenomenon of so-called pseudo-discrete eigenvalues which in experiments with crystalline media have been found to invade the continuum has recently been clarified by careful analysis of a suitable model.

Solutions of eigenvalue problems are needed for predicting the values of diffusion parameters. They are also a prerequisite for solving the initial-value problem by the Laplace transform technique. For the time-dependent Green's function this leads to a bi-linear form in terms of the eigenfunctions; to this a 'transient' term, in the form of an integral along the edge of the continuum, must be added. Unfortunately, many of the mathematical steps involved in this procedure are still tentative and the proofs are missing.

In the development of methods of solution, problems with slab geometry have as usual been predominant. Approximate methods have often produced satisfactory results. Also the exact methods of Wiener and Hopf, and of Case, have been generalized to energy-dependent transport theory. However, practical success has in both cases been limited to simple models. A reciprocity property of the Green's function (a generalization of the detailed balance relation) has helped to obtain from diffusion theory easy asymptotic solutions of a few standard problems.

Some methods have been exchanged with the kinetic theory of gases, where similar eigenvalue, initial-value and boundary-value problems have arisen. An occasional link to radiative transfer has also been established.

1. INTRODUCTION: DEFINITIONS AND NOTATION

Since the time of the Brookhaven Conference five years ago, several review papers on the theory of neutron thermalization and related subjects have been presented at various meetings [1-6]. Moreover, half of a recent monograph [7] has been devoted to this subject. To avoid repetition, therefore, this review will attempt neither completeness nor impartiality, both of which are difficult to achieve anyway.

The review is primarily devoted to rigorous results of a general character. Results from diffusion theory; multigroup, P_N and other

approximations; calculations for specific models; calculations of diffusion and thermalization parameters; and calculational procedures in general, are mentioned only occasionally as examples. Since restriction to a well-defined field seems advisable, problems involving a combination with slowing-down theory, such as thermalization problems for multiplying media, are not discussed.

Neutron thermalization theory can be specified as a special branch of neutron transport theory, dealing with neutrons in thermal equilibrium, or approaching equilibrium, with some moderating system. Hence we shall have to discuss solutions of, and methods of solving, the transport equation (a linearized version of the Boltzmann equation) in the energy range up to a few times $k_B T$, where T is the temperature of the moderator.

A shorthand statement of that equation is

$$\left(\frac{\partial}{\partial t} + \hat{A}\right) N(\vec{r}, \vec{v}, t) = S(\vec{r}, \vec{v}, t) \tag{1}$$

with the Boltzmann operator $\hat{A}$ defined as follows:

$$\hat{A} f(\vec{r}, \vec{v}) = \vec{v} \cdot \nabla f(\vec{r}, \vec{v}) + v\Sigma(\vec{v}) f(\vec{r}, \vec{v}) - \int v' \Sigma_s(\vec{v}' \to \vec{v}) f(\vec{r}, \vec{v}') d^3 v' \tag{2}$$

where f is a function from some functional space to be specified later. The last term in Eq. (2) defines the scattering operator.

Unless stated otherwise, we shall consider a bounded system with no neutrons coming from outside. (Incident neutron beams may be imagined as being substituted by sources located just beneath the surface.) Hence the domain of the operator $\hat{A}$ comprises functions $f(\vec{r}, \vec{v})$ which vanish for $\vec{r}$ on the surface of the system and for $\vec{v}$ pointing inward.

We have introduced the velocity variable $\vec{v}$ instead of the more common E and $\vec{\Omega}$. The neutron density N, the source density S, and the macroscopic differential scattering cross-section $\Sigma_s(\vec{v}' \to \vec{v})$ are defined per unit velocity space.

Invariance against time reversal is reflected in the relation

$$v' M(v') \Sigma_s(\vec{v}' \to \vec{v}) = v M(v) \Sigma_s(-\vec{v} \to -\vec{v}') \tag{3}$$

where

$$M(v) = \left(\frac{m}{2\pi k_B T}\right)^{3/2} \exp\left(-\frac{mv^2}{2k_B T}\right)$$

With the minus signs omitted, Eq. (3) is known as the detailed-balance relation. Such omission is usually permissible because, in general, neutron cross-sections are also parity invariant. We then have, also,

$$\Sigma(\vec{v}) = \Sigma(-\vec{v}) \tag{4}$$

The last relation is irrelevant whenever the medium is macroscopically isotropic, as will be assumed henceforth ($\Sigma = \Sigma(v)$). In such a case $\Sigma_s(\vec{v} \to \vec{v}')$ depends only on v, v' and the scattering angle δ, and we may write

$$\Sigma_s(\vec{v} \to \vec{v}')\, v'^2 = \sum_{\ell=0}^{\infty} \frac{2\ell+1}{4\pi} \Sigma_\ell(v \to v')\, P_\ell(\cos\delta) \tag{5}$$

and for the azimuth-integrated kernel,

$$\Sigma_s(v, \mu \to v', \mu') \equiv \int_0^{2\pi} \Sigma_s(\vec{v} \to \vec{v}')\, v'^2\, d\varphi'$$

$$= \sum_{\ell=0}^{\infty} \frac{2\ell+1}{2} \Sigma_\ell(v \to v')\, P_\ell(\mu)\, P_\ell(\mu') \tag{6}$$

In most problems to be reviewed, we shall deal with a macroscopically uniform system with time-independent properties, as already indicated in Eq. (2). However, more general cases are easily introduced, with little or no loss to the qualitative mathematical picture.

The detailed-balance relation makes it possible to symmetrize the kernel of the integral in Eq. (2). This is one of the reasons, aside from mathematical convenience, for usually considering solutions within a Hilbert space, namely the L_2 space corresponding to the symmetrized version of the equation. We shall follow this practice, but avoid symmetrization. To do this we define the scalar product in L_2 space with the aid of a weight function, equal to the reciprocal of the Maxwellian distribution function,

$$(f, g) = \iint f(\vec{r}, \vec{v})\, \overline{g(\vec{r}, \vec{v})}\, [M(v)]^{-1}\, d^3\vec{r}\, d^3\vec{v} \tag{7}$$

with the integrals taken over the volume of the system and over the whole velocity space, respectively.

It is important to know the exact lower bounds of the functions $\Sigma(v)$ and $v\,\Sigma(v)$

$$\kappa^* = \min.[\Sigma(v)]$$

$$\lambda^* = \min.[v\,\Sigma(v)]$$

For the usual monatomic gas model $\Sigma(v)$ is continuous and decreases monotonically from $\Sigma(0) = \infty$ to $\Sigma(\infty) = \kappa^* > 0$; whereas $v\,\Sigma(v)$ attains its minimum $\lambda^* > 0$ at $v = 0$, and increases monotonically for $v > 0$. Many other moderators show a similar behaviour, and we shall therefore say that this is the normal case, although exceptions of every kind are known (e.g. Bragg cut-offs).

2. SURVEY OF EIGENVALUE SPECTRA

Let us first turn to the eigenvalue problems, namely, special solutions of the homogeneous transport equation (S = 0), proportional to $e^{-\lambda t}$ (or $e^{-i\omega t}$), or to $e^{-\kappa x}$ (or e^{iBx}), or to a product of two or several such factors. Knowledge of these solutions, and of the corresponding eigenvalue spectra, is a prerequisite for an analytical treatment of initial-value problems and problems with given sources.

As can be seen from the Proceedings of the BNL Conference, more thorough investigation of eigenvalue problems was begun only at that time, chiefly by Corngold and his group [9] and by Nelkin [8, 10]. Further effort has more or less clarified the general picture, although it is too early to determine whether there are still problems to be solved. In many of those cases already solved the polish of mathematical rigour is still lacking.

In the time-eigenvalue problem we make the ansatz

$$N(\vec{r}, \vec{v}, t) = N(\vec{r}, \vec{v})e^{-\lambda t}$$

which leads to the equation

$$\hat{A}\, N(\vec{r}, \vec{v}) = \lambda\, N(\vec{r}, \vec{v}) \tag{8}$$

If a solution within the Hilbert space is sought, the decay constant λ must be an eigenvalue, i.e. it must belong to the point spectrum of the operator $\hat{A}$. Unfortunately, this is not the only part of the spectrum; another part, or even the whole spectrum, covers a continuum. It is often assumed, but by no means generally proved, that this part is a purely continuous spectrum, and in particular that it contains no embedded eigenvalues.

2.1. Relaxation of a uniform neutron distribution

If a uniform isotropic neutron distribution is assumed for an infinite medium, Eq. (8) simplifies to [9]

$$v\,\Sigma(v)\,N(v) - \int_0^\infty v'\Sigma_0(v' \to v)\,N(v')\,dv' = \lambda N(v) \tag{9}$$

where N(v) refers to the neutron density per unit speed interval. For a solid moderator only the inelastic part of the scattering cross-section is taken into account in $\Sigma(v)$ and $\Sigma_0(v' \to v)$.

Because the operator represented by the left-hand side of Eq. (9) is self-adjoint in the space $L_2(0, \infty)$, with the weight $[v^2M(v)]^{-1}$, the spectrum is confined to the real axis. All intervals covered by the values of $v\Sigma(v)$, i.e. normally the interval $\lambda^* \leq \lambda < \infty$, belong to the spectrum [9]. To the left of this interval we find an infinite or finite set of discrete eigenvalues, λ_n, if the moderator is a fluid or a solid, respectively [11]. In the first case the eigenvalues approach the accumulation point quite fast, roughly like a geometric progression.

For an absorbing medium, of course, all eigenvalues are positive. They are conveniently enumerated as follows,

$$0 \leq \lambda_0 < \lambda_1 \leq \lambda_2 \leq \ldots < \lambda^*$$

where the case $\lambda_0 = 0$ of a non-absorbing medium has also been included.

An apparent contradiction to these statements arises from the existence of solutions to the problem of Wigner and Wilkins (see Ref. [7]). These are solutions of Eq. (9) for an absorbing medium and for $\lambda = 0$, and are characterized by a Fermi tail, $N(v) \propto 1/v^2$ for $\frac{1}{2} mv^2 \gg k_B T$ if $\Sigma(v) = \text{const.}$ in this range. However, it would be wrong to accept $\lambda = 0$ as an eigenvalue, because the Wigner-Wilkins solution is outside our L_2 space (the normalization integral in the sense of Eq. (7) diverges). From the physical viewpoint we may add that the Wigner-Wilkins problem corresponds to sources at infinity of velocity space, and has nothing to do with eigenvalue problems.

Many details of the eigenvalue problem have been investigated for various models, and the first few of the eigenvalues λ_n have been computed [12-15]. Rigorous arguments for the gas case have been presented by Ukai [16] and in a simplified version in a recent paper on the closely related gas-kinetic problem [17]. The finer structure of the continuous part of the spectrum has been investigated by Shizuta [18].

Though for a fluid moderator we know that an infinite number of discrete eigenvalues below λ^* exist, only a few are resolvable by the computational methods used so far. Such methods give a fair picture of the first few eigenfunctions only. The ultimate reason for this limitation can be seen in the oscillatory behaviour of the higher eigenfunctions in the low-speed range. For the monatomic gas model a crude description (not valid for $v \to 0$) of this behaviour is given by [11, 17]

$$N \sim v^{-\frac{1}{2}} \sin\left(\tfrac{1}{2} \nu \ln v - \delta\right)$$

where $\nu = [6(1 + M^{-1})^2 - 1]^{\frac{1}{2}}$.

2.2. Relaxation of a distribution with buckling

To simulate the more realistic problem of a finite moderator, we may introduce a buckling by asking for solutions of the form [19]

$$N(x, v, \mu, t) = N(v, \mu)\, e^{iBx}\, e^{-\lambda t}$$

and by looking for eigenvalues λ_n as functions of B. This leads to the equation

$$[v\Sigma(v) + iBv\mu]\, N(v, \mu) - \int_0^\infty \int_{-1}^{1} v' \Sigma_s(v', \mu' \to v, \mu) N(v', \mu')\, dv'\, d\mu' = \lambda N(v, \mu) \tag{10}$$

The area in the complex plane of λ, covered by the values of the function $v\Sigma(v) + iBv\mu$ for $0 \leq v < \infty$ and $-1 \leq \mu \leq 1$, belongs to the spectrum

of the operator represented by the left-hand side of this equation [4], In the normal case this area is bounded by the hyperbola-like curve (Fig. 1)

$$\mathrm{Re}(\lambda) = v\Sigma(v), \quad \mathrm{Im}(\lambda) = \pm Bv, \quad 0 \leq v < \infty$$

To the left of this region there may be a set of discrete eigenvalues. Only for isotropic scattering has it been proved that this set lies on the real axis [19]. With the possible exception of a liquid moderator [20] this set is finite or empty.

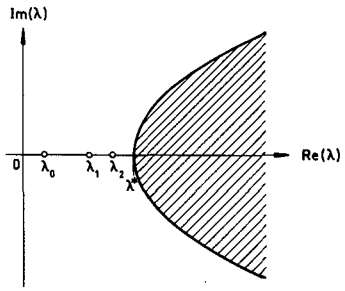

FIG. 1. Eigenvalues and continuous spectrum (shaded) for relaxation of a neutron distribution with buckling.

To demonstrate by a typical example the reasoning used in investigations of eigenvalue spectra, a sketch of a proof of the statement about the continuously distributed part of the spectrum will be described here [20]. The proof is based upon the following theorem [21]:

If for some operator $\hat{A}$ and for some λ a family of approximate normalized solutions φ_δ exists, in the sense that

$$\left\| (\hat{A} - \lambda)\varphi_\delta \right\| \to 0 \quad \text{for } \delta \to 0 \tag{11}$$

then λ belongs to the spectrum of $\hat{A}$.

Normalization is now understood in the two-dimensional L_2 space, $0 \leq v < \infty$, $-1 \leq \mu \leq 1$, with the weight $[v^2 M(v)]^{-1}$.

For the proof we choose some values λ, v_λ, and μ_λ, such that $\mathrm{Re}(\lambda) = v_\lambda \Sigma(v_\lambda)$, $\mathrm{Im}(\lambda) = iBv_\lambda \mu_\lambda$, and such that $v\Sigma(v)$ is continuous at this point. If the second term in Eq. (10) is omitted, a suitable approximate solution clearly is one, the square of which simulates a δ-function located at the chosen point in the (v, μ) plane:

$$\varphi_\delta(v, \mu) = [v^2 M(v)/\delta^2]^{1/2} \quad \text{for } v_\lambda \leq v < v_\lambda + \delta, \ \mu_\lambda \leq \mu < \mu_\lambda + \delta$$
$$= 0 \text{ outside this region.}$$

Indeed, we see that for this part of the operator condition (11) is fulfilled, because of the continuity of $v\Sigma(v)$, and the mentioned portion of the complex λ-plane therefore belongs to the spectrum. It is also easy to see that in this case there is no other spectrum.

It should take only a few more straightforward steps to verify that the addition of the second term in Eq. (10) does not destroy the validity of condition (11). We have to repeat this verification for each type of moderator (gas, liquid, amorphous solid, microcrystalline solid), taking into account the general properties of the scattering kernels.

For a gaseous moderator the verification can be by-passed by referring to a theorem of Weyl in Ref. [22], because in this case the scattering operator is compact, i.e. completely continuous. The latter fact has been proved by Montagnini et al. [23] and can also be inferred from the corresponding gas-kinetic result of Grad [24]. Weyl's theorem also assures for this case that only discrete eigenvalues can arise outside the mentioned, continuously distributed spectrum. If, however, the scattering operator is not compact, it may give rise to some additional continuous spectrum. Such a case has been established by Corngold for a solid moderator [20].

If it is assumed that all discrete eigenvalues λ_n are real, we may draw a tentative picture of the functions $\lambda_n(B^2)$ (Fig. 2). As long as buckling is small, perturbation theory can be applied. For the fundamental, i.e. the lowest, eigenvalue, and for 1/v absorption ($v\,\Sigma(v) = \alpha = \text{const.}$), this results in the well-known series

$$\lambda = \alpha + DB^2 - CB^4 + \ldots \tag{12}$$

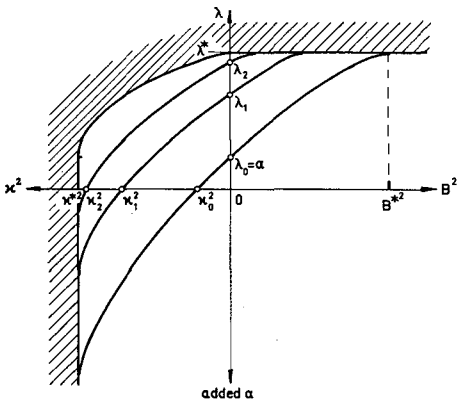

FIG. 2. Corngold's diagram showing the dependence of time-eigenvalues upon buckling and of space-eigenvalues upon the concentration of added absorber (1/v absorption law is assumed). Values in the shaded area belong to the continuous spectrum.

The eigenvalues $\lambda_n(B^2)$ have also been computed for a wider range of bucklings, and for a variety of models [13, 25-27].

If absorption does not follow the 1/v law, the formalism is somewhat more complicated, even for $B = 0$. In this case an expansion in powers of concentration of absorber is obtained. The discovery of a rather high discrepancy in the quadratic term, between theoretical predictions and observations, has aroused considerable interest [28, 29].

As indicated in Fig. 2, the bound λ^* of the continuum is not affected by the buckling. The situation is different, however, if instead of the oscillating spatial behaviour, a real exponential dependence is assumed

$$N(x, v, \mu, t) = N(v, \mu)e^{-\kappa x}\, e^{-\lambda t}$$

If the previous standard procedure is repeated, we find [25] that the bound of the continuum is lowered to the value min. $[v\,\Sigma(v) - \kappa v]$. In normal cases this gives a parabola-like boundary curve on the picture of the eigenvalues (Fig. 2).

2.3. Relaxation lengths

Instead of asking for time-eigenvalues λ_n as functions of the given B^2 or $-\kappa^2$, we may just as well ask for the space-eigenvalues (the reciprocal relaxation lengths) κ_n as functions of the given λ. Often we are interested only in the time-independent problem ($\lambda = 0$), which leads us to the equation

$$[\Sigma(v) - \kappa\mu]\Phi(v,\mu) = \int_0^\infty\int_{-1}^{1} \Sigma_s(v', \mu' \to v, \mu)\,\Phi(v', \mu')\,dv'\,d\mu' \tag{13}$$

with $\Phi(v,\mu) = v\,N(v,\mu)$.

Usually one or a few pairs of discrete eigenvalues $\pm\kappa_n$ exist, and there is a continuum on the real axis beyond $\pm\kappa^*$ [19]. It can be shown, with the use of detailed balance and by the fact that the absorption cross-section is non-negative, that all eigenvalues κ_n are real, and that none are embedded in the continuum. The pair of smallest eigenvalues ($\pm\kappa_0$) is again simple (except for a non-absorbing medium, when the pair merges at $\kappa_0 = 0$), and corresponds to the unique pair of non-negative eigensolutions $\Phi_0(v, \pm\mu)$. The reciprocal of κ_0 is called the diffusion length.

It is worthwhile to study the dependence of the diffusion length, and of space-eigenvalues in general, upon the amount of poisoning. If the poison is a $1/v$ absorber, the absorption rate is the mathematical equivalent of a negative decay constant. Hence in this way the above picture (Fig. 2) can be continued beneath the horizontal axis [19].

Several procedures for computing the κ_n have been used [15, 30]. For degenerate scattering kernels still another scheme is suggested by Case's method, where the κ_n are found from the zeros of a certain determinant [5], $\det \vec{\Lambda}(1/\kappa_n) = 0$.

2.4. Neutron waves

In recent years experiments with so-called neutron waves have been completed by the pulsed neutron technique. Transport-theoretical interpretations of such experiments have been given by Moore [33] and (in a multigroup version) by Travelli [34].

We again imagine an infinite medium and ask for solutions of the form

$$N(x, v, \mu, t) = N(v,\mu)\, e^{ikx} e^{-\beta x} e^{-i\omega t}$$

Obviously the only mathematical difference from the previous cases is that we now have an imaginary decay constant, $\lambda = i\omega$, and therefore a complex buckling $B = k + i\beta$, or a complex space-eigenvalue,

$$\kappa = \beta - ik$$

After these substitutions are made, the equation for $N(v, \mu)$ is the same as Eq. (10). We now ask for complex eigenvalues κ_n, that is, for both the wave numbers k_n and the damping factors β_n, as functions of frequency ω.

For a fixed ω we may get a set of discrete eigenvalues $\kappa_n(\omega)$. In addition to this, we find, by the same reasoning as before, that a continuously distributed spectrum is formed by the values of the fraction $[\Sigma(v) - i\omega/v]/\mu$ [20, 34-36]. In the normal case this part of the spectrum covers two sectors of the complex plane, bounded by the hyperbola-like curves (Fig. 3),

$$\mathrm{Re}(\kappa) = \pm\Sigma(v), \quad \mathrm{Im}(\kappa) = \pm\,\omega/v, \quad 0 \leq v < \infty$$

For crystalline media the picture is more complicated because of the Bragg cut-offs [20, 35].

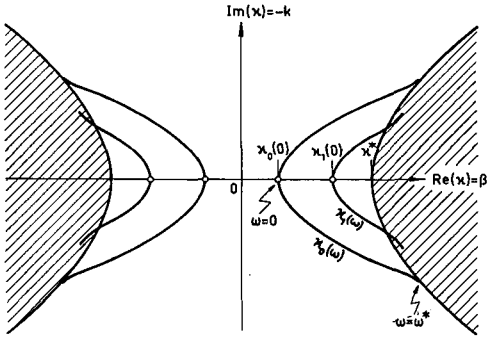

FIG. 3. Complex eigenvalues for neutron waves. The shaded area represents the continuous spectrum for $\omega = \omega^*$.

If the frequency is increased, the continuously distributed part of the spectrum spreads, until, in the limit of $\omega \to \infty$, it covers the half-planes $|\mathrm{Re}(\kappa)| > \kappa^*$. At the same time the discrete eigenvalues move upon curves in the complex plane of κ, as shown by Fig. 3. A portion of the curve $\kappa_0(\omega)$ near the real axis can be obtained from Eq. (12) in an obvious way. Other parameters of interest can then be deduced, such as the 'wave' velocity for $\omega \to 0$ [37]

$$c_0 \approx 2\left(\frac{\alpha}{D} - \frac{C\alpha^2}{D^3}\right)^{\frac{1}{2}}\left(\frac{1}{D} - \frac{2C\alpha}{D^3}\right)^{-1} \tag{14}$$

(The distinction between phase and group velocities vanishes in this limit.)

2.5. Bounded systems

The problems discussed so far represent highly idealized examples, because an infinite medium was assumed in all calculations. Neither the solution with a definite buckling, nor a combination of a finite number of such solutions, can give an exact picture of the decay modes in bounded systems. This is especially true for small systems where the concept of buckling becomes risky [19, 38].

Such an approach could possibly lead to exact results through a Fourier expansion of the distribution function, which would involve arbitrarily high values of buckling [39]. It seems plausible that the continuously distributed part of the spectrum is formed by superposition of a set of spectra such as shown by Fig. 2. In the resulting picture this

part of the spectrum is expected, in the normal case, to cover the half-plane $\mathrm{Re}(\lambda) \geq \lambda^*$.

A safer derivation of the spectrum requires a fresh start based on Eq. (8). In analogy with what was done before, we select some λ, $\mathrm{Re}(\lambda) > \lambda^*$, and choose a vector $\vec{v}_\lambda$, such that its magnitude satisfies the equation $v_\lambda \Sigma(v_\lambda) = \mathrm{Re}(\lambda)$. Then we try

$$\varphi_\delta(\vec{r}, \vec{v}) = [M(v)/V\delta^3]^{\frac{1}{2}} \quad \exp[i\,\mathrm{Im}(\lambda)\vec{r}\cdot\vec{v}/v^2]$$

$$\text{for } v_{\lambda i} \leq v_i < v_{\lambda i} + \delta, \quad i = 1, 2, 3$$

$$= 0 \quad \text{for } \vec{v} \text{ outside that region.}$$

A straightforward calculation shows that

$$\left|(\hat{A} - \lambda)\,\varphi_\delta(\vec{r}, \vec{v})\right| \lesssim \left|\varphi_\delta(\vec{r}, \vec{v})\right| \left[\frac{d(v\,\Sigma(v))}{dv}\right]_{v=v_\lambda} \delta + R\delta^a \tag{15}$$

where the reasoning has been shortened by assuming differentiability of $v\Sigma(v)$. The remainder term $R\delta^a$ comes from the scattering part of the operator $\hat{A}$. As in section 2.2, a more detailed estimate must be made for each type of moderator (gas, liquid, etc.). For each case we should show that R belongs to the L_2 space defined by Eq. (7), and that $a > 0$. This proves that condition (11) is fulfilled and that therefore λ belongs to the spectrum.

With some restrictions, it has been proved that the other half-plane, $\mathrm{Re}(\lambda) < \lambda^*$, contains at most a finite number of isolated eigenvalues (real for isotropic scattering) of finite multiplicity [39-43]. A case where the set of eigenvalues may be infinite is also known [42]. Vidav has shown recently [44] that some assertions about this part of the spectrum can be made under much weaker assumptions, by the aid of a very general theorem of Shmul'yan [45]. It is sufficient to assume that the scattering operator is bounded, and that the generalized Peierls operator, corresponding to the Laplace transform of Eq. (1), or an iterated or a certain intermediate operator, is compact. Whereas we may be fairly sure about the first condition, the validity of the second has been established only for a special case with isotropic scattering [41]. Still, there is reason to hope that it is also fulfilled more generally. Shmul'yan's theorem then would lead to the conclusion that the half-plane $\mathrm{Re}(\lambda) < \lambda^*$ contains only isolated eigenvalues. These are poles of the resolvent operator $(\hat{A} - \lambda)^{-1}$.

Gotusso et al. [46] have computed the fundamental decay constant for a monatomic gas sphere, using Feynman's perturbation technique. The related slab problem has been investigated (for several scattering models) by Kladnik [47], who applied Nelkin's variational method (previously used with Milne's problem). Čopič [48] has obtained higher approximations by polynomial expansions.

A simple consequence of detailed balance is that if $N_n(\vec{r}, \vec{v})$ is an eigensolution of Eq. (8), then $N_n(\vec{r}, -\vec{v})$ solves the adjoint equation, in the sense of definition (7) [49, 50]. Both solutions correspond to the same eigenvalue. It follows, by a standard procedure [51], that the $N_n(\vec{r}, \vec{v})$ and $N_n(\vec{r}, -\vec{v})$ form a biorthogonal set. If the normalization integral is posi-

tive (which again is generally believed, though proved only under very special restrictions) we may impose a normalization

$$(N_m^\dagger, N_n) \equiv \iint N_m(\vec{r}, -\vec{v})\, N_n(\vec{r}, \vec{v})\, [M(v)]^{-1}\, d^3\vec{r}\, d^3\vec{v} = \delta_{mn} \tag{16}$$

2.6. Disappearance of the discrete spectra

In all of the above cases it has been found that under certain circumstances the discrete eigenvalues merge into the continuum. It is generally assumed, but rarely proved, that after touching the edge of the continuum the eigenvalues truly disappear, and not that they wander into the continuum.

In the problem represented by Eq. (9), calculations predict such an effect if a sufficient amount of a very strongly non-$1/v$ poison of the "cooling" type is added to the moderator [11]. However, it is doubtful whether a complete disappearance of the discrete spectrum can be achieved with existing neutron-absorbing materials.

Buckling, which accounts in an approximate way for leakage, has a similar effect [13, 19]. With increasing buckling the eigenvalues λ_n one by one reach the edge λ^* of the continuum, as shown by Fig. 2, until finally only the latter part of the spectrum is left. The critical value B^{*2}, at which this happens, has been computed for simplified models [27].

As expected in view of the above results, we find for bounded systems that the discrete time-eigenvalues disappear whenever the size of the system becomes too small. An example of this kind was first presented by Nelkin [10], whereas rigorous proofs, under lesser restrictions, have been worked out by Albertoni and Montagnini [39, 40], and others [41-43].

The size of the system for which the last discrete time-eigenvalue disappears is sometimes well within the range of the usual pulsed-neutron experiments [52].

If scattering is isotropic, a sufficient condition for the disappearance of the discrete spectrum can be derived in the form of an inequality for the maximum diameter of the system [5],

$$d_{max} < \left\{ \int_0^\infty \int_0^\infty [\Sigma_0(v' \to v)]^2\, [v'^3 M(v')/v^3 M(v)]\, dv\, dv' \right\}^{-\frac{1}{2}}$$

For a better estimate the Hilbert-Schmidt norm used here should be replaced by the true norm of the same operator [42].

Computations for a sphere made of free carbon gas (with isotropic scattering) have shown that the last discrete eigenvalue disappears when the diameter becomes smaller than roughly 3.5 epithermal mean free paths [46].

The results for bounded systems do not directly apply to the slab problem. Doubts about this case [19] were removed by Ukai [53]; see also Refs. [54-56]. It has been found that here too, contrary to the situation in one-speed theory, the discrete time-eigenvalues disappear if the slab is made sufficiently thin.

Corngold [19] has found that the space-eigenvalues κ_n are also capable of disappearing by reaching the bound κ^* of the continuously

distributed spectrum. For realistic absorption laws the space eigenvalues disappear, as shown in Fig. 2, whenever the concentration of absorber is increased beyond a certain amount [57, 58]. Wood [27] has shown by calculations that this may happen within the range accessible to experiments.

A similar change of the spectrum is seen repeated in Fig. 3, where discrete eigenvalues κ_n are no longer present if the frequency exceeds a certain value ω^*. For a free gas of atomic mass 12, Travelli [34] has shown that the lowest eigenvalue κ_0 disappears at $\omega^* = 3.3\ \lambda^*$. (This value is extracted from Travelli's data by taking into account the relation $\lambda^* = \overline{v}_M \kappa^*$, valid for the monatomic gas model with small absorption, where $\overline{v}_M$ is the average speed of the atoms, $\overline{v}_M = (8k_B T/\pi M)^{1/2}$.)

Apparently for this case no general theorem about the disappearance of the discrete eigenvalues has so far been established.

2.7. Singular eigenfunctions

If the continuously distributed spectrum found in the above problems truly is a pure continuous spectrum, no eigensolution within the L_2 space can be associated with any point belonging to this continuum. However, singular eigenfunctions belonging to some broader functional space might be constructed. For the case of Eq. (9), Koppel [59] has used singular eigenfunctions involving δ-functions and belonging to the values $\lambda \geq \lambda^*$. These eigenfunctions have properties similar to those used by Case [60] in angle-dependent one-speed problems.

Travelli [34] has indicated that analogous singular eigenfunctions exist for the neutron-wave problem, and no doubt the same can be said for the rest of the above problems.

The interesting question arises: what happens to a regular eigensolution when the corresponding eigenvalue disappears? In particular: what happens to the non-negative eigensolution, corresponding in some of the problems to the lowest eigenvalue (λ_0 or κ_0)? We may suspect that in such cases, even after the disappearance of the discrete spectrum, a non-negative solution continues to exist, though singular in some way [11]. As before, such a solution would correspond to the lower bound of the spectrum which now is λ^* or κ^* for the time- and space-eigenvalue problems, respectively. Conjectures of this kind could possibly be proved on the basis of suitable generalizations of the Perron-Jentzsch theorem. (See Ref. [61].)

For the sake of better understanding, we may quote a 'physical' explanation, first for the problem described by Eq. (9). Too strong absorption cooling (produced by some non-1/v poison) causes a breakdown of the competition of two processes: thermalization (the reshuffling between the energy ranges), and absorption cooling. Therefore, after a very long time, any initial distribution will approach a singular distribution, containing a strong peak of cold neutrons [11]. For a bounded system, the same effect is expected to be produced by diffusion cooling.

The space-eigensolutions behave differently, since in the normal case the bound κ^* of the continuum is given by the epithermal limit of $\Sigma(v)$. Heating of the neutron gas is now responsible for the fundamental mode to become singular, and the singularity is expected to consist of an enhanced epithermal tail [58].

3. INITIAL-VALUE PROBLEMS

3.1. The Laplace-transform technique

One of the main tasks of thermalization theory is to predict the time-evolution of a given initial neutron distribution in a moderator; that is, we have to solve the homogeneous transport equation [Eq. (1) with S = 0] for t > 0 and for a given $N^{(0)} \equiv N(\vec{r}, \vec{v}, 0)$. Again a bounded system will be assumed.

Two methods have been used for proving the existence and uniqueness of the solution of this problem. Case and Zweifel [62] begin with the integral form of the transport equation (the generalized Peierls equation) and represent the solution by a Neumann series. Convergence is assured under quite broad conditions, which constitutes the required proof. It is clear that this approach, if applied to computations, would be useful only for short times, when convergence is fast.

There is little need to base this method upon a rigorous derivation of the integral equation from the integro-differential one (1), because both can be derived independently from physical arguments. Hence either one of them may be taken as the basis for further mathematical treatment.

The second method [53, 63-65], aimed at long-time approximations, consists in the application of the Laplace-transform technique to Eq. (1). To justify such a procedure, and to assure the existence and uniqueness of the solution, one must prove (by aid of the Hille-Yosida theorem) that $\hat{A}$ in Eq. (1) is the infinitesimal generator of a strongly continuous semigroup.

Only a rough description of this technique will be given in the following. The Laplace transform of N is defined by the integral

$$\mathcal{N}_\lambda(\vec{r}, \vec{v}) = \int_0^\infty N(\vec{r}, \vec{v}, t)\, e^{\lambda t}\, dt \qquad \text{for } \mathrm{Re}(\lambda) < \lambda_0$$

and by its analytic continuation. From (1) we derive the equation

$$(\hat{A} - \lambda)\mathcal{N}_\lambda = N^{(0)} \tag{17}$$

which has the form of an inhomogeneous time-independent transport equation, and should be solved by corresponding methods. In operator notation the result may be written as

$$\mathcal{N}_\lambda = (\hat{A} - \lambda)^{-1}\, N^{(0)} \tag{18}$$

The solution of the time-dependent problem is then obtained by inverse Laplace transformation,

$$N(\vec{r}, \vec{v}, t) = \lim_{\omega \to \infty} \frac{1}{2\pi i} \int_{\gamma - i\omega}^{\gamma + i\omega} \mathcal{N}_\lambda(\vec{r}, \vec{v})\, e^{-\lambda t}\, d\lambda \tag{19}$$

where $\gamma < \lambda_0$.

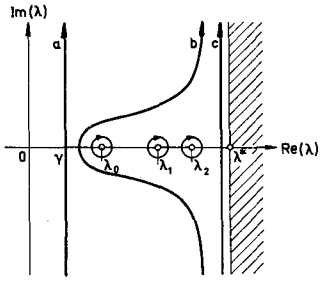

FIG.4. Integration paths (a,b,c) used in solving the initial-value problem for a bounded system. The shaded area shows the continuous spectrum.

The solution will assume a practically useful form only if we are able to shift and deform the path of integration as shown by Fig.4. The integration path then breaks up into circles enclosing the eigenvalues λ_n, which are poles of the integrand, and a remaining integral alongside the border of the continuum. The residue of the integrand at $\lambda = \lambda_n$ is proportional to the corresponding eigenfunction [49,50,53], namely equal to

$$(N_n^\dagger, N^{(0)}) N_n(\vec{r},\vec{v}) \exp(-\lambda_n t)$$

if the eigenfunctions are normalized according to Eq.(16). Thereby an expansion in terms of the decay-modes is derived,

$$N(\vec{r},\vec{v},t) = \sum_n (N_n^\dagger, N^{(0)}) N_n(\vec{r},\vec{v}) \exp(-\lambda_n t) + R(\vec{r},\vec{v},t) \tag{20}$$

The 'transient' term R, to be expressed by the mentioned remaining integral [53], presumably shows a long-time behaviour roughly like $\exp(-\lambda^* t)$.

Only for a special one-speed problem have all the mathematical steps involved in this procedure been legalized by rigorous proofs [63]. It will probably not be easy to generalize the proofs to velocity-dependent theory and to arbitrary geometry. Even if the previously mentioned uncertainties about the spectrum of the operator $\hat{A}$ are removed, and the full application of Shmul'yan's theorem is assured, one further difficulty remains: We must prove that the behaviour of the Laplace transform $\mathcal{N}_\lambda(\vec{r},\vec{v})$ at $\mathrm{Im}(\lambda) \to \pm\infty$, $\mathrm{Re}(\lambda) < \lambda^*$, is such that the shifting of the integration path is allowed.

3.2. Quasi-discrete decay constants

We have seen (section (2.6) that for a sufficiently small system the discrete terms in the expansion (20) are absent. Hence in such cases the decay rate of a neutron distribution should (slowly) approach the value λ^*. Contrary to this expectation, experiments with some crystalline materials, notably beryllium, have shown an exponential decay which for small samples was much faster than $e^{-\lambda^* t}$. Such observations appeared to "stand in direct contradiction to rather direct consequences of the Boltzmann equation" [46]. A lively discussion about the 'quasi-discrete decay modes' was started and resulted in a series of papers [66-76].

The multigroup computations of Ghatak and Honeck [26] left little doubt that the effect is genuine. Their well-known diagram of λ_n versus B^2 indicates something resembling discrete decay constants embedded in the continuum. Theorists had to explain these findings too, aside from the experimental facts.

An explanation, in line with earlier conjectures [4], has been given by Corngold and Durgun [73, 74]. Their calculation is based on a diffusion equation with prescribed buckling, and a simple model for the scattering kernel: isotropic scattering, a separable kernel for inelastic scattering, and a term accounting for elastic scattering. The latter term is missing below the Bragg cut-off, where $\Sigma_{inel}(v) \propto 1/v$; above the cut-off Σ_{el} and Σ_{inel} are constant.

Since the operator involved in the diffusion approximation is self-adjoint, the spectrum lies on the real axis. The continuously distributed part covers the interval $\lambda \geq \lambda^*$, instead of an area as in sections 2.2 and 2.5. In spite of this intrinsic spectral difference, physical arguments indicate that the diffusion approximation should fairly well reproduce the true time-evolution.

As before, there are no discrete eigenvalues below λ^* if buckling is sufficiently large. After the inverse Laplace transformation is carried out, the integration path is deformed, so that it runs along both sides of the line $\lambda^* \leq \lambda < \infty$. Hence the response of some array of detectors can be written in the form

$$R(t) = \int_{\lambda^*}^{\infty} K(\lambda)\, e^{-\lambda t}\, d\lambda \tag{21}$$

The continuous expansion-amplitude $K(\lambda)$ is related to $\mathcal{N}_\lambda$ in a simple way.

Further calculations have shown that the amplitude $K(\lambda)$ has a relatively sharp peak at some $\lambda_p > \lambda^*$, whereas below this value K is small. Thereby an intermediate decay, roughly proportional to $\exp(-\lambda_p t)$, is accounted for. Only after an exceedingly long waiting time could a decay such as $\exp(-\lambda^* t)$ be approached.

A striking interpretation stems from the observation that the line $\lambda \geq \lambda^*$ is a branch cut-off $\mathcal{N}_\lambda$ and of related functions. Corngold and Durgun have investigated the behaviour of these functions on the unphysical sheets, and found a pair of poles in the immediate vicinity of λ_p. This is a direct consequence of the Bragg cut-off, and of the low value of the total scattering rate below it. Nothing like this is found for models with smoothly varying cross-sections.

We may notice that if, following the proposal of Kothari [66], we ignore the inelastic scattering below the Bragg cut-off, the λ^* is shifted to a higher value $\lambda_{Bragg} = v_{Br}\, \Sigma(v_{Br})$. The previous unphysical pair of poles should then merge into one pole on the real axis below λ_{Bragg}, thereby becoming a discrete decay constant λ_0. Correspondingly, the peak of the integrand in Eq. (21) shrinks into a delta function, yielding a discrete decay mode.

Quite recently Corngold has given an even more satisfactory explanation based upon transport theory [20]. Because of the Bragg cut-off, a gap in the form of a vertical strip splits the continuously distributed spectrum (Fig. 1) into two segments. The left-hand segment is very thin,

and for a certain model it degenerates into a vertical line through the point λ^*. When buckling is sufficiently increased, the fundamental eigenvalue λ_0 jumps, in a way, across this segment. After that we have inside the gap a true discrete (not a 'quasi-discrete') eigenvalue.

3.3. The time-dependent Green's function

Let us now specialize the result (20) of section 3.1. Assuming that the mathematical difficulties mentioned there have been overcome, we may imagine that the initial distribution is created by a unit monokinetic instantaneous point source,

$$N^{(0)} = \delta(\vec{r} - \vec{r}_0)\,\delta(\vec{v} - \vec{v}_0)$$

The corresponding solution is a time-dependent Green's function of the transport equation, and will be denoted by $N(\vec{r}_0, \vec{v}_0 \to \vec{r}, \vec{v}; t)$. Its decay-mode expansion follows from Eq. (20) [49, 50],

$$N(\vec{r}_0, \vec{v}_0 \to \vec{r}, \vec{v}; t) = \sum_n \frac{N_n(\vec{r}_0, -\vec{v}_0)\, N_n(\vec{r}, \vec{v})}{M(v_0)} \exp(-\lambda_n t) + R(\vec{r}_0, \vec{v}_0 \to \vec{r}, \vec{v}; t) \tag{22}$$

A different expansion, useful especially in plane geometry, is that by a Fourier integral; in other words, the neutron pulse is expressed as a superposition of neutron waves. Such studies are useful in the description of pulse-propagation experiments [32, 36, 37].

An important symmetry property of the Green's function can be derived from the detailed-balance relation. First we show that the function $[M(v_0)/M(v)]\, N(\vec{r}_0, -\vec{v}_0 \to \vec{r}, -\vec{v}; t)$ satisfies an equation adjoint to Eq. (1). Then, in view of a general symmetry relationship among adjoint Green's functions [51], we immediately find the reciprocity theorem [5, 49, 50]:

$$M(v_0)\, N(\vec{r}_0, \vec{v}_0 \to \vec{r}, \vec{v}; t) = M(v)\, N(\vec{r}, -\vec{v} \to \vec{r}_0, -\vec{v}_0; t) \tag{23}$$

We may say that this is a generalization of detailed balance to macroscopic systems of uniform temperature. At the same time Eq. (23) represents an extension of a similar theorem in time-independent one-speed theory [77].

The reciprocity theorem relates the outcome of an experiment to another one with the source and detector interchanged. In some cases the theorem is useful for fitting diffusion approximations to initial conditions. Such examples are the time- and energy-dependent albedo problems for a semi-infinite medium and for a thick slab. In both cases long-time asymptotic solutions have been expressed in terms of the solution of the steady-state Milne problem [5, 49].

4. TIME-INDEPENDENT PROBLEMS IN SLAB GEOMETRY

4.1. The method of singular eigenfunction expansions

As is well known, two exact analytical methods have been successfully applied in one-speed transport theory, mainly in slab geometry: the technique of Wiener and Hopf, and the singular eigenfunction expansions of Case [60, 78]. More recently both methods have been generalized also to energy-dependent theory. However, except for certain simplified models, the practical success of these generalizations has not been very encouraging.

Although the two methods differ, they are equivalent at least in one respect: whatever has been solved by one method appears solvable by the other one too. Opinions occasionally voiced that the Wiener-Hopf technique is the better one fail to convince the users of Case's method, and vice versa. Quite in line with this state of affairs the present report is limited to the developments of only one of the two methods.

The generalization of Case's method to velocity-dependent transport theory is due to Bednarz and Mika [79]. They have simplified the formalism by introducing the collision density ψ (per unit solid angle and per unit speed interval) and the new variable

$$\xi = \kappa^{*}\mu/\Sigma(v).$$

As in section 2.3 we look for special solutions of the form

$$\psi(x, v, \xi) = \phi(v, \xi; \nu)e^{-x/\nu}.$$

(For the sake of consistency with the practice in one-speed theory, $1/\nu$ has been substituted for the parameter κ of section 2.3.

The equation obeyed by the eigenfunctions is essentially the same as Eq.(13). For isotropic scattering, and with κ^{*-1} as the unit of length, it reduces in the normal case to

$$(\nu - \xi)\phi(v, \xi; \nu) = \frac{\nu}{2}\int_{-1}^{1} d\xi' \int_{v_{\xi'}}^{\infty} \Sigma_0(v' \to v)\phi(v', \xi'; \nu)\,dv'. \tag{24}$$

where $v_{\xi'}$ is the root of the equation $|\xi'|\,\Sigma(v_{\xi'}) = 1$.

Besides the regular solutions of Eq.(24), already discussed in section 2.3, there is a continuous set of singular eigenfunctions, corresponding to the interval $-1 \leq \nu \leq 1$. These eigenfunctions are composed of an analytic term and a term proportional to $\delta(\nu - \xi)$. Bednarz and Mika have used un-normalized eigenfunctions and have built an extra arbitrariness into the coefficient of the δ-term. Thereby the whole set of eigenfunctions was made complete in the full-range, in the sense that the set can be used for expanding arbitrary functions $f(v, \xi)$, defined for $-1 \leq \xi \leq 1$ and $0 \leq v < \infty$. This property permits the solution of, for instance, the time-independent plane-geometry Green's function problem for an infinite medium.

For degenerate kernels it seems profitable to introduce normalized eigenfunctions, with the δ-term also standardized in a prescribed way. Completeness with respect to the variable v is lost thereby, and the expansion must be supplemented by an additional term, orthogonal in a certain sense to all other terms [5].

To solve Milne's and other problems for a semi-infinite medium, Leonard and Ferziger [80] have proved also half-range completeness, using a somewhat different formalism. Here only half of the set is used ($\nu>0$), and ξ is restricted to the interval $0<\xi\leq 1$. At least for a degenerate kernel a more traditional kind of proof of half-range completeness seems feasible [5]. Since half-range orthogonality can also be established, one has the deceptive impression that calculations should be just as easy as in one-speed theory. The impression is wrong, because the calculations involve matrices (mostly non-commuting) with as many rows and columns as there are terms in the kernel. For instance, the weight function $\mu H(\mu)$ of one-speed half-range orthogonality is replaced by a matrix $\xi\vec{H}(\xi)$. Whereas for Chandrasekhar's H-function (or for Case's $\gamma(\mu)$ and $X(\mu)$ closed-form expressions exist, the $\vec{H}$-matrix has to be computed numerically from a system of integral equations.

In view of this situation several authors have tried to find ways to evade the half-range formalism. Fuchs and Collatz [81, 82], and Żelazny [83] have argued that the iteration procedure used for slab problems can just as well be based on full-range expansions as on half-range ones. In velocity-dependent theory full-range expansions are by far easier, and should be preferred, unless a too high price is paid for slower convergence of the iteration. This remains to be seen.

A different way has been tried by Pahor [84], who applied the invariance arguments of Ambarzumian and Chandrasekhar to Case's eigensolutions. Thereby he derives the properties of the $\vec{H}$-matrix, in terms of which the emerging angular densities for the albedo and Milne problems are expressed. Hence we again face the task of computing this matrix.

There is one exceptional model (aside from the trivial constant cross-section approximation) which escapes all these difficulties, because closed-form solutions do exist, and all calculations are just as easy as in one-speed theory. This is the case of a separable kernel for isotropic scattering

$$\Sigma_0(v' \to v) = \langle v\Sigma_s \rangle^{-1}\, 4\pi v^3\, M(v)\Sigma_s(v)\Sigma_s(v')$$

It differs from one-speed theory only in that instead of the constant c (the number of secondaries per collision) a variable $c(\xi)$ has to be introduced

$$c(\xi) = \langle v\Sigma_s \rangle^{-1} \int_{v_\xi}^{\infty} 4\pi v^3 M(v)[\Sigma_s(v)]^2 dv \tag{25}$$

Mika [85] has investigated this model in detail, and solved the Milne problem as an example of application. His formalism can still be slightly simplified by the use of half-range orthogonality relations [86, 87].

Roughly the same difficulties found with the degenerate kernel are encountered in generalizations of Case's method to multigroup approximations. Such schemes, originally due to Żelazny and Kuszell [88], have been further developed for the separable case [89, 90], as well as for the more general models [91-94].

4.2. The thermal Milne problem

This problem continued to attract some interest not only for its own sake, but also because its solution is needed for a proper fit of diffusion approximations to boundary conditions.

Kallfelz and Reichardt [95] have further refined the method based on Nelkin's variational principle, which is specifically suited to thermal problems for a medium of uniform temperature. A different approach based on the knowledge of the one-speed solution was introduced by Schofield and Lancefield [96, 97]. Direct computational solutions for various realistic kernels have been worked out by Eisenhauer [98]. Mockel [99] has tested the method of invariant embedding, which leads to a system of non-linear integral equations.

For the separable kernel, solutions have been obtained, as already mentioned, by singular eigenfunction expansions, and also by the Wiener-Hopf technique [100, 101]. Williams has extended this technique to the two-term degenerate kernel [102] and to a two-group scheme [103]. On the other hand, for a kernel differing little from a separable one, a perturbation method has been found useful [104].

An interesting generalization of Milne's problem is obtained by introducing lateral buckling [105]. The purpose of such solutions is to simulate neutron distributions in prisms.

4.3. The Kottwitz problem

A non-uniformity in the temperature of the moderator tends to push the neutron gas to one side, which effect is known as thermal diffusion. If the temperature varies smoothly over long distances, a diffusion approximation can be used, once the thermal diffusion factor is known. A modified method for calculating this factor has recently been applied by Seghal [106].

In the Kottwitz problem an infinite-plane sharp-temperature discontinuity in an infinite medium is considered. In the vicinity of the discontinuity, the diffusion approximation is no longer applicable and a transport solution is required. For the heavy-gas model a solution of this kind has been worked out by Williams [107], and for the case of a constant cross-section by Gritton et al. [108].

5. RELATIONS TO OTHER FIELDS OF PHYSICS

5.1. Relations to radiative transfer

The mathematical aspects of neutron transport and of radiative transfer differ to a considerable extent, except in the one-speed and monochromatic cases, respectively, where we have a 1:1 equivalence.

However, also beyond these obvious cases equivalence has been established for a pair of particular models [86]: the separable kernel in velocity-dependent neutron transport, and the picket-fence model and its generalization, the uniform line-blanketing model, in non-grey radiative transfer. In the latter model, after integration over a certain set of spectral intervals, the transport equation becomes the same as that for a separable kernel in neutron thermalization. For solutions see Refs. [85-87, 89, 90, 100].

5.2. Relations to the kinetic theory of gases

Neutron thermalization theory can be considered a branch of the kinetic theory of gases. In many ways neutron thermalization is simpler because of the linearity of the transport equation. On the other hand, the moderator does not need to be a gas and may have quite complicated properties.

Contrary to a first impression, it is not true that this relationship was exhausted long ago. Again and again problems in neutron transport crop up which can be solved by borrowing some method or result from gas theory, and vice versa.

Some of the models used in neutron transport have their counterparts in gas theory. It is well known that the assumption of isotropic scattering in the centre-of-mass system is equivalent to the assumption of hard-sphere molecules. The heavy-gas model is the same as the Lorentz model of a gas mixture [109].

The discovery of continuous spectra in the relaxation problem was almost simultaneous in neutron thermalization [9] and in gas theory [24]. Some of the reasoning in the gas problem was later taken over to the neutron case [4]. In return, Ferziger and Buckner applied Koppel's analysis [59] and Case's method to the gas relaxation problem [110, 111]. The proof that for a gaseous moderator Eq. (9) has an infinite set of discrete time-eigenvalues was easily transferred to the corresponding relaxation problem of a single gas [17].

Some of the features of neutron waves are found again in the theory of sound propagation in rarefied gases [112]. As in the neutron case, no regular waves appear to exist if the frequency exceeds a certain critical value.

A counterpart of the Milne problem is the slip problem of a rarefied gas. In solving it, Shen [113] has applied the variational method, whereas other authors have used Case's and related techniques [114, 115].

The problem of determining the classical self-correlation function $G_s(\vec{r}, t)$ for a hard-sphere gas is the same as the problem of a point neutron-source in an infinite monatomic hydrogen moderator, and has been treated by corresponding methods [116, 117].

5.3. Relations to thermodynamics and statistical mechanics of irreversible processes

Since the discovery of the role of thermal diffusion in neutron transport, several authors have applied to it the laws of irreversible thermodynamics, in particular Onsager's reciprocity relation. Grmela [118-120] has also attempted to make use of Prigonine's principle of minimum

entropy production, which, under certain restrictive conditions, should single out the time-independent solution.

A statistical interpretation of the minimum entropy production principle can be used — just as in the kinetic theory of gases — for determining the velocity distributions associated with almost equilibrium time-independent neutron distributions [121]. Such a variational principle is not new, as it is equivalent to an integral equation already used earlier for the same purpose.

Occasionally Kubo's formalism has been tried for calculating the diffusion parameters of neutrons [5, 118, 120]. Again the final expressions are the same as those known from conventional procedures.

Investigations along these frontier lines have been slightly disappointing. They have produced little more than simplified examples illustrating the meaning and limitations of these general principles.

ACKNOWLEDGEMENTS

I am indebted to Professors Noel Corngold and Paul F. Zweifel and to Dr. Michael M.R. Williams, who have taught me a great deal about the problems and methods discussed here, and from whom I have received much encouragement and stimulation. My thanks are also due to Professor Ivan Vidav for his kind help with the functional analytic aspects of the eigenvalue problems.

REFERENCES

[1] CORNGOLD, N., in Lectures from the Second Neutron Physics Conference (Boyne Mountain, Michigan, 1962), Michigan Memorial Phoenix Project (1964) 186.
[2] NELKIN, M., in Reactor Physics (Summer School lectures, Zakopane 1964), IAEA, Vienna, internal publication (1966).
[3] KAZARNOVSKI, M.V., in Reactor Physics (Summer School lectures, Zakopane 1964), IAEA, Vienna, internal publication (1966).
[4] CORNGOLD, N., in Pulsed Neutron Research I (Proc. Symp. Karlsruhe 1965), IAEA, Vienna (1965) 199.
[5] KUŠČER, I., in Developments in Transport Theory (Summer School lectures, Ankara 1965), Academic Press, London (1967).
[6] CORNGOLD, N., in Reactor Physics in the Resonance and Thermal Regions (Proc. ANS Meeting, San Diego 1966), MIT Press, Cambridge, Mass. (1966).
[7] WILLIAMS, M.M.R., The Slowing Down and Thermalization of Neutrons, North-Holland Publ. Co., Amsterdam (1966).
[8] Several papers in Proc. Brookhaven Conf. on Neutron Thermalization 4, BNL-719 (C-32) (1966).
[9] CORNGOLD, N., MICHAEL, P., WOLLMAN, W., Nucl. Sci. Engng 15 (1963) 13.
[10] NELKIN, M., Physica 29 (1963) 261.
[11] KUŠČER, I., CORNGOLD, N., Phys. Rev. 139 (1965) A981; 140 (1965) AB5.
[12] OHANIAN, M.J., DAITCH, P.B., Nucl. Sci. Engng 19 (1964) 343.
[13] SHAPIRO, C.S., CORNGOLD, N., Phys. Rev. 137 (1965) A1686; SHAPIRO, C.S., Rep. BNL-8433 (1964).
[14] WOOD, J., J. Nucl. Energy (Parts A/B) 20 (1966) 143.
[15] WILLIAMS, M.M.R., Nucl. Sci. Engng 26 (1966) 262.
[16] UKAI, S., J. nucl. Energy (Parts A/B) 19 (1965) 833.
[17] KUŠČER, I., WILLIAMS, M.M.R., Phys. Fluids (to be published).
[18] SHIZUTA, Y., Progr. theor. Phys. (Kyoto) 32 (1964) 489.
[19] CORNGOLD, N., Nucl. Sci. Engng 19 (1964) 80.
[20] CORNGOLD, N., Symp. on Transport Theory (Amer. Math. Soc., New York, 1967) to be published.

[21] HILLE, E., PHILLIPS, R.S., Functional Analysis and Semigroups, Amer. Math. Soc., Providence, R.I. (1957).
[22] KATO, T., Perturbation Theory for Linear Operators, Springer-Verlag, Berlin (1966) 244, Theorem 5.35.
[23] MONTAGNINI, B., DEMURU, M.L., J. math. Analysis Applic. 12 (1965) 49.
[24] GRAD, H., Proc. 3rd Int. Symp. Rarefied Gas Dynamics I (Paris 1962), Acad. Press, New York (1963) 26.
[25] TRAVELLI, A., CALAME, G.P., Nucl. Sci. Engng 20 (1964) 414.
[26] GHATAK, A.K., HONECK, H.C., Nucl. Sci. Engng 21 (1965) 227.
[27] WOOD, J., in Pulsed Neutron Research I (Proc. Symp. Karlsruhe 1965), IAEA, Vienna (1965) 219; J. nucl. Energy (Parts A/B) 20 (1966) 219.
[28] CALAME, G.P., Nucl. Sci. Engng 20 (1964) 352.
[29] BECKURTS, K.H., in Pulsed Neutron Research I (Proc. Symp. Karlsruhe 1965), IAEA, Vienna (1965) 3.
[30] KLADNIK, R., Nucl. Sci. Engng 17 (1963) 185.
[31] PEREZ, R.B., UHRIG, R.E., Nucl. Sci. Engng 17 (1963) 90.
[32] Several papers in Pulsed Neutron Research I and II (Proc. Symp. Karlsruhe 1965), IAEA, Vienna (1965); and in Proc. Symp. on Neutron Noise, Waves, and Pulse Propagation (Gainesville, Florida 1966), USAEC Symposium Series, No.9 (1967).
[33] MOORE, M.N., Nucl. Sci. Engng 26 (1966) 354.
[34] TRAVELLI, A., Proc. Symp. on Neutron Noise, Waves, and Pulse Propagation (Gainesville, Florida 1966), USAEC Symposium Series, No.9 (1967).
[35] DUDERSTADT, J.J., Nucl. Sci. Engng 29 (1967) 156.
[36] Several papers in Trans. Amer. nucl. Soc. 10 (San Diego Meeting, 1967).
[37] CHEUNG, K.Y., MILEY, G.H., Nucl. Sci. Engng 24 (1966) 216.
[38] WOOD, J., WILLIAMS, M.M.R., J. nucl. Energy 21 (1967) 113.
[39] ALBERTONI, S., MONTAGNINI, B., in Pulsed Neutron Research I (Proc. Symp. Karlsruhe 1965) IAEA, Vienna (1965) 239.
[40] ALBERTONI, S., MONTAGNINI, B., J. math. Analysis Applic. 13 (1966) 19.
[41] BEDNARZ, R., Rep. INR 615/IX - A/R, Warsaw (1965); and in Pulsed Neutron Research I (Proc. Symp. Karlsruhe 1965), IAEA, Vienna (1965) 259.
[42] UKAI, S., J. math. Analysis Applic. 18 (1967) 297.
[43] BORYSIEWICZ, M., MIKA, J., Nukleonik (to be published).
[44] VIDAV, I., J. math. Analysis Applic. (to be published).
[45] SHMUL'YAN, YU.L., Doklady 101 (1955) 35; Amer. math. Soc. Translations (2) 10 (1958) 341.
[46] GOTUSSO, L., MONTAGNINI, B., PIERPAOLI, V., Nukleonik 8 (1966) 341.
[47] KLADNIK, R., Nucl. Sci. Engng 23 (1965) 291.
[48] ČOPIČ, M., Trans. Amer. nucl. Soc. 8 (1965) 507; and Rep. NIJS R-449, Ljubljana (1965).
[49] KUŠČER, I., McCORMICK, N.J., Nucl. Sci. Engng 26 (1966) 522.
[50] KUŠČER, I., Kernenergie (to be published).
[51] MORSE, P.M., FESHBACH, H., Methods of Theoretical Physics, McGraw-Hill, New York (1953).
[52] CORNGOLD, N., MICHAEL, P., Nucl. Sci. Engng 19 (1964) 91.
[53] UKAI, S., J. nucl. Sci. Technol. (Tokyo) 3 (1966) 430.
[54] MOCKEL, A., Nucl. Sci. Engng 26 (1966) 279.
[55] MIKA, J., STANKIEWICZ, R., Nukleonik (to be published).
[56] BEDNARZ, R.J., Trans. Amer. nucl. Soc. 10 (1967) 291.
[57] LEONARD, A., Nucl. Sci. Engng 22 (1965) 489.
[58] CORNGOLD, N., Nucl. Sci. Engng 24 (1966) 410.
[59] KOPPEL, J.U., Nucl. Sci. Engng 16 (1963) 101.
[60] CASE, K.M., Ann. Phys. (N.Y.) 9 (1960) 1.
[61] KREĬN, M.G., RUTMAN, M.A., Uspeki matem. nauk (N.S.) 3 (1948) 3; Amer. math. Soc. Translations, 2nd ed. (1) 10 (1962) 199.
[62] CASE, K.M., ZWEIFEL, P.F., J. math. Phys. 4 (1963) 1376.
[63] WING, G.M., Introduction to Transport Theory, J. Wiley & Sons, New York (1962).
[64] MARTI, J.T., Nukleonik 8 (1966) 159.
[65] MIKA, J., Nukleonik 9 (1967) 200, 303.
[66] KOTHARI, L.S., Nucl. Sci. Engng 23 (1965) 402.
[67] CORNGOLD, N., Nucl. Sci. Engng. 23 (1965) 403.
[68] Several papers in Pulsed Neutron Research I and II (Proc. Symp. Karlsruhe 1965), IAEA, Vienna (1965).

[69] GHATAK, A.K., GOYAL, I.C., KOTHARI, L.S., J. nucl. Energy (Parts A/B) 19 (1965) 679.
[70] WILLIAMS, M.M.R., J. nucl. Energy (Parts A/B) 20 (1966) 222.
[71] GOYAL, I.C., GHATAK, A.K., KOTHARI, L.S., J. nucl. Energy (Parts A/B) 20 (1966) 667.
[72] WOOD, J., J. nucl. Energy (Parts A/B) 20 (1966) 649.
[73] CORNGOLD, N., DURGUN, K., Nucl. Sci. Engng 25 (1966) 450.
[74] CORNGOLD, N., DURGUN, K., Nucl. Sci. Engng (in press).
[75] WOOD, J., Nukleonik (in press).
[76] JENKINS, J.D., DAITCH, P.B., Trans. Amer. nucl. Soc. 10 (1967) 177.
[77] CASE, K.M., Rev. mod. Phys. 29 (1957) 651.
[78] CASE, K.M., ZWEIFEL, P.F., An Introduction to Linear Transport Theory, Addison-Wesley, Reading, Mass. (in press).
[79] BEDNARZ, R.J., MIKA, J.R., J. math. Phys. 4 (1963) 1285.
[80] LEONARD, A., FERZIGER, J.H., Nucl. Sci. Engng 26 (1966) 170, 181.
[81] FUCHS, K., COLLATZ, S., Kernenergie 7 (1964) 386.
[82] COLLATZ, S., Kernenergie 9 (1966) 329.
[83] ŻELAZNY, R., Proc. 3rd UN Int. Conf. PUAE 2 (1964) 86.
[84] PAHOR, S., Nucl. Sci. Engng (to be published).
[85] MIKA, J., Nucl. Sci. Engng 22 (1965) 235.
[86] STEWART, J.C., KUŠČER, I., McCORMICK, N.J., Ann. Phys. (N.Y.) 40 (1966) 321.
[87] McCORMICK, N.J., KUŠČER, I., Trans. Amer. nucl. Soc. 9 (1966) 444.
[88] ŻELAZNY, R., KUSZELL, A., Ann. Phys. (N.Y.) 16 (1961) 81; Physics of Fast and Intermediate Reactors II IAEA, Vienna (1963) 55.
[89] SIEWERT, C.E., ZWEIFEL, P.F., Ann. Phys. (N.Y.) 36 (1966) 61.
[90] SIEWERT, C.E., ZWEIFEL, P.F., J. math. Phys. 7 (1966) 2092.
[91] ZUMBRUN, K., Rep. EIR 72 Würenlingen, Switzerland (1965).
[92] IVANOV, L.D., Zh. prikl. mekh. tekh. Fiz. (1966) 58.
[93] BARAN, W., Warsaw discussion (1966).
[94] SIEWERT, C.E., SHIEH, P.S., J. nucl. Energy 21 (1967) 383.
[95] KALLFELZ, J.M., REICHARDT, W., Nukleonik 9 (1967) 148.
[96] SCHOFIELD, P., UKAEA Rep. T.P. 99 (1963).
[97] LANCEFIELD, M.J., SCHOFIELD, P., UKAEA Rep. T.P. 282 (1967).
[98] EISENHAUER, C., Nucl. Sci. Engng 19 (1964) 95.
[99] MOCKEL, J., Trans. Amer. nucl. Soc. 10 (1967) 207.
[100] WILLIAMS, M.M.R., Nucl. Sci. Engng 18 (1964) 260.
[101] ARKUSZEWSKI, J., Nucl. Sci. Engng 27 (1967) 104.
[102] WILLIAMS, M.M.R., Nucl. Sci. Engng 27 (1967) 511.
[103] WILLIAMS, M.M.R., J. Math. Phys. 45 (1966) 64.
[104] WILLIAMS, M.M.R., Nucl. Sci. Engng 19 (1964) 353.
[105] WILLIAMS, M.M.R., Nukleonik 9 (1967) 305.
[106] SEGHAL, B.R., Nucl. Sci. Engng 24 (1966) 212.
[107] WILLIAMS, M.M.R., Brit. J. appl. Phys. 16 (1965) 1727.
[108] GRITTON, E.C., LEONARD, A., BARRETT, P.R., Trans. Amer. nucl. Soc. 10 (1967) 208.
[109] ANDERSEN, K., SHULER, K.E., J. chem. Phys. 40 (1964) 633.
[110] FERZIGER, J.H., Phys. Fluids 8 (1965) 426.
[111] BUCKNER, J.K., FERZIGER, J.H., Phys. Fluids 9 (1966) 2309.
[112] BUCKNER, J.K., FERZIGER, J.H., Phys. Fluids 9 (1966) 2315.
[113] SHEN, S.F., Proc. 5th Int. Symp. Rarefied Gas Dynamics I (Oxford 1966), Acad. Press, N.Y. (1967).
[114] CERCIGNANI, C., Ann. Phys. (N.Y.) 20 (1962) 219.
[115] LEONARD, A., MULLIKIN, T.W., Ann. Phys. (N.Y.) 30 (1964) 235.
[116] NELKIN, M., GATHAK, A.K., Phys. Rev. 135 (1964) A4.
[117] DESAI, R.C., NELKIN, M., Nucl. Sci. Engng 24 (1966) 142.
[118] GRMELA, M., J. nucl. Energy (Parts A/B) 19 (1965) 81.
[119] GRMELA, M., Rep. UJV 1354/65, Prague (1965).
[120] GRMELA, M., Prague Thesis (1966); and paper in preparation.
[121] KUŠČER, I., ČADEŽ, A., Physica (submitted for publication).

DISCUSSION

I. THORSON: Can the presence of a continuum of eigenvalues always be associated with a breakdown of the assumption that the solutions can be written as separable functions of space, time and energy?

I. KUŠČER: Separability depends on the choice of the functional space in which the eigensolutions are sought. If this is the L_2 space, the continuously distributed part of the spectrum is expected normally to be a pure continuous spectrum. This means that no exact eigenmodes can be attributed to such spectral points in the λ-plane (i. e. separability fails here). Yet in a broader functional space, e. g. in the space of distributions, this may sometimes still be possible. In cases where no discrete spectrum exists, we might still have a non-negative fundamental mode $N(\vec{r}, \vec{v}) \exp(-\lambda^* t)$ in this broader sense, with the $N(\vec{r}, \vec{v})$ being singular in some way. Of course this mode is approached only very slowly, because the spectrum is dense near λ^*.

J. MIKA: I should like to draw your attention to the fact that in some cases it might be impossible to attach a definite physical meaning to the so-called continuous eigenfunction. This can be seen, for instance, from the example considered by Wing in his code for a slab surrounded by a vacuum and purely absorbing material, respectively. Despite the fact that the physical situation inside the slab is the same in both cases, the continuous spectra are different.

I. KUŠČER: The interior of the continuously distributed part of the eigenvalue spectrum has no doubt little to do with what one observes in an experiment. However, the example with the slab should perhaps not be quoted in this connection. It would seem that in this case the change in the spectrum must be attributed to an additional mathematical assumption which is not necessarily a consequence of the change in the physical situation.

EXISTENCE OF A DIFFUSION LENGTH IN A FINITE PRISM OF PURE MODERATOR

M. M. R. WILLIAMS
NUCLEAR ENGINEERING DEPARTMENT,
QUEEN MARY COLLEGE,
UNIVERSITY OF LONDON,
LONDON, UNITED KINGDOM

Abstract

EXISTENCE OF A DIFFUSION LENGTH IN A FINITE PRISM OF PURE MODERATOR. An exact integral transport equation is derived for the neutron flux in a finite prism of pure moderator. Assuming that the prism is infinite in the z-direction, a trial solution $\exp(-\nu z)$ is inserted, and an eigenvalue problem for ν, the spatial relaxation constant, results.

The eigenvalue ν is studied as a function of the absorption and dimensions of the prism. It is shown that the discrete eigenvalues are bounded by Σ_{min} and that a minimum dimension exists below which a diffusion length can no longer be found. This result is much more restrictive than the maximum absorption theorem of Corngold, and the minimum dimension of the prism is shown to correspond to transverse bucklings of 10^{-3} cm^{-2} for beryllium, and 1.5×10^{-3}cm^{-2} for graphite, at 300°K. For poisoned and low-temperature moderators these values will be even smaller.

The angular distribution of the neutrons in the moderator has been calculated perpendicular and parallel to the axis, and it is found that a marked anisotropy of the spectrum exists, particularly in the neighbourhood of the Bragg cut-off.

On the basis of degenerate kernel approximation to the scattering process, it is shown that when the system is such that no diffusion length exists, then the asymptotic transverse flux shape is no longer of the cosine type, but becomes progressively flatter as the distance from the source increases. This is due to an increase in the proportion of cold neutrons which have longer mean free paths than the average. The well-known cold neutron filtering effect can be explained in terms of this phenomenon. The results obtained from the present analysis are in quantitative agreement with recent experiments performed by De Juren and Swanson.

1. INTRODUCTION

In recent years there has been a marked refinement in the theory associated with two basic experiments, viz. the pulsed neutron experiment and the diffusion length experiment. It has emerged for example that the fundamental time decay constant ceases to exist when the pulsed assembly exceeds a certain buckling; and in the diffusion length experiment it has been shown that, when the system is poisoned to beyond a certain value, a unique diffusion length ceases to exist [1]. In both of these cases the mathematical implication is that the discrete spectrum becomes empty under certain conditions.

In the present paper, this list of restrictions imposed upon the experimentalist by the theoretician will be extended. We shall in fact study the diffusion length problem in greater detail and in a more realistic situation. Thus, instead of the infinite medium considered by Corngold in his original investigations, we shall allow leakage from the sides of the system, i.e. we have the moderator in the form of a prism, finite in the x-y directions and infinite in the z-direction. The problem then is to discuss the existence of the exponential decay along the z-axis as a function of absorption and transverse dimensions.

This problem has been discussed by the author in a previous publication [2], wherein, by intuitive arguments, it was proposed that the spatial decay constant was bounded by Σ_{min}. This led to the conclusion that a maximum transverse buckling existed for the dimensions of the prism, and, for values exceeding this, no discrete spatial decay existed. In addition, it was shown that, when $B^2 < B^2_{max}$, transverse leakage had no effect on the total flux spectrum which retained the same form as in the infinite medium. This effect is explained by assuming that the additional diffusion heating arising from the increased negative flux curvature in the z-direction is completely cancelled out by the diffusion cooling arising from the transverse leakage.

Although the energy dependence of the total flux is unaffected by transverse leakage, this is certainly not true of the angular flux, which shows a marked variation with angle, particularly in the neighbourhood of the Bragg cut-off. Some examples of this phenomenon will be given later in the paper.

The general ideas developed in Ref. [2] are extended in the present work and made more rigorous. In particular, an exact integral equation is developed for the spatial decay in a prism of arbitrary cross-sectional shape, and it is shown that, when the cross-sectional area is less than a certain, finite value, a spatial relaxation length ceases to exist. Indeed, we go further and obtain an expression for the flux as a function of position from the source using a simple scattering model. It is shown that measurement of flux decay in a block of moderator may still have some meaning even though the transverse dimensions are less than the mathematically allowed ones. This part of the analysis is analogous to the interpretation of pulsed neutron experiments when $B^2 > B^2_{max}$ [3].

The simple theory developed here is in qualitative and sometimes quantitative agreement with the experiments of De Juren and Swanson [4], and, throughout the paper, reference will be made to these experiments.

2. THEORY

2.1. The eigenvalue problem

We commence with the Peierls integral equation, viz.

$$\rho(x, y, z, E) = \frac{1}{4\pi}\int_0^\infty dE'\Sigma(E' \to E)\int dx'\int dy'\int dz' \frac{\exp\{-\Sigma(E)\sqrt{\Delta^2 + (z-z')^2}\}}{\Delta^2 + (z-z')^2}\rho(x', y', z', E') \tag{1}$$

where $\Delta^2 = (x-x')^2 + (y-y')^2$, and $\rho(x, y, z, E)$ is the neutron flux. Now, we assume that our system is of arbitrary but non-re-entrant shape in the x-y plane, and infinite in the z-direction. Then inserting the ansatz:

$$\rho(x, y, z, E) = \Psi_\nu(x, y, E)\, e^{-\nu z} \tag{2}$$

Eq. (1) can be rewritten

$$\Psi_\nu(\vec{r}, E) = \frac{1}{2\pi}\int_0^\infty dE'\Sigma(E' \to E)\int_A d^2\vec{r}'\,\Psi(\vec{r}', E')\int_1^\infty \Sigma(E)\, K_0\left(\Delta\sqrt{\omega^2\Sigma^2(E) - \nu^2}\right)d\omega \tag{3}$$

where $d^2\vec{r}$ is an element of area in the x-y plane, $\Delta = |\vec{r} - \vec{r}'|$, and $K_0(x)$ is a modified Bessel function. In arriving at Eq. (3), use has been made of the relation [5]

$$\int_0^\infty \frac{\cosh \nu s}{\Delta^2 + s^2} \exp\{-\Sigma(E)\sqrt{\Delta^2 + s^2}\}\, ds = \Sigma(E) \int_1^\infty K_0(\Delta\sqrt{\omega^2 \Sigma^2(E) - \nu^2})\, d\omega \tag{4}$$

In addition to Eq. (3), the bound $\mathrm{Re}\{\nu\} \leqslant \Sigma_{min}$ is implicit, otherwise Eq. (3) does not exist.

Equation (3) defines an eigenvalue problem for ν, and our aim is to study the behaviour of ν as a function of the cross-sectional area (A) of the prism. We give below two proofs that there is a minimum transverse dimension for the existence of ν; one is rigorous, the other practical.

2.2. Practical proof

If we assume that the transverse flux distribution can be approximated by the asymptotic function $\exp(i\vec{B} \cdot \vec{r})$, then it may be shown that Eq. (3) reduces to

$$\Phi_0(E, B, \nu) = \frac{1}{2\sqrt{\nu^2 - B^2}} \log\left[\frac{\Sigma(E) + \sqrt{\nu^2 - B^2}}{\Sigma(E) - \sqrt{\nu^2 - B^2}}\right] \int_0^\infty \Sigma(E' \to E)\, \Phi_0(E', B, \nu) \tag{5}$$

where

$$\Psi_\nu(\vec{r}, E) = \Phi_0(E, B, \nu)\, e^{i\vec{B}\cdot\vec{r}}$$

By setting $\nu^2 = B^2 + \kappa^2$, we note that Eq. (5) becomes

$$\Phi_0(E, \kappa) = \frac{1}{2\kappa} \log\left[\frac{\Sigma(E) + \kappa}{\Sigma(E) - \kappa}\right] \int_0^\infty \Sigma(E' \to E)\, \Phi_0(E', \kappa)\, dE'$$

which is simply the infinite medium eigenvalue problem defining κ, the inverse diffusion length. Thus the spatial decay constant in the z-direction is given by the conventional diffusion theory form. However, we have shown that ν is bounded by Σ_{min}, and this implies that $B^2 \leqslant \Sigma^2_{min} - \kappa^2$. We therefore have an expression for the maximum transverse buckling, viz. $B^2_{max} = \Sigma^2_{min} - \kappa^2$.

For hydrogenous materials, Σ_{min} occurs at high energy and is equal to the free atom value; in water, for example, we find B^2_{max} = 2.04 cm^{-2}, corresponding to a square of side about 3 cm. For the crystalline moderators, Σ_{min} occurs at the Bragg cut-off energy and can be very small. For graphite and beryllium at 300°K we find that $B^2_{max} = 1.5 \times 10^{-3}$ and 10^{-3} cm^{-2}, respectively[1]. These values of buckling correspond to squares of sides 115 and 140 cm, respectively.

---

[1] The values of Σ_{min} used are read directly from the barn book and it should be noted that small errors in Σ_{min} can lead to substantial errors in B^2_{max} (~ 50% in the present case of crystalline moderators).

According to the theory presented here, all measurements of diffusion length must be performed on stacks exceeding these dimensions. Violation of this bound will lead to non-exponential decay and consequently an energy spectrum which changes continuously with increasing distance from the source. Such a phenomenon has been observed by De Juren and Swanson [4] in graphite at approximately the buckling predicted by the present theory.

2.3. Rigorous proof

Returning to Eq. (3), and using the first form of the identity in Eq. (4), we see that the equation can be written

$$\Psi_\nu(\vec{r}, E) = \int_0^\infty dE' \Sigma(E' \to E) \int_A d^2\vec{r}' \, H(\Delta, E, \nu) \Psi_\nu(\vec{r}', E') \tag{3'}$$

with

$$H(\Delta, E, \nu) = \frac{1}{2\pi} \int_0^\infty \frac{\cosh \nu s}{\Delta^2 + s^2} \exp\left\{-\Sigma(E)\sqrt{\Delta^2 + s^2}\right\} ds$$

But clearly

$$H < \frac{1}{2\pi} \int_0^\infty \frac{\cosh \Sigma_{min} s}{\Delta^2 + s^2} \exp\left\{-\Sigma_{min} s\right\} ds$$

$$= \frac{1}{4\pi} \int_0^\infty \left[1 + e^{-2\Sigma_{min} s}\right] \frac{ds}{\Delta^2 + s^2}$$

$$< \frac{1}{2\pi} \int_0^\infty \frac{ds}{\Delta^2 + s^2} = \frac{1}{4\Delta}$$

Introducing this approximation for the kernel on the right-hand side of Eq. (3'), we find

$$\Psi_\nu(\vec{r}, E) < \frac{1}{4} \int_A \frac{d^2\vec{r}'}{|\vec{r} - \vec{r}'|} \int_0^\infty \Sigma(E' \to E) \Psi_\nu(\vec{r}', E') \, dE' \tag{6}$$

Integrating Eq. (6) over A, and using

$$\int_A \frac{d^2\vec{r}}{|\vec{r} - \vec{r}'|} \leqslant 2\pi R$$

where 2R is the maximum chord length of the area A, we find

$$\Phi(E) < \frac{\pi}{2} R \int_0^\infty \Sigma(E' \to E) \Phi(E') \, dE' \tag{7}$$

with

$$\Phi(E) = \int_A d^2 \vec{r}\ \Psi_\nu(\vec{r}, E)$$

We must now show that for sufficiently small R, the inequality (7) is violated. One possible method is to symmetrize the kernel in (7), integrate the squares of both sides and make use of the Schwartz inequality. This method of proof, however, precludes liquids, and elastic scattering in crystals, since the symmetrized kernel is not quadratically integrable.

To make the proof more general, a method employed by Corngold [1] in another connection will be used. Thus, we multiply each side of the inequality by $\Sigma(E)$, the total cross-section, and integrate over energy. After some rearrangement we find

$$\int_0^\infty \Sigma(E)\Phi(E)dE < \frac{\pi}{2} R \int_0^\infty \Sigma(E)\Phi(E) g(E)\, dE \tag{8}$$

where

$$g(E) = \int_0^\infty \frac{\Sigma(y)}{\Sigma(E)} \Sigma(E \to y)\, dy$$

It has been shown by Corngold [1] that g(E) is bounded for a large class of scattering kernels, i.e. $g(E) < K$, where K depends only on moderator properties.

Thus Eq. (8) can be written

$$R > 2/\pi K$$

and consequently the existence of a minimum value of R follows.

We have shown, therefore, that there exists a critical value, denoted by $2R_c$, of the maximum chord length 2R such that for $R < R_c$, no discrete relaxation lengths exist in a finite prism.

It should be noted that the arguments presented above apply only to a body which has a finite cross-sectional area. If one of the chords in the cross-section of the prism is infinite, as for example in a slab, then a different proof is needed to show that the relaxation length ceases to exist at a critical slab thickness. However, when the necessary modifications to the proof are made, similar conclusions are reached.

A further assumption, implicit in the above proof, is that the lowest eigenvalue ν_0 corresponds to a non-negative solution. Physically, this can be taken for granted, but for full mathematical rigour it should be proved.

A possible physical explanation for the non-existence of a discrete relaxation length is as follows: due to the transverse leakage, the flux decays along the z-axis more rapidly than it would in the infinite medium case, and it is to be expected that the larger spatial decay will lead to additional diffusion hardening. This, however, does not arise for $R > R_c$ since, as we have shown, the total flux in the finite prism is the same as

that in the infinite prism. The explanation is that, for $R > R_c$, diffusion cooling arises from the transverse leakage (this has positive flux curvature) and just balances the additional diffusion heating. For $R < R_c$, however, the transverse leakage becomes dominant and there is no longer any equilibrium; thus we have a progressive cooling effect as a function of distance from the source. It should be added, however, that a minimum value of R still exists even in one-velocity theory; we may conclude, therefore, that transport as well as energy effects are involved in this problem.

2.4. Are the eigenvalues real?

If $g(\vec{r}, E)$ and the symmetric kernel $S(E'|E)$ are defined as follows:

$$g(\vec{r}, E) = \frac{\Psi(\vec{r}, E)}{\sqrt{M(E)}}$$

$$S(E'|E) = \sqrt{\frac{M(E')}{M(E)}}\,\Sigma(E' \to E)$$

then Eq. (3) may be written symbolically

$$g = K_\nu \hat{S}\, g$$

K_ν is the operator

$$\int_A d^2\vec{r}\,' \frac{\Sigma(E)}{2\pi} \int_1^\infty K_0\left(|\vec{r} - \vec{r}\,'|\sqrt{\omega^2\Sigma^2(E) - \nu^2}\right) d\omega$$

Now it is readily shown that $(g, \hat{S}g^*)$ is real, since $\hat{S}$ is symmetric. Thus

$$(K_\nu \hat{S}\, g,\ \hat{S}\, g^*) = (K_\nu \vartheta, \vartheta^*) \tag{9}$$

is also real. Expression (9) can also be written as

$$(K_\nu \vartheta, \vartheta^*) = \int_0^\infty dE \int_{V_\infty} dV_{\vec{k}}\ |\tilde{\vartheta}(\vec{k}, E)|^2\, \mathscr{F}\left\{ \frac{\Sigma(E)}{2\pi} \int_1^\infty K_0\left(|\vec{r}|\sqrt{\omega^2\Sigma^2(E) - \nu^2}\right) d\omega \right\} \tag{10}$$

where $\tilde{\vartheta}(\vec{k}, E)$ is the two-dimensional Fourier transform of $\vartheta(\vec{r}, E)$, assumed zero if $\vec{r}$ is not in A.

Now the Fourier integral becomes

$$\mathscr{F}\left\{\ldots\right\} = \Sigma(E) \int_1^\infty \frac{d\omega}{k^2 - \nu^2 + \omega^2\Sigma^2(E)}$$

Thus, observing that $(K_\nu \vartheta, \vartheta^*) \equiv (K_{\nu^*} \vartheta, \vartheta^*)$ we find

$$0 = \int_0^\infty dE \int_{V_\infty} dV_{\vec{k}} \, |\vartheta(\vec{k}, E)|^2 \, \Sigma(E) \int_1^\infty d\omega \left\{ \frac{1}{k^2 - \nu^2 + \omega^2 \Sigma^2} - \frac{1}{k^2 - \nu^{*2} + \omega^2 \Sigma^2} \right\} \tag{11}$$

The quantity in curly brackets may be rewritten as

$$\frac{(\nu - \nu^*)(\nu + \nu^*)}{(k^2 + \omega^2 \Sigma^2 + |\nu|^2)^2 - (k^2 + \omega^2 \Sigma^2)(\nu + \nu^*)^2} \tag{12}$$

Since $(\nu + \nu^*)$ is real and the denominator in Eq. (12) is real and positive, we may conclude that $\nu = \nu^*$, and hence that ν is real.

3. THE SPATIAL FLUX VIA SOME SIMPLE SCATTERING MODELS

To obtain greater insight into the mechanism leading to non-exponential decay, we shall employ a simple scattering kernel in an attempt to render Eq. (3) amenable to analytical solution.

In addition to a simplified scattering model, it will also be necessary to reduce the number of spatial variables. We shall consider, therefore, a slab-like system, infinite in the z-direction, with a plane source at $z = 0$ in the x-y plane. The slab is finite in the x-direction and infinite in the y-direction, and we shall calculate the flux variation along the z-axis and, simultaneously, the transverse flux distribution in the x-direction. This situation is shown in Fig. 1.

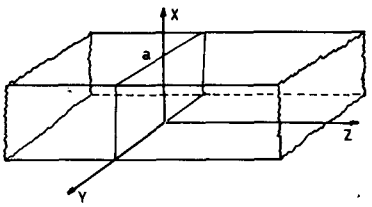

FIG. 1. Rectangular prism, infinite in y and z directions and of thickness a in the x direction.

Consider now the integral Eq. (1) with a source term. Defining the Fourier transform in the z-variable as

$$\Psi(\vec{r}, k, E) = \int_{-\infty}^{\infty} e^{-ikz} \, \Psi(\vec{r}, z, E) \, dz \tag{13}$$

and applying the transform to the integral equation, we find that $\Psi(\vec{r}, k, E)$ satisfies:

$$\Psi(\vec{r}, k, E) = \frac{\Sigma(E)}{2\pi} \int_A d^2\vec{r}\,' \int_1^\infty K_0\left(|\vec{r} - \vec{r}\,'| \sqrt{\omega^2 \Sigma^2(E) + k^2}\right) d\omega$$
$$\times \left\{ \int_0^\infty \Sigma(E' \to E) \Psi(\vec{r}\,', k, E') \, dE' + Q(\vec{r}\,', k, E) \right\} \tag{14}$$

In Eq. (14), $\vec{r}$ is the vector in the plane perpendicular to the z-direction, and Q is the source term.

Integration over the y-variable reduces Eq. (14) to

$$\Psi(x, k, E) = \frac{1}{2}\int_0^a dx' \int_1^\infty \frac{\Sigma(E)\exp\left\{-|x-x'|\sqrt{\omega^2\Sigma^2(E)+k^2}\right\}}{\sqrt{\omega^2\Sigma^2(E)+k^2}}\, d\omega$$

$$\times\left\{\int_0^\infty \Sigma(E'\to E)\Psi(x', k, E')\, dE' + Q(x', k, E)\right\} \tag{15}$$

where a is the width of the system in the x-direction.

Equation (15) is the basic equation for study.

3.1. Separable kernel

If we write

$$\Sigma(E'\to E) = \frac{1}{\bar{\Sigma}_s} M(E)\Sigma_s(E)\Sigma_s(E')$$

($\bar{\Sigma}_s$ is the Maxwellian average of $\Sigma_s(E)$) then Eq. (15) can be written

$$\Psi(x, k, E) = \frac{1}{2}\int_0^a dx' K(|x-x'|, E; k)\left[\frac{M(E)\Sigma_s(E)}{\bar{\Sigma}_s}\Phi(x', k) + Q(x', k, E)\right] \tag{16}$$

where

$$K(|y|, E; k) = \int_1^\infty \frac{\Sigma}{(\omega^2\Sigma^2+k^2)^{\frac{1}{2}}}\exp\left\{-|y|(\omega^2\Sigma^2+k^2)^{\frac{1}{2}}\right\} d\omega$$

and

$$\Phi(x, k) = \int_0^\infty \Sigma_s(E)\Psi(x, k, E)\, dE$$

For simplicity we shall assume that the source has the following energy dependence

$$Q(x, k, E) = Q(x, k)\frac{M(E)\Sigma_s(E)}{\bar{\Sigma}_s}$$

Then by multiplying Eq. (16) by $\Sigma_s(E)$ and integrating over $E(o, \infty)$, we find an equation for $\Phi(x, k)$, viz.

$$\Phi(x, k) = \int_0^a dx' H(|x-x'|; k)[\Phi(x', k) + Q(x', k)] \tag{17}$$

where

$$H(y; k) = \frac{1}{2\bar{\Sigma}_s}\int_0^\infty M(E)\Sigma_s^2(E)K(y, E; k)dE \tag{17a}$$

Finally, by setting

$$f(x, k) = \Phi(x, k) + Q(x, k)$$

we arrive at

$$f(x, k) = \int_0^a dx' \, H(|x-x'|; k) f(x', k) + Q(x, k) \tag{18}$$

As it stands, Eq. (18) cannot be solved in closed form. However, if a is allowed to become infinite, then the equation can be solved by the Wiener-Hopf technique with the finiteness of the body introduced via the 'end-point' approximation [6].

The details of the solution of Eq. (18), with $Q(x, z) = S\delta(z)$, will not be given due to their great length [see a forthcoming paper to be submitted to J. math. Phys.]. We shall, however, quote the final solution. Thus

$$\Psi(x, z, E) = \frac{S}{\Sigma_s} \beta M(E) \Sigma_s(E) \log\left(\frac{\Sigma(E)+\kappa}{\Sigma(E)-\kappa}\right) \sum_{n=0}^{N(a)} A_n \sin\left\{B_n(x+X_0(\nu_n))\right\} e^{-\nu_n z}$$

$$+ \frac{S}{\Sigma_s} M(E) \Sigma_s(E) \int_{\Sigma_{min}}^{\infty} A(E, s) \, e^{-sz} \, ds$$

$$+ \frac{S}{\Sigma_s} \beta M(E) \Sigma_s(E) \log\left(\frac{\Sigma(E)+\kappa}{\Sigma(E)-\kappa}\right) \int_{\Sigma_{min}}^{\infty} C(s) \cos\left\{\sqrt{s^2-\kappa^2}\left(x-\frac{a}{2}\right)\right\} e^{-sz} \, ds \tag{19}$$

where β, $A(E, s)$ and $C(s)$ are known functions, κ is the inverse infinite medium diffusion length, B_n is the transverse buckling of the nth mode of the slab, defined by

$$B_n = \frac{(2n+1)\pi}{a + 2X_0(\nu_n)} \tag{20}$$

$\nu_n^2 = \kappa^2 + B_n^2$, and $X_0(\nu_n)$ is the extrapolated endpoint. N(a) determines the number of discrete modes and can be found from a fairly simple formula.

3.2. Discussion of the solution

Eq. (19) divides naturally into three physically distinct terms. The first represents the fundamental decay and the higher spatial harmonics, with the integer N(a) determining the precise number of these. The second term is a direct source transient, and is unaffected by the size of the system. The third term is a transient which arises directly from the finiteness of the body and tends to zero as the thickness of the slab tends to infinity. We note that both first and third terms have the same energy spectra, but different spatial distributions.

In general, if the system is sufficiently large to permit at least one spatial eigenvalue ν_0, the flux will decay asymptotically with the form,

$$\Psi(x, z, E) \sim A_0 \frac{S}{\Sigma_s} \beta\, M(E)\, \Sigma_s(E) \log\left(\frac{\Sigma(E)+\kappa}{\Sigma(E)-\kappa}\right)$$

$$\times \sin\left\{B_0(x+X_0(\nu_0))\right\} e^{-\nu_0 z} \tag{21}$$

If, however, no spatial eigenvalues exist, then $\Psi(x, z, E)$ will not be separable in space and energy and will not decay exponentially. In addition, the transverse flux distribution will change progressively with distance from the source. Such behaviour has been observed experimentally by De Juren and Swanson, who show that to fit a $\sin\{B(x+X_0)\}$ function to the flux it is necessary that X_0 be an increasing function of z, thus indicating that the flux is becoming progressively flatter.

Another fact about the integral term is that the direct source transient part decays more rapidly than the other term. Thus, after a mean free path from the source, the solution is represented fairly well by

$$\Psi(x, z, E) \simeq \frac{S}{\Sigma_s} \beta\, M(E)\, \Sigma_s(E) \log\left(\frac{\Sigma(E)+\kappa}{\Sigma(E)-\kappa}\right)$$

$$\times \int_{\Sigma_{min}}^{\infty} C(s) \cos\left\{\sqrt{s^2-\kappa^2}\left(x-\frac{a}{2}\right)\right\} e^{-sz}\, ds \tag{22}$$

In this connection, the function C(s) is of extreme interest for it can be written as

$$C(s) = \frac{I(s)}{\cos^2\left\{\sqrt{s^2-\kappa^2}\left(\frac{a}{2}+X_1(s)\right)\right\} + \sinh^2\left\{\sqrt{s^2-\kappa^2}\; X_2(s)\right\}} \tag{23}$$

where $I(s) \neq 0$, for $\Sigma_{min} \leqslant s < \infty$.

Now, the 'sinh' term is never zero (except at s = 1), and when $a > a^*$ (i.e. a discrete mode exists) the 'cos' term is never zero. However, when $a < a^*$, and the solution has the form of Eq. (22), then we can find a value of s such that

$$\sqrt{s^2-\kappa^2}\left(\frac{a}{2} + X_1(s)\right) = \frac{\pi}{2} \tag{24}$$

i.e. the 'cos' term is zero. This leads to a maximum in the integrand about the root, s_0, of Eq. (24) given by

$$s_0^2 = \kappa^2 + \left(\frac{\pi}{a+2X_1(s_0)}\right)^2 \tag{25}$$

In the neighbourhood of the maximum, the integrand in Eq. (22) may be approximated by a Lorentzian function of the form

$$\vartheta(s_0)\,\frac{\gamma(s_0)\cos\left\{\sqrt{s^2-\kappa^2}\left(x-\frac{a}{2}\right)\right\}e^{-sz}}{(s-s_0)^2+\gamma^2(s_0)}$$

which, if the maximum is sharp, will allow Eq. (22) to be written approximately as

$$\Psi(x,z,E) \simeq \frac{S}{\Sigma_s}\,\beta\,M(E)\,\Sigma_s(E)\,\log\left(\frac{\Sigma(E)+\kappa}{\Sigma(E)-\kappa}\right)\vartheta(s_0)$$

$$\times\int_{\Sigma_{min}}^{\infty}\frac{\gamma(s_0)\cos\left\{\sqrt{s^2-\kappa^2}\left(x-\frac{a}{2}\right)\right\}e^{-sz}}{(s-s_0)^2+\gamma^2(s_0)}\,ds \qquad (22')$$

where $\gamma(s_0)$ is proportional to $X_2(s_0)$.

If $\gamma(s_0)$ is small, then the integrand will be highly peaked in the neighbourhood of $s = s_0$, and a first approximation to the integral term in Eq. (22') will be

$$e^{-s_0 z}\quad\cos\left\{\sqrt{s_0^2-\kappa^2}\,.\left(x-\frac{a}{2}\right)\right\}\int_{\Sigma_{min}}^{\infty}C(s)\,ds$$

or, using Eq. (24),

$$e^{-s_0 z}\quad\sin\left\{B_0^*\;(x+X_1(s_0))\right\}\int_{\Sigma_{min}}^{\infty}C(s)ds \qquad (26)$$

where

$$B_0^* = \frac{\pi}{a+2X_1(s_0)} \qquad (27)$$

The expression for the integral transient now reduces to a form which is identical to that of the fundamental mode decay, except that the buckling is now defined in terms of an effective extrapolated endpoint $X_1(s_0)$. A graph of the true extrapolated endpoint $X_0(\nu_0)$ and the effective one, $X_1(s_0)$, is shown in Fig. 2 for the one-speed case. $X_1(s_0)$ clearly appears to be the analytic continuation of $X_0(\nu_0)$ when $\nu_0 > \Sigma_{min}$, but we have not yet proved this.

Of course we have only assumed that Eq. (26) approximates the integral transient; clearly, for this to be a good approximation the value of $X_2(s_0)$ will have to be small. Only a numerical study will provide answers to these questions and to do this we have reduced our problem to the one-speed model.

Let us state at the outset, however, that in view of the experiments of De Juren and Swanson in graphite, it is not expected that Eq. (26) will be a very good approximation if $a \ll a^*$, since then the transverse flux shape changes markedly with z. However, for slab widths only slightly smaller than a^* we might expect Eq. (26) to be valid. This would

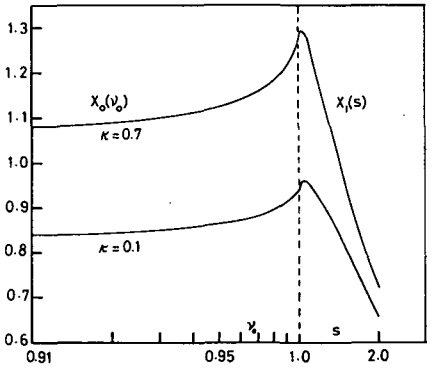

FIG. 2. Extrapolated endpoint of the fundamental mode as a function of the relaxation constant, and its analytic continuation for $\nu > \Sigma_{min}$ when the fundamental mode is absent.

certainly be a useful conclusion from an experimental point of view, since then the conventional methods of analysis could be employed to extract the infinite medium diffusion length from measurements of s_0.

3.3. Numerical results for one-speed model

We have already seen the behaviour of $X_0(\nu_0)$ and $X_1(s)$ in Fig. 2. Let us now examine numerically some other quantities of interest; namely, a^*, $X_2(s)$ and $C(s)$.

In terms of the one-velocity model, a^* in units of mean free path is given by the expression

$$a^* = \frac{\pi}{\sqrt{1-\kappa^2}} - 2\,X_0(1)$$

This is shown in Fig. 3 as a function of κ, and in absolute magnitude we see, therefore, that a^* is of the order of a few mean free paths. In an energy-dependent problem this would imply a few maximum mean free paths, and hence for crystalline materials a^* can be large, as suggested by the results of section 2.2.

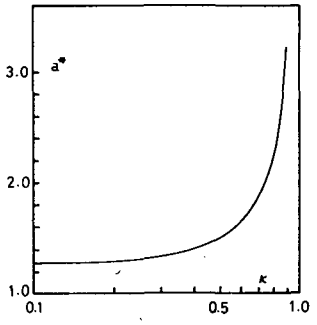

FIG. 3. Value of slab width a^* at which the fundamental mode disappears as a function of absorption.

The values of $X_2(s)$ for $\kappa = 0.1$ and 0.5 are given in Table I. $X_2(s)$ is seen to increase with s, but for s near zero it is small; we may conclude therefore that the integrand in Eq. (22') is highly peaked for s_0 near unity but becomes less peaked as s_0 increases, i.e. as the system gets smaller. Figure 4 shows the integrand of the continuum term for $\kappa = 0.1$ and $a = 1.0$. For this case, $a^* = 1.274$ and thus the

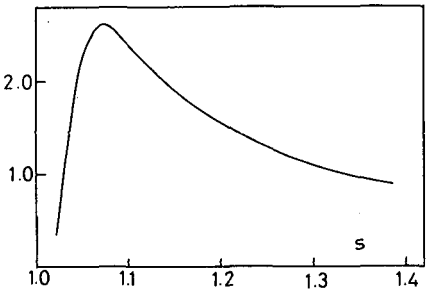

FIG.4. The integrand of the continuum integral for $a < a^*$. $\kappa = 0.1$.

maximum discussed earlier is present at $s_0 \approx 1.08$. It is quite clear from this figure that the approximation given by Eq. (26) is not a very good one. However, one must be careful in drawing general conclusions about energy-dependent problems from one-velocity results, and it is reasonable to conjecture, by analogy with the recent work of Corngold and Durgun [3] on the pulsed neutron experiment that we may expect the sharpness of the peak in Eq. (22') to be very sensitive to the presence of elastic coherent scattering with a Bragg cut-off. In this case the peak-to-half-width ratio should increase enormously and Eq. (26) should be applicable. It has not been found possible, however, to extend the present analytical work to such a case, even with a simple 'separable plus elastic' kernel of the type employed by Corngold and Durgun.

3.4. Angular distribution

As far as the energy spectrum is concerned, the most important effects are to be found in the angular distribution at various distances from the source. This distribution may be obtained from the integro-differential form of the transport equation once the total flux $\Psi(\vec{r}, E)$ is known. $\Psi(\vec{r}, E)$ is related to the angular flux in the following manner:

$$\Psi(\vec{r}, E) = \int_{-1}^{1} d\mu \int_{0}^{2\pi} d\psi\, \Phi(E, \vec{r}, \mu, \psi)$$

where $\mu = \cos\vartheta$, and the angular co-ordinates ϑ and ψ are shown in Fig. 5.

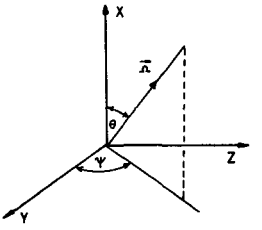

FIG. 5. Angular co-ordinates of the neutron motion.

After some manipulation, we arrive at the following result:

$$\Phi(E, x, z, \mu, \psi) = \Phi_{asymp}(E, x, z, \mu, \psi) + \Phi_{trans}(E, x, z, \mu, \psi) \qquad (28)$$

TABLE I. $X_2(s)$ AS A FUNCTION OF κ AND s

s	$\kappa = 0.1$	$\kappa = 0.5$
0	0	0
1.01	0.0310	0.0423
1.03	0.0658	0.0893
1.05	0.0932	0.1259
1.08	0.1278	0.1709
1.1	0.1478	0.1964
1.2	0.2256	0.2909
1.5	0.3477	0.4218
1.8	0.3975	0.4653
2.0	0.4126	0.4753

i.e. an asymptotic term plus a transient one. These are defined for the separable kernel model as

$$\Phi_{\text{asymp}} = \frac{SM(E)\,\Sigma_s(E)\,\kappa\beta}{2\pi\,\bar{\Sigma}_s}$$

$$\sum_{n=0}^{N(a)} A_n \frac{[(\Sigma(E)-\nu_n\sqrt{1-\mu^2}\,\sin\psi)\,\sin\{B_n(x+X_0(\nu_n))\} + \mu B_n \cos\{B_n(x+X_0(\nu_n))\}]}{(\Sigma(E)-\nu_n\sqrt{1-\mu^2}\,\sin\psi)^2 + \mu^2 B_n^2}\, e^{-\nu_n z} \tag{29}$$

and

$$\Phi_{\text{trans.}} = \frac{SM(E)\,\Sigma_s(E)}{8\pi\,\bar{\Sigma}_s^2}\int_{\Sigma_{min}}^{\infty} \frac{\epsilon(s)\,e^{-sz}\,ds}{(\Sigma(E)-s\sqrt{1-\mu^2}\,\sin\psi)} + \frac{SM(E)\,\Sigma_s(E)\,\kappa\beta}{2\pi\,\bar{\Sigma}_s}\int_{\Sigma_{min}}^{\infty} C(s)$$

$$\times\frac{\left[(\Sigma(E)-s\sqrt{1-\mu^2}\,\sin\psi)\cos\left\{\sqrt{s^2-\kappa^2}\left(x-\frac{a}{2}\right)\right\} - \mu\sqrt{s^2-\kappa^2}\,\sin\left\{\sqrt{s^2-\kappa^2}\left(x-\frac{a}{2}\right)\right\}\right]}{[\Sigma(E)-s\sqrt{1-\mu^2}\,\sin\psi]^2 + \mu^2(s^2-\kappa^2)}\,ds \tag{30}$$

Considering first the asymptotic term, i.e. the n = 0 term of Φ_{asymp} (when it exists), we find that the angular distribution becomes highly peaked in the forward direction ($\mu = 0$, $\sin\psi = 1$) as γ_0 approaches

Σ_{min}. Since Σ_{min} occurs at the Bragg cut-off in crystals, there is a marked forward bias of neutrons possessing energies at, and just below, this energy, i.e. the well-known preferential diffusion of cold neutrons.

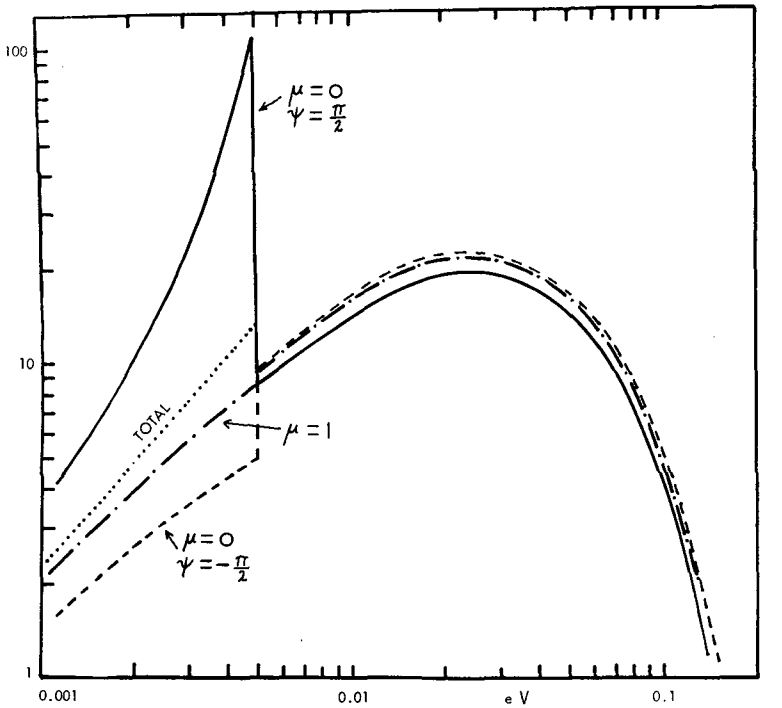

FIG. 6. The energy spectrum in beryllium at various angles.
$B^2 = 0.00035\ cm^{-2}$. $B_c^2 \doteq 0.001\ cm^{-2}$.

Figure 6 shows this effect in beryllium where we have plotted the asymptotic neutron spectrum at the centre of the system for three different directions; straight ahead in the positive z-direction, at right angles to the z-axis, and in the negative z-direction.

The large forward peak below the Bragg cut-off is a measure of the cold neutron build-up. It is interesting to note that, as we move away from the forward direction, this peak rapidly reduces in intensity and eventually disappears, becoming a depression, thus indicating an effect reminiscent of diffusion cooling.

The curves in Fig. 6 have not been obtained from the separable kernel but from a more accurate treatment of the asymptotic angular spectrum presented in a previous publication [2].

When the system is small enough, there is no asymptotic term, and the angular distribution is governed by the transient contribution. Arguments, similar to those used in arriving at Eq. (26), then lead to the conclusion that the angular distribution is of the same form as the asymptotic one, except that ν_0 is replaced by s_0. However, now it is possible for the denominator in Eq. (29) to be zero for $\mu = 0$ and

$$\psi = \sin^{-1}\left\{\frac{\Sigma(E)}{s_0}\right\}$$

for all values of E such that $s_0 \geqslant \Sigma(E) \geqslant \Sigma_{min}$. In general, s_0 is close to Σ_{min}, so that the spectrum consists of a highly singular beam of neutrons with energies in a range $E^* < E < E_B$, where E_B is the Bragg cut-off and E^* is such that $s_0 = \Sigma(E^*)$.

In practice, when the singularity arises, it will not be possible to approximate the integrand in Eq. (30), and the subsequent integration over s will smooth out the singularity, Nevertheless, there still exists a marked forward bias around a narrow range of energies, which increases in relative intensity as the distance from the source increases. Thus we again have the well-known crystalline filtering effect. Since most of the filters used by experimenters are too small to allow a discrete eigenvalue, it is likely that the continuum solution is mainly responsible for the selective filtering of cold neutrons.

ACKNOWLEDGEMENTS

The author is indebted to Professor Ivan Kuščer for suggestions which simplified the proof in section 2.3. Thanks are also due to J. Wood who performed the calculations which led to Fig. 6.

The programming of all the integrals leading to $X_1(s)$, $X_2(s)$, etc. was done by J. Spain, and his skill in performing these calculations is greatly appreciated.

The author is indebted to The Royal Society for financial support.

REFERENCES

[1] CORNGOLD, N., Nucl. Sci. Engng 19 (1964) 80.
[2] WILLIAMS, M. M. R., Nukleonik 9 (1967) 305.
[3] CORNGOLD, N., DURGUN, K., to appear in Nucl. Sci. Engng.
[4] DeJUREN, J. A., SWANSON, V. A., J. nucl. Energy 20 (1966) 905.
[5] DAVISON, B., AERE Rep. T/R 738 (1951).
[6] FRANKEL, S., GOLDBERG, S., Rep. AECD 2056 (1945),

DISCUSSION

L. S. KOTHARI: We have made some calculations to determine the eigenvalues in the time-dependent problem. We do observe peaking in the eigenvalue spectrum, but the value observed for the pseudo-fundamental mode is smaller than the value where the peak occurs. Are you sure your observations can be justified?

M. M. R. WILLIAMS: My observations are based on analogy with the results of Corngold and Durgun's paper (to be published in Nuclear Science and Engineering) on the pseudo-fundamental time eigenvalues. These authors do find that the pseudo-fundamental corresponds closely to the peak of the continuum. Their work is substantiated by some recent, as yet unpublished, work by Wood, who uses a more realistic scattering kernel.

W. E. REICHARDT: Your value of 1.5×10^{-3} cm^{-2} for the critical buckling of graphite is very close to the values used in several experiments for determination of the diffusion length. It is therefore desirable to have a reliable value for the minimum cross-section of graphite. There is a

discrepancy for this value between experiment and theory, the experimental values being higher than the calculated values by a factor of two. All the theoretical values calculated for different models agree relatively well. It may therefore be expected that the measured value is too high. In this case the critical buckling will be even smaller.

P. MICHAEL: Did you include the effect of an extrapolation distance in your calculation of the minimum 'safe' dimension?

M. M. R. WILLIAMS: No, I did not. However, I do not expect this to make any significant difference since the extrapolation distance will be roughly the average of the mean free path over the asymptotic spectrum, which is at most a few centimetres.

F. SHORE: Does the diffusion length connect smoothly with the pseudo-diffusion length across the critical dimension?

M. M. R. WILLIAMS: There appears to be a discontinuity of the slopes of the two curves above and below Σ_{min}. However, the details of this have not yet been worked out.

TIME-DEPENDENT THERMALIZATION WITH ELASTIC SCATTERING

M. BORYSIEWICZ AND J. MIKA
INSTITUTE OF NUCLEAR RESEARCH,
SWIERK k OTWOCKA, POLAND

Abstract

TIME-DEPENDENT THERMALIZATION WITH ELASTIC SCATTERING. The paper deals with the time-dependent transport equation describing the behaviour of thermal neutrons in a sample of moderator. The rigorous analysis of this problem with the assumption of isotropic scattering was reported by Albertoni and Montagnini for the free gas and by Bednarz for the crystalline moderator at the IAEA Symposium on Pulsed Neutron Research at Karlsruhe, May 1965. However, the results of Bednarz did not include the elastic scattering which plays an important role in crystals. In this paper the isotropic elastic scattering is included. The resulting scattering kernel is not square-integrable after symmetrization like the free gas kernel or the inelastic part of the scattering kernel in solids. However, it is shown in this paper that the essential features of the transport operator and, in particular, its spectrum, remain unchanged. This important fact enables the use of the transport theoretical interpretation of pulsed neutron experiments in solids.

1. INTRODUCTION

The solution of the time-dependent transport equation has been investigated in the last few years rather thoroughly. The problem of the time-dependent thermalization is of particular interest on account of the interpretation of pulsed neutron experiments in moderators. The investigation has proceeded along two main lines. The first is based on either the one Fourier component model or the diffusion approximation and the second on the exact treatment of the initial-value problem for the time-dependent transport equation. In many aspects approximate theories give similar physical results. However, it is obvious that the rigorous analysis is always of great value even if it only corroborates the results already predicted in the approximate treatment.

Among the papers devoted to the rigorous analysis of the initial-value problem for neutron thermalization, the most important is the paper of Albertoni and Montagnini [1] who investigated the free gas model and that of Bednarz [2] who generalized their results to include the inelastic part of scattering in solids. As a matter of fact, in both papers only the spectrum of the transport operator was found. The solution of the initial-value problem was discussed in a paper by Mika [3].

The important aspect of the mathematical analysis developed by Albertoni and Montagnini and, independently, by Bednarz was the square-integrability of the scattering kernel. This property is satisfied automatically for the free-gas model and obviously it is not true for the elastic part of scattering in solids. For this reason Bednarz' results for solids are to be restricted only to the inelastic scattering.

In this paper we include the isotropic elastic scattering and eventually show that it does not change the spectrum of the transport operator and that the solution to the initial-value problem exists under

the same requirements as those formulated in Ref. [3]. The assumption of the isotropy of the elastic scattering does not seem to change appreciably the physical situation, since the higher Legendre moments are strongly oscillating functions and the average effect should be small.

2. THE INITIAL-VALUE PROBLEM

In this paper the notation used by Bednarz [2] will be followed. Many details which can be found in Refs [1-3] will be omitted.

The time-dependent neutron transport equation in a finite moderating medium can be written in the form:

$$\frac{\partial \psi}{\partial t} = B\psi = (A + A_1)\psi \tag{2.1}$$

Here the function $\psi(\vec{r}, v, \vec{\Omega})$ is related to the neutron density so that

$$\psi(\vec{r}, v, \vec{\Omega}) = \sqrt{\frac{v}{m(v)}}\, N(\vec{r}, v, \vec{\Omega}) \tag{2.2}$$

where m(v) is the Maxwellian distribution. The function $\psi(\vec{r}, v, \vec{\Omega})$ satisfies the corresponding initial and boundary conditions.

The operator A includes the square integrable scattering kernel symmetrized with the use of detailed balance condition. It has the following form:

$$A\psi = -v\vec{\Omega}\,\mathrm{grad}\,\psi - v\,\Sigma(v)\,\psi + \frac{v}{4\pi}\int dv'k(v, v')\int d\vec{\Omega}'\,\psi(\vec{r}, v', \vec{\Omega}') \tag{2.3}$$

We acquire all the properties of the scattering kernel and the collision rate $h(v) = v\,\Sigma(v)$, assumed by Bednarz to be valid in our case.

The elastic scattering operator A_1 has the form

$$A_1\psi = \frac{1}{4\pi}\, v\, \Sigma_e\,(v)\int d\vec{\Omega}\,\psi(\vec{r}, v, \vec{\Omega}') \tag{2.4}$$

We assume that both $\Sigma_e(v)$ and $v\Sigma_e(v)$ are bounded functions for all v. Moreover $\lim_{v \to 0} v\,\Sigma_e(v) = 0$. These requirements are well satisfied in practice, e.g. for beryllium.

The operator A is defined in the Hilbert space H introduced by Bednarz. It is easily seen that these functions belong to the domain of A and hence the domains of B and A are identical, D(B)=D(A).

The initial-value problem for the initial distribution $\psi_0(\vec{r}, v, \vec{\Omega})$ belonging to D(B) has a unique solution if the operator B is an infinitesimal generator of a strongly continuous semi-group of operators.

It was shown by Mika [3] that if we restrict the definition of $\psi(\vec{r}, v, \vec{\Omega})$ to $v \leqslant w$ where w is a large but finite number, then the operator A is, in fact, generating a semi-group of operators. Now we see that, according to the definition, A_1 is bounded and has a dense domain in H. From this it follows that $B = A + A_1$ is also generating a semi-group of operators under exactly the same conditions as those formulated for A.

3. THE SPECTRUM OF B FOR Re $\lambda \leqslant -h_0$

It was shown by Bednarz that the half-plane Re $\lambda \leqslant -h_0 = \lim_{v \to 0} h(v)$ belongs to the spectrum of A. The proof is based upon the existence of a family of functions u_δ belonging to the domain of A and satisfying two conditions:

$$\| u_\delta \| \geqslant c > 0; \quad \lim_{\delta \to 0} \| (\lambda - A) u_\delta \| = 0 \tag{3.1}$$

The assumed properties of $\Sigma_e(v)$ are such that the value of h_0 is not changed. To prove that the half-plane Re $\lambda \leqslant -h_0$ for B also belongs to the spectrum it is sufficient to show that

$$\lim_{\delta \to 0} \| A_1 u_\delta \| = 0 \tag{3.2}$$

for the functions used by Bednarz. In fact, we see that

$$\| A_1 u_\delta \| \leqslant 4\pi \| u_\delta \| \int_{\delta^2}^{\delta} dv (v \Sigma_e(v))^2 \underset{\delta \to 0}{\to} 0 \tag{3.3}$$

Thus, we have established that the inclusion of the elastic scattering operator does not change the fact that the spectrum of the transport operator exists for Re $\lambda \leqslant -h_0$. However, its nature might be sensitive to the form of the scattering kernel.

4. THE INTEGRAL OPERATOR

To investigate the spectrum of the transport operator for Re$\lambda \geqslant -h_0$ we study the corresponding integral operator. With the elastic scattering included, it has the following form:

$$Q_\lambda = P_\lambda + F_\lambda = R_\lambda (K + E) \tag{4.1}$$

where

$$R_\lambda \phi = \int d\vec{r}' \frac{\exp\left[-\left(\frac{\lambda}{v} + \Sigma(v)\right)|\vec{r} - \vec{r}'|\right]}{4\pi |\vec{r} - \vec{r}'|} \phi(\vec{r}', v)$$

$$K\phi = \int dv' K(v, v') \phi(\vec{r}, v') \tag{4.2}$$

$$E\phi = \Sigma_e(v) \phi(\vec{r}, v)$$

The domain of these operators is the Hilbert space H_0 of square-integrable functions as defined by Bednarz [2].

The properties of P_λ have been investigated by Bednarz. He has shown that P_λ is a compact operator for Re $\lambda > h_0$. Moreover, it allows for the estimation

$$\| P_\lambda \| \leqslant ca \tag{4.3}$$

where a is the diameter of the body and c is some constant.

Let us proceed with the investigation of the operator F_λ. Denote its kernel by $F_\lambda(|\vec{r} - \vec{r}'|, v)$. We have for $\beta = \mathrm{Re}\,\lambda$

$$\int d\vec{r}' \, |F_\lambda(|\vec{r} - \vec{r}'|, v)| \leqslant \Sigma_e(v) \int_0^a ds \exp\left[-\left(\frac{\beta}{v} + \Sigma(v)\right)s\right]$$

$$= \frac{v\,\Sigma_e(v)}{\beta + h(v)} \left(1 - \exp\left[-\left(\frac{\beta}{v} + \Sigma(v)\right)a\right]\right) \leqslant \max_v \Sigma_e(v) a \tag{4.4}$$

Wee also see that

$$\int d\vec{r}' \, |F_\lambda(|\vec{r} - \vec{r}'|, v)| \leqslant \frac{v\Sigma_e(v)}{\beta + h(v)} < 1 \tag{4.5}$$

The last equation follows from the assumed properties of $\Sigma_e(v)$.

Now from Eqs (4.4) and (4.5) and from the theorem given on page 54 of Ref. [4] we see that

$$\| F_\lambda \| < \max_v \Sigma_e(v) a \tag{4.6}$$

and

$$\| F_\lambda \| < 1 \tag{4.7}$$

Now we will show that for Im $\lambda \neq 0$, 1 does not belong to the point or continuous spectrum of Q_λ, that is $1 \notin P\sigma Q_\lambda$ and $1 \notin C\sigma Q_\lambda$. Let us assume that this is not true. Then there exists a sequence $q_n \in H_0$ such that

$$\| q_n \| = 1; \quad \lim_{n \to \infty} \| (1 - Q_\lambda) q_n \| = 0. \tag{4.8}$$

From this it follows that for a sequence $f_n \in H_0$, such that $\| f_n \| \neq 0$, we have

$$\lim_{n \to \infty} ((1 - Q_\lambda) q_n, f_n) = 0. \tag{4.9}$$

Take $f_n = (K+E)q_n$. We see that $\|(K+E)q_n\| \neq 0$ for almost all n since in the opposite case we would have $\|Q_\lambda q_n\| = 0$ for almost all n, which is in contradiction with Eq. (4.8).

Now from Eq. (4.9) we have

$$\lim_{n \to \infty} [(q_n, (K+E)q_n) - (R_\lambda(K+E)q_n, (K+E)q_n)] = 0 \tag{4.10}$$

The first term of Eq. (4.10) is real. Therefore

$$\lim_{n\to\infty} \operatorname{Im}\,[R_\lambda f_n,\ f_n] = 0 \tag{4.11}$$

By using the Fourier transform technique (see, for instance, [1]) we can write

$$\operatorname{Im}\,(R_\lambda f_n,\ f_n) = \int_{-\infty}^{\infty} d\vec{k} \int dv\,[\operatorname{Im} M_\lambda(\vec{k},\ v)]\ |\tilde{f}_n(\vec{k}, v)]^2 \tag{4.12}$$

where

$$M_\lambda(\vec{k},\ v) = \frac{1}{kv}\ \arctan \frac{kv}{\lambda + h(v)} \tag{4.13}$$

is the Fourier transform of the kernel of R_λ and $\tilde{f}_n(\vec{k},\ v)$ the Fourier transform of $f_n(\vec{r}, v)$.

Now from the fact that $||f_n|| \neq 0$ it follows that $|\tilde{f}(\vec{k},\ v)|^2$ does not vanish identically. Since $\operatorname{Im} M_\lambda(\vec{k},\ v)$ has a constant sign and vanishes only if $\operatorname{Im}\lambda$ vanishes, Eq. (4.11) cannot be satisfied unless $\operatorname{Im}\lambda = 0$. This completes the proof of the assertion that 1 does not belong to $P\sigma Q_\lambda$ or $C\sigma Q_\lambda$ unless λ lies on the real axis.

Next we will show that 1 belongs to ρF_λ the resolvent set of F_λ for $\operatorname{Re}\lambda \geqslant -h_0$. Consider the equation

$$(\mu - F_\lambda) f = g;\quad f, g \in H_0 \tag{4.14}$$

We have

$$||g|| \cdot ||f|| \geqslant |(g, f)| \geqslant \operatorname{Re}(g, f) \tag{4.15}$$

On the other hand,

$$\operatorname{Re}((\mu - F_\lambda) f, f) = (\operatorname{Re}\mu\, ||f||^2 - \operatorname{Re}(F_\lambda f, f) \geqslant$$

$$||f||^2 = (\operatorname{Re}\mu - ||F_\lambda||) \tag{4.16}$$

From Eqs. (4.15) and (4.16) we see that for $\operatorname{Re}\lambda > -h_0$

$$||f|| = ||\ R(\mu, F_\lambda) g|| \leqslant (\operatorname{Re}\mu - ||F_\lambda||)^{-1} \cdot ||g|| \tag{4.17}$$

where $R(\mu, F_\lambda)$ denotes the resolvent operator of F_λ.

The above inequality holds for any $g \in H_0$. Therefore

$$||R(\mu, F_\lambda)|| \leqslant (\operatorname{Re}\mu - ||F_\lambda||)^{-1} \tag{4.18}$$

for $\operatorname{Re}\mu > ||F_\lambda||$. From Eqs. (4.7) we see that $1 \in \rho F_\lambda$.

Now we will prove that $1 \notin C\sigma Q_\beta$ for real β. To do this, assume that $1 \in C\sigma Q_\beta$ but does not belong to $P\sigma Q_p$. Then there exists a sequence q_n such that

$$||q_n|| = 1;\quad \lim_{n\to\infty} ||(1 - Q_\beta) q_n|| = 0 \tag{4.19}$$

If $1 \notin P\sigma Q_\beta$ then from the theorem given by Plesner [5] it follows that q_n is weakly convergent to zero. But since P_β is a compact operator, this means that $\lim_{n\to\infty} ||P_\beta q_n|| = 0$ and from Eq.(4.19) we have

$$\lim_{n\to\infty} ||(1-F_\beta)q_n|| = 0 \tag{4.20}$$

However, this is impossible since we have shown already that $1 \in \rho F_\beta$ for $\beta > -h_0$. This proves the assertion that 1 may belong only to the point spectrum of Q_β.

Our final task is to show that 1 does not belong to $R\sigma Q_\lambda$, the residual spectrum of Q_λ. Before we do so, let us consider the adjoint operator $Q^\dagger_\lambda$. Suppose that, for some λ, $1 \in P\sigma Q^\dagger_\lambda$. Then there exists $\phi_0 \in H_0$ such that $\phi_0 = Q^\dagger_\lambda \phi_0 = (K+E)R_{\bar\lambda}\phi_0$. Consider the expression

$$(R_{\bar\lambda}\phi_0,\ \phi_0) = (R_{\bar\lambda}\phi_0,\ (K+E)R_{\bar\lambda}\phi_0) = (\theta_0, (K+E)\theta_0) \tag{4.21}$$

where $\theta_0 = R_{\bar\lambda}\phi_0$ and $||\theta_0|| \neq 0$. Since the operators K and E are self-adjoint the expression (4.21) is real.

On the other hand, using the Fourier transform technique, we see that it can be real only if $\operatorname{Im}\lambda \neq 0$. This shows that $1 \in P\sigma Q^\dagger_\lambda$ only if $\operatorname{Im}\lambda = 0$.

For real β it can be easily shown that the point spectra of Q_β and $Q^\dagger_\beta$ are identical. In fact, let $\mu\,\phi_0 = Q_\beta\phi_0$. This implies that $(K+E)R_\beta(K+E)\phi_0 = \mu\,(K+E)\phi_0$ or $\mu\,\psi_0 = Q^\dagger_\beta\psi_0$ if we define $\psi_0 = (K+E)\phi_0 \neq 0$. Similarly we can prove the opposite implication.

Let us now return to the problem of the residual spectrum. The theorem proved in Ref. [4] states that if the domain of the operator is contained in the complete Hilbert space (this is satisfied in our case) then if some μ belongs to the residual spectrum of the operator then $\bar\mu$ belongs to the point spectrum of its Hilbert-adjoint operator. Therefore $1 \in R\sigma Q_\lambda$ implies $1 \in P\sigma Q^\dagger_\lambda$. However, we have shown that the latter is possible only for $\operatorname{Im}\lambda = 0$. But for real β, $1 \in P\sigma Q^\dagger_\beta$ implies $1 \in P\sigma Q_\beta$. As the same point cannot belong to the point and residual spectra simultaneously, we may state that for $\operatorname{Re}\lambda > -h_0$, $1 \notin R\sigma Q_\lambda$.

From the above discussion we see that 1 belongs to the resolvent set of Q_λ for all $\operatorname{Re}\lambda > -h_0$ and $\operatorname{Im}\lambda \neq 0$ and it may belong to the point spectrum for real λ. After Bednarz we can show that for the point spectrum the equations

$$\phi = Q_\lambda\phi \tag{4.22}$$

and

$$\lambda\psi = B\psi \tag{4.23}$$

are equivalent. That means that if there exists some $\phi \in H_0$ satisfying Eq. (4.22) then there exists $\psi \in H$ satisfying Eq. (4.23) and vice versa. In such a way, to investigate the point spectrum of B for $\operatorname{Re}\lambda > -h_0$ it is sufficient to find the values of λ for which $1 \in P\sigma Q_\lambda$.

It still remains to see what happens for the values of λ, $\operatorname{Re}\lambda > -h_0$ such that $1 \notin P\sigma Q_\lambda$. Since the continuous and residual spectra of Q_λ do not exist for $\operatorname{Re}\lambda > -h_0$ the Fredholm alternative is valid and $1 \notin P\sigma Q_\lambda$ implies $1 \in \rho Q_\lambda$. With this in mind and with the slight modification of the Bednarz approach we can easily show that, except for the point

spectrum of B, i.e. the values of λ such that $1 \in P\sigma Q_\lambda$ (this may happen only for real λ), the whole half-plane $\mathrm{Re}\,\lambda > -h_0$ belongs to the resolvent of B.

5. THE POINT SPECTRUM

The last problem is to investigate the nature of the point spectrum of B for $\mathrm{Re}\,\lambda > -h_0$. First, we notice that the spectrum is bounded for sufficiently large values of β, since in the opposite case the semi-group would not exist. This may be shown independently by estimating the norm of Q_λ in a way similar to that used to obtain Eq. (4.5).

It has been proved by Albertoni and Montagnini [1] that the family of operators P_β is strongly continuous for $\beta \in (-h_0, \infty)$. The same is obviously true for Q_β.

We will now prove that the point spectrum of B, which, according to what was stated above, is confined in the finite interval on the real axis $-h_0 \leqslant \beta \leqslant \beta_m < \infty$, has no accumulation points. To do so let us suppose that β^*, $-h_0 < \beta^* < \beta_m$ is an accumulation point of the eigenvalues of A, that is, there exists a sequence of eigenvalues β_n such that $\beta_n \to \beta^*$.

As the operator Q_β is strongly continuous in β, we can always choose a sequence of eigenfunctions q_n with the eigenvalues equal to unity, satisfying the equations $Q_{\beta_n} q_n = q_n$ in such a way that q_n tends to some function q^* in the norm. Then q^* satisfies the equation $q^* = Q_{\beta^*} q^*$.

Obviously $(K+E)q^* \neq 0$ since $(K+E)q^* = 0$ would imply $q^* = 0$. Consider the identity

$$(Q_{\beta_n} - Q_{\beta^*})\, q_n = (1 - Q_{\beta^*})\, q_n \tag{5.1}$$

If we multiply this by $(\beta_n - \beta^*)^{-1}$, we have

$$\frac{R_{\beta_n} - R_{\beta^*}}{\beta_n - \beta^*}\,(K+E)q_n = \frac{1}{\beta_n - \beta^*}\,(1 - R_{\beta^*}(K+E)q_n) \tag{5.2}$$

Since q^* is an eigenfunction of Q_{β^*}

$$((1 - R_{\beta^*}(K+E))\, q_n,\ (K+E)\, q^*) = 0 \tag{5.3}$$

hence

$$\left(\frac{R_{\beta_n} - R_{\beta^*}}{\beta_n - \beta^*}\,(K+E)\, q_n,\ (K+E)\, q^*\right) = 0 \tag{5.4}$$

Now we use once again the Fourier transform technique to express the scalar product on the right-hand side of Eq. (5.4). Then by letting $\beta_n \to \beta^*$ we obtain the equation

$$\int dv \int d\vec{k}\, \frac{\partial}{\partial \beta}\, M_\beta(\vec{k}, v)\Big|_{\beta = \beta^*} \left|\tilde{Q}^*(\vec{k}, v)\right|^2 = 0 \tag{5.5}$$

where $\tilde{Q}^*(\vec{k}, v)$ is the Fourier transform of $q^*(\vec{r}, v)$. As $|\tilde{Q}^*(\vec{k}, v)|^2$ does not vanish identically and

$$\frac{\partial}{\partial \beta} M_\beta(\vec{k}, v) = \frac{-2v}{(\beta + v\,\Sigma(v))^2 + v^2 k^2} < 0 \tag{5.6}$$

we see that Eq. (5.4) cannot be satisfied, which shows that our original proposition was wrong and the point spectrum of B does not have accumulation points.

In such a way we see that the point spectrum of B consists of the finite number of isolated points confined in the finite interval on the real axis. For the sufficiently small diameter of the body the point spectrum is empty as implied by Eqs. (4.3) and (4.6).

6. CONCLUSIONS

In the paper we have investigated the effect of the elastic scattering on the spectrum of the transport operator and the solution to the initial-value problem. We have shown that the inclusion of the elastic scattering does not change any of the results already obtained for the square-integrable kernels.

The spectrum of the transport operator consists of the half-plane $\mathrm{Re}\,\lambda \leqslant -h_0$ and of the finite number of isolated points of the point spectrum located on the real axis. For a sufficiently small diameter of the body the point spectrum disappears. The eigenvalue problem for the transport is equivalent to the eigenvalue problem, with the eigenvalue equal to unity, of the corresponding integral transport operator which is better suited to the numerical analysis.

As far as the initial-value problem is concerned, the solution with the elastic scattering included in the scattering operator exists under the same conditions as it does without the inelastic scattering.

REFERENCES

[1] ALBERTONI, S., MONTAGNINI, B., J. math. Analysis Applic. 13 (1966) 19.
[2] BEDNARZ, R., Pulsed Neutron Research I IAEA, Vienna (1965) 259.
[3] MIKA, J., The initial value problem for the neutron thermalization, Nukleonik (in print).
[4] STONE, M. H., Linear transformations in Hilbert space, Am. math. Soc. Colloq. Publ. 15 (1932).
[5] PLESNER, A. I., Spectral theory of the linear operators (in Russian).

DISCUSSION

H. G. KAPER: You gave a complete spectral analysis of the transport operator (A) under consideration. Did you prove the existence of a semi-group of operators T(t) = exp tA that solves the initial-value problem uniquely in the domain considered?

J. MIKA: Yes, this is sketched briefly in our paper.

H. G. KAPER: What is the effect of the residual spectrum on this semi-group?

J. MIKA: The residual spectrum, if it exists, is confined to the left-hand half-plane and its effect upon the semi-group is therefore not visible.

ИСПОЛЬЗОВАНИЕ СИСТЕМЫ ПОЛИНОМОВ ЛАГЕРРА И ПРИСОЕДИНЕННЫХ К НИМ ФУНКЦИЙ ДЛЯ РЕШЕНИЯ НЕКОТОРЫХ ТЕРМАЛИЗАЦИОННЫХ ЗАДАЧ

Н.И.ЛАЛЕТИН, И.Г.ПАСЫНКОВ
ИНСТИТУТ АТОМНОЙ ЭНЕРГИИ им. И.В.КУРЧАТОВА,
МОСКВА,
СССР
(Доклад представил Л.В.Майоров)

Abstract — Аннотация

USE OF A SYSTEM OF LAGUERRE POLYNOMIALS AND RELATED FUNCTIONS IN SOLVING VARIOUS THERMALIZATION PROBLEMS. The paper proposes a uniform and effective method of solving thermalization problems involving also fast neutron sources in the spatial region considered. In such problems the thermal neutron energy spectrum at energies much greater than kT becomes a Fermi spectrum, which cannot be satisfactorily represented by the product of the Maxwellian function and a linear combination of associated Laguerre polynomials. It is shown that in problems of this type the spectrum can be suitably represented by the expression:

$$\Phi(\epsilon) \cong \epsilon e^{-\epsilon} \sum_{n=0}^{N} [a_n L'_n(\epsilon) + b_n \varphi_n(\epsilon)]$$

where $[L'_n(\epsilon)]$ represents the associated Laguerre polynomials and $[\varphi_n(\epsilon)]$ represents the related functions, considered in an earlier work by one of the authors of the present paper. A method is proposed of determining the expansion coefficients a_n and b_n giving a reasonably uniform approximation of the known function over the whole energy range. The rate of convergence of the expansion is studied by comparing the neutron spectra in an infinite homogeneous medium obtained by direct numerical calculation and by using the proposed expansion. Spectra are considered for media with different dimensions and different absorption laws and for various thermalization models.

ИСПОЛЬЗОВАНИЕ СИСТЕМЫ ПОЛИНОМОВ ЛАГЕРРА И ПРИСОЕДИНЕННЫХ К НИМ ФУНКЦИЙ ДЛЯ РЕШЕНИЯ НЕКОТОРЫХ ТЕРМАЛИЗАЦИОННЫХ ЗАДАЧ. Предлагается единообразный и достаточно эффективный способ решения термализационных задач, в которых в рассматриваемой пространственной области находятся и источники быстрых нейтронов. В таких задачах энергетический спектр тепловых нейтронов при энергиях много больших кТ переходит в фермиевский и представление спектра в виде произведения максвелловской функции на линейную комбинацию сопряженных полиномов Лагерра оказывается непригодным. Показано, что в задачах указанного типа удобным является представление спектра в виде:

$$\Phi(\epsilon) \cong \epsilon e^{-\epsilon} \sum_{n=0}^{N} \left[a_n L'_n(\epsilon) + b_n \varphi_n(\epsilon) \right].$$

Здесь $[L'_n(\epsilon)]$ – сопряженные полиномы Лагерра, а $[\varphi_n(\epsilon)]$ – присоединенные к ним функции, рассматривавшиеся ранее одним из авторов настоящего доклада. В докладе предложен способ определения коэффициентов разложения a_n и b_n, дающий равномерную в некотором смысле аппроксимацию искомой функции во всем интервале энергий. Исследована скорость сходимости разложения путем сравнения спектров нейтронов в бесконечной однородной среде, сосчитанных прямым численным способом и с помощью предлагаемого разложения. Рассмотрены спектры в средах с различными величинами и законами поглощения и для разных моделей термализации.

В ряде термализационных задач оказалось удобным искать решение (энергетический спектр медленных нейтронов) в виде произведения максвелловской функции на конечный отрезок ряда полиномов (См.,

например, [1 – 4]). В частности, при использовании в качестве независимой переменной энергии нейтронов берется система обобщенных полиномов Лагерра первого порядка. (В дальнейшем для краткости будем называть их просто полиномами Лагерра). Такое представление удовлетворительно в тех случаях, когда спектр нейтронов не сильно отличается от максвелловского и не содержит "фермиевского хвоста". В большинстве задач реакторной физики, однако, интересуются спектром медленных нейтронов, образующихся в результате замедления быстрых нейтронов, которые возникают неподалеку от рассматриваемой области пространства и с энергиями много большими кТ. (Здесь Т – температура среды, к – постоянная Больцмана). В таких ситуациях представление решения с помощью полиномов Лагерра или совершенно невозможно или практически неприемлемо.

В работе [5] на примере решения типичной задачи указанного класса автор показал, что дополнение системы полиномов Лагерра системой присоединенных к ним функций исправляет положение.

Мы покажем ниже, что использование названной системы не ограничивается случаем рассмотренного в [5] тяжелогазового оператора и опишем более удовлетворительный по сравнению с использованным ранее способ определения коэффициентов разложения.

Покажем вначале, что любая функция $\Psi(\epsilon)$, определенная на интервале от 0 до ∞, которая не имеет особенностей в нуле и после умножения на $\epsilon e^{-\epsilon}$ становится квадратично интегрируемой, может быть как угодно точно представлена линейной суперпозицией полиномов Лагерра и присоединенных к ним функций. (Обозначим эту систему через $\{L\Lambda\}$).

Рассмотрим сначала такие функции $\Psi(\epsilon)$, которые могут быть представлены в виде суммы двух функций, из которых одна растет на бесконечности не быстрее конечной степени ϵ, а другая после умножения на $\epsilon e^{-\epsilon}$ может быть разложена вблизи бесконечно-удаленной точки в ряд Тейлора по обратным степеням ϵ.

Построим функцию $\Psi_F(\epsilon) = \sum_{n=0}^{\infty} b_n \varphi_n(\epsilon)$, где $\varphi_n(\epsilon)$ – присоединенная функция (см. [5]), а коэффициенты b_n определяются выражением

$$b_n = \lim_{\epsilon \to \infty} \frac{\Psi(\epsilon) - \sum_{k=0}^{n-1} b_k \varphi_k(\epsilon)}{\varphi_n(\epsilon)} \tag{1}$$

В силу свойств $\Psi(\epsilon)$ и $\varphi_n(\epsilon)$ все b_n существуют. Легко видеть, что разность $\Psi(\epsilon) - \Psi_F(\epsilon)$ растет на бесконечности не быстрее чем по степенному закону и, следовательно, может быть разложена в ряд по полиномам Лагерра

$$\Psi_M(\epsilon) = \Psi(\epsilon) - \Psi_F(\epsilon) = \sum_{n=0}^{\infty} a_n L_n^1(\epsilon) \quad \text{и}$$

$$\Psi(\epsilon) = \sum_{n=0}^{\infty} \{a_n L_n^1(\epsilon) + b_n \varphi_n(\epsilon)\} \tag{2}$$

Здесь

$$a_n = \int_0^{\infty} \epsilon e^{-\epsilon} L_n^1(\epsilon) \{\Psi(\epsilon) - \Psi_F(\epsilon)\} d\epsilon$$

Для вычисления a_n удобно воспользоваться тем обстоятельством, что n-ый полином Лагерра ортогонален с весом $\epsilon e^{-\epsilon}$ всем присоединенным функциям $\varphi_m(\epsilon)$ с номерами $m > n$. Это утверждение доказывается обычным способом, а именно, умножаем уравнение для m-ой присоединенной функции на $\epsilon e^{-\epsilon} L_n^1(\epsilon)$ и уравнение для n-го полинома Лагерра на $\epsilon e^{-\epsilon} \varphi_m(\epsilon)$, интегрируем оба уравнения в пределах от 0 до ∞, преобразовываем интегралы, содержащие вторые производные с помощью формулы интегрирования по частям и вычитаем одно получившееся равенство из другого. В результате имеем

$$\int_0^\infty \epsilon e^{-\epsilon} L_n^1(\epsilon)\, \varphi_m(\epsilon)\, d\epsilon = 0 \qquad \text{при } m > n$$

Используя эти соотношения, получим

$$a_n = \int_0^\infty \epsilon e^{-\epsilon} L_n^1(\epsilon)[\Psi(\epsilon) - \sum_{k=0}^{n} b_k \varphi_k(\epsilon)]\, d\epsilon \tag{3}$$

Пусть теперь $\epsilon e^{-\epsilon}\, \Psi(\epsilon)$ не разложима в ряд Тейлора по обратным степеням ϵ вблизи бесконечно-удаленной точки. В этом случае мы можем вначале апроксимировать ее удобной функцией, например, суперпозицией полиномов Лагерра от $1/\epsilon$, а затем провести ранее указанные операции.

Проведенное рассмотрение дает один возможный способ определения коэффициентов a_n и b_n. Он довольно прост, но имеет два существенных недостатка. Первый – предварительная апроксимация функции для получения нужного поведения вблизи бесконечно-удаленной точки. Второй недостаток заключается в том, что две части функции $\Psi_F(\epsilon)$ и $\Psi_M(\epsilon)$ приближаются по разному. Действительно, определение коэффициентов a_n формулой (3) означает, что $\Psi_M(\epsilon)$ в некотором смысле равномерно приближается во всем интервале энергий. Формулы (3) возникают из минимизации следующей величины

$$I = \int_0^\infty \epsilon e^{-\epsilon} [\Psi_M(\epsilon) - \sum_{n=0}^{N} a_n L_n^1(\epsilon)]^2 d\epsilon = I_{min},$$

$$I = \int_0^\infty \left[\frac{\Phi_M(\epsilon) - \epsilon e^{-\epsilon} \sum_{n=0}^{N} a_n L_n^1(\epsilon)}{\sqrt{\epsilon e^{-\epsilon}}} \right]^2 d\epsilon \simeq \int_0^\infty \left(\frac{\Delta\Phi_M}{\sqrt{\Phi_M}} \right)^2 d\epsilon.$$

Здесь $\Phi_M(\epsilon) = \epsilon e^{-\epsilon}\, \Psi_M(\epsilon)$; $\Delta\Phi_M(\epsilon) = \Phi_M(\epsilon) - \epsilon e^{-\epsilon} \sum_{n=0}^{N} a_n L_n^1(\epsilon)$ и учтено, что главный вклад дает член суммы с $n = 0$. Отсюда следует, что, грубо говоря, по всему интервалу энергий величина $(\Delta\Phi_M/\sqrt{\Phi_M})$ меняется мало.

С приближением части функции $\Psi_F(\epsilon)$ ситуация совершенно иная. Из формул (2) видим, что, ограничившись конечным числом присоединенных функций, мы сравнительно хорошо апроксимируем функцию при больших ϵ, но ошибка в области более малых ϵ может оказаться заметной. Обычно же наиболее интересным является интервал ϵ до 10 – 20.

Чтобы обойти это затруднение поступим следующим образом. Перепишем формулу (3) в виде

$$a_n = P \cdot f \cdot \int_0^\infty \epsilon e^{-\epsilon} \Psi(\epsilon) L_n'(\epsilon) d\epsilon - P \cdot f \cdot \int_0^\infty \epsilon e^{-\epsilon} L_n'(\epsilon) \sum_{\kappa=0}^{n} b_\kappa \varphi_\kappa(\epsilon) d\epsilon \qquad (4)$$

Здесь $P \cdot f$ означает "конечная часть", т.е. определенный способ выделения конечной части из расходящегося интеграла. Смысл и способы конкретного осуществления такой регуляризации для интегралов со степенной расходимостью подробно изложены в книгах [6, 7] (см. также приложение 2). Для коэффициентов b_κ, определенных формулой (1), выражение (4) совпадает с равенством (3), но, в отличие от последнего, выражение (4) будет иметь смысл и при других b_κ. Возьмем это выражение за определение a_n. Коэффициенты же b_n определим так, чтобы $\Psi_F(\epsilon)$ приближалась аналогично $\Psi_M(\epsilon)$. Так как главный вклад в $\Psi_F(\epsilon)$ дает $\varphi_0(\epsilon)$, то следует потребовать минимума интеграла

$$I' = \int_0^\infty \left(\frac{\Phi_F(\epsilon) - \epsilon e^{-\epsilon} \sum_{\kappa=0}^{N} b_\kappa \varphi_\kappa(\epsilon)}{\sqrt{\epsilon e^{-\epsilon}}\, \varphi_0(\epsilon)} \right)^2 d\epsilon = \int_0^\infty \frac{\epsilon e^{-\epsilon}}{\varphi_0(\epsilon)} \left(\Psi_F(\epsilon) - \sum_{\kappa=0}^{N} b_\kappa \varphi_\kappa(\epsilon) \right)$$

Отсюда

$$\frac{\partial I'}{\partial b_\kappa} = \int_0^\infty \epsilon e^{-\epsilon} \Lambda_\kappa(\epsilon) \left[\Psi_F(\epsilon) - \varphi_0(\epsilon) \sum_{n=0}^{N} b_n \Lambda_n(\epsilon) \right] = 0 \qquad (5)$$

Здесь $\Lambda_\kappa(\epsilon) = \varphi_\kappa(\epsilon)/\varphi_0(\epsilon)$.

Написанные равенства дают систему уравнений для определения b_κ с номерами от 1 до N. Коэффициент b_0 определяется из асимптотики $\Psi(\epsilon)$. Поскольку разбиение функции на компоненты $\Psi_M(\epsilon)$ и $\Psi_F(\epsilon)$ заранее неизвестно, формулы (4) и (5) дают общую систему уравнений для определения a_n и b_n.

В качестве примера рассмотрим решение следующей задачи. В бесконечной однородной среде имеются равномерно распределенные источники быстрых нейтронов. Энергию нейтронов источника можем считать бесконечной. Обмен энергией нейтронов с атомами среды описывается тяжелогазовым уравнением. Сечение поглощения меняется по закону $1/\sqrt{\epsilon}$. Требуется определить спектр нейтронов $\Phi(\epsilon)$, где ϵ – энергия, измеренная в единицах κT.

При указанных предположениях функции $\Psi(\epsilon) = \Phi(\epsilon)/\epsilon e^{-\epsilon}$ удовлетворяют уравнению:

$$\epsilon \frac{d^2}{d\epsilon^2} \Psi(\epsilon) + (2+\epsilon) \frac{d}{d\epsilon} \Psi(\epsilon) - \frac{c}{\sqrt{\epsilon}} \Psi(\epsilon) = 0 \qquad (6)$$

и условиям $\Psi(\epsilon)\epsilon e^{-\epsilon} = 0$ при $\epsilon = 0, \Psi(\epsilon)\epsilon e^{-\epsilon} \sim \frac{1}{\epsilon}$ при $\epsilon \to \infty$. (7)

Здесь $c = \sigma a(\kappa T)/(\xi \sigma_s)_{ac}$

Ищем решение в виде

$$\Psi(\epsilon) = \sum_{n=0}^{N} a_n L_n'(\epsilon) + \varphi_0(\epsilon) \sum_{n=0}^{N} b_n \Lambda_n(\epsilon). \qquad (8)$$

причем, в соответствии с условием (7), $b_0 = 1$. Подставляя выписанное разложение в уравнение (6), умножая затем его последовательно на $\epsilon e^{-\epsilon} L'_n(\epsilon)$ с номерами полиномов n от 0 до N и на функцию $\epsilon e^{-\epsilon} \Lambda_n(\epsilon)$ с $1 \le n \le N$, и интегрируя каждый раз в пределах от 0 до ∞, получим систему линейных алгебраических уравнений 2N+1 порядка*:

$$\vec{M}^{11}\vec{A} + \vec{M}^{12}\vec{B} = 0$$
$$\vec{M}^{21}\vec{A} + \vec{M}^{22}\vec{B} = 0 \qquad (9)$$

Здесь $\vec{A}$ вектор с компонентами $(a_0, a_1 \ldots a_n)$, $\vec{B}$ – вектор $(b_0, b_1 \ldots b_n)$, $\vec{M}^{ik}$ – субматрицы N-го порядка. Элементы матрицы $\vec{M}^{11}$ имеют вид:

$$\vec{M}^{11}_{nm} = \int_0^\infty \epsilon e^{-\epsilon} L'_n(\epsilon)\left[\hat{\epsilon} L'_m(\epsilon) - \frac{c}{\sqrt{\epsilon}} L'_m(\epsilon)\right] d\epsilon,$$

где $\hat{\epsilon} = \epsilon \frac{d^2}{d\epsilon^2} \ldots + (2-\epsilon)\frac{d}{d\epsilon}$, и так как $\hat{\epsilon} L'_m(\epsilon) = -m L'_m(\epsilon)$, то

$$M''_{nm} = -n(n+1)\delta_{nm} - c\left(L'_n(\epsilon)_1 \frac{L'_m(\epsilon)}{\sqrt{\epsilon}}\right).$$

Скалярные произведения $\left(L'_n(\epsilon)_1 \frac{L'_m(\epsilon)}{\sqrt{\epsilon}}\right) = \int_0^\infty \frac{\epsilon e^{-\epsilon} L_n L_m}{\sqrt{\epsilon}} d\epsilon$ выражаются через известные табулированные функции.

Элементы матрицы $\vec{M}^{12}$ представляются в виде:

$$M^{12}_{nm} = \int_0^\infty \epsilon e^{-\epsilon} L'_n(\epsilon)\left[\hat{\epsilon}\varphi_m(\epsilon) - \frac{c}{\sqrt{\epsilon}} \varphi_m(\epsilon)\right] d\epsilon \quad \text{и}$$

так как $\hat{\epsilon}\varphi_m(\epsilon) = -m\varphi_m(\epsilon) + L'_m(\epsilon)$, то

$$M^{12}_{nm} = -m(L'_{n_1}\varphi_m(\epsilon)) + n(n+1)\delta_{nm} - c\left(L_{n_1} \frac{\varphi_m}{\sqrt{\epsilon}}\right).$$

Как было отмечено ранее $(L_{n_1}\varphi_m) = 0$ при $m > n$. При $m \le n$ эти скалярные произведения представляют собой степенным образом расходящиеся интегралы и должны быть регуляризованы. Конечные части интегралов выражаются через табулированные функции. Скалярные произведения $(L_{n_1}(\varphi_m/\sqrt{\epsilon})$ – (при $m > n$ их конечные части) – также выражаются через известные функции.

Элементы матрицы M^{21}_{nm} равны

$$M^{21}_{nm} = \int_0^\infty \epsilon e^{-\epsilon} \Lambda_n(\epsilon)\left[\hat{\epsilon} L'_m(\epsilon) - \frac{c}{\sqrt{\epsilon}} L'_m(\epsilon)\right] d\epsilon = -m(\Lambda_{n_1} L_m) - c\left(\Lambda_{n_1} \frac{L_m}{\sqrt{\epsilon}}\right).$$

Входящие в это выражение регулярные интегралы считались численно.

---

* В данной работе в отличие от работы [5], мы пользуемся полиномами Лагерра, нормированными так же, как в справочнике [9].

Элементы матрицы

$$M^{22}_{nm} = \int_0^\infty \epsilon e^{-\epsilon} \Lambda_n(\epsilon) \left[\hat{\epsilon}\varphi_m(\epsilon) - \frac{c}{\sqrt{\epsilon}} \varphi_m(\epsilon) \right] = - m(\Lambda_n, \varphi_m) + (\Lambda_n, L'_m) - c\left(\Lambda_n, \frac{\varphi_m}{\sqrt{\epsilon}}\right)$$

также выражаются через сходящиеся интегралы, которые считались численно.

Из изложенного ясно, что все компоненты матричных элементов могут быть затабулированы и затем использованы для расчета спектров в средах с разными поглощениями.

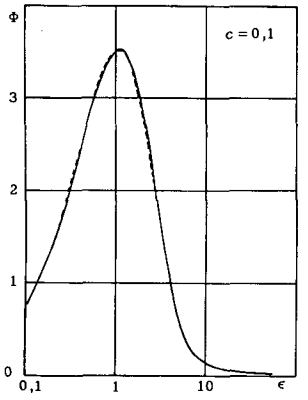

Рис. 1. Спектр нейтронов для значения c = 0,1.

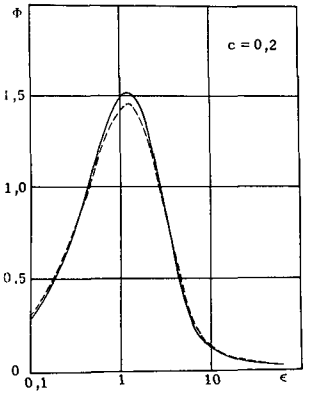

Рис. 2. Спектр нейтронов для значения c = 0,2.

На рис. 1 – 4 изображены спектры, сосчитанные для параметров c = 0,1; 0,2; 0,3 и 0,4. Расчеты были проведены для N от 0 до 6 ($(L\Lambda)_N$ – приближение). Для сравнения приведены спектры, сосчитанные прямым численным интегрированием уравнения (6) с помощью программы "СМЕНОБС"*.

* Программа "СМЕНОБС" предназначена для расчета спектра медленных нейтронов в однородной бесконечной среде с поглощением произвольным по величине и с произвольной зависимостью от энергии, причем интегрируется уравнение, рассмотренное в работе [8].

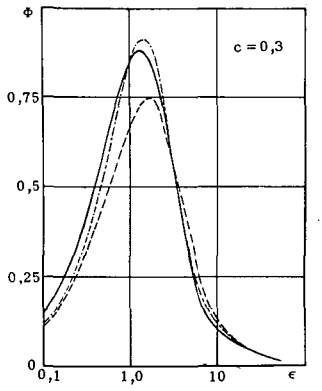

Рис. 3. Спектр нейтронов для значения c = 0,3.

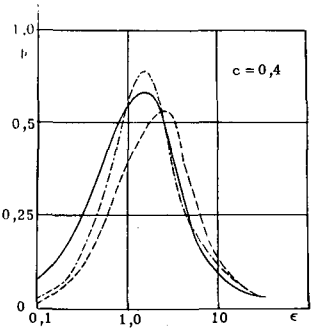

Рис. 4. Спектр нейтронов для значения c = 0,4.

На рисунках сплошными кривыми изображены результаты, полученные в $(L\Lambda)_6$ – приближении, которые на графиках совпадают с решениями, полученными по программе "СМЕНОБС". Штриховые кривые – решения, полученные в $(L\Lambda)_0$ – приближении. Штрих-пунктирные кривые – решения, полученные в $(L\Lambda)_2$-приближении и штрих-штрих-пунктирные кривые – решения в $(L\Lambda)_1$-приближении.

Видим, что для c = 0,1 заметный вклад дают лишь члены разложения (8) с n = 0.

ПРИЛОЖЕНИЕ 1

Рекуррентные формулы для полиномов Лагерра

$$L'_{n+1}(\epsilon) = \left(2 - \frac{\epsilon}{n+1}\right) L'_n(\epsilon) - L'_{n-1}(\epsilon) \qquad (П1-1)$$

$$(n+1) L'_{n+1}(\epsilon) = \epsilon \frac{d}{d\epsilon} L'_n(\epsilon) + (n+2-\epsilon) L'_n(\epsilon) \qquad (П1-2)$$

являются частным случаем соответствующих формул для вырожденной гипергеометрической функции $F(\lambda, 2, \epsilon)$ (См., например, [9]). Напомним, что $L'_n(\epsilon) = (n+1) F(-n, 2, \epsilon)$).

Присоединенные функции $\varphi_n(\epsilon)$ можно рассматривать как значения производных $\frac{\partial F(\lambda, 2, \epsilon)}{\partial \lambda}(n+1)$ при $\lambda = -n$, что позволяет легко написать рекуррентные формулы и для них:

$$\varphi_{n+1} = \left(2 - \frac{\epsilon}{n+1}\right)\varphi_n - \varphi_{n-1} + \frac{L'_n(\epsilon)}{n+2} - \frac{2L'_n}{n+1} + \frac{L_{n-1}}{n} \qquad (\text{П}1-3)$$

$$(n+1)\varphi_{n+1} = \epsilon\frac{d}{d\epsilon}\varphi_n + (n+2-\epsilon)\varphi_n + \frac{L_{n+1}}{n+2} - \frac{L_n}{n+1} \qquad (\text{П}1-4)$$

Зная явный вид нулевой присоединенной функции

$$\varphi_0(\epsilon) = \vec{E}_i(\epsilon) - \ln\gamma\epsilon - \frac{e^{\epsilon}}{\epsilon} + \frac{1+\epsilon}{\epsilon} \qquad (\text{П}1-5)$$

и воспользовавшись (П1 – 3, 4), легко получить выражения для последующих $\varphi_n(\epsilon)$. Присоединенные функции с произвольным номером могут быть представлены в виде:

$$\varphi_n(\epsilon) = L'_n(\epsilon)[\vec{E}_i;(\epsilon) - \ln\gamma\epsilon] - R_n(\epsilon)\cdot\frac{e^{\epsilon}}{\epsilon} + \frac{1}{\epsilon}Q_{n+1}(\epsilon), \qquad (\text{П}1-6)$$

где R_n – полиномы n-го порядка, определяемые по рекуррентной формуле типа (П1-1), исходя из $R_0 = 1$ и $R_1 = 1 - \epsilon$; Q – полиномы n порядка, определяемые по рекуррентной формуле, (П1-2), исходя из $Q_1 = 1 + \epsilon$, $Q_2 = 1 - 3/2\epsilon^2$;

2. Воспользовавшись представлением функции $\bar{E}_i(\epsilon) - \ln\gamma\epsilon$ в виде ряда Тейлора, легко найти поведение присоединенных функций в окрестности точки $\epsilon = 0$:

$$\varphi_n(\epsilon) = \frac{\epsilon^2}{2}(n+1) + \ldots \qquad (\text{П}1-7)$$

Для $\epsilon \gg 1$ имеет место асимптотическое представление

$$\epsilon e^{-\epsilon}\varphi_n(\epsilon) \sim (-1)^n\left[\frac{\prod_{p=0}^{n}(n+1-p)}{\epsilon^{n+1}} + \frac{(n+1)\prod_{p=0}^{n}(n+2-p)}{\epsilon^{n+2}} + \ldots\right] \qquad (\text{П}1-8)$$

ПРИЛОЖЕНИЕ 2

Как уже отмечалось, нам приходится иметь дело с интегралами типа $\int_0^{\infty}\epsilon e^{-\epsilon}\varphi_n(\epsilon)\epsilon^{\nu}d\epsilon = (\epsilon^{\nu}, \varphi_n)$, которые степенным образом расходятся на верхнем пределе при $\nu \geq n$ (ν – любое вещественное число). Отсылая

читателя за подробностями относительно обращения с интегралами подобного типа к книге [6], отметим лишь, что формально регуляризация этих интегралов сводится к вычитанию из $\varphi_n(\epsilon)$ такого числа первых членов асимптотического разложения (П1-8), которое необходимо, чтобы подинтегральное разложение стало интегрируемым.

Используя выражение (П1-5), получим следующие соотношения:

$$(\epsilon^{m-\alpha}, \varphi_0) = -\Gamma(m+2-\alpha)[\ln\gamma + (\delta_{\alpha_0}+1)\Psi(m+2-\alpha)] + \Gamma(m+1-\alpha) + \Gamma(m+2-\alpha), \qquad (\text{П2}-1)$$

где

$$\delta_{\alpha_0} = \begin{cases} 1 & \text{при } \alpha = 0 \\ 0 & \text{при } \alpha \neq 0 \end{cases}$$

Здесь m – целое число, α – вещественное число из интервала [(0, 1), $\Gamma(x)$ и $\Psi(x)$] соответственно, гамма-функция и ее логарифмическая производная.

В случае $n > 0$ имеем

$$(\epsilon^{\nu}, \varphi_m) = + \sum_{\ell=0}^{m} (-1)^{\ell+1} C_{n+1}^{n-\ell} \frac{\Gamma(m+2+\ell)}{m!} \left[\ln\gamma + 2\Psi(m+2+\ell)\right] + \sum_{\ell=0}^{m} q\Gamma(m+1+\ell).$$

Здесь q_ℓ - являются коэффициентами при степенях ϵ^ℓ в полиноме $Q_n(\epsilon)$ (См. П1-6).

ЛИТЕРАТУРА

[1] КАЗАРНОВСКИЙ М.В., СТЕПАНОВ А.В., ШАПИРО Ф.Л. II Международная конференция по мирному использованию атомной энергии. Доклады советских ученых. Ядерная физика, М., 1959, стр. 469.

[2] КАЗАРНОВСКИЙ М.В., ШАПИРО Ф.Л. Сборник "Нейтронная физика", стр. 169, Госатомиздат, М., 1961.

[3] ТАКАХАСИ Х. Термализация нейтронов. Сб. трудов Брукхэвенской конференции, стр. 258, Госатомиздат, М., 1964.

[4] KOTTWITZ D.A. . Nucl. Sci. and Engng. 7 (1960) 345.

[5] ЛАЛЕТИН Н.И. "Атомная энергия" 17 (1964) 193.

[6] ГЕЛЬФАНД И.М., ШИЛОВ Г.Е. Обобщенные функции, вып. 1, ГИФМЛ, Москва, 1958.

[7] ШВАРЦ Л. Математические методы для физических наук, Изд. "Мир", Москва, 1965.

[8] ЛАЛЕТИН Н.И. "Атомная энергия", 14 (1963) 458.

[9] ГРАДШТЕЙН И.С., РЫЖИК И.М. Таблицы интегралов, сумм, рядов и произведения, ГИФМЛ, Москва, 1963.

DISCUSSION

S.N. PUROHIT: As regards the use of Laguerre polynomials in the spectrum problem, might I say that I used the Laguerre polynomial expansion to calculate the thermal neutron spectrum for a heavy Debye

crystal, but found the method to break down in cases of large absorption. This work was reported at the American Nuclear Society Meeting at Boston in 1962, and has been published in the Society's transactions. Details of the spectrum results were also given in an unpublished report of the Brookhaven National Laboratory that same year.

I now have two questions. First, did the authors of the paper apply this method to a case other than that of a heavy gas? Secondly, what is the range of absorption values and how many polynomials did they use in their calculations?

L. V. MAIOROV: For this work they made a point of using the associated functions of the heavy gas equation, as well as the Laguerre polynomials, to describe the flux. Besides the heavy gas case, they also investigated the model of a gas moderator with arbitrary mass.

T. GOZANI: Did Dr. Laletin compare his expansion method with any measurement to see if he could reconstruct the experimental spectrum? It seems to me that the Friedmann non-$1/v$ absorption experiment might be a good example for comparison.

L. V. MAIOROV: The authors put forward a new method for solving the kinetic equation, rather than a new physical model. This should therefore be compared with other computational methods, not with experimental results.

E. U. VAUGHAN: As I see it, the functions $\varphi_n(\epsilon)$ do not satisfy the boundary conditions at zero energy. How is this situation handled?

L. V. MAIOROV: As $\epsilon \to 0$, $\varphi_n(\epsilon) \to \frac{1}{2}\epsilon^2 (n + 1) + \ldots$, which satisfies the boundary conditions.

P. MICHAEL: In certain problems, particularly time-dependent problems, it has been shown that velocity polynomials converge more rapidly. Have such polynomials been tried for the problems considered in this paper?

L. V. MAIOROV: Here, the main problem was to describe the transitional region of the spectrum by means of certain trial functions. If the velocity- or energy-dependent polynomials were to be used for this, a very large number of them would be required. However, the use of velocity-dependent polynomials seems to be a problem of minor importance.

ENERGY-DEPENDENT BOLTZMANN EQUATION WITH FISSION AND SLOWING-DOWN KERNELS

B. NICOLAENKO AND P.F. ZWEIFEL
UNIVERSITY OF MICHIGAN,
ANN ARBOR, MICHIGAN,
UNITED STATES OF AMERICA

Abstract

ENERGY-DEPENDENT BOLTZMANN EQUATION WITH FISSION AND SLOWING-DOWN KERNELS. This paper presents a study of the energy-dependent neutron transport equation, using Case's method of singular eigenfunctions and considering a continuous energy variable (rather than a multigroup scheme). Both fission and slowing-down kernels are included in the analysis. Under the assumption of simple cross-sections laws, and plane symmetry, a completeness theorem and the Green's function are found for the infinite medium, for both isotropic and anisotropic scattering, using rather general assumptions as to the slowing-down kernels (including convolution kernels) and, only in the anisotropic case, the generalized Greuling-Goertzel kernel. The crux of the completeness theorem is the inversion and analysis of the spectral properties of a continuous operator which acts upon the energy variable, and depends parametrically upon a complex variable z (with analyticity in some cut complex plane). For half-space problems, the Wiener-Hopf factorization of such an operator is a remarkably difficult problem. However, it can be performed if, for the slowing-down kernel, the Greuling-Goertzel approximation generalized to all its anisotropic components is used, in which case the Wiener-Hopf factorization gives another convolution operator. In this approximation the Milne problem is solved, and a study is made of the extrapolation length. There is a discussion of the difficulties introduced by fission kernels, with emphasis on the coexistence of space-energy separable modes with slowing-down transient modes.

I. INTRODUCTION

We deal in this paper with some aspects of the one-dimensional, static, energy-dependent neutron transport equation. We restrict our attention to the case that regeneration occurs only through fission and elastic scattering. In a future paper, inelastic scattering in the high-energy domain will be treated.

For many years, solutions of the energy-dependent Boltzmann equation were attempted only for simple elastic scattering models [1-8]. A number of authors have obtained solutions, in most cases based upon a double (Fourier-Laplace) transformation, leading to formidable inversion difficulties.

More recent work has been applied to the thermalization region [9-17, 21], but so far there are no exact or quasi-exact solutions in the fast region where fission and slowing-down coexist. In fact, even the earlier work dealing with elastic scattering in the fast region was only applied to full-space problems. The only exception to this is the work of Jacobs and MacInerney [19], but this approach, while excellent for the slowing-down problem they considered, cannot be readily extended to include fission or inelastic scattering.

As mentioned earlier, we treat elastic scattering plus fission in this paper, in the constant cross-section limit (unfortunately, the approximation of constant cross-sections is not easy to relax, but it is not a so bad approximation in the slowing-down domain as it is in the thermalization region). We are primarily concerned with isotropic elastic scattering, but the extension to the anisotropic case, using a Greuling-Goertzel kernel for each anisotropic component, will be indicated.

II. ISOTROPIC ELASTIC SCATTERING WITH FISSION

The basic transport equation that we consider is

$$\mu \frac{\partial\psi}{\partial x}(x,\mu,u) + \psi(x,\mu,u) = \frac{C_F}{2}\int_{-1}^{+1} d\mu'\chi(u)\int_{-\infty}^{+\infty}\psi(x,\mu',u')du'$$

$$+ \frac{C_S}{2}\int_{-1}^{+1} d\mu'\int_{-\infty}^{u} g(u-u')\psi(x,\mu',u')du' + \frac{1}{2}\delta(x-x_o)S(u) \qquad (1)$$

Here C_F represents the average number of fission secondaries per collision, while C_S is a similar quantity for elastic scattering. Also $\chi(u)$ is the fission spectrum and $g(u)$ the elastic-scattering kernel; S represents the extraneous source. Defining an operator O by

$$O\phi(u) = C_F\chi(u)\int_{-\infty}^{+\infty}\phi(u')du' + C_S\int_{-\infty}^{u} g(u-u')\phi(u')du' \qquad (2)$$

we see easily (by integration over lethargy) that O has only one eigenvalue equal to $C_F + C_S$ and a corresponding eigenfunction which satisfies the equation

$$O\mathscr{H}(u) = (C_F+C_S)\mathscr{H}(u) \qquad (3)$$

The explicit form of $\overline{\mathscr{H}}(u)$ can be found by a lethargy Fourier transform of Eq. (2) (k = transform variable)

$$\overline{\mathscr{H}}(k) = \frac{C_F\overline{\chi}(k)}{C_F+C_S(1-\overline{g}(k))} \qquad (4)$$

We see immediately that $\overline{\mathscr{H}}(0) = 1$.

If the source term [Eq. (1)] were of the form

$$S(u) = \mathscr{H}(u) \qquad (5)$$

then we see that Eq. (1) would reduce to a one-speed equation, because the solution is separable into a function of space and angle times $\mathscr{H}(u)$. Thus let us decompose the actual source as

$$S(u) = \mathscr{J}\mathscr{H}(u) + \Gamma(u) \tag{6a}$$

where

$$\mathscr{J} = \int_{-\infty}^{+\infty} S(u')du' \tag{6b}$$

and clearly

$$\int_{-\infty}^{+\infty} \Gamma(u')du' = 0 \tag{6c}$$

Since Eq. (1) is linear, its solution can be expressed as the one-speed solution due to $\mathscr{J}\mathscr{H}(u)$ plus the solution due to a source $\Gamma(u)$ of zero measure.

One can see very easily that the solution associated with the source $\Gamma(u)$ is also of zero measure, by referring to the integral form of the transport equation [20,21]. Call the former solution $\mathscr{H}(u)\ \phi_E(x,\mu)$ and the latter $\phi_{tr}(x,\mu,u)$

$$\psi(x,u,\mu) = \mathscr{H}(u)\ \phi_E(x,\mu) + \phi_{tr}(x,u,\mu) \tag{7}$$

Explicitly

$$\mu \frac{\partial\phi_E}{\partial x}(x,\mu) + \phi_E(x,\mu) = \frac{C_F+C_s}{2} \int_{-1}^{+1} d\mu'\phi_E(x,\mu') + \frac{1}{2}\delta(x)\mathscr{J} \tag{8a}$$

and

$$\mu \frac{\partial\phi_{tr}}{\partial x}(x,\mu,u) + \phi_{tr}(x,\mu,u) = \frac{C_s}{2} \int_{-1}^{+1} d\mu' \int_{-\infty}^{u} g(u-u')\phi_{tr}(x,\mu',u')du'$$

$$+ \frac{1}{2}\ \delta(x)\Gamma(u) \tag{8b}$$

The solution of (8a) is well known [23]. Equation (8b) is a plain slowing-down equation of the type solved by Jacobs and MacInerney [19]. Thus the present problem is completely solved.

The full-space and half-space Green's function will involve both solutions of Eq. (8a) (space-energy separable modes) and Eq. (8b) (nonseparable modes). These latter modes correspond to slowing-down transients, whose measure is zero; but such modes are physically present in integral experiments.

The Milne problem and criticality problems, on the other hand, involve only Eq. (8a).

We next turn to the anisotropic case which is much more complicated, because such a simple decomposition does not work. The reason is that energy transfer between different angular harmonics takes place. However, the work described above will serve as a guide, especially the idea of using slowing-down transient modes, whose total measure is zero.

III. THE ANISOTROPIC CASE

We will treat the case of a light elastic scatter, using a sequence of Greuling-Goertzel kernels to approximate the different angular harmonics. The general equation is

$$\begin{aligned}
\mu \frac{\partial\psi}{\partial x}(x,\mu,u) + \psi(x,\mu,u) &= \frac{1}{2} C_s \int_{-\infty}^{u} G_o(u-u')du' \int_{-1}^{+1} \psi(x,\mu',u')d\mu' \\
&+ \frac{1}{2} C_F \chi(u) \int_{-\infty}^{+\infty} du' \int_{-1}^{+1} \psi(x,\mu',u')d\mu' \\
&+ \frac{C_s}{2} \left\{ \sum_{n=1}^{\infty} (2n+1)P_n(\mu) \int_{-\infty}^{u} G_n(u-u')du' \right. \\
&(x) \left. \int_{-1}^{+1} P_n(\mu')\psi(x,\mu',u')d\mu' \right\} \\
&+ S(x,\mu,u)
\end{aligned} \tag{9}$$

The $P_n(\mu)$ are Legendre polynomials and $G_n(u)$ the Greuling-Goertzel kernels representing energy-transfer in the nth angular harmonic [22]. One could as well use the exact energy-transfer kernels of elastic scattering, since they are convolution kernels, too. However, if one uses Laplace or Fourier transforms of the lethargy variable, the inversion is made much easier with Greuling-Goertzel kernels.

If one now integrates Eq. (9) over the whole lethargy range, one obtains the one-speed anisotropic problem solved extensively by Mika [18]. By suppressing the fission kernel in Eq. (9), one finds the elastic slowing-down problem solved by Jacobs and MacInerney [19]. Though none of

these works can be straightforwardly extended to solve Eq. (9), we will refer to them for many techniques of calculation.

For the sake of brevity, we will deal with linear anisotropy. Extension to general anisotropy is readily made. The equations are

$$\mu \frac{\partial \psi}{\partial x}(x,\mu,u) + \psi(x,\mu,u) = \frac{C_s}{2} \int_{-\infty}^{u} G_o(u-u')du' \int_{-1}^{+1} \psi(x,\mu',u')d\mu'$$

$$+ \frac{C_F}{2} \chi(u) \int_{-\infty}^{+\infty} du' \int_{-1}^{+1} \psi(x,\mu',u')d\mu'$$

$$+ \frac{3}{2} C_s \mu \int_{-\infty}^{u} G_1(u-u')du' \int_{-1}^{+1} \psi(x,\mu',u')\mu' d\mu' + S(x,\mu,u) \tag{10a}$$

We transform Eq. (10a) by using a Fourier transform of the lethargy

$$\bar{\psi}(x,\mu,k) = \int_{-\infty}^{+\infty} \psi(x,\mu,u')e^{-iku'}du'$$

$$\mu \frac{\partial \bar{\psi}}{\partial x}(x,\mu,k) + \bar{\psi}(x,\mu,k) = \frac{C_s}{2} \bar{G}_o(k) \int_{-1}^{+1} \bar{\psi}(x,\mu',k)d\mu'$$

$$+ \frac{C_F}{2} \bar{\chi}(k) \int_{-1}^{+1} \bar{\psi}(x,\mu',0)d\mu'$$

$$+ \frac{3}{2} C_s \mu G_1(k) \int_{-1}^{+1} \bar{\psi}(x,\mu',k)\mu' d\mu' + \bar{S}(x,\mu,k) \tag{10b}$$

By setting $k = 0$

$$\bar{\psi}(x,\mu,0) = \int_{-\infty}^{+\infty} \psi(x,\mu,u')du'$$

we find Mika's one-speed equation

$$\mu \frac{\partial \bar{\psi}}{\partial x}(x,\mu,0) + \bar{\psi}(x,\mu,0) = \frac{C_F+C_s}{2} \int_{-1}^{+1} \psi(x,\mu',0)d\mu'$$

$$+ \frac{3}{2} \mu C_s B_1 \int_{-1}^{+1} \mu' \bar{\psi}(x,\mu',0)d\mu' + \bar{S}(x,\mu,0) \tag{10c}$$

(where $B_1 = \bar{G}_1(0)$).

Let us look for normal modes solutions of the homogeneous Eq. (10b), that is, solutions of the shape

$$\Phi(t,\mu,k)e^{-x/t} \tag{11a}$$

put

$$\Phi_o(t,k) = \int_{-1}^{+1} \Phi(t,\mu,k)d\mu \tag{11b}$$

$$\Phi_1(t,k) = \int_{-1}^{+1} \mu\Phi(t,\mu,k)d\mu \tag{11c}$$

Then, following a classical approach [18,23]

$$\begin{aligned}\Phi(t,\mu,k) &= \frac{t}{2} P \frac{1}{t-\mu} \{C_s\overline{G}_o(k)\Phi_o(t,k)+C_F\overline{\chi}(k)\Phi_o(t,0) \\ &+ 3\mu C_s\overline{G}_1(k)\Phi_1(t,k)\} \\ &+ \delta(t-\mu)\ \lambda(t,k)\end{aligned} \tag{12}$$

with

$$\begin{aligned}\lambda(t,k) &= \Phi_o(t,k) - tC_s\Phi_o(t,k)(Q_o(t)\overline{G}_o(k)) \\ &- tC_F\Phi_o(t,0)\overline{\chi}(k)Q_o(t) - 3t\ C_s\Phi_1(t,k)\{\overline{G_1}(k)Q_1(t)\}\end{aligned} \tag{13a}$$

$Q_o(z)$, $Q_1(z)$ are Legendre functions of the second kind

$$Q_o(z) = \frac{1}{2}\int_{-1}^{+1} \frac{d\mu}{z-\mu}, \quad Q_1(z) = \frac{1}{2}\int_{-1}^{+1} \frac{\mu d\mu}{z-\mu} \tag{13b}$$

If $\Phi_o(t,k)$ is arbitrary, then $\Phi_1(t,k)$ is readily obtained (see [18] and [19]

$$\Phi_1(t,k) = t\ \{\Phi_o(t,k)\ (1-C_s\overline{G_o}(k))-C_F\overline{\chi}(k)\ \Phi_o(t,0)\} \tag{14}$$

Let us look now for discrete regular modes. In general, there are only two such modes, corresponding to eigenvalues $\pm L_o$, such that (see Eqs. (12) and (13a))

$$\lambda(L_o,k) = 0 \tag{15a}$$

One sees at once that $\pm L_o$ are also the discrete eigenvalues of the one-speed equation (10c). For critical review of these eigenvalues, we refer to Mika [18].

The discrete modes will be

$$\Phi(\pm L_o,\mu,k)\ e(\mp x/L_o) \tag{15b}$$

with

$$\Phi(L_o,\mu,k) = \frac{1}{2}\frac{L_o}{L_o-\mu}\{C_s\overline{G_o}(k)\Phi_o(L_o,k) + C_F\bar{\chi}(k) + 3C_s\overline{G_1}(k)\mu\Phi_1(L_o,k)\} \tag{15c}$$

Here, we normalized

$$\Phi_o(L_o,0) = 1 \tag{15d}$$

And $\Phi_o(L_o,k)$ is solution of Eq. (15a), that is:

$$\frac{1}{L_o}\ \Phi_o(L_o,k) = C_s\overline{G_o}(k)\ Q_o(L_o)\ \Phi_o(L_o,k) + 3C_s\overline{G_1}(k)\ Q_1(L_o)\ \Phi_1(L_o,k) + C_F\bar{\chi}(k)Q_o(L_o) \tag{16}$$

Using Eq. (14), which yields $\Phi_1(L_o,k)$ in terms of $\Phi_o(L_o,k)$, Eq. (16) is very easily soluble. Then one can easily find the inverse Fourier transform of $\Phi_o(L_o,k)$, provided one has been using Greuling-Goertzel kernels.

Anticipating future developments, we can stress that the discrete regular modes $\Phi(\pm L_o,\mu,u)\ e^{\mp x/L_o}$ will be the only space-energy separable components of the complete solution. In an exponential experiment, one tries usually to measure these asymptotic separable modes, and an isotropic detector will be therefore sensitive to the "equilibrium" spectrum $\Phi_o(\pm L_o,u)$.

Now let us turn to the completeness of our set of normal modes, as defined by Eq. (12) and Eq. (15). As we shall see, these modes are not complete by themselves, and we shall have to add "slowing-down transients" of measure zero, for both full- and half-range completeness. First, the full-range hypothetical completeness theorem can be stated as

$$\psi(\mu,k) = \Sigma A_{o\pm}\Phi(\pm L_o,\mu,k) + \int_{-1}^{+1} \Phi(t,\mu,k)dt \tag{17}$$

where $\psi(\mu,k)$ is an arbitrary function of μ and of the lethargy-transformed variable K.

Checking Eq. (11b) and Eq. (12), where we define $\Phi(t,\mu,k)$, one sees immediately that we are taking $\Phi_o(t,k)$ as the unknown expansion coefficient of our continuum of singular modes, similar to the coefficient used by Mika and Jacobs-MacInerney in their respective completeness proofs [18,19]. Hence, for many intermediate steps in the following proof, the reader is referred to Mika's work [18].

So, applying Mika's procedure, we define, omitting many calculations

$$\begin{aligned}\psi''(\mu,k) &= \psi(\mu,k) - \Sigma A_{o\pm}\Phi(\pm L_o,\mu,k)\\ &- \frac{1}{2}\{C_s\overline{G_o}(k)\int_{-1}^{+1}\Phi_o(t,k)dt + C_F\overline{\chi}(k)\int_{-1}^{+1}\Phi_o(t,0)dt\}\\ &- \frac{3}{2}C_s\overline{G_1}(k)\mu\{(1-C_s\overline{G_o}(k))\int_{-1}^{+1}t\Phi_o(t,k)dt - C_F\overline{\chi}(k)\int_{-1}^{+1}t\Phi_o(t,0)dt\}\\ &- \frac{3}{2}\mu^2C_s\overline{G_1}(k)\{[1-C_s\overline{G_o}(k)]\int_{-1}^{+1}\Phi_o(t,k)dt - C_F\overline{\chi}(k)\int_{-1}^{+1}\Phi_o(t,0)dt\}\end{aligned} \tag{18}$$

Then define

$$F(z,k) = \frac{1}{2i\pi}\int_{-1}^{+1}\psi''(\mu,k)\frac{d\mu}{\mu-z} \tag{19}$$

also

$$\Omega_s(z,k) = 1-z\{C_s\overline{G_o}(k)Q_o(z)+3C_s\overline{G_1}(k)(1-C_s\overline{G_o}(k))Q_1(z)\} \tag{20}$$

$$\Omega_F(z,k) = -z\{C_F\overline{X}(k)Q_o(z)-3C_s\overline{G_1}(k)C_F\overline{X}(k)\ Q_1(z)\} \tag{21}$$

$$N(z,k) = \frac{1}{2\pi i}\int_{-1}^{+1}\frac{\Phi_o(t,k)dt}{t-z} \tag{22}$$

(let us recall that $\Phi_o(t,k)$ is the unknown expansion coefficient). The functions $N(z,k)$ and $F(z,k)$ are analytic in the z-complex plane cut from $[-1,+1]$. $\Omega_s(z,k)$ and $\Omega_F(z,k)$ are analytic in the z-complex plane cut from $[-1,+1]$, with the exception of possible poles.

Moreover,

$$\Omega_s(z,0) + \Omega_F(z,0) \equiv \Lambda(z) \tag{23}$$

$\Lambda(z)$ is the function used by Case and Mika [18,23] in the monokinetic case. This function is associated with the well-known solution of Eq. (10c).

Then, one can prove the following important fact: Eq. (17) is strictly equivalent to

$$F^+(\mu,k) - F^-(\mu,k) = \{\Omega_s^+(\mu,k)\ N^+(\mu,k) - \Omega_s^-(\mu,k)\ N^-(\mu,k)\}$$

$$+ \{\Omega_F^+(\mu,k)\ N^+(\mu,0) - \Omega_F^-(\mu,k)\ N^-(\mu,0)\} \tag{24}$$

(where $\pm$ means the value taken by an analytic function of z above and below the cut $[-1,+1]$. Thus

$$F(z,k) = \Omega_s(z,k)\ N(z,k) + \Omega_F(z,k)\ N(z,0) \tag{25}$$

Setting $k = 0$ in Eq. (25) and using Eq. (23), one finds at once $N(z,0)$

$$N(z,0) = \frac{F(z,0)}{\Lambda(z)} \tag{26}$$

And we get

$$N(z,k) = \frac{1}{\Omega_s(z,k)}\{F(z,k) - \frac{\Omega_s(z,k)\ F(z,0)}{\Lambda(z)}\} \tag{27}$$

Thus, the problem of finding $N(z,k)$ (that is the unknown expansion coefficient, see Eq. (22), seems to be solved. However $N(z,k)$ must <u>not</u>

have any singularities in z outside the cut [-1,+1]. Checking Eq. (27), we see that the delicate points are the zeros of $\Lambda(z)$ and $\Omega_s(z,k)$. First: $\Lambda(\pm L_o) = 0$; hence we must have

$$F(\pm L_o, 0) = 0 \tag{28}$$

Condition (28) is fulfilled through the discrete modes (15) introduced in Eqs. (17) and (18). One verifies easily that the discrete expansion coefficients $A_{o\pm}$ (Eqs. (17), (18), (19)) are exactly the same as those given by the well-known solutions of the monokinetic equation (10c) [18,23].

A more difficult problem lies in the zeros of $\Omega_s(z,k)$. For a fixed k, $\Omega_s(z,k)$ has zeros $z = J(k)$ such that

$$\Omega_s[J(k),k] = 0 \tag{29}$$

$z = J(k)$ is of course a function of k (possibly multivalued). However, we have exhausted our supply of discrete regular modes solution of Eq. (10b), in order to cope with the further singularities introduced by $\Omega_s(z,k)$. We should therefore conclude that the set of normal modes defined by Eqs. (11), (12), (13), (15), is incomplete.

But we can notice that $\Omega_s(z,k)$ is a function associated with the plain slowing-down problem (Eq. (10b) without fission) as solved extensively by Jacobs and MacInerney [19]. One can think of using the <u>discrete</u> regular normal modes of the plain slowing-down problem

$$\Psi(J(k),\mu,k) \quad e^{-x/J(k)} \tag{30}$$

with J(k) given by (29), as introduced by these former authors. Instead of expanding

$$\psi(\mu,k) - \Sigma A_{o\pm}\Phi(\pm L_o,\mu,k)$$

as in Eq. (17), one can try to expand

$$\psi(\mu,k) - \Sigma A_{o\pm}\Phi(\pm L_o,\mu,k) - B(k)\ \Psi(J(k),\mu,k) \tag{31a}$$

or, equivalently, instead of F(z,k), use

$$F(z,k) - \frac{B(k)}{2\pi i} \int_{-1}^{+1} \frac{\Psi(J(k),\mu,k)}{\mu - z}\, d\mu \tag{31b}$$

In order that the expressions (31a) and (31b) correspond to a solution of the complete transport equation with a fission kernel, one must have:

$$B(k) = 0 \quad \text{for} \quad k = 0 \tag{32}$$

That is, one is introducing discrete normal modes of the plain slowing-down equation, whose integral over the whole lethargy range (measure) is zero ("slowing-down transients"). One verifies indeed that this scheme works fully. For, if

$$\Omega_s(J(k),k) = 0 \tag{29}$$

we get immediately B(k) from Eq. (27)

$$B(k) = \{F(J(k),k) - \frac{\Omega_F(J(k),k)\ F(J(k),0)}{\Lambda(J(k))}\}$$

$$\times \{\frac{1}{2\pi i}\int_{-1}^{+1} \frac{\psi(J(k),\mu,k)}{\mu-J(k)}\, d\mu\}^{-1} \tag{33}$$

The crucial point is the verification of (32). Indeed, B(0) is proportional to

$$F(J(0),0) - \Omega_F(J(0),0)\ \frac{F(J(0),0)}{\Lambda(J(0))}$$

$$= F(J(0),0)\ \{\frac{\Lambda(J(0))-\Omega_F[J(0),0]}{\Lambda(J(0))}\}$$

$$= F(J(0),0)\ \frac{\Omega_s(J(0),0)}{\Lambda(J(0))} \tag{34}$$

(if we remember Eq. (23)). But, in Eq. (34), $\Omega_s(J(0),0) = 0$, because of Eq. (29). While $\Lambda(J(0)) \neq 0$. Hence

$$B(0) = 0 \tag{32}$$

To summarize, we have proved that the full-range completeness theorem must be stated as

$$\psi(\mu,k) = \Sigma A_{0\pm}\Phi(\pm L_0,\mu,k) + B(k)\Psi(J(k),\mu,k)$$

$$+ \int_{-1}^{+1} \Phi(t,\mu,k)dt \tag{35}$$

where $\Phi(\pm L_o,\mu,k)$ are the discrete regular modes of Eq. (10b), as defined in Eq. (15), and $\psi(J(k),\mu,k)$ are the discrete regular modes of the plain slowing-down problem, as introduced by Jacobs and MacInerney. The superposition of the latter modes has indeed a null measure, hence the name of "slowing-down transients."

The very same completeness theorem holds for the half-range domain, as it will be shown in the Appendix, although calculations are more involved.

$$\psi(\mu,k) = a_o\Phi(+L_o,\mu,k) + B(k)\Psi(J(k),\mu,k) + \int_0^1 \Phi(t,\mu,k)dt \quad (36)$$

And the solution of Milne's problem will be:

$$\psi(x,\mu,u) = \Phi(-L_o,\mu,u)e^{+x/L_o}$$

$$+ a_o\Phi(+L_o,\mu,u)e^{-x/L_o} + \frac{1}{2\pi}\int_{-\infty}^{+\infty} B(k)\Psi[J(k),\mu,k]e^{-x/J(k)}\, e^{iku}dk$$

$$+ \frac{1}{2\pi}\int_{-\infty}^{+\infty} e^{iku}\, dk \int_0^1 \Phi(t,\mu,k)e^{-x/t}\, dt \quad (37)$$

a_o and L_o will be identical to the equivalent parameters found in solving the one-speed equation (10c). The great difference lies in the presence of slowing-down transients.

IV. CONCLUSION

The present work has shown that the solution of the energy-dependent Boltzmann equation with elastic slowing-down <u>and</u> fission, is far from being straightforward. Neither prior works dealing with a monokinetic equation [18], nor works solving the plain slowing-down problem [19], could foretell the following basic features due to fission regeneration, that is, the coexistence, in the solution of any transport problem (half-space, full-space) of space-energy separable regular discrete modes, with nonseparable (but regular) "slowing-down transient" modes.

Basically similar features have been found in the fast-domain, with fission and <u>inelastic</u> slowing-down. Work will be published on this subject soon.

It has to be stressed that the "slowing-down transients," though decaying spatially faster than the separable modes, still decay more slowly

than the classical continuum transport transients. Hence, these effects will be important in the interpretation of integral experiments in the intermediate energy range; for instance, in an exponential experiment, one usually wishes to measure a well-defined, space-energy separable asymptotic (equilibrium) mode. However, experimentalists often acknowledged that they were not sure whether or not they had reached such an equilibrium distribution [24-27]. As far as we can know, the present work gives the first theoretical explanation of this experimental difficulty: there is competition between space-energy separable modes and slowing-down transients, the latter decaying sometimes rather slowly into space Some numerical work will be done soon on this transport-interpretation of exponential experiments.

APPENDIX

HALF-RANGE COMPLETENESS THEOREM IN THE ANISOTROPIC CASE

In this concise appendix complete familiarity will be assumed with the completeness theorem of Jacobs and MacInerney [19], though by no means will it be a straightforward extension.

We wish to prove half-range completeness. The starting point will be Eq. (24)

$$\psi''(\mu,k) = \{\Omega_s^+(\mu,k)\, N^+(\mu,k) - \Omega_s^-(\mu,k)\, N^-(\mu,k)\}$$

$$+ \{\Omega_F^+(\mu,k)\, N^+(\mu,0) - \Omega_F^-(\mu,k)\, N^-(\mu,0)\} \qquad (24)$$

With, this time

$$N(z,k) = \frac{1}{2\pi i} \int_0^1 \frac{\Phi_o(t,k)}{t-z}\, dt \qquad (38)$$

If we set $k = 0$ in Eq. (24), we find the solution of the associated one-speed equation (10c); hence $N(z,0)$ is perfectly well known from previous half-space one-speed solutions [18,23]. So, we are permitted to consider $N(z,0)$, $N^+(\mu,0)$, $N^-(\mu,0)$ as perfectly well-known functions. Hence, set

$$\psi'''(\mu,k) = \psi''(\mu,k) - \{\Omega_F^+(\mu,k)\, N^+(\mu,0) - \Omega_F^-(\mu,k)\, N^-(\mu,0)\} \qquad (39a)$$

and Eq. (24) becomes

$$\psi'''(\mu,k) = \Omega_s^+(\mu,k)\, N^+(\mu,k) - \Omega_s^-(\mu,k)\, N^-(\mu,k) \qquad (39b)$$

Define

$$X_s(z,k) = \frac{1}{1-z} \exp\left\{ \frac{1}{2\pi i} \int_0^1 \log\left\{ \frac{\Omega_s^+(\mu,k)}{\Omega_s^-(\mu,k)} \right\} \frac{d\mu}{\mu - z} \right\} \tag{40}$$

we have

$$\frac{X_s^+(\mu,k)}{X_s^-(\mu,k)} = \frac{\Omega_s^+(\mu,k)}{\Omega_s^-(\mu,k)} \tag{41}$$

Then Eq. (39b) can be rewritten as:

$$\frac{X_s^-(\mu,k)}{\Omega_s^-(\mu,k)} \quad \psi'''(\mu,k) = X_s^+(\mu,k)\, N^+(\mu,k) - X_s^-(\mu,k)\, N^-(\mu,k) \tag{42}$$

Define

$$S(z,k) = \frac{1}{2i\pi} \int_0^1 \frac{X_s^-(\mu,k)}{\Omega_s^-(\mu,k)} \quad \frac{\psi'''(\mu,k)}{\mu - z}\, d\mu \tag{43}$$

$S(z,k)$, $X_s(z,k)$, $N(z,k)$ are all functions analytic in z outside the cut $[0,+1]$. Thus from Eq. (42)

$$N(z,k) = \frac{S(z,k)}{X_s(z,k)} \tag{44}$$

$N(z,k)$ must behave as $1/z$ at infinity. This requires classically [23] that, instead of expanding $\psi'''(\mu,k)$, we expand

$$\psi'''(\mu,k) - B(k)\Psi(J(k),\mu,k) \tag{45}$$

$\Psi(J(k),\mu,k)$ being defined in (30). Classically, $B(k)$ will be given by

$$B(k) \quad \int_0^1 \frac{X_s^-(\mu,k)}{\Omega_s^-(\mu,k)} \quad \Psi(J(k),\mu,k)d\mu = \int_0^1 \frac{X_s^-(\mu,k)}{\Omega_s^-(\mu,k)} \quad \psi'''(\mu,k)d\mu \tag{46}$$

Again we must have condition (32): $B(0) \equiv 0$ (slowing-down transients). Equation (32) is equivalent to

$$\int_0^1 \frac{X_s^-(\mu,0)}{\Omega_s^-(\mu,0)} \psi'''(\mu,0)d\mu = 0 \tag{47a}$$

Using Eq. (42), Eq. (47a) becomes

$$\int_0^1 \{X_s^+(\mu,0)\, N^+(\mu,0) - X_s^-(\mu,0)\, N^-(\mu,0)\}d\mu = 0 \tag{47b}$$

This is indeed the crucial step; for $X_s(z,0)$ and $N(z,0)$ are perfectly well-known functions, analytic in the z-plane cut from [0,+1] and both behaving as $1/z$ at infinity. So

$$\int_0^1 \{X_s^+(\mu,0)\, N^+(\mu,0) - X_s^-(\mu,0)\, N^-(\mu,0)\}d\mu$$

$$= \oint_c X_s(z,0)\, N(z,0)dz \tag{47c}$$

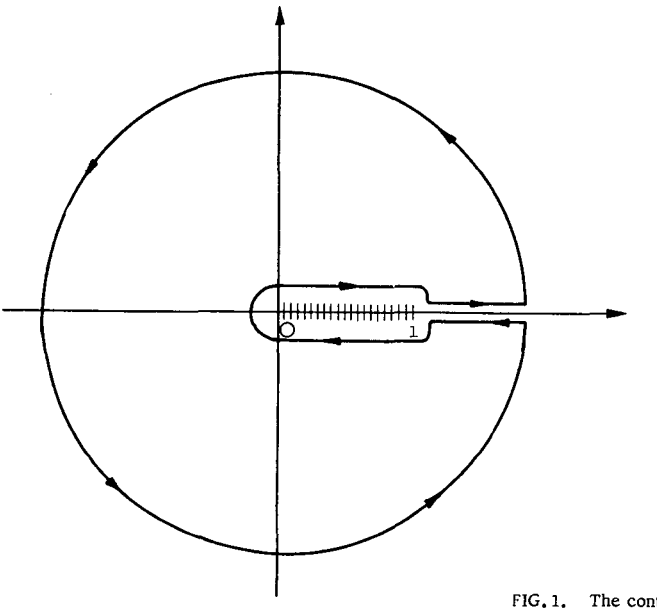

FIG. 1. The contour c in the z-complex plane.

where c is a contour in the complex z-plane (see Figure 1). Then from Cauchy's theorem (no singularities within c)

$$\oint_c X_s(z,0)\, N(z,0)dz \equiv 0 \tag{47d}$$

and, indeed

$$B(k) \equiv 0 \qquad \text{for } k \equiv 0 \tag{32}$$

So, we proved the following half-range completeness theorem, similar to the full-range one.

$$\psi(\mu,k) = a_o\Phi(L_o,\mu,k) + B(k)\Psi(J(k),\mu,k) + \int_0^1 \Phi(t,\mu,k)dt \tag{36}$$

The coefficient a_o is readily given by the solution of the associated one-speed equation (10c) [18,23].

REFERENCES

[1] MARSHAK, R. E., Rev. Mod. Phys. 19 (1947) 185.

[2] VERDE, M., WICK, G. C., Phys. Rev. 71 (1947) 852.

[3] WICK, G. C., Phys. Rev. 75 (1949) 738.

[4] HÖLTE, G., Arkiv for Fysik, Band 2 48 (1950).

[5] HÖLTE, G., Arkiv for Fysik, Band 2 14 (1951).

[6] HEJTMANEK, H., Atomkernenergie 6 (1961) 350.

[7] HEJTMANEK, H., Atomkernenergie 7 (1962) 359.

[8] PAPMUHL, N., Nucl. Sci. Engng. 22 (1965) 215.

[9] CORNGOLD, N., MICHAEL, P., WOLLMANN, W., Nucl. Sci. Engng. 15 (1963) 13.

[10] BEDNARZ, R. J., MIKA, J. R., J. Math. Phys. 4 9 (1963) 1285.

[11] STEWART, J. C., KUSCER, I., MacCORMICK, N. J., Ann. of Phys. 40 (1966) 321.

[12] WILLIAMS, M.M.R., Nucl. Sci. Engng. 18 (1964) 260.

[13] ARKUSZEWSKI, J., Nucl. Sci. Engng. 27 (1967) 104.

[14] WILLIAMS, M.M.R., Nucl. Sci. Engng. 27 (1967) 511.

[15] FERZIGER, J., LEONARD, A., Ann. of Phys. 22 (1963) 192.

[16] LEONARD, A., FERZIGER, J., Nucl. Sci. Engng. 26 (1966) 170.

[17] LEONARD, A., FERZIGER, J., Nucl. Sci. Engng. 26 (1966) 181.

[18] MIKA, J. R., Nucl. Sci. Engng. 11 (1961) 415.

[19] MacINERNEY, J. J., JACOBS, A. M., Nucl. Sci. Engng. 22 (1965) 215.

[20] DAVISON, B., Neutron Transport Theory, Oxford Univ. Press (1957).

[21] WILLIAMS, M.M.R., The Slowing Down and Thermalization of Neutrons, Wiley, New York (1966).

[22] FERZIGER, J., ZWEIFEL, P. F., The Slowing Down of Neutrons in Nuclear Reactors, Pergamon Press, New York (1965).

[23] CASE, K. M., ZWEIFEL, P. F., Neutron Diffusion: An Introduction to Linear Transport Theory, Addison-Wesley, Reading, Mass. (1967).

[24] LEIPUNSKY, A. E., Proc. 1st UN Int. Conf. PUAE 5 (1955) 342.

[25] OKRENT, D., Proc. 2nd UN Int. Conf. PUAE 12 (1958) 13.

[26] LEIPUNSKY, A. I., Proc. 2nd UN Int. Conf. PUAE 12 (1958) 3.

[27] LEIPUNSKY, A. I., Proc. 3rd UN Int. Conf. PUAE 6 (1964) 153.

DISCUSSION

N. J. McCORMICK: Have you attempted to relax your assumption of the constant cross-section by solving for the collision density and introducing the new variable used by Bednarz and Mika (J. Math. Phys. 4 (1963) 1285)?

B. NICOLAENKO: Attempts have been made, but it turned out that the completeness theorem proposed by Bednarz and Mika (for the energy-dependent Boltzmann equation) was incorrect. Completeness does not hold for a source term with an arbitrary energy spectrum because, in some cases, no discrete regular modes exist, while at the same time there is 'scattering of singularities' for the solution outside the classical cut

(-1, +1). This is typical of slowing-down problems, and details of our discoveries will be published soon.

H. G. KAPER: Could you give any information about the function J(k), e.g. is it analytic in the complex k-plane?

B. NICOLAENKO: The function J(k) is analytic in the complex k-plane, with the exception of a cut on the positive imaginary axis. J(k) is thus continuous on the real axis, which is the inversion path for k used in inverting the Fourier transform.

ASYMPTOTIC BEHAVIOUR OF NEUTRON TRANSPORT PROCESSES

J.H. HEJTMANEK
ATOMINSTITUT,
TECHNISCHE HOCHSCHULE,
VIENNA, AUSTRIA

Abstract

ASYMPTOTIC BEHAVIOUR OF NEUTRON TRANSPORT PROCESSES. The solution of the initial-value problem of the time-dependent linear Boltzmann equation corresponds to a semigroup of linear transformations:

Initial-value problem: $\frac{\delta n}{\delta t} = An \qquad n(\vec{x},\vec{v},0) = f(\vec{x},\vec{v})$

Solution: $n(\vec{x},\vec{v},t) = T_t f(\vec{x},\vec{v}) \qquad T_t = e^{At}$

Lehner and Wing were the first to use a Laplace transform technique for the study of the asymptotic behaviour of the solution. Mika, Bednarz, Albertoni, Kaper et al. extended this technique to more general problems. The main task is always to find the spectrum of the Boltzmann operator A. Asymptotic behaviour is closely related to the point spectrum of A, if the latter exists.

This paper uses a completely new approach, mean ergodic theory, the study of asymptotic properties of semigroups of bounded transformations in a Banach space. Two types of function spaces are considered: (1) The Banach space L^1_m of functions integrable on the six-dimensional μ-space of statistical mechanics. The Banach norm $\| f \|$ equals the total number of neutrons in the system; (2) The Hilbert space L^2_m of functions square integrable on the μ-space. The inner product (f, g) equals the total count rate of the neutron distribution f due to an array of neutron detectors described by the weight function g of the space dual to that of all neutron distributions.

Excluding the case of a super-critical system, the semigroup generated by the Boltzmann operator A is uniformly bounded $\| T_t \| \leq K$, $t \geq 0$. The splitting theorem of mean ergodic theory can be applied to T_t. The initial distribution is split uniquely into a sum of a reversible and a flight vector.

Now a special property of the semigroup generated by the Boltzmann operator A enters: there exists a characteristic time $t_0 > 0$ depending only on the geometry and chemistry of the system such that $T_t f(\vec{x},\vec{v}) > 0$ for all $(\vec{x},\vec{v})$, for all f and all $t \geq t_0$. From this property it is possible to deduce that an equilibrium distribution exists and is unique.

Taking the Hilbert space L^2_m, criticality of a reactor corresponds to strong mixing in the sense of ergodic theory; we define a reactor as critical if for all f and all g, positive almost everywhere, a positive limit $(T_t f, g)$ exists for $t \to \infty$. This definition corresponds to the Fermi experiment. Boundedness of T_t can be demonstrated.

Finally an attempt is made to define the mean entropy of a neutron transport process.

1. THE SEMIGROUP GENERATED BY THE BOLTZMANN OPERATOR

A neutron transport system is completely described by its total cross-section $\Sigma(\vec{v})$ and the collision kernel $c(\vec{v}')\Sigma_s(\vec{v}' \to \vec{v})$. Both will be assumed independent of $\vec{x}$. There is also a maximum velocity of all neutrons $|v| < v_{max}$, whereby v_{max} corresponds to the neutron energy of 10 MeV. The μ-space of the system is a six-dimensional bounded and open set P of points $(\vec{x},\vec{v})$. P is the Cartesian product of the geometry of the transport system M, a bounded and open convex set, and the sphere $V = \{\vec{v} | 0 < |v| < v_{max}\}$. There is no loss of generality,

if we assume $m(P) = 1$. The main problem in reactor theory is to find the behaviour of the neutron density $n(\vec{x}, \vec{v}, t)$ in the course of time, $n(\vec{x}, \vec{v}, 0) = f(\vec{x}, \vec{v})$ given at the instant $t = 0$.

It is necessary to specify the function space where the neutron density function is obtained. There are two ways:

(1) $n \in L_1$, i.e. n is absolutely integrable in P.

$$\|n\|_1 = \int |n(\vec{x}, \vec{v}, t)\, d\vec{x}\, d\vec{v}$$

L_1 is a Banach space with norm $\|n\|_1$, this norm means the total number of neutrons in P at time t.

(2) $n \in L_2$, i.e. n is square integrable in P. L_2 is a Hilbert space with the inner product

$$(n, g) = \int n(\vec{x}, \vec{v}, t)\, \overline{g(\vec{x}, \vec{v})}\, d\vec{x}\, d\vec{v}$$

meaning the total count rate of an array of detectors described by the weight function $g(\vec{x}, \vec{v})$. The inner product defines a norm

$$\|n\|_2 = \sqrt{(n, n)}$$

Since P has measure unity in the μ-space, $L_2 \leq L_1$, and because of the Schwartz inequality,

$$\|n\|_1 \leq \|n\|_2$$

holds. Thus $\|n\|_2$ is only an upper bound for the total number of neutrons in P. The solution of the initial-value problem leads to a semigroup of linear operators

$$G = \{T_t \mid t \geq 0\}$$

$$n(\vec{x}, \vec{v}, t) = T_t f(\vec{x}, \vec{v})$$

Purely physical reasoning implies that the semigroup must have the following properties:

(1) Every operator T_t is linear

$$T_t(f+g) = T_t f + T_t g \qquad T_t(\lambda f) = \lambda T_t f$$

because our transport problem is linear. Non-linear effects would enter by neutron-neutron encounters, but they are disregarded here. Therefore the superposition principle is valid.

(2) $T_0 f = f$, because $T_t f$ represents the solution of the initial-value problem.

(3) $T_{t_1}(T_{t_2} f) = T_{t_1+t_2} f$, because of the uniqueness of the solution. The T_t form an Abelian semigroup with parameter $t \geq 0$ containing the unit element T_0.

(4) The T_t are positive in the sense, if $f(\vec{x},\vec{v}) \geq 0$ and $\|f\|_2 = 1$ for all $(\vec{x},\vec{v}) \in P$, then $T_t f(\vec{x},\vec{v}) \geq 0$ for all $(\vec{x},\vec{v}) \in P$ and all $t \geq 0$.

(5) In the Banach algebra of linear operators T, a norm is defined by

$$\|T\|_i = \sup \|Tf\|_i$$

$$\|f\|_i \leq 1$$

If $\|T\|_i < \infty$, T is called a bounded linear operator. Let us assume $f(\vec{x},\vec{v}) \geq 0$ and $\|f\|_i = 1$. Then after a time t only a finite number $\|T_t f\|_i$ of neutrons can result from f. For a fixed t this number cannot become arbitrarily large, as we know from experience, for all $f(\vec{x},\vec{v}) \geq 0$ and $\|f\|_i = 1$. This means T_t is bounded for all $t \geq 0$, but not necessarily uniformly in t.

These properties of the semigroup are physically evident for any kind of transport process. The following property is characteristic for the neutron transport process:

(6) After the time $t_0 = dv_{max}^{-1}$ (d equals the diameter of M) $T_t f(\vec{x},\vec{v}) > 0$. $T_t f$ is strictly positive for all $(\vec{x},\vec{v}) \in P$, for all $f \geq 0$ and $\|f\|_i = 1$ and all $t \geq t_0$; t_0 is actually the time needed by the front of a neutron pulse to cross the system. If $c(\vec{v}')\Sigma_s(\vec{v}' \to \vec{v}) > 0$ for all $(\vec{v}',\vec{v}) \in V \times V$, then the above is true. In other words, all possible states $(\vec{x},\vec{v}) \in P$ a neutron can occupy are filled after a certain time characteristic to the system and are never again emptied completely.

2. PROPERTIES OF THE SEMIGROUP

These assumptions were obtained by purely physical reasoning, and we shall investigate now whether they are satisfied by the solution of the linear Boltzmann equation. $\Sigma(\vec{v})v$ and $c(\vec{v}')\Sigma_s(\vec{v}' \to \vec{v})v'$ are supposed to be continuous functions in $\overline{V}$, i.e. $\overline{V} \times \overline{V}$, and $c(\vec{v}')\Sigma_s(\vec{v}' \to \vec{v}) > 0$ to be strictly positive in $V \times V$. The linear Boltzmann equation has the form

$$\frac{\partial n}{\partial t} = An$$

A is called the Boltzmann operator

$$An = -\vec{v}\nabla n + In - v\Sigma(\vec{v})n$$

$$In = \int_V c(\vec{v}')\Sigma_s(\vec{v}' \to \vec{v})v' n(\vec{x},\vec{v}',t)d\vec{v}'$$

Working in the space L_2, the semigroup generated by A (i.e. $T_t = e^{At}$) was studied originally by Lehner and Wing [1] for a slab with isotropic scattering of monoenergetic neutrons. Their Laplace transform technique has been extended and computationally evaluated by several authors [2-8]. The Neumann series approach was first used by Case and Zweifel [9] and was made mathematically rigorous in Refs. [10, 11] by the method of successive approximation. Because of the continuity of $\Sigma(\vec{v})v$ and $c(\vec{v}')\Sigma_s(\vec{v}' \to \vec{v})$, the collision operator J is bounded in L_i.

Theorem 1: For the above conditions on the Boltzmann operator A, the semigroup T_t satisfies conditions (1) - (6) of section 1.

Proof: Existence and uniqueness of the initial-value problem have been proved in Refs. [10, 11]. (These papers are used in the following.) Condition (1) follows from the linearity of the Boltzmann equation, (2) and (3) from the uniqueness theorem. The following problems have a unique solution:

Problem 1: $\frac{\partial n}{\partial t} + \vec{v}\nabla n = -v\Sigma(\vec{v})\, n \qquad n(\vec{x},\vec{v},0) = f(\vec{x},\vec{v})$

Problem 2: $\frac{\partial n}{\partial t} + \vec{v}\nabla n = g(\vec{x},\vec{v},t) \qquad n(\vec{x},\vec{v},0) = 0$

Their solutions are

Solution of 1: $n(\vec{x},\vec{v},t) = \exp[-v\Sigma(\vec{v})t]\; S_t f(\vec{x},\vec{v})$

S_t is a group of positive contractions in L_i:

$$S_t f(\vec{x},\vec{v}) = f(\vec{x}-\vec{v}t,\vec{v}) \qquad \|S_t\|_i = 1$$

Solution of 2: $n(\vec{x},\vec{v},t) = \int_0^t S_{t-\xi}\, g(\vec{x},\vec{v},\xi)\, d\xi$

We can successively solve the system of equations:

$$i = 1 \qquad \frac{\partial n_1}{\partial t}\; \vec{v}\nabla n_1 = -v\Sigma(\vec{v})n \qquad n_1(\vec{x},\vec{v},0) = f(x,v)$$

$$\frac{\partial n_2}{\partial t} + \vec{v}\nabla n_2 = In_1 \qquad n_2(\vec{x},\vec{v},0) = 0$$

$$i \geq 2 \qquad \frac{\partial n_{2i-1}}{\partial t} + \vec{v}\nabla n_{2i-1} = -v\Sigma(\vec{v})n_i \qquad n_{2i-1}(\vec{x},\vec{v},0) = 0$$

$$\frac{\partial n_{2i}}{\partial t} + \vec{v}\nabla n_{2i} = In_i \qquad n_{2i}(\vec{x},\vec{v},0) = 0$$

$n = \sum_{i=1}^{\infty} n_i$ is obviously a solution of the Boltzmann equation. If $f \geq 0$, then all $n_i \geq 0$, hence (4) is proved.

To prove (6), it is sufficient to show that $n_4(\vec{x},\vec{v},t) > 0$ for all $(\vec{x},\vec{v}) \in P$ and a fixed $t \geq t_0$. We could do that by writing the explicit expression for n_4. But a heuristic argument will shorten this procedure considerably: n_4 is the contribution to the neutron density in $(\vec{x},\vec{v})$ at time t from the initial cloud of neutrons that reach $(\vec{x},\vec{v})$ after one collision between 0 and t and have their second collision in $(\vec{x},\vec{v})$ at time t. Then these neutrons occupy the state $(\vec{x},\vec{v})$, thus $n_4(\vec{x},\vec{v},t) > 0$. Boundedness of T_t has been proved in [11].

$$\| T_t \|_i \leq \sum_{k=0}^{\infty} \frac{t^k}{k!} \| I. - v\Sigma(\vec{v}). \|_i$$

This completes the proof of Theorem 1.

$T_t f$ is the solution of the initial-value problem for a set f, dense in L_i, e.g. the set of all polynomials in P.

In the next section we will confine ourselves to the case of the Hilbert space L_2, although $\|f\|_2$ is only an upper bound for the number of particles in P. The reason is that the theorems in mean ergodic theory are easily proved in that case.

3. THE SPLITTING THEOREM

Prerequisites for theorems in mean ergodic theory are the Hilbert space $H = L_2$ and a uniformly bounded semigroup of operators $G = \{T_t | t \geq 0\}$ in H. Our aim is to study the action of the Abelian semigroup G, generated by the Boltzmann operator A, for large times $t \to \infty$. The semigroup corresponds to a flow in H, every element $h \in H$ has an orbit $Gh = \{T_t h | t \geq 0\}$. In the following G will be assumed uniformly bounded, i.e. there exists a constant K such that we have $\| T_t \| \leq K$ for all $t \geq 0$. This excludes the case of a super-critical system. We extend G to its weak hull [13-15].

Definition: $\overline{G}$ is the set of all linear operators T in H with the additional property that for arbitrarily chosen $h_1, \ldots h_r$ and a weak neighbourhood U of 0, there exists at least one $T_t \in \overline{G}$ with

$$|((T - T_t) h_\rho, g_\sigma)| < \epsilon \qquad \rho = 1, \ldots r \qquad \sigma = 1, \ldots s$$

Theorem 2: (1) $\overline{G}$ is an Abelian semigroup of uniformly bounded linear operators

$$\| T \| \leq K \qquad T \in \overline{G} \qquad \| f \|$$

(2) Every $T \in \overline{G}$ is positive, i.e. for $f(x,v) \geq 0$ $\|f\| = 1$

$$Tf(\vec{x},\vec{v}) \geq 0$$

Proof: (1) has been proved in [14]. To prove (2), assume there can be found for $T \in \overline{G}$ an $h(\vec{x},\vec{v}) \geq 0$, $\|h\| = 1$, with the following properties:

$$E^+ = \{(\vec{x},\vec{v}) \mid Th(\vec{x},\vec{v}) > 0\}$$

$$E^- = \{(\vec{x},\vec{v}) \mid Th(\vec{x},\vec{v}) < 0\} \quad m(E^-) > 0$$

Let $\chi(\vec{x},\vec{v})$ be the characteristic function of E^-. Since T is in the weak hull of G, for every f, $g \in H$ and ϵ there exists a $T_t \in G$ with

$$|((T - T_t) f, g)| < \epsilon$$

For $f = h$, $g = \chi$ we obtain

$$\left| \int Th\chi - \int T_t h\chi \right| < \epsilon$$

$$\int Th\chi = \text{Constant} < \infty \qquad \int T_t h\chi \geq 0$$

This evidently leads to a contradiction; the left side cannot be arbitrarily small. This finishes the proof.

$\overline{G}h$, the weak orbit closure of Gh, is G-invariant, i.e. $G\overline{G}h \leq \overline{G}h$.

Definition: h is called a G-reversible vector, if $\overline{G}f = \overline{G}h$ for every $f \in Gh$. G acts like a group on a reversible vector: for every $T_t \in G$ there is a $T_s \in G$ such that $T_s(T_t h) = h$.
Trivial G-reversible vectors are 0 and at every fixed point h: $Gh = \{h\}$. Thus the set of all reversible vectors R is never empty.

Definition: h is called a flight vector, if $0 \in Gh$.
F is defined as the set of all G-flight vectors. The only vector that is simultaneously G-reversible and a G-flight vector, is 0.

Theorem 3 (splitting theorem): If G is an Abelian uniformly bounded semigroup, then R and F are linear G-invariant sub-spaces of H. Every $h \in H$ has a unique and orthogonal decomposition

$$h = r + f \qquad r \in R \qquad f \in F$$

The mappings $P_R : h \to r$ and $P_F : h \to f$ are orthogonal projections on R and F; they commute with every $T_t \in G$ and $P_R \in \overline{G}$.
$\overline{G}$ acts like a group in R.

Proof: See Refs. [14, 15].

Two cases are possible: (1) $H = F$ and (2) $H = R + F \quad R \neq \{0\}$.
Case (1): Every vector $h \in H$, $h(\vec{x},\vec{v}) \geq 0$, $\|h\| = 1$, is a G-flight vector, i.e.

$$\| T_t h \|_1 = \int T_t h = (T_t h, 1) \to 0$$

This apparently is the case for a sub-critical system.
Case (2): This is a critical system.

4. THE CRITICAL REACTOR

This section is devoted to the treatment of the critical system.

Theorem 4: For every $h(\vec{x},\vec{v}) \geq 0$, $\|h\| = 1$, P_R is strictly positive in the sense

$$P_R h(\vec{x},\vec{v}) > 0 \text{ for all } (\vec{x},\vec{v}) \in P$$

Proof: Assume

$$E^+ = \{(\vec{x},\vec{v}) \mid P_R h(\vec{x},\vec{v}) > 0\} \qquad m(E^+) > 0$$

$$E_0 = \{(\vec{x},\vec{v}) \mid P_R h(\vec{x},\vec{v}) = 0\} \qquad m(E_0) > 0$$

Then for $t \geq t_0$ $T_t P_R h(\vec{x},\vec{v}) > 0$ for all $(\vec{x},\vec{v}) \in P$.
In R,G acts like a group, so a T_s exists such that

$$T_s T_t P_R h(\vec{x},\vec{v}) > 0 \text{ for all } (\vec{x},\vec{v}) \in P$$

$$T_s T_t P_R h(\vec{x},\vec{v}) = P_R h(\vec{x},\vec{v}) \quad \text{Contradiction!}$$

$P_R h(\vec{x},\vec{v})$ is the critical equilibrium distribution the reactor will tend to.
Every G-flight must have positive and negative components

$$E^+ = \{(\vec{x},\vec{v}) \mid f(\vec{x},\vec{v}) > 0\} \qquad m(E^+) > 0$$

$$E^- = \{(\vec{x},\vec{v}) \mid f(\vec{x},\vec{v}) < 0\} \qquad m(E^-) > 0$$

The experiment, first performed by Fermi, to decide whether the system is critical or not, consists of a certain array of detectors described by the weight function $g(\vec{x},\vec{v}) \geq 0$, $\|g\| = 1$, and the initial distribution $h(\vec{x},\vec{v}) \geq 0$, $\|h\| = 1$.

Definition: G is called a critical semigroup, if

$$\lim (T_t h, g)$$

exists and is positive for all such h and g.

Theorem 5: If G is critical there exists a common upper bound for the norms of T_t

$$\| T_t \| \leq K$$

Proof: If the limit exists for all h and $g \geq 0$, $\|h\| = 1$, $\|g\| = 1$, then it exists for all $h, g \in H$, for every function $h \in H$ can be written in the form

$$h = h_1 - h_2 + i(h_3 - h_4)$$

$$h_i(\vec{x}, \vec{v}) \geq 0 \quad i = 1, 2, 3, 4$$

Due to a theorem of Banach-Steinhaus [12], a sequence of bounded linear functionals $L_t(h)$ is uniformly bounded, if $L_t(h)$ converges for every $h \in H$. This means, if

$$| L_t(h) | \leq K_t \| f \|$$

$$\lim L_t(h)$$

exists for every $h \in H$, then there is a constant K

$$K_t \leq K$$

In our case $(h|g)_t = (T_t f, g)$ is a sequence of bounded bi-linear forms in h and g. Using the Schwartz inequality we get

$$|(h|g)_t| \leq \| T_t \| \, \|h\| \, \|g\|$$

and this bound is exact and cannot be made smaller

$$\sup_{\|h\| \leq 1 \quad \|g\| \leq 1} |(h|g)_t| = \| T_t \|$$

The theorem of Banach-Steinhaus can be extended to bounded bi-linear forms, so we get

$$\| T_t \| \leq K$$

This completes the proof.

5. ENTROPY

If the μ-space of the system P is divided into a finite number n of equal cells, then the Hilbert space H reduces to an n-dimensional

Euclidean space R_n, the semigroup of operators to a set of $n \times n$ matrices

$$T_t = (T_{ik}^{(t)}) \quad i, k = 1, \ldots n$$

$T_{ik}^{(t)}$ is the expected number of neutrons in cell i at time t emerging from one neutron in cell k at time 0. In the discrete case the norms $\|.\|_1$ and $\|.\|_2$ are equivalent, therefore we can work in the Banach space L_1. Every neutron distribution is an n-dimensional vector

$$h = (h_1, \ldots h_n) \quad h_i \geq 0 \quad i = 1, \ldots n$$

$$\|h\|_1 = \sum_{i=1}^{n} |h_i|$$

The norm means the total number of neutrons in the system. The splitting theorem can be applied [16].

Theorem 6: (1) R has dimension one. The equilibrium distribution is unique (a fixed point). (2) The approach to equilibrium goes with exponential speed.

Proof: (1) Due to Theorem 4, every $r \in R$ has positive components

$$r = (r_1, \ldots r_n) \quad r_i > 0 \quad i = 1, \ldots n$$

Assume R is a linear sub-space of dimension at least two. Then it must intersect one of the co-ordinate planes $h_i = 0$. So we would get a G-reversible vector with a component zero. R has dimension one.
That R has only fixed points can be seen in the following way. Assume

$$\|T_t r\|_1 > \|r\|_1$$

for one t, then $\|T_t r\| \to \infty$ for $t \to \infty$. This is the excluded super-critical case, and similar for the sub-critical one.
(2) First we can show that there is a $T_s \in G$ that shrinks the intersection of the unit-sphere and F by a half. This follows from the compactness of the finite dimensional set.

$$\|T_s h - r\| \leq \tfrac{1}{2}$$

and from this

$$\|T_t h - r\| \leq K_1 e^{-K_2 t}$$

Numerical calculations have been done in the case of a slab where P reduces to a rectangle ($|x| < a$, $|\mu| < 1$). P has been divided into 41×11 cells, so H is a 451 dimensional space. The continuous time interval $t \geq 0$ has been split into a multiple of a certain time $t = \Delta t$.

TABLE I. ENTROPY AND THE KOLMOGOROFF-SINAI INVARIANT OF A SUB-CRITICAL SYSTEM

t	$\|T_t h\|_1$	H(t)	HK(t)
0	1.00000	-0.00000	0.91329
1	0.68541	0.95473	1.40081
2	0.56840	2.39485	1.36233
3	0.44031	3.46080	1.40966
4	0.35630	4.27341	1.40734
5	0.28583	4.84290	1.42333
6	0.23274	5.25288	1.42177
7	0.18821	5.53871	1.43448
8	0.15418	5.74582	1.39954
9	0.12144	5.89055	1.41852
10	0.09768	5.92882	1.41775
11	0.07844	5.94836	1.41984
12	0.06314	5.96011	1.41815
13	0.05070	5.96688	1.42002
14	0.04080	5.97129	1.41915
15	0.03279	5.97408	1.41981
16	0.02638	5.97595	1.41940
17	0.02120	5.97716	1.41976
18	0.01705	5.97798	1.41949
19	0.01371	5.97851	1.41977
20	0.01103	5.97887	1.41958
21	0.00887	5.97911	1.41971
22	0.00713	5.97926	1.41963
23	0.00573	5.97937	1.41970
24	0.00461	5.97945	1.41964
25	0.00371	5.97949	1.41969
26	0.00298	5.97953	1.41966
27	0.00240	5.97955	1.41968
28	0.00193	5.97956	1.41966
29	0.00155	5.97957	1.41968
30	0.00125	5.97958	1.41967
31	0.00100	5.97958	1.41967
32	0.00081	5.97958	1.41967
33	0.00065	5.97959	1.41967
34	0.00052	5.97959	1.41967
35	0.00042	5.97959	1.41967
36	0.00034	5.97959	1.41967
37	0.00027	5.97959	1.41967
38	0.00022	5.97959	1.41967
39	0.00018	5.97959	1.41967
40	0.00014	5.97959	1.41967
41	0.00011	5.97959	1.41967
42	0.00009	5.97959	1.41967
43	0.00007	5.97959	1.41967
44	0.00006	5.97959	1.41967
45	0.00005	5.97959	1.41967
46	0.00004	5.97959	1.41967
47	0.00003	5.97959	1.41967
48	0.00002	5.97959	1.41967
49	0.00002	5.97959	1.41967

TABLE II. ENTROPY AND THE KOLMOGOROFF-SINAI INVARIANT OF A SUPER-CRITICAL SYSTEM

t	$\|T_t h\|_1$	H(t)	HK(t)
0	1.00000	-0.00000	1.05976
1	0.87370	1.07793	1.68743
2	0.94800	2.64154	1.65457
3	0.96087	3.76195	1.71461
4	1.01904	4.53860	1.71803
5	1.07470	5.04634	1.73791
6	1.15045	5.38734	1.74106
7	1.22773	5.61513	1.75468
8	1.32496	5.77528	1.73688
9	1.40330	5.87118	1.74787
10	1.50097	5.90937	1.74796
11	1.60406	5.93239	1.74957
12	1.71681	5.94792	1.74897
13	1.83526	5.95827	1.75005
14	1.96406	5.96556	1.74971
15	2.10080	5.97062	1.75010
16	2.24792	5.97420	1.74996
17	2.40479	5.97669	1.75014
18	2.57310	5.97846	1.75005
19	2.75282	5.97969	1.75015
20	2.94544	5.98056	1.75010
21	3.15130	5.98118	1.75014
22	3.37171	5.98161	1.75012
23	3.60744	5.98192	1.75014
24	3.85974	5.98213	1.75013
25	4.12960	5.98228	1.75014
26	4.41840	5.98239	1.75013
27	4.72736	5.98246	1.75014
28	5.05794	5.98251	1.75014
29	5.41163	5.98255	1.75014
30	5.79006	5.98258	1.75014
31	6.19494	5.98260	1.75014
32	6.62815	5.98261	1.75014
33	7.09164	5.98262	1.75014
34	7.58755	5.98262	1.75014
35	8.11813	5.98263	1.75014
36	8.68582	5.98263	1.75014
37	9.29320	5.98263	1.75014
38	9.94306	5.98263	1.75014
39	10.63836	5.98264	1.75014
40	11.38228	5.98264	1.75014
41	12.17823	5.98264	1.75014
42	13.02983	5.98264	1.75014
43	13.94098	5.98264	1.75014
44	14.91585	5.98264	1.75014
45	15.95889	5.98264	1.75014
46	17.07487	5.98264	1.75014
47	18.26888	5.98264	1.75014
48	19.54640	5.98264	1.75014
49	20.91324	5.98264	1.75014

$G = \{T^t \mid t = 0, 1, \ldots\}$ is a cyclic semigroup generated by T. The matrix T has been constructed from first principles out of the neutron transport process. $\|T^t h\|_1$ has been computed for a sub-critical and a super-critical system, $h = (1, 0, \ldots 0)$ one neutron injected perpendicular from one side. Also the entropy and the Kolmogoroff-Sinai invariant [14] of the stochastic process

$$p_t = \|T^t h\|^{-1} T^t h$$

have been computed. The entropy

$$H(t) = -\sum_{i=1}^{n} p_i \log p_i$$

serves as a measure for the approach to the fundamental mode. $t_0 = 8$ is the time for a neutron pulse to cross the slab. For $t \geq 3t_0$ the entropy does not change any more; this is the time after which the transients have disappeared and the fundamental mode prevails. The Kolmogoroff-Sinai invariant can be explained as the information loss during one step Δt, or the amount of mixing of the stationary stochastic process.

$$HK(t) = -\sum_{i=1}^{n} p_i(t) \sum_{k=1}^{n} T_{ik} \log T_{ik}$$

It is larger in the case of a super-critical reactor, where better mixing occurs, because the dimensions are usually smaller than in the sub-critical case. (See Tables I and II.)

REFERENCES

[1] WING, G.M., An Introduction to Transport Theory, Wiley, New York (1962).
[2] MIKA, J., J. math. Phys. 7 (1966) 833.
[3] BEDNARZ, R., Pulsed Neutron Research I IAEA, Vienna (1965) 259.
[4] ALBERTONI, S., MONTAGNINI, B., Pulsed Neutron Research I IAEA, Vienna (1965) 239.
[5] MIKA, J., Nukleonik 9 1 (1967).
[6] MIKA, J., Nukleonik 9 4 (1967).
[7] KAPER, H.G., The initial value problem for monoenergetic neutrons in an infinite slab with delayed neutrons, Nucl. Engng Div. Stanford Univ.
[8] MARTI, J.T., Über Anfangs- und Eigenwertprobleme aus der Neutronentransporttheorie, Eidg. Inst. für Reaktorforschung, Würenlingen.
[9] CASE, K.M., ZWEIFEL, P.F., J. math. Phys. 4 11 (1963).
[10] HEJTMANEK, J.H., Nucl. Sci. Engng 25 (1966).
[11] HEJTMANEK, J.H., Linear Transport Theory, Academic Press (1967), Proc. Ankara Summer School in Transport Theory.
[12] RIESZ, F., NAGY, B.S., Vorlesungen über Funktionalanalysis, Deutscher Verlag der Wissenschaften, Berlin (1956).
[13] HILLE, E., Functional analysis and semigroups, Amer. math. Soc. Coll. 31, New York (1948).
[14] JACOBS, K., Neuere Methoden und Ergebnisse der Ergodentheorie, Springer Verlag, Berlin (1960).
[15] JACOBS, K., Lecture Notes on Ergodic Theory, Matematisk Institut, Aarhus Universitet (1962/63).
[16] HEJTMANEK, J.H., submitted for publication in J. math. Physics (1967).

DISCUSSION

H. G. KAPER: What dimension does your constant d refer to? Is it the maximum, minimum or some characteristic diameter?

J. H. HEJTMANEK: The maximum diameter of the system.

H. G. KAPER: How do you define d for the infinite slab?

J. H. HEJTMANEK: It is the width of the slab.

H. G. KAPER: Is your number 3 exact or approximate?

J. H. HEJTMANEK: Approximate. The error is then less than 1/1000.

M. M. R. WILLIAMS (Chairman): Is your problem a special case of a stochastic process, and if so could you explain this in more detail?

J. H. HEJTMANEK: The transport process is split into two parts: one contains the number of neutrons in the whole system, the other the distribution of neutrons over all cells normalized to one. This last part, of course, is a stochastic process.

NEUTRON WAVE PROPAGATION WITH A ONE-TERM DEGENERATE THERMALIZATION KERNEL

H.G. KAPER*, J.H. FERZIGER AND S.K. LOYALKA
STANFORD UNIVERSITY,
STANFORD, CALIFORNIA,
UNITED STATES OF AMERICA

Abstract

NEUTRON WAVE PROPAGATION WITH A ONE-TERM DEGENERATE THERMALIZATION KERNEL. The propagation of thermal neutron waves in a semi-infinite medium is studied by means of the Boltzmann equation with an isotropic one-term degenerate thermalization kernel. A complete set of eigenfunctions of this equation is found; the spectrum consists of a two-dimensional continuum and, at low frequencies and small absorption, a pair of discrete points. The neutron density in a half-space induced by an oscillating source at the free surface is expanded in terms of the eigenfunctions. The expansion coefficients are determined from the boundary conditions via a method, introduced by Cercignani in the kinetic theory of gases, in which one solves a two-dimensional integral equation with the aid of the theory of generalized analytic functions. The results of numerical calculations of the phase-velocity and attenuation length are compared with experimental data. At low frequencies the behaviour of the density is essentially that of the discrete term which decays at infinity. At higher frequencies the continuum terms become more important. Finally, above the frequency at which the discrete modes disappear (this region has not yet been reached by the experiments) the neutron distribution remains wave-like but the phase-velocity and attenuation length are mildly position-dependent. The experimental implications of this are discussed.

I. INTRODUCTION

In this paper we solve the problem of finding the neutron distribution in a half-space due to a modulated source of thermal neutrons at the free boundary. The analysis is based on the linearized Boltzmann equation for a system with plane symmetry, in which scattering is assumed to take place isotropically in the centre-of-mass co-ordinate system

$$[(\partial/\partial t) + v\mu(\partial/\partial x) + v\sigma(v)]N(x, v, \mu, t) = \frac{1}{2}\int_{-1}^{1} d\mu' \int_{0}^{\infty} dv' v' \sigma(v' \to v) N(x, v', \mu', t) \tag{1.1}$$

Here $N(x, v, \mu, t)dx\, dv\, d\mu$ is the time average at time t of the number of neutrons in the element $(x, x + dx; v, v + dv; \mu, \mu + d\mu)$ of phase space; $\sigma(v) = \sigma_s(v) + \sigma_a(v)$, where σ_s, σ_a and σ are the inverses of the scattering, absorption and total mean free path, respectively; $\sigma_s(v)$ is related to the thermalization kernel $\sigma(v' \to v)$ by the identity

$$\sigma_s(v) = \int_0^\infty \sigma(v \to v')\, dv' \tag{1.2}$$

* On leave of absence from the Mathematical Institute, University of Groningen, the Netherlands.

We look for a solution of Eq. (1.1), which is defined in the domain $V = \{(x, v, \mu) \mid 0 < x < \infty,\ 0 < v < \infty,\ -1 \leq \mu \leq 1\}$ for all values of $t > 0$, and which satisfies the conditions

$$N(x, v, \mu, t) < \infty \text{ for all } (x, v, \mu) \in V,\ t > 0 \tag{1.3a}$$

$$N(0, v, \mu, t) = e^{i\omega t} S(v, \mu) \text{ for all } t > 0,\ (v, \mu) \in R^+ \tag{1.3b}$$

where R^+ is the semi-infinite strip $R^+ = \{(v, \mu) \mid 0 < v < \infty,\ 0 < \mu \leq 1\}$ and S is any given function defined on R^+. In (1.3b), ω represents the frequency of the modulated source.

We assume that $\sigma(v' \to v)$ is a one-term degenerate kernel of the form

$$\sigma(v' \to v) = \gamma v \sigma_s(v) m(v) \sigma_s(v') \tag{1.4}$$

where $m(v)$ is the Maxwellian velocity distribution. Because of the relation (1.2) we have in the expression (1.4)

$$\gamma = \left(\int_0^\infty v\, m(v) \sigma_s(v)\, dv \right)^{-1} \tag{1.5}$$

The kernel (1.4) was first introduced by Corngold et al. [1]. We assume that $\sigma(v)$ is a positive, continuous function of v, which is monotonically non-increasing towards a limiting value $\sigma(\infty) > 0$ as $v \to \infty$, and that $v\sigma(v)$ is strictly increasing for $0 < v < \infty$.

The problem (1.1-1.3) can be reduced to a time-independent problem if we look for a solution of the form $e^{i\omega t} N_\omega(x, v, \mu)$. The spectrum of the transport operator, associated with this time-independent problem, depends on the parameter ω. It consists of a two-dimensional continuum and, at small values of ω and for $\sigma_s(v)/\sigma(v)$ sufficiently close to 1, a pair of discrete points in the complex spectral plane. The eigenfunctions can be shown to form a complete set for a certain class of complex-valued functions. Therefore, a normal mode expansion technique can be applied; the problem is then reduced to determining the expansion coefficients with the aid of the boundary conditions. Since the continuous spectrum occupies a two-dimensional region in the spectral plane, this implies that we have to solve a two-dimensional integral equation. Following Cercignani, who met a similar situation in the kinetic theory of gases [2], we reduce this integral equation to a boundary-value problem for a generalized analytic function and solve via a method described by Vekua [3].

The results of numerical calculations of the phase-velocity and attenuation length are given and compared with results for several approximate models as obtained by Travelli [4, 5] and with experimental data as given by Perez and Booth [6] for neutron wave propagation in graphite.

II. THE SPECTRUM OF THE TRANSPORT OPERATOR

If we consider solutions to Eq. (1.1) of the form

$$N(x, v, \mu)\, t) = e^{i\omega t} N_\omega(x, v, \mu) \tag{2.1}$$

and introduce the function

$$\Phi(x, v, \mu) = \frac{h(v) + i\omega}{m(v) h_s(v)} N_\omega(x, v, \mu) \tag{2.2}$$

where $h(v)$ and $h_s(v)$ represent the total and scattering collision frequency, respectively,

$$h(v) = v\sigma(v), \quad h_s(v) = v\sigma_s(v) \tag{2.3}$$

the original Eq. (1.1) with the kernel (1.4) is replaced by the time-independent equation

$$\left[1 + \frac{v\mu}{h(v) + i\omega} \frac{\partial}{\partial x}\right] \Phi(x, v, \mu)$$

$$= \tfrac{1}{2}\gamma \int_{-1}^{1} d\mu' \int_0^\infty dv' \frac{m(v') h_s^2(v')}{h(v') + i\omega} \Phi(x, v', \mu') \tag{2.4}$$

This equation constitutes the complex form of a system of two real equations. It is useful to define the complex variable

$$\zeta = \xi + i\eta \equiv \frac{v\mu}{h(v) + i\omega} = \frac{v\mu h(v)}{h^2(v) + \omega^2} - i \frac{v\mu\omega}{h^2(v) + \omega^2} \tag{2.5}$$

The relation (2.5) can be considered as defining a transformation of variables $(v, \mu) \Longrightarrow (\xi, \eta)$. One notices that $h(v) = -\omega\xi/\eta$, where $h(v)$ is a continuous and strictly increasing function of v. Therefore, we can solve for v in terms of $-\omega\xi/\eta$. Moreover, since $h(v) > 0$, we have $\operatorname{sgn}(\xi/\eta) = -\operatorname{sgn}(\omega)$. If we write

$$h(v) = -\omega\xi/\eta \Longleftrightarrow v = f(-\omega\xi/\eta) \tag{2.6}$$

f is a continuous, strictly increasing function of its argument. The transformation that is inverse to (2.5) is given by

$$v = f(-\omega\xi/\eta), \qquad \mu = -\frac{\omega(\xi^2 + \eta^2)}{\eta f(-\omega\xi/\eta)} \tag{2.7}$$

The Jacobian is

$$J(\xi, \eta) = \frac{\partial(v, \mu)}{\partial(\xi, \eta)} = -\omega^2 \frac{\xi^2 + \eta^2}{\eta^3} \frac{f'(-\omega\xi/\eta)}{f(-\omega\xi/\eta)} \tag{2.8}$$

Since J is always non-zero, the transformation (2.5) is a one-to-one mapping of the semi-infinite strip $R = R^+ \cup R^-$, where $R^\pm = \{(v,\mu) | 0<v<\infty,\ \mu \gtrless 0,\ 0<|\mu| \leq 1\}$, *onto a region* $G = G^+ \cup G^-$ *of the complex* ζ-plane. It is easily seen that the origin is a boundary point of G and that G is symmetric with respect to the origin. For $\zeta \in G^\pm$ one has $\xi \gtrless 0$; $G^\pm$ is bounded by the curve

$$\partial G \equiv \omega(\xi^2 + \eta^2) \pm \eta f(-\omega\xi/\eta) = 0 \tag{2.9}$$

The transformation of variables (2.5), together with the definition

$$\Psi(x,\zeta) \equiv \Psi(x,\xi,\eta) = \Phi(x,v,\mu) \tag{2.10}$$

gives the following form for Eq. (2.4):

$$\Psi(x,\zeta) + \zeta\frac{\partial\Psi}{\partial x} = \iint_G g(\zeta')\Psi(x,\zeta')\,d\xi' d\eta' \tag{2.11}$$

where we have abbreviated

$$g(\zeta) = \tfrac{1}{2}\gamma\,|J(\xi,\eta)|\left[\frac{m(v)h_s^2(v)}{h(v)+i\omega}\right]_{v(\xi,\eta)} \tag{2.12}$$

If Eq. (2.11) is formally written as $\partial\Psi/\partial x = A\Psi$, the transport operator A is defined by

$$(A\varphi)(\zeta) = -\zeta^{-1}\left[\varphi(\zeta) - \iint_G g(\zeta')\varphi(\zeta')\,d\xi' d\eta'\right] \tag{2.13}$$

for all φ belonging to the domain of A. Associated with this operator one may study the eigenvalue problem $A\varphi = -\nu^{-1}\varphi$:

$$(\nu-\zeta)\varphi(\nu,\zeta) = \nu\iint_G g(\zeta')\varphi(\nu,\zeta')\,d\xi'\,d\eta' \tag{2.14}$$

We shall normalize by choosing

$$\iint_G g(\zeta')\varphi(\nu,\zeta')\,d\xi'\,d\eta' = 1 \tag{2.15}$$

If we specify the domain of definition of the operator A as the space $\mathscr{E}'$ of distributions with support G on the (ξ,η)-plane, the eigenvalue problem (2.14) admits the following solution:

$$\varphi(\nu,\zeta) = \nu/(\nu-\zeta) + \{p(\nu)/g(\nu)\}\,\delta(\nu-\zeta) \tag{2.16}$$

where $p(\nu)$ is an arbitrary, complex-valued function.

Since $\zeta \in G$ we distinguish two cases:

1. $\nu \notin G$. From the relations (2.15) and (2.16) we obtain the dispersion relation

$$1 - \iint_G \frac{\nu g(\zeta)}{\nu - \zeta} \, d\xi \, d\eta = 0 \tag{2.17}$$

which determines the discrete spectrum of the operator A.

2. $\nu \in G$. The relations (2.15) and (2.16) lead to the following expression for $p(\nu)$:

$$p(\nu) = 1 - \iint_G \frac{\nu g(\zeta)}{\nu - \zeta} \, d\xi \, d\eta \tag{2.18}$$

Therefore, if we take $p(\nu)$ as in Eq. (2.18), the domain G belongs to the continuous spectrum of the operator A.

Let $L_1(\bar{G})$ denote the set of functions $f(z)$ defined and absolutely integrable over the domain G. After Vekua [3], we define, for $f \in L_1(\bar{G})$,

$$Tf(z) \equiv T_G f(z) = -\frac{1}{\pi} \iint_G \frac{f(\zeta)}{\zeta - z} \, d\xi \, d\eta \tag{2.19}$$

Among the properties of this function, we note

$$(\partial/\partial\bar{z}) \, Tf = 0 \qquad \text{if } z \notin \bar{G} \tag{2.20}$$

$$(\partial/\partial\bar{z}) \, Tf = f \qquad \text{if } z \in G \tag{2.21}$$

where $(\partial/\partial\bar{z}) = \frac{1}{2} \{(\partial/\partial x) + i(\partial/\partial y)\}$, $z = x + iy$.

Next we introduce the function

$$\Lambda(z) = 1 - \pi z \, Tg(z) \tag{2.22}$$

Since $g \in L_1(\bar{G})$, it follows that $\Lambda(z)$ exists for all z outside $\bar{G}$ and is holomorphic outside $\bar{G}$ with $\lim_{z \to \infty} \Lambda(z) = 1 - \int_G g(\zeta) \, d\xi \, d\eta$. Moreover, $\Lambda(z)$ exists almost everywhere inside G and $\Lambda \in L_p(\bar{G}_*)(1 \leq p < 2)$ if $z \in G$.

From (2.17) and (2.22) we conclude that the discrete spectrum of A is determined by the equation

$$\Lambda(z) = 0 \qquad \text{for } z \notin \bar{G} \tag{2.23}$$

On the other hand, in the case of the continuous spectrum it follows from (2.18) and (2.22) that

$$p(\nu) = \Lambda(\nu) \qquad \text{for } \nu \in G \tag{2.24}$$

In terms of the original variables, the dispersion relation (2.23) can be written as

$$\Lambda(z) \equiv 1 - \int_{-1}^{1} d\mu \int_{0}^{\infty} dv \frac{\rho(v)}{h(v) + i\omega - v\mu/z} = 0 \qquad \text{for } z \notin \bar{G} \tag{2.25}$$

with

$$\rho(v) = \tfrac{1}{2}\ \gamma m(v) h_s^2(v) \tag{2.26}$$

Since $\Lambda(-z) = \Lambda(z)$, the roots of Eq. (2.25) occur in pairs. The number of pairs of roots will, in general, depend on ω. Therefore, we shall write $\Lambda(z, \omega)$ instead of $\Lambda(z)$, while studying the discrete spectrum of the operator A.

In the limit $\omega = 0$, Eq. (2.25) becomes identical with the eigenvalue equation for the stationary transport problem, i.e. Eq. (1.1) with $\partial N/\partial t = 0$. It is well known that, in the latter case, the eigenvalue equation has exactly one pair of roots, $z = \pm\nu_0$, ν_0 real, if the ratio $\sigma_s(v)/\sigma(v)$ is sufficiently close to 1, and no roots otherwise, cf. Corngold [7], Leonard [8].

If ω is not zero, we consider Λ as a function of two complex variables and write

$$\Lambda(z, w) \equiv 1 - 2\int_{0}^{1} d\mu \int_{0}^{\infty} dv\, \rho(v) \frac{h(v) + w}{(h(v) + w)^2 - (v\mu/z)^2} \tag{2.27}$$

$\Lambda(z, w)$ is an analytic function ($z \notin \bar{G}$). Suppose that $\Lambda(\pm\nu_0, 0) = 0$. From the expression (2.27) it is evident that $\partial\Lambda/\partial z$ does not vanish at $(z, w) = (\pm\nu_0, 0)$ unless $|\nu_0| = \infty$. However, as one verifies from Eq. (2.25), $|\nu_0| = \infty$ occurs only if $\sigma_s(v) \equiv \sigma(v)$, which case is excluded. Then, the implicit function theorem for functions of several complex variables can be used, cf. Hörmander [9], Theorem 2.1.2. Thus, there exists an open neighbourhood of the origin, $|w| < \epsilon$, in which the equation $\Lambda(z,w) = 0$ can be solved for z: $z = z_1(w)$, $z = z_2(w)$; the functions z_1, z_2 are analytic and have the property $z_1(0) = \nu_0$, $z_2(0) = -\nu_0$. Moreover, from the parity of Λ it follows that $z_1(w) = -z_2(w)$.

Comparing Eq. (2.27) with (2.25), we see that the functions $z_1(w)$ and $z_2(w)$ can be interpreted as the eigenvalues of the operator A if $w = i\omega$. So there exists a value of ω, ω_c, which separates the interval $|\omega| < |\omega_c|$ where the discrete spectrum consists of one pair of eigenvalues $\nu = \pm\nu_0(\omega)$, from the interval $|\omega| > |\omega_c|$, where the discrete spectrum is empty.

The value $w_c = i\omega_c$ is reached when the functions $z_1(w)$ and $z_2(w)$ cannot be continued analytically. This happens when $\Lambda(z, w)$ is no longer analytic, i.e. if z meets the boundary ∂G.

The conclusion can now be stated as follows. The spectrum of the transport operator A, defined by the expression (2.13) on the space $\mathcal{S}'$ of distributions with support G on the (ξ, η)-plane, is composed of

(1) A discrete spectrum if (a) $|\omega| < |\omega_c|$ and (b) $\sigma_s(v)/\sigma(v)$ is sufficiently close to 1, otherwise the discrete spectrum is empty; if the discrete spectrum is not empty, it consists of one pair of complex

eigenvalues $\nu = \pm \nu_0(\omega)$, where $\pm \nu_0(\omega)$ are the roots of Eq. (2.23); the elementary solutions of Eq. (2.11) are $\varphi_\pm(x, \zeta) = e^{\mp x/\nu_0(\omega)} \varphi_\pm(\zeta)$ with

$$\varphi_\pm(\zeta) = \nu_0(\omega)/(\nu_0(\omega) \mp \zeta) \tag{2.28}$$

(2) A continuous spectrum, which consists of all $\nu \in G$; the elementary solutions of Eq. (2.11) are $\varphi_\nu(x, \zeta) = e^{-x/\nu} \varphi(\nu, \zeta)$ with

$$\varphi(\nu, \zeta) = \nu/(\nu - \zeta) + \{p(\nu)/g(\nu)\} \delta(\nu - \zeta) \qquad \nu \in G \tag{2.29}$$

where $p(\nu)$ is given by (2.24).

III. A COMPLETENESS THEOREM

In this section we prove the completeness theorem for the set of eigendistributions of the transport operator A, (2.28) and (2.29). We shall assume that $\Lambda(z)$ does not vanish for any value of z inside G. The case where this assumption does not hold will be treated in Appendix B.

Let H denote one of the following sets of the complex ζ-plane: G^+, G^- ('half-ranges'), $G = G^+ \cup G^-$ ('full-range'). If $H = G^+/G^-/G$, the set of eigendistributions $\{\varphi(\nu, \zeta)\}$, $\nu \in H$, supplemented by the eigendistribution(s) $\varphi_+(\zeta)/\varphi_-(\zeta)/\varphi_\pm(\zeta)$ if the discrete spectrum is non-empty, is complete for the class of generalized functions $\Psi(\zeta)$ with support H.

For the proof of this theorem we use the theory of generalized analytic functions, the details of which can be found in the monograph of Vekua [3]. The proof is based on the solution of the integral equation

$$\iint_H A(\nu)\varphi(\nu, \zeta)\, d\alpha d\beta = \widetilde{\Psi}(\zeta) \qquad \zeta \in H \tag{3.1}$$

for the generalized analytic function $A(\nu)$, $\nu = \alpha + i\beta$, where $\varphi(\nu, \zeta)$ is given by (2.29), $\widetilde{\Psi}$ is an arbitrary generalized function with support H. Substitution of $\varphi(\nu, \zeta)$ from Eq. (2.29) and use of the operator T_H, cf. Eq. (2.20), shows that Eq. (3.1) is equivalent to

$$\Lambda(z)A(z) - \pi g(z) T_H[zA(z)] = g(z)\widetilde{\Psi}(z) \qquad z \in H \tag{3.2}$$

According to Vekua, if a solution $A(\nu)$ of Eq. (3.1) exists in the space $L_1(\bar{H})$, then the function $T_H[zA(z)]$ exists for all points z outside $\bar{H}$, is holomorphic outside $\bar{H}$ and vanishes at infinity, while $T_H[zA(z)]$, regarded as a function of a point z in H, exists almost everywhere. Moreover, the derivative $\partial T_H[zA(z)]/\partial \bar{z}$ vanishes if $z \notin \bar{H}$ and is equal to $zA(z)$ if $z \in H$.

Since, in the half-range cases, the regions where $\Lambda(z)$ and $T_H[zA(z)]$ are holomorphic, are different, we introduce a new function $X(z)$ which has the following properties.

1. $X(z)$ exists for all points z outside $\bar{H}$, and is holomorphic outside $\bar{H}$, (3.3)

2. $X(z)$ exists almost everywhere in H and satisfies the condition

$$\Lambda(z)(\partial X/\partial \bar{z}) = -\pi z g(z) X(z) \qquad \text{if } z \in H \tag{3.4}$$

With Eq. (3.4), Eq. (3.2) becomes

$$(\partial/\partial \bar{z})[X(z) T_H[zA(z)]] = \gamma(z)\tilde{\Psi}(z) \qquad \text{for } z \in H \tag{3.5}$$

where we have defined

$$\gamma(z) = z g(z) X(z)/\Lambda(z) \qquad \text{for } z \in H \tag{3.6}$$

From the analyticity of X and $T_H(zA)$ outside $\bar{H}$ it follows that

$$(\partial/\partial \bar{z})[X(z) T_H[zA(z)]] = 0 \qquad \text{for } z \notin \bar{H} \tag{3.7}$$

A solution of the boundary-value problem, Eqs. (3.3) and (3.4), can be found by the method of Vekua [3], p. 147

$$X_0(z) = \exp \Gamma(z) \tag{3.8}$$

with

$$\Gamma(z) = T_H[-\pi z g(z)/\Lambda(z)] \tag{3.9}$$

Since the indefinite integral (with respect to $\bar{z}$) of $-\pi z g(z)/\Lambda(z)$ is equal to $\log \Lambda(z)$, we have according to Vekua [3] p. 26

$$\Gamma(z) = \log \Lambda(z) - \frac{1}{2\pi i} \int_{\partial H} \frac{\log \Lambda(\zeta)}{\zeta - z} d\zeta \qquad \text{if } z \in H \tag{3.10}$$

$$\Gamma(z) = -\frac{1}{2\pi i} \int_{\partial H} \frac{\log \Lambda(\zeta)}{\zeta - z} d\zeta \qquad \text{if } z \notin \bar{H} \tag{3.11}$$

The right-hand sides of the relations (3.10) and (3.11) are identical on the boundary ∂H, except possibly at the angular points of ∂H.

In the full-range case a solution of the boundary-value problem (3.3), (3,4) is evidently given by

$$X_0(z) = \Lambda(z) \tag{3.12}$$

However, the solution of the boundary-value problem (3.3), (3.4) is not unique. The general solution can be written as

$$X(z) = \Phi(z) X_0(z) \tag{3.13}$$

where $\Phi(z)$ is the so-called normal analytic divisor of $X(z)$, which is analytic in the whole complex plane with the possible exception of ∂H.

Uniqueness is obtained by the requirement that $X(z)$ does not vanish and $X \in L_1(\overline{H})$. Consider the behaviour of $X_0(z)$ in the neighbourhood of the angular point $z = 0$. Since $\Lambda(z)$ approaches 1 as $z \to 0$, it follows from Eqs (3.10) and (3.11) that a possible singularity of $X_0(z)$ at $z = 0$ must be due to the contribution from the integral along ∂H to $\Gamma(z)$.

First we discuss the half-range cases. Suppose that ∂H_0 is the open arc that is obtained from the oriented contour ∂H by deleting the point $z = 0$. The point $z = 0$ will be denoted by α or β, according to whether it is considered as the starting point or the end point of the arc ∂H_0. From the properties of Cauchy integrals, cf. Muskhelishvili [10] p. 74, it follows from Eqs (3.10) and (3.11) that

$$\text{if } z \to \alpha: \quad \Gamma(z) = \frac{\log \Lambda(\alpha)}{2\pi i} \log z + \Gamma_\alpha(z)$$

$$\text{if } z \to \beta: \quad \Gamma(z) = -\frac{\log \Lambda(\beta)}{2\pi i} \log z + \Gamma_\beta(z)$$

where $\Gamma_{\alpha\beta}(z)$ are bounded functions, tending to a definite limit when $z \to \alpha, \beta$ along any path. Since, for z near the origin, $\log \Lambda(z) = i\theta(z) + O(z)$, where $\theta(z) = \arg \Lambda(z)$, we have

$$\text{if } z \to \alpha: \quad X_0 = \widetilde{X}_\alpha(z)\, z^{\theta(\alpha)/2\pi}$$

$$\text{if } z \to \beta: \quad X_0 = \widetilde{X}_\beta(z)\, z^{-\theta(\beta)/2\pi}$$

where $\widetilde{X}_{\alpha\beta}(z)$ are bounded functions, tending to a definite limit as $z \to \alpha, \beta$ along any path.

The branch of $\log \Lambda(z)$, which is still arbitrary, shall now be fixed by the condition $\theta(\alpha) = 0$. Then $\theta(\beta)$ represents the change of $\arg \Lambda(z)$ as z moves around the oriented contour ∂H. Since, in the half-range cases, ∂H is either the contour of G^+ or the contour of G^-, where G^+ is the symmetric image of G^- with respect to the origin, it follows from the argument principle that $\theta(\beta)/2\pi$ is equal to $-\frac{1}{2}$ times the number of roots of $\Lambda(z) = 0$ in the complex plane outside $\overline{G}$: $\theta(\beta)/2\pi = 1$ if a discrete spectrum exists, $\theta(\beta)/2\pi = 0$ otherwise. Hence the requirement that $X(z)$ does not vanish and that $X \in L_1(\overline{H})$ can be met if $\Phi(z) = z^{-1}$ when a discrete spectrum exists, $\Phi(z) = 1$ otherwise.

For the full-range case ∂H is the union of the contour of G^+ and the contour of G^-. Hence, it is obvious that we have $\Phi(z) = z^{-2}$ when a discrete spectrum exists, $\Phi(z) = 1$ otherwise. Thus the solution to the boundary value problem, Eqs (3.3) and (3.4), is uniquely determined and given by

$$X(z) = z^{-\kappa} X_0(z) \tag{3.14}$$

with $\kappa = 1$ in the half-range cases and $\kappa = 2$ in the full-range case if a discrete spectrum exists; if the discrete spectrum is empty we have $\kappa = 0$ in all cases.

Returning to the boundary-value problem, Eqs. (3.5) and (3.7), we see that the unknown function $T_H[zA(z)]$ is given by

$$T_H[zA(z)] = [X(z)]^{-1} T_H[\gamma(z)\widetilde{\Psi}(z)] \tag{3.15}$$

provided that $T_H[zA(z)]$ vanishes at infinity. Since, from Eqs(3.14) and (3.15)

$$T_H[zA(z)] \sim z^{\kappa-1} \quad \text{as } z \to \infty \tag{3.16}$$

the latter condition can only be met if, in the cases $\kappa = 1$ or $\kappa = 2$,

$$\iint_H \zeta^i \gamma(\zeta)\widetilde{\Psi}(\zeta)\, d\xi\, d\eta = 0 \qquad \text{for } i = 0, \kappa - 1 \tag{3.17}$$

Hence if we write

$$\begin{aligned} \Psi(\zeta) &= \widetilde{\Psi}(\zeta) + a_\pm \varphi_\pm(\zeta) && \text{in the case } H = G^\pm \text{ and } \kappa = 1 \\ \Psi(\zeta) &= \widetilde{\Psi}(\zeta) + a_+\varphi_+(\zeta) + a_-\varphi_-(\zeta) && \text{in the case } H = G \text{ and } \kappa = 2 \end{aligned} \tag{3.18}$$

and require $a_\pm$ to satisfy the equations

$$a_\pm \iint_H \gamma(\zeta)\varphi_\pm(\zeta) d\xi\, d\eta = \iint_H \gamma(\zeta)\Psi(\zeta) d\xi\, d\eta \qquad \text{if } H = G^\pm \text{ and } \kappa = 1 \tag{3.19a}$$

and

$$a_+ \iint_H \zeta^i \gamma(\zeta)\varphi_+(\zeta) d\xi\, d\eta + a_- \iint_H \zeta^i \gamma(\zeta)\varphi_-(\zeta) d\xi\, d\eta$$

$$= \iint_H \zeta^i \gamma(\zeta)\Psi(\zeta) d\xi\, d\eta \qquad \begin{array}{l} \text{for } i = 0,1 \\ \text{if } H = G \text{ and } \kappa = 2 \end{array} \tag{3.19b}$$

then the function $T_H[zA(z)]$ as given by Eq. (3.15) meets all the requirements to yield $zA(z)$ upon differentiation with respect to $\bar{z}$ if $z \in H$. The result can be written as

$$zA(z) = (\partial/\partial\bar{z})\{[X(z)]^{-1} T_H[\gamma(z)\widetilde{\Psi}(z)]\}, \qquad z \in H \tag{3.20}$$

Thus, in the development of an arbitrary, given generalized function $\Psi(\zeta)$ with respect to the appropriate set of eigenfunctions, all the coefficients are uniquely determined. Since the arguments we used above can be reversed, the proof of the completeness property formulated in the theorem is complete.

IV. THE SOLUTION TO THE WAVE PROPAGATION PROBLEM

According to the results of the previous sections the general solution to the wave propagation problem, Eqs (1.1) and (1.3), is

$$N(x, v, \mu, t) = e^{i\omega t} \frac{m(v)h_s(v)}{h(v) + i\omega} \Psi\left(x, \frac{v\mu}{h(v)+i\omega}\right) \tag{4.1}$$

where

$$\Psi(x,\zeta) = \left\{a_+ e^{-x/\nu_0} \varphi_+(\zeta)\right\} H(\omega) + \iint_{G^+} A(\zeta')\varphi(\zeta',\zeta)e^{-x/\zeta'} d\xi' d\eta' \tag{4.2}$$

Here we have introduced the characteristic function $H(\omega)$,

$$H(\omega) = 1 \quad \text{if a discrete spectrum exists; } H(\omega) = 0 \text{ otherwise.} \tag{4.3}$$

The boundary condition (1.3a) has been used. The coefficients a_+ and $A(\zeta)$ must be determined from the boundary condition (1.3b), which gives

$$\Psi(0,\zeta) = \tilde{S}(\zeta) \qquad \text{for } \zeta \in G^+ \tag{4.4}$$

where

$$\tilde{S}(\zeta) = \left[\frac{h(v)+i\omega}{m(v)h_s(v)} S(v,\mu)\right]_{(v,\mu) \Longrightarrow (\xi,\eta)} \tag{4.5}$$

For convenience we shall suppose

$$\tilde{S}(\zeta) = \delta(\zeta - \zeta_0) = \delta(\xi - \xi_0)\,\delta(\eta - \eta_0) \tag{4.6}$$

Then $\Psi(x,\zeta)$ represents a Green's function, from which the density function due to any prescribed source function can be obtained by superposition. From Eqs(4.2), (4.4) and (4.6) we obtain the equation

$$\delta(\zeta - \zeta_0) = a_+\varphi_+(\zeta)H(\omega) + \iint_{G^+} A(\zeta')\varphi(\zeta'', \zeta)\, d\xi'\, d\eta' \qquad \text{for } \zeta \in G^+ \tag{4.7}$$

The solution to Eq. (4.7) is obtained by the method of section III. From Eqs (3.19) and (3.20) we find

$$\zeta A(\zeta) = (\partial/\partial\tilde{\zeta})\{[X(\zeta)]^{-1} T_{G^+}\{\gamma(\zeta)\{\delta(\zeta - \zeta_0) - a_+\varphi_+(\zeta)H(\omega)\}]\} \tag{4.8}$$

together with the condition

$$a_+\iint_{G^+} \gamma(\zeta)\varphi_+(\zeta)\, d\xi\, d\eta = \gamma(\zeta_0) \qquad \text{if } H(\omega) = 1 \tag{4.9}$$

Here the half-range X-function and the function $\gamma(z)$ are defined as

$$X(z) = \{1 + (z^{-1} - 1)H(\omega)\} \exp\{T_{G^+}[-\pi z g(z)/\Lambda(z)]\} \tag{4.10}$$

$$\gamma(z) = z g(z) X(z)/\Lambda(z) \qquad \text{for } z \in G^+ \tag{4.11}$$

Using the identities for the functions X and γ which we have listed in the Appendix, we can simplify Eqs (4.8) and (4.9). The result can be written as

$$\zeta A(\zeta) = -\frac{1}{\pi}\frac{\partial}{\partial\bar{\zeta}}\left\{\frac{1}{X(\zeta)}\left[\frac{\gamma(\zeta_0)}{\zeta_0 - \zeta} - a_+\nu_0\frac{X(\nu_0) - X(\zeta)}{\nu_0 - \zeta}H(\omega)\right]\right\} \tag{4.12}$$

together with the condition

$$a_+ = -\gamma(\zeta_0)/\nu_0 X(\nu_0) \qquad \text{if } H(\omega) = 1 \tag{4.13}$$

V. NUMERICAL CALCULATIONS

Calculations were performed using the scattering cross-section for a monatomic gas

$$\sigma_s(v) = \sigma_0 \frac{1}{\pi^{1/2}\beta v}\left\{\exp(-\beta^2 v^2) + \left(1 + \frac{1}{2\beta^2 v^2}\right)\operatorname{erf}(\beta v)\right\} \tag{5.1}$$

where $\beta = (m_g/2kT)^{1/2}$ m_g being the mass number of the scatterer; the absorption cross-section was taken to be α/v. Since the inelastic scattering cross-sections for all materials behave roughly like Eq. (5.1)

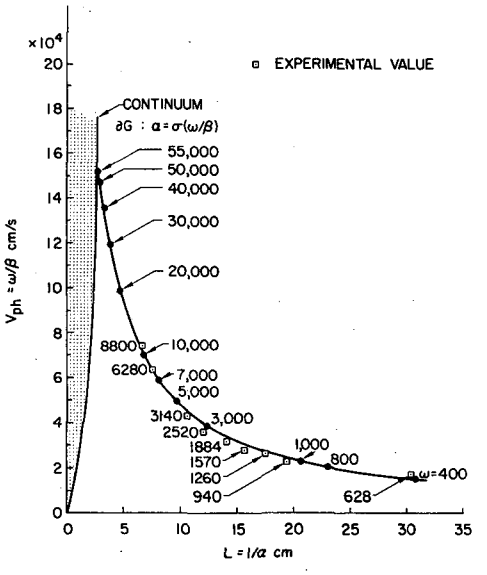

FIG. 1. Attenuation length and phase velocity as a function of frequency ω(rad/s). $\alpha + i\beta = \nu^{-1}$, the inverse relaxation length.
Attenuation length $L = 1/\alpha$ cm
Phase velocity $V_{ph} = \omega/\beta$ cm/s.

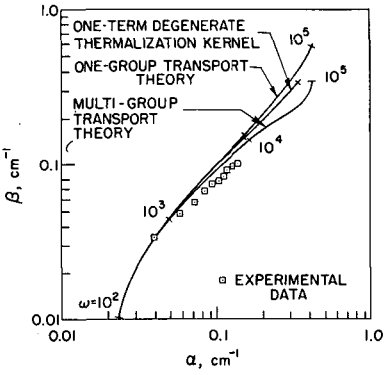

FIG. 2. Complex relaxation length as a function of frequency ω(rad/s).

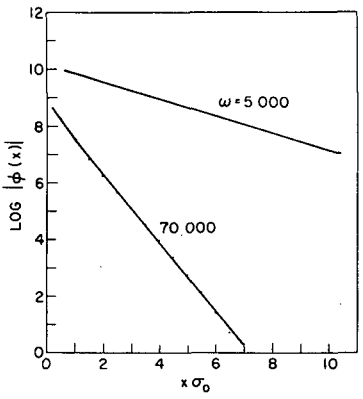

FIG. 3. Amplitude of neutron flux versus distance.

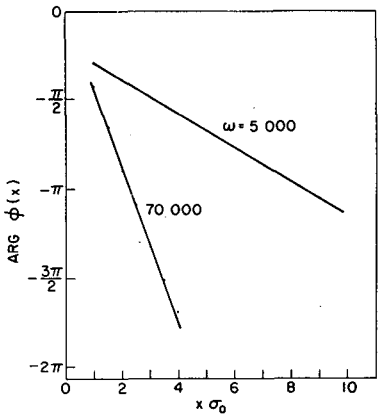

FIG. 4. Phase of neutron flux versus distance.

it is reasonable to compare the results with experiment. Of course, it must be remembered that the effect of elastic scattering, which can be quite important [11], is ignored. The value of σ_0 was taken to be 0.34 cm^{-1}; this gives an approximate representation of the inelastic cross-section of graphite ($T = 20°C$, $\alpha = 0.4048 \times 10^{-3}$ s/cm^2).

We have obtained numerical results for the solution of the dispersion relation (2.25). The critical value of ω, above which no such solution exists, was found to be approximately 58 000 rad/s. In Fig. 1, these results are compared with the experimental results of Perez and Booth [6]. In Fig. 2 we compare the same results with Travelli's results [5] for one-group and multigroup transport theory. Our results are in fair agreement with the results of Travelli; however, there is some disagreement with experimental results.

Now, to examine the effect of the continuum on the attenuation length and the phase velocity we calculated the total neutron flux for an isotropic Maxwellian source at the surface. The results of these calculations for two typical frequencies, $\omega = 5000$ and 70 000 rad/s, are given in Figs 3 and 4.

We note that for the former frequency, the function Λ has a zero embedded in the continuum and the method given in the Appendix B has been used.

It can be seen that at $\omega = 5000$ the effect of the continuum is negligible, i.e. an experiment should indeed measure the dispersion relation. In fact, it was found that this is roughly the case for all frequencies below the critical frequency. This differs from the results found in a similar analysis of the problem of sound propagation in gases [12], where the contribution of the continuum may become important if the critical frequency is approached.

At the critical frequency the discrete root disappears and therefore, in the final expression for the neutron flux, both the discrete term in Eq. (4.2) and the contribution to the continuum expansion coefficient from the discrete term, Eq. (4.8), vanish. Thus, the experimentally accessible results are not likely to change at the critical frequency.

ACKNOWLEDGEMENT

One of us (H. G. K.) is grateful to the Netherlands Organization for the Advancement of Pure Research (Z. W. O.) for making possible his stay at Stanford University through an award of a NATO Science Fellowship. Part of the present work has been supported by National Science Foundation Grant GK-737.

REFERENCES

[1] CORNGOLD, N., MICHAEL, P., WOLLMAN, W., Nucl. Sci. Engng 15 (1963) 13.
[2] CERCIGNANI, C., Ann. Phys. 40 (1966) 454.
[3] VEKUA, I.N., Generalized Analytic Functions, Pergamon Press, (1962).
[4] TRAVELLI, A., Trans. Am. nucl. Soc. 8 1 (1965) 293.
[5] TRAVELLI, A., Trans. Symp. on Neutron Noise, Waves and Pulse Propagation, Univ. of Florida (1966) 7.
[6] PEREZ, R.B., BOOTH, R.S., "Excitation of neutron waves by modulated and pulsed sources", Pulsed Neutron Research II IAEA, Vienna (1965) 701.
[7] CORNGOLD, N., Nucl. Sci. Engng 19 (1964) 80; ibid. 24 (1966) 410.
[8] LEONARD, A., Nucl. Sci. Engng 22 (1965) 489.
[9] HÖRMANDER, L., An Introduction to Complex Analysis in Several Variables, D. van Nostrand, Princeton, New Jersey (1966).
[10] MUSKHELISHVILI, N.I., Singular Integral Equations, P. Noordhoff, Groningen (1953).
[11] DUDERSTADT, J.J., private communication.
[12] BUCKNER, J.K., FERZIGER, J.H., Phys. of Fluids 9 (1966) 2315.

APPENDIX A

THE X-FUNCTION ASSOCIATED WITH COMPLETENESS ON G^+

From section IV we recall the definition of the half-range X-function and the related function $\gamma(z)$

$$X(z) = \{1 + (z^{-1} - 1)\, H(\omega)\} \exp\{T_{G^+}[-\pi z g(z)/\Lambda(z)]\} \tag{A.1}$$

$$\gamma(z) = z g(z) X(z)/\Lambda(z) \qquad \text{for } z \in G^+ \tag{A.2}$$

In this appendix we give some identities for these functions. Since the proofs are straightforward we omit them here.

1. $X(z) = 1 - H(\omega) - \pi T_{G^+}[\gamma(z)]$ for $z \notin G^+$ (A.3)

2. $X(z)(-z) = \Lambda(z)/\Lambda(\infty)\,\Pi(z)$ (A.4)

where $\Lambda(\infty) = 1 - \iint_G g(\zeta)d\xi\, d\eta$, $\Pi(z) = (z^2 - \nu_0^2)^{H(\omega)}$

3. $\gamma(z) = zg(z)/X(-z)\,\Lambda(\infty)\,\Pi(z)$ for $z \in G^+$ (A.5)

4. $X(0) = [\Lambda(\infty)\Pi(0)]^{-1/2} = 1 - H(\omega) + \iint_{G^+} \gamma(\zeta)\zeta^{-1}\, d\xi\, d\eta$ (A.6)

5. $\pi T_{G^+}[\gamma(z)] = 1 - H(\omega) - \Lambda(z)\gamma(z)/zg(z)$ for $z \in G^+$ (A.7)

6. $X(z)$ satisfies the non-linear integral equation

$$X(-z) = 1 - H(\omega) + T_{G^-}\left[\frac{-\pi z g(z)}{X(z)\Lambda(\infty)\Pi(z)}\right] \text{ for } z \in G^+ \tag{A.8}$$

7. If $H(\omega) = 1$, the function

$$\Omega(z) = [\{X(0)\}^{-1} - z]\, X(z) \tag{A.9}$$

satisfies the non-linear integral equation

$$\Omega(-z) = 1 + \pi z T_{G^-}\left[g(z)\frac{\Pi(0)}{\Pi(z)}\,\frac{1 - z^2\{X(0)\}^2}{\Omega(z)}\right] \text{ for } z \in G^+ \tag{A.10}$$

APPENDIX B

MODIFICATION OF THE THEORY FOR THE CASE THAT $\Lambda(z)$ HAS ZEROS INSIDE G

For reasons of simplicity we assumed in Section III that $\Lambda(z)$ does not vanish inside G. However, it may happen that the equation $\Lambda(z) = 0$ has a solution for certain values of $z \in G$, $z = \pm\nu_i$ say ($i = 1, 2, \ldots n$). It is easy to verify that none of the ν_i is equal to zero. These zeros of Λ are buried in the continuum and it follows from Eqs (2.16) and (2.24) that, at these points, the eigensolutions $\varphi(\nu,\zeta)$ do not involve the δ-function. When the multiplicity of a zero $z = \nu_i$ is m_i, the m_i linearly independent elementary solutions of Eq. (2.11) are

$$\varphi_{\pm ij}(x,\zeta) = [(\partial/\partial\nu)^j e^{-x/\nu}\,\varphi(\nu,\zeta)]_{\nu=\nu_i} \tag{B.1}$$

$(i = 1,2,\ldots n;\ j = 0,1,\ldots m_i - 1)$. At $x = 0$ this set of functions reduces to

$$\varphi_{\pm ij}(\zeta) = [(\partial/\partial\nu)^j \{\nu/(\nu-\zeta)\}]_{\nu=\nu_i} \tag{B.2}$$

These functions have to be taken into account in the completeness theory of section III. Full-range completeness now applies to the set of eigendistributions $\{\varphi(\nu,\zeta)\}$, $\nu \in G$, supplemented by $\varphi_\pm(\zeta)$ (if the discrete spectrum is not empty) and all $\varphi_{\pm ij}(\zeta)$. Partial-range completeness on the set G^+ applies to the set of eigendistributions $\{\varphi(\nu,\zeta)\}$, $\nu \in G^+$, supplemented by $\varphi_+(\zeta)$ (if the discrete spectrum is not empty) and all $\varphi_{+ij}(\zeta)$; similarly on the set G^-.

To prove the completeness properties we can use the arguments of section III. It is obvious from Eq. (3.4) that every zero $z = \nu_i$ (with multiplicity m_i) of $\Lambda(z)$ inside H corresponds to a zero $z - \nu_i$ (with multiplicity m_i) of $X(z)$. Now the solution of the boundary-value problem, Eqs (3.5) and (3.7), is given by

$$X(z)T_H[zA(z)] = T_H[\gamma(z)\tilde{\Psi}(z)] \tag{B.3}$$

Hence, this relation can only be solved for $T_H[zA(z)]$ if, inside H, the right member of Eq. (B.3) has the same zeros (with the same multiplicity) as $\Lambda(z)$, i.e. if the conditions

$$\{(\partial/\partial z)^j T_H[\gamma(z)\tilde{\Psi}(z)]\}_{z=\nu_i} = 0 \qquad (j = 0,1\ldots m_i - 1) \tag{B.4}$$

are satisfied for all i such that $\nu_i \in H$.

Hence, if we write instead of Eq. (3.18), for any arbitrary function Ψ,

$$\begin{aligned} \Psi(\zeta) &= \tilde{\Psi}(\zeta) + a_\pm\varphi_\pm(\zeta) + \sum_{ij} a_{\pm ij}\varphi_{\pm ij}(\zeta) \text{ in the case } H = G^\pm, \kappa = 1 \\ \Psi(\zeta) &= \tilde{\Psi}(\zeta) + a_+\varphi_+(\zeta) + a_-\varphi_-(\zeta) + \sum_{ij} a_{+ij}\varphi_{+ij}(\zeta) + \sum_{ij} a_{-ij}\varphi_{-ij}(\zeta) \\ &\qquad \text{in the case } H = G,\ \kappa = 2, \end{aligned} \tag{B.5}$$

omitting the terms involving $\varphi_+(\zeta)$ and $\varphi_-(\zeta)$ if $\kappa = 0$, and if we require that the coefficients $a_\pm$ and $a_{\pm ij}$ be chosen such that the conditions (3.17) and (B.4) are satisfied, then the solution $A(\zeta)$ of Eq. (3.1) is uniquely determined and given by Eq. (3.20) with $\tilde{\Psi}(\zeta)$ as in (B.5). The conditions (3.17) and (B.4) are equivalent to a set of linear algebraic equations, which can be solved uniquely for the expansion coefficients $a_\pm$ and $a_{\pm ij}$.

DISCUSSION

M. N. MOORE: I should like to ask a question and then to make a comment. Did you find explicit relations for the critical frequency and the critical absorption?

H. G. KAPER: We have no exact expressions for these conditions. However, it is possible to give an implicit equation from which the critical frequency can be calculated. The same is true for the critical absorption at zero frequency.

M. N. MOORE: In comparing theory with experiment you plotted the real against the imaginary part of the complex wave number K. We believe that a more sensitive test is to plot real and imaginary parts of K^2. This will be shown in our paper.

R. B. PEREZ: First, I should like to make a comment on nomenclature. The name 'dispersion relations' is usually given to the relationships between the real and imaginary part of a wave which, under suitable conditions, form a pair of Hilbert transforms.

Now, concerning the location of the continuum in the K-plane: previous calculations, using diffusion theory and Park's kernel for graphite, predicted a continuum around 5000 rad/s, which is widely different from your continuum starting at w = 58 000 rad/s. Is this due to the sensitivity of the location of the continuum to the model used for the kernel?

H. G. KAPER: As I mentioned earlier, a two-dimensional continuum is always present. Besides this continuum there may be a set of discrete eigenvalues if the frequency is sufficiently small. The point is that both the continuum and the discrete part vary with the frequency, and the variation will depend on the model used. Therefore, it is quite possible that different models give different values for the critical frequency, above which no discrete eigenvalues exist. We chose a simple model in order to be able to illustrate the effect of the continuum upon the neutron density itself and, as we have seen, this effect is only very weak and probably not observable.

L. S. KOTHARI: We have studied the problem of neutron wave propagation in beryllium – since the scattering kernel is better known here – in the diffusion theory approximation by rewriting the two coupled integral equations as a single integral equation, but in an energy range which is twice that of the original equations. This integral equation in the extended energy range is solved numerically. Apart from the various parameters (α, ξ), we can calculate the neutron spectrum as a function of space and time.

INVARIANT EMBEDDING AND PROPAGATION OF NEUTRON WAVES IN A SEMI-INFINITE MEDIUM

A. MOCKEL
UNIVERSITY OF FLORIDA,
GAINESVILLE, FLORIDA,
UNITED STATES OF AMERICA

Abstract

INVARIANT EMBEDDING AND PROPAGATION OF NEUTRON WAVES IN A SEMI-INFINITE MEDIUM. The experimental study of the propagation of neutron waves through a medium is of great interest in determining the characteristic of the medium and can often be applied in cases where the pulsed neutron experiments would be difficult or too long to perform. However, one of the main difficulties of the wave propagation method lies in the interpretation of the experimental results. The use of invariant embedding to compute the characteristics of the propagation allows one to overcome most of the difficulties involved in the theoretical prediction of numerical results.

As a preliminary problem, the study of the propagation of neutron waves in a semi-infinite non-multiplying medium has been performed, using invariant embedding. A degenerate kernel is used as the scattering kernel. Like the Milne problem, the method asks for solving first the equations giving the albedo of the semi-infinite medium. However, in the case of wave propagation, it is the Fourier transform of the time-dependent albedo which is of interest. Writing this Fourier transform, and solving the resulting set of integral equations, the asymptotic complex relaxation length can be easily found by solving an algebraic eigenvalue problem. It is easy to show that the complex relaxation length k (ω) also satisfies a system of integral equations. From these, the dispersion relation for the complex relaxation length was obtained.

1. INTRODUCTION

Neutron wave propagation has been extensively studied in the past five years. Several papers by Perez et al. (e.g. Ref.[1]) showed that it is possible to relate the coefficients of the expression of the inverse relaxation length in powers of ω to the thermalization parameters of the medium. However, no explicit theoretical expression of these coefficients using transport theory was available. Implicit expressions are given in Ref.[2].

In this paper we compute these coefficients using a method related to invariant embedding. The expression obtained correctly takes into account both the transport and thermalization effect. In the second part of the paper, the simplifications introduced by the use of a degenerate kernel are studied. Of course, in this case we do not treat correctly the thermalization effects. However, a study of the Milne problem by the same technique [3] showed that, in general, the inverse relaxation length is insensitive to the introduction of higher order corrections in the kernel.

Unfortunately, difficulties connected with a change of computer prevented us from obtaining numerical results.

2. EQUATION FOR THE INTERNAL FLUX

The quantity of interest in neutron wave experiments is the Fourier transform of the time-dependent flux caused by a sinusoidal source at $x = 0$, of frequency ω. It obeys the Boltzmann equation

$$\mu \frac{\partial \phi(x, \epsilon, \mu; \omega)}{\partial x} + [\Sigma_t(\epsilon) + i\omega\epsilon^{-\frac{1}{2}}]\phi(x, \epsilon, \mu; \omega)$$

$$= \int_0^\infty \int_{-1}^{+1} \Sigma(\epsilon, \mu \leftarrow \epsilon', \mu')\phi(x, \epsilon', \mu'; \omega)\, d\epsilon' d\mu' \tag{1}$$

$$\phi(0, \epsilon, \mu; \omega) = S(\epsilon, \mu)/\mu \qquad \mu > 0$$

$$\phi(\infty, \epsilon, \mu; \omega) = 0 \qquad \mu < 0$$

We will, in what follows, simplify slightly the derivation of our equation by assuming an isotropic scattering kernel. A generalization to an anisotropic kernel would not present any theoretical difficulties.

In view of the use of invariant embedding, we will rewrite the equation in terms of currents

$$I^+(x, \epsilon, \mu; \omega) = \mu\phi(x, \epsilon, \mu; \omega) \qquad \mu > 0$$

$$I^-(x, \epsilon, |\mu|; \omega) = |\mu|\phi(x, \epsilon, \mu; \omega) \qquad \mu < 0$$

The equation for I^+ is then (changing μ' in $-\mu'$ in the integral over I^-)

$$\frac{\partial I^+(x, \epsilon, \mu; \omega)}{\partial x} + \frac{\Sigma_t(\epsilon) + i\omega\epsilon^{-\frac{1}{2}}}{\mu} I^+(x, \epsilon, \mu; \omega)$$

$$= \frac{1}{2}\int_0^\infty \Sigma(\epsilon \leftarrow \epsilon') \int_0^1 I^+(x, \epsilon', \mu', \omega)\frac{d\mu'}{\mu'}\, d\epsilon'$$

$$+ \frac{1}{2}\int_0^\infty \Sigma(\epsilon \leftarrow \epsilon') \int_0^1 I^-(x, \epsilon', \mu', \omega)\frac{d\mu'}{\mu'}\, d\epsilon' \tag{2}$$

$$I^+(0, \epsilon, \mu; \omega) = S(\epsilon, \mu)$$

Instead of writing a similar equation for $I^-(x, \epsilon, \mu; \omega)$ we will make use of the fact that, due to the semi-infinite nature of the medium and to the absence of sources at infinity, we can directly relate I^- to I^+ through the reflection operator for the semi-infinite medium, at frequency ω

$$I^-(x, \epsilon, \mu; \omega) = \int_0^\infty \int_0^1 R^\infty(\epsilon, \mu | \epsilon', \mu'; \omega) I^+(x, \epsilon', \mu'; \omega)\, d\epsilon' d\mu' \tag{3}$$

Equation (2) can now be rewritten as an initial-condition integro-differential equation, rather than as a boundary-value equation

$$\frac{\partial I^+(x,\epsilon,\mu;\omega)}{\partial x} + \frac{\Sigma_t(\epsilon) + i\omega\epsilon^{-\frac{1}{2}}}{\mu} I^+(x,\epsilon,\mu;\omega)$$

$$= \frac{1}{2}\int_0^\infty d\epsilon'\,\Sigma(\epsilon \leftarrow \epsilon')\int_0^1 \frac{d\mu'}{\mu'}\int_0^\infty d\epsilon''\int_0^1 d\mu''\,A(\epsilon',\mu',\epsilon'',\mu'') \tag{4}$$

$$A(\epsilon',\mu',\epsilon'',\mu'') = \delta(\mu'-\mu'')\,\delta(\epsilon'-\epsilon'') + R^\infty(\epsilon',\mu' \mid \epsilon'',\mu'';\omega)\,I^+(x,\epsilon'',\mu'';\omega)$$

$$I^+(0,\epsilon,\mu,\omega) = S(\epsilon,\mu)$$

or, more concisely, by an operator notation

$$\Sigma = \frac{1}{2}\int_0^\infty\int_0^1 \Sigma(\epsilon \leftarrow \epsilon')\cdot d\epsilon'\,\frac{d\mu'}{\mu'}$$

$$R^\infty = \int_0^\infty\int_0^1 R^\infty(\epsilon,\mu \mid \epsilon',\mu')\cdot d\epsilon'\,d\mu'$$

$$I^+(x;\omega) = I^+(x,\epsilon,\mu;\omega)$$

$$\begin{cases} \dfrac{\partial I^+(x,\omega)}{\partial x} + \dfrac{\Sigma_t(\epsilon) + i\omega\epsilon^{-\frac{1}{2}}}{\mu} I^+(x,\omega) = \Sigma(\mathbf{I} + R^\infty)\,I^+(x;\omega) \\ I^+(0,\omega) = S \end{cases} \tag{5}$$

To solve the problem completely, we still have to know R^∞. But here we are provided, by invariant embedding, Eq. (1), with an equation for R^∞ which is (in operator notation)

$$\left(\frac{\Sigma_t(\epsilon) + i\omega\epsilon^{-\frac{1}{2}}}{\mu} + \frac{\Sigma_t(\epsilon') + i\omega\epsilon'^{-\frac{1}{2}}}{\mu}\right)R^\infty = (\mathbf{I} + R^\infty)\,\Sigma\,(\mathbf{I} + R^\infty) \tag{6}$$

Equation (6) has to be solved numerically. To solve Eq. (5) we will take its Laplace transform with respect to x

$$\left[k + \frac{\Sigma_t(\epsilon) + i\omega\epsilon^{-\frac{1}{2}}}{\mu}\right]\tilde{I}^+(k,\omega) = \Sigma(\mathbf{I} + R^\infty)\,\tilde{I}^+(k,\omega) + S \tag{7}$$

and examine the singularities in k of the operator

$$\mathbf{I} - \frac{\mu}{\Sigma_t(\epsilon) + i\omega\epsilon^{-\frac{1}{2}} + k\mu} \Sigma(\mathbf{I} + R^{\infty})$$

Obviously, any k such that

$$\begin{cases} \mu \operatorname{Re} k < -\Sigma_t(\epsilon) \\ \mu \left|\operatorname{Im} k\right| < \omega\epsilon^{-\frac{1}{2}} \end{cases} \quad \begin{matrix} 0 < \mu < 1 \\ 0 < \epsilon < \infty \end{matrix}$$

will be in the continuous spectrum. In addition, as pointed out by Duderstadt [4], an additional line could arise from the elastic part of the scattering kernel. Finally the zero of this operator (if any) will give rise to discrete modes.

It has been shown [3, 5] that, for zero frequency, at least one zero exists for sufficiently small absorption, and that this zero disappears when the absorption is increased.

The existence of a 'maximum frequency' theorem has, to the author's knowledge, not been proved in general. It has been proved for a separable kernel by Duderstadt [6]. For a general kernel, however, because of the presence of complex quantities, we cannot make use of the Jentsch theorem which enabled us to prove the 'maximum absorption' theorem in [3], and the author has not been able to find anything to replace it.

For small absorption and small frequencies, there exists at least one zero in k, which goes to the inverse relaxation length found in the study of the Milne problem when the frequency goes to zero.

3. EXPANSION IN POWERS OF ω FOR THE INVERSE RELAXATION LENGTH

The inverse relaxation length will be the (largest in modulus) eigenvalue of

$$I_0^+(k,\omega) = \frac{\mu}{\Sigma_t(\epsilon) + i\omega\epsilon^{-\frac{1}{2}} + k\mu} \Sigma(\mathbf{I} + R^{\infty}) I_0^+(k,\omega)$$

To expand k_0 in powers of $i\omega$, we will introduce the fictive eigenvalue equation

$$\lambda_0(k,\omega) I_0^+(k,\omega) = \frac{\mu}{\Sigma_t(\epsilon) + i\omega\epsilon^{-\frac{1}{2}} + k_0\mu} \Sigma(\mathbf{I} + R^{\infty}) I_0^+(k,\omega) \tag{8}$$

With the constraint

$$\lambda_0(k_0,\omega) = 1$$

k is now considered as a parameter, like ω

We will also introduce the adjoint equation

$$\bar{\lambda}_0(k,\omega)\, I_0^{+*}(k,\omega) = (R^{\infty *} + \mathbf{I})\Sigma^* \frac{\mu}{\Sigma_t(\epsilon) - i\omega\epsilon^{-\frac{1}{2}} + \bar{k}\mu}\, I_0^{+*}(k,\omega) \tag{9}$$

Multiplying Eq. (8) by $\overline{I_0^{+*}}\ (k_0,\omega)$ and integrating over ϵ and μ, we obtain

$$\lambda_0(I_0^{+*},\ I_0^{+}) = \left(I_0^{+*},\ \frac{\mu}{\Sigma_t(\epsilon) + i\omega\epsilon^{-\frac{1}{2}} + k\mu}\,\Sigma(\mathbf{I} + R^{\infty})\, I_0^{+}\right) \tag{10}$$

We can now take the variation of both sides of Eq. (10) for a variation of the parameter. Using the equation for I_0^+ at $\omega = 0$ and the fact that $d\lambda_0 = 0$ because of the constraint, we obtain

$$\left.\frac{dk_0}{di\omega}\right|_{\omega=0} = \frac{\left(I_0^{+*},\ \frac{\mu}{\Sigma_t(\epsilon) + k_0\mu}\,\Sigma\,\frac{dR^{\infty}}{di\omega}\, I_0^{+}\right) - \left(I_0^{+*},\ \frac{\epsilon^{-\frac{1}{2}}}{\Sigma_t(\epsilon) + k_0\mu}\, I_0^{+}\right)}{\left(I_0^{+*},\ \frac{\mu}{\Sigma_t(\epsilon) + k_0\mu}\, I_0^{+}\right)} \tag{11}$$

We can obviously obtain in a similar fashion every term in the expansion (though their expression becomes rapidly very cumbersome). For the second term

$$\left.\frac{d^2k_0}{d(i\omega)^2}\right|_{\omega=0} = -\frac{A}{\left(I_0^{+*},\ \frac{\mu^2}{(\Sigma_t(\epsilon) + k_0\mu)^2}\, I_0^{+}\right)} \tag{12}$$

$$A = -\frac{1}{2}\left(I_0^{+*},\ \frac{\mu}{\Sigma_t(\epsilon) + k_0\mu}\,\Sigma\,\frac{d^2R}{d(i\omega)^2}\, I_0^{+}\right) + \left(I_0^{+*},\ \frac{\mu\epsilon^{-\frac{1}{2}}}{(\Sigma_t(\epsilon) + k_0\mu)^2}\,\Sigma\,\frac{dR^{\infty}}{di\omega}\, I_0^{+}\right)$$

$$- \left(I_0^{+*},\ \frac{\epsilon^{-1}}{(\Sigma_t(\epsilon) + k_0\mu)^2}\, I_0^{+}\right)$$

$$+ \left.\frac{dk_0}{di\omega}\right|_{\omega=0}\left[\left(I_0^{+*},\ \frac{\mu^2}{(\Sigma_t(\epsilon) + k_0\mu)^2}\,\Sigma\,\frac{dR^{\infty}}{di\omega}\, I_0^{+}\right)\right.$$

$$\left. - 2\left(I_0^{+*},\ \frac{\mu\epsilon^{-\frac{1}{2}}}{\Sigma_t(\epsilon) + k_0\mu}\, I_0^{+}\right)\right]$$

We see that we have to know the derivative of R^∞ with respect to $i\omega$. This is easy to compute by derivation of Eq. (6). We will obtain linear integral equations for each derivative of order 1 or higher. The first is:

$$\frac{\Sigma_t(\epsilon)}{\mu} + \frac{\Sigma_t(\epsilon')}{\mu'} \frac{dR^\infty}{di\omega} + \left(\frac{\epsilon^{-\frac{1}{2}}}{\mu} + \frac{\epsilon'^{-\frac{1}{2}}}{\mu'}\right) R^\infty$$

$$= \frac{dR^\infty}{di\omega} \Sigma (\mathbf{I} + R^\infty) + (\mathbf{I} + R^\infty) \Sigma \frac{dR^\infty}{di\omega} \tag{13}$$

Obviously $\frac{dR}{di\omega}$ is real, and as a consequence, so is $\frac{dk_0}{di\omega}$

The second derivative is given by

$$\left(\frac{\Sigma_t(\epsilon)}{\mu} + \frac{\Sigma_t(\epsilon')}{\mu'}\right) \frac{d^2R^\infty}{d(i\omega)^2} + 2\left(\frac{\epsilon^{-\frac{1}{2}}}{\mu} + \frac{\epsilon'^{-\frac{1}{2}}}{\mu'}\right) \frac{dR^\infty}{di\omega}$$

$$= \frac{d^2R^\infty}{d(i\omega)^2} \Sigma(\mathbf{I} + R^\infty) + (\mathbf{I} + R^\infty) \Sigma \frac{d^2R^\infty}{d(i\omega)^2} + 2 \frac{dR^\infty}{di\omega} \Sigma \frac{dR^\infty}{di\omega} \tag{14}$$

Because of the real character of $\frac{dR^\infty}{di\omega}$, $\frac{d^2R^\infty}{d(i\omega)^2}$ is purely real, and so is $\frac{d^2k_0}{d(i\omega)^2}$.

By pursuing the expansion, one shows easily that all the derivatives with respect to $(i\omega)^n$ will be real, so that

$$k(\omega) = \sum_{n=0}^{\infty} \frac{(i\omega)^n}{n!} \left.\frac{d^nk}{d(i\omega)^n}\right|_{\omega=0}$$

and

$$k^2(\omega) = k^2(0) + 2i\,k(0) \left.\frac{dk(\omega)}{di\omega}\right|_{\omega=0}$$

$$- \left[k(0) \left.\frac{d^2k(\omega)}{d(i\omega)^2}\right|_{\omega=0} + \left(\left.\frac{dk(\omega)}{di\omega}\right|_{\omega=0}\right)^2\right] \omega^2 + \ldots$$

or, using the standard notation $k = \alpha + i\xi$

$$\alpha^2 - \xi^2 = k^2(0) - \left[k^2(0) \left.\frac{d^2k(\omega)}{d(i\omega)^2}\right|_{\omega=0} + \left(\left.\frac{dk(\omega)}{di\omega}\right|_{\omega=0}\right)^2\right] \omega^2 + \ldots$$

$$2\alpha\xi = \omega k(0) \left.\frac{dk(\omega)}{d(i\omega)}\right|_{\omega=0} + \ldots \tag{15}$$

On the other hand, in a semi-infinite medium, with no absorption, the square of the infinite relaxation length is given by

$$k^2(\omega) = \sum_{n=1}^{\infty} Q^{(n)}\left(\frac{\alpha_0 + i\omega}{D_0}\right)^n$$

and the $Q^{(n)}$ are related to the physical parameters D_0^W, C_0^W, and F_0^W by

$$\alpha_0 = v_0 \Sigma_{a0} \qquad C_0^W = -v_0 Q^{(2)}/(Q^{(2)})^3$$

$$D_0^W = v_0 / Q^{(1)} \qquad F_0^W = v/(Q^{(1)})^5[2(Q^{(2)})^2 - Q^{(1)}Q^{(3)}]$$

Besides (see Ref. [6]), the $Q^{(n)}$ are related to the coefficients of our expansion, $P^{(n)}$.

If we can assume that the expansion converges fast enough (small α and ω) to neglect any terms above the third, we have

$$Q^{(1)} = \frac{v_0}{\alpha_0}[P^{(2)}\alpha_0^2 - 2P^{(1)}\alpha_0 + 3P^{(0)}]$$

$$Q^{(2)} = -\frac{3v_0^2}{\alpha_0^2}\left[\frac{2}{3}P^{(2)}\alpha^2 - P^{(1)}\alpha + P^{(0)}\right]$$

$$Q^{(3)} = \frac{v_0^3}{\alpha_0^3}[P^{(2)}\alpha_0^2 - P^{(1)}\alpha_0 + P^{(0)}]$$

We are thus in a position to give rather cumbersome transport-thermalization expressions for the diffusion, diffusion cooling and F coefficients.

One could wonder why we did not take the derivative with respect to $z = \alpha_0 + i\omega$ rather than to $i\omega$. The reason is that the fictive eigenvalue (and the eigenfunctions) has a double degeneracy at $z = 0$. As a result [7] it is an analytic function of the principal part of $z^{\frac{1}{2}}$, and not of z, which makes the expansion rather difficult to perform.

4. DEGENERATE KERNEL

As is usual in invariant embedding, equations are drastically simplified when one uses a separable kernel

$$\Sigma = \frac{1}{2}\int_0^{\infty}\int_0^1 \Sigma(\epsilon \leftarrow \epsilon')\cdot d\epsilon' \frac{d\mu'}{\mu'} = \frac{1}{2}\sum_j \gamma_j g_j(\epsilon)\,\epsilon e^{-\epsilon}\int_0^{\infty}\int_0^1 g_j(\epsilon')\cdot d\epsilon' \frac{d\mu'}{\mu'} \qquad (16)$$

As we have shown in a previous paper [8] we can then define the H function as

$$H_j = \frac{1}{\epsilon e^{-\epsilon}}(\mathbf{I} + R^{\infty})\, g_j\, \epsilon' e^{-\epsilon'} \qquad (17)$$

which obeys the integral equation

$$H_i(\epsilon,\mu) = g_i(\epsilon)$$

$$+\frac{1}{2}\sum_j H_j(\epsilon,\mu)\int_0^\infty\int_0^1 \frac{H_j(\epsilon',\mu')\,g_i(\epsilon')\,\epsilon' e^{-\epsilon'}}{\frac{\Sigma_t(\epsilon)+i\omega\epsilon^{-\frac{1}{2}}}{\mu}+\frac{\Sigma_t(\epsilon')+i\omega\epsilon'^{-\frac{1}{2}}}{\mu'}}\,d\epsilon'\,\frac{d\mu'}{\mu'} \tag{18}$$

We can compute the successive derivatives of the H-function with respect to $i\omega$. The first one is

$$\left.\frac{dH_i(\epsilon,\mu)}{di\omega}\right|_{\omega=0} = -\frac{1}{2}\sum_j H_j(\epsilon,\mu)\int_0^\infty\int_0^1 \frac{H_j(\epsilon',\mu')\,g_i(\epsilon')\epsilon' e^{-\epsilon'}\left[\frac{\epsilon^{-\frac{1}{2}}}{\mu}+\frac{\epsilon'^{-\frac{1}{2}}}{\mu'}\right]}{\left[\frac{\Sigma_t(\epsilon)}{\mu}+\frac{\Sigma_t(\epsilon')}{\mu'}\right]^2}\,d\epsilon'\,\frac{d\mu'}{\mu'}$$

$$+\frac{1}{2}\sum_j H_j(\epsilon,\mu)\int_0^\infty\int_0^1 \frac{\left.\frac{dH_j(\epsilon',\mu')}{di\omega}\right|_{\omega=0} g_i(\epsilon')\,\epsilon' e^{-\epsilon'}}{\left[\frac{\Sigma_t(\epsilon)}{\mu}+\frac{\Sigma_t(\epsilon')}{\mu'}\right]}\,d\epsilon'\,\frac{d\mu'}{\mu'}$$

$$+\frac{1}{2}\sum_j \left.\frac{dH_j(\epsilon,\mu)}{di\omega}\right|_{\omega=0}\int_0^\infty\int_0^1 \frac{H_j(\epsilon',\mu')\,g_i(\epsilon')\epsilon' e^{-\epsilon'}}{\left[\frac{\Sigma_t(\epsilon)}{\mu}+\frac{\Sigma_t(\epsilon')}{\mu'}\right]}\,d\epsilon'\,\frac{d\mu'}{\mu'} \tag{19}$$

The computation of higher-order derivatives does not present any particular difficulty.

We will need, for the computation of the various derivatives of k, the expression for $\Sigma\frac{d^nR^\infty}{d(i\omega)^n}$. The easiest way to compute them is to make use of

$$\Sigma\,\frac{d^nR^\infty}{d(i\omega)^n} = \frac{d^n}{d(i\omega)^n}\{\Sigma\,(\mathbf{I}+R^\infty)\}$$

$$=\frac{d^n}{d(i\omega)^n}\left\{\frac{1}{2}\,\epsilon e^{-\epsilon}\sum_j \gamma_j\,g_j(\epsilon)\int_0^\infty\int_0^1 A\cdot d\epsilon'\,d\mu'\right\}$$

$$A = \int_0^\infty\int_0^1 g_j(\epsilon'')\left[\delta(\mu''-\mu')\,\delta(\epsilon''-\epsilon')+R^\infty(\epsilon'',\mu''\,|\,\epsilon',\mu';\omega)\right]d\epsilon''\,\frac{d\mu''}{\mu''}$$

Making use of detailed balance and reciprocity relation, we obtain

$$\Sigma \frac{d^n R^\infty}{d(i\omega)^n} = \frac{d^n}{d(i\omega)^n} \left\{ \frac{1}{2} \epsilon e^{-\epsilon} \sum_j \gamma_j g_j(\epsilon) \int_0^\infty \int_0^1 H_j(\epsilon', \mu') \cdot d\epsilon' \frac{d\mu'}{\mu'} \right\}$$

$$= \frac{1}{2} \epsilon e^{-\epsilon} \sum_j \gamma_j g_j(\epsilon) \int_0^\infty \int_0^1 \frac{d^n H_j(\epsilon', \mu')}{d(i\omega)^n} \cdot d\epsilon' \frac{d\mu'}{\mu'} \tag{20}$$

Besides, Eqs (8) and (9) can be reduced to matrix equations: for $\lambda = 1$ and $\omega = 0$ we get

$$I_0^+(\epsilon, \mu) = \frac{1}{2} \frac{\mu \epsilon e^{-\epsilon}}{\Sigma_t(\epsilon) + k\mu} \sum_j \gamma_j g_j(\epsilon) \int_0^\infty \int_0^1 H_j(\epsilon', \mu') I_0^+(\epsilon', \mu') d\epsilon' \frac{d\mu'}{\mu'}$$

or, by putting $C_j = \int_0^\infty \int_0^1 H_j(\epsilon', \mu') I_0^+(\epsilon', \mu') d\epsilon' \frac{d\mu'}{\mu'}$, we obtain

$$\begin{cases} C_i = \frac{1}{2} \sum_j \gamma_j C_j \int_0^\infty \int_0^1 \frac{\epsilon e^{-\epsilon} g_i(\epsilon) H_i(\epsilon, \mu)}{\Sigma_t(\epsilon) + k\mu} d\epsilon \, d\mu \\ I_0^+(\epsilon, \mu) = \frac{1}{2} \frac{\mu \epsilon e^{-\epsilon}}{\Sigma_t(\epsilon) + k\mu} \sum_j \gamma_j g_j(\epsilon) C_j \end{cases} \tag{21}$$

In the same way we obtain

$$I_0^{+*}(\epsilon, \mu) = \frac{1}{2\mu} \sum_j \gamma_j H_j(\epsilon, \mu) \int_0^\infty \int_0^1 g_j(\epsilon') \frac{\mu' \epsilon' e^{-\epsilon'}}{\Sigma_t(\epsilon') + k\mu'} I_0^{+*}(\epsilon', \mu') d\epsilon' d\mu'$$

Putting $C_j^* = \int_0^\infty \int_0^1 g_j(\epsilon') \frac{\mu' \epsilon' e^{-\epsilon'}}{\Sigma_t(\epsilon') + k\mu'} I_0^{+*}(\epsilon', \mu') d\epsilon' d\mu'$

we obtain

$$\begin{cases} C_j^* = \frac{1}{2} \sum_j \gamma_j C_j^* \int_0^\infty \int_0^1 \frac{\epsilon e^{-\epsilon} g_i(\epsilon) H_j(\epsilon, \mu)}{\Sigma_t(\epsilon) + k\mu} d\epsilon \, d\mu \\ I_0^{+*}(\epsilon, \mu) = \frac{1}{2\mu} \sum_j \gamma_j H_j(\epsilon, \mu) C_j^* \end{cases} \tag{22}$$

Introducing these values in the various integrals appearing in Eqs (11) and (12), we finally obtain the expression for the derivatives of the inverse relaxation length.

Normalizing the C so that $\frac{1}{2}\sum_i \gamma_i C_i^* C_i = 1$, we obtain

$$\frac{dk_0}{di\omega} = \frac{1}{4}\sum_i\sum_j \gamma_i C_i^* \left[\int_0^\infty\int_0^1 \frac{\left(-\epsilon^{-\frac{1}{2}} H_i(\epsilon,\mu) + \frac{dH_i(\epsilon,\mu)}{di\omega}\right) g_j(\epsilon)\,\epsilon e^{-\epsilon}}{\Sigma_t(\epsilon) + k_0\mu}\, d\epsilon\, d\mu\right]\gamma_j C_j \tag{23}$$

$$\frac{d^2k_0}{d(i\omega)^2} = \frac{A}{\frac{1}{4}\sum_i\sum_j \gamma_i C_i^* \left[\int_0^\infty\int_0^1 \frac{\mu\,\epsilon\, e^{-\epsilon} H_i(\epsilon,\mu) g_j(\epsilon)}{(\Sigma_t(\epsilon) + k\mu)^2}\, d\epsilon\, d\mu\right]\gamma_j C_j} \tag{24}$$

$$A = -\frac{1}{4}\sum_i\sum_j \gamma_i C_i^* \left[\alpha_{ij} - \frac{1}{2}\sum_\ell \beta_{i\ell}\gamma_{\ell j} + \frac{1}{2}\delta_{ij}\right]\gamma_j C_j$$

$$-\frac{1}{4}\frac{dk}{di\omega}\sum_i\sum_j \gamma_i C_i^* \left[2\epsilon_{ij} - \frac{1}{2}\sum_\ell \gamma_\ell \eta_{i\ell}\gamma_{\ell j}\right]\gamma_j C_j$$

$$\alpha_{ij} = \int_0^\infty\int_0^1 \frac{H_i(\epsilon,\mu) g_j(\epsilon) e^{-\epsilon}}{\mu[\Sigma_t(\epsilon) + k\mu]^2}\, d\epsilon\, d\mu$$

$$\beta_{ij} = \int_0^\infty\int_0^1 \frac{H_i(\epsilon,\mu) g_j(\epsilon)\,\epsilon^{\frac{1}{2}} e^{-\epsilon}}{[\Sigma_t(\epsilon) + k\mu]^2}\, d\epsilon\, d\mu$$

$$\gamma_{ij} = \int_0^\infty\int_0^1 \frac{\frac{dH_i(\epsilon,\mu)}{di\omega} g_j(\epsilon)\,\epsilon e^{-\epsilon}}{\Sigma_t(\epsilon) + k\mu}\, d\epsilon\, d\mu$$

$$\delta_{ij} = \int_0^\infty\int_0^1 \frac{\frac{d^2H_i(\epsilon,\mu)}{d(i\omega)^2} g_j(\epsilon)\,\epsilon e^{-\epsilon}}{\Sigma_t(\epsilon) + k\mu}\, d\epsilon\, d\mu$$

$$\epsilon_{ij} = \int_0^\infty\int_0^1 \frac{H_i(\epsilon,\mu) g_j(\epsilon)\,\epsilon^{\frac{1}{2}} e^{-\epsilon}}{\Sigma_t(\epsilon) + k\mu}\, d\epsilon\, d\mu$$

$$\eta_{ij} = \int_0^\infty\int_0^1 \frac{\mu H_i(\epsilon,\mu) g_j(\epsilon)\,\epsilon e^{-\epsilon}}{(\Sigma_t(\epsilon) + k\mu)^2}\, d\epsilon\, d\mu$$

ACKNOWLEDGEMENTS

The author would like to thank Dr. R. B. Perez for numerous discussions of the problem.

REFERENCES

[1] PEREZ, R. B., BOOTH, R. S., "Excitation of neutron waves by modulated and pulsed sources," Pulsed Neutron Research II IAEA, Vienna (1965) 701-28.

[2] MOORE, M. N., Nucl. Sci. Engng 26 (1966) 354.

[3] MOCKEL, A., "The Milne problem with absorption and the albedo of a semi-infinite medium," submitted for publication to Nucl. Sci. Engng.

[4] DUDERSTADT, J. J., "On the continuous eigenvalue spectrum of the neutron wave experiment," Nucl. Sci. Engng 29 (1967) 156.

[5] CORNGOLD, N., "On the maximum absorption theorem", Nucl. Sci. Engng 24 (1966) 410.

[6] DUDERSTADT, J. J., "A simple model of neutron wave propagation," Trans. Am. nucl. Soc. 10 (1967) 211.

[7] DUNFORD, N., SCHWARTZ, J. T., Linear Operators I Interscience, New York (1958) 587.

[8] MOCKEL, A., "Invariant imbedding and polyenergetic neutron transport theory, Part I, Theory," Nucl. Sci. Engng 29 (1961) 43.

RELATIONSHIP BETWEEN PULSED, POISONING AND WAVE EXPERIMENTS*

P. MICHAEL AND M.N. MOORE†
BROOKHAVEN NATIONAL LABORATORY,
UPTON, NEW YORK,
UNITED STATES OF AMERICA

Abstract

RELATIONSHIP BETWEEN PULSED, POISONING AND WAVE EXPERIMENTS. Two types of experiments that are used to determine integral neutron thermalization properties of moderators are the pulsed source (or die-away) experiment and the modulated source (or wave propagation) experiment. The diffusion length experiment can be considered the zero frequency limit of the modulated source experiment. We show here that from the theoretical point of view both experiments yield the same information about the moderator; the superiority of one type of experiment over the other must then be decided upon experimental considerations.

To exhibit the relationship between the two experiments, a perturbation solution for the fundamental eigenfunction and the inverse migration area is obtained by considering an expansion in powers of $i\omega$ of the transport equation, in slab geometry, for 1/v absorption. A comparison is made with the solution given by Nelkin for the die-away experiment, the latter being an expansion in terms of B^2. It is seen that individual terms in the expansion of the eigenfunction of one experiment can be written as a linear combination of the terms that appear in the other. In particular, it can be seen that while the spectrum in the pulsed experiment is softened, in the modulated experiment it is hardened.

From the equations that define the functions that appear in the expansion, one is able to see that the dependence of the parameters is in agreement with previous empirical results, namely that the imaginary part of the inverse migration area is less sensitive to thermalization properties than is the real part. It is clearly shown that relationships between the λ versus B^2 series and the η^2 versus $i\omega$ series are exact (and would be true also for a multiplying medium). These relationships have been used to relate experiments done with graphite.

1. INTRODUCTION

The aim of the work reported here is to exhibit the relation between the theory of the pulsed source experiment and that of the time-dependent exponential or neutron wave experiment.

Two different aspects of this relationship are developed. On the one hand, one recognizes the existence of a generalized dispersion law which characterizes the system and ultimately dictates the relationship between pulsed parameters and wave parameters. On the other hand, one recognizes that just as in the case of the pulsed experiment, the wave experiment explores an eigenvalue of the Boltzmann operator. Whereas the pulsed experiment eigenvalue depends upon the buckling, or the size of the system, the wave experiment eigenvalue depends upon the wave frequency. In a 1/v absorbing moderator, the wave experiment may be treated by a perturbation technique similar to that

* This work was performed under the auspices of the United States Atomic Energy Commission.

† Present address: Dept. of Physics, San Fernando Valley State College, Northridge, California

introduced by Nelkin [1] in his classical analysis of the pulsed experiment.

In section 2 we introduce a generalized dispersion law $Z(-\varkappa^2, if) = 0$ where $\varkappa$ and f are buckling-like and frequency-like complex parameters. The dispersion law may be solved for its roots $\varkappa_j^2 = \varkappa_j^2(if)$ or alternatively $if_j = f_j(-\varkappa^2)$. The first solution is explored by a wave experiment, whereas the second is explored by a pulsed experiment. We then find the relations between the coefficients of a MacLaurin series expansion of the two solutions of the dispersion law. These relations are always valid and represent a dictionary which translates the results of wave experiments into those of pulsed experiments and vice versa.

In sections 3 and 4 we restrict ourselves to moderating materials that scatter isotropically in the lab system and have an absorption cross-section that is inversely proportional to the speed of the neutron. In section 3, Nelkin's results are repeated, primarily to define notation. In section 4, we apply a perturbation method, analogous to that of Nelkin, to the wave experiment and obtain the same results as in section 1 relating the two eigenvalues and eigenfunctions.

In addition, a perturbation series for the fundamental eigenfunction is obtained and its relation to the eigenfunction for the pulsed problem is exhibited.

By considering the poisoning experiment as a special case of a wave experiment in a moderator, the connection between the three experiments, their characteristic parameters and their eigenfunctions is clearly exhibited.

In section 5, we abandon the model of the previous two sections which identifies the energy spectrum of the asymptotic wave or pulse as an eigenfunction of the Boltzmann operator and the decay constant or complex migration area as the corresponding eigenvalue. We return to the philosophy of section 2 which simply recognizes the existence of an energy spectrum defined by a complex decay constant (frequency) and a complex migration area (buckling) related through a dispersion law. Using these facts alone, we expand the spectrum in two perturbation series, one in the decay constant, the other in the migration area and, using the corresponding root of the dispersion law, find the wave experiment spectral perturbations in terms of the pulsed experiment perturbations. These latter relations are completely general and would also be valid in a multiplying medium.

2. THE GENERALIZED DISPERSION LAW

It was pointed out by one of us (M.N.M.) [2] that, because of the structure of the Boltzmann equation, solutions of

the form $n(f,\vec{\varkappa},v)\exp ift+i\vec{\varkappa}\cdot\vec{r}$,for the scalar flux, exist subject to the dispersion law $Z(-\varkappa^2,if) = 0$ where the exact form of the dispersion function Z depends upon the scattering, absorption and multiplying properties of the medium. Here $\varkappa$ and f, wave number-like and frequency-like parameters, are in general regarded as complex numbers. It was also shown [3] that, depending upon the boundary conditions selected by the experimenter, either $\varkappa = B = \varkappa^*$ or $f = \omega = f^*$. Thus, the real quantity (B or ω) becomes an independent variable of the experiment and the remaining complex quantity, measured in the experiment, becomes fixed and determined through the dispersion law. Due to the essentially diffusive nature of neutron propagation, the smallest value of f corresponding to a given real B is, in non-multiplying systems, imaginary, i.e. $f = i\lambda$, whereas the $\varkappa$ having the smallest imaginary part (least attenuated) for a given real ω, is complex, i.e. $\varkappa = -\xi + i\alpha$.

One sees immediately from the form of the dispersion law that λ has definite parity, being an even function of B. Furthermore, Moore has shown [4] that ξ and α also have definite parity with respect to ω, α being even and ξ odd. These parity properties are important for what is to follow.

Returning to the dispersion law

$$Z(-\varkappa^2,if) = 0 \tag{1}$$

we may solve for $\varkappa^2$ or for (if) whence

$$\varkappa^2 = \sum_n \varkappa_n (if)^n \tag{3}$$

$$if = \sum_m \lambda_m (-\varkappa^2)^m \tag{4}$$

where $\varkappa_n$ and λ_m are the expansion coefficients of the MacLaurin series for $\varkappa^2$ and (if), respectively.[1] It is clear that since Eqs. (3) and (4) are alternative ways of writing Eq. (1), the $\varkappa_n$ are related to the λ_m. Moreover, the relations between these two sets of parameters are not dependent upon the form of Z and hence independent of the nature of the system. We devote this section to obtaining these relations which relate wave parameters to pulsed parameters. One may eliminate $\varkappa^2$ from equations (3) and (4), thereby obtaining a series in (if). Since this series vanishes identically in f, the coefficients of each power of (if) vanish separately, resulting in the following relations for the $\varkappa_n$ in terms of the λ_n. These rela-

[1] The radii of convergence of these series for moderators depends upon the chemical state of the moderator and is still not completely understood.

tions are valid assuming the equations (3) and (4) may be truncated at 5th order in (if) and $(-\varkappa^2)$.

$$
\begin{aligned}
-\lambda_o &= -\lambda_1\varkappa_o + \lambda_2\varkappa_o^2 - \lambda_3\varkappa_o^3 + \lambda_4\varkappa_o^4 - \lambda_5\varkappa_o^5 \\
\varkappa_1 &= \left[-\lambda_1 + 2\lambda_2\varkappa_o - 3\lambda_3\varkappa_o^2 + 4\lambda_4\varkappa_o^3 - 5\lambda_5\varkappa_o^4\right]^{-1} \\
\varkappa_2 &= -\varkappa_1^3\left[\lambda_2 - 3\lambda_3\varkappa_o + 6\lambda_4\varkappa_o^2 - 10\lambda_5\varkappa_o^3\right] \\
\varkappa_3 &= 2\varkappa_2^2/\varkappa_1 - \varkappa_1^4\left[-\lambda_3 + 4\lambda_4\varkappa_o - 10\lambda_5\varkappa_o^2\right] \\
\varkappa_4 &= 5\varkappa_2/\varkappa_1^2\left[\varkappa_1\varkappa_3 - \varkappa_2^2\right] - \varkappa_1^5\left[\lambda_4 - 5\varkappa_o\lambda_5\right] \\
\varkappa_5 &= \varkappa_2/\varkappa_1^2\left[\frac{3\varkappa_1\varkappa_3^2}{\varkappa_2} + \frac{14\varkappa_2^2}{\varkappa_1} + 2\varkappa_4\varkappa_1 - 21\varkappa_2\varkappa_3\right] + 5\varkappa_1^6\lambda_5
\end{aligned}
\tag{5}
$$

This set is useful if one knows the λ_n and wishes to find the $\varkappa_n$. The first equation is solved for $\varkappa_o$ and then each equation is evaluated in succession for the remaining $\varkappa$'s. Hence Eq. (5) permits the calculation of wave parameters $\varkappa_n$, from pulsed parameters λ_n.

Alternatively, returning to Eqs. (3) and (4), one may eliminate (if) and obtain a series in $\varkappa^2$. By the previous argument, the coefficients of this series must each vanish resulting in the following relations for the λ_n in terms of the $\varkappa_n$.

$$
\begin{aligned}
\varkappa_o &= -\left\{\varkappa_1\lambda_o + \varkappa_2\lambda_o^2 + \varkappa_3\lambda_o^3 + \varkappa_4\lambda_o^4 + \varkappa_5\lambda_o^5\right\} \\
\lambda_1 &= -\left\{\varkappa_1 + 2\varkappa_2\lambda_o + 3\varkappa_3\lambda_o^2 + 4\varkappa_4\lambda_o^3 + 5\varkappa_5\lambda_o^4\right\}^{-1} \\
\lambda_2 &= \lambda_1^3\left[\varkappa_2 + 3\varkappa_3\lambda_o + 6\varkappa_4\lambda_o^2 + 10\varkappa_5\lambda_o^3\right] \\
\lambda_3 &= 2\lambda_2^2/\lambda_1 + \lambda_1^4\left[\varkappa_3 + 4\lambda_o\varkappa_4 + 10\lambda_o^2\varkappa_5\right] \\
\lambda_4 &= 5\lambda_2/\lambda_1^2\left[\lambda_1\lambda_3 - \lambda_2^2\right] + \lambda_1^5\left[\varkappa_4 + 5\lambda_o\varkappa_5\right] \\
\lambda_5 &= \lambda_2/\lambda_1^2\left[3\lambda_1\lambda_3^2/\lambda_2 + 14\lambda_2^2/\lambda_1 + 2\lambda_4\lambda_1 - 21\lambda_2\lambda_3\right] + 5\lambda_1^6\varkappa_5
\end{aligned}
\tag{6}
$$

This set is useful if one knows the $\varkappa_n$ and wishes to find the λ_n. Again, the first equation is solved for λ_o and from this value the successive λ_n are then computed.

2.1. The Application to Moderators

For the case of moderators the wave experiment expansion given by Perez and Booth [5] is

$$-\mathrm{Re}\ \varkappa^2 = \sum P_{2n}\ \omega^{2n} = \alpha^2 - \xi^2$$
$$-\mathrm{Im}\ \varkappa^2 = \sum P_{2n+1}\ \omega^{2n+1} = 2\alpha\xi \qquad (7)$$

upon comparison with Eq. (3) with $F = \omega$ and remembering the parity properties of α and ξ we have

$$(i)^{2n+2}\ \varkappa_{2n} = P_{2n}$$
$$(i)^{2n+2}\ \varkappa_{2n+1} = P_{2n+1} \qquad (8)$$

Moreover, the classical pulsed neutron expansion

$$\lambda = \alpha_o + D_o B^2 - CB^4 + FB^6 - GB^8 \qquad (9)$$

when compared with Eq. (4) with $if = -\lambda$ and $\varkappa^2 = B^2$ gives

$$\lambda_o = -\alpha_o\ ,\ \lambda_1 = D_o\ ,\ \lambda_2 = C,\ \lambda_5 = F,\ \lambda_4 = G,\ \lambda_5 = H$$

whence for a moderator, the equations (5) and (6) become

$$\alpha_o = D_o P_o + CP_o^2 + FP_o^3 + GP_o^4 + HP_o^5$$
$$P_1 = \left[D_o + 2CP_o + 3FP_o^2 + 4GP_o^3 + 5HP_o^4\right]^{-1}$$
$$P_2 = P_1^3\left[C + 3FP_o + 6GP_o^2 + 10HP_o^3\right]$$
$$P_3 = -2P_2^2/P_1 + P_1^4\left[F + 4GP_o + 10HP_o^2\right] \qquad (5')$$
$$P_4 = 5P_2/P_1^2\left[P_1P_3 + P_2^2\right] - P_1^5\left[G + 5P_oH\right]$$
$$P_5 = P_2/P_1^2\left[P_1P_3^2/P_2 + 14P_2^2/P_1 - 2P_1P_4 + 21P_2P_3\right] + 5P_1^6H$$

and

$$P_o = P_1\alpha_o + P_2(\alpha_o)^2 - P_3(\alpha_o)^3 - P_4(\alpha_o)^4 + P_5(\alpha_o)^5$$
$$D_o = \left\{P_1 + 2P_2(\alpha_o) - 3P_3(\alpha_o)^2 - 4P_4(\alpha_o)^3 + 5P_5(\alpha_o)^4\right\}^{-1}$$
$$C = D_o^3\left\{P_2 - 3P_3\alpha_o - 6P_4(\alpha_o)^2 + 10P_5(\alpha_o)^3\right\}$$
$$F = 2C^2/D_o + D_o^4\left[P_3 + 4P_4(\alpha_o) - 10P_5(\alpha_o)^3\right] \qquad (6')$$
$$G = 5C/D_o^2\left[D_oF - C^2\right] + D_o^5\left[-P_4 + 5P_5(\alpha_o)\right]$$
$$H = C/D_o^2\left[3D_oF^2/C + 14C^2/D_o + 2D_oG - 21CF\right] - 5D_o^6P_5$$

To use these last relations together with data acquired in a finite medium, it is necessary to correct the observed P_o. If the medium is so large in a direction perpendicular to the propagation axis that in the transverse dimension diffusion theory may be used, one replaces P_o in Eqs. (6') by $(P_o)_{observed} - B_t^2$. To compute $(P_o)_{observed}$ from the Eqs. (5'), one adds B_t^2 to the P_o obtained from Eqs. (5'), viz $(P_o)_{obs} = (P_o)_{calc} + B_t^2$. This correction for finite transverse dimension is discussed in references [2] and [6] .

The Eqs. (5') and (6') were obtained implicitly in parametric form by Perez and Booth, [5] , within the context of the diffusion approximation to the Boltzmann equation. The improvements due to our treatment are a) the relations are shown to be universally valid even in a multiplying medium as long as a dispersion law exists; b) the relations are obtained to higher order of approximation and c) the dependence of wave parameters upon pulsed parameters is now explicit.

As a consequence of property c), we are now in a position to clarify a longstanding mystery. By considering a hierarchy of models for neutron wave propagation in moderators, Perez and co-workers, [5,6] , have remarked that the frequency dependence of $\alpha^2-\xi^2$ was sensitive in first order to the thermalizing properties of the medium, whereas $2\alpha\xi$ appeared to be insensitive. This difference in sensitivity has been heretofore unexplained either physically or mathematically. Furthermore, as $\varkappa$ itself displays no such properties, the mystery is compounded. The explanation of this phenomenon is readily available from the expression for C Eq. (6'). If the system has small absorption one may keep the leading term and in first approximation

$$P_2 \approx \frac{C}{D_o^3} \tag{10}$$

Referring to Eq. (7) and remembering the even and odd parity of α and ξ we note that P_o is just the square of the attenuation constant as measured in an exponential experiment ($i\varkappa(0)$) and P_2 controls the first-order frequency dependence, thus to first order

$$\alpha^2-\xi^2 \approx \left(B_t^2 + \frac{1}{L^2}\right) + \frac{C}{D_o^3}\,\omega^2 \tag{11}$$

Similarly, using the same approximation in the second equation of (6') we see that $P_1 \approx 1/D_o$ and from Eq. (7)

$$2\alpha\xi \approx \omega/D_o \tag{12}$$

Clearly $2\alpha\xi$ is insensitive to thermalization and referring to Nelkin's analysis, [1] , which demonstrates the primary dependence of C upon the thermalization process, we see that

the Perez effect should be present in all lightly absorbing moderators.

It is of interest to note that the parameters P_j, $j = 0,1,2...n$, directly obtainable from experiment, have been measured in graphite [7] as have the parameters α_o, D_o, C and F in numerous experiments [8,9,10,11,12]. Using the approximate formulae, Perez and Booth, [5], have estimated the pulsed parameters from the wave parameters, with reasonable agreement. Using the same wave parameters, we have recalculated the pulsed parameters using the more exact Eqs. (6'). The results are given in Table I, together with a representative selection of pulsed parameters from the indicated sources. The close agreement with the experiment of Davis et al is striking. Moreover, when one considers the elaborate precautions taken in this latter to eliminate room-return background, a precaution unnecessary in wave experiments, the advantages of the wave experiment become numerous and may be summarized as follows: 1) the parameter varied in the experiment (ω) is accurately controlled and determined; 2) at each value of ω two quantities, α and ξ, are measured; 3) thermalization is a first order effect; 4) the range of frequencies over which an asymptotic mode exists appears to be greater than the corresponding range of bucklings, [13,14], thereby permitting the determination of a larger number of wave parameters; 5) the system geometry remains constant throughout the experiment; 6) room-return neutrons are incoherent with the measured wave and hence are automatically eliminated in the experiment; 7) using pulse propagation techniques, [5,15], one can in principle obtain frequency derivatives of α and ξ.

3. PERTURBATION TREATMENT OF THE PULSED EXPERIMENT IN MODERATORS

In this section, to facilitate referencing and to define notation, we summarize Nelkin's treatment [1] of the pulsed experiment in moderators. Nelkin shows that solutions to the Boltzmann equation which have the form $n(\lambda,B^2,v)\exp -\lambda t+i\vec{B}\cdot\vec{r}$ exist when $n(\lambda,B^2,v)$ satisfies the following "eigenvalue" equation

$$G(v,B^2,\lambda)n(\lambda,B^2,v) = S(v)n(\lambda,B^2,v) \tag{13}$$

where

$$G = 2iBv\left[\ln\frac{v\Sigma_T(v)-\lambda+iBv}{v\Sigma_T(v)-\lambda-iBv}\right]^{-1} - v\Sigma_s \tag{14}$$

and

$$Sn = \int dv'v'\Sigma_s(v'\to v)n(v') - v\Sigma_s(v)n(v) \tag{15}$$

assuming isotropic scattering. In what follows explicit func-

TABLE I

Computed Values of Thermal Diffusion Parameters for 1.60 g/cm^3 Graphite From Neutron Wave Experiments, Die-Away Experiments and the Parks Kernel

Reference	Source of Data	α_o s^{-1}	$D_o \times 10^{-5}$ cm^2/sec	$C \times 10^{-5}$ cm^4/sec	$F \times 10^{-7}$ cm^6/sec	$G \times 10^{-9}$ cm^8/sec
Perez & Booth[5]	wave exp't.	91.0 ±4	2.16±0.01	39.0±2	12.0±2	
This Work	wave exp't.	91.1 ±2	2.12±0.01	37.8±1.3	10.6±1.2	8.16±.8
Klose et al.[9]	die-away	88.6 ±1.6	2.11±0.02	16 ±5	-20 ±10	
Davis et al.[12]	die-away	77.59±0.6	2.091±.009	37.6±3.5	9.7±2.8	
Calculated values[5]	Parks kernel diffusion approx.		2.1104	20.1553	-5.0574	

tional dependence on v, λ and B^2 will be omitted when it is felt no confusion results. The notation is otherwise standard.

To solve for the fundamental eigenvalue, λ, and corresponding eigenfunction n, one expands n, λ and G in powers of B^2

$$n = N_o + N_2B^2 + N_4B^4 + N_6B^6 + \ldots \tag{16}$$

$$\lambda = \alpha_o + D_oB^2 - C\,B^4 + FB^6 + \ldots \tag{17}$$

$$G = G_o + G_2B^2 + G_4B^4 + G_6B^6 + \ldots \tag{18}$$

substitutes in Eq. (13), and obtains a power series in B^2 which vanishes identically. Since the coefficients of the series are independent of B^2, each separate coefficient vanishes and one obtains a set of coupled integral equations. Introducing neutron conservation

$$\int dv\ S\ q(v) = 0 \tag{19}$$

where q(v) is any neutron distribution and the principle of detailed balance

$$S\ M(v) = 0$$

where M(v) is the Maxwellian distribution , Nelkin then demonstrates assuming $\Sigma_a(v) = \lambda_o/v$, λ_o constant,

$$\alpha_o = \lambda_o = v\Sigma_a \quad \text{and} \quad N_o = M(v) \tag{20}$$

Furthermore, it follows that N_2 is a solution of

$$S\ N_2 = G_2N_o = \left(\frac{v}{3\Sigma_s} - D_o\right) N_o \tag{21}$$

which, when integrated over v, using Eq. (19), gives

$$D_o = \int \frac{v}{3\Sigma_s} N_o\ dv \Big/ \int N_o dv \tag{22}$$

Now Eq. (21) is a slowing-down problem with a source equal to $(D_o - v/3\Sigma_s)N_o$. Since this source (for all reasonable models) is positive at low energies and negative at high energies, N_2 is expected to be softer than a Maxwellian distribution. Moreover, this softened spectrum in addition to the Maxwellian N_o determines the diffusion cooling coefficient which is given by

$$C\int N_o dv = \int dvN_o\ \frac{v}{3\Sigma_s^2}\left(\frac{4}{15\Sigma_s} - \frac{D_o}{v}\right) + \int dvN_2\ v\left(\frac{D_o}{v} - \frac{1}{3\Sigma_s}\right) \tag{23}$$

The first term of the above expression for C is known as the "transport" contribution to the diffusion cooling coefficient. This is not to imply that it vanishes in diffusion theory. By diffusion theory we mean the result of retaining the first two terms in the expansion of the logarithm in Eq. (13). In such an approximation, the D_o/v contribution to the first term still survives.

Demanding the disappearance of terms of order B^4 shows that N_4 is a solution of

$$S\,N_4 = G_4 N_o + G_2 N_2$$
$$= \left\{ \frac{v}{3\Sigma_s^2}\left(\frac{D_o}{v} - \frac{4}{15\Sigma_s}\right) + C \right\} N_o + \left(\frac{v}{3\Sigma_s} - D_o\right) N_2 \tag{24}$$

whence integrating over v and using Eq. (19), the result Eq. (23) is obtained.

By proceeding in this same manner, viz. setting the B^6 term equal to zero and finding an integral equation for N_6 as a linear combination of N_o, N_2 and N_4, one can integrate over v and with the help of Eq. (19) find F where

$$F\int N_o dv = \int dv N_o \left[\frac{D_o^2}{v^2\Sigma_s} - \frac{C}{v} - \frac{4}{5}\frac{D_o}{v\Sigma_s^2} + \frac{44}{315\Sigma_s^2} \right] \frac{v}{3\Sigma_s^2}$$
$$+ \int dv\, N_2 \left[C + \frac{v}{3\Sigma_s^2}\left(\frac{D_o}{v} - \frac{4}{15\Sigma_s}\right) \right] \tag{25}$$
$$+ \int dv\, N_4 \left(\frac{v}{3\Sigma_s} - D_o \right)$$

Now although we have terminated the perturbation series, Eq. (16) at sixth order in B, the relations (20) through (25) are exact in the sense that carrying the calculation to the term in B^8 will leave these relations unchanged. Hence, they are exact to all orders in transport theory.

4. PERTURBATION TREATMENT OF THE WAVE EXPERIMENT IN MODERATORS

The Ansatz representing the decay of a neutron pulse leading to Eq. (13) may be transformed into that suitable to the representation of a wave by the prescription of section 2, i.e. $-\lambda \to i\omega$ and $\vec{B} \to \vec{\kappa}$ whence the associated "eigenvalue" problem becomes, using Eq. (13), (see reference [14])

$$G(v,\kappa^2,-i\omega)\,n(-i\omega,\kappa^2,v) = S(v)\,n(-i\omega,\kappa^2,v) \tag{26}$$

where

$$G = 2i\kappa v \;\; \ln\left[\frac{v\Sigma_T(v)+i\omega+i\kappa v}{v\Sigma_T(v)+i\omega-i\kappa v}\right]^{-1} - v\Sigma_s$$

If our interest were confined to a determination of the functional dependence of $\varkappa$ on ω, then reference would be made to Nelkin's results, Eqs. (20), (22), (23) and (25) for the pulsed parameters, together with Eqs. (5') for the wave parameters in terms of the pulsed parameters; however, we would like also to have the fundamental eigenfunction to give us spectral information. Therefore, we shall proceed in a manner analogous to that employed by Nelkin which provides both the eigenvalue and eigenfunction. The eigenvalue can be compared, under appropriate specialization, to the more general relations Eqs. (5') as a verification.

Following the usual procedure and assuming as before $v\Sigma_a = \alpha_o$, we expand n, G and $\varkappa$ in powers of $\alpha_o + i\omega$. Such an expansion is convenient because then the expansion coefficients are dependent only upon the scattering cross-section of the moderator. If desired (see ahead), the resulting series can always be transformed into a series in $i\omega$ only. Thus,

$$n = \sum_j n_j (i\omega+\alpha_o)^j \tag{27}$$

$$G = \sum_j T_j (i\omega+\alpha_o)^j \tag{28}$$

$$-\varkappa^2 = \sum_j \Gamma_j (i\omega+\alpha_o)^j \tag{29}$$

Demanding that these satisfy Eq. (26) we obtain from the zeroth-order term in $(i\omega+\alpha_o)$

$$T_o = \Gamma_o = 0 \quad \text{and} \quad n_o = N_o \tag{30}$$

where N_o is the Maxwellian distribution, from Eq. (20).

From the term first order in $(i\omega+\alpha_o)$, we obtain

$$S\, n_1 = T_1 n_o = (1 - v\Gamma_1/3\Sigma_s) n_o \tag{31}$$

and integrating over v, invoking the conservation condition Eq. (19), and remembering Eq. (30) there results

$$\Gamma_1^{-1} = \int dv\, N_o \frac{v}{3\Sigma_s} \Big/ \int dv N_o$$

or, using Eq. (22) we have

$$\Gamma_1 = 1/D_o \tag{32}$$

whence Eq. (31) with the help of Eq. (30) may be re-written in the form of Eq. (10).

$$S\, n_1 = -D_o^{-1} \left(\frac{v}{3\Sigma_s} - D_o \right) N_o$$

Thus, we see that n_1 is a solution to essentially the same slowing-down problem as is N_2, their sources being proportional. Whence, due to the linearity of the S operator,

$$n_1 = -\frac{N_2}{D_o} \tag{33}$$

Since N_2 softens the Maxwellian, n_1 hardens it and we see that a hardening of the steady-state spectrum is the first-order perturbation due to the frequency dependence.

Continuing with the examination of the coefficients of the $(i\omega+\alpha_o)$ series, the quadratic term yields

$$S\, n_2 = T_2\, n_o + T_1 n_1$$

with

$$T_2 = \frac{v}{3\Sigma_s^2} \left(\frac{1}{vD_o} - \frac{4}{15} \frac{1}{D_o^2 \Sigma_s} \right) - \frac{v}{3\Sigma_s} \Gamma_2$$

Employing the usual technique of integration over v and appealing to conservation of neutrons, one finds

$$\Gamma_2 = -\frac{C}{D_o^3} \tag{34}$$

and the integral equation satisfied by n_2 becomes, with the aid of Eq. (33)

$$S\, n_2 = \frac{1}{D_o^2} \left[\frac{v}{3\Sigma_s^2} \left(\frac{D_o}{v} - \frac{4}{15\Sigma_s} \right) + \frac{v}{3\Sigma_s} \frac{C}{D_o} \right] N_o - \frac{1}{D_o^2} \left(D_o - \frac{v}{3\Sigma_s} \right) N_2$$

which, referring to Eq. (24), is of the form

$$S\, n_2 = \frac{1}{D_o^2} G_4 N_o + \frac{C}{D_o^3} G_2 N_o + \frac{1}{D_o^2} G_2 N_2$$

This may be compared with Eqs. (21) and (24) and again invoking the uniqueness of the solution of a slowing-down problem, together with the linearity of the slowing-down operator, it is clear that

$$n_2 = D_o^{-2} \left\{ N_4 + CD_o^{-1} N_2 \right\} \tag{35}$$

Continuing in the same vein one finds that

$$\Gamma_3 = -D_o^{-4}\ (F-2D_o^{-1}C^2) \tag{36}$$

and that

$$n_3 = -D_o^{-4}\ \left\{D_oN_6-(F-2D_o^{-1}C^2)N_2+2CN_4\right\} \tag{37}$$

The Eqs. (33), (35) and (37) represent the first three corrections to a Maxwellian spectrum caused by the simultaneous addition of an α_o/v absorber and a periodic perturbation of the well-thermalized neutron population at frequency ω. Of course, to be exact, we are speaking of a deviation from the steady-state neutron population. The equations (32), (34) and (36) represent the first three corrections to the corresponding eigenvalue caused by exactly the same perturbation. All these corrections are exact to all orders of transport theory, subject, of course, to the restriction upon the scattering and absorption cross-sections already noted.

The fact that $-\varkappa^2$ at $\omega = \alpha_o = 0$, vanishes, could have been easily anticipated from the following physical argument. In an infinite, homogeneous, non-absorbing medium, the steady-state neutron distribution must also be the equilibrium distribution. The equilibrium distribution is the Maxwellian distribution but an equilibrium distribution must be spatially uniform, hence, infinite relaxation length. However, $\varkappa$ is the inverse of the relaxation length, hence $\varkappa^2$ corresponding to a Maxwellian must vanish, and $-\varkappa^2$ vanishes for $\omega = \alpha_o = 0$.

It is also clear on physical grounds, that a 1/v absorber must harden the spectrum but the hardening effect of a periodic perturbation of the neutron density is probably a mathematical idiosyncracy of the Boltzmann equation.

Having now evaluated the n_j and Γ_j, we use these in Eqs. (27) and (29), expand the binomial $(i\omega+\alpha_o)^j$, and collect all terms of like powers in $i\omega$, thereby finding the perturbation series due to frequency perturbations only. These two series, keeping just the leading terms, are reproduced below.

$$\begin{aligned} n = {} & N_o-\alpha_oD_o^{-1}N_2 + \alpha_o^2D_o^{-2}(N_4 + D_o^{-1}C\ N_2) + 0(\alpha_o^3) \\ & + i\omega\left\{-N_2D_o^{-1} + 2\alpha_oD_o^{-2}(N_4+D_o^{-1}CN_2) + 0(\alpha_o^2)\right\} \\ & + (i\omega)^2\left\{D_o^{-2}(N_4+D_o^{-1}CN_2) + 0(\alpha_o)\right\} \\ & + 0(i\omega)^3 \end{aligned} \tag{38}$$

also

$$
\begin{aligned}
-\kappa^2 = {} & (\alpha_o D_o^{-1} - \alpha_o^2 D_o^{-3} C - \alpha_o^3 D_o^{-4} (F - 2D_o^{-1} C^2) + 0(\alpha_o^4)) \\
& + i\omega \left\{ D_o^{-1} - 2\alpha_o D_o^{-3} C - 3\alpha_o^2 D_o^{-4} (F - 2D_o^{-1} C^2) + 0(\alpha_o^3) \right\} \\
& + (i\omega)^2 \left\{ -CD_o^{-3} - 3\alpha_o D_o^{-4} (F - 2D_o^{-1} C^2) + 0(\alpha_o^2) \right\} \qquad (39) \\
& + (i\omega)^3 \left\{ -D_o^{-4} (F - 2D_o^{-1} C^2) + 0(\alpha_o) \right\} \\
& + 0(i\omega)^4
\end{aligned}
$$

This gives, alternatively to Eq. (5')

$$
\begin{aligned}
P_o &= \alpha_o D_o^{-1} - \alpha_o^2 D_o^{-3} C - \alpha_o^3 D_o^{-4} (F - 2D_o^{-1} C^2) + 0(\alpha_o^4) \\
P_1 &= D_o^{-1} - 2\alpha_o D_o^{-3} C - 3\alpha_o^2 D_o^{-4} (F - 2D_o^{-1} C^2) + 0(\alpha_o^3) \\
P_2 &= CD_o^{-3} + 3\alpha_o D_o^{-4} (F - 2D_o^{-1} C^2) + 0(\alpha_o^2) \qquad (40) \\
P_3 &= -D_o^{-4} (2D_o^{-1} C^2 - F) + 0(\alpha_o)
\end{aligned}
$$

The only difference between Eqs. (40) and (5') is that the latter give each wave parameter in terms of the lower order ones, whereas here we eliminate all wave parameters of lower order and obtain the wave parameters in terms of the pulsed parameters only. One can also obtain the result Eq. (39) directly from a series reversion of Eq. (17) using the replacements $-\lambda = i\omega$ and $B^2 = -\varkappa^2$. This tells us that the inequalities (see section 4.2) that must be satisfied in order to obtain the results Eqs. (38) and (39) also guarantee that the series Eq. (39) has non-zero radius of convergence if the series Eq. (17) is similarly blessed.

The coefficients of $(i\omega)^j$ in the expression for the wave eigenfunction, Eq. (38), can also be obtained by starting from the pulsed eigenfunction Eq. (16) and replacing B^2 by $-\varkappa^2$ as given by Eq. (29) and then collecting powers of $i\omega$.

4.1 The Poisoning Experiment

The relation of the pulsed and wave experiment to the "poisoning" experiment [16] can be clarified by considering the latter as a special case of Eqs. (38) and (39). For if we set $\omega = 0$ in these equations, we reduce to an ordinary exponential experiment in a 1/v moderator and the experiment consists of varying the amount of 1/v absorber. Hence, at absorption α_o, the fundamental eigenfunction is, from Eq. (38)

$$n = N_o - \alpha_o D_o^{-1} N_2 + \alpha_o^2 D_o^{-2} (N_4 + D_o^{-1} C\, N_2) + 0(\alpha_o^3) \qquad (41)$$

while the corresponding square inverse relaxation length, from Eq. (39), is

$$-\varkappa^2_{\omega=0} = \alpha_o D_o^{-1} - \alpha_o^2 D_o^{-3} C - \alpha_o^3 D_o^{-4} (F - 2D_o^{-1} C^2) + 0(\alpha_o^4) \qquad (42)$$

This last agrees with the expression found by Honeck [16], who also obtained integral equations for n_o and n_1 but did not note the relation between the absorption perturbations and the leakage perturbations as per Eqs. (33) and (35).

4.2 Limitations

In the course of obtaining the major results of this section several restrictions were imposed during the analysis. Although some of these have been discussed already, we list them again to indicate the areas in which this analysis may be improved.

1. Isotropic scattering

In his original paper, Nelkin outlined a procedure to include anisotropies in the scattering kernel.

2. 1/v absorption

This limitation can be quite severe in moderator experiments. The relation between the wave and pulsed parameters as well as the wave parameters themselves are sensitive to the absorption cross-section, which in a moderator is small. Thus, a slight non- 1/v impurity can be serious. On the other hand, the relations (5') and (6') are perfectly general so that the restriction to 1/v absorption must be removable. We are continuing our efforts in this direction.

3. $\left| \dfrac{\alpha_o + i\omega}{v\Sigma_s} \right| < 1, \quad \left| \dfrac{v\varkappa}{v\Sigma_T + i\omega} \right| < 1 \quad$ for all v

Both these assumptions were made in the expansion of the function G, Eq. (14). The first limitation is present even in diffusion theory and is given by Perez and Uhrig (incorrectly), whereas the second was first quoted in reference [14] and is related to the region of the $\varkappa$-plane in which a dispersion law may be defined.

As usual, these limitations represent a situation in which the validity of the approximation to transport theory can be obtained only after the eigenvalue has been determined [17].

5. THE GENERAL RELATIONS BETWEEN THE WAVE SPECTRUM AND THE PULSED SPECTRUM

In section 2, we showed that if we only know that the system is characterized by a generalized dispersion law, viz both an asymptotic pulse and an asymptotic wave exist, then it is possible to find exact relations between the wave parameters and the pulsed parameters quite independently of the precise nature of this dispersion law. One is then led to the related question "Is it possible to relate the asymptotic wave spectrum to the asymptotic pulsed spectrum in a similarly tautological manner?"

To see that such is the case, we return to the dispersion Ansatz $n(f,\varkappa,v)\exp ift+i\vec{\varkappa}\cdot\vec{r}$ and remember that due to the existence of a dispersion law we may alternatively regard $n=n(f,v)$ or $n=n(\varkappa,v)$. We shall refer to the first as the wave representation and the second as the pulse representation. The neutron spectrum may be expanded as a power series in either representation. Thus,

$$n = \sum_j \bar{n}_j (if)^j = \sum_\ell \bar{N}_\ell (-\varkappa^2)^\ell \tag{43}$$

where both the wave expansion coefficients $\bar{n}_j$ and the pulse expansion coefficients $\bar{N}_\ell$ are functions of v only. In 1/v-absorbing, isotropically scattering moderators, these coefficients are simply related to the coefficients in Eqs. (16) and (27).

Referring to the perturbation series for the generalized decay constant Eq. (4) and the generalized migration area Eq. (3) we could eliminate either $(\varkappa^2)$ or (if) in Eq. (43), obtaining a series in (if) or $\varkappa^2$ respectively. Since the coefficients of the resulting series are functions of v but not of $\varkappa^2$ or f, these coefficients must vanish in all orders. Consequently, one may find relations between wave spectral perturbations $\bar{n}_j$ and the pulse spectral perturbations $\bar{N}_j$.

Eliminating $\varkappa^2$ from the pulse representation in Eq. (43), we obtain

$$\bar{n}_o = \sum_j (-1)^j \varkappa_o{}^j \bar{N}_j$$

$$\bar{n}_1 = \varkappa_1 \sum_j (-1)^j j\, \varkappa_o{}^{j-1} \bar{N}_j = \varkappa_1 \frac{d\bar{n}_o}{d\varkappa_o}$$

$$\bar{n}_2 = \varkappa_2 \frac{d\bar{n}_o}{d\varkappa_o} + \frac{\varkappa_1{}^2}{2} \frac{d^2\bar{n}_o}{d\varkappa_o{}^2}$$

$$\bar{n}_3 = \varkappa_3 \frac{d\bar{n}_o}{d\varkappa_o} + \varkappa_1\varkappa_2 \frac{d^2\bar{n}_o}{d\varkappa_o{}^2} + \frac{\varkappa_1{}^3}{3} \frac{d^3\bar{n}_o}{d\varkappa_o{}^3}$$

Eliminating (if) from the wave representation in Eq. (43), we obtain the inverse relations

$$\bar{N}_o = \sum_j \bar{n}_j (\lambda_o)^j$$

$$\bar{N}_1 = \lambda_1 \frac{d\bar{N}_o}{d\lambda_o}$$

$$\bar{N}_2 = \lambda_2 \frac{d\bar{N}_o}{d\lambda_o} + \frac{\lambda_1^2}{2} \frac{d^2\bar{N}_o}{d\lambda_o^2}$$

$$N_3 = \lambda_3 \frac{d\bar{N}_o}{d\lambda_o} + \lambda_1\lambda_2 \frac{d^2\bar{N}_o}{d\lambda_o^2} + \frac{\lambda_1^3}{3} \frac{d^3\bar{N}_o}{d\lambda_o^3}$$

which are exact. In moderators, using Eqs. (8) et seq., we obtain

$$\bar{n}_o = \sum_j P_o^j \bar{N}_j$$

$$\bar{n}_1 = P_1 \frac{d\bar{n}_o}{dP_o}$$

$$\bar{n}_2 = -P_2 \frac{d\bar{n}_o}{dP_o} + \frac{P_1^2}{2} \frac{d^2\bar{n}_o}{dP_o^2} \tag{44}$$

$$\bar{n}_3 = -P_3 \frac{d\bar{n}_o}{dP_o} - P_1P_2 \frac{d^2\bar{n}_o}{dP_o^2} + \frac{\varkappa_1^3}{3} \frac{d^3\bar{n}_o}{dP_o^3}$$

and for the pulse spectrum perturbations

$$\bar{N}_o = \sum_j (-\alpha_o)^j \bar{n}_j$$

$$\bar{N}_1 = -D_o \frac{d\bar{N}_o}{d\alpha_o} = D_o \sum_j (-1)^{j+1} j(\alpha_o)^{j-1} \bar{n}_j \tag{45}$$

$$\bar{N}_2 = -C \frac{d\bar{N}_o}{d\alpha_o} + \frac{D_o^2}{2} \frac{d^2\bar{N}_o}{d\alpha_o^2}$$

$$\bar{N}_3 = -F \frac{d\bar{N}_o}{d\alpha_o} + D_o C \frac{d^2\bar{N}_o}{d\alpha_o^2} - \frac{D_o^3}{3} \frac{d^3\bar{N}_o}{d\alpha_o^3}$$

These relations, Eqs. (44) and (45), are exact and can be compared to Eqs. (33), (35) and (37) which are also exact but limited to the 1/v absorbing, isotropically scattering moderator.

6. REMARKS

The principle purpose of this paper has been to explore the relation between the three classical asymptotic experiments. We have demonstrated that independently of any model, results from any one of the three can always be translated into the results of any other of the three and hence the three experiments are exactly equivalent from the point of view of the physical information contained in the experiment. From the point of view of feasibility in performing the experiment, however, there can be vast differences.

At the moment, in graphite and probably in multiplying media, the wave experiment appears preferable with a pulsed experiment in second place and a 1/v poisoning being, perhaps, the most difficult. However, this ordering is subject to change depending upon technological developments.

Because the relations between the three experiments are model independent, it is clearly seen that the function of a model is a) to calculate the basic parameters of any one of the three experiments in terms of the model parameters, and b) to define the domain of existence of asymptotic experiments altogether. We saw, for example, that the general results of sections 2 and 5 flowed from the assumption of the existence of a dispersion law. Whether this assumption is valid or not and what the form of the dispersion law is, can only be obtained with the aid of a model.

Because of the work here, it is now necessary to do a) once for any model and not three times as was previously the case. The translation of task b) from one experiment to the next, however, is still apparently not quite so automatic. However, for the 1/v absorbing, isotropically scattering moderator, the pulse and the wave problem have much in common, compare [13] and [14], and this may be indicative of the existence of a more fundamental, unifying relation.

REFERENCES

[1] NELKIN, MARK, Nucl. Sci. Engng 7 (1960) 210.

[2] MOORE, M. N., Nucl. Sci. Engng 21 (1965) 565. See also JOEST, K. H., Zeit. fur Physik 193 (1966) 202.

[3] MOORE, M. N., "Neutron Noise, Waves, and Pulse Progagation", USAEC Symposium Series 9 (1967) 21.

[4] MOORE, M. N., Nucl. Sci. Engng 28 (1967) 152.

[5] PEREZ, R. B., BOOTH, R. S., Pulsed Neutron Research II IAEA, Vienna (1965) 701.

[6] PEREZ, R. B., UHRIG, R. E., Nucl. Sci. Engng 17 (1963) 90.

[7] BOOTH, R. S., HARTLEY, R. H., PEREZ, R. B., Nucl. Sci. Engng 28 (1967) 404.

[8] STARR, E., PRICE, G. A., Proc. Brookhaven Conf. on Neutron Thermalization, BNL 719 III (1962) 1034.

[9] KLOSE, H., KÜCHLE, M., REICHARDT, W., ibid, BNL 719 III (1962) 935.

[10] SAGOT, M. et al., Exponential and Critical Experiments, IAEA, Vienna (1964) 163.

[11] LALANDE, G., Industries Atomiques 516 (1961) 71.

[12] DAVIS, S. K., DE JUREN, J. A., REIER, M., Nucl. Sci. Engng 23 (1965) 74.

[13] CORNGOLD, N., Nucl. Sci. Engng 19 (1964) 80.

[14] MOORE, M. N., Nucl. Sci. Engng 26 (1966) 354.

[15] MOORE, M. N., Nucl. Sci. Engng 25 (1966) 422.

[16] HONECK, H. C., Proc. Brookhaven Conf. on Neutron Thermalization, BNL 719 IV (1962) 1186.

[17] MICHAEL, P., Nucl. Sci. Engng 24 (1966) 93.

DISCUSSION

M.P. NAVALKAR: Could you explain how the F coefficient happens to be positive when calculations show that it is negative? We have done calculations in the case of BeO and we get F negative. Honeck's calculations indicate that this is the case with graphite, too.

M.N. MOORE: One of two possibilities must obtain – either at frequencies high enough to be F-sensitive there is significant continuum contamination, or the scattering kernels used in the calculation are simply wrong. I don't think the former is true, and I might add that the deviation is really not so large as one might be led to think simply on the basis of the sign change. One should remember that F is very small and the difference between $+\epsilon$ and $-\epsilon$ is only 2ϵ.

R.B. PEREZ: In connection with the wave values presented in Table I of your paper, I may mention that we used a set of similar relations, but to compare the 'neutron-wave' and 'die-away' experiments we put $\alpha_0 = 0$, which explains the differences in your table. In view of the low absorption of graphite the discrepancies are small, but nevertheless they are significant.

M.N. MOORE: Yes, your relations are essentially the same as ours. You obtained yours within the context of a diffusion theory model. Our purpose was two-fold: (1) to show that your implicit relations were valid independent of any model; and (2) to extend your relations to higher orders, as well as to make explicit the relation between the pulse and wave parameters.

P. MICHAEL: I should like to comment on Dr. Perez' remark about D_0. If one accepts the perturbation series, D_0 for the pulsed experiment is given exactly by an integration over a Maxwellian spectrum. It is in any case only an expansion coefficient around zero. And, for the wave experiment, the first coefficient of the $(\alpha + i\omega)$ series is exactly $(D_0)^{-1}$; therefore no other spectra need be considered.

P.G.M. D'OULTREMONT: Concerning the comparison between experimental results obtained by the pulsed or by the wave method. I would add that at Mol, in Belgium, the EURATOM-BelgoNucléaire – CEN association has made a careful check[1] on the agreement between reactivity measurements by the two methods in reflected water-moderated lattices. It is interesting to note the excellent quality of the agreement, especially since the transfer function of the reactor was measured directly in the case of the wave experiments, and by way of Fourier analysis for the pulsed experiments.

M.M.R. WILLIAMS (Chairman): I believe that the transverse buckling effect where there is a finite system, which I mentioned in my paper[2], may have a strong bearing on the interpretation of wave-type experiments. Clearly, if the system is too small from a transverse point of view, discrete waves will not exist since only a continuum will propagate.

M.N. MOORE: Indeed, it would be of great interest to repeat the wave experiment in graphite as a function of changing transverse buckling. One could study the onset of the continuum at successively lower frequencies, as the buckling increased.

R.B. PEREZ: I should like to comment on the effect of the transverse dimensions on the establishment of an asymptotic behaviour in either the diffusion length or the wave experiment.

Experiments in graphite have shown that a transverse buckling, i. e. a transverse dispersion law, with at least one discrete mode is established in systems smaller than predicted. However, I completely agree that the eigenvalue problem should indeed be studied in actual three-dimensional systems, since three-dimensional waves are excited in the system.

---

[1] Results to be published by W. Rotter and J.B. Russell in Nucl. Sci. Engng

[2] See WILLIAMS, M.M.R., SM-96/3, these Proceedings I.

НЕКОТОРЫЕ МЕТОДЫ РЕШЕНИЯ ЗАДАЧ ТЕОРИИ ТЕРМАЛИЗАЦИИ НЕЙТРОНОВ

Л.В.МАЙОРОВ, Г.Я.ТРУХАНОВ
ИНСТИТУТ АТОМНОЙ ЭНЕРГИИ им.И.В.КУРЧАТОВА,
МОСКВА,
СССР

Abstract — Аннотация

SOME METHODS OF SOLVING NEUTRON THERMALIZATION THEORY PROBLEMS. The paper deals with the basis of small-group methods, i.e. it indicates a way (collision method) of deriving that part of the total neutron spectrum which can be calculated with good accuracy using a small number of groups. As an example, an appropriate system of equations for the intersecting-group method is formulated.

The quasi-diffusion method of solving kinetic equations is generalized for thermalization problems. The suitability of the method for thermalization problems is discussed. The authors explain the influence of chemical bonds and kinetic effects on neutron thermalization in temperature gradient systems.

НЕКОТОРЫЕ МЕТОДЫ РЕШЕНИЯ ЗАДАЧ ТЕОРИИ ТЕРМАЛИЗАЦИИ НЕЙТРОНОВ. Дается обоснование малогрупповых методов, т.е. указывается способ (метод столкновений) выделения такой части полного спектра нейтронов, которая с хорошей точностью может быть вычислена небольшим числом групп. В качестве примера формулируется соответствующая система уравнений метода перекрывающихся групп.

Проводится обобщение квазидиффузионного метода решения кинетического уравнения на задачи термализации. Анализируется сходимость этого метода в задачах термализации. Выясняется влияние химических связей и кинетических эффектов на термализацию нейтронов в системах с градиентами температур.

1. ВВЕДЕНИЕ

В теории термализации нейтронов, как известно, приходится иметь дело с решением многоскоростного кинетического уравнения. В обзорном докладе на Брукхейвенской конференции [1] Нелкин выделил три основных направления исследования кинетического уравнения.

Первое направление связано с изучением наиболее существенных математических свойств уравнения переноса с ядром, подчиняющимся лишь общим ограничениям, следующим из теории взаимодействия нейтронов с веществом. Второе направление, – это прямое "точное" решение уравнений переноса на быстродействующих машинах. Третье направление охватывает исследование различных модельных задач, получение приближенных полуаналитических решений, основанное главным образом на физической интуиции. Последнее из этих направлений М.Нелкин, отдавая должное ряду интересных работ, оценил несколько пессимистически. Тем не менее, хорошо известно, что, несмотря на целый ряд возражений, которые можно представить автору почти любой работы этого направления, полуаналитические методы часто приводят к получению очень богатой информации. Нередко "точные" численные расчеты ценой больших усилий и затрат машинного времени позволяют получить лишь незначительные поправки к результатам полуаналитической теории. Более того, хорошо известны такие ситуации, когда полуаналитические методы наиболее эффективны там, где "точные" вычисления становятся наиболее трудоемкими и требуют большого числа действий. Проиллюст-

рируем это двумя примерами. Первый из них, расчет стационарного спектра тепловых нейтронов в бесконечной среде с источниками в области больших энергий. Для численного решения такой задачи можно воспользоваться, например, обычным методом итераций по источникам. С уменьшением поглощения резко падает скорость сходимости итераций. С другой стороны, чем меньше поглощение, тем с большей точностью спектр тепловых нейтронов является максвелловским. Отклонения от максвелловского спектра можно описать в рамках целого ряда полуаналитических моделей, например [2, 3]. Определение разницы, даже небольшой, между точным решением и его приближенной оценкой стоит очень дорого при численном итерационном решении.

Второй пример, это расчет критичности конечной плоской гетерогенной решетки с одинаковыми ячейками. Если размеры такой решетки велики, итерации Келлога при определении $K_{эфф}$ сходятся очень медленно. В то же время гомогенизация решетки приводит к простой задаче, имеющей аналитическое решение. Если размеры решетки достаточно большие, то точность этого решения возрастает. Также быстро с увеличением размеров уменьшается и скорость сходимости итераций Келлога.

Было бы странным, если бы как в первом, так и во втором примерах нельзя было бы использовать информацию, полученную из приближенных оценок для существенного ускорения процесса точного решения задачи.

С этой точки зрения, весьма перспективным для теории термализации нейтронов представляется круг идей, исследованных в работах Гольдина [4], Гермогеновой, Лебедева [5], Марчука и др. [6], Морозова [7], Николайшвили. Общим в этих работах является использование априорной информации об основных свойствах кинетического уравнения для существенного уменьшения количества операций, необходимого для "точного" численного решения уравнения. При этом некоторые из авторов получают эту информацию лишь из качественных оценок и интуитивных соображений. Тем не менее, даже те из перечисленных методов, которые математически строго не обоснованы, как правило, имеют очень высокую эффективность.

Мы рассмотрим возможность применения подобных идей в теории термализации нейтронов и попытаемся обосновать некоторые из вышеупомянутых методов с единой точки зрения.

2. СПЕКТР ТЕПЛОВЫХ НЕЙТРОНОВ В БЕСКОНЕЧНОЙ СРЕДЕ

Начнем с простого примера, расчета спектра тепловых нейтронов в бесконечной среде, и покажем, как можно существенно ускорить сходимость обычных итерационных методов, используя априорную информацию о спектре.

Поток нейтронов $\Phi(E)$ в бесконечной среде удовлетворяет кинетическому уравнению:

$$\Sigma_t(E)\Phi(E) = \int_0^{E_{гр}} \Sigma_s(E, E')\Phi(E')dE' + S(E) \qquad (1)$$

Здесь – $E_{гр}$ – граничная энергия, которая может быть сколь-угодно велика, например, 1 Бэв; остальные обозначения общепринятые.

Обычная итерационная схема для решения уравнения (1), например, такова:

$$\Sigma_t(E)\Phi^{(n+1)}(E) - \int_E^{E_{гр}} \Sigma_s(E, E')\Phi^{(n+1)}(E')dE' = \int_0^{E_{гр}} \Sigma_s(E, E')\Phi^{(n)}(E')dE' + S(E) \qquad (2)$$

Если $\Phi^{(0)}(E) = 0$, то очевиден физический смысл каждого приближения $\Phi^{(n)}(E)$. $\Phi^{(n)}(E)$ – это поток нейтронов, испытавших не более n таких соударений с ядрами замедлителя, после которых их энергия увеличивалась. В эпитепловой области энергий мало нейтронов, испытавших большое число соударений с приобретением энергии. Следовательно, уже при небольшом n в этой области энергий $\Phi^{(n)} \approx \Phi(E)$. Нейтроны с энергией порядка кТ испытывают примерно одинаковое число соударений с потерей и с приобретением энергии. Если поглощение в среде мало, то тепловые нейтроны могут испытывать очень большое число столкновений прежде, чем поглотятся. Поэтому только при больших n функция $\Phi^{(n)}(E)$ хорошо аппроксимирует точное решение кинетического уравнения $\Phi(E)$. Это и означает, что итерационный процесс (2) сходится очень медленно при $\Sigma_a \to 0$. С другой стороны, известно, что с уменьшением поглощения спектр тепловых нейтронов ($E \sim кT$) приближается к максвелловскому:

$$\Phi(E) \sim M(E) = E \exp(-E/кT) \qquad (3)$$

Используем эту априорную информацию для существенного ускорения зайделевских итераций (2) и построим новый итерационный процесс следующим образом. По функции $\Phi^{(n)}(E)$ найдем новое приближение к точному решению $\Phi^{(n+1/2)}(E)$ с помощью формулы (2). Следующее приближение $\Phi^{(n+1)}$ будем искать в виде:

$$\Phi^{(n+1)}(E) = \Phi^{(n+1/2)}(E) + \sum_{к=0}^{к_{max}} a_к L_к^{(1)}(E)M(E) \qquad (4)$$

Мы исходим из того, что зайделевские итерации (2) быстро сходятся в области больших энергий и медленно при $E \sim кT$. Последний шаг (4) нам необходим для ускорения сходимости итераций в этой области ($E \sim кT$). Для коэффициентов a_n напишем уравнение, минимизируя вариационный функционал, соответствующий уравнению (1). Этот функционал, как легко показать, имеет вид:

$$F(\Phi) = \int_0^{E_{гр}} \frac{dE}{M(E)} \left[\Phi(E)\Sigma_t(E) - \int_0^{E_{гр}} \Sigma_s(E, E')\Phi(E')dE'\right]\Phi(E) - 2\int_0^{E_{гр}} \frac{\Phi(E)S^0(E)}{M(E)}\, dE \qquad (5)$$

Поэтому уравнения для коэффициентов a_n таковы:

$$\frac{\partial F(\Phi^{(n+1)})}{\partial a_к} = 0 \qquad (6)$$

$$к = 1, 2, \ldots, к_{max}$$

Вычислив приближение $\Phi^{(n+1)}$ из уравнений (6), мы повторим итерационный цикл сначала. Он, как показано, состоит из двух этапов:
1-й этап: получение $\Phi^{(n+1/2)}$ (E) из $\Phi^{(n)}$(E) по формуле (2).
2-й этап: получение $\Phi^{(n+1)}$ (E) по $\Phi^{(n+1/2)}$ (E) из уравнений (6).

Построенный итерационный процесс, очевидно, сходится. В самом деле последовательность функций $\Phi^{(0)}$, $\Phi^{(1/2)}$, $\Phi^{(1)}$, ..., $\Phi^{(n)}$, $\Phi^{(n+1/2)}$, $\Phi^{(n+1)}$, ... минимизирует функционал (5): $F(\Phi^{(0)}) > F(\Phi^{(1/2)}) > \ldots > F(\Phi^{(n)}) > F(\Phi^{(n+1/2)}) \ldots$ Мы сознательно не останавливаемся на деталях доказательства сходимости процесса, чтобы более ясно выделить идею метода. Строгую постановку задачи и доказательство сходимости мы отложим до параграфа 4.

Приведем несколько примеров, характеризующих быстроту сходимости итераций (2), (6). Были рассчитаны спектры тепловых нейтронов в среде, заполненной газовым замедлителем (массы M = 1, M = 12) и нерассеивающим поглотителем. Отношение $\Sigma_a(кT)/\xi\Sigma_s$ варьировалось в широком диапазоне:

$$10^{-4} \le \Sigma_a(кT)/\xi\Sigma_s \le 1$$

Во всем интервале концентраций поглотителя скорость сходимости практически является постоянной и зависит только от закона поглощения и массы замедлителя. Рассматривались поглотители: а) с законом поглощения 1/v, б) резонансный поглотитель с поглощением, соответствующим по форме кадмиевому резонансу.

ТАБЛИЦА 1. ЗНАЧЕНИЯ $\lambda_{эфф}$

Поглощение	1/v		резонансное	
Размерность подпространства	M = 1	M = 12	M = 1	M = 12
$к_{max} = 1$	0,17	0,57	0,12	0,56
$к_{max} = 2$	0,12	0,31		
$к_{max} = 5$	0,09	0,24	0,09	0,22

В табл. 1 приведены значения $\lambda_{эфф}$, характеризующие скорость сходимости итераций. $\lambda_{эфф}$ определялось по результатам расчета из соотношения:

$$\int_0^{E_{гр}} \frac{[\Phi^{(n+1)}(E) - \Phi(E)]^2}{M(E)} dE \le \lambda^2_{эфф} \int_0^{E_{гр}} \frac{[\Phi^{(n)}(E) - \Phi(E)]^2}{M(E)} dE \qquad (7)$$

Из таблицы видно, что мы получаем при малых поглощениях колоссальный выигрыш по сравнению с обычным итерационным процессом (2). Следует также отметить, что итерации (2), (6) в действительности сходятся гораздо быстрей, чем это следует из завышенных оценок таблицы 1. В практически встречающихся задачах вклад в решение гармоник, соответствующих собственным числам $\lambda_{эфф}$, как правило, не превышает десятых долей процента. Поэтому для получения решения с точностью порядка 0,1% нужно сделать 3 – 4 итерации. Естественно, это число уменьшается с уменьшением поглощения.

В заключение заметим, что способ построения второго этапа нашего итерационного процесса в очень большой степени произволен. Можно гораздо лучше использовать априорную информацию о спектре, применяя для этого хорошо разработанные в теории термализации полуаналитические методы решения кинетического уравнения. Мы еще раз остановимся на этом в п.4.

3. МЕТОД ГЕРМОГЕНОВОЙ

Уже давно для ускорения итерационного решения задач термализации применяется метод баланса [8]. В этом методе каждое приближенное значение потока $\Phi^{(n+1)}(E)$, полученное в результате обычной итерации нормируется так, чтобы оно удовлетворяло интегральному соотношению баланса. Аналогично [9] ускорялись итерации в задачах с пространственной зависимостью. Метод интегрального баланса довольно эффективен. Однако его сходимость, насколько нам известно, ранее не была доказана. Гермогеновой удалось обобщить интегральный метод баланса и доказать сходимость своего метода для одногруппового кинетического уравнения. Коротко изложим ход ее рассуждений на примере задачи с плоской симметрией.

Пусть в результате обычной итерации получены векторные потоки $\varphi_+^{(n+1)}(x,\mu)$ и $\varphi_-^{(n+1)}(x,\mu)$ для нейтронов, летящих в положительном направлении вдоль оси $x(\varphi_+)$ и обратно (φ_-). Здесь μ косинус угла между направлением скорости нейтрона и осью x. Гермогенова ищет новое приближение $\tilde{\varphi}_+^{(n+1)} = c_+(x)\varphi_+^{(n+1)}(x,\mu)$ и $\tilde{\varphi}_-^{(n+1)} = c_-(x)\varphi_-^{(n+1)}(x,\mu)$, выбирая $c_-(x)$ и $c_+(x)$ так, чтобы минимизировать вариационный функционал Владимирова для плоской задачи [10]. Таким образом, Гермогенова строит последовательность функций, минимизирующих вариационный функционал, и, следовательно, сходящуюся к решению.

Продемонстрируем, как работает та же идея при решении задачи термализации для бесконечной среды. Пусть по формуле (2) мы нашли функцию $\Phi^{(n+1)}(E)$. Следующее приближение $\tilde{\Phi}^{(n+1)}(E)$ ищем в виде $\tilde{\Phi}^{(n+1)} = c\Phi^{(n+1)}$, где c определим, минимизируя вариационный функционал (5). Тогда получим:

$$c = \frac{\int_0^{E_{гр}} [\Phi^{(n+1)}(E)S(E)/M(E)]\,dE}{\int_0^{E_{гр}} dE\{\Sigma_t(E)\Phi^{(n+1)}(E) - \Phi^{(n+1)}(E)\int_0^{E_{гр}} \Sigma_s(E,E')\Phi^{(n+1)}(E')\,dE'\}/M(E)} \qquad (8)$$

Если решается задача с малым поглощением, то в оба интеграла формулы (8) при больших n основной вклад вносит максвелловская часть спект-

ра. Поэтому мы можем приближенно заменить отношение $\Phi^{(n+1)}(E)/M(E)$ единицей. Тогда, используя соотношение детального баланса для сечения рассеяния, получим:

$$c \sim \frac{\int_0^{E_{гр}} S(E)\,dE}{\int_0^{E_{гр}} \Phi^{(n+1)}(E)\Sigma_a(E)\,dE}$$

Отсюда следует, что функция $\widetilde{\Phi}^{(n+1)}(E)$ удовлетворяет приближенно интегральному соотношению баланса:

$$\int_0^{E_{гр}} \Sigma_a(E)\widetilde{\Phi}^{(n+1)}(E)\,dE = \int_0^{E_{гр}} S(E)\,dE$$

Так как по форме спектр довольно быстро приближается к максвелловскому (при обычных итерациях), то балансное соотношение эффективно ускоряет сходимость.

Однако мы привели здесь доказательство Гермогеновой не для того, чтобы обосновать давно практически используемый в теории термализации интегральный метод баланса. В ее рассуждениях нас привлекла открывающаяся возможность объединить обычные универсальные итерационные методы с полуаналитическими методами решения и выводами физического анализа кинетического уравнения теории термализации. В следующем параграфе мы попытаемся осуществить эту программу, сформулировав "принцип безопасности".

4. ПРИНЦИП БЕЗОПАСНОСТИ

Поставим задачу в общем виде.

А. Пусть в гильбертовом пространстве H задан самосопряженный положительно определенный оператор A с областью определения D_A и нам нужно решить уравнение:

$$A\varphi = f \qquad f \in H \tag{9}$$

Этому уравнению, как известно, соответствует вариационный функционал:

$$F(\varphi) = (A\varphi, \varphi) - 2(\varphi, f), \tag{10}$$

для которого справедлив следующий вариационный принцип. Для того, чтобы элемент $\overline{\varphi}$ был решением уравнения (9), необходимо и достаточно, чтобы он сообщал минимум функционалу (10). Любая последовательность элементов $\{\varphi^{(n)}\}$, минимизирующая функционал $F(\varphi)$, сходится к решению $\overline{\varphi}$, т.е. если $\lim_{n\to\infty} F(\varphi^{(n)}) = F(\overline{\varphi})$, то

$$(\overline{\varphi} - \varphi^{(n)}, A[\overline{\varphi} - \varphi^{(n)}]) > m^2(\overline{\varphi} - \varphi^{(n)}, \overline{\varphi} - \varphi^{(n)}) \to 0,$$

где

$$m^2 = \inf\{(A\varphi, \varphi)/(\varphi, \varphi)\}.$$

Б. Допустим, нам известен некоторый итерационный алгоритм:

$$\varphi^{(n+1)} = \varphi^{(n)} + H^{(n)}(f - A\varphi^{(n)}), \tag{11}$$

минимизируя функционал $F(\varphi)$:

$$(A[\varphi^{(n+1)} - \overline{\varphi}], \varphi^{(n+1)} - \overline{\varphi}) < |\lambda^{(n)}|(A[\overline{\varphi} - \varphi^{(n)}], \overline{\varphi} - \varphi^{(n)}), \tag{12}$$

где

$$\sup_n |\lambda^{(n)}| < 1.$$

В. Кроме того, предположим, что мы знаем какой-либо приближенный метод оценки решения уравнения $A\varphi = f$. Другими словами, если задан элемент $f \in H$, мы ставим ему в соответствие другой элемент $\widetilde{\varphi} \in D_A$, который и называем приближенным решением уравнения $A\varphi = f$. Таким образом, мы определяем в H оператор B:

$$\widetilde{\varphi} = Bf \tag{13}$$

Поставим задачу об улучшении итерационного процесса (11) за счет использования априорной информации, получаемой о решении с помощью приближенного уравнения. Обычно трудно оценить степень точности приближенных полуаналитических методов, и тем более, оценок, полученных на основании физического анализа задачи. Поэтому мы должны допускать вероятность сколь-угодно большой ошибки в приближенном решении (особенно, если мы мало доверяем его автору). Так как "улучшенный" итерационный процесс будет реализоваться на вычислительной машине без вмешательства человека, то в нем необходимо заложить возможность отбрасывания негодных оценок, получаемых из приближенного анализа. Учитывая эти замечания, организуем "улучшенный" итерационный процесс так, чтобы на каждом его шаге вариационный функционал по крайней мере не возрастал.

Пусть нам известно приближение с номером n, $\varphi^{(n)}$. По формуле (11) определим новый элемент $\varphi^{(n+1/2)}$:

$$\varphi^{(n+1/2)} = \varphi^{(n)} + H^{(n)}(f - A\varphi^{(n)}) \tag{14}$$

Разность между $\varphi^{(n+\frac{1}{2})}$ и точным решением $\overline{\varphi}$ удовлетворяет уравнению:

$$A[\overline{\varphi} - \varphi^{(n+\frac{1}{2})}] = f - A\varphi^{(n+\frac{1}{2})} = F \tag{15}$$

Оценим ее с помощью приближенного алгоритма B:

$$[\overline{\varphi} - \varphi^{(n+\frac{1}{2})}] \approx \epsilon^{(n+\frac{1}{2})} = BF \tag{16}$$

Следующий элемент минимизирующей $F(\varphi)$ последовательности будем искать в виде:

$$\varphi^{(n+1)} = \varphi^{(n+1/2)} + \alpha \epsilon^{(n+1/2)}, \tag{17}$$

где число α определим, минимизируя функционал $F(\varphi^{(n+1)})$

$$\alpha = \frac{(\epsilon^{(n+1/2)}, f) - (A\varphi^{(n+1/2)}, \epsilon^{(n+1/2)})}{(A\epsilon^{(n+1/2)}, \epsilon^{(n+1/2)})} \tag{18}$$

Если рецепт B для оценки приближенного решения не несет никакой полезной информации, то α обратится в нуль. При этом значение функционала $F(\varphi)$ не изменится. Если рецепт не вреден, число α будет порядка единицы (хотя естественно он может оказаться практически бесполезным, если функционал мало уменьшается).

Таким образом, в результате двух последовательных шагов нашего "улучшенного" итерационного процесса:

1. Функционал $F(\varphi)$ уменьшается, по крайней мере, в $\lambda^{(n)}$ раз, т.е. итерации сходятся к решению.

2. По сравнению с исходным итерационным процессом (11) максимальный проигрыш по числу операций будет не более, чем в два раза, если каждый дополнительный B-шаг окажется неэффективным (естественно, предполагается, что число операций, нужное для определения $\epsilon = BF$, пренебрежимо мало).

3. В случае хорошего алгоритма приближенного решения выигрыш может оказаться очень большим.

Метод, использованный нами для решения уравнения термализации в бесконечной среде, представляет частный случай применения принципа безопасности с несколькими неопределенными коэффициентами. В качестве оператора B там использовалась априорная информация о близости плохо сходящейся при обычных итерациях части спектра к максвелловскому распределению.

Естественно, что мы можем воспользоваться для построения B-шага итерационного процесса услугами нескольких физиков, имеющих различные мнения о приближенном решении задачи и предлагающих различные B-операторы, B_i. В этом случае n+1 приближение для решения ищется в виде*:

$$\varphi^{(n+1)} = \varphi^{(n+1/2)} + \sum_i \alpha_i \epsilon_i, \tag{19}$$

где $\epsilon_i = B_i F$, а неопределенные коэффициенты α_i определяются из условия минимума функционала $F(\varphi^{(n+1)})$:

$$\frac{\partial}{\partial \alpha_i} F(\varphi^{(n+1/2)} + \sum_i \alpha_i \epsilon_i) = 0 \tag{20}$$

$$i = 1, 2, \ldots$$

---

* В качестве неопределенных множителей можно ввести и матричные элементы конечномерных операторов, если искать $\varphi^{(n+1)}$ в виде $\varphi^{(n+1)} = \varphi^{(n+1/2)} + d\epsilon$, где d – конечномерный произвольный оператор.

В задачах теории термализации естественно использовать B-операторы, которые появляются в таких приближенных методах как, например, теория тяжелого газа (в том числе модифицированная), метод перекрывающихся групп, метод эффективной температуры и т.д.

В следующих параграфах мы проанализируем с точки зрения принципа безопасности упомянутые во введении эффективные методы ускорения сходимости Гольдина, Лебедева, Морозова.

5. КР – МЕТОД ЛЕБЕДЕВА [5]

Этот метод оказался очень эффективным при решении односкоростного кинетического уравнения. Применение принципа безопасности позволяет доказать сходимость КР-метода в общем случае и, на наш взгляд, существенно проясняет ее причины.

Как известно, для односкоростного кинетического уравнения можно написать вариационный функционал Владимирова [10], минимум которого реализуется при условии, что минимизирующая функция есть решение кинетического уравнения*. Если записать односкоростное уравнение в самосопряженном виде**:

$$(L_0 - S)u = f, \tag{21}$$

то итерационный процесс

$$u^{(n+1)} = L_0^{-1}Su^{(n)} + L_0^{-1}f \tag{22}$$

минимизирует вариационный функционал

$$F(u) = (L_0u, u) - (Su, u) - 2(u, f) \tag{23}$$

Приняв этот итерационный процесс в качестве основного, построим новый "улучшенный" следующим образом. Будем искать приближение $u^{(n+1)}$, используя результат предыдущей обычной итерации в виде:

$$u^{(n+1)} = u^{(n+1/2)} + \frac{1}{4\pi}\sum_{\kappa=0}^{N}(2\kappa+1)\sum_{i=-\kappa}^{\kappa} a_{\kappa,i}\epsilon_{\kappa,i}(\vec{p})\, Y_{\kappa,i}(\vec{S}), \tag{24}$$

где $Y_{\kappa,i}(\vec{S})$ – сферические гармоники, а $\epsilon_{\kappa,i}(\vec{p})$ пока не известные нам функции. Пользуясь стандартной процедурой получения уравнений сферических гармоник из условий минимизации вариационного функционала, мы получим для функций $\epsilon_{\kappa,i}(\vec{p})$ уравнения в P_{N+1} -приближении. Решив их, найдем новое значение приближенного решения кинетического уравнения $u^{(n+1)}$, которое используем в качестве исходного для следующего шага основного итерационного процесса. Построенный итерационный процесс эквивалентен итерационному процессу Лебедева. При этом доказана его сходимость для более общего случая (среда с разрывами и

---

* Как стало известно автору, Лебедевым получено аналогичное доказательство.

** Все обозначения в этом и следующем параграфах соответствуют обозначениям, принятым в работе [10].

с анизотропным рассеянием). В самом деле, в общих предположениях Владимировым доказано, что уравнения сферических гармоник с естественными граничными условиями получаются из условия минимизации функционала F(u) и, следовательно, построенная последовательность функций $u^{(0)}$, $u^{(\frac{1}{2})}$, ..., $u^{(n+1/2)}$, $u^{(n+1)}$, ... минимизируя функционал F(u), сходится к решению кинетического уравнения.

6. МЕТОД КВАЗИДИФФУЗИИ ГОЛЬДИНА

Не менее эффективным при решении односкоростного кинетического уравнения оказался метод квазидиффузии Гольдина [4]. Поскольку до сих пор не было дано доказательство его сходимости, проанализируем этот метод с точки зрения принципа безопасности.

Ограничимся для простоты рассмотрением односкоростного кинетического уравнения для задачи с плоской симметрией, которое в самосопряженной форме Владимирова имеет вид [10]:

$$-\mu^2\frac{\partial^2 u}{\partial z^2}+u=h(z)\int_0^1 u(z,\mu')d\mu'+\frac{f(z)}{2}, \tag{25}$$

а функция $u(z,\mu)$ связана с потоком нейтронов $\varphi(z,\mu)$ соотношениями:

$$\begin{aligned} u(z,\mu)&=\frac{1}{2}\Big[\varphi(z,\mu)+\varphi(z,-\mu)\Big]\\ -\mu\frac{\partial u}{\partial z}&=\frac{1}{2}\Big[\varphi(z,\mu)-\varphi(z,-\mu)\Big] \end{aligned} \tag{26}$$

Приведем также выражение для вариационного функционала F(u), соответствующего этой задаче:

$$\begin{aligned} F(u)=&\int_{-a}^{a}dz\int_0^1 d\mu\left[u^2(z,\mu)+\mu^2\left(\frac{\partial u}{\partial z}\right)^2\right]\\ &+\int_0^1 d\mu\mu[u^2(a,\mu)+u^2(-a,\mu)]-\int_{-a}^{a}dz\int_0^1 d\mu\int_0^1 d\mu' h(z)\,u(z,\mu)u(z,\mu')\\ &-\int_{-a}^{a}dz\int_0^1 d\mu\,u(z,\mu)\,(f(z)/2)) \end{aligned} \tag{27}$$

Предполагается для простоты, что сечение рассеяния изотропно, источники нейтронов также изотропны, а падающий на границы системы поток равен нулю.

Снова, как и в предыдущем параграфе, организуем улучшенный итерационный процесс, минимизируя на В-шаге вариационный функционал (27) и используя в качестве $u^{(n+1)}$ функцию в виде:

$$u^{(n+1)} = u^{(n+1/2)} + \frac{1}{2}\left[\epsilon_0(z)P_0(\mu) + 5\epsilon_2(z)P_2(\mu)\right] \tag{28}$$

Здесь $P_0(\mu)$ и $P_2(\mu)$ – полиномы Лежандра.
Подставив (28) в выражение для вариационного функционала (27), получим:

$$\begin{gathered}
2F(\epsilon_0, \epsilon_2) = \frac{1}{2}\int_{-a}^{a} dz\left\{\epsilon_0^2 + 5\epsilon_2^2 + \frac{1}{3}\left(\epsilon_0' + 2\epsilon_2'\right) + \frac{9}{7}\left(\epsilon_2'\right)^2\right. \\
\left. - h(z)\epsilon_0^2 - \epsilon_0\tilde{f}\right\} + \int_0^1 d\mu[\epsilon_0(a) + 5\epsilon_2(a)P_2(\mu)]^2 \cdot \mu \\
+ \int_0^1 d\mu\mu[\epsilon_0(-a) + 5\epsilon_2(-a)P_2(\mu)]^2 \\
\tilde{f}(z) = (h(z)/2)\int_{-1}^{1} d\mu[u^{(n+1/2)} - u^{(n)}]
\end{gathered} \tag{29}$$

Теперь мы можем пойти двумя различными путями.

1. Если считать функции $\epsilon_0(z)$ и $\epsilon_2(z)$ независимыми, то минимум функционала $F(\epsilon_0, \epsilon_2)$ реализуется на функциях $\tilde{\epsilon}_0(z)$ и $\tilde{\epsilon}_2(z)$, удовлетворяющих уравнениям Эйлера этой вариационной задачи:

$$-\frac{1}{3}\frac{d^2}{dz^2}\left(\epsilon_0 + 2\epsilon_2\right) + \epsilon_0(1 - h(z)) = \tilde{f}(z)$$

$$-\frac{d^2}{dz^2}\left[\frac{2}{3}\epsilon_0(z) + \frac{55}{21}\epsilon_2(z)\right] + 5\epsilon_2(t) = 0 \tag{30}$$

Но это, не что иное, как P_3 -уравнения KP_3 – метода Лебедева. Естественные граничные условия для этой системы также получаются из условия минимума функционала $F(\epsilon_0, \epsilon_2)$.

2. Второй путь приводит к модифицированному уравнению квазидиффузии, Гольдина. Наложим связь на функции $\epsilon_0(z)$ и $\epsilon_2(z)$, а именно:

$$\epsilon_2(z) = c(z)\epsilon_0(z)$$

Функцию $c(z)$ выберем так, чтобы выполнялось соотношение:

$$\frac{\int_{-1}^{1}\mu^2 u^{(n+1)}\,d\mu}{\int_{-1}^{1} u^{(n+1)}d\mu} = \frac{\int_{-1}^{1}\mu^2 u^{(n+1/2)}d\mu}{\int_{-1}^{1} u^{(n+1/2)}\,d\mu} = D^{(n+1/2)}(z)$$

откуда следует, что

$$c(z) = \frac{u_2^{(n+1/2)}}{u_0^{(n+1/2)}} = \frac{3D^{(n+1/2)} - 1}{2}$$

Итак, мы ищем $(n+1)$ приближение в виде:

$$u^{(n+1)}(z, \mu) = u^{(n+1/2)}(z, \mu) + \frac{1}{2}\epsilon_0(z)[P_0(\mu) + 5c(z)P_2(\mu)]$$

Минимизируя функционал $F(\epsilon_0, c\epsilon_0)$, придем к уравнению Эйлера для минимизирующей функции:

$$-\frac{1}{3}\frac{d^2}{dz^2}\left[\epsilon_0 + 2(\epsilon_0 c)\right] + (1-h)\epsilon_0 - \tilde{f}$$

$$-\frac{2}{3}c\frac{d^2\epsilon_0}{dz^2} - \frac{55}{21}c\frac{d^2}{dz^2}\left(\epsilon_0 c\right) + 5c^2\epsilon_0 = 0. \qquad (31а)$$

Это уравнение назовем модифицированным уравнением квазидиффузии. Построенный итерационный процесс, один цикл которого состоит из обычной итерации по источникам (22) и последующей минимизации функционала $F(\epsilon_0, c\epsilon_0)$, очевидно, сходится. Действительно последовательность функций $u^{(0)}, u^{(1/2)}, \ldots, u^{(n)}, \ldots$ минимизирует функционал, соответствующий поставленной задаче.

Модифицированный квазидиффузионный итерационный алгоритм по существу весьма схож с КР-методом. Однако скорость его сходимости все время возрастает по мере приближения $u^{(n)}(z, \mu)$ к точному решению. Это происходит из-за того, что чем точнее известно отношение $c(z)$, тем с большей точностью определяется $\epsilon_0(z)$.

Вопрос о граничных условиях для модифицированного уравнения квазидиффузии можно решить различными способами. Можно наложить связь на функции $\epsilon_0(\pm a)$, $\epsilon_2(\pm a)$ и получить граничные условия, минимизируя функционал. С другой стороны, так как достаточным условием сходимости итераций является $F(u^{(n+1)}) \le F(u^{(n+1/2)})$, можно положить на границах $\epsilon(\pm a) = 0$.

Связь между модифицированным квазидиффузионным алгоритмом и методом Гольдина очевидна. Покажем это. Будем минимизировать функционал (29), считая $\epsilon_2(z)$ заданной функцией. Тогда для любой $\epsilon_2(z)$ минимальное значение $F(\epsilon_0, \epsilon_2)$ реализуется на функции, удовлетворяющей первому из уравнений (30). Из всех возможных $\epsilon_2(z)$ выберем такую, чтобы между $\epsilon_0(z)$ и $\epsilon_2(z)$ сохранилось соотношение $\epsilon_2 = c\epsilon_0$. Тогда придем к квазидиффузионному уравнению Гольдина [4]:

$$-\frac{1}{3}\frac{d^2}{dz^2}\left(\left[1 + 2c\right]\epsilon_2^{(r)}\right) + \epsilon_0^{(r)}(1-h) = \tilde{f}(z) \qquad (31б)$$

Оно отличается от модифицированного квазидиффузионного уравнения членами, пропорциональными c. Значение функционала $F(\epsilon_0^{(r)}, c\epsilon_0^{(r)})$

заведомо больше, чем то, которое получается при использовании модифицированного уравнения, однако это совсем не означает, что метод Гольдина не является сходящимся. Расчеты, проведенные Гольдиным, показали высокую эффективность метода при решении односкоростных

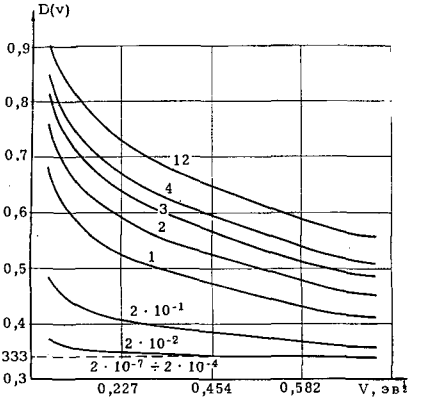

Рис. 1. Максимальные коэффициенты квазидиффузии в системе вода-поглотитель-вода (около каждой кривой указана оптическая толщина поглотителя для тепловых нейтронов).

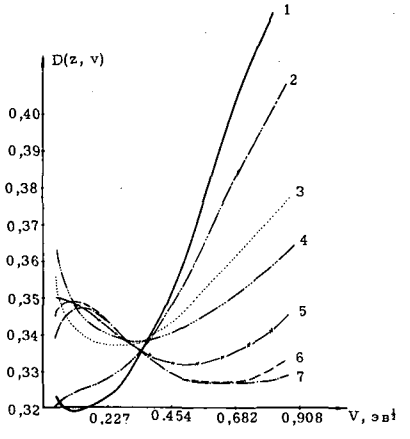

Рис. 2. Коэффициенты квазидиффузии в различных точках системы графит-центральная зона (тяжелый газ с малой плотностью)-вода (T_C=592°K; T_{H_2O} = 300°K). Около каждой кривой указано расстояние от границ графит-центральная зона и центральная зона-вода: 1 – H_2O – 0,1 см; 2 – H_2O – 0,025 см; 3 – центральная зона, 0,325 см от графита; 4 – центральная зона, 0,325 см от воды; 5 – C – 0,25 см; 6 – C – 1 см; 7 – C – 2 см.

задач. Нами была проведена большая серия расчетов с использованием метода Гольдина при решении задач термализации. Во всех случаях был получен существенный эффект ускорения сходимости по сравнению с обычными итерациями по источникам. Почти всегда желаемая точность в 0,1% достигалась после двух-трех итераций. Приведем некоторые иллюстрации. На рис. 1 изображены коэффициенты квазидиффузии:

$$D(z, v) = \int_{-1}^{1} \mu^2 \varphi(z, \mu, v) d\mu \Big/ \int_{-1}^{1} \varphi(z, \mu, v) d\mu,$$

полученные в результате решения ряда типичных задач термализации. На рис. 1 отражена степень анизотропии потока нейтронов в системе

вода-поглотитель при различной оптической толщине поглотителя (от $2 \cdot 10^{-7}$ до 12). Рис. 2 показывает тот же эффект в системе с малым поглощением графит-тяжелый газ с малой плотностью – вода ($T_C = 592°K$, $T_{H_2O} = 300°K$). Выводы о скорости сходимости итераций метода квазидиффузии, в частности, проверялись при изучении этих систем.

В заключение остановимся на методе ускорения сходимости, предложенном Морозовым [7]. Лебедеву удалось показать*, что возможны случаи, когда этот метод не приводит к сходящейся последовательности приближенных решений. Однако, используя принцип безопасности, поправки Морозова можно исправить еще раз так, чтобы гарантировать сходимость метода. В этом случае будут использованы положительные стороны его идеи и одновременно гарантирована сходимость.

ЗАКЛЮЧЕНИЕ

Последние достижения в развитии методов решения кинетического уравнения (обзор библиографии см. во введении) дают надежды на существенный прогресс, который может быть достигнут на пути улучшения численных методов решения задач термализации. При этом возрастает роль физического (полуаналитического) анализа этих задач. Особую важность, на наш взгляд, приобретает в связи с вышесказанным развитие вариационных принципов для кинетического уравнения термализации. Поэтому большую ценность имеют последние результаты Гермогеновой, которой удалось обобщить вариационный принцип Владимирова на случай многоскоростных задач.

ЛИТЕРАТУРА

[1] НЕЛКИН, М., "Термализация нейтронов", Атомиздат, М., 1965, стр. 201.
[2] ЛИНДЕНМЕЙЕР, С.У., Там же, стр. 252.
[3] SELENGUT, D.S., Nucl. Sci. Engng, 9, 94 (1961).
[4] ГОЛЬДИН, В.Я., ЖВМ и МФ 4, 1078 (1964).
[5] ЛЕБЕДЕВ, В.И., ЖВМ и МФ 6, 251 (1966).
[6] МАРЧУК, Г.И., СМЕЛОВ, В.В., ТУРЧИН, В.Ф., ИЛЯСОВА, Г.А., АЭ 13, 534 (1962).
[7] МОРОЗОВ, В.Н., "Теория и методы расчета реакторов". Госатомиздат, М., 1962.
[8] NELKIN, M.S., Nucl. Sci. Engng, 2, 199 (1957).
[9] HONECK, H.C., Nucl. Sci. Engng, 8, 193 (1960).
[10] ВЛАДИМИРОВ, В.С., Труды Математического института им. В.А.Стеклова, LXI, АН СССР, М., 1961.

DISCUSSION

F.C. SHURE: Is the second method equivalent to the use of Newton's method?

L.V. MAIOROV: Yes, indeed. An overall study was made and the specific neutron problems were also suitably investigated. Lebedev studied the transport equations; we examined the thermalization equations. As approximations one could use the heavy-gas equation, the overlapping group method, and so on.

---

* Для самосопряженного уравнения.

О НАХОЖДЕНИИ РЕШЕНИЙ НЕКОТОРЫХ ЗАДАЧ ПЕРЕНОСА

В.И.ЛЕБЕДЕВ
ИНСТИТУТ АТОМНОЙ ЭНЕРГИИ им.И.В.КУРЧАТОВА
МОСКВА,
СССР

(Доклад представил Л.В.Майоров)

Abstract — Аннотация

POSSIBLE SOLUTIONS OF VARIOUS TRANSPORT PROBLEMS. Let $x = (x_1, \ldots, x_q)$, $R_q(x)$ be the q-dimensional space ($q \geq 2$), s be the unit vector, and Ω the surface of the unit sphere.

The problem of solving transport equations with a degenerate scattering indicatrix is a multidimensional problem in $R_q x \Omega$; the nature of these problems calls for rapidly converging iterative methods which do not require all the information on the preceding step. The paper proposes a KP method: the idea consists in solving in R_q simplified problems of error determination using successive iterative steps of decreasing difficulty. Two operations are performed in the KP: the K-operation is a simple iteration in $R_q \times \Omega$ and operation $P = \{P_1(n_1), \ldots, P_\sigma(n_\sigma)\}$ is for the error with $P_k(n_k)$ representing the solution in R_q of the ultimate problem for a differential equation of order $2n_k$. P-operations are found and the convergence of the following methods is studied: $KP_1(n)$, $KP_1(n)P_2(0)$, $K^2P_1(n)$, cyclic $KP_1(1)$ and $KP_1(0)$ etc. For $2\pi T$ periodic problems the convergence is estimated, P(KP) (KP price) and cheap algorithms are found, and the non-improvability is shown. Numerical calculations indicated that the KP method is very efficient.

The Case results are generalized for the q-dimensional case: in $R_q \times \Omega$ a system of solutions is found for a homogeneous single-velocity transport equation with constant coefficients and an isotropic scattering indicatrix

$$\Phi_{\nu\omega}(s) \exp\left(\pm \frac{(x, \omega)}{\nu}\right)$$

These are generalized functions with $\nu \in \{[-1, 1], \pm \nu_0\}$ and $\omega \in \Omega$. Theorems are proved for the completeness of $\{\Phi_{\nu\omega}\}$ in $L_2(\Omega)$, for the partial orthogonality of $\{\Phi_{\nu\omega}\}$ and the possibility of representing $\psi \in L_2(\Omega)$ by $\{\Phi_{\nu\omega}\}$. For $q > 3$ the second component of ν can be missing.

$2\pi T$ periodic solutions of non-homogeneous transport equations are found for cells of different dimensions.

О НАХОЖДЕНИИ РЕШЕНИЙ НЕКОТОРЫХ ЗАДАЧ ПЕРЕНОСА. Пусть $x = (x_1, \ldots, x_q)$, $R_q(x)$ – q-мерное пространство ($q \geq 2$), s – единичный вектор, Ω – поверхность единичной сферы.

Задача решения уравнений переноса с вырожденной индикатрисой рассеяния является многомерной задачей в $R_q \times \Omega$; специфика таких задач требует разработки быстросходящихся итерационных методов, требующих запоминания не всей информации о проведенном итерационном шаге. Излагается КР-метод; идея его состоит в решении в R_q на каждом итерационном шаге последовательности убывающей трудности упрощенных задач для ошибки. В КР выполняется две операции: операция К-простая итерация в $R_q \times \Omega$, и операция $P = \{P_1(n_1), \ldots, P_\sigma(n_\sigma)\}$ для ошибки, здесь $P_k(n_k)$ означает решение в R_q краевой задачи для дифференциального уравнения $2n_k$-го порядка. Найдены операции Р и исследована сходимость методов: $KP_1(n)$, $KP_1(n)P_2(0)$, $K^2P_1(n)$, циклического $KP_1(1)$ и $KP_1(0)$ и др. Для $2\pi T$-периодических задач оценена сходимость, найдены Ц(КР) (цена КР) и дешевые алгорифмы, показана неулучшаемость. Численные расчеты показали высокую эффективность КР-метода.

Обобщены на q-мерный случай результаты Кейса: в $R_q \times \Omega$ найдена система решений однородного односкоростного уравнения переноса с постоянными коэффициентами и изотропной индикатрисой рассеяния

$$\Phi_{\nu\omega}(s) \exp\left(\pm \frac{(x, \omega)}{\nu}\right),$$

* Готическая "а".

являющихся обобщенными функциями, у которых $\nu\in\{[-1,1],\pm\nu_0\}$, $\omega\in\Omega$. Доказаны теоремы о полноте $\{\Phi_{\nu\omega}\}$ в $L_2(\Omega)$, о частичной ортогональности $\{\Phi_{\nu\omega}\}$, о представимости $\psi\in L_2(\Omega)$ через $\{\Phi_{\nu\omega}\}$. При $q>3$ вторая компонента множества ν может отсутствовать.

Найдены $2\pi T$-периодические решения неоднородных уравнений переноса, это решения для ячеек различной формы.

Задача по нахождению решений многогрупповых уравнений переноса с вырожденной индикатрисой рассеяния является типичной многомерной задачей. Как правило, число неизвестных значений функций в системах разностных уравнений, аппроксимирующих кинетические уравнения, столь велико, что при решении этих систем итерационными методами не представляется возможным запоминать все неизвестные, полученные на одном итерационном шаге; следовательно, требуется разработка таких быстросходящихся итерационных методов, которые требовали бы запоминания на каждом итерационном шаге не всей информации о решении, а только части ее существенно меньшей размерности. В докладе излагается предложенный в 1962 – 63 гг. автором КР-метод для решения задач переноса [1 – 4].

1. Условимся о критериях, по которым оценивается качество и сложность алгорифма. Напомним понятия цены и энтропии алгорифма, связанные со временем счета и объемом памяти ЭВМ, необходимыми для выполнения алгорифма.

Цена алгорифма $\mathfrak{A}^*$ для решения задачи $Tu=f$ в пространстве B с точностью ϵ определяется формулой

$$Ц(\mathfrak{A})=Ц(\mathfrak{A}/T,\ B,\ \epsilon)=\sup_{\|f\|=1,\|v\|=1} O(\mathfrak{A}/T,\ B,\ \epsilon), \tag{1.1}$$

где $O(\mathfrak{A}/T,\ B,\ \epsilon)$ – общее число приведенных действий ЭВМ, необходимых для решения алгорифмом $\mathfrak{A}$ задачи T с точностью ϵ в пространстве B, начиная с начального приближения $u^0=u-v$. Если $\mathfrak{A}=\mathfrak{A}(q)$, то $\mathfrak{A}_g=\mathfrak{A}(q_g)$, назовем дешевым, если

$$Ц(\mathfrak{A}_g)=\inf_q Ц(\mathfrak{A}(q)). \tag{1.2}$$

Энтропией $\mathfrak{A}$ назовем величину $Э(\mathfrak{A})=\log_2 N_0(\epsilon)$, где $N_0(\epsilon)=\inf N(\epsilon)$, $N(\epsilon)$ – количество ячеек памяти ЭВМ для хранения промежуточных данных, при котором возможна реализация $\mathfrak{A}$, а нижняя грань берется по всевозможным способам запоминания хранимой информации. Алгорифмы $\mathfrak{A}$ частично упорядочиваются по эффективности в соответствии со значениями некоторого функционала потерь $W(Ц(\mathfrak{A}),\ Э(\mathfrak{A}),\ \epsilon)$.

2. Сформулируем общий вид КР-метода применительно к разностным аналогам задач переноса. Пусть i, к, q, m, σ – целые, E_i – i-мерные пространства, $m\ll q$, $u\in E_q$, y, $f\in E_m$, $y=Su$ и в E_q задана система уравнений

$$L_0u=hy+df. \tag{2.1}$$

Пусть известно, что

$$Ц(SL_0^{-1}hy)=Ц_0,\qquad Ц(hy),\ Ц(df)\ll Ц_0.$$

Требуется решить (2.1) достаточно эффективным алгорифмом $\mathfrak{A}$, для которого

$$Э(\mathfrak{A})\le\log_2 m+O(1).$$

Для этого в E_m строим операторы $T_0 = SL_0^{-1}h$,

$$T_i = (B_i - C_i)^{-1}\,[(B_i - C_i(I - \tau_i))T_{i-1} - C_i\tau_i] \tag{2.2}$$

и уравнения

$$B_i W^{k+i/\sigma} = C_i(W^{k+i/\sigma} + \tau_i(y^{k+i/\sigma} - y^k)),$$

$$y^{k+(1+i)/\sigma} = y^{k+i/\sigma} + W^{k+i/\sigma}, \tag{2.3}$$

$$i = 1, 2, \ldots, \sigma - 1,$$

где операторы B_i, C_i, τ_i выбираем такими, чтобы в E_m

$$Ц((B_i - C_i)^{-1} C_i\tau_i) \ll Ц_0, \qquad B_i^{-1}C_i \approx T_{i-1},$$

$$Э((B_i - C_i)C_i\tau_i) \le \log_2 m + O(1),$$

и одна из норм $T_{\sigma-1}$ была бы мала.

Переход $y^k \to y^{k+1}$ делаем в две операции К и Р.
Операция К:

$$y^{k+1/\sigma} = SL_0^{-1}(hy^k + df). \tag{2.4}$$

Операция $P = (P_1, \ldots, P_{\sigma-1})$ состоит из набора операций P_i, $i = 1, 2, \ldots, \sigma - 1$, каждая из которых состоит в решении i-ой системы (2.3). Тогда $\eta^{k+1} = y - y^{k+1} = T_{\sigma-1}(y - y^k)$ и

$$\|\eta^{k+1}\| \le \|T_{\sigma-1}\|\,\|\eta^k\|. \tag{2.5}$$

За операцию Р может быть взято решение ряда модельных (упрощенных) задач для ошибки η^{k+1}, и если упрощенная задача достаточно хорошо отражает основные свойства задачи (2.1), то выбирая за малую цену на каждом итерационном шаге главную часть ошибки из решения упрощенной задачи, мы получим быстросходящийся КР-метод и

$$Ц(КР) = (Ц(К) + Ц(Р))\,(1 + |\ln\epsilon/\ln\|T_{\sigma-1}\||). \tag{2.6}$$

При типичных предположениях о росте при $\epsilon \to 0$ величин Ц(К), Ц(Р), $\ln\|T_{\sigma-1}\|$ найдены асимптотически дешевые алгорифмы и вычислены их цены. Найдено условие "0" (оптимальности), при котором КР-метод неулучшаем, т.е. $Ц(КР) = O(Ц(К))$ при $\epsilon \to 0$; это условие требует, чтобы $\lim\limits_{\epsilon\to 0} |\ln\epsilon/\ln\|T_{\sigma-1}\||\le \gamma < \infty$; оно накладывает определенные ограничения на вид разностных схем.

3. Пусть $x = (x_1, \ldots, x_q)$, $R_q(x)$ – q-мерное пространство, $q \ge 2$, s – единичный вектор, Ω – поверхность единичной сферы, $E_m(x)$ – m-мерное пространство вектор-функций $\varphi(x, s)$, $A(x) = \{A_1, \ldots, A_m\}$ – диагональная $m \times m$-матрица, $h(x, \mu)$ – $m \times m$-матрица, где $\mu = (s, s')$, $s, s' \in \Omega$, $h(x, -\mu) = h(x, \mu)$.

Рассмотрим m-групповое кинетическое уравнение

$$As\nabla\varphi+\varphi=Sh\varphi+f(x,\ s), \tag{3.1}$$

где

$$S\psi=\frac{\Gamma(q/2)}{(2\pi)^{q/2}}\int\limits_{\Omega}\psi(x,s')\,ds'.$$

Если φ-решение (3.1), то функция

$$u=\frac{1}{2}\Big(\varphi(x,\ s)+\varphi(x,\ -s)\Big)$$

удовлетворяет уравнению

$$-[As\nabla]^2u+u=Shu+F(x,s), \tag{3.2}$$

где

$$F=\frac{1}{2}\Big(f(x,s)+f(x,\ -s)\Big)+\frac{1}{2}As\nabla(f(x,\ s)-f(x,\ -s))$$

и

$$\varphi=u-As\nabla u. \tag{3.3}$$

Пусть для (3.2) поставлена некоторая краевая задача в области $D\in R_q(x)$, тогда рассматривая (3.2) как операторное уравнение, запишем его в виде

$$Lu+u=Shu+F \tag{3.4}$$

и положим $L_0=L+I$, $u_0=y=Su$.

4. Далее мы ограничимся рассмотрением $2\pi T$-периодических задач для $A=\mathrm{const}$, $h=h(x)$; это задачи для ячеек реактора (например, кубической, трехгранной, шестигранной формы) [3]. Пусть T – $q\times q$-матрица, $\det T=1$, $j=(j_1,\ \ldots,\ j_q)$, j_k – целые, $\beta_j=(T^{-1})^*j$, $\lambda_j=|\beta_j|A$, h^{ik} – элементы $h(x)$,

$$r(\lambda)=B_q\int\limits_{-1}^{1}\frac{(1-t^2)^{\rho}\,dt}{1+\lambda^2t^2}, \tag{4.1}$$

где $\rho=\frac{1}{2}\Big(q-3\Big)$, а B_q выбрано из условия: $r(0)=1$. Пусть функция $e(t)$ удовлетворяет условиям: $r(t)\le e(t)\le 1$, а

$$F = \Sigma F_j(s)\exp(i\beta_j x), \qquad F = \{F_j\},$$

$$h^{i'k} = \Sigma h_j^{i'k}\exp(i\beta_j x), \qquad \theta \geq 0,$$

$$\bar{A}(e, \theta) = \{h : [h]_e \leq \theta\}, \tag{4.2}$$

где $[h]_e = \sup_{ij} \sum_n \sum_{k=1}^m |h_n^{ik}|\, e(|\beta_{n+j}|A_k)$.

Для класса матриц $h \epsilon \bar{A}(r, \theta)$, $0 \leq \theta < 1$, найдено при $m \geq 1$, $q \geq 2$ $2\pi T$ – периодическое решение уравнения (3.2). При $h = \text{const}$ это решение запишется в виде:

$$u(x, s) = \Sigma (I + (s, \beta_j)^2 A^2)^{-1}[(I - hr(|\beta_j|A))^{-1} h\psi_j$$

$$+ F_j(s)]\ \exp(i\beta_j x),$$

$$u_0 = Su = \Sigma (I - r(|\beta_j|A)h)^{-1}\psi_j \exp(i\beta_j x), \tag{4.3}$$

где

$$\psi_j = S[(I + (s', \beta_j)^2 A^2)^{-1}\ F_j(s')].$$

Далее для простоты положим $m = 1$, $T = I$ и сформулируем различные варианты КР-метода, которые мы будем обозначать сокращенно, указывая лишь тип операций. Через $P_i(n)$ обозначим операцию P_i в КР-методе, если она сводится к решению в Σ дифференциального уравнения $2n$-го порядка. Обобщения предположенных схем очевидны на более общие краевые задачи для нестационарных или многогрупповых уравнений.

5. $KP_1(n)$-метод. За К берется решение уравнения

$$L_0 u^{k+1/2} = hu_0^k + F, \qquad u_0^{k+1/2} = Su^{k+1/2}$$

за $P_1(n)$-решение в Σ сильно эллиптического уравнения $2n$-го порядка при однородных краевых условиях:

$$Q_n W^{k+1/2} = P_n(hW^{k+1/2} + f_1) \tag{5.1}$$

где Q_n, P_n – дифференциальные операторы, а $f_1 = h(u_0^{k+1/2} - u_0^k)$. За Q_n, P_n могут быть взяты операторы метода сферических гармоник, P_{W1}-уравнений [2] и т.д.

Пусть $\|f\| = \max_n |f_n e^{-1}(\lambda_n)|$, $Q_n(t)$, $P_n(t)$ – полиномы степени n, $n-1$ относительно t^2, $P_n(0) = 1$ и $P_n(t) \geq 0$, $e(t)Q_n(t) - QP_n(t) > 0$ при $t^2 \geq 0$, $0 \leq \theta < 1$. За операцию $P_1(n)$ примем решение 2π-периодической задачи для (5.1) при $Q_n = Q_n(A_i\Delta^{1/2})$, $P_n = P_n(A_i\Delta^{1/2})$. Пусть $h \epsilon \bar{A}(e, \theta)$,

$$\psi(t) = (r - Q_n^{-1}P_n)(e - \theta Q_n^{-1}P_n)^{-1}, \qquad \|\psi\| = \max_t |\psi|,$$

$$E_n(e, \theta) = \inf_{Q_n, P_n} \|\psi\|, \qquad \eta^k = u_0 - u_0^k = \Sigma \eta_j^k \exp(i\beta_j x)$$

тогда

$$\|\eta^k\| \leq (\|\psi\|\theta)^k \|\eta^0\|. \tag{5.2}$$

Справедливы следующие утверждения:

1. Если $Q_n^{-1}P_n \le (e+r)(1+\theta)^{-1}$, то $\|\psi\| \le 1$, $E_n(e, \theta) \le 1$ при $n \ge 1$;
2. задача (5.1) с Q_n, P_n, реализующими $E_n(e, \theta)$, разрешима;
3. $E_n(e, \theta') \le E_n(e, \theta)$ при $0 \le \theta' \le \theta$; $E_n(e', \theta) \le E_n(e, \theta)$ при $e \le e' \le 1$.
4. если $Q_n(0) = 1$, то $KP_1(n)$-метод является балансным методом.

Подсчитано, что для балансных схем при $q = 3$ $E_1(1,1) = 0.186$; $E_2(1,1) = 0.029$; $E_1(1,0.99) = 0.172$; $E_2(1,0.99) = 0.027$. Для P_1 и P_2 -приближения метода сферических гармоник $\|\psi\| \le 0.23$, 0.11 соответственно. Для построения полиномов $Q_n(t)$, $P_n(t)$ предлагается алгорифм, основанный на разложении функции $r(t)$ в цепную дробь:

$$r(t) \approx P_n(t)/Q_n(t) \tag{5.3}$$

тогда $\|\psi\| \le 0(n^{-1+\beta})$, $0 \le \beta < 1$, для функций $e(t)$, убывающих как $0(t^{-\beta})$ при $t \to \infty$. При $h = \text{const}$ найдены асимптотически дешевые по n алгорифмы $KP_1(n)$-метода, для которых при $\epsilon \to 0$

$$Ц(KP_1(n_g)) \sim (1+\gamma)Ц(K)$$

при этом

$$n_g \sim 0(\gamma^2 \epsilon^{-1/\gamma} |\ln\epsilon|^{-1}(1+\gamma)^{-1}).$$

Рассмотрим варианты при $\sigma \ge 2$, в которых ускорение сходимости достигается за счет применения дополнительных сравнительно нетрудоемких операций. Пусть $q = 3$, $h = \text{const}$, $e \equiv 1$, α_k означает меняющийся с периодом N числовой параметр, $T_W(x)$-полином Чебышева 1-го рода на $[-1,1]$ N-ой степени, y_i – корни $T_W(x)$, $Q_W = |T_W(y_0)|^{-1}$, где $|y_0| > 1$. Для периодических задач будут справедливы равенства: $\eta_n^{k+1} = V(n)\eta_n^k$.

6. $KP_1(n)P_2(0)$-метод: $\sigma = 3$, операция $P_1(n)$ имеет вид:

$$Q_n W^{k+1/3} = P_n(hW^{k+1/3} + h(u_0^{k+1/3} - u_0^k)),$$

$$u_0^{k+2/3} = u_0^{k+1/3} + W^{k+1/3}.$$

Операция $P_2(0)$ имеет вид:

$$W^{k+2/3} = (1 - \alpha_k h)^{-1} \alpha_k h(u_0^{k+2/3} - u_0^k),$$

$$u_0^{k+1} = u_0^{k+2/3} + W^{k+2/3}.$$

Тогда, если $\alpha_k = \frac{1}{2}\Big(M + m + (M - m)y_k\Big)$, где $M = \max_t \psi(t)$, $m = \min_t \psi(t)$, то

$$|\eta_n^{k+w}| \le \theta_N |\eta_n^k|, \tag{6.1}$$

где $y_0 = (2 - (M+m)h)((M-m)h)^{-1}$.

Так при $n = 1$, $N = 1$, $Q_1(t) = t^2/3 + 1$ имеем $\theta_1 < h(8, 8 - h)^{-1}$.

7. K^2P-метод: в нем за один итерационный шаг делается две операции K и одна операция P. Так как собственные числа операций K^2 и $P_1(n)$ убывают асимптотически одинаково, то экономя на операциях P, можно добиться хорошей сходимости.

а) $K^2P_1(n)$-метод:

$$u_0^{k+1/3} = SL_0^{-1}(hu_0^k + F),$$

$$u_0^{k+2/3} = SL_0^{-1}(hu_0^{k+1/3} + F),$$

$$Q_n W^{k+2/3} = P_n h^2 (W^{k+2/3} + (u_0^{k+2/3} - u_0^k)),$$

$$u_0^{k+1} = u_0^{k+2/3} + W^{k+2/3}.$$

Так при $P_1(t) \equiv 1$, $Q_1(t) = 1 + q_{11}t^2$, $q_{11} = 2/3$ имеем $|V(n)| \le 0.049h^2$, а при $q_{11} = 0{,}643$ – $|V(n)| \le 0.038h^2$.

б) $K^2P_1(n)P_2(0)$-метод:

$$u_0^{k+1/4} = SL_0^{-1}(hu_0^k + F), \quad u_0^{k+1/2} = SL_0^{-1}(hu_0^{k+1/4} + F),$$

$$Q_n W^{k+1/2} = P_n h^2 (W^{k+1/2} + (u_0^{k+1/2} - u_0^k)),$$

$$u_0^{k+3/4} = u_0^{k+1/2} + W^{k+1/2},$$

$$W^{k+3/4} = (1 - \alpha_k h^2)^{-1} \alpha_k h^2 (u_0^{k+3/4} - u_0^k),$$

$$u_0^{k+1} = u_0^{k+3/4} + W^{k+3/4}.$$

Тогда при $\alpha_k = \frac{1}{2}\left(M_1 + m_1 + (M_1 - m_1)y_k\right)$, где $M_1 = \max_k \gamma_k$, $m_1 = \min_k \gamma_k$, а γ_k – собственные значения операции $K^2P_1(n)$, справедливо (6.1) при

$$y_0 = (2 - (M_1 + m_1)h^2)h^{-2}(M_1 - m_1)^{-1}.$$

Так, если $n = 1$, $q_n = 2/3$, то $|y_0| \ge 41h^{-2} - 1$, т.е. $\theta_1 \le h^2(41 - h^2)^{-1}$ для $N = 1$.

в) Обобщениями предложенных методов являются $S_e(K)P_1(n)$ и $S_e(K)P_1(n)P_2(0)$-методы, где $S_e(t)$ – полином e-ой степени. Эффективность этих методов зависит от соотношения между порядком аппроксимации функции $S_e(r(t))$ дробно-рациональными функциями P_n/Q_n и величиной $Ц(S_e(K) \sim \ell Ц(K)$.

8. $(K^2P_1(1))^m KP_2(n)$-метод. Операция $P_2(n)$ выполняется с Q_n, P_n, определенными в (5.3). Исследован вопрос о выборе фиксированной операции $P_1(1)$ и оптимальном выборе m как функции от n. Операция $P_1(1)$ задается операторами (см. (2.3))

$$B_1 = Q_1 = -\frac{4}{\pi^2}A^2\Delta + I, \qquad C_1 = P_1 h^2 = h^2 I, \qquad \tau_1 = I.$$

Показано, что при $m \sim \frac{1}{6}\ln n$ уменьшение ошибки на одну произведенную операцию K будет оптимальным, ошибка уменьшится в $O((n^{-1}\ln n)^{3/2} h)$ раза.

9. Циклический $KP_1(1)$-метод: считаем, что $P_1(t) \equiv 1$, $Q_1(t) = 1 + \alpha_k t^2/3$. На классе функций

$$H(C, \beta) = \{f : |f_n| \le c|n|^{-\beta}, n \ne 0, \beta \ge 0\}$$

оптимальные значения α_k определяются формулой:

$$\alpha_k = \left\{\frac{1+y}{2} : P_N^{(0,2(N+\beta))}(y) = 0\right\},$$

где $P_N^{(\alpha,\gamma)}(y)$ – полином Якоби. Тогда в (6.1)

$$\theta_N \le \frac{\Gamma(N+1)\Gamma(2N+2\beta+1)}{\Gamma(3N+2\beta+1)} \sim 2\sqrt{\frac{\pi}{3}}\left(\frac{2}{3}\right)^{2\beta} N^{1/2}\left(\frac{4N(N+\beta)^2 h}{(3N+2\beta)^3}\right)^N.$$

Указанный выбор α_k обеспечивает оптимальную сходимость метода на классе $H(c, \beta)$ в метрике, порожденной некоторым квадратичным функционалом. Если $F \in L_2(D) \cap H(c, \overline{\beta})$, то $\beta = \overline{\beta} + 1$. Для значений α_k справедливы асимптотические формулы:

$\alpha_k = \cos^2\frac{\theta_k}{2}$, где $\theta_1 = j_1(N(3N+2(1+\beta)) + \beta + 1/3)^{-1/2}$, j_1 – первый корень функции Бесселя $J_0(x)$, а при $K \ge 2$:

$$\theta_k = \theta_{k-1} + \pi g(\overline{\theta}_k), \qquad \overline{\theta}_k = \theta_{k-1} + \frac{\pi}{2} g\left(\theta_{k-1}\right),$$

где

$$g(\theta) = \left((3N+2\beta+1/2)(N+1/2) + \frac{1}{4\sin^2\theta} - (N+\beta)^2 \operatorname{tg}^2\frac{\theta}{2}\right)^{-1/2}$$

Аналогичным образом исследуется циклический $K^2P_1(1)$-метод, в нем оптимальные коэффициенты α_k выражаются через корни полинома $P_N^{(0,4N+2\beta)}(y)$.

10. Факторизованные операции P. Поскольку главную трудность в операции P составляет обращение оператора $R = Q - Ph$, то можно рассмотреть факторизованные операторы R, представимые в виде произведения одномерных дифференциальных операторов, тогда цена операции R^{-1} заметно снизится. Расчеты множителей сходимости в KP_1 и K^2P_1-методах для двумерных задач с использованием одномерных дифференциальных параметров 2-го порядка показали, что, например, для $h = 0.9$ ошибка уменьшается соответственно в 0.24; 0.14 раза.

11. Обобщены на q-мерный случай результаты Кейса [5]: найдена система решений однородного уравнения (3.1) при $h = \text{const}$, $A = \text{const}$, $m = 1$. Эти решения имеют вид:

$$\Phi_{\nu\omega}(s)\exp\left(\pm\frac{(x, \omega)}{A\nu}\right),$$

где ν-числовой параметр, а $\omega\in\Omega$. Функции $\Phi_{\nu\omega}$ являются обобщенными функциями, величина $\nu\in\mathcal{N}$, где $\mathcal{N}$-множество, состоящее вообще говоря из двух компонент: отрезка $[-1, 1]$ и двух точек $\pm\nu_0\notin[-1,1]$; при $q>3$ и достаточно малом $h>0$ второй компоненты у $\mathcal{N}$ нет. Решения, соответствующие значениям $\pm\nu_0$, имеют вид

$$\psi_{0\pm}(x, (s, \omega)) = \Phi_{0\pm}((s, \omega)) \exp\left(\pm\frac{(x, \omega)}{A\nu_0}\right),$$

где

$$\Phi_{0\pm}(\mu) = \frac{h\nu_0}{\nu\pm\mu},$$

а ν_0^{-1} – корень уравнения $hr(i\mu) = 1$, в котором взята та ветвь функции $r(t)$, для которой $r(0) = 1$; для $\nu\in[-1, 1]$ решения имеют вид:

$$\psi_\nu(x, (s,\omega)) = \Phi_\nu((s, \omega)) \exp\left(-\frac{(x, \omega)}{A\nu}\right),$$

где

$$\Phi_\nu(\mu) = P\frac{h\nu}{\nu-\mu} + \frac{\lambda(\nu)\delta(\mu-\nu)}{B_q(1-\nu^2)^\rho},$$

под Pf понимается регуляризированное значение f,

а
$$\lambda(\nu) = 1 - hB_q P\int_{-1}^{1}(1-\mu^2)^\rho/(\nu-\mu)d\mu,$$

справедливы.

Теорема 1. Для любого фиксированного $\omega\in\Omega$ и ν, $\nu'\in\mathcal{N}$

$$S\Big((s',\omega)\Phi_\nu((s', \omega))\,\Phi_{\nu'}((s', \omega)\Big) = 0 \qquad \text{при} \qquad \nu\neq\nu'.$$

Теорема 2. Система функций $\Phi_\nu((s, \omega))$, где $\nu\in\mathcal{N}, \omega\in\Omega$, образует полную систему функций в пространстве $L_2(\Omega)$.

По теореме 2 для любой $f(s)\in L_2(\Omega)$ найдутся такие функции $f_i(s) = 1, 2, 3$, $A(\nu)$, что функция

$$\psi(x, s) = S\Big[f_1(s')\Phi_{0+}((s, s'))\exp\left(-\frac{(s', x)}{A\nu_0}\right)$$
$$+ f_2(s')\Phi_{0-}((s, s'))\exp\left(\frac{(s', x)}{A\nu_0}\right)$$
$$+ f_3(s')\int_{-1}^{1}A(\nu)\Phi_\nu((s, s'))\exp\left(-\frac{(s', x)}{A\nu}\right)d\nu\Big]$$

является решением однородного уравнения (3.1) и $\psi(0, s) = f(s)$. Аналогичные результаты получены для однородного уравнения (3.2).

12. Пусть в произвольной выпуклой области D с кусочно гладкой границей рассматривается основная краевая задача переноса [6], коэффициенты кинетического уравнения предполагаются кусочно непрерывными функциями, а индикатриса рассеяния – четной по (s, s') функцией. Пусть за операцию P_1 взято решение P_{2n-1} -уравнений метода сферических гармоник с граничными условиями Маршака-Владимирова [6]. При ограничениях, наложенных на коэффициенты уравнения в п.16 работы [6], доказана сходимость построенного таким образом KP_1 -метода.

ЛИТЕРАТУРА

[1] ЛЕБЕДЕВ В.И., Метод характеристик для решения кинетического уравнения. Журн. вычисл. матем. и матем. физ., 6, 2 (1966) 251 – 275.

[2] ЛЕБЕДЕВ В.И., О КР-методе ускорения сходимости итераций при решении кинетического уравнения. Сборник "Численные методы решения задач матем. физ." М., "Наука", 1966.

[3] ЛЕБЕДЕВ В.И., О нахождении решений кинетических задач. Журн. вычисл. матем. и матем. физ., 6, 5 (1966) 895 – 912.

[4] ЛЕБЕДЕВ В.И., Итерационный КР-метод. Доклад на ICM (тезисы), М, 1966, Вычислительная матем., 14 (1966) 40.

[5] CASE M.K., Elementary Solutions of the Transport Equations and Their Applications. Ann. Phys. 9 (1960).

[6] ВЛАДИМИРОВ В.С., Математические задачи односкоростной теории переноса частиц. Тр. Матем. ин-та АН СССР, т.XI, 1961.

DECAY OF A THERMAL NEUTRON PULSE IN A FINITE COHERENT MODERATOR

V. ARDENTE AND G. ROSSI
CENTRE COMMUN DE RECHERCHE, EURATOM,
ISPRA, ITALY

Abstract

DECAY OF A THERMAL NEUTRON PULSE IN A FINITE COHERENT MODERATOR. To investigate the problem of the approach to equilibrium of a fast neutron pulse in a finite crystalline medium a phenomenological description of the decay process has been worked out, based on the concept of the energy-dependent neutron mean life. The time evolution of the neutron flux can be represented for $t > \bar{t}$ ($\bar{t}$ is connected with the time at which the thermal pulse is fully built up) by means of the ansatz $\varphi(E,t) = f(E) \exp[-\lambda(E)t]$. The same time moments of order 0 and 1 as in the rigorous solution of the time-dependent Boltzmann equation are imposed on this flux. The functions $f(E)$ and $\lambda(E)$ are thus obtained and from these the time evolution of the instantaneous slope of the so-called decay curve for the neutron population in the assembly considered (effective decay constant) is evaluated. The time moments are solutions of stationary Boltzmann equations and for this reason these functions can be determined by means of a suitable calculational method for stationary neutron spectrum problems. This approach has been used to analyse the decay process of a neutron pulse in coherent solid moderators, such as beryllium and graphite. For each of these moderators blocks of various dimensions have been considered, on which pulsed neutron measurements have been performed. The time moments $m_0(E)$ and $m_1(E)$ have been determined by means of the code GATHER in the framework of the $D(E)B^2\,\varphi(E,t)$ approximation for the leakage term of the Boltzmann equation. The 101 group energy scheme of GATHER has been adapted to the particular problem, which requires a very detailed analysis at very low energies (down to 0.5×10^{-4} eV). For the scattering kernel the incoherent approximation has been used, as given by the phonon expansion in the form contained in the SUMMIT code. Interference effects have been taken into account by evaluating the elastic (zero-phonon) term of the polycrystalline coherent scattering cross-section for a hexagonal lattice. To analyse the sensitivity to the details of the moderator dynamics of such integral quantities as the total neutron density and the effective decay constant, as a function of time, the same calculations have been made as for the case with the free-gas scattering matrix.

Our approach succeeds in predicting the experimental time evolution of the total neutron density for the cases in which a comparison has been possible. More generally it allows a deeper analysis of the moderator dynamics effects on the approach to equilibrium of the neutron pulse.

1. INTRODUCTION

A considerable amount of theoretical effort has been devoted in the last few years to the interpretation of pulsed neutron (die-away) experiments in finite crystalline moderators. Generally the discussion has been focused on the apparent contradiction between the results of die-away time measurements in beryllium and some properties of the eigenvalue spectrum of the Boltzmann operator [1, 2]. Lately the situation has been clarified, at least partly, on the basis of two simple considerations of a physical nature:

(a) The measured quantities (decay-constants) and the results of the mathematical analysis (eigenvalues of the Boltzmann operator) are, strictly speaking, two different things [3, 4].

(b) Experimental data in the case of small moderator blocks lead to decay curves, which are too poorly defined near the end of the observation time interval [5].

It is the authors' aim here to show that all the experimental results concerning decay curves for the neutron density and decay constants can be explained in a rather satisfactory way in the framework of the Boltzmann neutron transport equation. The calculations are based on a phenomenological model which retains the physical details of the approach to equilibrium of the neutron pulse [4]. More precisely our results indicate that, during the time which is usually considered by the experimentalist as long enough for a pure fundamental decay mode to appear, the pulse in a block of dimensions below a certain value is far from its asymptotic behaviour. As a consequence the decay constant during this time is time-dependent and the die-away time deduced from the data is always to be considered as a time-average.

Both the asymptotic behaviour and the time evolution of the pulse are strongly dependent on the moderator dynamics. Nevertheless an average value of the decay constant over the time interval during which measurements are performed turns out to be rather insensitive to the scattering model. The coarse nature of this quantity is clearly brought out by the fact that a quite satisfactory agreement with the experimental data is obtained even using a free-gas model, except of course in the case of very small samples.

A short description of the model is given in section 2, some details of the calculational method, with particular emphasis on the scattering matrices, in section 3 and finally numerical results and the conclusions that can be drawn from their analysis in section 4.

2. THE MODEL

The time evolution of a neutron pulse in a finite crystalline assembly can be analysed in terms of eigenvalues and eigenfunctions of the Boltzmann operator, or, alternatively, by means of a numerical solution of the time-dependent Boltzmann neutron transport equation [6-8]. A very detailed analysis of the energy exchange phenomena between neutrons and moderator at low energies is necessary; as a consequence, both methods lead to rather heavy calculational procedures. In particular, for the numerical analysis of the continuous spectrum, which, as is well known, plays an essential role here, one is faced with a series of delicate numerical problems which seem to have been dealt with only recently in a satisfactory way [9].

Our aim was to work out a simplified method for evaluating the energy-integrated neutron density in a finite crystalline moderator as a function of time, bearing in mind, however, all the physical details of the moderator dynamics down to very low energies. To accomplish this we introduced an energy-dependent decay constant, which takes into account in a phenomenological way the effect of the superposition of discrete and continuous decay modes on the time evolution of the neutrons belonging to a certain energy group. This is equivalent to assuming the following ansatz for the time and energy-dependence of the neutron flux:

$$\varphi(E, t) = f(E)e^{-\lambda(E)t} \tag{1}$$

Obviously such an assumption can be considered as a reasonable one only for $t > \bar{t}$ ($\bar{t}$ is connected with the time at which the thermal neutron pulse

is fully built up). To determine the functions f(E) and λ(E) we imposed on the flux (1) the same time moments of order 0 and 1 as for the rigorous solution of the time-dependent Boltzmann equation. We obtained

$$[\lambda(E)]^{-1} = \frac{\int_0^\infty t\varphi(E,t)dt}{\int_0^\infty \varphi(E,t)dt} \equiv \frac{m_1(E)}{m_0(E)} \equiv \tau(E)$$

$$f(E) = \frac{1}{\tau(E)} \int_0^\infty \varphi(E,t)dt \qquad (2)$$

where $\tau(E)$ is the so-called emission time for the neutrons of energy E in the assembly considered. From Eqs. (1) and (2) we found the activation of a 1/v neutron detector placed in the assembly, and eventually the quantity

$$\lambda_{eff}(t) = \frac{\int_0^\infty \frac{1}{\tau(E)} f(E)\, e^{-\frac{t}{\tau(E)}} \frac{1}{\sqrt{E}} dE}{\int_0^\infty f(E)\, e^{-\frac{t}{\tau(E)}} \frac{1}{\sqrt{E}} dE} \qquad (3)$$

i.e. the effective decay constant as a particular average value of the inverse neutron mean lifetimes.

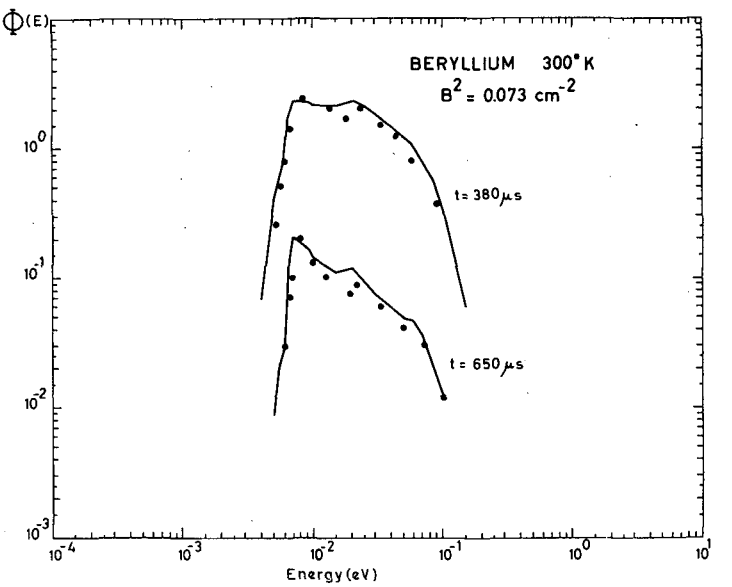

FIG. 1. Time-dependent spectra in beryllium. Experimental points from Ref. [10]. The times given are the mean chopping times.

To illustrate the reliability of the ansatz (1) a comparison between calculated and measured neutron spectra in a beryllium block ($B^2 = 0.073\ cm^{-2}$) at times $t = 378\ \mu s$ and $t = 649\ \mu s$ after the pulse is shown in Fig. 1. The calculations were performed on the basis of Eqs. (1) and (2) by the method to be described in section 3. The measurements are those of Gaerttner et al. at Rensselaer Polytechnic Institute [10]. The experimental points are from an average over the time interval in which the neutron chopper was open ($\approx 120\ \mu s$), while the theoretical curve corresponds to a well-defined time. For this reason a normalization procedure was repeated for each curve, with $E = 0.006$ eV as reference point. One can see that within the above-mentioned limits the agreement is quite satisfactory.

3. THE CALCULATIONAL METHOD

The time moments $m_0(E)$ and $m_1(E)$ are obtained by solving numerically two stationary Boltzmann equations, which in the diffusion approximation with space-energy separability read as follows:

$$[D(E)B^2 + \Sigma_a(E) + \Sigma_s(E)]\, m_0(E) = \int_0^\infty \Sigma_s(E' \to E) m_0(E') dE' + S(E)$$

$$[D(E)B^2 + \Sigma_a(E) + \Sigma_s(E)] m_1(E) = \int_0^\infty \Sigma_s(E' \to E) m_1(E') dE' + \frac{1}{v}\, m_0(E) \tag{4}$$

where $D(E) \equiv \{3[\Sigma_a(E) + \Sigma_s(E)]\}^{-1}$, B^2 is the fundamental eigenvalue of the Helmholtz equation for the geometry being considered and $S(E)$ the energy distribution of the source.[1]

To analyse the decay of a thermal neutron pulse in beryllium and graphite blocks of various dimensions, we have utilized the code GATHER [11], which solves Eqs. (4) in a 101 energy group scheme. The original mesh-points distribution of the GATHER library has been modified to describe in detail the low-energy region (down to 0.5×10^{-4} eV) and the region of the Bragg peaks; of the 101 groups about 30 are below the Bragg cut-off.

According to our fundamental assumption, Eq. (1), the origin of the time scale for our calculations is the time at which the thermal pulse is fully built up. As a consequence the source term in the first of Eqs. (4) should be a thermal energy distribution of more or less Maxwellian shape, as the experiments also indicate [5]. The temperature of such a Maxwellian distribution can be somewhat greater than the physical temperature of the moderator for blocks of small dimensions. Consequently we have introduced as a source in GATHER a Maxwellian density at the

[1] The correct time-dependent P_1 approximation leads to time-moment equations which differ from Eqs. (4) only in the source term of the second equation. The correction is of the order $\frac{D(E)B^2}{\Sigma_{tot}(E)}$, i.e. it is not negligible only in a restricted energy interval below the Bragg cut-off, where the diffusion approximation itself is not adequate.

physical moderator temperature (300°K) for all cases, except the greatest buckling values, for which (according to the indications of the measurements of Gaerttner et al. [10]) a temperature of 500°K has been adopted. As a matter of fact, the influence of the source temperature on the results is not negligible, but this uncertainty only affects the cases in which the measurements are less accurate. On the basis of the experimental information quoted, we can conclude that the origin of our time scale corresponds to $t \approx 150\ \mu s$ after the pulse for beryllium and $t \approx 500\ \mu s$ for graphite.

To analyse the sensitivity of integral quantities such as the total neutron density and the effective decay constant as a function of time, to the details of the moderator dynamics, the calculations have been performed for each moderator, both with the free-gas scattering matrix and taking into account all the details of the crystal dynamics.

The scattering kernel from polycrystalline beryllium was calculated at room temperature in the energy range 0.5×10^{-4} eV to 2.38 eV, on the basis of the following assumptions:

(i) For the contribution to the scattering from inelastic processes we have used the incoherent approximation as given by the phonon expansion in the form contained in the SUMMIT code [12], which gives the terms corresponding to phonon exchange, once the phonon frequency distribution $f(\omega)$ is known. The $f(\omega)$ function used was that obtained theoretically from a central force model [13].

(ii) Interference effects, giving rise to Bragg peaks, have been taken into account by evaluating the elastic (zero-phonon) term of the polycrystalline coherent scattering cross-section for a hexagonal lattice [14].

Only P_0 contributions have been considered. The value of $[v\Sigma_{tot}(E)]_{min.}$ for a density of 1.85 g/cm^3 is 4060 s^{-1}. The absorption cross-section has been taken as $1/v$ and normalized to 10 mb for $v = 2.200$ m/s. The total cross-section deduced on the basis of this model agrees very well with the experimental data reported in BNL-325, practically for the whole energy range.

For graphite, the 101×101 scattering matrix was calculated by means of a similar calculational procedure, both for incoherent and coherent terms. Compared with the previous one this calculation differs only in two points. Firstly, due to the highly anisotropic nature of vibrations in a graphite lattice, we have considered separately the parallel and perpendicular phonon spectra with respect to the hexagonal planar streets containing carbon atoms in graphite. Thus, the scattering kernel was obtained by averaging over orientations of the crystal. Secondly, the energy range was divided in two regions, 0.5×10^{-4} eV $< E <$ 1 eV and 1 eV $< E <$ 2.38 eV. Only in the first region was the matrix calculated, by taking into account the detailed crystalline structure, both for inelastic (incoherent approximation) and elastic (zero-phonon coherent term) scattering. In the high-energy region the scattering was evaluated on the basis of a free-gas model at an effective temperature

$$T_{eff} = \frac{1}{2} \int_0^{\omega_{max.}} f(\omega)\,\omega \coth\left(\frac{\omega}{2T}\right) d\omega$$

where

$$f(\omega) = \frac{1}{3} f_{\perp}(\omega) + \frac{2}{3} f_{\parallel}(\omega)$$

TABLE I. THEORETICAL AND EXPERIMENTAL DECAY CONSTANTS (s^{-1})

B^2 (cm^{-2})	Free-gas model	Crystalline model	Only inelastic	Lee and Daitch[a]		Experimental
				(A)	(B)	
0.025	2868	3243	-	3155	3242	3636
0.073	7668	7682	8776	7091	7728	9090
0.12	11559	10283	-	10156	11251	13333

[a]The results of Lee and Daitch [9] were obtained from the graphical plot of N(t) on the basis of the following hypotheses:
(A) Zero-flux boundary condition, bound-atom kernel normalization
(B) Zero-flux boundary condition, BNL-325 kernel normalization
These theoretical values and the experimental ones correspond to: $B^2 = 0.0263\ cm^{-2}$, $B^2 = 0.0753\ cm^{-2}$, $B^2 = 0.124\ cm^{-2}$.

This temperature, deduced from the average kinetic energy corresponding to the phonon spectrum of crystalline graphite, is equal to 702°K.

The phonon spectra $f_{\perp}$ and $f_{\parallel}$ were those calculated by means of the root sampling technique of Young and Koppel [15], which is much more accurate and detailed than the extrapolation technique in which the phonon spectrum is obtained directly from neutron scattering measurements.

The total cross-section deduced in this way is in quite good agreement with experimental BNL-325 data, apart from the very low energies below the first Bragg peak where it is smaller than the experimental total cross-section (which is very poorly known for that region) (A similar situation was found by Ghatak and Honeck [6] who used the Park's model for graphite). The value $[v\Sigma_{tot}(E)]_{min}$ is 765 s^{-1} for a density of 1.651 g/cm^3 and a 1/v absorption cross-section normalized to 4 mb for v = 2.200 m/s), but this fact could influence to some extent only the asymptotic behaviour of the pulse.

4. RESULTS AND CONCLUDING REMARKS

The results shown in the figures concern the following quantities:

(a) Neutron density as a function of time (Figs. 2, 3)

(b) Effective decay constant as a function of time (Figs. 4, 5)

(c) Mean effective decay constant as a function of buckling (Figs. 6, 7).

The last quantity has been obtained by averaging the effective decay constant over the time interval of the measurements. For beryllium this extends in all cases up to $t \approx 1.5$ ms after the pulse; for graphite it covers three or four decay times starting after a waiting time which depends on the block dimensions.

In Table I a comparison between the results of our calculations for beryllium with those from various scattering models and those recently published by Lee and Daitch [9] is shown. The experimental values for high bucklings quoted by these authors are deduced from decay curves in a time interval smaller than the total measurement time. This fact could explain the systematic under-evaluation of our mean values with respect to the experimental ones.

Some direct remarks can be made from an analysis of these results. The behaviour of every $\lambda_{eff}(t)$ curve can be related to the structure of the eigenvalue spectrum of the Boltzmann operator for the corresponding case. In other words, $\lambda_{eff}(t)$ for very great times tends to an asymptotic value λ_{asym} which is greater than, equal to, or smaller than $\lambda^* \equiv [v\Sigma_{tot}(E)]_{min}$ depending on the buckling value: for instance, for $\lambda_{asym} \geqslant \lambda^*$ the set of discrete eigenvalues appears as empty and the time evolution of the neutron pulse is asymptotically determined by the structure of the continuous spectrum.

The curves of $\lambda_{eff}(t)$ calculated by the free-gas model show an approximately horizontal straight-line behaviour also for rather high buckling values, due to the fact that the value of λ^* for free-gas is very high ($[v\Sigma_{tot}(E)]_{min} \approx 7.2 \times 10^4$ s^{-1} for beryllium, $\approx 2.8 \times 10^4$ s^{-1} for graphite) and a well-separated discrete fundamental eigenvalue exists for the smallest dimensions.

The decay curves always show a straight-line behaviour in a more or less extended time interval, although the related $\lambda_{eff}(t)$ curve indicates

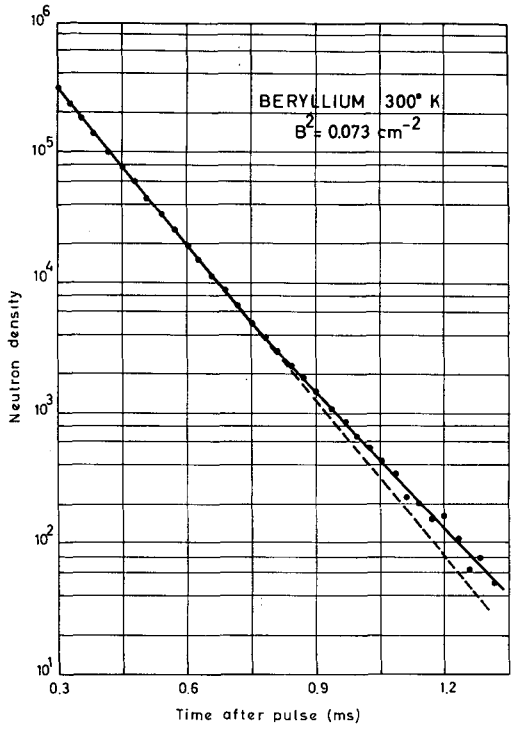

FIG. 2. Decay curves in beryllium. Experimental points and dotted straight line from Ref. [5].

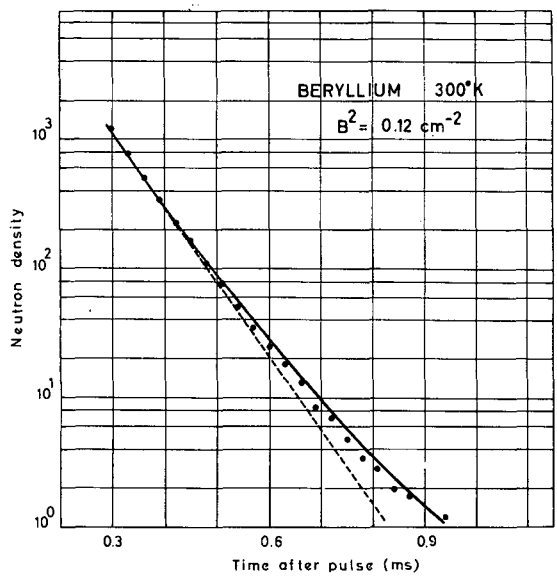

FIG. 3. Decay curves in beryllium. Experimental points deduced from Ref. [9].

in many cases a continuous variation of the slope; as a matter of fact, the mean variation of the slope of the decay curves in such a time interval is so small that the nature of the logarithmic plot of N(t) (where N(t) is quite large) can completely hide it. For this reason the comparison with experiments for $\lambda(B^2)$ has been done in terms of a time-averaged λ_{eff} .

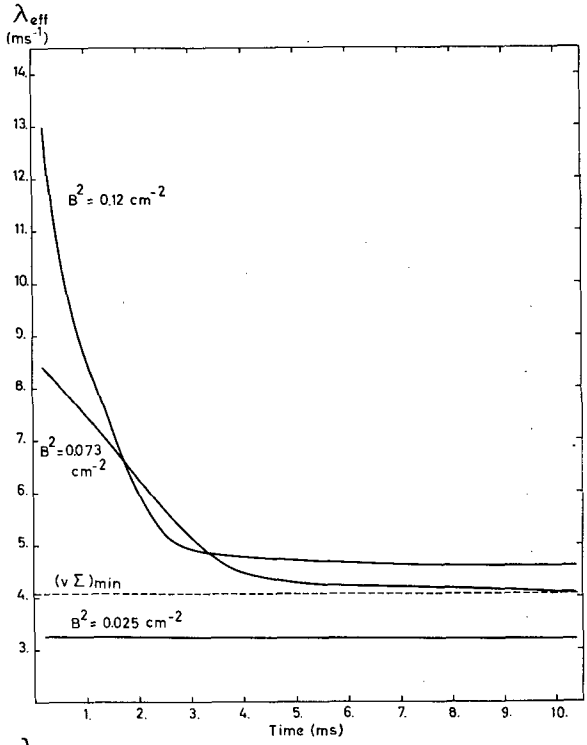

FIG. 4. Instantaneous slope of the decay curve in beryllium.

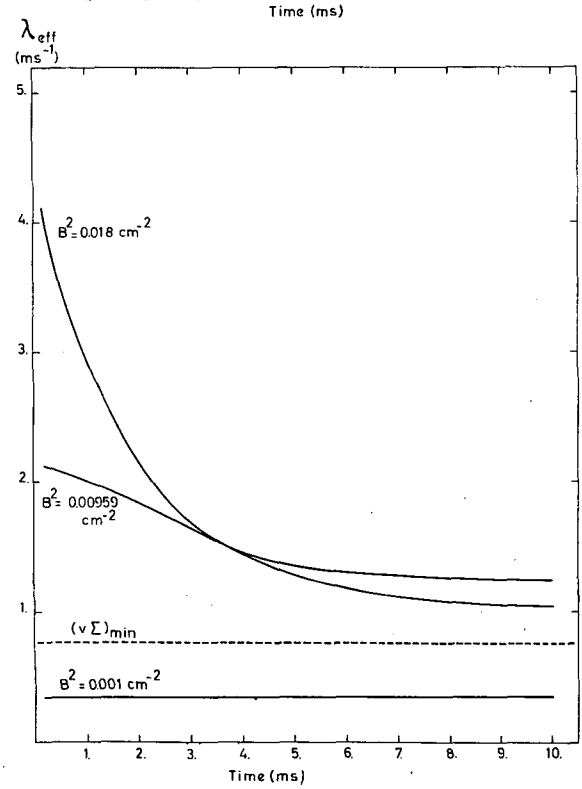

Fig. 5. Instantaneous slope of the decay curve in graphite.

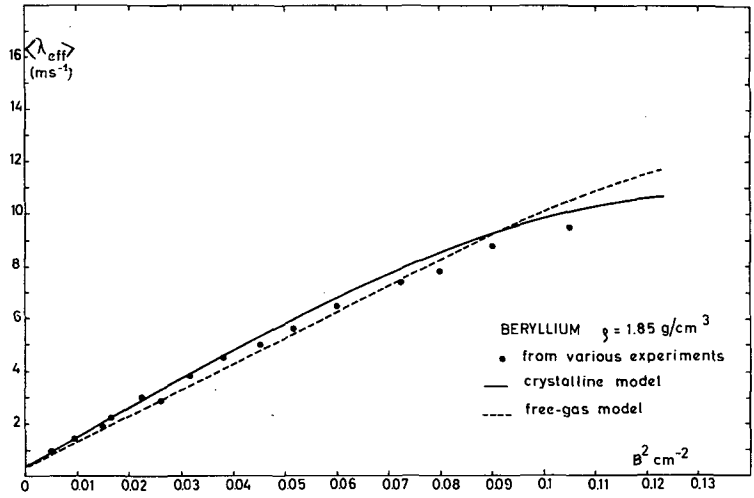

FIG. 6. Mean effective decay constant for various beryllium blocks.

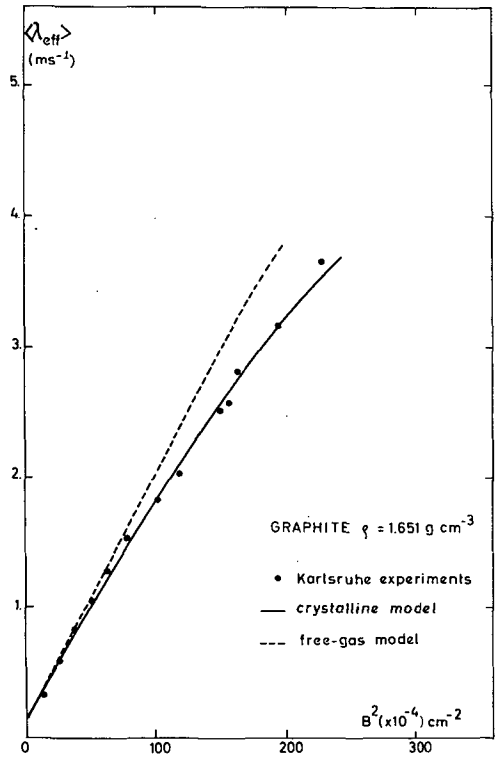

FIG. 7. Mean effective decay constant for various graphite blocks. Experimental points from Klose, H., Küchle, M. and Reichardt, W., Proc. Brookhaven Conf. on Neutron Thermalization, BNL-719, III (1962) 935.

Finally the comparison of the calculated mean effective decay constants as a function of buckling with the measured ones shows a reasonably good agreement with experiments, at least for not too great buckling values, this also being in the framework of the free-gas model.

Consequently we consider the following conclusions justifiable: The interpretation of pulsed neutron experiments available at the moment, as far as integral quantities such as N(t) and $\lambda(B^2)$ are concerned, is certainly possible in the framework of the Boltzmann neutron transport equation. No contradiction appears between the existence of the bound λ^* for the set of the discrete eigenvalues of the Boltzmann operator and the measurement of decay constants, which are greater than for bound.

In the time interval in which more or less accurate measurements are possible, the decay constant (calculated as a time average of the instantaneous slope of the decay curve in this interval) is rather slightly dependent on the moderator dynamics. As a matter of fact, the decay constant appears as a very poor and, in many cases, ambiguous basis of comparison, so that both experimental and theoretical effort should concern primarily more detailed quantities such as N(t) and $\varphi(E,t)$.

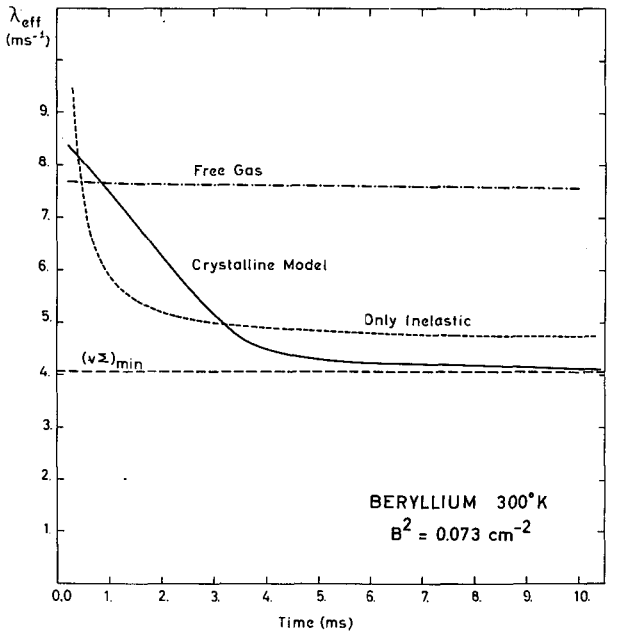

FIG. 8. Instantaneous slope of the decay curve in beryllium. Comparison between various scattering models.

By considering in fact the whole evolution of the neutron pulse one sees very clearly the paramount importance for the decay process of the various types of interactions (elastic, coherent, inelastic) between neutrons and moderator. This is shown by the λ_{eff} (t) curves; we give as a typical example in Fig. 8 the results for a beryllium block (B^2 = 0.073 cm^{-2}) obtained with three different scattering matrices, i.e. crystalline, free-gas, and an inelastic scattering matrix, which is realistic only at energies below the Bragg cut-off.

In the case of high buckling values the approach-to-equilibrium of the neutron pulse in its final stage is mainly determined by the competition between inelastic scattering processes and leakage. This low-energy trapping could be, as has already been pointed out by Wood [16] and by

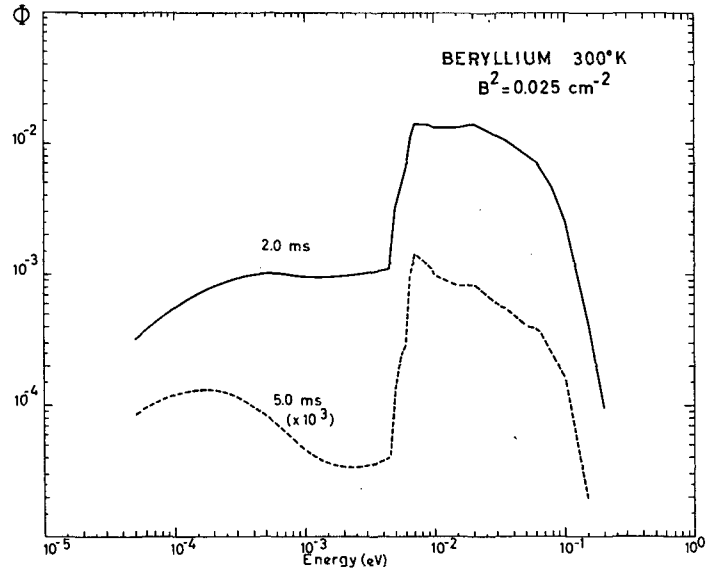

FIG. 9. Calculated time-dependent spectra in beryllium ($B^2 = 0.025\ cm^{-2}$).

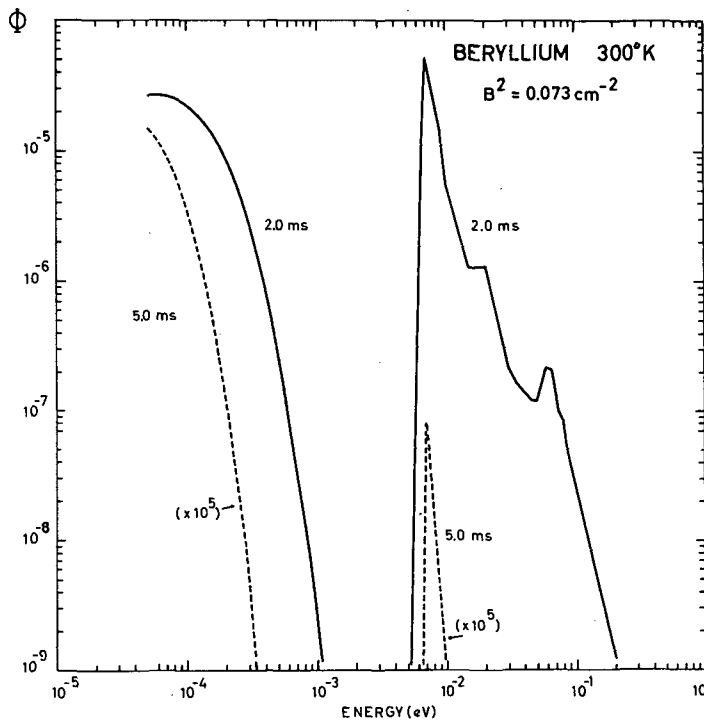

FIG. 10. Calculated time-dependent spectra in beryllium ($B^2 = 0.073\ cm^{-2}$).

Lee and Daitch [9], of great theoretical interest, but unfortunately it is beyond the possibilities of available experimental techniques.

The predominant role of cold neutrons in small beryllium blocks at very late times for a case in which a quasi-stationary situation is achieved, is shown in Figs 9 and 10, where the neutron spectra at t = 2 ms and t = 5 ms for two buckling values ($B^2 = 0.025$ cm^{-2} and $B^2 = 0.073$ cm^{-2}) are presented.

Since the effects from cold neutrons would be enhanced in the case of crystalline moderators at very low temperatures, there is, in this connection, a great interest in experimental data for such samples. On the other hand, the methods of theoretical analysis in this field should be improved beyond the diffusion approximation in its usual simple form; in fact, transport effects will certainly not be negligible for neutrons of energy below the Bragg cut-off.

ACKNOWLEDGEMENTS

The authors wish to thank Dr. A. Kind and the colleagues of the R.P.D. Theoretical Physics Group, Drs. E. Diana, H. Hembd and A. Scotti for several helpful discussions.

REFERENCES

[1] NELKIN, M., Physica 29 (1963) 261.
[2] BECKURTS, K H., Pulsed Neutron Research I IAEA, Vienna (1965) 3.
[3] CORNGOLD, N., Nucl. Sci. Engng 23 (1965) 403.
[4] ARDENTE, V., ROSSI, G., J. nucl. Energy (Parts A/B) (1967).
[5] FULLWOOD, R.R., et al., Nucl. Sci. Engng 18 (1964) 138.
[6] GHATAK, A.K., HONECK, H.C., Nucl. Sci. Engng 21 (1965) 227.
[7] CORNGOLD, N., DURGUN, K., Nucl. Sci. Engng 25 (1966) 450 and private communication.
[8] GOYAL, I.C., GHATAK, A.K., KOTHARI, L.S., J. nucl. Energy (Parts A/B) 20 (1966) 667.
[9] LEE, R.R., DAITCH, P.B., Nucl. Sci. Engng 28 (1967) 247.
[10] GAERTTNER, E.R. et al., Pulsed Neutron Research I IAEA, Vienna (1965) 483.
[11] JOANOU, G.D. et al., General Atomic Rep. GA-4132 (1963).
[12] BELL, J., General Atomic Rep. GA-2492 (1962).
[13] YOUNG, J.A., KOPPEL, J.U., Phys. Rev. 134 (1964) A 1476; Nucl. Sci. Engng 19 (1964) 367.
[14] NALIBOFF, Y.D., KOPPEL, J.U., General Atomic Rep. GA-6026 (1964).
[15] YOUNG, J.A., KOPPEL, J.U., J. chem. Phys. 42 (1965) 357.
[16] WOOD, J., J. nucl. Energy (Parts A/B) 20 (1966) 649.

DISCUSSION

A. I. M. RITCHIE: We have done some decay constant measurements in BeO, which show that the decay is either exponential, questionable or definitely not exponential. When the decay is not exponential the exponent derived from fitting an exponential to the decay curve decreases quite rapidly with time, in a manner similar in many respects to Dr. Rossi's curves. Hence there is no doubt that non-exponential behaviour exists and there is no need to define an 'average' decay constant.

G. E. ROSSI: May I just say that for all the 'supercritical' buckling values for which the experimentalists claim to obtain a decay constant, a comparison of the results of our model (λ_{eff} (t) curve) and of the experimental one can only be made through an 'average' decay constant.

A. I. M. RITCHIE: I should like to know what point there is in generating a $\lambda(B^2)$ curve with $\lambda > \lambda^*$ when there is ambiguity in assigning a value to the exponent.

G. E. ROSSI: Well, it has been found that until $B^2 = 0.06\ cm^{-2}$ there is practically exponential decay, and furthermore some division of exponential decay is found only for $B^2 = 0.08\ cm^{-2}$.

M. M. R. WILLIAMS (Chairman): One of the advantages of this method, surely, is that it does not matter whether decay is exponential or not.

M. P. NAVALKAR: Our calculations for BeO show that buckling corresponding to λ_{max} occurs somewhere between 0.02 and 0.03 cm^{-2}.

A. I. M. RITCHIE: Dr. Navalkar's calculations correspond very closely to what we observe experimentally – that once one gets beyond buckling of about 0.03 cm^{-2} one can no longer see discrete decay in BeO.

A. P. C. KIND: As a colleague of the authors I would explain that the model proposed is intended to be a very simple, but physically sound, tool for interpreting experimental data referring not to integral but to detailed time-dependent thermalization quantities.

T. GOZANI: I feel that the question of the existence or non-existence of a pure exponential is becoming somewhat subjective. There are two ways out of this awkward situation. One way consists of describing exactly how the least-squares fit to a single exponential was made, e. g. the time domain, statistical weights, and other statistical criteria; then this procedure should be applied to the calculated time-dependent flux by comparing the experimental decay constant with the calculated quantity.

Another way, which is independent of subjective judgements and does not demand time-dependent codes, is to compare integral quantities, such as the ratio of the first to the zero time moment, and higher moments which are the solutions of steady-state computations.

Did you compare your calculated time moments directly with any experimental time moment?

G. E. ROSSI: A comparison with stationary quantities such as 'experimental' time moments could perhaps be performed in order to ensure the reliability of the moments $m_0(E)$, $m_1(E)$, which come into our model. But our first aim was to obtain a satisfactory picture of <u>time-dependent</u> phenomena by analysing in detail the energy exchange processes with well-tested scattering matrices.

M. N. MOORE: Apropos of Dr. Gozani's remark, if one considers the full set of time moments, i. e. $m_n = \int_0^\infty dt\, t^n\, \varphi(E,t)$ for all n, these are exactly equivalent to $\varphi(E,t)$. These moments can be computed from experimental data as well as theoretically. I believe Dr. Gozani's point is that it is more sensible to compare time moments than approximate exponential decay constants.

MODEL FOR THERMALIZATION*

P.B. DAITCH AND J.D. JENKINS
RENSSELAER POLYTECHNIC INSTITUTE,
TROY, NEW YORK, UNITED STATES OF AMERICA

Abstract

MODEL FOR THERMALIZATION. The approach to thermal equilibrium and the equilibrium distribution of neutrons in a homogeneous pulsed neutron assembly may be qualitatively and quantitatively considered in terms of a time-dependent spectrum composed of three terms. First, a high-energy transient whose role is to fit the exact energy distribution of the pulsed source at t = 0. This decays with a time constant given by the neutron removal rate at the source energy. Second, a term suggested by monoenergetic diffusion theory consisting of a source divided by a removal rate. The source is represented by a scattering in source, based on a Maxwellian, and the removal rate by the energy-dependent interaction rate modified by leakage and the equivalent absorption due to the (λ/v) time derivative term. This term decays with the time dependence $\exp(-\lambda t)$ with λ constant. Third, a term which has an exponential time dependence at each energy with decay constant given by the removal rate at that energy. This term is adjusted such that when the entire solution is integrated over all time it yields the correct flux for the time-independent problem with an equivalent steady-state source.

A variational principle is used to determine λ and the amplitude associated with the second term. This term clearly shows the role and meaning of the fundamental or pseudo-fundamental mode. The trial function has the same general form regardless of whether or not λ is less than $(v\Sigma)_{min}$. When $\lambda > (v\Sigma)_{min}$ the coefficient of $\exp(-\lambda t)$ is no longer positive definite and it is then termed the pseudo-fundamental. The third term provides a direct interpretation for the contribution of transients to form the bulk of the difference between the fundamental or pseudo-fundamental and the associated steady-state problem.

INTRODUCTION

In this paper we develop an intuitive model for understanding thermalization phenomena. This model is not meant to supplant multigroup methods for accurate quantitative prediction nor is it meant to supplant integral representations for investigating the formal aspects of the problem. The model simply allows one to form an intuitive picture of the processes involved and identifies the essential features of the problem in a quantitative fashion. The method of this paper may be used for quantitative prediction and may even help shed light on some of the formal aspects.

One of the major limitations of the model is the description of leakage by a DB^2 term. This essentially fixes the model as energy-dependent diffusion theory. Since the model employs actual total, transport and energy exchange cross-sections various integrals have to be done by numerical quadrature. This should not, however, be considered a multigroup approximation which may be somewhat more restrictive.

The general approach here is to set up a model. The model is constructed in accord with our intuitive ideas. The parameters in the model are adjusted to fulfil boundary conditions, and by using a variational approach. The results of the model are tested against "exact" calculations.

* This work was supported by the United States Atomic Energy Commission under contract AT(30-3)-328.

THE MODEL

The model consists of a sum of a few terms; each term consists of a function of energy multiplied by an exponential function of time with "half-lives" which are not all energy-independent.

The first term is

$$\varphi(E, B^2)\, e^{-\lambda t} \tag{1}$$

This term is meant to represent the majority of neutrons in a regenerating mode. The regeneration here is due to up-scattering. We will fully specify the energy and buckling dependence of $\varphi(E, B^2)$ except for a multiplicative amplitude. The factor λ in the exponent is a constant. The amplitude and λ are eventually adjusted by means of a variational approach.

The second term is

$$\theta(E, B^2)\, e^{-\Lambda(E, B^2)t} \tag{2}$$

This term is meant to represent the majority of the transients. The function $\Lambda(E, B^2)$ is taken as

$$\Lambda(E, B^2) = v\,\Sigma_T(E) + vD(E)B^2 \tag{3}$$

This means that the neutrons described by the function $\theta(E, B^2)$ leave the system with an exponential time dependence given by the lifetime for removal at that energy. They are not sustained by a regenerative process such as those neutrons described by $\varphi(E, B^2)$. The function $\theta(E, B^2)$, in conjunction with the other terms, is used to fulfil an integral type of boundary condition on the time-dependence.

A third term of the form

$$\psi(E, B^2)e^{-\lambda_s t} \tag{4}$$

is present to enable the model to satisfy the source condition at $t = 0$. The constant λ_s is fixed at a value appropriate for the decay rate of source neutrons.

The sum of the above three terms gives our expression for the time- and energy-dependent neutron flux:

$$\Phi(E, B^2, t) = \varphi(E, B^2)e^{-\lambda t} + \theta(E, B^2)e^{-\Lambda(E, B^2)t} + \psi(E, B^2)e^{-\lambda_s t} \tag{5}$$

The regenerative mode is represented by taking φ explicitly as

$$\varphi(E, B^2) = A\,\frac{M(E)\,\Sigma_s(E)}{\Sigma_T(E) + D(E)B^2 - (\lambda/v)} \tag{6}$$

where $M(E)$ is a Maxwellian flux at the ambient temperature, $\Sigma_s(E)$ and $\Sigma_T(E)$ are the scattering and total cross-sections, and $D(E)$ is the diffusion coefficient. A is an amplitude and λ is constant, both to be determined later.

If the time-dependent source is written as $(1/v)S(E, B^2)\,\delta(t)$ and the flux is 0 at $t = 0^-$, then the flux at $t = 0^+$ should be $S(E)$. We ensure this condition on all the $\Phi(E, B^2, t)$ we consider by setting

$$S(E, B^2) = \varphi(E, B^2) + \theta(E, B^2) + \psi(E) \tag{7}$$

That is, we take

$$\psi(E, B^2) = S(E, B^2) - \varphi(E, B^2) - \theta(E, B^2) \tag{8}$$

At this point, except for the constants A and λ and the function $\theta(E, B^2)$, the energy, buckling and time-dependence of the model are fixed. The function θ is determined by insisting that the time integral of $\Phi(E, B^2, t)$ satisfy the steady-state diffusion equation with source $(1/v)S(E, B^2)$. Letting the solution of this steady-state problem be denoted by $\varphi_{ss}(E, B^2)$, we set

$$\varphi_{ss}(E, B^2) = (1/\lambda)\,\varphi(E, B^2) + (1/\Lambda(E, B^2))\,\theta(E, B^2) + (1/\lambda_s)\,\psi(E, B^2) \tag{9}$$

That is we take

$$\psi(E, B^2) = \lambda_s \varphi_{ss}(E, B^2) - (\lambda_s/\lambda)\,\varphi(E, B^2) - (\lambda_s/\Lambda(E, B^2))\,\theta(E, B^2) \tag{10}$$

This ensures that at every energy our model represents the correct number of neutrons when integrated over all time.

By solving Eqs. (7) and (9) simultaneously one has

$$\theta = \frac{\Lambda\lambda_s}{\lambda_s - \Lambda}\left[\varphi_{ss} - \frac{\lambda_s - \lambda}{\lambda_s \lambda}\,\varphi - \frac{1}{\lambda_s} S\right] \tag{11}$$

$$\psi = \frac{\Lambda\lambda_s}{\lambda_s - \Lambda}\left[\frac{1}{\Lambda} S - \varphi_{ss} - \frac{\lambda - \Lambda}{\lambda\Lambda}\,\varphi\right] \tag{12}$$

For a given S, φ_{ss} may be found by standard techniques – direct numerical matrix inversion and multiplication on a computer. Thus, with S and φ_{ss} known and φ given by Eq. (6), our expression given in Eq. (5) is determined except for the two constants A and λ.

The constants A and λ are determined from a simple least-squares variational principle. The quantity

$$f(A, \lambda) = \iint \left[H\Phi - \frac{1}{v}\frac{\partial \Phi}{\partial t}\right]^2 dE\,dt \tag{13}$$

is defined where $H(E, B^2)$ represents the appropriate energy-dependent diffusion operator and $\Phi(E, B^2, t)$ is given by our model. This quantity represents the square of the error by which we fail to satisfy the exact equation. By varying A and λ until $f(A, \lambda)$ is a minimum this becomes a least-squares variational principle. The values of A and λ which make this integral a minimum are those selected and used in $\Phi(E, B^2, t)$ as given by Eq. (5).

The variational functional $f(A, \lambda)$ gives an absolute rather than a relative error. For some of the cases considered this was too crude

since the absolute error could be minimized by forcing all the neutrons out of the system as quickly as possible with an ever increasing value for λ, thus decreasing the time integral. This was overcome by introducing a weighting factor of t^n into the integrand for the least-squares variational principle. For the problems considered the value of n was not critical and a value about n = 4 was usually satisfactory.

The time integrals represented in Eq. (13) with or without a time weighting factor were all done analytically. The energy integrals represented in Eq. (13) were all done numerically. The minimization of the variational functional was reduced to a one-dimensional numerical search since either A or λ could be eliminated in terms of the other by means of the solution of the least-squares equations found by taking derivatives of the functional with respect to A and λ.

AN EXAMPLE

The time-dependent flux in beryllium assemblies covering a wide range of bucklings has been used as a test of the intuitively based model described above. There are published [1] multi-group diffusion theory calculations available over the range of interest and these calculations have already been compared with both experiment and improved calculations. For the purpose of this paper we use the same cross-sections as those used in the calculations of Lee and Daitch [1] and legislate their multi-group diffusion theory results as "exact".

The bucklings considered range from 0.0131 to 0.124 cm^{-2}. At B^2 larger than about 0.026 cm^{-2} the lowest eigenvalue no longer describes the bulk of the neutrons available to the experiments, a well-established phenomenon [2]. It is for this range of $B^2 > 0.026$ cm^{-2} that the denominator of $\varphi(E, B^2)$ as given by Eq. (6) contains at least one change of sign and thus forces $\varphi(E, B^2)$ to lose its otherwise positive definite character. When $\varphi(E, B^2)$ does not have the positive definite character necessary for a fundamental it takes on the character of a pseudo-fundamental to which it is more or less closely related depending on the definition used for the pseudo-fundamental.

Since the denominator of $\varphi(E, B^2)$ may be zero for some values of E, it is necessary to investigate the singularities in the flux as given by the model. The zeros of the denominator of φ occur as shown by Eq. (6) for those values of E such that

$$\lambda = v\,\Sigma_T(E) + vD(E)\,B^2$$

In view of Eq. (3), $\Lambda(E, B^2)$ when evaluated for that energy which makes the denominator of $\varphi(E, B^2)$ zero is just equal to λ. Hence, at any energy at which a singularity may occur in $\varphi(E, B^2)$ the exponential time-dependence is the same for $\varphi(E, B^2)$ and $\theta(E, B^2)$. It is further noted that, as shown in Eq. (12) in the coefficient of $e^{-\lambda st}$, $\varphi(E, B^2)$ is multiplied by $\lambda - \Lambda(E, B^2)$ which cancels the denominator with the zeros of $\varphi(E, B^2)$. Thus at the energy in question and at time t = 0 all the singularities and other smooth functions must add up to give the source condition of Eq. (7) which is under all usual conditions not singular at this energy. Hence, the singularities in the coefficients of $e^{-\lambda t}$ and

$e^{-\Lambda(E,B^2)t}$ must cancel exactly at $t = 0$. Further, since at the singular energies $\lambda = \Lambda(E, B^2)$ this exact cancellation persists for all time. Thus $\Phi(E, B^2, t)$ is non-singular at all energies even in the cases when a zero appears in the denominator of $\varphi(E, B^2)$.

Similar arguments may be used to show that the flux remains positive as a function of time if the source is positive. The salient feature of the argument is that when $\varphi(E, B^2)$ changes sign the relative magnitude of $e^{-\lambda t}$ and $e^{-\Lambda t}$ also changes.

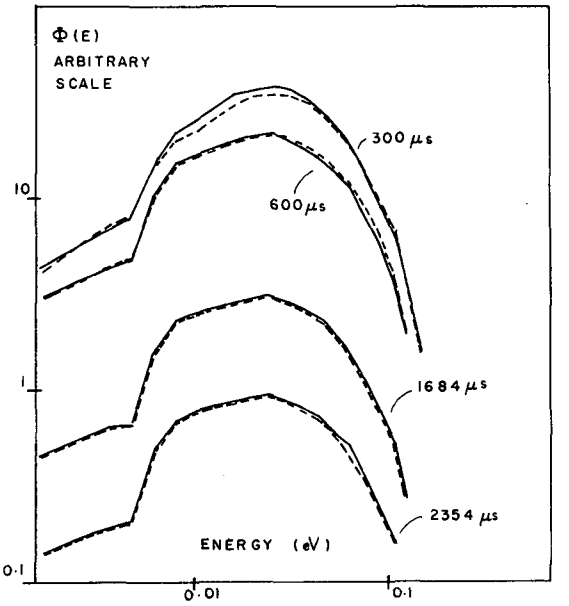

FIG. 1. The scalar flux is given as a function of energy at the times indicated for $B^2 = 0.0131\ cm^{-2}$. The solid curves are the 'exact' theory from Ref. [1] and the dashed curves are the results of the intuitive model of the present work. All results are given normalized to the same pulsed source.

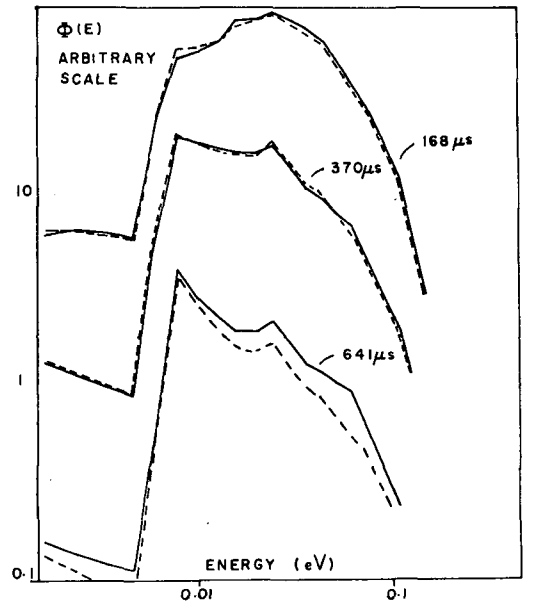

FIG. 2. The scalar flux is given as a function of energy at the times indicated for $B^2 = 0.0753\ cm^{-2}$. The solid curves are the 'exact' theory from Ref. [1] and the dashed curves are the results of the intuitive model of the present work. All results are given normalized to the same pulsed source.

Using the intuitive method the energy- and time-dependent flux for beryllium assemblies with $B^2 = 0.0131$, $B^2 = 0.0753$ and $B^2 = 0.124$ have been computed. These results are presented in Figs. 1, 2 and 3. It is clear that over the range of variables presented, the agreement is excellent. The range of parameters chosen was governed by the earlier work of Ref. [1]; the range covered in Ref. [1] was governed by the range covered by the Rensselaer Polytechnic Institute experiments [2]. For shorter times, the present method and the exact calculation disagree in that the build-up of the spectrum as given by the present calculations is too fast. This is shown in Fig. 4. The count rate for a 1/v counter is compared in Fig. 5 with the exact calculations over the range observed in the Rensselaer Polytechnic Institute experiments and the agreement is seen to be excellent; it should be noted that the times reached in Fig. 5 are well beyond those of Figs. 1, 2 and 3 which display the flux. It may be further emphasized that, although the ordinates on some of the figures are arbitrary, there is no arbitrary relative normalization introduced of the intuitive model calculations and the exact calculations.

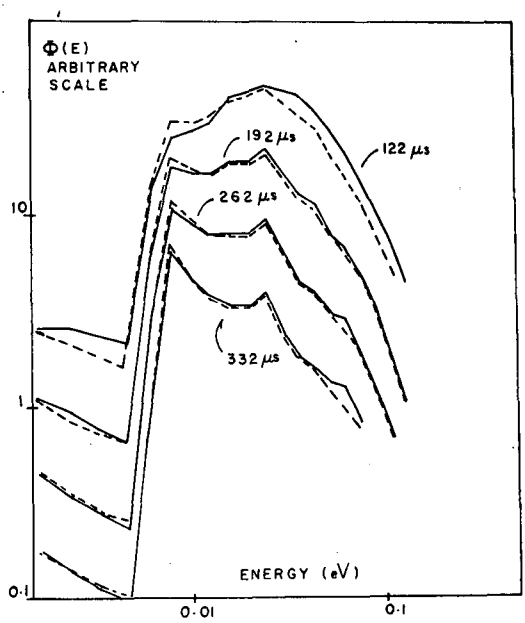

FIG. 3. The scalar flux is given as a function of energy at the times indicated for $B^2 = 0.124\ cm^{-2}$. The solid curves are the 'exact' theory from Ref. [1] and the dashed curves are the results of the intuitive model of the present work. All results are given normalized to the same pulsed source.

CONCLUSIONS

The intuitive model seems adequate to describe thermalization over a large range of energy, buckling and time. The shortcoming at very early times is partly due to a poor representation of the source transients in slowing down. This could probably be considerably improved by using a better value for λ_s; it could, for example, be variationally adjusted. For comparison with most thermalization experiments the simplest intuitive model appears adequate since it is correct over the area where experiments are usually performed and is also correct in an integrated sense.

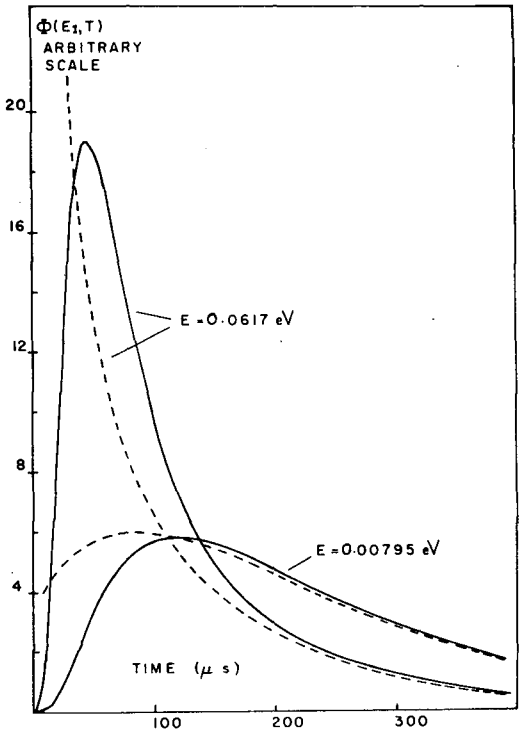

FIG. 4. The value of scalar flux at selected energies is given as a function of time for a system with a $B^2 = 0.0753$. The solid curves are the 'exact' theory from Ref. [1] and the dashed curves are the results of the intuitive model of the present work. All results are given normalized to the same pulsed source.

Regenerative mode

We would label the part of the solution represented by $\varphi(E, B^2)e^{-\lambda t}$ the regenerative mode. The name is chosen because it is in accord with a physical mechanism such that the number of neutrons at a given energy is influenced not only by the rate at which neutrons leave the energy in question but also by the rate at which they are regenerated at that energy by an energy transfer or regeneration mechanism. In large systems or systems where the losses (other than 1/v losses) are small relative to the regeneration rate, the regenerative mode is the true fundamental or asymptotic mode of the system.

In the smaller (non-1/v) systems the decay constant (λ) gets larger and the neutrons taking part in this regenerative (scattering in our Be example) process no longer have a positive definite distribution. The physical mechanism is still operative and important for these neutrons in the regenerative mode but their distribution can no longer serve as an asymptotic distribution. The lifetime in this type of regenerative mode is less than the lifetime for removal from some energy or energies and the neutrons at these energies become the asymptotic distribution. In this type of situation the regenerative mode assumes a role similar to a pseudo-fundamental. It will have a large amplitude rather independent of the particular shape of the source and represents a mechanism in the system much as the fundamental.

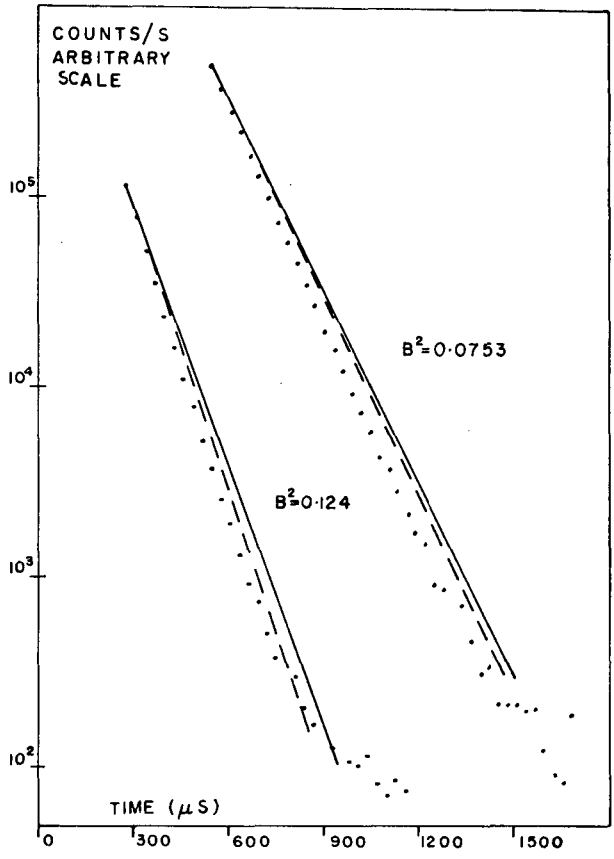

FIG. 5. The count rate in a (1/v) detector as a function of time as given by the 'exact' theory of Ref. [1] (solid curves) and the intuitive model of the present work (dashed curves) for the bucklings indicated. The theoretical results are given normalized to the same pulsed source but the normalization of the experimental results (dots) from Ref. [2] is arbitrary.

Removal lifetime

The lifetime for removal at any particular energy, $\Lambda^{-1}(E, B^2)$, appears to play a particularly important role in the time-dependence of the flux. It is a mono-energetic property in that for neutrons of any given energy its value is not dependent on what is occurring at any other energy. A whole system of transients appears in the intuitive model with this simple time-dependence. When $\varphi(E, B^2)$ is not positive definite the flux for large values of t is given by the coefficient of the smaller values of $\Lambda(E, B^2)$ and as t goes to infinity by the coefficient of $\Lambda(E, B^2)_{min}$. As already noted, $\Lambda(E, B^2)$ in comparison with λ determines the sign changes of $\varphi(E, B^2)$. It may be noted that $\theta(E, B^2)e^{-\Lambda(E, B^2)t}$ as time increases represents a loss of epithermal neutrons to the system and a gain of thermal neutrons in the vicinity of kT where $\theta(E, B^2) < 0$.

Other problems

The same intuitive reasoning may be applied to yield the time-dependence of fast pulsed assemblies [3]; in these problems the fission process furnishes the regenerative mechanism for the regenerative

mode. We also note that others are pursuing similar lines of approach to the thermalization problem [4].

The model strongly suggests that in the epithermal region the most important parameters in the time-dependence are the removal rate at each energy and an adequate description of the source. If there was a need to measure removal cross-sections in this region, the intuitive model would allow their extraction from pulsed experiments.

REFERENCES

[1] LEE, R.R., DAITCH, P.B., "An analysis of neutron thermalization in beryllium", Nucl. Sci. Engng 28 (1967) 247.

[2] GAERTTNER, E.R., DAITCH, P.B., FULLWOOD, R.R., LEE, R.R., SLOVACEK, R.E., Pulsed Neutron Research I IAEA, Vienna (1965).

[3] JENKINS, J.D., DAITCH, P.B., "Analysis of pulsed fast spectra", Nucl. Sci. Engng, in press.

[4] ARDENTE, V., ROSSI, G., "Energy-dependent neutron mean-life and pulsed experiments in crystalline moderators", J. nucl. Energy, in press.

DISCUSSION

P.F. ZWEIFEL: In your model you have the sum of three exponential decays, I believe: two constants in the exponent and one a function of energy and buckling. When B^2 is of such magnitude that there is a discrete eigenvalue, which of your three exponential terms dominates?

P.B. DAITCH: Different terms dominate at different times and energies. For example, with a high-energy source, at early times the λt and Λt terms cancel at low energies. At long times, and under the conditions you specify, the λt term dominates and actually gives the asymptotic mode.

P.F. ZWEIFEL: When, in the continuum, do you still have an exponential decay for the second term?

P.B. DAITCH: I assume you refer to the case where $\lambda > \Lambda_{min}$. At long times the Λt term dominates for energies such that $\lambda > \Lambda(E, B^2)$. For these energies and times there is a characteristic decay constant at each energy. Despite this there is no overall mode since $\theta(E,B^2)$ is multiplied by the non-separable term $e^{-\Lambda(E,B^2)t}$.

F.C. SHURE: Your paper stated that in the continuum region the regenerative mode takes on a singular behaviour, but that the singularity is cancelled by a singularity in the transient. How is this possible if the two modes have different time dependence? Does their time dependence coincide in the neighbourhood of the singularity?

P.B. DAITCH: Yes. The initial condition forces cancellation at that time. The singularities occur at just those points where the time dependence is the same, retaining the cancellation at all subsequent times.

D.H. DAY: Is this method of calculation suitable for the case of a point source, where one must consider higher harmonics as well as the fundamental in the lateral buckling?

P.B. DAITCH: This is an interesting problem and the ideas contained in the paper may be applied to it. A Fourier analysis might be useful in some cases. One might consider Λ as a function of E and $\vec{r}$ rather than E and B^2. In any case, it seems that it would be useful to focus on the actual lifetime of the neutrons as a function of energy and position.

СРЕДНЯЯ ПЛОТНОСТЬ НЕЙТРОНОВ В НЕОДНОРОДНЫХ СРЕДАХ

А.В.СТЕПАНОВ
ФИЗИЧЕСКИЙ ИНСТИТУТ им. П.Н.ЛЕБЕДЕВА,
АН СССР, МОСКВА,
СССР

Abstract — Аннотация

MEAN NEUTRON DENSITY IN HETEROGENEOUS MEDIA. The paper considers the passage of neutrons through a heterogeneous medium, which may be described using the Boltzmann equation with fluctuating parameters. An approximate expression is derived for the neutron flux averaged over the fluctuations in the medium, and is valid for small fluctuations. The mean neutron flux is analysed as a function of time and energy. A periodic reactor lattice is considered as an example of a heterogeneous medium.

СРЕДНЯЯ ПЛОТНОСТЬ НЕЙТРОНОВ В НЕОДНОРОДНЫХ СРЕДАХ. Рассмотрено прохождение нейтронов в неоднородной среде, которое можно описать с помощью уравнения Больцмана с флуктуирующими параметрами. Выведено приближенное уравнение для потока нейтронов, усредненного по флуктуациям в среде, справедливое в случае малого масштаба флуктуаций. Проведен анализ временной и энергетической зависимости среднего потока нейтронов. Найдены аналитические выражения для постоянных релаксации нейтронного распределения. В качестве примера неоднородной среды рассмотрена периодическая решетка реактора.

1. ВВЕДЕНИЕ

Одной из важных задач теории гетерогенных реакторов является отыскание $\langle\Phi\rangle$-потока нейтронов, усредненного по объему ячейки* (макроскопический поток). Подобная задача возникает и в теории термализации нейтронов. В настоящей работе развит универсальный метод отыскания $\langle\Phi\rangle$. Однако, ввиду того, что используется специфический математический аппарат, представляется целесообразным разъяснить постановку задачи и обсудить область применимости метода в рамках более простой односкоростной теории (разд. 2 – 6). Учету энергетической зависимости функции распределения нейтронов посвящен разд. 7.

Практически задачу об отыскании $\langle\Phi\rangle$ решают, заменяя реальную гетерогенную систему гомогенной средой с соответствующим образом подобранными диффузионными характеристиками**. Проиллюстрируем это утверждение простым примером. Рассмотрим среду с исчезающе малым поглощением. Тогда задача гомогенизации такой среды сводится к отысканию некоторого эффективного коэффициента диффузии $D_{эфф}$, который выступает в законе Фика для среднего тока нейтронов $\langle\vec{j}\rangle$

$$\langle\vec{j}\rangle = -D_{эфф}\langle\nabla\Phi\rangle \tag{1.1}$$

* Следует сразу же оговориться, что такое правило отыскания макроскопического потока справедливо, если только последний является константой. Если же макроскопический поток зависит от координат, то усреднение необходимо выполнять (при фиксированном расстоянии от источника нейтронов до детектора) по статистическому ансамблю решеток, отдельные представители которого отличаются друг от друга смещением в пространстве.

** Обширную библиографию по этому вопросу можно найти в монографиях [1 – 3].

Замечая, что формула (1.1) аналогична известному соотношению между вектором электрической индукции и электростатическим потенциалом, воспользуемся результатом расчета $\epsilon_{эфф}$ – эффективной диэлектрической проницаемости неоднородной среды [4] ($\epsilon_{эфф}$ – аналог $D_{эфф}$ в нашей задаче). Приведем результат. Если диффузия происходит вдоль слоев вещества, т.е. при "продольной" диффузии в слоистой среде, то

$$D^{\parallel}_{эфф} = \langle D \rangle \tag{1.2}$$

При поперечной диффузии в этой среде

$$D^{\perp}_{эфф} = \langle D \rangle \left[1 - \frac{\langle [D - \langle D \rangle]^2 \rangle}{\langle D \rangle^2} \right]. \tag{1.3}$$

Таким образом коэффициент диффузии $D_{эфф}$ зависит от направления диффузии в гетерогенной решетке. Это хорошо известный результат [5]. Аналогично при диффузии в направлении перпендикулярном оси двумерной решетки с квадратной ячейкой можно показать, что

$$D^{\perp}_{эфф} = \langle D \rangle \left[1 - \frac{1}{2} \frac{\langle [D - \langle D \rangle]^2 \rangle}{\langle D \rangle^2} \right], \tag{1.4}$$

а в случае изотропной среды

$$D^{изотр.}_{эфф} = \langle D \rangle \left[1 - \frac{1}{3} \frac{\langle [D - \langle D \rangle]^2 \rangle}{\langle D \rangle^2} \right]. \tag{1.5}$$

Разумеется, рассмотренный пример имеет лишь эвристическую ценность и необходимо более точное решение задачи о гомогенизации гетерогенной среды.

Точная задача об отыскании среднего потока нейтронов может быть сформулирована следующим образом. Сначала мы должны найти распределение нейтронов в среде с фиксированной зависимостью макроскопических поперечных сечений $\Sigma(\vec{r})$ от координат $\Phi(\vec{r}, \vec{v}, t; \Sigma(\vec{r}))$, а затем вычислить функциональный интеграл

$$\langle \Phi(\vec{r}, \vec{v}, t) \rangle = \int \Phi(\vec{r}, \vec{v}, t; \Sigma(\vec{r})) P(\Sigma) d\Sigma, \tag{1.6}$$

где $P(\Sigma)$ – закон распределения поперечных сечений Σ; $\vec{v}$ – скорость нейтронов. Разумеется, осуществить эту программу удается только в малом числе случаев, когда структура среды достаточно проста.

Универсальным методом является теория возмущений: в качестве нулевого приближения используется выражение для потока нейтронов в однородной среде, а неоднородность учитывается как возмущение. Пренебрегая в нулевом приближении неоднородностью, мы правильно учитываем лишь средние значения поперечных сечений Σ_0, которые предпола-

гаются постоянными (среда пространственно однородна). Тем самым реальный закон распределения $P(\Sigma)$ мы заменяем приближенным

$$P_0(\Sigma) = \delta(\Sigma - \Sigma_0) . \tag{1.7}$$

В первом неисчезающем приближении теории возмущений мы правильно учитываем вторые моменты закона распределения $P(\Sigma)$: рассматриваются корреляционные функции $\langle \Sigma_s(\vec{r})\Sigma_s(\vec{r}')\rangle, \langle \Sigma_s(\vec{r})\Sigma_a(\vec{r}')\rangle$, и т.д.; здесь Σ_s и Σ_a – макроскопические сечения рассеяния и поглощения, соответственно. Учет следующих членов ряда теории возмущений приводит к необходимости рассмотреть более высокие моменты $P(\Sigma)$.

Приближенное уравнение, которому удовлетворяет $\langle G(x/y)\rangle$ – средний поток нейтронов от элементарного источника (усредненная функция Грима кинетического уравнения) имеет следующий вид [6, 7]:

$$\hat{B}(x)\langle G(x/y)\rangle = -\delta(x-y) - \int M_1(x/x')\langle G(x'/y)\rangle dx' . \tag{1.8}$$

Здесь $x = \{\vec{r}, \vec{v}, t\}$ – совокупность переменных задачи, $y = \{\vec{r}_0, \vec{v}_0, t_0\}$ – переменные, характеризующие источник, $\hat{B}$ – оператор уравнения переноса. Уравнение (1.8) отличается от соответствующего уравнения с усредненными коэффициентами

$$\hat{B}G_0(x/y) = -\delta(x-y) \tag{1.9}$$

интегральным членом в правой части, который обусловлен наличием флуктуаций в среде*. Ядро M_1 этого интегрального оператора имеет вид

$$M_1(x/x') = \langle \hat{\mu}(x)G_0(x/x')\hat{\mu}(x')\rangle \tag{1.10}$$

$\hat{\mu}(x)$ – возмущение, связанное с флуктуациями поперечных сечений, причем

$$\langle \hat{\mu}(x)\rangle = 0 . \tag{1.11}$$

Вывод уравнения (1.8), которое мы будем называть уравнением в M_1-приближении, дан в приложении А**; решения этого уравнения для конкретных задач переноса нейтронов получены в разд. 3 – 5 (односкоростные задачи с непрерывно действующим источником нейтронов), в разд. 6 (односкоростная задача с импульсным источником) *** и в разд. 7 (многоскоростная задача со стационарным источником). В приложении Б получено уточнение приближения (1.8) для стационарной диффузии моноэнер-

---

* В дальнейшем отклонение значений поперечных сечений от соответствующих средних мы будем называть флуктуациями.

** Точное уравнение для среднего потока нейтронов в произвольной среде с флуктуирующими параметрами выведено в работе [7] методом функционального дифференцирования.

*** Анализ нестационарной диффузии нейтронов в гетерогенной решетке численным методом был проведен ранее в работе [8].

гетических нейтронов. Анализу свойств некоторых видов корреляционных функций, выступающих в выражении для $M_1(x/x')$ (1.10) посвящены следующий раздел и приложение В.

2. КОРРЕЛЯЦИОННЫЕ ФУНКЦИИ

В случае решетки гетерогенного реактора соответствующие корреляционные функции можно вычислить, используя разложение периодических функций $\mu_k(\vec{r})$, описывающих пространственную зависимость поперечных сечений для коэффициента диффузии, в ряд Фурье:

$$\mu_k(\vec{r}) = \frac{1}{v_я}\sum_{\vec{g}} A_k(\vec{g})e^{-i\vec{g}\vec{r}} \tag{2.1}$$

$$A_k(\vec{g}) = \int_{v_я}\mu_k(\vec{r})e^{i\vec{g}\vec{r}}d\vec{r} \tag{2.2}$$

$v_я$ – объем элементарной ячейки, $\vec{g}$ – вектор обратной решетки; индекс "k" характеризует вид возмущения (сечение поглощения и т.п.). Учитывая правило, по которому производится усреднение в случае среды с периодической структурой (см. Введение), получим, принимая во внимание (2.1) и (2.2)

$$\langle\mu_k(\vec{r})\rangle = \frac{1}{v_я}\int_{v_я} d\vec{r}'\mu_k(\vec{r}+\vec{r}')$$

$$= \frac{1}{v_я}\sum_{\vec{g}} A_k(\vec{g})e^{i\vec{g}\vec{r}}\frac{1}{v_я}\int_{v_я} e^{-i\vec{g}\vec{r}'}d\vec{r}'$$

$$= \frac{1}{v_я}\sum_{\vec{g}} A_k(\vec{g})e^{i\vec{g}\vec{r}}\,\delta_{g,0} = \frac{1}{v_я}A_k(0). \tag{2.3}$$

Вследствие нашего определения функций $\mu_k(\vec{r})$ среднее $\langle\mu_k(\vec{r})\rangle = 0$. Это означает, что

$$A_k(0) = 0. \tag{2.4}$$

Найдем выражение для корреляционной функции $K_{ij}(\vec{r}-\vec{r}')$. С помощью формул (2.1) и (2.2) получим

$$K_{ij}(\vec{r}-\vec{r}') = \frac{1}{v_я}\int\mu_i(\vec{r}+\vec{r}'')\mu_j(\vec{r}'+\vec{r}'')d\vec{r}''$$

$$= \frac{1}{v_я^2}\sum_{\vec{g}}\sum_{\vec{g}'} A_i(\vec{g})A_j(\vec{g}')e^{-i\vec{r}\vec{g}-i\vec{r}'\vec{g}'}$$

$$\times \frac{1}{v_я} \int d\vec{r}'' e^{-i\vec{r}(\vec{g}+\vec{g}')}$$

$$= \frac{1}{v_я^2} \sum_{\vec{g}} \sum_{\vec{g}'} A_i(\vec{g}) A_j(\vec{g}') e^{-i\vec{r}\vec{g} - i\vec{r}'\vec{g}'} \delta_{\vec{g}, -\vec{g}'}$$

$$= \frac{1}{v_я^2} \sum_{\vec{g}} A_i(\vec{g}) A_j^*(\vec{g}) e^{-i\vec{g}(\vec{r}-\vec{r}')} \quad . \tag{2.5}$$

Рассмотрим некоторые частные случаи. Корреляционная функция плоской решетки с периодом 2а зависит лишь от одной координаты. Например, в случае простой структуры типа

$$\mu_k(z) = \begin{cases} \mu_{k1} & a < z < 2a \\ \mu_{k2} & 0 < z < a \end{cases} \tag{2.6}$$

корреляционная функция $K_{ij}(z - z')$ имеет вид

$$K_{ij}(z - z') = \frac{2\mu_{j0}\mu_{j0}}{\pi^2} \sum_{n=1}^{\infty} \frac{\cos\frac{2n-1}{a}\pi\left(z - z'\right)}{(2n-1)^2} , \tag{2.7}$$

где

$$\mu_{i0} = \mu_{i1} - \mu_{i2} \tag{2.8}$$

Отметим, что из (2.6) следует $\langle \mu_k(z) \rangle = \frac{\mu_{k1} + \mu_{k2}}{2} \neq 0$. Это противоречит нашему определению функции $\mu_k(z)$, данному выше (см. (2.3) – (2.4). Однако, благодаря тому, что мы исключили из суммы, определяющей корреляционную функцию $K_{ij}(z - z')$ слагаемое с $n = 0$, последняя оказывается инвариантной относительно сдвига $\mu_k(z)$ на любую постоянную величину.

В более сложном варианте прямоугольной двумерной решетки с периодами 2а и 2в с полым круговым цилиндром в каждой элементарной ячейке (начало координат в ячейке совпадает с центром сечения цилиндра)

$$\mu_k(\rho) = \begin{cases} \mu_{k1} & r_1 < \rho < r_2 \\ \mu_{k2} & \rho < r_1, \ \rho > r_2 \end{cases} \tag{2.9}$$

корреляционная функция $K_{ij}(\vec{r} - \vec{r}')$ может быть представлена в виде

$$K_{ij}(\vec{r} - \vec{r}') = \frac{\mu_{i0}\mu_{j0}}{a^2 b^2} \sum_{n=0}^{\infty} \sum_{m=0}^{\infty} \lambda_{mn} \frac{\left[r_2 \mathcal{J}_1\left(\pi r_2 \sqrt{\frac{n^2}{a^2} + \frac{m^2}{b^2}}\right) - r_1 \mathcal{J}_1\left(\pi r_1 \sqrt{\frac{n^2}{a^2} + \frac{m^2}{b^2}}\right) \right]^2}{\frac{n^2}{a^2} + \frac{m^2}{b^2}}$$

$$\times \cos\frac{\pi}{a} n(x - x') \cos\frac{\pi}{b} m(y - y') , \tag{2.10}$$

где $\mathcal{J}_1(x)$ – функция Бесселя, а

$$\lambda_{mn} = \begin{cases} 0 & n = m = 0 \\ 1/2 & n = 0, \quad m \neq 0; \quad n \neq 0, \quad m = 0 \\ 1 & n \neq 0, \quad m \neq 0. \end{cases} \tag{2.11}$$

Если же в ячейке симметрично* расположены N одинаковых однородных цилиндрических стержней радиуса R, то для функции $K_{ij}(\vec{r} - \vec{r}\,')$ получим следующее выражение

$$K_{ij}(\vec{r} - \vec{r}\,') = \frac{\mu_{i0}\mu_{j0}\, R^2}{a^2 b^2} \sum_{n=0}^{\infty}\sum_{m=0}^{\infty} \lambda_{mn} \frac{\mathcal{J}_1^2\left(\pi R\sqrt{\frac{n^2}{a^2} + \frac{m^2}{b^2}}\right)}{\frac{n^2}{a^2} + \frac{m^2}{b^2}}$$

$$\times \cos\frac{\pi}{a} n(x - x')\cos\frac{\pi}{b} m(y - y')\varphi_N(n, m) \tag{2.12}$$

Здесь

$$\varphi_N(n, m) = \left|\sum_{k=1}^{N} e^{i\frac{\xi_k}{a}\pi n}\; e^{i\frac{\eta_k}{b}\pi m}\right|^2 \tag{2.13}$$

ξ_k и η_k определяют положение центра сечения $k^{ого}$ стержня относительно начала координат в ячейке. Свойства корреляционных функций для более сложных неоднородных систем (в частности для систем,не обладающих строгой периодичностью) обсуждаются в работе [7]. Корреляционная функция для полностью неупорядоченной среды вычислена в приложении "В" данной работы.

3. СТАЦИОНАРНАЯ ДИФФУЗИЯ ТЕПЛОВЫХ НЕЙТРОНОВ

Рассмотрение конкретных задач переноса нейтронов в гетерогенных средах мы начнем с анализа уравнения

$$\operatorname{div}\left[\frac{D(\vec{r})}{D_0}\operatorname{grad} G(\vec{r}/\vec{r}_0)\right] - \frac{\Sigma_a(\vec{r})}{D_0} G(\vec{r}/\vec{r}_0) = -\frac{S}{D_0}\delta(\vec{r} - \vec{r}_0), \tag{3.1}$$

описывающего стационарную диффузию тепловых нейтронов; S – мощность источника. В дальнейшем для простоты будем считать $S/D_0 = 1$. Макроскопическое сечение поглощения $\Sigma_a(\vec{r})$ и коэффициент диффузии D запишем, соответственно, в виде

$$\Sigma_a(\vec{r}) = \Sigma_{a0} + G_a(\vec{r}); \qquad \langle \Sigma_a(\vec{r})\rangle = \Sigma_{a0}, \qquad \langle G_a(\vec{r})\rangle = 0 \tag{3.2}$$

$$D(\vec{r}) = D_0 + d(\vec{r}); \qquad \langle D(\vec{r})\rangle = D_0; \qquad \langle d(\vec{r})\rangle = 0 \tag{3.3}$$

---

* Решетка обладает свойством инвариантности при зеркальных отражениях относительно осей 0x и 0y.

Как нетрудно проверить, подставляя (3.2) и (3.3) в уравнение (3.1) и сравнивая с (1.8), в данном случае

$$\hat{B} = \nabla^2 - \kappa_0^2 \tag{3.4}$$

$$\hat{\mu}(\vec{r}) = -\eta(\vec{r})\nabla^2 - (\nabla\eta(\vec{r}))\nabla + \nu(\vec{r}), \tag{3.5}$$

где

$$\kappa_0^2 = \frac{\Sigma_{a0}}{D_0}, \qquad \eta(\vec{r}) = \frac{d(\vec{r})}{D_0}, \qquad \nu(\vec{r}) = \frac{G_a(\vec{r})}{D_0} \tag{3.6}$$

В случае пространственно-однородной среды (т.е. однородной в среднем) уравнение (1.8) преобразованием Фурье относительно $\vec{r} - \vec{r}_0$ можно свести к алгебраическому

$$[p^2 + \kappa_0^2]\langle g(\vec{p})\rangle = 1 + m_1(\vec{p})\langle g(\vec{p})\rangle \tag{3.7}$$

Были введены обозначения

$$\langle g(\vec{p})\rangle = \int d\vec{r}\, e^{i\vec{p}\vec{r}} \langle G(\vec{r})\rangle \tag{3.8}$$

$$m_1(\vec{p}) = \int d\vec{r}\, e^{i\vec{p}\vec{r}}\, M_1(\vec{r}) \tag{3.8a}$$

Таким образом

$$\langle g(\vec{p})\rangle = [p^2 + \kappa_0^2 - m_1(\vec{p})]^{-1} \tag{3.9}$$

и, соответственно,

$$\langle G(\vec{r}/\vec{r}_0)\rangle = \frac{1}{(2\pi)^3}\int \frac{d\vec{p}\, e^{-i\vec{p}(\vec{r}-\vec{r}_0)}}{p^2 + \kappa_0^2 - m_1(\vec{p})} \tag{3.10}$$

В нулевом приближении $m_1(\vec{p}) = 0$ и

$$g_0(\vec{p}) = \frac{1}{p^2 + \kappa_0^2} \tag{3.11}$$

и поток нейтронов убывает по закону

$$G_0(\vec{r}/\vec{r}_0) = \frac{1}{4\pi\,|\vec{r} - \vec{r}_0|}\, e^{-\kappa_0|\vec{r}-\vec{r}_0|} \tag{3.12}$$

Подставим выражения для $G_0(\vec{r}/\vec{r}_0)$ (3.12) и $\hat{\mu}(\vec{r})$ (3.5) в формулу для $M_1(\vec{r}/\vec{r}\,')$ (1.10) и выполним преобразование Фурье относительно $\vec{r} - \vec{r}\,'$.

В результате получим [7, 9]

$$m_1(\vec{p}) = \frac{1}{(2\pi)^3}\int d\vec{\xi}\,\frac{[\vec{p}(\vec{p}-\vec{\xi})]^2 k_{\eta\eta}(\vec{\xi}) + 2\vec{p}(\vec{p}-\vec{\xi})k_{\eta\nu}(\vec{\xi}) + k_{\nu\nu}(\vec{\xi})}{(\vec{p}-\vec{\xi})^2 + \kappa_0^2}, \quad (3.13)$$

где

$$k_{\eta\eta}(\vec{\xi}) = \int d\vec{r}\, e^{i\vec{\xi}\vec{r}}\, K_{\eta\eta}(\vec{r}) \quad (3.14)$$

– Фурье-образ корреляционной функции флуктуаций $\eta(\vec{r})$. Остальные корреляционные функции определяются аналогичным образом.

В случае плоской решетки (2.6), когда все корреляционные функции зависят от координат одинаковым образом, при $\pi/a\kappa_0 \gg 1$ ($p \sim \kappa_0$) получим (условие $\pi/a\kappa_0 \gg 1$ подразумевается малый пространственный масштаб флуктуаций).

$$m_1(\vec{p}) \approx p^2\left\{\epsilon_{\eta\eta}\left(\frac{p_z^2}{p^2} - \frac{\kappa_0^2 a^2}{12}\right) + \frac{\epsilon_{\eta\nu}\, a^2}{6}\left(1 - \frac{2p_z^2}{p^2}\right)\right\} + \frac{\epsilon_{\nu\nu} a^2}{12} \quad (3.15)$$

Здесь

$$\epsilon_{ij} = K_{ij}(0) = \frac{1}{(2\pi)^3}\int d\vec{\xi}\, k_{ij}(\vec{\xi}). \quad (3.16)$$

Этот результат следует из точного расчета Шевелева [5] для данного частного случая. При $a\kappa_0 \to 0$ выражение (3.15) значительно упрощается.

$$m_1(\vec{p}) = \epsilon_{\eta\eta} p_z^2 \quad (3.17)$$

Для двумерной решетки (2.12) с одним поглощающим нейтроны стержнем ($\varphi_1 = 1$) в квадратной ячейке ($a = b$), получим из (3.13) при $\pi/a\kappa_0 \gg 1$, полагая для простоты, что флуктуирует только сечение поглощения*, следующее выражение для $m_1(\vec{p})$

$$m_1(\vec{p}) \approx \frac{\nu_0^2 R^2}{\pi^2}\sum_{n=0}^{\infty}\sum_{m=0}^{\infty}\lambda_{mn}\frac{\mathcal{J}_1^2\left(\pi\frac{R}{a}\sqrt{n^2+m^2}\right)}{(n^2+m^2)^2} \quad (3.18)$$

График двойной суммы в (3.18) как функции R/a приведен на рис. 1. Если же флуктуирует и коэффициент диффузии, то в предельном случае $a\kappa_0 \to 0$ получим аналог выражения (3.17)

$$m_1(\vec{p}) = \frac{\epsilon_{\eta\eta}}{2} p_\perp^2, \quad (3.19)$$

---

* При слабом поглощении ($\Sigma_a \ll \Sigma_s$) флуктуации сечения поглощения практически не сказываются на величине коэффициента диффузии, который при $\Sigma_s = \text{const}$ остается постоянным.

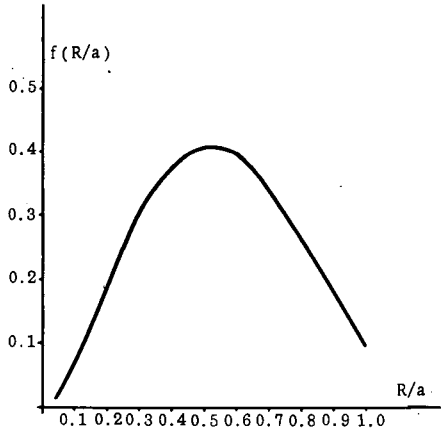

Рис. 1. График функции

$$f(R/a) = \sum_{n=0}^{\infty}\sum_{m=0}^{\infty} \lambda_{mn} \frac{\mathcal{J}_1^2\left(\frac{\pi R}{a}\sqrt{n^2+m^2}\right)}{(n^2+m^2)^2}$$

гед $p_\perp$ – проекция вектора $\vec{p}$ на плоскость, перпендикулярную оси симметрии решетки.

В случае изотропной среды для мелкомасштабных неоднородностей

$$m_1(\vec{p}) = \frac{\epsilon_{\eta\eta}\, p^2}{3} \tag{3.20}$$

Подставим выражения (3.17) – (3.20) в уравнение

$$p^2 + \kappa_0^2 - m_1(\vec{p}) = 0, \tag{3.21}$$

определяющее постоянные затухания среднего потока нейтронов (см. ур. (3.9)). Получим следующие результаты. Если флуктуирует только сечение поглощения, то диффузия нейтронов как в плоской так и в двумерной решетке оказывается практически изотропной (эффекты анизотропии проявляются в членах более высокого порядка по $(a\kappa_0)^2$, нежели учтенные нами в (3.15) и (3.18) и в предельном случае $a\kappa_0 \to 0$ постоянная релаксации стремится к значению, соответствующему гомогенной смеси. Например, в случае плоской решетки (2.6)

$$p^2 = -\kappa_0^2\left[1 - \frac{\epsilon_{\nu\nu} a^2}{12\kappa_0^2}\right], \tag{3.22}$$

т.е. ослабление потока происходит медленнее, чем в гомогенной среде ($\kappa_0 = \kappa_r$ при $D = \text{const}$). Если же флуктуирует и сечение рассеяния (а следовательно, и коэффициент диффузии), то и в плоской и в двумерной решетках при "продольной" диффузии (для простоты мы ограничимся рассмотрением предельного случая $a\kappa_0 \to 0$)

$$p_{\parallel}^2 = -\kappa_0^2, \tag{3.23}$$

причем

$$\kappa_0^2 = \frac{\Sigma_{a0}}{D_0} \neq \kappa_r^2 = 3\,\Sigma_{a0}\cdot\Sigma_{s0}\,; \qquad \Sigma_{s0} \text{ – среднее сечение рассеяния.}$$

В случае "поперечной" диффузии в плоской решетке

$$p_{\perp 1}^2 = -\frac{\kappa_0^2}{1-\epsilon_{\eta\eta}} \approx -3\,\Sigma_{a0}\,\Sigma_{s0} = -\kappa_r^2, \tag{3.24}$$

т.е. в предельном случае тонких слоев диффузия поперек слоев происходит так же как и в гомогенной среде.

Если же нейтроны диффундируют вдоль направления, перпендикулярного оси двумерной решетки, то

$$p_{\perp 2}^2 = -\kappa_0^2 \frac{1}{1-\epsilon_{\eta\eta}/2} \neq -\kappa_r^2, \tag{3.25}$$

а при диффузии в изотропной среде

$$p^2 = -\frac{\kappa_0^2}{1-\epsilon_{\eta\eta}/3} \neq -\kappa_r^2. \tag{3.26}$$

Формулы (3.23) – (3.26) совпадают с результатами, полученными в Введении другим методом. Характерной особенностью этих выражений является их независимость от пространственного масштаба неоднородностей, что ограничивает область применимости теории малыми (по амплитуде) флуктуациями. Чтобы устранить это ограничение, необходимо точно учесть все поправки к постоянной релаксации κ_0, не содержащие малого отношения масштаба неоднородности к длине диффузии в однородной среде, а не только первую из них $\sim \epsilon_{\eta\eta}$. Осуществив эту программу (см. приложение Б), получим, что выражение (3.23) остается неизменным, а вместо (3.24) – (3.26), соответственно, выступают

$$p_{\perp 1}^2 = -\kappa_0^2 \left\langle \frac{1}{1+\eta} \right\rangle = -\kappa_r^2 \tag{3.24a}$$

$$p_{\perp 2}^2 = -\frac{\kappa_0^2}{2} \frac{\left\langle \frac{1}{1+\eta/2} \right\rangle}{1-\frac{1}{2}\left\langle \frac{1}{1+\eta/2} \right\rangle} \neq -\kappa_r^2 \tag{3.25a}$$

$$p^2 = -\frac{\kappa_0^2}{3} \frac{\left\langle \frac{1}{1+\eta/3} \right\rangle}{1-\frac{2}{3}\left\langle \frac{1}{1+\eta/3} \right\rangle} \neq -\kappa_r^2 \tag{3.26a}$$

При малых флуктуациях эти выражения переходят, соответственно, в (3.24) – (3.26). Параметры анизотропии диффузии оказываются равными (при $a\kappa_0 \to 0$):

<u>плоская решетка</u>

$$\frac{L_{\parallel}^2}{L_{\perp}^2} = \frac{\kappa_r^2}{\kappa_0^2} = \left\langle \frac{1}{1+\eta} \right\rangle \approx 1 + \langle \eta^2 \rangle \tag{3.27}$$

двумерная решетка

$$\frac{L_{\parallel}^2}{L_{\perp}^2} = \frac{\left\langle \frac{1}{1+\eta/2} \right\rangle}{2 - \left\langle \frac{1}{1+\eta/2} \right\rangle} \approx 1 + \frac{\langle \eta^2 \rangle}{2} \tag{3.28}$$

Например, в частном случае двухкомпонентной среды с длинами свободного пробега λ_1 и λ_2 соответственно, из (3.28), получаем*

$$\frac{L_{\parallel}^2}{L_{\perp}^2} = \frac{\langle \lambda \rangle (\lambda_1 + \lambda_2)}{\langle \lambda \rangle^2 + \lambda_1 \lambda_2} \tag{3.29}$$

Поправки к результатам (3.23) – (3.29), зависящие от пространственного масштаба неоднородности, можно учесть в рамках M_1-приближения. Выражения, содержащиеся в (3.23) – (3.29) определяются лишь объемным содержанием компонент среды. Итак, решая задачу о релаксации среднего потока нейтронов в M_1-приближении и заменяя слагаемые в выражениях для постоянной затухания потока, не исчезающие при $ak_0 \to 0$, их значениями согласно формулам (3.23), (3.24а) – (3.26а), мы получаем результаты, справедливые при сильных (по амплитуде) мелкомасштабных флуктуациях коэффициента диффузии и сечения поглощения в среде.

Из выражений (3.27) и (3.28) следует, что анизотропия диффузии сохраняется и при исчезающе малом размере неоднородности. Этот физически бессмысленный результат является следствием необоснованного применения диффузионного уравнения в предельном случае $\ell / L_0 \to 0$ [5] (ℓ – размер неоднородности, L_0 – длина диффузии в гомогенной среде), который может быть проанализирован с помощью точного кинетического уравнения.

4. СТАЦИОНАРНОЕ ОДНОСКОРОСТНОЕ КИНЕТИЧЕСКОЕ УРАВНЕНИЕ

Функция Грина стационарного односкоростного кинетического уравнения в неорганической среде с изотропным рассеянием удовлетворяет уравнению

$$-\vec{n}\nabla G(\vec{r}\,\vec{n}/\vec{r}_0\,\vec{n}_0) - \Sigma_t(\vec{r}) G(\vec{r}, \vec{n}/\vec{r}_0, \vec{n}_0)$$

$$+ \frac{\Sigma_s(\vec{r})}{4\pi} \int d\vec{\Omega}' G(\vec{r}, \vec{n}'/\vec{r}_0, \vec{n}_0) = -\delta(\vec{r} - \vec{r}_0)\, \delta(\vec{n} - \vec{n}_0) \tag{4.1}$$

$\vec{n}$ – единичный вектор в направлении движения нейтрона; Σ_t и Σ_s – полное сечение и сечение рассеяния, соответственно:

---

* При малом объемном содержании одной из компонент выражения (3.27) – (3.29) совпадают с соответствующими результатами работы [10].

Оператор $\hat{B}$ и возмущение $\hat{\mu}$ определяются следующими очевидными соотношениями:

$$\hat{B}G(\vec{r}, \vec{n}/\vec{r}_0, \vec{n}_0) = -[\vec{n}\nabla + \Sigma_{t0}]G(\vec{r}, \vec{n}/\vec{r}_0, \vec{n}_0)$$

$$+ \frac{\Sigma_{s0}}{4\pi}\int d\vec{\Omega}' G(\vec{r}, \vec{n}'/\vec{r}_0, \vec{n}_0) \tag{4.2}$$

$$\hat{\mu}(\vec{r})\, G(\vec{r}, \vec{n}/\vec{r}_0, \vec{n}_0) = G_t(\vec{r}) G(\vec{r}, \vec{n}/\vec{r}_0, \vec{n}_0)$$

$$- \frac{G_s(\vec{r})}{4\pi}\int d\vec{\Omega}' G(\vec{r}, \vec{n}'/\vec{r}_0, \vec{n}_0) \tag{4.3}$$

Подставляя $\hat{\mu}(\vec{r})$, определенное соотношением (3.3) и $G_0(\vec{r}, \vec{n}/\vec{r}_0, \vec{n}_0)$ (см., например, монографию [1]) выражение для оператора $M_1(\vec{r}, \vec{n}/\vec{r}', \vec{n}')$ (1.10) можно найти M_1 и получить кинетическое уравнение для усредненной функции Грина.

Будучи преобразованным по Фурье относительно $\vec{r} - \vec{r}_0$ в случае изотропного источника это уравнение примет вид:

$$(i\vec{p}\vec{n} - \Sigma_{t0})\langle g(\vec{p}, \vec{n})\rangle + \frac{\Sigma_{s0}}{4\pi}\langle g(\vec{p})\rangle$$

$$= -1 - \frac{1}{(2\pi)^3}\int d\vec{\xi}\, k_{tt}(\vec{\xi})\int d\vec{\Omega}' g_0(\vec{p} - \vec{\xi}, \vec{n}/\vec{n}')\langle g(\vec{p}, \vec{n})\rangle$$

$$+ \frac{1}{(2\pi)^3}\int d\vec{\xi}\, \frac{k_{ts}(\vec{\xi})}{4\pi}\left[\int d\vec{\Omega}' g_0(\vec{p} - \vec{\xi}/\vec{n}') g(\vec{p}, \vec{n}') + g_0(\vec{p} - \vec{\xi}, \vec{n})\langle g(\vec{p})\rangle\right]$$

$$- \frac{1}{(2\pi)^3}\int d\vec{\xi}\, \frac{k_{ss}(\vec{\xi})}{16\pi^2} g_0(\vec{p} - \vec{\xi})\langle g(\vec{p})\rangle. \tag{4.4}$$

Здесь были введены следующие обозначения

$$\langle g(\vec{p}, \vec{n})\rangle = \int d\vec{r}\, e^{i\vec{p}\vec{r}}\langle G(\vec{r}, \vec{n})\rangle$$

$$\langle g(\vec{p})\rangle = \int d\vec{\Omega}\langle g(\vec{p}, \vec{n})\rangle$$

Фурье-образ функции Грина кинетического уравнения в нулевом приближении

$$g_0(\vec{p}, \vec{n}/\vec{n}') = -\frac{\delta(\vec{n} - \vec{n}')}{i\vec{p}\vec{n} - \Sigma_{t0}}$$

$$+ \frac{\Sigma_{s0}}{4\pi}\frac{1}{i\vec{p}\vec{n} - \Sigma_{t0}}\left[1 + \frac{\Sigma_{s0}}{4\pi}\int\frac{d\vec{\Omega}''}{i\vec{p}\vec{n}'' - \Sigma_{t0}}\right]^{-1}\frac{1}{i\vec{p}\vec{n}' - \Sigma_{t0}}, \tag{4.5}$$

$$g_0(\vec{p}, \vec{n}) = \int d\vec{\Omega}' g_0(\vec{p}, \vec{n}/\vec{n}') \quad \text{и т.д.}$$

Если устремить ℓ -характерный размер неоднородностей среды – к нулю (при неизменном уровне флуктуаций ϵ_{ij}), то интегралы в правой части (4.4) исчезают и это уравнение совпадает с кинетическим уравнением для гомогенной среды при произвольном направлении диффузии. Этот вывод можно получить, если учесть, что $\epsilon_{ij} = \frac{1}{(2\pi)^3}\int k_{ij}(\vec{\xi})\,d\vec{\xi}$ не зависит от размера неоднородностей, а функция $g_0(\vec{p}-\vec{\xi},\vec{n}/\vec{n}')$ при $\ell \to 0$ пропорциональна ℓ. Более точно: необходимо, чтобы

$$\vec{\xi}\vec{n} \sim \ell_{эфф}^{-1} \gg \Sigma_{t0} \gg \kappa_0$$

Здесь $\ell_{эфф}$ – эффективная длина пути, проходимого нейтроном в области, заполненной материалом определенного сорта; например, в случае плоской решетки $\ell_{эфф} = a/\sin\theta$, a – толщина слоя, θ – угол между направлением движения нейтрона (вектор $\vec{n}$) и плоскостью слоя. Это неравенство не удовлетворяется при $\vec{\xi}\vec{n} = 0$, т.е. для нейтронов, движущихся параллельно слоям решетки. В этом случае необходим более тщательный анализ [7].

Будем искать решение уравнения (4.4) методом сферических гармоник. В первом приближении

$$\langle g(\vec{p},\vec{n})\rangle = \frac{1}{4\pi}\left[\langle g(\vec{p})\rangle + 3\vec{n}\langle \vec{g}_1(\vec{p})\rangle\right] \tag{4.6}$$

С помощью стандартных преобразований (см., например, [1]) получим следующее уравнение, определяющее постоянную релаксации нейтронного потока:

$$\langle g(\vec{p})\rangle^{-1} = p^2 + \kappa_r^2 - \frac{3}{(2\pi)^3}\int\frac{d\vec{\xi}}{4\pi}\left\{\Sigma_{t0}\,k_{aa}(\vec{\xi})g_0^{00}(\vec{p}-\vec{\xi})\right.$$

$$\left. + 2k_{ta}(\vec{\xi})g_0^{10}(\vec{p}-\vec{\xi}) + \frac{k_{tt}(\vec{\xi})}{\Sigma_{t0}(\vec{\xi})}g_0^{11}(\vec{p}-\vec{\xi})\right\} = 0 \tag{4.7}$$

Здесь

$$g_0^{\ell j}(\vec{p}-\vec{\xi}) = \int d\vec{\Omega}\int d\vec{\Omega}'(i\vec{p}\vec{n})^{\ell} g_0(\vec{p}-\vec{\xi},\vec{n}/\vec{n}')(i\vec{p}\vec{n}')^j \tag{4.8}$$

При выводе уравнения (4.7) мы пренебрегли, как обычно в диффузионном приближении, вкладом в постоянную релаксации членов порядка $(\lambda_{s0}\kappa_r)^2 \sim \lambda_{s0}/\lambda_{a0}$. Влияние неоднородностей уравнение (4.7) учитывает с той же степенью точности, что и уравнение (3.4).

Фурье-компонента тока нейтронов $\langle \vec{g}_1(\vec{p})\rangle$ связана с Фурье-компонентой потока $\langle g(\vec{p})\rangle$ следующим соотношением

$$\langle \vec{g}_1(\vec{p})\rangle = \frac{\langle g(\vec{p})\rangle}{3\Sigma_{t0}}\left[i\vec{p} + \frac{3}{(2\pi)^3}\int\frac{d\vec{\xi}}{4\pi}k_{ta}(\vec{\xi})\int d\vec{\Omega}\,g_0(\vec{p}-\vec{\xi}_1\vec{n})\,\vec{n}\right.$$

$$\left. + \frac{3}{(2\pi)^3}\int\frac{d\vec{\xi}}{4\pi}\frac{k_{tt}(\vec{\xi})}{\Sigma_{t0}}\int\int d\vec{\Omega}\,d\vec{\Omega}'\vec{n}\,g_0(\vec{p}-\vec{\xi}_1\vec{n}/\vec{n}')(i\vec{p}\vec{n}')\right] \tag{4.9}$$

Первое слагаемое в скобках в правой части (4.9) соответствует диффузии в гомогенной среде. Второе слагаемое, как правило, мало по сравнению с остальными* и слабо зависит от направления диффузии: оно обусловлено локальными флуктуациями потока нейтронов. Третье слагаемое зависит от ориентации источника по отношению к слоям вещества: оно учитывает влияние флуктуаций потока нейтронов на макроскопический ток. Из выражения (4.9) следует, что в координатном представлении связь среднего тока нейтронов $\langle\vec{j}\rangle$ с потоком, усредненным по флуктуациям параметров среды, оказывается интегральной (хотя мы используем для $\langle g(\vec{p}, \vec{n})\rangle$ P_1 -приближение)

$$\langle\vec{j}(\vec{r})\rangle = \int d\vec{r}\,' \hat{\vec{R}}(\vec{r} - \vec{r}\,')\langle G(\vec{r}\,')\rangle \tag{4.10}$$

Таким образом использованное нами в Введении соотношение (1.1) оказывается неточным. Величина тока $\langle\vec{j}(\vec{r})\rangle$ в точке $\vec{r}$ зависит не только от поведения потока в той же точке, но и от значений $\langle G\rangle$ в области нелокальности оператора $\hat{\vec{R}}$. Размер этой области определяется пространственным масштабом флуктуаций в среде. Оператор $\hat{\vec{R}}$ в выражении (4.10) зависит от взаимной ориентации источника нейтронов и неоднородностей в среде. Вследствие этого, например, альбедо и экстраполированные размеры объема замедлителя могут зависеть от расположения неоднородностей вещества. Можно показать, используя (4.9), что в случае плоской решетки (2.6) при $a \ll \lambda_{s0}$

$$\frac{d_{\parallel}}{d_{\perp}} = 1 + \frac{6\epsilon_{ss}}{\pi^2}\frac{a}{\Sigma_{t0}}\sum_{n=1}^{\infty}\frac{1}{(2n-1)^3} \approx 1 + 0{,}64\frac{\epsilon_{ss}\,a}{\Sigma_{t0}}\ , \tag{4.11}$$

где $d_{\parallel}$ и $d_{\perp}$ – длины линейной экстраполяции в направлениях, параллельном и перпендикулярном слоям решетки, соответственно.

Рассмотрим уравнение (4.7) в следующих предельных случаях:

а) $\lambda_{t0} \approx \lambda_{s0} \ll \ell \ll \kappa_r^{-1} \equiv L_r$

В этом предельном случае знаменатели в выражении для $g_0(\vec{p} - \vec{\xi}, \vec{n}/\vec{n}\,')$ (4.5) можно разложить при $|\vec{p} - \vec{\xi}|$, p, $\ll \Sigma_{t0}$ в ряд по степеням малого отношения λ_{s0}/ℓ. Учитывая в этом разложении лишь главные члены, мы приходим к результату усреднения диффузионного уравнения (см. разд. 3).

В работе [7] приведены формулы, содержащие следующие члены ряда по степеням λ_{s0}/ℓ **

б) $\ell \ll \lambda_{s0} \approx \lambda_{t0} \ll \kappa_r^{-1} \equiv L_r$

Если флуктуирует только сечение рассеяния, т.е. $k_{aa} = k_{ta} \equiv 0$, то уравнение (4.7) упрощается.

---

* Это слагаемое необходимо учитывать, если флуктуирует только сечение поглощения.

** Уточнить диффузионное приближение можно иным путем, записывая функцию Грина нулевого приближения в виде суммы диффузионного ядра и ядра однократного столкновения (см. монографию Вейнберга и Вигнера) [2].

В приближении линейном относительно размера неоднородности ($\sim \ell / \lambda_{s0}$) это уравнение имеет вид [7, 9]

$$p^2 + \kappa_r^2 + \frac{3\pi^2}{\Sigma_{t0}} \frac{1}{(2\pi)^3} \int d\vec{\xi}\, \frac{k_{ss}(\vec{\xi})}{4\pi\xi} \left(p^2 - \frac{(\vec{p}\,\vec{\xi})}{\xi^2} \right)^2 = 0 \qquad (4.12)$$

Для решетки типа (2.6) в случае диффузии вдоль слоев

$$p_{\parallel}^2 = -\kappa_r^2 \left[1 + \frac{6}{\pi^2} \frac{\epsilon_{ss}\, a}{\Sigma_{t0}} \sum_{n=1}^{\infty} \frac{1}{(2n-1)^3} \right]^{-1}, \qquad (4.13)$$

тогда как для диффузии поперек слоев в этом приближении

$$p_{\perp}^2 = -\kappa_r^2 .$$

Таким образом, для этой системы эффект анизотропии диффузии определяется формулой

$$\frac{L_{\parallel}^2}{L_{\perp}^2} = 1 + \frac{6}{\pi^2} \frac{\epsilon_{ss}\, a}{\Sigma_{t0}} \sum_{n=1}^{\infty} \frac{1}{(2n-1)^3} \approx 1 + 0{,}64 \frac{\epsilon_{ss}\, a}{\Sigma_{t0}} \qquad (4.14)$$

При $a \to 0$ анизотропия диффузии исчезает.

В случае решетки типа (2.12) с одним стержнем в ячейке фактор анизотропии диффузии имеет вид

$$\frac{L_{\parallel}^2}{L_{\perp}^2} = 1 + \frac{3}{8} \frac{(\Sigma_{s1} - \Sigma_{s2})^2}{a\Sigma_{t0}} R^2 \sum_{n=0}^{\infty} \sum_{m=0}^{\infty} \lambda_{mn} \frac{\mathcal{J}_1^2\left(\frac{\pi R}{a} \sqrt{n^2 + m^2} \right)}{(n^2 + m^2)^{3/2}}$$

$$= 1 + \frac{3}{2\pi} \frac{\epsilon_{ss}\, a}{\Sigma_{t0}} \left[1 - \frac{\pi R^2}{4a^2} \right]^{-1} \sum_{n=0}^{\infty} \sum_{m=0}^{\infty} \lambda_{mn} \frac{\mathcal{J}_1^2\left(\frac{\pi R}{a} \sqrt{n^2 + m^2} \right)}{(n^2 + m^2)^{3/2}} . \qquad (4.15)$$

Дисперсия ϵ_{ss} равна

$$\epsilon_{ss} = \frac{\pi R^2}{4a^2} \left[1 - \frac{\pi R^2}{4a^2} \right] \left[\Sigma_{s1} - \Sigma_{s2} \right]^2 .$$

График суммы в (4.15) как функции R/a приведен на рис. 2.

В изотропной среде с корреляционной функцией

$$K_{ss}(\vec{r}) = \epsilon_{ss}\, e^{-\beta r} \qquad (4.16)$$

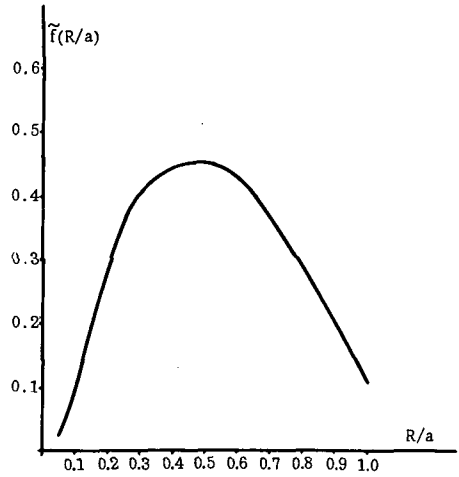

Рис. 2. График функции

$$\tilde{f}(R/a) = \sum_{n=0}^{\infty}\sum_{m=0}^{\infty} \lambda_{mn} \frac{\mathcal{J}_1^2\left(\frac{\pi R}{a}\sqrt{n^2+m^2}\right)}{(n^2+m^2)^{3/2}}$$

постоянная релаксации среднего потока нейтронов определяется выражением

$$p^2 = -\kappa_r^2 \frac{1}{1+\frac{\epsilon_{ss}}{\beta\Sigma_{t0}}} . \tag{4.17}$$

Воспользуемся этой формулой, чтобы оценить по порядку величины поправку к постоянной затухания потока нейтронов в кипящей жидкости. Пренебрегая рассеянием в пузырьке пара и полагая $\beta^{-1} \approx R_n$, R_n – радиус пузырька пара, получим из (4.17)

$$p^2 = -\kappa_r^2 \frac{1}{1+\rho\frac{R_n}{\lambda_{s0}}} , \tag{4.18}$$

где ρ – объемное паросодержание. Таким образом в практически интересных случаях поправка к κ_r может составлять несколько процентов.

В данном разделе мы рассмотрели кинетическое уравнение в среде с изотропным рассеянием. При наличии анизотропного рассеяния задача может быть решена аналогичным образом. При этом, однако, мы приходим к более громоздким выражениям. Приближенный учет анизотропии рассеяния сводится к замене Σ_s транспортным сечением рассеяния Σ_{tr}.

5. ДИФФУЗИЯ В МУЛЬТИПЛИЦИРУЮЩЕЙ СРЕДЕ

Уравнение, которому удовлетворяет поток нейтронов от элементарного источника в неоднородной размножающей среде, как известно [1, 2], имеет вид

$$\nabla^2 G(\vec{r}/\vec{r}_0) - \frac{1}{D_0}\Sigma_a(\vec{r})\, G(\vec{r}/\vec{r}_0)$$

$$+\int \frac{\tilde{k}(\vec{r}\,')}{D_0}\Sigma_a(\vec{r}\,')\, W(\vec{r}/\vec{r}\,')\, G(\vec{r}\,'/\vec{r}_0)\, d\vec{r}\,' = -\delta(\vec{r}-\vec{r}_0) \tag{5.1}$$

$\widetilde{k}(\vec{r})$ – количество быстрых нейтронов, рождающихся при поглощении одного теплового нейтрона; $W(\vec{r}/\vec{r}\,')$ – вероятность того, что быстрый нейтрон, возникший в точке $\vec{r}\,'$, замедлится до тепловой энергии в точке $\vec{r}$. Влияние гетерогенности среды на замедление не учитывается. Выше для простоты мы предположили, что коэффициент диффузии D_0 остается постоянным во всей диффузионной среде. В этом случае, очевидно,

$$BG(\vec{r}/\vec{r}_0) = [\nabla^2 - \kappa_0^2]\, G(\vec{r}/\vec{r}_0) + Q_0 \int W(\vec{r}/\vec{r}\,')\, G(\vec{r}\,'/\vec{r}_0)\, d\vec{r}\,' \qquad (5.2)$$

$$\mu G(\vec{r}/\vec{r}_0) = \nu(\vec{r}) G(\vec{r}/\vec{r}_0) - \int q(\vec{r}\,')\, W(\vec{r}/\vec{r}\,') G(\vec{r}\,'/\vec{r}_0) d\vec{r}\,' \qquad (5.3)$$

Были введены обозначения

$$Q(\vec{r}) = \frac{\widetilde{k}(\vec{r})\Sigma_a(\vec{r})}{D_0}, \qquad Q_0 = \langle Q(\vec{r})\rangle\,;$$

$$q(\vec{r}) = Q(\vec{r}) - Q_0\,; \qquad \nu(\vec{r}) = \frac{\Sigma_a(\vec{r}) - \Sigma_{a0}}{D_0} \qquad (5.4)$$

Если диффузионная среда однородна в среднем и занимает все пространство, то нетрудно, используя преобразование Фурье относительно $\vec{r} - \vec{r}_0$, получить следующее уравнение для постоянной релаксации потока нейтронов*:

$$p^2 + \kappa_0^2 - Q_0\omega(\vec{p}) - m_1(\vec{p}) = 0\,. \qquad (5.5)$$

Здесь

$$m_1(\vec{p}) = \frac{1}{(2\pi)^3}\int d\vec{\xi}\, \frac{k_{\nu\nu}(\vec{\xi}) - k_{\nu q}(\vec{\xi})[\omega(\vec{p}-\vec{\xi}) + \omega(\vec{p})] + k_{qq}(\vec{\xi})\omega(\vec{p})\omega(p-\xi)}{(\vec{p}-\vec{\xi})^2 + \kappa_0^2 - Q_0\,\omega(\vec{p}-\vec{\xi})} \qquad (5.6)$$

и

$$\omega(\vec{p}) = \int d(\vec{r} - \vec{r}\,')\, e^{i\vec{p}(\vec{r}-\vec{r}\,')}\, W(\vec{r} - \vec{r}\,') \qquad (5.7)$$

Принимая во внимание, что ℓ – характерный размер неоднородности в среде – мал по сравнению с κ_0^{-1} и возрастом нейтронов в однородной среде τ, можно упростить выражение для $m_1(\vec{p})$. С точностью до членов, квадратичных относительно ℓ, имеем**

$$m_1(\vec{p}) = \frac{1}{(2\pi)^3}\int \frac{d\vec{\xi}}{\xi^2}\left[k_{\nu\nu}(\vec{\xi}) - k_{\nu q}(\vec{\xi})\omega(\vec{p})\right] \qquad (5.8)$$

---

* Все выкладки аналогичны проведенным выше.

** В случае систем с периодической структурой функции k_{ij} обращаются в нуль в окрестности $\xi = 0$.

Таким образом, в случае размножающей среды функция $m_1(\vec{p})$ уже более не является положительно определенной и постоянная релаксации среднего потока может быть как меньше постоянной затухания нейтронного потока в однородной среде, так и больше ее.

В том случае, когда гетерогенная система занимает ограниченный объем, можно получить уравнение аналогичное (5.5) – характеристическое уравнение реактора:

$$\mathrm{Det}\,\|[\alpha_k^2+\kappa_0^2]\,\delta_{kn}-G_0\langle k|W|n\rangle-\langle k|M_1|n\rangle\|=0 \qquad (5.9)$$

Здесь

$$\langle k|W|n\rangle=\int\int d\vec{r}d\vec{r}'\varphi_k(\vec{r})\,W(\vec{r}/\vec{r}')\varphi_n(\vec{r}) \qquad (5.10)$$

$$\langle k|M_1|n\rangle=\int\int d\vec{r}d\vec{r}'\,\varphi_k(\vec{r})M_1(\vec{r}/\vec{r}')\,\varphi_n(\vec{r})$$

φ_n – собственные функции соответствующей краевой задачи:

$$\nabla^2\,\varphi_n(\vec{r})+\alpha_n^2\varphi_n(\vec{r})=0 \qquad (5.11)$$

6. НЕСТАЦИОНАРНАЯ ДИФФУЗИЯ ТЕПЛОВЫХ НЕЙТРОНОВ

В диффузионном приближении поток тепловых нейтронов от импульсного источника удовлетворяет уравнению

$$-\frac{1}{vD_0}\frac{\partial}{\partial t}G(\vec{r},t/\vec{r}_0t_0)+\mathrm{div}\left[\frac{D(\vec{r})}{D_0}\,\mathrm{grad}\,G(\vec{r},\,t/\vec{r}_0,\,t_0)\right]$$

$$-\frac{\Sigma_a(\vec{r})}{D_0}G(\vec{r},\,t/\vec{r}_0,\,t_0)=-\,\delta(\vec{r}-\vec{r}_0)\,\delta(t-t_0), \qquad (6.1)$$

где v – скорость нейтронов.

Возмущение, обусловленное неоднородностью среды, описывается выражением (3.5) и не зависит от времени. Поэтому с помощью преобразования Лапласа относительно $t-t_0$

$$G(\vec{r}/\vec{r}_0;\,\lambda)=\int_0^\infty d(t-t_0)\,e^{-\lambda(t-t_0)}\,G(\vec{r},t/\vec{r}_0,t_0) \qquad (6.2)$$

уравнение (6.1) можно записать в виде стационарного диффузионного уравнения (3.1). Таким образом усредненная функция Грина $\langle G(\vec{r}/\vec{r}_0;\lambda)\rangle$ удовлетворяет уравнению

$$\hat{B}_\lambda\langle G(\vec{r}/\vec{r}_0;\,\lambda)\rangle=-\,\delta(\vec{r}-\vec{r}_0)-\int d\vec{r}'M_1^\lambda(\vec{r}/\vec{r}')\langle G(\vec{r}'/\vec{r}_0;\lambda)\rangle \qquad (6.3)$$

Здесь

$$\hat{B}_\lambda = \nabla^2 - \kappa_\lambda^2 \tag{6.4}$$

$$\kappa_\lambda^2 = \kappa_0^2 + \frac{\lambda}{vD_0} \tag{6.5}$$

$$M_1^\lambda(\vec{r}/\vec{r}\,') = \langle \hat{\mu}(\vec{r}) G_0^\lambda(\vec{r}/\vec{r}\,') \hat{\mu}(\vec{r}\,') \rangle \tag{6.6}$$

Функция Грина нулевого приближения, как обычно, является решением уравнения

$$\hat{B}_\lambda G_0^\lambda(\vec{r}/\vec{r}_0) = -\delta(\vec{r} - \vec{r}_0) \tag{6.7}$$

В случае неограниченной пространственно однородной среды можно получить следующее выражение для Фурье-образа функции Грина $\langle G(\vec{r}/\vec{r}_0;\, \lambda) \rangle$

$$\langle g(\vec{p},\, \lambda) \rangle = [p^2 + \kappa_\lambda^2 - m_1(\vec{p},\, \lambda)]^{-1}\ , \tag{6.8}$$

где $m_1(\vec{p},\, \lambda)$ определяется выражением (3.13) с заменой κ_0^2 на κ_λ^2.

В случае периодической решетки (2.6), состоящей из очень тонких слоев ($a\kappa_0 \ll 1$, но $a/\lambda_s \gg 1$ так, что применима теория диффузии)

$$m_1(\vec{p},\, \lambda) = \epsilon_\eta p_z^2 \tag{6.9}$$

и при диффузии вдоль слоев

$$\langle G(x - x_0;\, t - t_0) \rangle = v D_0 \frac{e^{-\frac{(x - x_0)^2}{4vD_0(t - t_0)}}}{[4\pi v D_0 (t - t_0)]^{1/2}} e^{-vD_0\kappa_0^2(t - t_0)} \tag{6.10}$$

Если нейтроны диффундируют поперек слоев, то

$$\langle G(z - z_0;\, t - t_0) \rangle = v D_0 \frac{e^{-\frac{(z - z_0)^2}{4vD_r(t - t_0)}}}{[4\pi v D_r (t - t_0)]^{1/2}} e^{-vD_0\kappa_0^2(t - t_0)}$$

$$D_0 \cdot \kappa_0^2 = \Sigma_{a0} \tag{6.11}$$

Следовательно, в случае очень тонких слоев скорость убывания потока нейтронов во времени такая же, что в гомогенной среде, а скорость расплывания нейтронного импульса в пространстве оказывается зависящей от ориентации плоского источника по отношению к слоям решетки (см. также [8]).

Рассмотрим теперь диффузию нейтронов от нестационарного источника, помещенного в среду ограниченного объема. Будем искать реше-

ние уравнения (6.3) в виде разложения по полной системе функций $\varphi_n(\vec{r})$ соответствующей краевой задачи, т.е.

$$\langle G(\vec{r}/\vec{r}_0;\ \lambda)\rangle = \sum_n g_n(\vec{r};\ \lambda)\,\varphi_n(\vec{r}) \tag{6.12}$$

$$\nabla^2 \varphi_n(\vec{r}) + \alpha^2 \varphi_n(\vec{r}) = 0 \tag{6.13}$$

Граничные условия те же, что и для однородной среды.

Коэффициенты разложения $g_n(\vec{r}_0,\ \lambda)$ удовлетворяют следующей системе уравнений

$$\sum_n g_n(\vec{r}_0,\ \lambda)[(\kappa_\lambda^2 + \alpha_n^2)\,\delta_{kn} - m_{kn}^\lambda] = \varphi_k(\vec{r}_0), \tag{6.14}$$

где

$$m_{kn}^\lambda = \iint d\vec{r}'\,d\vec{r}\,\varphi_k(\vec{r}) M_1^\lambda(\vec{r}/\vec{r}')\varphi_n(\vec{r}') \tag{6.15}$$

В первом приближении коэффициент при основной гармонике имеет вид

$$g_1(\vec{r}_0,\ \lambda) = \frac{\varphi_1(\vec{r}_0)}{\kappa_\lambda^2 + \alpha_1^2 - m_{11}^\lambda}, \tag{6.16}$$

т.е. постоянная затухания основной гармоники уменьшается на m_{11}^λ (при $m_{11}^\lambda > 0$). Например, в случае плоского источника нейтронов в слоистой среде эта добавка зависит от ориентации источника по отношению к слоям и таким образом учитывает анизотропию диффузии нейтронов.

В заключение этого раздела отметим, что в предыдущей работе автора [6 б) была рассмотрена задача о нестационарном плоском источнике тепловых нейтронов в слое вещества со случайными неоднородностями. Предполагалось, что длина корреляции флуктуаций очень мала по сравнению с толщиной слоя (корреляционная функция $\sim \delta(z - z_0)$). Было показано, что основной пространственной гармонике отвечают две постоянные затухания. Этот результат является следствием предположения о специальном виде корреляционной функции. В случае периодической структуры расщепления основного собственного значения на два близко лежащих друг к другу нет: постоянная затухания уменьшается так же как и в стационарном случае.

7. УЧЕТ ЭНЕРГЕТИЧЕСКОЙ ЗАВИСИМОСТИ ФУНКЦИИ РАСПРЕДЕЛЕНИЯ НЕЙТРОНОВ

Перенос нейтронов в области энергий, превышающих тепловую, в возрастном приближении подчиняется уравнению диффузионного типа (6.1) и результаты предыдущего раздела могут быть использованы для анализа поведения среднего потока замедляющихся нейтронов.

Рассмотрим термализацию нейтронов в неоднородной среде, полагая для простоты, что флуктуирует только сечение поглощения. Предположим также, что соответствующая задача для однородной среды решена и известно выражение для функции Грина в нулевом приближении G_0.

Тогда для потока нейтронов от элементарного источника запишем в диффузионном приближении кинетическое уравнение

$$\nabla^2 G(\vec{r}, \vec{E} \,|\, \vec{r}_0, E_0) - \kappa_0^2(E)\, G(\vec{r}, E \,|\, \vec{r}_0, E_0) - \nu(\vec{r}, E)\, G(\vec{r}, E \,|\, \vec{r}_0, E_0)$$

$$+ \int G(\vec{r}, E' \,|\, \vec{r}_0, E_0) \frac{\Sigma_{s0}(E, E')}{D_0(E)} dE' = -\delta(E - E_0)\, \delta(\vec{r} - \vec{r}_0) \tag{7.1}$$

Здесь $\Sigma_{s0}(E, E')$ – ядро рассеяния, т.е. дифференциальное (относительно энергии) макроскопическое сечение рассеяния нейтронов с энергией E' в единичный интервал энергий вблизи E; $\kappa_0^2(E) = \frac{\Sigma_{t0}(E)}{D_0(E)}$, $\nu(\vec{r}, E) = \frac{\delta_a(\vec{r}, E)}{D_0(E)}$.

В M_1 – приближение Фурье-образ среднего потока нейтронов (преобразование Фурье выполнено относительно $\vec{r} - \vec{r}_0$) в случае неограниченной пространственно-однородной среды удовлетворяет уравнению

$$-[p^2 + \kappa_0^2(E)] \langle g(\vec{p}, E; E_0) \rangle + \int dE' \tilde{\Sigma}(E, E', \vec{p}) \langle g(\vec{p}, E'; E_0) \rangle = -\delta(E - E_0) \tag{7.2}$$

$$\langle g(\vec{p}, E; E_0) \rangle = \int d(\vec{r} - \vec{r}_0) e^{i\vec{p}(\vec{r} - \vec{r}_0)} \langle G(\vec{r}, E \,|\, \vec{r}_0, E_0) \rangle$$

$$\tilde{\Sigma}(E, E'; p) = \frac{1}{D_0(E)} \Sigma_{s0}(E, E') + \frac{1}{(2\pi)^3} \int d\vec{\xi}\, k_{\nu\nu}(\vec{\xi}, E; E') g_0(\vec{p} - \vec{\xi}, E; E') \tag{7.3}$$

Таким образом, флуктуации сечения поглощения в рассматриваемом приближении приводят к изменению ядра рассеяния.
Можно показать [7], что

$$\tilde{\Sigma}(E', E; \vec{p}) = \frac{D_0(E)}{D_0(E')} \frac{E'}{E} e^{\frac{E - E'}{k_Б T}} \tilde{\Sigma}(E, E'; \vec{p}) \tag{7.4}$$

Это отношение для $\tilde{\Sigma}(E, E'; \vec{p})$ эквивалентно принципу детального баланса для ядра рассеяния $\Sigma_{s0}(E, E')$

$$\Sigma_{s0}(E', E) = \Sigma_{s0}(E, E') e^{\frac{E' - E}{k_Б T}} \frac{E'}{E} \tag{7.5}$$

Решение уравнения (7.2) будем искать в виде разложения по полиномам Лагерра

$$\langle g(\vec{p}, E; E_0) \rangle = \sum_{i=0}^{\infty} \frac{E}{(k_Б T)^2} e^{-\frac{E}{k_Б T}} \frac{L_i^{(1)}(E/k_Б T)}{\sqrt{i!(i+1)!}} g_i(\vec{p}_1 E_0) \tag{7.6}$$

Для коэффициентов $g_i(p_1\ E_0)$ получаем следующую систему уравнений

$$\sum_{i=0}^{\infty}\{-[\delta_{ki}\,p^2+(\kappa_0^2(E)_{ki}]+\tilde{\gamma}_{ki}(\vec{p})\}\,g_i(\vec{p}_1E_0)=-\frac{L_k^{(1)}(E_0/k_БT)}{\sqrt{k!(k+1)!}} \tag{7.7}$$

$k=0,\ 1,\ 2\ldots$

$$(\kappa_0^2(E))_{ki}=\int\frac{dE\cdot E}{(\kappa_БT)^2}e^{-\frac{E}{k_БT}}\kappa_0^2(E)\,\frac{L_k^{(1)}\left(\frac{E}{k_БT}\right)L_i^{(1)}\left(\frac{E}{k_БT}\right)}{\sqrt{i!(i+1)!\ k!(k+1)!}} \tag{7.8}$$

$$(\tilde{\gamma}(\vec{p}))_{ki}=\int dE\int dE'\,\frac{E'}{(k_БT)^2}e^{-E'/k_БT}L_k^{(1)}\left(\frac{E}{k_БT}\right)L_i^{(1)}\left(\frac{E'}{k_БT}\right)\frac{\tilde{\Sigma}(E,\ E';\ \vec{p})}{\sqrt{i!\ (i+1)!\ k!(k+1)!}} \tag{7.9}$$

В одногрупповом приближении

$$g_1(\vec{p},\ E_0)=\frac{L_0^{(1)}(E/k_БT)}{p^2+(\kappa_0(E))_{00}-\tilde{\gamma}_{00}(\vec{p})} \tag{7.10}$$

Для области замедлителя, свободной от источников, можно сформулировать задачу на собственные значения

$$[p^2+\kappa_0^2(E)]\langle\Phi(E,\vec{p})\rangle-\int dE'\tilde{\Sigma}(E,E',\vec{p})\langle\Phi(E',\vec{p})\rangle=0 \tag{7.11}$$

Если энергетическую зависимость потока нейтронов $\langle\Phi(E,\vec{p})\rangle$ аппроксимировать максвелловским распределением $\frac{E}{k_БT}e^{-E/k_БT}$ то из (7.11) следует (см. также (7.10))

$$p^2=\tilde{\gamma}_{00}(\vec{p})-(\kappa_0^2(E))_{00}$$

$$=\iint dEdE'\,\frac{E'}{(k_БT)^2}e^{-\frac{E'}{k_БT}}\int\frac{d\vec{\xi}}{(2\pi)^3}k_{\nu\nu}(\vec{\xi},\ E,\ E')\,g_0(\vec{p}-\vec{\xi},\ E,\ E')-\left(\frac{\Sigma_{a0}(E)}{D_0(E)}\right)_{00}$$

Таким образом, как и в односкоростном случае, флуктуации сечения поглощения, приводят к уменьшению постоянной затухания потока нейтронов по сравнению с однородной средой.

Если характерный размер неоднородности $\xi_{эфф}^{-1}$ мал по сравнению с λ_{s0}, то диффузионное приближение неприменимо, и необходимо рассмотреть точное кинетическое уравнение, которое в M_1 – приближении для изотропного рассеяния – имеет вид (см. разд.4)

$$[i\vec{p}\vec{n}-\Sigma_{t0}(E)]\langle g(\vec{p},\ \vec{n},\ E;E_0)\rangle+\frac{1}{4\pi}\iint d\vec{\Omega}'dE'\Sigma_{s0}(E,\ E')\langle g(\vec{p},\ \vec{n}',\ E';\ E_0)\rangle$$

$$=-\delta(E-E_0)-\frac{1}{(2\pi)^3}\int d\vec{\xi}\int dE'k_{aa}(\vec{\xi},\ E,\ E')\int d\vec{\Omega}g_0(\vec{p}-\vec{\xi},\ \vec{n},\ \vec{n}';E,\ E')$$

$$\times\langle g(\vec{p},\ \vec{n}';\ E';\ E_0)\rangle. \tag{7.12}$$

Источник нейтронов в уравнении (7.12) изотропный, $\vec{n}$ – единичный вектор в направлении движения нейтрона. В первом приближении относительно $\xi^{-1}_{эфф}$ нулевую функцию Грина можно записать в виде*

$$g_0(\vec{p}-\vec{\xi},\ \vec{n};\ \vec{n}';\ E;\ E') \approx \frac{\delta(E-E')\,\delta(\vec{n}-\vec{n}')}{i(\vec{p}-\vec{\xi})\vec{n}-\Sigma_{t0}(E)} \tag{7.13}$$

Подставляя (7.13) в уравнение (7.12), получим

$$[i\vec{p}\vec{n}-\Sigma_{t1}(E)]\langle g(\vec{p},\ \vec{n};\ E;\ E_0)\rangle + \frac{1}{4\pi}\int\int d\vec{\Omega}dE'\,\Sigma_{s0}(E,\ E')$$

$$\times\langle g(\vec{p},\ \vec{n}',\ E';E_0)\rangle = -\,\delta(E-E_0), \tag{7.14}$$

где

$$\Sigma_{t1}(E) = \Sigma^{(E)}_{t0} - \frac{1}{(2\pi)^3}\int d\vec{\xi}\,\frac{k_{aa}(\vec{\xi},\ E;\ E)}{i(\vec{p}-\vec{\xi})\vec{n}-\Sigma_{t0}(E)}$$

$$\approx \Sigma^{(E)}_{t0} + \frac{1}{(2\pi)^3}\int d\vec{\xi}\,\frac{k_{aa}(\vec{\xi};\ E;\ E)}{i\vec{\xi}\vec{n}+\Sigma_{t0}(E)}$$

Итак, в линейном приближении относительно $\xi^{-1}_{эфф}$ – характерного размера неоднородности, поправка к постоянной затухания потока нейтронов оказывается такой же, как и в односкоростном случае (см. разд.4).

8. ЗАКЛЮЧЕНИЕ

В данной работе было выведено приближенное уравнение для среднего потока нейтронов от элементарного источника в диффузионной среде с флуктуирующими параметрами. Необходимая информация о структуре среды содержится в корреляционной функции флуктуаций, которая может быть найдена для широкого класса диффузионных сред от периодической структуры типа (2.6) до среды со случайно расположенными примесями** (см. приложение В).

В качестве характерного параметра, описывающего перенос нейтронов в гетерогенной среде, рассмотрено выражение для постоянной релаксации среднего потока нейтронов. Развитый выше подход позволяет проанализировать и другие важные величины, как, например, среднее сечение поглощения и т.п. (см. приложение А, формулу (А.18).

В заключение автор выражает глубокую признательность М.В.Казарновскому за постоянный интерес к работе и полезные замечания.

---

* Это приближение неприменимо для нейтронов, движущихся параллельно слоям плоской решетки, либо вдоль стержней в двумерной решетке (см. разд.4).

** Примерами неупорядоченной среды могут служить кипящая жидкость и горные породы. Рассмотрение последних представляет интерес в некоторых задачах ядерной геофизики.

ПРИЛОЖЕНИЕ А

Выводы основного уравнения

Однородное кинетическое уравнение, описывающее перенос нейтронов в среде без источников, можно записать в символической форме

$$\hat{A}\psi(x) = 0, \tag{A.1}$$

где $\hat{A}$ – линейный оператор, действующий на x совокупность переменных, от которых зависит функция распределения ψ. В случае неоднородной среды оператор $\hat{A}$ содержит компоненты, зависимость которых от пространственных координат $\vec{r}$ имеет нерегулярный характер. Выделим из оператора $\hat{A}$ флуктуирующую часть

$$\hat{A}(x) = \hat{B}(x) - \hat{\mu}(x), \tag{A.2}$$

где

$$\hat{B}(x) = \langle \hat{A}(x) \rangle \tag{A.3}$$

$$\langle \hat{\mu}(x) \rangle = 0 \tag{A.4}$$

Уголковые скобки означают вычисление среднего по ансамблю неоднородных сред. Для реактора это сводится к усреднению по объему элементарной ячейки (см. Введение).

Обозначим через $G(x/y)$ функцию Грина уравнения (A.1). Как известно,

$$\hat{A}(x)G(x/y) = -\delta(x-y), \tag{A.5}$$

где $\delta(x-y)$ – произведение δ-функций по отдельным переменным. Принимая во внимание (A.3), запишем (A.6) в интегральной форме

$$G(x/y) = G_0(x/y) - \int dx' G_0(x/x')\hat{\mu}/x')G(x'/y). \tag{A.6}$$

Функция $G_0(x/y)$, удовлетворяющая уравнению

$$\hat{B}(x)G_0(x/y) = -\delta(x-y), \tag{A.7}$$

есть функция Грина кинетического уравнения

$$\hat{B}(x)\psi_0(x) = 0, \tag{A.8}$$

описывающего перенос нейтронов в однородной среде. Как было показано ранее [6, 7], непосредственное применение метода последовательных приближений для отыскания решения уравнения (A.6), приводит к представлению $\langle G(x/y)\rangle$ в виде ряда, плохо сходящегося (или вообще расходящегося) на больших расстояниях от источника. Поэтому воспользуемся другим методом. А именно, усредним уравнение (A.6). Получим

$$\langle G(x/y)\rangle = G_0(x/y) - \int dx' G_0(x/x')\langle \hat{\mu}(x')\, G(x'/y)\rangle \qquad (A.9)$$

Ценой введения нового, пока неизвестного оператора $M(x'/x'')$, устраним коррелятор $\langle \hat{\mu}(x')G(x'/y)\rangle$ и получим замкнутое уравнение для функции $\langle G(x/y)\rangle$

$$\langle G(x/y)\rangle = G_0(x/y) + \int dx' \int dx'' G_0(x/x')\, M(x'/x'')\langle G(x''/y)\rangle, \qquad (A.10)$$

которое, принимая во внимание (A.7), можно переписать в следующем виде:

$$\hat{B}(x)\langle G(x/y)\rangle = -\delta(x-y) - \int dx' M(x/x')\langle Gx'/y)\rangle, \qquad (A.11)$$

Учитывая условие

$$\int dx' G(x/x')\, G^{-1}(x'/y) = \delta(x-y), \qquad (A.12)$$

определяющее обратную функцию Грина $G^{-1}(x/y)$, из (A.10) можно найти следующее соотношение для оператора $M(x/x')$

$$M(x/x') = G_0^{-1}(x/x') - \langle G(x/x')\rangle^{-1} \qquad (A.13)$$

Обращая разложение $\langle G(x/y)\rangle$ в ряд теории возмущений

$$\langle G(x/y)\rangle = G_0(x/y) + \int\int dx' dx'' G_0(x/x')\langle \hat{\mu}(x')\, G_0(x'/x'')\hat{\mu}(x'')\rangle\, G\,(x''/y) - \ldots \qquad (A.14)$$

с помощью (A.12) получим следующее приближенное выражение для функции $\langle G(x/y)\rangle^{-1}$

$$\langle G(x/y)\rangle^{-1} = G_0^{-1}(x/y) - \langle \hat{\mu}(x)\, G_0(x/y)\hat{\mu}(y)\rangle + \ldots \qquad (A.15)$$

Соответственно из (А.13) следует

$$M(x/y) \approx M_1(x/y) \equiv \langle \hat{\mu}(x)\, G_0(x/y) \hat{\mu}(y) \rangle \qquad (A.16)$$

Это выражение представляет собой первый член разложения оператора $M(x/y)$ по моментам функции $\hat{\mu}(x)$ [7] .

Подставляя $M(x/y)$ в виде (А.16) в уравнение (А.11) получим

$$\hat{B}(x) \langle G(x/y) \rangle = -\delta(x-y) - \int dx' \langle \hat{\mu}(x)\, G_0(x/x') \hat{\mu}(x') \rangle \langle G(x'/y) \rangle \qquad (A.17)$$

Это уравнение является основным в настоящей работе (уравнение M_1-приближения). Нетрудно показать, что другая важная в теории гетерогенных реакторов величина $\langle \hat{\mu}_1(x) G(x/y) \rangle$ в M_1-приближении определяется следующим соотношением

$$\langle \hat{\mu}_1 G(x/y) \rangle = \langle \hat{\mu}_1(x) \rangle \langle G(x/y) \rangle - \int dx' \langle \hat{\mu}_1(x) G_0(x/x') \hat{\mu}(x') \rangle \langle G(x'/y) \rangle,$$

где M_1 – некоторая функция макроскопических сечений.

ПРИЛОЖЕНИЕ Б

Уточнение M_1-приближения

Рассмотрим стационарное диффузионное уравнение для неограниченной среды

$$\left[\nabla^2 + \eta(\vec{r})\nabla^2 + \nabla\eta(\vec{r})\nabla\right] G(\vec{r}/\vec{r}_0) - \kappa_0^2 \left[1 + \frac{\nu(\vec{r})}{\kappa_0^2}\right] G(\vec{r}/\vec{r}_0) = -\delta(\vec{r} - \vec{r}_0) \qquad (Б.1)$$

Преобразуем его дважды по Фурье относительно $\vec{r} - \vec{r}_0$ и $\vec{r}$.

$$g(\vec{p}_1 \vec{r}) = \int d(\vec{r} - \vec{r}_0)\, e^{i\vec{p}(\vec{r} - \vec{r}_0)}\, G(\vec{r}/\vec{r}_0) \qquad (Б.2)$$

$$\tilde{g}(\vec{p}, \vec{k}) = \int d\vec{r}\, e^{i\vec{k}\vec{r}}\, g(\vec{p}, \vec{r}) \qquad (Б.3)$$

Преобразованное уравнение (Б.1) запишем в виде

$$[(\vec{k} + \vec{p})^2 + \kappa_0^2]\, \tilde{g}(\vec{p}, \vec{k}) + \frac{1}{(2\pi)^3} \int d\vec{k}'\, \tilde{g}(\vec{p}, \vec{k} - \vec{k}')$$

$$\times \{[(\vec{k} - \vec{k}' + \vec{p})^2 + \vec{k}(\vec{k} + \vec{p} - \vec{k}')]\, \eta_1(\vec{k}') + \nu_1(\vec{k}')\} = (2\pi)^3 \delta(\vec{k}) \qquad (Б.4)$$

Были введены обозначения

$$\eta_1(\vec{k}) = \int \eta(\vec{r})\, e^{i\vec{k}\vec{r}} d\vec{r} \qquad (Б.5)$$

$$\nu_1(\vec{k}) = \int \nu(\vec{r})\, e^{i\vec{k}\vec{r}} d\vec{r} \qquad (Б.6)$$

Запишем решение уравнения (Б.4) по методу последовательных приближений и выполним обратное преобразование Фурье относительно $\vec{k}$. В результате получим:

$$g(\vec{p}, \vec{r}) = \sum_{n=0}^{\infty} \frac{(-1)^n}{p^2+\kappa_0^2} \frac{1}{(2\pi)^{3n}} \int d\vec{k}_1 \ldots \int d\vec{k}_n e^{-i\vec{r}\sum_{i=1}^{n}\vec{k}_i} c_1(\vec{k}_1) \ldots c_1(\vec{k}_n)$$

$$\times \frac{[\vec{p}(\vec{p}+\vec{k}_1)\eta_0+\nu_0] \ldots [(\vec{p}+\sum_{i=1}^{n-1}\vec{k}_i)(\vec{p}+\sum_{i=1}^{n}\vec{k}_i)\eta_0+\nu_0]}{[(\vec{p}+\vec{k}_1)^2+\kappa_0^2] \ldots [(\vec{p}+\sum_{i=1}^{n}\vec{k}_i)^2+\kappa_0^2]} \qquad (Б.7)$$

Мы предположили, что функции η и ν одинаковым образом зависят от координат

$$\eta(\vec{r}) = \eta_0 c(\vec{r}) \qquad \eta_1(\vec{k}) = \eta_0 c_1(\vec{k})$$

$$\nu(\vec{r}) = \nu_0 c(\vec{r}) \qquad \nu_1(\vec{k}) = \nu_0 c_1(\vec{k}) \qquad (Б.8)$$

Усредняя выражение (Б.7), получим

$$\langle g(\vec{p})\rangle = \frac{1}{p^2+\kappa_0^2} - \sum_{n=1}^{\infty}\left(-\frac{1}{8\pi^3}\right)^{n-1} \int d\vec{k}_1 \ldots \int d\vec{k}_{n-1} \int d\vec{r}_1 \ldots \int d\vec{r}_{n-1} e^{i\sum_{j=1}^{n-1}\vec{k}_j\vec{r}_j}$$

$$\times K(\vec{r}_1 \ldots \vec{r}_{n-1}) \frac{[\vec{p}(\vec{p}+\vec{k}_1)\eta_0+\nu_0] \ldots [(\vec{p}+\sum_{j}^{n-1}\vec{k}_j)\vec{p}\eta_0+\nu_0]}{[(\vec{p}+\vec{k}_1)^2+\kappa_0^2] \ldots [p^2+\kappa_0^2]}, \qquad (Б.9)$$

где

$$K(\vec{r}_1 \ldots \vec{r}_{n-1}) = \langle c(\vec{\rho})c(\vec{r}_1+\vec{\rho}) \ldots c(\vec{r}_{n-1}+\vec{\rho})\rangle \qquad (Б.10)$$

– корреляционная функция n-ого порядка. Для пространственно однородной среды функция K зависит от n – 1 переменной.

Рассмотрим выражение (Б.9) для некоторых частных видов диффузионных сред, удерживая в разложении (Б.9) слагаемые, не содержащие малого отношения p/k_i. Если плоский источник нейтронов расположен перпендикулярно слоям плоской решетки, то вследствие $\vec{p}\vec{k}_i = 0$, получим из (Б.9)

$$\langle g(\vec{p})\rangle = \frac{1}{p^2+\kappa_0^2} \qquad (Б.11)$$

При "поперечной" диффузии в случае тонких слоев ($p \ll k_i$), обращая разложение функции $\langle g(\vec{p})\rangle$ (Б.9), находим

$$\langle g(\vec{p})\rangle^{-1} = p^2 + \kappa^2 - p^2[\langle\eta^2\rangle - \langle\eta^3\rangle + [\langle\eta^4\rangle - \langle\eta^2\rangle] - \ldots$$

$$= p^2\{1 - \langle\eta^2\rangle + \langle\eta^3\rangle - [\langle\eta^4\rangle - \langle\eta^2\rangle^2] + \ldots\} + \kappa_0^2$$

$$= \{p^2 + \kappa_0^2[1 - \langle\eta^2\rangle + \langle\eta^3\rangle - \ldots]^{-1}\}\{1 - \langle\eta^2\rangle + \langle\eta^3\rangle - \ldots\} \qquad (Б.12)$$

Принимая во внимание, что

$$\kappa_r^2 = 3\langle\Sigma_a\rangle\langle\Sigma_t\rangle = \kappa_0^2[1 + \langle\eta^2\rangle - \langle\eta^3\rangle + \langle\eta^4\rangle - \langle\eta^5\rangle + \ldots] \qquad (Б.13)$$

получаем из (Б.12) следующее уравнение для определения постоянной затухания среднего потока нейтронов

$$\langle g(\vec{p})\rangle^{-1} = p^2 + \kappa_r^2 = 0. \qquad (Б.14)$$

В системе с осевой симметрией диффузия вдоль оси симметрии происходит также, как и в случае "продольной" диффузии в плоской решетке. Диффузия в направлении, перпендикулярном оси, описывается уравнением

$$p^2 + \frac{\kappa_0^2}{2}\,\frac{\langle[1+\eta/2]^{-1}\rangle}{1 - 1/2\langle[1+\eta/2]^{-1}\rangle} = 0. \qquad (Б.15)$$

Аналогично в случае изотропной среды постоянная затухания среднего потока нейтронов определяется из уравнения

$$p^2 + \frac{\kappa_0^2}{3}\,\frac{\langle[1+\eta/3]^{-1}\rangle}{1 - 2/3\langle[1+\eta/2]^{-1}\rangle} = 0. \qquad (Б.16)$$

Поправки к этим результатам, пропорциональные p/k_i и более высоким степеням p/k_i, могут быть учтены в рамках M_1-приближения при соответствующем выборе нулевого приближения.

При выводе формул (Б.15) и (Б.16) мы приближенно заменили дробь в (Б.9) ее средним значением по области изменения угловых переменных $\vec{k}_i/\vec{k}_i$.

ПРИЛОЖЕНИЕ В

Корреляционная функция для диффузионной среды с случайными неоднородностями

В том случае, когда диффузионная среда содержит случайно расположенные локализованные неоднородности типа примесей (для простоты полагаем, что все примеси одинаковы), то

$$\mu_k(\vec{r}) = \sum_{\alpha=1}^{N} \Gamma_k(\vec{r} - \vec{R}_\alpha) - \left\langle \sum_{\alpha=1}^{N} \Gamma_k(\vec{r} - \vec{R}_\alpha) \right\rangle \qquad (B.1)$$

Суммирование выполняется по всем (N) примесям. Функция $\Gamma_k(\vec{r} - \vec{R}_\alpha)$ характеризует действие в точке $\vec{r}$ примеси, расположенной в области вблизи $\vec{R}_\alpha$. Выражение (B.1) удобно представить в виде интеграла

$$\mu_k(\vec{r}) = \frac{1}{(2\pi)^3} \int d\vec{q} e^{-i\vec{q}\vec{r}} \gamma_k(\vec{q}) [\rho(\vec{q}) - \langle \rho(\vec{q}) \rangle], \qquad (B.2)$$

где

$$\gamma_k(\vec{q}) = \int d\vec{r}\, \Gamma_k(\vec{r})\, e^{i\vec{q}\vec{r}} \qquad (B.3)$$

$$\rho(\vec{q}) = \sum_{\alpha=1}^{N} e^{i\vec{q}\vec{R}_\alpha} \qquad (B.4)$$

Предположим, что корреляция в расположении примесей отсутствует*. Тогда среднее от произвольной функции $f(\vec{R}_1 \ldots \vec{R}_N)$ имеет вид

$$\langle f \rangle = \frac{1}{V^N} \int d\vec{R}_1 \ldots d\vec{R}_N\, f(\vec{R}_1 \ldots \vec{R}_N), \qquad (B.5)$$

где V – объем замедляющего вещества. Усредняя произведение $\mu_k(\vec{r})\mu_j(\vec{r}\,')$, получим с точностью до членов, линейных по N/V следующее выражение для корреляционной функции [11] :

$$K_{ij}(\vec{r}) = \frac{N}{V} \frac{1}{(2\pi)^3} \int d\vec{q}\, e^{i\vec{q}\vec{r}} \gamma_i(\vec{q}) \gamma_j^*(\vec{q}) \qquad (B.6)$$

Такую корреляционную функцию можно использовать при описании диффузии нейтронов в кипящей жидкости. В качестве другого примера укажем на решетку реактора, у которой отверстия для стержней шире самих стержней и последние могут в них свободно перемещаться. Для

---

* Это предположение справедливо при достаточно низкой плотности примесей, когда можно пренебречь возможностью перекрытия двух и более примесей.

простоты предположим, что закон распределения $\vec{U}_e$ – смещения $e^{ого}$ стержня из узла решетки имеет гауссову форму

$$P(\vec{U}_c) = (\pi\theta)^{-3/2} e^{-U_c 2/\theta} \qquad (B.7)$$

Для такой системы Фурье-образ корреляционной функции имеет вид [7]

$$k_{ij}(\vec{p}) = [k_{ij}(\vec{p})]_{\theta=0}\, e^{-p^2\theta/2} + \frac{N}{V}\gamma_i(\vec{p})\gamma_j^*(\vec{p})\,[1 - e^{-p^2\theta/2}] \qquad (B.8)$$

Первое слагаемое в правой части (B.8) определяет вклад идеальной периодической структуры в корреляционную функцию. При $\theta \to \infty$ это слагаемое исчезает. Второе слагаемое обязано своим происхождением наличию разброса в координатах стержней: при $\theta = 0$ оно обращается в нуль.

ЛИТЕРАТУРА

[1] ГАЛАНИН А.Д., Теория ядерных реакторов на тепловых нейтронах. Атомиздат, Москва, 1959.
[2] ВЕЙНБЕРГ А., ВИГНЕР Е., Физическая теория ядерных реакторов. ИИЛ, Москва, 1961.
[3] ГРИГОРЬЕВ И.С., НОВИКОВ В.М., Диффузия нейтронов в гетерогенных системах. Атомиздат, Москва, 1966.
[4] ЛАНДАУ Л.Д., ЛИФШИЦ Е.М., Электродинамика сплошных сред. ГИИТЛ, Москва, 1957.
[5] ШЕВЕЛЕВ Я.И., Атомная энергия, 2 (1957) 224.
[6] СТЕПАНОВ А.В.: а) Pulsed Neutron Research, I.A.E.A., Vienna 1 (1965) 339; б) Атомная энергия, 20 (1966) 265.
[7] СТЕПАНОВ А.В., Труды ФИАН (в печати).
[8] HONECK, H.C., QUIQUEMELLE, B.C., Pulsed Neutron Research, I.A.E.A., Vinna 1 (1965) 309.
[9] СТЕПАНОВ А.В., Атомная энергия 22 (1967) 4.
[10] ГАЛАНИН А.Д., Атомная энергия 9 (1960) 89.
[11] СТЕПАНОВ А.В., Атомная энергия 21 (1966) 292.

SLOWING-DOWN AND HEATING-UP OF NEUTRONS IN BERYLLIUM

A.K. GHATAK
INDIAN INSTITUTE OF TECHNOLOGY, NEW DELHI
AND
I.C. GOYAL, P.S. GROVER AND L.S. KOTHARI
UNIVERSITY OF DELHI, DELHI,
INDIA

Abstract

SLOWING-DOWN AND HEATING-UP OF NEUTRONS IN BERYLLIUM. We report here the results of an extensive series of calculations made to understand quantitatively the approach to equilibrium of (i) a high-energy neutron pulse and (ii) a low-energy neutron pulse, introduced inside finite beryllium assemblies.

After a high-energy burst of neutrons at time $t \approx 0$, we have calculated the neutron spectra at subsequent times, and these have been compared with the experimental results. The agreement is found to be very good. We have also studied the rate at which the average neutron energy and the average neutron velocity approach equilibrium. From these studies, the thermalization time, τ_{th}, has been deduced and the possibility of its experimental measurement is discussed.

When a pulse of low-energy neutrons is introduced inside a moderating assembly, the average energy of the neutron distribution increases with time. For this heating-up process also, we have calculated the transient neutron spectra, the decay constant of the pulse and the heating-up relaxation time, τ_H. Unlike neutron slowing-down, where equilibrium is reached faster in larger assemblies, in the heating-up case we find that equilibrium is reached faster for smaller assemblies. The possible reasons for this behaviour are discussed.

I. INTRODUCTION

In recent years there has been considerable interest in the problem of measuring the fundamental-mode time decay constant, λ_0, in small moderating assemblies. The existing theories predict (both for bounded and unbounded media) that for any discrete mode the decay constant cannot exceed $(v\Sigma)_{min}$ and that for bucklings exceeding a certain critical buckling, B_c^2, no discrete mode will exist [1-4]. However, in beryllium assemblies at room temperature the experimentally reported values of λ_0 [5] apparently observe no bound and also give no indication of the existence of any critical buckling [5-6]; on the other hand, in small beryllium assemblies at low temperatures Silver [7] observed that the measured decay constant continued to decrease with time, indicating that equilibrium was not established. Fullwood et al. [8] have also reported that the time variation of the total neutron density at long times deviates from a single exponential.

In section II we report the results of calculations of time-dependent neutron spectra after a fast neutron burst in beryllium assemblies and compare these with the experimental results of Gaerttner et al. [9] and Fullwood et al. [8]. The possibility of measuring the thermalization time is also discussed.

In section III we discuss the approach to equilibrium of a pulse of low-energy neutrons introduced inside different moderating assemblies

of beryllium at room temperature. We have studied how the total neutron density and the average neutron energy change with time. In this case, the average energy of the distribution increases with time until it attains the equilibrium value. For this reason, we refer to this as the heating-up case. Compared with the slowing-down case, it is found that during heating-up, equilibrium is reached faster in smaller assemblies than in larger assemblies. The possible explanation for this behaviour has been discussed.

II. SLOWING-DOWN OF NEUTRONS

The time-dependent diffusion equation in the absence of any source is given by

$$\frac{\partial N(v,\vec{r},t)}{\partial t} = v D(v)\, \nabla^2 N - v\Sigma_s(v) N - v\Sigma_a(v) N + \int v'\Sigma_s(v'\to v) N(v',\vec{r},t)\, dv' \quad (1)$$

where the symbols have their usual meanings. If we look for solutions of the form $N(v)\exp(iBr - \lambda t)$ we get the following eigenvalue equation:

$$PN = \lambda N \quad (2)$$

where the operator P is defined by

$$PN \equiv (v\Sigma_s + v\Sigma_a + v DB^2) N - \int v'\Sigma_s(v' \to v) N(v')\, dv' \quad (3)$$

If $N_j(v)$ are the eigenfunctions of the operator P and λ_j are the corresponding eigenvalues, then the time-dependent neutron density can be expanded as

$$N(v,t) = \sum_j a_j N_j(v)\, e^{-\lambda_j t} \quad (4)$$

and the total neutron density $N(t)\,(= \int N(v,t)\, dv)$ will be given by

$$N(t) = \sum_j A_j e^{-\lambda_j t} \quad (5)$$

where

$$A_j = \int a_j N_j(v)\, dv \quad (6)$$

and a_j are expansion coefficients determined from the initial conditions.

The instantaneous average velocity and average energy of the neutron distribution are defined by the following equations

$$\bar{v}(t) = \frac{\int v\, N(v,t)\, dv}{\int N(v,t)\, dv} \tag{7}$$

$$\bar{E}(t) = \frac{\int E\, N(v,t)\, dv}{\int N(v,t)\, dv} \tag{8}$$

In our calculations we have used the multigroup approach and diagonalized P to obtain the eigenvalues and the corresponding eigenfunctions (for details see [10, 11]). We have used 30 energy groups in the thermal region and therefore obtained 30 discrete eigenvalues. The absorption cross-section σ_a is assumed to be of 1/v type and we have taken it to be 10.5 mb at 2200 m/s neutron velocity. For the scattering kernel we have used the first term of the Placzek expansion [12]. Transport cross-section data have been taken from the work of Goyal [13].

We report first the results of time-dependent spectra in a beryllium assembly corresponding to $B^2 = 0.075\ cm^{-2}$ at 305°K (density 1.86 g/cm^3). The values of buckling, temperature and density are chosen so that it is possible to compare our results with the experimental data of Gaerttner et al. [9]. The coefficients a_j were calculated so as to reproduce the spectra at some initial time (in this case at t = 176 μs). Spectra at subsequent times were calculated using Eq. (4).

The time-dependent spectra so obtained are plotted in Fig. 1. The fundamental-mode eigenfunction is also plotted. The normalization of curves at different times is arbitrary. Solid curves represent the theoretically calculated spectra. Experimental points are shown by circles and crosses. It is seen that the comparison between theory and experiments is very satisfactory. The trapping of neutrons at neutron energies corresponding to Bragg reflections is clearly seen. Calculated spectra for other buckling values also show similar satisfactory agreement with experimental results. This shows that multigroup diffusion theory is good enough for explaining the approach to equilibrium of a neutron pulse, though the predicted eigenvalue structure might be erroneous. It is to be noted that the fundamental-mode eigenfunction shows a peak at the lowest velocity group, which is a consequence of using diffusion theory [14].

By comparing our Fig. 1 with Fig. 3 of Lee and Daitch [15] we find that our calculations are just as satisfactory, if not better. The comparison shows that the time-dependent problem can be explained well by the simple kernel that we have used and multigroup diffusion theory.

Fullwood et al. have reported measurements on the change of neutron density with time in a beryllium assembly of $B^2 = 0.073\ cm^{-2}$ at 30°C (density of Be = 1.7 g/cm^3). Taking the same parameters and assuming the neutron spectrum to be a Maxwellian at 30°C at time t = 159 μs (c.f. Fig. 2 of Fullwood et al. [8]), we have calculated the coefficients a_j occurring in Eq. (4). If a_j is known, the total neutron

density as a function of time can be calculated. This is plotted as the solid curve in Fig. 2. The theoretical calculations are in excellent agreement with the experiment. The observed deviation from an exponential curve is very well explained by the present calculations.

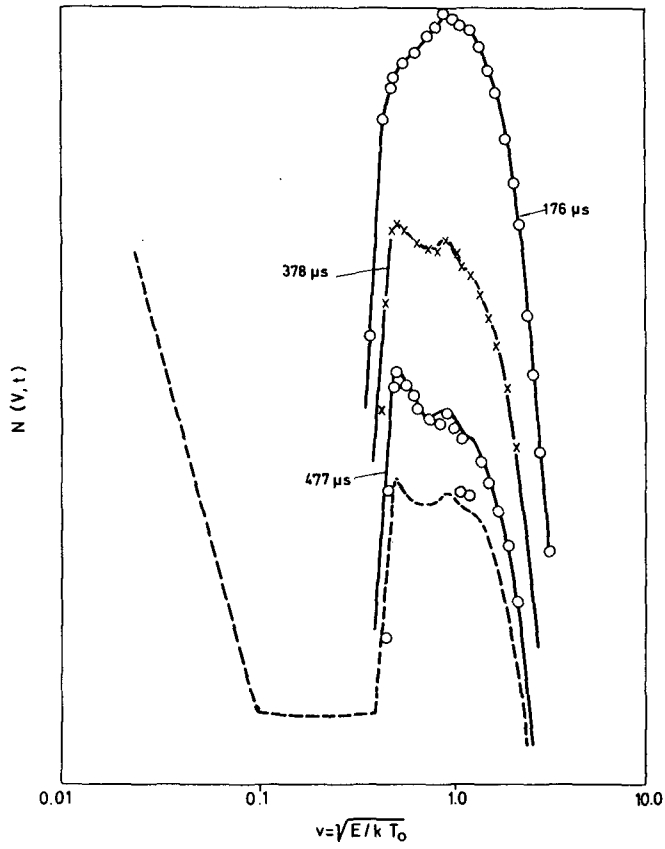

FIG. 1. Neutron density N(v,t) in a finite beryllium assembly ($B^2 = 0.075$ cm^{-2}) as a function of v for various values of t. The normalization at different times is arbitrary. Solid curves represent the theoretical results and the experimental points are shown by circles and crosses. The curve labelled ∞ represents the theoretically calculated fundamental mode eigenfunction.

Close to equilibrium, one may express the time-dependence of the average energy of the neutron distribution $\overline{E}(t)$, as

$$\overline{E}(t) - \overline{E}(\infty) = \{\overline{E}(0) - \overline{E}(\infty)\}\, e^{-t/\tau_{th}(t)} \tag{9}$$

where $\overline{E}(0)$ and $\overline{E}(\infty)$ are respectively the average neutron energies at time t = 0 and t = ∞. If the decay is a simple exponential, i.e. τ_{th} is a constant, independent of time, we refer to it as the slowing-down relaxation time or thermalization time.

To obtain the thermalization time in beryllium we have calculated the time-dependent spectra in an infinite assembly, i.e. $B^2 = 0\ cm^{-2}$ ($T = 300°K$, density $1.8\ g/cm^3$). After calculating the mean energy

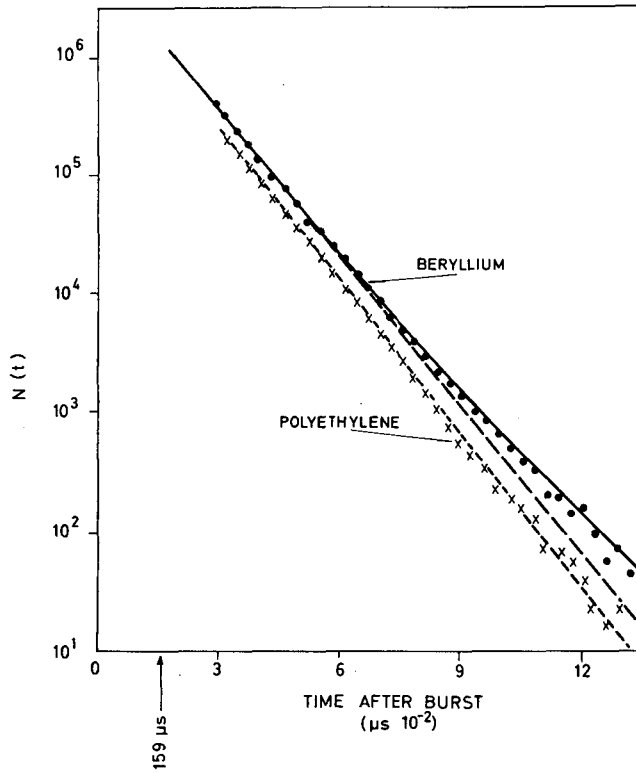

FIG.2. The variation of N(t) as a function of time. For beryllium ($B^2 = 0.073\ cm^{-2}$, $T = 30°C$), the solid curve corresponds to the theoretical calculations. Dots represent the experimental values of Fullwood et al. [8]. Dashed line is drawn to show deviation from exponential behaviour. For polyethylene the crosses indicate experimental results in the same environment.

(Eq.(8)) and mean velocity (Eq.(7)) at different times we have plotted (Fig.3) the instantaneous values of the slopes, i.e. $-\left[\frac{d}{dt}\{\ln(\overline{E}(t) - \overline{E}(\infty))\}\right]^{-1}$ and $-\left[\frac{d}{dt}\{\ln(\bar{v}(t) - \bar{v}(\infty))\}\right]^{-1}$ (For details of this analysis see Grover and Kothari [16]). When equilibrium is reached, both these slopes should become constant and equal to $\tau_{th} = (\lambda_1 - \lambda_0)^{-1}$. However, from our calculations we find that the asymptotic value is not reached before very large times. At 600 μs the slopes of the energy and velocity curves are shown to be 157 and 162 μs, respectively, whereas they are 165 and 169 μs, respectively, at 750 μs.

Experimentally τ_{th} in beryllium has been measured by Zhezherun et al. [6]. He has made measurements in two beryllium cubes, one of side 50 cm and another of 60 cm and finds the decay of $\overline{E}(t)$ to be exponential in the time interval of 300 and 1000 μs. He obtains the value of τ_{th} as 178 ± 25 μs for the cube with linear dimension of 60 cm and 170 ± 30 μs for the other cube. Extrapolating these results to the

case of $B^2 = 0\ cm^{-2}$, he obtains the value of thermalization time in an infinite assembly as $\tau_{th} = 185 \pm 20\ \mu s$. Our calculated values compare favourably with this experimental result.

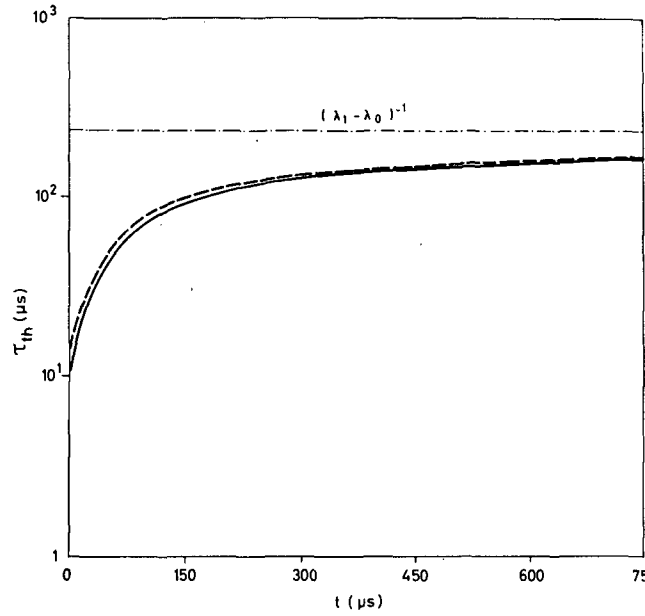

FIG. 3. The effective value of $\tau_{th}(t)$ as a function of time in an infinite beryllium assembly. Solid line represents $\left[-\frac{d}{dt} \ln \{\bar{E}(t) - \bar{E}(\infty)\}\right]^{-1}$ and the dashed line represents $\left[-\frac{d}{dt} \ln \{\bar{v}(t) - \bar{v}(\infty)\}\right]^{-1}$. The asymptotic value $(\lambda_1 - \lambda_0)^{-1}$ is also shown.

III. HEATING-UP OF NEUTRONS

The energy distribution of the initial neutron pulse introduced inside the assembly at t = 0 is assumed to be a Maxwellian distribution at temperature 100°K. Starting with this initial distribution, neutron spectra at subsequent times have been calculated by solving Eq. (1) by the time-step method. (For details, see Grover and Kothari [16, 17]). The one-phonon inelastic scattering cross-section has been used for the scattering kernel [18]. The values of buckling considered are 0, 0.006, 0.02 and $0.05\ cm^{-2}$.

In Figs (4) and (5) the time-dependent neutron spectra for $B^2 = 0.006$ and $0.05\ cm^{-2}$, respectively, are presented. The different curves in each figure show how the neutron energy distribution changes with time. The effect of elastic neutron scattering on the neutron spectra is clearly marked in this case also. The neutron spectra at long times (500 μs here) have been compared with equilibrium spectra (dashed curve) which is the fundamental mode eigenfunction of the operator P. Different curves have been normalized at neutron energy 500 k. By comparing

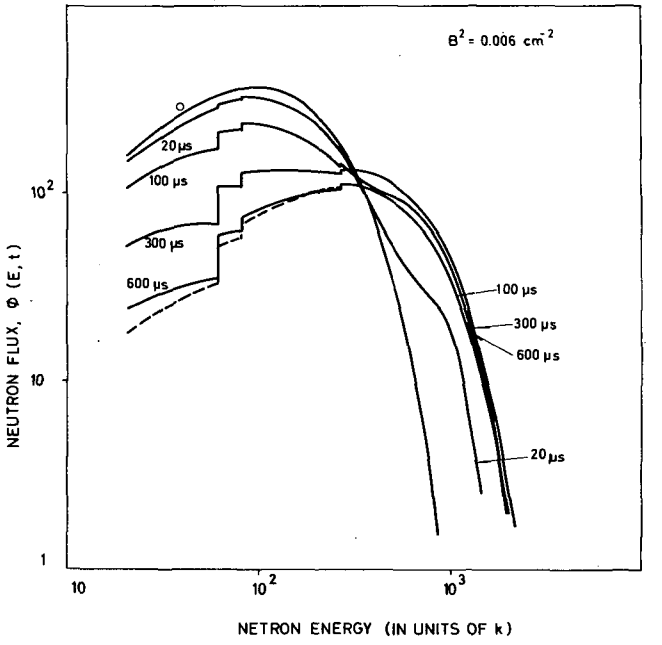

FIG.4. Neutron energy distributions at different times ($B^2 = 0.006\ cm^{-2}$). Dashed curve represents the asymptotic distribution (this curve is normalized to the curve for 600 μs at 500 k).

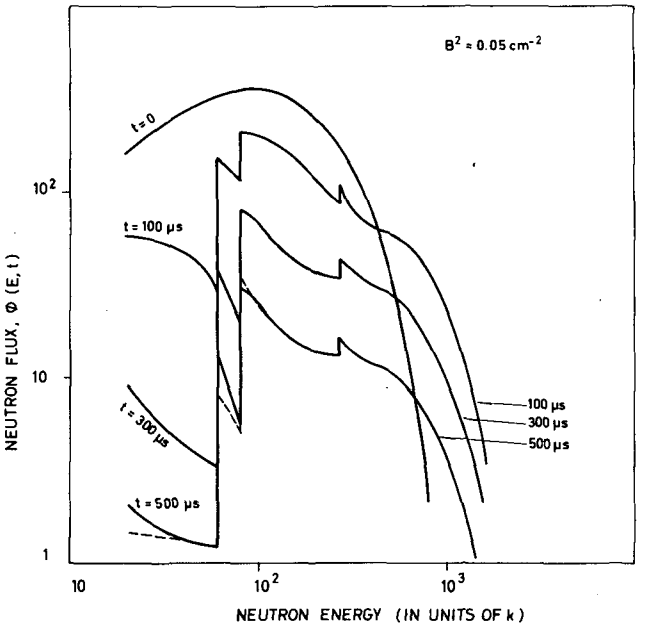

FIG.5. Neutron energy distributions at different times ($B^2 = 0.05\ cm^{-2}$). Dashed curve represents the asymptotic energy distributions (this curve is normalized to the curve for 500 μs at 500 k).

the dashed curve with the time-step spectra, we observe that for $B^2 = 0.05\ cm^{-2}$ equilibrium is reached faster than for $B^2 = 0.006\ cm^{-2}$. This implies that during heating-up, equilibrium is reached faster in smaller assemblies. In the slowing-down case thermalization becomes slower as B^2 increases. This may partially be explained by the fact that in a small assembly the mean energy of the equilibrium distribution is lower than $3/2\ kT_A$, T_A being the temperature of the assembly. (This is the so-called diffusion-cooling effect). Hence a pulse of neutrons of temperature lower than T_A attains equilibrium faster. As the assembly size increases, the final mean equilibrium energy also increases and a pulse of low-energy neutrons has to heat-up over a wider energy range, lengthening the whole process.

In Fig. 6 we report the dependence of total neutron density on time for $B^2 = 0$, 0.006, 0.02 and 0.05 cm^{-2}. It is seen that after some time, the curves become linear and the total neutron density decays as a single exponential. The slope of the linear part of the curve determines λ_0. We find that for $B^2 = 0$, 0.006, 0.02 and 0.05 cm^{-2}, the values of the decay constant are 284, 1052, 2540 and 5011 s^{-1}, respectively; while the fundamental mode eigenvalues are 270, 1060, 2555 and 5047 s^{-1}, respectively. The agreement indicates that the total neutron density decays as a single exponential about 50 μs after injecting the pulse inside the assembly.

Knowing the time-dependent neutron spectra, we have calculated average neutron energy (Eq. 8) as a function of time. The time variation of $\overline{E}(t)$ has been analysed in terms of a relation of the type

$$\overline{E}(\infty) - \overline{E}(t) = \{\overline{E}(\infty) - \overline{E}(0)\}\, e^{-t/\tau_H(t)}$$

where $-1/\tau_H(t)$ is the slope of the curve $\ln(\overline{E}(\infty) - \overline{E}(t))$ versus time, at time t. This slope gives information about the rate of gain of energy by the neutrons from the atoms of the moderator. At long times, if $\tau_H(t)$ becomes constant independent of time, we will refer to it as the heating-up relaxation time. $\overline{E}(\infty)$ is the average energy of the fundamental mode eigenfunction.

In Fig. (6) we have also plotted the time variation of $\ln\{\overline{E}(\infty) - \overline{E}(t)\}$ for $B^2 = 0$, 0.006, 0.02 and 0.05 cm^{-2}. We observe that for $B^2 = 0$, the time variation of $\{\overline{E}(\infty) - \overline{E}(t)\}$ even after 700 μs does not become a single exponential. The slope of the curve keeps changing with time. We find that $\overline{E}(700\ \mu s) = 444$ k (where $\overline{E}(\infty) = 450$ k), and the rate of increase is quite slow. During the last stages, the slope of the curve is nearly 260 μs. (It may be noted here that the slowing-down relaxation time, τ_{th}, is only 170 μs). We thus conclude that in an infinite medium a neutron pulse at a temperature higher than that of the moderator comes to equilibrium faster than a pulse whose temperature is less than that of the moderator.

This difference in behaviour may be due to the fact that mean-energy loss per collision for neutrons of energy greater than about 700 k is much larger than the mean-energy gain per collision for neutrons of energy less than about 500 k [18]. For the other cases, with $B^2 \neq 0$, the slope of each curve keeps changing continuously in the beginning but after some time, depending upon the value of B^2, it almost attains a constant value. This slope determines the heating-up relaxation time.

By comparing the curves for $B^2 = 0.006$ and $0.05\ cm^{-2}$, we find that the time beyond which the curve becomes linear, decreases with increases of buckling, i.e. equilibrium is set up faster in smaller assemblies[1]. The values of τ_H deduced from the linear part of the curves are nearly 189, 178 and 138 μs for $B^2 = 0.006$, 0.02 and 0.05 cm^{-2} respectively.

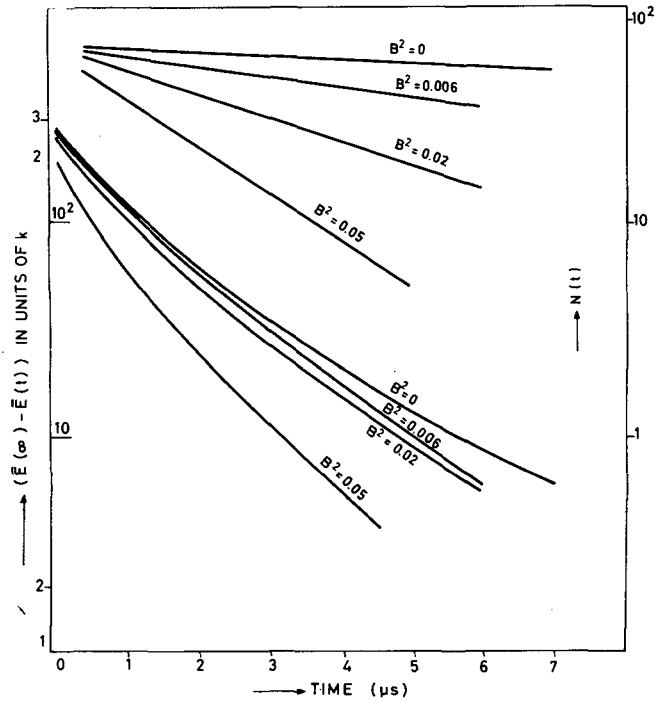

FIG. 6. Variation of total neutron density, N(t) and $\{\bar{E}(\infty) - \bar{E}(t)\}$ with time.

It will be of interest to pulse small crystalline assemblies with low-energy neutrons and study experimentally the process of heating-up of neutrons in moderators.

REFERENCES

[1] CORNGOLD, N., Nucl. Sci. Engng 19 (1964) 80.
[2] NELKIN, M., Physica 29 (1963) 261.
[3] SHAPIRO, S., CORNGOLD, N., Phys. Rev. 137 (1965) A 1686.
[4] WOOD, J.R., Pulsed Neutron Research I IAEA, Vienna (1965) 219.
[5] BECKURTS, K.H., Proc. Brookhaven Conference on Neutron Thermalization III, RE-1, BNL-718, C-32 (1962).
[6] ZHEZHERUN, I.F. et al., Proc. 3rd UN Int. Conf. PUAE 3 (1965) 260.
[7] SILVER, E.G., Proc. Brookhaven Conference on Neutron Thermalization III, 981, BNL-719, C-32, (1962).
[8] FULLWOOD, R.R., SLOVACEK, R.E., GAERTTNER, R.E., Nucl. Sci. Engng 18 (1964) 138.
[9] GAERTTNER, R.R. et al., Pulsed Neutron Research I IAEA, Vienna (1965) 483.

[1] Obviously, this observation cannot be pushed too far, since for very small assemblies the diffusion theory itself will not be applicable.

[10] GHATAK, A.K., HONECK, H.C., Nucl. Sci. Engng 21 (1965) 227.
[11] OHANIAN, M.J., DAITCH, P.B., Nucl. Sci. Engng 19 (1964) 343.
[12] KOTHARI, L.S., SINGWI, K.S., Solid State Phys. 8 (1959) 184.
[13] GOYAL, I.C., J. nucl. Energy Parts A/B 19 (1965) 103.
[14] GROVER, P.S., KOTHARI, L.S., GHATAK, A.K., sent for publication to J. nucl. Energy (May 1967).
[15] LEE, R.R., DAITCH, P.B., Nucl. Sci. Engng (to appear).
[16] GROVER, P.S., KOTHARI, L.S., J. nucl. Energy Parts A/B 20 (1966) 835.
[17] GROVER, P.S., KOTHARI, L.S., J. nucl. Energy parts A/B (to appear).
[18] KOTHARI, L.S., SINGWI, K.S., GHATAK, A.K., sent for publication to J. nucl. Energy (May 1967).

DISCUSSION

G. E. ROSSI: I should appreciate some further explanation of the fact that in your opinion the neutron peaking at low energy is due to the diffusion approximation. I think that any 'pseudo-eigenfunction', should have a singularity at the origin (E = 0) independently of the approximation used for the leakage term.

L. S. KOTHARI: We feel that the peaking essentially arises because of computational difficulties, rather than as a physical phenomenon.

P. MICHAEL: Is not the main difference between transport and diffusion theory that the former gives a logarithmic singularity at very low energy while the latter gives a '$1/\chi$'-like singularity?

L. S. KOTHARI: Off-hand I cannot recall the complete expression for φ, but in transport theory, for the case of isotropic scattering and in the iBr approximation, the expression for the flux involves λ in the following form:

$$\varphi \propto \frac{1}{B} \tan^{-1} \left(\frac{Bv}{-\lambda + v\Sigma_s} \right)$$

When the denominator goes to zero, $\tan^{-1}$ gives $\frac{\pi}{2}$ and φ does not diverge.

M. M. R. WILLIAMS (Chairman): I must say that for B^2 less than B^2_{max} I had always assumed that the flux went to zero there, but that when it was greater than B^2_{max} or approached it, then the flux started to go to infinity at the origin.

Professor Kuščer has done some work on this, and I wonder whether he would like to comment on the fact that the spectrum tends to peak at zero velocity as B^2 tends to B^2_{max}, or is greater than B^2_{max}.

I. KUŠČER: Well, if the discrete decay constant does not exist, so that λ^* is the slowest possible decay, then the peak is due to those neutrons not able to escape except by the minimum collision rate. All other neutrons escape faster by leakage.

M. M. R. WILLIAMS: So the peak would appear to be still there, even in transport theory, and this is not just an inaccuracy of diffusion theory.

SCATTERING LAW

(Session B)

SCATTERING LAW STUDIES FOR MODERATORS
A review

W. GLÄSER
KERNFORSCHUNGSZENTRUM,
KARLSRUHE, FEDERAL REPUBLIC OF GERMANY

Abstract

SCATTERING LAW STUDIES FOR MODERATORS: A REVIEW. Considerable progress has been made recently in the understanding of neutron scattering by condensed matter. This has influenced the investigations on neutron thermalization in moderators, where previously over-simplified models such as the free-gas kernel have been used for calculations.

Although measurements of scattering laws were started about eight years ago, it is only in the last few years that the experimental technique delivers consistent and accurate results. Parallel to and connected with this work, practicable, theoretical models for scattering kernels have been developed, taking into account the principal effects of chemical binding.

In this review the present state of the experimental technique is discussed. Progress has been achieved by including multiple scattering corrections and coherent effects in the interpretation of data. A detailed discussion of scattering law measurements for water, zirconium hydride and graphite is given. Measurements for other moderators are summarized. Finally a comparison of integral parameters calculated from experimental scattering law data and synthetic kernels with results derived from integral measurements is given.

I. INTRODUCTION

The problem we have to deal with is the scattering of neutrons with an energy below a few eV in condensed matter. In the last two decades it has been proved that neutrons of such energy are extremely versatile probes for studying the details of the structure and dynamics of atomic many-particle systems, and neutron scattering measurements have brought new insight into this behaviour. Also, the general theoretical picture describing the neutron scattering process has been developed and has been successfully used in many cases to explain experimental results. We have to restrict ourselves here to a small part of this work, namely, to the investigation of materials which are of interest as reactor moderators.

As an introduction it may be worthwhile to recall the basic formulae. In the first Born approximation, using the Fermi pseudo-potential, the double-differential scattering cross-section can be written

$$\frac{d^2\sigma}{d\Omega dE} = \frac{k}{k_0} \sum_{i,f} p_i \left| \langle f | \sum_n b_n e^{i\vec{\kappa}\vec{r}_n} | i \rangle \right|^2 \delta(E - E_0 + \hbar\omega)$$

$$\hbar\omega = E_f - E_i, \quad \hbar\kappa = \hbar(\vec{k}_0 - \vec{k}) \tag{1}$$

where i, f are the initial and final states of the scatterer, $E_{i,f}$ the corresponding energies, p_i is the population of the initial state and b_n is the bound scattering amplitude of the n-th nucleus, $\vec{k}_0$, $\vec{k}$ are the wave

vectors of the incident and scattered neutron and E_0, E the corresponding energies. For scatterers consisting of a single atomic species Eq. (1) can be written

$$\frac{d^2\sigma}{d\Omega dE} = \frac{\sigma_b}{4\pi}\frac{k}{k_0} S(\vec{\kappa},\omega) \tag{2}$$

where σ_b is the bound scattering cross-section.

$S(\vec{\kappa},\omega)$ depends only on the structure and dynamics of the scatterer and is called the scattering law of the system or its dynamical structure factor. From Eq. (2) it follows that $S(\vec{\kappa},\omega)$ can be derived directly from an absolute determination of the double-differential cross-section. If our discussion is further restricted to isotropic materials, which in general includes all moderators, Eq. (1) can be rewritten in the form

$$\sigma(E_0 \to E, \cos\vartheta) = \frac{\sigma_b}{2k_BT}\sqrt{\frac{E}{E_0}}\, e^{-\beta/2} S(\alpha,\beta) = \frac{1}{2k_BT}\sqrt{\frac{E}{E_0}}\, e^{-\beta/2}\left\{\sigma_b S_s(\alpha,\beta) + \sigma_c S_d(\alpha,\beta)\right\}$$

$$\alpha = \frac{m(E_0 + E - 2\sqrt{E_0 E}\cos\vartheta)}{M\, k_BT}, \quad \beta = \frac{E - E_0}{k_BT} \tag{3}$$

where ϑ is the scattering angle, σ_c the bound coherent cross-section, k_B is Boltzmann's constant, T the absolute temperature, M is the mass of the scattering atom, m the neutron mass and S_s, S_d are the 'self' and 'distinct' part of the scattering law. The introduction of the relative units α and β, now often used, is in principle only advantageous for a perfect gas. In the more general case $S(\alpha,\beta)$ still depends in a complicated way on the temperature.

A number of practicable theoretical models have been proposed to describe $S(\vec{\kappa},\omega)$ or $S(\alpha,\beta)$. For example, the scattering from isolated molecules, neglecting the interaction between rotations and vibrations, has been described in different approximations [1,2]. The scattering from ideal solids has been handled in the harmonic approximation taking multi-phonon processes into account for incoherent scattering [3] and restricting so far to one-phonon processes in the coherent case [4].

For liquids the situation is even more unsatisfactory. Several proposals to describe the diffusive motions of the constitutive particles quantitatively have been made [5]. First attempts have been made to treat the hindered rotation of molecules in liquids [6].

A large number of scattering law calculations for moderators start with the Gaussian approximation for the intermediate scattering function $I(\alpha,t)$ in the time-dependent formalism [7].

$$S_s(\alpha,\beta) = \frac{1}{2\pi}\int_{-\infty}^{+\infty} I(\alpha,t)\, e^{i\beta t}\, dt \tag{4}$$

where

$$I(\alpha,t) = \exp\left\{-\alpha\int \frac{\rho(\beta)}{\beta\sinh(\beta/2)}\left[\cosh(\beta/2) - \cos\beta t\right] d\beta\right\} \tag{5}$$

$\rho(\beta)$ is a generalized frequency distribution which, in the case of harmonic vibrating solids of cubic symmetry having one atom per unit cell, is identical to the normalized density of lattice vibration modes. $\rho(\beta)$ can be derived from $S(\alpha, \beta)$ by extrapolating $S(\alpha, \beta)/\alpha$ to $\alpha = 0$.

$$\rho(\beta) = \frac{\beta}{2} \sinh \frac{\beta}{2} \left(\frac{S_s}{\alpha}\right)_{\alpha=0} \tag{6}$$

For more general systems $\rho(\beta)$ is not directly the density of the vibration modes, e.g. because of the influence of polarization vectors in solids. But it still describes the spectral density of the motions of a single atom and can be defined quite generally as the Fourier transform of the imaginary part of the atom's velocity auto-correlation function [8]. From $\rho(\beta)$, $S_s(\alpha, \beta)$ can be completely reconstructed.

Much work remains to be done to get more satisfactory models for the different systems of condensed matter. It should be stressed, however, that in the field we are interested in here – the thermalization of neutrons in reactors – the integral quantities to be calculated often do not depend strongly on the details of the scattering law. This may be an advantage or disadvantage depending on the point of view. Calculations even with crude models often give sufficiently accurate results for these integral quantities of practical interest. This fact, on the other hand, makes it difficult to use, for example, measured thermalization properties as a check for the validity of models or the accuracy of measured scattering laws. This is a point which is discussed later. There are certain well-understood general properties of $S(\vec{\kappa}, \omega)$, which are more important to observe for neutron thermalization than the realistic description of details. These properties are expressed by the following relations.

(a) Principle of detailed balance

$$S(-\vec{\kappa}, -\omega) = e^{-\hbar\omega/k_B T} S(\vec{\kappa}, \omega) \tag{7}$$

This is a consequence of the microscopic reversibility of scattering processes. Although Eq. (7) is not a necessary condition, it guarantees that the solution of the Boltzmann equation for a non-absorbing infinite medium is a Maxwellian distribution. By extracting the factor $\exp(-\beta/2)$ and introducing the function $S(\alpha, \beta)$ (a symmetrical function in β), as was done in Eq. (3), the relation (7) is always fulfilled.

(b) Moment relations

The first few of these moment theorems originally derived by Placzek [9] are

$$\int S_s(\vec{\kappa}, \omega)\, d\omega = 1, \qquad \int S_c(\vec{\kappa}, \omega)\, d\omega = 1 + \gamma(\vec{\kappa}) \tag{8}$$

$$\int S(\vec{\kappa}, \omega)\omega\, d\omega = \frac{\kappa^2}{2M} \tag{9}$$

$$\int S(\vec{\kappa}, \omega)\omega^2 d\omega = \frac{\kappa^2}{M} k_B T \tag{10}$$

where $\gamma(\vec{\kappa})$ is the Fourier transform of the static pair-distribution in the coherent case. Equation (9) is well known as the 'sum rule, which says that for any system of chemically bound atoms the average energy transfer $\overline{\hbar\omega}$ for a momentum transfer $\hbar\kappa$ is the same as it would be if the atoms were free. Equations (8), (9) and (10) guarantee that the high-energy total-scattering cross-section will be the free-atom cross-section and should not be violated. In these equations only measurable quantities appear, allowing us to use them as a check for experimental results.

II. INTEGRAL PROPERTIES OF $S(\alpha, \beta)$

If the scattering law $S(\alpha, \beta)$ is complete (covering the whole α, β-range) and accurate enough, all physical properties influenced by the chemical binding of the atoms can be calculated. Here we are mainly interested in integral properties describing aspects of neutron thermalization which can be evaluated from $S(\alpha, \beta)$ and determined or derived more directly from measurements. Among these quantities are the total scattering cross-section $\sigma(E_0)$, the average cosine of the scattering angle $\bar{\mu}(E_0)$, the differential scattering cross-section $\sigma(E_0, \vartheta)$, the transport mean free path $\lambda_{tr}(E_0)$, the thermal diffusion constant D_0, the second moment of energy transfer M_2 for a Maxwellian distribution and others.

A method quite commonly used now for such calculations is to start from the generalized frequency distribution $\rho(\beta)$. $\rho(\beta)$ can be either measured directly using cold neutrons derived from $S(\alpha, \beta)$ or constructed from other experimental data on the dynamics of the scatterer, e.g. from interatomic force constants, available from dispersion curve measurements. If the incoherent approximation is valid, the phonon expansion [3] and the short-collision-time approximation [10] are sufficient to calculate $S(\alpha, \beta)$ for the whole α- and β-range of interest. Several computer programmes to do these calculations are now available, e.g. LEAP [11], SUMMIT [12], GAKER [13], UPRAS [14] and others.

Similarly programmes are in use for calculating P_n-scattering matrices, starting from $S(\alpha, \beta)$, e.g. PIXSE [15]. These are then used for the calculation of thermal spectra, for the numerical solution of transport problems and related topics.

From the LEAP output, KAPIXSE [16], for example, evaluates the coefficients of the expansion of $\sigma(E_0 \to E, \vartheta)$ in Legendre polynoms $P_\ell(\mu)$ ($\mu = \cos\vartheta$):

$$\sigma_\ell(E_0 \to E) = \frac{2}{2\ell+1} \int_{-1}^{+1} P_\ell(\mu)\, \sigma(E_0 \to E, \mu)\, d\mu \tag{11}$$

and further

$$\sigma(E_0) = \int dE\, \sigma_0(E_0 \to E), \quad \bar{\mu}(E_0) = \int dE\, \sigma_1(E_0 \to E)/\sigma(E_0) \tag{12}$$

The thermal diffusion constant is defined as

$$D_0 = \int_0^\infty M(E)\,\lambda_{tr}(E)\,dE \Big/ \left(3\int \frac{1}{v} M(E)\,dE\right) \quad . \tag{13}$$

where $M(E) = (k_BT)^{-2}\,E\,\exp(-E/k_BT)$ is the Maxwellian distribution.

Another important parameter is M_2, the second moment of energy transfer for a Maxwellian velocity distribution of the neutrons

$$M_2 = (k_BT)^{-2} \int_0^\infty dE_0 \int_0^\infty dE\, M(E)\,(E - E_0)^2\,\sigma(E \to E_0) \tag{14}$$

Within the Gaussian approximation for the scattering law, M_2 can be written [17]

$$M_2 = (15/16)(\sigma_b m/M) \int_{-\infty}^{+\infty} t\,\dot{w}(t)\,[0.25 + t^2 + mw(t)/\underline{M}\,]^{-7/2}\,dt \tag{15}$$

where

$$w(t) = \int_0^\infty [\,\rho(\beta)/\beta\,\sinh(\beta/2)]\,[\cosh(\beta/2) - \cos(\beta t)]\,d\beta \tag{16}$$

III. PRESENT STATE OF THE EXPERIMENTAL TECHNIQUE

1. Experimental arrangement, technique of measurement

For the measurement of double-differential cross-sections a double spectrometer is necessary. This is an apparatus consisting of a primary spectrometer, a monochromator selecting from a thermal neutron source spectrum a beam with a small energy band of neutrons, and a secondary spectrometer for analysing the energy and momentum of scattered neutrons.

Most of the scattering laws for materials we are interested in here are measured with the time-of-flight technique, using a pulsed monochromatic neutron beam and determining the energy after scattering by the time-of-flight of the neutrons. As sources, mainly thermal reactors with high fluxes have been used and a number of experiments have also been performed with linear accelerators.

The time-of-flight spectrometers in principle do not differ in the secondary part of the arrangement. The difference is mainly in the primary part, the production of the pulsed monochromatic beam. Because the phased rotor systems used at Harwell and Chalk River [18], at the MTR (Idaho) [19], and in Ann Arbor, Michigan [20] are already familiar, I would like to show you the principle of a rotating crystal time-of-flight spectrometer which in the last few years has become a strong competitor to the mechanical chopper systems. Fig. 1 shows a scheme of the rotating

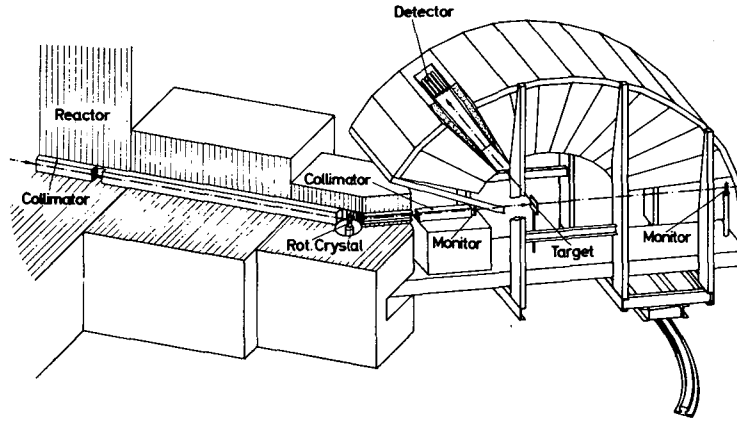

FIG. 1. Rotating crystal time-of-flight spectrometer at the FR 2.

crystal spectrometer in operation at the reactor FR 2 in Karlsruhe [21]. There are perhaps only two comments to be made.
(a) The rotating crystal is a relatively simple technical device compared with a phased chopper and it has the advantage of offering several monochromatic beams simultaneously.
(b) Considering intensity and resolution, crystal and double chopper are about equivalent. If the rotating crystal is optimized it is even superior to the chopper.

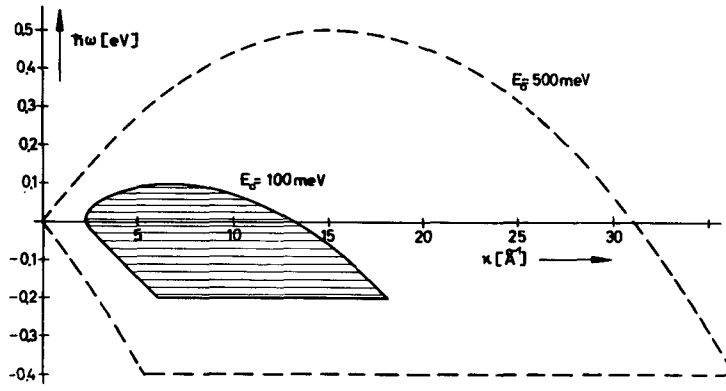

FIG. 2. Attainable κ, ω range for different incident energies E_0.

The present apparatus has a primary energy resolution of 2-5%. So far it was used for incident energies between 8 and 100 meV. Fig. 2 shows the part of the (κ, ω) plane covered by this instrument and the range one probably would like to cover to get complete scattering laws.

2. Data accumulation and reduction

Normally the large amount of data collected in such an experiment is stored in a multichannel analyser, sequentially written on magnetic tape or, as we are doing it now, handled by an on-line computer with large-

capacity storage media, such as tapes and magnetic discs, available. The totalized information for sample-in and -out runs normally available on a tape is converted in $S(\alpha, \beta)$ values on a larger computer. This data can be further condensed if the assumptions of a model like the generalized frequency distribution are valid, or at least a good approximation. In this case the way to interpolate and extrapolate the data is obvious.

3. Multiple scattering

Often the $S(\alpha, \beta)$ values derived in this way are not the quantities one really wishes to determine. Even with targets of transmission as high as 0.9 multiple scattering processes (neutron scattered twice or more often) contribute substantially to the measured cross-section $\sigma(E_0 \rightarrow E, \vartheta)$ especially for coherent scattering, a very complicated process. The correction for these contributions is in general, especially for coherent scattering, a very complicated process. The unknown quantity $S(\alpha, \beta)$ has to be known already for the correction. The approach we decided to make is to calculate this correction in the incoherent approximation. Space-, angle- and energy-dependent neutron currents $p_n(x, \vartheta, E)$ are defined in the probe. Up to three collisions which take into account all possible combinations of elastic and inelastic processes are considered.

An iterative procedure was developed which starts by describing the experimentally determined $S(\alpha, \beta)$ values by a phonon expansion (using a programme such as LEAP [11], e.g.). The currents $p_n(x, \vartheta, E)$ are then calculated. By comparing $p_1(x, \vartheta, E)$, the quantity we are really interested in, with $S(\alpha, \beta)$ derived from the measurement a correction is found which leads to a new choice for the frequency distribution of the phonon expansion.

A computer programme (VIPER) has been written to do these evaluations [22]. In practice it was found that one or two iterations are sufficient to obtain the multiple scattering correction. Fortunately one often finds already for p_2 the typical angular dependence of the elastic scattering, thus allowing an estimation of higher p_n terms and saving the large computer time necessary for $p_3(x, \vartheta, E)$. A typical result of such a procedure is shown in Fig. 3. Depending on α it was found that inelastic multiple scattering processes contribute substantially to the correction. Similar calculations, restricted sometimes to elastic contributions, however, have been done by others [23 - 25].

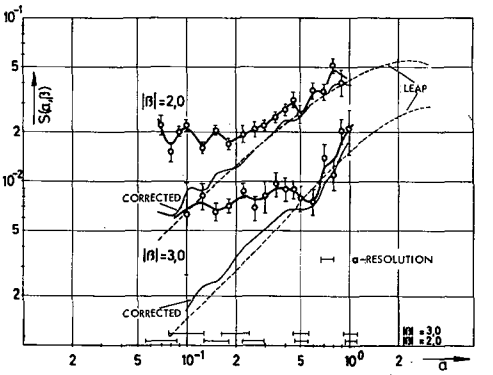

FIG. 3. Examples of multiple scattering corrections.

4. Resolution correction

Not much work has been done so far for correcting $S(\alpha, \beta)$ for the resolution of the spectrometer. A simple correction for lines unfolds two Gaussian distributions, giving again a Gaussian [26]. A more general procedure has been described by Maiorov et al. [27]. In this approach $S(\alpha, \beta)$ is calculated by direct time integration of the intermediate scattering function, introducing a Gaussian cut-off factor $\exp(-\delta^2 t^2/2)$. The result is a convolution of the true scattering distribution with a Gaussian of width δ and this is just the quantity measured.

IV. OTHER SOURCES OF INFORMATION

As we have seen, the present scattering law measurements with neutrons do not cover the whole part of interest of the (κ, ω) plane and often the energy resolution is not sufficient enough to measure excitation energies accurately enough. Therefore results of other experimental techniques have to be taken into consideration, especially for the more complicated molecular liquids and solids, in the construction of a complete scattering law. For instance the frequencies of intramolecular vibrations are largely available from infra-red and Raman measurements and can be used to complete $\rho(\beta)$.

For simple single crystals, phonon-dispersion relations in a few symmetry directions or planes can be measured with an accuracy of a few per cent using coherent neutron scattering or X-ray scattering. These measured dispersion curves are normally fitted with a several-neighbours Born-von Kármán model to determine interatomic force constants. Techniques have been developed to calculate from these force constants the density of lattice vibration modes. Probably the most accurate method is at present the root sampling technique [28]. Because of the higher accuracy attainable in dispersion measurements, a frequency distribution derived in this way seems to be more reliable than one derived from a measured $S(\alpha, \beta)$ using the incoherent approximation and the extrapolation procedure of Eq. (6). The $\rho(\beta)$ calculated by the root sampling technique for an irreducible part of the Brillouin zone can then be used as input information for the Gaussian approximation.

It should be kept in mind, however, that for more complicated crystals the spectral density of atomic motions is needed rather than that of normal modes. This essentially means that not $\rho(\beta)$ but $S(\alpha, \beta)$ has to be calculated with the root sampling technique.

Finally it should be mentioned that sometimes specific heat measurements allow the reconstruction of part of the frequency distribution or the determination of open parameters in a model assumption for $\rho(\beta)$ [29].

V. DISCUSSION OF MEASURED SCATTERING LAWS

It is impossible to cover in a review such as the present one all the scattering law data measured so far. Therefore only a few important materials such as water, zirconium hydride and graphite are selected. Other materials such as organics will be covered by other papers in this

session; also the few results mentioned in this paper will be supplemented by further contributions.

1. Light water

(a) Free H_2O molecules

Although the knowledge of the scattering properties of gaseous H_2O may not be of vital interest for direct reactor use, an experimental determination of $S(\alpha, \beta)$ may be a sensitive check of current theoretical models describing scattering from free molecules. Results of an experiment at 540°K and a pressure of 20 atm are shown in Fig. 4 [30]. It can be seen that the Krieger-Nelkin model calculations using an effective mass

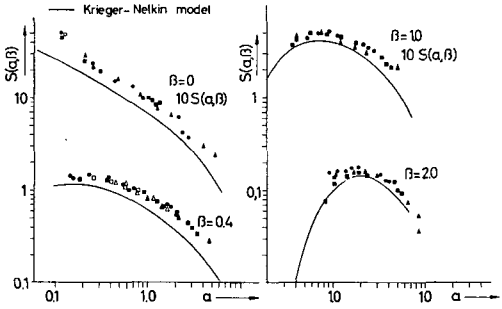

FIG. 4. Examples of $S(\alpha, \beta)$ for gaseous H_2O.

$\overline{M} = 1.9\ M_H$ do not agree with the experiment. Obviously the differential cross-section for scattering from a system of asymmetric tops has to be calculated in the H_2O case, which has been done so far only for low-incident energies [31].

(b) Liquid H_2O

A considerable amount of neutron scattering data has been collected for liquid H_2O. We restrict our discussion here to room temperature data; newer results for higher temperatures are also reported in these Proceedings. Examples of $S(\alpha, \beta)$ values from different authors [32 - 36] are shown in Fig. 5. The plot leads to an estimation of the consistency of the data of an order of about 20% for most of the α, β range covered.

Because of the mainly incoherent scattering of hydrogen the extrapolation technique leading to a generalized frequency distribution $\rho(\beta)$ may be a good model in this case if the harmonic approximation is still useful and if the influence of the difference in vibration amplitudes of H and O can be handled.

$\rho(\beta)$ was derived from the $S(\alpha, \beta)$ data shown above and further from several up-scattering experiments [37, 38] with cold neutrons, which have been converted directly to a frequency distribution on the basis of the same assumptions. A comparison of all these distributions is made in Fig. 6. The area below each of these curves is normalized to 0.5. Compared with the present attainable accuracy for such frequency distribution measurements for simpler systems such as vanadium the agreement is quite satisfactory. The cold neutron data have the advantage of better resolution, especially at low β-values, but it is difficult to correct them

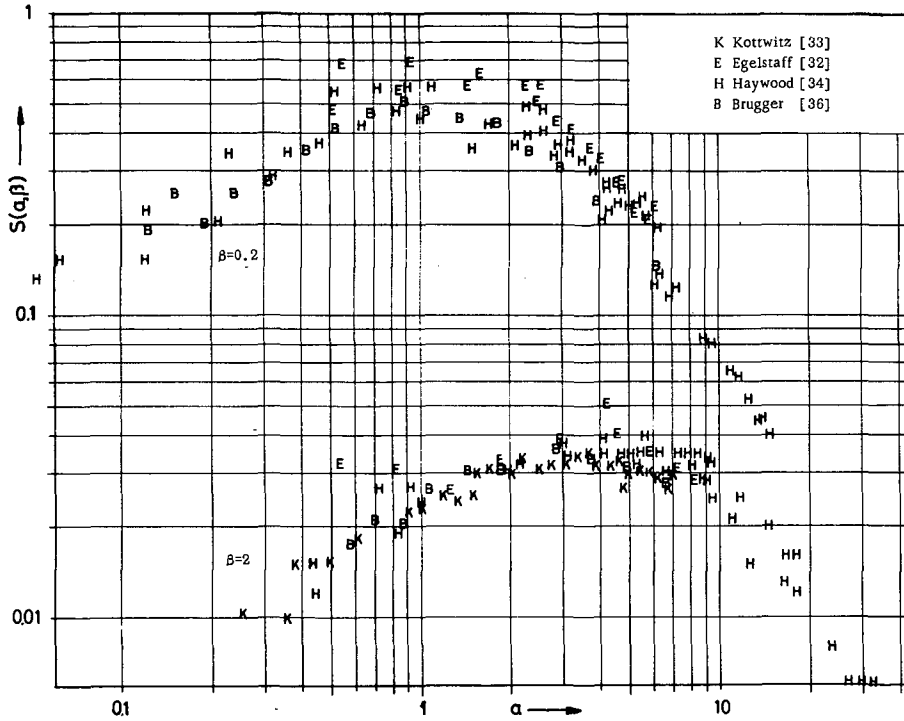

FIG. 5. $S(\alpha,\beta)$ data for H_2O at 295°K for two values of β.

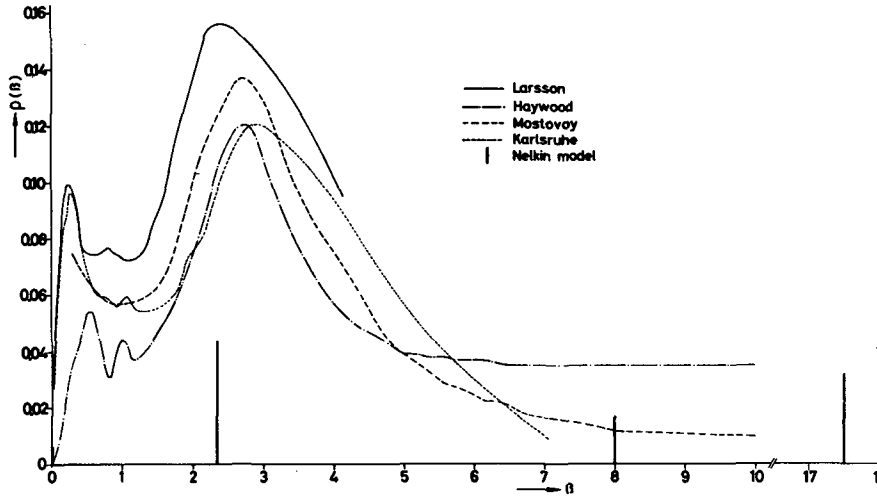

FIG. 6. Frequency distributions for room-temperature H_2O.

for multi-phonon processes. The energy range covered by this distribution is generally divided in 3 regions:

(i) Diffusive motions of molecules corresponding to small energy transfers. This effect does not show up in the given $\rho(\beta)$; it contributes also only a small part to the spectral density

(ii) The β-range up to $\beta = 1$ with bumps at about 8 meV and 22 meV is determined by vibrations of the whole molecules.

(iii) The region above $\beta = 1$ is thought to be mainly related to librational motions (hindered rotations) of the molecules.

Regions (i) to (iii) are approximated in the Nelkin model [39] by two δ-functions. The relative weights of these δ-functions at $\beta = 0$ and $\beta = 2.4$ are indicated in Fig. 6 by the height of the lines.

For the internal vibrations of the H_2O molecules which are assumed not to be disturbed much by liquid effects, energy levels at 0.205 eV, 0.428 eV and 0.450 eV have been derived from infra-red data. Only recently an indication of the binding mode at 0.205 eV was found in neutron scattering data [40]. The total weight of these levels in the spectral density should be about 0.5 because half of the six degrees of freedom of each pair of H atoms in the molecule has to be assigned to vibrations and half to the low-energy motions. This is essentially confirmed by the experimental results for the low-energy part of $\rho(\beta)$ and was used for normalizing the curves of Fig. 6.

Although the Nelkin model was a major step from a free-gas approximation to a realistic scattering kernel for H_2O, discrepancies remained between measured and calculated integral quantities. In fact this is not surprising if the low-energy part of $\rho(\beta)$ which shows a considerable structure is just approximated by two δ-functions. Part of this discrepancy has been removed by allowing for the spatial anisotropy of the internal H_2O vibrations [41].

Another extension of the Nelkin model recently proposed by McMurry and Russell [36] treats water as a mixture of free molecules and of aggregates of molecules of two sizes. Amplitudes of a set of vibrational energies below 0.125 eV have been selected to fit the MTR scattering law data for room-temperature H_2O. Although the general features of this model are reasonable, the selected amplitudes may depend on the large multiple scattering contributions at small α.

Integral data for H_2O

A few typical results evaluated from $S(\alpha, \beta)$ data for H_2O in comparison with measured quantities are discussed in this section. Figure 7 shows a comparison of experimental $\sigma(E_0)$ data for H_2O at room temperature [42, 43] with different model calculations. The dotted curve is calculated with the Nelkin model; the anisotropic model gives the dashed line and the solid line is a KAPIXSE calculation using $\rho(\beta)$ given by Haywood (see Ref. [44]). The general agreement of the various results is quite good; however, this indicates only that $\sigma(E_0)$ is not very sensitive to the details of $S(\alpha, \beta)$.

The agreement between the various models is quite satisfactory again for M_2 given in Table I. The differences are more pronounced in the differential cross-section $\sigma(E_0, \vartheta)$ and in the average cosine $\bar{\mu}(E_0)$. Experimental results [48, 49] and model calculations for both are given in Figs 8 and 9. The discrepancy can be partially reduced with the anisotropic vibration model for water [41] but it seems that the experimentally determined scattering kernel yields the best agreement with the measured α-values. Because $\bar{\mu}$ determines important quantities for reactor applications, such as the transport mean free path λ_{tr} and the thermal diffusion

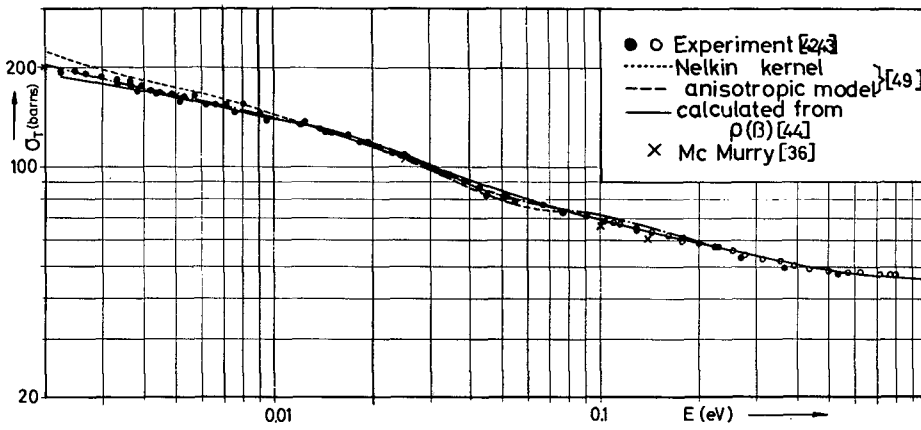

FIG. 7. Total cross-section of H_2O.

TABLE I. SECOND MOMENT OF ENERGY TRANSFER M_2 FOR H_2O

Model	M_2 (barns)	Refs
Nelkin	49.05	Honeck [45]
Nelkin	47.9	Kiefhaber [46]
Haywood	46.5	Gläser and Beckurts [47]

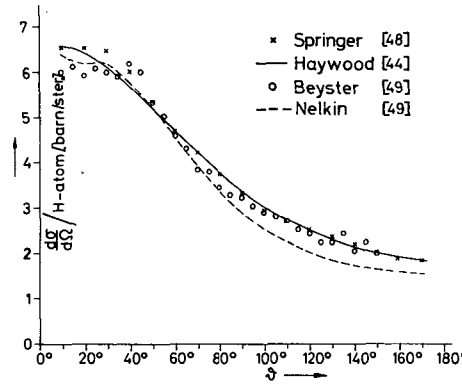

FIG. 8. Angular scattering of H_2O for an incident energy E = 44 meV.

constant D_0, the experimentally determined scattering data should be taken into account in the construction of a final scattering kernel.

Another check of the data is possible with diffusion parameters derived from pulsed neutron measurements. Here the time constant α of the decay

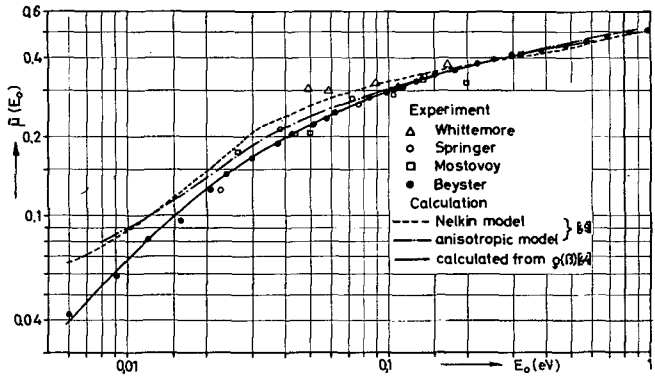

FIG. 9. Average cosine $\bar{\mu}$ (E_0) of H_2O.

of an asymptotic spectrum is correlated with the geometrical buckling B^2 of the moderator assembly by a series of the type

$$\alpha = \overline{v\Sigma_a} + D_0B^2 - CB^4 + FB^6 + \ldots \qquad (17)$$

Table II gives more recent results for the parameters.

TABLE II. DIFFUSION PARAMETERS IN H_2O AT 20°C

D_0 (cm²/s)	C(cm⁴/s)	F(cm⁶/s)	Refs
35 630 ± 80	3420 ± 170	214 ± 139	Experimental [50]
37 045	3361	169	Nelkin kernel [51]
34 520	4220	363	Haywood $\rho(\beta)$ [44]

Influence of the scattering law on thermal neutron spectra

Neutron spectra measurements also offer the possibility of comparing the various scattering models with experimental data. The type of experiment to be done depends on the property of the scattering model to be checked. If only the energy transfer $\Sigma(E_0 \rightarrow E)$ is of interest, spectra from large (poisoned) homogeneous systems which are not sensitive to the angular dependence of the scattering kernel can be measured. Spectra from the boundaries of moderators, however, depend in principle on the energy transfer and angular-dependent properties of $S(\alpha, \beta)$. The possibilities of time-dependent spectra measurements, which may be more sensitive to the details of the scattering model, have not been fully exploited yet.

Experiments of various types have been reviewed elsewhere [44, 52] and are discussed in these Proceedings. A typical example of the first type is given in Fig. 10, where a spectrum from boron-poisoned H_2O measured by Poole [44] is compared with calculations using the Nelkin model and

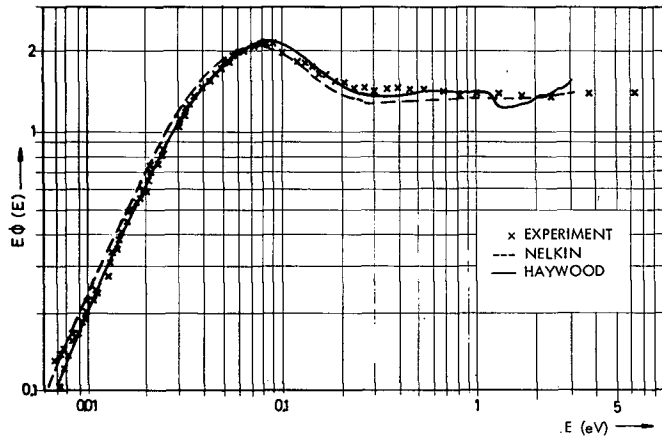

FIG. 10. Calculated spectra in comparison with experimental data for boron-poisoned H_2O [44].

the frequency distribution $\rho(\beta)$ derived by Haywood. Although the Nelkin kernel is a considerable improvement over the free-gas kernel, here, similarly as in the comparison of integral parameters we did above, a final discrepancy still exists which is reduced further by experimental scattering law data.

2. Zirconium hydride

In the ZrH_x lattice the H atoms are placed in the centre of a tetraeder formed by the heavy Zr atoms. Because of the high-bound hydrogen cross-section, neutrons see, in first approximation, a system of isotropic harmonic oscillators. Then from a theoretical point of view zirconium hydride or more generally the metal hydrides are perhaps the simplest of all moderators. The oscillator frequency $\hbar\omega$ has been experimentally determined by several workers to be about 0.14 eV. Up to four excited levels have been found with no substantial change in $\hbar\omega$. Further, a line width $\Delta\hbar\omega$ of about 30 meV was determined for the first level without a detectable angular and temperature dependence. Results for $\hbar\omega$ and $\Delta\hbar\omega$ of the first level are summarized in Table III.

By assuming a Debye spectrum with a cut-off at 20 meV for the acoustical modes of the zirconium hydride lattice and the line discussed above for the spectral density of optical modes a reasonably accurate scattering kernel has been constructed by Young et al. [60]. The weight to be assumed for the acoustical modes, although it is small, is somewhat arbitrary in this model. An attempt to determine this part of the frequency distribution from the specific heat was made by Reichardt [29]. He arrived at a cut-off energy of 27 meV. A direct determination of $\rho(\beta)$ from measured scattering law values for $ZrH_{1.08}$ at T = 210°C using the extrapolation technique has been made recently by Ehret [54]. The result of this measurement is compared with the constructed $\rho(\beta)$'s in Fig. 11. The area of the measured acoustical part, corresponding also approximately to a Debye spectrum with a cut-off at 27 meV, is about 0.006. From general arguments it follows that this area of $\rho(\beta)$ depends on the hydrogen concentration in ZrH_x. The experimentally determined total area of $\rho(\beta)$ is about 20% lower than the theoretical value 1. This deviation is thought to be

TABLE III. ENERGY AND LINE WIDTH OF THE OPTICAL LEVEL IN ZIRCONIUM HYDRIDE

Composition	$ZrH_{0.5}$	$ZrH_{1.08}$	$ZrH_{1.5}$	$ZrH_{1.5}$	—	ZrH_2	ZrH_2	ZrH_2
T(°C)	27	210	20	393	23	27	20	20
$\hbar\omega$ (meV)	140-145	138	130	130 ± 5	136	140-145	137	140
$\Delta\hbar\omega$ (meV)	28	36	29.5	31	28	28	29	26.4
Refs	[53]	[54]	[55]	[56]	[57]	[53]	[58]	[59]

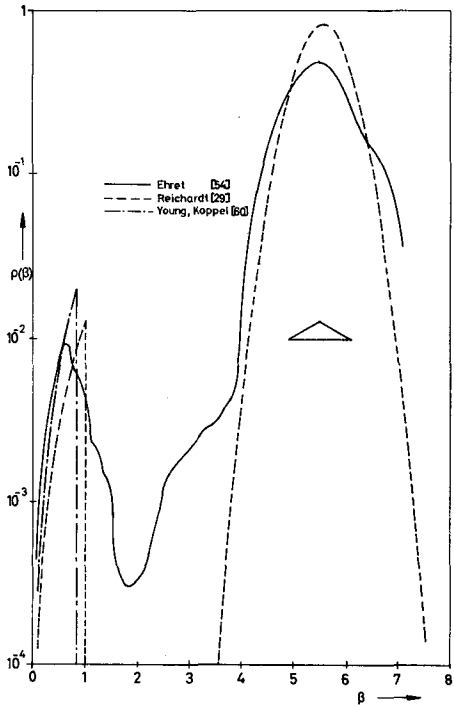

FIG. 11. Frequency distributions of zirconium hydride.

caused by the Zr atoms which have to be taken into account in principle with a different $\rho(\beta)$.

Integral properties for zirconium hydride

For the synthetical $\rho(\beta)$ models and the experimentally determined $\rho(\beta)$ various calculations of $\sigma(E_0)$, $\sigma(E_0, \vartheta)$ and $\bar{\mu}(E_0)$ have been made in the incoherent approximation. Results for $\sigma(E_0)$ at room temperature are compared with the experimental data in Fig. 12. Besides the coherent contribution of Zr to $\sigma(E_0)$ above 4 meV the agreement is better than a few per cent.

Experimentally determined $\sigma(E_0, \vartheta)$ values by Kornbichler [61] show a considerable structure, probably due to coherent Zr scattering, and there-

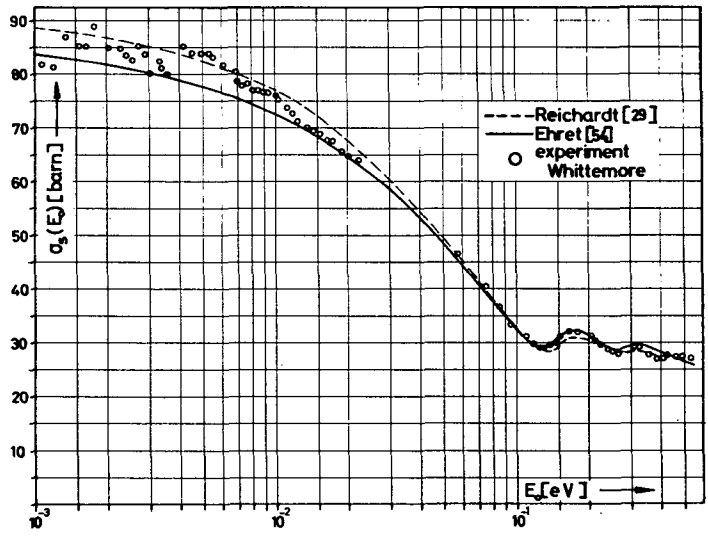

FIG. 12. Total cross-section of zirconium hydride.

fore can be described only on the average by the models given above. The degree of agreement is demonstrated in Fig. 13. Similar measurements have been made by Beyster et al. [49]. In the average cosine $\bar{\mu}(E_0)$ (Fig. 14) the coherent effects are smoothed out again. There is, however, a sudden change of $\bar{\mu}$ at the energy of the Einstein oscillator which is also reasonably well described by the models.

3. Graphite

Several experiments have been performed to measure the scattering of thermal neutrons from graphite at different temperatures [62-64]. The results of a more recent series of measurements by Carvalho [65] on different types of graphite at a temperature of 533°K are given in Fig. 15. Incident neutron energies E_0 have been between 17.5 and 95.5 meV. Again the symmetrical form of the scattering law $S(\alpha, \beta)$ is plotted. Because data for different E_0 and for positive and negative β have to be on the same curve this representation gives an impression of the experimental accuracy. The curves show a considerable amount of structure which is marked at low β and low α and tends to wash out at larger α and higher β values. This structure which has not been so clear in the earlier experiments has its origin of course in the predominant coherent scattering of carbon. All data have been corrected for multiple scattering. The correction is serious for small α, reducing $S(\alpha, \beta)$ almost by a factor 5 for the lowest α values measured.

To explain the details of the experimental results, the coherent scattering law has to be calculated. On the other hand, the simplest model one can try to compare with the measurement is a phonon expansion for the scattering law in the incoherent approximation. The result of such a calculation with a generalized frequency distribution derived from the experimental data in an iterative procedure is given by the dashed lines in Fig. 15. The corresponding frequency distribution is shown in Fig. 16

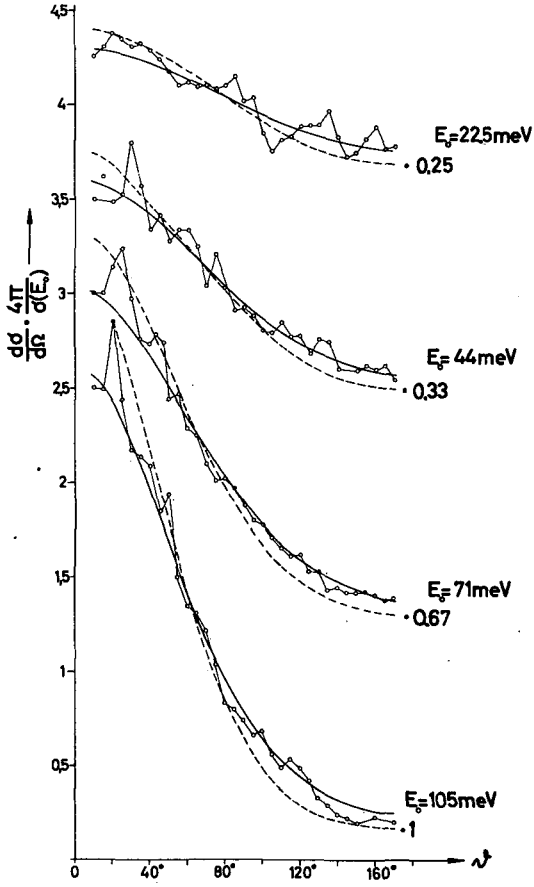

FIG. 13. $\sigma(E_0, \vartheta)$ of zirconium hydride. Calculations: - - - Young, —— Ehret

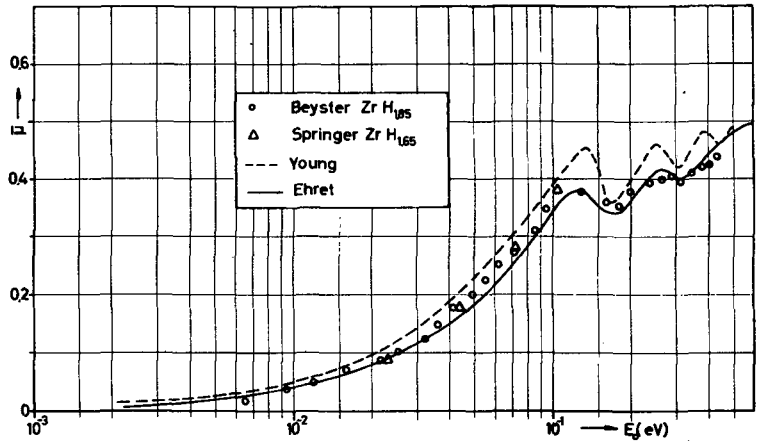

FIG. 14. Average cosine $\bar{\mu}(E_0)$ of zirconium hydride.

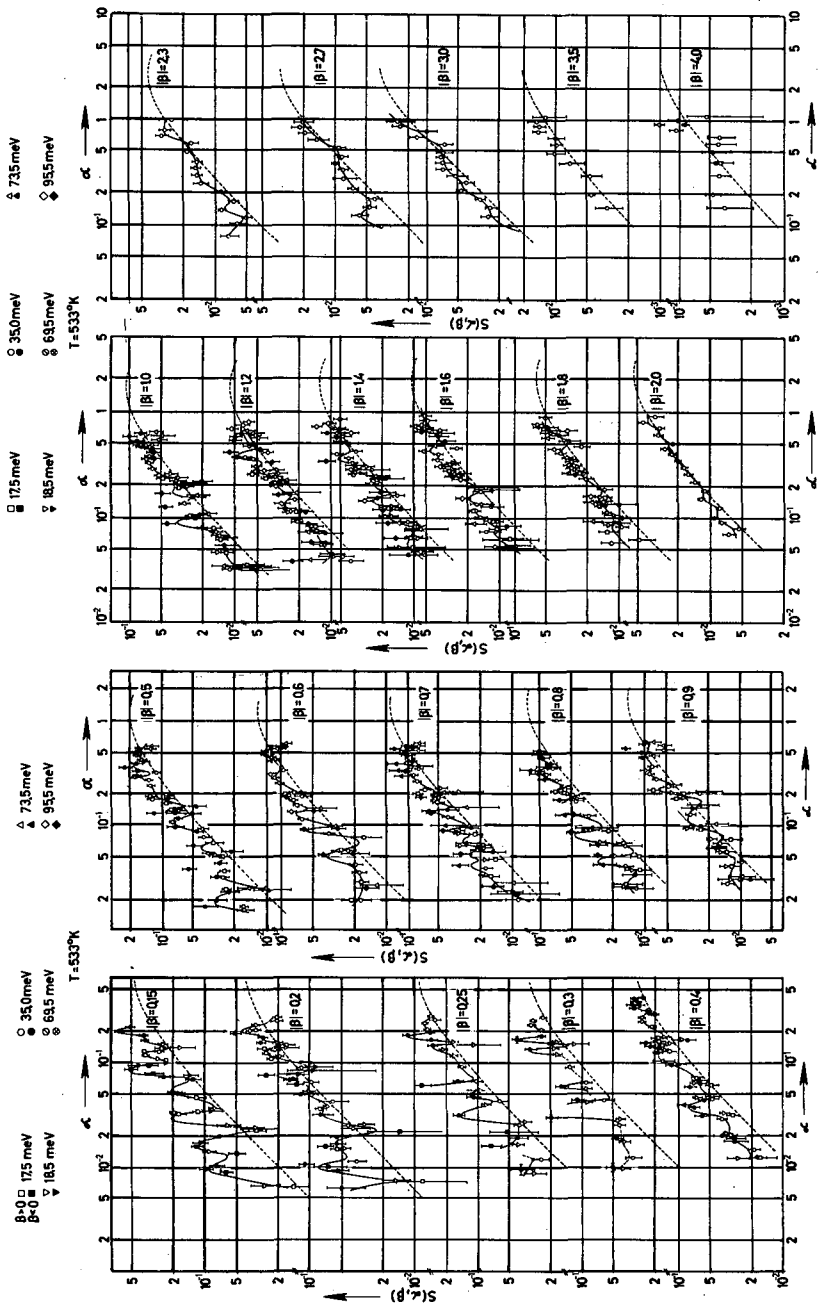

FIG. 15. Scattering law $S(\alpha, \beta)$ of graphite at $T = 533°K$.

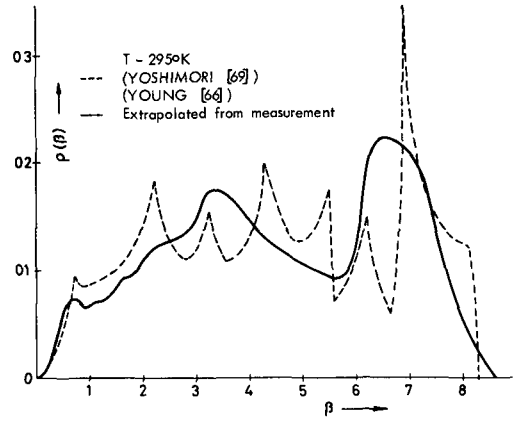

FIG. 16. Frequency distribution of graphite at room temperature.

where it is compared with the distribution calculated with the sampling technique for the Yoshimori-Kitano model [66]. The latter one was adjusted to get agreement with the measured specific heat of reactor-grade graphite. The demands on the extrapolated distribution should not be too high in view of all the approximations made. But it may be interesting that the specific heat of graphite can be described surprisingly well with this $\rho(\beta)$, which has no adapted parameters in it. Several other integral properties where directional effects are not very important can be reproduced with a similar accuracy.

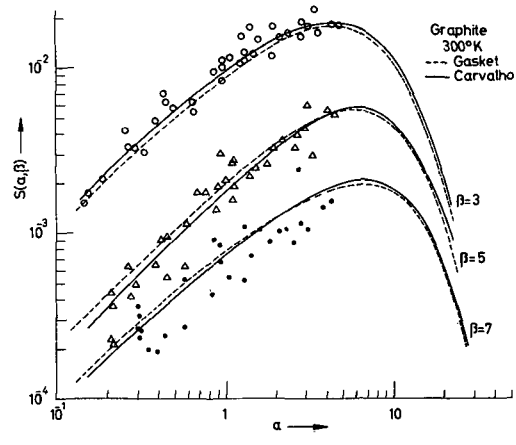

FIG. 17. $S(\alpha, \beta)$ for graphite at high α and β values.

Scattering law measurements for room-temperature reactor-grade graphite have been done recently by Whittemore [67] for higher energy and momentum transfers. These data, although they show less structure, can be well described with the frequency distribution derived above. Part of these data in comparison with calculations is shown in Fig. 17.

The actual behaviour of $S(\alpha, \beta)$ and angular-dependent phenomena described by $S(\alpha, \beta)$ cannot be understood in the incoherent approximation.

Takahashi [68] made a detailed theoretical study of the coherent one-phonon cross-section of polycrystalline graphite starting with the lattice model of Yoshimori and Kitano [69]. Besides the frequencies the polarization vectors of the phonons are needed for the calculation of the coherent scattering. $S(\alpha, \beta)$ has been separately calculated for in-plane and out-of-plane modes by sampling 675 values of the wave vector in an irreducible part of the first Brillouin zone. A typical result for a low β-value is shown in Fig. 18. In the same figure experimental data of Egelstaff [62] and temperature-converted data of Carvalho are shown. Unfortunately this conversion is not strictly allowed because of multiphonon contributions making the comparison somewhat arbitrary. However, at least an overall agreement between experiment and calculation can be seen. The difference between the two experimental set of points at small α may be largely due to multiple scattering.

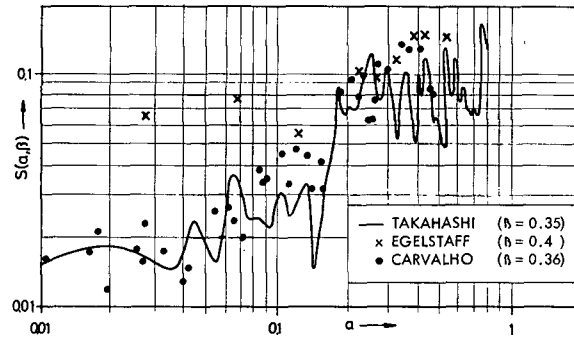

FIG. 18. Coherent one-phonon contribution to $S(\alpha, \beta)$ of graphite.

Integral data for graphite

To the author's knowledge no calculations of integral scattering properties of graphite have been done so far, taking coherent scattering into account. Several calculations have been done in the incoherent approximation either with the extrapolated $\rho(\beta)$ distributions or the frequency density derived from the Yoshimori-Kitano model. Here even the total cross-section, because of its coherent structure, cannot be used as a reasonable check. All model calculations yield below the Bragg cut-off an inelastic contribution to $\sigma(E_0)$ which is about a factor of two lower than the experimental points [42]. This discrepancy is not fully explained up to now.

The average cosine $\bar{\mu}(E_0)$ calculated for two $\rho(\beta)$'s is given in Fig. 19. No direct measurement of $\bar{\mu}$ (angular distribution type) has been done so far. Calculations of the second moment of energy transfer M_2 as a function of temperature are given in Fig. 20.

An experimental check of the graphite scattering kernel is possible, again by comparing the diffusion parameters derived from pulsed neutron measurements Eq. (17)] with the calculated values. Diffusion parameters for graphite derived from several experiments are compared in Table IV with results of calculations.

The agreement between experiment and theory perhaps can be judged more directly by comparing the different α versus B^2 curves which are shown in Fig. 21. The results of other measurements agree well with the two sets of experimental data plotted in Fig. 21.

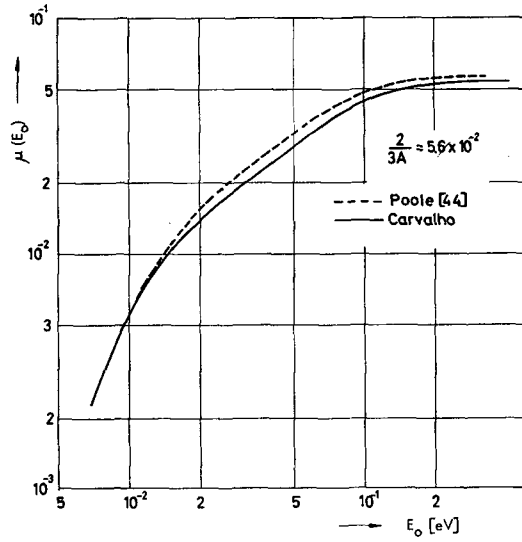

FIG. 19. Average cosine $\bar{\mu}$ (E_0) of graphite.

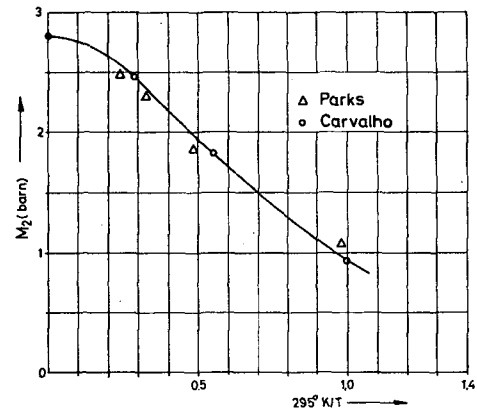

FIG. 20. M_2 for graphite (free gas).

4. Other moderators

(a) D_2O

Measurements of $S(\alpha, \beta)$ have been done by Haywood and Thorson [75] at 20°C and 150°C. The generalized frequency distribution $\rho(\beta)$ for different temperatures was determined also from cold neutron measurements [76]. An adjustment of the Nelkin model parameters for the description of D_2O in the incoherent approximation has been given by Honeck [77] which was successful in describing the total cross-section and measured spectra. A careful study of coherent scattering was made by Butler [78]. Butler and Koppel and Young [79] showed that the interference effects tend to cancel.

TABLE IV. DIFFUSION PARAMETERS OF GRAPHITE AT ROOM TEMPERATURE (density 1.6 g/cm^3)

D_0(10^5 cm^2/s)	C(10^5 cm^4/s)	F (10^7 cm^6/s)	Refs
			Experiment
2.13 ± 0.02	26 ± 5	-	Klose, Küchle and Reichardt [70]
2.11 ± 0.02	16 ± 5	-20 ± 10	
2.14 ± 0.01	39 ± 3	-	Starr and Price [71]
2.19 ± 0.03	37.9 ± 4	-	Sagot and Tellier [72]
			Calculation
2.178	24.6	-8.3	Honeck [73]
2.06	36.5	-14.7	Carvalho [74]

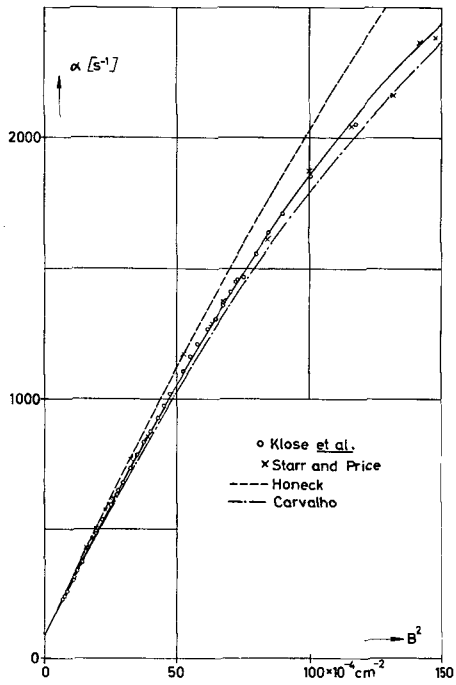

FIG.21. Experimental and calculated α versus B^2 curves for graphite.

(b) Beryllium and beryllium oxide

The only experimental determinations of $S(\alpha, \beta)$ for polycrystalline material of these two moderators have been made by Sinclair [80]. He tried also to derive a generalized frequency distribution using the extrapolation technique. Young and Koppel [81] used the results of phonon dispersion measurements of Schmunk et al. [82] to calculate the frequency

spectrum of beryllium with the sampling technique. There is a considerable difference between the calculated frequency distribution and the $\rho(\beta)$ extrapolated from $S(\alpha, \beta)$ measurements.

For beryllium oxide no theoretical calculation of the frequency distribution has been made so far. Such a calculation is more laborious than for Be because of the presence of two different atomic species in the lattice. On the other hand, the use of the incoherent approximation for calculating $S(\alpha, \beta)$ is even more doubtful than for beryllium. It seems that for beryllium oxide further theoretical and experimental investigations are needed.

VI. SUMMARY AND CONCLUSIONS

In the last few years scattering kernels became available, which take into account the influence of the different forms of chemical binding in matter on slow neutron scattering in a more realistic way than earlier. The experimental information used in constructing these kernels came from specific heat measurements, optical spectroscopy and inelastic neutron scattering experiments.

So far the scattering has been treated mainly in the incoherent approximation and the Gaussian approximation for the intermediate scattering function. Only in a few cases has coherent scattering been taken into account. For almost all the important moderators appropriate kernels are now available, which describe neutron thermalization in these materials in a satisfying way for many needs. A series of computer codes has been developed to make use of the available scattering law data to calculate scattering matrices.

A few typical examples of available scattering law data have been discussed in this paper and it has been shown that inelastic neutron scattering experiments contributed considerably to our knowledge of neutron behaviour in matter in the energy range which is most important for neutron thermalization in reactors.

The experimental technique of scattering law measurements has reached a stage to deliver consistent results within an accuracy of ± 10%. This accuracy is good enough to reproduce the results of simpler but more precise integral measurements. These measurements, mainly single-differential cross-section measurements, pulsed neutron experiments and, to some extent, spectra measurements offer valuable checks for the various scattering law data generated. The most sensitive check for synthetic kernels is to compare them with experimental scattering law data. But it seems that especially the differential cross-section data are also quite sensitive to details of the scattering law. More systematic studies of this type are worthwhile.

Less work has been done so far on the temperature dependence of $S(\alpha, \beta)$. Also further experimental studies of the coherently scattering moderators are desirable. Probably the progress made in phonon dispersion work with neutrons will form a sound basis for more accurate calculations for crystalline materials.

REFERENCES

[1] KRIEGER, T.J., NELKIN, M.S., Phys. Rev. 106 (1957) 290.
[2] GRIFFING, G.W., Inelastic Scattering of Neutrons in Solids and Liquids I IAEA, Vienna (1963) 435.
[3] SJÖLANDER, A., Ark. Fys. 14 (1958) 315.
[4] IIJIMA, S., J. nucl. Sci. Technol. 3 (1966) 160.
[5] SJÖLANDER, A., in Thermal Neutron Scattering (EGELSTAFF, P.A., Ed.) Academic Press, N.Y. (1965) 291.
[6] YIP, S., OSBORN, R.K., Phys. Rev. 130 (1963) 1860.
[7] EGELSTAFF, P.A., SCHOFIELD, P., Nucl. Sci. Engng 12 (1962) 260.
[8] RAHMAN, A., SINGWI, K.S., SJÖLANDER, A., Phys. Rev. 126 (1962) 986.
[9] PLACZEK, G., Phys. Rev. 86 (1952) 377.
[10] WICK, G.C., Phys. Rev. 94 (1954) 1228.
[11] McLATCHIE, R., Program description LEAP, AERE, Harwell (1962).
[12] BELL, J., USAEC Rep. GA-2492 (1962).
[13] HONECK, H.C., BNL-5826 (1961).
[14] MAIOROV, L.V., TURCHIN, V.F., YUDKEVICH, M.S., Proc. 3rd UN Int. Conf. PUAE 2 (1965) 379.
[15] MacDOUGALL, J.D., Rep. AEEW-M 318 (1963).
[16] STITTGEN, H., Internal report, Karlsruhe (1964).
[17] SCHOFIELD, P., Rep. BNL-770 (T-288) (1962).
[18] EGELSTAFF, P.A., COCKING, S.J., ALEXANDER, T.K., Inelastic Scattering of Neutrons in Solids and Liquids, IAEA, Vienna (1961) 165.
[19] BRUGGER, R.M., EVANS, J.E., Nucl. Instrum. Meth. 12 (1961) 75.
[20] ZWEIFEL, P.F., Rep. 03712-S-P, University of Michigan (1964).
[21] CARVALHO, F., EHRET, G., GLÄSER, W., RIPFEL, H., Rep. KFK-263 (1964).
[22] CARVALHO, F., EHRET, G., Internal report, Karlsruhe (1966).
[23] HONECK, H.C., Rep. GA-5968 (1964).
[24] COCKING, S.J., HEARD, C.R.T., Rep. AERE-R 5016 (1965).
[25] THORSON, I.M., Private communication.
[26] GREENSPAN, H., BAKSYS, I.G., ANL Reactor Physics Constants Center, Newsletter No.3 (1962).
[27] MAIOROV, L.V., TURCHIN, V.F., YUDKEVICH, M.S., Proc. 3rd UN Int. Conf. PUAE 2 (1965) 379.
[28] GILAT, G., RAUBENHEIMER, L.J., Phys. Rev. 144 (1966) 390.
[29] REICHARDT, W., SM-96/15, these Proceedings II.
[30] MERKEL, A., Internal report, Karlsruhe (1966).
[31] KHUBCHANDANI, P.G., RAHMAN, A., J. nucl. Energy 11 (1960) 89.
[32] EGELSTAFF, P.A., Rep. AERE-R 3931, Harwell (1962).
[33] KOTWITZ, D.A., LEONARD, J.R., Inelastic Scattering of Neutrons in Solids and Liquids I IAEA, Vienna (1963) 359.
[34] HAYWOOD, B.C., Rep. AERE-R 4484, Harwell (1964).
[35] MOSTOVOY, V.I. et al., Proc. 3rd UN Int. Conf. PUAE 2 (1965) 280.
[36] McMURRY, H.C., RUSSELL, G.J., BRUGGER, R.M., Nucl. Sci. Engng 25 (1966) 248.
[37] LARSSON, K.E., DAHLBORG, U., React. Sci. Technol. 16 (1962) 81.
[38] BLANCKENHAGEN, P.v., Karlsruhe (unpublished).
[39] NELKIN, M.S., Phys. Rev. 119 (1960) 741.
[40] HARLING, O.K., Phys. Lett. 22 (1966) 15.
[41] KOPPEL, J.U., YOUNG, J.A., Nucl. Sci. Engng 19 (1964) 412.
[42] Rep. BNL 325.
[43] Rep. GA-4659 (1963) 25.
[44] POOLE, M.J., Pulsed Neutron Research I IAEA Vienna (1965) 425.
[45] HONECK, H.C., Nucl. Sci. Engng 18 (1964) 49.
[46] KIEFHABER, E., Private communication.
[47] GLÄSER, W., BECKURTS, K.H., Nucl. Sci. Engng 20 (1964) 235.
[48] SPRINGER, T., HOFMEYER, C., KORNBICHLER, S., LEMMEL, H.D., Proc. 3rd UN Int. Conf. PUAE 2 (1965) 351.
[49] BEYSTER, J.R., YOUNG, J.C., NEILL, J.M., MOWRY, W.R., Pulsed Neutron Research I IAEA, Vienna (1965) 407.
[50] ARAI, E., KÜCHLE, M., Nukleonik 7 (1965) 416.
[51] GHATAK, A.K., HONECK, H.C., Nucl. Sci. Engng, 21 (1965) 227.
[52] BEYSTER, J.R., NEILL, J.M., USAEC Rep. CONF-660303 (1966) 91.

[53] WHITTEMORE, W., Rep. GA-4490 (Rev.).
[54] EHRET, G., Karlsruhe (unpublished) (1966).
[55] PELAH, I., EISENHAUER, C.M., HUGHES, D.J., PALEVSKY, H., Phys. Rev. 108 (1957) 1091.
[56] ANDRESEN, A., McREYNOLDS, A.W., NELKIN, M., ROSENBLUTH, M., WHITTEMORE, W., Phys. Rev. 108 (1957) 1092.
[57] WOODS, A.D.B., BROCKHOUSE, B.N., SAKOMOTO, M., SINCLAIR, R.N., Inelastic Scattering of Neutrons in Solids and Liquids, IAEA, Vienna (1961) 487.
[58] PAN, S.S., WEBB, F.J., Nucl. Sci. Engng 23 (1965) 188.
[59] HARLING, O.K., Rev. scient. Instrum. 37 (1966) 697.
[60] YOUNG, J.C., YOUNG, J.A., HOUGHTON, G.K., TRIMBLE, G.D., BEYSTER, J.R., Nucl. Sci. Engng 19 (1964) 230.
[61] KORNBICHLER, S., Nukleonik 7 (1965) 281.
[62] EGELSTAFF, P.A., COCKING, S.J., Inelastic Scattering of Neutrons in Solids and Liquids, IAEA, Vienna (1961) 25; and Rep. AERE-R 3931 (1962).
[63] DOLLING, G., BROCKHOUSE, B.N., Phys. Rev. 128 (1962) 1120.
[64] HAYWOOD, B.C., SINCLAIR, R.N., Rep. AERE-R 4732 (1964).
[65] CARVALHO, F., Doctor thesis, Karlsruhe (1967).
[66] YOUNG, J.A., KOPPEL, J.U., J. chem. Phys. 42 (1965) 357.
[67] WHITTEMORE, W., Private communication.
[68] TAKAHASHI, H., Private communication.
[69] YOSHIMORI, A., KITANO, Y., J. phys. Soc. Japan 11 (1956) 352.
[70] KLOSE, H., KÜCHLE, M., REICHARDT, W., Rep. BNL 719, Vol.III (1962) 935.
[71] STARR, E., PRICE, G.A., Rep. BNL 719, Vol.III (1962) 1034.
[72] SAGOT, M., TELLIER, H., Rapport C.E.A. 2210 (1963).
[73] HONECK, H.C., Rep. BNL 719, Vol. IV (1962) 1186.
[74] CARVALHO, F., Private communication.
[75] HAYWOOD, B.C., THORSON, I.M., Rep. BNL 719, Vol. I (1962) 27.
[76] DAHLBORG, U., GRESSHÖG, G., LARSSON, K.E., MÖLLER, E., PUROHIT, S.N., SJÖSTRAND, N.G., Proc. 3rd UN Int. Conf. PUAE 2 (1965) 336.
[77] HONECK, H.C., Trans. Am. nucl. Soc. 5 (1962) 47.
[78] BUTLER, D., Proc. phys. Soc. 81 (1962) 276 and 294.
[79] KOPPEL, J.U., YOUNG, J.A., Nukleonik 7 (1965) 408.
[80] SINCLAIR, R.N., Inelastic Scattering of Neutrons in Solids and Liquids, II IAEA, Vienna (1963) 199.
[81] YOUNG, J.A., KOPPEL, J.U., Phys. Rev. 134 (1964) 1476.
[82] SCHMUNK, R.E., BRUGGER, R.M., RANDOLPH, P.D., STRONG, K.A., Phys. Rev. 128 (1962) 562.

DISCUSSION

J.M. CARPENTER: May I express a few thoughts on the presentation of scattering law values as a function of α and β. As Dr. Gläser has mentioned, this method of presentation is primarily advantageous in the case of the perfect monatomic gas. Otherwise, the scaling of energy transfer to the sample temperature obscures the actual frequencies. Similarly, presentation in terms of α obscures the dependence of the coherent scattering on interatomic distances, while also forcing the choice of a scatterer mass.

W. GLÄSER: In principle, I agree with you. However, I do not believe it is of major significance whether you measure these quantities in the one set of units or in the other. You just have to become familiar with the different units and it seems that this is not very difficult. Of course, in using the relative units the generalized frequency distribution becomes temperature-dependent.

D. T. GOLDMAN: I should like to add that at the Brookhaven Conference Brugger presented experimental data plotted as $S(K^2, \omega)$, which seems very reasonable.

Another point perhaps worthy of mention is that one quantity which is easily obtainable from a variety of measurements or models is the effective temperature T. Since neutron thermalization is sensitive to large energy transfers it depends strongly on this quantity, which is therefore a rapidly derivable number for each moderator and can be used directly in reactor design calculations.

M. S. NELKIN (Chairman): From the water data given, it would appear that combining the Young-Koppel anisotropy correction in H_2O with a good choice of p (β) will impair the present good agreement of theory and experiment for $\bar{\mu}$(E).

CALCULATIONS OF THE THERMAL SCATTERING LAW FOR SOLIDS AND LIQUIDS

R. G. JARVIS
ATOMIC ENERGY OF CANADA LIMITED,
CHALK RIVER, ONTARIO,
CANADA

Abstract

CALCULATIONS OF THE THERMAL SCATTERING LAW FOR SOLIDS AND LIQUIDS. A method has been developed, based on the incoherent approximation, to describe scattering in solids and liquids. It deals with molecules which are made up of one or more types of scatterer, such as UO_2 and D_2O.

For each scatterer there is a scattering law

$$S(\alpha,\beta) = \frac{1}{2\pi}\int_{-\infty}^{\infty} \exp(-\alpha w(t))\exp(i\beta t)dt$$

in Egelstaff's notation. The width function w(t) corresponds to a 'generalized frequency distribution' $\rho(\beta)$ which, in its most complicated form, has five components. The first and second describe sharp peaks (such as the two main vibration levels in D_2O), the third and fourth represent broader peaks (such as the combined effects of minor vibration levels and the rotations and translations), the fifth is for diffusion and is omitted for solids.

The integral for S is expanded over the vibration terms and then evaluated by a combination of numerical methods and saddle-point integrations. Finally, the S's for the scatterers are combined to give an S for the molecule.

1. INTRODUCTION

This paper discusses two models, to represent the incoherent scattering of neutrons by liquids and solids respectively. They have been developed at Chalk River over a period of a few years to fit to scattering experiments with liquids such as light water and heavy water and solids such as uranium dioxide and zirconium hydride. The models are employed in two computer programs, LIK and SOL, for the CDC G-20 computer, written in APEX (an algebraic language similar to ALGOL).

2. GENERAL THEORY

For neutron scattering by a single scattering species the double-differential cross-section can be written [1], using Egelstaff's notation [2],

$$\frac{\partial^2\sigma}{\partial\Omega\partial E} = \frac{\sigma_b}{4\pi kT}\left(\frac{E}{E_o}\right)^{\frac{1}{2}} \exp\left(-\frac{\beta}{2}\right) S(\alpha,\beta) \qquad 2.1$$

E_o and E are the initial and final neutron energies for scattering into an element of solid angle $d\Omega$, through an angle θ. T is the temperature of the system and k is Boltzmann's constant. $S(\alpha,\beta)$ is the 'scattering law' for the particular

scatterer in terms of the dimensionless variables α and β where

$$\alpha = [E_o + E - 2(E_oE)^{\frac{1}{2}} \cos\theta]/AkT, \quad \beta = (E - E_o)/kT \qquad 2.2$$

Finally, σ_b the 'bound' cross-section is related to σ_f the 'free' cross-section by $\sigma_b = (1 + 1/A)^2 \sigma_f$, where A is the mass of the scatterer in units of neutron mass.

In what follows, the scattering is supposed to be incoherent. The time transform of $S(\alpha,\beta)$ is the intermediate scattering function $I(\alpha,t)$, defined by

$$S(\alpha,\beta) = \frac{1}{2\pi} \int_{-\infty}^{\infty} I(\alpha,t) \exp(i\beta t)\, dt \qquad 2.3$$

where t is in units of $\hbar/kT$ and $I(\alpha,t)$ is a real, analytic, even function of t [3]. Corresponding to Placzek's moment theorems [4], $I(\alpha,t)$ has the properties

$$I(\alpha,i/2) = 1, \qquad \frac{\partial}{\partial t} I(\alpha,i/2) = i \qquad 2.4$$

Then, using Vineyard's 'gaussian' approximation [5], $I(\alpha,t)$ may be written

$$I(\alpha,t) = \exp[-\alpha w(t)] \qquad 2.5$$

where $w(t)$, the width function, is a real analytic even function of t.

Finally, the width function may be related to $\rho(\beta)$, the generalized frequency distribution function, by the integral [2],

$$w(t) = \int_0^{\infty} \rho(\beta) \frac{\cosh(\beta/2) - \cos\beta t}{\beta \sinh(\beta/2)}\, d\beta \qquad 2.6$$

It is the description of $\rho(\beta)$ by particular models which forms the basis for this paper, leading to calculations of $S(\alpha,\beta)$ by 2.3,

$$S(\alpha,\beta) = \frac{1}{2\pi} \int_{-\infty}^{\infty} \exp[-\alpha w(t)] \exp[i\beta t]\, dt \qquad 2.7$$

For a molecule, composed of several scatterers, the effective $S(\alpha,\beta)$ for a given β (i.e., a given $(E - E_o)$) may be

defined in several ways. The definition used in the following calculations is

$$S_{Mol}\ (\alpha_o,\beta) = \left(\sum_i W_i\ \sigma_{bi}\ S_i\ (\alpha_i,\beta)\right) \Big/ \left(\sum_i W_i\ \sigma_{bi}\right) \qquad 2.8$$

In this formula α_o is the α-value for a mass of 1, $\alpha_i = \alpha_o/A_i$ where A_i is the mass of the i-th scatterer, σ_{bi} is the i-th bound cross-section and W_i is the number of scatterers of the i-th type. The S_i are not unconnected because the corresponding $\rho_i(\beta)$ depend upon the dynamic behaviour of the particular scatterers in the molecule. This definition of S_{Mol} has the advantage that the α's are clearly defined and leads eventually to a convenient prescription for quantities such as energy-transfer cross-sections which depend upon integrals of S.

3. A MODEL FOR LIQUIDS

The following model was designed to describe incoherent scattering in light water and heavy water but it is quite flexible and it could be used for other liquids. For each scatterer, the generalized frequency distribution $\rho(\beta)$ contains two components for sharp peaks (such as the major vibration levels in H_2O and D_2O), two components for broad peaks (such as the combined effects of minor vibrations, rotations and translations) and one component for diffusion

$$\rho(\beta) = A_{d1}\ \delta(\beta-\beta_1) + A_{d2}\ \delta(\beta-\beta_2)$$

$$+ A_{g_1}\ 2\beta\ \sinh\left(\frac{\beta}{2}\right)\ \exp\left(\frac{-\beta^2}{\beta_{g_1}^2}\right) + A_{g_2}\ 2\beta\ \sinh\left(\frac{\beta}{2}\right)\ \exp\left(\frac{-\beta^2}{\beta_{g_2}^2}\right)$$

$$+ \frac{4d}{\pi}\ (c^2 + \tfrac{1}{4})^{\frac{1}{2}}\ \sinh(\beta/2)\ K_1\left[(c^2 + \tfrac{1}{4})^{\frac{1}{2}}\ \beta\right] \qquad 3.1$$

The components are written in the same order, 2 sharp peaks (delta functions), 2 broad peaks (based on gaussians) and the diffusion term (a modified Bessel function of the second kind). The areas of the delta functions are A_{d1} and A_{d2} and the area of the diffusion term is d/c. If A_{gs_1} and A_{gs_2} are the areas of the broad peaks then

$$A_{g_1} = A_{gs_1}\ \frac{4\ \exp(-\beta_{g_1}^2/16)}{\sqrt{\pi}\ \beta_{g_1}^3}\ ,\ A_{g_2} = A_{gs_2}\ \frac{4\ \exp(-\beta_{g_2}^2/16)}{\sqrt{\pi}\ \beta_{g_2}^3} \qquad 3.2$$

The shape of the diffusion term was suggested by Egelstaff [2]. The first Placzek moment theorem results in the constraint that the sum of the areas is unity, that is $\int_0^\infty \rho(\beta)\ d\beta = 1$.

The distribution $\rho(\beta)$ is related to $p(\beta)$, the other commonly used distribution, by [2],

$$(\beta/2)\ \rho(\beta) = \sinh(\beta/2)\ p(\beta) \qquad 3.3$$

Carrying out the integration for w(t), 2.6 leads to

$$w(t) = \lambda - \Big[M_{g_1} \exp(-t^2\beta_{g_1}^2/4) + M_{g_2} \exp(-t^2\beta_{g_2}^2/4)$$

$$+ N_1 \cos(\beta_1 t) + N_2 \cos(\beta_2 t) + 2d\left(c-(c^2 + t^2 + \tfrac{1}{4})^{\frac{1}{2}}\right)\Big] \qquad 3.4$$

where

$$M_{g_1} = A_{g_1}\sqrt{\pi}\ \beta_{g_1}, \qquad M_{g_2} = A_{g_2}\sqrt{\pi}\ \beta_{g_2}$$

and

$$N_1 = A_1/[\beta_1 \sinh(\beta_1/2)], \quad N_2 = A_2/[\beta_2 \sinh(\beta_2/2)] \qquad 3.5$$

λ, the Debye - Waller factor, is the sum of the constant terms in w(t), with the exception of the diffusion component.

$$\lambda = M_{g_1} \exp(\beta_{g_1}^2/16) + M_{g_2} \exp(\beta_{g_2}^2/16)$$

$$+ N_1 \cosh(\beta_1/2) + N_2 \cosh(\beta_2/2) \qquad 3.6$$

4. THE CALCULATION OF S FOR A LIQUID

$S(\alpha,\beta)$ is obtained for each scatterer from 2.3, using 2.5 to give

$$S(\alpha,\beta) = \frac{1}{2\pi}\int_{-\infty}^{\infty} \exp[-\alpha w(t)]\ \exp(i\beta t)\ dt \qquad 4.1$$

and writing out w(t) more explicitly this becomes

$$s(\alpha,\beta) = \frac{e^{-\alpha\lambda}}{\pi}\int_0^{\infty} e^{\alpha[g_1(t)+g_2(t)+u_1(t) + u_2(t) - f(t)]}\cos(\beta t)\ dt \qquad 4.2$$

$$g_1(t) = M_{g_1} \exp(-t^2\beta_{g_1}{}^2/4), \quad u_1(t) = N_1 \cos(\beta_1 t)$$

$$f(t) = 2d\,[(c^2 + t^2 + \tfrac{1}{4})^{\frac{1}{2}} - c] \quad \text{etc.} \qquad 4.3$$

In general the envelope of this Fourier transform falls fairly steeply for small values of t (the $g_1(t)$ and $g_2(t)$ terms in the exponent) and then takes on a much slower asymptotic fall (the f(t) in the exponent). For typical H_2O and D_2O cases the $u_1(t)$ and $u_2(t)$ terms are very small (N_1 and N_2 of order 10^{-3} or less) but they have a strong influence on the transform for β-values near to sums and differences of integral multiples of β_1 and β_2.

The integral of 4.2 may be expanded over the vibration terms u_1 and u_2 to yield,

$$S(\alpha,\beta) = \frac{e^{-\alpha\lambda}}{\pi} \sum_s \sum_n C_s\left(\frac{\alpha N_1}{2}\right) C_n\left(\frac{\alpha N_2}{2}\right) \int_0^\infty e^{\alpha[g_1(t)+g_2(t)-f(t)]} \cos(\gamma t)dt \qquad 4.4$$

where $\gamma = \beta + s\beta_1 + n\beta_2$, with s and n taking all integer values. The coefficients C_s and C_n are series of powers of $(\alpha N_1/2)$ and $(\alpha N_2/2)$ respectively, convergent for all α, N_1 and N_2. For example, for the s series,

$$C_s\ (\alpha N_1/2) = C_{-s}(\alpha N_1/2)$$

where

$$C_s\left(\frac{\alpha N_1}{2}\right) = \sum_{r=0}^{\infty} \frac{(\alpha N_1/2)^{2r+s}}{(s+r)!\,r!} \quad \text{for positive s,} \qquad 4.5$$

The asymptotic behaviour is isolated by writing the kernel of 4.4 as

$$e^{\alpha[g_1(t) + g_2(t) - f(t)]} = \left[e^{\alpha[g_1(t) + g_2(t)]} - 1\right] e^{-\alpha f(t)} + e^{-\alpha f(t)} \qquad 4.6$$

and the integrals which result are then $S = S_o + S_{as}$, in the same order. S_{as}, the asymptotic integral, may be evaluated explicitly and the corresponding terms in the (s,n) expansion are

$$\frac{e^{-\alpha\lambda}}{\pi}\ e^{\alpha 2dc}\ \frac{2\alpha d(c^2 + \frac{1}{4})^{\frac{1}{2}}}{((2\alpha d)^2 + \gamma^2)^{\frac{1}{2}}}\ K_1\left[(c^2 + \tfrac{1}{4})^{\frac{1}{2}}\ \ (2\alpha d)^2 + \gamma^2)^{\frac{1}{2}}\right] \qquad 4.7$$

For small γ, S_o is integrated numerically by Filon's method [6] (parabolic fits to small segments of the envelope). For large γ, S_o is computed by contour integration in the complex plane, over a saddle-point on the imaginary axis. The explicit form of w(t) is of great help in the saddle-point integration.

Without 'insight', or a directed form of search, the double summation of 4.4 can be very time-consuming. In the two computer programs LIK and SOL a systematic search is made for the region in (s,n) space containing the significant contributions. Apart from the C-coefficients, the largest components of the transform correspond to integer values of s and n which lie near to the straight line $\gamma = \beta + s\beta_1 + n\beta_2 = 0$, forming a 'ridge'. The effect of the C-coefficients is to move the ridge towards or away from the (s,n) origin. The programs search in the direction roughly perpendicular to the line $\gamma = 0$ until a point on the ridge is found and then the effective length of the ridge is mapped and integrals are taken for (s,n) points on contours on both sides of the ridge, until convergence is attained.

5. A MODEL FOR SOLIDS

The model for solids has the same form of $\rho(\beta)$ as the above liquid model except that the diffusion terms are omitted. Again, incoherent scattering is assumed.

6. THE CALCULATION OF S FOR A SOLID

S is obtained as an expansion in the vibration terms, as above,

$$S(\alpha,\beta) = \frac{e^{-\alpha\lambda}}{\pi} \sum_s \sum_n C_s\left(\frac{\alpha N_1}{2}\right) C_n\left(\frac{\alpha N_2}{2}\right) \int_0^\infty e^{\alpha[g_1(t)+g_2(t)]} \cos(\gamma t)dt \qquad 6.1$$

To separate the asymptotic behaviour, write,

$$e^{\alpha[g_1(t) + g_2(t)]} = \left[e^{\alpha[g_1(t) + g_2(t)]} - 1\right] + 1 \qquad 6.2$$

The first integral is computed by Filon's method or by saddle-point, according to the size of γ. The asymptotic integral is now a delta function $\delta(\gamma)$ leading to the spectrum of delta functions

$$S_{as} = \frac{e^{-\alpha\lambda}}{\pi} \sum_s \sum_n C_s\left(\frac{\alpha N_1}{2}\right) C_n\left(\frac{\alpha N_2}{2}\right) \delta(\beta + s\beta_1 + n\beta_2) \qquad 6.3$$

To make use of this it is necessary to consider the integral of S over a finite range of β and in practice this could correspond to a finite experimental resolution in energy. The contributions from the appropriate delta functions can then be included.

7. CONCLUSION

The LIK and SOL programs are being used to calculate S values to compare with the results of the Scattering Law

Experiment at Chalk River [7]. They are also used in Thorson's corrections for multiple scattering in the experimental data [8].

Fig. 1 shows $\rho(\beta)$ distributions for the H and O components of the H_2O molecule, for typical values of the parameters. The total area of each distribution is unity.

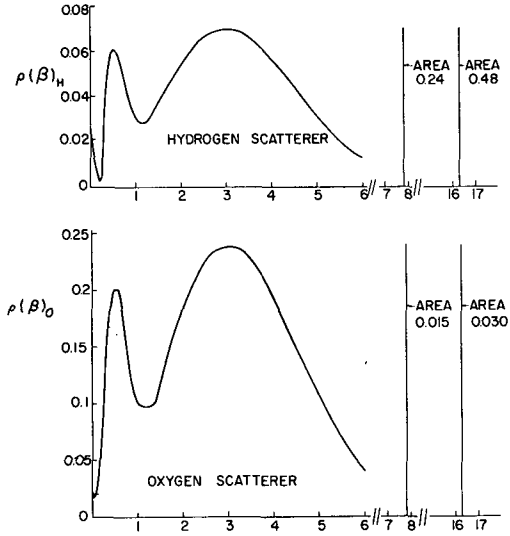

FIG. 1. $\rho(\beta)$ for H and O in H_2O.

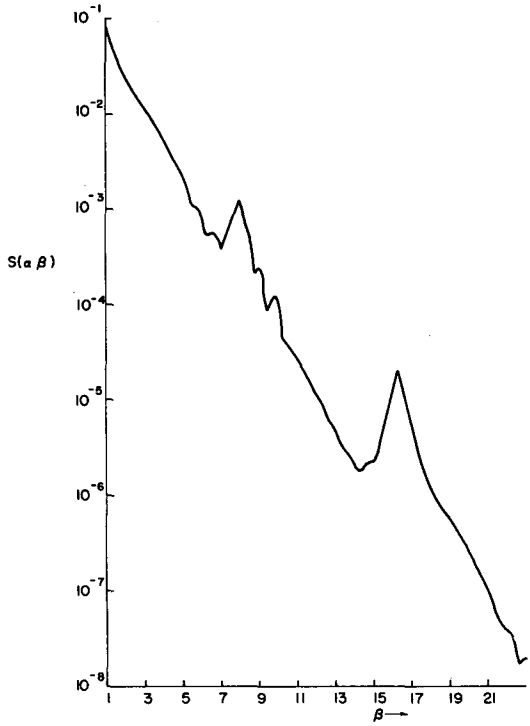

FIG. 2. $S(\alpha,\beta)$ for H_2O for $\alpha = 4$.

Fig. 2 and Fig. 3 are plots of $S(\alpha,\beta)$ vs. β for a given α value, for the H_2O molecule using the same typical parameters. The peaks corresponding to the vibration terms at $\beta_1 = 7.9$ and $\beta_2 = 16.3$ are very clear and nearby structure from multi-phonon terms can also be seen in Fig. 2.

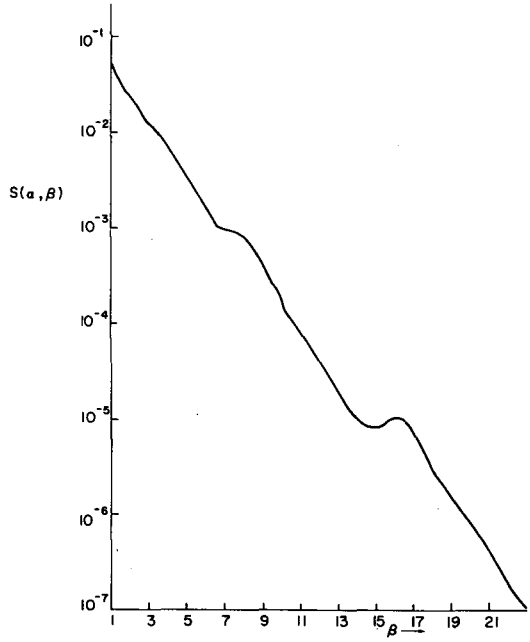

FIG. 3. $S(\alpha,\beta)$ for H_2O for $\alpha = 10$.

The two models, for liquid and solid, which have been described above, form the basis for a series of computer programs to calculate other moderator properties such as energy-transfer cross-sections, energy-moments and transport cross-sections.

The chosen form for $\rho(\beta)$ should be flexible enough to represent the significant properties of some important moderators. The fact that it leads to an explicit form for $w(t)$ is of great help in the integrations for S and particularly in the saddle point integrations needed for large β.

ACKNOWLEDGEMENTS

I am very grateful to P.A. Egelstaff, G.E. Lee Whiting, I.M. Thorson and G.W. Bluman for helpful discussions, and to R.M. Dunbar for a good deal of assistance with the computing.

REFERENCES

[1] VAN HOVE, L., Phys. Rev. 95 (1954) 249.

[2] EGELSTAFF, P.A., SCHOFIELD, P., Nuc. Sci. Engng 12 (1962) 39.

[3] SCHOFIELD, P., Inelastic Scattering of Neutrons in Solids and Liquids, IAEA, Vienna (1960) 39.

[4] PLACZEK, G., Phys. Rev. 86 (1952) 377.

[5] VINEYARD, G.H., Phys. Rev. 110 (1958) 999.

[6] FILON, L.N.G., Proc. Roy. Soc. Edinburgh XLIX (1928) 38.

[7] THORSON, I.M., JARVIS, R.G., to be published.

[8] THORSON, I.M., Paper SM-96/21, these Proceedings I.

DISCUSSION

S. N. PUROHIT: Your remarks concerning the determination of weights of different modes are interesting. However, in the case of D_2O coherent effects are present for small momentum and energy transfers. The presence of these effects will complicate your determination of the parameters for the Egelstaff width model, used in the description of diffusive modes.

R. G. JARVIS: I agree that such a determination would be difficult. We have estimated the diffusion parameters quite differently, by arguments based on properties such as thermal diffusion, viscosity, etc. I believe that the coherent effects in D_2O occur for momentum and energy transfers that are relatively unimportant for reactor spectrum calculations. Butler's calculations for the D_2O molecule lend support to this belief.

J. A. YOUNG: The extensive calculations which we have made on thermal neutron scattering from D_2O show that there is a fortunate cancellation of inter-molecular and intra-molecular effects which considerably reduces the importance of coherent scattering for D_2O, especially for spectral calculations.

ANALYTICAL EVALUATION OF THE LARGE TIME CONTRIBUTION TO NEUTRON SCATTERING CROSS-SECTIONS*

A. G. GIBBS AND C. W. LINDENMEIER
BATTELLE MEMORIAL INSTITUTE,
PACIFIC NORTHWEST LABORATORY,
RICHLAND, WASHINGTON,
UNITED STATES OF AMERICA

Abstract

ANALYTICAL EVALUATION OF THE LARGE TIME CONTRIBUTION TO NEUTRON SCATTERING CROSS-SECTIONS. In the incoherent Gaussian approximation, the differential cross-section for scattering of slow neutrons is evaluated from a time-dependent width function w(t). The behaviour of w(t) for large t determines the form of the quasi-elastic peak, and when the cross-section is evaluated as a numerical Fourier transform its contribution is slowly convergent. Since w(t) often approaches a simple analytical form at large t, the large time contribution may be evaluated directly, thus giving an analytical expression for the quasi-elastic peak and eliminating the slowly convergent part of the Fourier transform. This approach is used in a numerical code being developed at Battelle-Northwest. The experimental spectral function is fit by simple analytical expressions for which w(t) can be evaluated analytically. In the integral representation of $\sigma_s(E_0 \rightarrow E)$ as a cosine transform the values of the integrand with w(t) replaced by its asymptotic form are subtracted out and evaluated analytically. The difference is evaluated numerically by integrating over successive half-cycles of the cosine and summing the resulting series with a Euler transform.

The analytical contribution to $\sigma_s(E_0 \rightarrow E)$ can itself be integrated over final energies to obtain an analytical expression for the quasi-elastic contribution to $\sigma_s(E_0)$. The remaining slowly varying contribution can be evaluated with only a few energy points and the calculated $\sigma_s(E_0)$ can be used as a check on the parameters of the model.

Numerical results are given for a model of water in which it is assumed that $w(t) \sim Jt^2 + K/4$ for large t. The analytical contributions are then generalizations of the ideal gas results, and the numerical contribution converges rapidly.

At present the code accepts only the above asymptotic form for w(t), but it appears that the inclusion of a more realistic option width, $w(t) \sim 2Dt + L$, will present no difficulties.

I. INTRODUCTION

The computation of the Legendre moments of the scattering cross-section can be carried out in two ways: the scattering law $S(\alpha, \beta)$ may be calculated first and the moments of the cross-section obtained by integrating $S(\alpha, \beta)$ over angles or, as considered herein, the integral representation of $S(\alpha, \beta)$ may itself be integrated over angles, thus providing a representation of the moments of the cross-section as cosine transforms. The latter approach is particularly advantageous if the moments are required at only a few energy points since the necessity of evaluating $S(\alpha, \beta)$ at a much greater number of points is eliminated. While the cosine transform approach has also been considered by Turchin

* This paper is based on work performed under the United States Atomic Energy Commission Contract AT (45-1) 1830.

[1] and by Hutchinson and Schofield [2], the approach that we describe here differs from past treatments both in the method of evaluating the cosine transform and in the addition of a special treatment of the large time contribution.

II. BASIC THEORY

In the incoherent Gaussian approximation, the differential scattering cross-section is given by [3]

$$\sigma_s(E_0 \to E; \mu) = \frac{\sigma_b}{2kT} \left(\frac{E}{E_0}\right)^{\frac{1}{2}} e^{-\beta/2} S(\alpha, \beta) \tag{1}$$

where E_0 and E are the initial and final neutron energies, σ_b is the bound atom cross-section, μ is the cosine of the laboratory scattering angle and $S(\alpha, \beta)$ is the scattering law, which is a function of the variables

$$\alpha = \frac{E_0 + E - 2\mu\sqrt{EE_0}}{AkT} \tag{2}$$

and

$$\beta = \frac{E - E_0}{kT} \tag{3}$$

Here A is the atomic mass and T the temperature. As is well-known, $S(\alpha, \beta)$ can be expressed in terms of a function w(t) related to the time-dependent mean-square displacement of the scattering atom

$$S(\alpha, \beta) = \frac{1}{\pi} \int_0^\infty e^{-\alpha w(t)} \cos \beta t \, dt \tag{4}$$

The function w(t) is itself related to a spectral function $\rho(\beta)$

$$w(t) = \int_0^\infty \rho(\beta) \frac{[\cosh(\beta/2) - \cos \beta t]}{\beta \sinh(\beta/2)} d\beta \tag{5}$$

The function $\rho(\beta)$ can be obtained from model calculations or from experiment.

Reactor analysis generally employs the Legendre moments of the cross-section

$$\sigma_n(E_0 \to E) = \int_{-1}^{1} P_n(\mu) \, \sigma_s(E_0 \to E; \mu) \, d\mu \tag{6}$$

Since the μ-dependence of $S(\alpha, \beta)$ occurs only through α, which is linear in μ, the integration over μ in Eq. (6) can be carried out analytically by interchanging the order of the μ and t integrations. By defining

$$\alpha = B - C\mu \tag{7}$$

where

$$B(E, E_0) = \frac{E_0 + E}{AkT} \tag{8}$$

and

$$C(E_0, E) = \frac{2\sqrt{EE_0}}{AkT} \tag{9}$$

we obtain

$$\sigma_n(E_0 \to E) = \frac{\sigma_b}{\pi kT} \left(\frac{E}{E_0}\right)^{\frac{1}{2}} e^{-\beta/2} \times \int_0^\infty \cos \beta t \, e^{-Bw(t)} \, i_n(Cw(t))dt \tag{10}$$

Here $i_n(x)$ is the modified spherical Bessel function of the first kind [4]; that is,

$$i_n(x) = \left(\frac{\pi}{2x}\right)^{\frac{1}{2}} I_{n+\frac{1}{2}}(x) = \frac{1}{2} \int_{-1}^{1} P_n(\mu) \, e^{x\mu} \, d\mu \tag{11}$$

In particular,

$$\left.\begin{aligned} i_0(x) &= \frac{\sinh x}{x} \\ \text{and} \quad i_1(x) &= \frac{1}{x}\left(\cosh x - \frac{\sinh x}{x}\right) \\ \text{while} \quad i_{n+1}(x) &= i_{n-1}(x) - \frac{(2n+1)}{x} i_n(x) \qquad (n \geq 1) \end{aligned}\right\} \tag{12}$$

III. REPRESENTATION OF THE WIDTH FUNCTION

The width function w(t) can be obtained in two different ways. If experimental values of $\rho(\beta)$ are available at closely spaced points, the integral in Eq. (5) can be evaluated numerically for many values of t and w(t) can then be obtained by interpolating in the resulting table. An alternative approach has been suggested by Lindenmeier [5] and also by Hutchinson and Schofield [2]: the experimental $\rho(\beta)$ is fit by a sum of simple analytical functions for which the integral in Eq. (5) can be evaluated in closed

form; this provides an analytical expression for w(t). When $\rho(\beta)$ exhibits rather simple structure, the latter method will be preferred since it eliminates the computation time and inaccuracies of the numerical integration and interpolation and provides a means of generating $\rho(\beta)$ at different temperatures by interpolating on the fitting parameters.

As proposed in [5], we represent $\rho(\beta)$ as

$$\rho(\beta) = J\,\delta(\beta) + \sum_{i=1}^{N} \alpha_i\, \rho_i(\beta) \tag{13}$$

where

$$\rho_i(\beta) = N_i\, \beta \sinh(\beta/2) \left[e^{-\frac{(\beta-\gamma_i)^2}{4\delta_i}} + e^{-\frac{(\beta+\gamma_i)^2}{4\delta_i}} \right] \tag{14}$$

Here γ_i, δ_i, and the weights J and α_i are adjustable parameters and N_i are normalizing coefficients such that

$$\int_0^\infty \rho_i(\beta)\, d\beta = 1 \tag{15}$$

Since $\rho(\beta)$ is also normalized to unity the weights $\alpha_1 \ldots \alpha_n$ and J satisfy the constraint

$$J + \sum_{i=1}^{N} \alpha_i = 1 \tag{16}$$

Each function $\rho_i(\beta)$ has a resonance-like peak lying near $\beta_i = \gamma_i + \delta_i$ with a width of approximately $2\sqrt{\delta_i}$. As γ_i approaches zero or δ_i, respectively, $\rho_i(\beta)$ approaches the 'oscillator' or the 'Gaussian' form suggested by Hutchinson and Schofield [2]. The term $J\,\delta(\beta)$ in Eq.(13) arises from an approximate representation of the translational motion as a free translation with an effective mass of 1/J amu. In a gas or liquid, J will generally be less than the reciprocal atomic mass, and for a solid J is zero.

By substituting the assumed form for $\rho(\beta)$ into Eq.(5) we find that

$$w(t) = J(t^2 + \tfrac{1}{4}) + \sum_{i=1}^{N} \alpha_i \left[A_i - B_i\, e^{-\delta_i t^2} \cos \gamma_i t\right] \tag{17}$$

where A_i and B_i are known functions of γ_i and δ_i [5]. We note that for large t

$$w(t) \sim J t^2 + K/4 \tag{18}$$

where

$$K = J + \sum_{i=1}^{N} \alpha_i A_i \tag{19}$$

For $J = K = 1$ the asymptotic form of $w(t)$ is the same as for an ideal gas; however, in general J and K will differ substantially from unity. A more realistic treatment of the translational motion, such as that proposed by Egelstaff and Schofield [3], would lead to the alternate result at large t of

$$w(t) \sim 2Dt + L \tag{20}$$

IV. CALCULATION OF THE COSINE TRANSFORM

While $w(t)$ can either be obtained numerically or represented analytically, the computation of $\sigma_n(E_0 \to E)$ must generally be carried out by evaluating the cosine transform in Eq.(10) numerically. Even though the factor $e^{-Bw} i_n(cw)$ in the integrand of this equation approaches zero at large t, the integration may have to be extended over many cycles of the cosine before convergence is obtained. This is particularly true if β is large. To minimize the loss of significant figures due to near-cancellation of contributions from successive half-cycles of the cosine, we evaluate $\sigma_n(E_0 \to E)$ by first rewriting Eq.(10) as

$$\sigma_n(E_0 \to E) = \frac{\sigma_b}{\pi kT} \left(\frac{E}{E_0}\right)^{\frac{1}{2}} e^{-\beta/2} \sum_{j=0}^{\infty} g_j \tag{21}$$

where

$$g_j = \frac{1}{|\beta|} \int_{(j-\frac{1}{2})\pi}^{(j+\frac{1}{2})\pi} \cos\tau \; e^{-Bw\left(\frac{\tau}{|\beta|}\right)} i_n\left(Cw\left(\frac{\tau}{|\beta|}\right)\right) d\tau \tag{22}$$

(for $j = 0$ the lower limit is replaced by zero)

The terms g_j are evaluated by Simpson's rule, with successive refinement of the partition until some specified precision is obtained. The problem of evaluating the (perhaps) slowly convergent semi-infinite integral in Eq.(10) is thus reduced to one of summing the (perhaps) slowly convergent alternating series in Eq.(21). A particularly useful technique for summing such a series is provided by the Euler-Van Wijngaarden transformation [6], which can be written as

$$\sum_{j=0}^{\infty} g_j = g_0 + g_1 + \ldots + g_{n-1} + \tfrac{1}{2} \sum_{j=0}^{\infty} M^j g_n \tag{23}$$

TABLE I. VALUES OF $\sigma_0(E_0 \rightarrow E)$ AND $\sigma_1(E_0 \rightarrow E)$ FOR IDEAL GAS, A = 1, T = 300 °K
(Energies - eV; σ_0 and σ_1 - units of free atom cross-section)

E_0 \ E	0.001		0.01		0.1		1.0	
0.001	217.3	73.56						
	219.1	74.54						
0.01	21.91	2.357	61.92	24.63				
	21.91	2.357	62.09	24.80				
0.1	2.191	7.454×10^{-2}	6.209	0.7844	9.928	7.477		
	2.191	7.454×10^{-2}	6.209	0.7844	9.945	7.495		
1.0	0.2191	2.359×10^{-3}	0.6208	2.475×10^{-2}	0.9942	0.2362	0.9982	0.9724
	0.2191	2.357×10^{-3}	0.6209	2.480×10^{-2}	0.9945	0.2370	1.000	0.9742

σ_0-TISC	σ_1-TISC
σ_0	σ_1

where M is the forward mean operator defined by $M\, g_i' = \frac{1}{2}(g_i + g_{i+1})$. The algorithm (23) is equivalent to direct summation of the first n terms of the series followed by Euler transformation of the rest. The essence of the Euler transformation is the observation that when an alternating series is slowly convergent, the series composed of the averages of successive terms often converges much faster.

The technique outlined here for evaluating the integral in Eq.(10) has been used with success by Ekstrom [7] in a computer programme for evaluating general sine and cosine transforms. Since the Euler transform technique explicitly recognizes the problem of large cancellations, and is designed to minimize their effect, its use permits accurate evaluation of the transform in Eq.(10) for larger values of β than can be tolerated if the integral is evaluated by Filon's method [2] or similar methods which make no special provision to deal with cancellations.

Since the point $\beta = 0$ appears as a singularity of the integrals of Eq.(22) the Euler transform cannot be used for this point. However, since no cancellation problems arise for $\beta = 0$, the integral in Eq.(10) can then be evaluated numerically in a straightforward manner.

To demonstrate the accuracy of the Euler transform method we have evaluated $\sigma_0(E_0 \to E)$ and $\sigma_1(E_0 \to E)$ for an ideal gas of mass 1, using both Eq.(10) and the well-known analytical expressions for these quantities. The results are shown in Table I. In each box, the left-hand pair of numbers is σ_0 and the right-hand pair σ_1. The top pair was calculated by the Euler transform method (Programme TISC) and the bottom pair from the analytical expressions. The agreement is encouraging for both σ_0 and σ_1.

As an additional check, we have evaluated $\sigma_0(E_0 \to E)$ for Nelkin water using both Eq.(10) and the GAKER code. The results are shown in Table II, and good agreement is obtained, except for the elastic term at high energies, where Hutchinson and Schofield [2] have observed the same discrepancy.

V. THE LARGE TIME CONTRIBUTION

(a) The differential cross-sections $\sigma_n(E_0 \to E)$

When $\sigma_n(E_0 \to E)$ is calculated near the quasi-elastic peak (small β) the values of w(t) at large t contribute significantly to the integral in Eq.(10). As noted above, w(t) usually has a particularly simple asymptotic form at large t, and for small β it is advantageous to exploit this fact to evaluate the large time contribution to $\sigma_n(E_0 \to E)$ analytically.

Let $w_\infty(t)$ denote the asymptotic form of w(t) at large t (e.g. $w_\infty(t) = J\, t^2 + K/4$ for a gas-like translational mode). Then for small β we rewrite Eq.(10) as

$$\sigma_n(E_0 \to E) = \sigma_n^{(t)}(E_0 \to E) + \sigma_n^{(\infty)}(E_0 \to E) \tag{24}$$

TABLE II. VALUES OF $\sigma_0(E_0 \to E)$ FOR HYDROGEN IN NELKIN WATER, T = 293°K

(Energies – eV; σ_0 – units of free atom cross-section)

E_0 \ E	0.001	0.01	0.1	1.0
0.001	915.6 833.7			
0.01	23.66 23.57	261.2 259.2		
0.1	0.7019 0.6995	3.339 3.331	42.03 33.62	
1.0	0.0998 0.1009	0.3143 0.3137	0.8109 0.8273	4.266 1.220

TISC

GAKER

where

$$\sigma_n^{(t)}(E_0 \to E) = \frac{\sigma_b}{\pi kT}\left(\frac{E}{E_0}\right)^{\frac{1}{2}} e^{-\beta/2}$$

$$\times \int_0^\infty \cos\beta t \left\{ e^{-Bw(t)}\, i_n(Cw(t)) - e^{-Bw_\infty(t)}\, i_n(Cw_\infty(t)) \right\} dt \qquad (25)$$

and

$$\sigma_n^{(\infty)}(E_0 \to E) = \frac{\sigma_b}{\pi kT}\left(\frac{E}{E_0}\right)^{\frac{1}{2}} e^{-\beta/2}$$

$$\times \int_0^\infty \cos\beta t\; e^{-Bw_\infty(t)}\, i_n(Cw_\infty(t))\, dt \qquad (26)$$

This decomposition exhibits $\sigma_n(E_0 \to E)$ as the sum of a contribution $\sigma_n^{(t)}(E_0 \to E)$ due to the transient part of w(t) and a contribution $\sigma_n^{(\infty)}(E_0 \to E)$ due to the asymptotic part of w(t). It is often possible to evaluate $\sigma_n^{(\infty)}(E_0 \to E)$ analytically. For example, with $w_\infty(t) = J\,t^{1/2} + K/4$ the integral in Eq.(26) is easily evaluated (see e.g. [8]) and for n = 0 we obtain

$$\sigma_0^{(\infty)}(E_0 \to E) = \frac{\sigma_b}{\sqrt{JK}}\,\frac{A}{8E_0}\left\{ e^{-\left(1-\sqrt{\frac{K}{J}}\right)\frac{\beta}{2}}\left[\operatorname{erf}\left(\frac{\sqrt{K(B+C)}}{2} + \frac{\beta}{2\sqrt{J(B+C)}}\right)\right.\right.$$

$$\left. -\operatorname{erf}\left(\frac{\sqrt{K(B-C)}}{2} + \frac{\beta}{2\sqrt{J(B-C)}}\right)\right] + e^{-\left(1+\sqrt{\frac{K}{J}}\right)\frac{\beta}{2}}\left[\operatorname{erf}\left(\frac{\sqrt{K(B+C)}}{2} - \frac{\beta}{2\sqrt{J(B+C)}}\right)\right.$$

$$\left.\left. -\operatorname{erf}\left(\frac{\sqrt{K(B-C)}}{2} - \frac{\beta}{2\sqrt{J(B-C)}}\right)\right]\right\} \tag{27}$$

For J = K = 1, this result reduces to the well-known ideal gas cross-section. It is interesting to note that the single expression (27) holds both for $E_0 < E$ and $E_0 > E$ provided that the square roots are taken to be positive quantities, as is automatically done in machine computation. Expressions for $\sigma_n^{(\infty)}(E_0 \to E)$ with $n > 0$ can also be obtained for the gas-like translational model, and like the corresponding ideal gas results are all expressible in terms of error functions and simple exponentials.

For the more realistic asymptotic form $w_\infty(t) = 2\,D\,t + L$, similar results can be obtained, except that the $\sigma_n^{(\infty)}(E_0 \to E)$ are now expressible in terms of simple exponential functions and exponential integrals.

The moments can now be evaluated by adding the analytical value of $\sigma_n^{(\infty)}(E_0 \to E)$ to the integral in Eq.(25), which, when evaluated numerically by the methods of section IV, converges more rapidly for small values of β than the original integral of Eq.(10). In addition, the effects of round-off and cancellation errors are significantly reduced by treating the large time contribution separately.

(b) The integrated cross-sections $\sigma_n(E)$

In addition to the differential cross-sections $\sigma_n(E \to E')$, their integrals over final energy

$$\sigma_n(E) = \int_0^\infty \sigma_n(E \to E')\,dE' \tag{28}$$

are also required in reactor analysis and design. Two different situations arise:

(1) For hydrogenous materials, in which coherent scattering effects are slight, the $\sigma_n(E)$ can be compared to experimental data as an additional check on the parameters used to fit $\rho(\beta)$. Indeed, the parameters which describe $\rho(\beta)$ for very small β (e.g. J and D in Eqs (18) and (20)) can

probably best be determined by fitting $\sigma_n(E)$ and the quasi-elastic peak of $\sigma_n(E \to E')$ rather than $\rho(\beta)$ itself, since it is difficult to obtain accurate experimental values of $\rho(\beta)$ at small β.

(2) For materials in which coherent scattering is significant, integration of Eqs (10) or (24) over final energy provides only the incoherent contribution to $\sigma_n(E)$. A direct calculation of the coherent contribution is seldom practical, and for reactor analysis purposes, it is usually assumed that the coherent contribution is purely elastic, the appropriate amount of elastic scattering being added to the incoherent contribution so that $\sigma_n(E)$ agrees with experiment. In this case no additional check is provided for the parameters of the model.

In either of the above cases it is necessary to integrate the $\sigma_n(E \to E')$, given by Eqs (10) or (24), over final energy. Since the inelastic part of $\sigma_n(E \to E')$ is relatively smooth and slowly varying, only a few energy points are required for its numerical integration. However, many energy points would be required to determine the contribution of the quasi-elastic peak to $\sigma_n(E)$. Since it is the large time contribution which gives rise to this peak, this numerical difficulty can be avoided if $\sigma_n^{(\infty)}(E \to E')$ can be integrated analytically. Thus, we represent $\sigma_n(E)$ as

$$\sigma_n(E) = \sigma_n^{(t)}(E) + \sigma_n^{(\infty)}(E) \tag{29}$$

a decomposition obtained by integrating Eq. (24) over final energy.

To date, we have obtained results for $\sigma_n^{(\infty)}$ only for the simple case $w_\infty(t) = Jt^2 = K/4$. For this case, Eq. (27) for $\sigma_0^{(\infty)}(E \to E')$ can be integrated over E' to give

$$\sigma_0^{(\infty)}(E) = \sigma_b \left(\frac{A'T'}{E_0}\right)\left[\left(\frac{K}{K-J}\right)\mathrm{erf}\left(\frac{A'E_0}{T'}\right)^{\frac{1}{2}}\right.$$

$$\left. - \left(\frac{A' + \sqrt{J/K}}{2\left(1-\frac{J}{K}\right)\sqrt{A'g}}\right) e^{-\left(\frac{K-J}{4Kg}\right)\frac{E_0}{T}} \quad \mathrm{erf}\left(\frac{A' + \sqrt{J/K}}{2\sqrt{g}}\left(\frac{E_0}{T}\right)^{\frac{1}{2}}\right)\right] \tag{30}$$

where

$$A' = A/\sqrt{JK}, \quad T' = T\sqrt{J/K}, \quad g = \left(\frac{A'}{4} + \frac{1}{4A'} + \frac{1}{2}\sqrt{\frac{J}{K}}\right)$$

The use of L'Hopital's rule shows that this expression reduces to the familiar ideal gas result when $J = K = 1$. Since no analytical expression is known for $\sigma_1(E)$ for the ideal gas, it is not surprising that we have been unable to obtain $\sigma_1^{(\infty)}(E)$ for the more general case $J \neq K \neq 1$. However, our preliminary results for water indicate that the appropriate J for a liquid is rather small, $J \sim 10^{-3}$. Thus, it should be adequate to obtain $\sigma_1^{(\infty)}(E)$ as a power series expansion in J. Taking the limit as

$J \to 0$ in Eq.(10) with w(t) replaced by $Jt^2+K/4$, we obtain

$$\sigma_1^{(\infty)}(E) = \left(\frac{AT}{KE_0}\right)\left[\left(1-\frac{2AT}{KE_0}\right)+\left(1+\frac{2AT}{KE_0}\right)e^{-\left(\frac{KE_0}{AT}\right)}\right]+O(J) \tag{31}$$

We have also obtained the coefficient of the first power of J in this expansion. Thus, for $w_\infty(t) = Jt^2+K/4$, both $\sigma_0^{(\infty)}$ (E) and $\sigma_1^{(\infty)}$ (E) can be obtained. At present, we have not attempted the calculations of total moments for $w_\infty(t) = 2Dt+L$.

VI. COMPUTATIONS

As an example, the results of a calculation of $\sigma_0(E_0 \to E)$ for hydrogen in water are shown in Table III. For this calculation, $\rho(\beta)$ was represented as a sum of four $\rho_i(\beta)$ plus the delta function at the origin. The

TABLE III. VALUES OF $\sigma_0(E_0 \to E)$ FOR FOUR-RESONANCE MODEL OF WATER, T = 293°K

(Energies – eV; σ_0 – units of free atom cross-section)

E_0 \ E	0.001	0.01	0.1	1.0
0.001	10 730			
0.01	7.170	2551		
0.1	1.193	4.047	308.2	
1.0	0.08780	0.2912	0.7960	30.91

Model Parameters: J = 1/2500

i	α_i	β_i	γ_i	δ_i
1	1/36	0.056	1.40×10^{-9}	0.056
2	2654/5625	2.58	1.59×10^{-9}	0.98
3	1/6	8.08	7.60×10^{-9}	0.48
4	1/3	19.1	19.0×10^{-9}	0.077

fitting parameters, which are indicated at the bottom of the table, are preliminary and should not be considered optimum. The computation time for the ten energy points shown was 25 s on the UNIVAC 1108. The values of $\sigma_s(E_0 \rightarrow E)$ in the table differ considerably from the corresponding values for Nelkin water, particularly at small β. These values also check with another code which calculates $\sigma_s(E_0 \rightarrow E)$ integrating $S(\alpha, \beta)$ over angles [9].

REFERENCES

[1] TURCHIN, V.F., Calculation of the differential cross-section of slow neutrons by time integration, Report No.6, USSR State Committee on the Uses of Atomic Energy, Physics and Power Institute (1965), (In Russian).

[2] HUTCHINSON, P., SCHOFIELD, P., Computation of scattering cross sections for use in thermal neutron transport calculations, Conference on the Application of Computing Methods to Reactor Problems, USAEC Rep. ANL 7050 (1965).

[3] EGELSTAFF, P.A., SCHOFIELD, P., Nucl. Sci. Engng 12 (1962) 260.

[4] ABRAMOWITZ, M., STEGUN, I.A., Handbook of Mathematical Functions, National Bureau of Standards, Wash. D.C. (1964).

[5] LINDENMEIER, C.W., Scattering law for water I, II, in USAEC Reps. HW-77311 (1963) and HW-79054 (1963).

[6] Modern Computing Methods, Notes on Applied Science No.16, N.P.L., Her Majesty's Stationery Office, London.

[7] EKSTROM, P.A., Program FTRANS-numerical Fourier transformation routine, USAEC Rep. HW-84151 (1964).

[8] ERDÉLYI, A. et al., Tables of Integral Transforms 1 McGraw-Hill Book Co., New York (1954).

[9] LINDENMEIER, C.W., Program SCATMOM, unpublished.

DISCUSSION

P.F. ZWEIFEL: I should like to point out that there is considerable literature on the subject of numerical quadrature of Fourier transform integrals. Over ten years ago Hurwitz and myself published a paper in the MTAC journal in which we used a Gauss quadrature technique, taking the weight function as the cosine factor and summing by the same technique which you described. Later, Varga published details of another technique, and during the past year I have seen a preprint of a paper from Los Alamos on the same subject.

M.S. NELKIN: IBM is now paying much attention to a new way of doing Fourier transforms with a great saving of computer time. The method is not so much concerned with the actual numerical integration; its main feature is the use of an algorism which greatly reduces the redundancy in computing the needed numbers.

G.J. KIROUAC: You refer to the term J as $1/M_{eff}$ for translations. For practical calculations for water, what value do you give to J?

A.G. GIBBS: We use a very small number, 1/2500, but this is only a tentative figure.

QUASI-CLASSICAL APPROXIMATION FOR SCATTERING FROM MOLECULES

G.C. SUMMERFIELD AND P.F. ZWEIFEL
UNIVERSITY OF MICHIGAN,
ANN ARBOR, MICHIGAN,
UNITED STATES OF AMERICA

Abstract

QUASI-CLASSICAL APPROXIMATION FOR SCATTERING FROM MOLECULES. In a previous paper, an expression for the scattering cross-section from a molecular substance has been derived. This expression is based upon the so-called quasi-classical approximation. The scattering law is expressed in the form

$$S(\underset{\sim}{K}, \omega) \sim \int dt e^{-i\omega t} \langle \exp\{f(\underset{\sim}{K}, t)\} \rangle_T$$

It is further shown that if $f(\underset{\sim}{K}, t)$ is expanded in a power series in t, and only linear terms retained, the Krieger-Nelkin result is obtained. Such an expansion is inconsistent, however, because the thermal average in the above equation introduces some terms quadratic in the time but other quadratic terms have been ignored when $f(\underset{\sim}{K}, t)$ was expanded. In the present work we expand the quantity $\langle \exp\{f(\underset{\sim}{K}, t)\} \rangle_T$ in a similar series, but retain all terms of order t^2. A closed form expression is then obtained for the incoherent portion of the cross-section, and comparisons are made with the Krieger-Nelkin result and with some exact computer studies of molecular cross-sections.

Also, we derive an expression that is highly accurate for smaller values of the momentum transfer, where the approximations described above are not particularly good.

I. INTRODUCTION

A number of papers [1-9] have studied the contributions of molecular rotations to the scattering cross-sections for thermal neutrons. Several of these papers have attempted to set limits on the validity of the approximation introduced by Krieger and Nelkin in [4].

The Krieger-Nelkin approximation is in a sense a 'quasi-classical' approximation in that after certain manipulations are carried out the quantum rotational operators are replaced by classical variables. This has resulted in the general interpretation that the only approximation made by Krieger and Nelkin was to treat the rotations classically. This is not in fact the case. If one interprets the quasi-classical cross-sections in the sense of [10-12] then the Krieger-Nelkin approximation is not quasi-classical.

This explains why the Krieger-Nelkin approximation is not extremely good whenever the neutron energy is larger than the rotational level spacing (which is the case for essentially all neutron experiments that have been performed on molecular gases).

As was shown in an earlier paper [13] the Krieger-Nelkin approximation is actually a short-time approximation to the quasi-classical expression.

Here we examine the quasi-classical expression for neutron scattering from molecular gases using the results of [13]. In Section II we show that if the quasi-classical expression for the logarithm of the intermediate scattering function $\chi(\Delta\underset{\sim}{p},t)$ is approximated by a power series in t through terms in t^2, one obtains a result which does not satisfy detailed balance. Numerical computations have been carried out using this approximation, and it is seen to be no better (or worse) than Krieger-Nelkin. If the condition of detailed balance is applied to this result, the Krieger-Nelkin result is obtained.

In Section III, we describe another approach to the evaluation of the quasi-classical cross-section. This approximation is good for small momentum transfers. In particular, in Section IV some numerical results are compared with the exact results of [8] for diatomic molecules, and the agreement is seen to be strikingly good. In a subsequent paper, the restriction to small momentum transfers will be removed.

It should be stressed that all of the results given here apply to the noninterference scattering (i=j). Further effort is required for the interference terms.

II. THE SHORT-TIME EXPANSION

Using the notation of [13], the quasi-classical approximation for neutron scattering by a rotating molecule gives for the rotational part of the intermediate scattering function

$$\chi_{rot}(\Delta\underline{p},t) = N^{-1} \sum_j c_j^2 \chi_j(\Delta\underset{\sim}{p},t) \tag{1}$$

where

$$\begin{aligned}\chi_j(\Delta\underset{\sim}{p},t) = \langle \exp\{ & \frac{i}{\hbar} \Delta\underset{\sim}{p}\cdot[\underline{q}_j(t)-\underline{q}_j(0) \\ & - \frac{i\beta\hbar}{2}(\underset{\approx}{I}^{-1}\cdot\underset{\sim}{L})x\underline{q}_j(0)\ ] \\ & - \frac{\beta}{8}(\underset{\sim}{q}_j(0)x\Delta\underset{\sim}{p})\cdot\underline{\underline{I}}^{-1}\cdot(\underline{q}_j(0)x\Delta\underset{\sim}{p})\}\rangle_{TC}\end{aligned} \tag{2}$$

and c_j is the incoherent scattering length of the jth atom in the molecule.

Now if we write

$$\chi_j(\Delta\underline{p},t) = e^{z_j(t)} \tag{3}$$

and

$$z_j(t) \approx z_j(0) + \dot{z}_j(0)t + \ddot{z}_j(0)t^2/2$$

we can use the classical equation of motion

$$\dot{\underset{\sim}{q}}_j = (\underset{\approx}{I}^{-1} \cdot \underset{\sim}{L}) x \underset{\sim}{q}_j \tag{4}$$

and obtain

$$z_j(0) = 0$$

$$\dot{z}_j(0) = \frac{i\Delta_p^2}{6\hbar} \operatorname{Tr} \underset{\underset{=}{}}{K}_j$$

$$\ddot{z}_j(0) = -\frac{\Delta p^2}{3\beta\hbar^2} \operatorname{Tr} \underset{\underset{=}{}}{K}_j - \frac{\Delta p^4}{30\hbar^2} \{\operatorname{Tr} \underset{\underset{=}{}}{K}_j^2 - \frac{1}{3} (\operatorname{Tr} \underset{\underset{=}{}}{K}_j)^2\} \tag{5}$$

where

$$\underset{\underset{=}{}}{K}_j = \underset{\underset{=}{}}{D}_j^{\dagger} \cdot \underset{\underset{=}{}}{I}^{-1} \cdot \underset{\underset{=}{}}{D}_j \tag{6}$$

$$D_j = \begin{pmatrix} 0 & -z_j & y_j \\ z_j & 0 & -x_j \\ -y_j & x_j & 0 \end{pmatrix}$$

and x_j, y_j, z_j are the components of $\underset{\sim}{q}_j$.

Introducing the usual expression for χ_{trans} and performing the dt integration we obtain for the cross-section

$$\frac{d^2\sigma}{d\Omega d\varepsilon} = \frac{k'}{Nk} \sum_j \frac{c_j^2}{2} \sqrt{1/\pi\hbar^2 b_j}$$

$$(x) \exp\{-(\hbar a_j - \varepsilon)^2/4\hbar^2 b_j\} \tag{7}$$

where

$$a_j = \Delta p^2 \{ \frac{\operatorname{Tr} \underset{\underset{=}{}}{K}_j}{6\hbar} + \frac{1}{2M\hbar} \} \tag{8}$$

$$b_j = \Delta p^2 \{ \frac{\operatorname{Tr} \underset{\underset{=}{}}{K}_j}{6\beta\hbar^2} + \frac{1}{2M\beta\hbar^2} \}$$

$$+ \frac{\Delta p^4}{60\hbar^2} (\operatorname{Tr} \underset{\approx}{K}_j^2 - \frac{1}{3} (\operatorname{Tr} \underset{\underset{=}{}}{K}_j)^2) \tag{9}$$

and M is the mass of the entire molecule.

This result is similar to a result obtained by Kosaly and Solt [5] for a diatomic molecule. We have evaluated this expression for a diatomic molecule and compared the result to exact calculations [8] and the Krieger-Nelkin expressions. The results were found to be neither better nor worse than Krieger-Nelkin.

It should be noted that Eq. (7) does not satisfy the principle of detailed balance. It does however give the first two Placzek moments exactly and gives the exact quasi-classical expression [11] for the third Placzek moment.

If one writes the intermediate scattering functions in the form of Eq. (3) and insists that the results give the first two Placzek moments exactly and satisfy detailed balance the Krieger-Nelkin approximation is obtained. Thus we see that the Krieger-Nelkin approximation is implied by a short-time expansion which satisfies detailed balance.

The numerical results indicate that neither of these approximations is valid except at very high momentum transfers. (This is in agreement with the calculations quoted in [2] and [8].)

The reason for this is easily understood by taking the large time limit of Eq. (3). The left-hand side approaches a constant and the right-hand side vanishes. The expansion of X_{rot} is secular.

The appropriate conditions for the validity of this expansion is that X_{trans} decay sufficiently rapidly with time, since $X = X_{trans}\, X_{rot}$.

$$X_{trans}(\Delta \underline{p},t) = \exp\{i \frac{\Delta p^2}{2M\hbar} t - \frac{\Delta p^2}{2M\hbar^2\beta} t^2\}$$

We see that X_{trans} decays with a characteristic time

$$t_o = \sqrt{2M\hbar^2\beta/\Delta p^2}$$

Since the average periodicity of X_{rot} is the mean period for molecular rotations

$$\tau = \sqrt{2\pi^2 I\beta}$$

we have the conditions for the validity of a time expansion of X_{rot}

$$\frac{\Delta p^2}{2M} \gg \frac{1}{\pi^2}\frac{\hbar}{2I} = \frac{R}{\pi^2} \tag{10}$$

where R is called the rotational constant. This is again similar to a result of [5] which was obtained by comparing the Placzek moments of the Krieger-Nelkin expression with exact results for a diatomic molecule.

We feel that the analysis given here provides a physical insight into the validity of the short-time expansion method and, in particular, it has led up to the method to be described in the next section.

III. AN APPROXIMATION VALID FOR SMALLER Δp

In Section II we have discussed a time-expansion approximation to χ_{rot}, and pointed out why it was valid only for large momentum transfers. Therefore it is reasonable to attempt to extend the range of validity by performing an expansion of χ_{rot} in powers of Δp. Such an approach is described below. Volkin [3] has previously attempted such an expansion on the exact quantum mechanical expression for the cross-section, but our use of the quasi-classical expression vastly simplified the computations.

Including both translations and rotations we can write

$$\frac{d^2\sigma}{d\Omega d\varepsilon} = \frac{k'}{2\pi\hbar k} e^{\beta\varepsilon/2} \int_{-\infty}^{\infty} dt\, e^{-i\varepsilon t/\hbar} \exp\{-\frac{\Delta p^2\beta}{8M} - \frac{\Delta p^2 t^2}{2M\hbar^2\beta}\}$$

$$(x) \sum_j c_j^2 \langle \exp\{\frac{i}{\hbar} \Delta \underset{\sim}{p}\cdot(\underline{q}_j(t)-\underline{q}_j(0))$$

$$- \frac{\beta}{8} (\underline{q}_j(0)x\Delta \underset{\sim}{p})\cdot \underset{\approx}{I}^{-1}\cdot(\underline{q}_j(0)x\Delta \underline{p})\} \rangle_{TC} \tag{11}$$

If $\frac{\beta}{8} (\underline{q}_j \times \Delta \underline{p}) \cdot \underline{\underline{I}}^{-1} \cdot (\underline{q}_j \times \Delta \underline{p})$ is small we can approximate it by its average value

$$\langle \frac{\beta}{8} (\underline{q}_j x\Delta \underline{p})\cdot \underline{\underline{I}}^{-1}\cdot(\underline{q}_j x\Delta \underline{p})\rangle_{TC} = \frac{\beta\Delta p^2}{24} \mathrm{Tr}\underline{\underline{K}}_j \tag{12}$$

Then expanding the remaining exponential in the thermal average Eq. (11) in a power series we can write

$$\langle \exp\{\frac{1}{i} \Delta \underset{\sim}{p}\cdot(\underline{q}_j(t) - \underline{q}_j(0))$$

$$- \frac{\beta}{8} (\underline{q}_j(0)x\Delta \underline{p})\cdot \underline{\underline{I}}^{-1}\cdot(\underline{q}_j(0)x\Delta \underline{p})\} \rangle_{TC}$$

$$\simeq \exp\{-\frac{\beta\Delta p^2}{24} \mathrm{Tr}\underline{\underline{K}}_j\} \sum_{n=0}^{\infty} \{-\frac{\Delta p^2}{\hbar^2}\}^n \frac{1}{(2n)!(2n+1)}$$

$$(x) \langle(\underline{q}_j(\tau) - \underline{q}_j(0))^{2n}\rangle_{TC}$$

where we have used the fact that odd powers in the expansion vanish under the orientation average. Now we note that

$$(\underline{q}_j(t)-\underline{q}_j(0))^2 = -q_j^2(0)(e^{i\alpha(t)/2}-e^{-i\alpha(t)/2})^2 \tag{13}$$

where $\alpha(t)$ is the angle between $\underline{q}_j(0)$ and $\underline{q}_j(t)$. Using these results in (11), we obtain after some manipulations

$$\frac{\partial^2\sigma}{\partial\Omega d\varepsilon} = \sum_{r=0}^{\infty} \frac{\partial^2\sigma(r)}{\partial\Omega\partial\varepsilon} \tag{14}$$

where

$$\frac{\partial^2\sigma(0)}{\partial\Omega\partial\varepsilon} = \frac{k'}{k} \sqrt{M\beta/2\pi\Delta p^2}\, \exp\{ \frac{\beta\varepsilon}{2} - \frac{\Delta p^2\beta}{8M} - \frac{\varepsilon^2 M\beta}{2\Delta p^2} \}$$

$$(x) \sum_j c_j^2 \exp\{-\frac{\beta\Delta p^2}{24} \mathrm{Tr}\underline{\underline{K}}_j\}\{ \sum_{n=0}^{\infty} \{-\frac{\Delta p^2 q_j^2}{\hbar^2}\}^n /(n!)^2(2n+1)\} \tag{15}$$

and for $r \neq 0$

$$\frac{\partial^2\sigma(r)}{\partial\Omega\partial\varepsilon} = \frac{k'}{2\pi\hbar k} e^{\beta\varepsilon/2} \int_{-\infty}^{\infty} dt\, e^{-i\varepsilon t/\hbar}$$

$$(x) \exp\{-\frac{\Delta p^2\beta}{8M} - \frac{\Delta p^2 t^2}{2M\hbar^2\beta}\}$$

$$(x) \sum_j c_j^2 \exp\{-\frac{\beta\Delta p^2}{24} \mathrm{Tr}\underline{\underline{K}}_j\} \sum_{n=r}^{\infty} \left(\frac{\Delta p^2 q_j^2}{\hbar^2}\right)^n$$

$$(x) (-1)^{n+r} \frac{2\langle\cos r\alpha(t)\rangle_{TC}}{(2n+1)(n-r)!(n+r)!} \tag{16}$$

The basic problem has now been reduced to the determination of the angle $\alpha(t)$ for the terms involving $n > 0$, which can be evaluated in either the body- or space-fixed coordinate systems. For the $n = 0$ term, molecular information enters only in a trivial way.

The double sum in Eq. (14) can be readily performed for $\Delta p_j^2 q^2/\hbar^2$ up to a value of about 10 on a remote, time-sharing terminal. For larger Δp^2 one can use the short-time results as described in the previous sections.

IV. THE DIATOMIC MOLECULE

For the diatomic molecule

$$\alpha(t) = \omega t$$

and (17)

$$H_{rot} = I\omega^2/2$$

where I is the moment of inertia.

With these expressions, we can evaluate the thermal average in Eq. (16) and we obtain

$$\frac{\partial^2\sigma(r)}{\partial\Omega\partial\varepsilon} = \frac{k'}{k}\sqrt{\beta/4\pi\{\frac{\Delta p^2}{2M} + r^2R\}}\left\{1 - \frac{r^2R}{\{\frac{\Delta p^2}{2M} + r^2R\}}\right.$$

$$\left. + \frac{\varepsilon^2 r^2 R\beta}{2\{\frac{\Delta p^2}{2M} + r^2R\}^2}\right\}\exp\left\{\frac{\beta\varepsilon}{2} - \frac{\Delta p^2\beta}{8M}\right.$$

$$\left. - \frac{\varepsilon^2\beta}{4\{\frac{\Delta p^2}{2M} + r^2R\}}\right\}\sum_j c_j^2 \exp\{-\frac{\beta\Delta p^2}{24}\mathrm{Tr}\underline{\underline{K}}_j\}$$

$$(x)\quad \sum_{n=r}\left(\frac{\Delta p^2 q_j^2}{\hbar^2}\right)^n (-1)^{n+r}\frac{2}{(n-r)!(n+r)!(2n+1)}$$

$$r > 0 \qquad (18)$$

Using Eqs. (18) and (15) we have determined the cross-section for scattering from HCl and HF and compared with Lurie's [8] exact calculation. These results are shown in Figures 1 and 2. We note the good agreement particularly in the vicinity of the elastic peak where the time expansions are particularly poor. For larger scattering angles our results are not as good due to the increase in Δp. The only approximation here, aside from terminating the sums, is that of Eq. (12). This approximation will be removed in a subsequent paper, in which more numerical results will also be quoted.

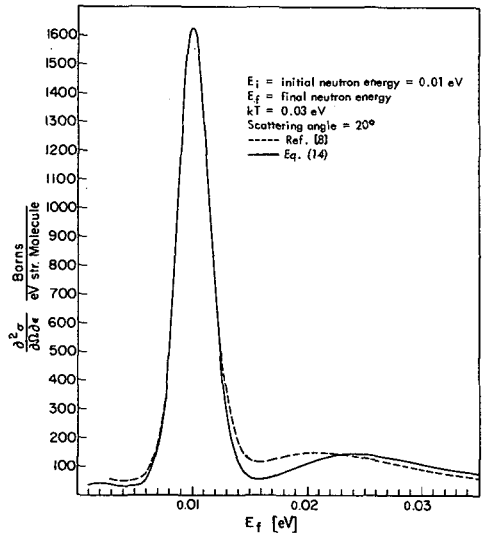

FIG. 1. Neutron cross-section for HCl gas.

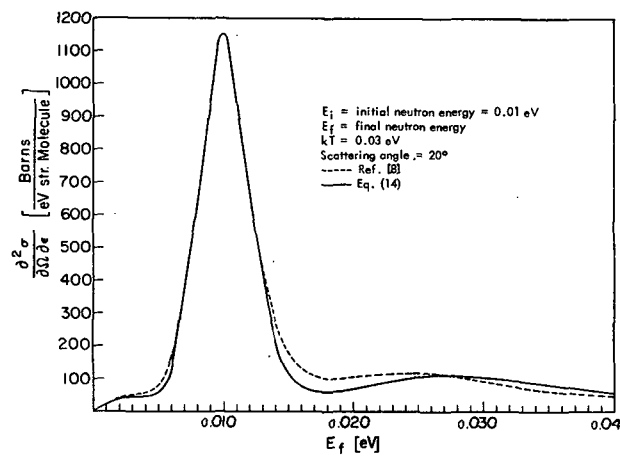

FIG. 2. Neutron cross-section for HF gas.

V. CONCLUSIONS

It appears that by judicious choice of the time-expansion method of Section II and the Δp expansion of Section III most of the range of interest in neutron-scattering experiments can be covered. Additional work remains to be done, however, before interference scattering can be treated adequately in either approximation.

ACKNOWLEDGEMENTS

This work was supported in part by the U. S. National Science Foundation. The computations were carried out on a remote terminal to the Ford Motor Company computer. We want to thank Ford for making the computer time

available. We are also indebted to Professor J. M. Carpenter and Mr. Norman Lurie for very helpful discussions.

REFERENCES

[1] ZEMACH, A. C., GLAUBER, R. J., Phys. Rev. 101 (1956) 118.

[2] GRIFFING, G. W., Phys. Rev. 124 (1961) 1489; and 127 (1962) 1179.

[3] VOLKIN, H. C., Phys. Rev. 113 (1959) 866; and 117 (1960) 1029.

[4] KRIEGER, T. J., NELKIN, M. S., Phys. Rev. 106 (1957) 290.

[5] KOSALY, G., SOLT, G., Phys. Letters 6 (1963) 51; 13 (1964) 223; and Physica 32 (1966) 16.

[6] DZYUB, I. P., Soviet Phys. JETP 22 (1966) 347.

[7] KOVALCHUK, V. G., Ukrainsky Fizychnyi Zhurnal 11 (1966) 581.

[8] LURIE, N., J. Chem. Phys. 46 (1967) 352.

[9] YOUNG, J. A., KOPPEL, J. U., Phys. Rev. 135 (1964) A603.

[10] AAMODT, R. et al., Phys. Rev. 126 (1962) 1165

[11] ROSENBAUM, M., ZWEIFEL, P. F., Phys. Rev. 137 (1965) B271.

[12] IMRE, K. et al., J. Math. Phys. (in press).

[13] SUMMERFIELD, G. C., ZWEIFEL, P. F., Phys. Rev. (in press).

AMPLITUDE OF THE TWO-QUANTUM TERM IN THE SCATTERING LAW FOR MOLECULAR GASES

J. M. CARPENTER AND R. A. SCHAEFER
UNIVERSITY OF MICHIGAN,
ANN ARBOR, MICHIGAN,
UNITED STATES OF AMERICA

Abstract

AMPLITUDE OF THE TWO-QUANTUM TERM IN THE SCATTERING LAW FOR MOLECULAR GASES. The orientation-averaged amplitude of the two-quantum term in the scattering law for coherent scattering of neutrons by molecular gases is computed in closed form. The phase factor $e^{i\vec{\kappa}\cdot\vec{b}}$ is averaged jointly with the amplitude factor $(\vec{\kappa}.\vec{f}_1)(\vec{\kappa}.\vec{f}_2)(\vec{\kappa}.\vec{f}_3)(\vec{\kappa}.\vec{f}_4)$. The resulting expression is appropriate for use in approximately calculating thermalization kernels, and for interpreting measurements of scattering laws for coherent molecular gases. Calculations are performed for C_2F_6, for the two-quantum combinations of the $\hbar\omega_{12} = 216\ cm^{-1} = 27$ meV mode with the $\hbar\omega_9 = 34.9\ cm^{-1} = 43.5$ meV and the $\hbar\omega_9 = 371\ cm^{-1} = 46.5$ meV modes. Calculations are also performed for the two-quantum overtone of Br_2. The results of the calculations show that interference-scattering effects are significant in comparison with the direct scattering amplitude. The possibility is discussed of a method of 'inelastic diffraction' by means of which maxima in measured scattering laws may be interpreted to assign the frequencies according to symmetry species.

Either in calculations of scattering kernels or in the interpretation of measurements of scattering laws for molecular gases, it is necessary to account for the influence of energy transfer with the modes of internal vibration of the molecule. Under certain circumstances, generally at small scattering angles, low-neutron energies and low temperatures, the scattering cross-section is expected to appear as a spectrum of broadened lines. There is a quasi-elastic peak centred about zero-energy transfer, and others of lower amplitude, centred about the energy transfer associated with excitation of one quantum in a vibrational mode, two quanta, etc. It is our purpose here to compute the areas of these peaks. This is done without reference to the shapes of the peaks, that is, without regard to the broadening due to centre-of-mass translation and free rotation about the centre of mass. Although the calculation has already been performed for incoherent scatterers, we treat here the general case for both coherent and incoherent scattering, including interference effects within a molecule, but neglecting intermolecular interference.

The scattering law is related to the cross-section, [1, 2, 3]

$$\frac{\partial^2\sigma}{\partial\Omega\partial\epsilon} = \frac{k_f}{k_0} S(\kappa, \epsilon) \tag{1}$$

with $\hbar\vec{k}_0$ and $\hbar\vec{k}_f$ the neutron initial and final momenta, $\hbar\kappa = \hbar|\vec{k}_f - \vec{k}_0|$ the momentum transfer and $\epsilon = \frac{\hbar^2}{2m}(k_f^2 - k_0^2)$ the neutron energy gain. It is use-

ful to write the scattering law as a sum

$$S(\kappa, \epsilon) = \sum_{\nu, \nu'} a^2_{\nu\nu'} S_{\nu\nu'}(\kappa, \epsilon) \tag{2}$$

where

$$a^2_{\nu\nu'} = A_\nu A_{\nu'} + C^2_\nu S_{\nu\nu'} \tag{3}$$

in which A_ν and C_ν are respectively the bound coherent and incoherent scattering lengths for the ν-th nucleus. For the present calculation, it is convenient to work in terms of the intermediate scattering functions $\chi_{\nu\nu'}(\kappa, t)$

$$S_{\nu\nu'}(\kappa, \epsilon) = (2\pi\hbar)^{-1} \int_{-\infty}^{\infty} dt e^{-i\epsilon t} \chi_{\nu\nu'}(\kappa, t) \tag{4}$$

In $\chi_{\nu\nu'}$ the influence of centre-of-mass translation is rigorously separable as a factor

$$\chi_{\nu\nu'}(\kappa, t) = \chi^{\text{Trans.}}(\kappa, t)\, \chi^{\text{Rot.-Vib.}}_{\nu\nu'}(\kappa, t) \tag{5}$$

where

$$\chi^{\text{Trans.}}(\kappa, t) = e^{-(it\hbar + k_B T t^2)\kappa^2/2M} \tag{6}$$

and

$$\chi^{\text{Rot.-Vib.}}_{\nu\nu'}(\kappa, t) = \langle \psi_{\text{Rot}} | e^{i\vec{\kappa}\cdot\vec{b}_\nu(t)} V_{\nu\nu'}(\vec{\kappa}, t) e^{-i\vec{\kappa}\cdot\vec{b}_{\nu'}(0)} | \psi_{\text{Rot.}} \rangle_T \tag{7}$$

Here, $\langle\ \rangle_T$ denotes a thermal average with respect to rotational states, $\vec{b}_\nu(t)$ is the time-dependent operator for the equilibrium position of the ν-th atom with respect to molecular centre-of-mass; and $V_{\nu\nu'}(\vec{\kappa}, t)$ describes the vibrational motions of the molecule.

We shall perform an orientation average related to that in Eq. (7) to obtain the areas of the peaks in the scattering law. McMurry et al. [4] have calculated a numerical orientation average of the corresponding quantities. Our procedure follows from a suggestion of Janik and Kowalska [2] that V be expanded in a power series in κ.

Arguments of considerable complexity can be avoided and the desired result obtained by adopting a form for V given by Zemach and Glauber [3] and ignoring the Debye-Waller factors.

$$V_{\nu\nu'}(\kappa, t) = \prod_\lambda V^\lambda_{\nu\nu'}(\kappa, t) \tag{8}$$

$$V^\lambda_{\nu\nu'}(\kappa, t) = e^{-h^\lambda_{\nu\nu'}} \exp\left[g^\lambda_{\nu\nu'}\left(e^{\omega^\lambda(it-\hbar/2k_BT)} + e^{-\omega^\lambda(it-\hbar/2k_BT)}\right)\right] \tag{8a}$$

where

$$h^{\lambda}_{\nu\nu'} = \frac{\hbar^2[(\vec{\kappa}\cdot\vec{\gamma}^{\lambda}_{\nu}(t))^2 + (\vec{\kappa}\cdot\vec{\gamma}^{\lambda}_{\nu'}(0))^2]}{4\hbar\omega^{\lambda}} \coth\frac{\hbar\omega^{\lambda}}{2k_BT} \tag{8b}$$

and

$$g^{\lambda}_{\nu\nu'} = \frac{\hbar^2(\vec{\kappa}\cdot\vec{\gamma}^{\lambda}_{\nu}(t))(\vec{\kappa}\cdot\vec{\gamma}^{\lambda}_{\nu'}(0))}{2\hbar\omega^{\lambda}} \operatorname{csch}\frac{\hbar\omega^{\lambda}}{2k_BT} \tag{8c}$$

Here, $\prod_{\lambda} e^{-h^{\lambda}_{\nu\nu'}}$ is the Debye-Waller factor which we shall take to be unity, $\vec{\gamma}^{\lambda}_{\nu}(t)$ is the displacement of the ν-th atom in the λ-th normal mode, with normalization

$$\sum_{\nu} m_{\nu}(\vec{\gamma}^{\lambda}_{\nu}(t))^2 = 1 \tag{9}$$

and ω^{λ} is the frequency of the λ-th normal mode. It is to be noted that the $\vec{\gamma}^{\lambda}_{\nu}(t)$ are time-dependent operators as the rotational eigenfunctions, and do not commute with one another or with the $\vec{b}_{\nu}(t)$ when evaluated at different times. Already in Eq.(8) the non-commuting property of these operators has been violated. The $\vec{\gamma}$ depend on t because they are measured in a co-ordinate system which rotates with the molecule. The more complex treatment in which the commutation rules are respected and the Debye-Waller factor is retained indicates that the results obtained below are correct in the sense of an expansion of $V_{\nu\nu'}$ in powers of κ.

The expansion of Zemach and Glauber,

$$V^{\lambda}_{\nu\nu'} = \sum_{n_{\lambda}=-\infty}^{\infty} I_{n_{\lambda}}(g^{\lambda}_{\nu\nu'})e^{n_{\lambda}\hbar\omega^{\lambda}/2k_BT}\, e^{-in_{\lambda}\omega^{\lambda}t} \tag{10}$$

(ignoring the Debye-Waller factor), where I_n are the modified Bessel functions, gives $V_{\nu\nu'}$ in a form which may be written

$$V_{\nu\nu'} = \sum_{\{n_{\lambda}\}} \left[\prod_{\lambda} I_{n_{\lambda}}(g^{\lambda}_{\nu\nu'})\right]\left[e^{n_{\lambda}\omega^{\lambda}\left(-it+\frac{\hbar}{2k_BT}\right)}\right] \tag{11}$$

The scattering law is then

$$S_{\nu\nu'}(\kappa,\epsilon) = \sum_{\{n_\lambda\}} \frac{1}{2\pi\hbar} \int_{-\infty}^{\infty} e^{-i(\epsilon-\sum_\lambda n_\lambda \hbar\omega^\lambda)t}$$

$$\times e^{\sum_\lambda n_\lambda \frac{\hbar\omega^\lambda}{2k_BT}} \chi^{\text{Trans.}}(\kappa,t)$$

$$\langle e^{i\vec{\kappa}\cdot\vec{b}_\nu(t)} \prod_\lambda I_{n_\lambda}(g^\lambda_{\nu\nu'}) e^{-i\vec{\kappa}\cdot\vec{b}_{\nu'}(0)} \rangle_T \, dt \tag{12}$$

$$\equiv \sum_{\{n_\lambda\}} S^{\{n_\lambda\}}_{\nu\nu'}(\kappa) = \sum_{\{n_\lambda\}} \int_{-\infty}^{\infty} e^{-i\epsilon t} \chi^{\{n_\lambda\}}_{\nu\nu'}(\kappa,t) \frac{dt}{2\pi\hbar} \tag{13}$$

Each term in the sum represents a contribution to S in the neighbourhood of ϵ around

$$\epsilon \sim \sum_\lambda n_\lambda \hbar\omega^\lambda. \tag{14}$$

In the above, $\sum_{\{n_\lambda\}}$ denotes the sum over all possible sets of n_λ's.

Consider now the area under one of these peaks,

$$S^{\{n_\lambda\}}_{\nu\nu'}(\kappa) = \int_{-\infty}^{\infty} S^{\{n_\lambda\}}_{\nu\nu'}(\kappa,\epsilon)d\epsilon \tag{15}$$

which is a function of κ alone.

$$S^{\{n_\lambda\}}_{\nu\nu'}(\kappa) = \int_{-\infty}^{\infty} d\epsilon \int_{-\infty}^{\infty} dt\, e^{-i\epsilon t} \frac{1}{2\pi\hbar} \chi^{\{n_\lambda\}}_{\nu\nu'}(\kappa,t) \tag{16}$$

$$= \chi^{\{n_\lambda\}}_{\nu\nu'}(\kappa,0) \tag{17}$$

$$= e^{\sum_\lambda n_\lambda \frac{\hbar\omega^\lambda}{2k_BT}} \langle \psi_{\text{Rot.}} \left| e^{i\vec{\kappa}\cdot\vec{b}_\nu(0)} \prod_\lambda I_{n_\lambda} e^{-i\vec{\kappa}\cdot\vec{b}_{\nu'}(0)} \right| \psi_{\text{Rot.}} \rangle_T \tag{18}$$

since $\chi^{\mathrm{Trans}}(\kappa, 0) = 1$. The factor $e^{\sum_\lambda n_\lambda \frac{\hbar\omega^\lambda}{2k_BT}}$ is the detailed balance factor, and the thermal average with respect to rotational states is now just an orientation average.

It is these peak areas on which we now focus our attention.

1. Quasi-elastic peak

When all the n_λ are zero, $S^{(0)}_{\nu\nu'}$ is the area of the quasi-elastic peak, at

$$\epsilon \sim \sum_\lambda n_\lambda \hbar\omega^\lambda = 0 \tag{19}$$

To first order in their arguments,

$$I_n(x) \approx \left(\frac{x}{2}\right) \frac{|n|}{|n|!} \tag{20}$$

and thus to first order $I_0 = 1$ and

$$S^{(0)}_{\nu\nu'} = \langle e^{i\vec{\kappa}\cdot\vec{b}_\nu(0)}\, e^{-i\vec{\kappa}\cdot\vec{b}_{\nu'}(0)} \rangle_\Omega = j_0(\kappa|\vec{b}_\nu - \vec{b}_{\nu'}|) \tag{21}$$

is the familiar result for diffraction from a molecular gas.

2. One-quantum peaks

When all the n_λ are zero except one, say the Λ-th, for which $n_\Lambda = \pm 1$

$$S^{(\pm 1)\Lambda}_{\nu\nu'}(\kappa) = e^{\pm\frac{\hbar\omega^\Lambda}{2k_BT}} \langle e^{i\vec{\kappa}\cdot\vec{b}_\nu} \prod_{\lambda\neq\Lambda} [I_0(g^\lambda_{\nu\nu'}]\, I_1(g^\Lambda_{\nu\nu'}) e^{-i\vec{\kappa}\cdot\vec{b}_{\nu'}} \rangle_\Omega \tag{22}$$

$$\approx e^{\pm\frac{\hbar\omega^\Lambda}{2k_BT}} \langle e^{i\vec{\kappa}\cdot\vec{b}_\nu} \frac{g^\lambda_{\nu\nu'}}{2} e^{-i\vec{\kappa}\cdot\vec{b}_{\nu'}} \rangle_\Omega \tag{23}$$

$$= e^{\pm\frac{\hbar\omega^\Lambda}{2k_BT}} \frac{\hbar^2}{4\hbar\omega^\Lambda} \operatorname{csch}\frac{\hbar\omega^\Lambda}{2k_BT} \langle e^{i\vec{\kappa}\cdot\vec{b}_\nu} (\vec{\kappa}\cdot\vec{\gamma}^\Lambda_\nu)(\vec{\kappa}\cdot\vec{\gamma}^\Lambda_{\nu'}) e^{-i\vec{\kappa}\cdot\vec{b}_{\nu'}} \rangle_\Omega \tag{24}$$

The problem then is to obtain the average value in Eq.(24). The average over orientations has been performed in an earlier paper [5] by use of a generating function.

3. Two-quantum peaks

When all the n_λ are zero except one, say the Λ-th, for which $n_\Lambda = \pm 2$, the result corresponding to Eq.(22) describes the scattering with exchange

of two quanta with the Λ-th mode. Then

$$S_{\nu\nu'}^{(\pm 2)\Lambda}(\kappa) = e^{\pm\frac{2\hbar\omega^{\Lambda}}{2k_BT}} \langle e^{i\vec{\kappa}\cdot\vec{b}_\nu} \prod_{\lambda\neq\Lambda} [I_0(g_{\nu\nu'}^{\lambda})] \times I_2(g_{\nu\nu'}^{\Lambda}) e^{-i\vec{\kappa}\cdot\vec{b}_{\nu'}} \rangle_\Omega \tag{25}$$

$$\approx e^{\pm\frac{2\hbar\omega^{\Lambda}}{2k_BT}} \frac{\hbar^4 \operatorname{csch}^2 \frac{\hbar\omega^{\Lambda}}{2k_BT}}{32(\hbar\omega^{\Lambda})^2} \langle e^{i\vec{\kappa}\cdot\vec{b}_\nu} (\vec{\kappa}\cdot\vec{\gamma}_\nu^{\Lambda})^2 (\vec{\kappa}\cdot\vec{\gamma}_{\nu'}^{\Lambda})^2 e^{-i\vec{\kappa}\cdot\vec{b}_{\nu'}} \rangle_\Omega \tag{26}$$

Similarly, when all the n_λ are zero except two, say the Λ_1-th and the Λ_2-th, for which $n_{\Lambda_1} = \pm 1$ and $n_{\Lambda_2} = \pm 1$, the result describes the scattering with simultaneous exchange of one quantum with each of the two modes.

$$S_{\nu\nu'}^{(\pm 1)\Lambda_1 (\pm 1)\Lambda_2}(\kappa) = e^{\frac{\pm\hbar\omega^{\Lambda_1} \pm\hbar\omega^{\Lambda_2}}{2k_BT}} \langle e^{i\vec{\kappa}\cdot\vec{b}_\nu}$$

$$\times \prod_{\lambda\neq\Lambda_1,\Lambda_2} [I_0(g_{\nu\nu'}^{\lambda})] I_1(g_{\nu\nu'}^{\Lambda_1}) I_2(g_{\nu\nu'}^{\Lambda_2}) e^{-i\vec{\kappa}\cdot\vec{b}_{\nu'}} \rangle_\Omega \tag{27}$$

$$\approx e^{\frac{\pm\hbar\omega^{\Lambda_1}\pm\hbar\omega^{\Lambda_2}}{2k_BT}} \frac{\hbar^4 \operatorname{csch} \frac{\hbar\omega^{\Lambda_1}}{2k_BT} \operatorname{csch} \frac{\hbar\omega^{\Lambda_2}}{2k_BT}}{16(\hbar\omega^{\Lambda_1})(\hbar\omega^{\Lambda_2})}$$

$$\langle e^{i\vec{\kappa}\cdot\vec{b}_\nu} (\vec{\kappa}\cdot\vec{\gamma}_\nu^{\Lambda_1})(\vec{\kappa}\cdot\vec{\gamma}_{\nu'}^{\Lambda_1})(\vec{\kappa}\cdot\vec{\gamma}_\nu^{\Lambda_2})(\vec{\kappa}\cdot\vec{\gamma}_{\nu'}^{\Lambda_2}) e^{-i\vec{\kappa}\cdot\vec{b}_{\nu'}} \rangle_\Omega \tag{28}$$

The average appearing in Eq.(26) is identical in form to that in Eq.(28). We therefore proceed to obtain an expression for the average of Eq.(28).

Just as the average for the one-quantum amplitude is conveniently performed using a generating function, so is the corresponding average in Eq.(28) for the two-quantum amplitude. Thus, noting that,

$$F_{\nu\nu'}^{(2)\Lambda_1\Lambda_2} = \frac{\partial^4}{\partial\alpha_1\,\partial\alpha_2\,\partial\beta_1\,\partial\beta_2} G_{\nu\nu'}^{(2)\Lambda_1\Lambda_2} \Bigg|_{\alpha_1=\alpha_2=\beta_1=\beta_2=0} \tag{29}$$

where

$$G_{\nu\nu'}^{(2)\Lambda_1\Lambda_2} = e^{i\vec{\kappa}\cdot\vec{b}} \tag{30}$$

and

$$\vec{b} = \vec{b}_\nu - \vec{b}_{\nu'} + \alpha_1\vec{\gamma}_\nu^{\Lambda_1} + \alpha_2\vec{\gamma}_\nu^{\Lambda_2} + \beta_1\vec{\gamma}_{\nu'}^{\Lambda_1} + \beta_2\vec{\gamma}_{\nu'}^{\Lambda_2}$$

and the desired result is now

$$\langle F^{(2)\Lambda_1\Lambda_2}_{\nu\nu'}\rangle_\Omega = \frac{\partial^4}{\partial\alpha_1\,\partial\alpha_2\,\partial\beta_1\,\partial\beta_2}\langle G^{(2)\Lambda_1\Lambda_2}_{\nu\nu'}\rangle_\Omega\Bigg|_{\alpha_1=\alpha_2=\beta_1=\beta_2=0}$$

$$= \frac{\partial^4}{\partial\alpha_1\,\partial\alpha_2\,\partial\beta_1\,\partial\beta_2}\, j_0(\kappa\,|b|)\Bigg|_{\alpha_1=\alpha_2=\beta_1=\beta_2=0} \tag{31}$$

and is obtained after straightforward but tedious application of simple differentiation and recurrence relations. We write the result

$$\langle F^{(2)\Lambda_1\Lambda_2}_{\nu\nu'}\rangle_\Omega = k^4\left\{\frac{X}{3\cdot 5}\, j_0 + \left(\frac{2X}{3\cdot 7} - \frac{B}{7}\right) j_2 + \left(\frac{X}{5\cdot 7} - \frac{B}{7} + P\right) j_4\right\} \tag{32}$$

where

$$j_\ell = j_\ell(\kappa\, b_{\nu\nu'}) \tag{32a}$$

and

$$\begin{aligned} X &= x_{12}\,x_{34} + x_{13}\,x_{24} + x_{14}\,x_{23} \\ B &= x_{12}b_3\,b_4 + x_{13}\,b_2 b_4 + x_{14}b_2 b_3 \\ &\quad + x_{23}b_1\,b_4 + x_{24}b_1 b_3 + x_{34}b_1\,b_2 \\ P &= b_1\,b_2\,b_3\,b_4 \end{aligned} \tag{32b}$$

in which

$$\begin{aligned} x_{12} &= \vec{\gamma}^{\Lambda_1}_{\nu}\cdot\vec{\gamma}^{\Lambda_2}_{\nu} \\ x_{13} &= \vec{\gamma}^{\Lambda_1}_{\nu}\cdot\vec{\gamma}^{\Lambda_1}_{\nu'} \\ x_{14} &= \vec{\gamma}^{\Lambda_1}_{\nu}\cdot\vec{\gamma}^{\Lambda_2}_{\nu'} \\ x_{23} &= \vec{\gamma}^{\Lambda_2}_{\nu}\cdot\vec{\gamma}^{\Lambda_1}_{\nu'} \\ x_{24} &= \vec{\gamma}^{\Lambda_2}_{\nu}\cdot\vec{\gamma}^{\Lambda_2}_{\nu'} \\ x_{34} &= \vec{\gamma}^{\Lambda_1}_{\nu'}\cdot\vec{\gamma}^{\Lambda_2}_{\nu'} \\ b_1 &= (1/b_{\nu\nu'})(\vec{b}_{\nu\nu'}\cdot\vec{\gamma}^{\Lambda_1}_{\nu}) \\ b_2 &= (1/b_{\nu\nu'})(\vec{b}_{\nu\nu'}\cdot\vec{\gamma}^{\Lambda_2}_{\nu}) \\ b_3 &= (1/b_{\nu\nu'})(\vec{b}_{\nu\nu'}\cdot\vec{\gamma}^{\Lambda_1}_{\nu'}) \\ b_4 &= (1/b_{\nu\nu'})(\vec{b}_{\nu\nu'}\cdot\vec{\gamma}^{\Lambda_2}_{\nu'}) \\ \vec{b}_{\nu\nu'} &= \vec{b}_{\nu} - \vec{b}_{\nu'};\quad b_{\nu\nu'} = |\,\vec{b}_{\nu\nu'}| \end{aligned} \tag{32c}$$

It is to be remarked that Eq.(32) is completely symmetric with respect to interchange of Λ_1 with Λ_2 and interchange of ν with ν'. The orientation average calculated according to Eq.(32) has been successfully checked against a computer evaluation of the orientation average, in which the average was performed by evaluating the function to be averaged for a large number of orientations, and summing the results. The limiting forms for $b \to 0$ are also correct.

The two-quantum amplitudes, Eqs (26) and (28), are then calculable using Eq.(32). Contributions from all ν, ν' to the scattering law then yield the amplitude of the two-quantum peaks in the scattering law. For two quanta to one mode, ('overtones', in the terminology of the optical spectroscopists)

$$S^{(\pm 2)\Lambda}(\kappa) = \sum_{\nu,\nu'} a^2_{\nu\nu'} S^{(\pm 2)\Lambda}_{\nu\nu'}(\kappa) \tag{33}$$

and for one quantum to each of two modes ('combinations')

$$S^{(\pm 1)\Lambda_1(\pm 1)\Lambda_2}(\kappa) = \sum_{\nu,\nu'} a^2_{\nu\nu'} S^{(\pm 1)\Lambda_1(\pm 1)\Lambda_2}_{\nu\nu'}(\kappa) \tag{34}$$

Calculations have been performed for several cases for hexafluoroethane, C_2F_6 (freon 116). The normal mode displacements were computed from force constants inferred by Pace [6] from optical spectroscopic data and were performed by H.L. McMurry. Frequencies computed from these force constants match the assigned observed optically-active modes

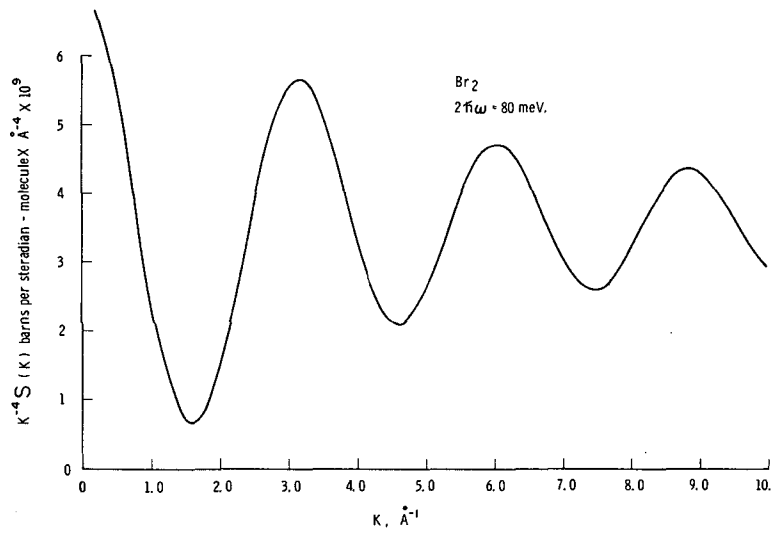

FIG. 1. The amplitude of the two-quantum term in the scattering law for Br_2, for $\epsilon = 2\hbar\omega = 80$ meV. The detailed-balance factor is not included.

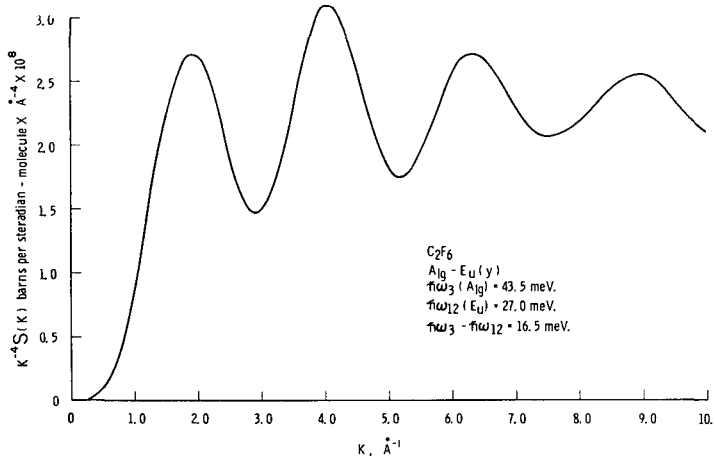

FIG.2. The amplitude of the two-quantum term in the scattering law for C_2F_6, for the two modes $\hbar\omega_3$ = 43.5 meV, species A_{1g}, and $\hbar\omega_{12}$ = 27.0 meV, species Eu. $\epsilon = \hbar\omega_3 - \hbar\omega_{12}$ = 16.5 meV. The detailed-balance factor is not included.

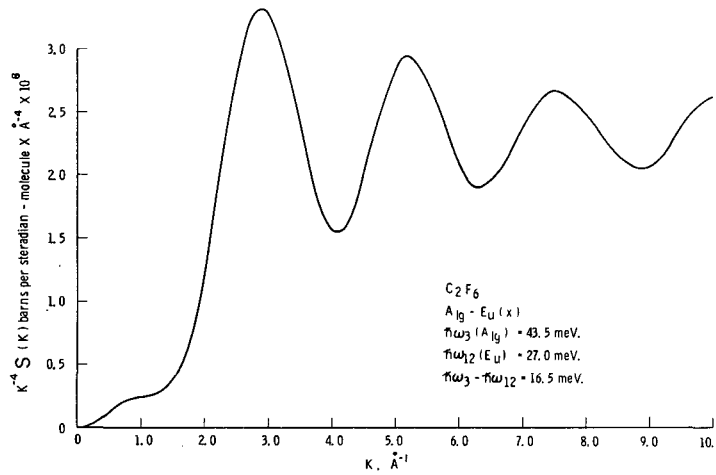

FIG.3. The amplitude of the two-quantum term in the scattering law for C_2F_6, for the two modes $\hbar\omega_3$ = 43.5 meV, species A_{1g}, and $\hbar\omega_{12}$ = 27.0 meV, species Eu. (The Eu species is two-fold degenerate.) $\epsilon = \hbar\omega_3 - \hbar\omega_{12}$ = 16.5 meV. The detailed-balance factor is not included. The amplitudes of Figs 2 and 3 must be added to account for interaction with the degenerate modes.

fairly well, but actual frequencies given below were taken from the more recent work of Carney et al. [7].

A calculation is also shown for the diatomic molecule Br_2, in which there is only one vibrational mode, of frequency 40 meV (323 cm^{-1}) [8]. For Br_2, the normal-mode displacements $\vec{\gamma}$ are of equal magnitude, oppositely directed and co-linear with the molecular axis and $|\vec{\gamma}| = 0.079$ $amu^{-\frac{1}{2}}$.

Figures 1-4 present the results for several two-quantum amplitudes. Since these are all proportional to κ^4, this factor is divided out to clarify the presentation. For these purposes, κ is expressed in $Å^{-1}$.

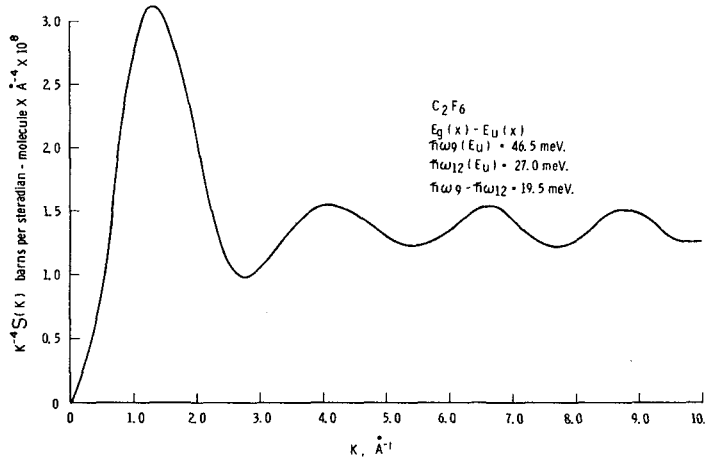

FIG.4. The amplitude of the two-quantum term in the scattering law for C_2F_6, for the two modes $\hbar\omega_9 = 46.5$ meV, species Eg, and $\hbar\omega_{12} = 27.0$ meV, species Eu. (Both Eg and Eu are two-fold degenerate.) $\epsilon = \hbar\omega_9 - \hbar\omega_{12} = 19.5$ meV. The detailed-balance factor is not included. The amplitudes of this and three similar terms must be added to account for interactions between all combinations of the degenerate modes.

Both the one-quantum and the two-quantum amplitudes show the ripply structure characteristic of diffraction by molecular gases. The maxima and minima do not necessarily correspond to those for scattering by the rigid molecule, since these depend not only on the interatomic spacings and scattering lengths, but also on the displacement vectors. It is therefore possible, in cases where vibrationally inelastic peaks are resolved, to compare measured areas with the present calculated ones, as an aid to assigning the peaks to given processes. The present calculations, with the results for the one-quantum terms from Ref. [5], then form the basis for a sort of 'inelastic diffraction' method of neutron spectroscopy on molecular gases.

ACKNOWLEDGEMENTS

We wish to express our gratitude to H. L. McMurry who computed the normal mode eigenvectors for C_2F_6, and to the Ford Motor Company, whose computing facilities at the Technical Computer Center were used in part for the present calculations. This work was partially supported by the National Science Foundation, under Grant No. GK-1647.

REFERENCES

[1] Van HOVE, L., Phys. Rev. 95 (1954) 111.
[2] JANIK, J. A., KOWALSKA, A., Thermal Neutron Scattering (EGELSTAFF, P. A., Ed.) Academic Press, New York (1965).
[3] ZEMACH, A.C., GLAUBER, R.J., Phys. Rev. 101 (1956) 118, 129.
[4] McMURRY, H. L., Nucl. Sci. Engng 15 (1963) 429; McMURRY, H. L., GANNON, L.J., HESTIR, W. A., ibid. 15 (1963) 483.
[5] CARPENTER, J.M., J. chem. Phys. 46 (1966) 465.
[6] PACE, E. L., ASTON, J. G., J. Amer. chem. Soc. 70 (1948) 566.
[7] CARNEY, R., PIATROWSKY, E.A., MEISTER, A.G., BRAUN, J.H., CLEVELAND, F.F., J. mol. Spec. 7 (1961) 209.
[8] MOELWYN-HUGHES, E. A., Physical Chemistry, Pergamon Press, Inc., New York (1961).

NEUTRON SCATTERING FROM MOLECULAR NITROGEN *

J.A. YOUNG
GENERAL ATOMIC DIVISION,
GENERAL DYNAMICS CORPORATION,
SAN DIEGO, CALIFORNIA,
UNITED STATES OF AMERICA

Abstract

NEUTRON SCATTERING FROM MOLECULAR NITROGEN. The scattering of slow neutrons by molecular nitrogen has been calculated. The purpose of this calculation was to obtain a formulation which would allow relatively accurate results and which would be easy to evaluate numerically. The latter criterion rules out an exact calculation. The approach used takes into account all the rotational, vibrational, and translational motions of the N_2 molecules but ignores spin correlations. The procedure utilizes the mass-tensor or Krieger-Nelkin approximation for the rotational motions. The vibrations are included also, but neglect upscattering since the vibrational level at 0.3 eV is high compared with the thermal energy. The translational motion is included, assuming a free gas of N_2 molecules. Interference scattering between the two nitrogen atoms in a molecule has been included for the sake of completeness. The scattering laws (α, β) have been evaluated and from the computer code FLANGE, the total cross-section, angular cross-sections, and slowing-down power have been obtained for initial neutron energies, ranging up to 1 eV. The total cross-section agrees quite well with experiment. The angular cross-section shows a fair degree of anisotropy but no experimental data are known for this cross-section.

1. INTRODUCTION

In recent years much work has been done towards calculating slow neutron scattering cross-sections from atoms bound in condensed matter. In some cases this work was done with the aim of using neutrons as a probe to study the target material, and in others because the cross-section itself was wanted. The purpose of this report is to give an approximate expression for computing the slow neutron cross-section from N_2 gas at room temperature, or to be more precise, at temperatures below that where an appreciable number of molecules have their vibrational states thermally excited. For N_2, this is a large temperature range since the molecular moment of inertia is large, and the vibrational level at 0.3 eV is high.

We want to be able to calculate both differential and integral cross-sections, and to take into account the vibrational motion as well as the rotations and translations of the molecule. The calculation could be done in this case exactly as was done for the case of H_2;[1] however, that would involve excessive amounts of machine computation time; therefore an appropriate and reliable approximation is desirable. The method we have chosen to use is to extend the theory of Krieger and Nelkin[2] to include the vibrational transitions of the molecule with a more precise orientation average. This greatly extends the neutron energy range that

* This work was sponsored by the Air Force Weapons Laboratory, USA.

can be considered, and furthermore it allows the cross-section to become that for free atoms in the limit of high incident neutron energies where thermal and chemical effects have no influence.

2. FORMULATION AND RESULTS

The standard expression for the scattering cross-section from a molecular system is [3]

$$\frac{d^2\sigma}{d\epsilon d\Omega} = \sqrt{\frac{E}{E_o}}\,\frac{1}{2\pi}\sum_{\nu\nu'} a^2_{\nu\nu'}\int_{-\infty}^{\infty} dt\, e^{-i\epsilon t} \langle \chi_{\nu\nu'}(t)\rangle_T$$

where the sum over ν runs over the nuclei in the molecule, E is the final neutron energy, E_o the initial neutron energy, the $a^2_{\nu\nu'}$, are bound scattering lengths, ϵ is the energy transfer ($\epsilon = E - E_o$), and $\langle \chi_{\nu\nu'}(t)\rangle_T$ is a correlation function

$$\langle \chi_{\nu\nu'}(t)\rangle_T = \langle e^{i\vec{\kappa}\cdot\vec{r}'_\nu(t)}\, e^{-i\vec{\kappa}\cdot\vec{r}_{\nu'}(0)}\rangle_T$$

where $\vec{r}'_\nu(t)$ is the position vector of the νth nucleus at time t, and the subscript T indicates that a thermal average is to be taken. We make the assertion that the translational motion can be separated from the rotational and vibrational motion

$$\langle \chi_{\nu\nu'}(t)\rangle_T = \langle \chi_{\nu\nu'}(t)\rangle_T^{trans}\, \langle \chi_{\nu\nu'}(t)\rangle_T^{\substack{rot\\vib}}$$

Now we have the usual result

$$\langle \chi_{\nu\nu'}(t)\rangle_T^{trans} = e^{-\frac{\kappa^2}{4M}(it + Tt^2)}$$

where M is the atomic mass and T the temperature in energy units. This is the monatomic free-gas result for mass 2M.

At this point we wish to treat the rotations and vibrations of an individual molecule. We write

$$\langle \chi_{\nu\nu'}(t)\rangle_T^{\substack{rot\\vib}} = \langle \psi_i^{\substack{rot\\vib}} \left| e^{i\vec{\kappa}\cdot\vec{R}_\nu(t)}\, e^{-i\vec{\kappa}\cdot\vec{R}_{\nu'}(0)} \right| \psi_i^{\substack{rot\\vib}}\rangle_T$$

Let

$$\vec{R}_\nu(t) = \vec{r}_\nu(t) + \vec{u}_\nu(t)/2$$

where $\vec{r}_\nu(t)$ is the instantaneous position of the νth atom referred to the molecular center-of-mass if there were no vibrations, i.e. $|\vec{r}_\nu(t)| = a/2$ where a is the equilibrium separation distance between the two nitrogen atoms. The quantity $\vec{u}_\nu(t)/2$ is the small departure of each atom from its equilibrium position. The assumption is that the vibrations are harmonic. Upon making the above substitution we can write

$$<\chi_{\nu\nu'}(t)>_T^{\substack{rot\\vib}} = <\psi_i^{rot.}\left| e^{i\vec{\varkappa}\cdot\vec{r}_\nu(t)} e^{-i\vec{\varkappa}\cdot\vec{r}_{\nu'}(0)}\right|\psi_i^{rot}>_T$$

$$\cdot<\psi_i^{vib}\left| e^{i\vec{\varkappa}\cdot\vec{u}_\nu(t)/2} e^{-i\vec{\varkappa}\cdot\vec{u}_{\nu'}(0)/2}\right|\psi_i^{vib}>$$

since only the rotational motion is thermally excited.

To evaluate the vibrational correlation function we have to evaluate

$$<0|e^{i\vec{\varkappa}\cdot\vec{u}_\nu(t)/2} e^{-i\vec{\varkappa}\cdot\vec{u}_{\nu'}(0)/2}|0>$$

where $\vec{u}_1 = -\vec{u}_2$ since we have a linear molecule. We expand $\vec{u}$ in normal modes in the following way

$$u(t) = \frac{i}{(M\omega)^{1/2}}\left[b e^{-i\omega t} - b^\dagger e^{i\omega t}\right]$$

where $u(t) = |\vec{u}(t)|$ and $\hbar\omega$ is the energy of the variation quanta. (Hereafter we set $\hbar = 1$.) If we let the polar angle between $\vec{\varkappa}$ and $\vec{r}_\nu$ be ϑ, then

$$\frac{\vec{\varkappa}\cdot\vec{u}_\nu(t)}{2} = \frac{\varkappa\mu i}{2(M\omega)^{1/2}}\left[b e^{-i\omega t} - b^\dagger e^{i\omega t}\right]$$

where $\mu = \cos\vartheta$. Now b and b^+ are the boson annihilation and creation operators respectively, and $[b, b^+] = 1$.

First consider the "self" terms ($\nu = \nu'$).

$$e^{i\varkappa\mu u(t)/2} e^{-i\varkappa\mu u(0)/2} = \exp\left\{-\frac{\varkappa\mu}{2\sqrt{M\omega}^{1/2}}\left[b\left(e^{-i\omega t}-1\right) - b^{\dagger}\left(e^{i\omega t}-1\right)\right]\right\}$$

$$\cdot \exp\left\{-\frac{\varkappa^2\mu^2}{8M\omega}\left[\left(b\,e^{-i\omega t} - b^{\dagger}\,e^{i\omega t}\right),\ b-b^{\dagger}\right]\right\}$$

where we have used

$$e^{A}e^{B} = e^{A+B}\,e^{\frac{1}{2}[A,B]}$$

Continuing,

$$e^{i\varkappa\mu u(t)/2}\ e^{-i\varkappa\mu u(o)/2} = \exp\left(\frac{-\varkappa^2\mu^2}{4M\omega}\left(1 - e^{-i\omega t}\right)\right)$$

$$\cdot \exp\left\{\frac{\varkappa\mu b^{\dagger}}{2(M\omega)^{1/2}}\left(e^{i\omega t}-1\right)\right\}\ \exp\left\{\frac{-\varkappa\mu b}{2(M\omega)^{1/2}}\left(e^{-i\omega t}-1\right)\right\}$$

Thus

$$\langle 0|e^{i\vec{\varkappa}\cdot\vec{u}(t)/2}\ e^{-i\vec{\varkappa}\cdot\vec{u}(o)/2}|0\rangle = e^{\frac{-\varkappa^2\mu^2}{4M\omega}\left(1-e^{-i\omega t}\right)}$$

since the annihilation operator operating on the vacuum state gives zero. This expression can be rewritten in the following form:

$$\langle 0|e^{i\vec{\varkappa}\cdot\vec{u}(t)/2}\ e^{-i\vec{\varkappa}\cdot\vec{u}(o)/2}|0\rangle = e^{\frac{-\varkappa^2\mu^2}{4M\omega}}\sum_{n=0}^{\infty}\frac{1}{n!}\left(\frac{\varkappa^2\mu^2}{4M\omega}\right)^n e^{-in\omega t}$$

If now we consider $\nu \neq \nu'$, we have

$$\langle 0|e^{i\varkappa\mu u(t)/2}\ e^{i\varkappa\mu u(o)/2}|0\rangle = e^{\frac{-\varkappa^2\mu^2}{4M\omega}}\sum_{n=0}^{\infty}\frac{(-1)^n}{n!}\left(\frac{\varkappa^2\mu^2}{4M\omega}\right)^n e^{-in\omega t}$$

At this point we use the results of Krieger and Nelkin[2] for the rotational motion, which in effect is the Sachs-Teller mass tensor con-

cept, and this approximation is expected to be valid whenever the incident neutron energy is large compared to the rotational level spacing. The derivation will not be repeated here, so we simply state the result

$$<\chi^{(t)}_{\nu\nu'}>^{rot}_{T} = \exp\left\{i\vec{\varkappa}\cdot(\vec{r}_{\nu}(o) - \vec{r}_{\nu'}(o)\right\} \exp\left\{-\frac{1}{2}\left(\Sigma_{\alpha\beta}\varkappa_{\alpha} R^{\nu\nu}_{\alpha\beta}\varkappa_{\beta}\right)(it + Tt^2)\right\}$$

where the tensor $R_{\alpha\beta}$ is given by

$$R_{\alpha\beta} = \sum_{\gamma,\epsilon} B^{\dagger}_{\alpha\gamma} I^{-1}_{\gamma\epsilon} B_{\epsilon\beta}$$

and

$$B = \begin{pmatrix} o & -z & y \\ z & o & -x \\ -y & x & o \end{pmatrix}$$

x, y, z are the components of $\vec{r}_{\nu}(0)$, also I^{-1} is the inverse moment of inertia tensor which in this case is defined as

$$I^{-1} = \frac{2}{Ma^2}\begin{pmatrix} 1 & 0 & 0 \\ 0 & 1 & 0 \\ 0 & 0 & 0 \end{pmatrix}$$

We find easily then that

$$\sum_{\alpha\beta}\varkappa_{\alpha} R^{\nu\nu}_{\alpha\beta}\varkappa_{\beta} = \frac{\varkappa^2}{2M}(1-\mu^2)$$

so for the rotations the correlation function can be written as

$$<\chi^{(t)}_{\nu\nu'}>^{rot}_{T} = \exp\left\{i\vec{\varkappa}\cdot(\vec{r}_{\nu}(o) - \vec{r}_{\nu'}(o)\right\} \exp\left\{-\frac{\varkappa^2}{4M}(1-\mu^2)(it + Tt^2)\right\}$$

The total correlation function becomes for ($\nu = \nu'$)

$$<\chi^{(t)}_{\nu\nu}>_{T} = e^{\frac{-\varkappa^2\mu^2}{4M\omega}} \exp\left\{-\frac{\varkappa^2}{4M}(2-\mu^2)(it + Tt^2)\right\} \sum_{n=0}^{\infty}\frac{1}{n!}\left(\frac{\varkappa^2\mu^2}{4M\omega}\right)^n e^{-in\omega t}$$

and for $\nu \neq \nu'$ the result is

$$\langle X_{\nu\nu'}(t)\rangle_T = e^{i\vec{\varkappa}\cdot(\vec{r}_\nu(o) - \vec{r}_{\nu'}(o))}\, e^{\frac{-\varkappa^2\mu^2}{4M\omega}} \exp\left\{-\frac{\varkappa^2}{4M}(2-\mu^2)(it + Tt^2)\right\}$$

$$\cdot \sum_{n=0}^{\infty} \frac{(-1)^n}{n!}\left(\frac{\varkappa^2\mu^2}{4M\omega}\right)^n e^{-in\omega t}$$

Next we observe that if $\nu = \nu'$

$$a_{\nu\nu'} = \frac{1}{4\pi}(\sigma_{coh} + \sigma_{incoh})$$

and if $\nu \neq \nu'$

$$a_{\nu\nu'} = \frac{1}{4\pi}\sigma_{coh}$$

where σ_{coh} is the bound coherent cross-section, and σ_{incoh} is the bound incoherent cross-section. The cross-section per atom for "self" scattering is then given by

$$\frac{d^2\sigma}{d\epsilon\, d\Omega} = \frac{(\sigma_{coh} + \sigma_{incoh})}{8\pi^2}\sqrt{\frac{E}{E_o}} \int_{-\infty}^{\infty} dt\, e^{-i\epsilon t} \int_0^1 d\mu\, e^{\frac{-\varkappa^2\mu^2}{4M\omega}}$$

$$\cdot \sum_{n=0}^{\infty} \frac{1}{n!}\left(\frac{\varkappa^2\mu^2}{4M\omega}\right)^n \exp\left\{\frac{-\varkappa^2}{4M}(2-\mu^2)(it + Tt^2) - in\omega t\right\}$$

where we have included an average over molecular orientations.

Note that for high neutron energies ($\gtrsim$1.0 eV) or short collision times t, the cross-section can be simplified to (putting μ^2 equal to its average value 1/3)

$$\frac{d^2\sigma}{d\epsilon\, d\Omega} = \frac{\sigma_{bound}}{8\pi^2}\sqrt{\frac{E}{E_o}} \int_{-\infty}^{\infty} dt\, e^{-i\epsilon t}\, e^{-i\frac{\varkappa^2}{2M}t}$$

which gives the free atom cross-section in this classical limit. The interference scattering has no such classical limit since it is a purely

quantum effect. At high energies it tends to wash out similar to a diffraction pattern disappearing with decreasing wave length.

The cross-section per atom for interference scattering is then given by

$$\frac{d^2\sigma}{d\epsilon d\Omega} = \frac{\sigma_{coh}}{8\pi^2}\sqrt{\frac{E}{E_o}}\int_{-\infty}^{\infty} dt\, e^{-i\epsilon t}\int_0^1 d\mu\, e^{-\varkappa^2\mu^2/4M\omega}$$

$$\cdot\cos(\varkappa a\mu/2)\sum_{n=0}^{\infty}\frac{(-1)^n}{n!}\left(\frac{\varkappa^2\mu^2}{4M\omega}\right)^n \exp\left\{\frac{-\varkappa^2}{4M}(2-\mu^2)(it + Tt^2) - in\omega t\right\}$$

The integrals over time t can be readily performed

$$\frac{d^2\sigma}{d\epsilon d\Omega} = \left(\frac{\sigma_{coh}+\sigma_{incoh}}{4\pi}\right)\sqrt{\frac{E}{E_o}}\int_0^1 d\mu\,\frac{e^{\frac{-\varkappa^2\mu^2}{4M\omega}}}{\sqrt{\frac{\pi\varkappa^2 T}{M}(2-\mu^2)}}$$

$$\cdot\sum_{n=0}^{\infty}\frac{1}{n!}\left(\frac{\varkappa^2\mu^2}{4M\omega}\right)^n e^{\frac{-(\epsilon+n\omega+\varkappa^2(2-\mu^2)/4M)^2}{T\varkappa^2(2-\mu^2)/M}}$$

for the "self" terms, and

$$\frac{d^2\sigma}{d\epsilon d\Omega} = \frac{\sigma_{coh}}{4\pi}\sqrt{\frac{E}{E_o}}\int_0^1 d\mu\,\frac{e^{\frac{-\varkappa^2\mu^2}{4M\omega}}}{\sqrt{\frac{\pi\varkappa^2 T}{M}(2-\mu^2)}}\cos\left(\frac{\varkappa a\mu}{2}\right)$$

$$\cdot\sum_{n=0}\frac{(-1)^n}{n!}\left(\frac{\varkappa^2\mu^2}{4M\omega}\right)^n e^{\frac{-(\epsilon+n\omega+\varkappa^2(2-\mu^2)/4M)^2}{T\varkappa^2(2-\mu^2)/M}}$$

for the interference terms.

As stated the interference terms are completely quantum mechanical and will not contribute significantly to the cross-section at high incident neutron energies ($\gtrsim$ 0.1 eV). Thus we make the approximation

of neglecting interference scattering for the numerical computations, with the idea that they can be included at a later stage if desired.

The double-differential "self" scattering cross-section per unit energy and solid angle, can be written in the following form:

$$\frac{d^2\sigma}{d\epsilon d\Omega} = \frac{\sigma_{coh}+\sigma_{incoh}}{4\pi T}\sqrt{\frac{E}{E_o}}\int_0^1 d\mu \frac{e^{\frac{-T\alpha\mu^2}{2\omega}}}{\sqrt{2\pi\alpha(2-\mu^2)}} \cdot$$

$$\cdot \sum_{n=0} \frac{1}{n!}\left(\frac{T\alpha\mu^2}{2\omega}\right)^n \exp\left\{\frac{-(\beta+n\omega/T+\alpha(2-\mu^2)/2)}{2\alpha(2-\mu^2)}\right\}$$

where $\alpha = \kappa^2/2MT$, and $\beta = \epsilon/T$. Note that aside from kinematical factors the cross-section depends only upon α and β the momentum and energy transfer. The above expression has been evaluated on the UNIVAC 1108 for room temperature (T = 0.0253 eV) by means of the machine program NITE. The integral cross-sections such as $d\sigma/dE$ and σ_T have been computed by integrating the formula for the angular and energy scattering over scattering angle and final energy. This has been done by using the machine program FLANGE. The total cross-section (including absorption) has been compared with the experimental curve found in BNL 325, and this comparison is shown in Fig. 1. The agreement is seen to be quite

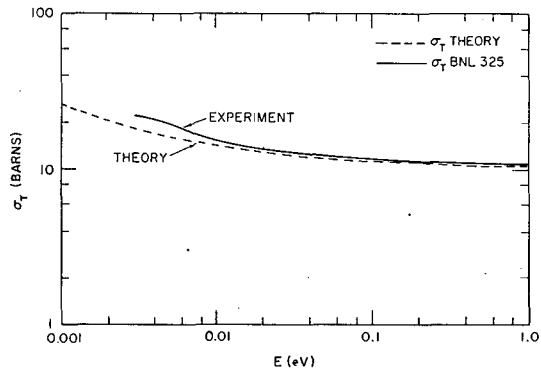

FIG. 1. Comparison of theory and experiment for the total cross-section of nitrogen at room temperature

good, with the discrepancy at low neutron energies being undoubtedly due to the absence of interference terms. The curves indicate, however, that the results should be quite adequate to compute neutron spectra in nitrogen gas.

REFERENCES

1. Young, James A., and Koppel, J. U., Phys. Rev. 134 A603 (1964).

2. Krieger, T.J., and Nelkin, M., Phys. Rev. 106 290 (1957).

3. Zemach, A.C., and Glauber, R.J., Phys. Rev. 101 118 (1956).

MULTIPLE SCATTERING IN NEUTRON DOUBLE-DIFFERENTIAL CROSS-SECTION MEASUREMENTS*

E. L. SLAGGIE
GENERAL ATOMIC DIVISION,
GENERAL DYNAMICS CORPORATION,
SAN DIEGO, CALIFORNIA,
UNITED STATES OF AMERICA

Abstract

MULTIPLE SCATTERING IN NEUTRON DOUBLE-DIFFERENTIAL CROSS-SECTION MEASUREMENTS. Calculations have been performed of multiple scattering corrections for several important experimental measurements of double-differential neutron scattering by hydrogenous materials, most notably room-temperature water. The calculations were carried out by the program MUSE, which solves the integral transport equation numerically to obtain the scattered neutron fluxes for single and multiple (up to four) collisions in a slab sample, using a theoretical kernel as input. In many cases these corrections turn out to be large and also quite sensitive to the theoretical model. Such results emphasize the fact that a quantitative treatment of multiple scattering is an absolutely essential step in the interpretation of double-differential data, but is not necessarily a straightforward and unique procedure.

To help clarify this situation we have investigated and compared ways of treating multiple scattering in double-differential experiments. Two methods of correcting for multiple scattering are considered. These are: (1) multiplying the data by a factor which is essentially the theoretically computed ratio of single-scattering to total-scattering; and (2) subtracting from the observed scattered flux a theoretically computed multi-collision flux. These correction methods are equivalent and the corrected data are consistent with the theoretical double-differential cross-sections only under stringent conditions relating the theoretical model to the experiment. When these conditions are not satisfied it is still sometimes possible to find circumstances which strongly favour the use of one method over the other. However, there is a possibility that large uncertainties and ambiguities will arise in corrections made by either method, primarily because of model sensitivity. Thus it is not always feasible to present experimental results in the form of corrected data. Instead, the uncorrected data should be used to check theoretical models by direct comparison of the theoretically calculated and observed scattered fluxes.

1. INTRODUCTION

Correcting double-differential data for multiple scattering is an exceedingly complicated problem. Basically one would like to find equations describing in terms of two-body scattering amplitudes the scattering centers. The equations must then somehow be inverted so that the two-body amplitudes are expressed in terms of total scattered fluxes, which are the measured quantities. Apart from the difficulty of inverting the equations, it is clear that even in principle this program cannot be performed for an experiment which covers only a restricted range of energy and momentum transfers. A theoretical model is thus needed to extract from observed scattered fluxes the single-collision contribution, from which cross-sections can be directly obtained. The fundamental dilemma is that reliable corrections are therefore difficult to obtain when they are most needed — in the case of scatterers for which the theory is not yet com-

* This work was sponsored by the United States Atomic Energy Commission.

plete. Such a scatterer is room-temperature water; therefore it is of special interest to apply to it methods which have been developed for making multiple scattering corrections in double-differential experiments. The object of such a study is to determine the importance of multiple scattering in typical measurements and to estimate the accuracy of the corrections using the best theoretical models available.

It has already been established[1] that in several important cases the corrections to water data are large (factors smaller than .6 are not uncommon) and very sensitive to the theoretical model. A further uncertainty is introduced by the existence of different and generally nonequivalent correction methods. The choice of correction methods depends both on characteristics of the theoretical model and on the condition of the experimental data with respect to error sources not directly associated with multiple scattering. While some guidelines have been given[1] for choosing the correction method, in many circumstances the choice is not clear and the accuracy of the corrected results is difficult to determine.

In this paper we wish to illustrate the correction methods and examine their accuracy in a realistic case for which it is nevertheless possible to avoid complications introduced by uncertainties in the data and lack of accurate knowledge of the true cross-sections. To do this we generate fictitious "data" for a hypothetical water double-differential measurement, using the McMurry-Russell[2] (MR) water model as input to the code MUSE,[3] which then calculates the scattered fluxes for different orders of collision (up to four collisions) in a slab sample. These calculated fluxes represent the data that would have been observed in an idealized experiment in which the only source of error is multiple scattering (assuming for the sake of the illustration, of course, that the water scattering is accurately given by the MR model). We then correct the "data", using corrections based on "Haywood II kernel", a model developed by Koppel.[4] This model uses a continuous frequency distribution obtained from experimental data by Haywood, using extrapolation techniques.[5] The "corrected data" can be compared with the "right answer", i.e., the MR model double-differential cross-section (ddc), as a way of studying the model sensitivity and the accuracy of the correction methods. This hypothetical case is in fact a realistic simulation of the actual problems involved in correcting water ddc data, since it is not unlikely that the discrepancies between the Haywood II and the MR model scattering laws are comparable to the discrepancies between the predictions of either model and the true water scattering law. The MR model and the Haywood II kernel are typical of the most advanced theoretical water scattering laws which have been developed. Nevertheless, uncertainties are associated with each model,[1] so that it is difficult to establish exactly how good these models are for general use in multiple scattering calculations. Thus until improved theoretical models become available, it is possible that actual corrected water data will sometimes contain inaccuracies comparable with those present in our hypothetical example.

After the discussion and example of correction methods, the usefulness of varying sample thickness as an experimental technique for estimating the importance of multiple scattering is discussed. An example of multiple scattering corrections for double-differential scattering by zirconium hydride is also given.

2. MULTIPLE SCATTERING CORRECTION METHODS

In this section we review some of the material given in Ref. 1 concerning multiple scattering in slab samples when interference between scattering centers can be neglected (a good approximation in hydrogenous material). In such cases the motion of neutrons through the sample can be described classically in terms of neutron fluxes (actually, flux densities) $\varphi(\vec{r}, E, \vec{\Omega})$ where $\varphi(\vec{r}, E, \vec{\Omega})dAdEd\Omega$ denotes the number of neutrons in the energy range E to E + dE at a point $\vec{r}$ in the sample that cross, per second, an area surface element of dA oriented perpendicular to $\vec{\Omega}$ at $\vec{r}$, while moving along a direction lying in the element of solid angle $d\Omega$ about $\vec{\Omega}$. The integral transport equation for φ can be solved by iteration in terms of orders of scattering, whereby φ_m, the flux of neutrons which have undergone m collisions, is found in terms of φ_{m-1}. The φ_m's (for $m \leq 4$) leaving a slab sample exposed to a monoenergetic and monodirectional unit incident flux are computed by the program MUSE,[3] using a theoretical kernel for the scatterer as input. For such a case, the double-differential cross-section (ddc) is directly related to the transmitted first collision flux as follows:

$$N_o\sigma(E_1, E_2, \vec{\Omega}_1 \cdot \vec{\Omega}_2) = (\mu_2/t)A(1,2)\varphi_1(t, E_2, \vec{\Omega}_2) \tag{1a}$$

where N_o denotes the number of scattering centers per unit volume; the terms E_1 and E_2 are the incident and final neutron energies; $\vec{\Omega}_1$ and $\vec{\Omega}_2$ denote unit vectors in the direction of neutron motion before and after the collision, respectively, so $\vec{\Omega}_1 \cdot \vec{\Omega}_2$ is the cosine of the scattering angle, μ_2 is the cosine of the angle between the outgoing neutron direction and the slab normal, and t is the slab thickness. For infinite slab geometry the φ_m's are functions only of z, where z is a coordinate chosen normal to the slab. Thus the transmitted first collision flux can be denoted by $\varphi_1(t, E_2, \vec{\Omega}_2)$. Final $A(1,2)$ represents an attenuation correction given by the equation

$$A(1,2) = (x_2 - x_1)[\exp(-x_1) - \exp(-x_2)]^{-1} \tag{2}$$

where $x_1 \equiv t N_o \sigma_T(E_i)/\mu_i$, where $\sigma_T(E_i)$ is the total cross-section for neutrons of energy E_i, and μ_i denotes the cosine of the angle between the slab normal and the incoming (i=1) or outgoing (i=2) neutrons.

The notation is somewhat simplified by introducing "response functions", $R_n(E, \vec{\Omega})$, defined as follows:

$$R_n(E, \vec{\Omega}) \equiv (\mu/t)\, \varphi_n(t, E, \vec{\Omega}) \tag{3}$$

where μ is the cosine of the angle between the slab normal and the unit vector $\vec{\Omega}$. Then Eq. (1a) can be written as

$$N_o\sigma(E_1, E_2, \vec{\Omega}_1 \cdot \vec{\Omega}_2) = A(1,2)R_1(E_2, \vec{\Omega}_2) \tag{1b}$$

In an experiment the quantity measured at the detector is the flux for all orders of scattering, which can be described as a "total experimental response" $R_x(E_2, \vec{\Omega}_2)$. A single-collision "corrected response" can be obtained from R_x either by multiplying R_x by a theoretically-computed ratio, $R_1\left(\sum_{n=1}^{\infty} R_n\right)^{-1}$ or by subtracting from R_x a theoretically-computed multiple scattering response, $\sum_{n=2}^{\infty} R_n$. These correction procedures as applied to slab samples can be conveniently formulated as follows:

a. Factor Method

The factor-corrected experimental ddc, $\sigma_{xF}(E_1, E_2, \mu_0)$, is related to the total experimental response by the equation,

$$\sigma_{xF}(E_1, E_2, \mu_0) \equiv C(1,2)\, R_x\,(E_2, \vec{\Omega}_2)\, N_o^{-1} \tag{4}$$

The correction factor C(1, 2) is given by

$$C(1,2) = N_o \sigma(E_1, E_2, \mu_0) \left[\sum_{n=1}^{\infty} R_n(E_2, \vec{\Omega}_2)\right]^{-1} \tag{5}$$

where $\mu_0 \equiv \vec{\Omega}_1 \cdot \vec{\Omega}_2$ and $\sigma(E_1, E_2, \mu_0)$ is the theoretical ddc.

b. Subtraction Method

The subtraction-corrected experimental ddc, $\sigma_{xS}(E_1, E_2, \mu_0)$, is related to the total experimental response by the equation,

$$\sigma_{xS}(E_1, E_2, \mu_0) \equiv A(1,2)\, N_o^{-1} \left[R_x(E_2, \vec{\Omega}_2) - \sum_{n=2}^{\infty} R_n(E_2, \vec{\Omega}_2)\right] \tag{6}$$

The theoretical responses R_n in Eqs. (5) and (6) can be obtained from the code MUSE[3] for $n \leq 4$. In most cases of interest the sums in Eqs. (5) and (6) are well approximated by omitting responses of order higher than fourth.[1]

For theory and experiment to be in agreement, the sum of theoretically calculated responses R_n should equal R_x (assuming that the data have been corrected for effects other than multiple scattering):

$$R_x(E_2, \vec{\Omega}_2) = \sum_{n=1}^{\infty} R_n(E_2, \vec{\Omega}_2) \text{ (theoretical)} \tag{7}$$

It is easily verified that when Eq. (7) is satisfied the factor and subtraction methods give identical corrected ddc's which equal the theoretical ddc. Failure to satisfy Eq. (7) indicates that something is amiss with the theory or at least with the way it is being applied to the experiment in question. Also the factor and subtraction methods in general then no longer give the same results, nor do the corrected ddc's equal the theoretical ddc's. In practical data correction problems this is the situation most likely to arise.

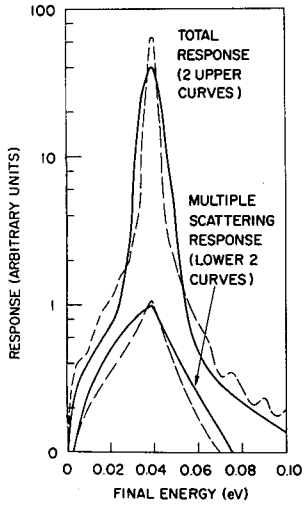

FIG. 1. Calculated total and multiple scattering responses for an idealized H_2O measurement using a slab sample of thickness 0.01 in., incident energy 0.039 eV, scattering angle 25.6°.

——— Based on Haywood II kernel
– – – Based on MR model

3. HYPOTHETICAL EXAMPLES OF MULTIPLE SCATTERING CORRECTION

We consider double-differential scattering of .039-eV neutrons by a slab sample of room-temperature water .01 inches thick, corresponding to a transmission of about .9 for neutrons incident at an angle of 45 degrees. This experimental setup was used by Brugger[2] in making the water double-differential measurements on which the MR model is based. Figure 1 shows as a function of final energy the total response $\left(\sum_{n=1}^{4} R_n\right)$ and multiple scattering response $\left(\sum_{n=2}^{4} R_n\right)$ calculated by MUSE[3] for a scattering angle 25.6 degrees (outgoing neutron direction at an angle 19.4 degrees from the slab normal), assuming a maximum of four collisions. The solid curves are based on the Haywood II kernel[4] while the dotted curves are based on the MR model. The narrower quasielastic peak for the MR results reflects the use in that model of heavy aggregates of water molecules[2] in contrast to the unphysical assumption of freely-recoiling water molecules made in constructing the Haywood II kernel. More structure is seen in the MR results than in the Haywood II curve, but it is important to note that this structure appears only in the first collision response, as is evi-

dent from the absence of structure in the multiple scattering response. This model insensitivity of the multiple scattering response is an important advantage of the subtraction method of correction. By contrast, the factor corrections are quite sensitive to the theoretical model, as is seen in Fig. 2, in which C(1, 2) defined by Eq. (5) is plotted for both models.

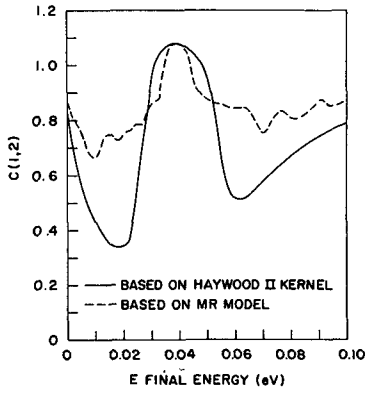

FIG. 2. Multiple scattering factor corrections for an idealized H_2O measurement using a slab sample of thickness 0.01 in. incident energy 0.039 eV, scattering angle 25.6°. Corrections for multiple scattering by a 10-mil H_2O sample.

E_1 = 0.039 eV
θ_1 = 45°; θ_2 = 19.4°; $\theta_{scattering}$ = 25.6°

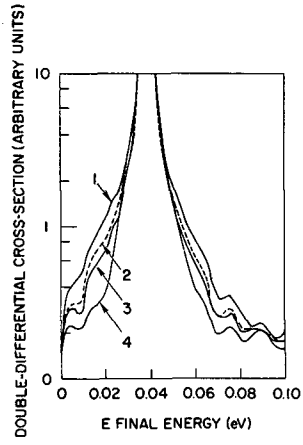

FIG. 3. MR model total response treated as hypothetical ddc data and "corrected" for multiple scattering using multiple scattering results based on the Haywood II kernel.

1 MR model total response, replotted from Fig. 1
2 Subtraction-corrected MR model 'data'
3 MR model ddc, the 'right answer'
4 Factor-corrected MR model 'data'

In order to exclude from the study of correction methods any uncertainties introduced by differences between an actual experiment and the idealized experiment used in MUSE computations, we shall treat the total response based on the MR model as "experimental data", i.e., as R_x in Eqs. (4) and (6). We then correct this fictitious data using Haywood II results. Figure 3 compares the factor- and subtraction-corrected "data" (Curves 4 and 2, respectively) with the actual MR-model ddc (Curve 3) and with the "uncorrected" MR-model total response replotted from Fig. 1 (Curve 1). (The curves are essentially in agreement in the peak around .039 eV, not plotted. The ddc is scaled by N_o, so that units are those of responses.) The difference between Curves 3 and 1 is substantial, indicating that according to the MR model multiple scattering cannot be assumed negligible (although this assumption was in fact made in constructing the MR model by

fitting Brugger's uncorrected data[2]). However, it is seen that correction by the factor method, using Haywood II results, leads to worse agreement with the actual ddc than no correction at all. The subtraction-corrected "data" (Curve 2) on the other hand represents a considerable improvement over simply neglecting multiple scattering.

For experiments involving higher incident energies (≥ .15 eV) calculations of total responses show the MR model and Haywood II results to be in better agreement than in the case we have considered here. The corrections as computed by the different models are in better agreement and for the most part do not exceed thirty percent for samples with fairly high transmissions. As in our example, the subtraction method in principle gives better results, but in practice may be difficult to apply.

4. FACTOR CORRECTIONS AS FUNCTIONS OF SAMPLE THICKNESS

In practice an experimental way of testing data for the presence of multiple scattering is to vary the sample thickness. Any significant sensitivity of the measured cross-sections to sample thickness is evidence that multiple scattering is important. It is not so clear, however, that lack of such sensitivity indicates the absence of multiple scattering, though this argument is not infrequently used. The possibility exists that double-differential multiple scattering corrections can be significant and also relatively insensitive to sample thickness. We can see this by writing the factor correction C(1, 2) in the form

$$C(1,2) = A(1,2)\left[1 + \sum_{n=2}^{\infty} R_n(E_2,\vec{\Omega}_2)/R_1(E_2,\vec{\Omega}_2)\right]^{-1} \qquad (8)$$

Increasing the thickness t increases the higher-order responses relative to R_1, tending to make C(1, 2) a smaller number. However, the attenuation factor A(1, 2) grows larger with increasing thickness, tending to increase C(1, 2). Thus a competition exists between multiple scattering as a mechanism for augmenting the scattered flux at a particular final angle and energy and multiple scattering as a mechanism for reducing this flux through attenuation in the sample. For very small t, A(1, 2) increases linearly with t, while in the special case of isotropic elastic scatterers the ratio R_2/R_1 goes as $t\ln t$ [6]. Thus C(1, 2) for a very thin sample becomes smaller when the thickness is increased. As the thickness is further increased, however, C(1, 2) rises back toward unity and must for thick samples, particularly when absorption is present, become large to correct for attenuation. Therefore C(1, 2) has a minimum as a function of t, in the vicinity of which C(1, 2) will change slowly with varying thickness.

For complicated double-differential scattering like that from water the behavior of C(1, 2) must be investigated numerically to determine the range and degree of insensitivity to thickness. We have studied a typical upscattering measurement, in which .0052 eV neutrons are incident normally on a slab sample. Figure 4 shows factor corrections calculated for a scattering angle of thirty degrees for three different thicknesses: .02 cm.

.05 cm, and .12 cm. The MR model was used. This experimental setup resembles that of Larsson, et al.[7] who noticed that the ratio of the total scattering fluxes observed with a .05 cm sample to those with a .02 cm sample was very roughly 2.5. While Larsson's reported results are consistent with the absence of multiple scattering, they are also consistent to the same degree of precision with the correction factors of Fig. 4, which show above .04 eV less than a 15 percent reduction when the thickness is varied from .02 cm to .05 cm. An even smaller change is observed on

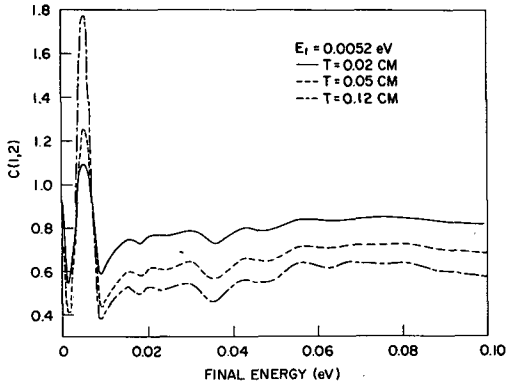

FIG. 4. Factor corrections for scattering by H_2O slab samples of varying thickness; incident energy 0.0052 eV, incident angle zero degrees; final angle 30°. Calculated based on MR model.

increasing the thickness to .12 cm, indicating that a minimum for C(1, 2) is being approached. (For thicknesses much greater than .12 cm the four-collision approximation used in MUSE[3] becomes inadequate; therefore this minimum cannot be calculated directly.) This example suggests that important corrections to the data will sometimes be overlooked if insensitivity to thickness is regarded as proof that multiple scattering is negligible.

5. MULTIPLE SCATTERING CORRECTIONS FOR ZIRCONIUM HYDRIDE MEASUREMENTS

The principal characteristic of double-differential scattering by ZrH_2 is that neutrons tend to gain or lose energy in amounts which are multiples of energies lying in a band centered roughly around .137 eV. A simple phenomenological frequency distribution consisting of a Debye spectrum with cutoff at .02 eV and a Gaussian of width .02 eV centered at .137 eV gives fair to good agreement with neutron data.[4, 8] It is possible to relate the shape of the frequency distribution to the lattice dynamics of ZrH_2, giving the model a quantitative physical basis.[9]

We have used a scattering kernel based on the lattice dynamical model as input to a MUSE calculation of factor corrections for .57 eV neutrons incident at 45 degrees on a .04 cm slab (transmission ~.9).[8] Results are shown in Fig. 5 for scattering through 25 degrees (final angle 20 degrees from the slab normal). These results are somewhat similar to those shown in Fig. 11 of Ref. 1 for water scattering corrections calculated using the Nelkin model.[10] The valleys between the peaks indi-

cate energy regions to which no single scattering is possible in this model. Some irregularity in the shape of the peaks comes from structure in the ddc as given by the lattice dynamical model.[9]

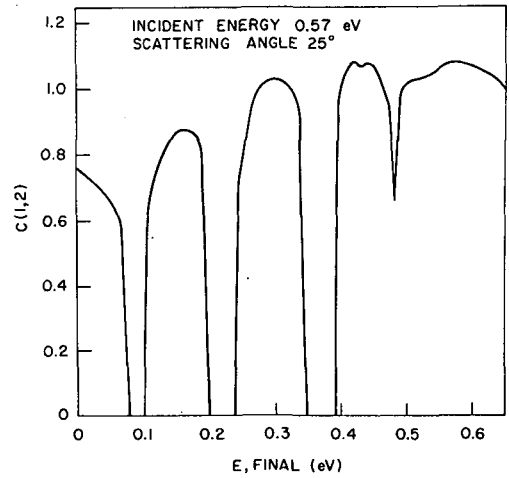

FIG. 5. Factor corrections for scattering of 0.570 eV neutrons by a ZrH_2 slab sample of thickness 0.04 cm. Incident angle 45°, final angle 20°, scattering angle 25°. Calculations based on a lattice dynamical model [9].

Calculations of total responses, not shown here, indicate that very little total scattering is to be expected in the "valleys" according to this model. However, it is simple to modify the model to provide for wider and even overlapping peaks,[9] should this be necessary to fit observed total responses when data become available.[11] In the regions of final energy in which the data are expected to be most significant, i.e. around the centers of the phonon peaks, the correction factors are seen to vary slowly and be close to unity, except for three-phonon scattering, which requires about a ten percent correction. In view of these results and considering the likelihood that the theoretical model is basically correct, it appears that multiple scattering is less important as a source of error in ZrH_2 double-differential measurements than in water measurements.

6. CONCLUSIONS

It has been seen in our example for water that unless the theoretical model leads to total responses substantially in agreement with the total experimental response, it is possible to make significant errors in multiple scattering corrections. The subtraction method of correction has, in principle, the advantage of reduced model sensitivity relative to the factor method. However in practical situations the presence of resolution broadening or experimental uncertainty can prevent use of the subtraction method.[1] Thus improved over-all precision of experimental data, in addition to improved theoretical models, particularly for water, is needed to make possible more accurate multiple scattering corrections. Theoretical studies are also needed to guide investigation of multiple scattering by experimental techniques, as is evident from the example of correction factor insensitivity to sample thickness. Because of ambiguity in experimental tests for multiple scattering, it is important that experimental designs

to minimize multiple scattering be subjected to careful theoretical analysis. However, the results of such an analysis may be very sensitive to the theoretical model used in the calculations, which are likely to be difficult if complicated geometries are involved. Thus it may sometimes be preferable to design an experiment so that the theoretical analysis can be made very precise, even though multiple scattering is not necessarily minimized. The experimental and calculated total responses can then be accurately compared, giving a good test of the theory, even when the data cannot be directly interpreted at cross-sections.

REFERENCES

[1] Slaggie, E. L., "Multiple Scattering in Double Differential Neutron Cross Section Measurements," General Atomic Report GA-7531 (1967). A condensed version of this report is to be published in Nuclear Science and Engineering.

[2] McMurry, H. L., Russell, G. J., and Brugger, R. M., Nucl. Sci. Eng. 25 248 (1966).

[3] Honeck, H. C., "MUSE, A Computer Code for Multiple Scattering Corrections," General Atomic Report GA-5968 (October 1, 1964).

[4] Koppel, J. U., "Neutron Scattering by Hydrogenous Moderators," USAEC Report GA-7055, General Atomic Division, General Dynamics Corporation, (March 22, 1966).

[5] Haywood, B. C., Journal of Nuclear Energy 21 249 (1967).

[6] Vineyard, G. H., Phys. Rev. 96 93 (1954).

[7] Larson, K. E., Holmryd, S., and Otnes, K., Inelastic Scattering of Neutrons in Solids and Liquids, IAEA, Vienna, (1960) 329.

[8] Pan, S. S., Moore, W. E., Yeater, M. L., Transactions of the American Nuclear Society 9 495 (1966).

[9] Slaggie, E. L., (to be published). See also Beyster, J. R., "Integral Neutron Thermalization Quarterly Progress Report for the period Ending March 31, 1967," USAEC Report GA-7898, General Atomic Division, General Dynamics Corporation (April 4, 1967).

[10] Nelkin, M., Phys. Rev. 119 741 (1960).

[11] Results for .57 eV were not shown in Ref. 8. Some preliminary results have appeared in the Linear Accelerator Progress Report for January 1966 through March 1966, Rensselaer Polytechnic Institute, Troy, New York.

DISCUSSION

W. GLÄSER: In your paper you mention that in the calculation of multiple scattering contributions you went up to the fourth collision term. Did you estimate the fourth collision contribution to the total scattered intensity?

E. L. SLAGGIE: Yes. The MUSE code calculates the collision fluxes for each separate collision and, in most of the cases we investigated, the fourth collision flux was about 10%, or less, of the third collision flux. I think that is a reasonable approximation.

W. GLÄSER: I should also like to comment on the difficulties involved in selecting a good model to start with. It seems to me that in cases where the extrapolation method is a good approximation it is advantageous to generate a generalized frequency distribution in an iterative procedure including multiple scattering corrections.

J. A. YOUNG: While such an iterative procedure may converge, there would appear to be no guarantee that it will converge to the correct answer.

D. T. GOLDMAN: Does Dr. Slaggie conclude that all double-differential cross-sections are suspect?

E. L. SLAGGIE: No. Our calculations indicate that multiple scattering corrections are large and very model-sensitive, primarily for small scattering angles and small incident energies. Of course, to some extent the remaining data are also suspect unless, or until, they are examined quantitatively for multiple scattering effects.

R. G. FLUHARTY: I feel it should be stated, on the subject of multiple-scattering corrections, that the results reported look very good; they prove that considerable progress has been made and show great promise. It would now appear that these codes, which have been discussed before, can become available for general use.

The need for such correction is greatest on the edges of the elastic scattering peak; past interpretations in this region should be considered suspect, but elsewhere the uncertainty should be less. I believe that more effort should be devoted to experimental verification of the corrections based both on a model and on a computational procedure. Where large corrections are being made, the implied iterative procedures can be very misleading and some experimental check of predictions should be attempted.

J. R. BEYSTER: Mr. Fluharty's remarks prompt me to say that some experiments have been done to check the multiple scattering analysis. We have carried out experiments on H_2O, D_2O and $ZrH_{1.8}$, varying the sample thickness and the angle between the neutron beam and the sample. We measured the single-differential cross-section and corrected the data using the MUSE procedure. This seems to work even for very thick samples.

G. J. KIROUAC: We have also made multiple scattering corrections for our data using the MUSE code. Our data cover incident neutron energies above 0.1 eV. Using the Haywood kernel and the McMurry-Russell model, we observe a maximum difference of about 10% between the correction factors for scattering angles from 25° to 150°. This maximum occurs for the small angle.

E. L. SLAGGIE: Our calculations likewise show that at higher incident energies the corrections are less extreme and the different models give better agreement. Dr. Kirouac's observation illustrates the importance of careful selection of energies and scattering angles in order to minimize the effects of multiple scattering.

TEMPERATURE EFFECT ON NEUTRON SCATTERING KERNELS

L. FINKELSTEIN
ISRAEL ATOMIC ENERGY COMMISSION,
SOREQ NUCLEAR RESEARCH CENTER,
SOREQ, ISRAEL

Abstract

TEMPERATURE EFFECT ON NEUTRON SCATTERING KERNELS. An explicit form of the neutron scattering kernel is derived for the case of resonant cross-section, elastic or inelastic scattering and nuclear thermal motion. The expression obtained is a one-dimensional integral over the variable cross-section, and it is shown to be useful in analysing various situations of practical interest, when used in conjunction with tables of Laplace transforms. In particular, when the cross-section is expanded in Laguerre polynomials, the integral can be evaluated analytically.

1. Introduction

The neutron scattering kernel was investigated for thermal neutrons by Wigner and Wilkins [1], Zemach and Glauber [2], Smelov [3] and many others. In those studies the scattering cross-section could be assumed constant, and the collision - elastic. The present study is devoted mainly to resonant cross-sections and elastic or inelastic scattering, isotropic in the center-of-mass system. These are of importance in the slowing-down region of reactor theory.

2. Notation

In the presence of nuclear thermal motion, the neutron transport equation reads

$$\left(\bar{v}\cdot\frac{\partial}{\partial\bar{r}}+\frac{\partial}{\partial t}\right) n(\bar{r},\bar{v},t) = -\, n(\bar{r},\bar{v},t)\int d_3\bar{V}\ \Phi(\bar{V})\,|\bar{V}-\bar{v}|\cdot\mu_t\left(\tfrac{1}{2}m_o|\bar{V}-\bar{v}|^2\right)$$

$$+\int d_3\bar{v}'\ n(\bar{r},\bar{v}',t)\int d_3\bar{V}\ \Phi(\bar{V})\,|\bar{V}-\bar{v}'|\left\{P(V,\bar{v}'\to\bar{v},0)\ \mu_n(E)\right.$$

$$\left.+\int_0^E dE^*P(\bar{V},v'\to\underline{v},E^*)\ \mu_n(E,E^*)\right\}$$

The notation adopted is as follows:

$\bar{v}'$ and $\bar{v}$	- pre and post-collisional laboratory velocities of a neutron
$\Phi(\bar{V})\ d_3\bar{V}$	- fraction of nuclei with laboratory thermal velocities within $d_3\bar{V}$ about $\bar{V}$
$n(\bar{r},\bar{v},t)\ d_3\bar{r}\ d_3\bar{v}$	- (expected) number of neutrons within $d_3\bar{r}\ d_3\bar{v}$ at point $\bar{r}$, velocity $\bar{v}$ and time t
A	- nucleus-to-neutron mass ratio
m_o	- reduced mass

E	- pre-collisional total kinetic energy of a nucleus-neutron pair, measured in their center-of-mass system
E^*	- excitation energy of the residual nucleus, measured in the center-of-mass system (= excitation energy of the compound nucleus less binding energy of the neutron)
$\mu_t(E), \mu_n(E), \mu_n(E,E^*)$	- total, elastic and inelastic scattering collision cross-sections
$P(\bar{V},\bar{v}' \to \bar{v},E^*)d_3\bar{v}$	- probability, that as a result of a collision between a nucleus and a neutron, travelling respectively with initial velocities $\bar{V}$ and $\bar{v}'$, the neutron will emerge with final velocity within $d_3\bar{v}$ about $\bar{v}$, provided that the excitation energy of the residual nucleus is E^*

Though not shown explicitly, the possible dependence of Φ and μ on $\bar{r}$ and t is tacitly assumed.

The expression $\mu_t^D(\bar{v}) = \frac{1}{v}\int d_3\bar{V}\ \Phi(\bar{V})\,|\bar{V}-\bar{v}|\cdot\mu_t(\frac{1}{2}m_o|\bar{V}-\bar{v}|^2)$ is known as the Doppler broadened cross-section. The kernel of equation (1), namely

$$K(\bar{v}' \to \bar{v}) \equiv \int d_3\bar{V}\ \Phi(\bar{V})\,|\bar{V}-\bar{v}'|\left\{P(\bar{V},\bar{v}' \to \bar{v},0)\ \mu_n(E) + \int_0^E dE^* P(\bar{V},\bar{v}' \to \bar{v},E^*)\ \mu_n(E,E^*)\right\} \tag{2}$$

is called the neutron scattering kernel, and is the subject of our investigation. Splitting $K(\bar{v}' \to \bar{v})$ into its elastic and inelastic components we write

$$K_{el}(\bar{v}' \to \bar{v}) = \int d_3\bar{V}\ \Phi(\bar{V})\,|\bar{V}-\bar{v}'|\,P(\bar{V},\bar{v}' \to \bar{v},0)\ \mu_n(E)$$

$$K_{in}(\bar{v}' \to \bar{v}) = \int d_3\bar{V}\ dE^*\ \Phi(\bar{V})\,|\bar{V}-\bar{v}'|\,P(\bar{V},\bar{v}' \to \bar{v},E^*)\,\mu_n(E,E^*) \tag{3}$$

Figure 1 illustrates the geometrical dependence of the various velocities involved in a collision, as measured in the laboratory and center-of-mass systems.

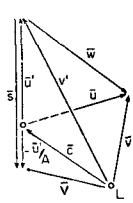

FIG. 1. Velocities involved in a collision.

Here

$$\bar{c} = \frac{1}{A+1}(A\bar{V}+\bar{v}'), \quad \bar{u}' = \bar{v}'-\bar{c}, \quad \bar{u} = \bar{v}-\bar{c} \tag{4}$$

are respectively the laboratory velocity of the nucleus-neutron center-of-mass, and pre-collisional and post-collisional neutron velocities, measured in the center-of-mass system.

$$\bar{s} = \bar{V}-\bar{v}' \quad \text{and} \quad \bar{w} = \bar{v}-\bar{v}' \tag{5}$$

are respectively the pre-collisional nucleus-neutron relative velocity, and the change of neutron velocity in a collision.

3. Transfer Function $P(\bar{V},\bar{v}' \rightarrow \bar{v},E^*)$

Consider a binary collision in the center-of-mass system. Since the total momentum in this system is zero, it follows that the velocity of the nucleus is $-\bar{u}'/A$ before collision, and $-\bar{u}/A$ after collision. With this in mind the equation of conservation of energy (with neglected relativistic effects) reads

$$\frac{m}{2}u'^2 + \frac{Am}{2}(u'/A)^2 = \frac{m}{2}u^2 + \frac{Am}{2}(u/A)^2 + E^*$$

where m is the neutron mass. This can be written as follows

$$u^2-u'^2 + \left(\frac{A}{A+1}g\right)^2 = 0 \text{ , where } g^2 = \frac{E^*}{m_o/2} \text{ and } m_o = \frac{A}{A+1}m \tag{6}$$

From Fig. 1 we see that (for given A) a collision is equally well specified by either triplet of vector parameters $(\bar{V},\bar{v}',\bar{v})$ or $(\bar{V},\bar{u}',\bar{u})$. As a result we may define

$$P_c(\bar{V},\bar{u}' \rightarrow \bar{u},E^*)\, d_3\bar{u} \equiv P(\bar{V},\bar{v}' \rightarrow \bar{v},E^*)\, d_3\bar{v} \tag{7}$$

Keeping $\bar{V}$ and $\bar{v}'$ constant we force $\bar{c}$ to remain constant. Varying now $\bar{v}$ we get, in view of $\bar{v} = \bar{c} + \bar{u}$,

$$d_3\bar{v} = d_3\bar{u} = d_2\bar{u}_o . u^2 du \tag{8}$$

Here $\bar{u}_o$ is a unit vector in the direction of $\bar{u}$, and $d_2\bar{u}_o$ is an elementary area described by $\bar{u}_o$ on a unit sphere.

It follows from (6) that the value of u is predetermined by the values of u' and $\frac{A}{A+1}g$, no matter what the direction of $\bar{u}_o$ is. That is to say, the event x , of a neutron's post-collisional speed being within du about u , is independent of the event y , that the direction of the neutron's post-collisional velocity is within $d_2\bar{u}_o$ about $\bar{u}_o$. Denoting the corresponding probabilities by $P_x . d(u^2)$ and $P_y . d_2\bar{u}_o$, we consequently have

$$P_c(\bar{V},\bar{u}' \rightarrow \bar{u},E^*) d_3\bar{u} = P_x d(u^2) . P_y d_2\bar{u}_o \tag{9}$$

Since $P_c d_3\bar{u}$, $P_y d_2\bar{u}_o$ and $P_x d(u^2)$ are probabilities, we get by integration over the corresponding full domains

$$\int P_c d_3\bar{u} = \int P_y d_2\bar{u}_o = \int P_x d(u^2) = 1 \tag{10}$$

Assuming that the scattering is isotropic in the center-of-mass system we get from (10)

$$P_y \cdot d_2\bar{u}_o = \frac{d_2\bar{u}_o}{4\pi} \tag{11}$$

Equation (6) in conjunction with the last equality of (10) implies

$$P_x d(u^2) = \delta\left[u^2 - u'^2 + \left(\frac{A}{A+1}\, g\right)^2\right] d(u^2) \tag{12}$$

where δ is the Dirac δ-function.

Collecting (7) to (12) we have

$$P(\bar{V},\bar{v}' \to \bar{v},E^*)\, d_2\bar{u}_o \cdot u^2 du = \delta\left[u^2 - u'^2 + \left(\frac{A}{A+1}\, g\right)^2\right] d(u^2) \cdot \frac{d_2\bar{u}_o}{4\pi}$$

or, after cancellation

$$P(\bar{V},\bar{v}' \to \bar{v},E^*) = \frac{1}{2\pi u}\, \delta\left[u^2 - u'^2 + \left(\frac{A}{A+1}\, g\right)^2\right] \tag{13}$$

Here $\bar{u}$ and $\bar{u}'$ are functions of $\bar{V}$, $\bar{v}'$ and $\bar{v}$ as given by (4). $\bar{V}$, $\bar{v}'$, $\bar{v}$ and E^* in (13) are arbitrary.

4. Explicit form of the scattering kernel

Elastic scattering is isotropic in the center-of-mass system if E is less than several MeV for light nuclei, and less than 100 keV for heavy nuclei. Taking into account that in the process of moderation by heavy nuclei, elastic scattering is less important than the inelastic one, and since the latter is isotropic in the center-of-mass system up to about 10 MeV, we may assume, for the sake of applications in reactor theory, that the angular distribution of the neutrons emerging from any scattering collision is isotropic in the center-of-mass system.

With the above motivation we insert (13) into (3), and assuming further Maxwellian $\Phi(\bar{V})$ we obtain

$$K_{in}(\bar{v}' \to \bar{v}) = \frac{(\beta/\pi)^{3/2}}{2\pi} \int d_3\bar{V}\, dE^*\, e^{-\beta V^2} \frac{|\bar{V}-\bar{v}'|}{\sqrt{u'^2 - \left(\frac{A}{A+1}\, g\right)^2}}\, \mu_n(E,E^*)\, \delta\left[u^2 - u'^2 + \left(\frac{A}{A+1} g\right)^2\right] \tag{14}$$

For $K_{el}(\bar{v}' \to \bar{v})$ we get a similar simpler expression. Here $\beta = \frac{Am}{2kT}$, where k is the Boltzmann constant and T is the temperature of the scatterer.

To carry out the integration we change the variable $\bar{V}$ to $s = \bar{V} - \bar{v}'$, and note that since $\bar{v}'$ is a constant parameter of the integration, we have $d_3\bar{s} = d_3\bar{V}$. From Fig.1 we see that $\bar{u}' = -\frac{A}{A+1}\bar{s}$ and $\bar{u} = \bar{u}' + \bar{w}$,

consequently $u^2-u'^2 = w^2 + 2\bar{u}'.\bar{w} = w^2 - \frac{2A}{A+1}\,\bar{s}.\bar{w}$. Finally, taking into account that $E = \frac{1}{2}m_o s^2$, we get

$$K_{in}(\bar{v}' \to \bar{v})$$

$$= \frac{(\beta\pi)^{3/2}}{2\pi}\int \mu_n\left(\tfrac{1}{2}m_o s^2, E^*\right) e^{-\beta(\bar{s}+\bar{v}')^2}\,\delta\left[w^2 - \frac{2A}{A+1}\,\bar{w}.\bar{s} + \left(\frac{A}{A+1}\,g\right)^2\right]\frac{s\,d_3\bar{s}\,dE^*}{\frac{A}{A+1}\sqrt{s^2-g^2}} \tag{15}$$

The domain of integration consists of the entire three-dimensional $\bar{s}$ space, and of values of E^* from the segment $0 \leqslant E^* \leqslant \frac{1}{2}m_o s^2$. To simplify further considerations we shall drop the restriction $E^* \leqslant \frac{1}{2}m_o s^2$. By this we do not change the value of the integral. Indeed, $E^* > \frac{1}{2}m_o s^2$ is equivalent [by (6)] to $g > s$. This, in turn, implies

$$w^2 - \frac{2A}{A+1}\,\bar{w}.\bar{s} + \left(\frac{A}{A+1}\,g\right)^2 > w^2 - 2\bar{w}\cdot\frac{A}{A+1}\,\bar{s} + \left(\frac{A}{A+1}\,\bar{s}\right)^2 = \left(\bar{w} - \frac{A}{A+1}\,s\right)^2 \geqslant 0$$

We see thus, that for $E^* > \frac{1}{2}m_o s^2$, the argument of the δ-function in (15) is strictly positive, and consequently the integrand of (15) is equal to zero.

It is convenient to carry out the integration in a cylindrical system of coordinates with the axis pointing in the direction of $\bar{w}$ (see Fig. 2).

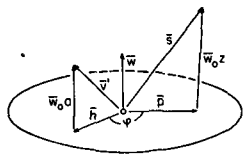

FIG. 2. Decomposition of $\bar{s}$ and $\bar{v}'$.

To this end we represent $\bar{s}$ and $\bar{v}'$ in the form

$$\bar{s} = \bar{w}_o z + \bar{p} \quad , \qquad \bar{v}' = \bar{w}_o a + \bar{h} \tag{16}$$

where $\bar{w}_o$ is a unit vector in the direction of $\bar{w}$, and $\bar{p}$, $\bar{h}$ are vectors normal to $\bar{w}$.

The elementary volume $d_3\bar{s}$ becomes $d_3\bar{s} = p\,dp\,d\phi\,dz$, and the limits of integration are:

$$0 < p < \infty \quad , \qquad 0 \leqslant \phi \leqslant 2\pi \quad , \qquad -\infty < z < +\infty$$

Also

$$(\bar{s}+\bar{v}')^2 = (\bar{p}+\bar{h})^2 + (\bar{w}_o z+\bar{w}_o a)^2 = p^2+h^2+2hp\cos\phi + (z+a)^2$$

Next we note, that since the integrand of (15) is non-negative, we may choose at will the order of integration. In this way (15) becomes

$$K_{in}(\bar{v}' \to \bar{v}) = (2\pi)^{-1}\,(\beta/\pi)^{3/2}\,\frac{A+1}{A}\,e^{-\beta h^2}\int_0^\infty dE^*\int_0^\infty p\,dp\,e^{-\beta p^2}\int_0^{2\pi} d\phi\,e^{-2\beta hp\cos\phi}$$

$$\cdot\int_{-\infty}^{+\infty} dz\,\mu_n\left(\frac{m_o}{2}\,z^2 + \frac{m_o}{2}\,p^2, E^*\right) e^{-\beta(z+a)^2}\,\delta\left[w^2 - \frac{2A}{A+1}\,wz + \left(\frac{A}{A+1}\,g\right)^2\right]\sqrt{\frac{z^2+p^2}{z^2+p^2-g^2}} \tag{17}$$

Integration over z gives

$$\frac{A+1}{2Aw}\,\mu_n\left(\frac{m_o}{2}q^2+\frac{m_o}{2}p^2,E^*\right)e^{-\beta(q+a)^2}\sqrt{\frac{q^2+p^2}{q^2+p^2-g^2}}\,,$$

where

$$q=\frac{A+1}{2A}\,\frac{w^2+\left(\frac{A}{A+1}g\right)^2}{w} \tag{18}$$

The integral over ϕ is a well-known representation of the zero-order Modified Bessel function

$$\int_0^{2\pi} e^{-2\beta hp\cos\phi}\,d\phi = 2\pi I_o(2\beta hp)$$

Finally, we change in (17) the variable of integration p to $E=\frac{m_o}{2}p^2$, and obtain

$$K_{in}(\bar{v}'\to\bar{v}) = \frac{1}{2m_o}(\beta/\pi)^{3/2}\left(\frac{A+1}{A}\right)^2\frac{1}{w}\,e^{-\beta h^2}\int_0^\infty dE^*\int_0^\infty dE\; e^{-\frac{2\beta}{m_o}E}\; I_o\left(2\beta h\sqrt{\frac{2E}{m_o}}\right)$$

$$e^{-\beta(q+a)^2}\sqrt{\frac{\frac{1}{2}m_oq^2+E}{\frac{1}{2}m_oq^2-E^*+E}}\;\mu_n\left(\tfrac{1}{2}m_oq^2+E,E^*\right) \tag{19}$$

It remains to give explicit expressions for h, $(q+a)^2$ and q^2 in terms of $\bar{v}'$, $\bar{v}$, $\bar{w}$ and E^*.

Fig. 3 illustrates the geometrical dependence between $\bar{v}'$, $\bar{v}$, $\bar{w}$, $\bar{w}_o$, $\bar{h}$ and $\bar{w}_o a$, as given by the latter relations of (5) and (16). Since $a=\bar{v}'\cdot\bar{w}_o$, we get from $v^2=v'^2+w^2+2\bar{v}'\cdot\bar{w}_o w$ the value of

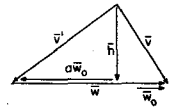

FIG. 3. Calculation of a and h.

$$a=\frac{1}{2w}\left(v^2-v'^2-w^2\right) \tag{20}$$

and also

$$h^2=v'^2-a^2$$

$$=v'^2-\frac{1}{4w^2}\left(v^2-v'^2-w^2\right)^2$$

From (18) we obtain

$$\tfrac{1}{2}m_oq^2=\tfrac{1}{4}\,\frac{\left[\frac{m_o}{2}\left(\frac{A+1}{A}w\right)^2+E^*\right]^2}{\frac{m_o}{2}\left(\frac{A+1}{A}w\right)^2}$$

From (18) and (20) follows the value of

$$q+a \quad \frac{1}{2w}\left(\frac{A}{A+1}\,g^2 + \frac{1}{A}\,w^2 + v^2 - v'^2\right)$$

Finally, we introduce the notation

$$\theta = \frac{2\beta}{m_o} = \frac{A+1}{kT} \tag{21}$$

$$W = \frac{m_o}{2}\left(\frac{A+1}{A}\,w\right)^2 \tag{22}$$

$$H = 2\beta\, h\sqrt{\frac{2}{m_o}} = \theta\sqrt{2m_o\left[v'^2 - \frac{1}{4w^2}\left(v^2-v'^2-w^2\right)^2\right]} \tag{23}$$

$$R = \frac{m_o}{2}\,\frac{A+1}{A}\left(\frac{1}{A}\,w^2+v^2-v'^2\right) \tag{24}$$

in terms of which (19) assumes the form

$$K_{in}(\bar{v}' \to \bar{v}) = \frac{m_o\left(\frac{A+1}{2A}\right)^3\left(\theta/\pi\right)^{3/2}}{\sqrt{W}}\, e^{-H^2/4\theta}\cdot\int_0^\infty dE^*\, \exp\left[-\frac{\theta}{4W}\,(R+E^*)^2\right]$$

$$\cdot\int_0^\infty dE\; e^{-\theta E}\cdot I_o(H\sqrt{E})\cdot\sqrt{\frac{[(W+E^*)^2/4W]+E}{[(W-E^*)^2/4W]+E}}\cdot\mu_n\left(\frac{(W+E^*)^2}{4W}+E,E^*\right) \tag{25}$$

Strictly speaking, the excitation energy of the compound nucleus can assume only a discrete set of values E_i^c, $i=1,2,3,\ldots$. It follows that the excitation energy of the residual nucleus, E^* assumes only the values $E_i^* = E_i^c - B$, where B is the binding energy of the neutron. We see thus that (25) should be replaced by

$$K_{in}(\bar{v}' \to \bar{v}) = \frac{m_o\left(\frac{A+1}{2A}\right)^3\left(\theta/\pi\right)^{3/2}}{\sqrt{W}}\, e^{-H^2}\, 4\theta\sum_i \exp\left|-\frac{\theta}{4W}\,(R+E_i^*)^2\right|$$

$$\cdot\int_0^\infty dE\; e^{-\theta E}\cdot I_o(H\sqrt{E})\cdot\sqrt{\frac{[(W+E_i^*)^2/4W]+E}{[(W-E_i^*)^2/4W]+E}}\cdot\mu_n\left(\frac{(W+E_i^*)^2}{4W}+E,E_i^*\right) \tag{26}$$

In the range in which the excitation energies of the compound nucleus cannot be resolved into a well-separated discrete spectrum, the spectrum is assumed continuous, and it can be taken into account by the use of (25).

$K_{el}(\bar{v}' \to \bar{v})$ is obtained from (26) by putting $E_i^* = 0$, replacing $\mu_n\left(\frac{(W+E_i^*)^2}{4W} + E, E_i^*\right)$ by $\mu_n(\frac{1}{4}W+E)$, and dropping the summation.

$$K_{el}(\bar{v}' \to \bar{v}) = \frac{m_o\left(\frac{A+1}{2A}\right)^3\left(\theta/\pi\right)^{3/2}}{\sqrt{W}} \exp\left[-\frac{1}{4}\left(\frac{H^2}{\theta} + \frac{\theta R^2}{W}\right)\right] \int_0^\infty dE\, e^{-\theta E}\, I_o(H\sqrt{E}) \cdot \mu_n(\tfrac{1}{4}W+E) \tag{27}$$ *)

5. Examples of application

It is sometimes possible to calculate exactly, or closely approximate the integral over E in situations of practical interest. One simple way to do this is to make use of a table of Laplace transforms. We shall illustrate the procedure by considering a few examples. The simplest is elastic scattering with constant scattering collision cross-section. The integral in (27) becomes

$$\mu_n \int_0^\infty e^{-\theta E}\, I_o(H\sqrt{E})\, dE = \frac{\mu_n}{\theta}\, e^{H^2/4\theta}$$

by Formula (25), p.185 of Ref. [4] (and using $\mathfrak{J}_o(iz) = I_o(z)$). We arrive thus at the well-known expression [3] (in different notation)

$$K_{el}(\bar{v}' \to \bar{v}) = \sqrt{\frac{m_o\theta}{2\pi^3}}\left(\frac{A+1}{A}\right)^2 \frac{\mu_n}{w} \exp\left[-\frac{m_o}{8}\,\theta\,\frac{1}{w^2}\left(\frac{w^2}{A} + v^2 - v'^2\right)^2\right] \tag{28}$$

Next consider resonant elastic scattering (given e.g. by the one-level Breit-Wigner formula). Here $\mu_n(E) = \mu_r(E) + p$, where p = const. represents the potential scattering, and $\mu_r(E) \ll p$ for sufficiently large $E(E > E_o)$. In the interval $0 < E < E_o$ we approximate the function $e^E\, \mu_r(E)$ by a sum of Tshebyshev polynomials. This results in

$$p + e^{-E} \sum_{n=0}^{N} C_n\, T_n(E) \approx \mu_n(E) \quad \text{for} \quad 0 \leqslant E \leqslant E_o$$

$$\approx p \approx \mu_n(E) \quad \text{for} \quad E > E_o$$

the latter line of the above approximation is caused by the exponential factor e^{-E} . After rearrangement we get

$$\mu_n\,(\tfrac{1}{4}W+E) \approx p + e^{-\frac{1}{4}W} \sum_{n=0}^{N} P_n(W)\, E^n\, e^{-E} \tag{29}$$

where $P_n(W)$ are polynomials in W . The different terms of (29) can now be integrated separately. The constant term is already given by

*) A different derivation of K_{el} developed independently by Blackshaw and Murray was published recently in Nucl.Sci.Eng. 27 (March 1967) 520.

the right-hand side of (28), with μ_n replaced by p. To all other terms we may apply Formula (33), p.185 of Ref. [4].

$$\int_0^\infty e^{-(\theta+1)} I_o(H\sqrt{E})\, E^n\, dE = (\theta+1)^{-n-1} \exp\left[\frac{H^2}{4(\theta+1)}\right] L_n\left(-\frac{H^2}{4\theta+4}\right) \qquad (30)$$

We note that the result obtained in this way can serve not only for numerical calculations, but has also some analytic value if the number of approximating polynomials, N in (29) can be made sufficiently small.

Next consider resonant inelastic scattering given by the cross-section $\mu_n(E,E_i^*)$. Denoting $\frac{(W-E_i^*)^2}{4W}$ by x we have

$$\sqrt{\frac{[(W+E_i^*)^2 \quad 4W]+E}{[(W-E_i^*)^2 \quad 4W]+E}}\ \mu_n\left(\frac{(W+E_i^*)^2}{4W}+E,E_i^*\right) = \sqrt{\frac{E_i^*+x+E}{x+E}}\ \mu_n(E_i^*+x+E,E_i^*)$$

The range of x is now split into 2 subintervals $0 \leqslant x \leqslant \epsilon$ and $x > \epsilon$. The integral of (26) is evaluated separately in each subinterval of x. For $x > \epsilon$, the function $\sqrt{\frac{E_i^*+x+E}{x+E}}$ is bounded, and therefore $\sqrt{\frac{E_i^*+x+E}{x+E}}\ \mu_n(E_i^*+x+E,E_i^*)$ can be expanded in Laguerre functions of the argument (E_i^*+x+E). As in (29) we rearrange the expansion in powers of E, and use (30) to integrate separately the different terms.

To evaluate the integral for $x < \epsilon$, we note that since this integral is a continuous function of x, it can be approximated in the whole interval $0 \leqslant x \leqslant \epsilon$ by its value at $x = 0$, if ϵ is sufficiently small. To this end we insert $x = 0$ into (26) and expand $\left\{\sqrt{E_i^*+E}\ \mu_n(E_i^*+E,E_i^*)\right\}$ into Laguerre functions of the argument (E_i^*+E). The expansion is again rearranged in powers of E, and the different terms of the expansion can be integrated separately by the application of the Formulae (29) and (33), p.185 of Ref. [4].

As a final example of application we observe that in case of narrow resonance scattering the collision cross-section can be approximated by a sum of a few δ-like narrow resonances, and a constant term, representing potential scattering

$$\mu_n(E,E_i^*) \approx \sum_j S_{ij}\ \delta(E-E_{ij}) + p$$

When this is inserted into (26), $K(\bar{v}' \to \bar{v})$ is obtained at once.

Acknowledgement

This investigation was partially supported by the KBB (Karlsruhe) - Euratom Association on Fast Reactors, Kernforschunsgzentrum, Karlsruhe.

References

[1] E. P. WIGNER and J. E. WILKINS, AECD-2275 (1944)
[2] A. ZEMACH and R. GLAUBER, Phys. Rev. 101 (1956) 118
[3] V. V. SMELOV, Dissertation (1959) unpublished, results and method described in G. J. Marchuk "Computational Methods in Nuclear Reactor Theory", (in Russian) (1961)
[4] A. ERDELYI, W. MAGNUS, F. OBERHETTINGER, F. G. TRICOMI, "Tables of Integral Transforms", Vol.I, McGraw Hill (1954)

NEUTRON SCATTERING IN BERYLLIUM*

J.U. KOPPEL AND J.A. YOUNG
GENERAL ATOMIC DIVISION,
GENERAL DYNAMICS CORPORATION,
SAN DIEGO, CALIFORNIA,
UNITED STATES OF AMERICA

Abstract

NEUTRON SCATTERING IN BERYLLIUM. To obtain more accurate scattering kernels for solid moderators a calculation has been attempted to calculate the neutron scattering from first principles. In other words, instead of using the usual force constant models based on experiments and fitted phenomenologically, we have computed the moderator dynamics independent of experiment. The results we have obtained are applicable at present only to the solid moderators and, in particular, to beryllium, which is the first moderator treated by this method. The method proceeds by using the adiabatic approximation to separate the electronic and ionic motions, and from there to an expansion of the energy to second order. The most difficult contribution to treat both analytically and numerically is the electronic contribution to the ion energy. The pure Coulomb potential presents only a computational problem. There are three contributions to the Hamiltonian: (1) the direct Coulomb interaction between ions, (2) the core-core exchange repulsion, and (3) the conduction electron energy. This last term is the most difficult to obtain. The expression for the second-order electronic contribution is quite complicated and involves an intricate sum over the electronic band structure of the static crystal. In effect, this sum is the theoretical dielectric function of the crystal. To compute the band structure of beryllium for this calculation the crystal potential of Loucks and Cutler was used. The band structure was obtained using 23 orthogonalized plane waves. It is anticipated that these calculations will result in more reliable scattering kernels.

Due to its favorable neutron moderation and low absorption properties beryllium metal is one of the most important materials in nuclear reactor technology. Hence, it is important to formulate an accurate model for calculating the energy spectrum of thermal neutrons in a beryllium moderator. The inelastic scattering of thermal neutrons in a crystalline material like beryllium is caused by their interaction and energy exchange with the normal modes of vibration of the crystal. Hence, in order to formulate a scattering kernel we need to know the frequency spectrum of beryllium.

Some time ago the authors have published[1] a frequency spectrum calculated from a Born-Von Karman model whose force constants were obtained by Schmunk, et al.[2] by fitting the phonon dispersion curves they had measured by coherent neutron scattering. In the present work we have the more ambitious goal of obtaining the dispersion curves, and hence the frequency spectrum for beryllium from first principles, that is without introducing empirical knowledge of any kind into the theory. The need for such a calculation has been pointed out by many authors because of the long range of the ion-conduction-electron-ion interaction in a metal. Owing to these long-range effects the fitting of the dispersion curves by a Born-Von Karman model requires too large a number of empirical force constants to be physically meaningful.

* This work was supported by the United States Atomic Energy Commission.

Ab initio calculations have been performed by other workers[3-5] with good results for simple metals like sodium. For other metals, however, good agreement between first-principle calculations and experiment has not yet been achieved. Beryllium, which is treated here, is a particularly difficult case. Being divalent, its metallic properties are due to band overlap and hence its Fermi surface is very complicated. Furthermore, beryllium crystallizes in the hcp structure, and thus has two atoms per unit cell; this introduces a structure factor which adds to the numerical difficulties of the calculation.

An important restriction has to be imposed at the start in order to make the theory manageable. We shall assume that the electronic energies (and wave functions) depend only parametrically on the coordinates R_ν of the ions, but not on their velocities. This is the so-called adiabatic approximation. We can then write the following Hamiltonian for the motion of the ions:

$$H = \frac{M}{2} \sum_{\nu} \dot{R}_\nu^{\,2} + \Phi(R_1, R_2, \ldots) \tag{1}$$

We shall calculate the lattice dynamics in the harmonic approximation. Hence we expand Φ in powers of the displacements $\vec{u}_\nu$ of the ions. The first-order term vanishes and the second-order term takes the form

$$\Phi^{(2)} = \frac{1}{2} \sum_{\substack{\ell\varkappa \\ \alpha}} \sum_{\substack{\ell'\varkappa' \\ \beta}} u_\alpha\begin{pmatrix}\ell \\ \varkappa\end{pmatrix} u_\beta\begin{pmatrix}\ell' \\ \varkappa\end{pmatrix} \varphi_{\alpha\beta}\begin{pmatrix}\ell & \ell' \\ \varkappa & \varkappa'\end{pmatrix} \tag{2}$$

where $u_\alpha\binom{\ell}{\varkappa}$ denotes the α-th cartesian component of the displacement of the ion characterized by lattice index ℓ and cell index $\varkappa$. The $\varphi_{\alpha\beta}\binom{\ell\ \ell'}{\varkappa\ \varkappa'}$ are the previously mentioned force constants.

If we express the displacements $\vec{u}$ in terms of normal coordinates Q_q

$$\vec{u}\begin{pmatrix}\ell \\ \varkappa\end{pmatrix} = \frac{1}{\sqrt{NM}} \sum_{qj} \vec{e}\left(\varkappa \middle| {q \atop j}\right) Q_{qj}\, e^{i\vec{g}\cdot\vec{R}\binom{\ell}{\varkappa}} \tag{3}$$

Eq. 2 takes the form

$$\Phi^{(2)} = \frac{1}{2M} \sum_{qjj'} Q_{qj} Q^*_{qj'} \sum_{\substack{\alpha\ \beta \\ \varkappa\ \varkappa'}} W_{\alpha\beta}\left(\varkappa\varkappa' \middle| {q \atop}\right) e_\alpha\left(\varkappa \middle| {q \atop j}\right) e^*_\beta\left(\varkappa' \middle| {q \atop j'}\right) \tag{4}$$

where

$$W_{\alpha\beta}\begin{pmatrix} q \\ \varkappa\varkappa' \end{pmatrix} = \sum_{\ell} e^{i\vec{q}\cdot\left[\vec{R}\begin{pmatrix}\ell\\ \varkappa\end{pmatrix} - R\begin{pmatrix}o\\ \varkappa'\end{pmatrix}\right]} \varphi_{\alpha\beta}\begin{pmatrix}\ell o\\ \varkappa\varkappa'\end{pmatrix} \tag{5}$$

In the preceding equations, $\vec{q}$ denotes the phonon wave vector, j is the branch index, N is the number of cells of the crystal, M is the ionic mass, and $\vec{e}(\varkappa|{}^{q}_{j})$ stands for the polarization vectors which satisfy the secular equation

$$\sum_{\beta\varkappa'} W_{\alpha\beta}\begin{pmatrix} q \\ \varkappa\varkappa' \end{pmatrix} e_{\beta}\left(\varkappa'|{}^{q}_{j}\right) = M\omega_j^2(q)\, e_{\alpha}\left(\varkappa|{}^{q}_{j}\right) \tag{6}$$

giving the phonon frequencies $\omega_j(q)$.

The elements of the dynamical matrix $W_{\alpha\beta}(\begin{smallmatrix} q \\ \varkappa\varkappa' \end{smallmatrix})$ can be expressed as a sum over three terms, stemming from each one of the three kinds of force constants which contribute to the potential function : 1. the direct Coulomb interaction between positive ions, 2. the short-range exchange repulsion between ion-cores and 3. the long-range ion-conduction electron-ion interaction mentioned above. The first two contributions are easily evaluated by conventional techniques. Concerning the third one, several methods have been developed by different authors, one of the first being the variational method used by Toya[3] for the case of sodium. Here we follow Sham's method[4] also originally applied to sodium after generalizing it to nonprimitive lattices as required for beryllium.

Sham's starting point is the adiabatic approximation and a Hartree-Fock-like expression for the electron ground state energy $\mathcal{E}(R)$ in the undistorted lattice

$$\mathcal{E}(R) = \sum_k n(k)E(k, R) - \frac{1}{2}\iint d^3r\, d^3r'\, v(|r-r'|)\rho(r, R)\rho(r'R)$$

$$+ \frac{1}{2}\iint d^3r\, d^3r' \mathcal{V}(r, r')\rho(r, r', R)\rho(r', r, R) \tag{7}$$

$$\rho(r, r', R) = \sum_k n(k)\, \psi_k(r, R)\, \psi_k^*(r', R) \tag{8}$$

Here R stands for the equilibrium ion coordinates, r is the electron coordinate, $E(k, R)$ are one-particle energies, n are occupational numbers,

v is the electron-electron Coulomb interaction and v is the shielded e-e interaction. The sum over k includes spin and it is in the extended zone. The wave functions $\psi_k(r,R)$ are the Bloch states satisfying the following Schrödinger equation:

$$H(r,R)\psi_k(r,R) = E(k,R)\psi_k(r,R) \tag{9}$$

$$H(r,R)\psi_k(r,R) \equiv \left\{-\frac{\hbar^2}{2m}\nabla_r^2 + V(r,R) + \int d^3r' v(|r-r'|)\rho(r',R)\right\}\psi_k(r,R)$$

$$-\int d^3r' \mathcal{V}(r,r')\rho(r,r',R)\psi_k(r',R) \tag{10}$$

$$V(r,R) = \sum_{\ell,\varkappa} U(r-R_{\ell\varkappa}) \tag{11}$$

The term V has the periodicity of the lattice and U is the unshielded ion-electron potential.

In order to find the electron ground state of the distorted lattice we expand everything in powers of the ion displacements, up to second order since we are concerned only with the harmonic approximation. Hence

$$\begin{aligned}
V(r,R+u) &= V(r,R) + V^{(1)} + V^{(2)} \\
\mathcal{E}(R+u) &= \mathcal{E}(R) + \mathcal{E}^{(1)} + \mathcal{E}^{(2)} \\
H(r,R+u) &= H(r,R) + H^{(1)} + H^{(2)} \\
\psi_k(r,R+u) &= \psi_k(r,R) + \psi^{(1)} + \psi^{(2)} \\
E(k,R+u) &= E(k,R) + E^{(1)} + E^{(2)}
\end{aligned}$$

Actually, we want to find $\mathcal{E}^{(2)}$. The wave function ψ_k and the one-particle energies E(k) are expanded by perturbation theory. Since the Hamiltonian H involves the ψ_k in its Hartree-Fock terms, we obtain a self-consistency condition which is expressed by the following integral equation for the electron-phonon matrix element.

$$\langle\psi_{k'}|H^{(1)}|\psi_k\rangle = \langle\psi_{k'}|V^{(1)}|\psi_k\rangle + \sum_{kk'} \frac{n(K)-n(K')}{E(K)-E(K')}\left(v_{k'KK'k} - \mathcal{V}_{k'KkK'}\right)$$

$$\cdot\langle\psi_{K'}|H^{(1)}|\psi_K\rangle \tag{12}$$

where

$$v_{k'KK'k} = \iint d^3r\, d^3r' \psi^*_{k'}(r)\psi^*_K(r')\, v(|r-r'|)\psi_{K'}(r')\psi_k(r) \qquad (13)$$

and a similar definition holds for $\mathcal{V}_{k'KkK'}$.

This equation clearly describes the shielding of the change of ion-electron potential $V^{(1)}$ as a consequence of the electron-electron interaction and defines a dielectric constant.

The exact solution of the integral equation is made extremely difficult by the exchange term. Hence it is necessary to treat the exchange by some approximation. Here we use Hubbard's approximation, which, if $\mathcal{V}(r, r')$ is approximated by a Fermi-Thomas potential, leads to

$$\mathcal{V}_{k'KkK'} = \frac{4\pi e^2}{N\Omega}\left[(k'-k)^2 + k_F^2 + k_S^2\right]^{-1} \qquad (14)$$

where k_F is the Fermi momentum and k_S is the inverse of the screening length.

The final result for the second-order total-conduction electron energy can be expressed in the same form as Eq. (4). The electronic contribution to the matrix elements $W_{\alpha\beta}\binom{q}{\varkappa\varkappa'}$ is then given by

$$W^E_{\alpha\beta}\binom{q}{\varkappa\varkappa'} = \sum_{GG'}\left[W^E_{\alpha\beta,\varkappa\varkappa'}(q+G,\ q+G') - \delta_{\varkappa\varkappa'}\sum_{\varkappa''} W^E_{\alpha\beta,\varkappa''\varkappa'}(G, G')\right] \qquad (15)$$

$$W^E_{\alpha\beta,\varkappa\varkappa'}(q+G,\ q+G') = \left\{Nv(q+G)\left[1-f(g+G)\right]\right\}^{-1}\left[\epsilon^{-1}(q+G, q+G') - \delta_{GG'}\right]$$

$$\cdot\, U(-q-G)U(q+G')e^{i(G\varkappa'-G'\varkappa)}(q_\alpha+G_\alpha)(q_\beta+G'_\beta) \qquad (16)$$

where G is a reciprocal lattice vector, U(G) stands for the Fourier transform of U(r), v(G) is the Fourier transform of v(r) and ϵ^{-1} is the inverse of the dielectric matrix obtained by solving the self-consistency integral equation given above. ϵ is given by the following expression

$$\epsilon(q+G, q+G') = \delta_{GG'} + \left[1-f(q+G)\right]Nv(q+G)\,\chi(q+G, q+G') \qquad (17)$$

$$\chi(q+G, q+G') = \frac{1}{N} \sum_{kk'} \frac{n(k)-n(k')}{E(k)-E(k')} \langle \psi_k | e^{-i(q+G)\cdot r} | \psi_{k'} \rangle \langle \psi_{k'} | e^{i(q+G')\cdot r} | \psi_k \rangle \tag{18}$$

$$f(q+G) = \frac{1}{2} \frac{(q+G)^2}{(q+G)^2 + k_F^2 + k_s^2} \tag{19}$$

Exchange between conduction electrons is treated in Hubbard's approximation. This leads to the term $-f(q+G)$ which reduces the shielding effect of the conduction electrons by a factor 1/2 in the limit of large wave vectors $q+G$. The expression for ε reduces to the free electron dielectric constant (random phase approximation) if the Bloch states are approximated by plane waves. The term χ then becomes diagonal and isotropic. The corresponding formula is

$$\chi(q) = \frac{3\bar{n}}{2E_F} \left[\frac{1}{2} + \frac{4k_F^2 - q^2}{8k_F q} \log \left| \frac{q+2k_F}{q-2k_F} \right| \right]$$

where $\bar{n}$ is the number of conduction electrons per unit cell and E_F is the Fermi energy.

This function is shown in Fig. 1 in terms of the variable $y = q/2k_F$. In the same figure we show the exact diagonal term $\chi(q+G, q+G)$ as obtained by a detailed energy band calculation for $q+G$ along the hexagonal axis of symmetry. The main difference between the two curves is the marked dip of the second curve at small values of q. This is due to the pronounced decrease of the density of states at the Fermi level, which is typical for divalent metals.

The band calculation was done by the orthogonalized plane waves method with a self-consistent potential obtained by Loucks and Cutler.[6] The Bloch states were calculated as a linear combination of 23 OPW's which gave reasonable convergence for the one-electron energies.

In view of the similarity between the two curves of Fig. 1 for most of the range of q, a first attempt to calculate the phonon frequencies using the free electron dielectric constant as given by Eq. (20) seems quite justified. In fact, the results turned out to be in fair agreement with experiment. The comparison of this free electron calculation with Schmunk's[2] measurements is shown in Figs. 2 and 3. For phonons propagating along the (0001) direction it is seen that three of the four branches are in good agreement with experiment; the transverse optical branch, however, deviates significantly from the measured curve at small values of q. The $(01\bar{1}0)$ curves are in poorer agreement with experiment although the fit for the highest optical branch which determines the cutoff of the frequency spectrum is still very good.

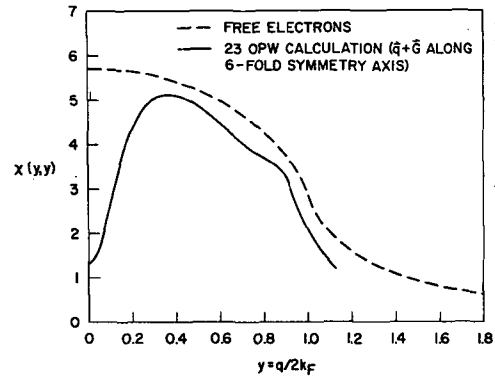

FIG. 1. Function χ and its exact diagonal term as a function of $q/2k_F$.

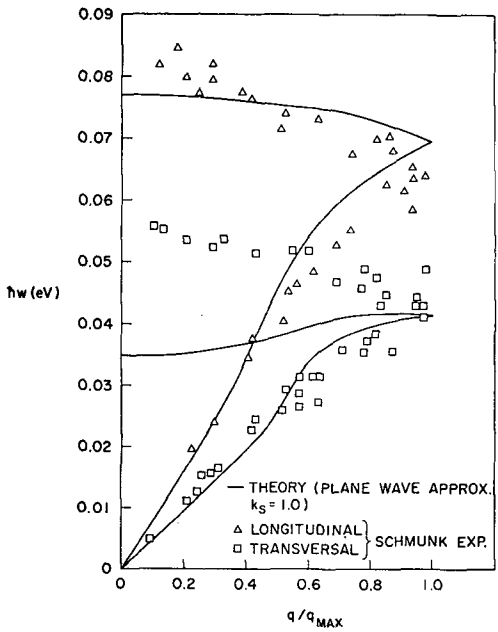

FIG. 2. Dispersion curves for beryllium (0001).

The bare ion potential U entering Eq. (16) was taken from Loucks and Cutler (contribution $h_a + h_b$ of Ref. 6) and core-core exchange repulsion was neglected in view of the smallness of the beryllium cores.

It was hoped that the use of the more accurate dielectric constant obtained from the OPW calculation would lead to much better agreement with experiment. Unfortunately this expectance was not borne out by our first numerical results. The main difficulty is believed to lie in the limited number of OPW considered so far. A much larger volume in reciprocal space is required in order to obtain reliable values for $\chi(q+G, q+G')$ in the important interval about $q+G \approx 2k_F$. Another serious difficulty is the alternating sign of terms in the sums over G in Eq. (15)

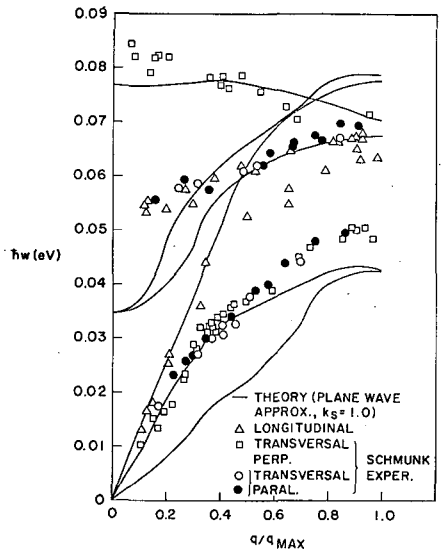

FIG. 3. Dispersion curves for beryllium $(01\bar{1}0)$.

which could increase the relative error of the sum by one or two orders of magnitude due to very close cancellation. With the 23 reciprocal lattice vectors corresponding to our 23 OPW band calculation we obtained values of $\chi(q+G, q+G')$ just beyond $q+G = 2k_F$. In order to get convergence of the sum over G in Eq. (16) it is necessary to go much further out in reciprocal space. Hence we extrapolated the diagonal terms with a tail having the asymptotic behavior of the free electron χ and neglected the off-diagonal terms which are between one and two orders of magnitude smaller than the diagonal terms. The result was quite insensitive to the form of the extrapolated tail. Further calculations with more OPW's are in progress. It is hoped that ultimately we shall get a good fit to the experimental dispersion curves and hence a good frequency spectrum to be used in the formulation of an improved neutron scattering kernel.

REFERENCES

[1] YOUNG, J.A., KOPPEL, J.U., Nucl. Sci. Engng 19 (1964) 367.
[2] SCHMUNK, R.E., et al., Phys. Rev. 128 (1962) 562.
[3] TOYA, T., Inelastic Scattering of Neutrons I IAEA, Vienna (1965) 29.
[4] SHAM, L.J., Proc. R. Soc. Ser. A 283 (1965) 33.
[5] VOSKO, S.H., et al., Canad. J. Phys. 43 (1965) 1187.
[6] LOUCKS, T.A., CUTLER, P.H., Phys. Rev. 133 (1964) A819.

DISCUSSION

H. TAKAHASHI: Is the dispersion relation sensitive to the exchange interaction?

J. A. YOUNG: The disperson relations are, I suppose, somewhat sensitive to the form of the exchange potential, especially at smaller

q-values, but we have not performed these calculations using different exchange potentials.

M. S. NELKIN (Chairman): How well does a similar approach work for simpler metals?

J. A. YOUNG: For sodium, especially, the results are satisfactory.

W. GLÄSER: I should like to comment in this connection that even for simple metals such as alkali metals the agreement between theoretical calculations and experimental dispersion curves is not so good as one would like. Some workers are therefore now trying to use the neutron data to fit, for example, a pseudo-potential model in order to get information on the behaviour of the electrons. For a system like beryllium, however, such a procedure is more elaborate. Do you believe that you can take proper account of the deviation from free electron behaviour?

J. A. YOUNG: Yes.

R. G. FLUHARTY: I'm not sure how appropriate it is at this point to mention the success that Solbrig and McMurry are having in fitting dispersion relations using a co-valent bond model based on molecular physics. In particular, they have found a detailed fit to the dispersion relations for diamond and are now attempting BeO.

J. A. YOUNG: The co-valent bond model is completely equivalent to the Born-Huang lattice dynamics, although it may possibly have computational advantages. At all events, they are both phenomenological – in contrast to the attempts here to perform a first principles calculation.

ИЗУЧЕНИЕ НЕУПРУГОГО РАССЕЯНИЯ НЕЙТРОНОВ В ГРАФИТЕ ПРИ РАЗЛИЧНЫХ ТЕМПЕРАТУРАХ

И.П.ЕРЕМЕЕВ, В.И.МОСТОВОЙ, И.П.САДИКОВ,
М.Н.СЕВЕРОВ, А.А.ЧЕРНЫШОВ
ИНСТИТУТ АТОМНОЙ ЭНЕРГИИ им.И.В.КУРЧАТОВА,
МОСКВА,
СССР

Abstract — Аннотация

STUDY OF INELASTIC NEUTRON SCATTERING IN GRAPHITE AT VARIOUS TEMPERATURES. The paper gives results of measurements of the double-differential neutron scattering cross-section for reactor graphite for temperatures of 15, 490, 1000 and 1370°C.

The measurements were made at the WWR-M reactor with an experimental device intended for studying the inelastic scattering of slow neutrons. Monochromatization and chopping of the primary neutron beam were achieved with the aid of a single crystal and a mechanical chopper. The scattered radiation is analysed in terms of energy using the time-of-flight method simultaneously for eight angles in the range 10°-115°.

The data obtained are represented in the form of the scattering cross-section $S(\epsilon, \kappa)$, which is compared with the result of calculations based on the frequency spectrum suggested by Egelstaff.

ИЗУЧЕНИЕ НЕУПРУГОГО РАССЕЯНИЯ НЕЙТРОНОВ В ГРАФИТЕ ПРИ РАЗЛИЧНЫХ ТЕМПЕРАТУРАХ. Представлены результаты измерения дважды дифференциального сечения рассеяния нейтронов для реакторного графита для температур: 15, 490, 1000 и 1370°С.

Измерения проведены на реакторе ВВР-М на экспериментальной установке, созданной для изучения неупругого рассеяния медленных нейтронов. Монохроматизация и прерывание первичного пучка нейтронов осуществляется с помощью монокристалла и механического прерывателя. Рассеянное излучение анализируется по энергии методом времени пролета одновременно под восемью углами в интервале 10° – 115°.

Полученные данные представлены в виде сечения рассеяния $S(\epsilon, \kappa)$, которое сравнивается с результатами расчетов, выполненных на основе частотного спектра, предложенного Энгельстаффом.

I. ВВЕДЕНИЕ

Дважды дифференциальное сечение рассеяния медленных нейтронов на графите применительно к проблеме термализации впервые измерили Эгельстафф и Кокин [1] при температурах графита 24°С и 610°С. При комнатной температуре графита подобные измерения проводились также Хейвудом и Сорсоном [2]. В узкой области передач энергии и импульса рассеяние медленных нейтронов графитом изучалось Вудсом и др. [3]. Все эти работы относятся еще к периоду Брукхейвенской конференции по термализации нейтронов. Позднее была опубликована работа [4] по неупругому рассеянию холодных нейтронов на графите при температуре 950°С, но она не преследовала цели получения данных для термализации.

Экспериментальная информация о дважды дифференциальных сечениях, получаемая в ограниченной области изменения переменных, может быть использована наиболее эффективно для расчетов термализационных задач посредством применения так называемого обобщенного частотного спектра [5, 6].

Предложенный Эгельстаффом довольно простой по форме частотный спектр для графита с граничной энергией, соответствующей температуре $\theta_D = 2100°K$, воспроизводит столь же удовлетворительно экспериментальные данные по дважды дифференциальному сечению в области не слишком больших передач импульсов, как и более детальный спектр Иосимори и Китано [7]. Однако согласие с данными по зависимости удельной теплоемкости графита от температуры можно получить, если принять для частотного спектра Эгельстаффа $\theta_D = 2600°K$. Расчеты спектров нейтронов в системах с графитом, выполненные на основе этого частотного спектра и спектра Иосимори и Китано, дают практически одинаковые результаты [7].

Как известно [8, 9], в системах с графитом при наличии поглощения и большого градиента температуры эффекты кристаллической связи в графите еще заметно влияют на формирование спектра тепловых нейтронов при температурах ~550°C. Поскольку практику современного реакторостроения интересуют расчеты систем с более высокой температурой графита и поскольку результаты, полученные в работе [1] для температур графита выше комнатной, являются единственными и не столь детальными, представлялось интересным измерить дважды дифференциальные сечения графита как в области температур, охватываемой упомянутыми экспериментами, так и при более высоких температурах. При этом важно было проверить применимость частотного спектра Эгельстаффа для вычисления закона рассеяния при более высоких температурах графита.

Следует отметить, что проверка применимости этого частотного спектра при высоких температурах путем сопоставления расчетных спектров нейтронов с измеренными не представляется возможной в связи с большими экспериментальными трудностями измерения спектров нейтронов в конкретных системах при высоких температурах графита и больших градиентах температуры.

В данной работе произведено измерение дважды дифференциального сечения графита при температурах 15°C, 490°C, 1000°C и 1370°C. Результаты измерений сравнены с расчетами, использующими частотный спектр Эгельстаффа.

II. ЭКСПЕРИМЕНТАЛЬНАЯ УСТАНОВКА

При выполнении точных расчетов по термализации нейтронов необходимо знать закон рассеяния для замедлителя в широких пределах изменения энергии и импульса нейтрона. Для этого необходимо выполнить измерения сечения рассеяния нейтронов при различных начальных энергиях и углах рассеяния с достаточно хорошим энергетическим разрешением.

Среди известных методов изучения неупругого рассеяния нейтронов, основанных на использовании стационарного источника нейтронов (реактора), наилучшим образом этим требованиям, на наш взгляд, отвечает комбинированный метод "кристалл + прерыватель", который объединяет преимущества метода трехосевого спектрометра (высокое разрешение) и методик, основанных на измерении времени пролета (достаточная светосила, особенно при использовании многодетекторной системы).

Суть метода состоит в следующем. Коллимированный "белый" пучок нейтронов из реактора падает на кристалл-монохроматор. Отра-

женный пучок монохроматических нейтронов с энергией E_0 прерывается механическим прерывателем и попадает на исследуемый образец. Спектры нейтронов, рассеянных образцом, измеряются методом времени пролета одновременно под несколькими углами с помощью системы детекторов, расположенных в вертикальной плоскости. Достаточно широкий диапазон изменения E_0 обеспечивается, во-первых, за счет изменения угла отражения и, во-вторых, за счет использования монокристаллов с различным межплоскостным расстоянием.

Установка смонтирована на горизонтальном пучке реактора ВВР-М Института Физики АН УССР в г.Киеве. Общий вид установки показан на рис. 1.

1. Кристаллический монохроматор

В качестве монохроматора нейтронов использовались монокристаллы свинца и кремнистого железа. Монокристалл свинца размерами $25 \times 8 \times 0{,}8$ см^3 применялся для получения монохроматических нейтронов в области $E_0 \leqslant 30$ мэв (миллиэлектронвольт) при отражении от плоскости (111) с межплоскостным расстоянием $d = 2{,}84$ Å. В связи с возрастанием фона при малых углах отражения для выделения нейтронов с $E_0 > 30$ мэв применялся тонкий (0,45 мм) монокристалл кремнистого железа ($d = 2{,}03$ Å), а также монокристалл свинца. В последнем случае кристалл устанавливался в положение "на пропускание" и использовалась отражающая плоскость (220) с $d = 1{,}68$ Å.

Пучок нейтронов сечением $5 \times 6{,}5$ см^2, падающий на кристаллмонохроматор, формировался системой сменных коллиматоров, позволяющей изменять расходимость пучка в пределах $6{,}5' \div 60'$.

2. Механический прерыватель

Для создания пульсирующего потока монохроматических нейтронов применялись механические прерыватели диаметром 150 мм с различной шириной и кривизной параболических щелей в зависимости от выделяемой энергии и требуемого разрешения. Профиль щели для каждого прерывателя рассчитывался так, чтобы получить максимальную светосилу в некотором энергетическом диапазоне при заданном разрешении по времени пролета. Степень монохроматизации роторов составляет $70 \div 100\%$, что заведомо обеспечивает дискриминацию нейтронов, соответствующих отражениям высших порядков. Форма функции пропускания показана на рис. 5.

3. Детекторы

Установка имеет 8 детекторов, расположенных под углами θ: 9,5; 25,1; 40,5; 55,7; 70,9; 86,1; 101,3 и 116,5°. Каждый детектор представляет собой двухрядный пакет из 15 счетчиков типа СНМ-8А длиной 100 см и диаметром 38 мм, наполненных обогащенным газом BF_3 до давления 700 мм рт. ст.*. Величина Σ_a для газа, наполняющего счетчики, которая необходима для вычисления эффективности детекторов, была найдена из измерений пропускания нескольких экземпляров счетчиков.

---

* В настоящее время проводятся подготовительные работы для замены борных счетчиков на счетчики с He^3 меньших размеров.

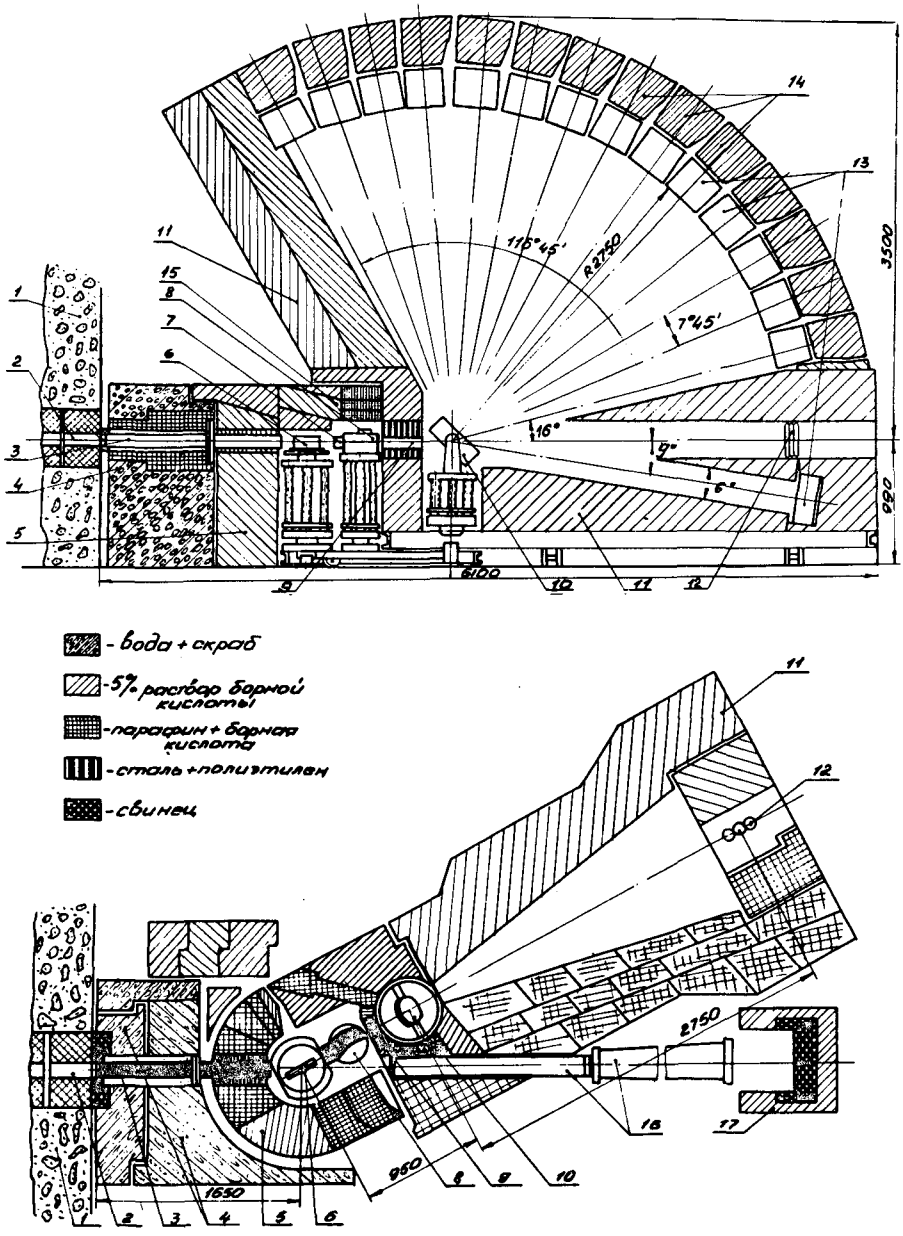

Рис. 1. Общий вид установки:
1 – защита реактора; 2 – 3 – 7 – 9 – система коллиматоров; 4 – 5 – 11 – 14 – 15 – различные части защиты установки; 6 – кристалл-монохроматор; 8 – механический прерыватель; 10 – образец; 12 – монитор монохроматического пучка; 13 – детекторы; 16 – вакуумная труба для прямого пучка; 17 – ловушка прямого пучка.

Импульсы с детекторов, усиленные однокаскадными предусилителями, поступали на входы соответствующих милливольтовых дискриминаторов и далее на вход системы многомерного временного анализа (рис. 2).

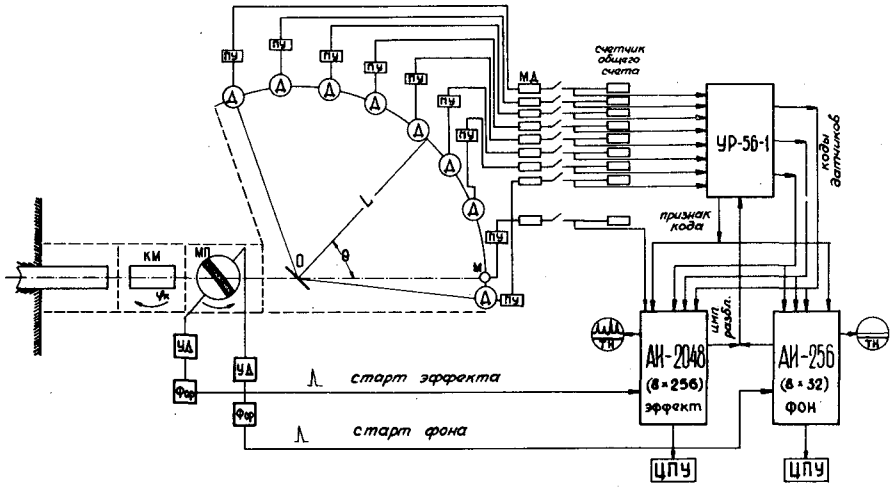

Рис. 2. Блок-схема временного анализа:
МП – механический прерыватель; УД – усилитель-дискриминатор; Д – детекторы; М – монитор; ПУ – предусилители; МД – милливольтовые дискриминаторы; УР-56 – блок кодирования импульсов; ЦПУ – цифропечатающее устройство; ТН – трубка наблюдения.

4. Система многомерного временного анализа

Регистрация рассеянного образцом излучения производилась одновременно для всех углов системой многомерного временного анализа, состоящей из двух многоканальных временных анализаторов и коммутационной приставки (рис. 2). В соответствии с числом детекторов система регистрации имеет 8 независимых входов. Анализатор АИ-2048 использовался для регистрации спектров рассеянных нейтронов, АИ-256 – для измерения фона. Анализаторы эффекта и фона запускались импульсами, поступавшими с магнитных головок механического прерывателя в момент открытия щелей и через полоборота, соответственно, что позволяло измерять эффект и фон практически одновременно.

5. Монитор отраженного пучка

Для контроля за интенсивностью монохроматических нейтронов, для измерения спектра нейтронов, падающих на образец, а также для выполнения некоторых вспомогательных операций (юстировка монокристаллов, коллиматоров и др.) служил монитор, расположенный на отраженном пучке на расстоянии ~280 см от образца. Монитор собран в виде пакета из 3 счетчиков BF_3 с таким же наполнением и той же эффективной толщиной, как и основные детекторы.

Для уменьшения фона все части экспериментальной установки окружены толстым слоем (~50 см) водной защиты, а внутренние полости облицованы кадмием.

6. Образец

Эксперименты при всех температурах были выполнены на одном и том же образце, представлявшем собой пластину размерами 130×70×49 мм^3, вырезанную из блока реакторного графита ($\rho = 1{,}60$ г/см^3) вдоль направления выдавливания.

В измерениях при комнатной температуре образец (находящийся на расстоянии $\ell = 62{,}5$ см от оси вращения прерывателя) был расположен под углом 53° к падающему пучку нейтронов, и рассеяние изучалось одновременно под всеми углами. При высоких температурах, когда образец находился в контейнере, измерения проводились поочередно для углов рассеяния $\theta \leq 86°$ и $\theta \geq 86°$; образец в этом случае был наклонен к пучку под углом 45° и 135° соответственно.

Доля нейтронов, рассеянных образцом, не превышала 25%.

Высокотемпературные измерения были проведены в специальном контейнере (рис. 3). Для уменьшения фона диафрагмы контейнера были изготовлены из дюралюминия минимально возможной толщины (1 – 1,5 мм). Нагрев графита осуществлялся в вакууме за счет джоулева тепла, выделяемого в образце при пропускании через него электрического тока. Электровводы, корпус контейнера и периферия диафрагм охлаждались проточной водой. Сами диафрагмы дополнительно охлаждались струей сжатого воздуха. Для уменьшения температуры диафрагм и создания более равномерного распределения температуры по образцу предусмотрен тепловой экран из молибдена. Следует отметить,

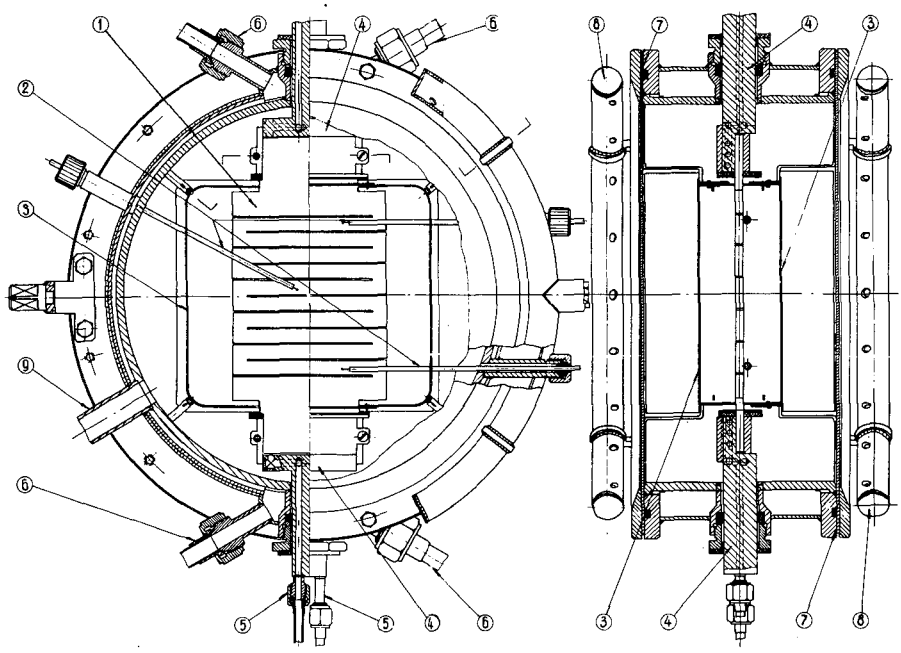

Рис. 3. Конструкция высокотемпературного контейнера:
1 – графитовый образец; 2 – термопары; 3 – молибденовые экраны; 4 – 5 – электровводы с водяным охлаждением; 6 – водяное охлаждение корпуса контейнера; 7 – алюминиевые диафрагмы; 8 – распределительные трубки воздушного охлаждения диафрагм; 9 – штуцер системы вакуумирования.

что постановка теплового экрана позволяет при одинаковой затрате электрической мощности значительно увеличить температуру графитового образца.

Предварительные стендовые испытания показали, что в отсутствии тепловых экранов при электрической мощности в 8 – 10 квт можно достичь температуры графита 1500° – 1600°С.

Для уменьшения неравномерности температуры вдоль образца, обусловленной значительным теплоотводом через медные электроконтакты, на концах образца делались специальные вырезы, приводившие к локальному увеличению тепловыделения и выравниванию температуры. Температура измерялась в центре и на краю образца с помощью иридий-родиевых термопар. Сечение рассеяния измерялось при следующих значениях температуры графита: 15° ± 3°, 490° ± 20°, 1000° ± 30° * и 1370° ± 30°С. Указанная неопределенность учитывает неравномерность температуры по образцу и нестабильность температуры во время измерений.

III. УСЛОВИЯ ИЗМЕРЕНИЙ И ОБРАБОТКА ЭКСПЕРИМЕНТАЛЬНЫХ ДАННЫХ

Измерения дважды дифференциальных сечений графита в указанном диапазоне температур выполнены при трех значениях энергии нейтронов, падающих на образец: 15 мэв, 45,2 мэв и 68 мэв и следующих углах рассеяния: 9,5° **, 21,1°, 40,5°, 55,7°, 70,9°, 86,1°, 101,3° и 116,5°. Разрешение по энергии падающих нейтронов для различных серий измерений составляло 6,5 – 12,5%. Анализ энергии нейтронов, рассеянных образцом графита, проводился методом времени пролета на базе L = 281,75см ± 0,5 см. Рис. 4 иллюстрирует экспериментальные данные по рассеянию нейтронов с энергией 15 мэв и 68 мэв на графите при температуре 15° и 1000°С, полученные непосредственно на каналах временных анализаторов. Более подробно условия измерений представлены в таблице.

На рис. 5 приведены измеренные на тонком образце ванадия спектры упругого рассеяния, характеризующие аппаратурное разрешение в данном эксперименте. Следует отметить, что выбранное разрешение, по-видимому, достаточно для изучения термализующих свойств графита.

В принятой методике измерений важным вопросом является относительная калибровка детекторов. Она была выполнена при помощи измерения интенсивности упругого рассеяния от тонкого образца ванадия, для которого можно довольно точно рассчитывать угловую зависимость рассеяния. Эта зависимость до некоторой степени определяется геометрией образца и сечением поглощения, но главным образом обусловлена фактором Дебая-Уоллера, который был вычислен с использованием экспериментально полученного частотного спектра ванадия [10]. Измерения рассеяния на ванадии были выполнены при трех энергиях нейтронов: 15; 45,2 и 68 мэв, что позволило проверить правильность проведенных вычислений.

---

* Сечение рассеяния при E_0 = 68 мэв измерено при температуре образца 970 ± 30°С.

** В связи со значительным уровнем фона экспериментальные данные для угла 9,5° в окончательных результатах представлены не полностью.

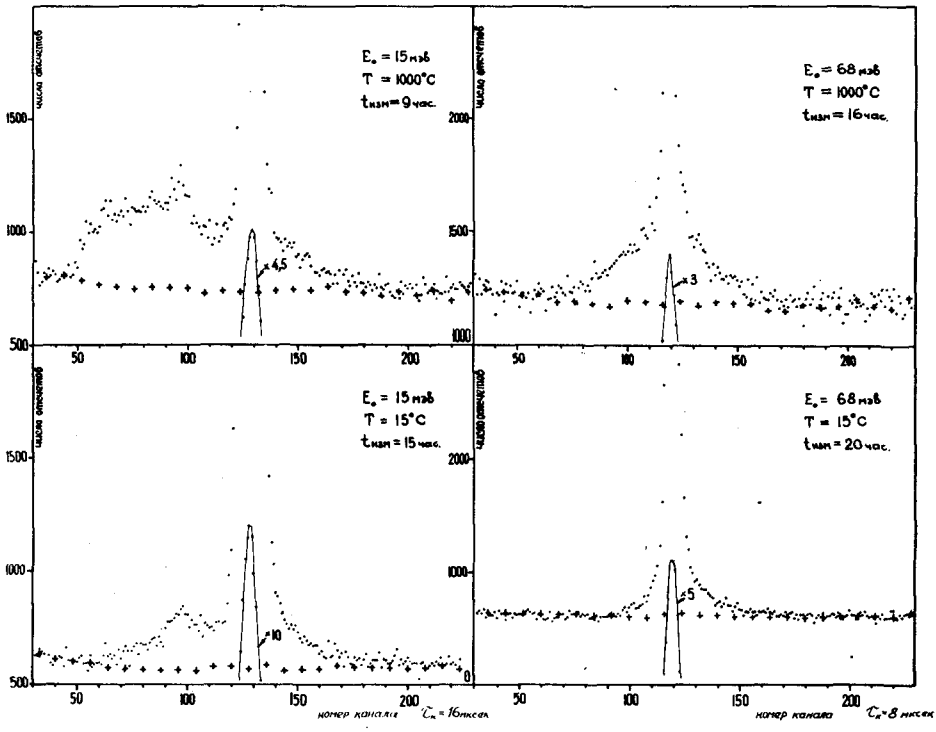

Рис. 4. Спектры нейтронов, рассеянных образцом графита на угол $\theta = 101{,}3°$. +++ – уровень фона.

УСЛОВИЯ ИЗМЕРЕНИЙ

E_0 МЭВ.	$2\varphi_Б$	КРИСТАЛ МОНОХРОМАТОР	(hkl)	α	η	n об/мин	$\tau_к^{эф}$ МКСЕК.	$\tau_к^{ф}$ МКСЕК.	$\frac{\Delta\lambda}{\lambda}$%	ΔE_0 МЭВ.	T ОБР.
15	48,5°	Pb	(111)	59′	22′	7000	16	128	5,4	1,6	15°C 490°± 20°C 1000°± 30°C 1570°± 30°C
45,2	39°	Fe	(110)	59′	17′	12800	8	64	6,3	0,3	15°C 1000°±30°C
68	36,2°	Pb	(220)	16,5′	22′	14300	8	64	3,3	4,5	15°C 490°± 20°C 970°± 30°C

$\varphi_Б$-Брэгговский угол отражения; α-расходимость падающего пучка;
η-мозаичность монокристалла-монохроматора; n-скорость вращения механического прерывателя с шириной щели 0,9 мм и противом 2,7 мм;
T-температура образца.

Известно, что одной из главных трудностей в экспериментах по неупругому рассеянию является высокий уровень фона. Основным источником фона в данном эксперименте были быстрые и промежуточные нейтроны пучка, проникающие сквозь защиту. Этот фон, измеряемый одновременно с эффектом, существенно возрастает с уменьшением угла рассеяния, но слабо зависит от времени пролета (рис. 4), что позволяет усреднять его по многим каналам для уменьшения статистической ошибки.

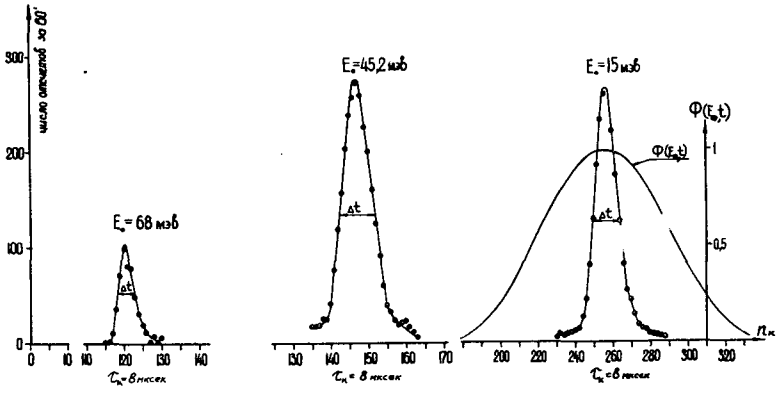

Рис. 5. Упругое рассеяние на ванадии; угол рассеяния $\theta = 86{,}1°$; доля рассеянных образцом нейтронов $R \approx 0{,}1$; $\Phi(E_0, t)$ – функция пропускания механического прерывателя.

Измерения в области высоких температур проводились в контейнере, диафрагмы которого создавали дополнительное рассеяние, сильно зависящее от угла и времени пролета. Эффект рассеяния на диафрагмах измерялся специально, в отсутствии образца и в области неупругого рассеяния составил $\sim 10\%$ от рассеяния на графите.

Как отмечалось выше, функция пропускания механического прерывателя обеспечивает дискриминацию отражения второго порядка от кристалла-монохроматора (рис. 5). Однако, вследствие неравномерности толщины слоя кадмия на стенках щелей ротора, предназначенного для измерений при 15 мэв, ротор пропускал незначительную (менее 1%) долю нейтронов с энергией 60 мэв, соответствующих отражению второго порядка от монокристалла Pb. В связи с этим были проделаны специальные измерения, позволившие оценить и учесть вклад от этих нейтронов в экспериментальных данных для $E_0 = 15$ мэв.

Скорость счета на каналах временного анализатора $N(t, \theta)$ за вычетом фона от перечисленных выше источников связана с дважды дифференциальным сечением $\sigma(E_0, E, \theta)$ для тонкого образца следующим соотношением:

$$\sigma(E_0, E, \theta)\left[\frac{\text{барн}}{\text{мэв стерад}}\right] = \frac{10^{24}}{n} \cdot \frac{N(t, \theta) \cdot \Delta(t)}{N_0} \cdot \frac{1}{\Omega_g} \cdot \frac{1}{\tau_k(t)}, \qquad (1)$$

где:
- n – число ядер графита на см^2 поверхности образца (при $T > 15°C$ учитывалось изменение n за счет теплового расширения образца);
- $\Delta(t)$ – множитель, учитывающий потерю нейтронов за счет их поглощения в воздухе и конструктивных материалах, а также эффективность регистрации нейтронов детектором;
- Ω_g – телесный угол с образца на детектор (стерад.);
- $\tau_k(t)$ – ширина канала временного анализатора, выраженная в энергетических единицах (мэв);
- N_0 – число нейтронов, падающих на образец.

Следует отметить, что величину N_0 целесообразно определять не непосредственно, а воспользоваться измерением полного числа нейтронов, рассеянных образцом с известным значением Σ_s и Σ_a:

$$N_s = \int_0^{\infty} dt \int_0^{\pi} \frac{N(t,\theta)\cdot\Delta(t)}{\Omega_g}\cdot 2\pi\cdot\sin\theta\, d\theta \qquad (2)$$

В этом случае отпадает необходимость в определении величины Ω_g и абсолютного значения эффективности детекторов.

К сожалению, получить N_s прямо из измерений с графитом трудно из-за резкой зависимости $N(\theta)$, обусловленной когерентными эффектами. Поэтому значения N_s были найдены из измерений с тонким образцом ванадия ($n = 1{,}56\cdot 10^{22}$ ядер/см^2). Поскольку у ванадия $\Sigma_a \approx \Sigma_s$, то при вычислении N_0 необходимо учитывать потерю нейтронов за счет их поглощения в образце. Для достаточно тонкого образца с точностью в несколько процентов можно определить N_0 по формуле:

$$N_0 = N_s \Big/ \frac{\Sigma_s}{\Sigma_t}\cdot\left(1 - e^{-\Sigma_t \ell_1}\right)\cdot e^{-\Sigma_a \ell_2}, \qquad (3)$$

где: ℓ_1 – толщина образца в направлении падающего пучка;
ℓ_2 – среднее расстояние, проходимое нейтронами в образце после первого столкновения.

О точности, с которой выполнена абсолютная калибровка сечений, можно судить по величине систематических отклонений в законе рассеяния, полученном из экспериментальных данных для различных значений E_0(рис. 8).

Удобно представить данные в виде, предложенном Браггером в обзорном докладе на Брукхейвенской конференции по термализации [11]. Для этого было вычислено приведенное сечение рассеяния $S(\epsilon, \kappa)$:

$$S(\epsilon,\kappa)\left[\frac{\text{барн}}{\text{мэв}\cdot\text{стерад}}\right] = \sqrt{\frac{E_0}{E}}\cdot e^{\frac{\epsilon}{2kt}}\cdot\sigma(E_0, E, \theta), \qquad (4)$$

где $\epsilon = E - E_0$ – изменение энергии нейтрона,
$\kappa = |\vec{K} - \vec{K}_0|$ – изменение импульса нейтрона (в Å^{-1}).

Область переменных ϵ и κ, охваченная в нашем эксперименте показана на рис. 6.

При переходе к переменным ϵ и κ ось энергии разбивалась на интервалы шириной ΔE, и значения S внутри интервала усреднялись. Это уменьшало статистический разброс и позволило провести через усредненные экспериментальные точки кривые наиболее "правдоподобным" способом.

Пример таких кривых дан на рис. 7.

Зависимости $S(\epsilon)$, приведенные на этих графиках, соответствуют экспериментальным спектрам, измеренным при определенном угле рассеяния, и относятся к тем значениям ϵ и κ, которые лежат на кривых $\theta = \text{const}$, показанных на рис. 6.

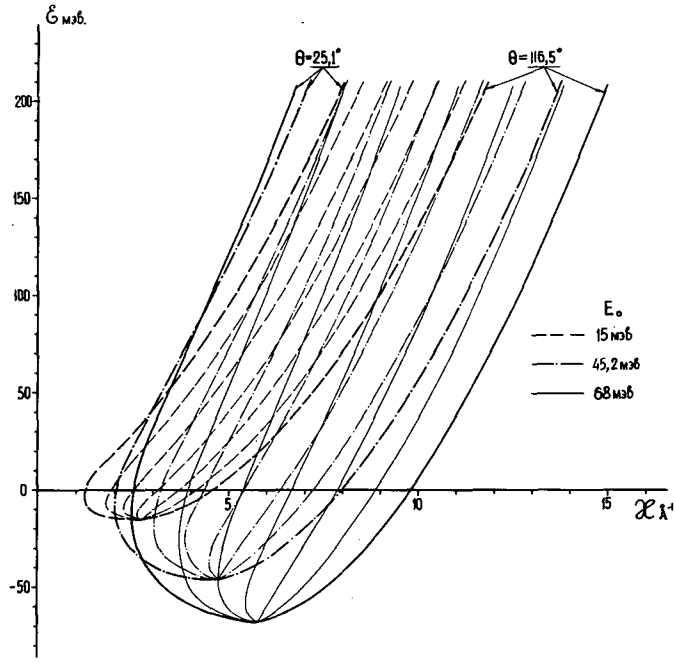

Рис. 6. Область изменения переменных ϵ и κ, в которой измерялось сечение рассеяния.

Для удобства сопоставления с результатами других измерений и расчетов с помощью графиков, соответствующих $\theta = \text{const}$, были построены зависимости $S(\kappa)$ при $\epsilon = \text{const}$. В этом виде и представлена полностью информация, полученная в данном эксперименте.

Вся описанная процедура обработки исходных данных, за исключением последней операции, выполнялась на ЭВМ М-20.

IV. ОБСУЖДЕНИЕ РЕЗУЛЬТАТОВ

Сечение рассеяния в виде $S_\epsilon(\kappa)$ для четырех температур графита приведены на рис. 8. Сечения, полученные из измерений при разных значениях E_0 и соответствующие положительным и отрицательным величинам ϵ, обозначены на графиках различными знаками. Указанные ошибки характеризуют статистическую точность измерений, но не учитывают таких возможных дополнительных источников ошибок, как влияние разрешения, изменение эффективности детекторов в процессе измерений и других, которые увеличивают разброс точек.

На рис. 8 для комнатной температуры приведены также данные других экспериментов, представленные в обзоре Браггера [11]. Наблюдается некоторое расхождение с нашими результатами, особенно при малых ϵ, которое, по-видимому, является следствием систематической ошибки в одном из экспериментов.

Зависимость $S(\kappa)$ имеет явно немонотонный характер, который свидетельствует о том, что усреднение когерентных эффектов в неупругом рассеянии за счет поликристалличности образца происходит неполностью

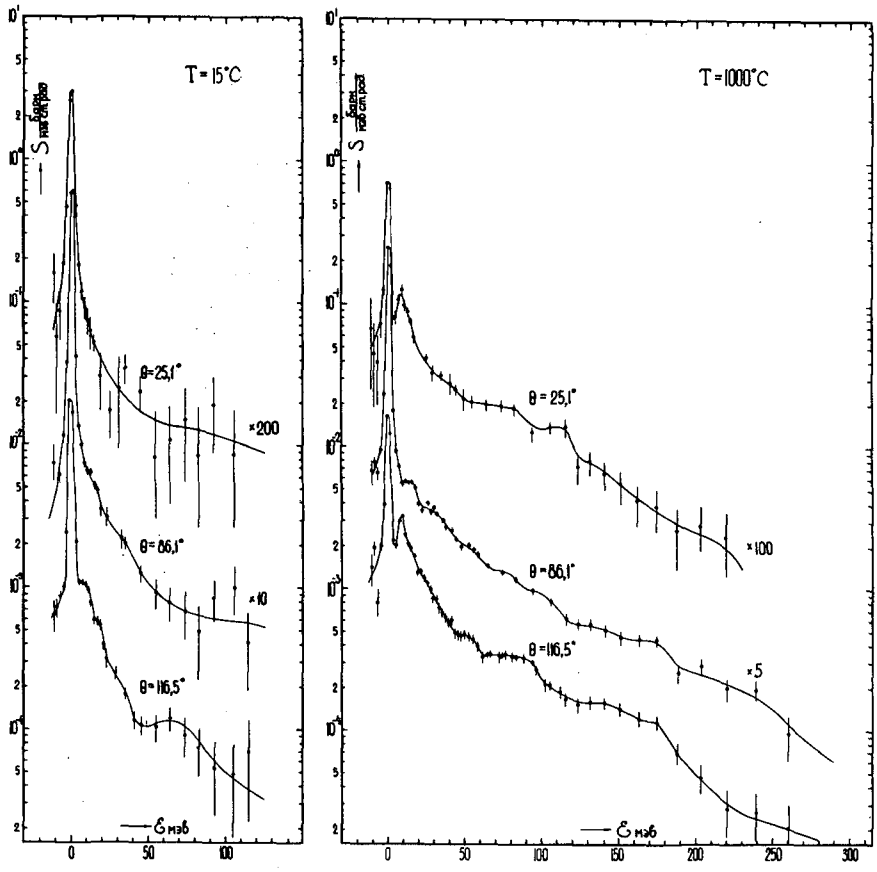

Рис. 7. Приведенные сечения $S(\epsilon, \kappa)$ при $\theta = \text{const}$ для $E_0 = 15$ мэв и двух значениях температуры.

в довольно большой области значений ϵ. Когерентные максимумы особенно отчетливо проявляются в кривых $S_\theta(\epsilon, \kappa)$ (рис. 7), где они в меньшей степени замаскированы разбросом экспериментальных точек.

Для того, чтобы воспроизвести расчетным путем отмеченные особенности сечения, необходимо проводить вычисления $S(\epsilon, \kappa)$ с учетом когерентных эффектов. Однако такой расчет весьма трудоемок и едва ли оправдан для целей термализации. Как отмечалось во введении, при расчете нейтронных спектров в системах с графитом удовлетворительные результаты получаются при использовании сечений, вычисленных в некогерентном гауссовском приближении на основе упрощенного частотного спектра графита, предложенного Эгельстаффом. Для того, чтобы сравнивать дважды дифференциальное сечение, получаемое в таком приближении, с измеренным на эксперименте, Майоровым по программе УПРАС [12] были выполнены расчеты $S(\epsilon, \kappa)$ в исследованной области переменных ϵ и κ при температурах графита 15, 500 и 1000°C. Как видно, вычисленные сечения близки к измеренным не только при комнатной, но и при более высокой температуре.

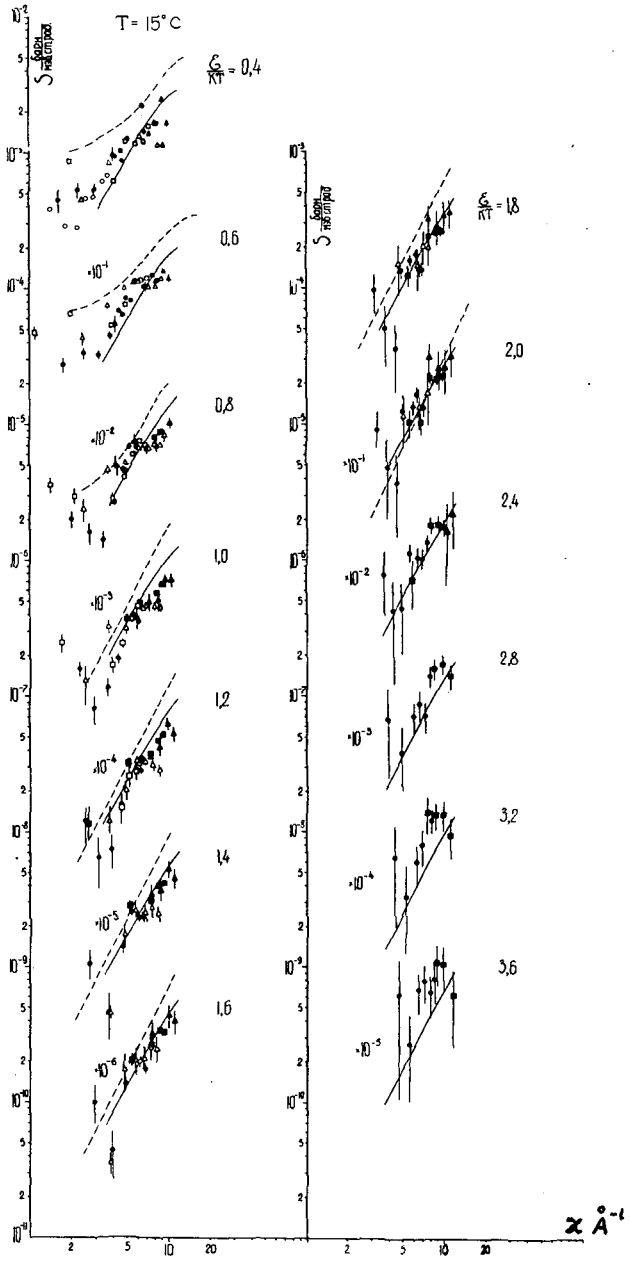

Рис. 8а. Приведенные сечения $S(\epsilon, \kappa)$ при $\epsilon = const$ для графита при температуре T = 15°C.
Экспериментальные значения:
♦ $\epsilon > 0$ ϕ $\epsilon < 0$ $E_0 = 15$ мэв; ♦ $\epsilon > 0$ ϕ $\epsilon < 0$ $E_0 = 45{,}2$ мэв ♦ $\epsilon > 0$ ϕ $\epsilon < 0$ $E_0 = 68$ мэв;
– – – данные, приведенные в обзоре [11];
——— расчет по частотному спектру, предложенному Эгельстаффом с $\theta_D = 2100°$.

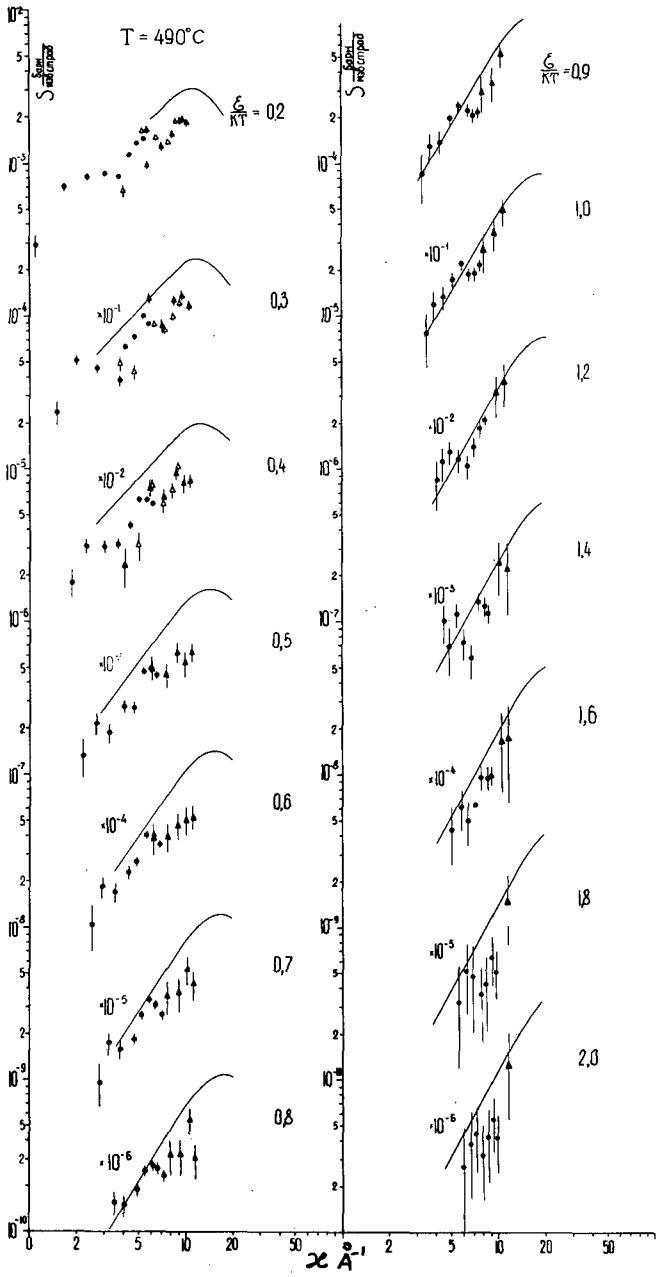

Рис. 8б. Сечения $S(\epsilon, \kappa)$ при $\epsilon = \text{const}$ для графита при $T = 490°C$.

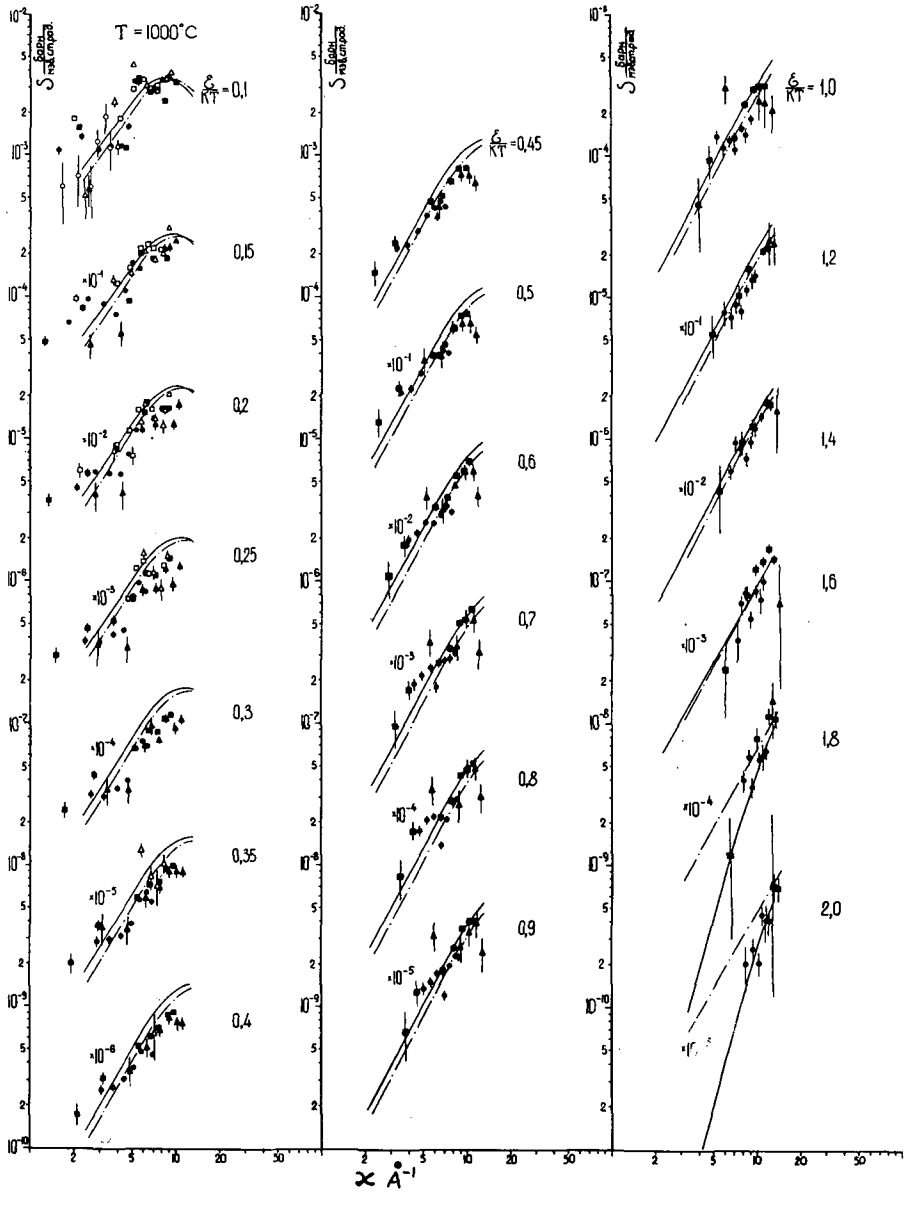

Рис. 8в. Сечения $S(\epsilon, \kappa)$ при ϵ=const для графита при T=1000°C.
— · — Расчет по спектру с θ_D = 2600°C.

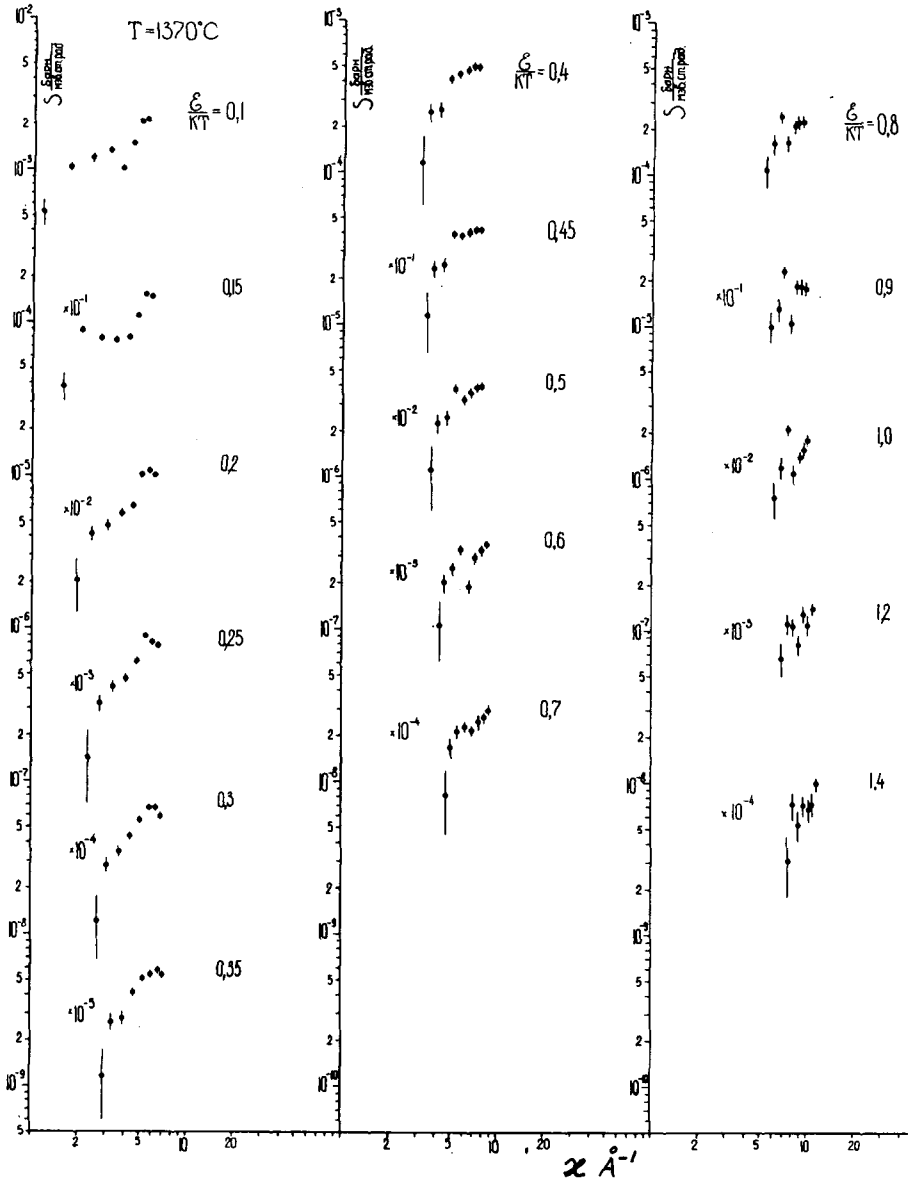

Рис. 8г. Сечения $S(\epsilon, \kappa)$ при $\epsilon = \text{const}$ для графита при T = 1370°C.

Однако эти расчеты не передают деталей зависимости сечения от κ, обусловленных когерентными эффектами, а также недостаточно точно описывают энергетическую зависимость сечения, что связано с принятой приближенной формой частотного спектра. Различие между вычисленной и измеренной энергетической зависимостями сечения несколько увеличивается при повышении температуры графита.

Детальное сопоставление измеренного сечения с результатами расчета дает возможность приблизить вид используемого частотного спектра к реальному путем вариации его параметров. Для примера на рис. 8 показаны две серии расчетных кривых для T = 1000°C, полученных при двух значениях граничной частоты спектра Эгельстаффа $\theta_D = 2100°$ и $\theta_D = 2600°$. Видно, что второе значение θ_D лучше описывает ход сечения, что согласуется с выводами работы [7].

В заключение считаем приятным долгом отметить, что наладка экспериментальной установки и изучение ее физических параметров проводилось совместно с сотрудниками Института физики АН УССР П.Г.Иваницким, В.Т.Кротенко, А.Цыбульником, Б.И.Горбачевым и А.Исаевым.

Авторы благодарны О.М.Воронцову, выполнившему проектно-конструкторские работы по созданию установки, Л.В. Майорову – за расчеты сечений графита и полезное обсуждение результатов, А.А.Осочникову и А.В.Смирнову – за наладку системы многомерного временного анализа, Л.А.Толмачевой, создавшей программу для обработки экспериментальных данных на ЭВМ, В.В.Головневу, О.Я.Ермолаеву, Е.Ф.Польникову и Н.А.Яковлеву – за помощь в измерениях и обработке данных.

ЛИТЕРАТУРА

[1] EGELSTAFF, P.A., COCKING, S.J., "Inelastic Scattering of Neutrons in Solids and Liquids", IAEA, Vienna (1961) 569.
[2] HAYWOOD, B.C., THORSON, I.M., "Inelastic Scattering of Neutrons in Solids and Liquids", IAEA, Vienna 2 (1963) 111.
[3] WOODS, A.D.B., BROCKHOUSE, B.N., SAKOMOTO, M., SINCLAIR, R.N., "Inelastic Scattering of Neutrons in Solids and Liquids", IAEA, Vienna (1961) 487.
[4] EGELSTAFF, P.A., HARRIS, D.H., Phys. Lett. 7 (1963) 220.
[5] EGELSTAFF, P.A., Nucl. Sci. Engng 12 (1962) 250.
[6] EGELSTAFF, P.A., SCHOFIELD, Nucl. Sci. Engng 12 (1962) 260.
[7] WIKNER, N.F., JOANOU, G.D., PARKS, D.E., Nucl. Sci. Engng 19 (1964) 108.
[8] PARKS, D.E., BEYSTER, I.R., WIKNER, N.F., Nucl. Sci. Engng 13 (1962) 306.
[9] МАЙОРОВ Л.В. и др. Proc. Symp. "Pulsed neutron research", IAEA, Vienna 1 (1965) 657.
[10] ЗЕМЛЯНОВ М.Г. и др., "Inelastic Scattering of Neutrons in Solids and Liquids", IAEA, Vienna 2 (1963) 125-142.
[11] БРАГГЕР Р.М., "Термализация нейтронов", Атомиздат, М., 1964, стр. 5 – 20.
[12] МАЙОРОВ Л.В., ТУРЧИН В.Ф., ЮДКЕВИЧ М.С., Доклад P/360 на III Женевской конференции, 1964, Proc. 3rd UN Int. Conf. PUAE, Vol. 2, p. 379.

DISCUSSION

H. TAKAHASHI: According to my calculations, which Dr. Gläser mentioned in his paper[1] the scattering law of parallel modes to the honeycomb graphite plane has a sharp coherent peak at small β, and this becomes broad as β increases. The scattering law of perpendicular modes has a finer coherent peak than that of the parallel mode. For small β, the perpendicular mode is predominant; then at β = 3.0 the parallel mode dominates. I realize that this tendency is indicated clearly in this experiment, but I would like to ask you one question: can you measure the scattering law for each mode separately, using pyrolitic

[1] Gläser, W., SM-96/104, these Proceedings I.

graphite? If this could be done, it would give much useful information about graphite.

A. CHERNYSHOV: Brockhouse has made measurements of this type on pyrolitic graphite. In our experiments on polycrystalline graphite it was not possible to determine the characteristics of separate modes in any detail. It would be better to work on monocrystalline graphite, using the whole crystal, but unfortunately it is not easy to obtain good single crystals of pyrolitic graphite.

SCATTERING LAWS FOR HEAVY WATER AT 540°K AND LIGHT WATER AT 550°K

B.C. HAYWOOD AND D.I. PAGE
ATOMIC ENERGY RESEARCH ESTABLISHMENT,
HARWELL, DIDCOT, BERKS,
UNITED KINGDOM

Abstract

SCATTERING LAWS FOR HEAVY WATER AT 540°K AND LIGHT WATER AT 550°K. Spectral density distributions have been calculated from scattering law measurements on heavy water at 540°K and light water at 550°K; these are compared with the light-water data at room temperature. The scattering laws over all energy and momenta transfers have been generated using the computer programme LEAP and discrepancies between the calculated and experimental results are discussed in terms of coherent and multiple scattering effects. The scattering law for light water at 550°K is used in the programme TRAP to calculate the total scattering cross-sections which are compared with the room-temperature data.

1. INTRODUCTION

Several models for the molecular motions of the water molecule have been used to predict the properties of water as a neutron moderator in reactor calculations [1,2]. In these models the vibrations of the molecules are idealized and represented by harmonic oscillators at a small number of frequencies. The positions and weightings of these oscillators are adjusted to predict some neutron transport property correctly. Calculations of the double-differential scattering cross-sections fail because of the simplicity of the models.

A model has been proposed [3] which represents the molecular motions in water by a continuous distribution of harmonic oscillators. This has been used to predict values of the double-differential scattering cross-sections for light water at room temperature which agree with the experimental values [4]. In this paper the work is extended to light water at 550°K and heavy water at room temperature and 540°K. The treatment of the data follows closely that given by Haywood [3].

2. DATA

A comprehensive set of double-differential scattering cross-sections for various moderators has been obtained using the phased rotor spectrometer on the NRU reactor at Chalk River Nuclear Laboratories. The set includes data for light water at 550°K [5], heavy water at 300°K [6] and heavy water at 540°K [7]. The apparatus is shown schematically in Figure 1 and is fully described by Egelstaff et al. [8] and Brugger [9]; the detailed data collection and data processing methods used on the spectrometer and experimental conditions are given in references [3-10]. The water measurements extend over a range of momentum transfer of 1 - 18 $Å^{-1}$ and energy transfers of 0 - 0.08 eV (D_2O at 295°K) 0 - 0.155 eV (H_2O at 550°K) and 0 - 0.19 eV (D_2O at 540°K).

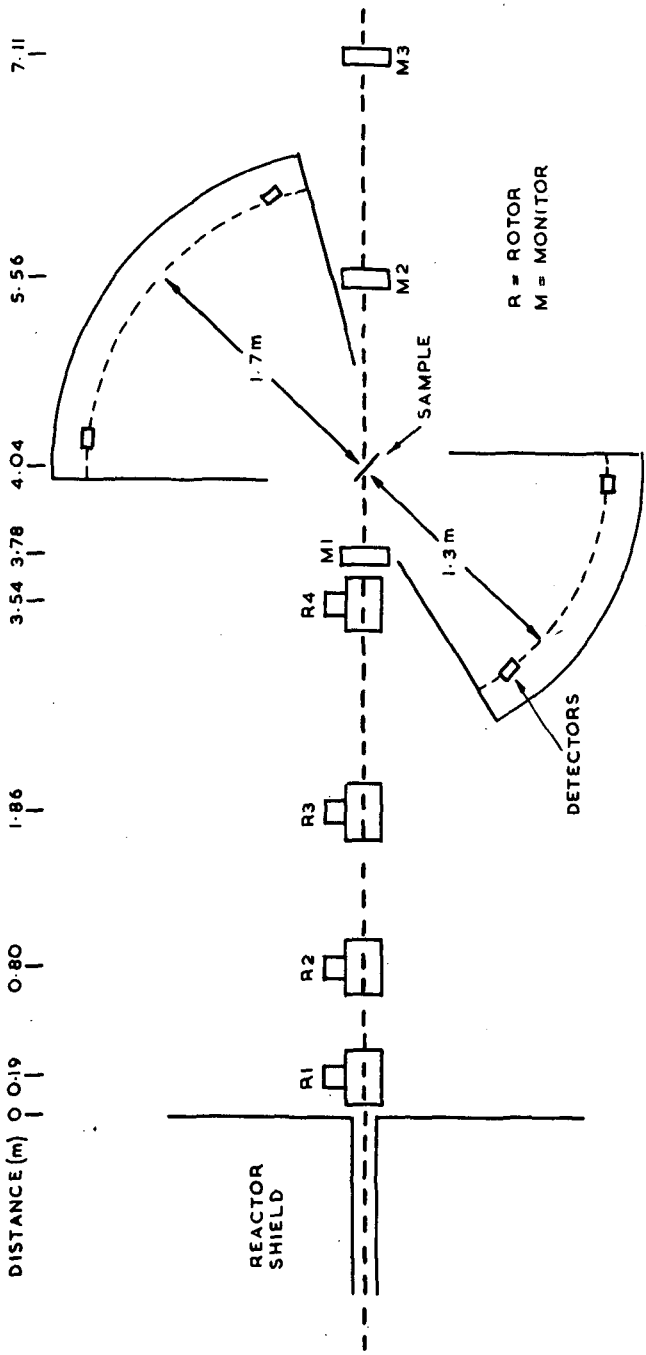

FIG. 1. Schematic diagram of the phased rotor spectrometer.

3. ANALYSIS OF THE DATA

3.1 Determination of the spectral density function

The data are presented in the form of compilations of scattering law $S(\alpha,\beta)$-values in terms of the dimensionless units α and β where S, α and β are defined in the appendix. It has been shown [11] that the spectral density function $\rho(\beta)$ is given by

$$\lim_{\alpha \to 0} \left({}^{S}/\alpha \right) = \frac{\rho(\beta)}{2\beta \sinh \beta/2}$$

and the plot of log $({}^{S}/\alpha)$ as a function of α at a fixed value of β is an almost straight line which can be extrapolated to $\alpha = 0$. By repeating this process at various values of β, an estimate of $\rho(\beta)$ can be obtained. This was done with the experimental data for light water. The estimated $\rho(\beta)$ extended only over the low-energy range (rotational and translational modes) of the spectral density function and did not include the vibrational modes of the molecules. These modes have been observed in light water at room temperature by Raman and infra-red spectroscopy at energy transfers of 0.205, 0.43 and 0.45 eV [12]. It is likely the width of the vibrational lines will increase with temperature but as no experimental evidence is available, the modes are represented as δ-functions in $\rho(\beta)$ at both low and high temperatures. These δ-functions were added at energies of 0.205, 0.43 and 0.45 eV for light water and $1/\sqrt{2}$ of these values (0.145, 0.305 and 0.32 eV) for heavy water. A weighting of 1/6 of the area of the whole $\rho(\beta)$ was assigned to each mode [13]. Self-diffusion was ignored in determining the spectral density functions. Values of the self-diffusion coefficient have been measured in light water up to 353°K [14] and extrapolation gives a value of $(4 \pm 1) \times 10^{-4}$ cm^2/sec at 550°K compared with a value of $1.8 \pm 0.1 \times 10^{-5}$ cm^2/sec at room temperature. Since for light water at room temperature the area of $\rho(\beta)$ allocated to the diffusion modes has been shown to be about 10^{-3} [15], the area at higher temperatures is unlikely to be significant.

For light water the contribution of the oxygen atoms to $\rho(\beta)$ was ignored since the fraction of $\rho(\beta)$ due to oxygen is estimated as 1.6×10^{-3} from the relative masses and cross-sections.

Thus the final $\rho(\beta)$ for light water consisted of a low-energy part derived from the experimental data and ascribed entirely to the motion of the hydrogen atoms, with the addition of the high-energy δ-functions to account for the vibrational levels.

For heavy water the oxygen contribution cannot be ignored and this leads to considerable difficulty when attempting to fit calculated S-values to the experimental data.

3.2 Regeneration of the scattering law S-values

The computer programme LEAP [16] calculates S-values for any given $\rho(\beta)$ using the gaussian approximation and ignoring interference effects due to coherent scattering. The two cases of light and heavy water will be considered separately.

3.2.1 Light water

The contribution of the oxygen atoms to the $\rho(\beta)$ obtained in the previous section is negligible and the scattering by light water is almost

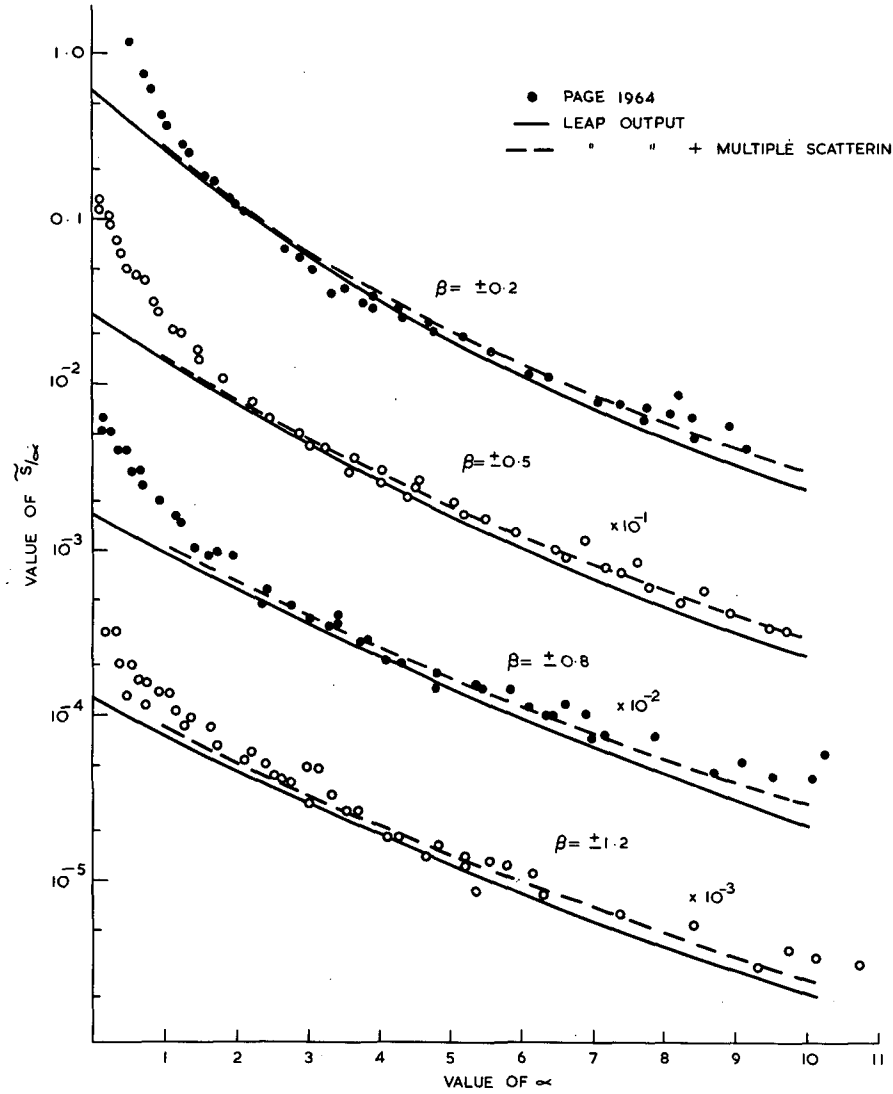

FIG.2. H_2O at 550°K; log (S/α) versus α for β < 1.5.

totally incoherent ($\sigma_{coh}/\sigma_{inc}$ < 3% [17]). Thus the S-values calculated from LEAP can be compared directly with the experimental data. In the published data no correction was made for multiple scattering of neutrons by the sample and this is considered to be the main source of error. Thorson [18] has written a computer programme to calculate multiple scattering effects from an assumed scattering law and this was carried out for light water at 550°K. The experimental points were corrected for multiple scattering and compared with the output from LEAP. An iterative procedure was followed to find the ρ(β) giving the optimum fit to the data. Figures 2 and 3 show the experimental data (S/α v α) for several values of β. The calculated values (LEAP) are shown as a solid line; the multiple

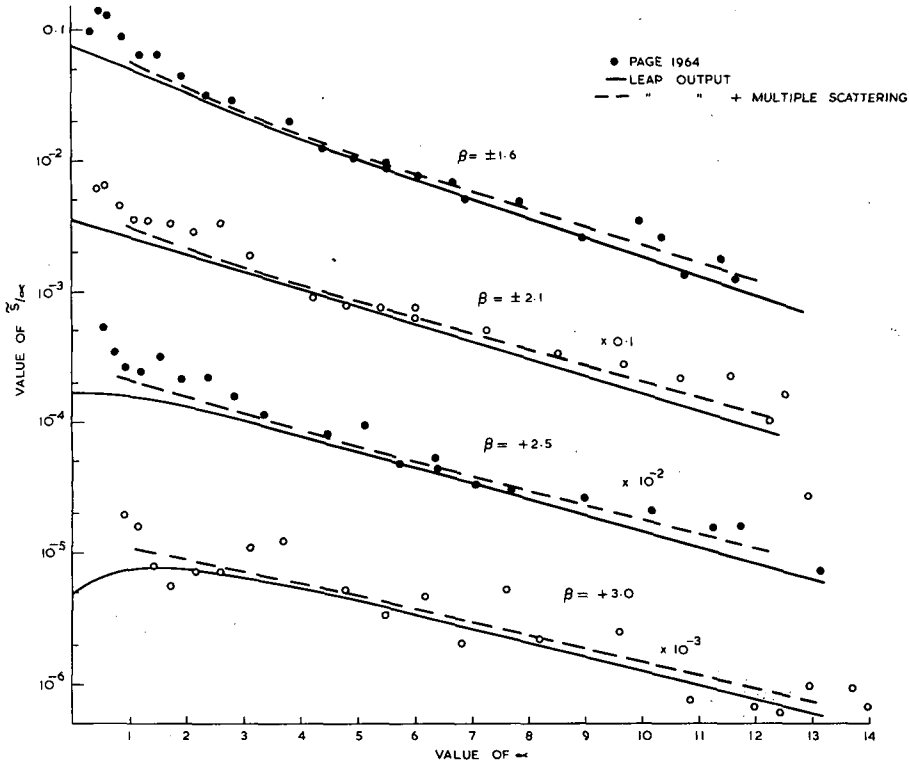

FIG. 3. H_2O at 550°K; log (S/α) versus α for β > 1.5.

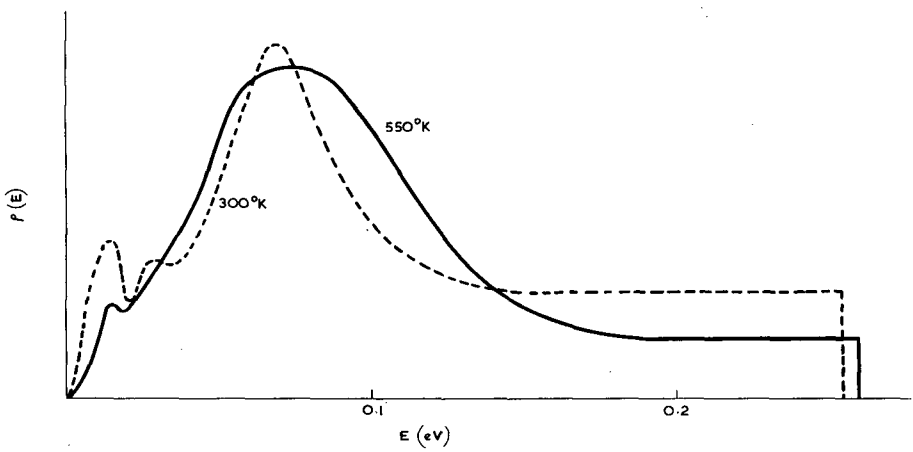

FIG. 4. Spectral density functions for H_2O at 550°K and 300°K.

scattering correction is added to this to give the broken line as the final calculated values. Figure 4 shows the final spectral density function used in the calculations together with that for water at room temperature [3].

3.2.2 Heavy water

The scattering by heavy water is complicated by two further processes. Firstly the oxygen contribution to $\rho(\beta)$ is not negligible and secondly deuterium scatters both coherently and incoherently.

(i) Contribution from the deuterium atoms. It is expected that the deuterium atoms in D_2O will behave in a similar manner to the hydrogen atoms in H_2O. Therefore initially the $\rho(\beta)$ for the deuterium atoms was taken to be the same as for the hydrogen atoms, after allowance for the difference in mass. The scattering law S-values were then calculated using LEAP. This is the incoherent contribution due to the deuterium atoms.

(ii) Contribution from the oxygen atoms. To a first approximation the scattering from the oxygen atoms may be considered as that from free molecules. Therefore the oxygen atoms were taken to be a perfect gas of mass 20. Values of the scattering law for a perfect gas have been calculated [19] and this contribution was added to that of the deuterium atoms, after adjusting the α-values for the mass difference.

(iii) Multiple scattering contribution. This was taken to be the same as for the multiple scattering by light water.

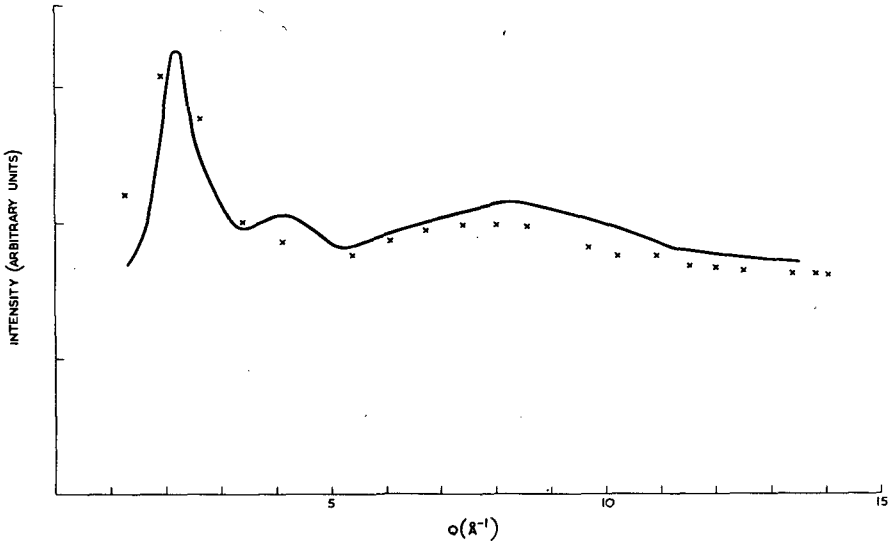

FIG.5. Diffraction pattern (total scattering) from D_2O at 300°K.

(iv) Coherent effects. The diffraction pattern for D_2O at room temperature is shown in Figure 5 [20]. After the first large peak extending up to $Q = 3.5$ Å^{-1} and which is due to intermolecular scattering, the pattern varies slowly about and with small deviation from a mean value. This mean value is the contribution from the incoherent scattering and the self term while the interference terms arise from the coherent scattering. A similar pattern was obtained from the 540°K data and the points corresponding to the 23 detector positions which were used are shown on the figure. Thus in fitting the data we shall expect the experimental points at values of α beyond the first peak ($\alpha > 0.3$, corresponding to $Q > 3.5$) to oscillate about the best line.

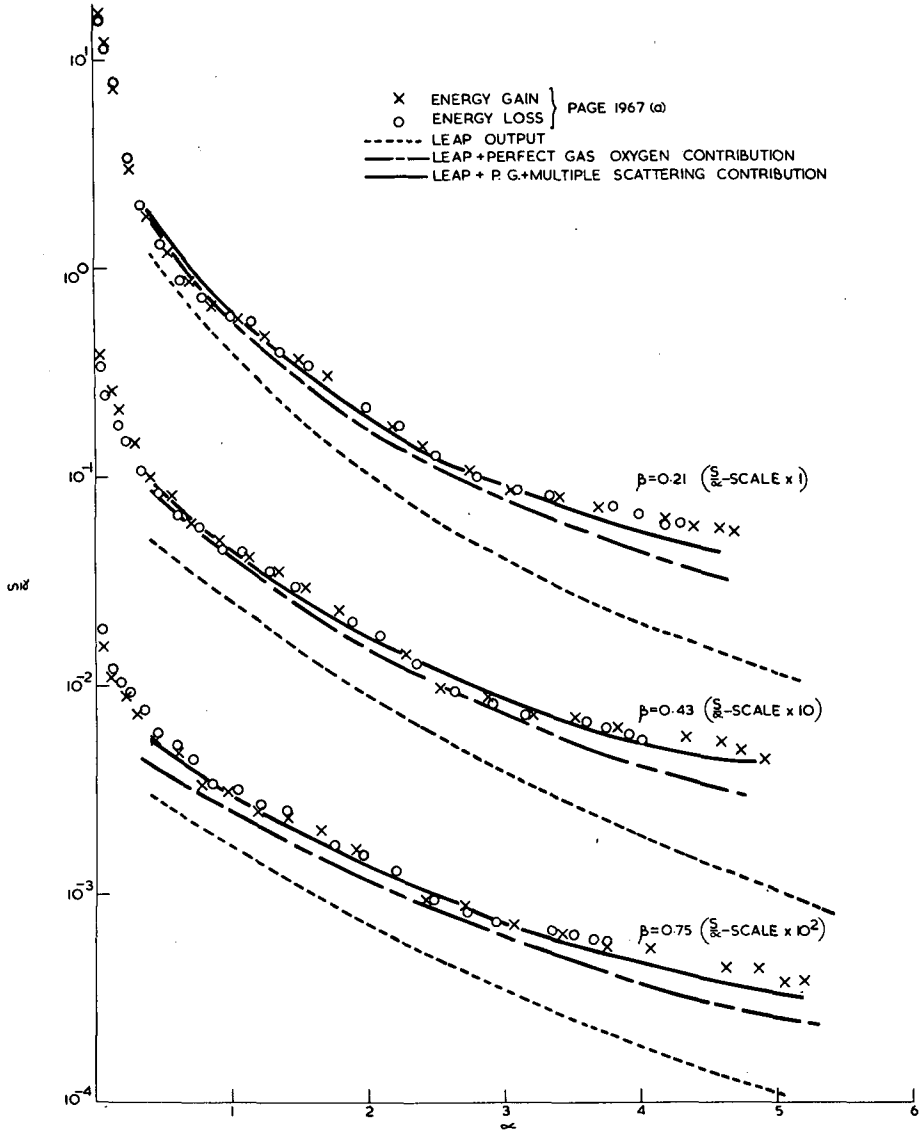

FIG. 6. D_2O at 540°K; $\log(S/\alpha)$ versus α for $\beta < 1.0$.

The S-values calculated by LEAP from the initial $\rho(\beta)$ (deuterium contribution) with the oxygen perfect gas values and multiple scattering corrections added, were compared with the experimental results. The usual iterative procedure was carried out to find the optimum $\rho(\beta)$.

Figures 6 and 7 show the data (S/α v. α) at several values of β for heavy water at 540°K. In each case the broken lines show the contribution due to the deuterium atoms as calculated by LEAP, the chain dotted lines show the addition of the contribution of the oxygen treated as a perfect gas and the solid lines show the final values when the multiple scattering

has been added. Similar curves were obtained for heavy water at room temperature. Figure 8 shows the spectral density functions used in the LEAP calculations.

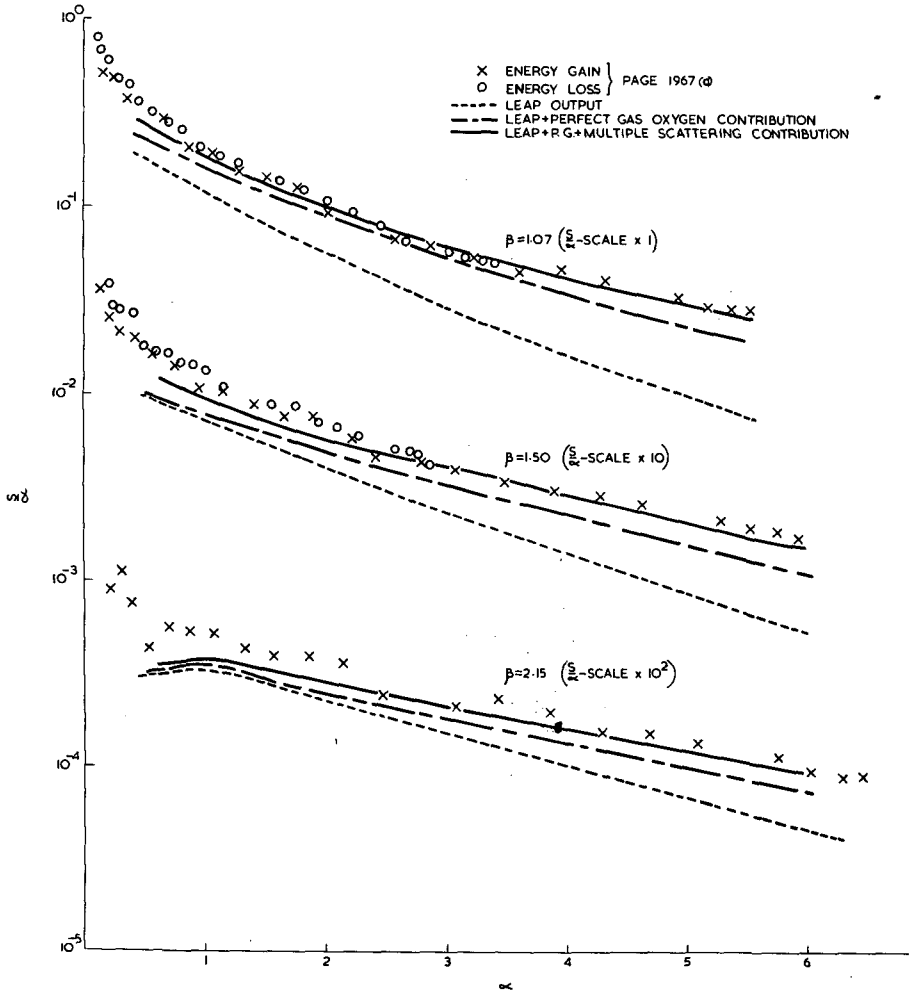

FIG. 7. D_2O at 540°K; $\log(S/\alpha)$ versus α for $\beta > 1.0$.

4. DISCUSSION

4.1 Goodness of fit to the data

For both light and heavy water the calculated curves fit the data within experimental error. The slight discrepancies in the case of heavy water at low values of α can be assigned to coherent scattering effects and this is confirmed by peaks in the diffraction pattern at $Q \simeq 4$ and 8.5 ($\alpha \simeq 0.4$ and 1.6) being apparent. The large first peak which extends to $Q \simeq 3.5$ ($\alpha \simeq 0.28$) means the fitting of the line below this value is not meaningful.

4.2 Comparison of the spectral density functions

The spectral density functions at room temperature and at high temperature are similar for both H_2O and D_2O. In both cases the hindered rotational level (0.07 eV for H_2O, 0.05 eV for D_2O) has increased slightly in energy, as expected. The increased thermal motions at the higher

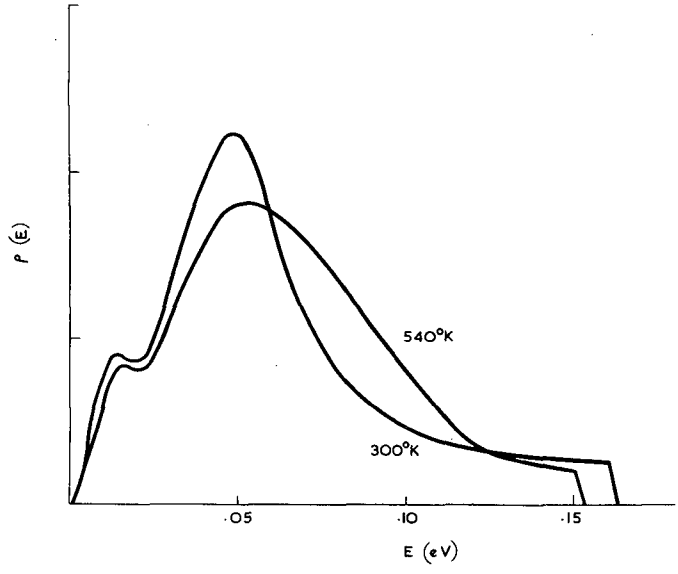

FIG. 8. Spectral density functions for D_2O at 540°K and 300°K.

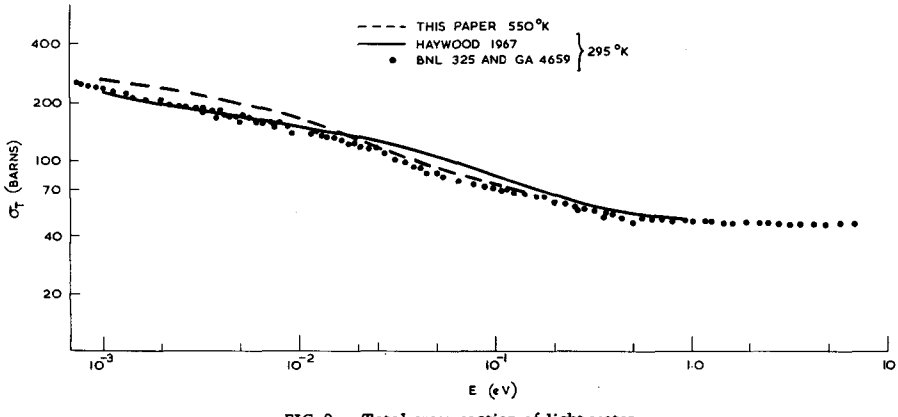

FIG. 9. Total cross-section of light water.

temperatures lead to a broadening of the level. The width of the hindered translational levels (0.025 eV for H_2O, 0.015 eV for D_2O) has also increased and the level merges more into the rotational peak. The peak at 0.012 eV in the room-temperature light water which may be related to the peak at 0.007 eV reported by Larsson [21] has decreased in intensity at the higher temperature, as noted by Larsson. There is possible evidence for the existence of a peak at about 0.1 eV reported by Sanalan [22]; this corresponds to the band found in Raman spectra at 800 cm^{-1} and attributed by Walrafen [23] to libration of the hydrogen bond.

5. CALCULATION OF THE TOTAL CROSS-SECTIONS

The total scattering cross-section (σ_T) can be calculated from the scattering law S-values by integration over all values of α and β. This was carried out for light water at 550°K using the computer programme TRAP [16] which calculates the scattering kernels $\sigma(E \rightarrow E')$ and then σ_T using a trapezoidal numerical integration method. The input data to TRAP was generated by LEAP from the spectral density function in Fig. 4. The results are shown in Fig. 9 together with the experimental [17, 24] and calculated [3] values for room-temperature light water. The calculated lines are similar at the two temperatures except at low energies where the increase in the high-temperature data is probably due to the water molecules being less tightly bound.

The total cross-sections for heavy water cannot be calculated by this method as LEAP does not generate the interference terms.

6. CONCLUSIONS

Spectral density functions for light water (550°K) and heavy water (540°K and 300°K) have been derived and used to calculate scattering law S-values which are in good agreement with the experimental data. The region in the distributions corresponding to large energy transfers ($\Delta E > 0.1$ eV) is not well defined due to the lack of accurate scattering law data but information from infra-red and Raman spectroscopy is used to overcome this. The total cross-sections for light water at 550°K calculated from the complete scattering law follows the values measured at room temperature quite closely. This fact and the similarity in the spectral density functions indicates there is only a small change in the scattering behaviour of water when it is raised from 300°K to 550°K.

APPENDIX

The Scattering Law $S(\alpha,\beta)$ is defined by

$$\frac{d^2\sigma}{d\Omega dE} = \frac{1}{k_B T} \cdot \frac{\sigma_b}{4\pi} \cdot \left(\frac{E'}{E}\right)^{1/2} \cdot e^{-\beta/2} \cdot S(\alpha,\beta)$$

$$\alpha = \frac{E + E' - 2(EE')^{1/2} \cos\theta}{Ak_B T}$$

$$\beta = \frac{E' - E}{k_B T}$$

$$\sigma_b = \sigma_f \cdot \left(\frac{A+1}{A}\right)^2$$

where $\frac{d^2\sigma}{d\Omega dE}$ is the differential scattering cross-section of the specimen

T is the absolute temperature of the specimen

σ_b is the bound atom cross-section

σ_f is the free atom cross-section

k_B is Boltzmann's constant

A is the ratio of the mass of the target atom to the mass of the neutron

E is the energy of the neutron before the interaction

E' is the energy of the neutron after the interaction

θ is the angle through which the neutron is scattered

The mass and bound atom cross-section for only the principal scatterer (deuterium: A = 2.01, σ_b = 7.6b; hydrogen: A = 1.00, σ_b = 81.5b) were used in the compilations.

REFERENCES

[1] NELKIN, M., Phys. Rev. 119 (1960) 741.

[2] McMURRAY, H.L., Idaho Nuclear Corporation Rep. IN-1020 (1966).

[3] HAYWOOD, B.C., J. Nuc. Energy 21 (1967) 249.

[4] HAYWOOD, B.C., UKAEA Rep. AERE - R 4484 (1964).

[5] PAGE, D.I. AECL Rep. 2093 (1965).

[6] HAYWOOD, B.C. UKAEA Rep. AERE - R 4582 (1964).

[7] PAGE, D.I., UKAEA Rep. AERE - R 5408 (1967).

[8] EGELSTAFF, P.A., COCKING, S.J. and ALEXANDER, T.K. AECL Rep. 1494 (1960).

[9] BRUGGER, R.M., "Thermal Neutron Scattering" Ch. 2 (EGELSTAFF, P.A. Ed.). Academic Press, London (1965).

[10] PAGE, D.I., Proc. Phys. Soc. 90 5(1967) (in the press).

[11] EGELSTAFF, P.A. and SCHOFIELD, P., Nuc. Sci. and Eng. 12 (1962) 260.

[12] HERZBERG, G., "Infra-red and Raman Spectra" Van Nostrand, N.Y. (1960).

[13] SCHOFIELD, P. Priv. comm.

[14] SIMPSON, J.H. and CARR, H.Y., Phys. Rev. 111 (1958) 1201.

[15] EGELSTAFF, P.A., Phil. Mag. Supp. 11 (1962) 203.

[16] McLATCHIE, R.C.F., Unpublished (1962).

[17] HUGHES, D.J. and SCHWARTZ, R.B., Brookhaven Nat. Lab. Rep. BNL 325 (1958).

[18] THORSON, I.M., Priv. comm. (1965).

[19] McLATCHIE, R.C.F., HEARD, C.R.T., EGELSTAFF, P.A. and SCHOFIELD, P., UKAEA Rep. AERE - R 3847 (1961).

[20] PAGE, D.I., Proc. Faraday Soc. (1967)(in the press).

[21] LARSSON, K.E. and DAHLBORG, U., Reactor Sci. Technol. (J. Nucl. Energy Parts A/B) 16 (1962) 81.

[22] SANALAN, Y., Priv. comm. (1967).

[23] WALRAFEN, G.E., J. Chem. Phys. 36 (1962) 1036.

[24] GENERAL ATOMIC PROGRESS REPORT GA-4659 (1964).

DISCUSSION

W. GLÄSER: You mentioned that one contribution to the enhanced slope of your S/α curves for H_2O at small α may come from anharmonic effects. Is there any serious or plausible explanation for having enhanced anharmonic contributions at small α?

D.I. PAGE: None of which I am aware.

W.E. REICHARDT: I think that for light water, too, the experimental double-differential cross-section should be corrected for the oxygen contribution, when Egelstaff's extrapolation technique is used. Although the corrections may well be smaller than the actual experimental errors of the individual points, neglecting the oxygen will introduce a systematic error, which will have an effect, for instance, on the total area under the generalized frequency distribution curve. Scattering law measurements have reached a stage where integral data calculated from their results agree with experimental data to within a few per cent. Further improvement cannot be expected if effects of several per cent magnitude are neglected.

EXPERIMENTAL SCATTERING LAW FOR VARIOUS REACTOR MATERIALS

I. M. THORSON
ATOMIC ENERGY OF CANADA LIMITED,
CHALK RIVER, ONTARIO, CANADA

Abstract

EXPERIMENTAL SCATTERING LAW FOR VARIOUS REACTOR MATERIALS. The double-differential neutron-scattering cross-sections for zirconium hydride and uranium dioxide have been measured on the Chalk River phased-rotor spectrometer at the NRU reactor. The results are presented in the scattering law, $S(\alpha, \beta)$ form. The UO_2 data were taken for four specimen temperatures; results at 27°C and 500°C cover an energy transfer range 0.005 - 0.09 eV and at 1310°C and 1480°C, a range of 0.01 - 0.18 eV. The ZrH_x data were taken with a specimen temperature of 27°C for x = 0, 0.63, 0.98 and 1.98; in all cases the cross-sections due to acoustical modes are negligible for energy transfers above 0.04 eV and the shape, if any, of the optical peak at 0.14 eV is not resolved because of intensity and resolution limitations. The accuracy with which the absolute normalization and important corrections for background, detector sensitivity and multiple scattering can be made is discussed. Multiple scattering is shown to be a significant effect for the low-momentum transfer measurements because it modifies the observed α-dependence and the extrapolated S/α value at $\alpha = 0$.

1. INTRODUCTION

The experimental, double-differential cross-section results given in this paper for UO_2 at several temperatures and for ZrH_x at several hydrogen concentrations are intended primarily for comparison with the predictions of models used for neutron spectrum calculations. The measurements were made on the joint Canada - UK phased-rotor spectrometer [1] on the NRU reactor. Most measurements were made with an incident neutron energy of 0.055 eV but some used 0.11-eV neutrons. Section 2 describes the more important spectrometer characteristics, calibration techniques and data collection and processing procedures as well as the apparatus.

In Section 3 the method of estimating the multiple scattering correction is outlined. Section 4 contains the results, $S(\alpha,\beta)$, in graphical form. The results are defined for fixed energy transfer by summing the experimental cross-sections between arbitrarily chosen energy boundaries. Space limitations necessitate energy groupings which are usually larger than the energy resolution of the spectrometer and sometimes significantly larger than the structure in the results. The more detailed results are available as a report [2] or tabulation on magnetic tape.

2. EXPERIMENTAL APPARATUS AND PROCEDURES

2.1. Experimental Apparatus

2.1.1. Phased-Rotor Spectrometer

The phased-rotor spectrometer [1] consists basically of two synchronous rotors which select the energy and time-of-

arrival at the specimen of the incoming neutrons and an electronic sorting device to define scattered neutron time-of-flight from the specimen to the detectors. All results presented here were taken with a rotor period of 2000 μs. With this period the standard deviations on the neutron arrival time at the specimen and the incident reciprocal velocity were 3.1 μs and 0.9 μs/m respectively [9]; they were not significantly increased by a long-term mean deviation of ± 1 μs from constant phase between the rotors.

The incident neutron beam intensity, resolution and reciprocal velocity were continuously monitored by flat thin-walled fission detectors placed directly in the beam on either side of the specimen; one was between the last rotor and the specimen and the other down-beam from the specimen. Scattered neutrons were detected in two banks of scintillator-photomultiplier detectors. Fifteen scintillators 7.6 x 15.2 cm were used in transmission geometry (scattered neutrons pass through the specimen) for scattering angles between 10° and 90°; nine scintillators, 12.1 cm square were placed in reflection geometry (neutrons emerge from the same side of specimen as incident) at scattering angles between -90° and -160°. All data except those for UO_2 at $510^{o}C$ were taken with specimen-to-detector flight path distances of 1.74 m for the 1st quadrant detectors and 1.29 m for the 3rd quadrant detectors. The $510^{o}C$ UO_2 data were taken with 1.29-m flight paths to all detectors.

2.1.2. Time-of-Flight Analyser and Data Recording System

The events from all scattered neutron and beam monitor detectors were sorted into 270 4-μs time channels according to time-of-arrival relative to an arbitrary phase point in the primary rotor cycle. Events were coded as to time-channel of arrival and detector of origin in 16-bit words; each word along with a 5-bit code defining the specimen positions was recorded on a magnetic tape. The magnetic tape was subsequently read back, sorting the events of 900 channels at each pass of the magnetic tape into a ferrite core store. The information was then punched on cards for input to a computer.

2.1.3. Specimens and Specimen Holders

Scattering specimens for all experiments were plane slabs placed with the specimen normal in the plane of the scattered neutron detectors and at 45° to the incident beam direction. In taking the uranium dioxide data the detector background count rates were measured in alternate 15-minute periods with an empty, identical specimen container. For the zirconium hydride data a four-step cycle was used: two zirconium hydride specimens, a vanadium specimen and a blank were placed in the beam sequentially.

The room-temperature results were taken with an evacuated specimen tank which had 0.3-mm aluminum ports for the incident, transmitted and scattered neutrons. The ambient temperature at the specimen position was 27 ± $3^{o}C$. The UO_2 results were all taken with pressed, sintered polycrystalline specimens in the form of slabs 0.20 x 5.1 x 6.3 cm.

The UO_2 results at 510°C were taken with a holder which heated the specimen by conduction from the clamped edges of the slab. A 0.1-mm thick cylindrical aluminum heat shield surrounded the specimen. The temperature was measured with an iron-constantan thermocouple at the edge of the specimen. The temperature gradient across the specimen was measured separately. The mean temperature of the in-beam portion of the specimen was 510 ± 10°C.

The UO_2 data at 1310°C and 1480°C were taken with a specimen holder furnace which heated the UO_2 slab by radiation from 0.71-mm diameter tungsten heater wires spaced 0.66 cm from the slab surfaces. The heater wires were parallel to both the specimen plane and the detector plane at a spacing between windings of 2.5 mm. Two tungsten heat shields surrounded the specimen and heaters; one 0.08-mm thick plane parallel to the specimen and a second cylindrical, 0.05-mm thick. Two cylindrical molybdenum heat shields both 0.08-mm thick and a 0.15-mm aluminum vacuum tank wall also intercepted both incident and scattered neutrons. The specimen temperature was measured with a tungsten-rhenium thermocouple at the edge of the specimen; the temperature variation at other points in the specimen was probably less than ± 25°C at 1480°C. Corrections for the neutron beam attenuation by the holder walls were applied as discussed in Section 4 below.

The zirconium specimen was made up of five 0.76-mm plates. The specimens of zirconium hydride were produced by gaseous hydriding of thin (0.4 to 0.8 mm) zirconium plates at ~800°C. The specimens warped appreciably but the ± 3-mm variation from the ideal plane should not affect the results significantly. The hydrogen concentration was estimated from the weight gain on hydriding.

2.2. Spectrometer Characteristics and Calibration

2.2.1. Intensity, Resolution and Velocity Calibration

For all experiments reported here the total beam intensity at the specimen was 1-2 x 10^4 n/s. The angular resolution of the incident neutron beam in the plane of the detectors is ~0.015 radians, full width; this is small compared to the azimuthal angular width of the detectors which range from 0.044 radians for the 7.6-cm wide detectors at 1.74-m flight path to 0.094 radians for 12.1-cm detectors at 1.29 m.

The reciprocal velocity resolution depends on the outgoing reciprocal velocity and the scattering angle. The variance of the reciprocal velocity measurement σ_R^2 is given by [9]

$$\sigma_R^2 = \frac{1}{x_{SD}^2}\left(\sigma_t^2 + \frac{a^2}{12}\left(\tau_o \tan\theta_N + \tau\,\frac{\sin(\theta-\theta_N)}{\cos\theta_N}\right)^2 + \left(x_{CS} + \left(\frac{\tau}{\tau_o}\right)^3 x_{SD}\right)^2\sigma_\tau^2\right) \qquad 1.$$

where

σ_t^2 is the variance on the time-of-arrival at the chopping point (mid point between the primary rotors) of the neutrons finally selected by the rotor system,

a is the beam width in the plane of the detectors,

τ_o is the incident neutron reciprocal velocity,

τ is the final neutron reciprocal velocity,

θ_N (= 45) is the angle between the specimen normal and the incident beam,

θ is the neutron scattering angle,

x_{CS} (= 1.87m) is the distance from the chopping point to the specimen,

x_{SD} is the distance from the specimen to the detector and

$\sigma_\tau{}^2$ is the variance on the reciprocal velocity of the neutrons selected by the rotor system.

The incident reciprocal velocity was calculated from the measured distance and mean time-of-arrival difference for the beam monitor detectors. The resolution parameters σ_t and σ_τ were also calculated from the distances and measured variances on the arrival times of the neutrons at the beam monitor detectors. The precise specimen-to-detector distances used in calculating the reciprocal velocity scales were deduced from the measured time-of-arrival of the neutrons elastically scattered by a vanadium specimen. Besides being convenient, this method compensates, to first order, for any inherent delay differences between time-of-arrival and detector pulse for the various detectors.

2.2.2. Detector Sensitivity

The scattered neutron detector sensitivities relative to the beam monitor sensitivity were also measured with a vanadium scattering specimen. For beam monitor count of C_m in a detector of sensitivity ε_m the relative macroscopic (including detector solid angle) sensitivity of a scattered neutron detector, $\varepsilon_d \Delta\Omega/\varepsilon_m$, is given by

$$\frac{\varepsilon_d \Delta\Omega}{\varepsilon_m} = \frac{C_d}{C_m} \; \frac{\sigma_T}{\sigma'} \; \frac{1}{1 - T} \qquad 2.$$

where

T is the transmission factor of the specimen,

σ_T is the total cross-section of specimen at the incident neutron energy.

C_d is the scattered neutron detector count coming from a component whose cross-section is σ'. This component can be any identifiable part of the scattered neutron distribution.

For incident neutron energies $E_o \geq 0.03$ eV the total scattering (elastic and inelastic) from vanadium was used; $\sigma'(\theta)$ is then given by a relation due to Placzek [3].

$$\sigma'(\theta) = \frac{\sigma_f}{4\pi} (1 + 2.6 \times 10^{-4}/E_o + 0.039 \cos \theta) \qquad 3.$$

where $\sigma_f = 4.93$ barns, the free atom scattering cross-section for vanadium. The detector sensitivity so deduced was associated with the incident neutron energy after making a correction to the measured inelastic component for the variation of detector sensitivity with energy.

For incident neutron energies below $E_o = 0.03$ eV the elastic component can be easily identified at all scattering angles and the angular distribution of this component is given by

$$\sigma'(\theta) = \frac{\sigma_b}{4\pi} e^{-\lambda\alpha} \qquad 4.$$

where $\sigma_b = 5.13$ barns, the bound atom cross-section for vanadium, $\alpha = 1.53\ E_o(1 - \cos \theta)$ and λ, the Debye - Waller factor, has the value 4.2 based on a weighted mean from several sources [4].

Expressions (3) and (4) define the angular distribution due to single scattering only. For the vanadium specimens used $T \sim 0.75$ and multiple scattering generally contributed $\sim 12\%$ to the scattered neutron intensity. Corrections were made to the detector sensitivities based on multiple scattering calculations similar to those described below for the results.

The detector sensitivities were measured at discrete neutron energies by taking vanadium results at different incident neutron energies. The detector efficiency results for each detector were then fitted by least squares to an expression of the form

$$\varepsilon(\tau) = \Sigma'(\tau) \cdot \frac{e^{-\Sigma(\tau)} - e^{-\mu}}{\mu - \Sigma(\tau)} \qquad 5.$$

to give the best values for μ. $\Sigma(\tau)$ is the macroscopic $Li^6(n,\alpha)H^3$ reaction cross-section for the plane slab scintillator and μ is an effective photon absorption parameter.

2.2.3. Data Processing and Reduction

Punched cards containing the data were processed on a G-20 computer. The initial operation subtracted the background

correction after normalizing by the monitor detector ratio, compared the daily results with previous results, and summed the current results with the previous results. The second operation applied corrections for the detector sensitivity and normalized the data to a double-differential cross-section scale using the relation

$$\sigma(\tau_o \rightarrow \tau,\theta) = \frac{C_\theta(tc)}{C_m} \cdot \frac{\varepsilon_m}{\varepsilon_d \Delta\Omega} \cdot \frac{\varepsilon(\tau_o)}{\varepsilon(\tau)} \cdot \frac{1}{g(\tau_o,\tau,\theta)} \cdot \frac{1}{\Delta\tau} \qquad 6.$$

$\varepsilon(\tau)$ and $\varepsilon(\tau_o)$ were calculated from (5) and $\varepsilon_m/\varepsilon_d\Delta\Omega$ from (2) both based on the vanadium results. $C_\theta(tc)$ is the count in time channel tc of width $\Delta\tau$ at a reciprocal velocity τ in a detector at a scattering angle θ. $g(\tau_o,\tau,\theta)$ is the effective number of scattering molecules in the specimen per unit beam area. It is given by

$$g(\tau_o,\tau,\theta) = \begin{cases} \dfrac{n}{\cos\theta_N} \cdot \dfrac{e^{-\frac{\sigma_T(\tau_o)n}{\cos\theta_N}} - e^{-\frac{\sigma(\tau)n}{\cos(\theta-\theta_N)}}}{\frac{\sigma(\tau)n}{\cos(\theta-\theta_N)} - \frac{\sigma_T(\tau_o)n}{\cos\theta_N}}, & \cos(\theta-\theta_N) > 0 \quad 6a. \\[2ex] \dfrac{n}{\cos\theta_N} \cdot \dfrac{1-e^{-\left(\frac{\sigma_T(\tau_o)n}{\cos\theta_N} - \frac{\sigma(\tau)n}{\cos(\theta-\theta_N)}\right)}}{\frac{\sigma_T(\tau_o)n}{\cos\theta_N} - \frac{\sigma(\tau)n}{\cos(\theta-\theta_N)}}, & \cos(\theta-\theta_N) < 0 \quad 6b. \end{cases}$$

where n is the slab thickness in molecules per unit area in the normal direction, usually based on the specimen transmission and total cross-section, $\sigma_T(\tau_o)$, at the incident reciprocal velocity τ_o. To derive the first-order cross-section values on the assumption that multiple scattering has no net effect $\sigma(t)$ is set equal to the absorption cross-section, $\sigma_a(T)$, for the specimens. For the final results, after subtraction of the multiple scattering component, $\sigma(\tau) = \sigma_T(\tau)$.

$S(\alpha,\beta)$ values are calculated from the cross-section results by integrating numerically over arbitrarily defined outgoing reciprocal velocity limits, τ_{min} and τ_{max}, corresponding to $\beta + \Delta\beta/2$ and $\beta - \Delta\beta/2$ from the relationship

$$S(\alpha,\beta) = \frac{4\pi}{\sigma_b} \frac{\tau}{\tau_o} e^{\beta/2} \frac{1}{\Delta\beta} \int_{\tau_{min}}^{\tau_{max}} \sigma(\tau_o \rightarrow \tau,\theta)\, d\tau \qquad 7.$$

where

$$\beta = \frac{E - E_o}{k_b T} = \frac{c}{k_b T} \left(\frac{1}{\tau^2} - \frac{1}{\tau_o^2}\right) \qquad 7a.$$

$$\alpha = \frac{c}{k_b T} \left(\frac{1}{\tau^2} + \frac{1}{\tau_o^2} - \frac{2 \cos \theta}{\tau \, \tau_o}\right) \qquad 7b.$$

$c = 5226.8$ for τ and τ_o in μs/m and $k_b T$, the specimen temperature, in eV. The σ_b value was arbitrarily chosen to be the sum of the bound atom cross-sections for the various components of the unit "molecule" of the scattering specimen.

3. MULTIPLE SCATTERING

3.1. Multiple Scattering Calculation

The double and triple scattering components emerging from the plane slab specimens have been calculated numerically from tabulated cross-sections. The computer code calculates the collision probability P for the j + 1 generation (number of previous collisions) neutrons in the solid angle segment Ω, layer ℓ and energy group e by integrating numerically over all (Ω,ℓ,e) groups of the jth generation collisions.

The basic equation is

$$P_{j+1}(\Omega,e,\ell) = T(\Omega,e)^{(|\ell-\ell'|-1)}(1-T(\Omega,e))$$

$$\int_\Omega \int_e \int_\ell P_j(\Omega',e',\ell') \cdot \frac{\sigma(e' \to e, \Omega' \to \Omega)}{\sigma_T(e')} \, d\ell' de' d\Omega' \qquad 8.$$

where $T(\Omega,e)$ is the average transmission factor for (Ω,e) neutrons through one of the equal thickness layers and $\sigma_T(e)$ is the total cross-section for neutrons of energy e. For $\ell' = \ell$ the effective transmission factor is calculated from the thin layer approximation. The elastic scattering term, i.e. $e = e'$, is calculated on the basis of the direct or incoherent scattering approximation for each component of the scattering system.

The inelastic component is calculated from tabulated S-values produced by the SOL code of R.G. Jarvis [5]. The "best fits" to the first order (i.e. without multiple scattering correction) experimental $S(\alpha,\beta)$ results have been used. Up to 30 energy groups can be used. Two energy group widths are used; one of ΔE at low energies and one of $3\Delta E$ at higher energies.

The solid angle grid is based on a spherical coordinate system with the polar axis coincident with the specimen normal. Up to 5 azimuthal intervals in 2π space and $4(\ell-1)$ co-latitude intervals in the ℓth azimuthal interval are used. All solid angle segments are equal size.

The code calculates second collision probabilities for all (Ω,e,ℓ) groups "exactly" by integrating over the azimuthal

angle in 1° steps and by using analytical expressions which take precise account of the single collision density within a layer. All succeeding calculations are based on the thin layer approximations. The results for each generation are punched on cards as macroscopic double-differential cross-sections for the specimen for arbitrarily chosen detector angles.

3.2. Multiple Scattering Correction

The multiple scattering of all orders is calculated from the 2nd and 3rd order scattering at each energy - angle point on the assumption of a constant ratio for successive generation beyond the first. As discussed previously [6] this condition should hold accurately for the total intensity integrated over energy at a given angle and should be adequate for the specimen thicknesses used here for the individual energy points. Summing the infinite series gives the following relation for MS, the multiple scattering

$$MS(\tau,\theta) = DS(\tau,\theta)/(1 - TS(\tau,\theta)/D(\tau,\theta)) \qquad 9.$$

where DS is the double and TS the triple scattering component.

The effective multiple scattering cross-sections per specimen molecule are then interpolated from the calculated reciprocal velocity distributions for each time channel of the experimental results. The corrections are applied by subtraction after normalizing the calculated inelastic contribution of all orders to the experimental inelastic component.

3.3. Multiple Scattering for UO_2 and ZrH_x

For all of the results shown here three azimuthal segments were used in calculating the multiple scattering corrections. For all the zirconium hydride results 15 energy groups covered the range from 0 to 0.245 eV. The $S(\alpha,\beta)$ tables were calculated with the SOL program with $\beta_G = 0.6$ and $\beta_d = 5.3$ for both the zirconium and hydrogen components. The A_d parameter for the zirconium component was 0.01 and for hydrogen in the range 0.992 to 0.995 depending on the hydrogen content.

The room temperature UO_2 multiple scattering corrections were calculated using 27 energy groups up to 0.215 eV and for the higher temperature UO_2 corrections 24 groups to 0.322 eV. For all UO_2 cases the S values for the oxygen were calculated with SOL using a single Maxwellian component only with $\beta_G \times k_BT = 0.045$ eV; the uranium values are calculated with two Maxwellian components of $\beta_G \times k_BT = 0.0135$ eV and 0.045 eV. The relative weighting to the lower energy component was 0.46 to give a Debye - Waller factor in agreement with neutron diffraction experiments [7].

4. EXPERIMENTAL RESULTS

4.1. Zirconium and Zirconium Hydride Results

The double-differential cross-sections for scattering 0.055 eV neutrons from $ZrH_{0.98}$ at angles of 44° and 144° are

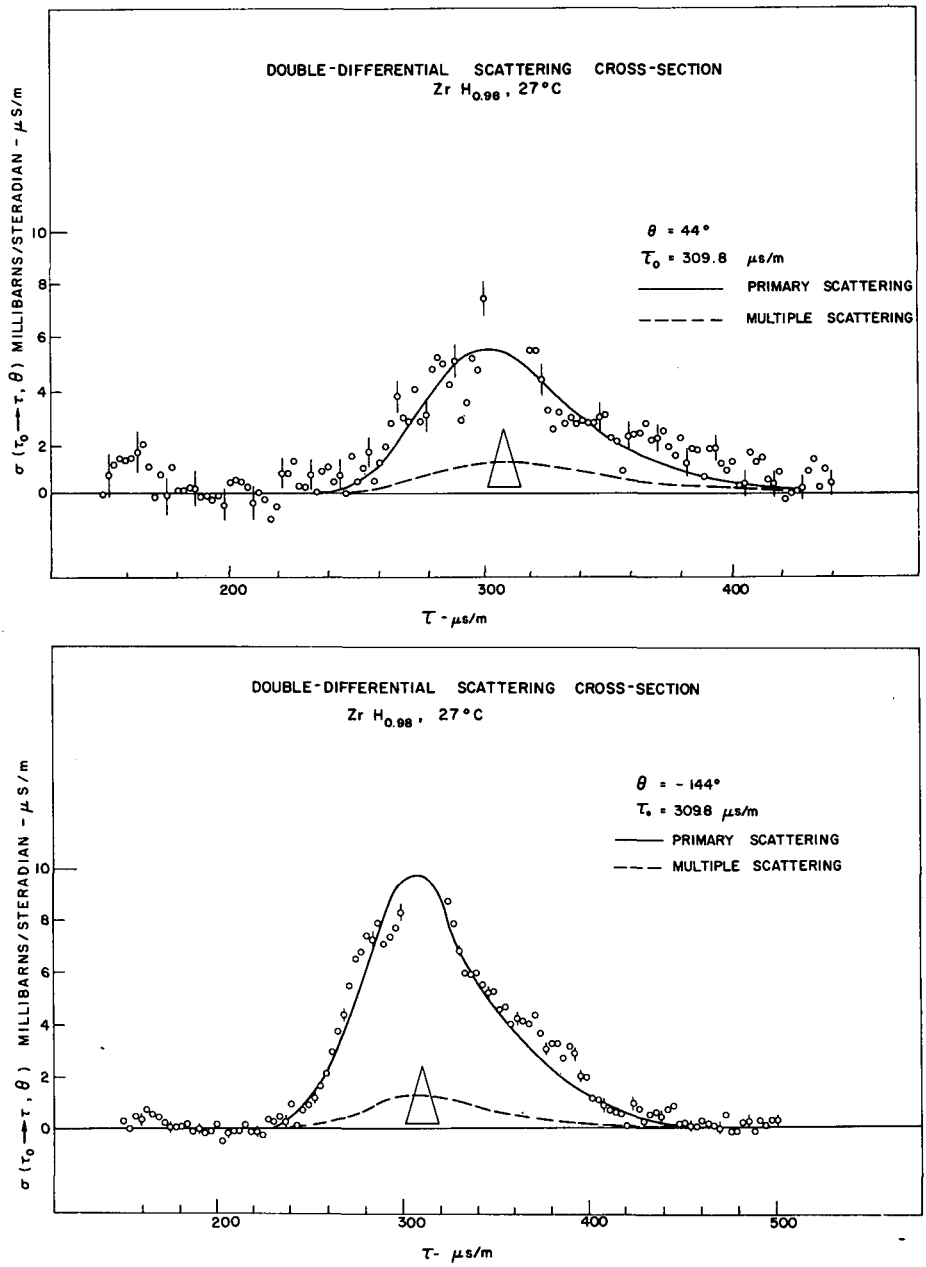

FIG. 1. The double-differential neutron scattering cross-sections for $ZrH_{0.98}$ at 27°C are shown for two scattering angles. The experimental points include a multiple scattering component.

shown in Fig. 1. The solid lines show the single scattering distributions estimated from the S-values used in calculating the multiple scattering corrections. The dotted lines show

the multiple scattering components. They are typical of the results at other angles and hydrogen concentrations, except, of course, of the pure zirconium results which have no component at $\tau \approx 165$ μs/m due to the optical modes. As can be inferred from Fig. 1 the multiple scattering component is essentially isotropic; thus this component of the measured inelastic distribution becomes dominant at small scattering angles. This can be seen more clearly in Fig. 4 where the $S(\alpha,\beta)/\alpha$ for $ZrH_{0.98}$ is plotted as a function of α; for some β-values points are shown both before and after multiple scattering corrections have been applied.

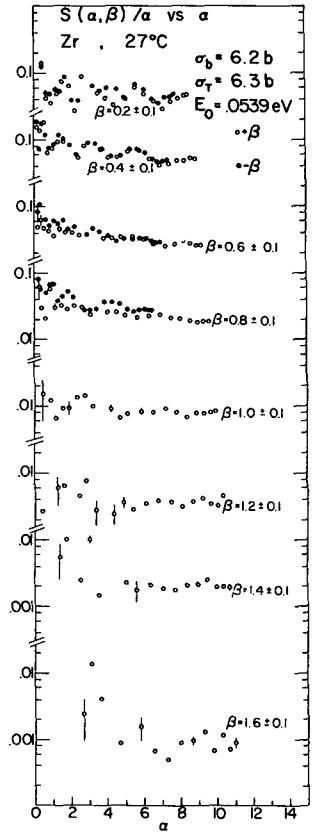

FIG. 2. The scattering law, in the form of $S(\alpha,\beta)/\alpha$ as a function of α, is shown for Zr at 27°C. The ranges of β shown are integration limits for equation (7), not error estimates.

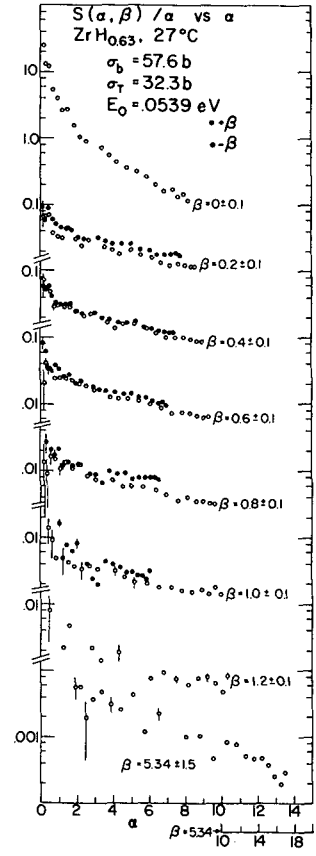

FIG. 3. The scattering law for $ZrH_{0.63}$ at 27°C.

No conclusions can be drawn from present results about the shape, if any, of the distribution due to optical modes because of the low-scattered intensity in these experiments. The present results should, however, be useful in estimating the multi-phonon contribution to the scattering distributions near the optical peaks taken with higher incident energies.

The results for Zr, $ZrH_{0.63}$, $ZrH_{0.98}$ and $ZrH_{1.98}$ are shown in Figs. 2, 3, 4 and 5 respectively as plots of $S(\alpha,\beta)/\alpha$ vs α. Note that α is not scaled by the neutron-to-scattering nucleus mass ratio. The number of scattering "molecules" per unit beam area was calculated in all cases from the measured transmission factors for the incident neutrons. The total cross-section values used in equations (6a) and (6b) to calculate g are shown on the figures. The bound atom cross-sections used in equation (7) are also shown on the figures.

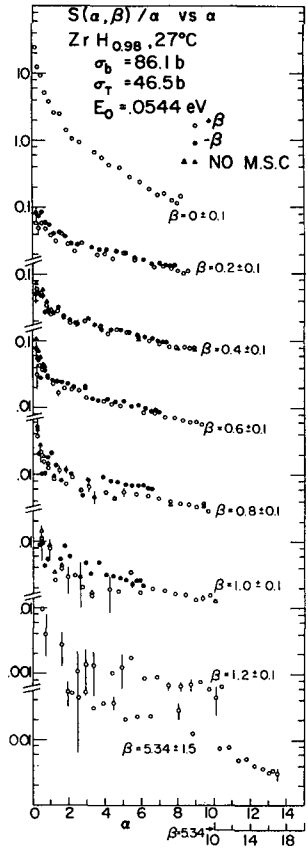

FIG.4. The scattering law for $ZrH_{0.98}$ at 27°C. The points marked No M.S.C. have not been corrected for multiple scattering except for setting $\sigma(\tau) = \sigma_a(\tau)$ in equations (6a) and (6b).

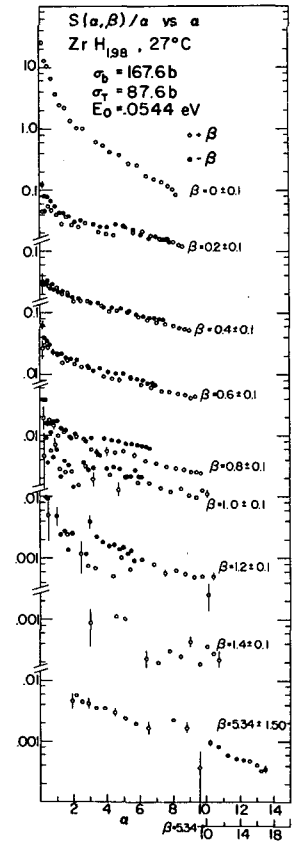

FIG.5. The scattering law for $ZrH_{1.98}$ at 27°C.

The sample error bars on all groups represent one standard deviation due to statistical counting errors only. Other factors introduce probable errors which are usually smaller than but sometimes comparable to the statistical errors. The detector sensitivity assignments involve errors of the order of 5% and the normalization factors, exclusive of total and bound atom cross-section values, can also contribute a few per-

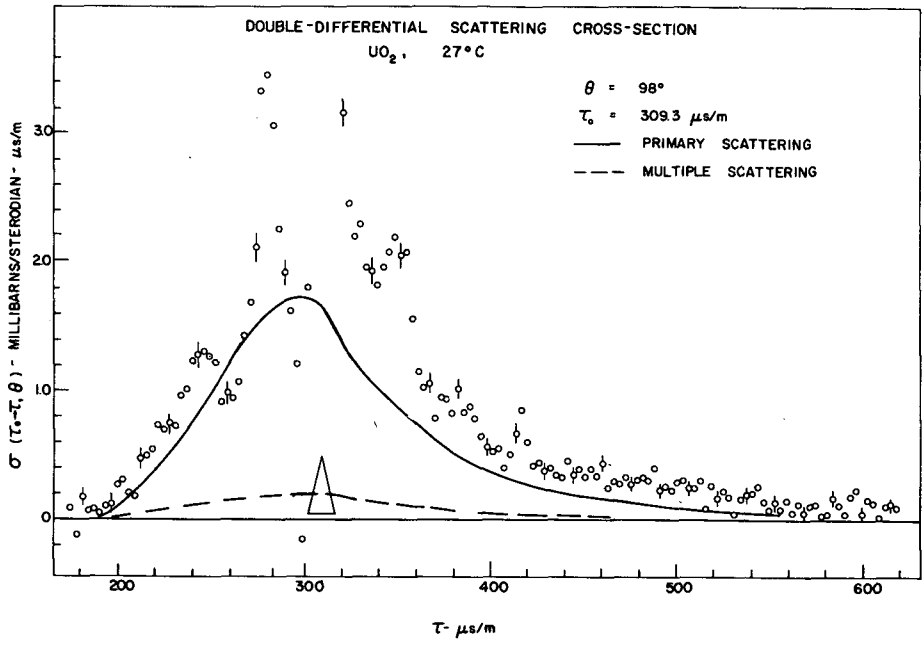

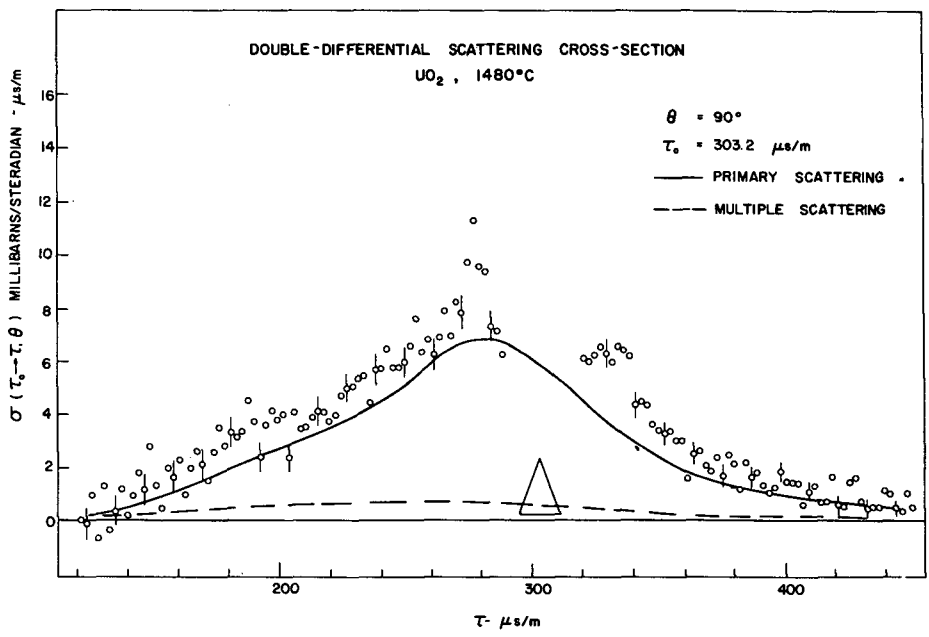

FIG. 6. The double-differential neutron scattering cross-sections for UO_2 at scattering angles near 90° are shown for specimen temperatures of 27°C and 1480°C. The experimental points include a multiple scattering component.

cent. Multiple scattering correction errors cannot be determined with any precision but probably do not contribute significantly beyond the counting statistic errors; where the multiple scattering correction, and, thus potential error, is largest the statistical accuracy is worst. Most points are likely accurate to the quadrature sum of the statistical error plus a 10% standard error from all other sources.

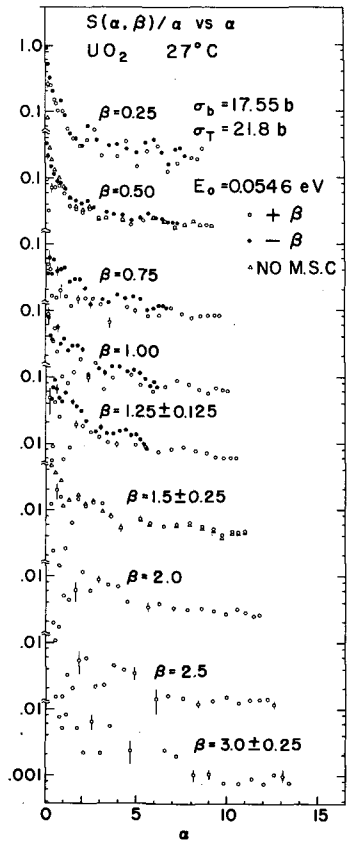

FIG. 7. The scattering law, in the form of $S(\alpha,\beta)/\alpha$ as a function of α, is shown for UO_2 at 27°C. The ranges of β shown are integration limits for equation (7), not error estimates. The points marked No M.S.C. have not been corrected for multiple scattering except for setting $\sigma(\tau) = \sigma_a(\tau)$ in Eqs.(6a) and (6b).

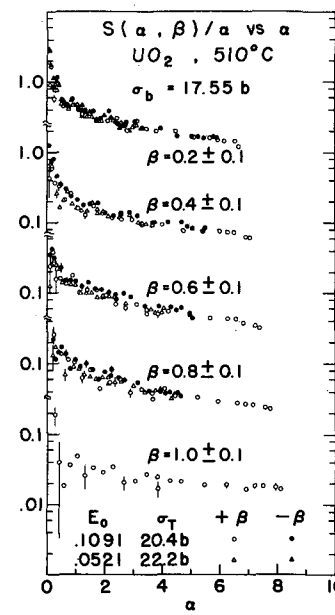

FIG. 8. The scattering law for UO_2 at 510°C.

4.2 UO_2 Results

Fig. (6a) shows the double-differential cross-sections of UO_2 at room temperature for 0.055 eV neutrons at a scattering angle $\theta_D = 98^o$. Fig. (6b) shows the results for UO_2 at 1480°C

and $\theta_D = 90^o$. The single and multiple scattering components are shown as solid and dotted lines respectively, estimated from the S-values produced by SOL.

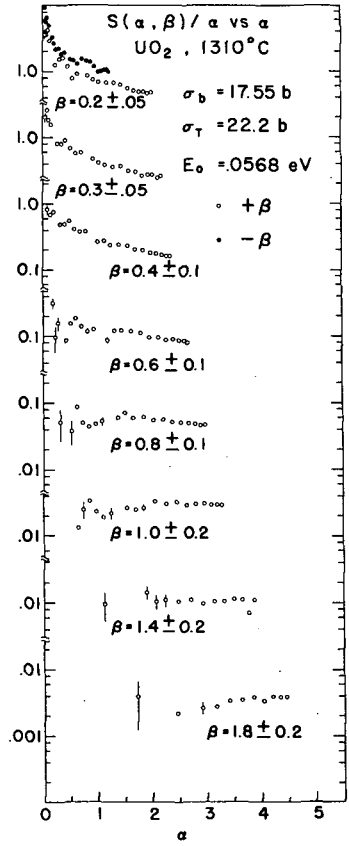

FIG. 9. The scattering law for UO_2 at 1310°C.

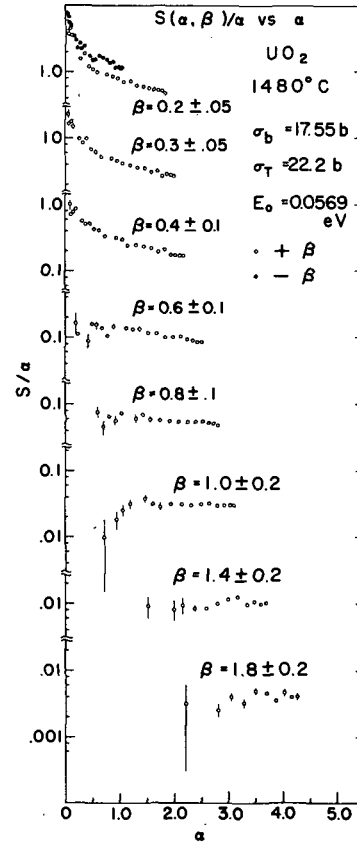

FIG. 10. The scattering law for UO_2 at 1480°C.

The results, especially at room temperature, show considerable structure at energy transfers which correlate quite well with peaks in the frequency distribution of UO_2 deduced from single crystal - single phonon measurements [8]. Interference effects, however, would never allow a precise measurement of the frequency distribution. The results do, however, give considerable support to the procedure of estimating the inelastic double-differential cross-sections for spectrum calculations on the basis of direct scattering only. The interference effects in the coherent scatterer UO_2 are mostly smoothed by orientation averaging at larger α's to give the relatively smooth α-dependence to the S-function in Fig. 7.

At higher temperatures the structure in S(α,β) in both the α and β directions is smaller than at room temperature as can be seen in Figs. 8, 9, and 10. At the highest temperatures the results at low β-values were unreliable because of large

background components from the specimen furnace; these results have been discarded. From Fig. (6b) it can be seen that the results for UO_2 at high temperature show a smooth β-dependence as would be expected from the approach to gas-like conditions for the scattering nuclei.

For the 27°C and 510°C results the error discussion given above at 4.1 for the zirconium hydride results is applicable. For the UO_2 results at the two highest temperatures a fairly large (10 to 20%) correction for the scattering and attenuation by the specimen heaters was necessary. This correction was very difficult to determine accurately and probably makes the dominant error contribution, except for statistical counting errors. The over-all accuracy should be given adequately by the quadrature sum of a 20% relative error on any point and the statistical counting errors.

5. CONCLUSIONS AND ACKNOWLEDGEMENTS

5.1. Conclusions

The experimental results given in this paper are intended for comparison with the predictions of models used in spectrum calculations. These models are always necessary since direct use of the experimental double-differential cross-sections is generally not practical for several reasons. The models are usually based on gross simplifications of the physics of the solid or liquid state but they should be adequate for spectrum calculation provided they are in reasonable agreement with the experimental double-differential cross-section results such as those given above for zirconium hydride and uranium dioxide.

ACKNOWLEDGEMENTS

The author wishes to thank Dr. P.A. Egelstaff who was the driving force in organizing the group and apparatus by which these results were taken. He has also contributed substantially to the author's understanding and appreciation of the entire neutron scattering field.

Thanks are also due to W.J. McKay for extensive help over the years in handling the routine data processing work and to many other technical and scientific staff from CRNL and AERE Harwell for a wide variety of contributions to the scattering law program.

Particular thanks are due to R.B. Turner of CRNL for supervising the design, construction and operation of the high temperature UO_2 specimen furnace and to Dr. R.G. Jarvis for the use of the SOL program.

REFERENCES

[1] EGELSTAFF, P.A., COCKING, S.J., ALEXANDER, T.K., Inelastic Scattering of Neutrons in Solids and Liquids, IAEA, Vienna (1961) 165.
THORSON, I.M., Can. Nucl. Technol. II 2 (1963) AECL-1758.

[2] To be published as an AECL report.
[3] PLACZEK, G., Phys. Rev. 86 (1952) 377.
[4] BROCKHOUSE, B.N., Can. J. Phys. 33 (1955) 889;
GLASER, W., CARVALHO, F., EHRET, G., Inelastic Scattering of Neutrons I IAEA, Vienna (1965) 99.
[5] JARVIS, R.G., SM-96/23, these Proceedings I.
[6] BROCKHOUSE, B.N., CORLISS, L.M., HASTINGS, J.M., Phys. Rev. 98 (1955) 1721.
[7] WILLIS, B.T.M., LAMBE, K.A.D., VALENTINE, T.M., A neutron diffraction study of the thermal motion of the atoms in urania and thoria, Harwell report AERE-R4001 (1962).
[8] DOLLING, G., COWLEY, R.A., WOODS, A.D.B., Can. J. Phys. 43 (1965) 1397.
[9] ROYSTON, R.J., Nucl. Instrum. Meth. 30 (1964) 184.

DISCUSSION

W.E. REICHARDT: I agree with Dr. Thorson that the shape of the low-frequency acoustic modes of zirconium hydride are not influenced appreciably by the number of hydrogen atoms in the unit cell. However, the weight of the acoustic part of the generalized frequency distribution will depend on the hydrogen concentration.

I.M. THORSON: Yes, that is so. The fraction that goes into the optical part over the entire range from 0.63 to 1.98 of the hydrogen concentration changes from 0.992 to 0.995.

A.A. CHERNYSHOV: What is the frequency density in the range between the acoustic and optical parts of the vibration spectrum in zirconium hydride, according to your data? Is it affected by the concentration of hydrogen and the temperature of the sample?

I.M. THORSON: Within the limits of accuracy of the experimental data, the double-differential cross-sections are zero for energy transfers between $\Delta E \approx 0.04$ and 0.11 eV, using incident neutron energies of 0.055 eV, and are independent of the hydrogen concentration. Thus, to an upper limit, which I do not know off-hand but which can easily be found from the experimental data, the frequency distribution is zero between these limits of 0.04 and 0.11 eV. As for your last point, I cannot comment as the experiments were done at room temperature only.

EPITHERMAL NEUTRON INELASTIC SCATTERING AND SCATTERING LAW FOR H_2O

G.J. KIROUAC, W.E. MOORE, L.J. ESCH AND K.W. SEEMANN
KNOLLS ATOMIC POWER LABORATORY *
SCHENECTADY, NEW YORK
AND
M.L. YEATER
RENSSELAER POLYTECHNIC INSTITUTE,
TROY, NEW YORK
UNITED STATES OF AMERICA

Abstract

EPITHERMAL NEUTRON INELASTIC SCATTERING AND SCATTERING LAW FOR H_2O. A new double-differential scattering system at the Rensselaer Linear Accelerator Laboratory has been used to study the interactions of neutrons with liquid H_2O through energy-loss scattering. Measurements have been recently made at six scattering angles and several incident neutron energies in the range 0.15 to 0.63 eV. Room temperature data have been reduced to the cross-section $\partial^2\sigma/\partial\Omega\partial E$, and the scattering law $S(\alpha, \beta)$. All of the results have been corrected for multiple scattering using the Honeck (MUSE) code. The generalized frequency distribution $P(\beta)$ has been derived from the scattering law.

Comparison of these measurements with calculations based on several different theoretical molecular models provides a sensitive test of the scattering kernels used for reactor thermalization problems. A model based upon the Haywood frequency distribution and the McMurry-Russell model are compared with the experimental results. The McMurry-Russell model appears to overpredict scattering from the hindered rotational band of the water molecules. The Haywood model is in fairly good agreement with experiment for most of the energy and angular range, although substantial disagreements remain for the quasi-elastic energy region.

1. INTRODUCTION

A large part of the thermalization research in reactor physics has centred on the construction and evaluation of scattering models for reactor moderator materials. The accuracy of particular models has been tested by experimental and theoretical comparisons of such quantities as asymptotic, time-dependent, and poisoned neutron spectra, and differential and integral cross-sections. All of these methods of study have yielded important information on the thermalization process. However, the detailed knowledge of molecular dynamics required for the construction of realistic scattering models can best be obtained by a study of the experimental scattering law and inelastic scattering cross-section.

A joint programme, by the Department of Nuclear Engineering and Science at Rensselaer Polytechnic Institute (RPI) and the Knolls Atomic Power Laboratory, for the measurement of scattering law and inelastic scattering cross-sections has been in progress for several years. Some of our earlier work with a less sophisticated scattering system has been

* Operated for the United States Atomic Energy Commission by the General Electric Company, Contract No. W-31-109-Eng.-52.

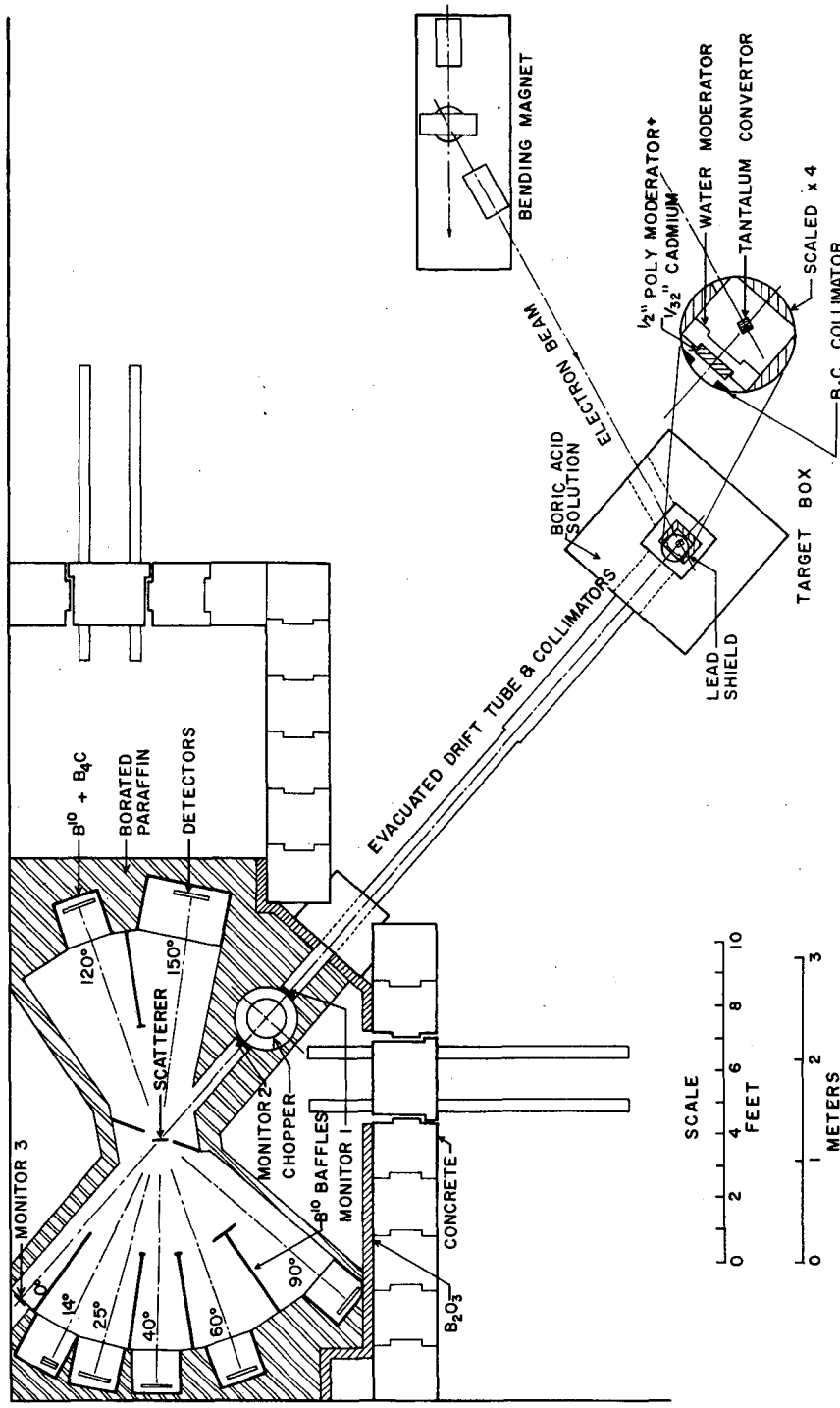

FIG. 1. Experimental layout of RPI-KAPL double-differential scattering spectrometer.

reported elsewhere [1]. The present work on liquid water was performed with the new epithermal neutron spectrometer used by our group at the Linear Accelerator Laboratory at RPI. This high-resolution spectrometer produces monochromatic bursts of neutrons in the energy range from 0.1 eV to several eV and is ideally suited for the study of energy transfer modes from about 0.02 eV up to the incident neutron energy.

Several other studies of the inelastic scattering by liquid water have been reported previously [2-5]. Most of this work has been done for neutron energies below a few tenths of an eV, although chemical binding effects are known to influence thermalization properties at energies as high as a few eV. The present work covered a range of incident neutron energy from 0.15 eV to 0.63 eV. Double-differential cross-sections have been measured at 300°K for five incident energies in this range and at six scattering angles from 14° to 120°. From these data, the scattering law, $S(\alpha,\beta)$, has been obtained and the frequency function, $P(\beta)$, extracted. Cross-sections and scattering law have been compared with various theoretical models. These cross-sections have been integrated to provide a check with the differential scattering measurements of Beyster [6].

2. EXPERIMENTAL METHOD

The room-temperature water specimen was a 0.010-in. slab, held between 0.013-in. aluminium foils which were reinforced by a thin aluminium honeycomb; transmission at 0.15 eV was about 95%. Some measurements were also made with a 0.028-in. specimen in order to check the effects of multiple scattering. All cross-section calculations were normalized by separate measurements using a 0.102-in. vanadium scattering specimen.

Interaction of the pulsed electron beam of the RPI accelerator with an electron-neutron convertor target provided an intense neutron source. A thin water moderator adjacent to the convertor target slowed the neutrons to the epithermal energy range. At a distance of 6 m from the source, a monochromatic neutron burst was selected by a large aperture fast chopper. An evacuated neutron drift tube reduced the intensity loss due to air scattering along the flight path. The chopped beam passed through the scattering specimen, and the scattered neutrons were detected in six banks of high-efficiency ^{3}He counters arrayed at various angles; the spectrum of scattered neutrons was deduced from their time-of-flight. Extensive use of B_4C and ^{10}B shielding along the flight paths and around the detector banks had an important effect in reducing the background. Three thin fission counters monitored the neutron beam incident on the chopper and at two points after the chopper. The first served to normalize various runs to the same source intensity and the last two provided an accurate determination of the incident energy selected by the chopper. A diagram of the experimental layout is shown in Fig. 1, and pertinent details of the spectrometer operation are listed in Table I.

In this experiment the accelerator was synchronized with the neutron chopper; the phase between the two determined the neutron velocity selected by the chopper. The procedure for taking data was to make a run measuring the water specimen scattering and the background, a run with the empty specimen holder, and a vanadium run. During a background measurement the accelerator-chopper phase was shifted by

TABLE I. PARAMETERS FOR RPI-KAPL DOUBLE-DIFFERENTIAL NEUTRON SCATTERING SPECTROMETER

Source: RPI Linear Electron Accelerator

Repetition Rate	- 180-240 burst/s
Pulse Width	- 4.5 μs
Neutron Moderator	- 1 in. × 3 in. × 8 in. H_2O slab

Spectrometer: 15 000-20 000 rev/min Neutron Chopper

Aperture	- 8 in^2
Chopping Slits	- B^{10} impregnated epoxy-fibreglass
Slit Width	- 1/16 in
Burst Width	- 6.8 s at 20 000 rev/min
Incident Flight Path	- 5.97 m
Scattered Flight Path	- 2.36 m

Incident Energy Resolution: Full width at half maximum measured at chopper exit

E_0(eV)	ΔE_0 (eV)	% $\Delta E_0/E_0$
0.23	0.0051	2.2
0.33	0.0087	2.6
0.50	0.014	2.8
0.63	0.019	3.0

Scattered Energy Resolution: Full width at half maximum at neutron detectors

E_0 = 0.23 eV		E_0 = 0.33 eV		E_0 = 0.63 eV	
E_n(eV)	ΔE_n(eV)	E_n(eV)	ΔE_n(eV)	E_n (eV)	ΔE_n (eV)
0.17	0.011	0.26	0.026	0.43	0.046
0.11	0.0084	0.13	0.014	0.18	0.025

half the chopper period. Therefore, when neutrons of the desired incident energy reached the chopper slits the curvature was reversed and the transmission dropped to zero; the experimental configuration was otherwise identical to that of a normal water specimen measurement.

By using appropriate gating circuitry for the combined specimen-background run, every fifth source burst was phased as a background measurement. This procedure of interleaving foreground and background effectively eliminated normalization problems. Vanadium and empty specimen holder runs were made every few minutes. Data were routed into a PDP-7 computer according to scattering angle and type of run. The computer provided programmed time-channel compression, an approximate cross-section versus energy display, and programmed sample changes. A block diagram of the data accumulation system is shown in Fig. 2.

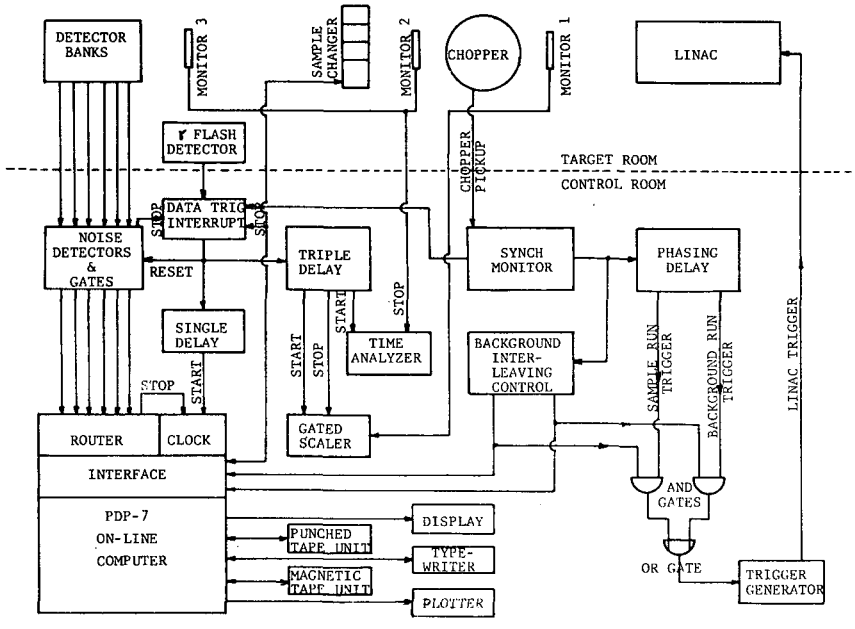

FIG. 2. Block diagram of data accumulation system.

3. RESULTS

Data reduction was accomplished by a system of Fortran IV codes written for a CDC-6600 computer [7]. Raw time-of-flight data were corrected for background and specimen holder scattering. The double-differential scattering cross-section was calculated from the following expression:

$$\frac{\partial^2\sigma(E_i \to E_n,\theta)}{\partial\Omega\,\partial E_n} = \frac{D(E_i \to E_n,\theta)}{D'(E_i,\theta)} \cdot \frac{N'\eta(E_i)}{N\eta(E_n)C_a\Delta E_n} \cdot \frac{\partial\sigma'(E_i,\theta)}{\partial\Omega} \cdot f(E_i \to E_n,\theta) \tag{1}$$

where $D(E_i \to E_n,\theta)$ = normalized water scattering counts in the n'th time channel, $D'(E_i,\theta)$ = total normalized counts in the vanadium scattering peak, N' and N = scattering atoms/cm^2 for vanadium and water samples, $\eta(E_i)$ and $\eta(E_n)$ = detection efficiency for vanadium and water scattering

events, and ΔE_n = energy width of the n' th time channel. Correction for neutron beam attenuation in the vanadium sample was made by the factor C_a. The vanadium scattering cross-section $\partial\sigma'(E_i, \theta)/\partial\Omega$ was represented as a function of the form A + B cos θ. Multiple scattering in the water specimen was included in the factor $f(E_i \rightarrow E_n, \theta)$. The data reduction codes interpolated a table of multiple scattering corrections to obtain the factor at the required values of the energy and angle arguments.

Calculated cross-sections were transformed to the scattering law, $S(\alpha, \beta)$, by the usual formulas [8],

$$S(\alpha,\beta) = \frac{4\pi T}{\sigma_b}\left(\frac{E_i}{E_n}\right)^{\frac{1}{2}} e^{\beta/2} \frac{\partial^2 \sigma}{\partial\Omega \partial E_n} (E_i \rightarrow E_n, \theta) \tag{2}$$

$$\alpha = \frac{E_n + E_i - 2(E_n E_i)^{\frac{1}{2}} \cos\theta}{MT}$$

$$\beta = \frac{(E_n - E_i)}{T}$$

where E_i = incident neutron energy, E_n = final neutron energy, σ_b = bound atom scattering cross-section (81.44 b for hydrogen), T = specimen temperature in eV, θ = lab scattering angle, and M = ratio of principal scatterer mass to the neutron mass (unity for hydrogen). Graphs of the cross-section and scattering law results were obtained directly from the computer output through the use of a Calcomp plotter. Curves were also drawn on the same graphs using a stored table of theoretical results.

Multiple scattering corrections for the experimental data were calculated with the transport code MUSE-2, written by Honeck [9]. This code and the general problems associated with multiple scattering have been extensively studied by Slaggie [10]. Independent calculations of multiple scattering corrections, using Monte Carlo techniques, have been made by Bischoff and Kalos [11], and these have largely confirmed the results obtained with the transport code. To calculate these correction factors, a theoretical scattering kernel must be used, and the corrections will vary somewhat depending on the kernel. For the 0.010-in. water specimen, typical correction factors using different kernels are shown in Fig. 3. It can be seen that the corrections are about 10-25%. The corrections which were applied to the data were based upon the scattering model developed by Koppel [12] from the experimental frequency spectrum of Haywood and Thorson [2].

Corrected experimental results for the double-differential scattering cross-section are shown in Figs 4 and 5. Theoretical curves which are also shown in these illustrations will be considered in another section of this paper. The ordinate of the graphs represents the water cross-section in units of barns/eV steradian molecule, and the abscissa is the scattered neutron energy in eV. Dashed vertical lines indicate the expected location of known excitations of the water molecules, such as the broad rotational band centred near 0.06 eV. Data and theory have been omitted for the quasi-elastic peak at 14° for clarity of presentation. The error bars incorporate the uncertainties due to counting statistics in the background and specimen runs. Systematic errors which may enter

the cross-section calculation have also been estimated. These are: uncertainty in the vanadium cross-section ~ 3%, scattering kernel dependence of the multiple scattering corrections ~ 10%, uncertainty of the incident neutron energy ~ 2%, and sample thickness uncertainty ~ 10%.

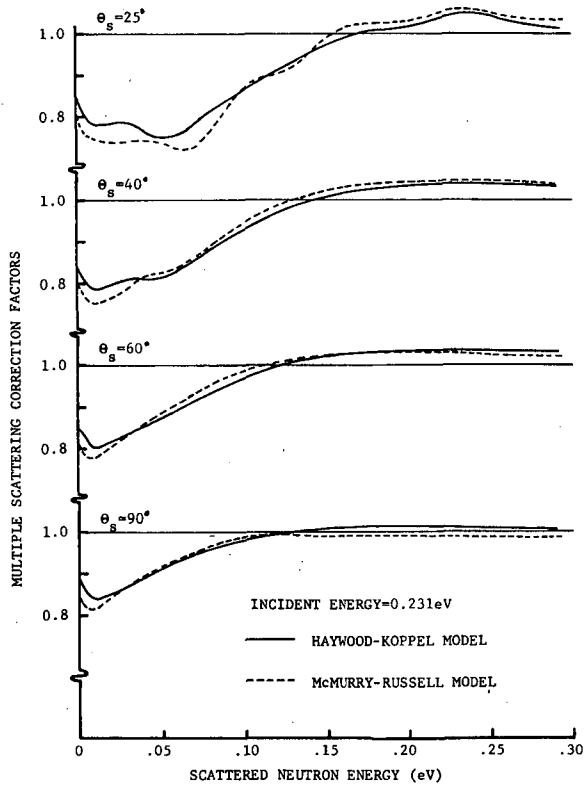

FIG. 3. Multiple scattering corrections at 0.23 eV using the McMurry-Russell model and the Haywood-Koppel model.

Two of the lower energy runs (Fig. 4) demonstrate a strong neutron interaction with the hindered rotation states located near 0.06 eV excitation energy. In agreement with other neutron scattering measurements, the rotational band appears to be wide. Data obtained with 0.332 eV incident neutrons show evidence of the H-O-H angle bending mode at about 0.21-eV excitation. In this case the cross-section profile is influenced by multi-phonon contributions from the rotation band. Preliminary calculations indicate that the multi-phonon content in this energy region varies from about 30% at 14° to 70% at 40°. These calculations emphasize the importance of using low scattering angles to observe the transitions of interest.

Cross-section measurements at incident neutron energies of 0.499 eV and 0.631 eV are shown in Fig. 5. In these runs the rotation band is not resolved from the quasi-elastic peak. The highest energy run illustrates the excitation of the two hydrogen-bond stretching modes near 0.45-eV

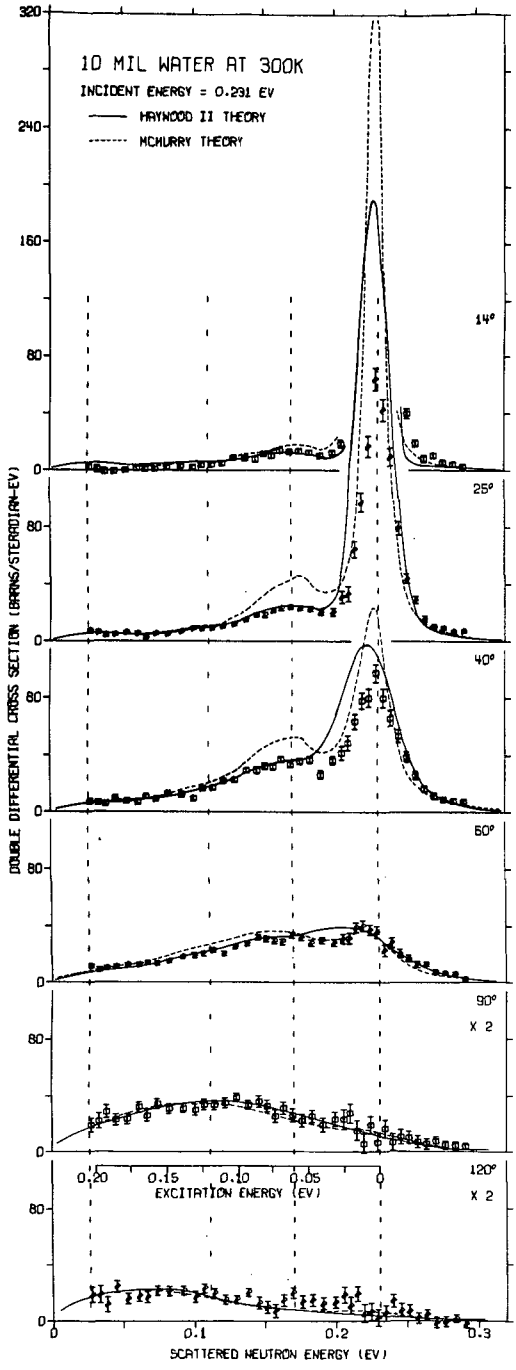

FIG. 4. Double-differential scattering cross-section for H_2O at 300°K for incident neutron energies 0.231 eV and 0.332 eV.

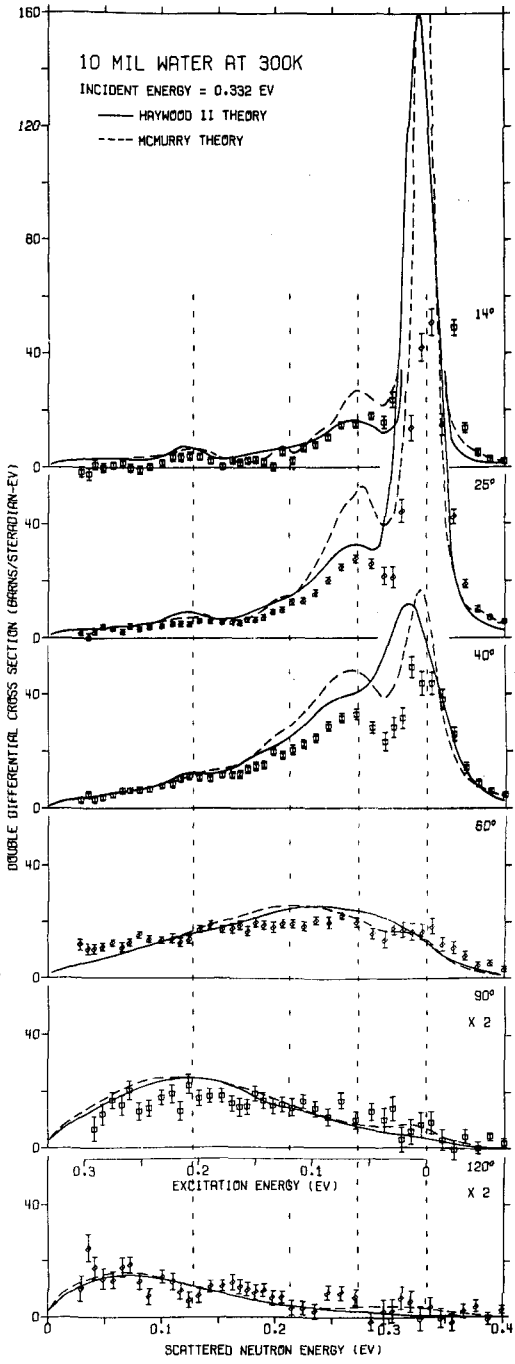
10 MIL WATER AT 300K
INCIDENT ENERGY = 0.332 EV
HAYWOOD II THEORY
MCMURRY THEORY
DOUBLE DIFFERENTIAL CROSS SECTION (BARNS/STERADIAN-EV)
14°
25°
40°
60°
90°
X 2
120°
X 2
EXCITATION ENERGY (EV)
SCATTERED NEUTRON ENERGY (EV)

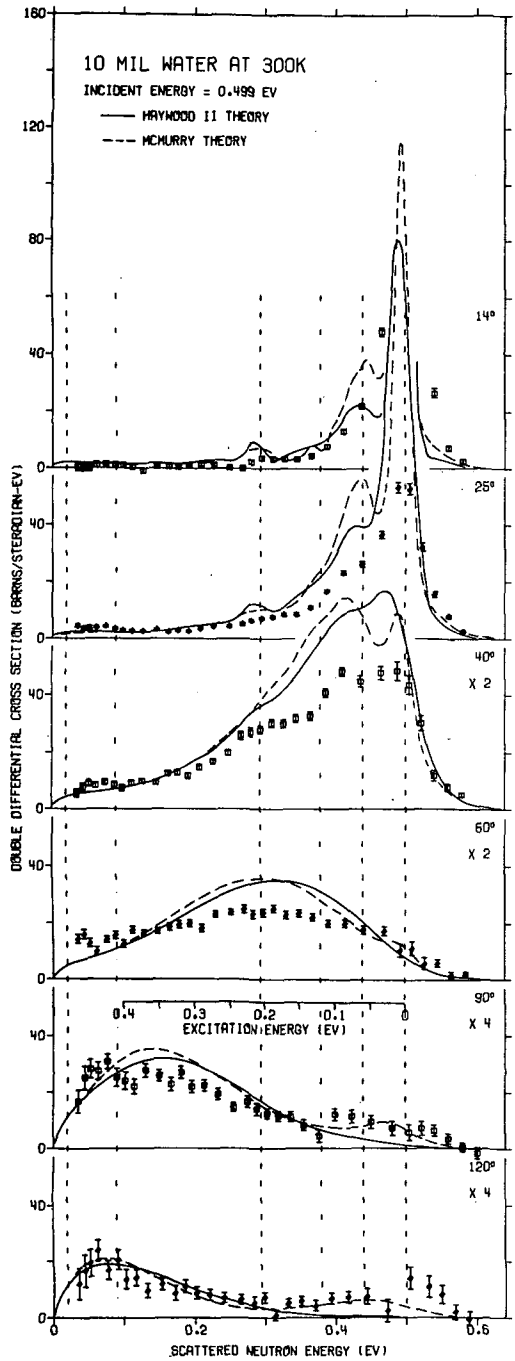

FIG. 5. Double-differential scattering cross-section for H_2O at 300°K for incident neutron energies of 0.499 eV and 0.631 eV.

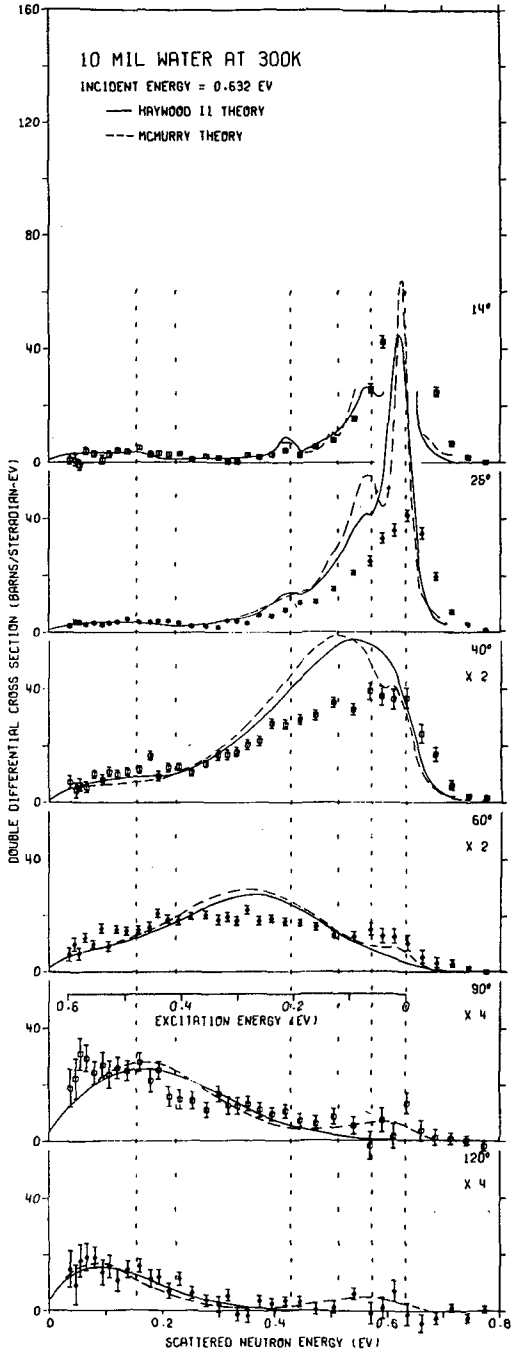
10 MIL WATER AT 300K
INCIDENT ENERGY = 0.632 EV
HAYWOOD II THEORY
MCMURRY THEORY
14°
25°
40°
X 2
60°
X 2
90°
X 4
120°
X 4
DOUBLE DIFFERENTIAL CROSS SECTION (BARNS/STERADIAN-EV)
EXCITATION ENERGY (EV)
SCATTERED NEUTRON ENERGY (EV)
160
120
80
40
0
0.6
0.4
0.2
0.8

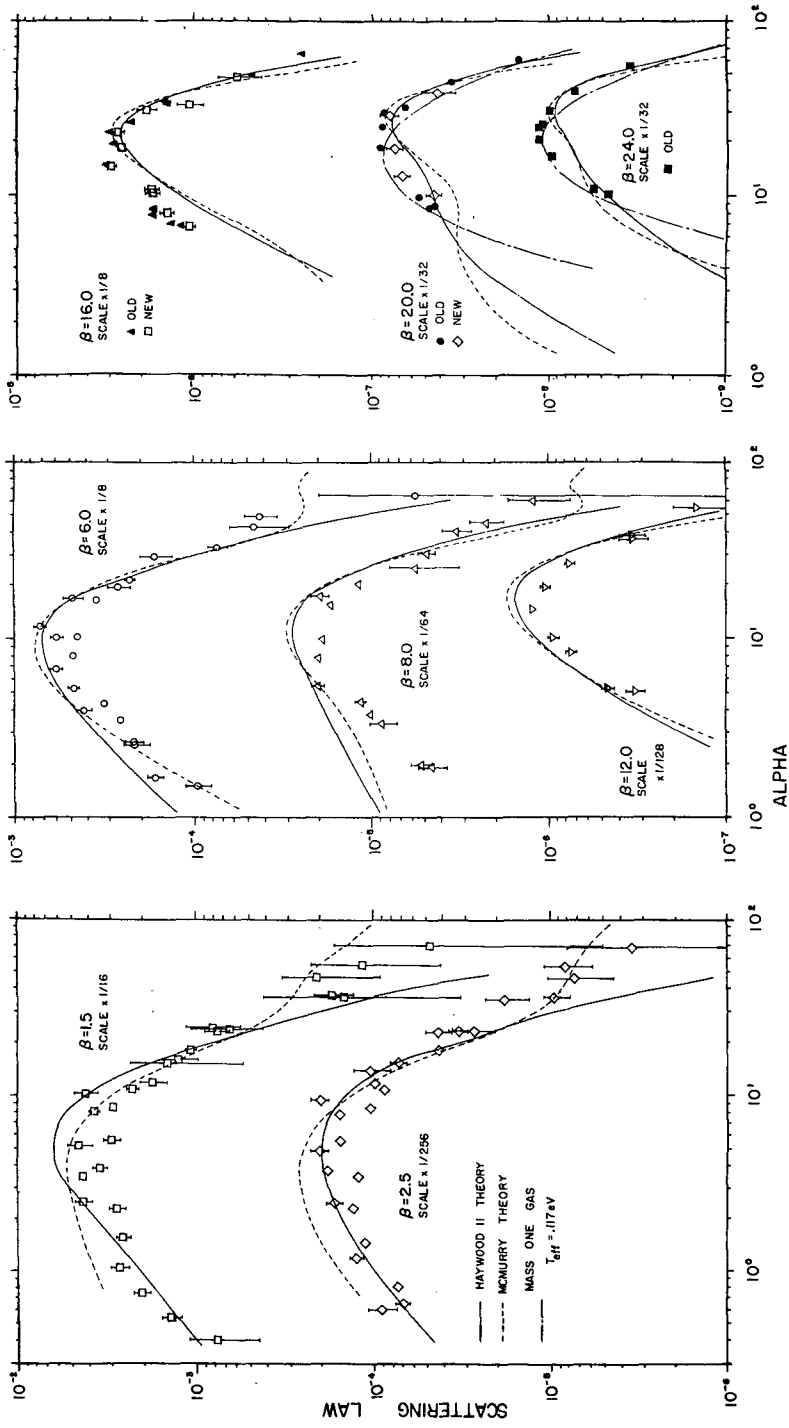

FIG. 6. Scattering law for H_2O at 300°K.

energy transfer. The modes are not well defined in the cross-section profile due to the influence of experimental resolution broadening and multiphonon excitations of the lower energy modes.

The double-differential cross-section has been integrated over scattered neutron energies to obtain the differential scattering cross-section $\partial\sigma/\partial\Omega$. In Table II these results are compared with direct measurements made by Beyster [6]. Discrepancies are attributed primarily to systematic uncertainties in the present measurements. The integrated results generally agree with Beyster's values to about 10%.

Some of the cross-section data have been illustrated in the form of scattering law, $S(\alpha,\beta)$, in Fig. 6. These data extend to much higher α and β-values than previous measurements. The error bars indicate only the statistical uncertainties (including background corrections). A rough measure of the systematic errors present in the experiment is afforded by the self consistency of data at a constant β-value. These data are obtained from six scattering angles and several experimental runs, each at a different incident energy. The theoretical curves shown in Fig. 6 will be discussed in the next part of this paper.

Using the extrapolation technique introduced by Egelstaff [8], a generalized frequency spectrum may be obtained

$$P(\beta) = \beta^2 \lim_{\alpha \to 0} [S(\alpha,\beta)/\alpha] \tag{3}$$

TABLE II. INTEGRATED DOUBLE-DIFFERENTIAL SCATTERING COMPARED WITH DIFFERENTIAL SCATTERING CROSS-SECTION MEASURED BY BEYSTER [6]

Scattering angles	Differential scattering cross-section (barns eV^{-1} steradian^{-1})				
	Incident neutron energy (eV)				
	0.154	0.231	0.332	0.499	0.631
40°	8.3	7.7	7.0	6.9	7.4
(45°)	(7.7)	(7.4)	(7.0)	(6.6)	(6.9)
60°	4.8	5.8	6.0	4.8	5.1
	(6.0)	(5.6)	(5.2)	(5.0)	(5.2)
90°	4.4	3.2	2.4	2.1	2.3
	(3.9)	(3.2)	(2.7)	(2.5)	(2.4)

[a] ( ) Data of Beyster

For liquids, $P(\beta)$ is the Fourier transform of the velocity correlation function for the scattering atoms. In the case of a crystalline solid, it is directly related to the phonon frequency spectrum $\rho(\beta)$

$$\rho(\beta) = P(\beta) \frac{\sinh(\beta/2)}{\beta/2} \tag{4}$$

Since the integral of $\rho(\beta)$ must equal unity for correct normalization, a useful check on the accuracy of $P(\beta)$ is available.

Scattering law results have been plotted as $\log[\beta^2 S(\alpha,\beta)/\alpha]$ versus α at constant β, and fitted straight lines have been extended to zero α. For β-values less than 5, the derived $P(\beta)$ is in good agreement with the results obtained by Kottwitz and Leonard [3] and by Haywood and Thorson [2]. This is shown in Fig. 7. At larger β-values, straight lines could no longer be drawn through the points since the values of $\log[S(\alpha,\beta)/\alpha]$ began to decrease at small α-values. If these points were ignored, a $P(\beta)$ was obtained which was in good agreement with previous results. Thus far, a satisfactory method has not been found to perform the extrapolation for larger β-values, although it is certain that the values of $P(\beta)$ will be much lower than those obtained by Kottwitz and Leonard. It is possible that earlier results for $P(\beta)$ have failed to satisfy the required normalization condition because of the large values obtained by straight line extrapolations.

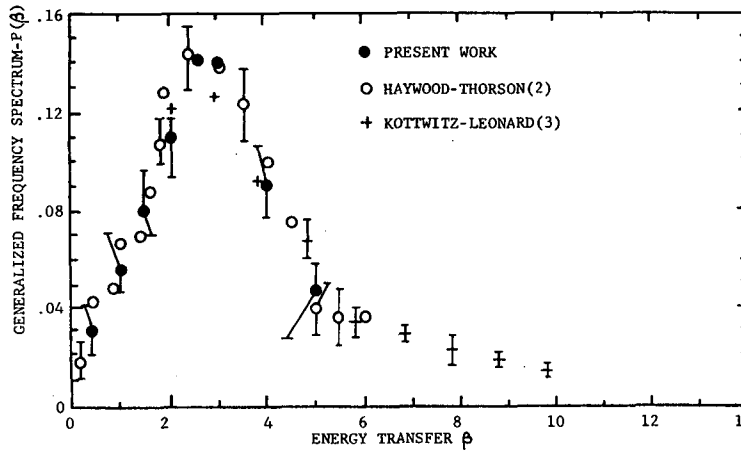

FIG. 7. Generalized frequency distribution for H_2O at room temperature.

4. WATER MODELS FOR REACTOR CALCULATIONS

All water models which have been proposed have used the incoherent scattering approximation ($\sigma_{inc}/\sigma_{coh} \sim 40$ for hydrogen). The scattering

law, $S(\alpha,\beta)$, is the Fourier transform of the intermediate scattering function, $\chi(\alpha,t)$ which is assumed to have a Gaussian form,

$$S(\alpha,\beta) = \int_{-\infty}^{+\infty} e^{i\beta t}\,\chi(\alpha,t)\,dt \tag{5}$$

$$\chi(\alpha,t) = \exp \alpha[g(t) - g(0)]$$

where $\alpha g(0)$ is the Debye-Waller factor. The width function $g(t)$ is related to the phonon frequency spectrum $f(\omega)$ through the integral transform,

$$\gamma(t) = \int_{-\infty}^{+\infty} \frac{f(|\omega|)\, e^{\omega/2T}}{2\omega/T\, \sinh(\omega/2T)}\, e^{i\omega t}\, d\omega \tag{6}$$

In this development of the scattering law, all of the basic information required for a particular scattering material is contained in the frequency spectrum.

The first scattering model specifically designed for water was proposed by Nelkin [13] in 1960. The model uses a frequency spectrum consisting of delta-function lines at 0.06, 0.20 and 0.48 eV to represent hindered rotations, H-O-H angle bending and O-H bond stretching vibrations of the water molecule. The Nelkin model provided much more accurate thermalization calculations than the free hydrogen gas model, and has been used extensively. Recently the availability of accurate differential and integral cross-section measurements for water has encouraged the development of more detailed models. Two of these, the McMurry-Russell model [4], and the model designed by Koppel [12] from the Haywood experimental frequency spectrum [2], are described here and compared with our results.

The McMurry-Russell model makes use of the quasi-crystalline theory of water [14] which assumes that hydrogen bonding between molecules leads to the formation of quasi-crystalline aggregates of various sizes. This model represents the liquid as a mixture of free H_2O molecules, and two heavier aggregates of mass 75 and 150. Each aggregate is given a rotational and translational frequency spectrum consisting of 8 or 9 discrete delta-function lines with frequencies $0 < \omega \leq 0.125$ eV. The amplitude of individual lines is adjusted to satisfy certain normalization requirements and to give agreement with Brugger's scattering law measurements [4]. Each of the aggregates is allowed to undergo free translations, and within any aggregate, all molecules have discrete spectral lines at 0.20 eV and 0.46 eV which represent the internal angle bending and O-H bond stretching vibrations. With this discrete representation of the frequency spectrum, scattering law is obtained in the familiar form of multi-phonon expansions. One of the most interesting features of the McMurry-Russell model is that it provides a convenient method of incorporating temperature dependence of the frequency spectrum by variation of the aggregate sizes and their fractional abundance.

In the model introduced by Koppel, the rotational frequency band of the water molecules is represented by a modified form of the experimental frequency distribution obtained by Haywood and Thorson from their scattering law measurements. Since this spectrum is continuous rather than discrete, the model necessitated development of a computer code, GASKET [15], to carry out numerically the integral transforms indicated by Eqs (5) and (6). The spectrum used by Koppel differed from the Haywood spectrum in that an ω^2 behaviour was introduced at the origin and the spectrum was cut off at 0.165 eV. After renormalization, free translations of mass 18 molecules, and discrete lines at 0.205 eV and 0.45 eV were added. The weights of individual portions of the frequency spectrum are only slightly modified from the Nelkin model. Those parts of the spectrum which are represented as discrete lines are analytically integrated by the GASKET code to give the scattering law as a series of phonon terms. This discrete part of the scattering law can then be convolved with the continuous part obtained from the direct numerical inversions.

In Figs 4 and 5, the McMurry-Russell and the Haywood-Koppel models are compared with our cross-section results. These models have not been broadened for experimental energy resolution before comparison. The figures illustrate that the most significant disagreements occur for the low (< 0.03 eV) energy transfers in the Haywood-Koppel model, and for the rotational energy region in the McMurry-Russell model. The quasi-elastic scattering peaks predicted by the Haywood-Koppel model are considerably broader than the experimental results. This disagreement would be more severe if the theory had been resolution broadened. It seems reasonable to assume that the discrepancy is related to the assumption of free mass-18 translations. The width of the quasi-elastic scattering peaks is more accurately given by the McMurry-Russell model in which much heavier aggregates of water molecules were assumed. While the McMurry-Russell theory leads to sharp quasi-elastic peaks at small scattering angles which are not seen in the data, this disagreement can be explained by the limitations of experimental resolution. Figures 4 and 5 demonstrate that the McMurry-Russell model overestimates the scattering from the broad band of rotational levels centred near 0.06 eV energy transfer. It is possible that this difficulty may result from the fact that model parameters were determined in part by fitting to scattering data which were not corrected for multiple scattering.

In Fig. 6, the two models are compared with the experimental scattering law. Both models are in good agreement with experiment at large β-values. A hydrogen gas model, with an effective proton temperature of 0.11 eV is also shown in the illustration. It is particularly interesting that for $\beta > 20$ (~ 0.5 eV), the gas model with an effective temperature provides as good agreement as either of the other models.

5. CONCLUSIONS

Extensive cross-section and scattering law data have been obtained for room-temperature water. The scattering law has been used to derive a generalized frequency spectrum $P(\beta)$ for $\beta \leq 5$ which is in good agree-

ment with previous results. Although the present measurement extends to much larger β-values than previous experiments, a meaningful frequency spectrum could not be obtained for the large β-values due to the difficulties in performing the required extrapolation to zero α.

The McMurry-Russell and Haywood-Koppel models were compared with the experimental results. Good agreement was obtained for limited ranges of the energy and angle variables. Substantial disagreements were observed at low-energy transfers in the Haywood-Koppel model and for scattering from the rotational levels in the McMurry-Russell model.

Good agreement with a simple gas model at an effective proton temperature was observed for $\beta > 20$. The use of such a model would greatly simplify scattering kernel calculations, and further experimental investigation of the accuracy and range of application of the model seems warranted.

It has been demonstrated that inelastic scattering and scattering law measurements can provide an extremely sensitive test of scattering models. While these experiments are more difficult than integral measurements, and due caution must be exercised in the application of multiple scattering corrections, the increased sensitivity to chemical binding effects appears to make the effort worthwhile.

ACKNOWLEDGEMENTS

The authors would like to thank Dr. H. L. McMurry for providing his model calculations, and Dr. S. Pearlstein for supplying the Haywood-Koppel model from the Brookhaven Evaluated Nuclear Data File. We also thank Dr. F. Feiner for his technical advice and assistance.

REFERENCES

[1] KIROUAC, G.J., MOORE, W.E., SEEMANN, K.W., YEATER, M.L., Proc. Conf. Neutron Cross Section Technology, TID-4500 Conf. 660303 (1966) 122; KIROUAC, G.J., USAEC Rep. KAPL-3196 (1966).

[2] HAYWOOD, B.C., THORSON, I.M., Proc. BNL Conf. on Neutron Thermalization (1962); EGELSTAFF, P.A., HAYWOOD, B.C., THORSON, I.M., Inelastic Scattering of Neutrons in Solids and Liquids I, IAEA, Vienna (1963) 343.

[3] KOTTWITZ, D.A., LEONARD, B.R., Jr., Inelastic Scattering of Neutrons in Solids and Liquids I IAEA, Vienna (1963) 359.

[4] McMURRY, H.L., RUSSELL, G.J., BRUGGER, R.M., Nucl. Sci. Engng 19 (1964) 248.

[5] LARSSON, K.E., DAHLBORG, U., Inelastic Scattering of Neutrons in Solids and Liquids I IAEA, Vienna (1963) 317.

[6] BEYSTER, J.R., MOWRY, W.R., USAEC Rep. GA-5373 (1964).

[7] ESCH, L.J., MOORE, W.E., USAEC Rep. KAPL-3356 (1967).

[8] EGELSTAFF, P.A., SCHOFIELD, P., Nucl. Sci. Engng 12 (1962) 260.

[9] HONECK, H.C., USAEC Rep. GA-5968 (1964).

[10] SLAGGIE, E.L., USAEC Rep. GA-7480 (1966) Appendix G; submitted to Nucl. Sci. Engng.

[11] BISCHOFF, F., KALOS, M.H., Private communications (1966).

[12] KOPPEL, J.U., Reactor Physics in the Resonance and Thermal Regions (GOODJOHN, A.J., POMRANIG, G.C., Eds.), MIT Press, Cambridge, Mass. (1966) 27.

[13] NELKIN, M.S., Phys. Rev. 119 (1960) 741.

[14] BERNAL, J.D., FOWLER, R.H., J. chem. Phys. 1 (1933) 515. Recent articles include; NEMETHY, G., SHERAGA, H.A., J. chem. Phys. 36 (1962) 3382, and BUIJS, K., CHOPPIN, G.R., J. chem. Phys. 39 (1963) 2035.

[15] KOPPEL, J.U., TRIPLETT, J.R., NALIBOFF, Y.D., USAEC Rep. GA-7417 (1966).

DISCUSSION

W. GLÄSER: Is not the bending of your S/α curves at small α, as happens for the high β-values, just a consequence of large multi-phonon contributions? If this is the case, the use of a straight line in the extrapolation simply has no meaning. Rather one should compare a calculation of S with the experimental points, perhaps in an iterative way.

G. J. KIROUAC: Yes, I quite agree. That is why we did not give values of the $P(\beta)$ function for β larger than 5. However, if one has to rely on theory to derive a spectral density, I think the concept of S/α extrapolation loses some of its usefulness.

A. J. H. GODDARD: With reference to your calculated $S(\alpha, \beta)$ for $\beta = 20$ and $\beta = 24$, there seems to be some structure in $S(\alpha, \beta)$ as calculated from the McMurry-Russell and Hayward models. We observed a similar structure when we were calculating $S(\alpha, \beta)$ for terphenyl, but when we increased the number of terms in the phonon series this structure disappeared. Do you have any comments on this?

G. J. KIROUAC: I assume that this structure is due to the high-energy vibrational modes near 0.45 eV, which is quite close to $\beta = 20$. Increasing the number of terms in the phonon expansion for this level should therefore have no influence on the structure. I am afraid I cannot usefully comment further on the effect you observe.

I. M. THORSON: Can you estimate the integrated intensities of the vibrational modes at 0.2 and 0.45 eV?

G. J. KIROUAC: Perhaps we can by estimating the contribution to this area from the multi-phonon excitations of the rotational band. At any rate, we plan to attempt these calculations.

INELASTIC NEUTRON SCATTERING IN METAL HYDRIDES, UC AND UO_2, AND APPLICATIONS OF THE SCATTERING LAW*

S.N. PUROHIT, S.S. PAN, F. BISCHOFF,
W.A. BRYANT, C. LAJEUNESSE AND M.L. YEATER
RENSSELAER POLYTECHNIC INSTITUTE,
TROY, NEW YORK
AND
W.E. MOORE, G.J. KIROUAC, L.J. ESCH
AND N.C FRANCIS
KNOLLS ATOMIC LABORATORY,
SCHENECTADY, NEW YORK, UNITED STATES OF AMERICA

Abstract

INELASTIC NEUTRON SCATTERING IN METAL HYDRIDES, UC AND UO_2, AND APPLICATIONS OF THE SCATTERING LAW. This paper describes the measurement of inelastic neutron scattering in metallic hydrides, UC and UO_2, the calculation of their scattering laws, and discusses scattering law applications. Measurements based on the energy loss method are made at the Rensselaer Linear Accelerator Laboratory.

Measurements on ZrH_x (with varying hydrogen concentration), NbH and ThH_2 have been made at room temperature. The ZrH_2 and NbH measurements were repeated at liquid nitrogen temperature. For ZrH_x, the variation of optical level width caused by changing sample temperature, momentum transfer and concentration of hydrogen atoms has been studied. NbH data exhibit a doublet at 0.12 and 0.164 eV. This is believed to arise from splitting of the 1-0 transition in the optical band into transverse and longitudinal modes. For metal hydrides the Einstein model is found to be a poor representation of the frequency spectrum.

Differential scattering cross-sections have been obtained for UC, using an 85%-transmission powder sample, 0.134-eV incident energy and six scattering angles (14° to 150°). A peak at 0.045 eV excitation is observed.

UO_2 data were obtained on a depleted powder sample having approximately 95% transmission, for incident energies of 0.341 eV, and scattering angles of 25° to 150°. Evidence of inelastic scattering from excitations beyond 0.1 eV, the limit of previous measurements, is observed.

Theoretical scattering laws have been calculated for ZrH_2, UC and UO_2. The UC scattering data were compared with theoretical results based on a Debye acoustic mode at 0.014 eV and a Gaussian distribution at 0.045 eV. Agreement between theory and experiment is good. For ZrH_2 and UO_2 the frequency spectra reported in the literature were employed. A treatment of proposed multiple scattering corrections is described.

The paper also discusses applications of scattering laws. The importance of the experimental and theoretical study of Placzek moments is stressed. We especially emphasize the role of these moments, including the effective temperature, in the study of Doppler broadening of resonances of fissile, fertile and structural materials. This broadening may play a significant role in temperature coefficients of fast reactors.

INTRODUCTION

This paper reviews the current low-energy neutron scattering research at the Rensselaer Polytechnic Institute. This work involves the measurement of neutron scattering cross-sections for materials of a wide range of

* This work was supported by the United States Atomic Energy Commission under contract number AT(30-3)-328.

interest (such as uranium compounds, metallic hydrides and hydrogenous compounds), the theoretical calculation of scattering laws and cross-sections, the comparison between theoretical and experimental results to test a given frequency spectrum, and the application of temperature-dependent scattering laws in reactor physics problems.

In section I, experimental results on the differential inelastic scattering of neutrons in metallic hydrides and uranium compounds are presented. These measurements have been undertaken with the RPI-KAPL high-resolution neutron scattering facility at the Rensselaer Linear Accelerator Laboratory. The scattering experiments are based upon the energy loss method, in contrast to the conventional energy gain experiments utilizing the cold neutrons from a nuclear reactor. Use is made of relatively high incident-energy neutrons (0.1 to 0.6 eV) to permit a careful study of the high-energy transfer modes in molecular systems.

Theoretical results obtained with the available scattering law codes are described in section II. For illustration, we present a set of scattering laws for ZrH_2, UO_2, and UC. Comparison between measured and theoretical cross-sections are also discussed in this section.

Finally, in section III the importance of small-energy and large-momentum transfer experiments in obtaining the Placzek moments of the frequency spectrum is emphasized. In addition, the problem of the Doppler broadening of neutron resonances in a bound nucleus is also discussed. The theoretical formalism emphasizes the role of Placzek moments and the necessity of obtaining improved knowledge of frequencies and amplitudes of normal modes in the study of resonance line shape.

I. DIFFERENTIAL CROSS-SECTION MEASUREMENTS

A. Experimental method

To obtain good resolution and an adequate count rate for inelastic scattering measurements in the epithermal region, it is important to use an intense pulsed source, a large-aperture fast chopper, and high efficiency neutron detectors. Because count rates are inherently very small, only one or two events per second, extensive and complex shielding is required to sufficiently reduce background. The Rensselaer Linear Accelerator provides 0.6-A 4.5-μs electron bursts, which are converted to fast neutrons in a tantalum target. Short bursts of epithermal neutrons are extracted from a thin moderator placed near the linac target. A multi-slit neutron chopper, having an 8-in^2 aperture, is positioned at a distance of 6 m from this source to obtain a chopped neutron beam of the desired incident energy. The chopping slits have 1/16-in. spacing and 8-in. length, and produce a 6.8-μs FWHM (full-width at half maximum) burst at 20 000 rev/min.

In this experiment the accelerator is synchronized with the neutron chopper; the desired neutron velocity is selected from the source spectrum by fixing the time delay between the source burst and the moment when the chopping slits are aligned with the collimated neutron beam. The chopped beam passes through the sample under study, and scattered neutrons are detected by banks of 10-atm ^{3}He proportional counters arrayed at six angles. The flight times of detected neutrons are recorded by an on-line computer; detected events are routed to different memory areas according

to the scattering angle (detector bank) and type of experimental run. The normal sequence of runs, which is repeated every few minutes under computer control, is: (1) a 'foreground' run measuring the sample scattering, (2) a 'background' run made with the linac-chopper phase electronically shifted by half the chopper period, (3) an empty sample holder run, and (4) a run measuring the scattering from a vanadium standard sample. The latter serves as a repetitive detector calibration. All runs are normalized by means of thin beam monitor counters.

A CDC-6600 computer is used to subtract the background, sample holder and air scattering, and to correct for the energy dependence of the detector efficiency. The data are reduced to differential cross-sections, normalized by the vanadium (angular-dependent) cross-section. Automatic plots of the data and the standard deviations are obtained. Comprehensive Monte Carlo codes are being developed to provide reliable corrections for multiple scattering in the sample and for deriving a realistic experimental resolution function. Further description of the scattering facility is given in Ref. [1].

B. Metallic hydrides [2, 3, 4]

(1) Zirconium hydride

Typical differential cross-sections for zirconium hydride are shown in Figs 1 and 2. The structure which appears in the energy distribution comes from various phonon states which absorb that quantum of energy appropriate to a particular mode. Optical multiphonon peaks can be seen

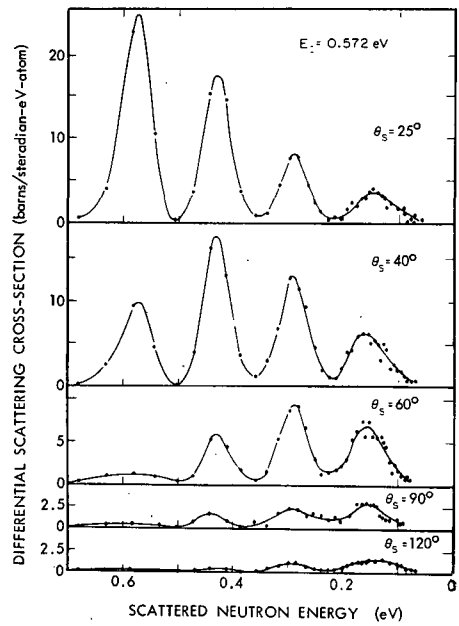

FIG. 1. Double-differential scattering cross-sections of ZrH_2 for 0.572-eV incident neutron energy at 295°K.

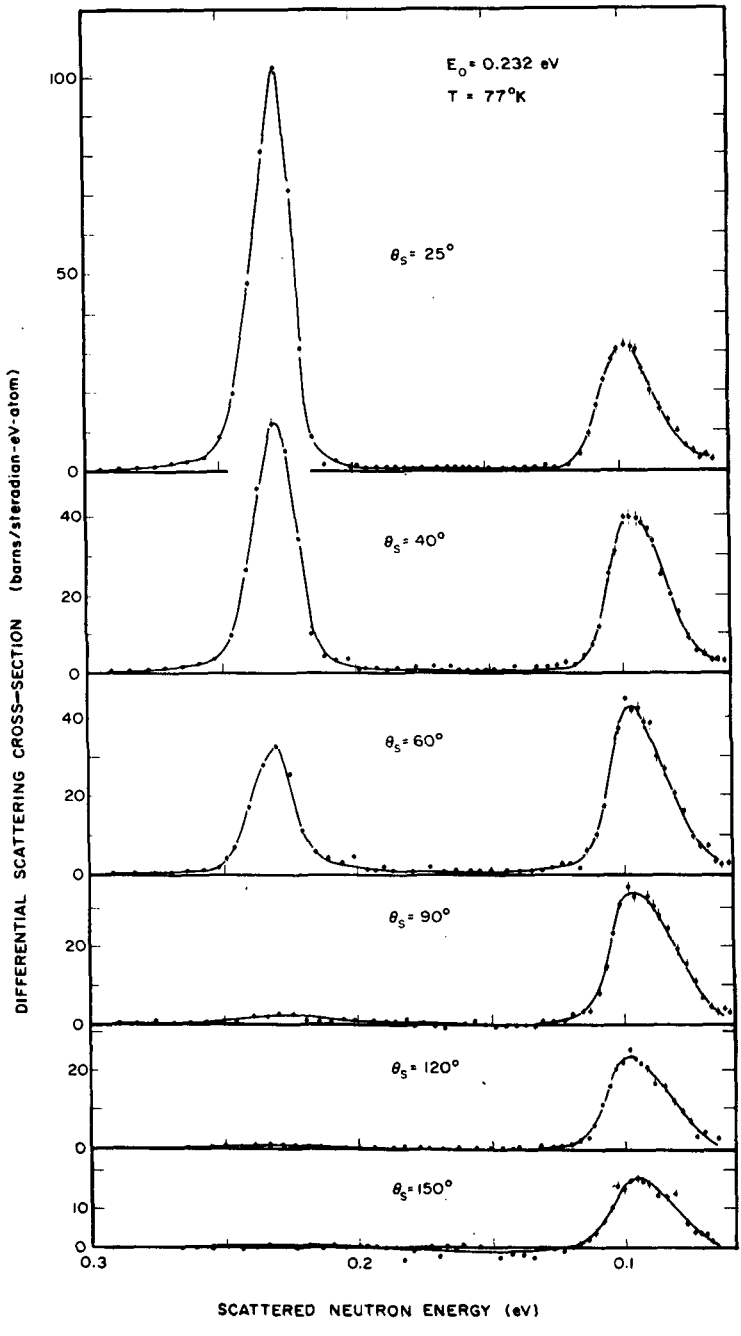

FIG. 2. Double-differential scattering cross-sections of ZrH_2 for 0.232-eV incident neutron energy at 77°K.

clearly in the energy distribution of inelastically scattered neutrons. The contributions due to acoustic vibrations are also evident, on examining the asymmetry of the elastic peaks. However, separation of this inelastic component from the elastic scattering is difficult due to resolution limitations.

Our experimental results are summarized and compared in Table I with those obtained from the other laboratories. The results of Whittemore [5] indicate narrower and approximately equal widths for the first and second peaks. Since he had to make a large resolution correction in going from observed widths to true widths, his corrected widths could be substantially influenced by very small errors in his resolution function. Our experimental data are in good agreement with Harling and Leonard's measurement [6] at room temperature.

The elastic scattering cross-section of the bound hydrogen atom decreases with increasing momentum transfer. Since the inelastic cross-section from the acoustic vibration always produces a contribution near the elastic region, these inelastic components must be subtracted in order to determine the elastic scattering cross-section. Figure 3 shows a plot of $d\sigma/d\Omega$ versus $4E_0 \sin^2(\theta/2)$. From the slope of the curve the value of the Debye-Waller factor for ZrH_2 equal to 1.37 $Å^2$ has been obtained.

The optical frequency distribution derived from experiment has been compared with Slaggie's calculation [7]. He has used the central force model to obtain the frequency distribution from the dynamical equations. His result gives the same shape of asymmetry of the optical peak as our experiment. The observed energy distribution of the optical modes is also in agreement with Brockhouse's measurements on ZrH_2 [8]. By comparing measurements made at liquid nitrogen and room temperature, it is concluded that the width observed at 295°K is not due to the Doppler broadening effect.

(2) Titanium hydride

The vibrational energies and level widths of titanium hydride also have been measured (Fig. 4). The level energies for the first, second and third phonon are approximately equally spaced; the levels are rather broad, but there is no clear departure from regular spacing to indicate anharmonic behaviour. The observed widths are larger than the corresponding widths of zirconium hydride. This is expected because the atomic mass of the zirconium is higher than that of titanium, thus the hydrogen-to-hydrogen interaction through the coupling with lighter metal atoms (titanium in this case) will be stronger.

Comparing our results with those of other laboratories, the one-phonon energy is found to be in good agreement with the results of Saunderson and Cocking [9] and Whittemore and McReynolds [10]. The width of the one-phonon peak is in fair agreement with the results of Saunderson and Cocking. The heat capacity measurement [11] of TiH_2 gives the proton vibrational energy at 0.145 eV which is also in good agreement with the present neutron scattering results. The root-mean-square displacement of the proton from its equilibrium position is about 0.12 Å.

TABLE I ZIRCONIUM HYDRIDE RESULTS

COMPARISON OF RESULTS WITH OTHER LABORATORIES

E_o	First Level		Second Level		Third Level		Fourth Level
(meV)	$\hbar\omega_o$ *	σ_1 **	$2\hbar\omega_o$	σ_2	$3\hbar\omega_o$	σ_3	$4\hbar\omega_o$
159	138±2.0						
238	137±2.9	26.2±2.5					
396	137±8.7	29.0±2.7	273±5.9	54.2±6.1			
572	137±15.0	31.8±6.0	277±11.3	54.4±8.5	421±8.8	76±15	
665	140±18.2		277±14.2		421±11.5		553±9.5
Averages	137.6±3.5	27.4±1.9	274±7.1	54.3±5	417±7	76±15	553±9.5
Pelah, et al. [8]	130±15						
Woods, et al. [5]	140	26					
Whittemore [6]	140	18	280	20			
Harling, et al.	141.4±3	26.4±0.6	280.9±8	52.2±3.7	411±19	72±6	

* Energy in 10^{-3}eV unit.

** σ measures the full-width at half-maximum.

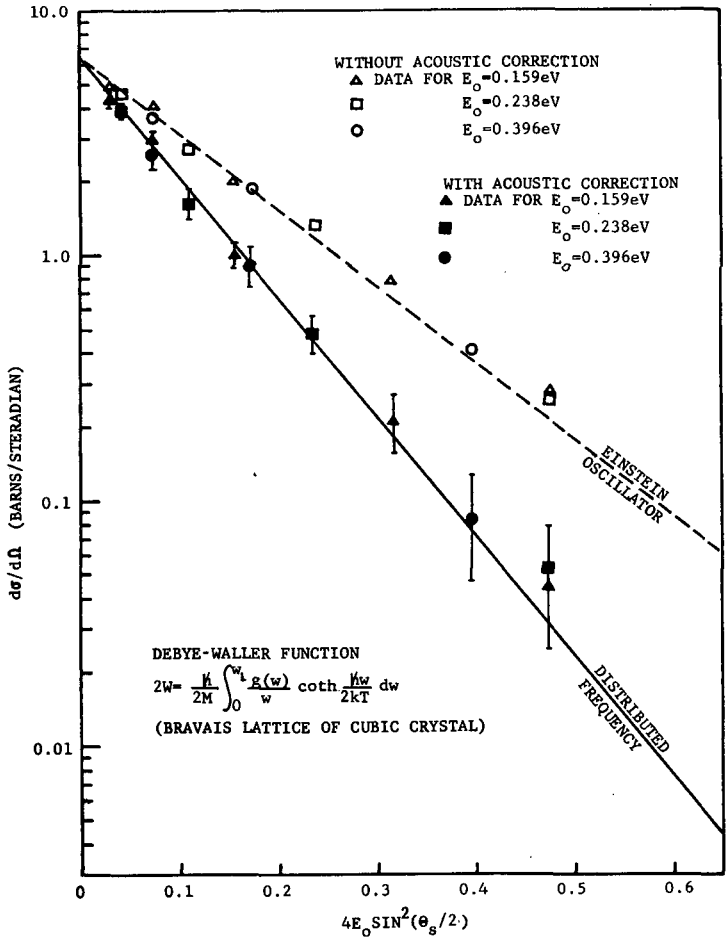

FIG. 3. Purely elastic scattering cross-sections for ZrH_2 compared with theory.

(3) Niobium hydride

The double-differential scattering cross-sections of niobium hydride have been measured at room temperature and liquid nitrogen temperature (Fig. 5). They exhibit two well-separated optical peaks corresponding to energy transfers of 0.120 and 0.164 eV. Both are attributed to the 1 - 0 transitions of hydrogen atoms in the metal lattice. The second peak at 0.164 eV cannot be explained as 2 - 0 transition of the optical mode, since this energy level is not a multiple of the energy of the first peak at 0.120 eV. For a detailed explanation of the splitting, see Pan [2]. The root-mean-square displacements of the hydrogen atoms in the niobium lattice are calculated to be 0.110 and 0.132 Å, based on the independent Einstein oscillator approximation.

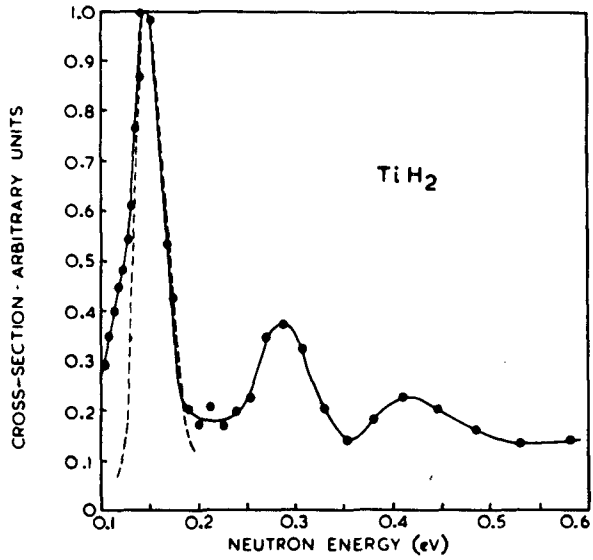

FIG. 4. Double-differential scattering cross-sections of TiH_2 (84% transmission) by filter difference method.

(4) Thorium hydride

The energy distribution of scattered neutrons in thorium hydride is similar to that of niobium hydride; both demonstrate the splitting of the optical levels. Figure 6 exhibits a narrow optical level at 0.076 eV and a broader level around 0.126 eV, observed by the filter difference method [2, 12]. The cold neutron experiment by Bergsma and Geodkoop [13] for thorium hydride gives one proton vibrational frequency as 0.079 eV, in good agreement with our measurement.

C. Uranium compounds

In view of the importance of reactor fuels such as UO_2 and UC and the lack of adequate scattering cross-section information, it is appropriate to undertake neutron inelastic scattering measurements on these materials. One can expect to derive a phonon frequency distribution from the inelastic scattering data; on the basis of this the scattering law as a function of temperature can be generated. Combined with an intensive theoretical study, one could make a critical assessment of the chemical binding effects on the temperature-dependent Doppler coefficients in thermal and fast reactors. Some survey runs have been made to assess the feasibility of this programme.

(1) Uranium carbide

Differential scattering cross-sections have been obtained for polycrystalline UC, using a rather thick (85% transmission) normal uranium sample and 0.134-eV incident energy; these results are shown in Fig. 7.

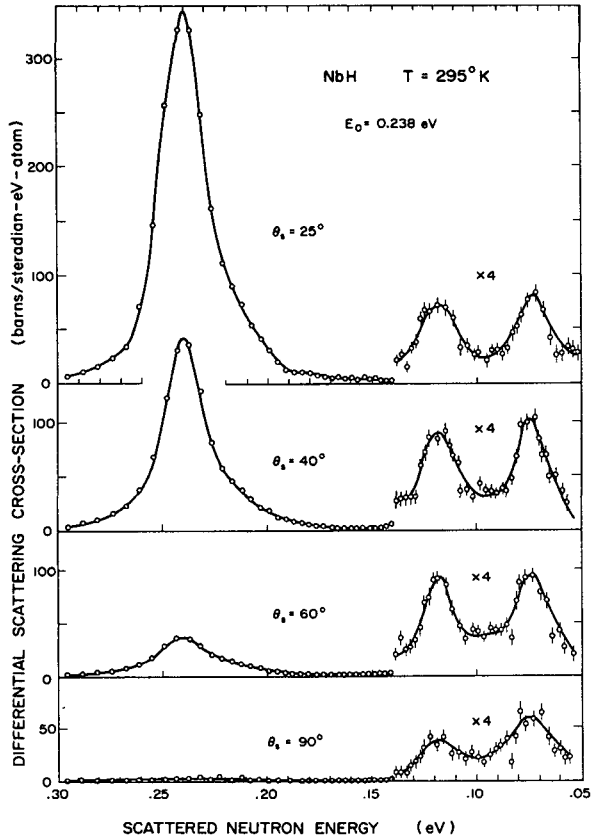

FIG. 5. Double-differential scattering cross-sections for niobium hydride.

Pronounced structure in the inelastic spectra is observed, with a well-defined isolated peak appearing at 0.045-eV excitation. A corresponding, smaller peak is observed in the up-scattering part of the spectra. Some evidence is seen in the scattered energy distribution for the two-phonon excitation of this 0.045-eV mode, combined with a probable contribution from multiple inelastic scattering. Two additional features of the data are noteworthy: A low-energy mode is observed, just resolved from the elastic scattering peak in both up and down scattering, corresponding to approximately 0.014-eV excitation; and the elastic intensity appears to fluctuate as a function of angle, which may reflect the coherent effects expected in UC. The elastic peak cross-sections at 14°, 25°, 60°, 90°, 120° and 150° are 8, 92, 95, 55, 45 and 58 barns/steradian-eV, respectively. The high diffraction peak appears to be around 40° scattering angle. In Fig. 7 the elastic data points have been omitted, except for 14°, to avoid the confusion of overlapping spectra. No correction has been made yet for resolution broadening or multiple scattering. The theoretical inelastic scattering curves shown in Fig. 7 are discussed in section II.

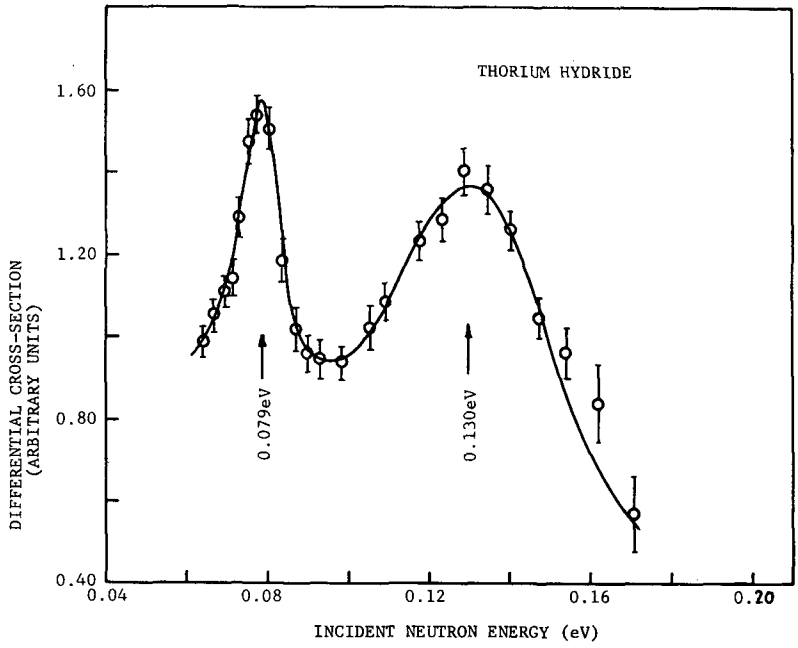

FIG. 6. Double-differential scattering cross-sections of ThH_2 (87% transmission) by filter difference method.

(2) Uranium dioxide

Some data have also been obtained for UO_2; incident energies of 0.134 eV and 0.341 eV were used on a thin depleted uranium polycrystalline sample having approximately 95% transmission. These runs will be repeated with the higher resolution attained for the UC run (about a factor of two better). However, these data do show important qualitative features.

The differential cross-sections for $E_0 = 0.134$ eV are pictured in Fig. 8. The data show a distinct structure near 0.085- and 0.100-eV scattered neutron energy. These peaks may correspond to maxima of Dolling's frequency distribution [14] at about 0.050 and 0.035 eV excitation. The Haywood-Thorson data [15] also indicate excitations in this energy range. The strong modes below 0.020 eV in Dolling's theory may contribute to the so-far unresolved region near the elastic peak. The cross-section profiles for $E_0 = 0.341$ eV are also shown in Fig. 8. Evidence for the same energy modes from 0.03 to 0.08 eV studied by others [14, 15] is also seen near the 'quasi-elastic' peak. As this incident energy may be high enough to include most of the crystalline binding effects within the 'quasi-elastic' peak through the multiphonon process, we are attempting to extract the important quantity, the effective temperature, from the width of this peak at the back angles, by a gas model fit.

II. THEORETICAL SCATTERING LAWS

Measured neutron cross-sections have been compared with the theoretical results obtained with the GASKET [16] and FLANGE codes [17].

The GASKET programme calculates the neutron scattering law, in the incoherent approximation, by evaluating the time integral for a given frequency spectrum of dynamical modes. In our calculations for UC and UO_2 we assumed the isotropic nature of the system. This assumption makes the polarization vector, for a normal mode per unit mass, independent of the nature of the atom. This approximation enables us to introduce the frequency spectrum of the whole lattice.

For an i-th atom, the scattering law is given by

$$S_i(K,\omega) = \frac{1}{2\pi} \int_{-\infty}^{\infty} \exp i\omega t \, \chi_i(K^2, t) dt \qquad (1)$$

The intermediate scattering function χ_i, a function of momentum transfer $\hbar K$, is explicitly given in terms of the frequency spectrum of harmonic vibrations, $f(\xi)$ for the whole lattice and the mass of scatterer M_i.

$$\chi_i = \exp \frac{\hbar K^2}{2M_i} \left\{ \int_{-\infty}^{\infty} \frac{f(\xi)(\exp(-i\xi t)-1)}{\xi\left(\exp\frac{\hbar\xi}{k_B T} - 1\right)} d\xi \right\} \qquad (2)$$

The FLANGE code finally calculates the neutron cross-sections with the GASKET scattering law output. In the following section we describe the frequency spectra for ZrH_2, UC and UO_2 employed in the calculation of scattering laws and cross-sections.

A. Frequency spectra

In Figs 9 and 10, frequency spectra for ZrH_2, UC and UO_2 are shown. These frequency spectra have been employed in the scattering law calculations. All these frequency spectra consist of the low-energy-transfer acoustic modes representing the motion of the heavier atom, and the high-energy-transfer modes, which account for the presence of the lighter element.

For ZrH_2 two frequency spectra are shown in Fig. 9. The frequency spectrum employed in the scattering law calculations consists of an acoustic mode with a Debye cut-off at 0.02 eV, and an optical mode represented by a Gaussian of 0.025-eV width centred at 0.135 eV.

The frequency spectrum employed in the UC calculations is given in Fig. 10. The basis for this frequency spectrum is the measured cross-section data shown in Fig. 7. An acoustic mode with a Debye temperature corresponding to 0.014 eV, and a high-energy-transfer mode represented by a Gaussian of 0.003-eV width centred at 0.045 eV characterized this frequency spectrum. Mathematically one may express the frequency spectrum as a sum of two components $f_1(\xi)$ and $f_2(\xi)$ representing two modes.

$$f(\xi) = a_1 f_1(\xi) + a_2 f_2(\xi) \qquad (3)$$

By varying the weights a_1 and a_2 in the cross-section calculations it has been found that the ratio $a_1/a_2 = 1/12$ gives a good fit to the present

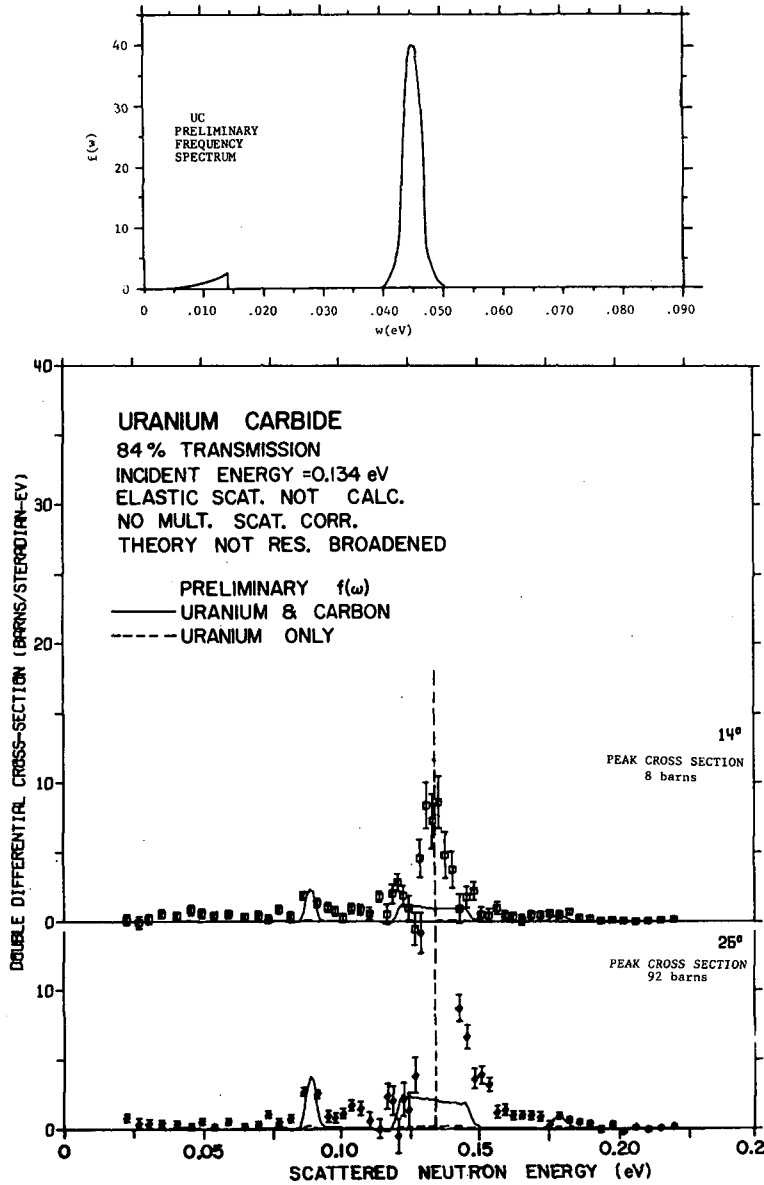

FIG. 7. Preliminary differential scattering cross-sections for uranium carbide theory calculated with frequency distribution of Fig. 10.

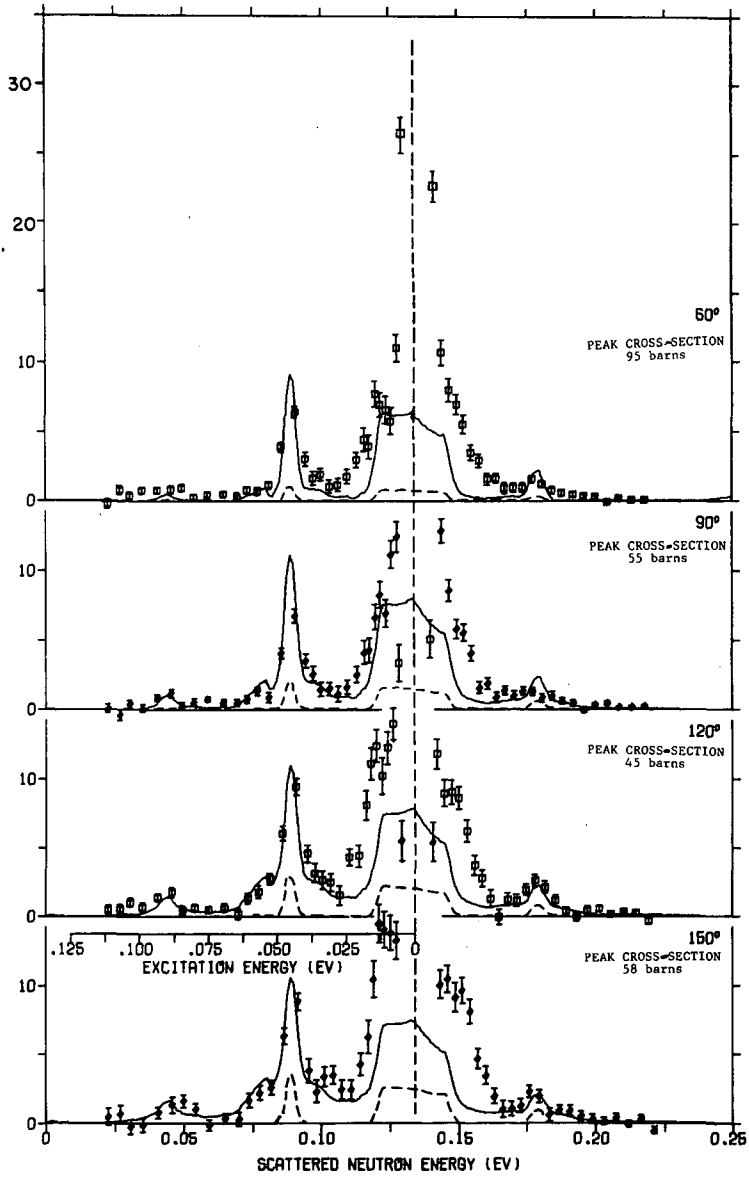
60°
PEAK CROSS-SECTION
95 barns
90°
PEAK CROSS-SECTION
55 barns
120°
PEAK CROSS-SECTION
45 barns
150°
PEAK CROSS-SECTION
58 barns
.125 .100 .075 .050 .025 0
EXCITATION ENERGY (EV)
0 0.05 0.10 0.15 0.20 0.25
SCATTERED NEUTRON ENERGY (EV)

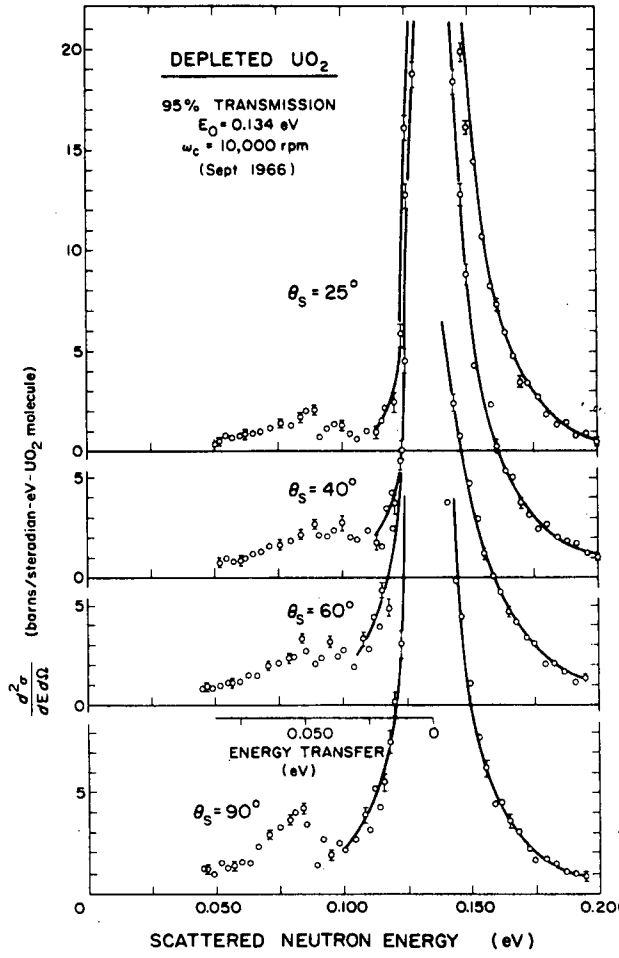

FIG. 8. Preliminary differential scattering cross-sections for depleted uranium dioxide.

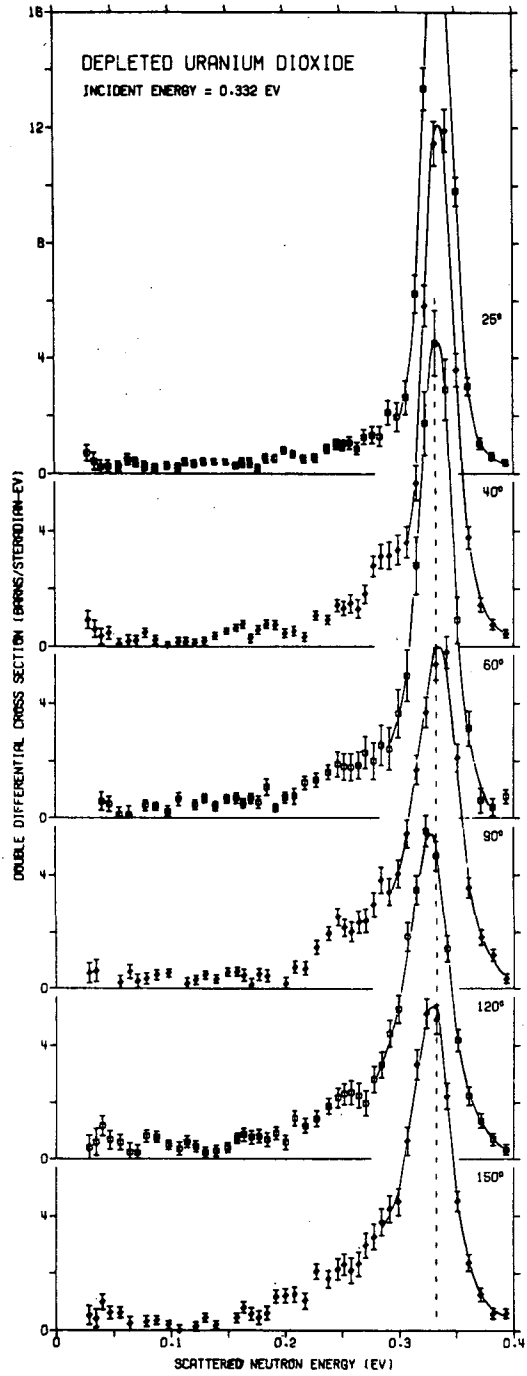
DEPLETED URANIUM DIOXIDE
INCIDENT ENERGY = 0.332 EV
25°
40°
60°
90°
120°
150°
DOUBLE DIFFERENTIAL CROSS SECTION (BARNS/STERADIAN-EV)
SCATTERED NEUTRON ENERGY (EV)
0
4
8
12
16
0.1
0.2
0.3
0.4

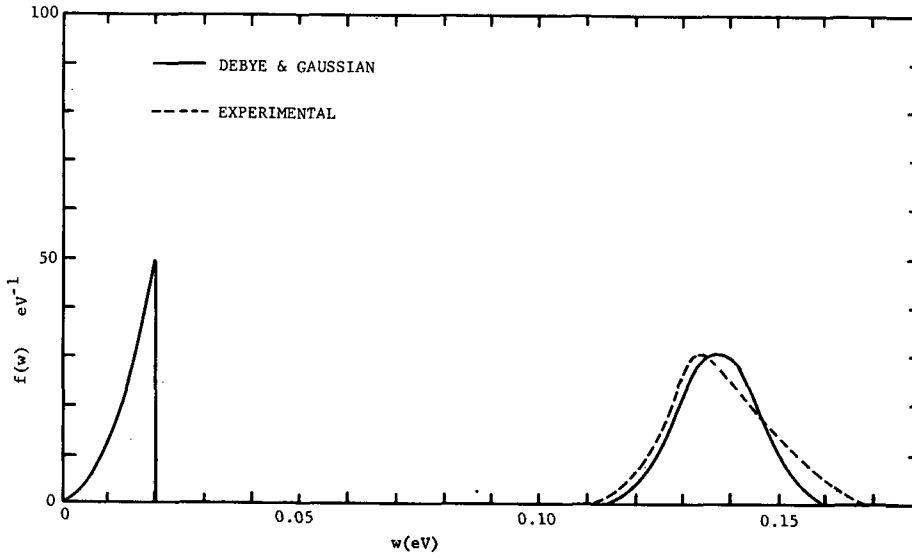

FIG. 9. Frequency spectrum for zirconium hydride.

neutron scattering data. At present there does not exist any frequency spectrum for UC in the literature. An attempt is now being made to obtain the frequency spectrum for UC from the lattice vibration studies.

Several frequency spectra of uranium dioxide have been reported in the literature. In Fig. 10 two frequency spectra employed in our UO_2 studies are shown. These spectra are based on cold neutron scattering measurements. Dolling et al. [14] obtained their frequency spectrum from dispersion law measurement and the shell model studies. Haywood and Thorson [15], on the other hand, derived a frequency spectrum from inelastic neutron scattering data using the incoherent approximation. Dolling et al. also calculated temperature-dependent Debye temperature from the specific heat studies. At room temperature the Debye temperature was found to be 600°K.

B. Scattering laws $S(\alpha, \beta)$

Theoretical scattering laws for ZrH_2, UC and UO_2 based on the frequency spectra discussed above, are shown in Figs 11, 12 and 13. $S(\alpha, \beta)$ as a function of β for different values of α are plotted. $\alpha = \hbar^2K^2/2Mk_BT$ and $\beta = \hbar\omega/k_BT$ are the Egelstaff variables. One may observe the following facts from these curves.

(1) For small values of α which correspond to $\alpha < 1$ for UO_2 and UC and $\alpha < 10$ for ZrH_2, the $S(\alpha, \beta)$ is strongly influenced by the structure in the frequency spectrum. Peaks and breaks at the phonon excitation energies corresponding to the optical and acoustic modes are clearly demonstrated.

(2) For large values of α (for UC and UO_2 $\alpha > 2$ and for ZrH_2 $\alpha > 48$), $S(\alpha, \beta)$ smooths out and can be very well represented by the short collision-time expansion result. The latter is valid for large-momentum transfers at high-incident energies.

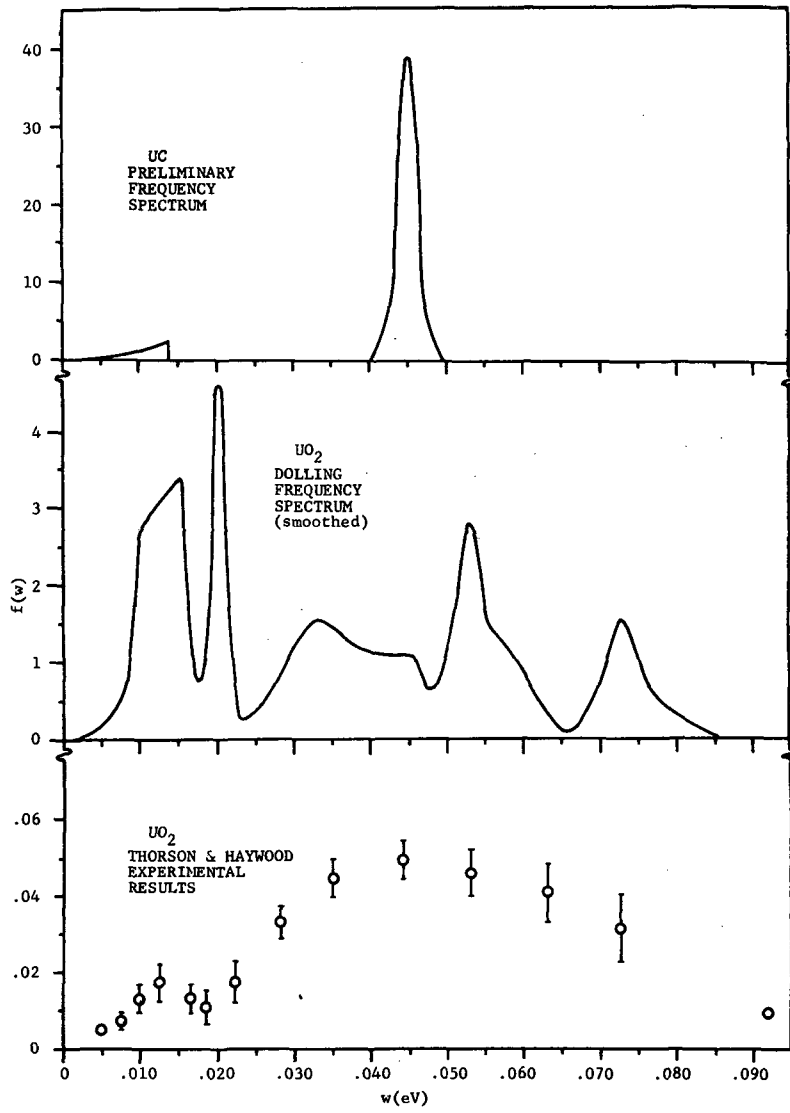

FIG. 10. Frequency distributions used for theoretical calculations for UC and UO_2

In the case of UO_2, we have also calculated $S(\alpha, \beta)$ for the Dolling et al. frequency spectrum, and for an empirical frequency spectrum consisting of an acoustic mode with a Debye cut-off at 0.014 eV and three Gaussian distributions at 0.035, 0.05 and 0.07 eV. The weights of the Gaussians have been taken as free parameters to be obtained from the neutron scattering data. The empirical frequency spectrum gives a detailed structure compared with the Haywood spectrum but smooths out the details of the Dolling spectrum. It may, therefore, constitute an intermediate spectrum between the broad Haywood spectrum and the detailed Dolling spectrum.

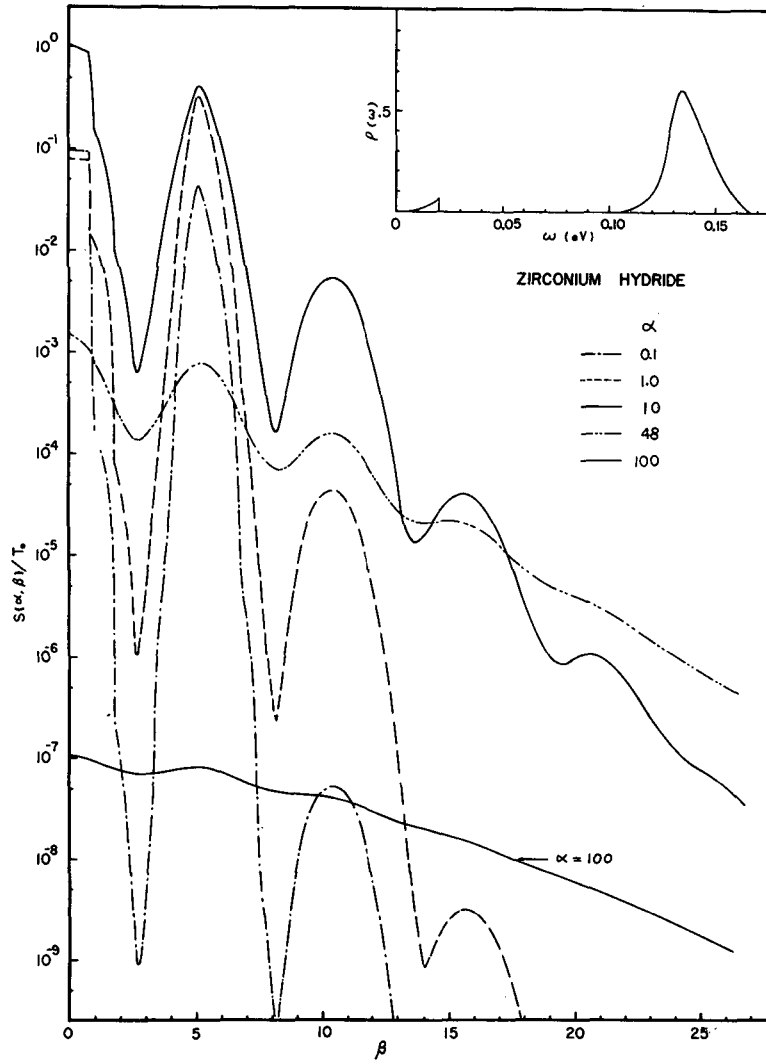

FIG. 11. Scattering law calculated for zirconium hydride.

C. Comparison between theoretical and experimental results

We discuss a direct comparison between theoretical and experimental cross-sections in this section. In the case of ZrH_2, theoretical and measured differential cross-sections have been compared. These results have been discussed in detail elsewhere [2].

Theoretical cross-sections for UC, based on our empirical frequency spectrum presented in Fig. 10, are plotted along with the experimental results for 0.134-eV incident energy in Fig. 7. One must add the contribution of the elastic scattering cross-section to the theoretical results

from the FLANGE output to obtain the total cross-section. In our calculations, we varied the ratio a_1/a_2 between the low- and high-energy transfer modes to obtain the best fit with the neutron scattering data. For a_1/a_2 equal to 1/12 the agreement between theory and experiment is found to be good. The contribution of uranium has also been plotted in Fig. 7. It is of interest to note that the major contribution in the neighbourhood of the elastic region is due to the neutron scattering by uranium atoms. On the other hand, the neutron scattering by the carbon atom is responsible for the major contribution in the inelastic region.

An attempt has also been made to compare theoretical results for the Dolling, Haywood, and the empirical (three Gaussian) frequency spectrum described earlier, with the experimental data. The theoretical results provided by the Haywood as well as Dolling frequency spectra overestimate the inelastic cross-section, in comparison with the measured cross-sections. The Debye plus three Gaussian frequency spectra with arbitrary weights of 1, 2, 7 and 5 have been attempted to give a better fit to the present data. However, considerable further theoretical and experimental studies are required to construct a frequency spectrum which would reproduce the neutron scattering data for UO_2.

D. Multiple scattering correction

Multiple scattering correction calculations are being undertaken using a Monte Carlo code. This code calculates the multiple scattering correction factor (C), defined as

$$C = \frac{\varphi_s(E, \vec{\Omega})}{\varphi_t(E, \vec{\Omega})} \tag{4}$$

$\varphi_s(E, \vec{\Omega})$ = flux at energy E which would be observed at a detector in a direction $\vec{\Omega}$ if only single interactions occurred, or

$$\varphi_s(E, \vec{\Omega}) = \varphi_{inc.}(E', \vec{\Omega}') \times \Sigma_s(E' \rightarrow E, \vec{\Omega}' \rightarrow \vec{\Omega}) \times t \tag{5}$$

$\varphi_t(E, \vec{\Omega})$ = flux at energy E which would be observed at a detector in a direction $\vec{\Omega}$ if multiple interactions were allowed in thickness t.

This code at present is being used for the gas kernel calculations. However, the extension of this code to arbitrary kernels is in progress [18].

Correction factors have been generated for ^{238}U gas and ^{16}O gas. The scatterer is assumed to have the same thickness and number density as the UO_2 sample. An effective correction for UO_2 has been obtained based on the following formula

$$C = \frac{\varphi_s^O(E, \vec{\Omega}) + \varphi_s^U(E, \vec{\Omega})}{\varphi_t^O(E, \vec{\Omega}) + \varphi_t^U(E, \vec{\Omega})} \tag{6}$$

where the superscripts U and O refer to uranium and oxygen respectively.

The multiple scattering correction factor for the elastic region is plotted in Fig. 13. As can be seen, the correction is almost constant over the elastic peak for the large scattering angles. This implies that any shape

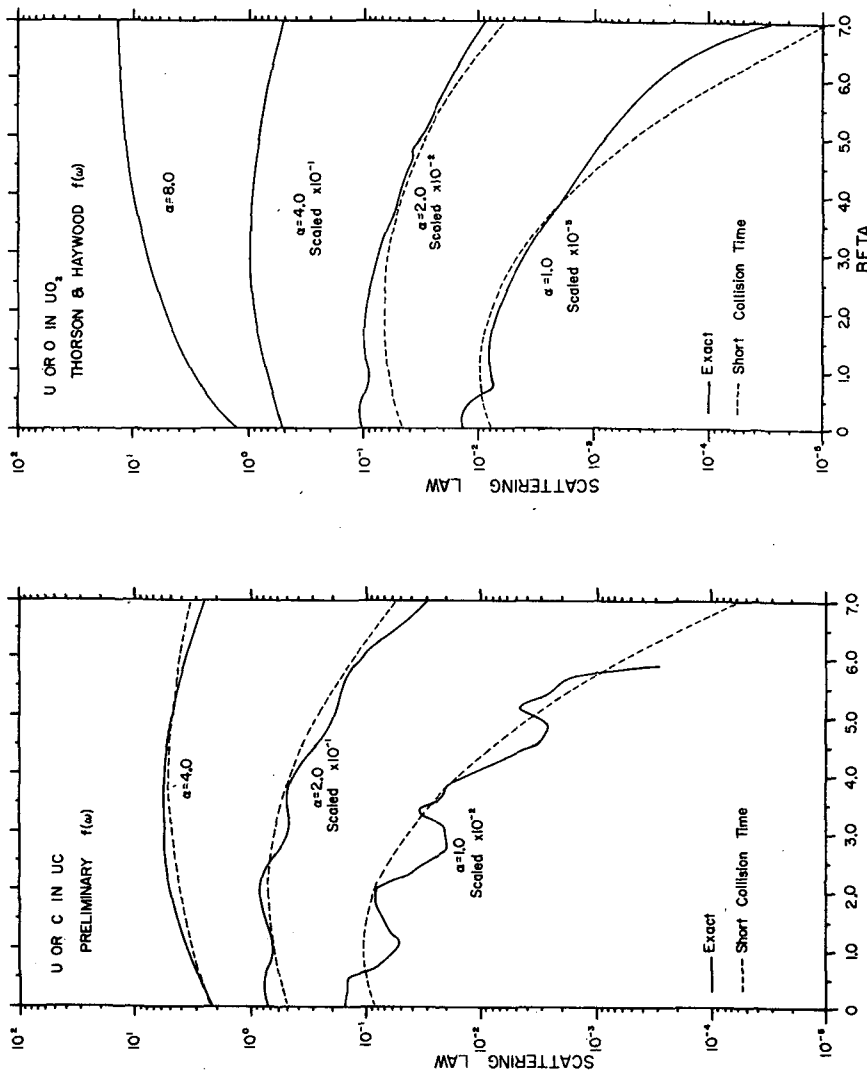

FIG. 12. Scattering law calculated for uranium carbide and uranium dioxide with frequency distributions of Fig. 10.

analysis we do in this region will not be affected very much by multiple scattering.

E. Limitations of incoherent approximation

Theoretical results presented here have been obtained from the GASKET code in the Placzek incoherent approximation. As far as ZrH_2 is concerned, this approximation holds true since the hydrogen atom, the main scatterer, is an incoherent scatterer. However, in the case of UC and UO_2 this approximation breaks down since U, C and O are coherent scatterers. The presence of the coherent effects considerably complicates the analysis problem.

In addition, the concept of frequency spectrum introduced to simplify the calculations is only rigorously valid for an isotropic cubic Bravais lattice. In the case of di- and tri-atomic systems the assumptions involved in the use of frequency spectra may not be completely justified due to the non-isotropic nature of the system. For example, the experimental values of the temperature-dependent Debye-Waller factor given by the X-ray scattering data of Willis [19] tend to confirm the importance of anisotropy and anharmonicity of vibrations in UO_2. The treatment of coherent scattering, and the anisotropy and anharmonicity of the lattice vibrations, is extremely complicated. At high temperatures the anharmonic effects strongly determine the thermodynamic properties of the system, such as specific heat and thermal conductivity.

III. APPLICATIONS OF SCATTERING LAW

The major objective of the neutron scattering law measurements is to provide realistic scattering kernels for a wide range of reactor physics problems. These involve the analysis of the pulsed slow-neutron spectra in finite media, the prediction of space-dependent thermal neutron spectra in homogeneous and heterogeneous media, the determination of the temperature-dependent resonance integrals, and the calculation of Doppler coefficients for thermal and fast reactors. It is well known that a scattering kernel can be theoretically constructed, provided the frequencies and amplitudes of vibrational modes in a scattering system are available.

A. Determination of frequency spectrum

Frequency spectra employed in the construction of the scattering kernel have been obtained by three methods: (i) cold neutron scattering experiments, (ii) phenomenological models, and (iii) thermodynamic data on specific heat. Each method has its limitations and does not necessarily yield the same frequency spectrum.

Egelstaff [20] proposed the determination of the frequency spectrum by extrapolating the scattering law to zero momentum transfer.

$$\left[\frac{S(\alpha,\beta)}{\alpha}\right]_{\alpha\to 0} = \frac{f(\beta)\exp\left(-\frac{\beta}{2}\right)}{2\beta\sinh\frac{\beta}{2}} \tag{7}$$

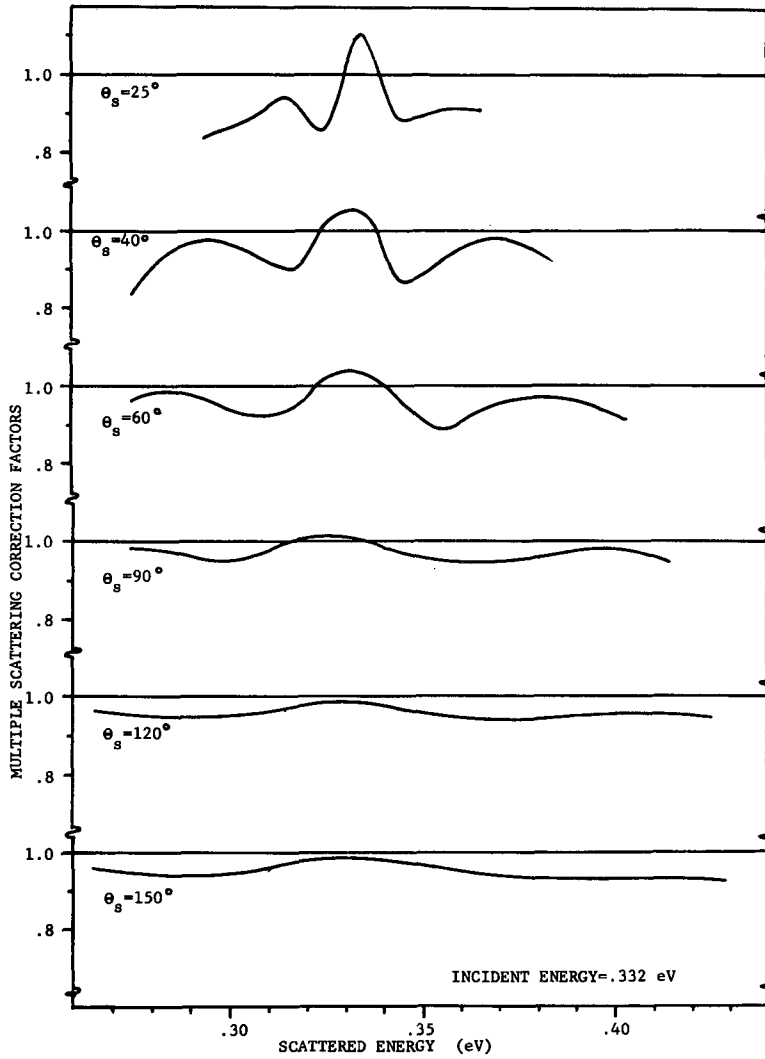

FIG. 13. Monte Carlo calculations of multiple scattering corrections for uranium dioxide free-gas approximation.

This procedure has been widely applied to the cold neutron scattering data obtained from a reactor by the energy gain method. The neutron scattering data in the extrapolation range need to be corrected for the experimental resolution, the multiple scattering and coherent effects. As mentioned in section II, the evaluation of these factors is extremely complicated; this puts some limitation on this method.

Neutron scattering data presented in the earlier sections may not be suitable for deriving the realistic frequency spectrum by the extrapolation procedure, as the corrections in the small-momentum transfer region are large. However, these data can be compared with a theoretical scattering

law constructed from a given frequency spectrum as shown in earlier sections for UC, UO_2 and ZrH_2. Therefore, indirectly they do provide a test for that frequency spectrum. In addition, we are of the opinion that energy-loss experiments at high-incident energies provide useful data for obtaining the Placzek moments of a frequency spectrum from the energy-transfer moments of the experimental scattering law.

B. Determination of Placzek moments

We define the n-th Placzek moment

$$\langle \xi^n \rangle = \int_{-\infty}^{+\infty} \frac{\xi^n f(\xi) d\xi}{\left(\exp \frac{\hbar\xi}{k_B T} - 1\right)} \tag{8}$$

These moments govern the deviations from the Fermi slowing-down spectrum, on the high-energy end, whenever the intermediate scattering function is represented by the short-collision time expansion of Placzek [21] and Wick [22]. Corngold [23] introduced the use of this expansion to study the high-energy end of the thermal neutron spectrum.

Placzek [21] derived the energy-transfer moments of the scattering law $S(\vec{K}, \omega)$ for a fixed momentum transfer $(\vec{K})$ in terms of $\langle \xi^n \rangle$ moments. Due to the variation of $\vec{K}$ for fixed angle, the application of the Placzek results requires considerable rearrangement of the scattering data. To avoid this rearrangement, theoretical results for the energy-transfer moments of $S(\vec{K}, \omega)$, for a fixed angle, $\cos^{-1}\mu$, have been obtained. These moments can be expressed in terms of the Placzek moments [24].

$$\langle \xi^n \rangle = \sum_{p=0}^{\infty} \frac{1}{p!} \left[\frac{\hbar m}{M} (1-\mu)\right]^p I_{n+p} \tag{9}$$

where

$$I_{n+p} = (i)^{n+p} \left[\frac{\partial^{n+p} \chi_p(E_0, t)}{\partial t^{n+p}}\right]_{t=0} \tag{10}$$

and

$$\chi_p(E_0, t) = [\gamma(t)]^p \exp\left\{\frac{\hbar m}{M} (1-\mu) E_0 \gamma(t)\right\} \tag{11}$$

$$\gamma(t) = \int_{-\infty}^{+\infty} \frac{f(\xi)[\exp(-i\xi t) - 1]}{\xi\left(\exp \frac{\hbar\xi}{k_B T} - 1\right)} \tag{12}$$

where $\gamma(t)$ is the Vineyard width function [25].

In the case of a heavy scatterer the convergence of the above expansion is extremely rapid, as $m/M \ll 1$.

An attempt is being made to fit the experimental data for high-incident energy with a gas model, using the temperature as a free parameter. At small angles the determination of T_{eff} (effective temperature) is complicated due to the domination of the width by the experimental resolution.

However, at back angles corresponding to the large-momentum transfer, the Doppler width is comparable to the resolution function width. Therefore, the back angle data may be suitable to obtain T_{eff}.

In Table II we present T_{eff} values and Debye-Waller factors for ZrH_2, UC and UO_2 based on the frequency spectra described in an earlier section. Mathematically T_{eff} is defined by the first Placzek moment.

$$\frac{T_{eff}}{2T} = \frac{\langle \xi \rangle}{2T} = \int_0^\infty \frac{\xi}{2T} f(\xi) \coth \frac{\hbar \xi}{2k_B T} d\xi \tag{13}$$

TABLE II

DEBYE-WALLER FACTORS AND EFFECTIVE TEMPERATURES

DEBYE-WALLER FACTOR ($Å^2$)					
Materials	Model	Temperature 300°K	600°K	1200°K	Ref.
UO_2 (U Only)	Shell Model	.2	.4	.7	[14]
	X-Ray Diff.	.25	.5	.85	[19]
	3 Gaussians + Debye	.15	.28	.56	*
ZrH_2	1 Gaussian + Debye	1.37	—	—	2

EFFECTIVE TEMPERATURES AT 300°K			
Material	Model	T_{eff}/T	
UO_2	Dolling, et al.	1.25	[14]
	Haywood-Thorson	1.40	[15]
	3 Gaussians + Debye	1.24	*
UC	1 Gaussian + Debye	1.34	*
ZrH_2	1 Gaussian + Debye	2.82	2

* Calculated in this work.

C. Doppler broadening of neutron resonances in a bound nucleus

Lamb [26] in his classical paper studied the problem of the resonance absorption of neutrons in a nucleus bound in a lattice. This paper emphasized the importance of the knowledge of the neutron scattering law or the intermediate scattering function in the study of the resonance line shape. As proposed by Lamb, the gas model formula with an effective temperature has been extensively used in the analysis of the Doppler broadened resonances. It is well known that the gas model is valid for large-momentum and small-energy transfers. For high-energy neutron resonances the expansion of the scattering law by a modified short collision-time expansion where the gas model with an effective temperature represents a leading term, may be quite satisfactory. However, for low-energy resonances the short collision time expansion is of doubtful value. In this energy range, either the Bessel function expansion, the phonon or the mass expansion of the intermediate scattering function must be employed. As a matter of fact, Jackson and Lynn [27] employed the Bessel function expansion to study 6.65-eV resonance in U metal and U_3O_8.

In this paper, we describe in brief the theoretical results in another study [28]. The resonance absorption cross-section (for neutrons or gamma rays) can be represented by a time integral involving the intermediate scattering function. (See Nelkin and Parks [29] and Singwi and Sjölander [30]):

$$\sigma(E) = \frac{\sigma(E_0)\Gamma}{4\hbar} \int_{-\infty}^{\infty} \chi_i(K^2, t) \exp\left\{ i(E - E_0)t - \frac{\Gamma}{2} |t| \right\} dt \tag{14}$$

where E_0 is neutron resonance energy, Γ is the nuclear width and $\sigma(E_0)$ is the cross-section at energy E_0. We discuss two cases.

(1) Modified short-collision time expansion

We shall now expand $\chi(K^2, t)$ using the modified short-collision time expansion.

$$\chi_i(K^2, t) = \exp \frac{\hbar K^2}{2M} (it - k_B T_{eff} t^2) \sum_{n=0}^{\infty} q_n \left\{ \frac{\hbar K^2}{2M} it \right\}^n \tag{15}$$

The coefficients a_n are explicitly given in terms of the Placzek moments. (See Sjölander [31]).

Substituting the above expansion in $\sigma(E)$ we obtain after some calculation

$$\sigma(E) = \frac{\sigma(E_0)\Gamma}{4\hbar} \left[\left(\frac{\Gamma}{2}\right)^2 \psi(X, \theta) + \sum_{n=3}^{\infty} a_n \left(\frac{\Gamma}{2}\right)^{2-n} \frac{\partial^n \psi(x, \theta)}{\partial x^n} \right] \tag{16}$$

where

$$\psi(x, \theta) = \frac{1}{2\sqrt{\pi\theta}} \int_{-\infty}^{\infty} \frac{\exp - \frac{(x-y)^2}{4\theta}}{(1+y^2)} dy \tag{17}$$

$$\chi = \frac{E - E_0 - \hbar^2 K^2/2M}{\Gamma/2} \text{ and } \theta = \frac{2k_B T_{eff} \hbar^2 K^2}{MT^2} \tag{18}$$

To obtain $\partial^n \psi(x, \theta)/\partial x^n$ we define an integral I_r with the following recurrence relation

$$I_n = J_{n-2} - I_{n-2} \tag{19}$$

where

$$I_n = \int_{-\infty}^{\infty} \frac{y^n \exp - \frac{(x-y)^2}{4\theta}}{(1+y^2)} dy \tag{20}$$

and

$$J_n = \int_{-\infty}^{\infty} y^n \exp - \frac{(x-y)^2}{4\theta} dy \tag{21}$$

After a series of calculations, we can finally show that

$$\sigma(E) = \frac{\sigma(E_0)\Gamma}{4\hbar} [A\psi(x, \theta) + B\chi(x, \theta) + C] \tag{22}$$

In the above expression the coefficients A, B and C involve the Placzek moments of the frequency spectrum other than T_{eff}. The ψ and χ functions involve only T_{eff}. The function $\chi(x, \theta)$, which appears in the study of the interference scattering cross-section using a gas model, is defined as follows:

$$\chi(x, \theta) = \frac{\partial\psi(x, \theta)}{\partial x} \tag{23}$$

It is of interest to note that the above expression for the cross-section is exactly identical to the form given by Adler and Adler [32], who used the R-matrix theory for studying the contribution of the multilevel interferences. In the Adler formalism the coefficients depend only on the nuclear parameters. On the other hand, in our formalism they depend on the moments of frequency spectrum of the vibrational modes. These coefficients also govern the wings of the resonance line. This emphasizes the importance of studying the Placzek moments other than T_{eff} in the study of the resonance line shape.

(2) Bessel function expansion

For harmonic vibrations, one may expand χ_i by a Bessel function expansion. (See for details Ref.[33])

$$\chi_i(K^2, t) = \exp - 2W \prod_{\lambda} \sum_{n_\lambda=-\infty}^{+\infty} I_{n_\lambda} \left[\frac{\hbar(\vec{K}\cdot\vec{e}_\lambda)^2}{2NM\sinh\frac{\hbar\omega_\lambda}{2k_BT}} \right]$$

$$\times \left(\exp\left\{ \frac{\hbar n_\lambda \omega_\lambda}{2k_BT} + i n_\lambda \omega_\lambda t \right\} \right) \tag{24}$$

In the above expression,

$$2W = \sum_{\lambda} \left(\frac{\hbar}{2M\omega_\lambda N} \right) (\vec{K}\cdot\vec{e}_\lambda)^2 \coth\frac{\hbar\omega_\lambda}{2k_BT} \quad \text{(Debye-Waller factor)} \tag{25}$$

$\vec{e}_\lambda$ = polarization vector for the λ-th normal mode.
ω_λ = frequency of the λ-th normal mode.

Employing the above expression in Eq.(23), we finally obtain

$$\sigma(E) = \frac{\sigma(E_0)\Gamma \exp - 2W}{4\hbar} \sum_{n_\lambda=-\infty}^{+\infty} I_{n_\lambda} \left(\frac{\hbar(\vec{K}\cdot\vec{e}_\lambda)^2}{2NM\sinh\frac{\hbar\omega_\lambda}{2k_BT}} \right)$$

$$\times \left\{ \frac{\exp(\hbar n_\lambda \omega_\lambda / 2k_BT)}{(E - E_0 - n_\lambda\omega_\lambda)^2 + (\Gamma/2)^2} \right\} \tag{26}$$

The modified Bessel function expansion is valid for large-momentum transfers; it may therefore, be preferable to the phonon or mass expansions which are valid for low-momentum transfers only.

A theoretical programme at Rensselaer is in progress to study the importance of binding effects on the narrow resonances based on the above formalisms.

REFERENCES

[1] KIROUAC, G.J., et al., "Epithermal neutron inelastic scattering and scattering law for H_2O", these proceedings, paper SM-96/64.

[2] PAN, S.S., Ph.D. Thesis, Rensselaer Polytechnic Institute (1967).

[3] PAN, S.S., MOORE, W.E , YEATER, M.L., Trans. Am. nucl. Soc. 9 (1966) 495.

[4] PAN, S.S., WEBB, F.J., Nucl. Sci. Engng 23 (1965) 188.

[5] WHITTEMORE, W.L., Inelastic Scattering of Neutrons II IAEA, Vienna (1965) 305.

[6] HARLING, O.K., LEONARD, B.R., Jr., Rep. BNL-940 (1965).

[7] SLAGGIE, E.L., General Atomics, private communication.

[8] WOODS, A.D.B , BROCKHOUSE, B.W., SAKAMOTO, M., SINCLAIR, R.N., Inelastic Scattering of Neutrons in Solids and Liquids, IAEA, Vienna (1961) 487.

[9] SAUNDERSON, D.H., COCKING, S.J., Inelastic Scattering of Neutrons in Solids and Liquids II IAEA, Vienna (1963) 265.

[10] WHITTEMORE, W.L., McREYNOLDS, A.W., Inelastic Scattering of Neutrons in Solids and Liquids, IAEA, Vienna (1961) 511.
[11] STALINSKI, B., BIEGANSKI, F., Bull. Acad. Pol. Sci. Ser. Sci. chim. 8 (1960) 243.
[12] PAN, S.S., WEBB, F.J., YEATER, M.L., Nucl. Instrum. Meth. 42 (1966) 197.
[13] BERGSMA, J., GEODKOOP, J.A., Inelastic Scattering of Neutrons in Solids and Liquids, IAEA, Vienna (1961) 501.
[14] DOLLING, G., COWLEY, R.A., WOODS, A.D.B., Can. J. Phys. 43 (1965) 1397.
[15] THORSON, I.M , HAYWOOD, B.C., Inelastic Scattering of Neutrons in Solids and Liquids II IAEA, Vienna (1963) 213.
[16] KOPPEL, J.U., TRIPLETT, J.R., NALIBOFF, Y.D., General Atomic Rep., GA-7417 (1966).
[17] BEYSTER, J.R., USAEC Rep., GA-6824 (1965).
[18] BISCHOFF, F., KALOS, M., private communication.
[19] WILLIS, B.T.M., Proc. roy. Soc. (London), Ser. A, 274 (1963) 122, 134.
[20] EGELSTAFF, P.A., Inelastic Scattering of Neutrons in Solids and Liquids, IAEA, Vienna, (1961) 25.
[21] PLACZEK, G., Phys. Rev. 86 (1962) 377.
[22] WICK, G.C., Phys. Rev. 94 (1954) 1228.
[23] CORNGOLD, N., Ann. Phys. 6 (1959) 368; ibid 11 (1960) 338.
[24] LAJEUNESSE, C., private communication.
[25] VINEYARD, G., Phys. Rev. 110 (1958) 999.
[26] LAMB, W.E., Phys. Rev. 55 (1939) 190.
[27] JACKSON, H E., LYNN, J.E., Phys. Rev. 127 (1962) 461.
[28] PUROHIT, S.N., private communication.
[29] NELKIN, M.S., PARKS, D.E., Phys. Rev. 119 (1960) 1060.
[30] SINGWI, K.S., SJÖLANDER, A., Phys. Rev. 120 (1960) 1093.
[31] SJÖLANDER, A., Ark. Fys. 14 (1958) 315.
[32] ADLER, F.T., ADLER, D.B., Reactor Physics in the Resonance and Thermal Regions II MIT Press Mass. (1966) 47.
[33] PUROHIT, S.N., Neutron Scattering and Thermalization Lectures, AB ATOMENERGI Rep. S-333, Sweden (1965).

DISCUSSION

H. TAKAHASHI: You used Dolling's frequency spectrum to analyse your UO_2 data, but this is essentially a spectrum for the whole UO_2 crystal. I should have thought it better to use two frequency spectra, to take account of the amplitudes of the atomic vibrations.

S. N. PUROHIT: Well, when we use the incoherent approximation, we are employing a frequency spectrum concept. Dolling has given a frequency spectrum which implies not only the energies of the normal modes but also the amplitudes.

Now, in our calculations we used the GASKET code, which computes $S(\alpha,\beta)$, for a given frequency spectrum, in the incoherent approximation. We assumed that the intermediate scattering function for the ith scatterer could be given by a simple expression involving $f(\omega)$, that is:

$$\chi_i = \exp \frac{\hbar K^2}{2M_i} \left[\int_{-\infty}^{+\infty} \frac{f(\omega)(\exp(-i\omega t)-1)}{\omega\left(\exp \frac{\hbar\omega}{k_B T} - 1\right)} d\omega \right]$$

This formula is exact for an isotropic cubic lattice, with one atom per unit cell. In the case of UO_2 we assumed that the sum of the polarization vectors can be replaced by an integral over the frequency spectrum of

the whole lattice, so

$$\sum_{\lambda} \frac{(\underline{K}C^{i}{}_{\lambda})^2}{M_i} g(\omega_\lambda) \longrightarrow \frac{K^2}{2M_i} \int f(\omega)g(\omega)d\omega$$

This mathematical statement contains the physical assumptions of our calculations.

I. M. THORSON: I would disagree with what Dr. Purohit has just said about an amplitude-frequency spectrum for UO_2. As I see it, no amplitudes of any kind are involved. The essential problem lies in deducing the separate quasi-frequency distributions to be used for calculating the scattering law for two-component systems, when these quasi-frequency distributions are to be computed from the conventional frequency distribution of normal modes for the system.

S. N. PUROHIT: We discussed this problem in some detail before doing our calculations, and we assumed that the lattice vibrations in the whole system could be replaced by a rotational frequency spectrum. This means that as far as the neutron is concerned it is scattered by either uranium or oxygen; momentum is transferred and the required energy is transferred. I would not want to divide this one-phonon frequency spectrum for the whole lattice into quasi-frequency spectra and I maintain that for isotropic cubic systems our treatment is justified. I do not quite see how to take into account the points you mention, unless one goes into detailed calculations and abandons the incoherent approximation.

J. A. YOUNG: In line with what Dr. Takahashi and Dr. Thorson have said, I should like to mention that we have performed calculations in the incoherent approximation for non-isotropic systems, using the polarization vectors and frequencies rather than simply the phonon spectrum. I would emphasize that the slow neutron scattering cross-section depends on the phonon spectrum solely for cubic solids with one atom per unit cell, which scatter only incoherently.

S. N. PUROHIT: Yes, I agree. The GASKET code in the present form only accepts frequency spectra of the normal modes, and so we decided to do the UO_2 calculations using the available Dolling frequency spectrum, but we do intend to undertake detailed calculations for UO_2 using the polarization vectors and frequencies and so eliminate the use of the idealized concept of the frequency spectrum.

SLOW NEUTRON SCATTERING AND THERMALIZATION BY BENZENE *

D. SPREVAK†, J.U. KOPPEL AND J.A. YOUNG
GENERAL ATOMIC DIVISION,
GENERAL DYNAMICS CORPORATION,
SAN DIEGO, CALIFORNIA,
UNITED STATES OF AMERICA

Abstract

SLOW NEUTRON SCATTERING AND THERMALIZATION BY BENZENE. The moderation of neutrons in benzene has been studied and a kernel for benzene was obtained. The cross-sections were calculated in the incoherent approximation. The dynamics of the benzene molecule were determined, assuming a model of the molecule in which the atoms make harmonic oscillations about the equilibrium position. The harmonic potential was formed with the set of force constants calculated by Crawford and Miller from the assigned frequency spectrum. The vibrational frequencies and the amplitude vectors determined in this way were used in the calculation of the scattering law. The hindered translations and rotations corresponding to the liquid state were included as free translations of the molecule with an associated effective mass. The numerical calculations of the scattering law for benzene were performed with the code GASKET, which calculates the scattering law from the vibrational spectrum of the molecule.

The total cross-section, the average of the scattering angle, and the single-differential cross-section were obtained and compared with experimental data. The agreement between theory and experiment is very good.

1. INTRODUCTION

In this paper we present calculations of the double-differential scattering cross-section, the single-differential scattering cross-section, the total cross-section, and the average of the cosine of the scattering angle for benzene. Our results are compared with previous calculations and with experimental data.

Section 2 contains the general basis and physical assumptions which we have made in these calculations. In Section 3 the cross-section is expressed in terms of the dynamical state of the atoms forming the molecule. Section 4 deals with the dynamics of the benzene molecule and gives the resulting normal mode amplitudes. In section 5 we discuss and present our results for the cross-sections.

2. SCATTERING OF NEUTRONS BY BENZENE

The differential cross-section for the scattering of neutrons from any molecular system with initial wave functions ψ_i and final wave func-

* This work was sponsored by the United States Atomic Energy Commission.

† Visiting scientist from Bariloche, Argentina, under the auspices of the United States Agency for International Development.

tions ψ_f is*

$$\frac{d^2\sigma}{d\Omega dE} = \frac{1}{2\pi}\frac{k}{k_0}\sum_f \int_{-\infty}^{\infty} dt\, e^{iEt}\left[e^{-i(E_i-E_f)t}\,|<\psi_f|\sum_m \exp(i\vec{\varkappa}\cdot\vec{x}_m)C_m|\psi_i>|^2\right]_T \quad (1)$$

Here k_0, and k are initial and final neutron moments, respectively, E_i, E_f are the initial and final energies of the molecular system, E is the neutron energy transfer, $\vec{\varkappa}$ the neutron momentum transfer, $\vec{x}_m$ and C_m the position vector and scattering amplitude of the mth atom, respectively, and the subscript T implies that a thermal average is to be taken over initial states.

If in Eq. (1) we neglect the contribution to the scattering from the interference terms, we have what is called the incoherent approximation. This is a good approximation for the hydrogen atoms in benzene, because of the approximate cancellation of the neutron scattering amplitudes in the triplet and singlet states of the n-p system. Since the interaction of the neutrons with the hydrogen atoms is the main mechanism of thermalization of the neutrons, this approximation is also good for the benzene molecule.

The cross-section in the incoherent approximation will be

$$\frac{d^2\sigma}{d\Omega dE} = \frac{1}{8\pi^2}\frac{k}{k_0}\int_{-\infty}^{\infty} e^{iEt}\,dt\sum_{k=1}^{n}\sigma_k^b\, X_k(\vec{\varkappa},t) \quad (2)$$

The sum is over all the atoms in the molecule and σ_k^b is the bound atom cross-section of the kth atom; the function $X_k(\vec{\varkappa},t)$, which contains the dependence of the scattering on the dynamics of the atoms in the molecule, is given by

$$X_k(\vec{\varkappa},t) = <e^{i\vec{\varkappa}\cdot\vec{x}_k(t)}\, e^{-i\vec{\varkappa}\cdot\vec{x}_k(0)}>_T \quad (3)$$

where $\vec{x}_k(t)$, the time-dependent position operator of the kth nucleus in the molecule at the time t, satisfies the Heisenberg equation of motion

$$i\frac{d}{dt}\vec{x}_k(t) = \vec{x}_k(t)\,H - H\vec{x}_k(t) \quad (4)$$

in which H is the molecular Hamiltonian. The symbol $<\ldots>_T$ means that an average is to be taken over the equilibrium distribution of initial states of the molecule.

---

*We are using a system of units where $\hbar$ (Planck's constant divided by 2π) = 1 and k_b (Boltzman's constant) = 1.

Even in this approximation the calculation of the cross-sections constitutes a difficult problem. The main difficulty is in the exact determination of the dynamics of the molecule on which the cross-section depends.

We shall obtain an expression for $\vec{x}(t)$ from a model that avoids some of the difficulties of the problem but keeps the essential features of the molecular dynamics as far as the neutron scattering is concerned.

In the simplified model we ignore all the interactions between molecules, and between rotations and vibrations. The first one is an approximation that can only be justified by comparing the results with experimental data. At present there is no theoretical method to treat the liquid state in an exact way. The second approximation is justified by the large differences between the frequencies corresponding to vibrational states and rotational states, due to the large moment of inertia of the benzene molecule. We also neglect spin correlation effects which are not important at room temperature.

Basically, the model is a vibrating molecule in which the carbon and hydrogen atoms make harmonic oscillations about their equilibrium positions. The hindered translations and rotations corresponding to the liquid state are treated as free translations of the whole molecule to which we associate an effective mass.

3. MATHEMATICAL FORMULATION

The instantaneous position of the sth nucleus in the molecule may be expressed as

$$\vec{x}_s(t) = \vec{X}(t) + \vec{b}_s(t) + \vec{u}_s(t) \tag{5}$$

where $\vec{X}(t)$ is the position vector of the molecular center of mass, $\vec{b}_s(t)$ is the distance of the equilibrium position of the sth nucleus from the center of mass, and $\vec{u}_s(t)$ is the instantaneous displacement of the nucleus from its equilibrium position due to vibration.

If we neglect interaction between rotation and vibration the molecular Hamiltonian can be expressed as the sum of three parts

$$H = H_{tr} + H_{vib} + H_{rot} \tag{6}$$

which are, separately, the Hamiltonians for the translation, vibrational and rotational motions of the molecule.

For small vibrations we may separate the displacement due to vibrations into normal modes and write

$$\vec{u}_s(t) = \sum_{j=1}^{3n-6} \left(\frac{1}{2M_s\omega_j}\right)^{1/2} \vec{C}_j^s \left(A_j e^{-i\omega_j t} + A_j^+ e^{i\omega_j t}\right) \tag{7}$$

where M_s is the mass of the sth particle in the molecule, n is the number of atoms in the molecule, ω_j and $\vec{C}_j^s$ are the frequency and the amplitude vector, respectively, of the sth particle in the jth mode of vibration, A_j and its Hermitian conjugate A_j^+ are the annihilation and creation operators, respectively, associated with the normal mode identified by the index j.

If we use the fact that during the time of interaction of the neutron with the molecule the atoms of the molecule change their position mainly by vibration, we can separate vibration and rotation in the cross-section.[1] Under this condition Eq. (3) takes the form

$$X_k(\vec{\varkappa}, t) = X^{tr}(\vec{\varkappa}, t)\, X_k^{vib}(\vec{\varkappa}, t)\, X_k^{rot}(\vec{\varkappa}, t) \tag{8}$$

Furthermore, if we approximate translations and rotations of the molecule as free translations with an effective mass, Eq. (8) takes the form

$$X_k(\vec{\varkappa}, t) = X_k^{tr}(\vec{\varkappa}, t)\, X_k^{vib}(\vec{\varkappa}, t) \tag{9}$$

where[2]

$$X_k^{tr}(\varkappa, t) = \exp\left[\frac{\varkappa^2}{2M_k^*}(it - Tt^2)\right] \tag{10}$$

M_k^* is the effective mass associated with the atom k and T is the absolute temperature.

Furthermore,[2]

$$X_s^{vib}(\varkappa, t) = \left\langle \exp\left\{\frac{1}{2M_s}\sum_{j=1}^{3n-6}(\vec{\varkappa}\cdot\vec{C}_j^s)^2\left[g(\omega_j, t) - g(\omega_j, 0)\right]\right\}\right\rangle_\Omega \tag{11}$$

with

$$g(\omega, t) = \frac{\left[\bar{n}(\omega) + 1\right] e^{i\omega t} + \bar{n}(\omega) e^{-i\omega t}}{\omega} \tag{12}$$

and

$$\bar{n}(\omega) = (e^{\omega/T} - 1)^{-1} \tag{13}$$

The symbol $<\ldots>_\Omega$ indicates an average over-all molecular orientation.

Here we make another approximation. Instead of averaging the exponential in Eq. (11) we take the average of the exponent, that is

$$X_s^{vib}(\varkappa, t) = \exp\left\{ < \frac{1}{2M_s} \sum_{j=1}^{3n-6} (\vec{\varkappa} \cdot \vec{C}_j^s)^2 \left[g(\omega_j, t) - g(\omega_j, 0)\right] >_\Omega \right\} \tag{14}$$

This averaging procedure is generally satisfactory, since it gives the exact result in the limits $\varkappa^2 \to 0$ and $\varkappa^2 \to \infty$.

Performing the average we get

$$\begin{aligned} &< \frac{1}{2M_s} \sum_{j=1}^{3n-6} (\vec{\varkappa} \cdot \vec{C}_j^s)^2 \left[g(\omega_j, t) - g(\omega_j, 0)\right] >_\Omega \\ &= \frac{\varkappa^2}{6M_s} \sum_{j=1}^{3n-6} (C_j^s)^2 \cdot \left[g(\omega_j, t) - g(\omega_j, 0)\right] \end{aligned} \tag{15}$$

If we write

$$\rho_s(\omega) = \frac{1}{3} \sum_{\omega_j} \delta(\omega - \omega_j) \left(\vec{C}_j^s\right)^2 \tag{16}$$

Eq. (14) becomes

$$X_s^{vib}(\varkappa, t) = \exp\left\{ \frac{\varkappa^2}{2M_s} \int_0^\infty \rho_s(\omega)\, d\omega \left[g(\omega, t) - g(\omega, 0)\right] d\omega \right\} \tag{17}$$

Due to the six-fold symmetry axis of the benzene molecule all six hydrogen as well as all six carbon atoms are equivalent. Hence there are only two different frequency spectra, ρ_H and ρ_C, leading to only two different X-functions, X_H and X_C, the index H referring to hydrogen and C to hydrogen.

Hence the cross-section per hydrogen and carbon atom takes the form

$$\frac{d^2\sigma}{d\Omega dE} = \frac{1}{8\pi^2}\frac{k}{k_0}\int_{-\infty}^{\infty} e^{iEt}dt\left(\sigma_H^b X_H(\varkappa, t) + \sigma_c^b X_C(\varkappa, t)\right) \tag{18}$$

where X_H and X_C are given by Eqs. (9), (10) and (17).

4. THE MOLECULAR DYNAMICS OF BENZENE

In the previous sections of this report the importance of molecular dynamics with regard to neutron scattering became apparent. Here we discuss in some detail the dynamics of the benzene molecule.

In the equilibrium configuration the benzene molecule has an hexagonal structure with symmetry D_{6h}. Two parameters describe the geometry of the molecule: R_o, the distance between two nearest carbons, taken as 1.39 Å and r_o, the distance between a carbon and the nearest hydrogen, taken as 1.08 Å. Figure 1 shows this arrangement; the small and the large circles represent the hydrogen and the carbon atoms respectively.

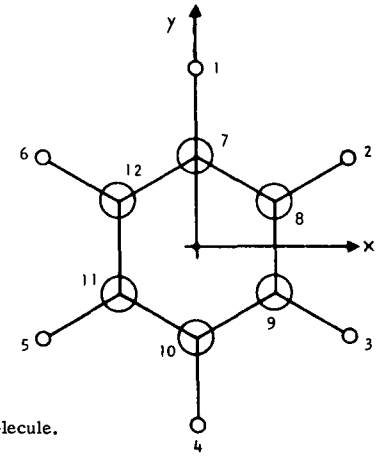

FIG. 1. Benzene molecule.

The following set of internal coordinates were used for describing the dynamics of the molecule:

R_j : The carbon-carbon bond stretching

r_j : The carbon-hydrogen bond stretching

α_j : The change in the CCC ring angle

β_j : The angle between the CH bond and the bisector of the outer CCC angle.

γ_j : The bending of the CH bond out of the plane of the three nearest carbons.

δ_j : The torsion of the type CCCC.

Since we only consider quadratic terms in the energy the internal coordinates are linearly related to the cartesian displacements of the atoms. Thus, calling $\{S_t\}$ the set of internal coordinates we have

$$S_t = \sum_{k=1}^{n} \vec{r}_{tk} \cdot \vec{u}_k \tag{19}$$

where the vectors $\vec{r}_{tk}$ depend on the geometry of the molecule.

The normal vibrations of benzene separate into two kinds. One set of normal vibrations has amplitude vectors that are perpendicular to the plane of the molecule and the other set has amplitude vectors that are parallel to the plane of the molecule. Altogether there are 3n-6 = 30 normal modes of vibrations. Of these 2n-3 = 21 are of the parallel type. The remaining nine modes belong to the perpendicular type.

The structure of the representation formed by the cartesian coordinates of benzene is

$$\Gamma_i = 2A_{1g} + A_{2g} + 4E_{2g} + 2B_{1u} + 2B_{2u} + 3E_{1u}$$

for the 21 in-plane modes, and

$$\Gamma_o = 2B_{2g} + E_{1g} + A_{2u} + 2E_{2u}$$

for the nine out-of-plane modes.

It follows that there are seven double degenerate in-plane normal modes and three double degenerate out-of-plane normal modes.

The symmetry properties have been utilized in the assignment of the fundamental frequencies of vibration that have been found experimentally from the infrared and Raman techniques. The assigned experimental frequencies are then used to calculate the force constants. The force field for benzene has been determined in this way by many workers[3,4,5] with substantial agreement. In this work we use the set of force constants obtained by Crawford and Miller.[3,4]

The set of internal coordinates defined by Eq. (19) is not the most convenient for calculating the normal modes of vibration. From the knowledge of the molecular symmetry it is possible to find a new set $\{D_i\}$ called symmetry coordinates, which lead to a factorization of the secular equation. The transformation from internal to symmetry coordinates is [6,7]

linear and unitary

$$D_i = \sum_j T_{ij} S_j \tag{20}$$

In terms of the symmetry coordinates the vibrational Hamiltonian takes the form

$$H_{vib} = \frac{1}{2} \sum_{tt'} \left[G^{-1}_{tt'} \dot{D}_t \dot{D}_{t'} + F_{tt'} D_t D_{t'} \right] \tag{21}$$

where F and G are the Wilson matrices. F is the matrix formed by the force constants when the potential energy is expressed in symmetry coordinates. G^{-1} is the inverse of the matrix G whose elements can be obtained from Eqs (19)-(21)

$$G_{tt'} = \sum_{k,\ell,\ell'} \frac{1}{M_k} T_{t\ell} \vec{r}_{\ell k} \cdot \vec{r}_{\ell' k} T_{t'\ell'} \tag{22}$$

The molecular vibrations may be expressed in terms of normal modes by introducing the set of normal coordinates $\{Q_j\}$. The normal coordinates can be written as a linear combination of the symmetry coordinates

$$Q_j = \sum_i L_{ji} D_i \tag{23}$$

The elements L_{ij} of the square matrix L are determined by the condition that the Hamiltonian of Eq. (21) be diagonal if expressed in terms of normal coordinates. This leads to the matrix equation

$$LGF = \Lambda L$$

where Λ is diagonal. Since both F and G are symmetric this equation can also be put in the form

$$FGL^+ = L^+ \Lambda \tag{24}$$

The elements λ_j of Λ are obtained by solving the secular equation

$$\det[FG - \lambda I] = 0 \tag{25}$$

where I is the unit matrix.

The roots of the secular equation give the normal mode frequencies ω_j appearing in Eq. (7) through the relation

$$\lambda_j = \omega_j^2 \quad (j = 1, 2 \ldots, 3n-6) \tag{26}$$

The amplitude vectors $\vec{C}_j^s$ appearing in Eq. (7) are directly related to the

normal coordinates Q_j. In fact defining the mass-weighted cartesian displacement coordinates

$$\vec{q}_k = \sqrt{M_k}\,\vec{u}_k \qquad (k = 1, 2 \ldots n) \tag{27}$$

we have

$$\left.\begin{aligned} \vec{q}_k &= \sum_j \vec{C}_j^k Q_j \\ &\text{or} \\ Q_j &= \sum_k \vec{C}_j^k \cdot \vec{q}_k \end{aligned}\right\} \tag{28}$$

since the $\vec{C}_j^k$ satisfy the orthogonality relations

$$\sum_k \vec{C}_j^k \cdot \vec{C}_{j'}^k = \delta_{jj'} \tag{29}$$

Now from Eqs. (19) and (20) we can rewrite Eq. (23) in the form

$$Q_j = \sum_{i,k,\ell} L_{ji}\, T_{ik}\, \vec{r}_{k\ell} \cdot \vec{q}_\ell / \sqrt{M_\ell} \tag{30}$$

which compared to Eq. (28) yields the following expression for the amplitude vectors

$$\vec{C}_j^k = \sum_{i,\ell} L_{ji}\, T_{i\ell}\, \vec{r}_{\ell k} / \sqrt{M_k} \tag{31}$$

The preceding formula together with the normalization imposed by Eq. (29) completely determine the amplitude vectors to be used in Eq. (11).

In Tables I, II and III we list the values of the x, y and z components of the vectors $\vec{C}_j^k$. From these numbers* the frequency spectra ρ_H and ρ_C can be calculated according to Eq. (16). It is easily seen that the resulting frequency spectra are the same for all six hydrogen as well as for all six carbon atoms. However, for maximum numerical accuracy it is convenient to calculate ρ_H and ρ_C from the average over-all equivalent atoms.

---

*In an earlier calculation Boffi, et al.,[8] using the same force field obtained slightly different results. However, we feel that our values are more reliable since their amplitudes do not satisfy Eq. (29) very accurately.

Table I

X-COMPONENTS OF THE AMPLITUDE VECTORS $\vec{C}_j^k$

j/k	1	2	3	4	5	6	7	8	9	10	11	12
1	0	.1186	.1186	0	-.1186	-.1186	0	.3331	.3331	0	-.3331	-.3331
2	0	.3331	.3331	0	-.3331	-.3331	0	-.1186	-.1186	0	.1186	.1186
3	.3630	.1815	-.1815	-.363	-.1815	.1815	-.1869	-.0934	.0934	.1869	.0934	-.0934
4	0	-.1181	.1181	0	-.1180	.1181	0	-.3333	.3333	0	-.3333	.3333
5	0	-.3333	.3333	0	-.3331	.3333	0	.1181	-.1181	0	.1181	-.1181
6	.3545	-.1772	-.1772	.3545	-.1772	-.1772	-.2026	.1013	.1013	-.2026	.1013	.1013
7	.2026	-.1013	-.1013	.2026	-.1013	-.1013	.3544	-.1772	-.1772	.3544	-.1772	-.1772
8	0	-.1083	-.1083	0	.1083	.1083	0	.1146	.1146	0	-.1146	-.1146
9	0	-.2375	-.2375	0	.2375	.2375	0	.068	.068	0	-.068	-.068
10	0	.1179	-.1179	0	.1179	.1179	0	-.3241	-.3241	0	.3241	.3241
11	0	-.2073	-.2073	0	.2073	.2073	0	.0466	.0466	0	-.0466	-.0466
12	.1530	.0345	-.0345	-.1530	-.0345	.0345	-.4967	.2981	-.2981	.4967	-.2981	.2981
13	.0003	.4110	.4110	.0003	-.4110	.4110	.0231	-.1408	.1408	-.0231	.1408	-.1408
14	.1320	.0722	-.0722	-.1320	-.0722	.0722	.2847	.2767	-.2767	-.2847	-.2767	.2767
15	.5408	-.1817	.1817	-.5408	.1817	-.1817	.071	-.1518	.1518	-.071	.1518	-.1518
16	0	-.1654	.1654	0	-.1654	.1654	0	.2164	-.2164	0	.2164	-.2164
17	0	.2102	-.2102	0	.2102	-.2102	0	.2658	-.2658	0	.2658	-.2658
18	0	.2312	-.2312	0	.2312	-.2312	0	-.0868	.0868	0	-.0868	.0868
19	-.4410	-.1545	-.1545	-.4410	-.1545	-.1545	.3223	-.0525	-.0525	.3223	-.0525	-.0525
20	.3547	-.0094	-.0094	.3547	-.0094	-.0094	.2744	-.1859	-.1859	.2744	-.1859	-.1859
21	-.0137	-.4141	-.4141	-.0137	-.4141	-.4141	-.0189	.1314	.1314	-.0189	.1314	.1314

Table II

Y-COMPONENTS OF THE AMPLITUDE VECTORS $\vec{C}_j^k$

j/k	1	2	3	4	5	6	7	8	9	10	11	12
1	.1369	.0684	-.0684	-.1369	-.0684	.0684	.3846	.1923	-.1923	-.3846	-.1923	.1923
2	.3846	.1923	-.1923	-.3846	-.1923	.1923	-.1369	-.0684	.0684	.1369	.0684	-.0684
3	0	-.3143	-.3143	0	.3143	.3143	0	.1618	.1618	0	-.1618	-.1618
4	.1363	-.0682	-.0682	.1364	-.0682	-.0682	.3848	-.1924	-.1924	.3848	-.1924	-.1924
5	.3847	-.1924	-.1924	.3849	-.1923	-.1924	-.1363	.0682	.0682	-.1364	.0682	.0682
6	0	.3070	-.3070	0	.3070	-.3070	0	-.1754	.1754	0	-.1754	.1754
7	0	.1754	-.1754	0	.1754	-.1754	0	.3070	-.3070	0	.3070	-.3070
8	.097	.0905	-.0905	-.097	-.0905	.0905	.2320	-.4305	.4305	-.2320	.4305	-.4305
9	.5481	-.1368	.1368	-.5481	.1368	-.1368	-.1800	.06231	-.06231	.1800	-.06231	.06231
10	.1403	.0639	-.0639	-.1403	-.0639	.0639	.4639	.0976	-.0976	-.4639	-.0976	.0976
11	-.0620	.4211	-.4211	.0620	-.4211	.4211	-.1787	.098	-.098	.1787	-.098	.098
12	0	.1083	.1083	0	-.1083	-.1083	0	-.1146	-.1146	0	.1146	.1146
13	0	.2375	.2375	0	-.2375	-.2375	0	-.068	-.068	0	.068	.068
14	0	.1179	.1179	0	-.1179	-.1179	0	.3241	.3241	0	-.3241	-.3241
15	0	.2073	.2073	0	-.2073	-.2073	0	-.0466	-.0466	0	.0466	.0466
16	.0589	.3455	.3455	.0589	.3455	.3455	.1775	-.1974	-.1974	.1775	-.1974	-.1974
17	.1308	-.2333	-.2333	.1308	-.2333	-.2333	.3393	-.1210	-.1210	.3393	-.1210	-.1210
18	.5476	.1472	.1472	.5476	.1472	.1472	-.1815	-.0312	-.0312	-.1815	-.13112	-.03112
19	0	.1654	-.1654	0	.1654	-.1654	0	-.2164	.2164	0	-.2164	.2164
20	0	-.2102	.2102	0	-.2102	.2102	0	-.2657	.2657	0	-.2657	.2657
21	0	-.2312	.2312	0	-.2312	.2312	0	.0868	-.0868	0	.0868	-.0868

Table III

Z-COMPONENTS OF THE AMPLITUDE VECTORS $\vec{C}_j^k$

k/j	1	2	3	4	5	6	7	8	9
1	.3921	.3699	.1727	.0000	0	-.3268	-.4759	0	-.5133
2	.3921	-.3699	-.1727	-.2830	-.4122	.1634	.238	.4445	-.2567
3	.3921	.3699	.1727	.2830	.4122	.1634	.238	.4445	.2567
4	.3921	-.3699	-.1727	.0000	0	-.3268	-.4759	0	.5133
5	.3921	.3699	.1727	-.2830	-.4122	.1634	.238	-.4445	.2567
6	.3921	-.3699	-.1727	.2830	.4122	.1634	.238	-.4445	-.2567
7	-.1136	-.1727	.3699	0	0	-.476	.3268	0	.2642
8	-.1136	.1727	-.3699	-.4122	.2830	.238	-.1634	-.2289	.1322
9	-.1136	-.1727	.3699	.4122	-.2830	.238	-.1634	-.2289	-.1322
10	-.1136	.1727	-.3699	0	0	.476	.3268	0	-.2642
11	-.1136	-.1727	.3699	-.4122	.2830	.238	-.1634	.2289	-.1322
12	-.1136	.1727	-.3699	.4122	-.2830	.238	-.1634	.2289	.1322

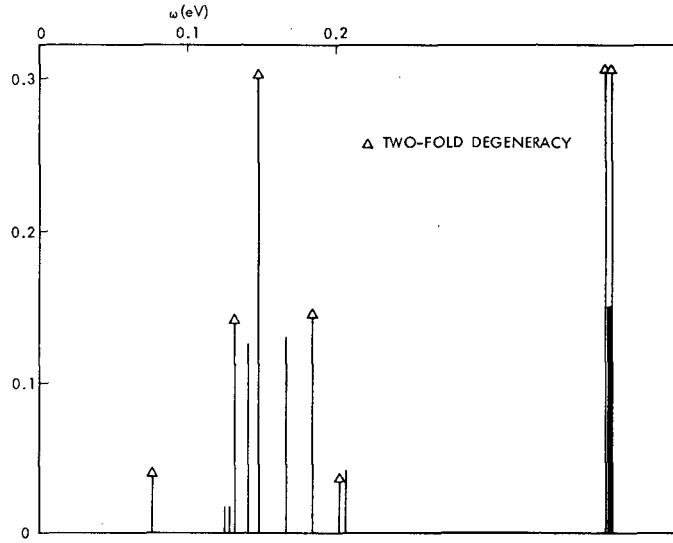

FIG. 2a. In-plane vibration in benzene.

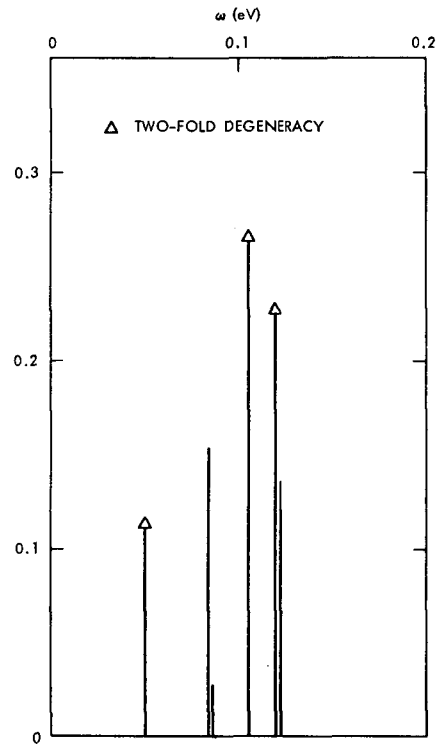

FIG. 2b. Out-of-plane vibrations in benzene.

Table IV

J-INDEX FROM TABLES I, II AND III AND THE CORRESPONDING FREQUENCY

J	FREQ.	J	FREQ.	J	FREQ.
1	678	1	996	12	1617
2	993	2	3061	13	3050
3	693	3	1323	14	599
4	403	4	1017	15	1180
5	958	5	3058	16	1053
6	403	6	1112	17	1469
7	958	7	1647	18	3082
8	851	8	1617	19	1053
9	851	9	3050	20	1469
		10	599	21	3082
		11	1180		
For the out-of-plane vib.		For the in-plane vib.			

Figures 2-a and 2-b show the fundamental frequencies of vibration for benzene. The height of the lines shown in these figures indicates the average of $|C_j^H|^2$ over all hydrogen atoms.

The correspondence between the j-index in Tables I, II and III and the frequency is given in Table IV. The frequencies are given in cm^{-1}.

5. SCATTERING CROSS-SECTION IN BENZENE

The frequencies and amplitude vectors which we have calculated in the previous sections have been used with Eq. (18) to obtain the scattering law for the benzene molecule.

The numerical calculations for the scattering law were carried out using the code GASKET.[9]

The availability of this code has made it possible to improve on an earlier scattering kernel obtained by Boffi, et al.[8] In GASKET the translational and rotational modes can be treated as free translations according to Eq. (10). Furthermore using GASKET the cluster of frequencies closely spaced about 0.38 eV can be treated as one single discrete oscillator. This considerably improves the numerical accuracy since very narrow peaks in the frequency spectrum lead to large numerical errors if treated as distributed modes. For the same reason, the remaining part of the discrete frequency spectrum, that is, the part be-

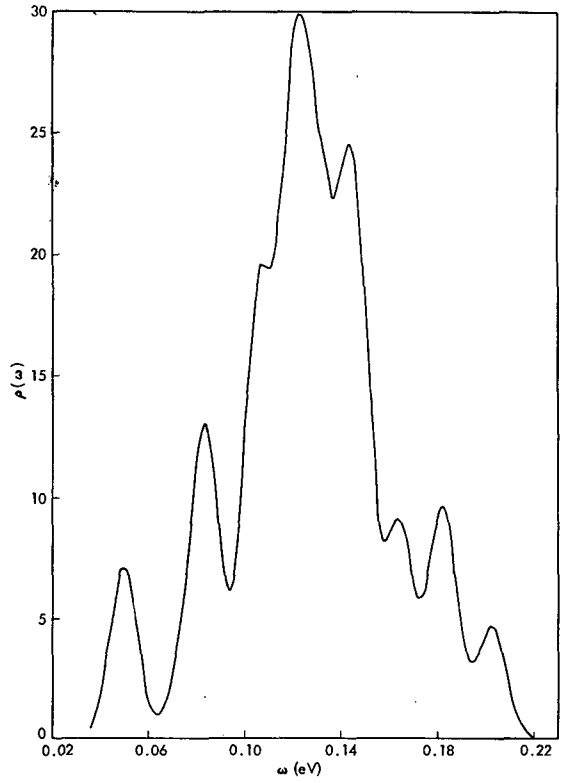

FIG. 3. Vibrational spectrum of the hydrogen atoms used to calculate benzene kernel. (The set of frequencies about 0.38 eV are not shown.)

low .38 eV, had to be artificially broadened. The resulting continuous spectra for the hydrogen and carbon atoms, as used in our calculations, are shown in Figs 3 and 4.

The effective translational mass associated with the hydrogen atoms to be used in Eq. (10) is

$$M_H^* = \frac{1}{1 - \frac{1}{18} \sum_{j=1}^{3n-6} \sum_{k=1}^{6} |\vec{C}_j^k|^2} = 20.94$$

For the carbon atoms

$$M_c^* = \frac{1}{1 - \frac{1}{18} \sum_{j=1}^{3n-6} \sum_{k=7}^{12} |\vec{C}_j^k|^2} = 42.2$$

The total cross-section obtained with the present calculations is shown in Fig. 5. Also shown for comparison is the cross-section obtained by

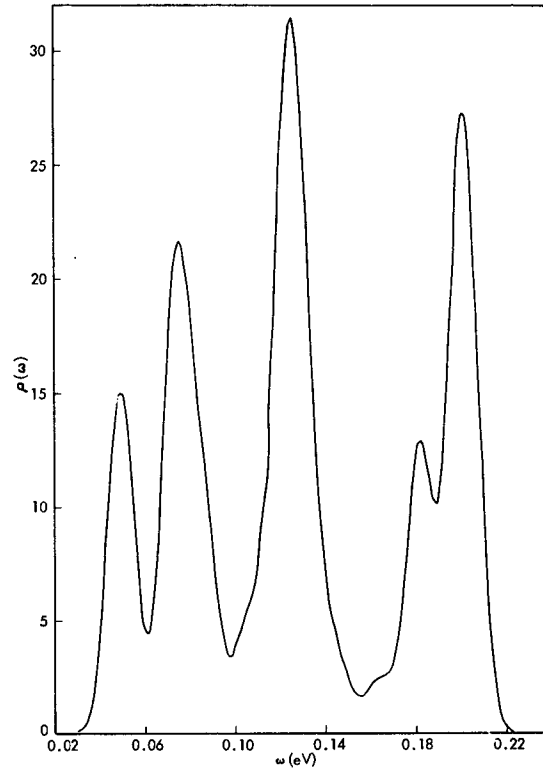

FIG. 4. Vibrational spectrum of the carbon atoms used to calculate benzene kernel. (The set of frequencies about 0.38 eV are not shown.)

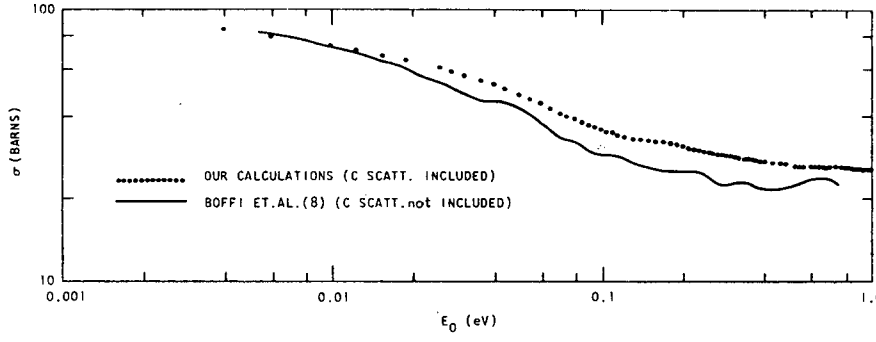

FIG. 5. Total cross-section.

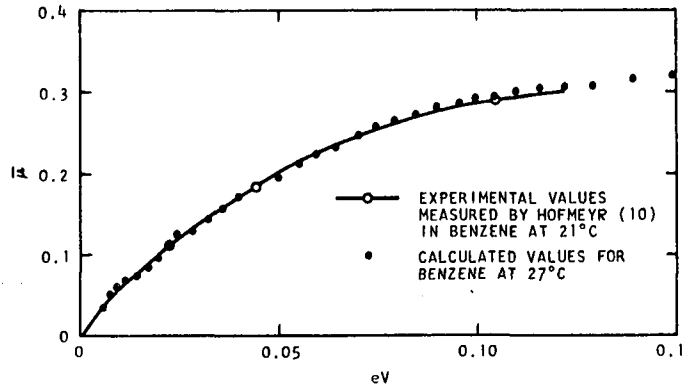

FIG. 6. Average of the cosine of the scattering angle.

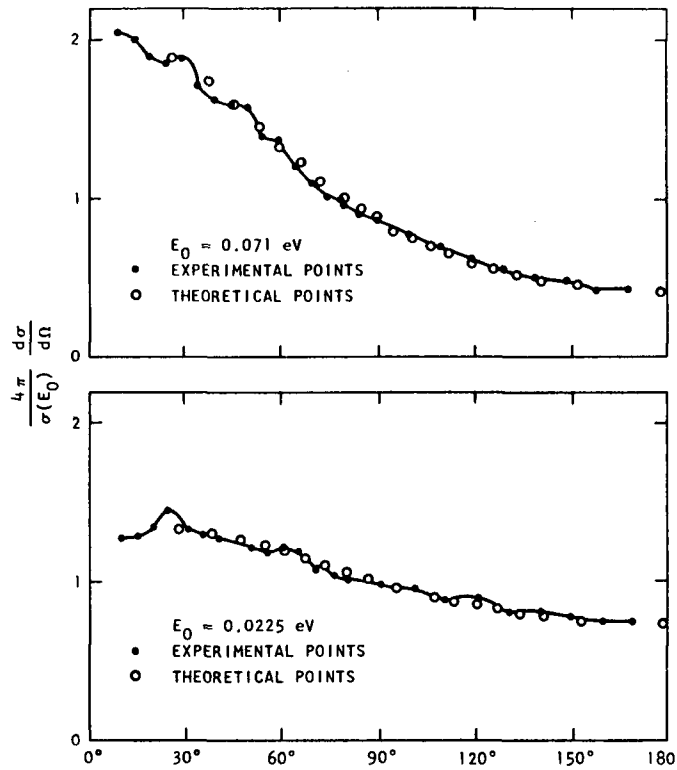

FIG. 7. The experimental values were measured by C. Hofmeyr [10] in benzene at 21°C. Our calculations were made considering a temperature of 27°C.

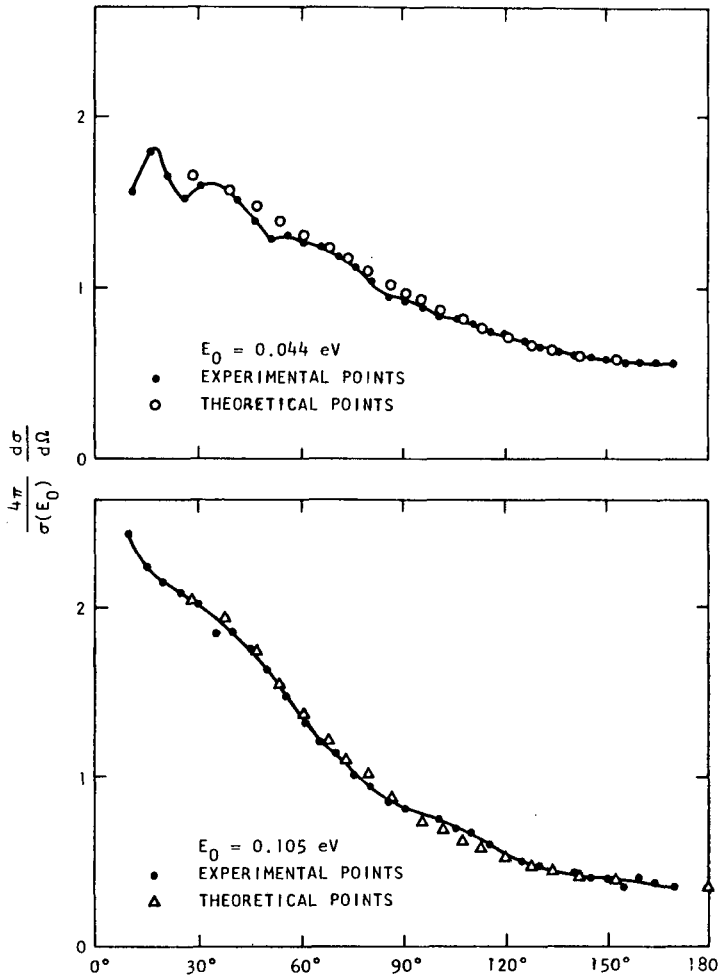

FIG. 8. Single-differential cross-section.

Boffi, et al. Their results, however, do not include the scattering due to the carbon atoms.

The calculated single-differential cross-section and the average cosine of the scattering angle are compared with experimental values obtained by C. Hofmeyr. [10] As it can be seen in Figs. 6, 7 and 8 the agreement with the experimental values is fairly good except for the peaks corresponding to the coherent scattering in the single-differential cross-section but coherent scattering was not considered in these calculations.

REFERENCES

[1] Parks, D. E., Nelkin, M. S., Wilkner, N. F., and Beyster, J. R., "Neutron Thermalization and its Application to Reactors Design," Chapter 2, General Atomic Report GA-4023 (1965).

[2] Zemach, A. C., and Glauber, C. T., Phys. Rev. 101 118 (1956).

[3] Miller, F. A., and Crawford, Jr., B. L., J. chem. Phys. 14 282 (1946).

[4] Crawford, Jr., D. L., and Miller, F. A., J. chem. Phys. 17 249 (1949).

[5] Kovner, M. A., Bogomolov, A. M., Opt i Spektr 4 301 (1958).

[6] Wilson, E. B. et al., Molecular Vibrations, McGraw-Hill (1955).

[7] Nielsen, J. R., and Berryman, L. H., J. chem. Phys. 17 659 (1949).

[8] Boffi, V. C., Molinari, V. G., Parks, D. E., "Slow Neutron Scattering and Thermalization by Benzene and Other Polyphenyls," General Atomic Report GA-3024, (April 1962).

[9] Koppel, J. U., Triplett, J. R., and Naliboff, Y. D., "GASKET, A Unified Code for Thermal Neutron Scattering," USAEC Report GA-7417, General Atomic Division, General Dynamics Corporation (1966).

[10] Hofmeyr, C., Nucleonik 7 265 (1965).

CALCULATED SCATTERING LAW AND THERMAL NEUTRON SPECTRUM FOR BENZENE *

R.S. MARSDEN AND H.L. McMURRY
IDAHO NUCLEAR CORPORATION,
IDAHO FALLS, IDAHO,
UNITED STATES OF AMERICA

Abstract

CALCULATED SCATTERING LAW AND THERMAL NEUTRON SPECTRUM FOR BENZENE. The Egelstaff scattering law, $S(\alpha, \beta)$, has been calculated for benzene using a complete set of normal modes and associated characteristic vibrational energies. Intermolecular interactions have been neglected. The data compare favorably with the measurements of Gläser, Ehret, and Merkel except that for $\beta < 2$, the calculated $S(\alpha, \beta)$ functions fall below the data at low α values. This is attributed to neglect of intermolecular interactions.

The total cross-sections calculated as a function of neutron energy are in good agreement with the data of Rush. Calculated values of $\bar{\mu}(E)$, the average cosine of the scattering angle, are generally a few percent higher than Hofmayr's data.

A spectrum calculated for benzene poisoned to 5.9 b per H atom agrees fairly well with measurements made at General Atomic, although the calculated distribution is high for energies below the peak of the $E\,\phi(E)$ function. The calculated parameters, λ_0, D, and C, appearing in the equation, $\lambda = \lambda_0 + DB^2 - CB^4$, are higher than the results of Pál, Kisdi-Koszó, Szatmáry, and Vizi; but λ_0 and C lie within the error limits given for the data.

1. INTRODUCTION

The potential use of Santowax and other phenyl compounds as reactor moderator materials has focused attention on the understanding of scattering properties of benzene, which is the basic structural unit of these materials. To this end we have calculated the normal modes of benzene, and we have used them and the measured vibrational energies to calculate the slow neutron scattering. Although the treatment neglects intermolecular interaction, this could be included in refining the model. Indeed, preliminary work indicates that improved agreement will be possible, by inserting suitable low frequencies with properly chosen vibrational amplitudes, to describe the effect of the intermolecular interactions.

2. FUNDAMENTAL FREQUENCIES AND NORMAL MODES

The fundamental frequencies and normal modes of benzene required for the determination of the scattering have been calculated using computer programs based on the methods of McMurry[1]. The benzene molecule is assumed to be planar and to have the symmetry of the D_{6h} group as designated by Wilson et al[2]. Calculations have been made for two sets of assigned frequencies. The first set uses the assignments of Crawford and Miller[3] for the planar vibrations and those selected by Herzberg for the nonplanar vibrations[4]; the second set uses the assignments selected by Shimanouchi[5]. For the nonplanar vibrations, the assignments of Herzberg agree quite well with those of Miller and Crawford[6]. The assigned and calculated frequencies are compared in Table I. In the calculation of $S(\alpha,\beta)$, the input data uses the assigned frequencies, but the amplitude factors correspond to the calculated frequencies.

* This work was performed under contract with the United States Atomic Energy Commission.

TABLE I

COMPARISON OF ASSIGNED AND CALCULATED FUNDAMENTAL FREQUENCIES FOR BENZENE

Planar Vibrations						
	Crawford and Miller	Calculated (this paper)	Shimanouchi Assignment	Calculated (this paper)	$\langle \Delta r^2 \rangle$[a] $(A^\circ)^2 \times 10^{-4}$ (this paper)	
Symmetry Species	Wave Number (cm^{-1})	Wave Number (cm^{-1})	Wave Number (cm^{-1})	Wave Number (cm^{-1})	$\langle \Delta r_H^2 \rangle$	$\langle \Delta r_C^2 \rangle$
A_{1g}	3062	3060	3062	3060	8.0	0.09
A_{1g}	992	996	992	996	3.2	2.1
A_{2g}	1326	1330	1326	1330	16.5	0.4
E_{2g}	3047	3047	3047	3047	16.8[b]	0.1[b]
E_{2g}	1596	1559	1596	1559	18.9[b]	1.4[b]
E_{2g}	1178	1166	1178	1166	21.4[b]	2.1[b]
E_{2g}	606	597	606	597	7.0[b]	7.0[b]
B_{1u}	3060	3058	3068	3058	8.0	0.1
B_{1u}	1010	1015	1010	1015	3.1	2.1
B_{2u}	1648	1644	1310	1306	1.3	1.3
B_{2u}	1110	1112	1150	1147	23.1	0.2
E_{1u}	3080	3075	3063	3075	16.6[b]	0.1[b]
E_{1u}	1485	1482	1486	1482	14.7[b]	1.9[b]
E_{1u}	1037	1031	1038	1031	32.5[b]	1.8[b]

Nonplanar Vibrations						
	Herzberg Assignment	Calculated (this paper)	Shimanouchi Assignment	Calculated (this paper)	$\langle \Delta r^2 \rangle$[a] $(A^\circ)^2 \times 10^{-4}$ (this paper)	
Symmetry Species	Wave Number (cm^{-1})	Wave Number (cm^{-1})	Wave Number (cm^{-1})	Wave Number (cm^{-1})	$\langle \Delta r_H^2 \rangle$	$\langle \Delta r_C^2 \rangle$
B_{2g}	1520	1508	995	993	5.7	1.1
B_{2g}	538	541	703	693	35.4	1.4
E_{1g}	849	851	849	851	51.6[b]	1.1[b]
A_{2u}	671	670	673	670	38.1	0.3
E_{2u}	1160	1160	975	971	20.8[b]	2.3[b]
E_{2u}	404	404	410	420	77.7[b]	5.0[b]

[a] Calculated from Equation (28), Reference 1.

[b] The $\langle \Delta r_\nu^2 \rangle$ for the degenerate modes is the sum of the values for the partners.

3. SCATTERING FUNCTION

The scattering function for a free gas of benzene molecules at 295°K has been calculated by means of a computer program based on the methods described by McMurry[7,8]. The program computes the reduced partial-differential scattering cross-section (RPDC), $S(\kappa^2,\beta)$, which is defined in terms of the partial-differential scattering cross-section, $\sigma(E_o,E,\vec{\Omega})$, by the following relation:

$$S(\kappa^2,\beta) = (k_o/k)\ e^{\beta/2}\ \sigma(E_o,E,\vec{\Omega}) \tag{1}$$

In Equation (1), E_o and E are the incident and scattered neutron energies, respectively, and $\beta = (E - E_o)/k_B T$, where k_B is the Boltzmann constant in eV/deg and T is the absolute temperature. The k_o and k are the magnitudes of the incident and scattered neutron wave vectors and $\vec{\kappa} = \vec{k} - \vec{k}_o$. For direct comparison with the measurement of Gläser[9], the results of the calculations are presented in Figure 1 in the form of the Egelstaff scattering law (ESL), $S(\alpha,\beta)$, which is related to $S(\kappa^2,\beta)$ by the equation

$$S(\kappa^2,\beta) = \frac{\sigma_b}{4\pi k_B T}\ S(\alpha,\beta) \text{ with } \alpha = \frac{\kappa^2\hbar^2}{2M\beta T} \tag{2}$$

where

σ_b = 6.49 barns (the bound atom cross-section for hydrogen)

T = 295°K

As is usual for hydrogenous moderators, the value M = 1 atomic unit is used in defining α.

McMurry's procedures for calculation of the scattering function require the assumption of a structure for the scattering system which is amenable to calculation. Then the motions of the atoms can be calculated and an approximation to the formalism of Zemach and Glauber[10] used to calculate the scattering functions in Equations (1) and (2). In the present case the structure is the free benzene molecule, and an atom's motion is the resultant of the internal vibrations and the free translations and rotations of the molecule; the effects of interactions between molecules upon the atomic motion are not considered. In addition to the fundamental frequencies and the amplitude factors derived from the normal modes of vibration, the calculation also requires the bound atom cross-sections and the masses of the atoms. The following values have been used:

<u>Hydrogen</u>

σ_b = 6.49 barns

M_H = 1.008 atomic units

<u>Carbon</u>

σ_b = 0.41 barns

M_c = 12.011 atomic units

Figure 1 displays the comparison between the data of Gläser, Ehret, and Merkel and our calculations[9]. The calculated values are considered to be in satisfactory agreement with measurements when β = 2.0 or higher, and also for the higher α values at lower β's. However, as expected, for the low β's the values at $S(\alpha,\beta)$

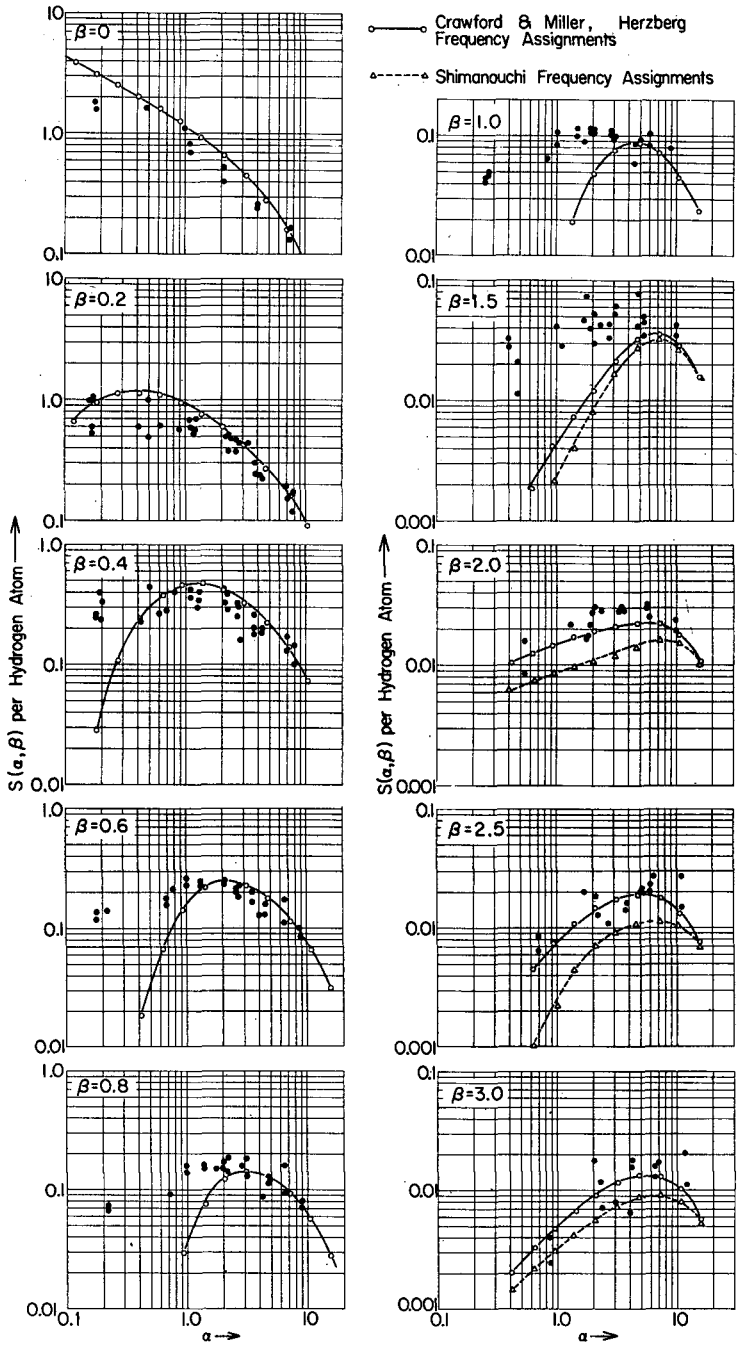

Fig. 1 Comparisons of calculated $S(\alpha,\beta)$ per hydrogen atom in benzene with Gläser's data.

calculated for low α's are much lower than the data. These departures are attributed to the neglect of intermolecular interactions. As in the case of water [11], the assumption of lower frequencies arising from intermolecular interactions will probably be necessary to improve the agreement between the calculations and measurements. Indeed, preliminary work in this direction supports this view. In Figure 1 it can be seen that for $\beta = 1.5$ or greater the choice of the Crawford and Miller-Herzberg frequency assignments gives considerably better agreement with the measurements than if the Shimanouchi assignments are used. Therefore, all subsequent calculations use the Crawford and Miller-Herzberg assignments.

4. LEGENDRE MOMENTS AND DERIVED QUANTITIES

The Legendre moments, defined as $\sigma_\ell(E_o) = \int_0^\infty \int_{-1}^{1} \sigma(E_o,E,\mu)\ P_\ell(\mu)\ d\mu dE$, have been calculated for ℓ equal to zero and one and are listed in Table II for a set of E_o in the range $0.00062 \leq E_o \leq 1.0$ eV. The zeroth moments, $\sigma_o(E_o)$, are the total scattering cross-sections. All values for $\sigma_o(E_o)$ and $\sigma_1(E_o)$ include the contributions to the scattering cross-section from both hydrogen and carbon even when values are given per hydrogen atom; however, no contributions from absorption are included.

In Figure 2 the calculated values of the total cross-section are compared with the measured values of Rush [12, 13]. The measured data are consistent with the calculations in including the scattering cross-section from carbon, in not including absorption, and in being for essentially the same temperature. A number of other measurements of the total cross-section of benzene have been made, but usually are either reported with the carbon scattering removed, or are ambiguous as to whether or not it has been removed. Antonini and Paoletti [14], who have removed the carbon contribution in their reported values, state that Rush's results are in very good agreement with theirs. Thus, the data of Rush provide a valid basis for comparison of calculations and measurements.

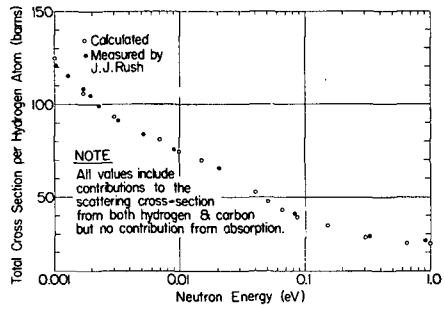

Fig. 2 Comparison of calculated total cross-section per hydrogen atom in benzene with Rush's data.

The agreement is good. In fact, the free-gas model of benzene gives much better agreement with observed values of the total cross-section than the free-gas model of water as reported by McMurry et al.[11]. Undoubtedly, this is due largely to the fact that the effective mass for scattering by H atoms in benzene (21.1) is considerably larger than for free H_2O molecules (1.88). Thus, the recoil effects are less important in benzene. This is supported by the fact that the Nelkin model for water in which $M_H = 18$ gives quite good total cross-sections.

The integration errors for $\sigma_o(E)$ and $\sigma_1(E)$ have been investigated by determining the effects of finer angular and energy meshes for $E_o = 0.007$, 0.085, and 1.0 eV. Essentially identical results were obtained with the finer meshes, indicating the meshes used for all E_o were sufficiently fine.

TABLE II

CALCULATED CROSS-SECTION, AVERAGE COSINE OF THE SCATTERING ANGLE, AND DIFFUSION COEFFICIENT AS A FUNCTION OF ENERGY FOR A FREE GAS OF BENZENE MOLECULES AT 295°K

Incident Neutron Energy E_o (eV)	Total Cross-Section		$\sigma_1(E_o)$		$\bar{\mu}(E_o)$	$D(E_o)$ (cm)	$(\overline{\Delta E})_o$	$(\overline{\Delta E})_1$	$(\overline{\overline{\Delta E}})_o$	$(\overline{\overline{\Delta E}})_1$
	Barns per Molecule	Barns per H Atom	Barns per Molecule	Barns per H Atom						
0.00062	884	147.3	8.0	1.3	0.009	0.055	7.51×10^{-3}	-7.54×10^{-2}	2.98×10^{-4}	-1.66×10^{-3}
0.001	749	124.8	8.3	1.4	0.011	0.065	7.60×10^{-3}	-7.25×10^{-2}	3.27×10^{-4}	-1.64×10^{-3}
0.0017	635	105.8	13.9	2.3	0.022	0.078	6.85×10^{-3}	-4.02×10^{-2}	2.61×10^{-4}	-0.94×10^{-3}
0.00225	596	99.4	15.4	2.6	0.026	0.084	6.57×10^{-3}	-3.59×10^{-2}	2.40×10^{-4}	-0.85×10^{-3}
0.003	559	93.2	19.1	3.2	0.034	0.090	6.29×10^{-3}	-2.79×10^{-2}	2.28×10^{-4}	-0.68×10^{-3}
0.0051	507	84.5	28.0	4.7	0.055	0.102	5.72×10^{-3}	-1.61×10^{-2}	2.19×10^{-4}	-0.44×10^{-3}
0.007	482	80.3	31.6	5.3	0.065	0.108	5.57×10^{-3}	-1.32×10^{-2}	2.42×10^{-4}	-0.38×10^{-3}
0.01	451	75.2	37.9	6.3	0.084	0.118	4.93×10^{-3}	-0.90×10^{-2}	2.22×10^{-4}	-0.31×10^{-3}
0.015	420	70.0	43.5	7.3	0.104	0.130	4.29×10^{-3}	-0.54×10^{-2}	2.28×10^{-4}	-0.24×10^{-3}
0.04	317	52.8	62.9	10.5	0.198	0.192	1.48×10^{-3}	0.12×10^{-2}	2.62×10^{-4}	-0.091×10^{-3}
0.05	287	47.8	64.4	10.7	0.224	0.220	0.071×10^{-3}	0.20×10^{-2}	2.84×10^{-4}	-0.079×10^{-3}
0.065	260	43.3	67.7	11.3	0.260	0.255	-2.30×10^{-3}	0.27×10^{-2}	3.99×10^{-4}	-0.051×10^{-3}
0.085	237	39.5	70.7	11.8	0.298	0.295	-6.52×10^{-3}	0.27×10^{-2}	6.39×10^{-4}	-0.022×10^{-3}
0.15	196	32.7	70.2	11.7	0.358	0.388	-26.8×10^{-3}	-0.27×10^{-2}	27.0×10^{-4}	0.27×10^{-3}
0.3	169	28.2	70.6	11.8	0.417	0.498	-80.6×10^{-3}	-3.27×10^{-2}	144×10^{-4}	3.98×10^{-3}
0.65	153	25.5	72.5	12.1	0.473	0.609	-225×10^{-3}	-14.1×10^{-2}	901×10^{-4}	44.4×10^{-3}
1.0	150	25.0	75.4	12.6	0.502	0.657	-382×10^{-3}	-27.3×10^{-2}	2390×10^{-4}	142×10^{-3}

The average cosine of the scattering angle, $\bar{\mu}(E_o)$, and the diffusion coefficient, $D(E_o)$, have been calculated from the relations

$$\bar{\mu}(E_o) = \frac{\sigma_1(E_o)}{\sigma_o(E_o)} \tag{3}$$

and

$$D(E_o) = \frac{1}{3\,[\Sigma_a(E_o) + \Sigma_o(E_o) - \Sigma_1(E_o)]} \quad . \tag{4}$$

The values are listed in Table II and compared with values calculated by Hofmeyr [15] from his differential cross-section measurements in Figures 3 and 4. While

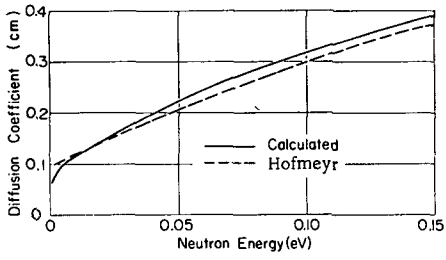

Fig. 3 Comparison of calculated diffusion coefficient of benzene with Hofmeyr's results.

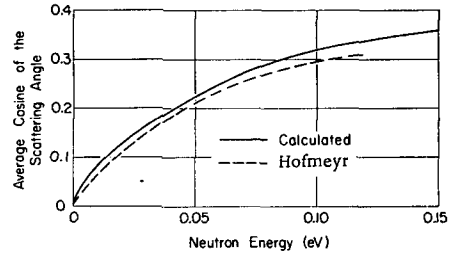

Fig. 4 Comparison of calculated average cosine of the scattering angle with Hofmeyr's results.

the agreements are reasonably good, our calculated values for $\bar{\mu}(E_o)$ and $D(E_o)$ lie above those deduced from the scattering. This was also true for water [11]. At the lowest energies, part of the difference for the $D(E_o)$ results arises because our definition of $D(E_o)$ includes absorption. Whereas Hofmeyr defines $D(E_o)$ without including $\Sigma_a(E_o)$; viz,

$$D(E_o) = \frac{1}{3\,\Sigma_s(E_o)\,[1 - \bar{\mu}(E_o)]} \quad \text{(Hofmeyr).} \tag{5}$$

However, most of the differences may result, as for water, because the integration to give $\bar{\mu}$ involves important contributions from regions where α and β are both small. It is in these regions that the model fails.

Also included in Table II are values computed for the energy-transfer moments, $(\overline{\Delta E})_\ell$ and $(\overline{\overline{\Delta E}})_\ell$ for $\ell = 1, 2$, defined by

$$(\overline{\Delta E})_\ell = \int_0^\infty \frac{(E - E_o)\,\sigma_\ell(E_o,E)dE}{\sigma_o(E_o)} \; ; \; (\overline{\overline{\Delta E}})_\ell = \int_0^\infty \frac{(E - E_o)^2\,\sigma_\ell(E_o,E)dE}{\sigma_o(E_o)} \quad . \tag{6}$$

Experimental comparisons with these results are not available.

Plots of $\bar{\sigma}_0(E_0,E)$ versus E are shown in Figures 5, 6, and 7 for $E_0 = 0.007$, 0.085, and 0.3 Ev, respectively. These plots show how this function peaks near the incident neutron energy, E_0.

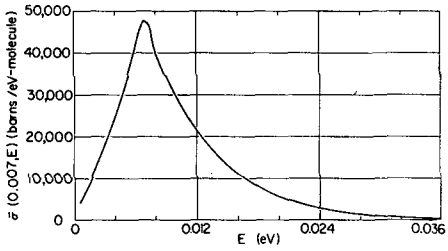

Fig. 5 Calculated $\bar{\sigma}(E_0,E)$ versus E of benzene for $E_0 = 0.007$ eV.

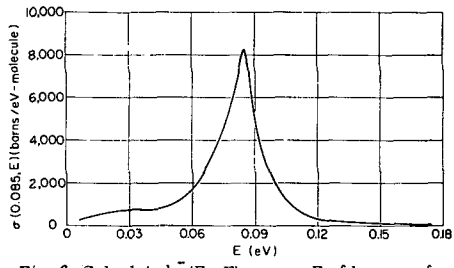

Fig. 6 Calculated $\bar{\sigma}(E_0,E)$ versus E of benzene for $E_0 = 0.085$ eV.

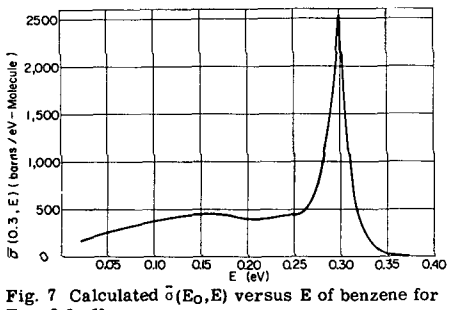

Fig. 7 Calculated $\bar{\sigma}(E_0,E)$ versus E of benzene for $E_0 = 0.3$ eV.

Figure 8 displays an infinite medium spectrum for C_6H_6 poisoned with boron to 5.9 b/H[16]. The comparison is with data from General Atomic[17]. The agreement is fairly good, but improvement is needed for energies below the peak of the $E\phi(E)$ function.

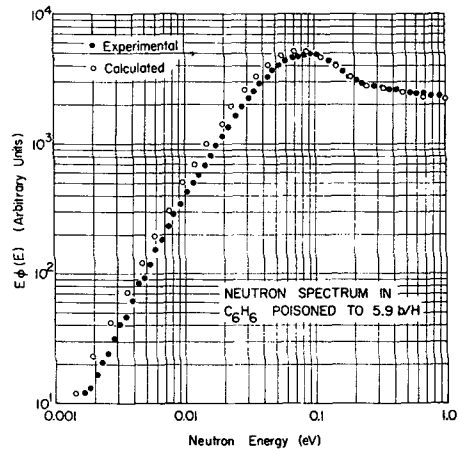

Fig. 8 Thermal neutron spectrum in benzene poisoned to 5.9 b/H.

Pál, Kisdi-Koszó, Bod, Szatmáry, and Vizi[18] have used pulsed neutron techniques to measure the thermal neutron parameters appearing in the equation.

$$\lambda = \lambda_o + DB^2 - CB^4 \quad . \tag{7}$$

Table III compares their results with those computed from a 33-group kernel calculated from our $S(\alpha,\beta)$ for benzene[19]. The calculated λ_0, D, and C are consistently higher than the measured data, but λ_0 and C fall within the error limits given.

TABLE III

THERMAL DIFFUSION PARAMETERS

	$\lambda_o(sec^{-1})$	$D(cm^2/sec)$	$C(cm^4/sec)$
Calculated	2,973	52,500	17,200
Experiment	2,886 ± 111	48,649 ± 1,373	13,869 ± 3,849

REFERENCES

[1] McMURRY, H.L., Spectrochim. Acta 21 (1965) 2091.
[2] WILSON, E.B., Jr., DECIUS, J.C., CROSS, P.C., Molecular Vibrations, McGraw-Hill, N.Y. (1955) Appendix X.
[3] CRAWFORD, B.L., Jr., MILLER, F.A., J. chem. Physics 17 (1949) 249.
[4] HERZBERG, G., Infrared and Raman Spectra, Van Nostrand, New York (1945) 362-69.
[5] SHIMANOUCHI, T., Tables of Molecular Vibration Frequencies, Part I - National Bureau of Standards Rep., NSRDS-NBS6, U.S. Dept. of Commerce, Wash., D.C. (1967).
[6] MILLER, F.A., CRAWFORD, B.L., Jr., J. chem Phys. 14 (1946) 282.
[7] McMURRY, H.L., Nucl. Sci. Engng 15 (1963) 429.
[8] McMURRY, H.L., GANNON, L.J., A Machine Program for Calculating Slow Neutron Scattering Cross Sections with Application to Water, USAEC Rep. IDO-16984 (1964).
[9] GLÄSER, W., EHRET, G., MERKEL, A., Inelastic Scattering of Neutrons II, IAEA, Vienna (1965) 167; GLÄSER, W., recent experimental data.
[10] ZEMACH, A.C., GLAUBER, R.J., Phys. Rev. 101 (1956) 118.
[11] McMURRY, H.L., RUSSELL, G.J., BRUGGER, R.M., Nucl. Sci. Engng 25 (1966) 248.
[12] RUSH, J.J., TAYLOR, T.I., HAVENS, W.W., Jr., J. chem. Phys. 37 (1962) 234.
[13] RUSH, J.J., Investigation of Rotational and Vibrational Freedom in Molecules by Cross-Section Measurements with Slow Neutrons, Thesis, Columbia University (1962).
[14] ANTONINI, B., PAOLETTI, A., Physica 30 (1964) 1647.
[15] HOFMEYR, C., Untersuchungen über die Streuung langsamer Neutronen an den Protonen in Phenylen und in Wasserdampf, Thesis, Technische Hochschule, München (1964).
[16] The authors are indebted to Mr. R.L. CURTIS for making this calculation.
[17] YOUNG, J.C., TRIMBLE, G.D., NALIBOFF, Y.D., HOUSTON, D.H., BEYSTER, J.R., Nucl. Sci. Engng 18 (1964) 376.
[18] PÁL, L., KISDI-KOSZÓ, É., BOD, L., SZATMÁRY, Z., VIZI, I., Proc. 3rd UN Int. Conf. PUAE 2 (1965) 310.
[19] The authors are indebted to Dr. G.W. GRIFFING for making these calculations.

MOLECULAR MODEL FOR POLYPHENYLS AND ITS USE IN CALCULATING REACTOR PARAMETERS

V. ARDENTE, R. CUNIBERTI, A. KIND AND G. ROSSI
CENTRE COMMUN DE RECHERCHE,
EURATOM,
ISPRA, ITALY

Abstract

MOLECULAR MODEL FOR POLYPHENYLS AND ITS USE IN CALCULATING REACTOR PARAMETERS. A molecular model previously proposed by one of us (V.A.) to describe the slow neutron scattering by polyphenyls has been applied to the evaluation of spectral indices and thermal reactivity parameters in organic-cooled heavy-water lattices. To predict the interaction between slow neutrons and bound nuclei in polyphenyls the single benzene molecule was regarded as the basic dynamic unit. The idea in this molecular model was to replace the very complicated and anisotropic vibrational spectrum of the average proton bound in the benzene molecule by a highly simplified isotropic one: two vibrational oscillators at 0.12 eV and 0.38 eV. Free molecular translations and hindered rotations are also included. The hindered rotations are formally replaced by a torsional isotropic oscillation with a single frequency at 0.02 eV and with a rotational mass $M_r = 21.3$.

The model was able to predict successfully experimental results on integral scattering quantities for benzene and diphenyl at room temperature, showing in this way that such quantities are not excessively dependent on the structure of the molecule or on the vibrational details of various polyphenyls. Hence we assume that this model can be applied for a quantitative understanding of thermal reactor parameters. To investigate the sensitivity of the mentioned reactor quantities to the description of the neutron interaction the calculations have also been performed with the free-gas model. We have employed two completely independent numerical methods for solving the Boltzmann transport equation (THERMOS, WDSN). The aim was to compare the sensitivity to the scattering law with the differences in the results connected with the adopted numerical method, by using the same nuclear data library. The calculations concern such quantities as spectral indices (^{239}Pu-^{235}U and ^{176}Lu-Mn reaction rate ratios), coolant temperature coefficients, thermal fission and thermal utilization factors and are referred to a typical ORGEL lattice, with clustered uranium carbide fuel element.

INTRODUCTION

Temperature coefficients related to the fuel channel must be carefully taken into account in the design of pressure-tube D_2O-moderated reactors, since they may play a determinant role in the dynamics of the whole system. A careful choice of the scattering model is necessary, too to determine the effects of the thermal part of the neutron spectrum. For the research on organic-cooled lattices at Ispra, a model for describing scattering by polyphenyls was developed. Furthermore, it was felt that a detailed analysis of the importance of the scattering model for the evaluation of the thermal lattice parameters was necessary. To do this, refined numerical programmes had to be used. However, as is well known, for detailed and, possibly, small effects, the results from any computer programme must be regarded with caution. Thus, to demonstrate clearly the magnitude of the effects caused by the scattering model, as compared with the numerical discrepancies resulting from the use of different transport codes, a series of calculations with a typical

heavy-water-moderated organic-cooled lattice were performed, by two completely independent numerical methods (the codes THERMOS [1] and WDSN [2]) using exactly the same set of cross-sections. The scattering models analysed here are the Nelkin-Honeck model for D_2O and the Nelkin-Ardente model for organic liquids; the results are compared with those obtained from a simple free-gas model. On the basis of a preliminary numerical analysis, the so-called Brown and St. John model was excluded from the study reported in this paper, because it gave unreliable results due to the presence of a discontinuity in the scatterer mass used to describe epithermal and thermal effects.

SCATTERING MODEL

The data for the reactor cell are given in Table I. HB-40 was chosen as organic coolant.

The dynamics of the proton bound in the organic molecule have been described in the related scattering model [3], following the general lines adopted by Nelkin [4] for the H_2O molecule and extended by Honeck [5] to the D_2O molecule. To predict the interaction between slow neutrons and bound nuclei in polyphenyls the single benzene molecule was regarded as the basic dynamic unit. Hence, it was assumed that results on benzene

TABLE I. URANIUM CARBIDE 7-RODS CLUSTER DATA

Fuel	Natural Uranium Carbide ρ = 13.54 g/cm^3 Fuel pins diameter ϕ = 25.2 mm Distance between fuel pins d = 29.5 mm
Canning	Aluminium ρ = 2.70 g/cm^3 Internal diameter ϕ_i = 25.50 mm, thickness = 1 mm
Pressure tube	Aluminium ρ = 2.70 g/cm^3 Internal diameter ϕ_i = 91 mm, thickness = 2 mm
Insulating layer	Air
Calandria tube	Aluminium ρ = 2.70 g/cm^3 Internal diameter ϕ_i = 101 mm, thickness = 1.5 mm
Coolant	HB 40 (26.5% Diphenyl, 73,5% Diphenyl Oxide) $\rho = 1.-6.5\times10^{-4}\ (T(^oC) - 25)$ g/cm^3
Moderator	D_2O purity 100%
Square lattice pitch 28 cm	

provide sufficient basis for a quantitative understanding of scattering by polyphenyls, at least about integral quantities of interest in thermal neutron problems.

In the 'molecular' model adopted the very complicated and anisotropic vibrational spectrum of the proton in the benzene is replaced by a highly simplified isotropic one: the simple assumption is that there are two vibrational oscillators at 0.12 and 0.38 eV, corresponding to a grouping of frequencies in the benzene spectrum. The hindered rotations are formally replaced by a torsional isotropic oscillation with a single frequency ω_r tentatively made equal to 0.02 eV. This value is substantially confirmed by the low-energy peak in the generalized frequency distribution $p(\beta)$ derived by extrapolation technique from scattering law measurements [6]. With this very simplified spectrum the benzene molecule is considered from the same point of view as that adopted by Nelkin [4] for light water, for which numerical codes are available [7].

Thus, the scattering model is a single molecule, free to move like a gas atom of the same mass, able to oscillate about a rotational axis with a freely rotating mass M_r = 21.3 amu, and also able to vibrate internally, according to two vibration modes. The reliability of the model is shown by the comparison with experimental data of Antonini and Paoletti [8] on the total scattering cross-section, and with the average angle cosine $\mu(E) = \langle \cos\theta(E) \rangle_{av.}$ data presented by Springer et al. [9] at the third Geneva Conference.

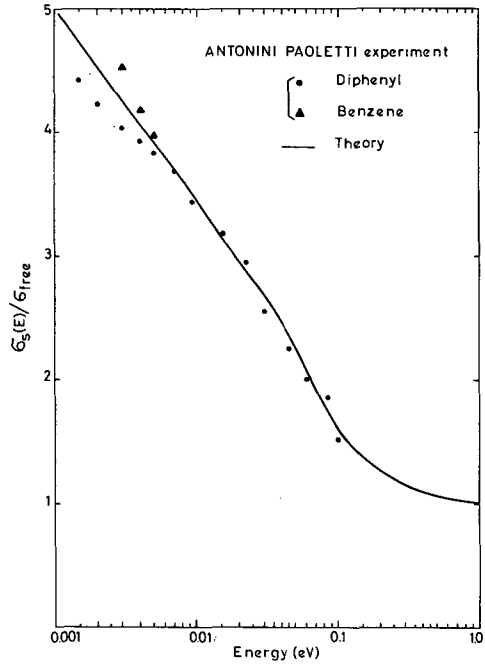

FIG. 1. Total scattering cross-section for one proton of polyphenyls as a function of incident neutron energy at T = 300°K. σ_{free} = 20.36 b is the free-proton scattering cross-section.

Figure 1 shows the total scattering cross-section for one proton of benzene as a function of the incident neutron energy. Experimental points are for benzene and diphenyl at the same room temperature; benzene points for energies higher than 0.005 eV were not plotted, since the measured transmission values were experimentally indistinguishable from those of diphenyl. The theoretical curve, calculated for benzene and adopted as valid for an 'average' polyphenyl molecule, fits so well with the experimental values that the hypothesis of the model is confirmed, at least in a strictly thermal region.

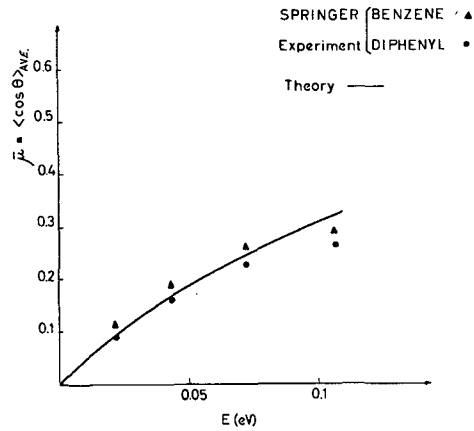

FIG.2. Average scattering cosine $\langle\cos\theta\,(E)\rangle$ for one proton of polyphenyls as a function of incident neutron energy at T = 300°K. Theory neglects carbon effects.

Figure 2 refers to another integral quantity of interest in thermal neutron problems, the average cosine $\mu(E)$. Carbon effects are not included in the theoretical curve. Figure 2 shows substantial equivalence between benzene and diphenyl and considerable agreement between theory and experiments.

Finally, the theoretical value $M_2 = 0.607\ cm^{-1}$ for the second moment of the energy transfer can be compared with the value $M_2 = 0.62 \pm 0.05\ cm^{-1}$ obtained experimentally by pulsed neutron technique [10].

CONCLUSIONS

These results show that it is possible to use a fairly simple model to calculate the scattering behaviour of polyphenyls and they give information about the sensitivity of the slow neutron scattering to the details of the dynamics and of the structural features of the molecule. The scattering matrices for hydrogen at various temperatures, calculated on the basis of this model, have been introduced in the GATHER II [11] library, which is the source of all nuclear data for both calculational methods.

The results concerning ^{239}Pu-^{235}U fission rate ratio, ^{176}Lu-^{55}Mn absorption rate ratio (average values in the cluster and in the moderator)

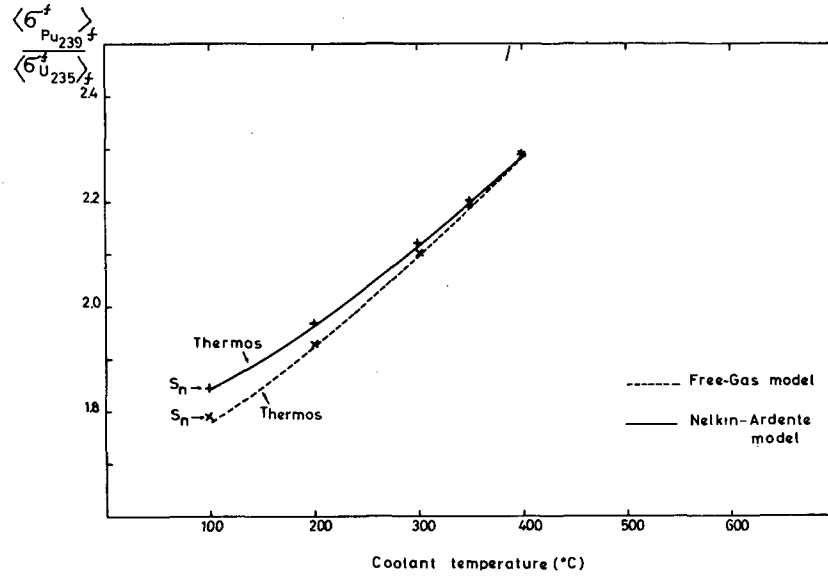

FIG. 3. ^{239}Pu-^{235}U fission rate ratio (cluster average) as a function of coolant temperature.

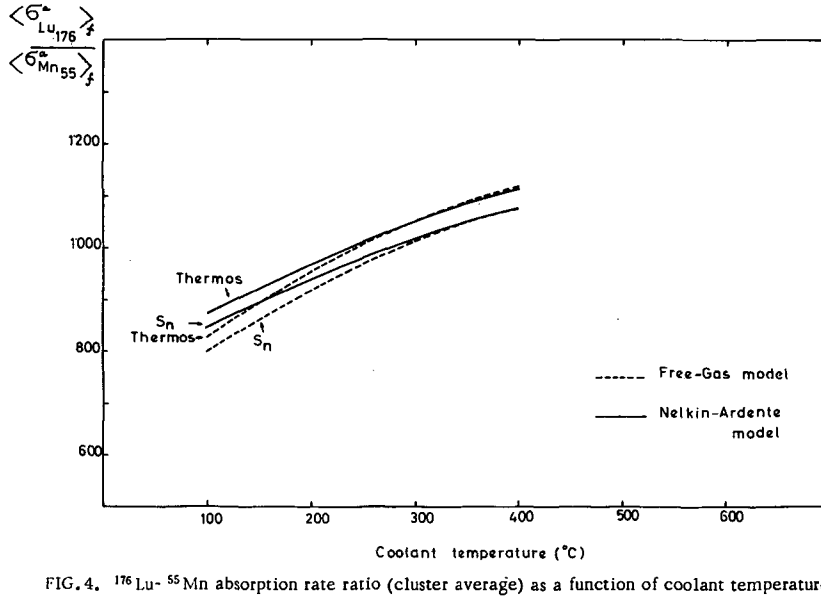

FIG. 4. ^{176}Lu-^{55}Mn absorption rate ratio (cluster average) as a function of coolant temperature.

and ηf are presented in Figs 3-5 and in Tables II-XV. (In the tables all temperatures for fuel, coolant and moderator are given in °C; NA = Nelkin-Ardente model; FG = free-gas model.) These results refer to the following lattice conditions:

(a) Room temperature

(b) Operating temperature for fuel and moderator, coolant temperature varying from 100 to 400°C.

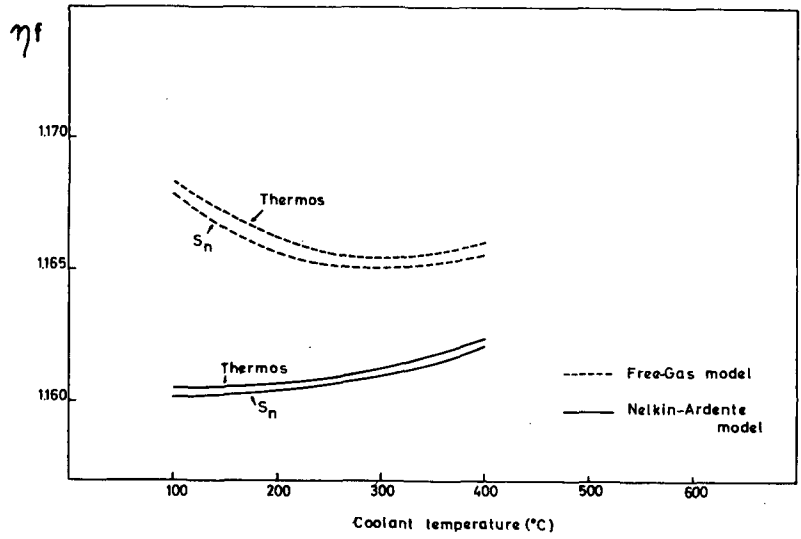

FIG. 5. ηf as function of the coolant temperature.

TABLE II. ηf FOR VARIOUS LATTICE CONDITIONS

	T_f=25, T_m=25, T_c=25			T_f=700, T_m=60, T_c=100			T_f=700, T_m=60, T_c=200		
	FG	NA	Δ %	FG	NA	Δ %	FG	NA	Δ %
THERMOS	1.1719	1.1620	0.85	1.1684	1.1605	0.68	1.1663	1.1607	0.48
WDSN	1.1712	1.1614	0.84	1.1679	1.1602	0.66	1.1657	1.1605	0.45
Δ %	0.06	0.06		0.04	0.025		0.05	0.02	

TABLE III. ηf FOR VARIOUS LATTICE CONDITIONS

	T_f=700, T_m=60, T_c=300			T_f=700, T_m=60, T_c=350			T_f=700, T_m=60, T_c=400		
	FG	NA	Δ %	FG	NA	Δ %	FG	NA	Δ %
THERMOS	1.1655	1.1613	0.36	1.1658	1.1618	0.36	1.1662	1.1624	0.33
WDSN	1.1651	1.1608	0.37	1.1653	1.1616	0.32	1.1660	1.1621	0.33
Δ %	0.03	0.04		0.04	0.02		0.02	0.025	

TABLE IV. ^{239}Pu-^{235}U FISSION RATE RATIO
(AVERAGE VALUES IN THE CLUSTER)

	T_f=25, T_m=25, T_c=25			T_f=700, T_m=60, T_c=100			T_f=700, T_m=60, T_c=200		
	FG	NA	Δ %	FG	NA	Δ %	FG	NA	Δ %
THERMOS	1.1663	1.6981	3.64	1.7792	1.8403	3.3	1.9256	1.9641	1.96
WDSN	1.6381	1.6998	3.63	1.7819	1.8424	3.3	1.9290	1.9680	1.98
Δ %	0.11	0.10		0.15	0.11		0.18	0.20	

TABLE V. ^{239}Pu-^{235}U FISSION RATE RATIO
(AVERAGE VALUES IN THE CLUSTER)

	T_f=700, T_m=60, T_c=300			T_f=700, T_m=60, T_c=350			T_f=700, T_m=60, T_c=400		
	FG	NA	Δ %	FG	NA	Δ%	FG	NA	Δ %
THERMOS	2.0987	2.1176	0.89	2.1907	2.2008	0.46	2.2832	2.2852	0.0875
WDSN	2.1042	2.1222	0.85	2.1973	2.2063	0.41	2.2932	2.2922	0.044
Δ %	0.26	0.22		0.30	0.25		0.44	0.305	

TABLE VI. Lu-Mn ABSORPTION RATE RATIO
(AVERAGE VALUES IN THE CLUSTER)

	T_f=25, T_m=25, T_c=25			T_f=700, T_m=60, T_c=100			T_f=700, T_m=60, T_c=200		
	FG	NA	Δ %	FG	NA	Δ %	FG	NA	Δ %
THERMOS	658.37	720.34	8.99	827.075	875.075	5.44	975.475	969.96	1.60
WDSN	642.41	700.18	8.61	801.00	847.46	5.48	920.40	939.67	2.07
Δ %	2.45	2.84		3.20	3.16		3.57	3.12	

TABLE VII. Lu-Mn ABSORPTION RATE RATIO
(AVERAGE VALUES IN THE CLUSTER)

	T_f=25, T_m=25, T_c=300			T_f=700, T_m=60, T_c=350			T_f=700, T_m=60, T_c=400		
	FG	NA	Δ %	FG	NA	Δ%	FG	NA	Δ %
THERMOS	1051.57	1051.28	0.027	1088.66	1084.755	0.36	1118.69	1113.23	0.49
WDSN	1013.73	1019.00	0.52	1049.78	1051.57	0.17	1079.60	1079.61	0.001
Δ %	3.60	3.07		3.57	3.06		3.50	3.02	

TABLE VIII. ^{235}U MICROSCOPIC FISSION CROSS-SECTION (AVERAGE VALUES IN THE CLUSTER)

	T_f=25, T_m=25, T_c=25			T_f=700, T_m=60, T_c=100			T_f=700, T_m=60, T_c=200		
	FG	NA	Δ %	FG	NA	Δ %	FG	NA	Δ %
THERMOS	439.17	412.42	6.085	392.19	375.56	4.24	362.22	355.16	1.94
WDSN	436.31	412.31	5.50	390.65	375.42	3.90	361.53	354.77	1.87
Δ %	0.645	0.026		0.39	0.037		0.19	0.11	

TABLE IX. ^{235}U MICROSCOPIC FISSION CROSS-SECTION (AVERAGE VALUES IN THE CLUSTER)

	T_f=25, T_m=25, T_c=300			T_f=700, T_m=60, T_c=350			T_f=700, T_m=60, T_c=400		
	FG	NA	Δ %	FG	NA	Δ %	FG	NA	Δ %
THERMOS	339.87	337.31	0.75	330.79	329.47	0.40	322.85	322.36	0.15
WDSN	339.51	336.87	0.78	330.05	329.02	0.31	321.63	321.84	0.065
Δ %	0.11	0.13		0.22	0.14		0.37	0.16	

TABLE X. ^{239}Pu MICROSCOPIC FISSION CROSS-SECTION

	T_f=25, T_m=25, T_c=25			T_f=700, T_m=60, T_c=100			T_f=700, T_m=60, T_c=200		
	FG	NA	Δ %	FG	NA	Δ %	FG	NA	Δ %
THERMOS	717.87	700.35	2.44	697.89	691.13	0.97	695.67	695.67	0.15
WDSN	714.71	700.83	1.94	696.12	691.66	0.64	697.40	698.20	0.115
Δ %	0.44	0.069		0.25	0.08		0.18	0.087	

TABLE XI. ^{239}Pu MICROSCOPIC FISSION CROSS-SECTION

	T_f=25, T_m=25, T_c=300			T_f=700, T_m=60, T_c=350			T_f=700, T_m=60, T_c=400		
	FG	NA	Δ %	FG	NA	Δ %	FG	NA	Δ %
THERMOS	715.45	714.29	0.16	727.21	725.09	0.29	740.0	736.67	0.45
WDSN	714.40	714.91	0.072	726.18	725.93	0.035	737.55	737.71	0.02
Δ %	0.15	0.087		0.14	0.116		0.33	0.14	

TABLE XII. Lu-Mn ABSORPTION RATE RATIO
(AVERAGE VALUES IN THE MODERATOR)

	T_f=25, T_m=25, T_c=25			T_f=700, T_m=60, T_c=100			T_f=700, T_m=60, T_c=200		
	FG	NA	Δ %	FG	NA	Δ %	FG	NA	Δ%
THERMOS	586.72	591.48	0.80	659.19	661.18	0.30	663.60	665.19	0.24
WDSN	573.24	578.22	0.86	642.72	644.72	0.39	646.03	648.57	0.39
Δ %	2.30	2.24		2.58	2.49		2.68	2.50	

TABLE XIII. Lu-Mn ABSORPTION RATE RATIO
(AVERAGE VALUES IN THE MODERATOR)

	T_f=700, T_m=60, T_c=300			T_f=300, T_m=60, T_c=350			T_f=700, T_m=60, T_c=400		
	FG	NA	Δ %	FG	NA	Δ%	FG	NA	Δ%
THERMOS	667.25	669.01	0.26	668.785	670.70	0.29	670.16	672.33	0.32
WDSN	649.45	651.57	0.326	650.88	653.18	0.35	652.60	654.70	0.32
Δ %	2.67	2.61		2.68	2.61		2.62	2.62	

TABLE XIV. ^{239}Pu-^{235}U FISSION RATE RATIO
(AVERAGE VALUES IN THE MODERATOR)

	T_f=25, T_m=25, t_c=25			T_f=700, T_m=60, T_c=100			T_f=700, T_m=60, T_c=200		
	FG	NA	Δ %	FG	NA	Δ %	FG	NA	Δ %
THERMOS	1.5238	1.5305	0.44	1.5741	1.5804	0.40	1.5767	1.5837	0.44
WDSN	1.5233	1.5306	0.48	1.5739	1.5811	0.455	1.5761	1.5845	0.53
Δ %	0.033	0.01		0.013	0.044		0.038	0.050	

TABLE XV. ^{239}Pu-^{235}U FISSION RATE RATIO
(AVERAGE VALUES IN THE MODERATOR)

	T_f=700, T_m=60, T_c=300			T_f=700, T_m=60, T_c=350			T_f=700, T_m=60, T_c=400		
	FG	NA	Δ %	FG	NA	Δ%	FG	NA	Δ %
THERMOS	1.5809	1.5879	0.44	1.5830	1.5903	0.46	1.5854	1.5928	0.46
WDSN	1.5799	1.5874	0.47	1.5821	1.5897	0.48	1.5854	1.5923	0.43
Δ %	0.063	0.031		0.057	0.038		0.0	0.031	

Generally speaking one can say that the differences between the results obtained with the two scattering models are nearly independent of the numerical programme used. In particular, the sensitivity of the temperature coefficients to the different physical models is the same for both numerical techniques. However, the discrepancies between the absolute values of the results obtained with the two programmes may, in some cases, be larger than the differences from the different scattering models.

With regard to the effects caused by the scattering model, the following comments may be made:

(1) With the free-gas model the behaviour of both spectral indices as a function of the coolant temperature is determined by the over-evaluation of the rethermalization effect due to collisions with coolant nuclei.
(2) The different behaviour of the $\eta f(Tc)$ curve with the two scattering models (Fig. 5) is determined by the competition between rethermalization and density effects.

A comparison with experimental results was possible only for the ^{176}Lu-^{55}Mn spectral index in the lattice at room temperature. The theoretical results obtained with THERMOS for the cluster average (normalized to the values at the cell edge) are 1.1259 and 1.2219 for the free-gas and the Nelkin-Ardente model respectively, to be compared with the measured value 1.2416 (±0.7%) [12]. With respect to this value the relative error of the reaction rate calculated with the Nelkin-Ardente model is ≈ 1.6% (discrepancy between THERMOS and WDSN: ≈ 0.55%). With the free-gas model the relative error is 9.9% (discrepancy between THERMOS and WDSN: ≈ 0.2%).

The agreement obtained with the Nelkin-Ardente model is rather satisfactory, taking into account also the fact that the measurements were performed inside the fuel pins, while the calculations refer to a homogenized region including fuel and coolant.

REFERENCES

[1] HONECK, H.C., Rep. BNL-5826 (1961).
[2] FRANCESCON, S., Rep. AEEW-R 273 (1963).
[3] ARDENTE, V., J. de Phys. 25 (1964) 64.
[4] NELKIN, M., Phys. Rev. 119 (1960) 741.
[5] HONECK, H.C., Trans. Am. nucl. Soc. 5 (1962) 47.
[6] GLÄSER, W., BECKURTS, K.H., Nucl. Sci. Engng 20 (1964) 235;
GLÄSER, W. et al., Inelastic Scattering of Neutrons II IAEA, Vienna (1965) 167.
[7] In our calculations we have used the Honeck GAKER code (see THERMOS report, BNL-5826 (1961)).
[8] ANTONINI, B., PAOLETTI, A., Physica 30 (1964) 1647.
[9] SPRINGER, T., HOFMEYR, C., KORNBICHLER, S., LEMMEL, H.D., Proc. 3rd UN Int. Conf. PUAE 2 (1965) 351.
[10] SANCHO, L., GARCIA-CASTAÑER, B., VERDAGUER, F., Pulsed Neutron Research I IAEA, Vienna (1965) 185.
[11] JOANOU, G.D. et al., Rep. GA-4132 (1963).
[12] KAY, R.E., GREEN, R.E., Rep. AECL-2651 (1966).

INELASTIC SCATTERING OF NEUTRONS FROM BENZENE AND WATER

D.K. ROSS, F.P. SZABO* AND Y. SANALAN
PHYSICS DEPARTMENT, UNIVERSITY OF BIRMINGHAM,
BIRMINGHAM, UNITED KINGDOM

Abstract

INELASTIC SCATTERING OF NEUTRONS FROM BENZENE AND WATER. From measurements with the Birmingham University cold neutron scattering apparatus, values have been obtained for the upscattering cross-sections of benzene and water. The apparatus has a resolution of 0.0015 eV and the measurements are made at eight angles of between 20° and 90° to the beam direction. Measurements were made on benzene at room temperature and on water at room temperature and 234°C. Although it is intended to further improve the resolution and statistics of the results, these already show some interesting features. The data have been reduced to the form $S(\alpha, \beta)$ and the extrapolation technique of Egelstaff has been used to extract the spectral density function $\rho(\beta)$. From neutron measurements at higher incident energies and other data, the rest of the $\rho(\beta)$ curve can be constructed and hence the scattering law regenerated using the LEAP-ADDELT programme. The regenerated results were compared with the experimental ones and where necessary the process was iterated until a good fit was obtained. The resultant $\rho(\beta)$ provides a good basis for the calculation of the scattering matrix required for reactor calculations. Benzene, which was chosen because of its similarity to a number of organic moderators and the existence of a theoretical model for its vibrations and rotations, gave a $\rho(\beta)$ which agreed to some extent with that obtained by Gläser but with a peak at lower energy. The results for water are similar to those obtained at Chalk River but there is some evidence for an extra peak in the derived function. This is reasonable because the cold neutron technique yields rather better energy resolution in the low-energy region as compared with the multirotor system used at Chalk River.

1. INTRODUCTION

In the energy range where neutron velocities are comparable with the thermal velocities of atoms, the moderating behaviour of isotropic incoherent materials may be calculated from the 'frequency distribution function' of their atomic motions. Part of this frequency function is accessible experimentally by the extrapolation technique of Egelstaff and Schofield [1] which is described briefly below, but the higher frequency region, in particular the internal vibrations of molecules, has not yet been measured as a function of momentum change. This region must therefore be estimated from other data and the methods used have varied from case to case. In general the energies of the vibrational levels are available from infra-red or Raman data. The amplitudes of the different levels can either be assumed to be a proportion of those which exist in the gas phase (e.g. benzene [2]) or be adjusted to (a) give the correct Debye-Waller factor and mean kinetic energy and to (b) satisfy the various moments relations (e.g. water [3]). The present measurements have been performed on benzene at room temperature and on water at room temperature and 234°C using the Birmingham University Cold Neutron apparatus on the reactor Herald at Aldermaston Weapons Research Establishment (A.W.R.E.), Aldermaston [4, 5]. Although it is appreciated that the main function of cold neutron measurements in this field is in improvement

* Present address: Defence Chemical, Biological and Radiation Laboratories, Ottawa, Ontario, Canada.

of the resolution of measurements of the frequency distribution at small energy changes and that the direct effect of these finer details on the overall thermalization behaviour of a moderator will be small, nevertheless so long as direct measurements are not possible at high-energy transfers, this type of experiment will have considerable importance because of the sensitivity of the Debye-Waller factor to changes in this region. Thus if the total Debye-Waller factor is known, either from the elastic scattering or by comparison of the experimental scattering law with that calculated from an assumed frequency distribution, and if that part of the factor due to the measurable region can be calculated, a further constraint is placed on the distribution in the unmeasurable region.

It is perhaps worth mentioning in this context that the internal vibrations of the water molecule have been recently measured with satisfactory resolution using the Herald Fast Chopper and an inverted filter, time-of-flight, technique [6]. While this technique provides only one momentum transfer for each energy transfer it seems that for simple distributions with only a few vibrational levels it will be possible to assign relative weights.

The results obtained so far are of a rather tentative nature. Experiments on benzene [4] were performed before the cold source came into operation and suffered badly from poor statistics and high background. It is intended to repeat the measurements in the near future. The water experiments were made possible by the availability of a high-pressure water sample designed at Harwell [7] and have only recently been completed [5]. Some aspects of the analysis, in particular the multiple scattering, are still under consideration and further experiments are planned to investigate these points. It is anticipated, however, that the basic conclusions will remain unchanged.

2. APPARATUS

The Birmingham University Cold Neutron Scattering Apparatus was first commissioned in 1965 but has since been subject to considerable modification. A full description can be found elsewhere [8] and so the present account will be brief and confined to the present configuration, although the benzene measurements were made with the original equipment.

The apparatus, which is shown in Fig. 1, uses neutrons from a tangential tube on HERALD, a 5-MW light-water-moderated reactor with highly enriched ^{235}U fuel. The available flux has been enhanced by a factor of 8 at 4 Å by the operation of a liquid-hydrogen-filled cold source and it is hoped that this can be further improved by adding a proportion of D_2. The source is inserted from the top of the reactor and also supplies an experiment at the opposite end of the beam tube. The beam is filtered by an 8-in. length of polycrystalline beryllium and a 4-in.-long bismuth crystal, both maintained at liquid nitrogen temperatures to minimize thermal diffuse scattering. The beryllium serves to scatter out of the beam all incident neutrons with energies greater than 0.005 eV ($\lambda = 4$Å) and the bismuth crystal serves partly to cut down the γ-flux and partly to enhance the resolution of the system because of a dip in its transmission at 4.4Å (due to Bragg scattering from a crystal plane). The intensity of the filtered beam falling on the chopper is approximately 5×10^6 n/cm^2 s when the cold source is in operation.

The chopping system is similar to that described by Harris et al. [9]. The rotor is made of a magnesium alloy containing 10% cadmium and is suspended from a Harwell type spinning head [10]. The rotor contains five curved slits of width 0.270 in. and height 1 in. with 0.094 in. of material between the slits. The central slit has a radius of curvature of 6.45 in. and the other slits are milled with the same centre of curvature. Such a slit system passes a range of reciprocal velocities ± 25%, about the value of the reciprocal velocity that corresponds to the maximum transmission probability (τ_0), where

$$\tau_0 = \tfrac{1}{2}\,\omega R_c \qquad (1)$$

ω is the angular velocity of the rotor and R_c is the radius of curvature of the central slit. With the rotor running at 481 c/s the peak transmission occurs at 1010 μs/m. The largest reciprocal velocity transmitted is about 1260 μs/m but because of the beryllium filter the minimum is 1002 μs/m. Because of the various Bragg edges and the effect of the bismuth dip, the shape of the spectrum is far from Gaussian and this considerably complicates the combination of the various resolution effects. (See below.) The full width at half height is 120 μs/m.

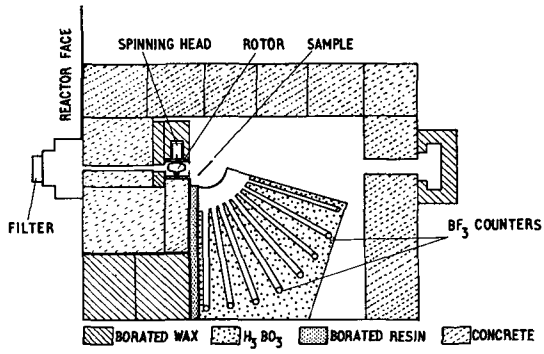

FIG. 1. The Birmingham University Cold Neutron Scattering Apparatus.

The pulses of neutrons from the chopper strike the sample at a distance of 29 cm from the rotor axis and are scattered into a ring of eight enriched BF_3 counters of 2-in. diameter and 16-in. active length. These counters lie at angles of between 20° and 90° to the horizontal direction on a vertical circle of radius 1.6 m centred at the sample. They are enclosed in a steel tank filled with H_3BO_3 which is itself surrounded by a concrete cell to reduce the local fast neutron background. The average count rate due to background is 0.25 counts per detector per minute. The experimental data, which for each event consists of a 7-bit binary word representing neutron time-of-flight and a 5-bit word representing sample and detector number (up to 10 detectors and three samples), are accumulated in a 4096 (2^{12}) channel magnetic core-store with a capacity of 2^{16} events per channel, built by Electrical Musical Industries Limited. This analyser provides a continuous monitoring of the accumulated data on an oscilloscope screen and the final data are punched out on to paper tape.

The total flux falling onto the sample is 10^6 n/min. For a similar rotor on DIDO, operating in a similar way Harris [9] quotes 5×10^6 n/min. The total vanadium count rate from a sample scattering about 8% of the beam is 17 counts/min per detector.

Resolution

The overall resolution of the apparatus is made up of a number of components which, it has been assumed, may be compounded as normal standard deviations. These components can be split into three groups depending on the way in which their effect varies with the energy change on scattering.

(1) Effects which give rise to a time uncertainty t_0 which is independent of energy change.

These components are:

(a) chopper burst width = 23 μs
(b) chopper scan time = 10 μs
(c) time spread due to the velocity spread of neutrons travelling from the rotor axis to the sample position = 40 μs
(d) time spread due to the flight path uncertainty before scatter = 25 μs
(e) time channel width = 16 μs.

Thus t_0 = 55 μs.

(2) Effects due to the uncertainty in flight path after scatter, yielding a time uncertainty proportional to the final reciprocal velocity (τ_f)

(a) sample dimension, $\Delta t = 0.018\ \tau_f$.
(b) departure of detectors from Debye-Sherrer cones $\Delta t = 0.015\tau_f$.
(c) detector depth $\Delta t = 0.05\ \tau_f$.

Thus $t_1 = 0.055\ \tau_f$

(3) Effect of initial reciprocal velocity spread on final reciprocal velocity τ_f after a given energy change

$$\Delta\tau_f = (\tau_f^3/\tau_0^3)\Delta\tau_0$$

Combining these effects and expressing them as a fractional uncertainty in τ_f we have

$$\frac{\Delta\tau_f}{\tau_f} = \sqrt{\left[\frac{t_0}{L\tau_f}\right]^2 + \left[\frac{t_1}{L\tau_f}\right]^2 + \left[\frac{\tau_f^2}{\tau_0^3}\Delta\tau_0\right]^2} \qquad (2)$$

where L is the distance from sample to detector (1.6 m). Substituting the appropriate values

$$\frac{\Delta\tau_f}{\tau_f} = \sqrt{\frac{1180}{\tau_f^2} + 0.00118 + 1.36 \times 10^{-14} \times \tau_f^4} \qquad (3)$$

which yields 13% for $\tau_f = \tau_0$ in agreement with the figure derived from vanadium scattering results, and gives 9% for a final energy of 0.025 eV.

Sample holders

The benzene being at room temperature was contained in a simple aluminium holder with walls 0.015-in. thick which defined a plane slab 0.010-in. thick. When placed at 45° to the beam this sample scattered 15% of the incident neutrons. Scatter attributable to aluminium alone was allowed for using observations of scattering from an empty sample holder.

The high-pressure water sample was manufactured from a single length of stainless steel tubing of 0.020-in. outer diameter and wall thickness 0.002 in. The tube was bent to and fro so that the middle portions of each run formed parts of a plane surface of area 2 in. × 2.5 in. which consisted altogether of 64 parallel lengths of tubing. The tubes were separated by a nominal 0.008 in. using an asbestos former and were heated electrically in a vacuum. 150 W were necessary to heat them to 200°C. Some difficulty was found, as the temperature was raised, in preventing distortion of the tubes from causing short circuits. Rather than reduce the number of tubes in the beam, it was decided to separate them with a 0.003-in. sheet of PTFE passed successively above and below the tubes. This solved the insulation problem and only contributed 0.3% to the total scattering. It did, however, produce a remarkably sharp elastic coherent reflection in the 50° counter (corresponding to a plane spacing of 4.7 Å) which, although removed by the background subtraction technique, contributes to the statistical uncertainty in that counter.

The sample is connected to a reservoir which is separated from a second volume containing compressed air by flexible bellows. This dual system serves both as a convenient way of applying the pressure (originally from a compressed air cylinder) and as a means of taking up the thermal expansion of the liquid. The whole system, including a second empty sample which is maintained at the same temperature, is mounted on a piston which can be driven to and fro pneumatically so that either the sample or the blank lies in the beam. The applied pressure can be taken up to 2000 lb/in^2, sufficient to prevent the boiling of water up to the critical temperature. In fact, because of loss of scattering, presumably from local boiling, the highest stable temperature obtained was 234°C. The temperatures of the samples are monitored by a number of thermocouples, and one of these serves to control the electrical power supplied. The control system, in addition to regulating the temperature of the samples, operates the sample change mechanism at preset intervals, indicates to the data analyser which sample is in the beam and cuts off the power supplies should the temperature or the water pressure vary unduly or the air pressure fall. While the sample is being changed and also if the sample conditions deviate from the preset values, data input to the analyser is halted.

3. EXPERIMENTAL RESULTS AND DISCUSSION

Some experimental results on vanadium at room temperature are shown in Fig. 2. Scattering from vanadium, which is almost entirely incoherent with a relatively high Debye temperature, shows a distinct elastic peak which can be used for the intercalibration of the detector efficiencies and as a measure of the elastic resolution of the apparatus.

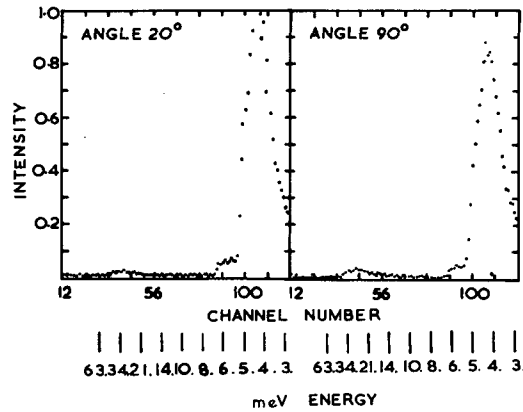

FIG. 2. The distribution of neutrons scattered from vanadium at 20°C.

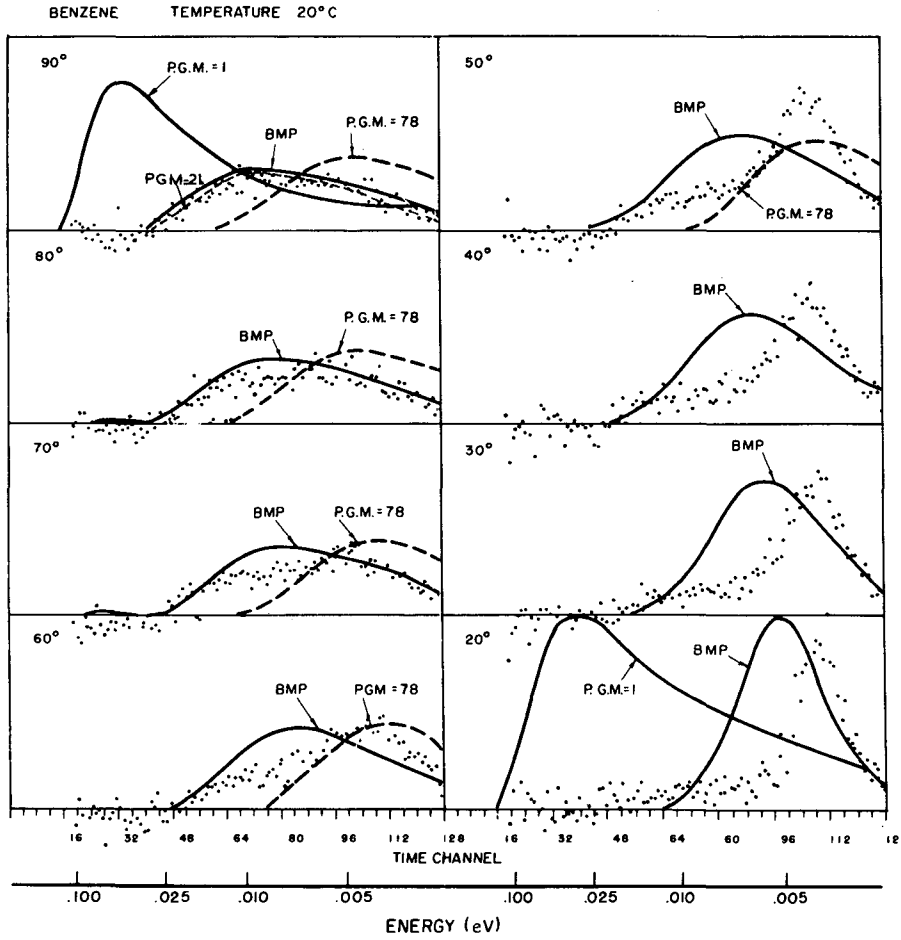

FIG. 3. Experimental data and theoretical predictions of the scattering from liquid benzene.

BMP = Boffi, Molinari and Parks theory. PGM = Perfect Gas Model for quoted mass ratio.

The diagram also shows the contribution of the acoustical modes in vanadium (Channels 34-56) and that the 20° counter has a noticeably higher background due to air scatter.

The benzene results are shown in Fig. 3. The points show the time-of-flight data corrected for background, dead-time and detector efficiency. At low angles the scattering is similar to that from vanadium in that it can be easily divided into an elastic and an inelastic region although the elastic region is broadened due to the diffusive motions of the molecules. At higher angles the distinction becomes less clear and at 90° there is virtually no sign of two peaks in the scattering. Also shown in Fig. 3 are the distributions that would be expected from the perfect gas model using relative masses of 1 (hydrogen alone) and 78 (the molecular weight of benzene). In addition there are curves calculated from the model suggested by Boffi, Molinari and Parks (BMP model) [2]. This model makes the assumption that the motions of hydrogen in liquid benzene can be represented as a combination of translational and rotational motions and of the vibrational motions of the free benzene molecule. It is further assumed that the rotations can be accounted for by using the Sachs-Teller mass tensor concept which recognizes the fact that molecules will take up recoil energy partly as translational and partly as rotational energy. This is done by putting the appropriate effective mass (M*) into the short-collision time approximation.

$$N_{ij} = \frac{1/i^4}{T} S(\alpha_{ij}, \beta_i) e^{-\beta i/2} \tag{4}$$

where N_{ij} is proportional to the number of counts in time channel i of counter j and where $S(\alpha, \beta)$ is the scattering law.

Using the fact that 0.005-eV neutrons would be detected in channel 100, we may define the scattering law variables in terms of the channel numbers as follows

$$\alpha_{ij} = \frac{1}{T}\left(\frac{50}{i^2} + \frac{50}{i_0^2} - \frac{100}{ii_0} \cos\theta_j\right)$$

$$\beta_i = 50\,(1/i^2 - 1/i_0^2)/T$$

θ_j is the angle of scatter into the jth counter

T is the absolute temperature in eV

and i_0 is the time channel of the elastically scattered neutrons. Using this relation one can write $S(\alpha, \beta)$ in terms of the BMP model (including only the first term of the phonon expansion)

$$S(\alpha_{ij}, \beta_i) = S_0(\alpha_{ij}, \beta_i) e^{-2w} \left(1 + C(\alpha_{ij}, \beta_i)\right) \tag{5}$$

where $S_0(\alpha_{ij}, \beta_i) = \sqrt{\frac{M^*}{4\pi\alpha_{ij}}} \exp\left[-\frac{M^*}{4\alpha_{ij}}\left(\frac{\alpha_{ij}^2}{M^{*2}} + \beta_i^2\right)\right]$ is the perfect gas law

for a gas of mass M* and where

$$2W = \frac{1}{3}\alpha_{ij}\sum_{k=1}^{30}\frac{A_k}{\beta_k}\coth(\beta_k/2)$$

is the Debye-Waller factor summed over the vibrational modes, and the term $(C(\alpha_{ij}, \beta_i)$ may be written

$$C(\alpha_{ij}, \beta_i) = \frac{2}{3}\alpha_{ij}\sum_{k=1}^{30}\frac{A_k e^{[-\beta_k/2\, M^*/[4\alpha_{ij}(\beta_k-1)]]}}{\beta_k(e^{\beta_k}-1)}\cosh\left[\frac{M^*\beta_i\beta_k}{2\alpha_{ij}}\right]$$

where the values of β_k and A_k, the energies and amplitudes of the normal modes in benzene can be found in Ref. [11].

The N_{ij} calculated from this formula are plotted in Fig. 3. As would be anticipated, the calculation does not reproduce the quasi-elastic peak and agreement at low angles is poor. In the case of the 90° counter, however, where the quasi-elastic peak has completely merged with the inelastic portion, the agreement is very reasonable. This reflects the fact that the short-collision time approximation is accurate in this case, that is to say that the neutron interaction is completed before the motion of the molecule is influenced by the interaction with its neighbours. However, because the lowest energy vibration in benzene has a value of $\beta_k = 2$ the value of $C(\alpha_{ij}, \beta_i)$ is fairly small, being controlled by the term in $e^{-\beta_k 2}$, and therefore since the normalization is arbitrary, equally good agreement can be obtained using the perfect gas formula with the Sachs-Teller effective mass (= 21.3). This can be seen from the 90° results in Fig. 3 where a perfect gas calculation (M = 21.3) is plotted for comparison. Thus probably the only conclusion that can be drawn from this form of analysis is that when the short-collision time approximation is appropriate, the molecules behave as a gas of atoms of mass about 20, in agreement with the Sachs-Teller effective mass concept. To test the model more fully one would have to use higher incident energies.

4. ANALYSIS OF THE INELASTIC SCATTERING OF MOLECULAR LIQUIDS IN TERMS OF THE SPECTRAL DENSITY FUNCTION $\rho(\beta)$

Any more realistic analysis of the scattering from liquid benzene or from any other molecular liquid must take the intermolecular forces into account. Thus if the molecule vibrates in a given position for a finite time before diffusing to another position, neutrons which have an interaction time rather greater than the period of vibrational frequencies but less than that necessary to observe the specifically liquid properties of diffusion and molecular reorientation, will be scattered as if from a solid. It is therefore reasonable to try to represent the motions of molecules in a liquid in a way analogous to the frequency distribution that exists in a solid even though these vibrations may be short-lived. Such an analysis has been performed by Egelstaff and Schofield [1] who have shown that in the 'Gaussian approximation' a generalized spectral density distribution

function $\rho(\beta)$ can be defined in terms of the width function w(t) so as to include both oscillatory and diffusive motions. They further showed that for incoherent scatterers (with one effective type of scattering centre) the function $\rho(\beta)$ can be derived from measurements of $S_s(\alpha, \beta)$, the 'self' part of the scattering law, in the range of β accessible to experiment. Thus in theory the complete scattering law can be derived from the Fourier transform

$$S_s(\alpha, \beta) = \tfrac{1}{2}\pi \int_{-\infty}^{\infty} \exp\,(-\alpha\, w(t) + i\beta t)\, dt \qquad (6)$$

where the width function is derived from a Fourier transform of $\rho(\beta)$. However, such transformations are impossible to perform with any accuracy and it is therefore necessary to use more particular methods. Thus the width function can be divided into an oscillatory part and a diffusive part. The oscillatory component can be dealt with starting from the experimentally defined $\rho(\beta)$ and building up $S(\alpha, \beta)$ the bound part of the scattering law from appropriate series. The diffusive part can be represented by a model that gives the correct asymptotic behaviour, from which $S_D(\alpha, \beta)$ the diffusive part of the scattering law can be derived. Then using the convolution theorem of Fourier analysis the total scattering law can be produced by folding the two parts of the scattering law together. Now S_D is known to have the form of a broadened elastic peak, the width of which is proportional to α for small α. Its effect is therefore similar to resolution broadening and the effect on the thermalization behaviour is likely to be small.

The quasi-phonon expansion starts from the spectral density $\rho(\beta)$ and gives the scattering law as a sum of the various phonon terms.

Thus

$$S(\alpha, \beta) = \exp\,(-\alpha\lambda)\; 1/n!\;\; (B\alpha)^n\, T_n(\beta) \qquad (7)$$

where

$$B = \int_0^{\infty} \frac{\rho(\beta)}{2\beta \sinh\,(\beta/2)}$$

and

$$T_1(\beta) = 1/B\; \frac{\rho(\beta)}{2\beta \sinh\,(\beta/2)}$$

and

$$T_n(\beta) = \int_{-\infty}^{\infty} T_{n-1}(\beta')\, T_1(\beta-\beta')\, d\beta'$$

λ, the coefficient in the Debye-Waller factor is given by

$$\lambda = 2\int_0^{\infty} 1/\beta\;\; \coth\,(\beta/2)\rho(\beta)\, d\beta$$

From the above, $\rho(\beta)$ can be derived from the experimental values of $S(\alpha, \beta)$ by extrapolating $S(\alpha, \beta)/\alpha$ to $\alpha = 0$ in order to isolate the 1 phonon term. Thus

$$\underset{\alpha \to 0}{S(\alpha, \beta)/\alpha} = \rho(\beta)/2\beta \sinh(\beta/2) \tag{8}$$

As would be expected gently curving lines are obtained and the extrapolation is performed fairly easily. The importance of the technique is not only that it produces a correctly normalized $\rho(\beta)$ but that the smearing effect of the multi-phonon terms and also of S_d will be minimized and that the effective statistical accuracy of the result is improved. It thus happens that a frequency distribution can be produced with structure that is obscured in the raw data. (Compare Figs 5 and 7).

Extensive experiments have been performed along these lines using multirotor [3] and rotating crystal [12] spectrometers. These systems can provide a wide range of α-values over the whole range of β-values, in contrast to the cold neutron apparatus which can produce only eight α-values for each β-value and where the values of α become increasingly displaced from $\alpha = 0$ as β increases. The only advantage of the cold neutron technique is therefore at small β-values ($\beta < 2$) where the higher resolution can show up more detail in $\rho(\beta)$.

Equation (7) can be used to regenerate $S(\alpha, \beta)$ from a given $\rho(\beta)$ and the programme LEAP-ADDELT has been written to perform this operation [3]. This programme uses a 'steepest descent' method (an expansion in terms of $1/\alpha$) for regions in which the phonon expansion does not converge quickly. It will also fold the resultant scattering law with a diffusive component and a component derived from δ-function vibrations at higher energies. However, only a limited part of $\rho(\beta)$ is accessible to experiment and therefore assumptions have to be made about the form of $\rho(\beta)$ above $\beta = 6$. For molecular liquids the unobservable contributions are mainly due to internal vibrations whose energy is known. If some assumption is made about the relative weights of these vibrations then $S(\alpha, \beta)$ can be calculated for specified values of α and β for comparison with the experimental values. The process of iteration for the case of water is fully described by Haywood [3]. The analysis has also been performed for benzene by Gläser [12].

The spectral density for benzene

The results of performing the extrapolation technique for benzene are shown in Fig. 4, where it is actually the related function $\rho(\beta)$ that is plotted [1]. The present statistical accuracy does not warrant successive iterations with LEAP-ADDELT. Preliminary runs, however, giving the experimental part of $\rho(\beta)$ a weight of 0.077 and the remaining weight to the internal vibrations, yielded roughly the correct slope for S/α but much higher intercepts. This is perhaps due to the fact that a second peak in $\rho(\beta)$ caused by intermolecular modes has been obscured by the background. Raman spectroscopy measurements by Fruhling [14] on solid benzene show peaks at $\beta = 0.31$ and $\beta = 0.52$. The former agrees well with the experimental distribution while the distribution found by Gläser, also

shown in Fig. 4 and renormalized to our peak height, might perhaps include both peaks (cf. Egelstaff [15]). The situation here is far from satisfactory and firm conclusions must await new experimental results.

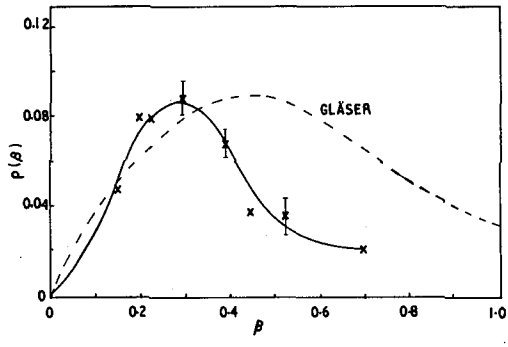

FIG. 4. Experimental values of $\rho(\beta)$ for benzene compared with those of Gläser et al.

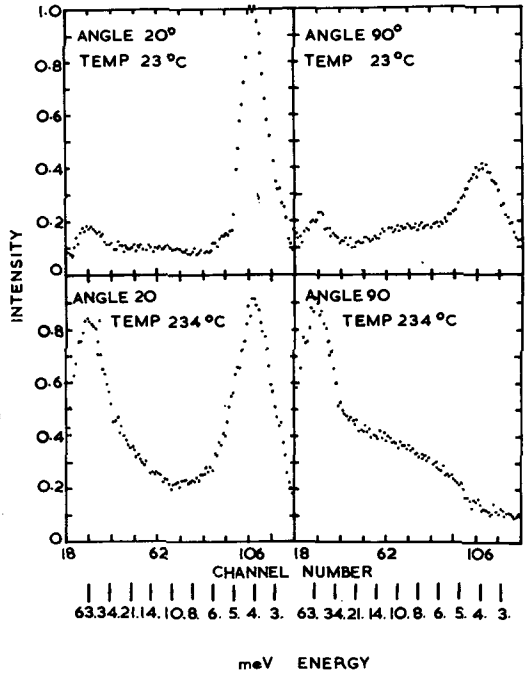

FIG. 5. Distributions of neutrons scattered from water.

The scattering from water

Typical results for room temperature and 234°C water are shown in Fig. 5 where appropriate corrections have been made for background, counter sensitivity and analyser dead-time. The room temperature results show good agreement with those of Larsson et al. [16] except at lower

energies where the shape of the incident spectrum is important. The broadening of the elastic peak as a function of angle also agrees with Larsson's results [5]. In the high-temperature run the peak at 60 meV has become extremely prominent while the elastic peak has virtually disappeared.

In converting the data to the scattering law form the product of the number of incident neutrons and the number of scattering atoms per square centimetre must be known. This has been derived in two ways:

(i) By estimating the total number of neutrons scattered in the sample. (A carefully measured detector efficiency function is used to calculate the number of neutrons scattered towards each counter and the other directions are estimated graphically.)

(ii) By calculating the number of hydrogen atoms from the fraction of neutrons scattered out of the beam (by means of a monitor beyond the sample) and separately estimating the total number of incident neutrons (using a low-efficiency fission chamber that covers the whole area of the beam at the exit from the chopper housing).

These estimates differed by 8%. The absolute value therefore is in doubt to at least 10%.

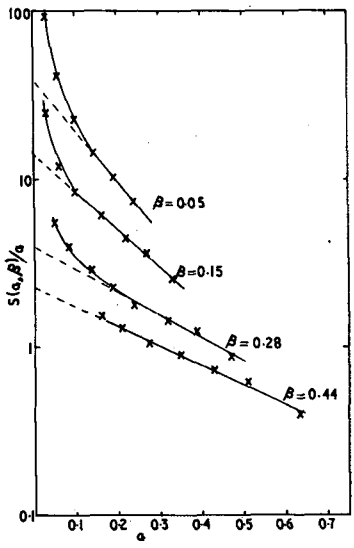

FIG. 6. Extrapolations of $S(\alpha, \beta)/\alpha$ for water at 234°C.

Some examples of the extrapolated curves of $S(\alpha, \beta)/\alpha$ are shown in Fig. 6. They all show a characteristic tendency to rise at small α-values. This tendency has been noted by other authors and in fact in Haywood's results [3] the rise begins with $\alpha \sim 2$ in contrast to the present results ($\alpha \sim 0.3$). It must clearly be due to some factor that is finite at $\alpha = 0$. Further if one extrapolates $S(\alpha, \beta)$ to $\alpha = 0$ and subtracts the value obtained from the values of $S(\alpha, \beta)$, the revised $S(\alpha, \beta)/\alpha$ curves now tend to a straight line at low α. The effect is therefore fairly independent of angle at low angle. Of the factors neglected in the above theory, the only ones that would be expected to have this form are multiple scattering and resolution broadening of the elastic peak although the latter effect would decrease rapidly with increasing β [17]. Both might be expected to appear

at higher α when higher incident energies are in use. It is hoped to perform more detailed calculations on the present results, but the uncorrected values have been used in the extrapolation at this stage.

The values of $\rho(\beta)$ so produced are plotted in Fig. 7 for room temperature and 234°C.

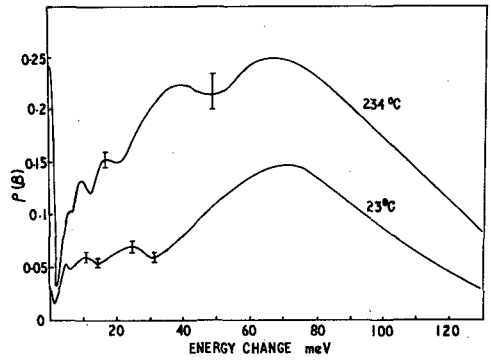

FIG. 7. The function $\rho(\beta)$ for water derived from experimental results at 23°C and 234°C.

The smallest peak at 6 meV has been reported by Larsson [16] and Golikov [18]. Also Pope and Nation [19] have derived a frequency distribution from the results of Sakamoto et al. [20], which shows a small peak at 8 meV. Hughes [21] also observed a small peak at 5 meV. Haywood's analysis of the results of the Chalk River multirotor data does not resolve this peak but that is not surprising because of the lower energy resolution. There is also some evidence from Raman spectroscopy for a peak at about 8 meV. The high-temperature curve also has a peak at 6 meV although it is less well-defined presumably due to broadening caused by increased damping of the motion.

The second peak occurs at 12 meV and this corresponds to the lowest peak observed in the multirotor experiments [3]. This might also correspond to a peak at 8 meV noted by Hughes. The high-energy curve again contains a peak at the same energy.

The third peak at room temperature shows up at about 25 meV at the same energy as found by Larsson [16], Haywood [3] and Golikov [18]. The corresponding peak at high energy however appears at 18 meV.

The remaining peak in the ambient run is the well-known hindered rotation peak at 70 meV which shows up clearly in the raw data. At high temperatures, however, it appears to have become split and shifted to lower energies. However, because of the errors at this β-value due to the length of the extrapolation involved it would be just possible to draw a single peak through the point. The indications are therefore of either two peaks at about 36 and 67 meV or possibly of one in the region of 50 meV. The possibility of a higher energy peak at room temperature was suggested by Larsson [22] on the basis of his results on D_2O. If the same peak were to be present in water it would be expected at about 100 meV, well above the range of present neutron techniques but at approximately the energy of an absorption observed in Raman and infra-red results. It is possible that Egelstaff's [23] observation (in H_2O at 150°C) of a peak in $\rho(\beta)$ at 65 meV could be a combination of these two peaks shifted to lower energies but it

is difficult to be sure about energy shifts until measurements have been made at intermediate temperatures, although the tendency has also been observed by Larsson [16].

Preliminary Leap runs have been performed using the $\rho(\beta)$ used by Haywood [3] outside the present experimental range. The $S(\alpha, \beta)/\alpha$ values produced, however, do not give the same slopes and the absolute values are significantly different. It is hoped that adjustment of the relative magnitude of the observable parts of the curve to give the correct Debye-Waller factor will improve the fit. The difference in the Debye-Waller factor between our calculation and Haywood's is due to the sensitivity of this factor to the low-energy region. It is felt therefore that the present results will be of use in deducing the parts of $\rho(\beta)$ beyond the experimental range.

5. CONCLUSION

Measurements made on the scattering of cold neutrons from benzene and water have been described and preliminary analyses of the results have been presented using the concept of the spectral density function. Although further work is necessary, it is clear from the results that cold neutron measurements have a significant part to play in the process of predicting the complete scattering law needed for reactor calculations.

ACKNOWLEDGEMENTS

The authors would like to thank the staff of the HERALD reactor, in particular Mr. G.S.B. Tuckey, for their continued assistance, Professor J. Walker and Dr. B.C.D. Haywood for many helpful discussions and Dr. P.A. Egelstaff for making the high-pressure water sample available. They are also much indebted to the Science Research Council, London for financial support.

REFERENCES

[1] EGELSTAFF, P.A., SCHOFIELD, P., Nucl. Sci. Engng 12 (1962) 260.
[2] BOFFI, V., MOLINARI, V.G., PARKS, D.E., Inelastic Scattering of Neutrons in Solids and Liquids II IAEA, Vienna (1963) 285.
[3] HAYWOOD, B.C., J. nucl. Engng 21 (1967) 249.
[4] SZABO, F.P., Ph. D. Thesis, Birmingham University, Birmingham, England (1965).
[5] SANALAN, Y., Ph. D. Thesis, Birmingham University, Birmingham, England.
[6] BEGG, M.M., ROSS, D.K., to be published.
[7] COCKING, S.J., BALL, A.R., J. Sci. Instrum. 41 (1964) 376.
[8] ROSS, D.K., to be published.
[9] HARRIS, et al., Inelastic Scattering of Neutrons in Solids and Liquids I IAEA, Vienna (1963) 107.
[10] EGELSTAFF, P.A., et al., J. Instn electr. Engrs 108 B (1961) 26.
[11] BOFFI, V.C. et al., Rep. GA-3024 (1962).
[12] GLÄSER, W. et al., Karlsruhe Report KFK 264 (1964).
[13] McLATCHIE, R.F., to be published.
[14] FRUHLING, A., Annls Phys. 6 (1951) 401.
[15] EGELSTAFF, P.A., J. nucl. Engng 17 (1963).
[16] LARSSON, K.E., DAHLBORG, U., Inelastic Scattering of Neutrons in Solids and Liquids I IAEA, Vienna (1963) 317.

[17] THORSON, I., to be published.
[18] GOLIKOV, V.V., Inelastic Scattering of Neutrons II IAEA, Vienna (1965) 201.
[19] POPE, N.K., NATION, R., Inelastic Scattering of Neutrons II IAEA, Vienna (1965) 141.
[20] SAKAMOTO, M. et al., J. phys. Soc. (Japan) Suppl. Bull, 17 (1962) 370.
[21] HUGHES, D.J. et al., Phys. Rev. 119 (1960) 872.
[22] LARSSON, K.E. et al., Reactor Sci. Technol. 16 (1962) 81.
[23] EGELSTAFF, P.A. et al., Inelastic Scattering of Neutrons in Solids and Liquids I IAEA, Vienna (1963) 343.

ANGULAR SCATTERING BY CH_2, $ZrH_{1.85}$ AND C_6H_6 *

J.R. BEYSTER, G. M. BORGONOVI AND G.W. CARRIVEAU
GENERAL ATOMIC DIVISION,
GENERAL DYNAMICS CORPORATION,
SAN DIEGO, CALIFORNIA,
UNITED STATES OF AMERICA

Abstract

ANGULAR SCATTERING BY CH_2, $ZrH_{1.85}$ AND C_6H_6. A study of the single-differential angular scattering cross-section has been made for a number of moderators. The linear electron accelerator at General Atomic was used to produce bursts of neutrons in a wide energy range. The cross-sections were determined for incident energies ranging from the sub-thermal region up to 10 eV and for angles from 10° to 150°.

The data are corrected for elastic and inelastic multiple scattering using the code MUSE, and are then compared to the values obtained from a theoretical model.

The results from a 15-mil thick sample of polyethylene (MARLEX 6050) at room temperature have been compared with the values calculated by the model of Koppel and Young, which uses a frequency spectrum lumped in four discrete oscillators.

The agreement with the theory is quite satisfactory and within the experimental errors, except for very low angles (less than 30°). At these low angles the problem of computing the correcting factors from a theoretical model becomes delicate, because of numerical difficulties associated with the sharp elastic component. The average cosine of the scattering angle ($\bar{\mu}$), calculated from the experimental angular cross-sections, is in good agreement over the entire energy range with that evaluated from the theory of Koppel and Young.

Angular scattering data have also been taken for $ZrH_{1.85}$ both at room temperature and at 700°K. During the course of these measurements the main difficulty was that of obtaining a chemically stable sample, since it is very easy to lose hydrogen in the process of heating. Even a small loss of hydrogen can seriously affect the measurements and particular care had to be taken to observe the temperature dependence of the cross-section. The temperature dependence is predicted by the Parks-broadened Einstein oscillator model.

The collection of a new set of angular data in C_6H_6 at room temperature has been motivated by a simultaneous theoretical study performed at this laboratory to derive a new kernel for the scattering law in this moderator.

1. INTRODUCTION

The single-differential angular cross-sections for scattering of neutrons by polyethylene, zirconium hydride, and benzene have been measured using a time-of-flight technique at the General Atomic electron linear accelerator facility.

Theoretical models are available for the atomic motions responsible for the thermalization of neutrons in these moderators. These models allow the calculation, in the scattering law formalism, of the double-differential cross-section and from this the single-differential cross-section can be computed and compared with the experimental data. The experimental technique which was used in collecting the scattering information in time-of-flight form is described in Section 2. Section 3 describes the

* This work was sponsored by the United States Atomic Energy Commission.

data reduction procedure and gives some details about the corrections which must be applied, namely a correction for multiple scattering and for a geometrical effect due to the finite length of the flight path after scattering.

Sections 4, 5, and 6 contain the experimental results for the cases of CH_2, $ZrH_{1.85}$, and C_6H_6 respectively.

The measurements in CH_2 and C_6H_6 were made at room temperature, while the measurements in $ZrH_{1.85}$ were made at room temperature and at 700°K. Details about the characteristics of the samples and a few comments on the model employed in the comparison are included in each section.

2. EXPERIMENTAL TECHNIQUE

Figure 1 shows the experimental setup used for these measurements. A periodically pulsed electron beam from the linear accelerator strikes a water-cooled, fansteel target and produces fast neutrons through a (γ, n) reaction. The neutrons are slowed down in a water moderator shaped to give a source of rather constant surface emissivity.

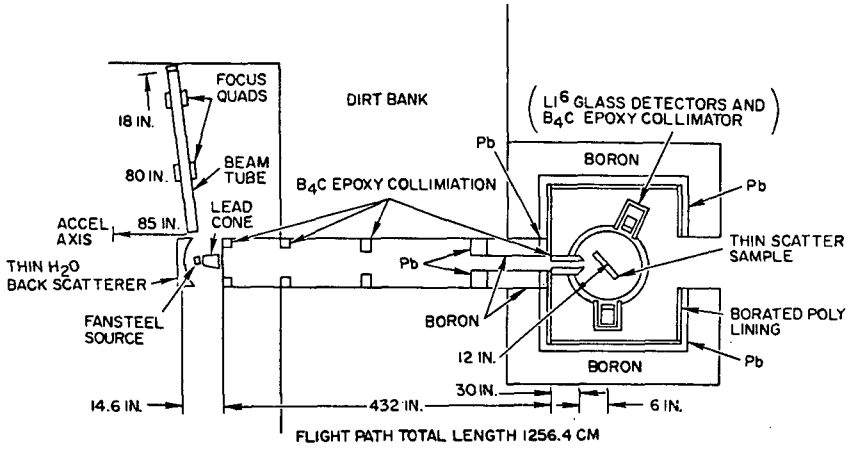

FIG. 1. Geometry for angular scattering measurements.

The time width of the electron pulse striking the target is 4.5 μsec, the frequency of operation is 60 pulses/sec, the energy of the electrons is 28 MeV, and the average current is 500 mA.

After the electron beam hits the target a strong "gamma flash" is produced. In order to limit the effect of this gamma flash on the electronics the target is shielded by a lead cone which is slightly larger than the target itself.

The water moderator forms a pulsed source of neutrons in a large energy region. The dieaway time for this source, which has an average thickness of 5 cm, has a value of about 64 μsec.

The neutrons travel along a 12-meter evacuated flight path, whose diameter is gradually reduced by boron carbide collimators. The flight path ends with a boron nitride collimator having a diameter of 5 cm.

At the end of the flight path the sample and the detectors are contained in an experimental vault heavily shielded with lead and lined with borated polyethylene.

The sample is in the form of a slab oriented at 45° with respect to the incident beam.

The average neutron flux in the total energy range available at the sample position during normal operation of the accelerator is 10^5 neutrons/min. cm^2. The detectors used in the measurements are two Li^6 glasses, followed by photomultiplier tubes and shielded with boron carbide epoxy sleeves. The Li^6 glasses have a thickness of 1.25 cm and their efficiency is very near to one for neutron energies up to 1 eV. The distance from the center of the sample to the detectors is 30 cm, which is small compared with the total distance from the source to the detectors.

The two detectors can be positioned with an accuracy of $\pm 0.5^{\circ}$ on both sides of the incident beam, over an angular range from 0° to 155°.

Several types of monitor systems have been tried. The one which has given the best results consists of two $B^{10}F_3$ detectors located near the end of the flight path and on both sides, one flat fission chamber in the beam before the sample, and one BF_3 bank located also in the direct beam but 5 meters beyond the sample. The fission chamber can monitor the complete beam area. The output from the monitors is fed into scalers and, for two of the monitors, the output is also fed to graphic recorders so that the operation of the monitors can be continuously checked. In normally operating conditions the monitors track each other to within three per cent.

Several checks of the experimental details have been made and are described elsewhere.[1]

The zero for the time-of-flight measurements is given by a pulse in phase with the electron beam pulse. The signals from the Li^6 detectors, after amplification, are fed to two separate TMC time-of-flight analyzers. The time-of-flight spectra are both printed and punched on tape for successive numerical analysis.

3. DATA CORRECTION PROCEDURE

3.1 COLLECTION AND TREATMENT OF DATA

The measurements are usually taken in angular steps of 5° with the sample in and out of the beam. The ratio background-to-signal changes with angle and sample thickness but it usually does not exceed ten per cent. A standard computer code, which includes corrections for

mean emission time in the source and losses in the analyzer system, transforms the measured time-of-flight spectra into fluxes as a function of energy.

The incident flux is measured with the same detector positioned at zero degrees, so that the experimental information can be readily put in the form of a ratio $R(\theta, E)$ of the scattered intensity at an angle θ to the incident intensity.

The *single-differential* cross-section can be written

$$d\sigma/d\Omega\,(\theta, E) = C_G\, R(\theta, E)\, C_M\, C_P$$

Here, C_G is a constant dependent on the geometry. This constant can be evaluated, in which case absolute cross-sections are measured, or it can be deduced by fitting the measurements to the known total cross-section.

For several reasons it is difficult to measure with the necessary accuracy all the geometrical parameters; therefore, the normalization to the total cross-section was preferred.

The factors C_M and C_P are respectively the multiple scattering correction and the finite flight path correction. These are angle- and energy-dependent corrections and to be computed require that a model for the scattering law be available.

3.2 MULTIPLE SCATTERING CORRECTION

The C_M factor is included to account for multiple collisions in the scatterer. Several methods[2, 3, 4] have been proposed to correct for multiple scattering. Slaggie[5] has pointed out that it is possible to express the correction in form of a factor only if the multiple scattering contribution is small, otherwise a more elaborate type of correction method involving the difference between the measured scattered flux and the flux due to multiple collisions has to be employed.

The amount of multiple scattering depends strongly on the thickness of the sample and will be discussed separately for the three moderators. In all cases we have employed the correction as calculated by the code MUSE[4] for the case of the single-differential cross-section.

The code MUSE, which is based on the integral transport theory, uses a theoretical kernel for the scattering law to evaluate the contributions from collisions to the fourth order.

The corrections evaluated by MUSE are accurate for scattering angles larger than 30°. Below 30° the theoretical kernel itself is not very dependable because of the finite mesh employed in the integrations. For this reason, in the treatment of the data which will be described later we have limited the multiple scattering correction to angles above 30 degrees.

3.3 FINITE FLIGHT PATH CORRECTION

When the neutrons are inelastically scattered the total time-of-flight t from the source to the detectors is the sum of a time t_0 and a time t_1. Here t_0 is the time-of-flight over ℓ_0, distance source-sample, and t_1 is the time-of-flight over the distance ℓ_1 from sample to detector. In our experiments the distance ℓ_1 is much smaller than ℓ_0 (30 cm compared to 1220 cm) so that in first approximation we can disregard the difference between t and t_0 and assume that the neutrons have an incident energy corresponding to the time $t_0 + t_1$ over the distance $\ell_0 + \ell_1$.

If we do not want to make this approximation we must evaluate the correct quantity which we are measuring by the time-of-flight method. This is easily obtained by changing from the variables E_0 and E_1 (initial and final energies) to the variables t_0 and t (time-of-flight before scattering and total time-of-flight).

In this new system the double-differential cross-section $\sigma(E_0, E_1, \theta)$ is expressed as $\sigma_1(t_0, t, \theta)$ and the number of counts in a channel of width Δt centered at a time t is

$$N(t)\Delta t = \Delta t \int_0^{t_0} \varphi_1(t_0)\sigma_1(t_0, t, \theta)\,|J|\,dt_0$$

where $\varphi_1(t_0)$ is the incident spectrum and J is the Jacobian of the transformation.

We obtain the single-differential cross-section by multiplying the experimental quantity $C_G\ R(\theta, E)$ by the factor

$$C_P = \frac{m(\ell_0+\ell_1)^2\,\varphi(E)\int_0^{\infty}\sigma(E, E_1, \theta)\,dE_1}{t^3\int_0^{t_0}\varphi_1(t_0)\sigma_1(t_0, t, \theta)\,|J|\,dt_0}$$

where m is the mass of the neutron, $\varphi(E)$ is the incident flux as a function of energy and t is connected to E by

$$E = \frac{m}{2}\,\frac{(\ell_0+\ell_1)^2}{t^2}$$

As with the C_M factor, the evaluation of the C_P factor requires the knowledge of the scattering law. Usually the C_P factor is very near to one, but in some cases, as in $ZrH_{1.85}$ near the oscillator level, where the neutrons are slowed down to very low energies, the difference between the single-differential cross-section and the time integral can reach 10 per cent.

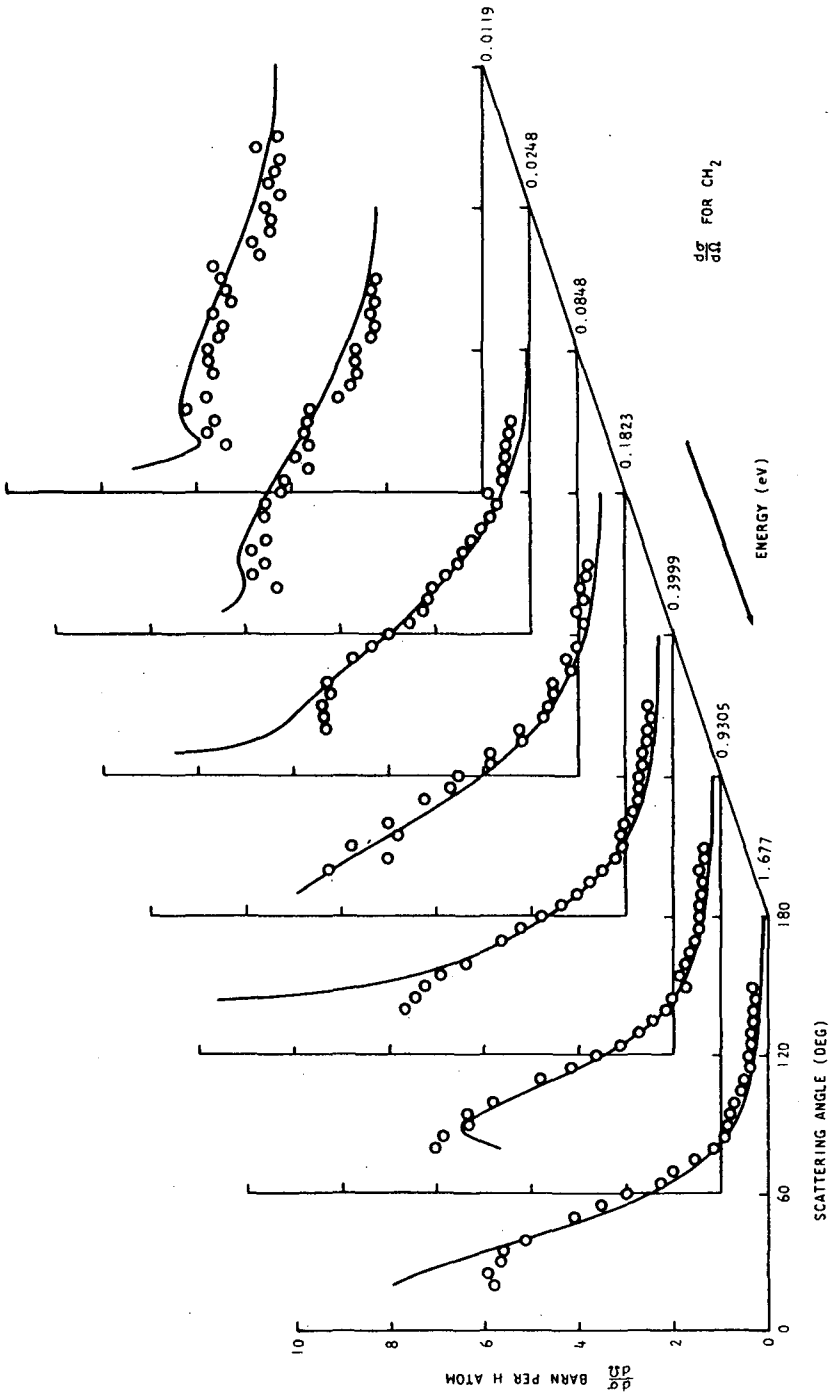

FIG. 2. Angular scattering cross-sections of polyethylene.

4. SINGLE-DIFFERENTIAL CROSS-SECTION OF CH_2

The sample of polyethylene used was MARLEX 6050 which was obtained from Phillips Petroleum Company. The density was 0.963 g/cc (at 20°C), the crystallinity 93 per cent and the average thickness 0.0375 cm. The data were treated with the technique previously described with normalization to the total cross-section.

The experimental cross-section is shown plotted in Fig. 2 for a group of seven selected energies as a function of scattering angle. The continuous curves show the theoretical cross-section calculated with a scattering kernel due to Koppel.[6] This scattering kernel was evaluated with the code GASKET[7] using a frequency spectrum based on the infrared absorption information.

This frequency spectrum consists of a number of lines which are weighted by the squares of the amplitudes of the corresponding modes of vibration. Since a detailed calculation of the polarization vectors for polyethylene is not available some assumptions had to be made in choosing the weighting factors. This scattering kernel was also used to evaluate the correcting factors.

It appeared clear that some difficulties are encountered at small scattering angles, say below 30 degrees. In this region, due to the narrow elastic peak, the results for $d\sigma/d\Omega$, for the multiple scattering correction and for the finite path correction depend very much on the energy mesh. While it is easy to use a fine energy mesh in the calculation of the single-differential cross-section, the angular and energy meshes contained in the code MUSE cannot be increased beyond a certain limit, so that the accuracy in the numerical integration is limited.

The product Σd, Σ being the total macroscopic scattering cross-section and d the thickness of the sample, was 0.21 for an energy of 0.01 eV, so that the transmission at this energy was about 81 per cent. The amount of multiple scattering, as calculated by MUSE, did not exceed 30 per cent.

In the results shown in Fig. 2 the dimension of the points is about 50 per cent bigger than the pure statistical error, to account for uncertainties in the measurement of the angles and in the neutron monitoring system. Only a general agreement exists. It appears difficult to draw conclusions about the details of the scattering model for a moderator having a complicated frequency spectrum like polyethylene when disagreements are observed.

For the reasons mentioned before, agreement between experimental and theoretical results for polyethylene has to be sought in the region above 30° scattering angle. Also it should be noted that coherent effects due to scattering from carbon atoms are observable at low energies.

From the experimental data $\bar{\mu}$, the average cosine of the scattering angle has been calculated. Figure 3 shows the experimental value of $\bar{\mu}$,

together with the theoretical curve taken from Ref. 7. The agreement is satisfactory.

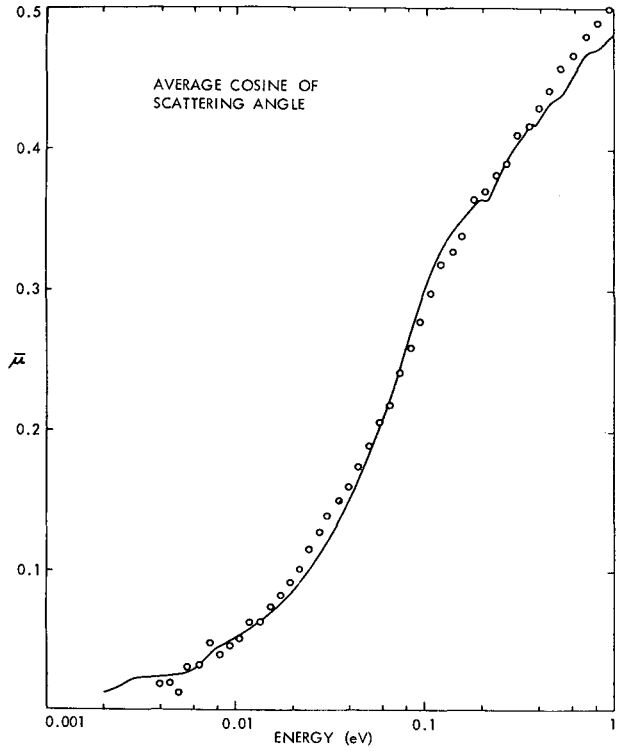

FIG. 3. Average cosine of the scattering angle for polyethylene.

5. SINGLE-DIFFERENTIAL CROSS-SECTION OF $ZrH_{1.85}$ AT ELEVATED TEMPERATURES

The angular scattering cross-section for zirconium hydride at 700°K has been measured. These data were taken to complement previous room temperature data.[8] The choice of elevated temperature was made in order to approximate reactor operating conditions. A series of room-temperature scattering data was also taken using the same sample so that the temperature effect on angular scattering cross-section could be studied.

A specially designed sample holder was needed for these measurements. This was necessary because of possible changes in sample composition at high temperature. Results from data collected using an unsealed sample holder have shown serious effects produced from loss of bound hydrogen and surface contamination in the sample.[9] The sample holder[10] consists of thin stretched aluminum windows held by stainless steel rings with knife edge seals and evacuated to reduce trapped air

contamination and pressure bulging when the sample is heated. The thin (0.125 mm) aluminum windows hold the 3.6-mm-thick, pressed zirconium hydride powder sample. Sample transmission measurements were performed before and after heating and the results indicate a negligible change in sample composition. The sample thickness was increased over previously reported measurements:[8] from 1 mm to 3.6 mm. This thick sample has a transmission of 64 per cent at 0.1 eV. Comparison of results from data taken using the thick and the thin samples at 296°K show that the multiple scattering correction methods are valid when applied to thick sample measurements.

The experimental angular scattering cross-section is compared to predictions from the theoretical model for zirconium hydride (described in Ref. 7) as shown in Fig. 4. The model used, which uses a frequency spectrum composed of a gaussian distribution centered at 0.137 eV and a Debye spectrum cut-off at 0.02 eV, predicts the temperature effect shown by the solid line in Fig. 5. The experimental points in this figure compare very well except near the oscillator levels where the theory predicts more pronounced dips. This effect is evident at both temperatures. Apart from this, the variation of the angular scattering cross-section with temperature agrees to within 5% with the corresponding calculated quantity. A comparison of the data at 296°K with thin sample data taken previously[8] is shown in Fig. 6.

6. SINGLE-DIFFERENTIAL CROSS-SECTION OF C_6H_6

The single-differential cross-section has been measured for benzene using a sample having an average thickness of 0.119 cm.

The sample was contained in a sealed holder consisting of an Al ring and two stretched Al foils having a thickness of 0.0125 cm. The sample thickness was carefully checked for possible bulging after filling. The maximum variation in sample thickness did not exceed 5%.

The product Σd, Σ being the total macroscopic scattering cross-section and d the thickness of the sample, was 0.362 for an energy of 0.01 eV, so that the transmission at this energy was about 70 per cent. The maximum amount of multiple scattering as calculated by MUSE did not exceed 45 per cent.

Figure 7 shows the measured single-differential cross-section for seven selected energies as a function of scattering angle. The continuous curves in the figure are the result of a calculation using a kernel computed by Sprevak and Koppel.[11] This kernel was evaluated with the code GASKET assuming a single oscillator for the cluster of frequencies near 0.38 eV and an artificially broadened frequency spectrum for the part below 0.38 eV. The scattering from the hydrogen atoms and from the carbon atoms in the benzene ring was included in the computation and treated in the incoherent approximation.

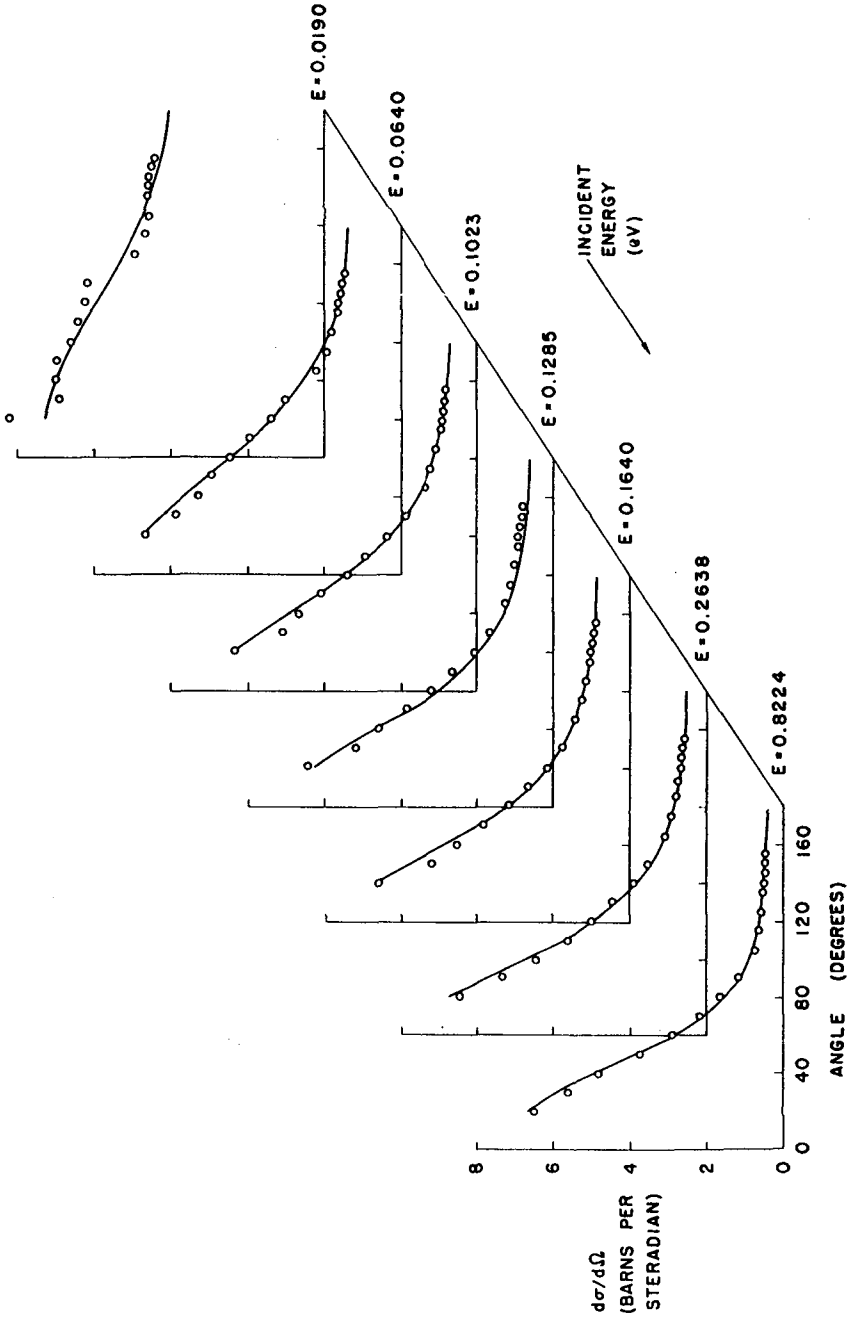

FIG. 4. Angular scattering cross-sections for $ZrH_{1.85}$.

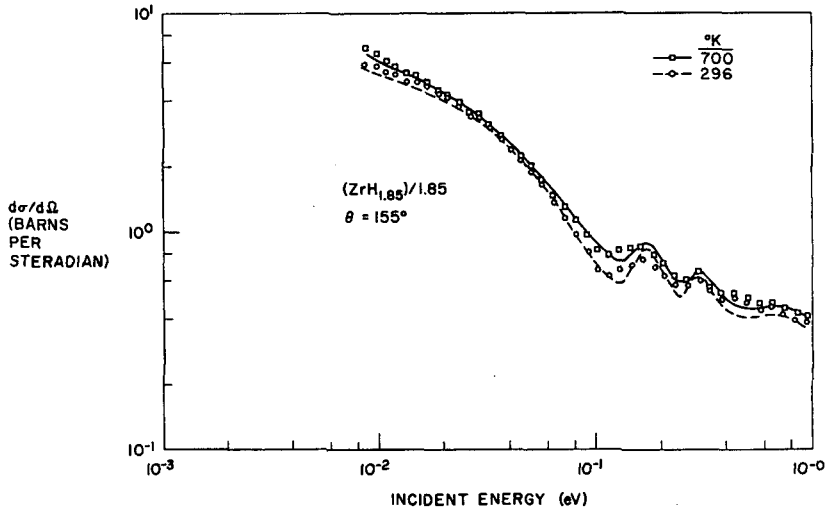

FIG. 5. Angular scattering cross-section for zirconium hydride; θ = 155°.

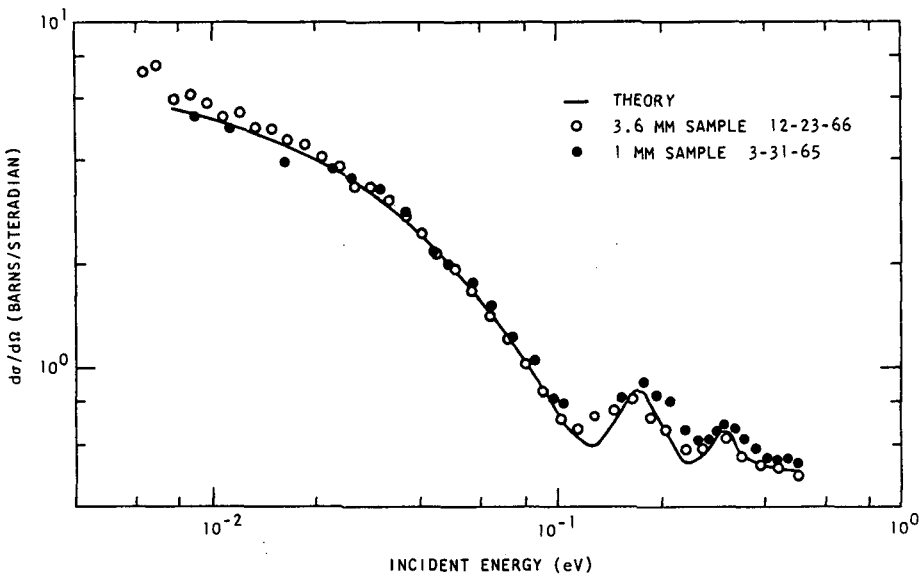

FIG. 6. Angular scattering cross-section for zirconium hydride; θ = 150°.

The kernel was used to compute the corrections for multiple scattering and finite flight path.

As in the case of polyethylene the results are dependable in an angular range above 30 degrees. The geometrical constant which gives the absolute values of the cross-section was determined by normalization to the total cross-section. The angular integration over the experimental results to obtain the normalization constant is only slightly influenced by

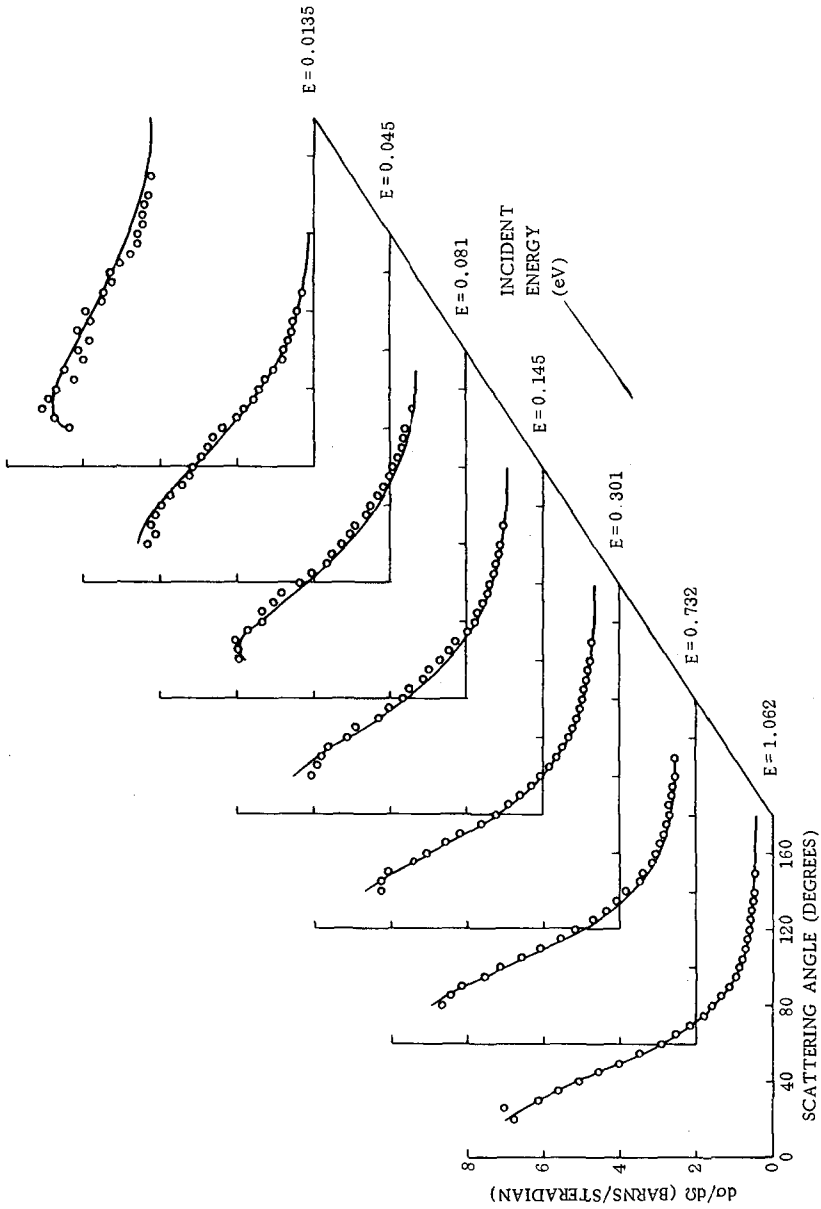

FIG. 7. Angular scattering cross-sections for benzene.

the uncertainty in the correction factors below 30 degrees. However, because of the presence of the factor sinθ in the integrand which gives the total cross-section, the low angle values do not affect the results too much. The values of the normalization constant including or not including the corrections for angles below 30 degrees differ at most by 3%.

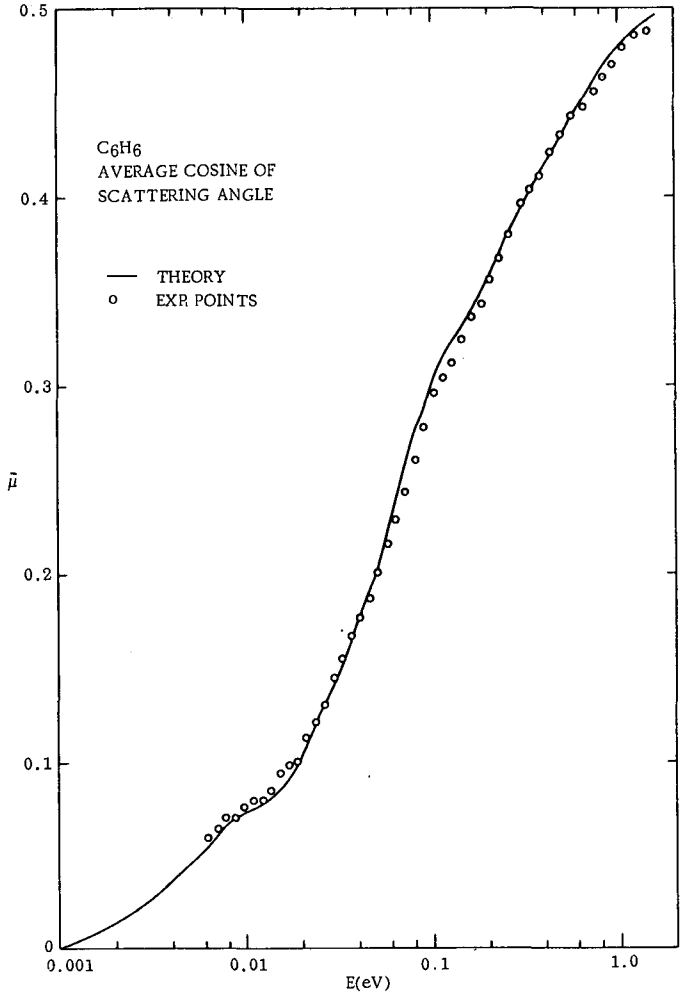

FIG. 8. Average cosine of the scattering angle for benzene.

Because of improvement in the data collection procedure, the experimental errors in the benzene measurement are believed to be smaller than in the previous cases. The dimension of the experimental points in Fig. 7 corresponds to the statistical error.

Some oscillations due to coherent effects, which cannot be accounted for by the model, are visible at low energies.

The average cosine of the scattering angle $\bar{\mu}$ was computed and is shown in Fig. 8 together with the computed theoretical curve of Sprevak and Koppel. The agreement is good. Measurements of the single-differential cross-section of benzene have been reported by Hofmeyr [12] at four incident energies, using a monochromatic beam obtained by crystal diffraction from a reactor beam. Also the procedure of correcting for multiple scattering was different, using the approximation of isotropic multiple scattering (Vineyard[2]).

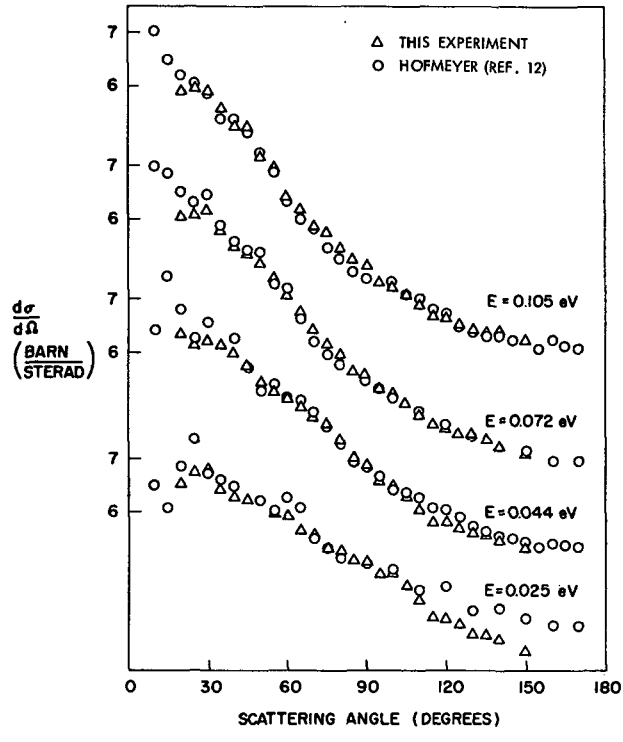

FIG. 9. Angular scattering cross-sections for benzene; comparison of two experimental results.

Figure 9 shows a comparison between the results of Hofmeyr and our results at comparable energies.

The two sets of measurements agree well except at high scattering angle for an incident energy of 0.025 eV. The difference is believed to be due to the different way of treating the multiple scattering.

REFERENCES

[1] Beyster, J. R., "Neutron Scattering from Light Water," USAEC Report GA-7608, General Atomic Division, General Dynamics Corporation (January 6, 1967).

[2] Vineyard, G.H., "Multiple Scattering of Neutrons," Physical Review 96 93 (1954).

[3] Lemmel, H. D., Nukleonik 7 (1965) 265.

[4] Honeck, H. C., "MUSE, A Computer Code for Multiple Scattering Corrections," General Atomic Report GA-5968 (October 1, 1964).

[5] Slaggie, E. L., "Multiple Scattering in Neutron Double-Differential Cross-Section Measurements," SM-96/53, these Proceedings I.

[6] Koppel, J. U., "Neutron Scattering by Hydrogeneous Moderators," USAEC Report GA-7055, General Atomic Division, General Dynamics Corporation (March 22, 1966).

[7] Koppel, J. U., et al., "GASKET, A Unified Code for Thermal Neutron Scattering," USAEC Report GA-7417 (Rev.), General Atomic Division, General Dynamics Corporation (March 10, 1967).

[8] Beyster, J. R., et al., "Differential Neutron Scattering from Hydrogeneous Moderators," USAEC Report GA-6245, General Atomic Division, General Dynamics Corporation (March 6, 1965).

[9] Beyster, J. R., et al., "Integral Neutron Thermalization Quarterly Progress Report for the Period Ending March 31, 1966," USAEC Report GA-7091, General Atomic Division, General Dynamics Corporation (April 22, 1966).

[10] Beyster, J. R., et al., "Integral Neutron Thermalization, Quarterly Progress Report for the Period Ending December 31, 1966," USAEC Report GA-7673, General Atomic Division, General Dynamics Corporation (January 25, 1967).

[11] Sprevak, D., Koppel, J. U., and Young, J. A., "Slow Neutron Scattering and Thermalization by Benzene", SM 96/76, these Proceedings I.

[12] Hofmeyr, C., Nukleonik 7 (1965) 286.

DISCUSSION

D. H. DAY: I would like to mention one experimental point. I notice you use a source moderator behind the source. Have you done any experiments to find out how the results differ when the moderator block is put in front of the source? Could you say how the two methods compare for total source strength and time resolution?

G. M. BORGONOVI: We experimented with various slabs of polyethylene of different thickness and in different positions, but found that the best intensity was obtained using an average moderator thickness of about 3 in. We also found it convenient to have this shape of moderator in our case, because on monitoring the surface of the beam we discovered that the profile was rather flat and so we wanted essentially to obtain a concentrated emission from the source.

NEUTRON THERMALIZATION IN DIPHENYL*

J.M. NEILL, H. ANTUNEZ† AND D. SPREVAK‡
GENERAL ATOMIC DIVISION,
GENERAL DYNAMICS CORPORATION,
SAN DIEGO, CALIFORNIA,
UNITED STATES OF AMERICA

Abstract

NEUTRON THERMALIZATION IN DIPHENYL. The organic coolant often considered for certain types of D_2O-moderated reactors usually consists of a mixture of polyphenyls, principally diphenyl and terphenyl. The thermalization in these moderating coolants is not yet well described and a possible treatment has been to use the scattering model by Boffi et al. for benzene, the simplest polyphenyl. More recently a new scattering model for benzene has been formulated by Sprevak. This model is compared here with integral measurements (total cross-section and quasi-infinite medium spectrum) in benzene, and the agreement is found to be very good. In addition, spectral measurements in molten diphenyl are reported. The measurements have been made at the General Atomic LINAC using standard time-of-flight methods. One set of measurements comprised the determination of the quasi-infinite medium spectra in diphenyl as a function of poison concentration. The other set of measurements comprised the spectral variation of the energy-dependent flux across an interface dividing poisoned diphenyl at 80°C from cadmium-poisoned D_2O at the same temperature. The measurements are compared with calculations based on the Sprevak model and comments on their agreement are made.

1. INTRODUCTION

There has been considerable interest in the thermalization of neutrons in diphenyl since it has potentialities as a coolant for nuclear reactors, particularly D_2O-moderated systems. No bound scattering model for diphenyl presently exists, although one is under development.[1] It has been common practice instead to utilize the description of scattering by bound hydrogen in benzene, which is the simplest of the polyphenyls. The scattering model used for benzene heretofore has been that due to Boffi, et al.[2] More recently, Sprevak[3] has developed an improved scattering model for benzene that has been tested predominantly against differential scattering data. It has therefore been appropriate to perform integral checks of Sprevak's model against data from both benzene and diphenyl. In this paper we describe the comparisons of theory to measurements that have been made of the total cross-section of benzene, of the quasi-infinite medium spectrum in benzene and in diphenyl as a function of poison, and of the position-dependent thermal neutron spectra at a D_2O-diphenyl interface. These comparisons have permitted some useful conclusions to be drawn.

2. MEASUREMENTS IN BENZENE

The motivation for studying the total cross-section σ_T of benzene is that σ_T is an integral check of the theoretical scattering kernel for that

* This work was sponsored by the United States Atomic Energy Commission.
† Visitor from Centro Atómico Bariloche, Argentina.
‡ Visitor from U.S.A.I.D.

moderator. Although σ_T is not as sensitive to the details of the scattering kernel as is a spectrum measurement, it can generally be performed with greater precision; moreover σ_T is a property of the material that is independent of geometry, density, or poison additions. The total cross-section of benzene was therefore measured using the geometry illustrated in Fig. 1. A pulsed electron beam from the General Atomic LINAC was made to impinge on a water-cooled target producing a burst of photoneutrons which were quickly thermalized by an adjacent moderator (H_2O tank). The neutrons were timed over the evacuated flight path to their detection by a bank of four BF_3 counters located 18 meters from the target. The neutron spectra were measured with benzene and dummy samples in position. A single measurement was made with a background plug at the sample location but the count rate was negligibly low and the background was not taken for further runs. The intensity of the neutron source for each run was monitored by means of gold foils and various live monitors.

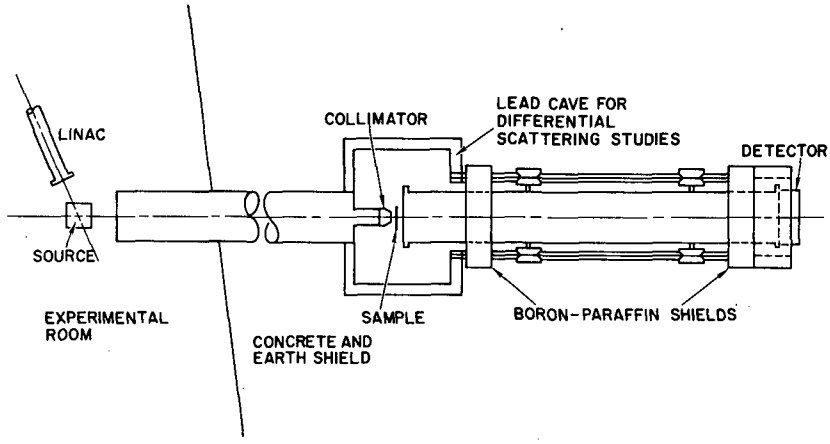

FIG. 1. Experimental arrangement for total cross-section measurements.

The samples consisted of a ring of aluminum covered with a skin of 0.0125 cm thick stretched aluminum foil, and filled with benzene. Three sample thicknesses were used - 0.2265 cm, 0.4906 cm and 0.8168 cm, and two runs were made with each sample. The observed transmissions were corrected for inscattering and multiple scattering using the simple procedures described in Ref. 4. The resulting total cross-sections for each run, weighted according to their statistical uncertainty, were averaged. The average of these measured σ_T is compared to the predictions of the Sprevak model[3] in Fig. 2. The theoretical model has a similar shape and magnitude to the observed data. Some structure in the calculations around 0.15 eV is borne out by the measurements. The theoretical data are consistently lower than the observed data though not by a constant amount or a ratio that would permit speculation on the cause of the discrepancy. The discrepancy is generally larger than the statistical uncertainties in the measurements. Generally, the experiment and theory agree to better than 2-1/2% and thus provide support for the adequacy of the Sprevak model for benzene.

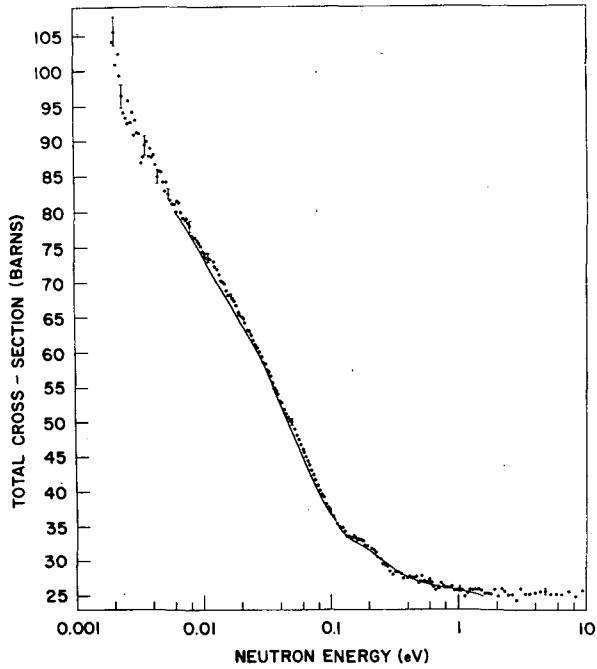

FIG. 2. Comparison of experimental and calculated total cross-sections for benzene.

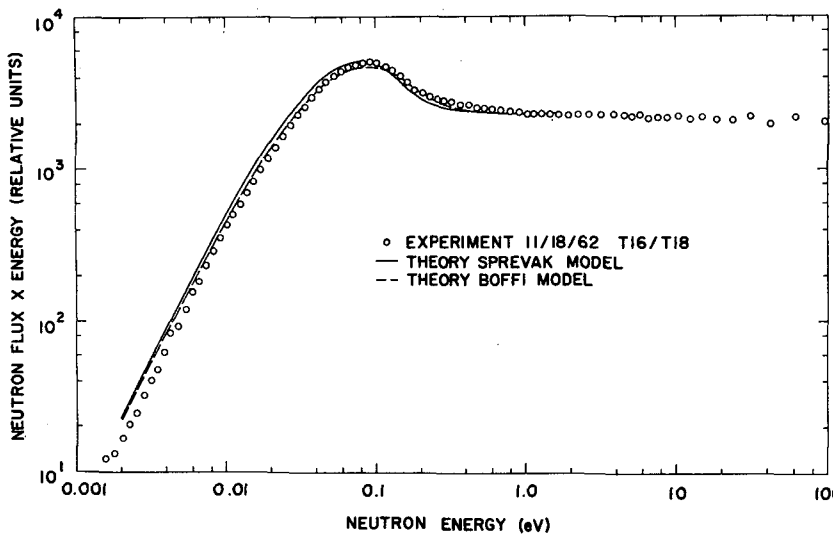

FIG. 3. Comparison of experimental and calculated neutron spectra in benzene (5.9 barns/H atom; infinite medium) $B^2 = 0$.

A further integral check of the Sprevak scattering kernel was made by using it to compute an infinite medium neutron spectrum in benzene poisoned by methyl borate to 5.9 barns/H atom at 2200 m/sec. This spec-

trum was measured and compared previously[5] to the predictions of the Boffi model.[2] The calculations made using the Sprevak model are superimposed on this old comparison in Fig. 3. At first it appears that the new model does not give as good agreement with the measurements as does the Boffi model. This is surprising since the angular scattering cross-sections are better predicted by Sprevak's model. A possible explanation for this discrepancy lies in the different treatments of the hindered rotations and translations. In the Boffi treatment these motions were represented by a Debye spectrum. In the Sprevak treatment these motions were represented by a free gas with an appropriate effective mass. The latter would lead to a calculated softer neutron spectrum. Moreover, no foil measurements in that experimental study in benzene had been performed so that there was no information on the local leakage. Consequently, the local buckling had been taken as zero in the comparative calculation. Thus it is possible that the agreement between the experimental values and the older calculated data in Fig. 3 may have been fortuitous. In spite of this the agreement of the spectrum calculated with the Sprevak model to the measured spectrum is quite reasonable (within ~15%). This provided reasonable confidence for proceeding with thermal spectrum measurements in diphenyl and using this same benzene model for comparative purposes.

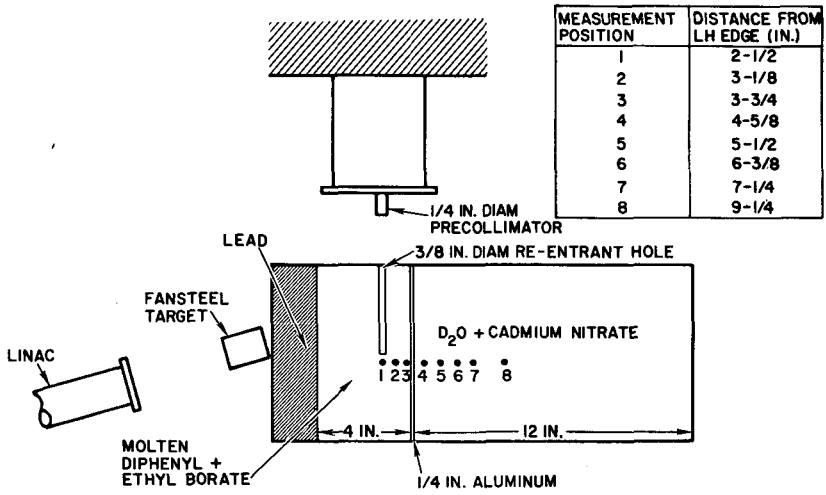

FIG. 4. Geometrical arrangement for spectral measurements at a D_2O-diphenyl interface.

3. MEASUREMENTS IN DIPHENYL

The spectral measurements in diphenyl were performed in a similar fashion to those in benzene that are described in Ref. 5. The procedure is discussed here briefly for the sake of completeness. A pulsed photoneutron source is allowed to excite an assembly of the moderator under study on the other side of a lead shield which serves to spread the incident neutrons. Figure 4 illustrates the general arrangement though it details a later experiment. The fast neutrons slow down

and are extracted from the point of interest via a reentrant hole. The neutrons are timed over a 16-m flight path to their detection by a calibrated bank of 32 BF_3 counters. The counts are analyzed by the TMC 1024 channel data reduction code HECTO.[6] Corrections for background, count rate losses, detector sensitivity, flight path transmission, and mean emission time are made with this code. The mean emission times are computed as the first time moment of the flux by the code GATHER.[7] The buckling for this calculation and also for infinite medium spectral calculations performed by this same code was determined from spatial foil activities. These were measured in each assembly using dysprosium-aluminum- and cadmium-covered indium foils. The diphenyl had to be kept molten since this is the form appropriate for its use as a reactor coolant. This was achieved by strapping electrical heaters to the aluminum tank. A temperature of 80 ± 7°C was maintained.

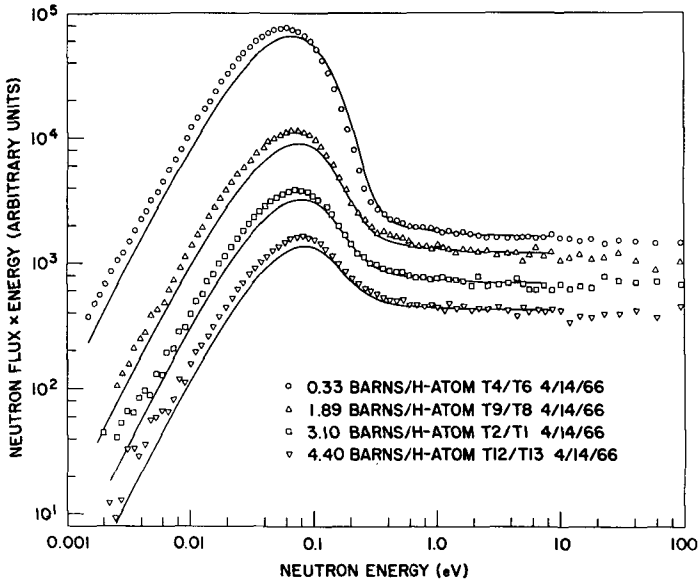

FIG. 5. Neutron spectra in diphenyl at 80°C.

Neutron spectra were measured in a 10 in. x 10 in. x 10 in. tank of diphenyl at various 1/v poison concentrations. The poison was ethyl borate dissolved in the molten diphenyl. The measurements were performed successively with poison being added progressively. The final mixture was analyzed for boron content and was found to agree with the quantity inserted thus confirming the intermediate concentrations. This could have been a problem due to losses of ethyl borate by evaporation (boiling point 120°C).

The neutron spectra are compared in Fig. 5 to the calculations made with the GATHER code in the B_1 approximation using the Sprevak bound scattering kernel for hydrogen in benzene (at 80°C). The agreement is not very good and discrepancies of up to 30% are present. In the past[8] the agreement of measured and calculated spectra in an unpoisoned hydrogenous moderator has not been very good simply because the leak-

age effects which dominate the shape of the thermal spectrum here are not treated properly in the B_1 approximation. The calculated spectrum shows a very strong dependence on B^2 for the unpoisoned case. This dependence is significantly lower for the poisoned systems, yet here the agreement is not much, if at all, better. This stands in contrast to the comparison in benzene alone shown in Fig. 2. It thus seems reasonable to conclude that the discrepancies may be due to the use of the benzene kernel for the calculation of diphenyl spectra.

The disagreement between the measured spectra in diphenyl and the spectrum calculated with the benzene scattering kernel can be discussed in terms of the differences between the benzene[3] and diphenyl[9] frequency spectra. The vibrational frequency spectrum in both diphenyl and benzene can be divided into two frequency zones that are well separated from each other. The high-frequency zone in both moderators comprises a small number of closely spaced frequencies around 0.38 eV. The low-frequency zones in both moderators are similar in that they both end at about 0.22 eV and there are no vibrational frequencies from that point to the high-frequency zone. However, in benzene the average spacing of the frequencies below 0.22 eV is about 0.007 eV and the largest spacing between successive frequencies is 0.025 eV. In diphenyl the average spacing in the same region is about 0.0035 eV and the largest spacing is 0.02 eV. The diphenyl vibrational spectrum also has some low frequencies of about 0.012 eV that are not present in the benzene spectrum, which ends around 0.05 eV. These lower frequencies of the diphenyl favor energy transfers leading to softer neutron spectra. This is consistent with the discrepancies between theory and measurement shown in Fig. 5.

4. MEASUREMENTS AT A DIPHENYL-D_2O INTERFACE

It is clear from the results described in Section 3 that the benzene scattering kernel is not adequate for the computation of thermal neutron spectra in diphenyl. Nevertheless, a diphenyl scattering kernel is being developed[1] and spectral data to check the transport properties of this scattering kernel when available would be useful. Spectrum measurements were therefore made as a function of position at an interface between molten diphenyl and D_2O at the same temperature (80°C). Figure 4 illustrates the geometry of the measurement. The measured flux at 90° to the source assembly axis was extracted from a reentrant tube whose position could be changed. The tank was rotated so that the reentrant tube could be removed without having to empty the contained fluids. The diphenyl was poisoned by ethyl borate to 3.90 barns/H-atom at 2200 m/sec and the D_2O was poisoned by cadmium nitrate to 2.44 barns/D-atom at 2200 m/sec. The spectrum in a homogeneous assembly of the latter poisoned moderator had been measured previously[10] and had agreed well with the theoretical values. Flux plots were made with various foils in the diphenyl and the D_2O to determine the local buckling at the measurement positions and to provide a basis for the calculation of the spatially-dependent slowing down source. Figure 6 illustrates the spatial activities along the source assembly axis. It is evident from this figure that the neutron flux is much more thermal in the diphenyl than it is in the D_2O.

The theoretical angular flux in this system was calculated using the 1DF transport theory code[11] in an S_8 representation. Broad group cross-sections were obtained from the GATHER code.[7] These were

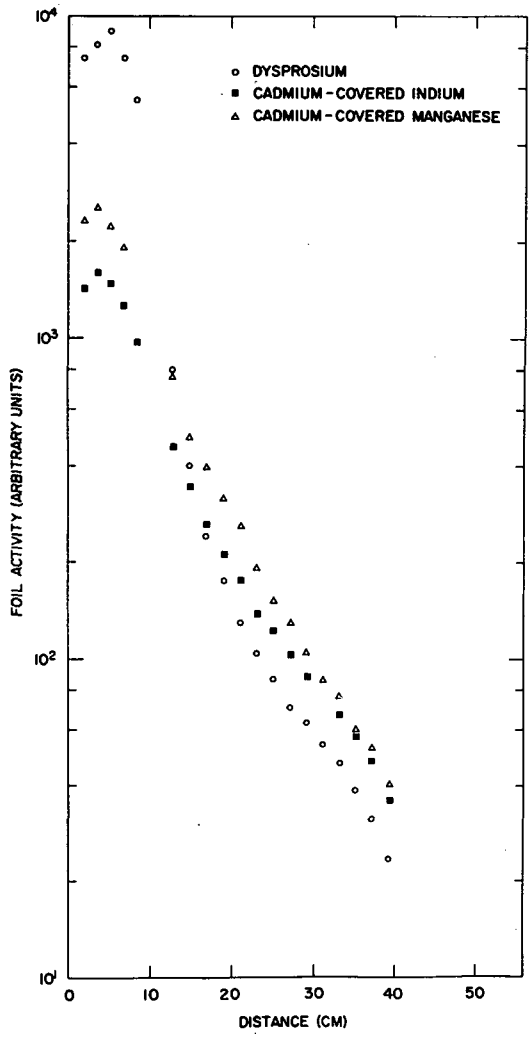

FIG. 6. Spatial distribution of activities along the diphenyl-D_2O assembly axis.

based on the Sprevak[3] model for hydrogen in benzene for the diphenyl and utilized an incoherent scattering model for D_2O based on Haywood's distributed rotational frequency spectrum.[12] A P_0 and P_1 source from the DSZ code[13] was utilized. P_0 and P_1 scattering were considered. The experimental and calculated angular fluxes are compared in Fig. 7. The agreement is not very good but the discrepancies are consistent with the observations made in Section 3. The calculated neutron spectra are

too hard in the diphenyl, and at the interface the peak in the $E\varphi(E)$ display is 40% in error. This error is larger than that observed in the homogeneous studies. The discrepancy gradually lessens as the distance into the D_2O becomes greater until at Position 8, which is the furthest from the interface, the agreement becomes quite fair. This observation is consistent with the aforementioned good agreement between theory and experiment in this poisoned D_2O.[10]

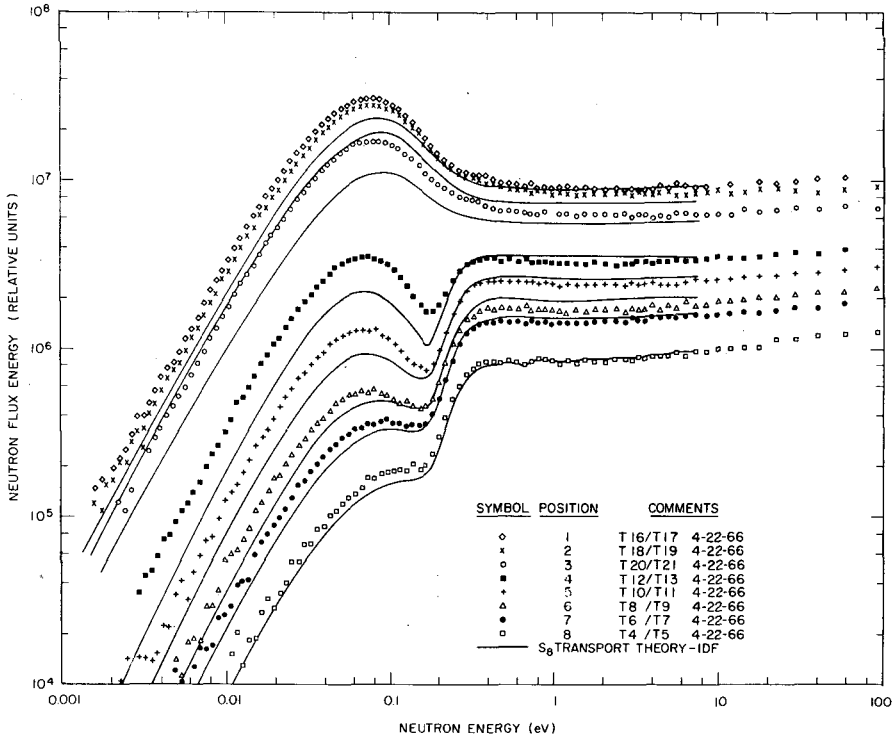

FIG. 7. Neutron spectra in the diphenyl-D_2O assembly at 80°C.

5. CONCLUSIONS

The integral data presented in this paper have demonstrated that the Sprevak model for hydrogen[3] in benzene predicts σ_T and thermal neutron spectra in that moderator reasonably well. The differences between that model and the Boffi model[2] for thermal spectrum calculations are not large. Differential measurements[14] however, strongly support the adequacy of Sprevak's model. Finally the Sprevak model for hydrogen in benzene predicts a thermal neutron spectrum in molten diphenyl that is too hard. This provides motivation for developing a force model and scattering kernel for diphenyl itself.

REFERENCES

[1] BEYSTER, J.R. et al., Integral Neutron Thermalization, Quarterly Progress Report to March 31, 1967, USAEC Rep. GA-7898 (4 April 1967).

[2] BOFFI, V.C., MOLINARI, V.G., PARKS, D.E., Slow Neutron Scattering and Thermalization by Benzene and Other Polyphenyls, Proc. Symp. Neutron Thermalization, Brookhaven, 1962; General Atomic Rep. GA-3024.
[3] SPREVAK, D., KOPPEL, J.U., YOUNG, J.A., Neutron thermalization in benzene, SM-96/76, these Proceedings I; USAEC Rep. GA-7674.
[4] RUSSELL, J.L., Jr., NEILL, J.M., BROWN, J.R., Total Cross Section Measurements of H_2O, USAEC Rep. GA-7581 (Dec. 1966).
[5] YOUNG, J.C. et al., Neutron spectrum measurements in H_2O, CH_2 and C_6H_6, Nucl. Sci. Engng 18 (1964) 376.
[6] NALIBOFF, Y.D., "HECTO", unpublished data.
[7] JOANOU, G.D., SMITH, C.V., VIEWEG, H.A., GATHER-II, An IBM-7090 FORTRAN II Program for the Computation of Thermal Neutron Spectra and Associated Multigroup Cross Sections, General Atomic Rep. GA-4132 (July 1963).
[8] YOUNG, J.C. et al., Neutron thermalization in light water, Nucl. Sci. Engng 28 (1967) 259.
[9] PEREGUDOV, G.V. Optics and Spectroscopy 9 (1960) 155.
[10] YOUNG, J.C., NEILL, J.M., Neutron spectrum measurements in H_2O and D_2O, Nucl. Sci. Engng 23 (1965) 34.
[11] Private communication from B. ROOS to R. DAHLBERG, December 1966; LATHROP, K.P., DTF-IV Code, USAEC Rep. LA-3373 (July 1965).
[12] HAYWOOD, B.C., Pulsed Neutron Research I IAEA, Vienna (1965) 433.
[13] BEYSTER, J.R. et al., Integral Neutron Thermalization, Annual Summary Report through Sept. 30, 1962, USAEC Rep. GA-3542 (1962).
[14] BEYSTER, J.R., BORGONOVI, G.M., CARRIVEAU, G.W., Angular scattering by CH_2, $ZrH_{1.85}$ and C_6H_6, SM-96/75, these Proceedings I.

DISCUSSION

D.H. DAY: Have you made integral measurements of the lateral flux distribution? I feel that by position 1 it may have relaxed to the fundamental mode.

H.M. ANTUNEZ: We have made transverse flux studies with foils in H_2O, and even at smaller distances cosine distributions have been obtained. Anyway, we have used the estimated leakage for the transverse dimensions, and this is incorporated in the calculations.

ANGULAR, SPACE, TEMPERATURE AND TIME DEPENDENCE OF NEUTRON SPECTRA

(Session C)

METHODS CURRENTLY USED TO COMPUTE SPATIALLY DEPENDENT THERMAL NEUTRON SPECTRA

A review

H.C. HONECK*
UNITED STATES ATOMIC ENERGY COMMISSION,
WASHINGTON, D.C.,
UNITED STATES OF AMERICA

Abstract

METHODS CURRENTLY USED TO COMPUTE SPATIALLY DEPENDENT THERMAL NEUTRON SPECTRA: A REVIEW. The methods used to compute the angular and spatial dependence of thermal neutron spectra were reviewed by the author at the BNL Neutron Thermalization Conference in 1962. At that time a wide variety of techniques were being proposed and used. These techniques included discrete ordinate, integral transport, spherical harmonics, and Monte Carlo to describe the spatial and angular behaviour. Treatment of the energy variable included multigroup, overlapping group, and differential equation methods. Unfortunately, in most cases, the methods had not been extensively applied to the calculation of thermal neutron spectra, and it was not possible to comment on their relative advantages or shortcomings.

In the last five years, considerable experience has been gained using these methods, and much more experimental data is now available. The purpose of this paper is to again look at the methods proposed and used in 1962, compile the experience of using them over the past five years, and comment on the relative merits of each method and how well they meet the needs of both the reactor designer and the neutron physicist.

Introduction

Several reviews of the methods for computing spatially dependent thermal spectra have been published during the past five years. Reviews by this author in 1962 [1] and 1963 [2] attempted to classify the theoretical methods which had been developed. A review by Beyster et al.[3] in 1965 described the combined theoretical and experiment aspects of the problem. An excellent review by Pomraning [4] in 1966 presented the basic theoretical considerations in some detail. Another review of this type would serve little purpose since no new methods have been developed. For this reason a different approach will be taken in this review. The purpose here will be to explore those methods which have been implemented as computer codes, and try to assess how well these codes satisfy the needs of the reactor designer and the neutron physicist.

There are, of course, many other aspects of spatially dependent thermal neutron spectra which are both interesting and important, but which will not be discussed here because of limitations on time and

---

* Present address: E.I. du Pont, Savannah River Laboratory, Aiken, South Carolina.

Table I - Thermalization Codes

Number of Spatial Dimensions	Treatment of the Energy Variable						
	Differential Eq.	Overlapping Groups	Multigroup				
			Diffusion Theory	P_n & DP_n	Discrete Ordinate	Integral Transport	Monte Carlo
0	TEMPEST-II [5] KATE-1 [6]					GAHTER-II [7] TAME [8] INCITE [9] SPECTRUM-V [10]	
1	SPECTROX [11] SPM055 [12] SEN143 [12] TERMIDOR [13]	SWAKRAUM [14] TFS [15]	GAZE-II [16] TNS [17]	SLO-P1 [18]	TET [19] ANISN [20] DTF4 [21] WDSN [22] BAM-IV [23]	THERMOS [24] HAMMER [25] GRAFA [26] LASER [27] TONG [28]	
2			GAMBLE-IV [29]		DOT [30]	CLEF [31]	
3							DRAM [32] MARC [33] THERMOPILE [34] SAFE [35] RBU [36]

space. An attempt has been made to include them in an extensive bibliography which has been subdivided in the following way:

[1- 4]	General references
[5-36]	Computer codes
[37-58]	Applications of the codes
[59-69]	The Milne Problem
[70-74]	Temperature Discontinuities
[75-85]	Other references

Several other topics which are related to spatially dependent spectra have been omitted on the grounds that they belong to another session in this Symposium. The most notable are those which concern the approach to equilibrium of a time or space distribution of neutrons.

A paper which tries to review the experience of using certain methods should not be based on the author's experience alone. To gather the experience of others, a brief questionnaire was sent to fifteen U. S. laboratories (time did not permit sending them to other countries). The author is indebted to the following individuals for their helpful replies:

B. R. Sehgal	A. W. Brown	G. R. Dalton
C. W. Lindenmeier	R. A. Grimesey	C. W. Craven
R. C. Liikala	W. A. Wittkopf	J. M. Neill
P. G. Aline	A. J. Goodjohn	R. A. Blaine
E. U. Vaughan	L. B. Levitt	B. J. Toppel
E. M. Pennington	D. H. Shaftman	C. N. Kelber
C. Mills	R. J. LaBauve	J. R. Suich

Thermalization Codes

The first question asked in the survey was "What codes are used in your laboratory for computing thermal neutron spectra?" The results have been compiled in Table I. Some comments on the groupings used in this table are appropriate.

My original idea was to present tables as in [2] giving the name of the code, the installation, the computer, the programming language, number of energy groups, treatment of anisotropy, etc. It soon became clear that there are so many versions of the same code that a detailed table would be meaningless. For example, there is the original BNL version of THERMOS for the IBM 7094, an expanded ANL version for the CDC-3600, a K-7 THERMOS developed in Norway, a Univac 1108 version at BNWL, a WAPD version included in LASER, and ORNL version included in TONG, a BNL-SRL version included in HAMMER, and probably others. For this reason, the classification scheme used in Table I describes only the number of spatial dimensions, the treatment of the energy variable, and the approximation to the transport equation. Even this crude categorization is not unique. I arbitrarily assigned the cross-section generating codes GATHER-II, TAME, INCITE, and SPECTRUM-V to integral transport theory because they do a B_n spectrum calculation. Since Monte Carlo codes are inherently capable of treating three-dimensional geometry, they were put into that category, even though some of the codes may contain simplifying assumptions about the third dimension.

The literature survey uncovered the names of other codes such as SPM055, SEN143, TERMIDOR, TFS, TNS, and CLEF. These were included in the table. Unfortunately, there are probably many other important European codes that have been omitted.

If one compares Table I with the similar table in [2], one discovers that very little has changed in the intervening four years. Many of the new codes are local versions of an older code. For example, TAME, INCITE, and SPECTRUM-V all perform a function similar to GATHER-II. HAMMER, GRAFA, LASER, TONG, AND CLEF are derivaties of THERMOS differing mainly in their treatment of collision probabilities and group structures, GAZE-II, GAMBLE-IV, ANISN, DTF4, and DOT were existing diffusion and transport codes which were modified to include upscattering. The older Monte Carlo code TRAM has been replaced by a newer version DRAM.

Unfortunately, Table I gives no indication of the popularity of the various codes. The survey yielded information on how many laboratories used a particular code, but not how often it is used. The following remarks are then largely my personal opinions.

The development of a particular method or use of a particular code depends on several factors: the reactor concept, the computer available, and whether the laboratory is predominantly research or design oriented. The U. S. and U. K. laboratories have large fast computers available to them and are more design oriented. It is not surprising then that these countries have led the development of multigroup transport theory, diffusion theory, collision probabilities, and Monte Carlo. What little use has been made of differential equations (Wilkins or Wigner-Wilkins) is now largely historical. The trends in the U. S. are toward more energy groups, more spatial detail, and more precise transport descriptions. If any single trend stands out, it is the increased popularity of Monte Carlo methods. These trends are tied very closely to the increases in computer size and speed over the last few years.

Four years ago, the continental European groups were developing analytical (as opposed to numerical) methods using diffusion theory, collision probabilities, and a differential energy operator. This trend continues, but numerical methods are becoming more popular. Groups in Norway and Sweden make extensive use of multigroup collision probabilities. These methods are also popular in Japan.

Typical Applications

The second question asked in the survey was "What are typical applications?" This is an important question to consider, because future developments in the codes and methods will be aimed at solving practical design problems, whereas much of the earlier development was aimed at the understanding of the thermalization problem. There appears to be four classes of applications which I will designate as: the simple lattice, the lattice of clusters, the complex cell, and the multi-zone reactor. A rough sketch of these four configurations is shown in Figure 1.

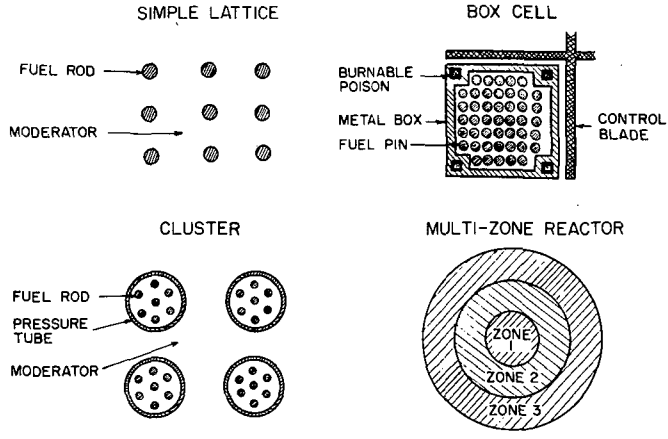

FIG. 1. Four classes of typical applications.

The simple lattice is a regular array of identical fuel rods in a moderator. This problem has been widely investigated and is probably the best understood problem in spatially dependent neutron thermalization theory. The most popular code is THERMOS which is based on multigroup, multi-region collision probabilities in one spatial dimension. A newer code GRAFA is similar to THERMOS but has exact boundary conditions for square and hexagonal lattices. Neither code treats anisotropic scattering in a rigorous manner. Multigroup S_n codes (WDSN, DTF-IV) are also used, but again suffer from approximate boundary conditions. They can, however, treat anisotropic scattering. Monte Carlo codes are capable of an exact treatment of both geometry and anisotropic scattering. In many cases, the treatment of anisotropic scattering has not been fully implemented in the codes.

The lattice of clustered fuel elements is a more complicated problem because there is no resemblance to one-dimensional geometry. Attempts have been made to reduce the problem to that of the simple lattice by homogenization of the cluster into annular rings. This technique has not yet been proven. A promising approach is the CLEF code which computes collision probabilities for the actual cluster geometry. Monte Carlo methods are ideal for this case and are beginning to be used.

The most complex structure that a reactor designer must consider is a box containing fuel pins of differing composition. To further add to the complexity of the problem, there may be lumped burnable poisons in corners of the box, and the space between boxes may contain either water or a control blade. This type of complex structure is of great practical importance and is used in PWR and BWR reactors. A typical procedure is to calculate the fine structure within the box with a THERMOS calculation assuming the fuel pins form an infinite lattice. These results are then used to homogenize regions inside the box. Next, the flux in the box and its vicinity is calculated with a few group, 2-D diffusion or S_n code. The procedure is completed by applying a few experimentally obtained corrections. The Monte Carlo

codes are ideal for this type of geometrically complex cell and are frequently used.

The last application is that of the multi-zone reactor. Within each zone, cell calculations as outlined above are performed and few thermal group cross-sections and transfer matrices are obtained. These are then used in diffusion theory codes such as GAZE-II, GAMBLE-IV, and SLO-P1 to calculate flux and power distributions throughout the reactor. Control elements are usually included at this stage, their effective cross-sections having been obtained by suitable modification of the cell calculational procedures. The overlapping group methods are also useful for multi-zoned reactors since each zone is usually large enough to establish an equilibrium spectrum.

Accuracy, Ease of Use, and Flexibility

The third question asked in the survey was "Do they provide the accuracy, ease of use, and flexibility that you would like?" Let me discuss each of these three topics separately.

Accuracy in the context used here means the ability to predict reaction rate distributions in a reactor. Obviously, this is the most important quantity from a reactor designers viewpoint. It is remarkable that nearly every reply to the questionnaire stated that adequate accuracy was obtained provided that the most sophisticated scattering kernels and codes were used. The implication is that if one used the best scattering kernels in a full Monte Carlo calculation, the predicted reaction rate distributions would be sufficiently accurate for reactor design. For simple geometrical situations, the collision probability and S_n methods are also reported to be sufficiently accurate, although minor discrepancies still exist.

Accuracy of computed spectra in heterogeneous assemblies is often inferred from spectral indices deduced from foil measurements. The interpretation is often difficult (especially since the foil activation cross-sections are not well known). There are still few direct measurements of spectra in lattices, but those that have been made appear to agree well with the calculations. In short, while there is no strong experimental evidence that our spectrum calculations in lattices are correct, there is no strong experimental evidence that they are not correct. In view of our ability to calculate infinite-media spectra, and our ability to solve the transport equation, the above conclusion is not surprising.

There is no consensus on whether the codes are as easy to use as one would like. Generally a code is written for a specific application. When that code is used at another laboratory for another application, it frequently is not easy to use. Several laboratories have linked codes together into larger, automated design codes such as HAMMER, TONG, and LASER. This linking of codes has introduced several new problems which will be discussed in the next section.

Flexibility of the existing codes is also a controversial area. The neutron physicist wants a highly flexible tool; the core designer wants a fast, moderately accurate, special purpose tool; the university professor wants something in between which will run on a small computer.

I would like to summarize this section as follows. We have a good understanding of the physics of spatially dependent neutron thermalization. The attainable accuracy is limited mainly by our knowledge of cross-sections, but these appear to be well enough known for reactor design purposes. Unfortunately, the implementation of the physics in the form of computer codes leaves much to be desired. The fast convenient codes omit too much of the essential physics, and the codes which do contain most of the physics are too slow and often awkward to use. Many of these shortcomings are discussed in detail in the next section.

Shortcomings of the Methods

The last question asked in the survey was "What are the shortcomings of the methods you use, and what would you like to have?" The comments can be divided into the following topics:

1. Data preparation
2. The transition region
3. Leakage calculations
4. Two-dimensional calculations
5. Anistropy treatment
6. Speed versus accuracy

The most frequent complaint is that the preparation of input data for thermalization codes is time-consuming, inconvenient, awkward and inefficient. This complaint is largely directed at the thermal scattering kernels. At the present time one starts with a few ($\sim 10^2$) data (masses, phonon distributions) and generates some 10^5 values of the scattering law which occupy the better part of a magnetic tape. Next, one computes the scattering kernel for a particular energy mesh and again generates some 10^4 values. The kernels are used in a spectrum calculation to obtain a few reaction rates (10^1). Since the trend in the U. S. is to use more groups and more detail, the quantity of data will increase even more. There are two approaches to the problem. Since larger and faster computers are now available, we can make much better use of modern data processing techniques to generate and process these data with a minimum of human intervention. The other approach is to compress these data and retain only the "necessary" part. Approximation of the integral thermalization operator by differential operator is an example of this approach. Unfortunately, much work will have to be done before we understand what the "necessary" part of the scattering kernel really is.

Some cutoff energy is usually selected to separate the thermal and epithermal energy regions. A historical choice is about 0.6 eV, but this now appears to be too low. Thermalization effects occur up to a few eV and a strong Pu-240 resonances lies at 1 eV. Raising the thermal cutoff introduces several problems. Extra energy groups must be added, the number depending on how much detail is desired for the Pu-240 resonance. Adding more groups is not a trivial detail for numerical difficulties occur in generating scattering kernels at high incident energies. A second problem is the coupling of the thermal and epithermal calculations. Most epithermal calculations describe the homogenized cell and cannot provide a suitable spatially-dependent slowing-down source for the thermal calculation. At best one computes

a decent energy distribution for the epithermal flux, but spatial dependence and anisotropy are ignored. Exceptions are HAMMER which provides the spatial dependence of the scalar epithermal flux, and Monte Carlo codes which do not use a thermal cutoff.

Thermal neutron leakage can be treated for homogeneous systems by the B_ℓ method as is done in GATHER-II. It is quite difficult to include leakage in heterogeneous cells. Of particular importance is anisotropic leakage in cells with void or low-density regions. It is possible to calculate directional collision probabilities which then can be used to estimate leakage and its effect on the neutron spectrum. Directional spatial moments of the birth-to-capture distribution can be estimated by Monte Carlo, but the calculation of the effect of leakage on the spectrum is difficult.

Most reactor cells are inherently two-dimensional configurations. Except for computing foil perturbations, it is rarely necessary to consider three dimensions. This is the gray area where it is not clear whether numerical methods (clearly better for 1-D situations) or statistical methods (clearly better for 3-D situations) are better. Collision probability methods work well for simple 2-D configurations (simple cell or cluster) but will doubtlessly be too slow for the complex cells. There is a definite need for a fast and accurate 2-D code.

Anistropic scattering is frequently ignored or treated in a very approximate manner. Even when the code used is capable of a rigorous treatment of anisotropic scattering, a simplified approximation is often used. Part of the difficulty is again the problem of data handling and storage, in this case the data are the large scattering matrices for the higher Legendre moments. The importance of including anisotropic scattering depends strongly on the application. Studies have demonstrated both that it is very important and that it can be completely ignored. It is clear, however, that whenever leakage is an important factor it is necessary to properly account for at least the P_1 component of the scattering matrix.

There is universal agreement that codes should run faster. The matter of speed cannot be dismissed too lightly for the reactor designer is often faced with the choice of running an accurate slow code or a fast approximate code. Increases in speed can be obtained by using a simplified (but still accurate) model, and by improving the numerical methods for a given model. There is a continuing need for work on both approaches. The ideal code would be one with an adjustable speed and accuracy trade-off.

General References

[1] HONECK, H., Thermal neutron spectra in heterogeneous assemblies, Proc. of the Brookhaven Conf. on Neutron Thermalization, Brookhaven National Laboratory Report BNL-719 (1962).

[2] HONECK, H.C., A review of the methods for calculating spatially dependent thermal-neutron spectra, Brookhaven National Laboratory Report BNL-821 (1963).

[3] BEYSTER, J. et al., Neutron thermalization and reactor applications, Proc. 3rd UN Int. Conf. PUAE 5 (1965) 405.

[4] POMRANING, G., "Transport methods for the calculation of spatially dependent thermal spectra", Reactor Physics in the Resonance and Thermal Regions (GOODJOHN, A., POMRANING, G., Eds.), The MIT Press (1966).

Computer Codes

[5] SHUDDE, R., DYER, J., TEMPEST-II, a neutron thermalization code, North American Aviation Report NAA-SR-MEMO-189 (1964).

[6] AMSTER, H., CALLAGHAN, J., KATE-1 a program for calculating Wigner-Wilkins and Maxwellian averaged thermal constants on the Philco-2000, Westinghouse Electric Corporation Report WAPD-TM-232 (1960).

[7] JOANOU, G., SMITH, C., VIEWEG, H., GATHER-II, an IBM 7090 program for the computation of thermal neutron spectra and associated multigroup cross sections, General Atomic Report GA-4132 (1963).

[8] NEUHOLD, R., Introduction to and programming manual for TAME and its service routines, Babcock and Wilcox Report BAW-TM-420 (1965).

[9] CURTIS, R., GRIMESEY, R., INCITE, an IBM 7040 program to generate thermal neutron spectra and multigroup constants using arbitrary scattering kernels, Idaho Nuclear Corporation Report IN-1062 (1967).

[10] SCHLOSSER, J., SPECTRUM V - infinite medium thermal flux spectrum program, General Electric Company Report HW-71953 (1961).

[11] LESLIE, D., The SPECTROX method for thermal spectra in lattice cells, J. Nucl. Energy 17 (1963) 293.

[12] CADILHAC, M. et al., "A simple model for the calculation of neutron spectra in thermal reactors", Reactor Physics in the Resonance and Thermal Regions (GOODJOHN, A., POMRANING, G., Eds.), The MIT Press (1966).

[13] KIND, A., ROSSI, G., "Application of a phenomenological thermalization model to irradiated heavy-water lattices", Reactor Physics in the Resonance and Thermal Regions (GOODJOHN, A., POMRANING, G., Eds.), The MIT Press (1966).

[14] FEDERIGHI, F., RENO, T., SWAKRAUM, a spatially dependent thermal spectrum program for the Philco-2000, General Electric Company Report KAPL-M-6413 (1964).

[15] HEMBD, H., "Determination of the neutron spectrum in a thermal reactor by flux synthesis method", Reactor Physics in the Resonance and Thermal Regions (GOODJOHN, A., POMRANING, G., Eds.), The MIT Press (1966).

[16] LENIHAN, S., GAZE-II, a one-dimensional multi-group neutron diffusion theory code for the IBM 7090, General Atomic Report GA-3152 (1962).

[17] KATSURAGI, S., SAITO, R., TNS - the thermal neutron spectrum in multi-region system, Japanese Atomic Energy Research Institute Report JAERI-1050.

[18] BOHL, H., GELBARD, E., BUERGER, P., CULLPEPPER, G., SLOP-1 a thermal multigroup program for the IBM-704, Westinghouse Electric Corporation Report WAPD-TM-188 (1960).

[19] EDGAR, K., RENO, J., TET, thermal energy transport program, General Electric Company Report KAPL-M-6123 (1964).

[20] ENGLE, W., Jr., A users manual for ANISN, a one-dimensional discrete ordinates code with anisotropic scattering, Oak Ridge National Laboratory Report K-1693 (1967).

[21] LATHROP, K., DTF4, a Fortran-IV program for solving the multigroup transport equation with anisotropic scattering, Los Alamos Scientific Laboratory Report LA-3373 (1965).

[22] FRANCESCON, S., The Winfrith DSN Programme, UKAEA Report AEEW-R273 (1963).

[23] BLAINE, R., BAM IV, Extension and conversion of the BAM code to Fortran IV, Atomics International Report AI-64-MEMO-261 (1964).

[24] HONECK, H.C., THERMOS - a thermalization transport theory code for reactor lattice calculations, Brookhaven National Laboratory Report BNL-5826 (1961).

[25] SUICH, J., HONECK, H., The HAMMER system, E. I. duPont, Savannnah River Laboratory Report DP-1062 (1967).

[26] TAKAHASHI, H. et al., GRAFA, an IBM-7044 FORTRAN IV code for calculation of the neutron spectrum for square and hexagonal lattices, Japanese Atomic Energy Research Institute Report JAERI-1097 (1965).

[27] PONCELET, C., LASER - a depletion program for lattice calculations based on MUFT and THERMOS, Westinghouse Electric Corporation Report WCAP-6073 (1966).

[28] VONDY, D., FOWLER, T., Computer code TONG for zero-dimensional reactor depletion calculation, Oak Ridge National Laboratory Report ORNL-TM-1633.

[29] DORSEY, J., GAMBLE-IV, a program for the solution of the multigroup neutron diffusion equations in two dimensions, General Atomic Report GA-6540 (1965).

[30] MYNATT, F., ENGLE, W., Jr., A users manual for DOT, a two-dimensional discrete ordinates code with anisotropic scattering, Oak Ridge National Laboratory Report K-1694.

[31] JONSSON, A., PEKAREK, H., "Multi-group collision probability theory in cluster geometry - comparison with experiments," Reactor Physics in the Resonance and Thermal Regions (GOODJOHN, A., POMRANING, G., Eds.), The MIT Press (1966).

[32] HABETLER, G., PFEIFFER, R., TUECKE, J., DRAM - a Monte Carlo program for the calculation of capture probabilities, General Electric Company Report KAPL-3013 (1964).

[33] GELBARD, E., ONDIS, H., SPANIER, J., MARC - a multigroup Monte Carlo program for the calculation of capture probabilities, Westinghouse Electric Corporation Report WAPD-TM-273 (1962).

[34] NAKACHE, F., KELLMAN, S., "Operating experience with UNC-THERMOPILE, an advanced Monte Carlo program for the evaluation of thermal assemblies", Reactor Physics in the Resonance and Thermal Regions (GOODJOHN, A., POMRANING, G., Eds.), The MIT Press (1966).

[35] HAUSKNECHT, D., Monte Carlo evaluation of a homogenization procedure for nuclear calculation of a heavy water organic cooled cell, Atomics International Report AI-CE-MEMO-38 (1966).

[36] TRIPPLET, J., MERRILL, E., BURR, J., The RBU reactor-burnup code: formulation and operating procedures, General Electric Company Report HW-70049.

Applications of the Codes

[37] GELBARD, E., "Monte Carlo methods for the calculation of thermal-neutron fluxes", Reactor Physics in the Resonance and Thermal Regions (GOODJOHN, A., POMRANING, G., Eds.), The MIT Press (1966).

[38] BITELLI, G. et al., Analysis of critical experiments with organic moderated assemblies, Nucl. Sci. Engng. 28 (1967) 270.

[39] HONECK, H.C., CRANDALL, J.L., "The physics of heavy water lattices", Reactor Technology, Selected Reviews-1965, USAEC Report TID-8541 (1965).

[40] HONECK. H.C., The calculation of thermal neutron lattice parameters of uranium-water lattices, Nucl. Sci. Engng. 18 (1964) 49.

[41] CROWTHER, R. et al., The physics of non-uniform BWR lattices, Int. Conf. on the Physics Problems in Thermal Reactor Design (1967).

[42] BAER, W. et al., Study of a slightly enriched UO_2 lattice with H:U=0.42 - measurement and analysis, Nucl. Sci. Engng. 23 (1965) 361.

[43] DUNN, F., Flux dipping and peaking in foils used in thermal disadvantage factor measurements, Trans. Am. Nucl. Soc. 9 (1966) 189.

[44] GLICKSTEIN, S. et al., Thermal disadvantage factors and fast advantage factors in uranium-233-thorium seed-blanket assemblies, Trans. Am. Nucl. Soc. 9 (1966) 178.

[45] TASSAN, S., Thermal spectrum measurements in slightly enriched uranium, light-water-moderated lattices, by the Lutetium activation method, Nucl. Sci. Engng. 26 (1966) 271.

[46] SMIT, J., STAM'LER, R., On the variation of the Lu:Dy activation ratio in reactor cells, Nucl. Sci. Engng. 24 (1966) 90.

[47] SALAH, S., PARKINSON, T., Differential and integral thermal-neutron spectra in D_2O-moderated lattices, Nucl. Sci. Engng. 26 (1966) 59.

[48] JOHANSSON, E. et al., Neutron spectra in uranium tubes, Nucl. Sci. Engng. 22 (1965) 157.

[49] JOHANSSON, E., JONSSON, E., LINDBERG, M., Neutron spectra in light or heavy water within a container located inside a uranium tube, Nucl. Sci. Engng. 25 (1966) 21.

[50] JOHANSSON, E., JONSSON, E., The spectrum of the angular neutron flux in a heavy-water natural-uranium lattice, Nucl. Sci. Engng. 25 (1966) 157.

[51] JOHANSSON, E. et al., The neutron spectrum in a UO_2 tube at different temperatures, Nucl. Sci. Engng. 26 (1966) 47.

[52] HAUBERT, P., MEYVAERT, N., "Approximate treatment of neutron thermalization in heterogeneous systems", Reactor Physics in the Resonance and Thermal Regions (GOODJOHN, A., POMRANING, G., Eds.), The MIT Press (1966).

[53] Physics research quarterly report, General Electric Company, Hanford Works Reports HW-81659 (1964), HW-80020 (1964), HW-84600 (1965), HW-77871 (1963), HW-84369 (1964), HW-79977 (1964).

[54] Physics research quarterly report, Battelle Memorial Institute, Pacific Northwest Laboratory Reports BNWL-95 (1965), BNWL-149 (1965), BNWL-284 (1966), BNWL-193 (1965), BNWL-340 (1966).

[55] KIER, P., Slow neutron spectrum studies by neutron activation, Argonne National Laboratory Report ANL-7110 (1965).

[56] KIER, P., TOPPEL, B., JONES, R., Initial critical experiments of the EBWR plutonium recycle program, Trans. Am. Nucl. Soc. 9 (1966) 446.

[57] McWHIRTER, A., GOODJOHN, A., The physics characteristics of the experimental beryllium oxide reactor, General Atomic Report GA-4413 (1965).

[58] WIKNER, N., JAYE, S., Energy dependent and spectrum average thermal cross sections for heavy elements and fission products for various temperatures and C/U-235 atom ratios, General Atomic Report GA-2113 (1965).

The Milne Problem

[59] WILLIAMS, M.M.R., A solution of the thermal-neutron Milne problem by perturbation theory, Nucl. Sci. Engng. 19 (1964) 353.

[60] EISENHAUER, C., Some results on the energy-dependent Milne problem for thermal neutrons and light gases, Nucl. Sci. Engng. 19 (1964) 95.

[61] ANDERSON, C.A., Jr., THOMPSON, J.J., Measurements of leakage - neutron energy spectra, Nucl. Sci. Engng. 18 (1964) 474.

[62] WILLIAMS, M.M.R., The energy-dependent Milne problem with a simple scattering kernel, Nucl. Sci. Engng. 18 (1964) 260.

[63] KLADNIK, R., The asynptotic angular-dependent leakage spectrum of thermal neutrons, Nucl. Sci. Engng. 23 (1965) 291.

[64] WOOD, D.E., Measurement of the angular distribution of thermal neutrons at the surface of cadnium rods, Nucl. Sci. Engng. 21 (1965) 515.

[65] VERBINSKI, V., Angular distribution of low-energy neutrons leaking from various scattering materials, Nucl. Sci. Engng. 27 (1967) 67.

[66] BIGHAM, C.B., Thermal neutron spectra near absorbers, Nucl. Sci. Engng. 21 (1965) 106.

[67] ARKUSZEWSKI, J., Milne problem for thermal neutrons with absorption, Nucl. Sci. Engng. 27 (1967) 104

[68] WILLIAMS, M.M.R., The thermal-neutron Milne problem with a two-term degenerate kernel, Nucl. Sci. Engng. 27 (1967) 511.

[69] KALLFELZ, J., BECKURTS, K., The influence of chemical binding on Milne problem neutron leakage spectra, Nucl. Sci. Engng. 28 (1967) 450

Temperature Discontinuities

[70] BENNETT, R.A., Neutron rethermalization in graphite and water, Nucl. Sci. Engng. 17 (1963) 131

[71] PEARCE, R.M., KENNEDY, J.M., Thermal neutron spectrum in a moderator with a temperature discontinuity, Nucl. Sci. Engng. 19 (1964) 102.

[72] SAASTAMOINEN, J., Thermal-neutron spectrum in water with temperature discontinuity, Nucl. Sci. Engng. 25 (1966) 261.

[73] SEHGAL, B., Neutron thermalization and diffusion in nonisothermal media, Nucl. Sci. Engng. 24 (1966) 212.

[74] BARDES, R. et al., Graphite interface studies - technical report, General Atomic Report GA-5305 (1964).

Other References

[75] SUICH, J.E., HONECK, H.C., Transport-theory calculations of temperature coefficients in heterogeneous reactor lattices, Nucl. Sci. Engng. 20 (1964) 93.

[76] MIKA, J., The thermalization theory with a simple scattering kernel, Nucl. Sci. Engng. 22 (1965) 235.

[77] KUNZE, H., On the theory of space-dependent neutron spectra in heterogeneous reactors, Nucl. Sci. Engng. 15 (1963) 1.

[78] KUNZE, H., On the theory of space-dependent neutron spectra in heterogeneous reactors II, Nucl. Sci. Engng. 23 (1965) 90.

[79] LALETIN, N., Spatial energy distribution of thermal neutrons in a heterogeneous reactor, J. Nucl. Energy 19 (1965) 652.

[80] ROBINSON, A., FERZIGER, J., "An energy-dependent calculation of the disadvantage factor", Reactor Physics in the Resonance and Thermal Regions (GOODJOHN, A., POMRANING, G., Eds.), The MIT Press (1966).

[81] WALKER, J.V., The effects of flux anisotropy on thermal-neutron flux perturbations, Nucl. Sci. Engng. 22 (1965) 94.

[82] STEWART, J.D., The definition of neutron diffusion parameters for a uniform reactor lattice, Nucl. Sci. Engng. 25 (1966) 266.

[83] COPIC, M. et al., Anisotropy of diffusion constant in media with empty channels, Nucl. Sci. Engng. 19 (1964) 74.

[84] PAGE, R., An investigation of neutron streaming using the pulsed neutron source technique, J. Nucl. Energy 21 (1967) 403.

[85] MENDELSON, M., The effect of anisotropic scattering in plane-geometry transport theory and Monte Carlo calculations, Nucl. Sci. Engng. 28 (1967) 127.

DISCUSSION

I. THORSON: What was the criterion used to judge the 'best' scattering law? Is the definition of 'best' dependent on the method of solving the transport equation?

H. C. HONECK: I should point out straightaway that the scattering law has only really been thoroughly tested for light and heavy water and graphite, and so all my comments relate to these few materials. I used 'best' to mean 'most sophisticated'. Only a few highly sophisticated scattering laws have been widely used in the United States of America, and these have been generated by the General Atomic code GASKET.

H. TAKAHASHI: I believe, Dr. Honeck, that you said it was almost impossible to include the anisotropic scattering in the first flight collision probability method. However, this is quite easily done. I have written a code, namded FIRST II, in which the anisotropic scattering is treated by generalized first flight collision probability.

H. C. HONECK: Yes, but I would also point out that in your paper on that very subject you demonstrated that this treatment was not necessary.

D. EMENDÖRFER: Mr. U. A. Schmid from the Stuttgart Technische Hochschule made a comparison of computing times for the first collision theory and the S_N approximation, in the case of a multiregion cell problem. He discovered that the first collision method is faster than the S_N method, if one restricts the problem to dealing with less than 10 to 15 space regions. I might add that in the case of a highly absorbing cell, one needs a fairly high order of S_N approximation ($N \geq 12$), in order to achieve the same accuracy as with the first collision theory.

L. V. MAIOROV: How do you account for the discrepancies between results obtained by the THERMOS programme and by the S_N method?

H. C. HONECK: This is certainly a difficult matter, and the results do show a systematic disagreement in a number of cases. However, by and large, if the input data is identical, the THERMOS and S_N programmes give very close results over a fairly wide range; S_N is much better when the lattice is more dilute and THERMOS when the lattice is highly absorbing.

L. V. MAIOROV: I have compared results obtained in the United States of America by the two methods, and recent studies would seem to indicate that the S_N method is less accurate than that based on the THERMOS programme.

D. EMENDÖRFER: I have here a diagram which may clarify the facts to some extent. It gives the disadvantage factor and the eigenvalue $\lambda = 1/k_\infty$ for a highly absorbing reactor cell, showing that the S_N approximation converges more slowly than the first collision method. It is clear, however, that the S_N value will converge to the best results of the first collision method if the order of the S_N approximation is sufficiently high. (See Fig. 1)

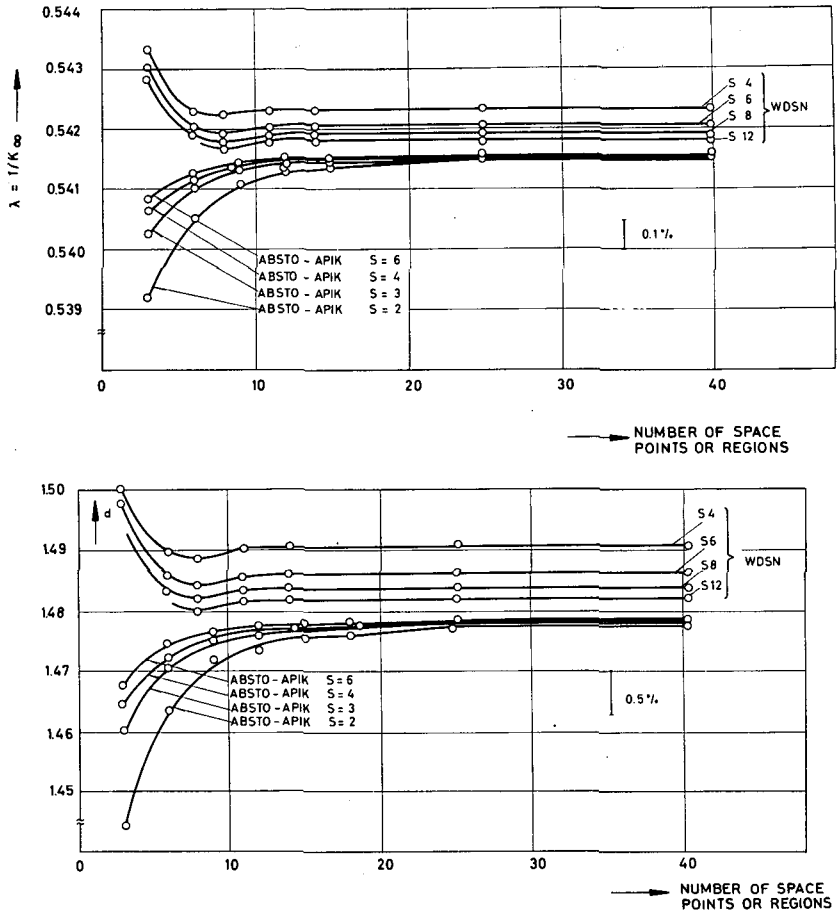

FIG. 1. Convergence of disadvantage factor d and eigenvalue $\lambda = 1/k_\infty$ calculated by means of ABSTO-APIK (first collision theory) and WDSN for a reactor cell.

R. G. JARVIS: You pointed out, Dr. Honeck, and I wrote in my paper[1] too, that one should not abandon one's detailed scattering model at too low an energy, because the spectrum in the region of the lower Pu resonances may still be sensitive to details of the scattering law. You also found that, on the whole, users of the various codes were satisfied with the results. Now, looking at these two statements together, the conclusion would seem to be that the models have not yet been severely tested in lattices containing appreciable amounts of Pu, and that one must be prepared still to consider the details of the scattering kernel in energy ranges up to about 2 or 3 eV.

H. C. HONECK: I quite agree.

J. J. DORNING: Concerning the future development of scattering kernels, to make them more accurate in the eV region for calculating Pu

[1] JARVIS, R.G., SM-96/23, these Proceedings I.

systems, I think that instead of further investigation of the very low energy behaviour, e. g. the diffusive modes in water, more emphasis should perhaps be placed on accurate inclusion of a number of the higher oscillatory modes. GAKER, for instance, treats only the highest oscillator of the Nelkin model exactly, at energies above about 5 eV.

H. C. HONECK: This is a good point. One must be very careful in one's treatment of the oscillators in the electron volt region, but the newer codes, like GASKET, will convolute in the higher oscillators exactly.

D. T. GOLDMAN: Several years ago we made a computational study of exactly how the Nelkin or extended Nelkin model should be treated, in a variety of energy groupings. It turned out that so long as the oscillator energies are sufficiently far apart in relation to the energy mesh chosen, the simpler one-oscillator-at-a-time computational scheme is satisfactory, as it is for water.

IMPORTANCE OF UPSCATTERING IN THE CALCULATION OF NEUTRON SPECTRA *

D. BOLLACASA
UNITED NUCLEAR CORPORATION,
WHITE PLAINS, NEW YORK
AND
D. T. GOLDMAN
NATIONAL BUREAU OF STANDARDS,
WASHINGTON, D.C.,
UNITED STATES OF AMERICA

Abstract

IMPORTANCE OF UPSCATTERING IN THE CALCULATION OF NEUTRON SPECTRA. A study has been made of the effect of raising the thermal energy cut-off higher than 0.625 eV. In most neutron thermalization calculations, the assumption is made that there is no upscattering above 0.625 eV. This may be a poor assumption especially for moderator models with chemically bound hydrogen even at room temperature. In the study, a thermal cut-off energy of 3.06 eV was chosen. This was done because the upscattering above this energy is small and this energy corresponds to that of a group in a slowing-down programme used in the calculations. Neutron spectra and group-averaged cross-sections were computed and the inadequacy of a thermal cut-off of 0.625 eV was manifested by comparisons between calculations at these energy cut-offs. A discontinuity can be observed in joining the thermal and epithermal fluxes at 0.625 eV, while the joining is smooth at 3.06 eV. This provides the possibility of directly normalizing the thermal neutron source to the slowing-down density from the epithermal energy region. Thus, neutron spectra in the thermal and epithermal energy regions can be calculated in one process. Comparisons were made in group constants with no upscattering included between 0.625 and 3.06 eV and with upscattering included up to 3.06 eV. Differences up to 9% were observed. These effects could become significant in the calculation of criticality factors if large resonances were present or if systems with large metal-to-water ratios were considered. A spectrum calculation for a SHA (a small homogeneous assembly) fuel element was compared to a measurement made of its asymptotic spectrum. Even though the agreement between calculation and experiment was not exact, the calculated spectrum closely matched the measured spectrum above 0.625 eV.

I. INTRODUCTION

The equation governing the behaviour of neutrons in a medium is usually called the Boltzmann transport equation. Many solutions of this equation have been proposed, of different complexities and differing orders of generality. For use in reactor assemblies, though by no means limited to these special cases, the domain of the general energy-dependent equation is usually divided into two regions denoted by the terms thermal and epithermal with an energy E_c separating the two. The dividing line, although not always explicitly stated, is the energy above which it is assumed that neutrons undergoing scattering collisions with moderating nuclei do not gain energy. This is the same as considering the target particles at rest relative to incident neutrons with energy greater than

* The work reported in this paper was performed while the authors were employed at Knolls Atomic Power Laboratory.

E_c Reasonable estimates for the value of E_c depend strongly upon the nature of the chemical state of the system, as well as upon the identity of the target particles themselves, and it will be seen that this variation can introduce errors into spectrum calculations.

A study was made of the importance of the inclusion of upscattering in the energy region above 0.625 eV, which is a typical thermal energy cut-off. Neutron spectra and group-averaged cross-sections were calculated using the LINK [1] programme which permits upscattering up to 3.06 eV. LINK is an amalgamation of two separate programmes, MUFT [2] and SWAK [3], with appropriate modifications, and is the basis for the results reported in this paper. In the following sections we begin with the infinite medium diffusion equation which is separated into thermal and epithermal regions. The effective thermal source is calculated and motivation is then provided for a high value of the cut-off energy. The computer programme which calculates the complete neutron spectrum is then briefly described. Typical examples of the calculation of a neutron spectrum for moderation by pure hydrogen, water and polyethylene are presented with emphasis on the thermal energy cut-off region. Finally comparisons with a particular experimental measurement are given.

II. THEORY

The specific problem of neutrons diffusing through an infinite medium was considered in the study. The behaviour of the neutrons can be represented by the following equation

$$\Sigma_t(E)\varphi(E) = \int_0^{E_c} \Sigma_s(E' \to E)\varphi(E')\,dE' + \int_{E_c}^{\infty} \Sigma_s(E' \to E)\varphi(E')\,dE' + S(E) \qquad (1)$$

which can be divided into thermal and epithermal energy regions

$$\Sigma_t(E)\varphi(E) = \int_{E_c}^{\infty} \Sigma_s(E' \to E)\varphi(E')\,dE' + S(E) \quad \text{for } E > E_c \qquad (2)$$

and

$$\Sigma_t(E)\varphi(E) = \int_0^{E_c} \Sigma_s(E' \to E)\varphi(E')\,dE' + \int_{E_c}^{\infty} \Sigma_s(E' \to E)\varphi(E')\,dE' \quad \text{for } E < E_c \qquad (3)$$

where $\Sigma_s(E' \to E)$ is the macroscopic scattering cross-section from energy E' to energy E and Σ_t is the total macroscopic cross-section $\Sigma_t(E) = \Sigma_s(E) + \Sigma_a(E)$. The cut-off energy E_c is chosen as described below, such that the upscattering can be neglected. Thus in Eq.(2) $\Sigma_s(E' \to E)$ is set equal to zero for $E' < E_c < E$ in calculating the spectrum shape and $S(E)$, the fission source, is realistically zero for $E < E_c$. Equation (2) is the prototype of the epithermal equations and Eq.(3) is the equation for the thermal energy region. The second term on the right-hand side of Eq.(3)

is the slowing-down source into the thermal region and its magnitude will be adjusted to conserve neutron balance in the two regions. We rewrite Eq.(3) as:

$$\Sigma_t(E)\,\varphi(E) = \int_0^{E_c} \Sigma_s(E' \to E)\,\varphi(E')\,dE' + \alpha\,S(E) \qquad E < E_c \tag{4}$$

where

$$\alpha\,S(E) = \int_{E_c}^{\infty} \Sigma_s(E' \to E)\,\varphi(E')\,dE' \tag{5}$$

The integral of S(E) over the thermal region is chosen to be unity, i.e.

$$\int_0^{E_c} S(E)\,dE = 1 \tag{5a}$$

and α will be determined so that neutron balance is guaranteed. The total number of neutrons entering the thermal energy region is the integral over E of Eq.(5). To determine the magnitude of α, we examine the number of neutrons slowing down below E_c; we consider the slowing-down density $q(E_c)$, defined as the difference between neutrons scattered from above E_c to below E_c and the neutrons scattered from below E_c to above E_c. An implicit assumption is made here that all neutrons scattered to energies above E_c eventually reappear as source neutrons and that none are absorbed. That is,

$$\begin{aligned} q(E_c) &= \int_0^{E_c} dE \int_{E_c}^{\infty} \Sigma_s(E' \to E)\,\varphi(E')\,dE' - \int_0^{E_c} dE' \int_{E_c}^{\infty} \Sigma_s(E' \to E)\,\varphi(E')\,dE \\ &= \alpha - \int_0^{E_c} \Sigma_s^{up}(E)\,\varphi(E)\,dE \end{aligned} \tag{6}$$

where we have made use of Eqs.(5) and (5a) and

$$\Sigma_s^{up}(E) \equiv \int_{E_c}^{\infty} \Sigma_s(E \to E')\,dE' \qquad E < E_c$$

The calculation of $\Sigma_s^{up}(E)$ under the assumption of scattering from a perfect gas of mass M and temperature $\overline{T}$ is given in the Appendix. $q(E_c)$ can be calculated by means of a slowing-down programme providing that the up-scattering term, the second term of Eq.(6), which is usually ignored in the slowing-down calculation is properly accounted for. The most direct way of achieving this is to extend the cut-off energy to a sufficiently high value so that $\Sigma_s(E \to E')$ for $E' > E$ is effectively zero. An alternative way of proceeding, as suggested by Federighi and Goldman [4], follows from the substitution of α from Eq.(6) into the thermalization

Eq.(4). Thus

$$\Sigma_t(E)\varphi(E) = \int_0^{E_c} \Sigma_s(E' \to E)\varphi(E')\,dE' + S(E)\left[q(E_c) + \int_0^{E_c} \Sigma_s^{up}(E')\varphi(E')\,dE'\right]$$

or

$$\Sigma_t(E)\varphi(E) = \int_0^{E_c} [\Sigma_s(E' \to E) + S(E)\Sigma_s^{up}(E')]\,\varphi(E')\,dE' + S(E)\,q(E_c) \tag{7}$$

Comparing Eqs (7) and (4) we note that if α is set equal to $q(E_c)$, the scattering kernel must be replaced by

$$\Sigma_s(E' \to E) \to \Sigma_s(E' \to E) + S(E)\,\Sigma_s^{up}(E')$$

To show that conservation of neutrons still holds, we integrate Eq.(7) over the thermal energy region and interchange the order of integration

$$\int_0^{E_c} \Sigma_t(E)\varphi(E)\,dE = \int_0^{E_c} dE'\ \varphi(E')\left[\int_0^{E_c} \Sigma_s(E' \to E)\,dE + \Sigma_s^{up}(E')\right] + q(E_c) \tag{8}$$

where we have made use of the normalization of S(E), Eq.(5a). It immediately follows from Eq. (8) that

$$\int_0^{E_c} \Sigma_a(E)\varphi(E)\,dE = q(E_c) \tag{9}$$

'neutron balance', where $\Sigma_t(E) = \Sigma_s(E) + \Sigma_a(E)$. Note, however, that for Eq.(9) to hold, the exact same numerical integration scheme must be used in evaluating $\Sigma_s(E) = \int_0^{\infty} \Sigma_s(E \to E')\,dE'$ as in solving the diffusion Eq.(7). A too small value of E_c, however, distorts the shape of the neutron spectrum.

If upscattering is neglected in computing the slowing-down source then the inhomogeneous term in Eq.(4) will be too large. The neutron flux calculated by a thermalization programme joined to a slowing-down programme will then have the correct shape, but will be too large in magnitude. This result is common to most calculations as is explicitly shown in the analysis reported here.

A measure of the validity of the assumption that there is no up-scattering above E_c can be estimated by examining the total scattering cross-section for the scattering from a mass one gas at an effective temperature $\overline{T}$. We can write the microscopic cross-section as [see Eq.(A.6) of the Appendix]

$$\sigma_s(E) = \sigma_f\left[\left(1 + \frac{\overline{T}}{2E}\right)\operatorname{erf}\sqrt{\frac{E}{\overline{T}}} + \sqrt{\frac{\overline{T}}{\pi E}}\ e^{-E/\overline{T}}\right] \qquad \left(\operatorname{erf} x = \frac{2}{\sqrt{\pi}}\int_0^x e^{-t^2}dt\right) \tag{10}$$

where σ_f is the free hydrogen cross-section. Table I lists values of Eq.(7) in units of free hydrogen cross-section for several effective temperatures with energies corresponding to cut-off energies. The effective temperatures chosen are those of a free gas, for which $T \approx \overline{T}$, and of particular moderator models of water and polyethylene which reduce in the limit of high incident energy to that of the scattering from mass one gas with effective temperatures $\overline{T} = 0.117$ and $\overline{T} = 0.136$, respectively [5]. It is quite evident from this simple display that it is desirable to raise the thermal cut-off to a value higher than $E_c = 0.625$ eV.

TABLE I. THE SCATTERING CROSS-SECTION FROM EQUATION (10) IN UNITS OF σ_f

Moderator	$\overline{T}$	$E_c = 0.625$ eV	$E_c = 3.06$ eV
Free Gas	0.0253	1.020	1.004
Water	0.117	1.094	1.019
Polyethylene	0.136	1.109	1.022

III. CALCULATIONAL METHOD

The Eqs (2) and (3) corresponding to the epithermal and thermal diffusion equations, respectively, can be solved in a variety of ways; however, the nature of $\Sigma_s(E' \to E)$ suggests two standard methods of solution for these two equations. A multigroup structure is usually employed in Eq.(2) and point-by-point values are used in solving Eq.(3). The integrals are replaced by summations. The matrix representing $\Sigma_s(E' \to E)$ in Eq.(2) is triangular, hence the equation can be solved by a recursion formula. The matrix representing $\Sigma_s(E' \to E)$ in Eq.(3) or its generalization in Eq.(7) is a full matrix and an inversion is necessary to obtain the solution.

The programme used to solve Eq.(2) has been described in another report [1, 2]. It makes use of the Greuling-Goertzel approximation to calculate the slowing-down density past each energy group boundary. For the purposes of this work the slowing-down density $q(E_c)$ was calculated and used as the coefficient α for the thermal source (cf. Eqs.(4) and (6)). For simplicity no anisotropic slowing-down source was considered. The source shape can be determined from Eq.(5) by making use of the fact that for hydrogenous moderators the scattering cross-section can be approximated by that of a mass one gas at an effective temperature $\overline{T}$. Then from Eq.(A.4) of the Appendix,

$$\Sigma_s(E' \to E) = \frac{N_s \sigma_f}{E'} \operatorname{erf} \sqrt{\frac{E}{\overline{T}}} \tag{11}$$

for $E' \geq E_c \geq E$, and a mass one target.

Substituting Eq.(11) into Eq.(5), we find

$$S(E) = \int_{E_c}^{\infty} \frac{C_1 \varphi(E')}{E'} \operatorname{erf}\sqrt{\frac{E}{T}}\, dE'$$

or

$$S(E) = C_2 \operatorname{erf}\sqrt{\frac{E}{T}}$$

The value of C_2 is determined from the normalization condition (5a) so that

$$S(E) = \frac{\operatorname{erf}\sqrt{\frac{E}{T}}}{\int_0^{E_c} \operatorname{erf}\sqrt{\frac{E}{T}}\, dE}$$

$$= \operatorname{erf}\sqrt{\frac{E}{T}} \left\{\left(E_c - \frac{T}{2}\right) \operatorname{erf}\sqrt{\frac{E_c}{T}} + \sqrt{\frac{E_c T}{\pi}}\, e^{-E_c/T}\right\}^{-1} \qquad (12)$$

Eq.(12) and the epithermal slowing-down density were used to solve the thermalization equation, appropriately modified to include geometrical buckling. The effect of raising the cut-off energy between thermal and epithermal regions for particular systems is shown in the next section.

IV. CALCULATIONAL RESULTS

A. Group-averaged cross-sections

A series of problems was run using the LINK programme to ascertain whether or not there was any difference in group-averaged constants when upscattering was included up to 3.06 eV and when no upscattering was included from 0.625 eV and 3.06 eV. Three problems were run using a pure moderator only, free hydrogen gas, water and polyethylene. Two problems were run for two different fuel types of SHA, a small homogeneous assembly. The composition of the two SHA fuels is given in Table II. In both cases the buckling was 0.010578. Table III shows the results of the calculations where A means no upscattering from 0.625 eV to 3.06 eV and B means upscattering up to 3.06 eV.

Table III clearly demonstrates that the assumption that there is no upscattering above 0.625 eV may be a poor one but not necessarily a crucial one since for criticality calculations we roughly have

$$k \approx \frac{\nu \Sigma_f}{-DB^2 + \Sigma_a}$$

where k is an effective eigenvalue. There is a noticeable effect in the values of the spectrum-averaged cross-sections, all becoming smaller over the complete (3.06 eV) thermal range for realistic scattering models.

TABLE II. COMPOSITION OF SHA FUELS

Isotopes	Type I, Number density (atoms/barn cm)	Type II, N.
H	0.02555	0.024429
C	0.01235	0.011987
Zr	0.01565	0.015475
U-238	0.835×10^{-5}	0.3703×10^{-4}
O	0.03156	0.032371
U-235	0.1116×10^{-3}	0.51706×10^{-3}
B		0.20425×10^{-4}

TABLE III. COMPARISON OF GROUP-AVERAGED CONSTANTS AT 68°F

	D	Σ_a	Σ_f
I. Free Hydrogen			
A	0.501577	6.86126×10^{-3}	0
B	0.503217	6.895×10^{-3}	0
Difference	+0.3%	+0.5%	
II. Hydrogen in Water			
A	0.48738	6.88022×10^{-3}	0
B	0.47395	6.83994×10^{-3}	0
Difference	-2.6%	-0.6%	
III. Hydrogen in Polyethylene			
A	0.416299	6.78114×10^{-3}	0
B	0.40446	6.75298×10^{-3}	0
Difference	-2.8%	-0.4%	
IV. SHA Fuel Type I			
A	0.385944	0.486442	8.69478×10^{-2}
B	0.3741062	0.475484	8.44676×10^{-2}
Difference	-3.0%	-2.3%	-3.0%
V. SHA Fuel Type II			
A	0.505385	0.131708	0.20835
B	0.462379	0.125404	0.19605
Difference	-9%	-5%	-6%

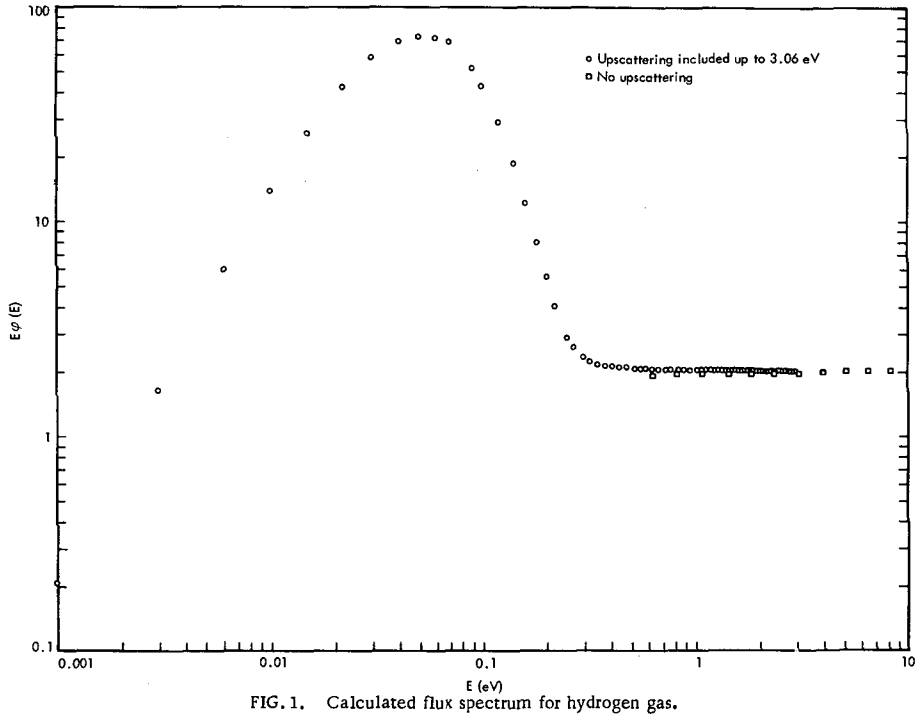

FIG. 1. Calculated flux spectrum for hydrogen gas.

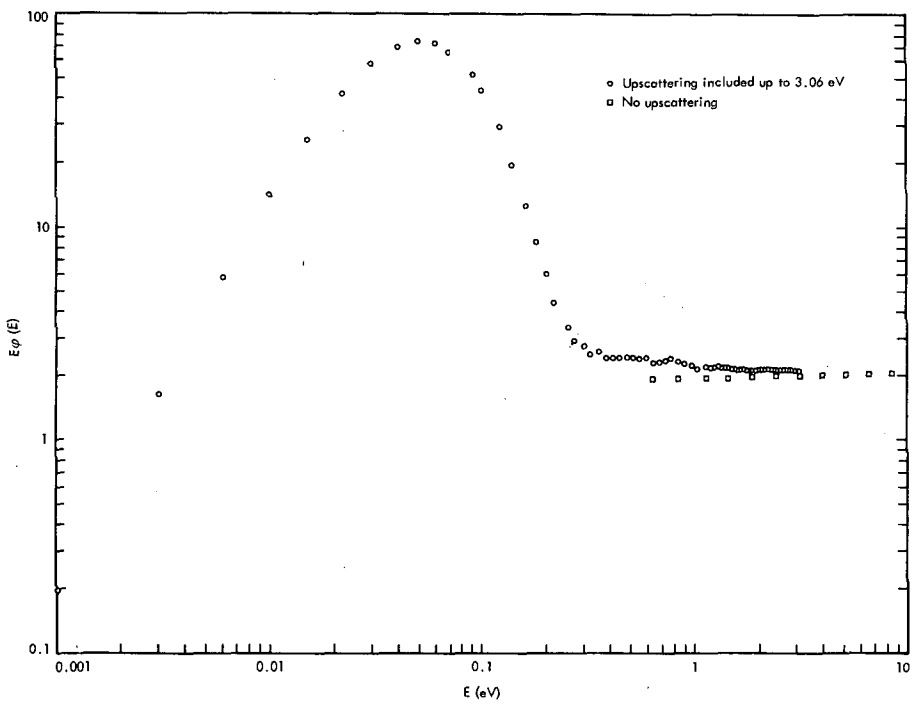

FIG. 2. Calculated flux spectrum for water scattering kernel.

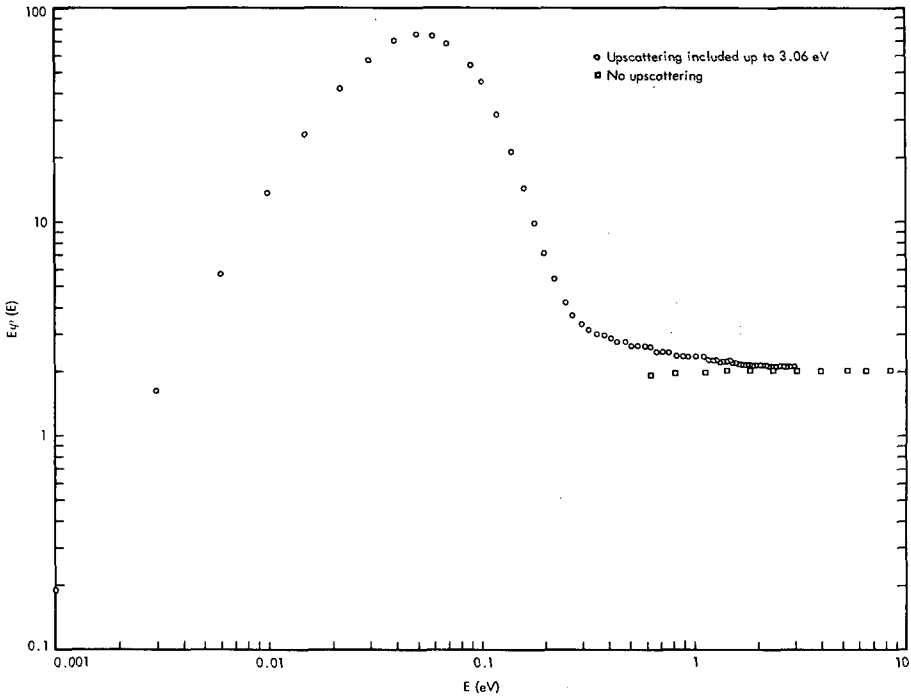

FIG. 3. Calculated flux spectrum for polyethylene scattering kernel.

However, this effect becomes of second order since the change in the averaged cross-sections are always in the same direction and a ratio of two quantities is required as in the calculation of the eigenvalue. Nevertheless, this change may still be significant if large resonances are present in the thermal region, or if the metal-to-water ratio is high.

B. Spectra

The spectra calculated for the five problems described above are reproduced in Figs 1-6. The mismatch of the epithermal flux and the thermal flux at 0.625 eV is evident. Not only are the magnitudes not the same, but also the shape is different. At 3.06 eV the shapes of the thermal and epithermal fluxes are the same. The magnitudes however are not the same partially because of the fact that, as previously mentioned, α has been set equal to $q(E_c)$ throughout these calculations and no correction for the upscattering beyond E_c has been made.

A measurement of the asymptotic spectrum of a SHA Type I fuel element was performed by Cerbone et al. [6]. The results are shown together with the flux calculated by the LINK programme and the agreement is rather good.

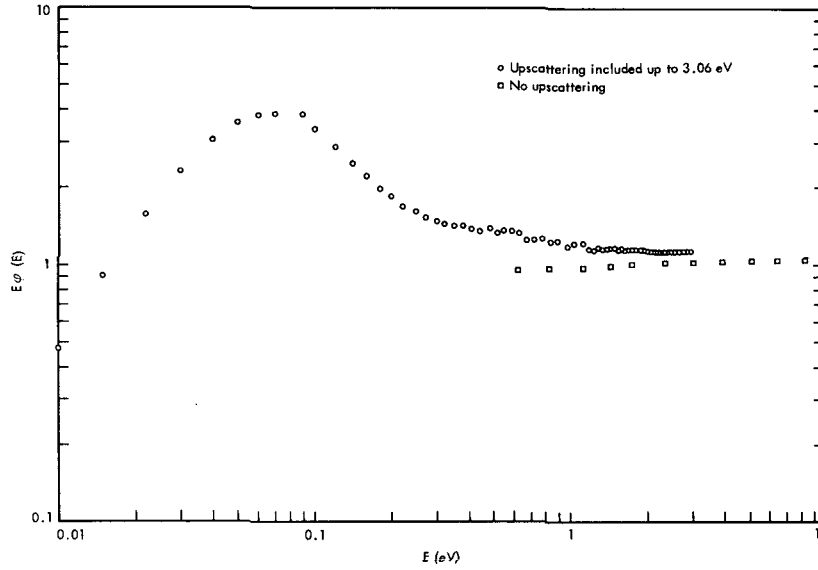

FIG.4. Calculated flux spectrum for old SHA fuel element.

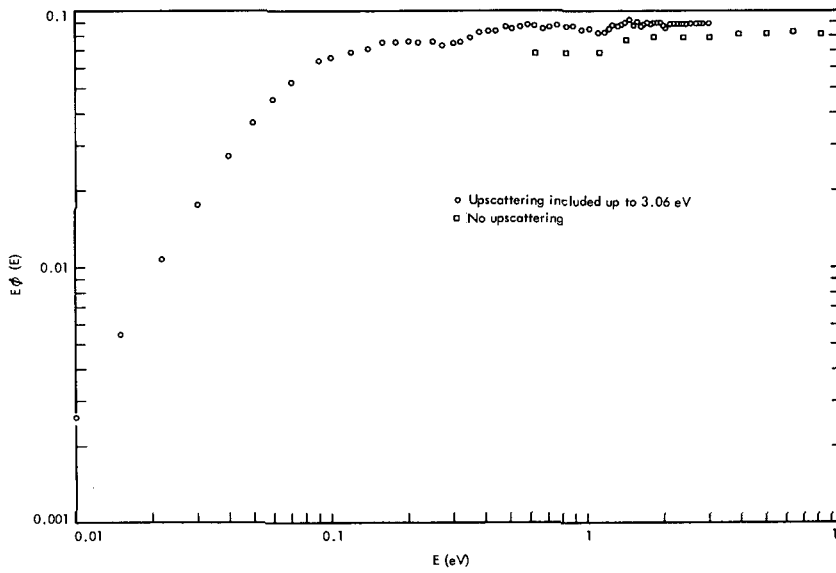

FIG.5. Calculated flux spectrum for new SHA element.

V. CONCLUSIONS

We have demonstrated that to calculate a neutron spectrum from thermal to fission energies subject to the triple conditions of neutron balance, correct spectral shape, and continuity of the spectrum at the

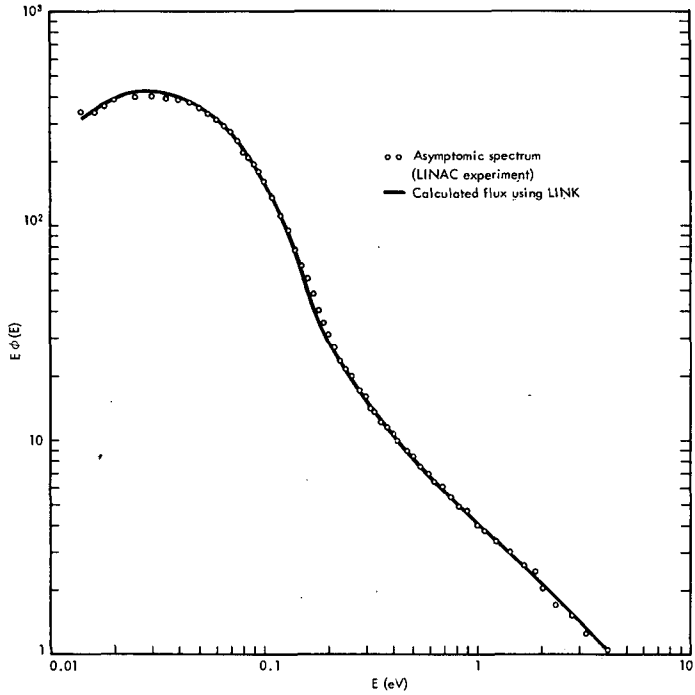

FIG. 6. Calculated and experimental thermal neutron asymptotic flux spectrum.

thermalization slowing-down boundary, it is necessary to use a rather high cut-off energy for realistic moderating materials. At one time this energy might have appeared high relative to the calculational tools available. It would seem that at present with demonstrated capabilities of digital computers in terms of programme storage size and speed of execution of operations one is no longer so limited. It is therefore, possible to perform necessary reactor physics calculations. However, in terms of reactor design calculations, which involve averages of cross-sections and fluxes over rather broad energy bands the case is not so clear. A particular example is the calculation of infinite dilute resonance integrals, for which a simple calculational model appears adequate [7]. It seems that the effect of chemical binding in this intermediate energy region will have to be examined for each particular case subject to appropriate design characteristics and would be expected to be most important when there is large resonance absorption in the region in question.

APPENDIX

CALCULATION OF THE UPSCATTERING CONTRIBUTION TO THE SLOWING-DOWN SOURCE

In section II of the text, the (microscopic) upscattering cross-section is defined as

$$\sigma_s^{up}(E_1) = \int_{E_c}^{\infty} \sigma_s(E_1 \to E_2)\, dE_2 \qquad \text{for } E_1 < E_c \tag{A.1}$$

It is possible to show that realistic models of the scattering cross-section, for large-energy transfers, corresponding to large values of incident energy, reduce to the scattering from a mass M gas at an effective temperature $\overline{T}$ [5]. The integral of interest, however, involves the scattering from an initial energy E_1 to a higher energy E_2. The technique we have used to guarantee that the scattering cross-section possesses the property of conserving detailed balance, involves the calculation of the down-scattering cross-section and evaluating the up-scattering directly from the detailed neutron balance relation,

$$\sigma(E_1 \to E_2) = \frac{E_2}{E_1}\, e^{-\frac{E_2 - E_1}{T}}\, \sigma(E_2 \to E_1) \tag{A.2}$$

where $E_1 < E_2$, and T is room temperature in energy units. We are considering the limit where the energy change is sufficiently large that $\sigma(E_2 \to E_1)$ can be replaced by the scattering cross-section from a perfect gas of mass M at a temperature $\overline{T}$. It is easy to show that the perfect gas scattering cross-section satisfies detailed balance with a temperature $\overline{T}$. Thus

$$\sigma(E_2 \to E_1) = \frac{E_1}{E_2}\, e^{-\frac{E_1 - E_2}{\overline{T}}}\, \sigma_{\overline{T}}(E_1 \to E_2)$$

Substituting this value into Eq. (A.2) one obtains

$$\sigma(E_1 \to E_2) = e^{-(w_2^2 - w_1^2)\gamma}\, \sigma_{\overline{T}}(E_1 \to E_2) \tag{A.3}$$

where

$$w_1 = \sqrt{\frac{E_1}{\overline{T}}}, \qquad w_2 = \sqrt{\frac{E_2}{\overline{T}}}, \qquad \text{and } \gamma = \frac{\overline{T}}{T} - 1$$

$\sigma_{\overline{T}}$ has been referred to often, for example by Kothari and Duggal [8] as

$$\sigma_{\overline{T}}(E_1 \to E_2) = \frac{\sqrt{\pi}\, a^2}{E_1} \frac{M}{m}\, e^{w_1^2} [e^{-w_2^2} I(dw_1 - cw_2) + e^{-w_1^2} I(dw_2 - cw_1)$$

$$- \left| e^{-w_2^2} I(dw_1 + cw_2) - e^{-w_1^2} I(dw_2 + cw_1) \right|] \tag{A.4}$$

where

$$I(x) = \int_0^x e^{-t^2}\,dt, \quad c = \tfrac{1}{2}\left(\sqrt{\frac{M}{m}} - \sqrt{\frac{m}{M}}\right), \quad d = \tfrac{1}{2}\left(\sqrt{\frac{M}{m}} + \sqrt{\frac{m}{M}}\right)$$

and a is the scattering amplitude defined by

$$\sigma_f = \pi a^2$$

where σ_f is the free-atom (high-energy) scattering cross-section.

Instead of immediately evaluating the integral of Eq. (A. 4) substituted into Eq. (A. 3) over energies E_2 between E_c and ∞, we shall for illustrative purposes first perform the integral of Eq. (A. 4) over all energies. We replace

$$\int_0^\infty dE_2 \qquad \text{by} \qquad 2\,\overline{T}\int_0^\infty w_2\,dw_2$$

and divide the integral into two parts:

$$w_2 < w_1 \qquad e^{-w_2^2} I(dw_1 + cw_2) > e^{-w_1^2} I(dw_2 + cw_1)$$

and $w_2 > w_1$ where the reverse is true.

We divide the total integral into $2\,\overline{T}\,\frac{\sqrt{\pi}\,a^2}{E_1}\,\frac{M}{m}\,e^{w_1^2}$ multiplied by the sum of four separate integrals:

$$A = \int_0^{w_1} w_2\,dw_2\,e^{-w_2^2}[I(dw_1 - cw_2) - I(dw_1 + cw_2)]$$

$$B = e^{-w_1^2}\int_0^{w_1} w_2\,dw_2\,[I(dw_2 - cw_1) + I(dw_2 + cw_1)]$$

$$C = \int_{w_1}^\infty w_2\,dw_2\,e^{-w_2^2}[I(dw_1 - cw_2) + I(dw_1 + cw_2)]$$

$$D = e^{-w_1^2}\int_w^\infty w_2\,dw_2[I(dw_2 - cw_1) - I(dw_2 + cw_1)]$$

After a fair amount of mathematical manipulation, we find

$$A = \tfrac{1}{2}\,e^{-w_1^2}\left[-I\left(\sqrt{\frac{m}{M}}\,w_1\right) + I\left(\sqrt{\frac{M}{m}}\,w_1\right)\right] - \frac{c}{2d}\,e^{-w_1^2}\left[I\left(\sqrt{\frac{m}{M}}\,w_1\right) + I\left(\sqrt{\frac{M}{m}}\,w_1\right)\right]$$

$$B = \frac{w_1^2}{2}\,e^{-w_1^2}\left[I\left(\sqrt{\frac{m}{M}}\,w_1\right) + I\left(\sqrt{\frac{M}{m}}\,w_1\right)\right] - \frac{e^{-w_1^2}}{4d^2}\left[I\left(\sqrt{\frac{m}{M}}\,w_1\right)\right.$$

$$+ I\left(\sqrt{\frac{M}{m}}\, w_1\right) - (d+c)\, w_1\, e^{-(d-c)^2 w_1^2} - (d-c)\, w_1 e^{-(d+c)^2 w_1^2} + 2c^2 w_1^2 I\left(\sqrt{\frac{M}{m}}\, w_1\right)$$

$$+ 2\, c^2 w_1^2 I\left(\sqrt{\frac{m}{M}}\, w_1\right)\Bigg]$$

$$C = \frac{e^{-w_1^2}}{2}\left[I\left(\sqrt{\frac{m}{M}}\, w_1\right) + I\left(\sqrt{\frac{M}{m}}\, w_1\right)\right] + \frac{c}{2d}\, e^{-w_1^2}\left[I\left(\sqrt{\frac{m}{M}}\, w_1\right) - I\left(\sqrt{\frac{M}{m}}\, w_1\right)\right]$$

$$D = -\frac{w_1^2}{2}\, e^{-w_1^2}\left[I\left(\sqrt{\frac{m}{M}}\, w_1\right) - I\left(\sqrt{\frac{M}{m}}\, w_1\right)\right] - \frac{e^{-w_1^2}}{4d^2}\Bigg\{\Bigg[I\left(\sqrt{\frac{M}{m}}\, w_1\right)$$

$$- I\left(\sqrt{\frac{m}{M}}\, w_1\right)\Bigg](1 + 2\, c^2 w_1^2) + (d+c)\, w_1\, e^{-(d-c)^2 w_1^2} - (d-c)\, w_1 e^{-(d+c)^2 w_1^2}\Bigg\}$$

Adding A + B + C + D, and making use of the relationship that

$$2\, d^2 = \tfrac{1}{2}\, \frac{M}{m}\left(1 + \frac{m}{M}\right)^2$$

we find the scattering cross-section from a gas to be

$$\sigma_s(E_1) = \frac{4\pi\, a^2}{\sqrt{\pi}\, \beta^2 \left(1 + \frac{m}{M}\right)^2}\left[\beta\, e^{-\beta^2} + (1 + 2\beta^2)\, I(\beta)\right] \tag{A.5}$$

where

$$\beta^2 = \frac{M}{m}\, w_1^2 = \frac{M}{m}\, \frac{E_1}{\bar{T}}$$

or

$$\sigma_s(E_1) = \sigma_f\left[\left(1 + \frac{\bar{T}}{2E_1}\right) \operatorname{erf}\sqrt{\frac{E_1}{\bar{T}}} + \sqrt{\frac{\bar{T}}{\pi E_1}}\, e^{-E_1/\bar{T}}\right] \tag{A.6}$$

The integral we wish to perform is, from Eqs. (A. 1) and (A. 3)

$$\sigma^{up}(E_1) = e^{w_1^2 \gamma} \int_{E_c}^{\infty} e^{-w_2^2 \gamma}\, \sigma_{\bar{T}}(E_1 \to E_2)\, dE_2 \qquad E_1 < E_c \tag{A.7}$$

This can be calculated in a straightforward manner using the fact that we require $E_1 < E_c$, which implies $E_1 < E_2$. We can make use of the calculation of the integrals C and D given above with the lower limit replaced by $w_1 \to \sqrt{E_c/\bar{T}}$. The integrals A and B, for which $E_2 < E_1$, do not

contribute to this calculation. We find

$$C' = \frac{e^{w_1^2\gamma}}{2(1+\gamma)} \left\{ e^{-\frac{E_c}{\overline{T}}(1+\gamma)} \left[I\left(dw_1 - c\sqrt{\frac{E_c}{\overline{T}}}\right) + I\left(dw_1 + c\sqrt{\frac{E_c}{\overline{T}}}\right)\right] \right.$$

$$\left. + \frac{c\, e^{-w_1^2 d^2 \left[1 - \frac{c^2}{d^2+\gamma}\right]}}{\sqrt{d^2+\gamma}} \left[I\left(\sqrt{(d^2+\gamma)\frac{E_c}{\overline{T}}} - \frac{c\,d\,w_1}{\sqrt{d^2+\gamma}}\right) - I\left(\sqrt{(d^2+\gamma)\frac{E_c}{\overline{T}}} + \frac{c d w_1}{\sqrt{d^2+\gamma}}\right)\right]\right\}$$

$$D' = e^{-w_1^2(1-\gamma)} \left\{ e^{-\frac{E_c}{\overline{T}}\gamma} \left[I\left(d\sqrt{\frac{E_c}{\overline{T}}} - cw_1\right) - I\left(d\sqrt{\frac{E_c}{\overline{T}}} + c\,w_1\right)\right] \right.$$

$$\left. + \frac{d e^{-c^2 w_1^2 \left[1 - \frac{d^2}{d^2+\gamma}\right]}}{\sqrt{d^2+\gamma}} \left[-I\left(\sqrt{(d^2+\gamma)\frac{E_c}{\overline{T}}} - \frac{c\,d\,w_1}{\sqrt{d^2+\gamma}}\right) + I\left(\sqrt{(d^2+\gamma)\frac{E_c}{\overline{T}}} + \frac{c\,d\,w_1}{\sqrt{d^2+\gamma}}\right)\right]\right\}$$

and the upscattering integral is

$$\frac{2\overline{T}\sqrt{\pi}\,a^2}{E_1} \frac{M}{m} e^{E_1/\overline{T}}$$

multiplied by the sum of C' and D'. The resulting equation is rather complicated to write explicitly. Instead of doing this explicitly we shall consider the special case of $m = M = 1$, which applies for the high-energy transfer limit of scattering from hydrogenous materials. Here $d = 1$, $c = 0$ and an especially simple result occurs

$$\sigma_s^{up}(E_1) = \int_{E_c}^{\infty} \sigma(E_1 \to E_2)\, dE_2$$

$$= \frac{2\overline{T}\sqrt{\pi}\,a^2}{E_1(1+\gamma)} e^{(1+\gamma)\frac{E_1 - E_c}{\overline{T}}} I\left(\sqrt{\frac{E_1}{\overline{T}}}\right)_{\substack{M=m=1 \\ E_1 < E_c}} \qquad (A.8)$$

We re-examine Eq.(A.4) for $m = M = 1$ and $E_1 < E_2 = E_c$, and compare the resulting equation with Eq.(A.8). It is possible to write

$$\sigma_s^{up}(E_1) = \frac{\overline{T}}{1+\gamma}\left[\sigma_{\overline{T}}(E_1 \to E_c)\right]$$

$$= \overline{T}\,\sigma_{\overline{T}}(E_1 \to E_c) \qquad (A.9)$$

where $\sigma_{\overline{T}}(E_1 \to E_c)$ is calculated by Eq.(A.4). In fact since, for terms near the diagonal of the scattering matrix, the gas at an effective temperature approximation may not be valid, it is more correct to use the actual $\sigma_{\overline{T}}(E_1 \to E_c)$ value calculated by the KERNEL [9] programme, for example, and multiply by $\overline{T}$ to evaluate the upscattering cross-section for inclusion with the scattering kernel to arrive at an effective kernel.

REFERENCES

[1] BOLLACASA, D., GOLDMAN, D.T., LINK - a combined slowing-down and thermalization program with a thermal cutoff of 3.06 eV, Rep. KAPL-3098 (1965).
[2] BOHL, H., Jr., HEMPHILL, A.P., MUFT-5 - a fast neutron spectrum program for the Philo-2000, Rep. WAPD-TM-218 (Feb. 1961). A FORTRAN version of this program, written by REITER, R.A., was utilized.
[3] FEDERIGHI, F.D., RENO, T.J., Jr., SWAK, a thermal cross-section program, Rep. KAPL-M-6145 (April 1964).
[4] FEDERIGHI, F.D., GOLDMAN, D.T., The slowing down source into thermal flux calculations is not quite the slowing down density, Rep. KAPL-M-6471 (April 1965).
[5] GOLDMAN, D.T., FEDERIGHI, F.D., Nucl. Sci. Engng 16 (1963) 165.
[6] CERBONE, R.J., SLOVACEK, R.E., GAERTTNER, E.R., Trans. Am. nucl. Soc. 10 (1967) 291.
[7] HARDY, J., Jr., Nucl. Sci. Engng 27 (1967) 135.
[8] KOTHARI, L.S., DUGGAL, V.P., Adv. nucl. Sci. Technol. 2 (1964) 186.
[9] FEDERIGHI, F.D., GOLDMAN, D.T., KERNEL and PAM, programs for use in the calculation of the thermal scattering matrix for chemically bound systems, Rep. KAPL-2225 (1962).

DISCUSSION

M. N. MOORE: I note that in your calculation upscattering contributed significantly at an energy as high as 3 eV (120 kT). Several years ago, in a paper by Vaughan, Cohen and myself, we considered the problem of thermalization in a heavy-gas moderator with an absorption resonance lying at an energy higher than kT. We evaluated the effect of upscattering by investigating the resonance escape probability, with and without thermalization, and found that if the resonance lay at 20 kT upscattering contributed 8% to the resonance integral. In view of this, I am surprised that you find noticeable effects at an energy six times higher than ours.

D. T. GOLDMAN: As co-author of the paper, I should like to reply to this point, and here again the answer hinges on the concept of effective temperature, $\overline{T}$. Since $\overline{T}$ is approximately 6 T for the bound hydrogen models considered in this paper, Dr. Moore's question should be reformulated in terms of this quantity. Then, an examination of the results presented in our paper will reveal that they are completely consistent with the heavy-mass results of Cohen, Moore and Vaughan, which show that the upscattering still produces an effect above about 20 $\overline{T}$. I can only stress that the effective temperature, rather than the ambient temperature, must be used here.

A. P. C. KIND: A year ago we were faced with the problem of evaluating ^{240}Pu resonance absorption in different types of reactor. We did a systematic analysis with an accurate numerical programme – I no longer remember which it was – and came to the conclusion that the upscattering does not need to be taken into account in the case of heavy-water reactors, but that its effect is quite important for high-temperature graphite reactors.

L. V. MAIOROV: Earlier work by Corngold does much to facilitate estimation of the thermal region correction, and I wonder whether the authors of the paper have compared their results with Corngold's predictions.

D. BOLLACASA: No, we have not made that comparison.

L. V. MAIOROV: It seems to me that shifting the thermal neutron boundary towards higher energies should not substantially worsen the

spectrum calculations in complex systems. This is bound up with the fact that the usual methods for solving the kinetic equation for thermal neutrons are basically iterative. Since, as a rule, iterations involve a quantity of neutrons having undergone one, two, three or more collisions, and in this thermal region the probability of upscattering is small, the number of iterations which have to be made in order to calculate slow neutron scattering at energies higher than 0.3 eV must be two, three, four, etc. Therefore, once the number of neutrons undergoing two or three collisions with upscattering of the higher region has been calculated, the thermal group boundary can be shifted again to 0.6. This is one possibility; another is as follows: the spectrum in the region of 0.6 eV and above can be readily approximated with the linear or square function of inverse powers of the energy. This then means that one or two, but not more, groups are added when the neutron scattering calculation is attempted in this large region.

D. BOLLACASA: I maintain that it follows from our paper that one just cannot forget about the upscattering in the region above 0.625 eV.

M. LIVOLANT: The upscattering in the flux derives from two phenomena: energy increase due to thermal agitation, and decrease in the slowing-down efficiency due to the effect of interatomic binding. For moderators such as water and graphite the second effect is predominant. Therefore, the effect calculated in this paper is not an energy increase effect alone, except in the case of hydrogen gas, but a mixture of this and the other component I have mentioned. Would you care to comment on this, please?

D. T. GOLDMAN: Perhaps I might again answer this point. In the high-energy transfer limit, the effect on neutron inelastic scattering by the intramolecular binding of the target particle appears to be the same as that of the scattering of the incident particle by a target consisting of a gas at an effective temperature. On this basis we estimated the contribution of the upscattering to the source from the epithermal region. The higher the incident energy, the more likely it is that a larger amount of energy in relation to the highest optical level of the system will be transferred. For the spectrum calculation in the thermal region, Dr. Bollacasa and I used the scattering kernel calculated from the model.

INTEGRAL AND ANGULAR CHARACTERISTICS OF THERMAL NEUTRON LEAKAGE SPECTRA

J.M. KALLFELZ
GEORGIA INSTITUTE OF TECHNOLOGY,
ATLANTA, GEORGIA
and
R. KLADNIK*
KANSAS STATE UNIVERSITY,
MANHATTAN, KANSAS,
UNITED STATES OF AMERICA

Abstract

INTEGRAL AND ANGULAR CHARACTERISTICS OF THERMAL NEUTRON LEAKAGE SPECTRA. The energy-dependent Milne problem for thermal neutrons has been investigated with increased experimental accuracy and more advanced theory in the past several years. Based on previously reported calculations and experiments of the authors and others, certain aspects of the Milne problem for a non-absorbing medium are sufficiently understood that semi-empirical expressions can be given for the dependence of various quantities. This paper gives the development of such expressions. Furthermore, a variational-iterative method used by the authors and others to solve the Milne problem is described briefly, and a further improvement to earlier solutions is given.

Simple semi-empirical expressions are given for the average energy of the angular-dependent leakage spectra (energy distribution of neutrons leaking from the moderator surface into the vacuum) which depend on the value of the second energy-exchange moment (M_2) of the scattering kernel, and on the space-asymptotic solution. The change near the moderator surface in the average energy of the current can also be described by a simple expression involving M_2. Since the space-asymptotic solutions are easy to obtain numerically, this provides a simple method for calculating approximately the average energies of the leakage spectra and current. The validity of the semi-empirical expressions is supported by showing qualitatively through the transport equation that the dependence on M_2 is to be expected.

Calculations were made for realistic scattering kernels for H_2O, benzene, Dowtherm A, and $ZrH_{1.7}$, as well as for the free gas and Corngold separable scattering kernels. Agreement with the experimental results available (primarily for H_2O) is good.

1. INTRODUCTION

The energy-dependent Milne problem for thermal neutrons has been the subject of many theoretical and experimental investigations in the past few years. Theoretical studies with simple scattering kernels yielded much qualitative information on the neutron spectrum [1-6]. Calculations with more realistic scattering kernels [7-10] agree satisfactorily with the experimental results available [11-13].

Due to the increased amount of experimental information available and the improved accuracy of the theoretical solutions, certain aspects of the Milne problem are becoming well understood. Using the variational-iterative method described by the authors and others in [1] and [8], calculations were made for four realistic scattering kernels representing hydrogenous moderators, and for several simplified scattering kernels which had scattering cross-sections similar to those of hydrogenous moderators [8]. Based on the results of these calculations, semi-empirical expressions can be determined for the behavior of the angular dependence

* On leave from the University of Ljubljana, Yugoslavia.

of the leakage spectra average energy, and for the average energy of the leakage current. These values are related through the second energy-exchange moment, M_2, to those of the space-asymptotic solution, which is easy to calculate.

Section 2 describes briefly the method used in [8], and discusses an improvement made to this solution. Section 3 gives the determination of the semi-empirical expressions. Section 4 supports the validity of these expressions by showing qualitatively through the transport equation that the dependence on M_2 is to be expected.

2. METHOD OF SOLUTION

The method of solution is discussed in [1] and [8] . The notation of [8] is used here. The transport equation for the absorption-free Milne problem has the form

$$\left[\mu \frac{\partial}{\partial x} + \Sigma_s(E)\right] \phi(x,E,\mu) = \int_0^\infty \int_{-1}^{1} \Sigma(E',\mu' \to E,\mu)\, \phi(x,E',\mu')\, dE'\, d\mu' \tag{1}$$

where μ is the cosine of the angle between the positive x-axis and the neutron velocity vector. The moderator is in the half-space $x > 0$.

The solution for $\Phi(x,E,\mu)$ is obtained using the spatial asymptotic solution

$$\phi_{as}(x,E,\mu) = C \cdot M(E)\left[x + x_0 - \mu U(E)\right] \tag{2}$$

x_0 is the extrapolated endpoint, and U(E) is a function defined in [1], which is approximately equal to $\lambda_{tr}(E)$. The entire solution is written in the form

$$\phi(x,E,\mu) = C \cdot M(E)\left[x - \mu U(E) + q(x,E,\mu)\right] \tag{3}$$

where M(E) is the Maxwellian flux distribution, and $q(x,E,\mu)$ is a function which describes the effect of the surface on the solution. An integral equation is obtained for $q(x,E,\mu)$ using the integral form of the transport equation. An approximate solution to this equation is obtained using a trial function with parameters determined by a variation method. The accuracy of the solution for $q(x,E,\mu)$ is improved by several iterations in its defining equation. The form of the trial function used in [8] was[1]

$$q_{20}(x,E,\mu) = b_1 - \left[b_2 + b_3 \mu U(E) + b_4 U(E)\right] e^{-x/l_s} \tag{4}$$

where l_s is the high-energy limit for the scattering mean free path, $l_s(E)$, and b_i are the variational parameters. The use of l_s as the relaxation length was rather arbitrary, but the solution was improved by two iterations. In [8] , results are given for the program IMALS, which calculates leakage spectra using equation (3), with $q_{22}(0,E,\mu)$, the second iteration of the trial function given in Eq. (4). Various comparisons are made to support the accuracy of this solution.

---

[1]The trial function is designated by q_{mj}, where m refers to the form of the trial function, and j designates the number of iterations in the defining equation.

It was desired to improve this solution further by changing the value for the relaxation length. This form of spatial dependence of the transient flux is, of course, only a rough approximation; the actual dependence is not expected to be exponential [6,10] . However, there should be a value of the relaxation length which describes the spatial dependence reasonably well in the range near x = 0, where the transient flux is most important.

In a previous paper [14] one of the authors has shown that for the monokinetic case better agreement is obtained with exact values using a relaxation length of 0.3 l_s.

To investigate the influence of this relaxation length on the IMALS results, the following trial function was used:

$$q_{3c}(x,E,\mu) = b_1 - [b_2 + b_3\mu U(E) + b_4 U(E)]e^{-\frac{x}{rl_s}} \tag{5}$$

where r is an arbitrary constant. Two approaches were used: firstly, the first iteration, $q_{31}(x,E,\mu)$, was used to calculate the x-dependent solution, which was compared with other results. Secondly, for x = 0 leakage spectra were calculated using $q_{32}(0,E,\mu)$, and compared with the IMALS results. (The extensive calculational effort needed to obtain the general second iteration, $q_{32}(x,E,\mu)$, was deemed too great.)

The first iteration has the following form:

$$\begin{aligned} \mu<0: \quad & q_{31}(x,E,\mu) = b_1 - D(E,\mu)e^{-x/rl_s} \\ \mu>0: \quad & q_{31}(x,E,\mu) = b_1 - D(E,\mu)e^{-x/rl_s} \\ & \quad + [D(E,\mu) - b_1 + \mu U(E)]\exp[-x/\mu l_s(E)] \end{aligned} \tag{6}$$

where $D(E,\mu) = \dfrac{b_2 + b_4 U^*(E) + \mu b_3[U(E) - l_s(E)]}{1 - \mu l_s(E)/rl_s}$

and U* (E) is a slowly increasing function of E defined in [8]. This solution satisfies the boundary condition exactly, i.e. $q_{31}(x,E,\mu)$ in Eq. (3) gives $\Phi(0,E,\mu) = 0$ for $\mu > 0$. Fig. 1 shows the spatial dependence of the energy-integrated solution $\Phi(x,\mu)$ for the Goldman-Nelkin kernel [15] for several μ-values.

The variational parameter b_1 is equivalent to x_0 in the asymptotic solution. Hence, if the solution is divided into the asymptotic (as) and transient (T) part:

$$\phi(x,E,\mu) = \phi_{as}(x,E,\mu) - \phi_T(x,E,\mu) \tag{7}$$

where $$\phi_{as}(x,E,\mu) = C\cdot M(E)[x + b_1 - \mu U(E)] \tag{8}$$

then $$\phi_T(x,E,\mu) = -C\cdot M(E)[q_{31}(x,E,\mu) - b_1] \tag{9}$$

Table I shows the results for the energy and μ-integrated transient flux, $\Phi_T(x)$, for r = 1.0 and 0.3 for an isotropically scattering hydrogen gas (free gas with a mass of 1). These values are compared to results of a numerical solution of EISENHAUER [6], which should be fairly accurate. As can be seen, $\Phi_T(x)$ for r = 0.3 agrees with the values of Eisenhauer much better for the small values of x, where the transient portion is most important to the total solution.

As mentioned above, b_1 takes the place of x_0 in the asymptotic solution. From Table II it can be seen that the b_1 values for r = 0.3 agree better with the values of x_0 calculated with the program ADALS [16]. The scattering kernels for the organic moderators are those of Gläser [17]. Thus, these results substantiate the findings of [14] that a relaxation length of 0.3 l_s is more appropriate for the trial function.

The question of particular interest is how much the choice of relaxation length affects the twice-iterated solution of IMALS for the angular-dependent leakage spectra. From Table III, it can be seen that the results for r = 1.0 and 0.3 are practically the same. Hence, the IMALS values (r = 1.0) will be used in the next section to determine the semi-empirical expressions.

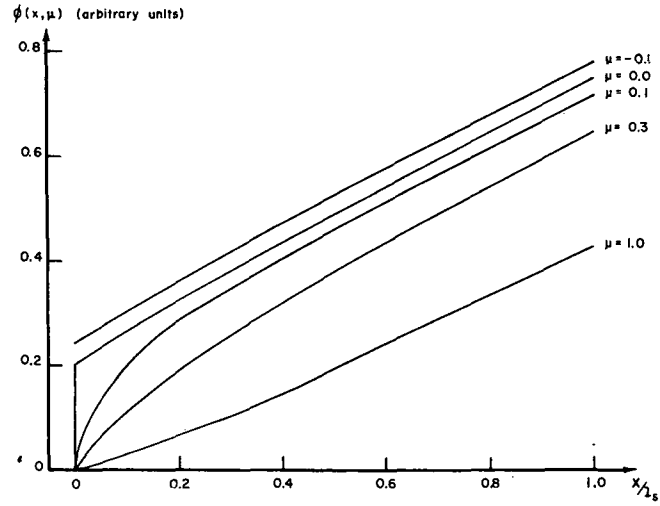

FIG. 1. Spatial dependence of the energy-integrated solution $\Phi(x,\mu)$ using Eq. (6) in Eq. (3), for the Goldman-Nelkin kernel.

TABLE I

TRANSIENT FLUX, $\Phi_T(x)$, FOR AN ISOTROPICALLY SCATTERING HYDROGEN GAS[a]

x/l_s	Eq. (9) r = 1.0	EISENHAUER [6]	Eq. (9) r = 0.3
0.125	1.000	1.000	1.000
0.375	.678	.480	.441
0.625	.531	.274	.206
1.125	.347	.107	.038

[a]Values normalized to that at x = 0.125.

TABLE II

VALUES OF b_1 AND x_o

Kernel	b_1/l_s (r = 1.0)	x_0/l_s [a]	b_1/l_s (r = 0.3)
Free Gas, mass = 1	.9684	.9343	.9260
Goldman-Nelkin	.5302	.5047	.5059
Benzene	.4646	.4405	.4425
Dowtherm A	.4403	.4169	.4191

[a]Calculated with the program ADALS [16].

TABLE III

VALUES OF $\bar{E}^N(\mu)$ USING $q_{32}(0,E,\mu)$ IN EQ. 3

Kernel	r	$\bar{E}^N(-1.0)$	$\bar{E}^N(-0.5)$	$\bar{E}^N(0.0)$
Goldman-Nelkin	1.0	1.1792	1.1515	1.1060
	0.3	1.1758	1.1516	1.1135
Benzene	1.0	1.1785	1.1524	1.1092
	0.3	1.1740	1.1507	1.1146
Hydrogen Gas, Isotropic Scattering	1.0	1.1027	1.0817	1.0328
	0.3	1.1018	1.0817	1.0343

3. EXPRESSIONS FOR AVERAGE ENERGIES

The IMALS results were shown in [13] to agree well with experimental results for H_2O, benzene, and Dowtherm A. Based on the IMALS results, the behavior of certain average energies can be related to M_2 and U(E) through simple expressions, which make it quite simple to calculate the average energies for any hydrogenous moderators. The two parameters, M_2 and U(E), are associated roughly with thermalization and transport effects, respectively.

3.1. Leakage Current

The average energy of the asymptotic current $\bar{E}_{Jas}$ is determined by the energy dependence of U(E) through the relationship [8]

$$\bar{E}_{Jas} = \int_0^\infty E\,M(E)\,U(E)\,dE \Big/ \int_0^\infty M(E)\,U(E)\,dE \qquad (10)$$

In the transient zone near the moderator surface, the average energy of the current changes because of the preferential leakage of fast neutrons. The magnitude of this change depends on how closely the moderator and neutron gas are "coupled," i.e. how well a moderator thermalizes. The thermalization power of a moderator can be represented by $M_2/\bar{\sigma}_s$, where $\bar{\sigma}_s$ is $\sigma_s(E)$ averaged over M(E). Table IV gives the average energy of the asymptotic and leakage current, in terms of $\bar{E}_M^\Phi = 2kT$, the average energy of a Maxwellian flux distribution. The scattering kernel for $ZrH_{1.7}$ is that of REICHARDT [18]. The delta function kernel

$$\Sigma(E' \to E) = \Sigma_s(E)\,\delta(E - E')$$

and the Corngold separable kernel

$$\Sigma(E' \to E) = \Sigma_s(E)\,\Sigma_s(E')\,M(E)/\bar{\Sigma}_s$$

represent limits for weak and strong energy exchange, respectively [5]. For both of these kernels, Σ_s (E) used for the calculations was that of a hydrogen gas.

TABLE IV

AVERAGE ENERGY[a] OF ASYMPTOTIC CURRENT, $\bar{E}_{Jas}$,

AND OF LEAKAGE CURRENT, $\bar{E}_J(0)$

Kernel	$M_2/\bar{\sigma}_s$	$\bar{E}_J(0)$	$\bar{E}_{Jas}$	$\frac{\bar{E}_J(0) - 1}{\bar{E}_{Jas} - 1} = CR$
Delta function	0.	1.088	1.105	.838
$ZrH_{1.7}$	.271	1.241	1.323	.747
Dowtherm A	.722	1.142	1.220	.646
Benzene	.948	1.131	1.214	.612
Goldman-Nelkin	1.065	1.122	1.201	.607
Hydrogen gas	1.93	1.087	1.159	.547
Corngold	3.75	1.055	1.105	.524

[a]In units of $\bar{E}_M^\Phi = 2kT$.

We can define the following ratio:

$$CR = [\bar{E}_J(0) - 1] / [\bar{E}_{Jas} - 1] \tag{11}$$

where $\bar{E}_J(x) = 2\pi \int_0^\infty \int_{-1}^{1} E\,\phi(x,E,\mu)\,\mu\, dE\, d\mu / J(x)$

and $J(x) = 2\pi \int_0^\infty \int_{-1}^{1} \phi(x,E,\mu)\,\mu\, dE\, d\mu$

The values of CR for the different kernels are given in Table IV. For the delta function kernel this ratio should be 1.0, as can be seen from the following. By integrating the transport equation the following equation can be derived [8]:

$$\frac{\partial}{\partial x} I(x) + \bar{E}_{g\to m}(x) = 0$$

where $I(x) = \bar{E}_J(x)\, J(x)$

and $\bar{E}_{g\to m}(x) = \int_0^\infty \int_0^\infty \Sigma(E' \to E)(E' - E)\,\phi(x,E')\, dE\, dE'$

Since J(x) is constant for zero absorption, and $\bar{E}_{g\to m}(x) = 0$ for the delta function kernel, $\bar{E}_J(x)$ is constant for this case.

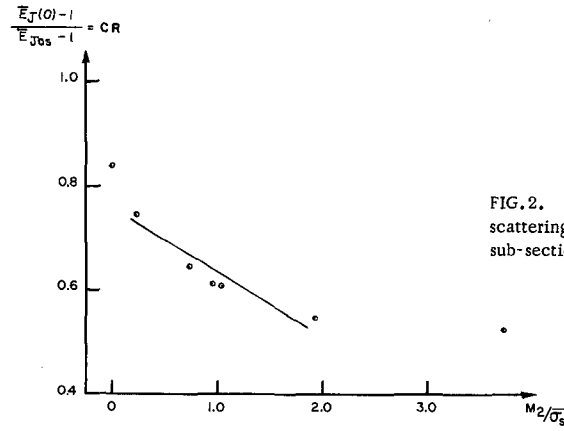

FIG. 2. The ratio CR for various scattering kernels, from IMALS. (See sub-section 3.1. and Table IV.)

Fig. 2 shows the results for CR graphically. The relation between CR and $M_2/\bar{\sigma}_s$ can be represented fairly well by the shown straight line in the range of applicability for realistic moderators. The equation of this line

$$CR = 0.75 - 0.12\, M_2/\bar{\sigma}_s \tag{12}$$

should be appropriate for calculating $\bar{E}_J(0)$ for non-crystalline moderators, if their $M_2/\bar{\sigma}_s$ and U(E) are known.

3.2. Perpendicular Leakage Spectrum

The variation of the perpendicular leakage spectrum, $\Phi(0,E,-1)$, from a Maxwell distribution is determined primarily by transport effects

TABLE V

AVERAGE ENERGY[a] OF PERPENDICULAR LEAKAGE FLUX FROM IMALS, $\bar{E}^{\Phi}(0, -1)$ AND FROM THE ASYMPTOTIC SOLUTION, $\bar{E}^{\Phi}_{as}(0, -1)$

Kernel	$\bar{E}^{\Phi}(0, -1)$	$\bar{E}^{\Phi}_{as}(0, -1)$	$\frac{\bar{E}^{\Phi} - \bar{E}^{\Phi}_{as}}{\bar{E}^{\Phi}_{as} - 1} = FR$
Delta function	1.0876	1.0603	.4527
$ZrH_{1.7}$	1.2455	1.1751	.4021
Dowtherm A	1.1519	1.1227	.2380
Benzene	1.1428	1.1197	.1930
Goldman-Nelkin	1.1332	1.1131	.1777
Hydrogen gas	1.0983	1.0906	.0850
Corngold	1.0648	1.0603	.0746

[a]In units of $\bar{E}^{\Phi}_{M} = 2kT$.

associated with the energy dependence of U(E). The difference between $\Phi(0, E, -1)$ from IMALS and $\Phi_{as}(0, E, -1)$ was found to be rather small in general, and to depend on $M_2/\bar{\sigma}_s$. $\Phi_{as}(0, E, \mu)$ was calculated using Eq. (8). Table V gives

$$\bar{E}^{\Phi}(x, \mu) = \int_0^{\infty} E\phi(x, E, \mu)\,dE \Big/ \int_0^{\infty} \phi(x, E, \mu)\,dE$$

for perpendicular leakage, i.e. $x = 0$, $\mu = 1$, for these two solutions, as well as the ratio FR, defined as

$$FR = [\bar{E}^{\Phi}(0,-1) - \bar{E}^{\Phi}_{as}(0,-1)] \Big/ [\bar{E}^{\Phi}_{as}(0,-1) - 1]$$

The straight line in Fig. 3 has the equation

$$FR = 0.45 - 0.23\, M_2/\bar{\sigma}_s \tag{13}$$

and fits the points fairly well in the range of interest for realistic moderators. Since the difference between $\bar{E}^{\Phi}$ and $\bar{E}^{\Phi}_{as}$ is small, the perpendicular leakage spectrum form is influenced primarily by the form of $U(E) \approx \lambda_{tr}(E)$, and the associated transport effects.

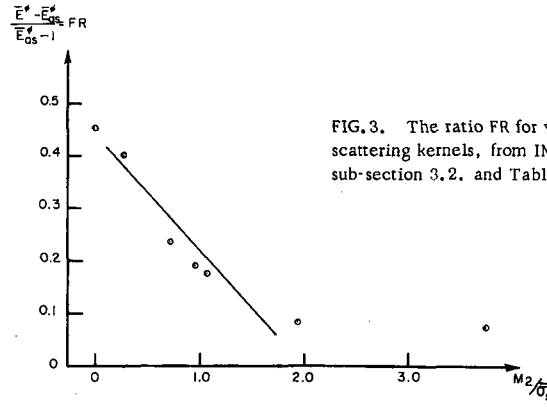

FIG. 3. The ratio FR for various scattering kernels, from IMALS. (See sub-section 3.2. and Table V.)

3.3. Angular Dependence of Leakage Spectra

For the angular dependence of the leakage spectrum, thermalization effects have a strong influence. This can be understood most easily by considering the limiting case of $\mu = 0$, for which there is no gradient and hence no net transport. For this case the transport equation becomes

$$\phi(0, E, 0) = \int_0^\infty \int_{-1}^{1} f(E', \mu' \to E, \mu)\, \phi(0, E', \mu')\, dE'\, d\mu' \qquad (14)$$

Making the following Legendre polynomial expansion

$$f(E', \mu' \to E, \mu) = \frac{1}{\Sigma_s(E)} \Sigma(E', \mu' \to E, \mu)$$

$$= \sum_{n=0}^{\infty} \frac{2n+1}{2} P_n(\mu)\, P_n(\mu')\, f_n(E' \to E) \qquad (15)$$

and writing

$$\phi(x, E, \mu) = M(E)\, \psi(x, E, \mu)$$

it is easy to show that for linearly anisotropic scattering

$$\psi(0, E, 0) = \tfrac{1}{2} \int_0^\infty f_0(E \to E')\, \psi_L(0, E')\, dE' \qquad (16)$$

where

$$\psi_L(0, E) = \int_{-1}^{0} \psi(0, E, \mu)\, d\mu$$

Eq. (16) illustrates the influence of the thermalization power of the moderator on the $\mu = 0$ spectrum. For the limiting case of the Corngold kernel, it is well-known that $\Phi(0, E, 0)$ is a Maxwellian, regardless of the form of the spectrum at other angles [4]. As pointed out in [8], the neutrons at $\mu = 0$ come from scattering collisions at the surface; since $\Phi_L(0, E)$ is not a Maxwellian, the variation of the $\mu = 0$ spectrum from a Maxwellian depends on the energy exchange in this last collision.

Eq. (16) provides a check for the consistency of results for calculated leakage spectra. The right hand side of Eq. (16) was calculated

TABLE VI

RELATIVE HEATING $RH^{\Phi}(\mu)$ FOR LEAKAGE SPECTRA, FROM IMALS

Kernel	$M_2/\bar{\sigma}_s$	$\bar{E}^N(0, -1)$[a]	$\bar{E}^{\Phi}(0, -1)$[b]	$RH^{\Phi}(-.7)$	$RH^{\Phi}(-.5)$	$RH^{\Phi}(-.3)$	$RH^{\Phi}(0)$
Delta function	.0	1.137	1.0876	.998	1.000	1.009	1.028
$ZrH_{1.7}$	.271	1.295	1.2455	.980	.968	.958	.944
Dowtherm A	.722	1.188	1.1519	.939	.887	.824	.716
Benzene	.948	1.178	1.1428	.926	.862	.783	.645
Goldman-Nelkin	1.065	1.179	1.1332	.923	.854	.769	.613
Hydrogen gas	1.93	1.135	1.0983	.894	.801	.678	.412
Corngold	3.75	1.097	1.0648	.872	.747	.565	.000

[a]In units of $\bar{E}^N_M = 1.5$ kT.

[b]In units of $\bar{E}^{\Phi}_M = 2$kT.

and compared to the left side. With the IMALS results for the Goldman-Nelkin kernel, the ratio of the two sides was 0.99±0.01, for all values of E.

Table VI shows the IMALS results for the relative heating $RH^{\Phi}(\mu)$ of the leakage spectra, where

$$RH^{\Phi}(\mu) = \frac{\bar{E}^{\Phi}(0,\mu)-1}{\bar{E}^{\Phi}(0,-1)-1} \tag{17}$$

and all $\bar{E}^{\Phi}$ are in units of $\bar{E}^{\Phi}_M = 2$ kT. $RH^{\Phi}(-1)$ is obviously 1.0 for all kernels. Since the form of the leakage spectrum is quite different from a Maxwellian over a wide energy range, the density-averaged energy, $\bar{E}^N(0,-1)/\bar{E}^N_M$ differs from that of $\bar{E}^{\Phi}(0,-1)/\bar{E}^{\Phi}_M$. The behaviour of $RH^{\Phi}(\mu)$ is practically the same as that of $RH(\mu)$ given in [8] , which is defined with $\bar{E}^N$. This behaviour is fitted fairly well in the $M_2/\bar{\sigma}_s$ range applicable for realistic moderators by the expression:

$$RH^{\Phi}(\mu) = 1 - (\mu+1)^2 \frac{M_2/\bar{\sigma}_s}{3} \tag{18}$$

Fig. 4 shows $RH^{\Phi}(0)$ vs. $M_2/\bar{\sigma}_s$, along with the straight line represented by Eq. (18).

To compare with values of $\bar{E}^{\Phi}(\mu)$ obtained from the experimental results of [13], calculations were made with Eqs. (18) and (13). The steps are

the following. Presuming $U(E) \approx \lambda_{tr}(E)$ and x_o are known for a particular scattering kernel, $\bar{E}^{\Phi}_{as}$ can be calculated using Eq. (2). Then, presuming M_2/σ_s is known, $\bar{E}^{\Phi}(0,-1)$, the average energy of the perpendicular leakage spectrum can be calculated using Eq. (13). Knowing $\bar{E}^{\Phi}(0,-1)$, $\bar{E}^{\Phi}(0,\mu)$ for any leakage direction can be calculated using Eq. (18). Table VII shows that the calculated results of the semi-empirical expressions agree with the experimental values within the experimental accuracy.

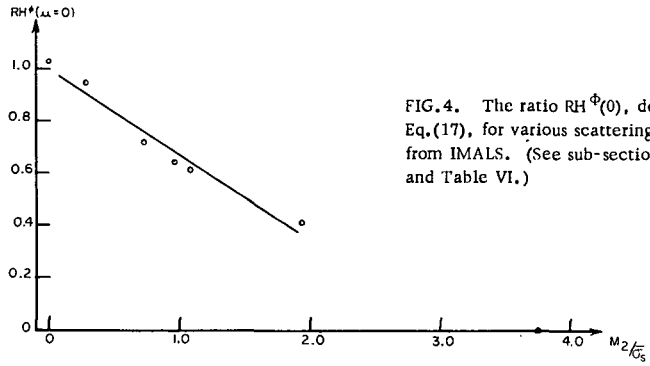

FIG.4. The ratio $RH^{\Phi}(0)$, defined by Eq.(17), for various scattering kernels from IMALS. (See sub-section 3.3. and Table VI.)

TABLE VII

RESULTS[a] OF $\bar{E}^{\Phi}(0,\mu)$ FOR SEMI-EMPIRICAL EXPRESSIONS

Moderator	Dowtherm A	Benzene	H_2O			
μ	-1.0	-1.0	-1.0	-0.5	-0.2	0.0
Calculated[b] $\bar{E}^{\Phi}(\mu)$	1.158	1.147	1.134	1.123	1.103	1.086
Experimental[c] $\bar{E}^{\Phi}(\mu)$	1.143±.02	1.145±.02	1.140±.02	1.122±.02	1.090±.02	1.080±.03

[a]In units of $\bar{E}^{\Phi}_M = 2kT$.

[b]Calculated using Eqs. (18) and (13).

[c]From results of [13].

4. TRANSPORT EQUATION CONSIDERATIONS

It can be shown qualitatively through the transport equation that the relations between the average energies for the actual and asymptotic spectra at the surface involve M_2. The integral form of the transport equation for $x = 0$, $\mu < 0$, is

$$\phi(0,E,-\mu) = \int_0^\infty \frac{dx'}{\mu}\left\{\int_0^\infty\int_{-1}^{1}\Sigma(E',\mu' \to E,-\mu)\phi(x',E',\mu')\,dE'\,d\mu'\right\} e^{-\frac{x'}{\mu}\Sigma(E)} \tag{19}$$

If we write

$$\phi(x,E,\mu) = \phi_{as}(x,E,\mu) - M(E)h(x,E,\mu) \tag{20}$$

where $M(E)h(x,E,\mu)$ is the transient flux, then

$$\phi(0,E,-\mu) = M(E)\int_0^\infty \frac{dx'}{\mu}\left\{\int_0^\infty\int_{-1}^{1}\Sigma(E,-\mu \to E',\mu') \cdot \left[x' + x_0 - \mu' U(E') - h(x',E',\mu')\right]dE'\,d\mu'\right\} e^{-\frac{x'\Sigma(E)}{\mu}} \tag{21}$$

From Eq. (21) it is easy to show that

$$\phi(0,E,-\mu) - \phi_{as}(0,E,-\mu) = -M(E)\int_0^\infty \frac{dx'}{\mu}\left\{\int_0^\infty\int_{-1}^{1}\Sigma(E,-\mu \to E',\mu')h(x',E',\mu')\,dE'\,d\mu'\right\} e^{-\frac{x'\Sigma(E)}{\mu}} \tag{22}$$

We then make the following assumption for the transient function

$$h(x',E',\mu') \approx \frac{1}{2}(a - bE')e^{-cx'} \tag{23}$$

where a, b and c are arbitrary constants. $b > 0$ will give a heated leakage spectrum. The approximation given by Eq. (23) can be obtained from Eq. (5), for $b_3 \ll b_4$ (which was the case for all kernels) and for $U(E) \sim E$ (which is a reasonable approximation in the energy range of interest). $h(x,E,\mu)$ from Eq. (23) in Eq. (22) gives

$$\phi(0,E,-\mu) - \phi_{as}(0,E,-\mu) = \Delta\phi = -M(E)\int_0^\infty \frac{dx'}{\mu}\left\{a\Sigma(E) - b\int_0^\infty \Sigma(E \to E')E'\,dE'\right\} e^{-\left(c + \frac{\Sigma(E)}{\mu}\right)x'} \tag{24}$$

Integrating over x and using

$$\frac{1}{c\mu + \Sigma(E)} = \frac{1}{c\mu} - \frac{\Sigma(E)}{c\mu(c\mu + \Sigma(E))} \tag{25}$$

we obtain

$$\Delta\phi = -\frac{M(E)\Sigma(E)}{c\mu + \Sigma(E)}\left[a + \frac{b}{c\mu}\int_0^\infty \Sigma(E \to E')E'\,dE'\right] + \frac{bM(E)}{c\mu}\int_0^\infty \Sigma(E \to E')E'\,dE' \tag{26}$$

Multiplying Eq. (26) by EdE and integrating over E gives

$$\bar{E}^{\phi}(0,-\mu) - \bar{E}^{\phi}_{as}(0,-\mu)\,k_1(\mu) = A(\mu) + \frac{k_2(\mu)\,b}{c\mu} \cdot \int_0^\infty E\,M(E)\,dE \int_0^\infty \Sigma(E\to E')E'dE' \tag{27}$$

where

$$A(\mu) = -k_2(\mu)\int_0^\infty \frac{E\,M(E)\Sigma(E)dE}{c\mu+\Sigma(E)}\left[a + \frac{b}{c\mu}\int_0^\infty \Sigma(E\to E')E'dE'\right]$$

$$k_1(\mu) = \int_0^\infty \phi_{as}(0,E,-\mu)\,dE \Big/ \int_0^\infty \phi(0,E,-\mu)\,dE$$

and

$$k_2(\mu) = 1\Big/\int_0^\infty \phi(0,E,-\mu)\,dE$$

Rewriting Eq. (27), and noting that

$$\int_0^\infty\int_0^\infty M(E)\,\Sigma(E\to E')E(E'-E)\,dE\,dE' = -\frac{(kT)^2}{2}M_2$$

we obtain

$$\bar{E}^{\phi}(0,-\mu) = k_1(\mu)\bar{E}^{\phi}_{as}(0,-\mu) + A(\mu) + \frac{bk_2(\mu)}{c\mu}\int_0^\infty E^{-2}M(E)\Sigma(E)\,dE - \frac{bk_2(\mu)kT^2}{2c\mu}M_2 \tag{28}$$

From Eq. (28), it can be seen that $\bar{E}^{\phi}(0,-\mu)$ and $\bar{E}^{\phi}_{as}(0,-\mu)$ are related through an expression involving M_2, as was expected based on the results of section 3. (If Eq. (28) is to be used for $\mu=0$, it should be rewritten by replacing Eq. (25) by

$$1/[c\mu + \Sigma(E)] = 1/c - [\Sigma(E) - c(1-\mu)]/c[c\mu + \Sigma(E)]\ )$$

Since $\bar{E}_J(0) = \int_0^1 \mu\,\bar{E}^{\phi}(0,-\mu)\,d\mu$

Eq. (28) can also be used to relate $\bar{E}_J(0)$ and $\bar{E}_{Jas}(0)$ through an equation containing M_2.

5. SUMMARY

The thermal neutron Milne problem for zero absorption has been investigated for various scattering kernels. It has been shown that a more appropriate relaxation length for the trial function describing the transient flux is 0.3 l_s, rather than the value of 1.0 l_s used in IMALS. However, after the second iteration of this trial function, the leakage spectra are practically the same for both values of the relaxation length.

The average energies of the perpendicular leakage spectrum and the leakage current can be related to the average energies of the asymptotic solutions for these quantities through the parameter $M_2/\bar{\sigma}_s$. The angular dependence of the leakage spectra average energy was shown to be related to the same parameter. Semi-empirical expressions were derived which allow the calculation of these average energies for non-crystalline moderators presuming that U(E) [$\approx\lambda_{tr}(E)$], x_o and $M_2/\bar{\sigma}_s$ are known for the scattering kernel. Average energy values obtained using these semi-empirical expressions agree satisfactorily with experimental values.

REFERENCES

[1] KLADNIK, R., KUŠČER, I., Nucl. Sci. Engng 11 (1961) 116.
[2] KLADNIK, R., KUŠČER, I., Nucl. Sci. Engng 13 (1962) 149.
[3] WILLIAMS, M.M.R., J. Nucl. Energy 17 (1963) 55.
[4] WILLIAMS, M.M.R., Nucl. Sci. Engng 18 (1964) 260.
[5] WILLIAMS, M.M.R., Nucl. Sci. Engng 19 (1964) 353.
[6] EISENHAUER, C., Nucl. Sci. Engng 19 (1964) 95.
[7] KIEFHABER, E., Nukleonik 6 (1964) 262.
[8] KALLFELZ, J.M., REICHARDT, W., Nukleonik 9 (1967) 148.
[9] WOOD, J., WILLIAMS, M.M.R., J. Nucl. Energy 21 (1967) 113.
[10] LANCEFIELD, M.J., SCHOFIELD, P., A.E.R.E. Harwell Rep. T.P. 282 (1967).
[11] RENZ, K., Nukleonik 9 (1967) 312.
[12] BECKURTS, K.H., Z. Naturforsch. 16a (1961) 611.
[13] KALLFELZ, J.M., Nukleonik 9 (1967) 273.
[14] KLADNIK, R., Proc. 3rd UN Int. Conf. PUAE 2 (1965) 142.
[15] FEDERIGHI, F.D., GOLDMAN, D.T., Knolls Atomic Power Laboratory Rep. KAPL-2225 (1962).
[16] KLADNIK, R., Nucl. Sci. Engng 23 (1965) 291.
[17] GLÄSER, W., BECKURTS, K.H., Nucl. Sci. Engng 20 (1964) 235.
[18] REICHARDT, W., Paper SM-96/15, these Proceedings II.

DISCUSSION

N.J. McCORMICK: In your curves of CR, FR, and RH against $M_2/\bar{\sigma}_s$, is there any reason why an exponential fit could not be used?

J.M. KALLFELZ: There are certainly other expressions which would fit the points better than the linear expressions we chose. However, the accuracy of the numerically calculated values from IMALS would not justify making too many refinements in the fit of the curve. We wanted the simplest expression which would fit the points reasonably well in the $M_2/\bar{\sigma}_s$ range of interest for realistic moderators. The ratios CR, FR and RH are very sensitive functions. For example, a 5% difference in CR would only cause a difference of something like 0.5% in the quantity to be calculated, $\bar{E}_{Jas}$ (0).

J.J. DORNING: With reference to Dr. McCormick's comment, and despite your reservations, I think it would still be very interesting to fit the curve in your first figure with a smooth curve to see whether there is further improvement on the excellent agreement you have already obtained using the linear fit. This might show an unexpected indirect dividend in the analysis of simple models such as the δ-function and Corngold models.

J.M. KALLFELZ: This might be possible. Nevertheless, I must again stress that attempts to obtain too 'exact' a fit could go beyond the numerical accuracy of the calculated IMALS values. We wanted a fairly simple expression, which would then be easier to support through the transport equation. Furthermore, the experimental values for $E^{\Phi}(o, \mu)$, with which we wanted to compare our calculated values, are only accurate to several per cent.

W. REICHARDT: Is formula 18 of your paper purely empirical or can it be justified to some extent directly from the transport equation?

J. M. KALLFELZ: This formula is semi-empirical, that is, it was obtained by fitting the calculated values for $RH^{\phi}(\mu)$. It is given qualitative support in section 4, where it is shown from the transport equation that the expression for $\overline{E}^{\phi}(0,\mu)$ involves M_2. However, there are several μ-dependent integral expressions containing unknown constants. Therefore the μ-dependence unfortunately cannot be given explicitly.

S. N. PUROHIT: I should like to make a point about the presence of M_2 in the energy expression. If one were to represent U(E) in your expression for $\overline{E}$ by a polynomial in E containig terms involving higher powers of E than 1, then one would get other matrix elements of the scattering operator, in addition to M_2.

J. M. KALLFELZ: For the numerically calculated (IMALS) values for $\overline{E}$ the exact values for U(E) were used. Of course, other matrix elements would be obtained in the analytic expression for $\overline{E}$ (section 4) if a more involved expression were used for the transient flux. However, we wanted a simple expression for the dependency, involving as few parameters as possible. From our results, M_2 probably has the most influence, since for realistic moderators the dependency can be described quite well using this parameter.

EFFECT OF SCATTERING ANISOTROPY ON THE CALCULATION OF PULSED-NEUTRON DECAY CONSTANTS*

J. DORNING
BROOKHAVEN NATIONAL LABORATORY,
UPTON, LONG ISLAND, NEW YORK
and
COLUMBIA UNIVERSITY,
NEW YORK CITY, NEW YORK,
UNITED STATES OF AMERICA

Abstract

EFFECT OF SCATTERING ANISOTROPY ON THE CALCULATION OF PULSED-NEUTRON DECAY CONSTANTS. In this paper the effect of including various orders of scattering anisotropy in the calculation of pulsed-neutron (die-away) experiment discrete time-decay constants is examined. The fundamental mode thermal neutron decay constants for spherical light-water systems are computed using realistic scattering models for the bound hydrogen atoms of the H_2O molecule. (Separate calculations were performed using the Nelkin model and the Young and Koppel model.) The results of extensive computations of decay constants for small systems using the discrete S_n method are presented. By the use of this method the introduction of an $e^{i\vec{B}.\vec{r}}$ Ansatz and the accompanying vagueness and difficulties in assigning extrapolation distances for small systems are avoided. Comparison with experiment shows that retention of the linearly anisotropic (P-1) term in the scattering kernel is essential and indeed considerably more important than model refinement. The inclusion of higher order scattering anisotropies (P-2, P-3), however, leads to extremely small changes in the computed decay constants. These results are physically very acceptable since the flux decay in small systems is dominated by leakage. As demonstrated by the calculations, the isotropic scattering approximation underestimates the leakage, whereas the P-1 approximation results in a rather accurate determination of this dominating factor.

The use of 'transport-corrected' P-0 cross-sections results in surprisingly accurate values for the decay constants of systems in the experimental range, and the computations show that this simple efficient method of accounting for scattering anisotropy is adequate for decay constant calculations in H_2O.

Additional information obtained from the calculations include the space-dependent energy spectra. The energy spectrum throughout a typical small system is significantly diffusion cooled, the spectrum at the center being softer than that at the surface. The spectra resulting from P-0 scattering calculations are not cooled quite as much as those obtained by transport-corrected P-0 and higher-order scattering computations which yield almost identical energy distributions for systems in the experimental range.

The effects of completely neglecting chemical binding are shown to be significant by comparing decay constants resulting from calculations based on the proton gas model with those obtained for the more realistic anisotropic model.

1. Introduction

The calculation of the fundamental mode decay constant α_0 of a thermalized neutron pulse has been the center of a considerable amount of interest for more than a decade now since von Dardel and Sjostrand [1] first employed pulsed-source techniques to measure neutron diffusion parameters. The original interpretation of the experiment based on one-velocity diffusion theory led to a linear relationship between α_0 and

* This work was performed under the auspices of the United States Atomic Energy Commission.

B^2. This proved adequate only when experiment and computations were restricted to very large systems. For more moderate system sizes it was realized that because of the preferential leakage of fast neutrons the spectrum of the flux remaining within such systems was "diffusion cooled", and that meaningful calculations would necessarily have to be based upon a formulation which included energy dependence. Finally, for small systems the diffusion approximation with or without energy dependence is not valid. Thus, when it is desired to calculate pulse-neutron experiment asymptotic time-decay constants for the full experimental range of system sizes it is necessary to solve the energy-dependent neutron transport equation. Analysis of the spectrum of the energy-dependent transport operator [2,3,4,5] has elucidated the nature of these decay constants. It has been shown that there is a continuum of decay constants extending from $\alpha^* = [v\Sigma(v)]_o = [v\Sigma(v)]_{min}$ to infinity regardless of system size, and zero, one, or more discrete decay constants below α^* depending upon the size of the pulsed medium. The radius (for a spherical system) above which there is always at least one discrete decay constant has been estimated to be approximately one Maxwell-averaged transport mean free path [6].

The aim of this paper was to calculate the fundamental mode thermal neutron decay constants for spherical light systems of various radii for the purpose of comparison with experiment, and to investigate the effect of including various orders of scattering anisotropy in kernels based on realistic H_2O models.

2. Method of Computation

Most calculations of pulsed-neutron decay constants using realistic scattering models have been done in the buckling approximation. For example, in many investigations the streaming operator $\vec{\Omega}\cdot\nabla$ in the integro-differential neutron transport equation has been replaced by $-DB^2$. Or, at the very least, the spatial dependence of the flux has been assumed to have the form $e^{i\vec{B}\cdot\vec{r}}$ permitting the replacement of the complicated streaming term $\vec{\Omega}\cdot\nabla\phi(\vec{r},E,\vec{\Omega})$ by $\vec{\Omega}\cdot\vec{B}\phi(E,\vec{\Omega})$ leaving the transport equation with no spatial dependence except through the vector $\vec{B}$. For large systems where the extrapolation distance is clearly defined and in general indistinguishable from the "Milne problem" value this Ansatz is acceptable and in fact desirable from the standpoint of facility in computation. However, for small systems the extrapolation distance varies with size, especially in the velocity-dependent problem, and the $e^{i\vec{B}\cdot\vec{r}}$ theory breaks down. But it is just these small systems, in which the asymptotic flux spectra are diffusion-cooled by the large amount of leakage, that hold the greatest interest for us both as a test of the scattering models at low energies and as a check on the less reliable portion of the experimentally accessible range of radii. Thus, a calculation

without introducing buckling in any way of the asymptotic decay constant as a function of system dimension which extends to extremely small sizes for realistic scattering models is desirable. Other solution methods such as P_ℓ multi-group calculations and Laguerre polynomial approaches have been attempted with some degree of success, but these methods are cumbersome when high-order approximations are required as is the case in small systems.

Because of the limitations on these techniques in thermal neutron decay calculations, we turned, in this work, to a very reliable and powerful method which has been well proven in numerous fixed-source and eigenvalue-type problems associated with reactor design studies, yet until now has remained untried as a tool in pulsed-neutron analysis. We employed the "discrete S_n approximation" to the transport equation to compute the asymptotic decay constant. The actual calculations to solve the multi-group discrete S_n equations for α_0 were carried out using the neutron transport code ANISN [7].

Since the S_n method is a source iteration method and the code thereby requires a fission source it was necessary to artificially introduce fission neutrons into the calculations. This was done with a minimum of effort and without altering the code in the slightest manner by merely juggling the cross-sections. It was desired to introduce a non-zero fission cross-section in order to obtain non-zero fission sources, but this had to be done in such a way as to leave the physics (at least the physics seen by the multi-group transport equations) of neutron energy transfer unchanged. To accomplish this we chose a group, say the ith group, and decreased the macroscopic scattering cross-sections $\Sigma(i\to j)$ to a number of other (j^{th}) groups by an amount a_j forming an adjusted energy transfer cross-section $\Sigma'(i\to j) = \Sigma(i\to j)a_j$. The additional requirement that $\sum_j a_j = 1.0$ was also included for reasons which will become evident below. The total scattering cross-section for the ith group was decreased by one cm^{-1}, and the absorption cross-section for this group increased by the same amount. That is

$$\Sigma_s'(i) = \Sigma_s(i) - 1.0$$

$$\Sigma_a'(i) = \Sigma_a(i) + 1.0$$

Finally, the zero value for $\nu\Sigma_f$ for the ith group was replaced by $(\nu\Sigma_f)' = 1.0$ for that group and the fission spectrum which had been zero was replaced by $\chi_j' = a_j/(\nu\Sigma_f)'$ thus introducing "fake fission". The fact that the fission spectrum is normalized and $(\nu\Sigma_f)'$ is set equal to one cm^{-1} is the reason that the a_j were normalized above. This cross-section juggling gave the code a fission source (which was necessary to determine the convergence of the outer iterations) while

enabling it to transfer neutrons from one group to another properly, according to the physical cross-sections for the process. It merely caused the task to be accomplished artificially via fission. Since only the P-0 part of the cross-sections was subjected to this juggling, and fission neutrons are emitted isotropically, this artificial treatment should be exact.

Admittedly, we used a rather large mace to attack the problem, but when numerical values for the purpose of comparison with experiment in complicated real physical systems are desired, the turn to large computing machines and extensive codes is unavoidable.

3. Realistic H_2O Models

The problems involved in determining the scattering kernel $\Sigma_s(E',\vec{\Omega}'\rightarrow E,\vec{\Omega})$ for realistic scattering materials are both fundamental and difficult. Their treatment requires a knowledge of the basic structure of matter, and a detailed understanding of the dynamics of atomic motions. Nevertheless, acceptable, and in some cases highly accurate, models have been developed for most common moderating materials. One such model is the Nelkin model [8] which is a purely incoherent (since $\sigma_{inc} >> \sigma_c$ for hydrogen) model for light water. In this model the motions of the bound hydrogen atoms are considered in terms of the H_2O molecule as the basic dynamical unit and the hindered molecular translation or diffusion through the liquid is replaced by free translation. Thus, the Nelkin model is basically a molecular gas model. In the development of the model it is assumed that the separation of the atomic motions into vibrations, hindered rotations and free translation of the molecule adequately describes the motion of the hydrogen atoms in the liquid. Further, the hindered rotations are replaced by a torsional oscillation of a single frequency. (This and the assumption that the vibrations of the stretching modes along the O-H bonds are isotropic are the most drastic assumptions of the model with respect to thermal neutron scattering.) Although the assumptions of free molecular translation and torsional oscillation avoid the problems of fundamental interest in liquid-state physics, most of the physical features of the dynamical structure of light water important to thermal neutron scattering are retained in the model. The energies characteristic of the diffusive modes of the water molecules are sufficiently low that neglecting these modes has little effect on neutron scattering cross-sections. This model which has met with a great deal of success is quite accurate when comparison with experiment is based on the total energy-dependent scattering cross-section for hydrogen in water. However, since a small but definite discrepancy between measured spectra and infinite medium spectrum calculations based on this model has been noted and as a result a more detailed model has been developed we in-

cluded this improved model as well as the Nelkin model in our decay constant calculations.

The anisotropic model which represents a refined version of the Nelkin model has been introduced by Young and Koppel [9]. The improvement of this model over the original Nelkin model is brought about by carrying out the averaging procedure over random molecular orientation more accurately. In particular, the anisotropy of the vibrational modes in the direction of the O-H bond is treated rigorously. Hence the model name. The total energy-dependent scattering cross-section predicted by this model is in better agreement with experiment than is that predicted by the original model. Because of the probable lack of sensitivity of the decay constants to the finer details of the models more elaborate models were not attempted. Two sets of decay-constant calculations were carried out for H_2O systems. The first set was done using the original Nelkin model, and the second using the anisotropic model. In both calculations the small contribution to scattering due to oxygen, the cross-section of which is low compared with hydrogen ($\sigma_b^O \approx 3.76$b, $\sigma_b^H \approx 81.6$b), was accounted for by including it as a free gas of mass sixteen. Absorption was taken as one-over-v. The fortran program GAKER [10] was used to compute the Nelkin model differential scattering cross-sections and a modified version of the same program was employed to determine the anisotropic model cross-sections.

4. Results of Calculations and Comparison with Experiment

Calculations were carried out for spherical homogeneous light-water systems ranging in radius from 10.182 cm to 0.6 cm using thirty velocity groups, P-3 scattering, forty spatial intervals, and the S_4 approximation. This range of radii extends from the largest systems of experimental interest to systems considerably smaller than the minimum practical experimental sizes. Although the fundamental mode decay constant increases very rapidly as system size is decreased (especially for very small systems) the computed value of α_0 for the smallest system investigated (radius = 0.6 cm) was less than $[v\Sigma(v)]_{min}$ for the Nelkin model which has been calculated [11] to be 290,000 sec^{-1}. Thus α_0 was still discrete. This system of course is larger than one Maxwell-averaged transport mean free path (~0.43535 cm). It was desired to emphasize the portion of the energy spectrum around and below 1kT since the spectrum should be cooler than a Maxwellian. To this end the multi-group structure was chosen to be the same as that used in the THERMOS code [10] which has been used very successfully in numerous thermal lattice calculations. Forty spatial intervals were used because this number appeared to yield a sufficiently fine mesh to result in convergence for the larger systems while still not requiring more computer time than coarser spatial meshes for the small systems. Although each iteration was faster when a coarse mesh was used, a larger

number of iterations were required to converge a given calculation. This can be partially attributed to the fact that when the same number of mesh intervals is used for all system sizes an excellent initial flux guess based on the converged values of the previous calculation is available. The S_4 approximation has proven to be sufficient in most S_n calculations and since energy spectrum cooling appears to be the most important effect of reducing system size quadrature points were sacrificed in favor of energy groups. The convergence as a function of all of these computational parameters was examined and is discussed below.

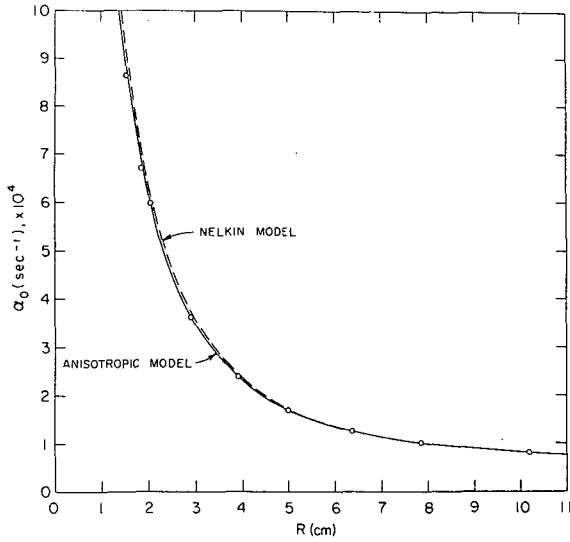

FIG. 1. The fundamental mode decay constant α_0 as a function of the radius R of homogeneous spherical light-water systems. Experimental values (circles) are taken from GON et al. [12].

Curves of the decay constant α_0 versus system radius R based on the two models were calculated using the exact same group structure, scattering anisotropy, quadrature points and weights, and spatial mesh, and are plotted along with experimental points [12] in Fig. 1. The better agreement of the curve based on the anisotropic model with experiment tends to support its already proven superiority over the Nelkin model. However, both of the calculated curves shown in Fig. 1 are in good agreement with experiment, and when one considers the steep slope of the α_0 vs. R curves along with the experimental difficulties encountered especially in extremely small systems where the discrepancies are greatest it is difficult to state that the computational results show that one model is superior to the other. Moreover, the close agreement with experiment which results from both models confirms the widely-held feeling that pulsed-neutron experiments are not sufficiently sensitive to test the fine details of scattering models for light water. The decay constants are accurately predicted without

including such details as the broad band of frequencies covered by the rotational modes of the molecule instead of the single frequency used by these models or the very low-energy behavior (i.e. diffusion of the H_2O molecules or complexes of molecules instead of the free translations assumed by these models).

The convergence of the computed values for α_0 was examined with regard to a number of calculational parameters. The number of groups was increased from 30 to 45 with all of the additional groups formed by dividing those groups of the original thirty which spanned the energy interval between 0.25 kT and 1.69 kT. Thus, the emphasis which already existed on the region where the diffusion-cooled energy spectrum peaked (below 1kT) was increased. The discrepancy between the 30-group and 45-group calculated decay constants was less than 0.06% in all cases. The number of S_n quadrature points was also varied. S_{16} calculations were done for the three smallest experimental systems (R = 1.53 cm, 1.859 cm, 2.061 cm). The maximum percent discrepancy between S_{16} and S_4 eigenvalues (which occurred for the smallest experimental system) was less than 1%. As a final check on the convergence of the calculations the number of spatial mesh intervals was doubled for the larger systems and halved twice for some of the smaller systems. No change in the computed decay constants occurred as a result of these variations.

5. The Effect of Scattering Anisotropy

Perhaps the most physically interesting computational parameter of the decay constant calculations is the order of the scattering anisotropy included. For this reason the effect of including various orders of anisotropy on the calculation was investigated. Since the decay of the thermal neutron flux in small systems is dominated by leakage, and the angular flux in such systems is likely to be peaked in a direction pointing outward from the center of the system a calculation which includes only the isotropic part of the scattering kernel should underestimate the leakage and therefore the decay constant. This is indeed the case as is shown in Fig. 2 which is a copy of Fig. 1 to which the results of calculations which included only the P-0 component of the scattering kernel based on the anisotropic model have been added. From this figure we see that inclusion of some degree of scattering anisotropy is essential and in fact more important than further model refinement. (The Nelkin model results are in considerably better agreement with experiment than are the P-0 anisotropic model results.) However, since the correct leakage is the essential feature, the extension to include the P-1 term and thus account for any preferentially forward scattering is the important consideration. This is clearly shown in Table I in which the calculated values of α_0 based on the anisotropic model for various orders of scattering anisotropy are tabu-

TABLE I

The Effect of Scattering Anisotropy on the Decay Constants

Sphere Radius (cm)	α_o (% Discrepancy)[a]			
	Order of Scattering Anisotropy Included			
	P-0	P-1	P-2	P-3
1.859[b]	60,081.1(13.367)	69,441.5(-.1298)	69,348.3(.00461)	69,351.5(---)
1.859[c]	60,430.7(13.650)	70,060.2(-.1103)	69,982.9(.00029)	69,983.1(---)
1.000[c]	141,774.0(8.477)	155,086.0(-.1173)	154,904.3(.00013)	154,904.5(---)

[a] P-3 value is taken as the correct solution.

[b] S_4 , 30 Group, anisotropic model plus oxygen gas. (Plotted in figure 3).

[c] S_{16} , 45 Group, anisotropic model plus oxygen gas.

lated. The P-0 scattering calculation for a small system (R = 1.859 cm) in the experimental range results in a decay constant which is more than 13% below the value computed using P-3 scattering. On the other hand the number arrived at using linearly anisotropic scattering is in rather good agreement with the P-3 value, the discrepancy being less than two tenths of a percent. The P-2 scattering result is almost identical to the P-3 value. Thus, we see, although isotropic scattering calculations are inadequate and result in considerable error, computations including only P-1 scattering are quite accurate and certainly sufficient for comparison with experiment.

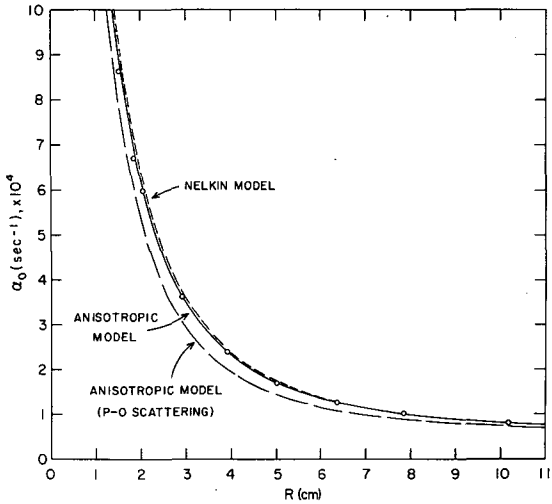

FIG. 2. The fundamental mode decay constant α_0 as a function of sphere radius R based on the P-0 scattering approximation compared with the results of computations including anisotropic scattering. Experimental values (circles) are taken from Gon et al. [12].

Further evidence in support of the physical argument placing importance on linearly anisotropic scattering can be found among some of the additional results of the calculations. For example, the ratio of the total leakage from a system to the total flux within the system is almost identical for the P-3, P-2, and P-1 scattering calculations, whereas this ratio is considerably lower when the computations are done in the P-0 scattering approximation.

6. "Transport Corrected" Cross-Sections

An extension of the "transport approximation" to energy-dependent problems can be easily made by assuming the scattering kernel can be represented in the form

$$\Sigma_s(E',\vec{\Omega}'\to E,\vec{\Omega}) \cong \sum_{\ell=0}^{L} \frac{(2\ell+1)}{4\pi}\,\Sigma_\ell(E';E)\,P_\ell(\vec{\Omega}\cdot\vec{\Omega}') + \Sigma_\delta(E')\,\delta(\vec{\Omega}\cdot\vec{\Omega}')\,\delta(E'-E)$$

Physically, this results in the division of the scattering kernel into a truncated expansion in Legendre polynomials of the scattering angle cosine plus a term which represents forward scattering with no energy degradation. The coefficient of the forward scattering term $\Sigma_\delta(e)$ has been shown [13] by requiring the conservation of certain moments to be the $(L+1)^{th}$ coefficient of the Legendre expansion $\Sigma_{L+1}(E';E)$ integrated over all final energies. For L=0 this assumption implies that the anisotropy of the scattering kernel is well represented by forward elastic scattering. When incorporated into a P-0, multi-group, discrete S_n calculation, this "transport approximation" results in decreasing the total scattering cross-section as well as the isotropic self-scattering cross-section of each group by the amount Σ_1 for that group. Actually, in a multi-group discrete S_n calculation the same results are achieved by less stringent physical requirements on the scattering. Under these circumstances, since the discrete representation of both the energy and angular variables has already been made all that is necessary is that the anisotropic component of the scattering result in energy changes which are insufficient to transfer a neutron out of its original energy group and that the alteration of its direction of motion be sufficiently small that its final direction cosine is within the range represented by its initial discrete direction. Thus, in such discrete type transport calculations one would expect that approximating the anisotropic part of the scattering in this manner may result in less inaccuracy (when compared with anisotropic calculations) than the original assumption would imply.

Indeed the discrepancies between the results of the isotropic scattering calculations using "transported corrected" cross-sections and those obtained by higher order scattering (P-1, P-3) calculations are extremely small, indicating that a large amount of the scattering anisotropy is associated "almost" forward, "almost" elastic scattering. The results of the P-0 transport approximation α-calculations are presented in Table II where they are compared with results of calculations using various orders of scattering. In this set of computations only the anisotropic model was considered. It is clear from Table II and perhaps more dramatically illustrated in Fig. 3 which is a plot of the computed decay constant for a sphere of 1.859 cm in radius against the order of scattering anisotropy included that the transport approximation (represented in Fig. 3 by an isolated point at "P-½") is extremely accurate. For example, for the smaller systems in the experimental range (1.530 cm to 3.904 cm) the percents of discrepancy between the P-0 transport approximation results and those obtained by P-3 scattering calculations are considerably less than 1%, while ordinary P-0 calculations result in discrepancies as high as 15% in this range. Yet, the same computational effort is required in P-0 and P-0 transport corrected calculations, while higher order calculations are considerably more time consuming. Thus, the transport approximation definitely represents an efficient method of computa-

tion in this case. Once again, our knowledge that the flux decay in these systems is dominated by leakage leads us to examine the ratio of total leakage to total system flux. As before in the P-1 case, these ratios for the transport corrected P-0 calculations are close to the P-3 values, while for the ordinary P-0 calculations they disagree considerably

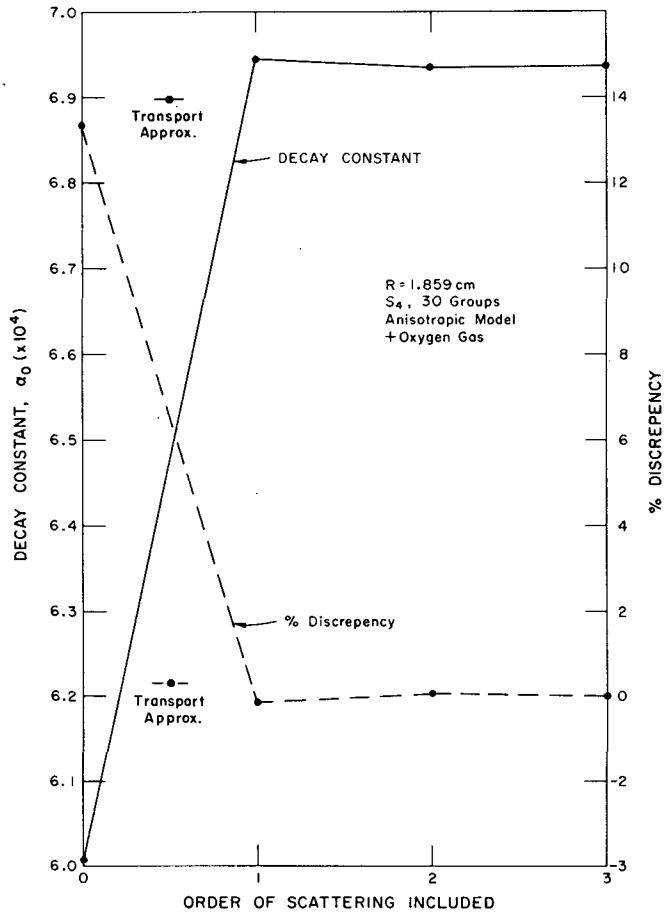

FIG. 3. The effect of including various orders of scattering anisotropy on the calculation of the decay constant.

with the P-3 values. For a system with a radius of 1.859 cm the P-1 scattering calculation overestimated the leakage to total flux ratio by 0.156%, and the P-0 transport corrected computation underestimated it by 0.75% while the straight P-0 calculation was below the P-3 value by more than 15.9%. As one would expect, the errors in these ratios are not far from the percents of discrepancy in the computed α-values shown in Table II.

TABLE II

Results of P-0 "Transport Approximation" Calculations

Sphere Radius (cm)	α_o [a] (% Discrepancy) [b]			
	Order of Scattering Anisotropy Included			
	P-0	P-0 (Transport)	P-1	P-3
0.600	243,217(4.773)	252,006(1.3316)	255,622(-0.0842)	255,407
0.750	195,036(6.042)	205,441(1.0295)	207,744(-0.0800)	207,578
1.000	140,398(8.259)	151,844(0.7802)	153,188(-0.0980)	153,038
1.530	79,687(11.931)	89,886(0.6587)	90,599(-0.1293)	90,482
1.859	60,080(13.369)	68,916(0.6287)	69,442(-0.1298)	69,352
2.910	30,786(15.356)	36,188(0.5031)	36,407(-0.0990)	36,371
3.904	20,148(15.384)	23,730(0.3402)	23,828(-0.0714)	23,811
4.988	14,562(14.607)	16,996(0.3343)	17,053	
6.363	10,974(13.050)	12,591(0.2377)	12,621	
7.846	8,941(11.282)	10,060(0.1786)	10,078	
10.182	7,309(8.820)	8,005(0.1372)	8,016	

[a] Based on 30 group, S_4, 40 mesh interval ANISN calculations for anisotropic model plus oxygen gas.

[b] The underscored values are taken as the correct.

One might have expected that such an integral parameter as the decay constant would be accurately calculated using a low-order scattering anisotropy or even transport corrected cross-sections; however, more detailed properties of the neutron field such as the energy distribution should be less apt to be correct. In Fig. 4 the energy spectra of the volume-integrated flux in a very small (radius = 0.60 cm) system based on P-3, P-0 transport corrected and ordinary P-0 scattering calculations are plotted. Even in such an extremely small system the discrepancy between the P-3 and P-0 trans-

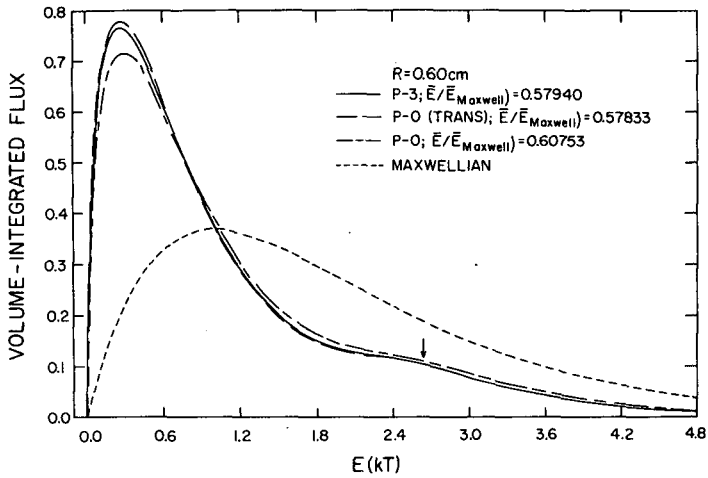

FIG.4. Diffusion-cooled energy spectra based on P-3 scattering, P-0 transport-corrected, and ordinary P-0 scattering calculations for a very small system. Note the "one-phonon" secondary peak (arrow).

port spectra is almost negligibly small. Although the spectrum resulting from the isotropic scattering calculations is strongly "diffusion cooled" ($\bar{E}/\bar{E}_{Maxwellian}$ = 0.60753) it is not as cool as that computed using P-3 scattering ($\bar{E}/\bar{E}_{Maxwellian}$ = 0.57940) indicating once again that the leakage is underestimated. A very interesting additional characteristic common to all three of these spectra is the secondary peak (arrow) which is centered about 2.65 kT. This secondary peak has an important physical origin. It represents a local (in energy) increase in the neutron flux caused by collisions of the large number of neutrons having energies near the main peak of the spectrum (~0.28 kT) with hydrogen atoms in which the rotational oscillatory modes of the H_2O molecule undergo one-phonon de-excitations imparting $\hbar\omega_r$ = 0.06 eV (~2.37 kT) to the neutrons. It is interesting to recall here that this broad secondary peak is a result of a "delta-function" in the original microscopic model [9]. This observation emphasizes the "smoothing" which occurs as one proceeds from the scattering model to the neutron flux distribution, and supports our conclusion that the pulsed-source experiment is insensititive to minor details of the scattering model. Cer-

tainly the inclusion of the broad band of rotational frequencies around 0.06 eV would have changed the results very little. Perhaps it might have broadened this secondary peak a small amount, but the effect on the decay constant would doubtlessly be extremely small. Further, the secondary peak does not appear at all in calculated spectra in systems large enough to be in the experimental range. The spectra in the smallest system which was compared with experiment (radius = 1.53 cm) based on P-3, P-0 transport, and P-0 scattering are shown in Fig. 5. They too, are softened by diffusion cooling; however, no "one-phonon" secondary peak can be observed in them. It can also be seen in Fig. 5 that for systems in the experimental range the discrepancy between the P-3 spectrum and P-0 transport spectrum is negligible while the ordinary P-0 spectrum differs from them significantly.

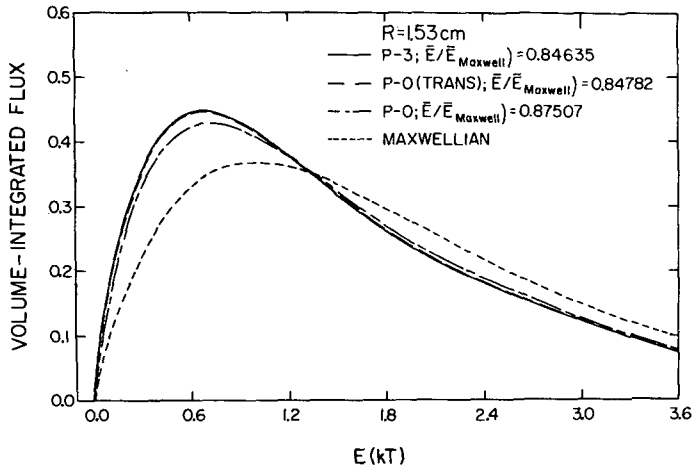

FIG. 5. Diffusion-cooled energy spectra based on P-3 scattering, P-0 transport-corrected, and ordinary P-0 scattering calculations for the smallest system in the experimental range.

One minor additional point is that the α-values resulting from the P-0 transport approximation calculations yield an extra dividend in that they should be extremely good estimates of $\alpha_1^{(slab)}$, the decay constants of the first spatial harmonic in slabs with half-thickness equal to the radii reported in Table II, since for an isotropic scattering kernel $\alpha_1^{(slab)} = \alpha_0^{(sphere)}$.

7. The Neglect of Chemical Binding

Although it was demonstrated above that calculations of such integral parameters as decay constants do not require more sophisticated models for H_2O than the Nelkin model or the anisotropic model (e.g. models which include the observed band of rotational frequencies account for diffusive motion of molecules, etc.) and that the inclusion of scattering anisotropy

at least in the form of transport-corrected cross-sections, is more important than further model development, the total neglect of chemical binding effects could not be tolerated. To show that the free proton model for hydrogen in water is too crude even for decay-constant calculations we performed a third set of computations for the H_2O systems considered above, using a mass-one free-gas model with the proper light-water hydrogen atomic density. Scattering by oxygen, and absorption were accounted for in the same manner as in the above calculations. The resulting α_0 vs. R curve shown in Fig. 6 (broken line) is

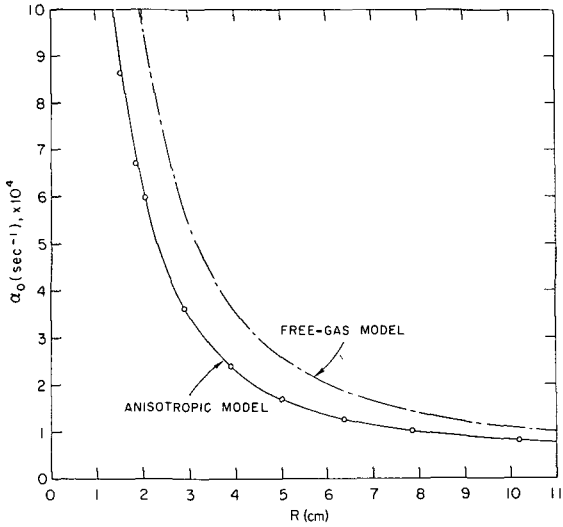

FIG. 6. The decay constants calculated neglecting chemical binding effects (free gas model) compared with those calculated using the more realistic anisotropic model. Experimental values are taken from Gon et al. [12].

in rather poor agreement with experiment compared to the curve (solid line) based on the anisotropic model, and exhibits approximately a 50% error for small system sizes when compared with either the experimental values or the anisotropic model calculations. This error decreases to about 30% for the largest spheres considered. One notes that the slopes of the two curves differ even for large systems, yet both appear to be approaching the same asymptotic value. When interpreted in terms of the simple small "B^2" (large system) theory these results seem quite natural. In the context of that theory [14] the two α_0 curves should have slopes of $\langle vD(v)\rangle$ near $B^2=0$ (i.e. for large systems). Although the energy spectra in these large systems for the two sets of calculations are both very near to Maxwellians, the diffusion coefficients D(v) which depend upon the scattering laws are different for the two models. Thus, the average values of vD(v) for the two models also differ. On the other hand, the asymptotic values of these curves corresponding to the values of α_0 at $B^2=0$ on an α_0 vs. B^2 plot should be the same since the $\Sigma_a(v)$ used

in both calculations were identical and the spectra in these large systems are almost Maxwellians regardless of the scattering laws. Thus, the asymptotic values of α_0 which are equal to $\langle v\Sigma_a(v)\rangle$ are in agreement. That the decay of the neutron flux in a system of a given size should be more rapid (larger α_0) for the gas model than for the anisotropic model becomes obvious when one considers that a fixed dimension represents fewer average transport mean free paths for the free-gas model than it does for the anisotropic model. (for example, $\lambda_{tr}^{-0.75}$ = 0.71384 cm for the gas model while $\lambda_{tr}^{-0.75}$ = 0.35453 cm for the anisotropic model.) Thus, a given size sphere is a "smaller" and therefore more leaky system for the gas model than for the anisotropic model and naturally will permit more rapid flux decay for the former.

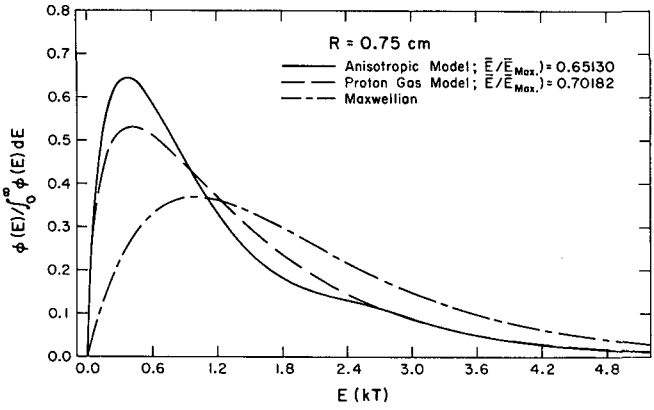

FIG. 7. The energy spectra of the volume-integrated fluxes based on the anisotropic model and proton gas model for a 0.75-cm radius sphere compared with a Maxwellian distribution.

The energy spectra of the volume-integrated fluxes in 0.75-cm radius spheres based on calculations for these two models along with a Maxwellian are shown in Fig. 7. Both energy distributions are considerably cooler than the Maxwellian, the proton gas model spectrum (average energy = 0.70182 $\bar{E}_{max}$) being not quite as cool as the anisotropic model spectrum (average energy = 0.65130 $\bar{E}_{max}$). On the basis of the system dimensions expressed in mean free paths we should expect the gas model spectrum to be cooler. (The simple reasoning being a smaller system implies more leakage and therefore more diffusion cooling. This reasoning is verified by our calculations in that the ratio of the total leakage to the volume-integrated total flux based on the gas model calculations is 1.6710 while this ratio for the anisotropic model calculations is only 1.1420.) However, there is another important factor to be included when considering the energy spectrum within a system. This is the thermalizing power of the scattering material. This thermalizing power is indicated

by the mean-square energy exchange between moderator and thermal spectrum,

$$M_2 = \frac{1}{\sigma_b T^4} \iint dE\, dE_o (E_o - E)^2 E_o\, e^{-E_o/kT}\, \sigma(E_o \to E)$$

The value of M_2 for the gas model is 1.9970, almost twice its value of 1.0226 for the anisotropic model. Thus, the greater thermalizing power of the proton gas model tends to "boost" the energy spectrum up toward a Maxwellian more than the realistic H_2O model does. This accounts for the result that the spectrum of the gas model system is not softer than that of the anisotropic model system in spite of the fact that the neutrons in the latter "see" a larger system.

The "one-phonon" secondary peak shows up clearly again in Fig. 7 and at its height actually rises above the gas model spectrum. No such secondary peak is observed for the gas model since it does not include an oscillator of any kind.

8. Summary

In summarizing the effect of scattering anisotropy on H_2O decay-constant calculations, we may state that the inclusion of anisotropic scattering at least in the form of "transport-corrected" cross-sections is essential and in fact more important than model refinement. (See Fig. 2 and Table I). However, in view of the good agreement with experiment obtained in this work and the uncertainties in die-away experiments in small systems it appears that neither higher order calculations nor more detailed models are necessary for the numerical determination of decay constants in light water.

On the other hand the use of an extremely crude model for H_2O which completely neglects the chemical binding effects such as the proton gas model leads to results which could hardly even be considered to be applicable to the problem.

We point out here that our statement that the use of transport-corrected cross-sections or at most P-1 scattering is sufficient in the calculation of decay constants only applies to light-water systems. Although it probably extends to other "incoherent" scattering materials, it definitely does not apply for crystals such as beryllium and graphite and other materials with significant coherent scattering cross-sections. In these materials coherent effects become important and the inclusion of a high order of scattering anisotropy may be essential to accurate decay constant calculations for small systems.

Acknowledgements

It is indeed a pleasure to acknowledge numerous stimulating discussions with Professor Noel Corngold (BNL and California Institute of Technology) under whose direction this work was done. The author also wishes to express his gratitude to Drs. Brian Clancy (AAEC) and Paul Michael (BNL) and other past and present members of the Yaphank Philosophical Society for their constant interest in this work, to Professor Herbert Goldstein (Columbia) and Mr. Jack Chernick (BNL) for arranging for his stay at Brookhaven, and to Professor Goldstein for originally suggesting the research topic.

REFERENCES

[1] VON DARDEL, G., SJOSTRAND, N., Diffusion parameters of thermal neutrons in water, Phys. Rev. 96 5 (1954) 1245.

[2] CORNGOLD, N., Some transient phenomena in thermalization, I. theory, Nucl.Sci. Engng. 19 (1964) 80.

[3] BEDNARZ, R., Spectrum of the Boltzmann operator with an isotropic thermalization kernel, Proc. IAEA Symp. Pulsed Neutron Research, Karlsruhe, Germany, Vol. I, p. 259, IAEA, Vienna (1965).

[4] ALBERTONI, S., MONTAGNINI, B., "Some spectral properties of the transport equation and their relevance to the theory of pulsed neutron experiments", Pulsed Neutron Research I IAEA, Vienna (1965) 239.

[5] DORNING, J., Thermal neutron decay constants for a simple scattering kernel, Trans. Am. Nucl. Soc. 9 1 (1966) 176.

[6] DORNING, J., Thermal neutron decay in small systems, (to be submitted).

[7] ENGLE, W. W., A user's manual for ANISN, a one-dimensional discrete ordinates transport code with anisotropic scattering, Report No. K-1693, Union Carbide Corp. Computing Technology Center, Oak Ridge (1967).

[8] NELKIN, M., Scattering of slow neutrons by water, Phys. Rev. 119 2 (1960) 741.

[9] KOPPEL, J. U., YOUNG, J. A., Neutron scattering by water taking into account the anisotropy of the molecular vibrations, Nucl. Sci. Engng. 19 (1964) 412.

[10] HONECK, H. C., THERMOS, a thermalization transport theory code for reactor lattice calculations, BNL Rep. BNL 5826, Brookhaven National Laboratory (1961).

[11] SHAPIRO, C., CORNGOLD, N., Approach to equilibrium of a neutron gas, Phys. Rev. 137 6A (1965) A1686.

[12] GON, E., LIDOFSKY, L., GOLDSTEIN, H., Pulsed-source measurements of neutron-diffusion parameters in water, Trans. Am. Nucl. Soc. 8 (1965) 274.

[13] POMRANING, G., Transport methods for the calculation of spatially dependent thermal spectra, "Reactor Physics in the Resonance and Thermal Regions", (GOODJOHN, A., POMRANING, G., Eds.), Vol. I, p. 207, MIT Press, Cambridge (1966).

[14] CORNGOLD, N., "Theoretical interpretation of pulsed neutron phenomena", Pulsed Neutron Research I IAEA, Vienna (1965) 199.

DISCUSSION

A. G. GIBBS: Have you tried gas model calculations using an effective temperature rather than the actual temperature?

J. J. DORNING: No, I have not considered these, since in using the proton gas model my aim was rather to show that neglecting chemical binding was seriously wrong. Using an effective temperature would indirectly include such effects and therefore defeat my purpose. At best it would give me results in which I could not have much faith and which I would therefore want to check using the more realistic models anyway.

S. N. PUROHIT: May I just say that if one were to use the effective temperature in the gas model, one would be violating the detailed balance theorem, and this, of course, should not be done in thermal spectra calculations.

P. F. ZWEIFEL: Can you explain what would happen if these calculations were carried out at very low temperatures?

J. J. DORNING: Well, I have not done such calculations, but at the moment it seems to me that in this case I should have doubts about the applicability of both the Nelkin model and the anisotropic model. At low temperatures the low-energy behaviour of the liquid water would become much more important and therefore the broad band of rotational frequencies would become significant. The liquid properties of water would also have a bearing on the problem under these circumstances, and the diffusive modes such as those shown in the Hayward-Thorson phonon frequency spectrum would have to be included. Both the Nelkin and anisotropic models treat molecular translations in the free gas approximation. At extremely low temperatures the translational motion is definitely not free and perhaps some local intermolecular order may begin to appear. Certainly, a model including free molecular translation for ice would be rather poor. In doing calculations for H_2O at low temperatures, but above freezing, I think that at present the best approach would be to use the Hayward-Thorson spectrum via the GASKET-FLANGE code or some similar one.

EFFET DE LA NON-UNIFORMITE DU FLUX EN RALENTISSEMENT SUR L'INTEGRALE DE RESONANCE

P. BENOIST, A. KAVENOKY ET M. LIVOLANT
CEA, CENTRE D'ETUDES NUCLEAIRES DE SACLAY, FRANCE

Abstract — Résumé

THE EFFECT OF NON-UNIFORMITY OF SLOWING-DOWN FLUX ON THE RESONANCE INTEGRAL. The effect of non-uniformity of the flux in the moderator on the effective resonance integral is studied. This non-uniformity may result either from the localized presence of the fission-neutron source in the fuel, or from capture in the fuel at resonance energy. To calculate these effects use is made of a simplified slowing-down model, with which moderator and fuel can be treated separately, and which is characterized by a fundamental function. The basic approximations of this model are studied separately and numerical applications of the resonance integral corrections are given in a few special cases.

EFFET DE LA NON-UNIFORMITE DU FLUX EN RALENTISSEMENT SUR L'INTEGRALE DE RESONANCE. On étudie l'influence de la non-uniformité du flux dans le modérateur sur l'intégrale effective de résonance; cette non-uniformité peut provenir, soit de la présence de la source de neutrons de fission localisée dans le combustible, soit de la capture dans le combustible à l'énergie des résonances. On utilise pour calculer ces effets un modèle simplifié de ralentissement permettant de traiter séparément modérateur et combustible, et caractérisé par une fonction fondamentale. Les approximations de base de ce modèle sont étudiées séparément et on donne des applications numériques des corrections à l'intégrale de résonance dans quelques cas particuliers.

INTRODUCTION

Nous nous proposons dans cette étude de calculer l'influence de la non-uniformité du flux dans le modérateur sur l'intégrale de résonance dans une cellule de réacteur. Cet effet de non-uniformité, qui est pratiquement négligeable dans les réseaux à eau légère, peut prendre une importance très grande dans les réseaux à graphite et à eau lourde. Pour le mettre en évidence, nous utiliserons une méthode permettant de traiter séparément le modérateur et le combustible. Ce modèle, qui repose sur plusieurs approximations, donne une bonne compréhension physique des phénomènes et permet des calculs assez rapides.

I. EXPOSE DE LA METHODE

Soit une cellule composée d'un modérateur et d'un canal cylindrique contenant un élément combustible. Nous supposerons que la section efficace et les propriétés de ralentissement du modérateur sont indépendantes de l'énergie, et que sa capture est nulle.

Nous allons tout d'abord définir une fonction $\Gamma(u)$ représentant l'«opacité» de la région du canal; ce sera la probabilité pour un neutron entrant dans le canal à la léthargie u, avec une densité angulaire que nous supposerons isotrope, d'être capturé dans le combustible. Il est entendu que cette capture peut avoir lieu à une léthargie supérieure à u, à la suite

de chocs ralentisseurs dans le combustible, mais nous supposerons pour simplifier que, si le neutron échappe à la capture, il pénétrera à nouveau dans le modérateur à la léthargie u à laquelle il est entré; en d'autres termes nous supposons que le ralentissement dans le combustible peut, compte tenu des résonances, jouer un rôle important pour le calcul de $\Gamma(u)$, mais qu'il est négligeable vis-à-vis du gain de léthargie dans un choc contre le modérateur. Cette hypothèse exclut évidemment la présence de noyaux trop légers à l'intérieur du canal. Nous définirons la «section effective» par la relation

$$\Gamma(u) = \frac{4V_u}{S} N_u \sigma_{eff}(u)$$

où V_u est le volume du combustible, S la surface du canal (par unité de longueur de celui-ci) et N_u le nombre de noyaux de combustible par unité de volume.

Nous allons maintenant définir une fonction $\beta(u, u')$ de la manière suivante: soit $\beta(u, u')$ le courant entrant dans le canal à la léthargie u, pour un neutron pénétrant dans le modérateur à la léthargie u' (nous préciserons plus loin sa distribution angulaire d'entrée) étant entendu que le combustible a une section de capture nulle.

On peut montrer que la fonction $\beta(u, u')$ est relativement peu sensible au choix de la distribution angulaire d'entrée dans le modérateur, pour les distributions angulaires rencontrées en pratique; nous choisirons donc une distribution angulaire d'entrée unique indépendante de u', que nous définirons plus loin.

On peut montrer d'autre part que la fonction $\beta(u, u')$ est assez peu sensible à la valeur adoptée à chaque léthargie pour la section de diffusion du combustible; nous calculerons donc $\beta(u, u')$ en faisant le choix une fois pour toutes d'une section de diffusion du combustible indépendante de la léthargie; dans ces conditions, la fonction $\beta(u, u')$ ne dépend plus que de $u - u'$ et nous n'avons à calculer qu'une fonction d'une variable.

Cette fonction $\beta(u)$ possède pour les faibles valeurs de u des transitoires généralisant les transitoires de Placzek; une fois cette zone transitoire franchie elle est constamment décroissante et tend asymptotiquement vers $S/4V\xi\Sigma_m$ quand u tend vers l'infini (Σ_m étant la section totale du modérateur); la fonction $\beta(u)$ jouera un rôle fondamental dans cette étude.

(Il est possible, en s'aidant des propriétés de la transformation de Laplace, de ramener le calcul de la courbe $\beta(u)$ à un calcul de cellule monocinétique. En particulier, on peut exprimer l'intégrale de $\zeta(u)$ au moyen de la méthode ABH [1] avec une bonne approximation:

$$\int_0^\infty \zeta(u)\, du = \rho + \gamma\beta(\infty)$$

où γ est le paramètre intervenant dans le modèle de Greuling-Goertzel et où, dans les notations de [1]

$$\rho = \frac{3}{2} \Sigma_{trm} \frac{b^2 c}{b^2 - c^2} C + \frac{3}{4} \lambda - 1$$

Il est possible également de calculer $\zeta(0)$ au moyen de l'albedo de premier choc du modérateur.)

Soit $J_-(u)$ le courant de neutrons entrant dans le canal par unité de surface et $J_{+0}(u)$ le courant de neutrons entrant pour la première fois dans le modérateur (neutrons provenant directement de la fission) supposé normalisé à l'unité; soit d'autre part $q(u)$ la moyenne sur le volume du modérateur de la densité de ralentissement à la léthargie u. L'équation du bilan s'écrit:

$$V_m \frac{dq}{du} + S J_- \Gamma = S J_{+0} \tag{1}$$

Le courant $J_-(u)$ peut s'exprimer à l'aide de la fonction de Green sans capture $\beta(u-u')$:

$$J_-(u) = \int_0^u \beta(u-u')[J_{+0}(u') - J_-(u')\,\Gamma(u')]\,du'$$

d'où une relation, indépendante de la capture, qui lie $J_-(u)$ et $q(u)$:

$$\frac{S}{V_m} J_-(u) = \int_0^u \beta(u-u')\frac{dq}{du'}\,du' = \beta(\infty)\,q + \int_0^u \zeta(u-u')\frac{dq}{du'}\,du' \tag{2}$$

en posant $\beta(\infty) = S/4V_m \xi \Sigma_m$ et $\zeta(u) = \beta(u) - \beta(\infty)$.

La fonction $\zeta(u)$ tend vers zéro quand u tend vers l'infini.

L'équation qui régit $q(u)$ s'écrit, par combinaison de (1) et (2):

$$\frac{dq}{du} + \beta(\infty)\Gamma q + \Gamma \int_0^u \zeta(u-u')\frac{dq}{du'}\,du' = \frac{S}{V_m} J_{+0} \tag{3}$$

Si le terme en ζ était négligé on obtiendrait pour le facteur antitrappe p à la léthargie u_0 (en admettant que l'intervalle 0, u_0 ne contient pas de sources)

$$p = V_m q(u_0) = \exp\left(-\beta(\infty)\int_0^{u_0}\Gamma(u)\,du\right) = \exp\left(-\frac{V_u N_u}{V_m \xi \Sigma_m} I_{eff}\right)$$

l'intégrale de résonance effective I_{eff} ayant pour valeur

$$I_{eff} = \frac{S}{4V_u N_u}\int_0^{u_0}\Gamma(u)\,du = \int_0^{u_0}\sigma_{eff}(u)\,du$$

Cette intégrale effective correspond à un flux uniforme dans le modérateur et indépendant de u. La présence du terme en ζ dans l'équation va rendre compte des phénomènes transitoires, les uns d'origine énergétique

(du type des transitoires de Placzek), les autres d'origine spatiale (effets de non-uniformité du flux dans le modérateur). Nous allons nous intéresser à deux effets corrosifs importants dus à la présence de ce terme.

a) Effet de relèvement du flux à haute énergie[1]

Aux hautes énergies les neutrons provenant des fissions dans le combustible se groupent dans le modérateur autour de la frontière du canal, et leur répartition tend peu à peu vers l'uniformité au fur et à mesure que la léthargie augmente; il en résulte une augmentation du courant entrant dans le canal, donc de l'intégrale effective. A ces énergies, la section de capture du combustible est suffisamment faible pour qu'on puisse considérer qu'elle n'affecte pas le courant entrant; on peut donc, dans le terme en ζ de l'équation (3), remplacer dq/du', par $(S/V_m)J_{+0}(u')$, conformément à (1). Il en résulte, à une bonne approximation près, que le relèvement du flux conduit à l'augmentation suivante de l'intégrale effective:

$$\Delta I_{eff} = \frac{V_m \xi \Sigma_m}{V_u N_u} \int_0^{u_0} du\, \Gamma(u) \int_0^u \zeta(u-u')\, S\, J_{+0}(u')\, du'$$

$$= \frac{1}{\beta(\infty)} \int_0^{u_0} du\, \sigma_{eff}(u) \int_0^u \zeta(u-u')\, S\, J_{+0}(u')\, du' \qquad (4)$$

Si $S\,J_{+0}(u') = \delta(u')$

$$\Delta I_{eff} = \frac{1}{\beta(\infty)} \int_0^{u_0} \sigma_{eff}(u)\, \zeta(u)\, du \qquad (5)$$

b) Effet d'interaction des résonances

A plus basse énergie, il apparaîtra un effet d'ombre des résonances les unes sur les autres; en d'autres termes la capture dans une résonance créera une dépression de flux dans le modérateur au voisinage de la frontière du canal, qui tendra à disparaître avec l'augmentation de la léthargie; d'où une diminution de l'intégrale effective pour les résonances suivantes. C'est en quelque sorte le phénomène inverse du précédent.

Pour calculer la correction du 1er ordre, nous remplacerons, dans le terme en ζ de l'équation (3), dq/du' par sa valeur non perturbée:

$$\frac{dq}{du'} + \beta(\infty)\,\Gamma(u')\,q(u') = \beta(\infty)\,\Gamma(u') \exp\left(-\beta(\infty) \int_{u'}^{u} \Gamma(u')\, du'\right) q(u) \qquad (6)$$

[1] Cet effet a été étudié en particulier par Naudet [2].

d'où une correction à l'intégrale effective, de signe contraire à la précédente

$$\delta I_{eff} = \frac{-S}{4V_u N_u} \int_0^{u_0} du\, \Gamma(u) \int_0^{u} du'\, \Gamma(u')\, \zeta(u-u') \exp\left(\beta(\infty) \int_{u'}^{u} \Gamma(u')\, du'\right) \qquad (7)$$

Le facteur exponentiel est en pratique très voisin de l'unité dans l'intervalle de léthargie où ζ est différent de 0; en introduisant les sections effectives, on a donc:

$$\delta I_{eff} = -\frac{4V_u N_u}{S} \int_u^{u_0} du\, \sigma_{eff}(u) \int_0^{u} du'\, \sigma_{eff}(u')\, \zeta(u-u') \qquad (8)$$

Le problème est maintenant de déterminer la fonction $\zeta(u)$ ou, ce qui revient au même, $\beta(u)$.

II. CALCUL DE $\beta(u)$

Méthodes de calcul et aspect physique de $\beta(u)$

Comme nous l'avons vu il existe deux ambiguïtés dans la détermination de $\beta(u)$, celle relative au choix de la distribution angulaire d'entrée dans le modérateur, et celle relative au choix de la section de diffusion du combustible, que nous avons supposée constante, en fonction de la léthargie.

Avant d'étudier l'influence de ces deux approximations, nous allons passer en revue rapidement les moyens de calcul dont nous disposons et donner quelques-uns des résultats obtenus; nous avons utilisé trois codes fondés sur la théorie du transport:

1° Le code de ralentissement TIBET [3] utilisant la théorie intégrale de transport, dans l'hypothèse du choc isotrope dans le système du laboratoire;

2° Le code JANVIER III de Amouyal et Tariel [4], utilisant l'approximation double P_2 de Yvon, admettant une loi de choc à un harmonique avec corrélation angle-énergie

$$\Sigma_s(u' \to u, \mu) = \tfrac{1}{2}\Sigma_s^0(u' \to u) + \tfrac{3}{2}\mu\, \Sigma_s^1(u' \to u)$$

3° Le code ALBEMOD [5], utilisant la méthode de Monte-Carlo, permettant de tenir compte de la loi de choc exacte avec corrélation angle-énergie (choc isotrope dans le système du centre de masse).

Dans l'hypothèse du choc isotrope, les deux codes TIBET et JANVIER III donnent pour la fonction $\beta(u)$ des résultats équivalents à 1% près. Ces résultats sont confirmés par le calcul de Monte-Carlo. La figure 1 représente la fonction $\beta(u)$ obtenue au moyen du code TIBET, pour la cellule à eau lourde suivante (cellule 1):

Rayon de la barre combustible	2	cm
Rayon de la cellule	11,46	cm

Section efficace totale du modérateur [2]	0,401 cm^{-1}
Section efficace totale du combustible (supposé non capturant)	0,4 cm^{-1}

On voit que la fonction $\beta(u)$ décroît asymptotiquement et tend vers $S/4V_m \xi \Sigma_m$ d'une manière exponentielle (l'asymptote correspond à un flux uniforme dans le modérateur) et qu'il existe pour les faibles valeurs de u des transitoires de même nature que les transitoires de Placzek. Il apparaît une première discontinuité correspondant au transfert maximal de léthargie par choc dans l'oxygène ($\epsilon_0 \simeq 0,250$), et une seconde discontinuité de même type correspondant au deutérium ($\epsilon_D \simeq 2,20$). On voit que pour u = 0 la fonction $\beta(u)$ a une valeur finie et qu'au voisinage de u = 0, cette fonction atteint des valeurs beaucoup plus élevées que la valeur asymptotique.

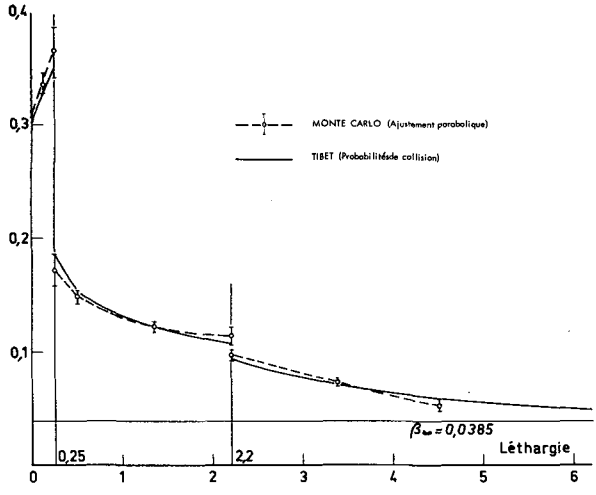

FIG. 1. Fonction β (u) – Cellule 1, D_2O, choc isotrope.

Dans la réalité le choc sur les atomes de modérateur est fortement anisotrope et la corrélation angle-énergie joue un rôle important. Seul le code ALBEMOD permet de prendre en compte cet effet de manière exacte. Nous avons testé d'autre part deux approximations de cette loi de choc: loi de choc à un harmonique, au moyen du code JANVIER III, et correction de transport, au moyen du code TIBET; cette correction revient à choisir comme loi de choc

$$\Sigma_s(u' \to u, \mu) = \tfrac{1}{2}\left[\Sigma_s^0(u' \to u) - \Sigma_s^1(u')\,\delta(u-u')\right]$$
$$+ \Sigma_s^1(u')\,\delta(u-u')\,\delta(\mu-1)$$

ce qui permet l'emploi d'un code avec loi de choc isotrope.

La figure 2 montre la fonction $\beta(u)$ obtenue dans les trois cas. L'usage de la loi de choc exacte ne change évidemment pas l'ordonnée

[2] Cette valeur ne correspond pas exactement à la section efficace totale de l'eau lourde dans le domaine épithermique, mais nous ne nous intéressons qu'à la comparaison des méthodes.

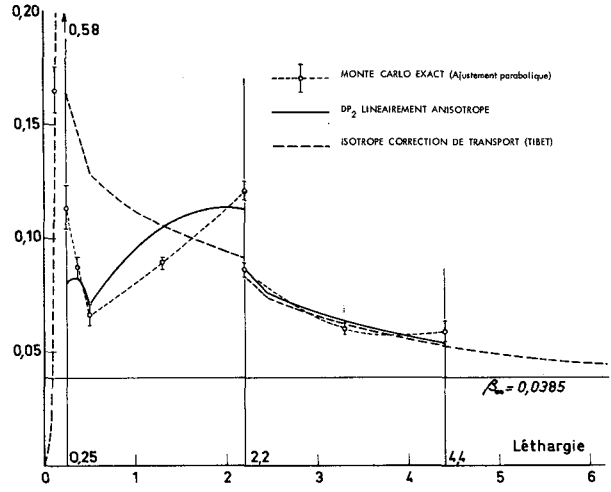

FIG. 2. Fonction β (u) – Cellule 1, D_2O.

de l'asymptote; dans la zone asymptotique ($u > \epsilon_D$) il diminue $\beta(u)$, bien que l'allure générale de la décroissance soit sensiblement la même; dans cette zone, la loi de choc à un harmonique et la correction de transport conduisent à des résultats en bon accord avec ceux obtenus à l'aide de la loi de choc exacte. Par contre, dans la zone transitoire ($u < \epsilon_D$), la présence d'une corrélation angle-énergie modifie complètement le comportement de $\beta(u)$; en particulier, au lieu de partir d'une valeur finie pour $u = 0$, la courbe part de zéro; la loi de choc à un harmonique représente assez bien l'allure de la courbe dans la zone transitoire, par contre la correction de transport donne des résultats complètement aberrants. Pour le calcul pratique de $\beta(u)$, nous utiliserons donc un calcul isotrope avec correction de transport dans la zone $u > \epsilon_D$ (code TIBET), et un calcul de Monte-Carlo rendant compte de la loi de choc exacte dans la zone $u < \epsilon_D$ (code ALBEMOD).

Nous avons d'autre part étudié une cellule type de réacteur à graphite français refroidi au gaz (réacteur Bugey) dont les caractéristiques sont les suivantes (cellule 2):

Rayon intérieur du tube combustible	4,25	cm
Rayon extérieur du tube combustible (tube homogénéisé)	5,15	cm
Rayon du canal	7	cm
Rayon de la cellule	21,66	cm
Section efficace totale du modérateur	0,405	cm^{-1}
Section efficace totale du combustible (supposé non capturant)	0,4	cm^{-1}

Dans le calcul, nous avons représenté le tube par une barre homogène de même rayon extérieur et comportant le même nombre de noyaux de combustible. On donne sur la figure 3 la fonction $\beta(u)$ correspondant à la loi de choc exacte, et celle correspondant à la correction de transport. La courbe présente une seule discontinuité, correspondant au gain

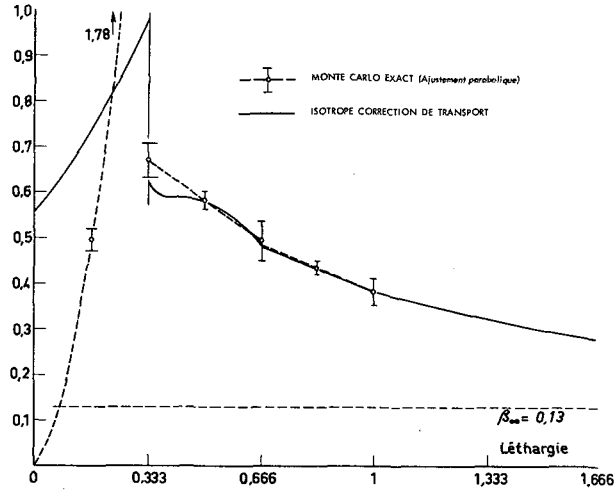

FIG. 3. Fonction β (u) – Cellule 2, graphite.

maximal de léthargie du graphite (ϵ = 0,333); d'autre part, bien que les dimensions de la cellule soient beaucoup plus grandes que dans le cas de l'eau lourde, la courbe tend plus rapidement vers son asymptote.

Influence de la distribution angulaire d'entrée dans le modérateur et de la section efficace du combustible

Dans la définition de $\beta(u, u')$ nous n'avons pas précisé la distribution angulaire des neutrons entrant dans le modérateur à u = 0. En réalité, cette distribution angulaire, dans les deux problèmes envisagés (relèvement du flux à haute énergie et interaction des résonances), est fonction de la léthargie u'. Nous admettrons qu'il est légitime d'utiliser dans tous les cas une distribution angulaire commune, que nous allons choisir maintenant.

Une autre ambiguïté concerne la section efficace de diffusion à attribuer au combustible pour le calcul de $\beta(u)$. Dans le problème réel il est évident que cette section efficace dépend de la léthargie, mais nous sommes conduits à choisir une section efficace indépendante de u afin que la fonction $\beta(u, u')$ ne dépende que de u – u'.

Pour fixer les idées, nous choisirons provisoirement une source de 1 neutron entrant dans le modérateur suivant une densité angulaire isotrope. D'autre part, nous prendrons comme section efficace de référence du barreau la section potentielle du combustible.

Nous allons d'ailleurs examiner dans quelle mesure le choix de la section du combustible influe sur $\beta(u)$. Le tableau I donne, dans le cas de la cellule 1, les valeurs, calculées par ALBEMOD, de l'intégrale de $\beta(u)$ dans plusieurs domaines de léthargie, pour une densité entrante isotrope et deux valeurs différentes de la section efficace du combustible. Les marges d'erreur indiquées correspondent à un intervalle de confiance de 95%.

TABLEAU I. VALEURS DE L'INTEGRALE $\int\beta(u)\,du$ DANS DIFFERENTS INTERVALLES DE LETHARGIE INFLUENCE DE LA SECTION EFFICACE INTERNE DU COMBUSTIBLE ET DE LA DISTRIBUTION ANGULAIRE D'ENTREE DANS LE MODERATEUR

u	Source isotrope		Source en volume
	$\Sigma_{su} = 0,04$ (cm^{-1})	$\Sigma_{su} = 0,4$ (cm^{-1})	$\Sigma_{su} = 0,4$ (cm^{-1})
0			
	0,0533 ± 0,0017	0,0536 ± 0,0016	0,0518 ± 0,0015
0,25			
	0,0245 ± 0,0011	0,0238 ± 0,0011	0,0224 ± 0,0010
0,50			
	0,157 ± 0,003	0,156 ± 0,003	0,153 ± 0,003
2,2			

TABLEAU II. VALEURS DE L'INTEGRALE $\int\beta(u)\,du$ DANS DIFFERENTS INTERVALLES DE LETHARGIE INFLUENCE DE LA SECTION EFFICACE INTERNE DU COMBUSTIBLE

u	Source en volume		
	$\Sigma_{su} = 0,01$ (cm^{-1})	$\Sigma_{su} = 0,1$ (cm^{-1})	$\Sigma_s = 1$ (cm^{-1})
0			
	0,3593	0,3470	0,3277
2,20			
	0,1655	0,1630	0,1586
4,40			

D'autres types de distributions angulaires d'entrée dans le modérateur ont été étudiés. En particulier, on peut prendre la distribution angulaire correspondant à une source en volume répartie uniformément dans le combustible. Cette distribution angulaire se rapproche de celle des neutrons provenant directement de la fission et est par suite assez bien adaptée au calcul de l'effet de relèvement à haute énergie. La troisième colonne du tableau I donne les intégrales de $\beta(u)$ calculée par ALBEMOD dans le cas d'une source en volume.

Le tableau II montre, dans le cas d'une source en volume, les variations de certaines intégrales de $\beta(u)$ lorsque la section efficace du

combustible varie. (Ce calcul a été fait au moyen du code TIBET dans l'hypothèse du choc isotrope.) Mais avec ce type de source la variation de la section efficace du combustible influe sur la distribution angulaire des neutrons entrant dans le modérateur. On voit que l'écart est plus important que dans le tableau I, ce qui tend à prouver que la distribution angulaire de la source a plus d'influence que le choix de la section efficace du combustible. L'examen de ces deux tableaux montre que l'effet de la distribution angulaire des neutrons entrant dans le modérateur est prépondérant.

Nous constatons que la fonction $\zeta(u)$ varie de quelques pour cent lorsque l'on fait varier, soit la distribution angulaire des neutrons entrant dans le modérateur, soit la section efficace du combustible supposé purement diffusant.

Les calculs des corrections à l'intégrale effective que nous effectuerons maintenant utiliseront une fonction $\zeta(u)$ définie pour une source uniforme dans le volume du combustible; ce choix, probablement très bon pour le calcul de l'effet à haute énergie, est peut être plus discutable pour l'effet d'interaction des résonances.

III. CALCUL DES CORRECTIONS A L'INTEGRALE EFFECTIVE

Nous allons maintenant calculer les corrections ΔI_{eff} et δI_{eff} données par (4) et (8). Pour cela nous avons besoin de la fonction $\Gamma(u)$. Compte tenu du fait que nous nous intéressons à un combustible métallique, ne contenant pas de noyaux légers, nous avons, au stade actuel de cette étude, calculé $\Gamma(u)$ en négligeant tout ralentissement dans le barreau, ce qui ramène le calcul à un calcul monocinétique; ceci est probablement justifié pour le calcul des corrections, mais ne le serait pas pour le calcul de l'intégrale effective elle-même. Nous avons utilisé dans le domaine compris entre 2 eV et 1015 eV une bande de sections efficaces calculée par le code GAROL [6] qui utilise 6670 points dans cet intervalle. Aux énergies supérieures à 30 keV, on a utilisé des sections efficaces données par Schmidt [7]. Nous avons exclu provisoirement de notre étude la zone comprise entre 1015 eV et 30 keV, où l'on ne connaît que la répartition statistique des résonances, bien que son influence sur l'effet de relèvement à haute énergie puisse être assez sensible. La fonction $\Gamma(u)$ a été obtenue au moyen du code de probabilités de collision ALCOLL [3], en décomposant le barreau en plusieurs zones coaxiales.

Dans le cas de la cellule 1, les corrections à apporter à l'intégrale effective sont les suivantes:

Effet de relèvement à haute énergie (au-dessus de 30 keV):

$$\Delta I_{eff} = 0,953 \text{ b}$$

Effet d'interaction des résonances (au-dessous de 1015 eV):

$$\delta I_{eff} = -0,173 \text{ b}$$

A titre d'indication l'intégrale effective calculée par la formule d'Hellstrand [8] vaut 8,92 b.

TABLEAU III. DETAIL DES INTERACTIONS DANS LA CELLULE 1 (D_2O) POUR LES QUATRE PRINCIPALES RESONANCES A BASSE ENERGIE

Energie (eV)	δI_{eff} Résonances précédentes (b)	δI_{eff} Résonance sur elle-même (b)	δI_{eff} Total de la résonance (b)
76,51			
	- 0,004	0	- 0,004
52,97			
	- 0,010	- 0,003	- 0,013
27,73			
	- 0,019	- 0,007	- 0,026
12,78			
	- 0,068	- 0,050	- 0,118
2,00			

TABLEAU IV. DETAIL DES INTERACTIONS DANS LA CELLULE 2 (GRAPHITE) POUR LES QUATRE PRINCIPALES RESONANCES A BASSE ENERGIE

Energie (eV)	δI_{eff} Résonances précédentes (b)	δI_{eff} Résonance sur elle-même (b)	δI_{eff} Total de la résonance (b)
76,51			
	- 0,016	0	- 0,016
52,97			
	- 0,039	- 0,007	- 0,046
27,73			
	- 0,076	- 0,017	- 0,093
12,78			
	- 0,199	- 0,163	- 0,362
2,00			

Dans le cas de la cellule 2, nous avons:

$\Delta I_{eff} = 0,907$ b

$\delta I_{eff} = -0,556$ b

La formule d'Hellstrand [8] conduit ici à 9,55 b.

Les tableaux III et IV donnent le détail de l'effet d'interaction pour les quatre principales résonances à basse énergie, dans le cas des

cellules 1 et 2 respectivement. On voit que l'effet d'interaction pour ces quatre résonances représente environ 93% de l'effet d'interaction global; il y a donc lieu d'attacher une importance particulière à ces quatre résonances; pour les résonances à plus haute énergie, on peut se contenter d'un traitement moins élaboré, du moins en ce qui concerne l'effet correctif considéré.

Un calcul de Monte-Carlo de référence a été effectué à l'aide du code RESCAPE [5]; ce code permet de calculer le facteur antitrappe pour une ou plusieurs résonances sans approximation, ainsi que les effets d'interaction envisagés; il résout, non pas le problème direct, mais le problème adjoint, ce qui permet d'obtenir les effets d'interaction avec une bonne précision. Ce code a fourni, pour l'interaction de la résonance à basse énergie avec elle-même, une valeur de 0,05 b, en bon accord avec celle donnée dans le tableau III.

REMERCIEMENTS

Ce travail a été effectué avec la collaboration de MM. D. Pillard et B. Micaux, que nous désirons remercier ici.

REFERENCES

[1] AMOUYAL, A., BENOIST, P., HOROWITZ, J., Nouvelle méthode de détermination du facteur d'utilisation thermique d'une cellule, J. Nucl. Energy 6 (1957) 79.

[2] NAUDET, R., Calcul du facteur antitrappe dans les réseaux à eau lourde, Rapport CEA-R-2475 (1965).

[3] KAVENOKY, A., LIVOLANT, M., Calcul et utilisation des probabilités de collision, Rapport à paraître.

[4] AMOUYAL, A., TARIEL, H., Programme de résolution de l'équation du transport multigroupe à une dimension en géométrie plane, cylindrique et sphérique dans l'approximation double P_n, Rapport CEA à paraître.

[5] LIVOLANT, M., PILLARD, D., Code pour le calcul de l'intégrale effective par la méthode Monte-Carlo, Rapport à paraître.

[6] STEVENS, C.A., SMITH, C.V., GAROL – A Computer Program for Evaluating Resonance Absorption Including Resonance Overlap, Rep. GA-6637 (1965).

[7] SCHMIDT, J.J., Neutron Cross-Sections for Fast Reactors Materials, Rep. KFK-120 (EANDC-E-35U) (1962).

[8] HELLSTRAND, E., LUNDGRE, G., The Resonance Absorption of Uranium Metal and Oxide, Rep. AE-77 (1962).

THERMALIZATION CALCULATIONS IN A CYLINDRICAL SHELL

S.A. KUSHNERIUK, C.S. KALMAN* AND A.M. MALECKI
CHALK RIVER NUCLEAR LABORATORIES,
ONTARIO, CANADA

Abstract

THERMALIZATION CALCULATIONS IN A CYLINDRICAL SHELL. An approximate, semi-analytical procedure for determining the distribution and energy spectrum of the thermal and epithermal neutron flux in a weakly neutron capturing, cylindrical shell medium is considered. The shell medium is taken to represent the moderator surrounding a fuel rod in a thermal reactor. The basis for calculating the flux in most of the moderator is the energy-dependent diffusion equation. Transient corrections to the diffusion approximation are added near the medium boundaries. The effects of adjoining media are taken into account through the boundary conditions imposed on the diffusion and transient fluxes. At the inner boundary these effects are calculated by collision probability methods. Activation fluxes are derived from the calculated neutron flux distributions and compared with measurements made in the D_2O moderator surrounding a uranium metal rod in the ZEEP reactor.

1. INTRODUCTION

The objective in this investigation has been to look into some possible methods of determining the "thermal" neutron flux distribution in a reactor cell and to see how sensitive the energy spectrum of the flux is to the forms assumed for the energy dependence of the transport and transfer cross-sections.

The reactor cell considered is assumed to have cylindrical symmetry, to be of infinite length and to be embedded in an environment such that there is no current of neutrons at the outer cell boundary of radius R. The cell itself consists of an inner region of radius b which absorbs most of the neutrons generated by the sources in the cell and a shell of thickness R-b, the moderator, in which most of the neutron slowing down and thermalization is carried on.

Our main concern in this report is the detailed specification of the flux distribution, $\phi(r,E)$, in the region R-b. The flux is written as the sum of two components

$$\phi(r,E) = \phi_{trans}(r,E) + \rho(r,E) \tag{1.1}$$

in which $\phi_{trans}(r,E)$ is a "transient" flux, important only near the boundary of the neutron-absorbing inner region and $\rho(r,E)$ is the flux obtained, possibly in an approximate form, from the solution of the energy-dependent diffusion equation

$$\nabla^2\rho(r,E) - G\rho(r,E) = -3\Sigma_{tr}(E)\ q(E) \tag{1.2}$$

---

* Summer student, 1965; now at the University of Rochester, Rochester, N.Y., United States of America.

where G is a linear integral operator defined as

$$G\psi(E) = 3\Sigma_{tr}(E)\left[\Sigma(E)\psi(E) - \int_0^{E_M} \Sigma(E'\to E)\psi(E')dE'\right] \tag{1.3}$$

E_M, in the above, is the maximum energy for which the solution (1.1) is considered (in our case 1.44 eV) while $\Sigma_{tr}(E)$ and $\Sigma(E) = \Sigma_a(E) + \Sigma_s(E)$ are the usual transport and total macroscopic cross-sections in the shell medium. $\Sigma(E'\to E)$ is the transfer cross-section which satisfies the detailed balance relation

$$\Sigma(E'\to E)M(E') = \Sigma(E\to E')M(E) \tag{1.4}$$

where M(E) is the Maxwellian spectrum and also

$$\Sigma_s(E) = \int \Sigma(E\to E')dE' \tag{1.5}$$

q(E) is the source spectrum which we have taken to be uniformly distributed in the shell.

The neutron fluxes and sources outside the shell medium are coupled to the fluxes inside the shell via the boundary conditions imposed on the diffusion flux at r = b and r = R. We assume that the neutron current in the moderating region R-b is adequately given everywhere by the diffusion theory expression $j(r,E) = -\rho'(r,E)/3\Sigma_{tr}(E)$. Since transient effects at the outer shell boundary are assumed negligible and we have taken $j(R,E) \equiv 0$ for all E it follows that the boundary condition on the diffusion flux at r = R is

$$\phi'(R,E) \equiv \rho'(R,E) = 0, \text{ all } E \tag{1.6}$$

At the inner boundary we write

$$\frac{1}{3\Sigma_{tr}(E)}\rho'(b,E) = J^{in}(b,E) - J^{out}(b,E) \tag{1.7}$$

where J^{in} and J^{out}, the neutron incurrent and outcurrent at r = b, are to be calculated directly by collision probability methods.

Equation (1.7) is the second boundary condition on the diffusion flux. In general this equation will be rather complicated, particularly if the inner region is also a thermalizing region. In this investigation we limit ourselves to elementary interior regions, those containing no neutron sources and such that scattering collisions have negligible effect on the neutron energy, at least in the energy range of interest. Such is nearly the case for natural uranium metal fuel elements sheathed in zirconium or aluminum. In these systems J^{out} may be described simply as

$$J^{out}(b,E) = [1-\beta(b,E)]\ J^{in}(b,E) \tag{1.7'}$$

where $\beta(b,E)$ is the blackness of the interior region to neutrons of energy E. The boundary condition (1.7) then reduces to

$$\rho'(b,E) = 3\Sigma_{tr}(E)\ \beta(b,E)\ J^{in}(b,E) \tag{1.8}$$

These elementary systems are of some practical interest. They are ideally suited for our purposes, that of investigating the possible approximations

to $\phi(r,E)$ and determining the sensitivity of the solutions to the forms assumed for $\Sigma_{tr}(E)$ and $\Sigma(E'\to E)$.

The moderator of interest to us is D_2O. We have used two types of $\Sigma_{tr}(E)$ and $\Sigma(E'\to E)$ each in our calculations.

(A) $\Sigma_{tr}(E)$ based on the Wick theory in the short collision time approximation [1],

$$\Sigma_{tr}^{(W)}(E) = \Sigma_s(E)\ [1-b(E)] \tag{1.9}$$

with $b(E) \simeq 0.240\ (2 - \sigma_s(E)/\sigma_s(E_M))$ in which $\Sigma_s(E)$ is the measured macroscopic scattering cross-section, $\Sigma_s(E) = N\sigma_s(E)$. BNL-325[2] data was used to give $\sigma_s(E)$.

(B) $\Sigma_{tr}(E)$ based on Nelkin's[3] model of neutron scattering. The data actually used here was obtained from Honeck's calculations as outlined in the program GAKER[4].

(C) $\Sigma(E'\to E)$ and hence also $\Sigma_s(E)$ based on the monatomic gas model using an effective mass of 3.6 amu for $DO_{\frac{1}{2}}$ as suggested by Brown and St. John[5].

(D) $\Sigma(E'\to E)$ and hence also $\Sigma_s(E)$ based on the Nelkin model as indicated in (B) above.

The possible approximations to the diffusion and transient fluxes and further details concerning the boundary condition (1.8) are discussed in section 2. Section 3 contains the specification of the source function $q(E)$ and some detail about the neutron fluxes in the inner region. In section 4 the calculated manganese activations based on our approximations to $\phi(r,E)$ are compared with the manganese activations measured in the D_2O moderated ZEEP reactor containing a lattice array of Aℓ sheathed, uranium metal rods.

2. DISCUSSION OF THE SOLUTION OF THE DIFFUSION EQUATION, THE ASSOCIATED BOUNDARY CONDITION AND THE APPROXIMATIONS TO THE TRANSIENT FLUX

For purposes of investigating an elementary approximation to the diffusion flux $\rho(r,E)$ and evaluating the boundary condition (1.8) we consider a series expansion solution of the equation (1.2) of the type

$$\rho(r,E) = \sum_{m=o}^{\infty} C_{2m}(E)\ r^{2m} + \sum_{m=o}^{\infty} B_{2m}(E)\ r^{2m} \log r/b \tag{2.1}$$

It is easy to verify that this series satisfies the equation (1.2) provided a suitable coupling of the coefficients $C_n(E)$ and $B_n(E)$ is made via energy-dependent integral equations. The expansion (2.1) which satisfies also the boundary $\rho'(R,E) = 0$ may be rewritten, with the aid of the diffusion equation, as

$$\rho(r,E) = A(E) + f_o(r)\ B(E) + \sum_{m=1}^{\infty} f_m(r)\ G^m B(E) \tag{2.2}$$

in which

$$f_o(r) = -(r^2 + 2R^2 \log R/r)/2R^2 \tag{2.3}$$

and $f_m(r)$ are particular solutions of the equations

$$\nabla^2 f_m(r) = f_{m-1}(r) + \theta_m, \quad m \geq 1 \tag{2.4}$$

in which the θ_m are so chosen that the condition $f_m'(R) = 0$ holds. In (2.2) G^m implies m repeated applications of the operator G defined by (1.3), i.e. $G^m\psi(E) = G \cdot G \cdots G\psi(E)$. The functions A(E) and B(E) satisfy a consistency relation

$$GA(E) = 3\Sigma_{tr}(E)q(E) - \frac{2}{R^2} B(E) + \sum_{m=1}^{\infty} \theta_m G^m B(E) \tag{2.5}$$

From (2.3) and (2.4), $f_1(r)$ and θ_1, for instance, are

$$f_1(r) = (r^4 + 2r^2R^2 - 8r^2R^2 \log R/r)/32R^2; \; \theta_1 = 3/4 \tag{2.6}$$

To completely specify the solution (2.2) for $\rho(r,E)$ we need one further equation to connect the functions A(E) and B(E). This is obtained from the boundary condition (1.8) which we now examine in greater detail. Let $T^{in}[S(r)]$ be the contribution to the incurrent at the surface r = b due to an isotropic source distributed as S(r) in the medium surrounding the surface b. If S(r) is defined over the range $b \leq r < \infty$, $T_\infty^{in}[S(r)] = 1/\pi \int_0^{\pi/2} \cos\phi d\phi \int_0^\infty S(r)Ki_2(\Sigma y)dy$ with $r^2 = b^2 + y^2 + 2by \cos\phi$, Σ being the macroscopic cross-section in the uniform medium surrounding the surface. For $S(r) \equiv q$, $T_\infty^{in}[q] = q/4\Sigma$. For $S(r) = r^2$, $T_\infty^{in}[r^2] = b^2(1+3/2b^2\Sigma^2 + 4/3b\Sigma)/4\Sigma$. When $S(r) = \Sigma \log r/b$, $T_\infty^{in}[\Sigma \log r/b]$ is denoted as $J_{in}(\log)$ in CRT-712[6] where tables of $J_{in}(\log)$ are given. When S(r) is defined over a limited range of r, $T^{in}[S(r)]$ is similar in form to $T_\infty^{in}[S(r)]$. We do not give it in detail.

In the case of interest to us the sources of neutrons for the incurrent at r = b are the distributed sources q(E), the scattered neutrons $\int\Sigma(E'\to E)\rho(r,E')dE'$ and $\int\Sigma(E'\to E)\phi_{trans}(r,E')dE'$ and the "boundary" source at the interface $r = R^\dagger$. Using the diffusion equation (1.2) we can write $J^{in}(b,E)$ as

$$J^{in}(b,E) = \frac{\rho(b,E)}{4} + T^{in}\left[\Sigma(E)(\rho(r,E)-\rho(b,E)) - \frac{1}{3\Sigma_{tr}(E)} \nabla^2\rho(r,E) + \int\Sigma(E'\to E)\, \phi_{trans}(r,E')dE'\right] + \alpha^{in} \tag{2.8}$$

in which α^{in} is a small correction term associated with the direct contribution to $J^{in}(b,E)$ by the "boundary" source less the contribution of a source term $\Sigma(E)\rho(b,E)$ extending to ∞ beyond the boundary r = R, the latter arising because to get the first term on the R.H.S. of (2.8) the source $\Sigma(E)\rho(b,E)$ had been extended beyond r = R. Using (2.8), the boundary condition (1.8) may now be written

$$\lambda(b,R,E) \equiv \frac{\rho(b,E)}{\rho'(b,E)} = \frac{4}{3\Sigma_{tr}(E)\beta(b,E)} - \frac{4T^{in}[\quad] + 4\alpha^{in}}{\rho'(b,E)} \tag{2.9}$$

---

† At r=R the boundary source is $J^{in}(E,R)$ which $\approx \frac{\rho(R,E)}{4} + \frac{q(E)}{4\Sigma(E)}$.

where, for convenience, the "extrapolation length" λ has been introduced to signify $\rho(b,E)/\rho'(b,E)$.

We now introduce explicitly the first order terms

$$\rho_F(r,E) = A(E) + f_o(r)\ B(E) \tag{2.10}$$

in the expansion (2.2) of $\rho(r,E)$ and write (2.9) as

$$\lambda(b,R,E) = \frac{\rho(b,E)}{\rho'(b,E)} = \lambda^*(b,R,E) + \xi(b,R,E) \tag{2.11}$$

in which

$$\lambda^*(b,R,E) = \frac{4}{3\Sigma_{tr}(E)\beta(b,E)} - \frac{4T^{in}[\Sigma(E)(\rho_F(r,E)-\rho_F(b,E))-\nabla^2\rho_F(r,E)/3\Sigma_{tr}(E)]}{\rho_F'(b,E)}$$

$$- \frac{4T^{in}[\int\Sigma(E'\to E)\phi_{trans}(r,E')dE'] + 4\alpha^{in}}{\rho'(b,E)} \tag{2.12}$$

and

$$\xi(b,R,E) = \frac{4T^{in}[\Sigma(E)(\rho_F(r,E)-\rho_F(b,E)) -\nabla^2\rho_F(r,E)/3\Sigma_{tr}(E)]}{\rho_F'(b,E)}$$

$$- \frac{4T^{in}[\Sigma(E)(\rho(r,E)-\rho(b,E))-\nabla^2\ \rho(r,E)/3\Sigma_{tr}(E)]}{\rho'(b,E)} \tag{2.13}$$

We note particularly that the 2nd term on the R.H.S. of (2.12) does not depend on the functions A(E) and B(E) but only on the function $f_o(r)$.

We recall also that in the one velocity limit in the case when the moderator is of finite thickness R-b, the moderator captures no neutrons and contains a uniform distribution of sources, the flux distribution in the moderator $\rho_F(r)$ satisfying the boundary condition $\rho_F'(R) = 0$ is $\rho_F(r) = A + f_o(r)B$ in which A and B are constants and $f_o(r)$ is the same as the $f_o(r)$ given by (2.3). The boundary condition $\lambda(b,R) = \rho_F(b)/\rho'_F(b)$ in this case is derived from

$$\lambda(b,R) = \frac{4}{3\Sigma_{tr}\beta(b)} - \frac{4T^{in}[\Sigma(\rho_F(r)-\rho_F(b))-\nabla^2\rho_F(r)/3\Sigma_{tr}]}{\rho_F'(b)}$$

$$- \frac{4T^{in}[\Sigma\phi_{trans}(r)] + 4\alpha_F^{in}}{\rho_F'(b)} \tag{2.14}$$

where again we note that the 2nd term on the R.H.S. of (2.14) depends only on the function $f_o(r)$. This term in fact is identical with the 2nd term on the R.H.S. of (2.12), the only difference being that the Σ in (2.12) is implicitly a function of E. This identity also applies to the first term on the R.H.S.'s of (2.12) and (2.14). We make the assumption that the third term on the R.H.S. of (2.12) is well enough approximated by its counterpart in (2.14) and conclude that $\lambda^*(b,R,E)$ is very nearly an energy-dependent equivalent of the one velocity $\lambda(b,R)$[7], i.e.

$$\lambda^*(b,R,E) \equiv \lambda^*(b,E) + \frac{b^2}{R^2-b^2}\left[\frac{1}{12b\Sigma(E)} + \frac{0.252}{0.378 + b\Sigma(E)}\right]/\Sigma_{tr}(E) \tag{2.15}$$

in which $\lambda^*(b,E)$ is the "infinite medium" extrapolation length

$$\lambda^*(b,E) = \left[\frac{4}{3\beta(b,E)} - g(b\Sigma_{tr}(E))\right]/\Sigma_{tr}(E) \tag{2.16}$$

Explicit formulae for $g(x)$ are given in [7]. The boundary condition (1.8) is then given by (2.11) with $\lambda^*(b,R,E)$ defined by (2.15) and $\xi(b,R,E)$ by (2.11).

If we now substitute the series expansion (2.2) explicitly into (2.11) and solve for $A(E)$ we obtain

$$A(E) = -\sum_{m=0}^{\infty} f_m(b)G^m B(E) + \lambda^*(b,R,E)\sum_{m=0}^{\infty} f_m'(b)G^m B(E) + \Delta(b,R,E) \tag{2.17}$$

in which $\Delta(b,R,E)$ is the product $\Delta(b,R,E) = \xi(b,R,E)\rho'(b,E)$, i.e.

$$\Delta(b,R,E) = 4\sum_{m=1}^{\infty} T^{in}\left[\Sigma(E)\left\{f_m(b)-f_m(r) + \frac{bR^2}{R^2-b^2}\left(\frac{b^2-r^2}{2R^2} + \log r/b\right)f_m'(b)\right\}\right.$$
$$\left. + \frac{1}{3\Sigma_{tr}(E)}\left\{f_{m-1}(r) + \theta_m + \frac{2b}{R^2-b^2} f_m'(b)\right\}\right]G^m B(E) \tag{2.18}$$

On substituting for $A(E)$ into (2.5) we see that $B(E)$ is a solution of the linear integral equation

$$3\Sigma_{tr}(E)q(E) - \frac{2}{R^2} B(E) + \sum_{m=1}^{\infty}\theta_m G^m B(E) + \sum_{m=0}^{\infty} f_m(b)G^{m+1}B(E)$$
$$= G\lambda^*(b,R,E)\sum_{m=0}^{\infty} f_m'(b)G^m B(E) + G\Delta(b,R,E) \tag{2.19}$$

This completes the formal specification of the solution of the diffusion equation (1.2). We see that we can proceed, at least in principle, in two ways. We could attempt to solve equation (2.19) directly for $B(E)$ by some iteration procedure. Having $B(E)$, $A(E)$ follows from (2.18) and then $\rho(r,E)$ from (2.2). Alternatively equation (1.2) may be solved directly for $\rho(r,E)$ by a numerical iteration procedure. The problem here is that the boundary condition, which $\rho(r,E)$ must satisfy, depends on knowing the solution $\rho(r,E)$, as is evident by inspecting the equation (2.13) for $\xi(b,R,E)$†.

---

† It should be noted here that the dependence on $\rho(r,E)$ arises only because of the way we have chosen to calculate $J^{in}(b,E)$. An approximation which has sometimes been used is the "diffusion" theory estimate of $J^{in}(b,E)$,

$$J^{in}(b,E) = \rho(b,E)/4 + \rho'(b,E)/6\Sigma_{tr}(E). \tag{2.20}$$

If we substitute into (1.8) we can solve for $\rho(b,E)/\rho'(b,E)$ and obtain for $\lambda(b,R,E) = \rho(b,E)/\rho'(b,E)$,

$$\lambda_{"diff"}(b,R,E) = [4/3\ \beta(b,E) - 2/3]/\Sigma_{tr}(E). \tag{2.21}$$

A similar approximation to λ in the one velocity limit was found to be inadequate[8].

One would proceed in a stepwise fashion. Assume, to begin with, that $\lambda(b,R,E) = \lambda^*(b,R,E)$, calculate the flux $\rho(r,E)$ on this basis, use the flux so calculated to obtain a correction $\xi(b,R,E)$ to the first estimate of $\lambda(b,R,E)$, recalculate the flux and so on.

Part of our investigation is to see how well the first few terms in the expansion (2.2), i.e. the distribution $\rho_F(r,E)$ given by (2.10), approximates to the exact solution. To this order $\xi(b,R,E) \equiv 0$ and hence $\lambda(b,R,E) \equiv \lambda^*(b,R,E)$ so that

$$A(E) = \frac{R^2-b^2}{R^2}\left\{\frac{\lambda^*(b,R,E)}{b} - \frac{1}{2(R^2-b^2)}\,(b^2+2R^2 \log R/b)\right\}B(E) \tag{2.22}$$

and B(E) is a solution of an "infinite medium"-like, linear integral equation

$$-\frac{2}{R^2}\,B(E) + 3\Sigma_{tr}(E)q(E) = \frac{R^2-b^2}{R^2}\,G\left\{\frac{\lambda^*(b,R,E)}{b} + \frac{1}{2(R^2-b^2)}(b^2-\frac{3}{2}R^2+2R^2\log R/b)\right\}B(E) \tag{2.23}$$

In the calculations we have performed we obtained first the solution $\rho_F(r,E)$ using the equations (2.22) to specify A(E) and B(E), then obtained the exact solution $\rho(r,E)$ by iterating directly on (1.2) as outlined in the preceding paragraph using $\rho_F(r,E)$ as the initial trial function.

Our specification of the transient flux is based entirely on making a simple energy-dependent generalization of the transient flux correction obtained in the one velocity limit [7], i.e. we write

$$\phi_{trans}(r,E) = \phi_{trans}(b,E)\;\frac{K_o(\nu\Sigma_{tr}(E)r)}{K_o(\nu\Sigma_{tr}(E)b)} \tag{2.24}$$

with $\nu \approx 4.0$. $\phi_{trans}(b,E)$ is given in further detail in section 3.

3. FURTHER SPECIFICATION OF THE SOURCE FUNCTION q(E), THE EXTRAPOLATION LENGTH $\lambda^*(b,R,E)$, THE TRANSIENT FLUX $\phi_{trans}(b,E)$ AND THE NEUTRON CAPTURE RATE IN THE INNER MEDIUM

We take the source spectrum to be the neutrons which end up with energies below the energy E_M following a collision in the D_2O of neutrons with energies greater than E_M. The distribution of neutrons with energies $E > E_M$, $\psi(E)$, is assumed to be

$$\psi(E) = Q/\xi\,\Sigma_m E \tag{3.1}$$

where ξ is the average logarithmic energy decrement per collision in the D_2O ($\xi \approx 0.506$). The source q(E) is then

$$q(E) = \frac{Q}{\xi\Sigma_m}\left\{\frac{\Sigma_O}{1-p_O}\left[\frac{1}{E_M} - \frac{p_O}{E}\right] + \frac{\Sigma_D}{1-p_D}\left[\frac{1}{E_M} - \frac{p_D}{E}\right]\right\} \tag{3.2}$$

$$p_O E_M \le E \le E_M \qquad p_D E_M \le E \le E_M$$

where the subscript O refers to oxygen, D to deuterium and $p = ((A-1)/(A+1))^2$.

The extrapolation length $\lambda^*(b,R,E)$, as we see from (2.15) and (2.16), depends on the blackness $\beta(b,E)$ and the latter depends on the detailed properties of the inner medium. Our calculations were performed for ZEEP rods. These consist of a natural uranium metal fuel region, 1.63 cm radius, surrounded by 2/10 mm thick air gap, 1 mm thick Aℓ sheath. The blackness of the rod assembly is written as

$$\beta(b,E) = \beta_{rod}(E) + \beta_{sh}(E) \tag{3.3}$$

where $\beta_{rod}(E)$ represents the fraction of the neutron incurrent at the surface b which is captured by the uranium metal fuel, $\beta_{sh}(E)$ the fraction captured in the sheath region,

$$\beta_{rod}(E) \approx \frac{a}{b}\,\beta(a,E)\theta;\ \theta = \exp(-2\Sigma_{sh}(E)(b-a)\left[1-\frac{4}{3\pi}\sqrt{2(b-a)/a}\right] \tag{3.4}$$

$$\beta_{sh}(E) = 1 - \exp(-4(b-a)\Sigma_{sh}(E)) - \frac{a}{b}\,\beta(a,E)(1-\theta)\theta \tag{3.5}$$

Here $\Sigma_{sh}(E)$ is the average macroscopic absorption cross-section for neutrons of energy E in the sheath region b-a, $\beta(a,E)$ is the blackness to neutrons of energy E of the homogeneous fuel region of radius a. The blackness $\beta(a)$ is defined in detail in [6] and numerical fits which may be used to evaluate it are given in [7].

Noting that the neutron absorption rate per unit length of inner medium may be equivalently described by either $2\pi b\, J^{in}(b,E)\beta(b,E)$ or $2\pi b\rho'(b,E)/3\Sigma_{tr}(E)$, (see (1.8)), and bearing in mind the significance of $\beta_{rod}(E)$ and $\beta_{sh}(E)$ in the definition of $\beta(b,E)$, we have also the following for the average neutron fluxes in the fuel and sheath media, (to within the approximations we are working with)

$$\langle\phi_F(E)\rangle \equiv 4J^{in}(b,E)\,\frac{\theta\beta(a,E)}{2a\Sigma_{aF}(E)} = \frac{2}{a\Sigma_{aF}(E)}\,\theta\,\frac{\rho'(b,E)}{3\Sigma_{tr}(E)}\,\frac{\beta(a,E)}{\beta(b,E)} \tag{3.6}$$

$$\langle\phi_{sh}(E)\rangle \equiv 4J^{in}(b,E)\,\frac{\beta_{sh}(E)}{4(b-a)\Sigma_{sh}(E)} = \frac{1}{(b-a)\Sigma_{sh}(E)}\,\frac{\beta_{sh}(E)}{\beta(b,E)}\,\frac{\rho'(b,E)}{3\Sigma_{tr}(E)} \tag{3.7}$$

where $\Sigma_{aF}(E)$ is the macroscopic absorption cross-section in the fuel medium for neutrons of energy E.

The transient flux $\phi_{trans}(b,E) \equiv [\phi(b,E)-\rho(b,E)]$ is written as

$$\phi_{trans}(b,E) = \rho(b,E)\left[\frac{\phi(b,E)}{\phi(a,E)}\,\frac{\phi(a,E)}{\rho'(b,E)}\,\frac{\rho'(b,E)}{\rho(b,E)} - 1\right] \tag{3.8}$$

Now $\rho'(b,E)/\rho(b,E)$ is just $\lambda(b,R,E)$. From (3.6) we can relate $\rho'(b,E)$ to $\langle\phi_F(E)\rangle$ and the ratio $\phi(a,E)/\langle\phi_F(E)\rangle$ is just the ratio of surface to average flux in the fuel, $G(a,b,R,E)$. Thus we write

$$\phi_{trans}(b,E) = \rho(b,E)\left[W\,G(a,b,R,E)\,\frac{2\theta\,\beta(a,E)}{\beta(b,E)a\Sigma_{aF}(E)}\,\frac{1}{3\Sigma_{tr}(E)\lambda(b,R,E)} - 1\right] \tag{3.9}$$

All quantities in (3.9) are now defined except $W = \phi(b,E)/\phi(a,E)$ and G and these we take to be the energy-dependent generalization of the corresponding one velocity results given in [7].

In so far as the energy dependences of the actual cross-sections are concerned, the ^{235}U cross-section was taken to be that given in CRRP-960[9]. ^{238}U absorption was taken as

$$\sigma_{a8}(E) = 2.72 \sqrt{E_0/E}\ [1 + 0.186E + 0.020E^2] \text{ barns} \tag{3.10}$$

with E in eV. Aℓ, D and O were assumed to have 1/v-type absorption cross-sections.

4. DISCUSSION OF THE RESULTS

As mentioned in the previous sections we evaluated the neutron flux spectrum and the manganese activation in the rod and moderator using the approximate solution $\rho_F(r,E)$ and its associated boundary value $\lambda^*(b,R,E)$ and the exact solution $\rho(r,E)$ and its associated boundary value $\lambda(b,R,E)$. The calculations were performed for two $\Sigma_{tr}(E)$, $\Sigma_{tr}^{(W)}(E)$ and $\Sigma_{tr}^{(N)}(E)$, and two $\Sigma(E'\to E)$, the monatomic gas transfer $\Sigma_G(E'\to E)$ with A = 3.6 and the Nelkin transfer, $\Sigma_N(E'\to E)$. Here we summarize the main features of the results. First, however, we indicate how the manganese activations were evaluated.

For $E < E_M = 1.44$ eV, the manganese detectors were assumed to have 1/v absorption cross-sections and the activation at position r is accordingly written as

$$A_{mn}^{(1)}(r) = A_0 \int_0^{E_M} \sqrt{E_0/E}\ \phi(E,r)\ \chi(E)dE \tag{4.1}$$

in which A_0 is an overall normalizing factor, $\chi(E)$ is the detector self-shielding factor for neutrons of energy E. Since the measured activation extends over the complete energy range activations due to neutrons with $E > E_M$ must, for purposes of comparison, be added to (4.1). To do this we take the neutron flux in the moderator for $E > E_M$ to be $\psi(E)$ given by (3.1). The added activation $A_{mn}^{(2)}(r)$ is then

$$A_{mn}^{(2)}(r) \approx A_0 \frac{Q}{\xi\Sigma_m} [2 \sqrt{E_0/E_M}\ \chi_f G_f + \sqrt{\pi/4}\ s_0\ \chi_R\ G_R] \tag{4.2}$$

in which s_0 is the manganese s factor[9], χ_f and χ_R the epithermal and resonance self-shielding factors for the detector and G_f and G_R the depression of the neutron fluxes at position r relative to the flux $\psi(E)$. We have taken $s_0\chi_R = 0.49$[10], $\chi_f \approx 1.0$, G_f and $G_R \equiv 1.0$ in the moderator, $G_f = G_R = 0.86$ in the fuel and $G_f = G_R = 0.95$ in the sheath.

One of the most clear cut results which has been obtained concerns the boundary condition (2.11). It is found that for the type of system considered $\lambda(b,R,E)$ is very nearly equal to $\lambda^*(b,R,E)$ except at the lowest energies. Typical values are given in Table I.

TABLE I: Values of λ, λ^*

E(eV)	λ^*(cm)	λ(cm)
0.000225	0.940	0.887
0.000625	1.072	1.050
0.003025	1.692	1.705
0.011025	2.799	2.811
0.024025	4.234	4.234
0.060025	7.507	7.510
0.245025	14.317	14.316

This aspect of the results would seem to have some significance in the establishment of good boundary conditions in the application of multigroup calculations to similar systems.

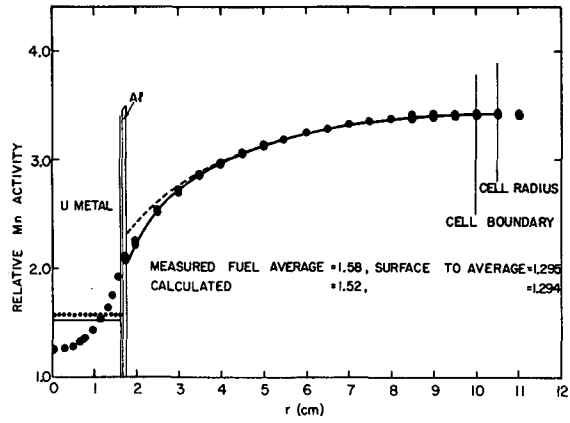

FIG. 1. Mn activity distributions

● Measured activity in a 20-cm hexagonal ZEEP rod lattice array [Green, R.E., CRNL, Nov. 1963]

——— Calculated activity using $\Sigma_{tr}^{(W)}$, $\Sigma_G(E' \to E)$, $\rho_F(r,E)$ and $\lambda^*(b,R,E)$

- - - - Calculated activity as above but with no transient correction.

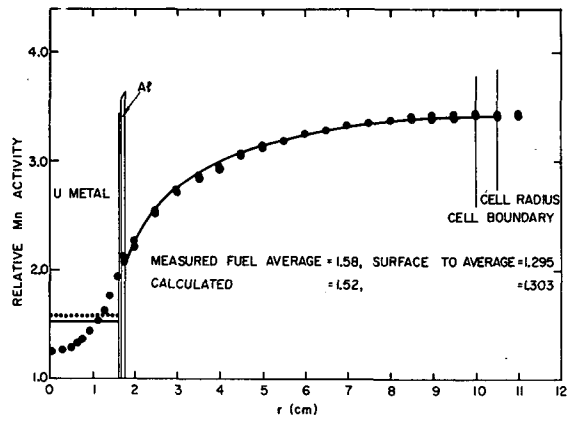

FIG. 2. Mn activity distributions

● Measured activity as in Fig. 1

——— Calculated activity using $\Sigma_{tr}^{(W)}$, $\Sigma_G(E' \to E)$, $\rho(r,E)$ and $\lambda(b,R,E)$.

We consider next the applicability of the approximation $\rho_F(r,E)$ to $\rho(r,E)$. It is found that, in so far as the calculated Mn activations are concerned, the values derived from the exact solution $\rho(r,E)$ are only slightly better than those derived from the approximation $\rho_F(r,E)$. This is illustrated in figures 1, 2, and 3. The two solutions $\rho_F(r,E)$ and $\rho(r,E)$ do have somewhat different energy spectra as is illustrated in figure 4

where the incurrent spectra at the rod surface are plotted. We conclude that, on the whole, $\rho_F(r,E)$ is a good approximation to $\rho(r,E)$, However, the deviations in the neutron spectra may be more significant if the cross-sections in the fuel medium deviate more from 1/v cross-sections.

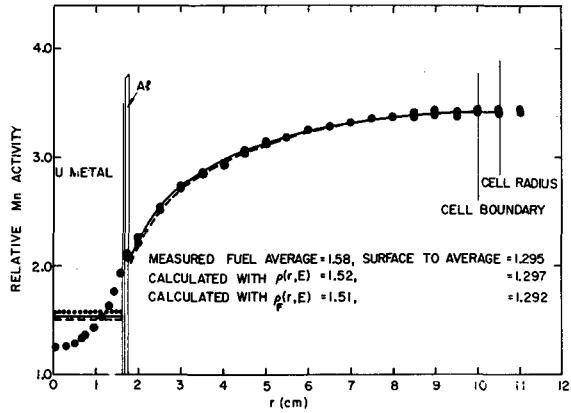

FIG. 3. Mn activity distributions

● Measured activity as in Fig. 1
——— Calculated activity using $\Sigma_{tr}(N)$, $\Sigma_N(E' \to E)$, $\rho(r,E)$ and $\lambda(b,R,E)$
- - - - Calculated activity using $\Sigma_{tr}(N)$, $\Sigma_N(E' \to E)$, $\rho_F(r,E)$ and $\lambda^*(b,R,E)$.

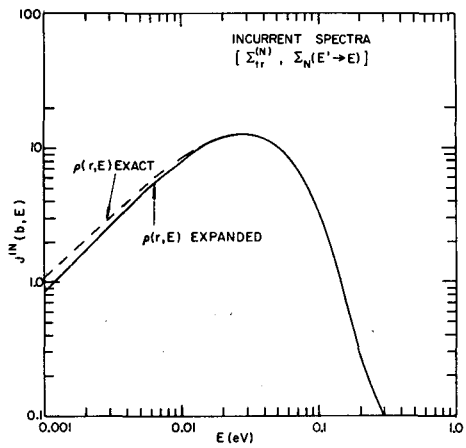

FIG. 4. Neutron incurrent spectra at the rod assembly surface.

A breakdown of a typical, calculated incurrent spectrum into a thermal "Maxwellian" component and an epithermal $\Delta(E)/E$ type component is indicated in figure 5. The effective temperature of the Maxwellian component is T = 313°K as derived on the basis of arguments presented in [11], extended to heterogeneous assemblies. This component represents the calculated thermal spectrum quite well. The joining function $\Delta(E)$ exhibits some of the properties of Westcott's $\Delta_4(E)$ [9].

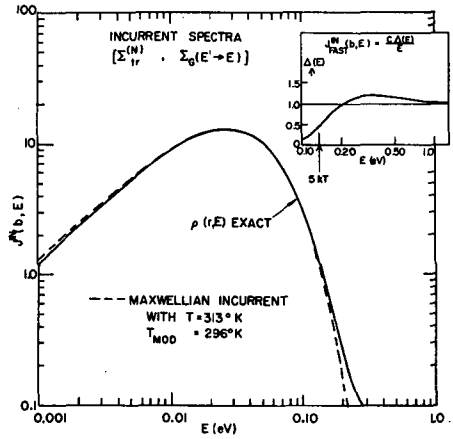

FIG. 5. Breakdown of the neutron incurrent spectrum into a thermal "Maxwellian" spectrum and $C\Delta(E)/E$ type epithermal spectrum.

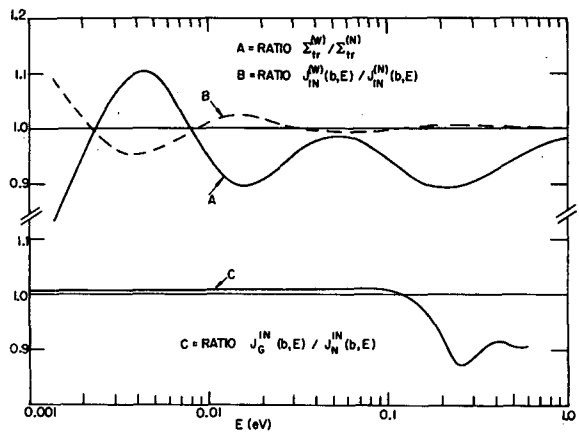

FIG. 6. Dependence of the incurrent spectrum on the choice of $\Sigma_{tr}(E)$ and $\Sigma(E' \to E)$
$J_{in}^{(W)}(b,E)$ calculated using $\Sigma_{tr}^{(W)}$, $\Sigma_G(E' \to E)$
$J^{(N)}(b,E)$ calculated using $\Sigma_{tr}^{(N)}$, $\Sigma_G(E' \to E)$
$J_G^{in}(b,E)$ calculated using $\Sigma_{tr}^{(N)}$, $\Sigma_N(E' \to E)$
$J_N^{in}(b,E)$ calculated using $\Sigma_{tr}^{(N)}$, $\Sigma_N(E' \to E)$.

A surprising feature of our results is the closeness of the calculated Mn activations for the various combinations of $\Sigma_{tr}(E)$ and $\Sigma(E' \to E)$ used (figures 1, 2, and 3). The calculated Mn activation in the fuel region is consistently lower than the measured activation by 3-4%. No reason has been established for this discrepancy. The neutron energy spectra calculated for the various $\Sigma_{tr}(E)$, $\Sigma(E' \to E)$ combinations do differ as is illustrated in figure 6. To indicate the dependence of the spectrum on $\Sigma_{tr}(E)$ we have plotted, curve A, the variation of the ratio $\Sigma_{tr}^{(W)}(E)/\Sigma_{tr}^{(N)}(E)$ as used in our calculations and the variation in curve B of the resultant ratio of the incurrent spectra at the rod surface, $J_{in}^{(W)}(b,E)/J_{in}^{(N)}(b,E)$, the tran fer

cross-sections in both instances being $\Sigma_G(E' \to E)$. At the lower energies there is evidence of dependence on $\Sigma_{tr}(E)$ (i.e. the larger $\Sigma_{tr}(E)$ the lower $J_{in}(b,E)$) but at the higher energies the two incurrents are quite similar. In curve C we plot the ratio of the incurrents $J_G{}^{in}(b,E)/J_N{}^{in}(b,E)$ where $J_G{}^{in}$ and $J_N{}^{in}$ are calculated using the monatomic gas and Nelkin transfer cross sections respectively, $\Sigma_{tr}(E)$ being the Nelkin $\Sigma_{tr}(E)$ in both instances. The departures of the two incurrent spectra are significant only in the epithermal energy region.

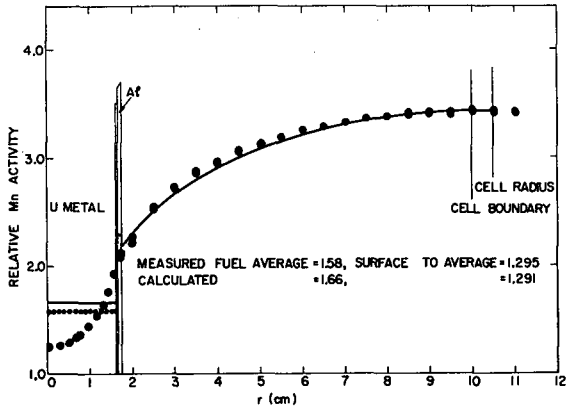

FIG. 7. Mn activity distributions

● Measured activity as in Fig. 1.

——— Calculated activity using $\Sigma_{tr}{}^{(N)}$, $\Sigma_N(E' \to E)$, $\rho_F(r,E)$ and $\lambda_{"diff"}(b,R,E)$

To illustrate the effect of the type of boundary condition used at the rod surface we have plotted in figure 7 the calculated Mn activation derived from $\rho_F(r,E)$ in combination with the "diffusion" theory boundary condition (2.21). The calculated activation in the fuel is now overestimated. The Mn activation in the moderator does not follow the measured activation as well as do the calculated activations given in figures 1, 2, and 3.

REFERENCES

[1] WILLIAMS, M.M.R., Nucl. Sci. Engng. 19 1 (1964) 132.
[2] HUGHES, D.J., SCHWARTZ, R.B., BNL-325, 2nd ed. (1958).
[3] NELKIN, M.S., Phys. Rev. 119 (1960) 791.
[4] HONECK, H.C., Description of the Code GAKER, BNL Internal Memorandum (1964).
[5] BROWN, H.D., ST.JOHN, D.S., Du Pont Report DP-33 (1954).
[6] KUSHNERIUK, S.A., Chalk River Report CRT-712 (AECL-462), 1957.
[7] KUSHNERIUK, S.A., Chalk River Report CRT-1258 (1967).
[8] KUSHNERIUK, S.A., JIRLOW, K., Reactor Sci. & Tech. 16 (1962) 464.
[9] WESTCOTT, C.H., Chalk River Report CRRP-960 (AECL-1101), 1962.
[10] GREEN, R.E., Chalk River Nuclear Laboratories, private communication (1967).
[11] COVEYOU, R.R., BATE, R.R., OSBORN R.K., Journ. Nucl. Energy 2 (1956) 153.

DISCUSSION

M. M. R. WILLIAMS (Chairman): In your generalization of the one-velocity results to energy dependence, you simply replaced the cross-section by the energy-dependent cross-section. This is also the basis of the SPECTROX code, is it not? How does your approach differ from SPECTROX?

S. A. KUSHNERIUK: Many formal aspects of my method and of SPECTROX are similar. Thus, the diffusion flux distribution $\rho(r, E)$ in both SPECTROX and my calculations satisfies the boundary conditions $\rho'(R, E) = 0$ at the cell boundary and, for the fuel assembly I have considered, $\frac{1}{3\Sigma_{tr}(E)} \rho'(b, E) = \beta(b, E) J^{in}(b, E)$ at the inner boundary, where in the latter $\beta(b, E)$ is calculated by similar collision probability methods. The differences, if my memory of the SPECTROX code does not fail me, are as follows:

1. The moderator flux $\phi(r, E)$ in my method contains a transient flux as well as the diffusion (i. e. asymptotic) flux $\rho(r, E)$.
2. In my method $J^{in}(b, E)$ is calculated by collision probability methods. SPECTROX uses a diffusion theory estimate for this incurrent. Note that since I also have a transient flux in the moderator my calculated $J^{in}(b, E)$ contains contributions from this flux.
3. SPECTROX limits the diffusion flux distribution $\rho(r, E)$ to the form which I have labelled $\rho_F(r, E)$. I have made calculations using both the exact solution to the diffusion equation and the approximation $\rho_F(r, E)$ and have shown that insofar as calculated Mn activations are concerned, and for the system considered, $\rho_F(r, E)$ is a good approximation to $\rho(r, E)$.
4. For my calculations it was convenient to rewrite the boundary condition at the inner boundary in terms of what I call the 'extrapolation length' $\lambda(b, R, E)$. I believe that the SPECTROX assumption with regard to the incurrent $J^{in}(b, E)$ is equivalent to using the extrapolation length denoted as $\lambda_{diff.}(b, R, E)$ in my text and this can be quite different from the 'exact' extrapolation length $\lambda(b, R, E)$ which I use. Note that I find that $\lambda(b, R, E) \simeq \lambda^*(b, R, E)$ where $\lambda^*(b, R, E)$ is a simple energy-dependent generalization of the one-velocity extrapolation length calculated for similar systems.

MONTE CARLO ANALYSES OF TIME-DEPENDENT NEUTRON THERMALIZATION IN ORGANIC MODERATOR

E. CUPINI AND V.G. MOLINARI
COMITATO NAZIONALE PER L'ENERGIA NUCLEARE,
CENTRO DI CALCOLO,
BOLOGNA, ITALY

Abstract

MONTE CARLO ANALYSES OF TIME-DEPENDENT NEUTRON THERMALIZATION IN ORGANIC MODERATOR. The slowing-down, thermalization and diffusion of a neutron pulse in benzene is studied by the Monte Carlo method. The time dependence of the neutron spectrum, total neutron density and spatial neutron distribution are obtained for homogeneous spheres as well as for infinite medium. The benzene scattering kernel was derived from the incoherent approximation assuming harmonic oscillation.

The value of the diffusion coefficient obtained is in perfect agreement with the theoretical and experimental data. It is found that the neutron distribution for the sphere with radius R= 1 cm, shows a very different behaviour in comparison with the spheres with R >1.5 cm. It is likely that only a continuous spectrum of eigenvalues exists for R <1.3 cm (B^2 >3.31 cm^{-2}).

1. INTRODUCTION

In recent years the approach to equilibrium of a neutron pulse in a finite moderating sample has been a problem of considerable interest. A large number of experimental and theoretical works has been devoted to this subject (see the reviews by Beckurts [1] and Corngold [2]). Much experimental research has been based upon the exponential behaviour of the neutron density at times long after the pulse has ceased. In other words, these experiments have dealt with the fundamental decay constant for various moderators as a function of size and shape. Recently measurement of time-dependent spectra n(v, t) has been reported. The measurement of transient spectra in small samples provides information which can be compared with theoretical models of the scattering kernel, and which clarifies the properties of the Boltzmann equation. But a complete and realistic description of the history of the velocity spectrum is difficult to obtain experimentally, especially for really small systems (small in terms of mean free paths)

Theoretical investigation [3, 4] has shown that the solution for the time, velocity-dependent neutron density can be expressed as:

$$n(v,t) = \sum_{i=0}^{i_{max}} a_i n_i(v)\, e^{-\lambda_i t} + \int_{\lambda^*}^{\infty} a(v,\lambda) e^{-\lambda t}\, d\lambda \qquad (1)$$

where $\lambda_i < \lambda^* = |v\Sigma(v)|_{min}$, and λ^* is a finite upper bound to the discrete decay constants λ_i. It has also been shown [3, 4] that there exists a maximum buckling value, B^2_{max} , beyond which no discrete decay constant

can exist. Computing investigations of this problem have been carried out [2]. But almost all the numerical methods used for systems of finite geometry work on the basis of the diffusion approximation that, as is well known, is valid as long as the geometry is not too small.

The Monte Carlo (M.C.) method, since it simulates the physical situation, requires no further assumption other than the neutron nucleus interaction, and is a powerful tool for investigating the thermalization in small samples (particularly when the discrete spectrum is empty), for predicting the value of B^2_{max}, and for comparing the results of the transient spectra measurements directly with the theory.

In a previous work [5] the M.C. method was applied to the case of the free proton gas scattering kernel to emphasize the most relevant properties of neutron thermalization. In the present paper we wish to present the results for benzene. The time dependence of the neutron velocity spectrum, the total neutron density and the spatial neutron distribution following a neutron burst at $t = 0$, are obtained for homogeneous spheres of benzene, as well as for the infinite medium. The benzene scattering kernel, derived from the incoherent approximation assuming harmonic oscillation [6], was obtained using the SUMMIT computer code [7].

In section 2 a brief outline of the M.C. programme is given. The results for the infinite medium are presented in section 3. Section 4 deals with thermalization in finite media.

2. CALCULATIONAL PROCEDURE

The calculation was performed assuming a temperature of 300°K and a benzene density equal to 0.871 g/cm^3.

Several time values and concentric spheres were considered, as well as the infinite medium. A point source of neutrons was assumed at the centre of the spherical system, emitting a burst of neutrons of energy $E = 10$ eV at the time $t = 0$. A $1/v$ type absorption cross-section was assumed, taking $v\,\Sigma_a(v) = 2992\ s^{-1}$.

The transfer cross-section $\sigma(E_0 \rightarrow E, \cos\vartheta)$ was calculated by the SUMMIT code using the model described in [6]. The transition matrix for the energy transfer and cosine of the scattering angle were then obtained. The energy and motion direction of a neutron emerging from a collision were computed from the transition matrix by means of linear interpolations. For energy greater than 0.70 eV the atoms of the medium are supposed to be free and at rest.

A neutron history, followed by means of the standard M.C. technique using a weight for the absorption, was stopped when the last target time was attained or the neutron escaped the system. A different M.C. technique was used for very small spheres, forcing a neutron emerging from a collision to make the next collision inside the system. A statistical weight was used to keep account of this device. The Monte-Carlo programme was developed for the IBM 7094 computer.

3. INFINITE MEDIUM

An infinite sample of benzene has been considered with a view to investigating various aspects of the thermalization problem and to know

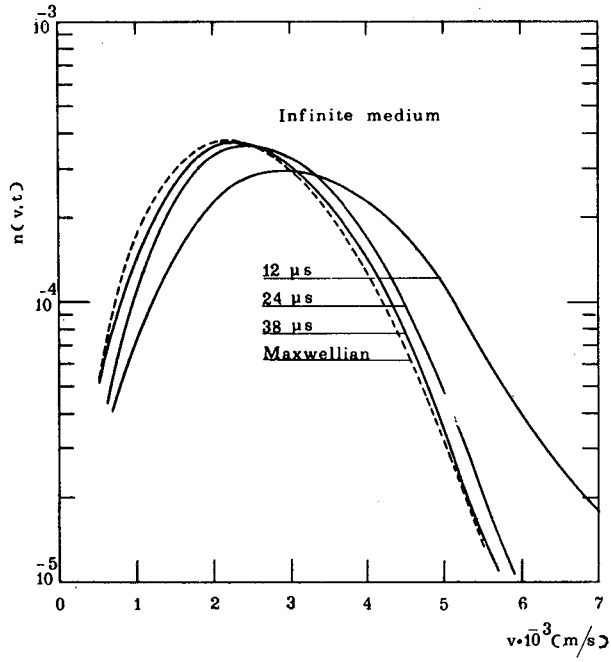

FIG. 1. Neutron velocity distribution at different times in infinite benzene assembly. Time in microseconds after initial pulse. The curves are obtained by smoothing the M.C. points.

how, and how fast, thermal equilibrium is approached. The time evolution of a neutron distribution was analysed at different times in the interval from 8 to 80 μs, after the introduction of the initial pulse.

In Fig. 1 the time development of the spectrum is shown. It can easily be seen that transitional spectra converge into the Maxwellian distribution and retain this distribution at all further times.

This result is also seen in Fig. 2 where the average neutron velocity $\bar{v}(t)$, defined as:

$$\bar{v}(t) = \frac{\int_0^\infty \int_0^\infty v\, n(\vec{r}, \vec{v}, t)\, d\vec{r}\, d\vec{v}}{\int_0^\infty \int_0^\infty n(\vec{r}, \vec{v}, t)\, d\vec{r}\, d\vec{v}} \qquad (2)$$

is plotted versus time. After about 60 μs the average velocity becomes constant and attains the asymptotic value $\bar{v}(\infty) = 2540$ m/s.

In Fig. 2 are also shown the values of the time behaviour of the total number of neutrons n(t) defined as:

$$n(t) = \int_0^\infty \int_0^\infty n(\vec{r}, \vec{v}, t)\, d\vec{r}\, d\vec{v} \qquad (3)$$

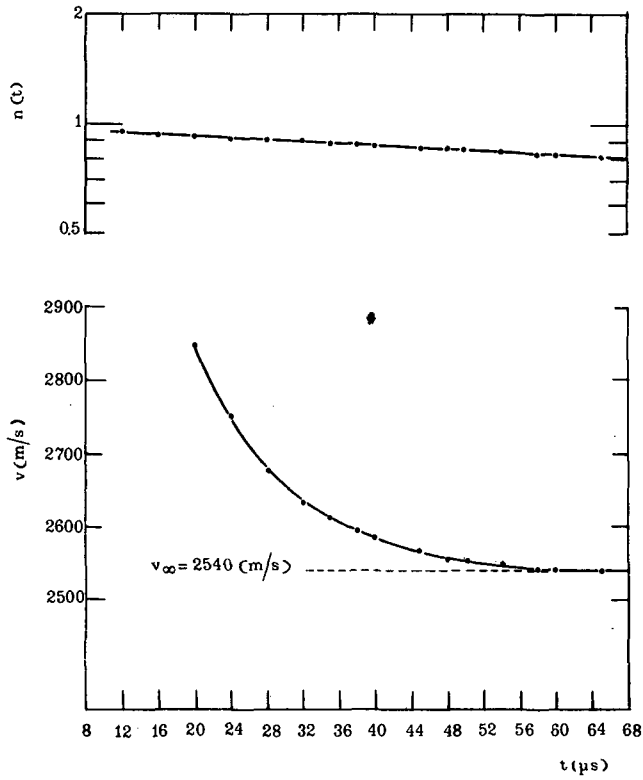

FIG. 2. Variation in time of average neutron velocity $\bar{v}(t)$ and total neutron density $n(t)$ for an infinite benzene assembly.

The values are well fitted to the curve $n(t) = e^{-\lambda_0 t}$ when $\lambda_0 = 2.99 \times 10^{-3}$ $\mu s^{-1} = v\,\Sigma_a$ as is to be expected from the theory.

4. FINITE MEDIUM

To give an insight into the features of the thermalization process for finite geometry, the time dependence of the neutron velocity spectrum, average velocity, spatial neutron distribution, average neutron distance and total neutron density are computed for homogeneous spheres.

In Figs 3 and 4 the time behaviour of the neutron velocity spectrum integrated over the whole sample for the spheres with R = 3 and 5 cm is shown. The dotted line represents the Maxwellian distribution at 300°K. We can see how the spectra converge into a distribution similar to the Maxwellian shifted towards the low velocity side. This softening furnishes a direct proof of diffusion cooling, due to the preferential leakage of neutrons of higher velocity. The spectra for the other spheres (with $R \geq 1.5$ cm) are similar to the former with the softening which always increases as the radius decreases. After some time, depending on the

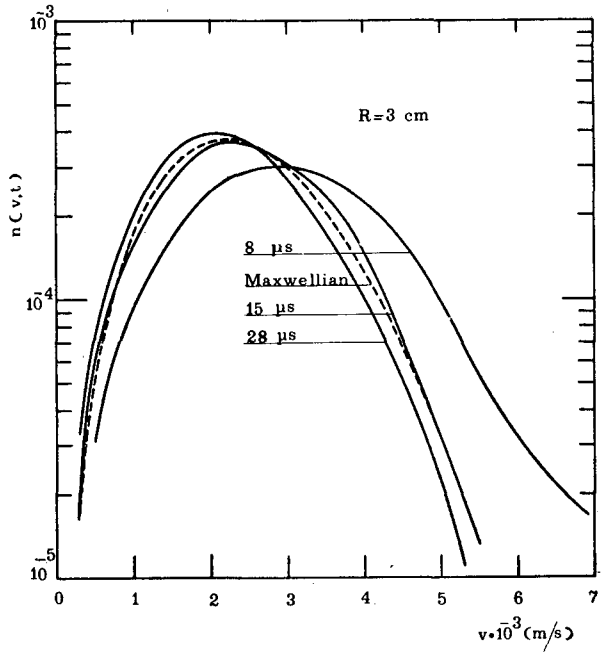

FIG. 3. Time variation of neutron spectrum in benzene, with R = 3 cm. Time in micro-seconds after initial pulse.

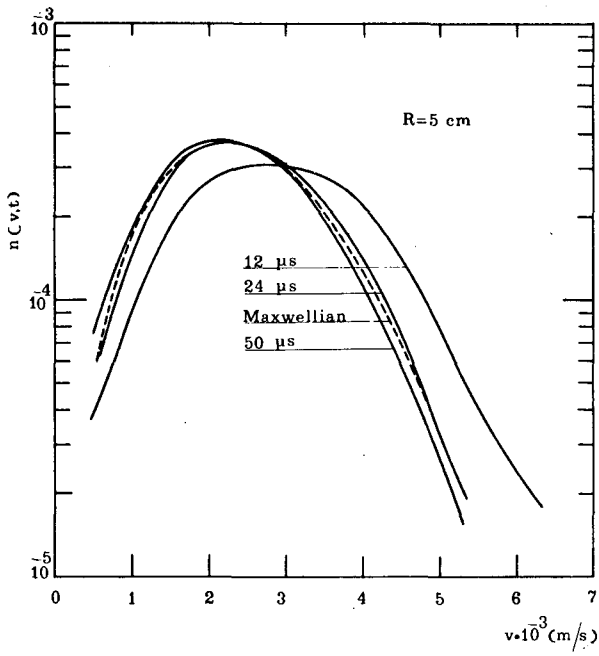

FIG. 4. Time variation of neutron spectrum in benzene, with R = 5 cm. Time in micro-seconds after initial pulse.

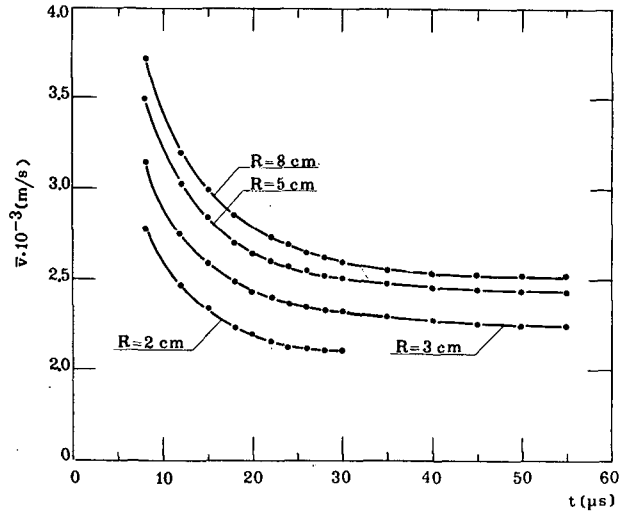

FIG. 5. Time variation of average neutron velocity, for various spheres of benzene.

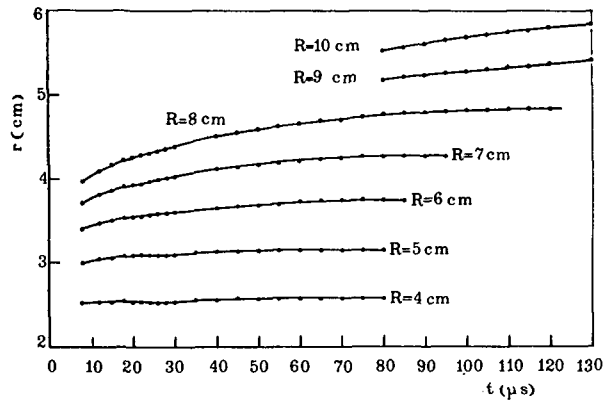

FIG. 6. Time variation of average neutron distance, for various spheres of benzene.

values of R, the spectra attain the asymptotic distribution, and the time behaviour of the neutron density is characterized by a single decay constant. To determine the time required for the spectra to achieve the asymptotic distribution as a function of R, and to analyse the last stage of neutron thermalization, it is useful to consider some integral parameters. Hence in Figs 5 and 6 the average neutron velocity and distance are plotted as time functions for various spheres. It will be observed that the time required for the average velocity to become constant diminishes with the decrease in radius.

On the other hand, the larger systems take longer to reach a state of equilibrium of the spatial distribution. It must be noted that for large spheres (R > 6 cm) a constant spatial distribution takes longer to achieve than that required for the energy distribution to become constant. In

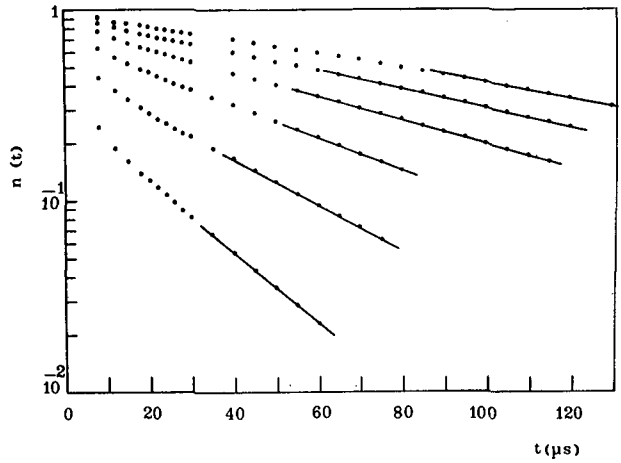

FIG. 7. Time behaviour of neutron density for benzene spheres of various radius.

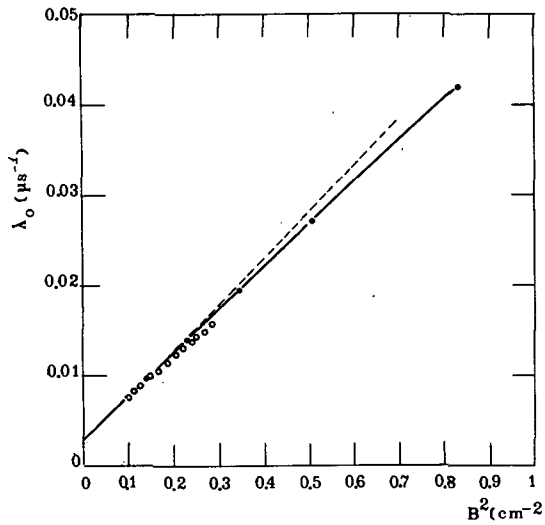

FIG. 8. Dependence of the decay constant for benzene on buckling.

other words, for the spheres with R > 6 cm the higher spatial modes play an important role in the establishment of the asymptotic distribution.

In Fig. 7 the time dependence of the total neutron density n(t) is given. After some time, depending on the radius, a simple exponential decay is attained. This time is in agreement with the previous results, as shown in Figs 5 and 6 . From the time behaviour of neutron density, the decay constant λ_0 is obtained for various spheres.

The values of the decay constants are plotted in Fig. 8 as a function of the buckling B^2 and compared with the experimental values of

Pál et al. [8] (the measurements are at 22°C). By fitting the values of the decay constants against B^2 with the expression

$$\lambda_0 = v\Sigma_a + D_0B^2 - CB^4 + FB^6 \tag{4}$$

TABLE I. ASYMPTOTIC VALUES OF $\bar{v}$ AND $\bar{r}$

R (cm)	$\bar{v}$(M.C.) (m/s)	$\bar{r}$ (M.C.) (cm)	$\bar{r}$ (Diffusion theory) (cm)
∞	2540	-	-
10	2520	-	6.17
8	2515	4.85	4.97
7	2500	4.28	4.37
6	2480	3.75	3.77
5	2430	3.15	3.17
4	2360	2.55	2.56
3	2260	1.94	1.96
2	2115	1.33	1.34
1.5	1970	1.00	1.02

TABLE II. DIFFUSION PARAMETERS OF C_6H_6

	$D_0\left(\frac{cm^2}{s}\right)$	$C\left(\frac{cm^4}{s}\right)$	$F\left(\frac{cm^6}{s}\right)$
M.C. (T = 300°K)	5.0×10^4	6.6×10^3	3.5×10^3
Theoretical (T = 300° K)	4.95×10^4 [9]	9.8×10^3 [11]	
Experimental (T = 295° K)	4.86×10^4 [8]	1.38×10^4 [8]	
Experimental (T = 297° K)	4.98×10^4 [10]		

we obtain for the diffusion coefficient D_0, for the diffusion cooling coefficient C, and for F, the values quoted in Table I. The value of D_0 is in perfect agreement with the theoretical [9] and experimental [8, 10] ones. The results obtained for C and F by fitting the M.C. points with the expression (4) are only qualitative. In fact the fit procedure ensures an agreement between the points and the curve, but the values of the parameters may be not allowed to have a physical meaning.

In Table II the asymptotic values of the average neutron velocity (see also Fig. 9) and radius are given. A comparison with the diffusion theory is also shown.

The critical value λ^* was calculated taking $v\Sigma(v)$ as constant for $v < 280$ m/s. We obtain $\lambda^* = 0.145\ \mu s^{-1}$. From Fig. 9 , where λ_0 is plotted as a function of R, it can be seen that λ^* should be reached for a radius of $R \simeq 1.3$ cm to which corresponds $B^2_{max} = 3.31\ cm^{-2}$. Thus for spheres with $R < 1.3$ cm no discrete eigenvalue should exist. It is therefore interesting to examine the thermalization process for spheres with $R < 1.3$ cm. We have considered a sphere of radius R = 1 cm and the results, compared with other spheres with $R > 1.3$ cm, are given in Figs 10 and 11 . In these figures the very different behaviour for the sphere with R = 1 cm can be seen. In fact, while for the spheres with R = 1.5; 1.8; 2 cm an asymptotic distribution in a time which decreases as the radius decreases is attained, the sphere with R = 1 cm shows a continuous decrease of the neutron average velocity and shows that the total neutron density has no exponential decay.

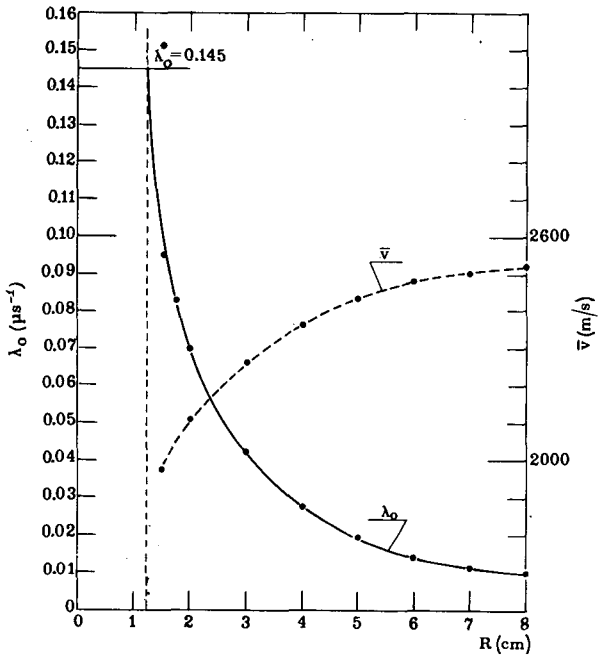

FIG. 9. Dependence of the decay constant and average velocity for benzene on sphere radius.

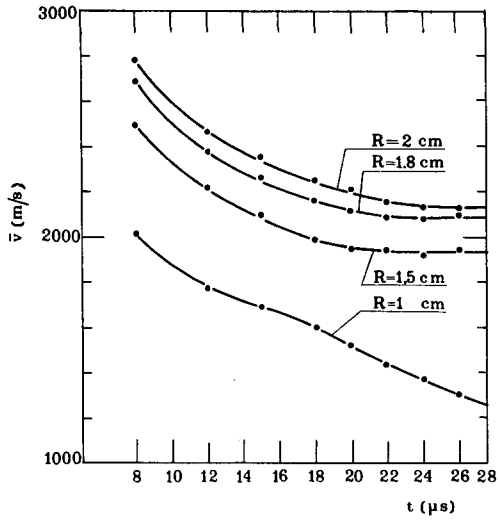

FIG. 10. Time variation of average neutron velocity for various spheres of benzene.

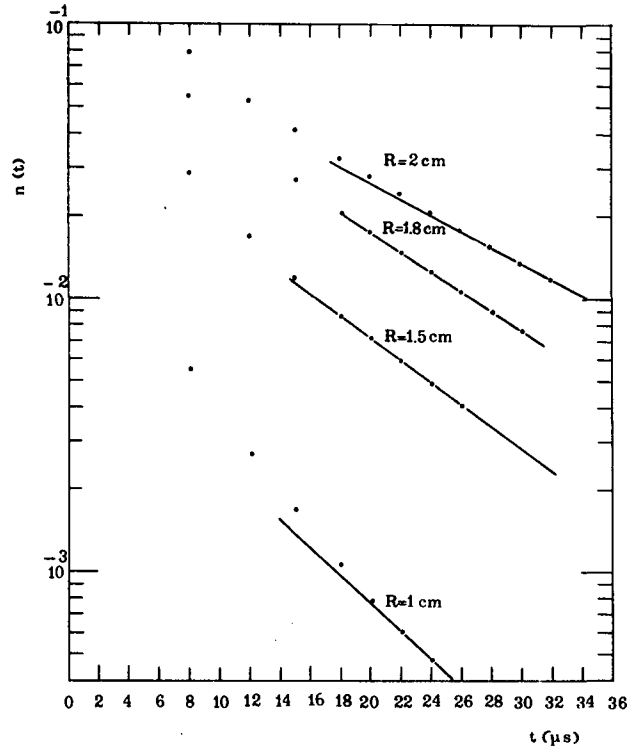

FIG. 11. Time behaviour of neutron density for benzene spheres of various radius.

5. CONCLUSIONS

A detailed and complete knowledge of neutron thermalization and diffusion is required both to better our understanding of the properties of the Boltzmann equation and to describe the approach to thermodynamic equilibrium, and also to design nuclear reactors on a more realistic basis. We believe that the M.C. can serve as a bridge between experiment and theory, and that it is in itself a powerful method for investigating the behaviour of a neutron population in a sample.

In this paper some results obtained for benzene systems have been reported. In particular the M.C. value of D_0 and the theoretical and experimental ones are in agreement. We have shown that for systems with R greater than about 1.5 cm (B^2 less than 2.66 cm^{-2}) the time behaviour of the neutron density is determined, at long times by an exponentially decaying mode. On the contrary the sphere with R = 1 cm (B^2 = 4.84 cm^{-2}) does not give an exponential decay of the neutron density, and the spectra do not show convergence into an equilibrium distribution.

REFERENCES

[1] BECKURTS, K.H., Pulsed Neutron Research I, IAEA, Vienna (1965) 3.
[2] CORNGOLD, N., Pulsed Neutron Research I, IAEA, Vienna (1965) 199.
[3] NELKIN, M.S., Physica 29 (1963) 261; KOPPEL, J., Nucl. Sci. Engng 16 (1963) 101.
[4] CORNGOLD, N., Nucl. Sci. Engng 19 (1964) 80; CORNGOLD, N., MICHAEL, P., WOLLMAN, W., Nucl. Sci. Engng 15 (1963) 13.
[5] CUPINI, E., MOLINARI, V.G., SOLINAS, G., Nukleonik 9 6 (1967) 295.
[6] BOFFI, V.C., MOLINARI, V.G., PARKS, D.E., Proc. Brookhaven Conf. on Neutron Thermalization, CNL-719 (1962) 69.
[7] BELL, J., Rep. GA-2492 (1962).
[8] PÁL, L., KISDI-KOSZÓ, E., BOD, L., SZATMÁRY, Z., VIZI, I., Proc. 3rd. UN Int. Conf. PUAE 2 (1965) 310.
[9] BOFFI, V.C., MARSICO, B., MOLINARI, V.G., SCOZZAFAVA, R., Nucl. Sci. Engng 24 (1966) 211.
[10] DEMANINS, F., private communication.
[11] SCOZZAFAVA, R., TRAVERSA, G., Rep. C.N.E.N. RT/FI (62)57 (1962).

DISCUSSION

T. GOZANI: I gather that λ measured or calculated by the least-squares fit over a certain time interval, in spheres of $B^2 \geq B^2_{max.}$, is larger than λ^* for all practical time. By 'practical' time I mean a period in which a measurable amount of neutrons becomes available, without the use of an infinitely strong source or very large neutron histories in the Monte Carlo calculation.

There is one question I should like to ask. Is it correct that in your calculation you assumed a point source of 10 eV at the centre of the spheres?

V.G. MOLINARI: Yes, that is correct.

I. KUŠČER: What, in your opinion, is the advantage of the Monte Carlo method over a step-by-step integration of the time-dependent transport equation?

V. G. MOLINARI: Deterministic methods usually necessitate certain assumptions, for instance about the boundary conditions, or the use of multigroup methods. In any case, in deciding which method to use for a particular problem it is also important to take into account the computer time needed to obtain the results.

NEUTRON RETHERMALIZATION STUDIES IN H_2O AND ZrH_n

J. SAASTAMOINEN
DEPARTMENT OF TECHNICAL PHYSICS,
TECHNICAL UNIVERSITY OF HELSINKI,
OTANIEMI, FINLAND

Abstract

NEUTRON RETHERMALIZATION STUDIES IN H_2O AND ZrH_n. The theoretical model used for calculation of the neutron spectrum in the vicinity of a medium and temperature discontinuity is based on the presentation of every P_N-component of the flux as a combination of the two equilibrium fluxes with space-dependent amplitudes. If the two first energy moments of the P_N-equations are exact, and every component of the flux is continuous at the interface, then these amplitudes are determined. P_3-calculations in plane geometry have been performed for the systems of $H_2O(20°C)$-$H_2O(80°C)$. The results obtained for the Nelkin and the McMurry-Russell scattering models have been compared with the experimental results. The one relaxation length model cannot be used to describe the neutron spectrum. The three relaxation lengths given by the P_3-calculations are all smaller than $(\Sigma_s)^{-1}_{min}$. Thus it appears that no discrete relaxation lengths exist in light water. The apparent discrepancy between the results of several experiments which have been reported can largely be attributed to the angle anisotropy of the spectrum.

Measurements have been performed for the H_2O-ZrH_2-system by the chopper time-of-flight method using the thermal column of FiR 1 (TRIGA Mark II) as the neutron source and extracting the neutron beam from the water side at various distances from the discontinuity. The perturbation introduced by the extraction channel and the connection between the beam spectrum and the real spectrum is discussed.

1. INTRODUCTION

The main justification for the study of transient phenomena in neutron thermalization is that they provide a good test for the accuracy of the approximations to the energy-dependent Boltzmann equation and give information about the thermalization properties of moderators.

The time-dependent transient phenomenon which has been studied most is the evolution of a fast neutron pulse in a moderator, whereas the Milne problem is the most-studied space-dependent problem. Though neutron rethermalization has not received quite so much attention, it is, however, a subject of considerable interest. The first investigation in this field was that of Kottwitz [1], in which he considered the 'two temperature problem', which consists of two adjacent half-spaces at different temperatures. Kottwitz was able to solve the problem analytically in the P_1-approximation using the heavy-gas scattering model which changes the integral thermalization operator of the Boltzmann equation to a second-order differential operator. Later the problem was studied by several authors [2-6]. In all these papers the gas model is chosen for the scattering kernel. This somewhat restricts drawing conclusions on the results obtained, which are valid for realistic moderators also. However, these investigations have greatly elucidated the general behaviour of the neutron flux. Williams' paper, in which he gave the transport theoretical solution for the energy moments of the scalar flux, should be especially mentioned in this respect. According to the picture formed on

the basis of that paper the spatial behaviour of the average energy of the scalar flux is composed of an exponential function and a transient term. The latter decays rather quickly, being of importance only in the immediate neighbourhood of the discontinuity. The former term dominates farther from the interface. The relaxation length connected with this term is called the rethermalization length. This general behaviour certainly applies also for realistic moderators. There are a number of discrete eigenvalues (relaxation lengths) and a continuum. Cases may also occur where no discrete eigenvalues exist. The limit-point between these two parts is $(\Sigma_s)_{min}$, which is analogous to the limit-point of $(v\Sigma_s)_{min}$ for the time eigenvalues.

However, the heavy-gas model is too simple for describing the actual situation in most of the common moderators. The energy dependence of the total scattering cross-section and the angle anisotropy in scattering are the most important features neglected by this model. In addition, the effect of chemical binding is not taken into account. The use of realistic scattering models, however, greatly complicates the solution. An analytical treatment becomes impossible and use must be made of direct numerical methods or some semi-analytical method for solving the transport equation. Direct numerical calculations, such as those based on the S_N method, require much computer time. Thus some semi-analytical method is desirable for reducing computer time.

Some measurements of the neutron flux in the vicinity of a large temperature gradient have been performed using either the foil activation or the time-of-flight method [7-11]. The former provides information about the scalar flux in the form of the spatial behaviour of some spectral index from which one can infer for example, the 'effective neutron temperature'. A more detailed picture of the flux may be obtained by the time-of-flight method which enables the measurement of the angular flux. But then problems connected with beam extraction arise. It is necessary either to make an extraction channel to a point where the flux is strongly position-dependent or to measure the spectrum of the leakage flux in the direction of the interface [11]. In the first case the channel may disturb the flux in the vicinity of the channel and the beam may contain neutrons coming from elsewhere than the point of extraction. In the second case the connection between the spectrum inside the moderator and the leakage spectrum must be known. The corrections to be applied to the measured spectrum are in both cases very difficult to evaluate. The moderators used in these measurements are graphite and light water. There are, especially in the case of water, rather large discrepancies between the results reported.

In the present paper a solution based upon the representation of the flux as a linear combination of two known spectra with space- and angle-dependent coefficients is given. The angle dependence is described by the Legendre polynomials and the solutions are derived in the P_1 - and P_3-approximations. A comparison of these solutions with the results obtained by various approximations to the angle dependence of the flux and scattering and by different scattering models gives information about the influence of the transport effects and the scattering kernel. The results are also compared with the experimental results obtained by various authors. The measurements of the present author in a system containing light water and zirconium hydride are also described.

2. THEORY

It is assumed that the right and the left half-spaces, separated by a plane at $x = 0$, are occupied by two moderators at the temperatures T_1 and T_2, respectively. If it is assumed that both moderators are non-absorbing and free from sources, the Boltzmann equation may be written as follows:

$$\mu \frac{\delta\phi(x,E,\mu)}{\delta x} + \Sigma_s(x,E)\phi(x,E,\mu) = \int_{-1}^{+1} d\mu' \int_0^\infty dE' \Sigma_s(x,E'\to E,\mu'\to\mu)\phi(x,E',\mu') \quad (1)$$

$\phi(x,E,\mu)$ is the neutron flux depending on the space-co-ordinate x, on the energy E, and on the direction cosine μ between the direction of neutron flight and the x-axis. $\Sigma_s(x,E'\to E,\mu'\to\mu)$ is the scattering cross-section from an energy E' to an energy E and from a direction characterized by μ' to a direction given by μ. $\Sigma_s(x,E)$ is the total scattering cross-section.

$\phi(x,E,\mu)$ is presented as a combination of two overlapping spectra with space- and angle-dependent coefficients, i.e.

$$\phi(x,E,\mu) = \sum_{i=1}^{2} \phi_i(x,\mu)\, M_i(E) \quad (2)$$

where $M_i(E)$ are known functions.

The angle-dependence of the flux and the scattering cross-section are expanded into the Legendre polynomials, i.e.

$$\phi_i(x,\mu) = \sum_{l=0}^{N} \left(\frac{2l+1}{2}\right) \phi_{il}(x)\, P_l(\mu) \quad (3)$$

and

$$\Sigma_s(x,E'\to E,\mu'\to\mu) = \sum_{l=0}^{N_l} \left(\frac{2l+1}{2}\right) \Sigma_{sl}(x,E'\to E)\, P_l(\mu_0) \quad (4)$$

Here μ_0 is the cosine of the scattering angle. The unknown functions are the coefficients $\phi_{il}(x)$. The number of these functions is $2(N+1)$. Multiplication of Eq.(1) with some energy-dependent function g(E) implies a balance equation for $g(E)\phi(x,E,\mu)$. Integration of this over E gives a balance equation for $\int_0^\infty g(E)\phi(x,E,\mu)\,dE$. Two balance equations of this kind may be satisfied by the trial function of Eq.(2). If $g(E) = 1$ the balance equation is the neutron conservation equation. $g(E) = E$ corresponds to the energy balance. The equations obtained with these g-functions are the same as those obtained by a variational method [12] when the adjoint flux is assumed to be a linear function of energy. Formally these equations are obtained from the P_N-equations by multiplying every equation by the two g-functions and integrating them over the energy.

The equations form a homogeneous differential equation system of first degree with constant coefficients. A solution in the form

$$\phi(x) = \{\phi_{10}, \phi_{20}, \phi_{11}, \phi_{21}, \phi_{22}, \ldots\ldots, \phi_{1N}, \phi_{2N}\} = \tilde{\phi}\, e^{\lambda x} \tag{5}$$

results in the equation

$$A(\lambda)\tilde{\phi} = 0 \tag{6}$$

In the P_1-approximation in region 1 ($T = T_1$, $x > 0$), when the $M_i(E)$-functions are taken to be the Maxwellians at T_1 and T_2, the following matrix is obtained for $A(\lambda)$:

$$A(\lambda) = A_1(\lambda) = \begin{bmatrix} 0 & 0 & \lambda & \lambda \\ \lambda & \lambda & 3a_{11} & 3a_{21} \\ 0 & b_{20} & 2T_1\lambda & 2T_2\lambda \\ 2T_1\lambda & 2T_2\lambda & 3b_{11} & 3b_{21} \end{bmatrix} \tag{7}$$

Similarly, in the P_3-approximation one obtains

$$A_3(\lambda) = \begin{bmatrix} 0 & 0 & \lambda & \lambda & 0 & 0 & 0 & 0 \\ \lambda & \lambda & 3a_{11} & 3a_{21} & 2\lambda & 2\lambda & 0 & 0 \\ 0 & 0 & 2\lambda & 2\lambda & 5a_{12} & 5a_{22} & 3\lambda & 3\lambda \\ 0 & 0 & 0 & 0 & 3\lambda & 3\lambda & 7a_{13} & 7a_{23} \\ 0 & b_{20} & 2T_1\lambda & 2T_2\lambda & 0 & 0 & 0 & 0 \\ 2T_1\lambda & 2T_2\lambda & 3b_{11} & 3b_{21} & 4T_1\lambda & 4T_2\lambda & 0 & 0 \\ 0 & 0 & 4T_1\lambda & 4T_2\lambda & 5b_{12} & 5b_{22} & 6T_1\lambda & 6T_2\lambda \\ 0 & 0 & 0 & 0 & 6T_1\lambda & 6T_2\lambda & 7b_{13} & 7b_{23} \end{bmatrix} \tag{8}$$

The abbreviations a_{il} and b_{il} have the following meaning:

$$\begin{aligned} a_{il} &= \int_0^\infty M(E/T_i)(\Sigma_s(x,E) - \Sigma_{sl}(x,E))\, dE \\ b_{il} &= \int_0^\infty EM(E/T_i)\,(\Sigma_s(x,E) - \Sigma_{sl}(x,E))\, dE + M_{1,l}(x, T_i, T_m) \end{aligned} \tag{9}$$

where

$$M_{1,1}(x, T_i, T_m) = \int_0^\infty M(E/T_i)\overline{\Delta E}_1(x,E)dE$$

$$= \int_0^\infty M(E/T_i) \int_0^\infty (E-E')\Sigma_{s1}(x, E \to E')\, dE'\, dE \tag{10}$$

T_m is the temperature of the moderator at x ($T_m = T_1$, when $x > 0$). The possible values of λ are obtained by setting det $(A(\lambda)) = 0$. In the P_1-approximation we obtain

$$\lambda_0 = 0; \quad \lambda_{1,2}^2 = \frac{3}{4}\frac{\Delta c_1}{\Delta T}\frac{b_{20}}{\Delta T} \tag{11}$$

where $\Delta c_1 = c_{21} - c_{11} = (b_{21} - 2T_1 a_{21}) - (b_{11} - 2T_1 a_{11})$ and $\Delta T = T_2 - T_1$. In the P_3-approximation one obtains the following equation for λ:

$$\lambda^2[(\lambda^2)^3 + A_4(\lambda^2)^2 + A_2(\lambda^2) + A_0] = 0 \tag{12}$$

where

$$A_4 = \frac{1008(2T_1\,\Delta a_3 - \Delta b_3)b_{20} - 1260(2\,\Delta e_3\,\Delta a_2 + 4\,\Delta d_3\Delta d_2)}{1296\,\Delta T^2}$$

$$\frac{-1260(\Delta b_2\Delta b_3 + 2\,\Delta a_3\Delta e_2) - 972\,b_{20}\Delta c_1}{1296\,\Delta T^2}$$

$$A_2 = \frac{945(2\,\Delta e_3\Delta a_2 + 4\,\Delta d_3\Delta d_2 + \Delta b_2\Delta b_3 + 2\,\Delta a_3\,\Delta e_2)\,b_{20}\Delta c_1}{1296\,\Delta T^4}$$

$$\frac{+[3920\,a_{12}b_{20} + 4900(b_{22}a_{12} - b_{12}a_{22})]\,(a_{13}b_{23} - a_{23}b_{13})}{1296\,\Delta T^2} \tag{13}$$

$$A_0 = \frac{3675(a_{22}b_{12} - a_{12}b_{22})\,(a_{13}b_{23} - a_{23}b_{13})\,b_{20}\Delta c_1}{1296\,\Delta T^4}$$

and

$$\Delta a_1 = a_{21} - a_{11}$$

$$\Delta b_1 = b_{21} - b_{11}$$

$$\Delta d_1 = T_2 a_{11} - T_1 a_{21} \tag{14}$$

$$\Delta e_1 = T_2 b_{11} - T_1 b_{21}$$

The result for $\phi(x)$ may be written in the form

$$\phi(x) = B_0\phi_0 + \sum_j B_j\phi_j e^{-\lambda_j x}; \quad (x > 0, \lambda_j > 0) \tag{15}$$

ϕ_j is the eigenvector connected to λ_j and B_j are constants. The corresponding solution may be written for the region 2 ($T = T_2$, $x < 0$). Requiring the flux to be continuous at the interface results in the continuity of every component of $\phi(x)$. $2(N+1)$ equations are obtained for determining the constants B_j on both sides of the interface. From these equations the two, being connected with both components of the P_1-angular dependence, i.e. ϕ_{11} and ϕ_{21}, are identical, for they have the same magnitude but reversed sign. When the solution is normalized so that, for example, $B_0 = 1$ for the region 1, $2N+1$ equations are left for the undetermined $2N+1$ B_j-values.

The described method is applied for a case where both half-spaces contain light water at temperatures 20 and 80°C respectively. The scattering cross-sections needed were calculated by the GAKER code [13] for the Nelkin model [14]. The energy integrations were performed in an evenly spaced z-variable which is defined by

$$z = \frac{E/T_0}{1+E/T_0}$$

where T_0 = 0.0253 eV; thirty-nine z-values from 0 to 1 were chosen.

TABLE I. RELAXATION LENGTHS ACCORDING TO THE NELKIN MODEL

Approximation	T = 20°C			T = 80°C		
	l_1/mm	l_2/mm	l_3/mm	l_1/mm	l_2/mm	l_3/mm
P 1	4.50	-	-	4.25	-	-
P 1[a]	3.91	-	-	3.74	-	-
P 3	5.33	2.39	1.39	5.04	2.45	1.37
P 3[a]	4.55	2.17	1.37	4.37	2.25	1.35

[a] Anisotropy of scattering is neglected.

The change of the integration variable simplifies the numerical integration procedure by allowing us to use only one step size over the whole integration region. In addition, there are more points in the region where the Maxwellians are changing most rapidly, i.e. in the small-energy region.

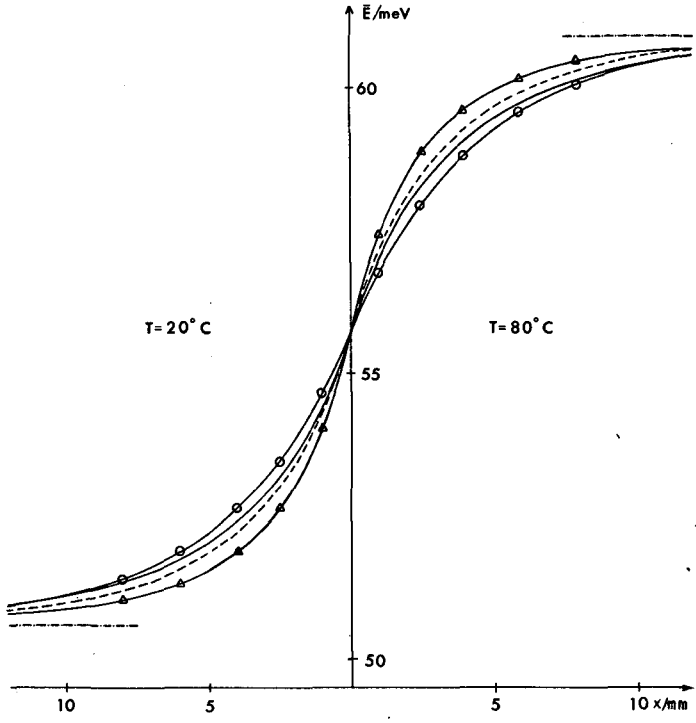

FIG. 1. Calculated spatial variation of average energy of scalar flux in $H_2O(80°C)$ - $H_2O(20°C)$ system.

——— P_3-approximation
— — P_3-approximation with isotropic scattering
○ ○ P_1-approximation
△ average energy of $\Phi(x,E,0)$

To evaluate the influence of the transport effects and the anisotropic scattering, calculations were made in the P_1 - and P_3-approximation with and without taking the anisotropic scattering into account. The relaxation lengths obtained are given in Table I. The behaviour of the flux-weighted average energy of the scalar flux is presented in Fig. 1. In this figure the average energy of $\Phi(x,E,0)$ is also plotted. The relaxation seems to be more rapid in the P_3 -approximation than in the P_1 -approximation. The anisotropy of scattering seems to have a rather small effect on the scalar flux. All the relaxation lengths are smaller than $(\Sigma_{s,min})^{-1}$ which is 7.34 mm. This indicates that there are probably no discrete relaxation lengths in light water but all the relaxation lengths obtained try to describe the continuum of the eigenvalues.

Though the P_N-approximation, especially for small N, is not expected to give good results for the angular flux, it, however, gives a qualitative picture of the real situation. Figure 2 describes the average energy of the angular flux for $\mu = -1$. The rather large discontinuity in the derivative at the interface may be due to the boundary conditions. The anisotropy of scattering seems also to have a rather large effect on the angular flux, as is to be expected. When one compares Figs 1 and 2, one observes

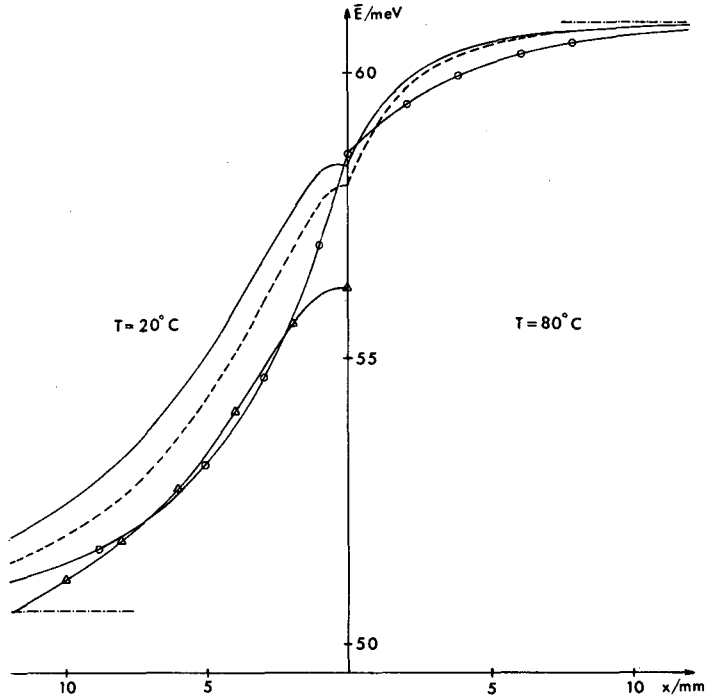

FIG. 2. Calculated spatial variation of average energy of $\Phi(x,E,-1)$ in $H_2O(80°C)$-$H_2O(20°C)$ system.

——— P_3-approximation
— — P_3-approximation with isotropic scattering
○ ○ P_1-approximation
△ Streaming effect accounted.

that the spectrum is strongly angle-dependent. A large part of this is caused by the transport factors as can be seen from the strong angular dependence obtained also for the heavy-gas model [15]. A part is due to anisotropic scattering and energy dependence of the total scattering cross-section.

To examine the sensitivity of the flux to the scattering model, calculations for light water were also made with the McMurry-Russell model [16]. These calculations were made for water at 20°C assuming the adjacent side to be at 270°C. This choice was made for analysing the measurements which are described later on. The results obtained for the relaxation lengths are compared with the results of the Nelkin model in Table II. In these results the P_2- and P_3-components of scattering are not taken into account because calculations show that they have little influence. The difference in the largest relaxation length is rather small, being mainly caused by the too strong thermalization power of the Nelkin model. As the comparison between Tables I and II shows, the relaxation lengths change somewhat when the temperature of the adjacent moderator changes. This also shows that the largest relaxation length is not a true rethermalization length, but rather a discrete eigenvalue trying to describe the continuum.

TABLE II. RELAXATION LENGTHS IN LIGHT WATER AT T = 20°C, WHEN THE ADJACENT SIDE HAS THE TEMPERATURE T = 270°C

Model	l_1/mm	l_2/mm	l_3/mm
Nelkin	5.90	2.27	1.47
McMurry-Russell	6.13	2.33	1.44

3. EXPERIMENTAL

The experimental approach includes two principal methods, viz. the foil activation method and the time-of-flight method. The former gives the spatial variation of some spectral index, whereas the latter gives the spatially-dependent neutron energy spectrum. Though the latter method seems to be superior, there is one serious problem connected with it, viz. the beam extraction. This is because one must make a channel to the point of extraction and this channel removes moderator material, thus changing the situation in the neighbourhood of this point. The channel may change the neutron energy spectrum at this point and cause streaming of neutrons from the walls of the channel to its bottom, thus making it possible for these neutrons to enter the beam. Naturally the disturbing effect depends on the size of the channel as compared with the mean free path of scattering and on the spatial dependence of the energy spectrum. Investigations of the influence of the channel width on the measured spectrum have been made when the spectrum is independent of position [17]. These show that in an infinite water moderator a channel measuring 5 cm in diameter only slightly deforms the spectrum. There are no measurements, known to the author, for studying the disturbing effect of the extraction channel when the spectrum is space dependent.

In spite of this lack of knowledge of the correction due to finite channel width this method was chosen for measuring the neutron spectrum in a system consisting of zirconium hydride at 270°C and light water at 10°C. Zirconium hydride was chosen because of its peculiar scattering properties caused by the nearly Einstein oscillator behaviour of the hydrogen atoms, and also because rethermalization may have an effect on the temperature coefficient of reactivity of zirconium hydride-moderated reactors. In the phonon frequency spectrum of zirconium hydride there is a very pronounced optical peak at 0.137 eV. (The weight factor of the acoustic part which extends to about 0.040 eV [18, 19] is not accurately known but is at most some per cents.) It was to be expected that there might be some abrupt change in the spectrum caused by this peak. Figure 3 presents the experimental set-up. The moderator chamber, consisting of two separate parts, one of which contained zirconium hydride at 270°C and the other light water at 10°C, was inserted into the middle of the graphite thermal column of FiR 1 (of type Triga Mark II). This was made by removing one graphite block of cross-section 10 cm × 10 cm from the column and placing the chamber to the hole thus formed. The width of both parts was 5 cm. These dimensions are too small for the

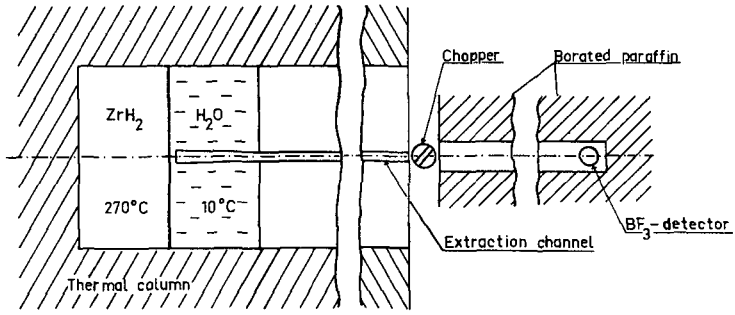

FIG. 3. Experimental arrangement for ZrH_2(270°C)-H_2O(10°C) measurements.

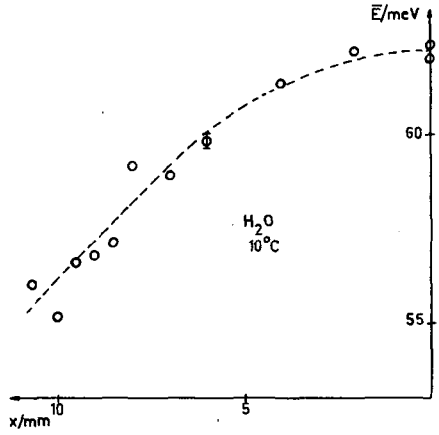

FIG. 4. Measured spatial variation in water of average energy of neutrons streaming perpendicular to the interface from ZrH_2 to H_2O.

zirconium hydride part to be considered as infinite. The part containing zirconium hydride in powder form (density 2.8 g/cm^3) was nearer to the reactor core. To the part containing water, an extraction channel was made, measuring 7 mm in diameter at the bottom and being a little conical. The distance from the bottom of the channel to the interface might be controlled from the outside of the reactor with an accuracy of 0.1 mm. The spectrum of the extracted beam was measured by a standard time-of-flight spectrometer [20] with a resolution of about 80 μs. Zirconium hydride with chemical composition ZrH_2 was heated by electric resistors. The temperature distribution of zirconium hydride was measured and a minimum value of 240°C at the interface was found when the temperature in the middle was 270°C. The temperature was controlled with an accuracy of 5°C. In the second part of the chamber, which was thermally insulated from the zirconium hydride part, a circulation of water was arranged. The temperature of the water was measured and found to be practically constant throughout the water chamber.

The time-of-flight spectra measured from different distances to the interface were corrected, after subtracting a very small epithermal background, for scattering in air in the flight path of neutrons, for the

dynamic and static transmissions of the chopper, and for the deviation of the efficiency of the BF_3-detector from the 1/v law. The resolution correction was neglected, due to its smallness, for the greatest part of the spectrum. The effect of neutrons coming to the beam directly from the graphite by scattering in air was measured by placing a cadmium plate to the beam tube just outside the moderator chamber. The contribution of these neutrons was also subtracted. From the corrected spectra, after smoothing the curves and taking the average of three adjacent points, the flux-weighted average energy was calculated numerically.

With the resolution used no abrupt change was found at about 0.137 eV. The average energy as a function of the distance from the interface is plotted in Fig.4. The error indicated is due to the statistical error of about 2% at the top of the spectrum. Evidently there has been some instability in the system causing the points to scatter more than the statistical error.

These results show much slower relaxation than that found by the present author in earlier measurements [11]. This is due to the strong angular dependence of the spectrum; in the earlier measurements the beam was taken as a leakage beam in the direction of the interface.

The influence of the extraction channel on the measured spectrum is difficult to evaluate, especially as to the spectrum disturbance at the point of extraction. The effect of the neutrons streaming down from the walls of the channel to the bottom and then scattering to the beam was calculated roughly. If the flux at a point on the wall of the channel was given by theoretical calculations, the average energy of the neutrons at this point, having a direction of flight toward the bottom of the channel, was determined. Then, for a neutron having this energy and direction, the average energy after scattering to the direction of the beam was determined. Then by weighting this energy with the probability for the neutron concerned to come to the beam after one scattering event and with the number of neutrons having the required direction, and integrating over the wall of the channel we obtained the contribution of these neutrons to the average energy of the beam. The curve marked with Δ in Fig.2 gives the average energy of the beam in the direction $\mu = -1$ when the streaming down of neutrons is taken into account as explained above. The effect is rather large, giving an idea of the difficulties involved in performing measurements of this kind which are reliable enough for comparison with theory.

4. CONCLUSIONS

It has been shown that the flux near a large-temperature gradient is highly anisotropic. This means that the rethermalization lengths or rethermalization cross-sections inferred from different experiments are not directly comparable. This explains at least partially the discrepancy found between the results reported. Of course the anisotropy becomes smaller for heavier moderators, leading to better agreement between results from different experiments.

Though the time-of-flight method gives principally much more information than the foil activation method, there is a serious drawback to the former method, which concerns corrections for the beam extraction.

This indicates that its use is questionable, especially in hydrogenous moderators. To obtain reliable experimental data for comparison with theory one must use the foil activation method in spite of much less information.

Use of the one relaxation length model does not seem to be suitable for hydrogenous moderators. The results obtained indicate that in water there are probably no discrete space-eigenvalues but the whole relaxation is determined by a continuum of eigenvalues. Williams' results [21] show that in a gas with mass number 2 there is no rethermalization length. Because the 'effective mass' of the hydrogen atom in water is of the same magnitude, non-existence of eigenvalues is therefore to be expected. This is also in agreement with the results of Wood [22] for the effective width model.

The study of the sensitivity of the flux to the scattering model is being considered for an analysis of the zirconium hydride-light water measurements. It is rather difficult to separate the effects of the anisotropic scattering and the energy transfer properties. However, it is found that the scalar flux is rather insensitive to the anisotropic scattering, whereas the angular flux shows greater sensitiveness.

In every case a highly developed experimental technique is required for a comparison of theory with experiment.

ACKNOWLEDGEMENTS

The author wishes to thank Professor Pekka Jauho for encouragement and interest in the present work. For the scattering kernel calculations he wishes to thank Mr. L.G. Larsson at AB Atomenergi, Studsvik, Sweden, Dr. H.L. McMurry at Idaho Nuclear Corporation, Idaho Falls, Idaho, U.S.A., and Northern Europe University Computing Centre, at Copenhagen, Denmark, for providing computer time. He is also grateful to Dr. M.M.R. Williams for reading the manuscript and for the remarks he made on it.

REFERENCES

[1] KOTTWITZ, D.A., Nucl. Sci. Engng 7 (1960) 345.
[2] SELENGUT, D.S., Nucl. Sci. Engng 9 (1961) 94.
[3] LESLIE, D.C., J. nucl. Energy 16 (1962) 303.
[4] PEARCE, R.M., KENNEDY, J.M., Nucl. Sci. Engng 19 (1964) 102.
[5] WILLIAMS, M.M.R., Brit. J. appl. Phys. 16 (1965) 1727.
[6] JAUHO, P., VIRJO, A., to be published in Nucl. Sci. Engng.
[7] BENNETT, R.A., USAEC Rep. BNL-719 3 (1962) 838.
[8] POOLE, M.J., SCHOFIELD, P., SINCLAIR, R.N., Exponential and Critical Experiments III IAEA, Vienna (1964) 87.
[9] MAIOROV, L.V., MOSTOVOI, V.J., SAFIN, Yu.A., TRUHANOV, G.Ya., Pulsed Neutron Research I IAEA, Vienna (1965) 657.
[10] SPRINGER, T., Nukleonik 4 (1960) 144.
[11] SAASTAMOINEN, J., Nucl. Sci. Engng 25 (1966) 261.
[12] SELENGUT, D.S., "Variational methods in neutron thermalization", Neutron Physics (YEATER, M.L., Ed.), Academic Press, New York and London (1962) 162-86.
[13] HONECK, H.C., USAEC Rep. BNL-5826 (1961).
[14] NELKIN, M., Phys. Rev. 119 (1960) 741.
[15] Unpublished work of the author.

[16] McMURRY, M.L., RUSSELL, G.J., BRUGGER, R.M., Nucl. Sci. Engng 25 (1966) 248.
[17] POOLE, M.J., Pulsed Neutron Research I IAEA, Vienna (1965) 425.
[18] YOUNG, J.C., YOUNG, J.A., HOUGHTON, G.K., TRIMBLE, G.D., BEYSTER, J.R., Nucl. Sci. Engng 19 (1964) 230.
[19] GLÄSER, W., EHRET, G., MERKEL, A., Inelastic Scattering of Neutrons II IAEA, Vienna (1965) 167.
[20] PALMGREN, A., Nucl. Instrum. Meth. 36 (1965) 88.
[21] WILLIAMS, M.M.R., Nucl. Sci. Engng 26 (1966) 262.
[22] WOOD, J., private communication by M.M.R. Williams.

CALCULATIONS ON THE FUNDAMENTAL TIME-DECAY CONSTANT OF WATER AND POLYETHYLENE *

G. W. GRIFFING
IDAHO NUCLEAR CORPORATION,
IDAHO FALLS, IDAHO,
UNITED STATES OF AMERICA

Abstract

CALCULATIONS ON THE FUNDAMENTAL TIME-DECAY CONSTANT OF WATER AND POLYETHYLENE. The computed time-decay spectrum of the Nelkin, GIN, and MR scattering kernels for water are compared. The spectrum for the Nelkin and GIN kernels were found to be nearly the same. However, the two discrete higher time eigenvalues of the MR kernel, which is in closer agreement with the experimental data on the partial-differential cross-section, are more closely spaced and smaller in magnitude than the corresponding eigenvalues for the other two kernels. In addition, the limit of the discrete spectrum as given by $(v\Sigma_s)_{min}$ is approximately 0.22 μsec^{-1} for the MR kernel and 0.32 μsec^{-1} for the other scattering kernels.

Deviations of less than one percent were found between the calculated and experimental results for the fundamental time-decay constant of water in spherical geometry. The experiments were done by Gon, who made measurements on various-sized systems with bucklings ranging from 0.09 to approximately 3.0 cm^{-2}. The magnitude of the computed fundamental time-decay constant was found not to be particularly sensitive to the kernel used.

Comparisons of the calculated and experimentally observed fundamental time-decay constant for polyethylene in cylindrical geometry were also made. For bucklings less than 0.15 cm^{-2}, deviations of less than one percent were noted. For larger bucklings, deviations of approximately two percent were found, except for the largest buckling of approximately 1.5 cm^{-2} which deviated by six percent. The McMurry scattering kernel was used in the computations on polyethylene.

1. INTRODUCTION

Experimental investigations by Gon [1] on the fundamental time-decay constant of water extended the measurements to much larger bucklings than had been done in previous experiments. Spherical geometry was used with the smallest sample having a radius of 1.5 cm. For this sample, the observed fundamental time-decay constant was 86,350 sec^{-1}. This observed value for the decay constant is still much below its upper bound given by $(v\Sigma)_{min}$. This bound has been estimated by various authors [2-4] to be approximately 300,000 sec^{-1}. Using the MR (for McMurry-Russell) scattering kernel [5], this bound is estimated to be about twenty-five percent smaller as will be seen in Section 3. One motive of this work was to ascertain whether the diffusion approximation to the Boltzmann equation was an adequate approximation in predicting the fundamental time-decay constant for these larger bucklings. Our results indicate that it is sufficient. Another objective was to compare the time-decay spectra of three different scattering kernels (see Section 3) which are progressively more satisfactory in their ability to predict the experimental details on the partial-differential scattering cross-section.

* This work was performed under the auspices of the United States Atomic Energy Commission.

Experiments on polyethylene using cylindrical geometry were done several years ago by Sjöstrand, Mednis, and Nilsson [6] in which the fundamental time-decay constant was measured for various bucklings. Apparently, there have been no theoretical computations confirming these measurements. Thus, results for this moderating material are also of interest. Fair to excellent agreement was obtained.

With a few minor modifications to the code, the computations were performed by making use of a code called TIDES [7]. It is applicable for the computations of time-dependent spectra for an isotropic, homogeneous, non-multiplying medium which can be described by a buckling B^2. Section 2 gives a brief discussion of the relevant work of Ohanian and Daitch [8] on which the code is based. In the remaining Sections, the results of the computations are given and discussed.

2. COMPUTATIONAL METHOD

In the diffusion approximation to the Boltzmann equation, the time-dependent spectrum is given by the solution of

$$\frac{1}{v}\frac{\partial\Phi(E,t)}{\partial t} = -[\Sigma_s(E) + \Sigma_a(E) + D(E)B^2]\Phi(E,t) + \int_0^\infty \Sigma_s(E'\to E)\Phi(E',t)dE' + S(E,t) \qquad (1)$$

where $\Phi(E,t)$ is the neutron flux density as a function of the neutron energy E (or velocity v) and time t. $\Sigma_s(E)$, $\Sigma_a(E)$ and $\Sigma(E'\to E)$ are the macroscopic scattering, absorption and energy transfer cross-sections, respectively. $S(E,t)$ is the source and $D(E)$ is the energy-dependent diffusion coefficient. If the scattering kernel is put into symmetrized form by making use of detailed balance, Eq. (1) can be written as

$$\frac{\partial X(E,t)}{\partial t} = PX(E,t) + \xi(E,t) \qquad (2)$$

where

$$X(E,t) = \Phi(E,t)/\sqrt{M(E)}$$

$$\xi(E,t) = S(E,t)/\sqrt{M(E)}$$

and

$$PX(E,t) = \int_0^\infty \left\{K(E',E) - v[\Sigma_s(E) + \Sigma_2(E) + D(E)B^2]\delta(E-E')\right\} X(E',T)dE'$$

$$K(E',E) = \Sigma_s(E'\to E)\sqrt{M(E')}\,/\sqrt{M(E)}$$

with

$$M(E) = (E/kT)\exp(-E/kT)$$

The solution of the homogeneous part of Eq. (2) is formally given by

$$\chi(E,t) = \sum_j A_j \psi_j(E)\, e^{-\lambda_j t} \quad . \tag{3}$$

In Eq. (3), the sum is over the discrete set together with an integration over a continuous set of eigenfunctions. The expansion coefficients are determined by the initial conditions. The eigenvalue equation to be solved is

$$P\psi_n(E) = -\lambda_n \psi_n(E) \tag{4}$$

An approximate numerical solution may be obtained by making use of a discrete energy representation. For greater detail the reader is referred to the paper of Ohanian and Daitch.

3. RESULTS OF CALCULATIONS

3.1. Comparisons with previous calculations

Various scattering kernels [4,8,9] have been used in studies on the thermalization problem of water. Here, we consider yet another. It is the MR scattering kernel. Essentially the MR scattering kernel is an elaborate extension of the Nelkin model [10]. It was designed to give a much better fit to the experimental data on the partial-differential cross-section. In general, the Nelkin and MR scattering kernels are in better agreement with each other for large neutron momentum transfers than for small neutron momentum transfers. This is not surprising since it is well known that details of the neutron scattering are much more sensitive to the various interactions at small neutron momentum transfers [11]. The motivation for the MR model was to better account for such interactions to obtain better agreement with the experimental data.

In the calculations of Ohanian and Daitch [8], the GIN (for Goldman improved Nelkin) scattering kernel [12] was used. The GIN kernel is also a modification of the Nelkin model which was designed to better fit the experimental data. However, since the modifications in the GIN model are not nearly so extensive as for the MR model, it would be expected agreement with the experimental data for scattering would be less satisfactory.

Table I compares some of the time eigenvalues obtained using the computer code TIDES for the Nelkin, GIN, and MR scattering kernels. The results for the GIN kernel are those of Ohanian and Daitch with a temperature of 20°C. The results for the Nelkin and MR kernels are for a temperature of 22°C. In all of these results the same thirty-three discrete energy points were used which ranged from 1.95×10^{-5} to 1.72 eV.

As will be observed, the results for the Nelkin and GIN kernels are quite similar. Indeed, it may be possible that there is no difference within the accuracy of the computations. In both there is

TABLE I

TIME EIGENVALUES AND $(v\Sigma_s)_{min}$ OF THE NELKIN, GIN, AND MR KERNELS

	NELKIN* (μsec^{-1})	GIN (μsec^{-1})	MR (μsec^{-1})
λ_1	0	0	0
λ_2	0.1769	0.1721	0.1494
λ_3	0.2740	0.2677	0.1957
λ_4	0.3223	0.3135	0.2260
λ_5	0.3252	0.3161	0.2307
λ_6	0.3323	0.3232	0.2452
λ_7	0.3390	0.3299	0.2583
λ_8	0.3529	0.3438	0.2772
λ_9	0.3639	0.3548	0.2989
λ_{10}	0.3835	0.3746	0.3161
λ_{11}	0.3985	0.3892	0.3422
$(v\Sigma_s)_{min}$	0.322	0.315	0.223

$\Sigma_a = 0.0$ $B^2 = 0.0$ H atom density = 0.0668×10^{24} atoms/cm^3

*Ghatak and Honeck [4] have done calculations at 20°C using a somewhat different version of the Nelkin model obtaining values of 0.1772 and 0.2759 μsec^{-1} for the two higher discrete eigenvalues. Our calculations are for 22°C based on a version of the Nelkin model described in Ref. [5].

an ambiguity of whether the 4th eigenvalue belongs to the discrete or the continuum spectrum. As pointed out by Ohanian and Daitch, this decision can be made by an examination of the corresponding eigenfunction. On the other hand, the spectrum for the MR kernel is decidedly different. There is no ambiguity about the 4th eigenvalue as it definitely belongs to the continuum. The two higher discrete eigenvalues (0.1494 and 0.1957 μsec^{-1}) are smaller and are more closely spaced than the corresponding eigenvalues for the other two kernels. The limit point of the discrete spectrum (0.223 μsec^{-1}) is even smaller than the 2nd higher discrete eigenvalue for the other two kernels. Since the MR kernel more closely fits the experimental data for the partial-differential cross-section, it would be expected that the MR eigenvalues would be more reliable.

The question arises regarding the possibility of measuring the higher time-decay constants. It was the hope in the reaction rate experiments of Möller and Sjöstrand [13] that the thermalization time constant (reciprocal of λ_2) was being measured. Doubt that this quantity is actually measured in those experiments, but rather an effective decay constant, has resulted from the study of Ghatak and Honeck [4]. In support of that conclusion, the author examined the computed time-dependent flux for an energy of 0.18 eV as obtained from TIDES using the MR kernel with a delta source at 1.7 eV. This gave a curve not

unlike the reaction rate curve for cadmium obtained by Möller and Sjöstrand. Starting at 22 μsec, the computed values of the flux at later times could be fitted to an accuracy of five percent or less by a function of the form

$$\Phi(t) = \Phi_1 + \Phi_2 e^{-\mu_2 t} \tag{5}$$

The value of μ_2 varied, depending on the range chosen to make the fit, having an average value of approximately 0.20 μsec^{-1}. Clearly, the reciprocal of μ_2 can only be considered as an effective value for the reciprocal time constant. This apparent thermalization time constant results simply because Eq. (5) does not represent the magnitude of the flux accurately enough. At least another exponential type term is needed to represent the flux more accurately. This procedure appears to be of little practical use in pulse type experiments for the determination of the thermalization time. It is mentioned that, in principle, the above analysis does not differ from the type of analysis used in the reaction rate experiments [13] to determine the thermalization time.

Purohit [14] has made an extensive study of the reaction rate problem. He found some dependence of the reaction rate on the scattering models. It would be of interest to repeat this work using the MR kernel.

3.2. Comparison with experimental results on water

Since water is an important neutron moderator, there has been much experimental and theoretical work done on this material. In general, it

TABLE II

EXPERIMENTAL AND THEORETICAL FUNDAMENTAL DECAY CONSTANTS OF WATER FOR VARIOUS BUCKLINGS

$B^2(cm^{-2})$	EXPERIMENT (sec^{-1})	THEORY (sec^{-1})	Per Cent Deviation
0.08906	8,050	8,084	0.4
0.1472	10,230	10,150	0.1
0.2195	12,600	12,690	0.1
0.2197	12,650	12,700	0.0
0.3038	15,560	15,600	0.0
0.3482	17,100	17,120	0.0
0.4889	21,830	21,840	0.0
0.5500	23,990	23,850	0.6
0.6162	26,010	25,840	0.0
0.7340	29,600	29,540	0.2
0.9472	36,210	36,000	0.6
(1.776)	59,700	59,500	0.3
(2.058)	65,790	65,340	0.7
(3.029)	86,350	86,040	0.4

Note: The experimental results are for a temperature of 24.5°C. The calculations are for a temperature of 22°C using the MR kernel. The bucklings in parentheses were assigned by the author.

would appear that there is fairly good agreement between the experiments and calculations for the diffusion parameters [15]. Concerning the fundamental decay constant, experimental results suggest a dependence upon the geometrical shape of the moderator [16-18] for large bucklings ($B^2 > 0.4$ cm^{-2}). To further elucidate the question regarding the geometrical shape and to obtain data on a more rigorously calculable geometry, Gon [1] performed some very careful experiments on spheres with radii ranging between 1.5 to 10.2 cm. For their common range of bucklings, these experiments are in agreement with those of Lopez and Beyster [16] on cubes.

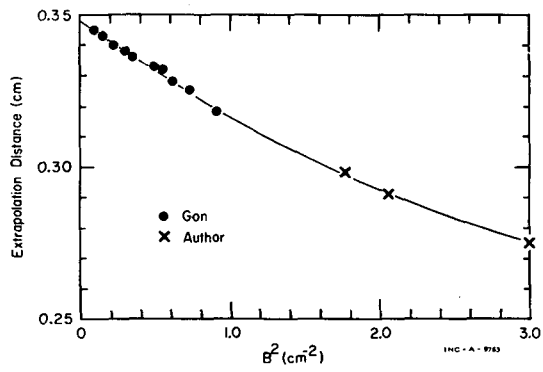

FIG. 1. Extrapolation distances for spheres. The solid curve has been drawn as a guide to the eye.

Table II compares the results obtained using TIDES with the experimental results of Gon. The agreement is excellent. The energy-dependent diffusion coefficient D(E) used was that computed by Ohanian [19]. In his study, Gon did not attempt to assign bucklings for $B^2 > 1.0$ cm^2, one reason being that the extrapolated distances as given by Gelbard and Davis [20] were not extended beyond $B^2 = 1.0$ cm^{-2}. Rather than attempt to compute the extrapolation distance, the author used the stratagem of first plotting the given extrapolated distances against the effective radii. This curve was then extended by "eyeball" to smaller radii. This gave approximate extrapolation distances from which a buckling was computed. This buckling was then used to compute the fundamental decay constant. Fig. 1 gives the variation of the extrapolation distance as a function of buckling. The depicted variation of the extrapolation distance with buckling is reasonable [21]. However, it can only be considered as an empirical curve.

De Juren [22] has reported some measurements on the fundamental time-decay constant for cylinders of water at 23°C. The calculated and measured results for the fundamental time-decay constant were not in as good agreement as our previous comparisons with Gon's measurements. For instance, at $B^2 = 0.6458$ cm^{-2} the computed value was 26,780 sec^{-1} while the observed value is quoted as 27,320 $\pm$ 130 sec^{-1}. This is a deviation of about two percent.

In concluding this section on water, a comparison is made in Fig. 2 of the first four time eigenvalues as a function of buckling for the MR and Nelkin kernels. It is to be noted that, whereas there is little

difference for the fundamental time eigenvalue, there are considerable differences for the higher time eigenvalues. It is of interest to note that the discrete time eigenvalues show a greater variation on the buckling than eigenvalues belonging to the continuum.

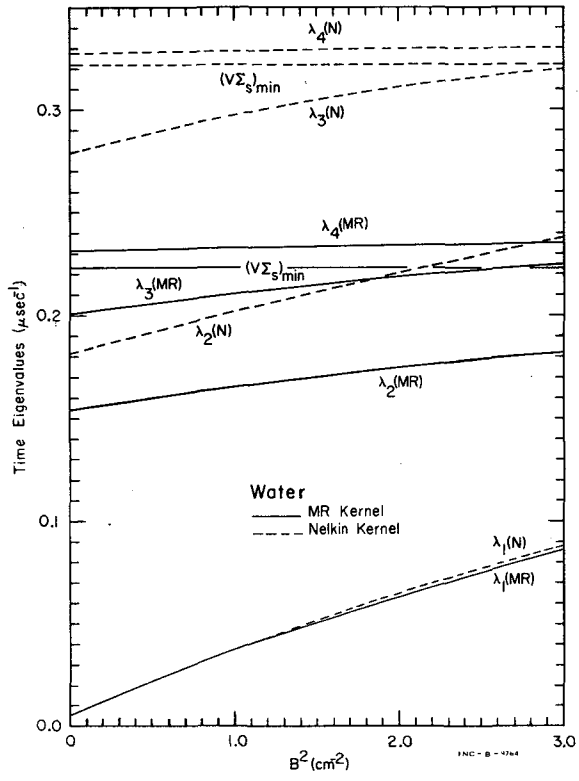

FIG. 2. Variation of time eigenvalues with B^2.

3.3. Comparison with experimental results on polyethylene

Before comparing the experimental and calculated results, we will comment briefly on the kernel used. This kernel was obtained by methods developed by McMurry [23,24]. Essentially, the method consisted of first doing normal coordinate analyses of n-butane which contains radicals of CH_3 and CH_2. The motions of the CH_2 radicals are taken to be representative of CH_2 radicals in polyethylene. Knowing these motions, the partial-differential cross-section is computed. It would not be expected that the partial-differential cross-section would be predicted in all details. Nevertheless, Whittemore [25] has found that this procedure is a realistic approximation, at least in those cases where checks could be made, to his experiments on the partial-differential cross-section of polyethylene.

Table III compares the computed fundamental time-decay constants with the experimentally observed decay constants [6] for cylinders of various bucklings. The energy-dependent diffusion coefficient D(E) used

TABLE III

EXPERIMENTAL AND THEORETICAL FUNDAMANTAL TIME-DECAY CONSTANTS OF POLYETHYLENE FOR VARIOUS BUCKLINGS

$B^2(cm^{-2})$	EXPERIMENT (sec^{-1})	THEORY (sec^{-1})	Per Cent Deviation
0.0981	8,493 ± 40	8,467	0.3
0.1070	8,772 ± 120	8,710	0.7
0.1206	9,008 ± 50	9,079	0.8
0.1427	9,725 ± 50	9,678	0.5
0.1825	10,517 ± 50	10,749	2.2
0.2645	12,675 ± 60	12,929	2.0
0.4835	18,220 ± 90	18,583	2.2
1.4844	39,440 ± 400	41,820	5.7

Note: Experimental results are for 20°C and the theoretical results are for 22°C. The hydrogen density was taken as 7.86×10^{22} atoms cm^{-3}.

TABLE IV

EXPERIMENTAL AND THEORETICAL DIFFUSION PARAMETERS OF POLYETHYLENE

	$\lambda(B^2=0)(sec^{-1})$	$D_0(cm^2 sec^{-1})$	$C(cm^4 sec^{-1})$
Sjöstrand, Mednis and Nilsson	5900 ± 90	26,500 ± 600	2600 ± 800
Three-Parameter Fit	5761	27,799	2368

Note: Experimental values are for 20°C and calculated values for 22°C.

in the calculations were obtained from the computer code SWAK [26]. The same thirty-three energy points were used as in water.

A striking feature in this comparison is that for the first four bucklings the experimental and theoretical results differ by less than one percent while the remaining cases differ by two percent or greater. It is suggestive that this is due, at least in part, to experimental reasons.

The same method as employed by the experimentalist may be used to find the diffusion parameters of polyethylene. Thus, the computed values for the fundamental time-decay constant is fitted to a curve of the form $\lambda(B^2) = \lambda(0) + D_0B^2 - CB^4$. The calculated results are compared with

experimental results in Table IV. The agreement appears to be satisfactory.

Finally, in Fig. 3 the first five time eigenvalues are shown as a function of the buckling. The quantity $(v\Sigma_s)_{min}$ was found to be approximately 0.36 μsec^{-1}. From an inspection of the eigenfunctions, the fourth eigenvalue (λ_4) appears to be in the discrete spectrum. However, with a more accurate kernel it would not be surprising if it actually belonged to the continuum.

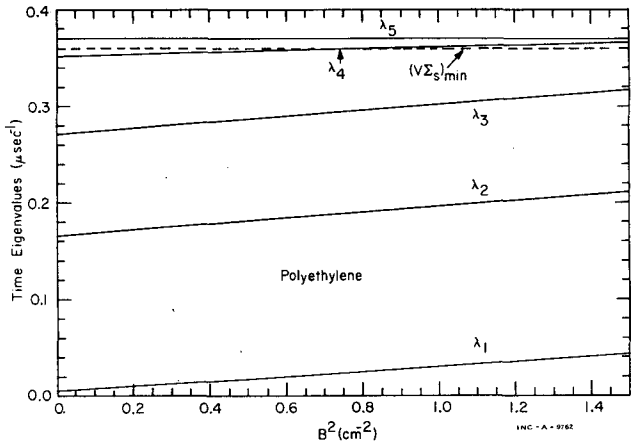

FIG. 3. Variation of time eigenvalues with B^2.

4. CONCLUDING REMARKS

In our calculations, it was found that the higher time eigenvalues obtained by using the MR scattering kernel for water are considerably smaller in magnitude than the magnitude of the corresponding eigenvalues using the Nelkin or GIN kernels. If the time-decay eigenvalue spectrum of water as predicted by the MR scattering kernel is approximately correct, the concept of a thermalization time as given by the reciprocal of the first higher eigenvalue is even more dubious than with other scattering kernels. A somewhat indirect experimental possibility of obtaining the first eigenvalue would be to subtract out the flux component of the fundamental mode from an appropriate neutron life history plot ($\Phi(E,t)$ against t for a fixed E) obtained in a pulse type experiment and analyze the resulting curve. However, for the reasons given earlier, this procedure appears to hold little promise.

Excellent agreement with Gon's measured fundamental time-decay constant on water spheres was found. This comparison does not permit a preference for the MR, Nelkin or GIN scattering kernels since each would give approximately the same value for the fundamental time-decay constant.

During the course of the analysis an empirical curve of the extrapolated distance as a function of buckling, for much larger bucklings than has been theoretically investigated, was obtained. This dependence should be theoretically investigated.

The agreement with the measured fundamental time-decay constant for polyethylene cylinders appeared to be satisfactory except, perhaps, for the largest buckling. Experiments on polyethylene spheres such as those for water would be worthwhile.

ACKNOWLEDGEMENTS

The author is indebted to Dr. H. L. McMurry who furnished the Nelkin and MR scattering kernels for water and the scattering kernel for polyethylene. The author is also indebted to Mr. J. Menzel, who acquainted the author with the computer code TIDES. The many conversations with Dr. R. G. Fluharty are gratefully acknowledged.

REFERENCES

[1] Gon, E. (1963), D. Sc. Eng., Columbia University, New York.
[2] Corngold, N. and Michael, P., Nucl. Sci. Eng. 19 (1964) 91.
[3] Williams, M. M. R. and Wood, J., J. Nucl. Energy 19 (1965) 601.
[4] Ghatak, A. K. and Honeck, H. C., Nucl. Sci. Eng. 21 (1965) 227.
[5] McMurry, H. L., Russell, G. J., and Brugger, R. M., Nucl. Sci. Eng. 25 (1966) 248.
[6] Sjöstrand, N. G., Mednis, J., and Nilsson, T., Arkiv Fysik 15 (1959) 483.
[7] Lee, R. R., Linac Internal Rpt., Rensselar Polytechnic Institute, Troy, New York (1966).
[8] Ohanian, M. J. and Daitch, P. B., Nucl. Sci. Eng. 19 (1964) 343.
[9] Wood, J., Pulsed Neutron Research I IAEA, Vienna (1965) 219.
[10] Nelkin, M. S., Phys. Rev. 119 (1960) 741.
[11] Griffing, G. W., Inelastic Scattering of Neutrons in Solids and Liquids I IAEA, Vienna (1963) 435.
[12] Goldman, D. T. and Federighi, F. D., Nucl. Sci. Eng. 16 (1963) 165.
[13] Möller, E. and Sjöstrand, N. G., Arkiv Fysik 27 (1964) 501.
[14] Purohit, S. N., A. B. Atomenergi Rpt. AE, 226 (1966).
[15] Beckurts, K. H., Pulsed Neutron Research I IAEA, Vienna (1965) 3.
[16] Lopez, W. M. and Beyster, J. R., Nucl. Sci. Eng. 12 (1962) 190.
[17] Küchle, M., Nukleonik 2 (1960) 131.
[18] Hall, R. S., Scott, S. A., and Walker, J., Proc. Phys. Soc. (London) 79 (1962) 257.
[19] Ohanian, M. J. (1963), Ph.D. Thesis, Rensselar Polytechnic Institute, Troy, New York.
[20] Gelbard, E. M. and Davis, J. A., Nucl. Sci. Eng. 13 (1962) 237.
[21] Beckurts, K. H., Proc. Brookhaven Conf. on Neutron Thermalization, BNL-719 (1962) Vol. III.
[22] De Juren, J. A., Pulsed Neutron Research I IAEA, Vienna (1965) 323.
[23] McMurry, H. L., Spectrochim. Acta 21 (1965) 2091.
[24] McMurry, H. L. and Speas, D., Spectrochim. Acta 21 (1965) 2105.
[25] Whittemore, W. L., Nucl. Sci. Eng. 24 (1966) 394.
[26] Federighi, F. D. and Reno, T. J., SWAK, A Thermal Cross Section Program, KAPL-M-RPC-6 (15 Mar. 1963).

DISCUSSION

D. H. DAY: I notice that the time-dependent experiments reported for water are for the decay of total flux. I should just like to mention that Sinclair, at Harwell, has measured the time decay at several

discrete energies, selected by using various orders of reflection from a crystal. Analysis of this work requires consideration of the time-dependent buckling, after completion of which the work will be published.

R. B. RAZMINAS: With regard to Table III of your paper, would you please comment on the extrapolation distances used for the B^2 correlation with λ for the polyethylene? Do you think that discrepancies between experiment and calculation at high B^2 may be due to lack of knowledge of the extrapolation distance?

G. W. GRIFFING: Sjöstrand's buckling values, as quoted in his paper, were used. It is indeed quite possible that the discrepancies at large B^2 were due to the factor you mention.

SYMPOSIUM ON NEUTRON THERMALIZATION AND REACTOR SPECTRA

HELD AT ANN ARBOR, MICHIGAN, 17-21 JULY 1967

CHAIRMEN OF SESSIONS

Session A	K.M. CASE	University of Michigan, Ann Arbor, Michigan
	M.M.R. WILLIAMS	Queen Mary College, University of London, London
Session B	M.S. NELKIN	Cornell University, Ithaca, New York
	R.K. OSBORN	University of Michigan, Ann Arbor, Michigan
Session C	K.W. KOFINK	Technische Hochschule, Karlsruhe
Session D	J. SALMON	Commissariat à l'énergie atomique, Paris
	A.P.C. KIND	Centre Commun de Recherche, Ispra
Session E	S.N. PUROHIT	Rensselaer Polytechnic Institute, Troy, New York
	J. MIKA	Institute of Nuclear Research, Swierk

SECRETARIAT OF THE SYMPOSIUM

Scientific Secretaries:	J. DOLNICAR	Division of Research and Laboratories, IAEA
	S. SANATANI	Division of Nuclear Power and Reactors, IAEA

Administrative Secretary:	P. GHELARDONI	Division of Scientific and Technical Information, IAEA
Editor:	M. BROWN	Division of Scientific and Technical Information, IAEA
Records Officer:	D.J. MITCHELL	Division of Languages, IAEA

IAEA SALES AGENTS

Orders for Agency publications can be placed with your bookseller or any of our sales agents listed below :

ARGENTINA
Comisión Nacional de
Energía Atómica
Avenida del Libertador
General San Martin 8250
Buenos Aires - Suc. 29

AUSTRALIA
Hunter Publications,
23 McKillop Street
Melbourne, C.1

AUSTRIA
Georg Fromme & Co.
Spengergasse 39
A-1050, Vienna V

BELGIUM
Office international de librairie
30, avenue Marnix
Brussels 5

BRAZIL
Livraria Kosmos Editora
Rua do Rosario, 135-137
Rio de Janeiro

Agencia Expoente Oscar M. Silva
Rua Xavier de Toledo, 140-1° Andar
(Caixa Postal No. 5.614)
São Paulo

BYELORUSSIAN SOVIET SOCIALIST REPUBLIC
See under USSR

CANADA
The Queen's Printer
Ottawa, Ontario

CHINA (Taiwan)
Books and Scientific Supplies
Service, Ltd.,
P.O. Box 83
Taipei

CZECHOSLOVAK SOCIALIST REPUBLIC
S.N.T.L.
Spolena 51
Nové Město
Prague 1

DENMARK
Ejnar Munksgaard Ltd.
6 Nörregade
Copenhagen K

FINLAND
Akateeminen Kirjakauppa
Keskuskatu 2
Helsinki

FRANCE
Office international de
documentation et librairie
48, rue Gay-Lussac
F-75, Paris 5e

GERMANY, Federal Republic of
R. Oldenbourg
Rosenheimer Strasse 145
8 Munich 8

HUNGARY
Kultura
Hungarian Trading Co. for Books
and Newspapers
P.O.B. 149
Budapest 62

ISRAEL
Heiliger and Co.
3 Nathan Strauss Street
Jerusalem

ITALY
Agenzia Editoriale Internazionale
Organizzazioni Universali (A.E.I.O.U.)
Via Meravigli 16
Milan

JAPAN
Maruzen Company Ltd.
6, Tori Nichome
Nihonbashi
(P.O. Box 605)
Tokyo Central

MEXICO
Librería Internacional
Av. Sonora 206
Mexico 11, D.F.

NETHERLANDS
N.V. Martinus Nijhoff
Lange Voorhout 9
The Hague

NEW ZEALAND
Whitcombe & Tombs, Ltd.
G.P.O. Box 1894
Wellington, C.1

NORWAY
Johan Grundt Tanum
Karl Johans gate 43
Oslo

PAKISTAN
Karachi Education Society
Haroon Chambers
South Napier Road
(P.O. Box No. 4866)
Karachi 2

POLAND
Ośrodek Rozpowszechniana
Wydawnictw Naukowych
Polska Akademia Nauk
Pałac Kultury i Nauki
Warsaw

ROMANIA
Cartimex
Rue A. Briand 14-18
Bucarest

SOUTH AFRICA
Van Schaik's Bookstore (Pty) Ltd.
Libri Building
Church Street
(P.O. Box 724)
Pretoria

SPAIN
Librería Bosch
Ronda de la Universidad 11
Barcelona

SWEDEN
C.E. Fritzes Kungl. Hovbokhandel
Fredsgatan 2
Stockholm 16

SWITZERLAND
Librairie Payot
Rue Grenus 6
1211 Geneva 11

TURKEY
Librairie Hachette
469, Istiklâl Caddesi
Beyoğlu, Istanbul

UKRAINIAN SOVIET SOCIALIST REPUBLIC
See under USSR

UNION OF SOVIET SOCIALIST REPUBLICS
Mezhdunarodnaya Kniga
Smolenskaya-Sennaya 32-34
Moscow G-200

UNITED KINGDOM OF GREAT BRITAIN AND NORTHERN IRELAND
Her Majesty's Stationery Office
P.O. Box 569
London, S.E.1

UNITED STATES OF AMERICA
National Agency for
International Publications, Inc.
317 East 34th Street
New York, N.Y. 10016

VENEZUELA
Sr. Braulio Gabriel Chacares
Gobernador a Candilito 37
Santa Rosalía
(Apartado Postal 8092)
Caracas D.F.

YUGOSLAVIA
Jugoslovenska Knjiga
Terazije 27
Belgrade

IAEA publications can also be purchased retail at the United Nations Bookshop at United Nations Headquarters, New York, at the news-stand at the Agency's Headquarters, Vienna, and at most conferences, symposia and seminars organized by the Agency.

In order to facilitate the distribution of its publications, the Agency is prepared to accept payment in UNESCO coupons or in local currencies.

Orders and inquiries from countries where sales agents have not yet been appointed may be sent to:

Distribution and Sales Group, International Atomic Energy Agency,
Kärntner Ring 11, A-1010, Vienna I, Austria

INTERNATIONAL
ATOMIC ENERGY AGENCY
VIENNA, 1968

PRICE: US $13.50
Austrian Schillings 349,-
(£4.15.4; F.Fr. 66,20; DM 54,-)